

Vaidy S. Sunderam  
Geert Dick van Albada  
Peter M. A. Sloot  
Jack J. Dongarra (Eds.)

LNCS 3516

# Computational Science – ICCS 2005

**5th International Conference  
Atlanta, GA, USA, May 2005  
Proceedings, Part III**

**3**  
Part III

 Springer

*Commenced Publication in 1973*

Founding and Former Series Editors:

Gerhard Goos, Juris Hartmanis, and Jan van Leeuwen

## Editorial Board

David Hutchison

*Lancaster University, UK*

Takeo Kanade

*Carnegie Mellon University, Pittsburgh, PA, USA*

Josef Kittler

*University of Surrey, Guildford, UK*

Jon M. Kleinberg

*Cornell University, Ithaca, NY, USA*

Friedemann Mattern

*ETH Zurich, Switzerland*

John C. Mitchell

*Stanford University, CA, USA*

Moni Naor

*Weizmann Institute of Science, Rehovot, Israel*

Oscar Nierstrasz

*University of Bern, Switzerland*

C. Pandu Rangan

*Indian Institute of Technology, Madras, India*

Bernhard Steffen

*University of Dortmund, Germany*

Madhu Sudan

*Massachusetts Institute of Technology, MA, USA*

Demetri Terzopoulos

*New York University, NY, USA*

Doug Tygar

*University of California, Berkeley, CA, USA*

Moshe Y. Vardi

*Rice University, Houston, TX, USA*

Gerhard Weikum

*Max-Planck Institute of Computer Science, Saarbruecken, Germany*

Vaidy S. Sunderam Geert Dick van Albada  
Peter M.A. Sloot Jack J. Dongarra (Eds.)

# Computational Science – ICCS 2005

5th International Conference  
Atlanta, GA, USA, May 22-25, 2005  
Proceedings, Part III

## Volume Editors

Vaidy S. Sunderam  
Emory University  
Dept. of Math and Computer Science  
400 Dowman Dr, W430, Atlanta, GA 30322, USA  
E-mail: vss@mathcs.emory.edu

Geert Dick van Albada  
Peter M.A. Sloot  
University of Amsterdam  
Department of Mathematics and Computer Science  
Kruislaan 403, 1098 SJ Amsterdam, The Netherlands  
E-mail: {dick,sloot}@science.uva.nl

Jack J. Dongarra  
University of Tennessee  
Computer Science Department  
1122 Volunteer Blvd., Knoxville, TN 37996-3450, USA  
E-mail: dongarra@cs.utk.edu

Library of Congress Control Number: 2005925759

CR Subject Classification (1998): D, F, G, H, I, J, C.2-3

ISSN           0302-9743  
ISBN-10       3-540-26044-7 Springer Berlin Heidelberg New York  
ISBN-13       978-3-540-26044-8 Springer Berlin Heidelberg New York

This work is subject to copyright. All rights are reserved, whether the whole or part of the material is concerned, specifically the rights of translation, reprinting, re-use of illustrations, recitation, broadcasting, reproduction on microfilms or in any other way, and storage in data banks. Duplication of this publication or parts thereof is permitted only under the provisions of the German Copyright Law of September 9, 1965, in its current version, and permission for use must always be obtained from Springer. Violations are liable to prosecution under the German Copyright Law.

Springer is a part of Springer Science+Business Media

[springeronline.com](http://springeronline.com)

© Springer-Verlag Berlin Heidelberg 2005  
Printed in Germany

Typesetting: Camera-ready by author, data conversion by Scientific Publishing Services, Chennai, India  
Printed on acid-free paper   SPIN: 11428862   06/3142   5 4 3 2 1 0



# Preface

The Fifth International Conference on Computational Science (ICCS 2005) held in Atlanta, Georgia, USA, May 22–25, 2005, continued in the tradition of previous conferences in the series: ICCS 2004 in Krakow, Poland; ICCS 2003 held simultaneously at two locations, in Melbourne, Australia and St. Petersburg, Russia; ICCS 2002 in Amsterdam, The Netherlands; and ICCS 2001 in San Francisco, California, USA.

Computational science is rapidly maturing as a mainstream discipline. It is central to an ever-expanding variety of fields in which computational methods and tools enable new discoveries with greater accuracy and speed. ICCS 2005 was organized as a forum for scientists from the core disciplines of computational science and numerous application areas to discuss and exchange ideas, results, and future directions. ICCS participants included researchers from many application domains, including those interested in advanced computational methods for physics, chemistry, life sciences, engineering, economics and finance, arts and humanities, as well as computer system vendors and software developers. The primary objectives of this conference were to discuss problems and solutions in all areas, to identify new issues, to shape future directions of research, and to help users apply various advanced computational techniques. The event highlighted recent developments in algorithms, computational kernels, next generation computing systems, tools, advanced numerical methods, data-driven systems, and emerging application fields, such as complex systems, finance, bioinformatics, computational aspects of wireless and mobile networks, graphics, and hybrid computation. Keynote lectures were delivered by John Drake – High End Simulation of the Climate and Development of Earth System Models; Marian Bubak – Towards Knowledge – Based Computing: Personal Views on Recent Developments in Computational Science and the CrossGrid Project; Alok Choudhary – Large Scale Scientific Data Management; and David Keyes – Large Scale Scientific Discovery through Advanced Computing.

In addition, four invited presentations were delivered by representatives of industry: David Barkai from Intel Corporation, Mladen Karcic from IBM, Steve Modica from SGI and Dan Fay from Microsoft. Seven tutorials preceded the main technical program of the conference: Tools for Program Analysis in Computational Science by Dieter Kranzlmüller and Andreas Knüpfer; Computer Graphics and Geometric Modeling by Andrés Iglesias; Component Software for High Performance Computing Using the CCA by David Bernholdt; Computational Domains for Explorations in Nanoscience and Technology, by Jun Ni, Deepak Srivastava, Shaoping Xiao and M. Meyyappan; Wireless and Mobile Communications by Tae-Jin Lee and Hyunseung Choo; Biomedical Literature Mining and Its Applications in Bioinformatics by Tony Hu; and Alternative Approaches to

Grids and Metacomputing by Gunther Stuer. We would like to thank all keynote, invited and tutorial speakers for their interesting and inspiring talks.

Aside from the plenary lectures, the conference included 10 parallel oral sessions and 3 poster sessions. Ever since the first meeting in San Francisco, ICCS has attracted an increasing number of researchers involved in the challenging field of computational science. For ICCS 2005, we received 464 contributions for the main track and over 370 contributions for 24 originally-proposed workshops. Of these submissions, 134 were accepted as full papers accompanied by oral presentations, and 89 for posters in the main track, while 241 papers were accepted for presentations at 21 workshops. This selection was possible thanks to the hard work of the 88-member Program Committee and 362 reviewers. The author index contains 1395 names, and over 500 participants from 41 countries and all continents attended the conference. The ICCS 2005 proceedings consists of three volumes. The first volume, LNCS 3514, contains the full papers from the main track of the conference, while volumes 3515 and 3516 contain the papers accepted for the workshops and short papers. The papers cover a wide range of topics in computational science, ranging from numerical methods, algorithms, and computational kernels to programming environments, grids, networking and tools. These contributions, which address foundational and computer science aspects are complemented by papers discussing computational applications in a variety of domains. ICCS continues its tradition of printed proceedings, augmented by CD-ROM versions for the conference participants. We would like to thank Springer for their cooperation and partnership. We hope that the ICCS 2005 proceedings will serve as a major intellectual resource for computational science researchers for many years to come. During the conference the best papers from the main track and workshops as well as the best posters were nominated and commended on the ICCS 2005 Website. A number of papers will also be published in special issues of selected journals.

We owe thanks to all workshop organizers and members of the Program Committee for their diligent work, which led to the very high quality of the event. We would like to express our gratitude to Emory University and Emory College in general, and the Department of Mathematics and Computer Science in particular, for their wholehearted support of ICCS 2005. We are indebted to all the members of the Local Organizing Committee for their enthusiastic work towards the success of ICCS 2005, and to numerous colleagues from various Emory University units for their help in different aspects of organization. We very much appreciate the help of Emory University students during the conference. We owe special thanks to our corporate sponsors: Intel, IBM, Microsoft Research, SGI, and Springer; and to ICIS, Math & Computer Science, Emory College, the Provost's Office, and the Graduate School at Emory University for their generous support. ICCS 2005 was organized by the Distributed Computing Laboratory at the Department of Mathematics and Computer Science at Emory University, with support from the Innovative Computing Laboratory at the University of Tennessee and the Computational Science Section at the University of Amsterdam, in cooperation with the Society for Industrial and Applied Mathe-

matics (SIAM). We invite you to visit the ICCS 2005 Website (<http://www.iccs-meeting.org/ICCS2005/>) to recount the events leading up to the conference, to view the technical program, and to recall memories of three and a half days of engagement in the interest of fostering and advancing computational science.

June 2005

Vaidy Sunderam  
on behalf of  
G. Dick van Albada  
Jack J. Dongarra  
Peter M.A. Sloot

# Organization

ICCS 2005 was organized by the Distributed Computing Laboratory, Department of Mathematics and Computer Science, Emory University, Atlanta, GA, USA, in cooperation with Emory College, Emory University (USA), the University of Tennessee (USA), the University of Amsterdam (The Netherlands), and the Society for Industrial and Applied Mathematics (SIAM). The conference took place on the campus of Emory University, in Atlanta, Georgia, USA.

## Conference Chairs

Scientific Chair – Vaidy Sunderam (Emory University, USA)

Workshops Chair – Dick van Albada (University of Amsterdam, The Netherlands)

ICCS Series Overall Chair – Peter M.A. Sloot (University of Amsterdam, The Netherlands)

ICCS Series Overall Co-Chair – Jack Dongarra (University of Tennessee, USA)

## Local Organizing Committee

Dawid Kurzyniec (Chair)

Piotr Wendykier

Jeri Sandlin

Erin Nagle

Ann Dasher

Sherry Ebrahimi

## Sponsoring Institutions

Intel Corporation

IBM Corporation

Microsoft Research

SGI Silicon Graphics Inc.

Emory University, Department of Mathematics and Computer Science

Emory University, Institute for Comparative and International Studies

Emory University, Emory College

Emory University, Office of the Provost

Emory University, Graduate School of Arts and Sciences

Springer

## Program Committee

Jemal Abawajy, Deakin University, Australia  
David Abramson, Monash University, Australia  
Dick van Albada, University of Amsterdam, The Netherlands  
Vassil Alexandrov, University of Reading, UK  
Srinivas Aluru, Iowa State University, USA  
Brian d'Auriol, University of Texas at El Paso, USA  
David A. Bader, University of New Mexico, USA  
Saeid Belkasim, Georgia State University, USA  
Anne Benoit, University of Edinburgh, UK  
Michele Benzi, Emory University, USA  
Rod Blais, University of Calgary, Canada  
Alexander Bogdanov, Institute for High Performance Computing and Information Systems, Russia  
Anu Bourgeois, Georgia State University, USA  
Jan Broeckhove, University of Antwerp, Belgium  
Marian Bubak, Institute of Computer Science and ACC Cyfronet – AGH, Poland  
Rajkumar Buyya, University of Melbourne, Australia  
Tiziana Calamoneri, University of Rome “La Sapienza”, Italy  
Serge Chaumette, University of Bordeaux, France  
Toni Cortes, Universitat Politècnica de Catalunya, Spain  
Yiannis Cotronis, University of Athens, Greece  
Jose C. Cunha, New University of Lisbon, Portugal  
Pawel Czarnul, Gdansk University of Technology, Poland  
Frederic Desprez, INRIA, France  
Tom Dhaene, University of Antwerp, Belgium  
Hassan Diab, American University of Beirut, Lebanon  
Beniamino Di Martino, Second University of Naples, Italy  
Jack Dongarra, University of Tennessee, USA  
Craig Douglas, University of Kentucky, USA  
Edgar Gabriel, University of Stuttgart, Germany  
Marina Gavrilova, University of Calgary, Canada  
Michael Gerndt, Technical University of Munich, Germany  
Yuriy Gorbachev, Institute for High Performance Computing and Information Systems, Russia  
Andrzej Goscinski, Deakin University, Australia  
Eldad Haber, Emory University, USA  
Ladislav Hluchy, Slovak Academy of Science, Slovakia  
Alfons Hoekstra, University of Amsterdam, The Netherlands  
Yunqing Huang, Xiangtan University, China  
Andrés Iglesias, University of Cantabria, Spain  
Hai Jin, Huazhong University of Science and Technology, China  
Peter Kacsuk, MTA SZTAKI Research Institute, Hungary  
Jacek Kitowski, AGH University of Science and Technology, Poland

Dieter Kranzlmüller, Johannes Kepler University Linz, Austria  
Valeria Krzhizhanovskaya, University of Amsterdam, The Netherlands  
Dawid Kurzyniec, Emory University, USA  
Domenico Laforenza, Italian National Research Council, Italy  
Antonio Lagana, University of Perugia, Italy  
Francis Lau, The University of Hong Kong, China  
Laurent Lefevre, INRIA, France  
Bogdan Lesyng, ICM Warszawa, Poland  
Thomas Ludwig, University of Heidelberg, Germany  
Emilio Luque, Universitat Autònoma de Barcelona, Spain  
Piyush Maheshwari, University of New South Wales, Australia  
Maciej Malawski, Institute of Computer Science AGH, Poland  
Michael Mascagni, Florida State University, USA  
Taneli Mielikäinen, University of Helsinki, Finland  
Edward Moreno, Euripides Foundation of Marilia, Brazil  
Wolfgang Nagel, Dresden University of Technology, Germany  
Genri Norman, Russian Academy of Sciences, Russia  
Stephan Olariu, Old Dominion University, USA  
Salvatore Orlando, University of Venice, Italy  
Robert M. Panoff, Shodor Education Foundation, Inc., USA  
Marcin Paprzycki, Oklahoma State University, USA  
Ron Perrott, Queen's University of Belfast, UK  
Richard Ramarosan, ONERA, France  
Rosemary Renaut, Arizona State University, USA  
Alistair Rendell, Australian National University, Australia  
Paul Roe, Queensland University of Technology, Australia  
Dale Shires, U.S. Army Research Laboratory, USA  
Charles Shoniregun, University of East London, UK  
Magda Slawinska, Gdansk University of Technology, Poland  
Peter Sloot, University of Amsterdam, The Netherlands  
Gunther Stuer, University of Antwerp, Belgium  
Boleslaw Szymanski, Rensselaer Polytechnic Institute, USA  
Ryszard Tadeusiewicz, AGH University of Science and Technology, Poland  
Pavel Tvrđik, Czech Technical University, Czech Republic  
Putchong Uthayopas, Kasetsart University, Thailand  
Jesus Vigo-Aguiar, University of Salamanca, Spain  
Jerzy Waśniewski, Technical University of Denmark, Denmark  
Greg Watson, Los Alamos National Laboratory, USA  
Peter H. Welch, University of Kent, UK  
Piotr Wendykier, Emory University, USA  
Roland Wismüller, University of Siegen, Germany  
Baowen Xu, Southeast University Nanjing, China  
Yong Xue, Chinese Academy of Sciences, China  
Xiaodong Zhang, College of William and Mary, USA  
Alexander Zhmakin, SoftImpact Ltd., Russia

Krzysztof Zielinski, ICS UST / CYFRONET, Poland

Zahari Zlatev, National Environmental Research Institute, Denmark

Elena Zudilova-Seinstra, University of Amsterdam, The Netherlands

## Reviewers

Adrian Kacso	Bastien Chopard	David Green
Adrian Sandu	Behrooz Shirazi	David Lowenthal
Akshaye Dhawan	Ben Jackson	David Roberts
Alberto	Beniamino Di Martino	Dawid Kurzyniec
Sanchez-Campos	Benjamin N. Jackson	Dick van Albada
Alex Tiskin	Benny Cheung	Diego Javier Mostaccio
Alexander Bogdanov	Biju Sayed	Dieter Kranzlmüller
Alexander Zhmakin	Bogdan Lesyng	Dirk Deschrijver
Alexandre Dupuis	Bogdan Smolka	Dirk Roekaerts
Alexandre Tiskin	Boleslaw Szymanski	Domenico Laforenza
Alexandros Gerbessiotis	Breannan O’Nuallain	Donny Kurniawan
Alexey S. Rodionov	Brian d’Auriol	Eddy Caron
Alfons Hoekstra	Brice Goglin	Edgar Gabriel
Alfredo Tirado-Ramos	Bruce Boghosian	Edith Spiegl
Ali Haleeb	Casiano Rodriguez León	Edward Moreno
Alistair Rendell	Charles Shoniregun	Eldad Haber
Ana Ripoll	Charles Stewart	Elena Zudilova-Seinstra
A. Kalyanaraman	Chen Lihua	Elisa Heymann
Andre Merzky	Chris Homescu	Emanouil Atanassov
Andreas Hoffmann	Chris R. Kleijn	Emilio Luque
Andrés Iglesias	Christian Glasner	Eunjoo Lee
Andrew Adamatzky	Christian Perez	Eunjung Cho
Andrzej Czygrinow	C. Schaub Schlaeger	Evarestov
Andrzej Gościński	Christoph Anthes	Evghenii Gaburov
Aneta Karaivanova	Clemens Grelck	Fabrizio Silvestri
Anna Morajko	Colin Enticott	Feng Tan
Anne Benoit	Corrado Zoccolo	Fethi A. Rabhi
Antonio Lagana	Craig C. Douglas	Floros Evangelos
Anu G. Bourgeois	Craig Lee	Francesco Moscato
Ari Rantanen	Cristina Negoita	Francis Lau
Armelle Merlin	Dacian Daescu	Francisco J. Rosales
Arndt Bode	Daewon W. Byun	Franck Cappello
B. Frankovic	Dale Shires	Frank Dehne
Bahman Javadi	Danica Janglova	Frank Dopatka
Baowen Xu	Daniel Pressel	Frank J. Seinstra
Barbara Glut	Dave Roberts	Frantisek Capkovic
Bartosz Baliś	David Abramson	Frederic Desprez
Bas van Vlijmen	David A. Bader	Frederic Hancke

Frédéric Gava	Jinling Yang	Massimo Coppola
Frédéric Loulergue	John Copeland	Mathilde Romberg
Frederick T. Sheldon	John Michopoulos	Mathura Gopalan
Gang Kou	Jonas Latt	Matthew Sottile
Genri Norman	Jongpil Jeong	Matthias Kawski
George Athanasopoulos	Jose L. Bosque	Matthias Müller
Greg Watson	Jose C. Cunha	Mauro Iacono
Gunther Stuer	Jose Alberto Fernandez	Michał Malafiejski
Haewon Nam	Josep Jorba Esteve	Michael Gerndt
Hai Jin	Jun Wu	Michael Mascagni
Hassan Diab	Jürgen Jähnert	Michael Navon
He Jing	Katarzyna Rycerz	Michael Scarpa
Holger Bischof	Kawther Rekabi	Michele Benzi
Holly Dail	Ken Nguyen	Mikhail Zatevakhin
Hongbin Guo	Ken C.K. Tsang	Miroslav Dobrucky
Hongquan Zhu	K.N. Plataniotis	Mohammed Yousoof
Hong-Seok Lee	Krzysztof Boryczko	Moonseong Kim
Hui Liu	Krzysztof Grzda	Moshe Sipper
Hyoung-Key Choi	Krzysztof Zieliński	Nageswara S. V. Rao
Hyung-Min Lee	Kurt Vanmechelen	Narayana Jayaram
Hyunseung Choo	Ladislav Hluchy	NianYan
I.M. Navon	Laurence T. Yang	Nicola Tonello
Igor Mokris	Laurent Lefevre	Nicolas Wicker
Igor Schagaev	Laurent Philippe	Nikolai Simonov
Irina Schweigert	Lean Yu	Nisar Hundewale
Irina Shoshmina	Leigh Little	Osni Marques
Isabelle Guérin-Lassous	Liang Cheng	Pang Ko
Ivan Dimov	Lihua Chen	Paul Albuquerque
Ivana Budinska	Lijuan Zhu	Paul Evangelista
J. Kroc	Luis M. Portela	Paul Gray
J.G. Verwer	Luoding Zhu	Paul Heinzlreiter
Jacek Kitowski	M. Mat Deris	Paul Roe
Jack Dongarra	Maciej Malawski	Paula Fritzsche
Jan Broeckhove	Magda Sławińska	Paulo Afonso Lopes
Jan Glasa	Marcin Paprzycki	Pavel Tvrđik
Jan Humble	Marcin Radecki	Paweł Czarnul
Jean-Luc Falcone	Marcin Sntek	Paweł Kaczmarek
Jean-Yves L'Excellent	Marco Aldinucci	Peggy Lindner
Jemal Abawajy	Marek Gajcki	Peter Brezany
Jens Gustedt	Maria S. Pérez	Peter Hellinckx
Jens Volkert	Marian Bubak	Peter Kacsuk
Jerzy Waśniewski	Marina Gavrilova	Peter Sloot
Jesus Vigo-Aguiar	Marios Dikaiakos	Peter H. Welch
Jianping Li	Martin Polak	Philip Chan
Jing He	Martin Quinson	Phillip A. Laplante



Pierre Fraigniaud	Samira El Yacoubi	Tomasz Gubała
Pilar Herrero	Sang-Hun Cho	Tomasz Szeplieniec
Piotr Bala	Sarah M. Orley	Toni Cortes
Piotr Wendykier	Satoyuki Kawano	Ulrich Brandt-Pollmann
Piyush Maheshwari	Savio Tse	V. Vshivkov
Porfidio Hernandez	Scott Emrich	Vaidy Sunderam
Praveen Madiraju	Scott Lathrop	Valentina Casola
Putchong Uthayopas	Seong-Moo Yoo	V. Krzhizhanovskaya
Qiang-Sheng Hua	Serge Chaumette	Vassil Alexandrov
R. Vollmar	Sergei Gorlatch	Victor Malyshekin
Rafał Wcisło	Seungchan Kim	Viet D. Tran
Rafik Ouared	Shahaan Ayyub	Vladimir K. Popkov
Rainer Keller	Shanyu Tang	V.V. Shakhov
Rajkumar Buyya	Sibel Adali	Włodzimierz Funika
Rastislav Lukac	Siegfried Benkner	Wai-Kwong Wing
Renata Słota	Sridhar Radharkrishnan	Wei Yin
Rene Kobler	Srinivas Aluru	Wenyuan Liao
Richard Mason	Srinivas Vadrevu	Witold Alda
Richard Ramarosan	Stefan Marconi	Witold Dzwinel
Rob H. Bisseling	Stefania Bandini	Wojtek Gościński
Robert M. Panoff	Stefano Marrone	Wolfgang E. Nagel
Robert Schaefer	Stephan Olariu	Wouter Hendrickx
Robin Wolff	Stephen Gilmore	Xiaodong Zhang
Rocco Aversa	Steve Chiu	Yannis Cotronis
Rod Blais	Sudip K. Seal	Yi Peng
Roeland Merks	Sung Y. Shin	Yong Fang
Roland Wismüller	Takashi Matsuhisa	Yong Shi
Rolf Rabenseifner	Taneli Mielikäinen	Yong Xue
Rolf Sander	Thilo Kielmann	Yumi Choi
Ron Perrott	Thomas Ludwig	Yunqing Huang
Rosemary Renaut	Thomas Richter	Yuriy Gorbachev
Ryszard Tadeusiewicz	Thomas Worsch	Zahari Zlatev
S. Lakshminarayanan	Tianfeng Chai	Zaid Zabanoot
Saeid Belkasim	Timothy Jones	Zhenjiang Hu
Salvatore Orlando	Tiziana Calamoneri	Zhiming Zhao
Salvatore Venticinque	Todor Gurov	Zoltan Juhasz
Sam G. Lambrakos	Tom Dhaene	Zsolt Nemeth

## Workshops Organizers

### High Performance Computing in Academia: Systems and Applications

Denis Donnelly – Siena College, USA

Ulrich Rude – Universität Erlangen-Nürnberg

**Tools for Program Development and Analysis in Computational Science**

Dieter Kranzlmüller – GUP, Joh. Kepler University Linz, Austria

Arndt Bode – Technical University Munich, Germany

Jens Volkert – GUP, Joh. Kepler University Linz, Austria

Roland Wismüller – University of Siegen, Germany

**Practical Aspects of High-Level Parallel Programming (PAPP)**

Frédéric Loulergue – Université Paris Val de Marne, France

**2005 International Workshop on Bioinformatics Research and Applications**

Yi Pan – Georgia State University, USA

Alex Zelikovsky – Georgia State University, USA

**Computer Graphics and Geometric Modeling, CGGM 2005**

Andrés Iglesias – University of Cantabria, Spain

**Computer Algebra Systems and Applications, CASA 2005**

Andrés Iglesias – University of Cantabria, Spain

Akemi Galvez – University of Cantabria, Spain

**Wireless and Mobile Systems**

Hyunseung Choo – Sungkyunkwan University, Korea

Eui-Nam Huh Seoul – Womens University, Korea

Hyoung-Kee Choi – Sungkyunkwan University, Korea

Youngsong Mun – Soongsil University, Korea

**Intelligent Agents in Computing Systems -The Agent Days 2005 in Atlanta**

Krzysztof Cetnarowicz – Academy of Science and Technology AGH, Krakow, Poland

Robert Schaefer – Jagiellonian University, Krakow, Poland

**Programming Grids and Metacomputing Systems - PGaMS2005**

Maciej Malawski – Institute of Computer Science, Academy of Science and Technology AGH, Krakow, Poland

Gunther Stuer – Universiteit Antwerpen, Belgium

**Autonomic Distributed Data and Storage Systems Management – ADSM2005**

Jemal H. Abawajy – Deakin University, Australia

M. Mat Deris – College University Tun Hussein Onn, Malaysia

**GeoComputation**

Yong Xue – London Metropolitan University, UK

**Computational Economics and Finance**

Yong Shi – University of Nebraska, Omaha, USA

Xiaotie Deng – University of Nebraska, Omaha, USA

Shouyang Wang – University of Nebraska, Omaha, USA

**Simulation of Multiphysics Multiscale Systems**

Valeria Krzhizhanovskaya – University of Amsterdam, The Netherlands

Bastien Chopard – University of Geneva, Switzerland

Yuriy Gorbachev – Institute for High Performance Computing & Data Bases, Russia

**Dynamic Data Driven Application Systems**

Frederica Darema – National Science Foundation, USA

**2nd International Workshop on Active and Programmable Grids Architectures and Components (APGAC2005)**

Alex Galis – University College London, UK

**Parallel Monte Carlo Algorithms for Diverse Applications in a Distributed Setting**

Vassil Alexandrov – University of Reading, UK

Aneta Karaivanova – Institute for Parallel Processing, Bulgarian Academy of Sciences

Ivan Dimov – Institute for Parallel Processing, Bulgarian Academy of Sciences

**Grid Computing Security and Resource Management**

Maria Pérez – Universidad Politécnica de Madrid, Spain

Jemal Abawajy – Deakin University, Australia

### **Modelling of Complex Systems by Cellular Automata**

Jiri Kroc – Helsinki School of Economics, Finland

S. El Yacoubi – University of Perpignan, France

M. Sipper – Ben-Gurion University, Israel

R. Vollmar – University of Karlsruhe, Germany

### **International Workshop on Computational Nanoscience and Technology**

Jun Ni – The University of Iowa, USA

Shaoping Xiao – The University of Iowa, USA

### **New Computational Tools for Advancing Atmospheric and Oceanic Sciences**

Adrian Sandu – Virginia Tech, USA

### **Collaborative and Cooperative Environments**

Vassil Alexandrov – University of Reading, UK

Christoph Anthes – GUP, Joh. Kepler University Linz, Austria

David Roberts – University of Salford, UK

Dieter Kranzlmüller – GUP, Joh. Kepler University Linz, Austria

Jens Volkert – GUP, Joh. Kepler University Linz, Austria

# Table of Contents – Part III

## Workshop on “Simulation of Multiphysics Multiscale Systems”

Multiscale Finite Element Modeling of the Coupled Nonlinear Dynamics of Magnetostrictive Composite Thin Film <i>Debiprosad Roy Mahapatra, Debi Prasad Ghosh, Gopalakrishnan Srinivasan</i> .....	1
Large-Scale Fluctuations of Pressure in Fluid Flow Through Porous Medium with Multiscale Log-Stable Permeability <i>Olga Soboleva</i> .....	9
A Computational Model of Micro-vascular Growth <i>Dominik Szczerba, Gábor Székely</i> .....	17
A Dynamic Model for Phase Transformations in 3D Samples of Shape Memory Alloys <i>D.R. Mahapatra, R.V.N. Melnik</i> .....	25
3D Finite Element Modeling of Free-Surface Flows with Efficient $k - \epsilon$ Turbulence Model and Non-hydrostatic Pressure <i>Célestin Leupi, Mustafa Siddik Altınakar</i> .....	33
Cluster Computing for Transient Simulations of the Linear Boltzmann Equation on Irregular Three-Dimensional Domains <i>Matthias K. Gobbert, Mark L. Breitenbach, Timothy S. Cale</i> .....	41
The Use of Conformal Voxels for Consistent Extractions from Multiple Level-Set Fields <i>Max O. Bloomfield, David F. Richards, Timothy S. Cale</i> .....	49
Nonlinear OIFS for a Hybrid Galerkin Atmospheric Model <i>Amik St.-Cyr, Stephen J. Thomas</i> .....	57
Flamelet Analysis of Turbulent Combustion <i>R.J.M. Bastiaans, S.M. Martin, H. Pitsch, J.A. van Oijen, L.P.H. de Goey</i> .....	64
Entropic Lattice Boltzmann Method on Non-uniform Grids <i>C. Shyam Sunder, V. Babu</i> .....	72

A Data-Driven Multi-field Analysis of Nanocomposites for Hydrogen Storage <i>John Michopoulos, Nick Tran, Sam Lambrakos</i> .....	80
Plug and Play Approach to Validation of Particle-Based Algorithms <i>Giovanni Lapenta, Stefano Markidis</i> .....	88
Multiscale Angiogenesis Modeling <i>Shuyu Sun, Mary F. Wheeler, Mandri Obeyesekere, Charles Patrick Jr</i> .....	96
The Simulation of a PEMFC with an Interdigitated Flow Field Design <i>S.M. Guo</i> .....	104
Multiscale Modelling of Bubbly Systems Using Wavelet-Based Mesh Adaptation <i>Tom Liu, Phil Schwarz</i> .....	112
Computational Study on the Effect of Turbulence Intensity and Pulse Frequency in Soot Concentration in an Acetylene Diffusion Flame <i>Fernando Lopez-Parra, Ali Turan</i> .....	120
Application Benefits of Advanced Equation-Based Multiphysics Modeling <i>Lars Langemyr, Nils Malm</i> .....	129
Large Eddy Simulation of Spanwise Rotating Turbulent Channel and Duct Flows by a Finite Volume Code at Low Reynolds Numbers <i>Kursad Melih Guleren, Ali Turan</i> .....	130
Modelling Dynamics of Genetic Networks as a Multiscale Process <i>Xilin Wei, Roderick V.N. Melnik, Gabriel Moreno-Hagelsieb</i> .....	134
Mathematical Model of Environmental Pollution by Motorcar in an Urban Area <i>Valeriy Perminov</i> .....	139
The Monte Carlo and Molecular Dynamics Simulation of Gas-Surface Interaction <i>Sergey Borisov, Oleg Sazhin, Olesya Gerasimova</i> .....	143
<b>Workshop on “Grid Computing Security and Resource Management”</b>	
GIVS: Integrity Validation for Grid Security <i>Giuliano Casale, Stefano Zanero</i> .....	147

On the Impact of Reservations from the Grid on Planning-Based Resource Management <i>Felix Heine, Matthias Hovestadt, Odej Kao, Achim Streit</i> . . . . .	155
Genius: Peer-to-Peer Location-Aware Gossip Using Network Coordinates <i>Ning Ning, Dongsheng Wang, Yongquan Ma, Jinfeng Hu, Jing Sun, Chongnan Gao, Weiming Zheng</i> . . . . .	163
DCP-Grid, a Framework for Conversational Distributed Transactions on Grid Environments <i>Manuel Salvadores, Pilar Herrero, María S. Pérez, Víctor Robles</i> . . . .	171
Dynamic and Fine-Grained Authentication and Authorization Architecture for Grid Computing <i>Hyunjoon Jung, Hyuck Han, Hyungsoo Jung, Heon Y. Yeom</i> . . . . .	179
GridSec: Trusted Grid Computing with Security Binding and Self-defense Against Network Worms and DDoS Attacks <i>Kai Hwang, Yu-Kwong Kwok, Shanshan Song, Min Cai Yu Chen, Ying Chen, Runfang Zhou, Xiaosong Lou</i> . . . . .	187
Design and Implementation of DAG-Based Co-scheduling of RPC in the Grid <i>JiHyun Choi, DongWoo Lee, R.S. Ramakrishna, Michael Thomas, Harvey Newman</i> . . . . .	196
Performance Analysis of Interconnection Networks for Multi-cluster Systems <i>Bahman Javadi, J.H. Abawajy, Mohammad K. Akbari</i> . . . . .	205
Autonomic Job Scheduling Policy for Grid Computing <i>J.H. Abawajy</i> . . . . .	213
A New Trust Framework for Resource-Sharing in the Grid Environment <i>Hualiang Hu, Deren Chen, Changqin Huang</i> . . . . .	221
An Intrusion-Resilient Authorization and Authentication Framework for Grid Computing Infrastructure <i>Yuanbo Guo, Jianfeng Ma, Yadi Wang</i> . . . . .	229

## 2nd International Workshop on Active and Programmable Grids Architectures and Components (APGAC2005)

An Active Platform as Middleware for Services and Communities Discovery <i>Sylvain Martin, Guy Leduc</i> . . . . .	237
p2pCM: A Structured Peer-to-Peer Grid Component Model <i>Carles Pairo, Pedro García, Rubén Mondéjar, Antonio F. Gómez Skarmeta</i> . . . . .	246
Resource Partitioning Algorithms in a Programmable Service Grid Architecture <i>Pieter Thysebaert, Bruno Volckaert, Marc De Leenheer, Filip De Turck, Bart Dhoedt, Piet Demeester</i> . . . . .	250
Triggering Network Services Through Context-Tagged Flows <i>Roel Ocampo, Alex Galis, Chris Todd</i> . . . . .	259
Dependable Execution of Workflow Activities on a Virtual Private Grid Middleware <i>A. Machì, F. Collura, S. Lombardo</i> . . . . .	267
Cost Model and Adaptive Scheme for Publish/Subscribe Systems on Mobile Grid Environments <i>Sangyoon Oh, Sangmi Lee Pallickara, Sunghoon Ko, Jai-Hoon Kim, Geoffrey Fox</i> . . . . .	275
Near-Optimal Algorithm for Self-configuration of Ad-hoc Wireless Networks <i>Sung-Eok Jeon, Chuanyi Ji</i> . . . . .	279
<b>International Workshop on Computational Nano-Science and Technology</b>	
The Applications of Meshfree Particle Methods at the Nanoscale <i>Weizuan Yang, Shaoping Xiao</i> . . . . .	284
Numerical Simulation of Self-heating InGaP/GaAs Heterojunction Bipolar Transistors <i>Yiming Li, Kuen-Yu Huang</i> . . . . .	292
Adaptive Finite Volume Simulation of Electrical Characteristics of Organic Light Emitting Diodes <i>Yiming Li, Pu Chen</i> . . . . .	300



Characterization of a Solid State DNA Nanopore Sequencer Using Multi-scale (Nano-to-Device) Modeling <i>Jerry Jenkins, Debasis Sengupta, Shankar Sundaram</i> . . . . .	309
Comparison of Nonlinear Conjugate-Gradient Methods for Computing the Electronic Properties of Nanostructure Architectures <i>Stanimire Tomov, Julien Langou, Andrew Canning, Lin-Wang Wang, Jack Dongarra</i> . . . . .	317
A Grid-Based Bridging Domain Multiple-Scale Method for Computational Nanotechnology <i>Shaowen Wang, Shaoping Xiao, Jun Ni</i> . . . . .	326
Signal Cascades Analysis in Nanoprocesses with Distributed Database System <i>Dariusz Mrozek, Bożena Małysiak, Jacek Fraczek, Paweł Kasprowski</i> . . . . .	334
<b>Workshop on “Collaborative and Cooperative Environments”</b>	
Virtual States and Transitions, Virtual Sessions and Collaboration <i>Dimitri Bourilkov</i> . . . . .	342
A Secure Peer-to-Peer Group Collaboration Scheme for Healthcare System <i>Byong-In Lim, Kee-Hyun Choi, Dong-Ryeol Shin</i> . . . . .	346
Tools for Collaborative VR Application Development <i>Adrian Haffegge, Ronan Jamieson, Christoph Anthes, Vassil Alexandrov</i> . . . . .	350
Multicast Application Sharing Tool – Facilitating the eMinerals Virtual Organisation <i>Gareth J. Lewis, S. Mehmood Hasan, Vassil N. Alexandrov, Martin T. Dove, Mark Calleja</i> . . . . .	359
The Collaborative P-GRADE Grid Portal <i>Gareth J. Lewis, Gergely Sipos, Florian Urmetzer, Vassil N. Alexandrov, Peter Kacsuk</i> . . . . .	367
An Approach for Collaboration and Annotation in Video Post-production <i>Karsten Morisse, Thomas Sempf</i> . . . . .	375

A Toolbox Supporting Collaboration in Networked Virtual Environments <i>Christoph Anthes, Jens Volkert</i> .....	383
A Peer-to-Peer Approach to Content Dissemination and Search in Collaborative Networks <i>Ismail Bhana, David Johnson</i> .....	391
<b>Workshop on “Autonomic Distributed Data and Storage Systems Management – ADSM2005”</b>	
TH-VSS: An Asymmetric Storage Virtualization System for the SAN Environment <i>Da Xiao, Jiwu Shu, Wei Xue, Weimin Zheng</i> .....	399
Design and Implementation of the Home-Based Cooperative Cache for PVFS <i>In-Chul Hwang, Hanjo Jung, Seung-Ryoul Maeng, Jung-Wan Cho</i> ...	407
Improving the Data Placement Algorithm of Randomization in SAN <i>Nianmin Yao, Jiwu Shu, Weimin Zheng</i> .....	415
Safety of a Server-Based Version Vector Protocol Implementing Session Guarantees <i>Jerzy Brzeziński, Cezary Sobaniec, Dariusz Wawrzyniak</i> .....	423
Scalable Hybrid Search on Distributed Databases <i>Jungkee Kim, Geoffrey Fox</i> .....	431
Storage QoS Control with Adaptive I/O Deadline Assignment and Slack-Stealing EDF <i>Young Jin Nam, Chanik Park</i> .....	439
High Reliability Replication Technique for Web-Server Cluster Systems <i>M. Mat Deris, J.H. Abawajy, M. Zarina, R. Mamat</i> .....	447
An Efficient Replicated Data Management Approach for Peer-to-Peer Systems <i>J.H. Abawajy</i> .....	457
<b>Workshop on “GeoComputation”</b>	
Explore Disease Mapping of Hepatitis B Using Geostatistical Analysis Techniques <i>Shaobo Zhong, Yong Xue, Chunxiang Cao, Wuchun Cao, Xiaowen Li, Jianping Guo, Liqun Fang</i> .....	464

eMicro: A Grid-Based Spatial Epidemiology Application <i>Jianping Guo, Yong Xue, Chunxiang Cao, Wuchun Cao, Xiaowen Li, Jianqin Wang, Liqun Fang</i> .....	472
Self-organizing Maps as Substitutes for K-Means Clustering <i>Fernando Bação, Victor Lobo, Marco Painho</i> .....	476
Key Technologies Research on Building a Cluster-Based Parallel Computing System for Remote Sensing <i>Guoqing Li, Dingsheng Liu</i> .....	484
Grid Research on Desktop Type Software for Spatial Information Processing <i>Guoqing Li, Dingsheng Liu, Yi Sun</i> .....	492
Java-Based Grid Service Spread and Implementation in Remote Sensing Applications <i>Yanguang Wang, Yong Xue, Jianqin Wang, Chaolin Wu, Yincui Hu, Ying Luo, Shaobo Zhong, Jiakui Tang, Guoyin Cai</i> .....	496
Modern Computational Techniques for Environmental Data; Application to the Global Ozone Layer <i>Costas Varotsos</i> .....	504
PK+ Tree: An Improved Spatial Index Structure of PK Tree <i>Xiaolin Wang, Yingwei Luo, Lishan Yu, Zhuoqun Xu</i> .....	511
Design Hierarchical Component-Based WebGIS <i>Yingwei Luo, Xiaolin Wang, Guomin Xiong, Zhuoqun Xu</i> .....	515
<b>Workshop on “Computational Economics and Finance”</b>	
Adaptive Smoothing Neural Networks in Foreign Exchange Rate Forecasting <i>Lean Yu, Shouyang Wang, Kin Keung Lai</i> .....	523
Credit Scoring via PCALWM <i>Jianping Li, Weixuan Xu, Yong Shi</i> .....	531
Optimization of Bandwidth Allocation in Communication Networks with Penalty Cost <i>Jun Wu, Wuyi Yue, Shouyang Wang</i> .....	539

Improving Clustering Analysis for Credit Card Accounts Classification <i>Yi Peng, Gang Kou, Yong Shi, Zhengxin Chen</i> .....	548
A Fuzzy Index Tracking Portfolio Selection Model <i>Yong Fang, Shou-Yang Wang</i> .....	554
Application of Activity-Based Costing in a Manufacturing Company: A Comparison with Traditional Costing <i>Gonca Tuncel, Derya Eren Akyol, Gunhan Mirac Bayhan, Utku Koker</i> .....	562
Welfare for Economy Under Awareness <i>Ken Horie, Takashi Matsuhisa</i> .....	570
On-line Multi-attributes Procurement Combinatorial Auctions Bidding Strategies <i>Jian Chen, He Huang</i> .....	578
<b>Workshop on “Computer Algebra Systems and Applications, CASA 2005”</b>	
An Algebraic Method for Analyzing Open-Loop Dynamic Systems <i>W. Zhou, D.J. Jeffrey, G.J. Reid</i> .....	586
Pointwise and Uniform Power Series Convergence <i>C. D’Apice, G. Gargiulo, R. Manzo</i> .....	594
Development of SyNRAC <i>Hitoshi Yanami, Hirokazu Anai</i> .....	602
A LiE Subroutine for Computing Prehomogeneous Spaces Associated with Complex Nilpotent Orbits <i>Steven Glenn Jackson, Alfred G. Noël</i> .....	611
Computing Valuation Popov Forms <i>Mark Giesbrecht, George Labahn, Yang Zhang</i> .....	619
Modeling and Simulation of High-Speed Machining Processes Based on Matlab/Simulink <i>Rodolfo E. Haber, J.R. Alique, S. Ros, R.H. Haber</i> .....	627
Remote Access to a Symbolic Computation System for Algebraic Topology: A Client-Server Approach <i>Mirian Andrés, Vico Pascual, Ana Romero, Julio Rubio</i> .....	635

Symbolic Calculation of the Generalized Inertia Matrix of Robots with a Large Number of Joints <i>Ramutis Bansevicius, Algimantas Čepulkauskas, Regina Kulvietienė, Genadijus Kulvietis</i> .....	643
Revisiting Some Control Schemes for Chaotic Synchronization with Mathematica <i>Andrés Iglesias, Akemi Galvez</i> .....	651
Three Brick Method of the Partial Fraction Decomposition of Some Type of Rational Expression <i>Damian Slota, Roman Witula</i> .....	659
Non Binary Codes and “Mathematica” Calculations: Reed-Solomon Codes Over GF ( $2^n$ ) <i>Igor Gashkov</i> .....	663
Stokes-Flow Problem Solved Using Maple <i>Pratibha, D.J. Jeffrey</i> .....	667
<b>Workshop on “Intelligent Agents in Computing Systems” – The Agent Days 2005 in Atlanta</b>	
Grounding a Descriptive Language in Cognitive Agents Using Consensus Methods <i>Agnieszka Pieczynska-Kuchtiak</i> .....	671
Fault-Tolerant and Scalable Protocols for Replicated Services in Mobile Agent Systems <i>JinHo Ahn, Sung-Gi Min</i> .....	679
Multi-agent System Architectures for Wireless Sensor Networks <i>Richard Tynan, G.M.P. O’Hare, David Marsh, Donal O’Kane</i> .....	687
ACCESS: An Agent Based Architecture for the Rapid Prototyping of Location Aware Services <i>Robin Strahan, Gregory O’Hare, Conor Muldoon, Donnacha Phelan, Rem Collier</i> .....	695
Immune-Based Optimization of Predicting Neural Networks <i>Aleksander Byrski, Marek Kisiel-Dorohinicki</i> .....	703
Algorithm of Behavior Evaluation in Multi-agent System <i>Gabriel Rojek, Renata Cięciwa, Krzysztof Cetnarowicz</i> .....	711

Formal Specification of Holonic Multi-agent Systems Framework  
*Sebastian Rodriguez, Vincent Hilaire, Abder Koukam* ..... 719

The Dynamics of Computing Agent Systems  
*M. Smolka, P. Uhruski, R. Schaefer, M. Grochowski* ..... 727

**Workshop on “Parallel Monte Carlo Algorithms for Diverse Applications in a Distributed Setting”**

A Superconvergent Monte Carlo Method for Multiple Integrals on the Grid  
*Sofiya Ivanovska, Emanouil Atanassov, Aneta Karaivanova* ..... 735

A Sparse Parallel Hybrid Monte Carlo Algorithm for Matrix Computations  
*Simon Branford, Christian Weihrauch, Vassil Alexandrov* ..... 743

Parallel Hybrid Monte Carlo Algorithms for Matrix Computations  
*V. Alexandrov, E. Atanassov, I. Dimov, S. Branford, A. Thandavan, C. Weihrauch* ..... 752

An Efficient Monte Carlo Approach for Solving Linear Problems in Biomolecular Electrostatics  
*Charles Fleming, Michael Mascagni, Nikolai Simonov* ..... 760

Finding the Smallest Eigenvalue by the Inverse Monte Carlo Method with Refinement  
*Vassil Alexandrov, Aneta Karaivanova* ..... 766

On the Scrambled Sobol’ Sequence  
*Hongmei Chi, Peter Beerli, Deidre W. Evans, Micheal Mascagni* ..... 775

**Poster Session I**

Reconstruction Algorithm of Signals from Special Samples in Spline Spaces  
*Jun Xian, Degao Li* ..... 783

Fast In-place Integer Radix Sorting  
*Fouad El-Aker* ..... 788

Dimension Reduction for Clustering Time Series Using Global Characteristics  
*Xiaozhe Wang, Kate A. Smith, Rob J. Hyndman* ..... 792

On Algorithm for Estimation of Selecting Core <i>Youngjin Ahn, Moonseong Kim, Young-Cheol Bang, Hyunseung Choo</i> . . . . .	796
A Hybrid Mining Model Based on Neural Network and Kernel Smoothing Technique <i>Defu Zhang, Qingshan Jiang, Xin Li</i> . . . . .	801
An Efficient User-Oriented Clustering of Web Search Results <i>Keke Cai, Jiajun Bu, Chun Chen</i> . . . . .	806
Artificial Immune System for Medical Data Classification <i>Wiesław Wajs, Piotr Wais, Mariusz Święcicki, Hubert Wojtowicz</i> . . . .	810
EFoX: A Scalable Method for Extracting Frequent Subtrees <i>Juryon Paik, Dong Ryeol Shin, Ungmo Kim</i> . . . . .	813
An Efficient Real-Time Frequent Pattern Mining Technique Using Diff-Sets <i>Rajanish Dass, Ambuj Mahanti</i> . . . . .	818
Improved Fully Automatic Liver Segmentation Using Histogram Tail Threshold Algorithms <i>Kyung-Sik Seo</i> . . . . .	822
Directly Rasterizing Straight Line by Calculating the Intersection Point <i>Hua Zhang, Changqian Zhu, Qiang Zhao, Hao Shen</i> . . . . .	826
PrefixUnion: Mining Traversal Patterns Efficiently in Virtual Environments <i>Shao-Shin Hung, Ting-Chia Kuo, Damon Shing-Min Liu</i> . . . . .	830
Efficient Interactive Pre-integrated Volume Rendering <i>Heewon Kye, Helen Hong, Yeong Gil Shin</i> . . . . .	834
Ncvtk: A Program for Visualizing Planetary Data <i>Alexander Pletzer, Remik Ziemiński, Jared Cohen</i> . . . . .	838
Efficient Multimodality Volume Fusion Using Graphics Hardware <i>Helen Hong, Juhee Bae, Heewon Kye, Yeong Gil Shin</i> . . . . .	842
G <sup>1</sup> Continuity Triangular Patches Interpolation Based on PN Triangles <i>Zhihong Mao, Lizhuang Ma, Mingxi Zhao</i> . . . . .	846
Estimating 3D Object Coordinates from Markerless Scenes <i>Ki Woon Kwon, Sung Wook Baik, Seong-Whan Lee</i> . . . . .	850

Stochastic Fluid Model Analysis for Campus Grid Storage Service <i>Xiaofeng Shi, Hui Feng Xue, Zhiqun Deng</i> .....	854
Grid Computing Environment Using Ontology Based Service <i>Ana Marilza Pernas, Mario Dantas</i> .....	858
Distributed Object-Oriented Wargame Simulation on Access Grid <i>Joong-Ho Lim, Tae-Dong Lee, Chang-Sung Jeong</i> .....	862
RTI Execution Environment Using Open Grid Service Architecture <i>Ki-Young Choi, Tae-Dong Lee, Chang-Sung Jeong</i> .....	866
Heterogeneous Grid Computing: Issues and Early Benchmarks <i>Eamonn Kenny, Brian Coghlan, George Tsouloupas, Marios Dikaiakos, John Walsh, Stephen Childs, David O'Callaghan, Geoff Quigley</i> .....	870
GRAMS: Grid Resource Analysis and Monitoring System <i>Hongning Dai, Minglu Li, Linpeng Huang, Yi Wang, Feng Hong</i> .....	875
Transaction Oriented Computing (Hive Computing) Using GRAM-Soft <i>Kaviraju Ramanna Dyapur, Kiran Kumar Patnaik</i> .....	879
Data-Parallel Method for Georeferencing of MODIS Level 1B Data Using Grid Computing <i>Yincui Hu, Yong Xue, Jiakui Tang, Shaobo Zhong, Guoyin Cai</i> .....	883
An Engineering Computation Oriented Grid Project: Design and Implementation <i>Xianqing Wang, Qinhuai Zeng, Dingwu Feng, Changqin Huang</i> .....	887
Iterative and Parallel Algorithm Design from High Level Language Traces <i>Daniel E. Cooke, J. Nelson Rushton</i> .....	891
An Application of the Adomian Decomposition Method for Inverse Stefan Problem with Neumann's Boundary Condition <i>Radosław Grzymkowski, Damian Słota</i> .....	895
Group Homotopy Algorithm with a Parameterized Newton Iteration for Symmetric Eigen Problems <i>Ran Baik, Karabi Datta, Yoopyo Hong</i> .....	899
Numerical Simulation of Three-Dimensional Vertically Aligned Quantum Dot Array <i>Weichung Wang, Tsung-Min Hwang</i> .....	908



Semi-systolic Architecture for Modular Multiplication over $GF(2^m)$ <i>Hyun-Sung Kim, Il-Soo Jeon</i> .....	912
---	-----

## Poster Session II

Meta Services: Abstract a Workflow in Computational Grid Environments <i>Sangkeon Lee, Jaeyoung Choi</i> .....	916
CEGA: A Workflow PSE for Computational Applications <i>Yoonhee Kim</i> .....	920
A Meta-heuristic Applied for a Topologic Pickup and Delivery Problem with Time Windows Constraints <i>Jesús Fabián López Pérez</i> .....	924
Three Classifiers for Acute Abdominal Pain Diagnosis – Comparative Study <i>Michal Wozniak</i> .....	929
Grid-Technology for Chemical Reactions Calculation <i>Gabriel Balint-Kurti, Alexander Bogdanov, Ashot Gevorkyan, Yuriy Gorbachev, Tigran Hakobyan, Gunnar Nyman, Irina Shoshmina, Elena Stankova</i> .....	933
A Fair Bulk Data Transmission Protocol in Grid Environments <i>Fanjun Su, Xuezheng Pan, Yong lv, Lingdi Ping</i> .....	937
A Neural Network Model for Classification of Facial Expressions Based on Dimension-Suk Model <i>Young-Suk Shin</i> .....	941
A Method for Local Tuning of Fuzzy Membership Functions <i>Ahmet Çinar</i> .....	945
QoS-Enabled Service Discovery Using Agent Platform <i>Kee-Hyun Choi, Ho-Jin Shin, Dong-Ryeol Shin</i> .....	950
A Quick Generation Method of Sequence Pair for Block Placement <i>Mingxu Huo, Koubao Ding</i> .....	954
A Space-Efficient Algorithm for Pre-distributing Pairwise Keys in Sensor Networks <i>Taekyun Kim, Sangjin Kim, Heekuck Oh</i> .....	958

An Architecture for Lightweight Service Discovery Protocol in MANET <i>Byong-In Lim, Kee-Hyun Choi, Dong-Ryeol Shin</i> .....	963
An Enhanced Location Management Scheme for Hierarchical Mobile IPv6 Networks <i>Myung-Kyu Yi</i> .....	967
A Genetic Machine Learning Algorithm for Load Balancing in Cluster Configurations <i>M.A.R. Dantas, A.R. Pinto</i> .....	971
A Parallel Algorithm for Computing Shortest Paths in Large-Scale Networks <i>Guozhen Tan, Xiaohui Ping</i> .....	975
Exploiting Parallelization for RNA Secondary Structure Prediction in Cluster <i>Guangming Tan, Shengzhong Feng, Ninghui Sun</i> .....	979
Improving Performance of Distributed Haskell in Mosix Clusters <i>Lori Collins, Murray Gross, P.A. Whitlock</i> .....	983
Investigation of Cache Coherence Strategies in a Mobile Client/Server Environment <i>C.D.M. Berkenbrock, M.A.R. Dantas</i> .....	987
Parallel Files Distribution <i>Laurentiu Cucos, Elise de Doncker</i> .....	991
Dynamic Dominant Index Set for Mobile Peer-to-Peer Networks <i>Wei Shi, Shanping Li, Gang Peng, Xin Lin</i> .....	995
Task Mapping Algorithm for Heterogeneous Computing System Allowing High Throughput and Load Balancing <i>Sung Chune Choi, Hee Yong Youn</i> .....	1000
An Approach for Eye Detection Using Parallel Genetic Algorithm <i>A. Cagatay Talay</i> .....	1004
Graph Representation of Nested Software Structure <i>Leszek Kotulski</i> .....	1008
Transaction Routing in Real-Time Shared Disks Clusters <i>Kyungoh Ohn, Sangho Lee, Haengrae Cho</i> .....	1012

Implementation of a Distributed Data Mining System <i>Ju Cho, Sung Baik, Jerzy Bala</i> .....	1016
Hierarchical Infrastructure for Large-Scale Distributed Privacy-Preserving Data Mining <i>Jinlong Wang, Congfu Xu, Hui Feng Shen, Yunhe Pan</i> .....	1020
<b>Poster Session III</b>	
Prediction of Protein Interactions by the Domain and Sub-cellular Localization Information <i>Jinsun Hong, Kyungsook Han</i> .....	1024
Online Prediction of Interacting Proteins with a User-Specified Protein <i>Byungkyu Park, Kyungsook Han</i> .....	1028
An Abstract Model for Service Compositions Based on Agents <i>Jinkui Xie, Linpeng Huang</i> .....	1032
An Approach of Nonlinear Model Multi-step-ahead Predictive Control Based on SVM <i>Weimin Zhong, Daoying Pi, Youxian Sun</i> .....	1036
Simulation Embedded in Optimization – A Key for the Effective Learning Process in (about) Complex, Dynamical Systems <i>Elżbieta Kasperska, Elwira Mateja-Losa</i> .....	1040
Analysis of the Chaotic Phenomena in Securities Business of China <i>Chong Fu, Su-Ju Li, Hai Yu, Wei-Yong Zhu</i> .....	1044
Pulsating Flow and Platelet Aggregation <i>Xin-She Yang</i> .....	1048
Context Adaptive Self-configuration System <i>Seunghwa Lee, Eunseok Lee</i> .....	1052
Modeling of Communication Delays Aiming at the Design of Networked Supervisory and Control Systems. A First Approach <i>Karina Cantillo, Rodolfo E. Haber, Angel Alique, Ramón Galán</i> .....	1056
Architecture Modeling and Simulation for Supporting Multimedia Services in Broadband Wireless Networks <i>Do-Hyeon Kim, Beongku An</i> .....	1060

Visualization for Genetic Evolution of Target Movement in Battle Fields  
*S. Baik, J. Bala, A. Hadjarian, P. Pachowicz, J. Cho, S. Moon* . . . . . 1064

Comfortable Driver Behavior Modeling for Car Following of Pervasive Computing Environment  
*Yanfei Liu, Zhaohui Wu* . . . . . 1068

A Courseware Development Methodology for Establishing Practice-Based Network Course  
*Jahwan Koo, Seongjin Ahn* . . . . . 1072

Solving Anisotropic Transport Equation on Misaligned Grids  
*J. Chen, S.C. Jardin, H.R. Strauss* . . . . . 1076

The Design of Fuzzy Controller by Means of Evolutionary Computing and Neurofuzzy Networks  
*Sung-Kwun Oh, Seok-Beom Roh* . . . . . 1080

Boundary Effects in Stokes' Problem with Melting  
*Arup Mukherjee, John G. Stevens* . . . . . 1084

A Software Debugging Method Based on Pairwise Testing  
*Liang Shi, Changhai Nie, Baowen Xu* . . . . . 1088

Heuristic Algorithm for Anycast Flow Assignment in Connection-Oriented Networks  
*Krzysztof Walkowiak* . . . . . 1092

Isotropic Vector Matrix Grid and Face-Centered Cubic Lattice Data Structures  
*J.F. Nystrom, Carryn Bellomo* . . . . . 1096

Design of Evolutionally Optimized Rule-Based Fuzzy Neural Networks Based on Fuzzy Relation and Evolutionary Optimization  
*Byoung-Jun Park, Sung-Kwun Oh, Witold Pedrycz, Hyun-Ki Kim* . . . 1100

Uniformly Convergent Computational Technique for Singularly Perturbed Self-adjoint Mixed Boundary-Value Problems  
*Rajesh K. Bawa, S. Natesan* . . . . . 1104

Fuzzy System Analysis of Beach Litter Components  
*Can Elmar Balas* . . . . . 1108

Exotic Option Prices Simulated by Monte Carlo Method on Market Driven by Diffusion with Poisson Jumps and Stochastic Volatility  
*Magdalena Broszkiewicz, Aleksander Janicki* . . . . . 1112

Computational Complexity and Distributed Execution in Water Quality Management <i>Maria Chtepen, Filip Claeys, Bart Dhoedt, Peter Vanrolleghem, Piet Demeester</i> .....	1116
Traffic Grooming Based on Shortest Path in Optical WDM Mesh Networks <i>Yeo-Ran Yoon, Tae-Jin Lee, Min Young Chung, Hyunseung Choo</i> . . . .	1120
Prompt Detection of Change point in the Operation of Networked Systems <i>Hyunsoo Kim, Hee Yong Youn</i> .....	1125
<b>Author Index</b> .....	1131

# Table of Contents – Part I

## Numerical Methods

Computing for Eigenpairs on Globally Convergent Iterative Method for Hermitian Matrices <i>Ran Baik, Karabi Datta, Yoopyo Hong</i> .....	1
2D FE Quad Mesh Smoothing via Angle-Based Optimization <i>Hongtao Xu, Timothy S. Newman</i> .....	9
Numerical Experiments on the Solution of the Inverse Additive Singular Value Problem <i>G. Flores-Becerra, Victor M. Garcia, Antonio M. Vidal</i> .....	17
Computing Orthogonal Decompositions of Block Tridiagonal or Banded Matrices <i>Wilfried N. Gansterer</i> .....	25
Adaptive Model Trust Region Methods for Generalized Eigenvalue Problems <i>P.-A. Absil, C.G. Baker, K.A. Gallivan, A. Sameh</i> .....	33
On Stable Integration of Stiff Ordinary Differential Equations with Global Error Control <i>Gennady Yur'evich Kulikov, Sergey Konstantinovich Shindin</i> .....	42
Bifurcation Analysis of Large Equilibrium Systems in MATLAB <i>David S. Bindel, James W. Demmel, Mark J. Friedman, Willy J.F. Govaerts, Yuri A. Kuznetsov</i> .....	50
Sliced-Time Computations with Re-scaling for Blowing-Up Solutions to Initial Value Differential Equations <i>Nabil R. Nassif, Dolly Fayyad, Maria Cortas</i> .....	58
Application of the Pseudo-Transient Technique to a Real-World Unsaturated Flow Groundwater Problem <i>Fred T. Tracy, Barbara P. Donnell, Stacy E. Howington, Jeffrey L. Hensley</i> .....	66
Optimization of Spherical Harmonic Transform Computations <i>J.A.R. Blais, D.A. Provins, M.A. Soofi</i> .....	74

Predictor-Corrector Preconditioned Newton-Krylov Method for Cavity Flow  
*Jianwei Ju, Giovanni Lapenta* . . . . . 82

**Algorithms and Computational Kernels**

A High-Order Recursive Quadratic Learning Algorithm  
*Qi Zhu, Shaohua Tan, Ying Qiao* . . . . . 90

Vectorized Sparse Matrix Multiply for Compressed Row Storage Format  
*Eduardo F. D’Azevedo, Mark R. Fahey, Richard T. Mills* . . . . . 99

A Multipole Based Treecode Using Spherical Harmonics for Potentials of the Form  $r^{-\lambda}$   
*Kasthuri Srinivasan, Hemant Mahawar, Vivek Sarin* . . . . . 107

Numerically Stable Real Number Codes Based on Random Matrices  
*Zizhong Chen, Jack Dongarra* . . . . . 115

On Iterated Numerical Integration  
*Shujun Li, Elise de Doncker, Karlis Kaugars* . . . . . 123

Semi-Lagrangian Implicit-Explicit Two-Time-Level Scheme for Numerical Weather Prediction  
*Andrei Bourchtein* . . . . . 131

Occlusion Activity Detection Algorithm Using Kalman Filter for Detecting Occluded Multiple Objects  
*Heungkyu Lee, Hanseok Ko* . . . . . 139

A New Computer Algorithm Approach to Identification of Continuous-Time Batch Bioreactor Model Parameters  
*Suna Ertunc, Bulent Akay, Hale Hapoglu, Mustafa Alpbaz* . . . . . 147

Automated Operation Minimization of Tensor Contraction Expressions in Electronic Structure Calculations  
*Albert Hartono, Alexander Sibiryakov, Marcel Nooijen, Gerald Baumgartner, David E. Bernholdt, So Hirata, Chi-Chung Lam, Russell M. Pitzer, J. Ramanujam, P. Sadayappan* . . . . . 155

Regularization and Extrapolation Methods for Infrared Divergent Loop Integrals  
*Elise de Doncker, Shujun Li, Yoshimitsu Shimizu, Junpei Fujimoto, Fukuko Yuasa* . . . . . 165

Use of a Least Squares Finite Element Lattice Boltzmann Method to Study Fluid Flow and Mass Transfer Processes <i>Yusong Li, Eugene J. LeBoeuf, P.K. Basu</i> .....	172
--	-----

## Nonnumerical Algorithms

On the Empirical Efficiency of the Vertex Contraction Algorithm for Detecting Negative Cost Cycles in Networks <i>K. Subramani, D. Desovski</i> .....	180
Minimal Load Constrained Vehicle Routing Problems <i>İmdat Kara, Tolga Bektaş</i> .....	188
Multilevel Static Real-Time Scheduling Algorithms Using Graph Partitioning <i>Kayhan Erciyes, Zehra Soysert</i> .....	196
A Multi-level Approach for Document Clustering <i>Suely Oliveira, Sang-Cheol Seok</i> .....	204
A Logarithmic Time Method for Two's Complementation <i>Jung-Yup Kang, Jean-Luc Gaudiot</i> .....	212

## Parallel Algorithms

The Symmetric–Toeplitz Linear System Problem in Parallel <i>Pedro Alonso, Antonio Manuel Vidal</i> .....	220
Parallel Resolution with Newton Algorithms of the Inverse Non-symmetric Eigenvalue Problem <i>Pedro V. Alberti, Victor M. García, Antonio M. Vidal</i> .....	229
Computational Challenges in Vector Functional Coefficient Autoregressive Models <i>Ioana Banicescu, Ricolindo L. Cariño, Jane L. Harvill, John Patrick Lestrade</i> .....	237
Multi-pass Mapping Schemes for Parallel Sparse Matrix Computations <i>Konrad Malkowski, Padma Raghavan</i> .....	245
High-Order Finite Element Methods for Parallel Atmospheric Modeling <i>Amik St.-Cyr, Stephen J. Thomas</i> .....	256



## Environments and Libraries

Continuation of Homoclinic Orbits in MATLAB <i>M. Friedman, W. Govaerts, Yu.A. Kuznetsov, B. Sautois</i> .....	263
A Numerical Tool for Transmission Lines <i>Hervé Bolvin, André Chambarel, Philippe Neveux</i> .....	271
The COOLFluiD Framework: Design Solutions for High Performance Object Oriented Scientific Computing Software <i>Andrea Lani, Tiago Quintino, Dries Kimpe, Herman Deconinck, Stefan Vandewalle, Stefaan Poedts</i> .....	279
A Problem Solving Environment for Image-Based Computational Hemodynamics <i>Lilit Abrahamyan, Jorrit A. Schaap, Alfons G. Hoekstra, Denis Shamonin, Frieke M.A. Box, Rob J. van der Geest, Johan H.C. Reiber, Peter M.A. Sloot</i> .....	287
MPL: A Multiprecision MATLAB-Like Environment <i>Walter Schreppers, Franky Backeljauw, Annie Cuyt</i> .....	295

## Performance and Scalability

Performance and Scalability Analysis of Cray X1 Vectorization and Multistreaming Optimization <i>Sadaf Alam, Jeffrey Vetter</i> .....	304
Super-Scalable Algorithms for Computing on 100,000 Processors <i>Christian Engelmann, Al Geist</i> .....	313
“gRpas”, a Tool for Performance Testing and Analysis <i>Laurentiu Cucos, Elise de Doncker</i> .....	322
Statistical Methods for Automatic Performance Bottleneck Detection in MPI Based Programs <i>Michael Kluge, Andreas Knüpfer, Wolfgang E. Nagel</i> .....	330

## Programming Techniques

Source Templates for the Automatic Generation of Adjoint Code Through Static Call Graph Reversal <i>Uwe Naumann, Jean Utke</i> .....	338
--	-----

A Case Study in Application Family Development by Automated Component Composition: h-p Adaptive Finite Element Codes <i>Nasim Mahmood, Yusheng Feng, James C. Browne</i> . . . . .	347
Determining Consistent States of Distributed Objects Participating in a Remote Method Call <i>Magdalena Sławińska, Bogdan Wiszniewski</i> . . . . .	355
Storage Formats for Sparse Matrices in Java <i>Mikel Luján, Anila Usman, Patrick Hardie, T.L. Freeman, John R. Gurd</i> . . . . .	364
Coupled Fusion Simulation Using the Common Component Architecture <i>Wael R. Elwasif, Donald B. Batchelor, David E. Bernholdt, Lee A. Berry, Ed F. D’Azevedo, Wayne A. Houlberg, E.F. Jaeger, James A. Kohl, Shuhui Li</i> . . . . .	372
<b>Networks and Distributed Algorithms</b>	
A Case Study in Distributed Locking Protocol on Linux Clusters <i>Sang-Jun Hwang, Jaechun No, Sung Soon Park</i> . . . . .	380
Implementation of a Cluster Based Routing Protocol for Mobile Networks <i>Geoffrey Marshall, Kayhan Erciyas</i> . . . . .	388
A Bandwidth Sensitive Distributed Continuous Media File System Using the Fibre Channel Network <i>Cuneyt Akinlar, Sarit Mukherjee</i> . . . . .	396
A Distributed Spatial Index for Time-Efficient Aggregation Query Processing in Sensor Networks <i>Soon-Young Park, Hae-Young Bae</i> . . . . .	405
Fast Concurrency Control for Distributed Inverted Files <i>Mauricio Marín</i> . . . . .	411
An All-Reduce Operation in Star Networks Using All-to-All Broadcast Communication Pattern <i>Eunseuk Oh, Hongsik Choi, David Primeaux</i> . . . . .	419
<b>Parallel and Distributed Computing</b>	
$S^2F^2M$ - Statistical System for Forest Fire Management <i>Germán Bianchini, Ana Cortés, Tomàs Margalef, Emilio Luque</i> . . . . .	427

Concurrent Execution of Multiple NAS Parallel Programs on a Cluster  
*Adam K.L. Wong, Andrzej M. Goscinski* ..... 435

Model-Based Statistical Testing of a Cluster Utility  
*W. Thomas Swain, Stephen L. Scott* ..... 443

Accelerating Protein Structure Recovery Using Graphics Processing Units  
*Bryson R. Payne, G. Scott Owen, Irene Weber* ..... 451

A Parallel Software Development for Watershed Simulations  
*Jing-Ru C. Cheng, Robert M. Hunter, Hwai-Ping Cheng,  
 David R. Richards* ..... 460

**Grid Computing**

Design and Implementation of Services for a Synthetic Seismogram Calculation Tool on the Grid  
*Choonhan Youn, Tim Kaiser, Cindy Santini, Dogan Seber* ..... 469

Toward GT3 and OGSINET Interoperability: GRAM Support on OGSINET  
*James V.S. Watson, Sang-Min Park, Marty Humphrey* ..... 477

GEDAS: A Data Management System for Data Grid Environments  
*Jaechun No, Hyoungwoo Park* ..... 485

SPURport: Grid Portal for Earthquake Engineering Simulations  
*Tomasz Haupt, Anand Kalyanasundaram, Nisreen Ammari,  
 Krishnendu Chandra, Kamakhya Das, Shravan Durvasula* ..... 493

Extending Existing Campus Trust Relationships to the Grid Through the Integration of Pubcookie and MyProxy  
*Jonathan Martin, Jim Basney, Marty Humphrey* ..... 501

Generating Parallel Algorithms for Cluster and Grid Computing  
*Ulisses Kendi Hayashida, Kunio Okuda, Jairo Panetta,  
 Siand Wun Song* ..... 509

Relationship Networks as a Survivable and Adaptive Mechanism for Grid Resource Location  
*Lei Gao, Yongsheng Ding* ..... 517

Deployment-Based Security for Grid Applications  
*Isabelle Attali, Denis Caromel, Arnaud Contes* ..... 526

Grid Resource Selection by Application Benchmarking for Computational Haemodynamics Applications <i>Alfredo Tirado-Ramos, George Tsouloupas, Marios Dikaiakos, Peter Sloot</i> . . . . .	534
--	-----

AGARM: An Adaptive Grid Application and Resource Monitor Framework <i>Wenju Zhang, Shudong Chen, Liang Zhang, Shui Yu, Fanyuan Ma</i> . . .	544
---	-----

## Failure Handling

Reducing Transaction Abort Rate of Epidemic Algorithm in Replicated Databases <i>Huaizhong Lin, Zengwei Zheng, Chun Chen</i> . . . . .	552
--	-----

Snap-Stabilizing $k$ -Wave Synchronizer <i>Doina Bein, Ajoy K. Datta, Mehmet H. Karaata, Safaa Zaman</i> . . . . .	560
---	-----

A Service Oriented Implementation of Distributed Status Monitoring and Fault Diagnosis Systems <i>Lei Wang, Peiyu Li, Zhaohui Wu, Shangjian Chen</i> . . . . .	568
--	-----

Adaptive Fault Monitoring in Fault Tolerant CORBA <i>Soo Myoung Lee, Hee Yong Youn, We Duke Cho</i> . . . . .	576
--	-----

## Optimization

Simulated Annealing Based-GA Using Injective Contrast Functions for BSS <i>J.M. Górriz, C.G. Puntonet, J.D. Morales, J.J. delaRosa</i> . . . . .	585
--	-----

A DNA Coding Scheme for Searching Stable Solutions <i>Intaek Kim, HeSong Lian, Hwan Il Kang</i> . . . . .	593
--	-----

Study on Asymmetric Two-Lane Traffic Model Based on Cellular Automata <i>Xianchuang Su, Xiaogang Jin, Yong Min, Bo Peng</i> . . . . .	599
---	-----

Simulation of Parasitic Interconnect Capacitance for Present and Future ICs <i>Grzegorz Tosik, Zbigniew Lisik, Malgorzata Langer, Janusz Wozny</i> . . .	607
--	-----

Self-optimization of Large Scale Wildfire Simulations <i>Jingmei Yang, Huoping Chen, Salim Hariri, Manish Parashar</i> . . . . .	615
---	-----

## Modeling and Simulation

Description of Turbulent Events Through the Analysis of POD Modes in Numerically Simulated Turbulent Channel Flow  
*Giancarlo Alfonsi, Leonardo Primavera* . . . . . 623

Computational Modeling of Human Head Conductivity  
*Adnan Salman, Sergei Turovets, Allen Malony, Jeff Eriksen, Don Tucker* . . . . . 631

Modeling of Electromagnetic Waves in Media with Dirac Distribution of Electric Properties  
*André Chambarel, Hervé Bolvin* . . . . . 639

Simulation of Transient Mechanical Wave Propagation in Heterogeneous Soils  
*Arnaud Mesgouez, Gaëlle Lefeuve-Mesgouez, André Chambarel* . . . . . 647

Practical Modelling for Generating Self-similar VBR Video Traffic  
*Jong-Suk R. Lee, Hae-Duck J. Jeong* . . . . . 655

## Image Analysis and Processing

A Pattern Search Method for Image Registration  
*Hong Zhou, Benjamin Ray Seyfarth* . . . . . 664

Water Droplet Morphing Combining Rigid Transformation  
*Lanfen Lin, Shenghui Liao, RuoFeng Tong, JinXiang Dong* . . . . . 671

A Cost-Effective Private-Key Cryptosystem for Color Image Encryption  
*Rastislav Lukac, Konstantinos N. Plataniotis* . . . . . 679

On a Generalized Demosaicking Procedure: A Taxonomy of Single-Sensor Imaging Solutions  
*Rastislav Lukac, Konstantinos N. Plataniotis* . . . . . 687

Tile Classification Using the CIELAB Color Model  
*Christos-Nikolaos Anagnostopoulos, Athanassios Koutsonas, Ioannis Anagnostopoulos, Vassily Loumos, Eleftherios Kayafas* . . . . . 695

## Graphics and Visualization

A Movie Is Worth More Than a Million Data Points  
*Hans-Peter Bischof, Jonathan Coles* . . . . . 703

A Layout Algorithm for Signal Transduction Pathways as Two-Dimensional Drawings with Spline Curves <i>Donghoon Lee, Byoung-Hyon Ju, Kyungsook Han</i> .....	711
Interactive Fluid Animation and Its Applications <i>Jeongjin Lee, Helen Hong, Yeong Gil Shin</i> .....	719
ATDV: An Image Transforming System <i>Paula Farago, Ligia Barros, Gerson Cunha, Luiz Landau, Rosa Maria Costa</i> .....	727
An Adaptive Collision Detection and Resolution for Deformable Objects Using Spherical Implicit Surface <i>Sunhwa Jung, Min Hong, Min-Hyung Choi</i> .....	735

## Computation as a Scientific Paradigm

Automatic Categorization of Traditional Chinese Painting Images with Statistical Gabor Feature and Color Feature <i>Xiaohui Guan, Gang Pan, Zhaohui Wu</i> .....	743
Nonlinear Finite Element Analysis of Structures Strengthened with Carbon Fibre Reinforced Polymer: A Comparison Study <i>X.S. Yang, J.M. Lees, C.T. Morley</i> .....	751
Machine Efficient Adaptive Image Matching Based on the Nonparametric Transformations <i>Bogusław Cyganek</i> .....	757
Non-gradient, Sequential Algorithm for Simulation of Nascent Polypeptide Folding <i>Lech Znamirowski</i> .....	766

## Hybrid Computational Methods

Time Delay Dynamic Fuzzy Networks for Time Series Prediction <i>Yusuf Oysal</i> .....	775
A Hybrid Heuristic Algorithm for the Rectangular Packing Problem <i>Defu Zhang, Ansheng Deng, Yan Kang</i> .....	783
Genetically Dynamic Optimization Based Fuzzy Polynomial Neural Networks <i>Ho-Sung Park, Sung-Kwon Oh, Witold Pedrycz, Yongkab Kim</i> .....	792

Genetically Optimized Hybrid Fuzzy Neural Networks Based on Simplified Fuzzy Inference Rules and Polynomial Neurons  
*Sung-Kwun Oh, Byoung-Jun Park, Witold Pedrycz, Tae-Chon Ahn . . .* 798

Modelling and Constraint Hardness Characterisation of the Unique-Path OSPF Weight Setting Problem  
*Changyong Zhang, Robert Rodosek . . . . .* 804

**Complex Systems**

Application of Four-Dimension Assignment Algorithm of Data Association in Distributed Passive-Sensor System  
*Li Zhou, You He, Xiao-jing Wang . . . . .* 812

Using Rewriting Techniques in the Simulation of Dynamical Systems: Application to the Modeling of Sperm Crawling  
*Antoine Spicher, Olivier Michel . . . . .* 820

Specifying Complex Systems with Bayesian Programming. An Alife Application  
*Fidel Aznar, Mar Pujol, Ramón Rizo . . . . .* 828

Optimization Embedded in Simulation on Models Type System Dynamics – Some Case Study  
*Elżbieta Kasperska, Damian Słota . . . . .* 837

A High-Level Petri Net Based Decision Support System for Real-Time Scheduling and Control of Flexible Manufacturing Systems: An Object-Oriented Approach  
*Gonca Tuncel, Gunhan Mirac Bayhan . . . . .* 843

**Applications**

Mesosopic Simulation for Self-organization in Surface Processes  
*David J. Horntrop . . . . .* 852

Computer Simulation of the Anisotropy of Fluorescence in Ring Molecular Systems  
*Pavel Heřman, Ivan Barvík . . . . .* 860

The Deflation Accelerated Schwarz Method for CFD  
*J. Verkaik, C. Vuik, B.D. Paarluis, A. Twerda . . . . .* 868

The Numerical Approach to Analysis of Microchannel Cooling Systems <i>Ewa Raj, Zbigniew Lisik, Malgorzata Langer, Grzegorz Tosik, Janusz Wozny</i> . . . . .	876
Simulation of Nonlinear Thermomechanical Waves with an Empirical Low Dimensional Model <i>Linxiang Wang, Roderick V.N. Melnik</i> . . . . .	884
A Computational Risk Assessment Model for Breakwaters <i>Can Elmar Balas</i> . . . . .	892
Wavelets and Wavelet Packets Applied to Termite Detection <i>Juan-José González de-la-Rosa, Carlos García Puntonet, Isidro Lloret Galiana, Juan Manuel Górriz</i> . . . . .	900
Algorithms for the Estimation of the Concentrations of Chlorophyll A and Carotenoids in Rice Leaves from Airborne Hyperspectral Data <i>Yanning Guan, Shan Guo, Jiangui Liu, Xia Zhang</i> . . . . .	908
Multiresolution Reconstruction of Pipe-Shaped Objects from Contours <i>Kyungha Min, In-Kwon Lee</i> . . . . .	916
<b>Biomedical Applications</b>	
Multi-resolution LOD Volume Rendering in Medicine <i>Kai Xie, Jie Yang, Yue Min Zhu</i> . . . . .	925
Automatic Hepatic Tumor Segmentation Using Statistical Optimal Threshold <i>Seung-Jin Park, Kyung-Sik Seo, Jong-An Park</i> . . . . .	934
Spatio-Temporal Patterns in the Depth EEG During the Epileptic Seizure <i>Jung Ae Kim, Sunyoung Cho, Sang Kun Lee, Hyunwoo Nam, Seung Kee Han</i> . . . . .	941
Prediction of Ribosomal Frameshift Signals of User-Defined Models <i>Yanga Byun, Sanghoon Moon, Kyungsook Han</i> . . . . .	948
Effectiveness of Vaccination Strategies for Infectious Diseases According to Human Contact Networks <i>Fumihiko Takeuchi, Kenji Yamamoto</i> . . . . .	956



## Data Mining and Computation

A Shape Constraints Based Method to Recognize Ship Objects from High Spatial Resolution Remote Sensed Imagery  
*Min Wang, Jiancheng Luo, Chenghu Zhou, Dongping Ming . . . . .* 963

Statistical Inference Method of User Preference on Broadcasting Content  
*Sanggil Kang, Jeongyeon Lim, Munchurl Kim . . . . .* 971

Density-Based Spatial Outliers Detecting  
*Tianqiang Huang, Xiaolin Qin, Chongcheng Chen, Qinmin Wang . . . . .* 979

The Design and Implementation of Extensible Information Services  
*Guiyi Wei, Guangming Wang, Yao Zheng, Wei Wang . . . . .* 987

Approximate B-Spline Surface Based on RBF Neural Networks  
*Xumin Liu, Houkuan Huang, Weixiang Xu . . . . .* 995

Efficient Parallelization of Spatial Approximation Trees  
*Mauricio Marín, Nora Reyes . . . . .* 1003

## Education in Computational Science

The Visualization of Linear Algebra Algorithms in Apt Apprentice  
*Christopher Andrews, Rodney Cooper, Ghislain Deslongchamps, Olivier Spet . . . . .* 1011

A Visual Interactive Framework for Formal Derivation  
*Paul Agron, Leo Bachmair, Frank Nielsen . . . . .* 1019

ECVlab: A Web-Based Virtual Laboratory System for Electronic Circuit Simulation  
*Ouyang Yang, Dong Yabo, Zhu Miaoliang, Huang Yuewei, Mao Song, Mao Yunjie . . . . .* 1027

MTES: Visual Programming Environment for Teaching and Research in Image Processing  
*JeongHeon Lee, YoungTak Cho, Hoon Heo, OkSam Chae . . . . .* 1035

## Emerging Trends

Advancing Scientific Computation by Improving Scientific Code Development: Symbolic Execution and Semantic Analysis  
*Mark Stewart . . . . .* 1043

Scale-Free Networks: A Discrete Event Simulation Approach <i>Rex K. Kincaid, Natalia Alexandrov</i> .....	1051
Impediments to Future Use of Petaflop Class Computers for Large-Scale Scientific/Engineering Applications in U.S. Private Industry <i>Myron Ginsberg</i> .....	1059
The SCORE Cluster Enabled OpenMP Environment: Performance Prospects for Computational Science <i>H'sien. J. Wong, Alistair P. Rendell</i> .....	1067
<b>Author Index</b> .....	1077

## Table of Contents – Part II

### Workshop On “High Performance Computing in Academia: Systems and Applications”

Teaching High-Performance Computing on a High-Performance Cluster <i>Martin Bernreuther, Markus Brenk, Hans-Joachim Bungartz, Ralf-Peter Mundani, Ioan Lucian Muntean</i> . . . . .	1
Teaching High Performance Computing Parallelizing a Real Computational Science Application <i>Giovanni Aloisio, Massimo Cafaro, Italo Epicoco, Gianvito Quarta</i> . . .	10
Introducing Design Patterns, Graphical User Interfaces and Threads Within the Context of a High Performance Computing Application <i>James Roper, Alistair P. Rendell</i> . . . . .	18
High Performance Computing Education for Students in Computational Engineering <i>Uwe Fabricius, Christoph Freundl, Harald Köstler, Ulrich Rüde</i> . . . . .	27
Integrating Teaching and Research in HPC: Experiences and Opportunities <i>M. Berzins, R.M. Kirby, C.R. Johnson</i> . . . . .	36
Education and Research Challenges in Parallel Computing <i>L. Ridgway Scott, Terry Clark, Babak Bagheri</i> . . . . .	44
Academic Challenges in Large-Scale Multiphysics Simulations <i>Michael T. Heath, Xiangmin Jiao</i> . . . . .	52
Balancing Computational Science and Computer Science Research on a Terascale Computing Facility <i>Calvin J. Ribbens, Srinidhi Varadarjan, Malar Chinnusamy, Gautam Swaminathan</i> . . . . .	60
Computational Options for Bioinformatics Research in Evolutionary Biology <i>Michael A. Thomas, Mitch D. Day, Luobin Yang</i> . . . . .	68
Financial Computations on Clusters Using Web Services <i>Shirish Chinchalkar, Thomas F. Coleman, Peter Mansfield</i> . . . . .	76

“Plug-and-Play” Cluster Computing: HPC Designed for the Mainstream Scientist <i>Dean E. Dager, Viktor K. Decyk</i> . . . . .	84
Building an HPC Watering Hole for Boulder Area Computational Science <i>E.R. Jessup, H.M. Tufo, M.S. Woitaszek</i> . . . . .	91
The Dartmouth Green Grid <i>James E. Dobson, Jeffrey B. Woodward, Susan A. Schwarz, John C. Marchesini, Hany Farid, Sean W. Smith</i> . . . . .	99
Resource-Aware Parallel Adaptive Computation for Clusters <i>James D. Teresco, Laura Effinger-Dean, Arjun Sharma</i> . . . . .	107
 <b>Workshop on “Tools for Program Development and Analysis in Computational Science”</b>	
New Algorithms for Performance Trace Analysis Based on Compressed Complete Call Graphs <i>Andreas Knüpfer and Wolfgang E. Nagel</i> . . . . .	116
PARADIS: Analysis of Transaction-Based Applications in Distributed Environments <i>Christian Glasner, Edith Spiegl, Jens Volkert</i> . . . . .	124
Automatic Tuning of Data Distribution Using Factoring in Master/Worker Applications <i>Anna Morajko, Paola Caymes, Tomàs Margalef, Emilio Luque</i> . . . . .	132
DynTG: A Tool for Interactive, Dynamic Instrumentation <i>Martin Schulz, John May, John Gyllenhaal</i> . . . . .	140
Rapid Development of Application-Specific Network Performance Tests <i>Scott Pakin</i> . . . . .	149
Providing Interoperability for Java-Oriented Monitoring Tools with JINEXT <i>Włodzimierz Funika, Arkadiusz Janik</i> . . . . .	158
RDVIS: A Tool That Visualizes the Causes of Low Locality and Hints Program Optimizations <i>Kristof Beyls, Erik H. D’Hollander, Frederik Vandeputte</i> . . . . .	166

CacheIn: A Toolset for Comprehensive Cache Inspection <i>Jie Tao, Wolfgang Karl</i> . . . . .	174
Optimization-Oriented Visualization of Cache Access Behavior <i>Jie Tao, Wolfgang Karl</i> . . . . .	182
Collecting and Exploiting Cache-Reuse Metrics <i>Josef Weidendorfer, Carsten Trinitis</i> . . . . .	191
<b>Workshop on “Computer Graphics and Geometric Modeling, CGGM 2005”</b>	
Modelling and Animating Hand Wrinkles <i>X.S. Yang, Jian J. Zhang</i> . . . . .	199
Simulating Wrinkles in Facial Expressions on an Anatomy-Based Face <i>Yu Zhang, Terence Sim, Chew Lim Tan</i> . . . . .	207
A Multiresolutional Approach for Facial Motion Retargetting Using Subdivision Wavelets <i>Kyungha Min, Moon-Ryul Jung</i> . . . . .	216
New 3D Graphics Rendering Engine Architecture for Direct Tessellation of Spline Surfaces <i>Adrian Sfarti, Brian A. Barsky, Todd J. Kosloff, Egon Pasztor, Alex Kozlowski, Eric Roman, Alex Perelman</i> . . . . .	224
Fast Water Animation Using the Wave Equation with Damping <i>Y. Nishidate, G.P. Nikishkov</i> . . . . .	232
A Comparative Study of Acceleration Techniques for Geometric Visualization <i>Pascual Castelló, José Francisco Ramos, Miguel Chover</i> . . . . .	240
Building Chinese Ancient Architectures in Seconds <i>Hua Liu, Qing Wang, Wei Hua, Dong Zhou, Hujun Bao</i> . . . . .	248
Accelerated 2D Image Processing on GPUs <i>Bryson R. Payne, Saeid O. Belkasim, G. Scott Owen, Michael C. Weeks, Ying Zhu</i> . . . . .	256
Consistent Spherical Parameterization <i>Arul Asirvatham, Emil Praun, Hugues Hoppe</i> . . . . .	265

Mesh Smoothing via Adaptive Bilateral Filtering <i>Qibin Hou, Li Bai, Yangsheng Wang</i> .....	273
Towards a Bayesian Approach to Robust Finding Correspondences in Multiple View Geometry Environments <i>Cristian Canton-Ferrer, Josep R. Casas, Montse Pardàs</i> .....	281
Managing Deformable Objects in Cluster Rendering <i>Thomas Convard, Patrick Bourdot, Jean-Marc Vézien</i> .....	290
Revolute Quadric Decomposition of Canal Surfaces and Its Applications <i>Jinyuan Jia, Ajay Joneja, Kai Tang</i> .....	298
Adaptive Surface Modeling Using a Quadtree of Quadratic Finite Elements <i>G. P. Nikishkov</i> .....	306
MC Slicing for Volume Rendering Applications <i>A. Benassarou, E. Bittar, N. W. John, L. Lucas</i> .....	314
Modelling and Sampling Ramified Objects with Substructure-Based Method <i>Weiwei Yin, Marc Jaeger, Jun Teng, Bao-Gang Hu</i> .....	322
Integration of Multiple Segmentation Based Environment Models <i>SeungTaek Ryoo, CheungWoon Jho</i> .....	327
On the Impulse Method for Cloth Animation <i>Juntao Ye, Robert E. Webber, Irene Gargantini</i> .....	331
Remeshing Triangle Meshes with Boundaries <i>Yong Wu, Yuanjun He, Hongming Cai</i> .....	335
SACARI: An Immersive Remote Driving Interface for Autonomous Vehicles <i>Antoine Tarault, Patrick Bourdot, Jean-Marc Vézien</i> .....	339
A 3D Model Retrieval Method Using 2D Freehand Sketches <i>Jiantao Pu, Karthik Ramani</i> .....	343
A 3D User Interface for Visualizing Neuron Location in Invertebrate Ganglia <i>Jason A. Pamplin, Ying Zhu, Paul S. Katz, Rajshekhar Sunderraman</i> .....	347

## Workshop on “Modelling of Complex Systems by Cellular Automata”

The Dynamics of General Fuzzy Cellular Automata <i>Angelo B. Mingarelli</i> .....	351
A Cellular Automaton SIS Epidemiological Model with Spatially Clustered Recoveries <i>David Hiebeler</i> .....	360
Simulating Market Dynamics with CD++ <i>Qi Liu, Gabriel Wainer</i> .....	368
A Model of Virus Spreading Using Cell-DEVS <i>Hui Shang, Gabriel Wainer</i> .....	373
A Cellular Automata Model of Competition in Technology Markets with Network Externalities <i>Judy Frels, Debra Heisler, James Reggia, Hans-Joachim Schuetze</i> ....	378
Self-organizing Dynamics for Optimization <i>Stefan Boettcher</i> .....	386
Constructibility of Signal-Crossing Solutions in von Neumann 29-State Cellular Automata <i>William R. Buckley, Amar Mukherjee</i> .....	395
Evolutionary Discovery of Arbitrary Self-replicating Structures <i>Zhijian Pan, James Reggia</i> .....	404
Modelling Ant Brood Tending Behavior with Cellular Automata <i>Daniel Merkle, Martin Middendorf, Alexander Scheidler</i> .....	412
A Realistic Cellular Automata Model to Simulate Traffic Flow at Urban Roundabouts <i>Ruili Wang, Mingzhe Liu</i> .....	420
Probing the Eddies of Dancing Emergence: Complexity and Abstract Painting <i>Tara Krause</i> .....	428
 <b>Workshop on “Wireless and Mobile Systems”</b>	
Enhanced TCP with End-to-End Bandwidth and Loss Differentiation Estimate over Heterogeneous Networks <i>Le Tuan Anh, Choong Seon Hong</i> .....	436

Content-Aware Automatic QoS Provisioning for UPnP AV-Based Multimedia Services over Wireless LANs <i>Yeali S. Sun, Chang-Ching Yan, Meng Chang Chen</i> . . . . .	444
Simulation Framework for Wireless Internet Access Networks <i>Hyoung-Kee Choi, Jitae Shin</i> . . . . .	453
WDM: An Energy-Efficient Multi-hop Routing Algorithm for Wireless Sensor Networks <i>Zengwei Zheng, Zhaohui Wu, Huaizhong Lin, Kougen Zheng</i> . . . . .	461
Forwarding Scheme Extension for Fast and Secure Handoff in Hierarchical MIPv6 <i>Hoseong Jeon, Jungmuk Lim, Hyunseung Choo, Gyung-Leen Park</i> . . . . .	468
Back-Up Chord: Chord Ring Recovery Protocol for P2P File Sharing over MANETs <i>Hong-Jong Jeong, Dongkyun Kim, Jeomki Song, Byung-yeub Kim, Jeong-Su Park</i> . . . . .	477
PATM: Priority-Based Adaptive Topology Management for Efficient Routing in Ad Hoc Networks <i>Haixia Tan, Weilin Zeng, Lichun Bao</i> . . . . .	485
Practical and Provably-Secure Multicasting over High-Delay Networks <i>Junghyun Nam, Hyunjue Kim, Seungjoo Kim, Dongho Won, Hyungkyu Yang</i> . . . . .	493
A Novel IDS Agent Distributing Protocol for MANETs <i>Jin Xin, Zhang Yao-Xue, Zhou Yue-Zhi, Wei Yaya</i> . . . . .	502
ID-Based Secure Session Key Exchange Scheme to Reduce Registration Delay with AAA in Mobile IP Networks <i>Kwang Cheol Jeong, Hyunseung Choo, Sang Yong Ha</i> . . . . .	510
An Efficient Wireless Resource Allocation Based on a Data Compressor Predictor <i>Min Zhang, Xiaolong Yang, Hong Jiang</i> . . . . .	519
A Seamless Handover Mechanism for IEEE 802.16e Broadband Wireless Access <i>Kyung-ah Kim, Chong-Kwon Kim, Tongsok Kim</i> . . . . .	527
Fault Tolerant Coverage Model for Sensor Networks <i>Doina Bein, Wolfgang W. Bein, Srilaxmi Malladi</i> . . . . .	535



Detection Algorithms Based on Chip-Level Processing for DS/CDMA Code Acquisition in Fast Fading Channels <i>Seokho Yoon, Jee-Hyong Lee, Sun Yong Kim</i> .....	543
Clustering-Based Distributed Precomputation for Quality-of-Service Routing <i>Yong Cui, Jianping Wu</i> .....	551
Traffic Grooming Algorithm Using Shortest EDPs Table in WDM Mesh Networks <i>Seungsoo Lee, Tae-Jin Lee, Min Young Chung, Hyunseung Choo</i> .....	559
Efficient Indexing of Moving Objects Using Time-Based Partitioning with R-Tree <i>Youn Chul Jung, Hee Yong Youn, Ungmo Kim</i> .....	568
Publish/Subscribe Systems on Node and Link Error Prone Mobile Environments <i>Sangyoon Oh, Sangmi Lee Pallickara, Sunghoon Ko, Jai-Hoon Kim, Geoffrey Fox</i> .....	576
A Power Efficient Routing Protocol in Wireless Sensor Networks <i>Hyunsook Kim, Jungpil Ryu, Kijun Han</i> .....	585
Applying Mobile Agent to Intrusion Response for Ad Hoc Networks <i>Ping Yi, Yiping Zhong, Shiyong Zhang</i> .....	593
A Vertical Handoff Decision Process and Algorithm Based on Context Information in CDMA-WLAN Interworking <i>Jang-Sub Kim, Min-Young Chung, Dong-Ryeol Shin</i> .....	601
<b>Workshop on “Dynamic Data Driven Application Systems”</b>	
Dynamic Data Driven Applications Systems: New Capabilities for Application Simulations and Measurements <i>Frederica Darema</i> .....	610
Dynamic Data Driven Methodologies for Multiphysics System Modeling and Simulation <i>J. Michopoulos, C. Farhat, E. Houstis, P. Tsompanopoulou, H. Zhang, T. Gullaud</i> .....	616

Towards Dynamically Adaptive Weather Analysis and Forecasting in LEAD <i>Beth Plale, Dennis Gannon, Dan Reed, Sara Graves, Kelvin Droegemeier, Bob Wilhelmson, Mohan Ramamurthy</i> . . . . .	624
Towards a Dynamic Data Driven Application System for Wildfire Simulation <i>Jan Mandel, Lynn S. Bennethum, Mingshi Chen, Janice L. Coen, Craig C. Douglas, Leopoldo P. Franca, Craig J. Johns, Minjeong Kim, Andrew V. Knyazev, Robert Kremens, Vaibhav Kulkarni, Guan Qin, Anthony Vodacek, Jianjia Wu, Wei Zhao, Adam Zornes</i> . . . . .	632
Multiscale Interpolation, Backward in Time Error Analysis for Data-Driven Contaminant Simulation <i>Craig C. Douglas, Yalchin Efendiev, Richard Ewing, Victor Ginting, Raytcho Lazarov, Martin J. Cole, Greg Jones, Chris R. Johnson</i> . . . . .	640
Ensemble-Based Data Assimilation for Atmospheric Chemical Transport Models <i>Adrian Sandu, Emil M. Constantinescu, Wenyuan Liao, Gregory R. Carmichael, Tianfeng Chai, John H. Seinfeld, Dacian Dăescu</i> . . . . .	648
Towards Dynamic Data-Driven Optimization of Oil Well Placement <i>Manish Parashar, Vincent Matossian, Wolfgang Bangerth, Hector Klie, Benjamin Rutt, Tahsin Kurc, Umit Catalyurek, Joel Saltz, Mary F. Wheeler</i> . . . . .	656
High-Fidelity Simulation of Large-Scale Structures <i>Christoph Hoffmann, Ahmed Sameh, Ananth Grama</i> . . . . .	664
A Dynamic Data Driven Grid System for Intra-operative Image Guided Neurosurgery <i>Amit Majumdar, Adam Birnbaum, Dong Ju Choi, Abhishek Trivedi, Simon K. Warfield, Kim Baldridge, Petr Krysl</i> . . . . .	672
Structure-Based Integrative Computational and Experimental Approach for the Optimization of Drug Design <i>Dimitrios Morikis, Christodoulos A. Floudas, John D. Lambris</i> . . . . .	680
Simulation and Visualization of Air Flow Around Bat Wings During Flight <i>I.V. Pivkin, E. Hueso, R. Weinstein, D.H. Laidlaw, S. Swartz, G.E. Karniadakis</i> . . . . .	689

Integrating Fire, Structure and Agent Models <i>A.R. Chaturvedi, S.A. Filatyev, J.P. Gore, A. Hanna, J. Means, A.K. Mellema</i> .....	695
A Dynamic, Data-Driven, Decision Support System for Emergency Medical Services <i>Mark Gaynor, Margo Seltzer, Steve Moulton, Jim Freedman</i> .....	703
Dynamic Data Driven Coupling of Continuous and Discrete Methods for 3D Tracking <i>Dimitris Metaxas, Gabriel Tsechpenakis</i> .....	712
Semi-automated Simulation Transformation for DDDAS <i>David Brogan, Paul Reynolds, Robert Bartholet, Joseph Carnahan, Yannick Loitière</i> .....	721
The Development of Dependable and Survivable Grids <i>Andrew Grimshaw, Marty Humphrey, John C. Knight, Anh Nguyen-Tuong, Jonathan Rowanhill, Glenn Wasson, Jim Basney</i> .....	729
On the Fundamental Tautology of Validating Data-Driven Models and Simulations <i>John Michopoulos, Sam Lambrakos</i> .....	738
<b>Workshop on “Practical Aspects of High-Level Parallel Programming (PAPP)”</b>	
Managing Heterogeneity in a Grid Parallel Haskell <i>A. Al Zain, P.W. Trinder, H-W. Loidl, G.J. Michaelson</i> .....	746
An Efficient Equi-semi-join Algorithm for Distributed Architectures <i>M. Bamha, G. Hains</i> .....	755
Two Fundamental Concepts in Skeletal Parallel Programming <i>Anne Benoit, Murray Cole</i> .....	764
A Formal Framework for Orthogonal Data and Control Parallelism Handling <i>Sonia Campa</i> .....	772
Empirical Parallel Performance Prediction from Semantics-Based Profiling <i>Norman Scaife, Greg Michaelson, Susumu Horiguchi</i> .....	781

Dynamic Memory Management in the *Loci* Framework  
*Yang Zhang, Edward A. Luke* ..... 790

**Workshop on “New Computational Tools for Advancing Atmospheric and Oceanic Sciences”**

On Adaptive Mesh Refinement for Atmospheric Pollution Models  
*Emil M. Constantinescu, Adrian Sandu* ..... 798

Total Energy Singular Vectors for Atmospheric Chemical Transport Models  
*Wenyuan Liao, Adrian Sandu* ..... 806

Application of Static Adaptive Grid Techniques for Regional-Urban Multiscale Air Quality Modeling  
*Daewon Byun, Peter Percell, Tanmay Basak* ..... 814

On the Accuracy of High-Order Finite Elements in Curvilinear Coordinates  
*Stephen J. Thomas, Amik St.-Cyr* ..... 821

Analysis of Discrete Adjoints for Upwind Numerical Schemes  
*Zheng Liu and Adrian Sandu* ..... 829

The Impact of Background Error on Incomplete Observations for 4D-Var Data Assimilation with the FSU GSM  
*I. Michael Navon, Dacian N. Daescu, Zhuo Liu* ..... 837

**2005 International Workshop on Bioinformatics Research and Applications**

Disjoint Segments with Maximum Density  
*Yen Hung Chen, Hsueh-I Lu, Chuan Yi Tang* ..... 845

Wiener Indices of Balanced Binary Trees  
*Sergey Bereg, Hao Wang* ..... 851

What Makes the Arc-Preserving Subsequence Problem Hard?  
*Guillaume Blin, Guillaume Fertin, Romeo Rizzi, Stéphane Vialette* ... 860

An Efficient Dynamic Programming Algorithm and Implementation for RNA Secondary Structure Prediction  
*Guangming Tan, Xinchun Liu, Ninghui Sun* ..... 869

Performance Evaluation of Protein Sequence Clustering Tools <i>Haifeng Liu, Loo-Nin Teow</i> .....	877
A Data-Adaptive Approach to cDNA Microarray Image Enhancement <i>Rastislav Lukac, Konstantinos N. Plataniotis, Bogdan Smolka,, Anastasios N. Venetsanopoulos</i> .....	886
String Kernels of Imperfect Matches for Off-target Detection in RNA Interference <i>Shibin Qiu, Terran Lane</i> .....	894
A New Kernel Based on High-Scored Pairs of Tri-peptides and Its Application in Prediction of Protein Subcellular Localization <i>Zhengdeng Lei, Yang Dai</i> .....	903
Reconstructing Phylogenetic Trees of Prokaryote Genomes by Randomly Sampling Oligopeptides <i>Osamu Maruyama, Akiko Matsuda, Satoru Kuhara</i> .....	911
Phylogenetic Networks, Trees, and Clusters <i>Luay Nakhleh, Li-San Wang</i> .....	919
SWAT: A New Spliced Alignment Tool Tailored for Handling More Sequencing Errors <i>Yifeng Li, Hesham H. Ali</i> .....	927
Simultaneous Alignment and Structure Prediction of RNAs Are Three Input Sequences Better Than Two? <i>Beeta Masoumi, Marcel Turcotte</i> .....	936
Clustering Using Adaptive Self-organizing Maps (ASOM) and Applications <i>Yong Wang, Chengyong Yang, Kalai Mathee, Giri Narasimhan</i> .....	944
Experimental Analysis of a New Algorithm for Partial Haplotype Completion <i>Paola Bonizzoni, Gianluca Della Vedova, Riccardo Dondi, Lorenzo Mariani</i> .....	952
Improving the Sensitivity and Specificity of Protein Homology Search by Incorporating Predicted Secondary Structures <i>Bin Ma, Lieyu Wu, Kaizhong Zhang</i> .....	960
Profiling and Searching for RNA Pseudoknot Structures in Genomes <i>Chunmei Liu, Yinglei Song, Russell L. Malmberg, Liming Cai</i> .....	968

Integrating Text Chunking with Mixture Hidden Markov Models for Effective Biomedical Information Extraction <i>Min Song, Il-Yeol Song, Xiaohua Hu, Robert B. Allen</i> .....	976
k-Recombination Haplotype Inference in Pedigrees <i>Francis Y.L. Chin, Qiangfeng Zhang, Hong Shen</i> .....	985
Improved Tag Set Design and Multiplexing Algorithms for Universal Arrays <i>Ion I. Măndoiu, Claudia Prăjescu, Dragoș Trincă</i> .....	994
A Parallel Implementation for Determining Genomic Distances Under Deletion and Insertion <i>Vijaya Smitha Kollı, Hui Liu, Michelle Hong Pan, Yi Pan</i> .....	1003
Phasing and Missing Data Recovery in Family Trios <i>Dumitru Brinza, Jingwu He, Weidong Mao, Alexander Zelikovsky</i> ...	1011
Highly Scalable Algorithms for Robust String Barcoding <i>B. DasGupta, K.M. Konwar, I.I. Măndoiu, A.A. Shvartsman</i> .....	1020
Optimal Group Testing Strategies with Interval Queries and Their Application to Splice Site Detection <i>Ferdinando Cicalese, Peter Damaschke, Ugo Vaccaro</i> .....	1029
Virtual Gene: A Gene Selection Algorithm for Sample Classification on Microarray Datasets <i>Xian Xu, Aidong Zhang</i> .....	1038
 <b>Workshop on “Programming Grids and Metacomputing Systems – PGaMS2005”</b>	
Bulk Synchronous Parallel ML: Modular Implementation and Performance Prediction <i>Frédéric Loulergue, Frédéric Gava, David Billiet</i> .....	1046
Fast Expression Templates <i>Jochen Härdtlein, Alexander Linke, Christoph Pflaum</i> .....	1055
Solving Coupled Geoscience Problems on High Performance Computing Platforms <i>Dany Kemmler, Panagiotis Adamidis, Wenqing Wang, Sebastian Bauer, Olaf Kolditz</i> .....	1064

H2O Metacomputing - Jini Lookup and Discovery <i>Dirk Gorissen, Gunther Stuer, Kurt Vanmechelen, Jan Broeckhove</i> .....	1072
User Experiences with Nuclear Physics Calculations on a H2O Metacomputing System and on the BEgrid <i>P. Hellinckx, K. Vanmechelen, G. Stuer, F. Arickx, J. Broeckhove</i> ...	1080
<b>Author Index</b> .....	1089

# Multiscale Finite Element Modeling of the Coupled Nonlinear Dynamics of Magnetostrictive Composite Thin Film

D. V. S. S. S. S., D. V. S. S. S.,  
National Institute of Science

ARDB Center for Composite Structures, Department of Aerospace Engineering,  
Indian Institute of Science, Bangalore 560012, India

**Abstract.** A multiscale nonlinear finite element model for analysis and design of the deformation gradient and the magnetic field distribution in Terfenol-D/epoxy thin film device under Transverse Magnetic (TM) mode of operation is developed in this work. A phenomenological constitutive model based on the density of domain switching (DDS) of an ellipsoidal inclusion in unit cell of matrix is implemented. A sub-grid scale homogenization technique is employed to upwind the microstructural information. A general procedure to ensure the solution convergence toward an approximate inertial manifold is reported.

## 1 Introduction

In this paper, a multiscale nonlinear finite element model for analysis and design of the deformation gradient and the magnetic field distribution in Terfenol-D/epoxy thin film device under Transverse Magnetic (TM) mode of operation is developed in this work. A phenomenological constitutive model based on the density of domain switching (DDS) of an ellipsoidal inclusion in unit cell of matrix is implemented. A sub-grid scale homogenization technique is employed to upwind the microstructural information. A general procedure to ensure the solution convergence toward an approximate inertial manifold is reported.

The nonlinear finite element model (FEM) is developed for the analysis and design of the deformation gradient and the magnetic field distribution in Terfenol-D/epoxy thin film device under Transverse Magnetic (TM) mode of operation. The model is based on the density of domain switching (DDS) of an ellipsoidal inclusion in unit cell of matrix. A sub-grid scale homogenization technique is employed to upwind the microstructural information. A general procedure to ensure the solution convergence toward an approximate inertial manifold is reported.



... n i o in n , x n l l i o l x i n w i i ,  
 o in i o w , in x i n l o n n , i i l y i l  
 o l n in n i v o i o n . B o o l n n o n l i n n  
 o y n i , v l o i o n l i l i x i w i i i l  
 n i o n .  
 v i n i o n l i n v i o n l l y o n i n l i l n i  
 l n o w o o y H *et al.* [ ], n o o n  
 o n n n l i y . A o n v l o o o  
 l v o l v i n l y o l x l i y i o i o n l n i o l ,  
 v y w o n l y o o n i o n o [ ,9] , l i l v l  
 i i l n i l n o [10] , l v l o [11] n w o -  
 o i i n . In o n x o i - n n o l , o n o  
 o n i n o l i n i o n [1] i w o n o i n , w i x n i l y o n  
 l i l n o i o n o w i n i n . S n l y , w i l i n o n l y  
 n o n l i n n o l o l , v n i n o i n l o w - i n i o n l  
 n i o l o n o i o i o i i n i o n [ ,13] y  
 n o . In n w o n w v i o n l l y o n i n l i l  
 n i o l w i o l l o w i n w o : (1) - i l o w i n i n  
 i o l i n o i o n n ( ) n o x i n i o l o o i i -  
 n l y i n i y i n n i l n o l i o n , w i  
 i n l i l o i n o l l o w i n o n v n i o n l y o i  
 o o n i o n .  
 n o l n i o i o n i n o i o n i n n -  
 o i o n o o l i l l n i o i n w i i n , w i o  
 i n i o o i l . In o o i l , y n i i o v n  
 o o l i n w n l i i y n l o n i . T o l x i y  
 i n i l o l i n i o - o l : (1) i i n n o n i i v  
 o l i n n o n o l i l w o . H w o l o n  
 n i y o o i n w i i n (DDS) [1] , w i x n i o n o i  
 n y n i o n l o i n o n o l y l l i n L v i i o n  
 w i i o n i o i n o o i v o o i n  
 l o n l n n i l v o ( ) i n l i n f f o v o l  
 i o n o n o i i v i n i l o o i n i o -  
 l n (3) i n i n o n l o i o l l l n  
 n o n l i y n ( ) o n i n v i o n l l y o n i n n i l n o l  
 n o l v i n i i i v l y .

## 2 Constitutive Model Based on Density of Domain Switching (DDS)

W o n i n n i l l o w o o o i o w n i n F i . 1 , i n w i  
 l l i o i l i n l i o n ( B ) i n i x ( A ) i o n o o i -  
 i v o i n . T f f i v o i n i o n o n i l l i n o i n i  
 o n n n l  $\theta$  w i i l o j o x i o l l i o i . W

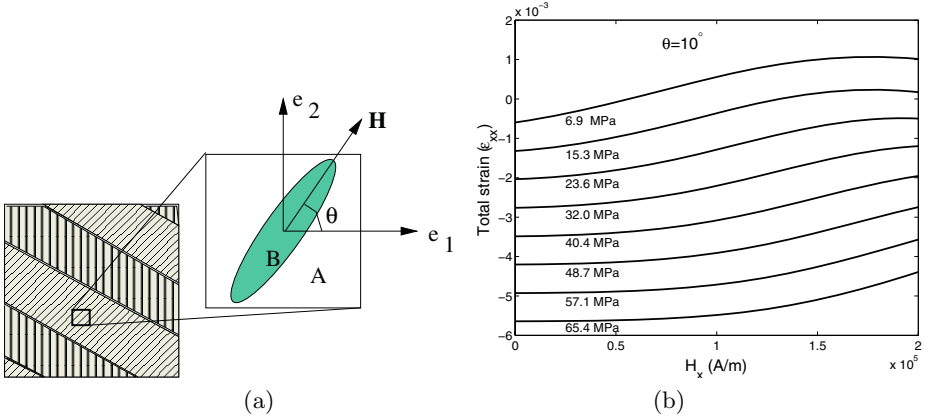


**Fig. 1.** (a) Unit cell with oriented magnetostrictive phase  $B$  in epoxy matrix phase  $A$  (b) strain vs. applied magnetic field in the unit cell with  $\epsilon = 0.5$ ,  $\theta = 10^\circ$  under varying stress

on i , n ff iv ly on - i n ion l on i iv , o lo A lon . jo ,  
xi o lli oi . Al o , i jo , xi i o o lin wi  
l n n i l  $\mathbf{H}$  n , ili i . U in DDS o l [1] i i  
o il o , ff o l , n o i ion o , ff iv ly n  
o o l . A o in o DDS o l , i o n i o in o ,  
B n w i n .

$$d = \left[ \frac{\partial \varepsilon}{\partial H} \right]_{\sigma} = \tilde{d} e^{-(z-1)^2/A}, \quad (1)$$

w , i o n i o in  $\tilde{d} = \tilde{d}_{cr} + a\Delta\sigma + b(\Delta\sigma)^2$ , ov ,  
 $\Delta\sigma = \sigma - \sigma_{cr}$ ,  $z = |H|/\tilde{H}$ ,  $\tilde{H} = \tilde{H}_{cr} + \zeta\Delta\sigma$ ,  $A = \sigma_{cr}/\sigma$ ,  $\sigma$  i ,  
 $\varepsilon$  i , in  $\sigma_{cr}$  i i lin , n o o in wi in . a ,  
 $b$ ,  $\tilde{d}_{cr}$ ,  $\tilde{H}_{cr}$  n  $\zeta$  , il on n o in y , l in i ,  
n , y n in x i n l i in [1]. L  $\epsilon \in (0, 1]$   
vol , ion o B . A ly in ix , l o , n-on l in  
n , li o on n  $\{\sigma_{11}, \sigma_{22}, \sigma_{12}\}$  n n i l  
o on n  $\{H_1, H_2\}$  in ni ll , on i iv o li o in , wi  
i x , in i-lin i o .

$$\sigma = \bar{Q}_{AB}\varepsilon - \bar{e}_B H, \quad B = \bar{\mu}_{AB} H + \bar{e}'_B \varepsilon, \quad (2)$$

w ,  $\varepsilon$  i lon i in l , in lon xi o lli oi , B i n i  
fl x ni y in l l n ,  $\bar{Q}_{AB}$  i ff iv n n i ff n ,  $\bar{e}_B$  n  $\bar{e}'_B$  ,  
n n o in o , n o i ion n  $\bar{\mu}_{AB}$  i ff iv , ili y .  
W o i-lin i ion o , in i in o , vo-  
l ion o o o lo y in o o i l . H , w w i o in  
in on i iv o lin . ( ) i t =  $t_i$  in o o in  
o , vio i t =  $t_{i-1} = t_i - \Delta t$   $\bar{e}_B^i = \bar{e}_B(\epsilon, \sigma^{i-1}, H^{i-1})$ ,



We in o low l ( $L_0$ ) n l ( $L_1$ ) wi n n v i l n in iv ly  $(\cdot)_0$  n  $(\cdot)_1$ .

$$\mathbf{x}_1 = \mathbf{x}/\epsilon, \quad t_1 = t/\epsilon, \quad \mathbf{u} = \mathbf{u}_0 + \epsilon \mathbf{u}_1, \quad \mathbf{H} = \mathbf{H}_0 + \epsilon \mathbf{H}_1 \quad (8)$$

T yn i o in l n now i in o n on- v ion l w

$$\left( \nabla_0 + \frac{1}{\epsilon} \nabla_1 \right) \cdot \boldsymbol{\sigma} = \bar{\rho} \frac{\partial^2 \mathbf{u}_0}{\partial t^2} + \frac{1}{\epsilon} \bar{\rho} \frac{\partial^2 \mathbf{u}_1}{\partial t_1^2}, \quad (9)$$

n o , M xw ll' ion

$$\left( \nabla_0 + \frac{1}{\epsilon} \nabla_1 \right) \cdot \mathbf{B} = 0. \quad (9)$$

In o o in o ff o x o o o i , w o o o n i ion. Si li yin  $(\cdot)$  wi l o  $(3)$  n  $(5)$  n o o ni in ov , i  $S$  wi no  $j = 1, \dots, n$ , n , i x ,

$$\theta^i(x_s, y_s) = \sum_{j=1}^n \psi_{\theta j}(x_s, y_s) \theta_j^i, \quad \epsilon = \sum_{j=1}^n \psi_{\epsilon j}(x_s, y_s) \epsilon_j^i, \quad (10)$$

w

$$\begin{aligned} & \frac{1}{\Omega_S} \int_{\Omega_S} \left[ \bar{\mathbf{Q}}^i : \nabla_0 \boldsymbol{\varepsilon} - \nabla_0 \bar{\mathbf{e}}^i \cdot \mathbf{H} - \bar{\mathbf{e}}^i : \nabla_0 \mathbf{H} + \frac{1}{\epsilon} \nabla_1 \bar{\mathbf{Q}}^i : \boldsymbol{\varepsilon} + \frac{1}{\epsilon} \bar{\mathbf{Q}}^i : \nabla_1 \boldsymbol{\varepsilon} \right. \\ & \left. - \frac{1}{\epsilon} \nabla_1 \bar{\mathbf{e}}^i \cdot \mathbf{H} - \frac{1}{\epsilon} \bar{\mathbf{e}}^i : \nabla_1 \mathbf{H} \right] d\Omega_S = \frac{1}{\Omega_S} \int_{\Omega_S} \left[ \bar{\rho} \frac{\partial^2 \mathbf{u}_0}{\partial t^2} + \frac{1}{\epsilon} \bar{\rho} \frac{\partial^2 \mathbf{u}_1}{\partial t_1^2} \right] d\Omega_S \quad (11) \end{aligned}$$

Si il ly, o o ni ion o  $(9)$  iv

$$\begin{aligned} & \frac{1}{\Omega_S} \int_{\Omega_S} \left[ \nabla_0 \bar{\mathbf{e}}^{iT} : \boldsymbol{\varepsilon}_0 + \bar{\mathbf{e}}^{iT} : \nabla_0 \boldsymbol{\varepsilon}_0 + \frac{1}{\epsilon} \nabla_1 \bar{\mathbf{e}}^{iT} : \boldsymbol{\varepsilon}_0 + \nabla_1 \bar{\mathbf{e}}^{iT} : \boldsymbol{\varepsilon}_1 + \frac{1}{\epsilon} \bar{\mathbf{e}}^{iT} : \nabla_1 \boldsymbol{\varepsilon}_1 \right. \\ & \left. + \nabla_0 \bar{\boldsymbol{\mu}}^i : \mathbf{H}_0 + \bar{\boldsymbol{\mu}}^i : \nabla_0 \mathbf{H}_0 + \frac{1}{\epsilon} \nabla_1 \bar{\boldsymbol{\mu}}^i : \mathbf{H}_0 + \nabla_1 \bar{\boldsymbol{\mu}}^i : \mathbf{H}_1 + \frac{1}{\epsilon} \bar{\boldsymbol{\mu}}^i : \nabla_1 \mathbf{H}_1 \right] d\Omega_S \\ & = 0 \quad (12) \end{aligned}$$

T o y o x in  $(9)$  i iv n in o n own i i ion n ion  $\psi_{\theta}$  n  $\psi_{\epsilon}$ . W il v l in  $(11)$ - $(12)$  w n o j ion o no l v i l on i no . T i i on y l , ov , ni l n no l v i l  $\mathbf{u}^{e(i-1)}$ ,  $\mathbf{H}^{e(i-1)}$  i  $t = t_{i-1}$  o l n ov l in wi  $S$  n y w i in

$$\mathbf{u}_k = \sum_{j=1}^n \psi_{u_j}(x_k, y_k, t_{i-1}) \mathbf{u}_j^e, \quad \boldsymbol{\varepsilon}_k = \sum_{j=1}^n \psi_{\varepsilon_j}(x_k, y_k) \boldsymbol{\varepsilon}_j^e,$$

$$\mathbf{H}_k = \sum_{j=1}^n \psi_{H_j}(x_k, y_k, t_{i-1}) \mathbf{H}_j^e, \quad (13)$$

w  $k$  i n in ion oin , i e in i ni l n no l n i i  $\psi_{u_j}^e$ ,  $\psi_{\varepsilon_j}^e$  n  $\psi_{H_j}^e$  n ion o in o l on no l n i i , v i o n v i  $t = t_{i-1}$ .

### 3.1 Finite Element Formulation

So, we will consider a volume element  $\Omega$  with nodes  $\mathbf{v}_i$  and edges  $\Gamma_i$ . The displacement  $\mathbf{u}$  and the stress  $\mathbf{p}$  are assumed to be constant over the element. In order to solve the problem, we will use the following finite element formulation. The weak form of the problem is given by

$$\mathcal{L}_1(\partial_t, \partial_{t_1})\mathbf{g}(\mathbf{u}_0, \mathbf{u}_1) - \mathcal{L}_2(\nabla_0, \nabla_1)\mathbf{p}(\boldsymbol{\varepsilon}_0, \boldsymbol{\varepsilon}_1, \mathbf{H}_0, \mathbf{H}_1) = 0, \quad (1)$$

$$\mathcal{L}_3(\nabla_0, \nabla_1)\mathbf{g}(\boldsymbol{\varepsilon}_0, \boldsymbol{\varepsilon}_1, \mathbf{H}_0, \mathbf{H}_1) = 0, \quad (15)$$

The natural boundary conditions are given by

$$\delta \int_{\Omega} \mathbf{u} \cdot [\mathcal{L}_1\mathbf{g} - \mathcal{L}_2\mathbf{p}] d\Omega + \delta \int_{\Omega} \mathbf{H} \cdot \mathcal{L}_3\mathbf{g} d\Omega = 0, \quad (16)$$

with the following boundary conditions

$$\mathbf{M}_0\ddot{\mathbf{q}}_0^e + \mathbf{M}_1\ddot{\mathbf{q}}_1^e + \mathbf{K}_0\mathbf{q}_0^e + \mathbf{K}_1\mathbf{q}_1^e = \mathbf{f}. \quad (1)$$

(1) is a second order ordinary differential equation in time. The displacement  $\mathbf{u}$  is given by

$$\begin{Bmatrix} H_x \\ H_y \end{Bmatrix} = (\bar{\boldsymbol{\mu}}^i)^{-1} : \begin{Bmatrix} \int_{t_{i-1}}^{t_i} \frac{\partial E_z}{\partial t} dt \\ \int_{t_{i-1}}^{t_i} \frac{\partial E_z}{\partial x} dt \end{Bmatrix} - (\bar{\boldsymbol{\mu}}^i)^{-1} : \bar{\mathbf{e}}^{iT} : \boldsymbol{\varepsilon}. \quad (1)$$

In the limit  $\epsilon \rightarrow 0$ , the problem reduces to a linear problem in  $(\mathbf{u}, \mathbf{H})$ . The problem is linear in  $\mathbf{u}$  and  $\mathbf{H}$  because the constitutive law is linear. However, the problem is nonlinear in  $\boldsymbol{\varepsilon}$  because of the presence of the term  $\epsilon \nabla \cdot \mathbf{H}$ . A linear problem in  $\mathbf{u}$  and  $\mathbf{H}$  can be solved analytically. The nonlinear problem can be solved numerically using the finite element method. The finite element method is used to discretize the domain  $\Omega$  into a mesh of elements. The displacement  $\mathbf{u}$  and the stress  $\mathbf{p}$  are assumed to be constant over each element. The finite element method is used to solve the problem (1)-(15) numerically.

$$\mathbf{u} = \mathbf{u}_0 + \epsilon \mathbf{u}_1 = \mathbf{u}_0 + \epsilon \mathbf{h}(\mathbf{u}_0), \quad (19)$$

where  $\mathbf{h}(\mathbf{u}_0)$  is a function of  $\mathbf{u}_0$ . In order to solve the problem (1)-(15) numerically, we will use the finite element method. The finite element method is used to discretize the domain  $\Omega$  into a mesh of elements. The displacement  $\mathbf{u}$  and the stress  $\mathbf{p}$  are assumed to be constant over each element. The finite element method is used to solve the problem (1)-(15) numerically. The finite element method is used to discretize the domain  $\Omega$  into a mesh of elements. The displacement  $\mathbf{u}$  and the stress  $\mathbf{p}$  are assumed to be constant over each element. The finite element method is used to solve the problem (1)-(15) numerically.

$$\nabla_1 \boldsymbol{\varepsilon}_1 = \mathbf{R}_1^i : \boldsymbol{\varepsilon} + \mathbf{R}_2^i : \mathbf{H}_1, \quad \nabla_1 \mathbf{H}_1 = \mathbf{R}_3^i : \boldsymbol{\varepsilon} + \mathbf{R}_4^i : \mathbf{H}, \quad (0)$$

where  $\mathbf{R}_1^i, \mathbf{R}_2^i, \mathbf{R}_3^i$  and  $\mathbf{R}_4^i$  are the constitutive tensors. The constitutive tensors are given by

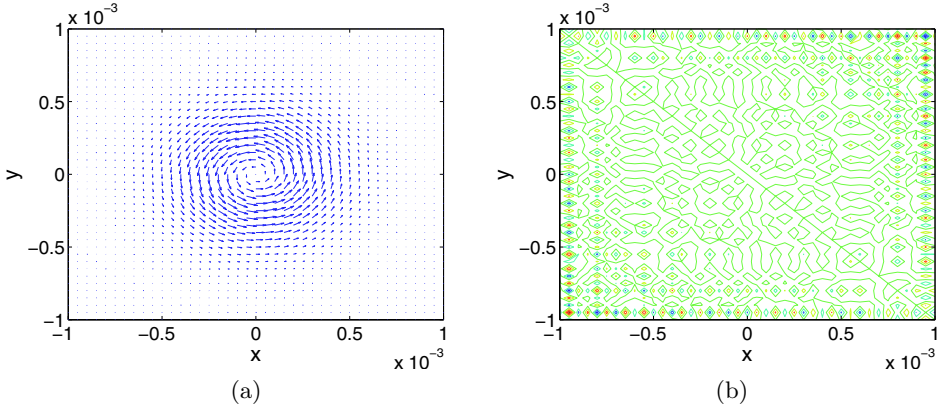


**Fig. 2.** (a) Orientation of  $\mathbf{H}$  field vectors and (b) shear strain contour under normally applied short pulse  $E_z(t)$  and captured at  $t = 50ns$

$$\begin{aligned} \left( \frac{\partial}{\partial t_1} + \epsilon \nabla_1 \right) (|\epsilon_1|^2 + |\mathbf{H}_1|^2) &= \epsilon_1 : \frac{\partial \epsilon_1}{\partial t_1} + \epsilon \epsilon_1 : \nabla_1 \epsilon_1 \\ &+ \mathbf{H}_1 : \frac{\partial \mathbf{H}_1}{\partial t_1} + \epsilon \mathbf{H}_1 : \nabla_1 \mathbf{H}_1 \end{aligned} \quad (1)$$

U in . . . ( 0) in . . . ( 1) n . . . lyin . . . l . . . n , y in . . . li y  $uv \leq \beta u^2 + v^2/\beta$ , . . . n lly w

$$\left( \frac{\partial}{\partial t_1} + \epsilon \nabla_1 \right) (|\epsilon_1|^2 + |\mathbf{H}_1|^2) \leq -\gamma_1^i |\epsilon_2|^2 - \gamma_2^i |\mathbf{H}_1|^2 - \gamma_3^i |\dot{\epsilon}_1|^2 - \gamma_4^i |\dot{\mathbf{H}}_1|^2, \quad (2)$$

w . . . ( ) :=  $\partial/\partial t_1$ ,  $\gamma_1^i$ ,  $\gamma_2^i$ ,  $\gamma_3^i$ ,  $\gamma_4^i$  . . . n ion o  $(\epsilon, \theta^i, \sigma^{i-1}, \mathbf{H}^{i-1})$ . In . . . in . . . ( ) lon . . . i i lin  $\partial/\partial t_1 + \epsilon \nabla_1 =$  on n , w n in . . . v l  $(t_{i-1}, t_i)$ , n . . . y . . . in . . . on  $(x, y) \in S^1$ , w . . . v

$$\begin{aligned} \|\epsilon_1\|^2 + \|\mathbf{H}_1\|^2 &\leq e^{-\gamma_1^i \Delta t} \|\epsilon_1^{i-1}\|^2 + e^{-\gamma_2^i \Delta t} \|\mathbf{H}_1^{i-1}\|^2 \\ &+ e^{-\gamma_3^i \Delta t} \|\dot{\epsilon}_1^{i-1}\|^2 + e^{-\gamma_4^i \Delta t} \|\dot{\mathbf{H}}_1^{i-1}\|^2. \end{aligned} \quad (3)$$

W . . . ( 3) n N w . . . ni iff . . . in i o olv . . . ( 1) on . . . n ly in  $(\mathbf{q}_0^e, \mathbf{q}_1^e)$ . Fi . . . ow . . . n o . . . olv . . . l . . . n i - l . . . in . . . o T 0.27 Dy0.73 F 1.95- oxy(30% y vol.) l . . . n no on l . . . i l l . . . li . . . n . . .

### 4 Concluding Remarks

B . . . on . . . no nolo i l . . . i o o i . . . o l o . . . n o o i iv o ly . . . o o i . . . i l , n . . . o o i yn . . . i , . . . li l l ni l . . . n o l wi . . . i - l o o ni ion i o . . . l . . . o . . . i . . . iv . . . N . . . i l l i l ion o . . . i - olv . . . l . . . n in T . . . nol-D o ly . . . i . . . o . . .

## References

1. Ghoniem, N.M., Busso, P., Kioussis, N. and Huang, H.: Multiscale modelling of nanomechanics and micromechanics: an overview. *Phil. Mag.* **83**(31-34) (2003) 3475–3528
2. Melnik, R.V.N. and Roberts, A.H.: Computational models for multi-scale coupled dynamic problems. *Future Generation Computer Systems* **20** (2004) 453–464
3. Quandt, E., Ludwig, A., Mencik, J. and Nold E.: Giant magnetostrictive TbFe/Fe multilayers. *J. Alloys Compounds* **258** (1997) 133–137
4. Kumar, D., Narayan, J., Nath, T.K., Sharma, A.K., Kvit, A. and Jin, C.: Tunable magnetic properties of metal ceramic composite thin film. *Solid State Communications* **119** (2001) 63–66
5. Liu, T., Burger, C. and Chu B.: Nanofabrication in polymer matrices. *Prog. Polym. Sci.* **2003** 5–26
6. Hommema, J. A.: Magnetomechanical behavior of Terfenol-D particulate composites. MS Thesis, University of Illinois at Urbana-Champaign (1999)
7. Hughes, T.J.R., Feijoo, G.R., Mazzei, L., and Quincy, L.B.: The variational multiscale method – a paradigm for computational mechanics. *Computer Methods in Applied Mechanics and Engineering* **166** (1998) 3–24
8. Babuska, I.: Homogenization approach in engineering, in: Lions, R., Glowinski (Eds.), *Computing Methods in Applied Sciences and Engineering, Lecture Notes in Economics and Mathematical Systems* **134** (1976) Springer, Berlin
9. Terada, K. and Kikuchi, N.: A class of general algorithms for multiscale analysis of heterogeneous media. *Comput. Methods Appl. Mech. Engrg.* **190** (2001) 5427–5464
10. Calgero, C., Laminie, J. and Temam, R.: Dynamical multilevel schemes for the solution of evolution equations by hierarchical finite element discretization. *Appl. Numer. Math.* **23** (1997) 403–442
11. Chessa, J. and Belytschko, T.: Arbitrary discontinuities in space-time finite elements by level sets and X-FEM. *Int. J. Numer. Meth. Engrg.* **61** (2004) 2595–2614
12. Bottasso, C.L.: Multiscale temporal integration. *Comput. Methods Appl. Mech. Engrg.* **191** (2002) 2815–2830
13. Margolin, L.G., Titi, E.S. and Wynne, S.: The postprocessing Galerkin and non-linear galerkin methods - A truncation analysis point of view. *SIAM J. Numer. Anal.* **41** (2003) 695–714
14. Wan, Y., Fang, D., Hwang, K.-C.: Non-linear constitutive relations for magnetostrictive materials. *Int. J. Non-linear Mechanics* **38** (2003) 1053–1065
15. Steindl, A. and Troger, H.: Methods for dimension reduction and their application in nonlinear dynamics. *Int. J. Solids Struct.* **38** (2001) 2131–2147
16. Menon, G. and Haller, G.: Infinite dimensional geometric singular perturbation theory for the Maxwell-Bloch equations. *SIAM J. Math. Anal.* **33** (2001) 315–346

# Large-Scale Fluctuations of Pressure in Fluid Flow Through Porous Medium with Multiscale Log-Stable Permeability

Olga Soboleva

Institute of Computational Mathematics and Mathematical Geophysics, Novosibirsk  
630090, pr. Lavrentieva 6, Russia  
olga@nmsf.sccc.ru

**Abstract.** In this paper, we consider subgrid modeling of a filtration flow of a fluid in a nonhomogeneous porous medium. An expression for the effective permeability coefficient for the large-scale component of the flow is derived. The permeability coefficient possesses a log-stable distribution. The obtained formulas are verified by the numerical modeling.

## 1 Introduction

Field and laboratory observational data imply that such parameters as permeability field and porosity have rather an irregular varying character. In this case small-scale details of permeability and porosity are unknown. The latter are taken into consideration in the statistical models [1],[2], [3],[5], using effective coefficients. In [2], [3], based on the ideas of the renormalized group (RG) by Wilson [4], the subgrid formulas for the effective permeability coefficient were derived, and the diffusion of the interface of liquids in their combined current in a scale-invariant porous medium for log-normal permeability distributions was studied. The Landau-Lifshits formula for the effective permeability within a strict field RG was calculated in Teodorovich [5]. In particular, there are mentioned arguments from monograph [6], according to which the RG methods partially take into account higher orders of the perturbation theory and are to improve the accuracy of the formulas to be obtained. The same arguments are also applicable to the subgrid modeling. If a medium is assumed to satisfy the improved similarity hypothesis by Kolmogorov [2], [7] the RG equations take a very simple form. In this paper, the Wilson RG ideas are used for deriving the subgrid modeling formulas when solving problems of filtration in a multiscale porous medium with a log-stable distribution of permeability. The differential equations for obtaining effective constants were also derived for the media that do not satisfy the improved similarity hypothesis. The formulas obtained are verified by the numerical modeling.

## 2 Statement of Problem

For small Reynolds' numbers, the filtration velocity  $\mathbf{v}$  and the pressure are connected by the Darcy law  $\mathbf{v} = -\varepsilon(\mathbf{x})\nabla p$ , where  $\varepsilon(\mathbf{x})$  is a random coordinate



function - the permeability coefficient. An incompressible liquid flows through the medium. The incompressibility condition brings about the equation

$$\nabla [\varepsilon(\mathbf{x}) \nabla p(\mathbf{x})] = 0. \quad (1)$$

Let a permeability field be known. This means that at each point  $\mathbf{x}$ , the permeability is measured by pushing the liquid through a pattern of a very small size  $l_0$ . A random function of spatial coordinates  $\varepsilon(\mathbf{x})$  is regarded as permeability limit at  $l_0 \rightarrow 0$ ,  $\varepsilon(\mathbf{x})_{l_0} \rightarrow \varepsilon(\mathbf{x})$ . In order to turn to a coarser grid  $l_1$ , it is impossible just to smooth the obtained field  $\varepsilon(\mathbf{x})_{l_0}$  in the scale  $l_1 > l_0$ . The field obtained is not a true permeability, which describes filtration in the domain of scales  $(l_1, L)$ , where  $L$  is the largest scale. In order that permeability be defined on a coarser grid, measurements should be taken again by pushing the liquid through larger samples of the size  $l_1$ . The necessity of fulfilling this procedure is due to the fact that the permeability fluctuations from the limit  $(l_0, l_1)$  have correlations with the pressure fluctuations induced by them. Similar to Kolmogorov [7], we consider the dimensionless field  $\psi$  equal to the relation of permeabilities smoothed in two different scales  $(l, l_1)$ . This approach is described in detail in [2]. Let us denote by  $\tilde{\varepsilon}(\mathbf{x})_l$  the smoothed in scale  $l$  the permeability  $\varepsilon(\mathbf{x})_{l_0}$ , then  $\psi(\mathbf{x}, l, l_1) = \tilde{\varepsilon}(\mathbf{x})_{l_1} / \tilde{\varepsilon}(\mathbf{x})_l$ . When  $l_1 \rightarrow l$ , the field  $\varphi(\mathbf{x}, l) = \left. \frac{d\psi(\mathbf{x}, l, l\lambda)}{d\lambda} \right|_{\lambda=1}$  is obtained that defines all statistical attributes of a porous medium. The relation obtained represents a differential equation, whose solution yields the permeability as function of the field  $\varphi$

$$\varepsilon(\mathbf{x})_{l_0} = \varepsilon_0 \exp \left[ - \int_{l_0}^L \varphi(\mathbf{x}, l) \frac{dl}{l} \right]. \quad (2)$$

The permeability is assumed to have inhomogeneities of the scales  $l$  from the interval  $l_0 < l < L$ , and the field  $\varphi$  is isotropic and homogeneous. The fields  $\varphi(\mathbf{x}, l)$ ,  $\varphi(\mathbf{y}, l')$ , with different scales for any  $\mathbf{x}$ ,  $\mathbf{y}$  are statistically independent. This hypothesis is generally assumed to be correct for different models and reflects the fact that the statistical dependence attenuates when fluctuations of scales differ in value [7]. The scale properties of a model are defined from the field  $\varphi(\mathbf{x}, l)$ . For the scale-invariant models, the condition  $\varphi(\mathbf{x}, l) \rightarrow \varphi(K\mathbf{x}, Kl)$  should be fulfilled. According to the theorem of sums of independent random fields [8] if the variance  $\varphi(\mathbf{x}, l)$  is finite, then for large  $l$ . Integral in (2) tends to the field with a normal distribution. However, if the variance is infinite and there exists a non-degenerate, limiting distribution of a sum of random values, then such a distribution will be stable. For simplicity, the field  $\varphi(\mathbf{x}, l)$  is assumed to have a stable distribution. With  $L/l_0 \gg 1$ , it is impossible to calculate the pressure from equation (1) or if it is, then it demands large computer costs. Therefore, we pose the problem to obtain effective coefficients in equations for the large-scale filtration components. For the subgrid modeling we use ideas of the Wilson RG.

### 3 A Log-Stable Permeability

The growth of irregularity, chaotic state and intermittence in the behavior of physical fields with increasing the scale of measuring made many researchers to reject the log-normal model and consider a general case of log-stable distributions. In [9], distributions of permeability fields and some statistical characteristics were obtained using the experimental borehole data. Also, it was shown that the permeability fields can have log-stable distributions. Stable distributions depend on the four parameters  $\alpha$ ,  $\beta$ ,  $\mu$ ,  $\sigma$ , [10]. The parameter  $\alpha$  is within the domain  $0 < \alpha \leq 2$ , where  $\alpha = 2$  corresponds to the Gauss distribution. Statistical moments of order  $m$  for  $m \geq \alpha$  do not exist except for the case  $\alpha = 2$ , for which all the statistical moments are determined. Thus, the variance is infinite for  $\alpha < 2$ , and the mean value - for  $\alpha < 1$ . For modeling the field  $\varphi(\mathbf{x}, l)$ , having a stable distribution law, the approach from [11] is used. At the points  $(\mathbf{x}_j, l)$ , the field  $\varphi$  is defined by the sum of random independent values having stable distributions with the same parameters  $\alpha$ ,  $\beta$ ,  $\mu = 0$ ,  $\sigma = 1$  (the form  $A$  [10]):

$$\varphi(\mathbf{x}_j, l) = \left( \frac{\Phi_0(l)}{2(\delta\tau \ln 2)^{\alpha-1}} \right)^{\frac{1}{\alpha}} a_{\mathbf{j}\mathbf{i}}^l \zeta_{\mathbf{i}}^l + \varphi_0(l), \quad (3)$$

where  $l = 2^\tau$ ,  $\delta\tau$  - is a discretization step, the coefficients  $a_{\mathbf{j}\mathbf{i}}^l$  have a support of size  $l^3$ , depend only on the module of difference of indices ( in the sequel the index  $j$  can be omitted )  $a_{\mathbf{j}\mathbf{i}}^l \equiv a^l(|\mathbf{i} - \mathbf{j}|)$ , and for all  $l$  the condition  $\sum_{k_x} \sum_{k_y} \sum_{k_z} \left( a_{k_x k_y k_z}^l \right)^\alpha = 1$  holds. For  $1 \leq \alpha \leq 2$ , the thus constructed field  $\varphi$  can be stable, homogeneous and isotropic in spatial variables [11]. If the coefficients  $a_{\mathbf{j}\mathbf{i}}^l$  satisfy the condition  $a_{\mathbf{j}\mathbf{i}}^l \equiv a^l \left( \frac{|\mathbf{i} - \mathbf{j}|}{l} \right)$  and the constants  $\Phi_0(l)$ ,  $\varphi_0(l)$  are the same for all  $l$ , then the field  $\varphi$  will be invariant with respect to the scale transformation. The mean of the field  $\varphi$  exists and is equal to  $\varphi_0(l)$ . As for the second moments, they are infinite for  $\alpha \neq 2$ . This complicates carrying out the correlation analysis, applied, for example, in [2] and the approach used in [5]. Nevertheless, for an extreme point  $\beta = 1$  the second moments for the permeability field itself exist despite of the absence of variance of the field  $\varphi$ . This case is of interest, because it was experimentally verified [9]. As  $l_0$  is a minimum scale, we can set  $\varepsilon(\mathbf{x}) = \varepsilon(\mathbf{x})_{l_0}$ . Thus, the permeability field  $\varepsilon(\mathbf{x})$  within the above-described model has the form:

$$\varepsilon(\mathbf{x}) = \varepsilon_0 \exp \left[ - \left( \ln 2 \sum_{\widehat{l}_0}^{\widehat{L}} \varphi(\mathbf{x}, \tau_l) \delta\tau \right) \right], \quad (4)$$

where  $L = 2^{\widehat{L}\delta\tau}$ ,  $l_0 = 2^{\widehat{l}_0\delta\tau}$ , and the integral in formula (2) is replaced by the sum. For the calculation of moments of first and second orders we use formulas from [11] for  $\langle e^{-b\zeta} \rangle$ . For the correlation permeability function we have the estimation:

$$\langle \varepsilon(\mathbf{x}) \varepsilon(\mathbf{x} + \mathbf{r}) \rangle \simeq C \exp \left[ 2\delta\tau \ln 2 \left( -2^{\alpha-2} \sum_{\widehat{l}_r}^{\widehat{L}} \Phi_0(\widehat{l}) \left[ \cos \left( \frac{\pi\alpha}{2} \right) \right]^{-1} - \varphi_0(\widehat{l}) \right) \right] \quad (5)$$

where  $r = 2^{\widehat{l}_r \delta \tau}$ . For the self-similar permeability

$$\begin{aligned} \langle \varepsilon(\mathbf{x}) \varepsilon(\mathbf{x} + \mathbf{r}) \rangle &\simeq C \exp \left[ 2 \left( -2^{\alpha-2} \Phi_0 \left[ \cos \left( \frac{\pi}{2} \alpha \right) \right]^{-1} - \varphi_0 \right) (\ln L - \ln r) \right] \quad (6) \\ &\simeq C \left( \frac{L}{r} \right)^{-2 \left( 2^{\alpha-2} \Phi_0 \left[ \cos \left( \frac{\pi}{2} \alpha \right) \right]^{-1} + \varphi_0 \right)} \end{aligned}$$

The constant  $C$  is not universal, and the exponent for the self-similar permeability in (6) is universal and according to [12] can be measured.

## 4 A Subgrid Model

Let us divide the permeability function  $\varepsilon(\mathbf{x}) = \varepsilon(\mathbf{x})_{l_0}$  into two components with respect to the scale  $l$ . The large-scale component  $\varepsilon(\mathbf{x}, l)$  is obtained by statistical averaging over all  $\varphi(\mathbf{x}, l_1)$  with  $l_1 < l$ , while the small-scale component is equal to:  $\varepsilon'(\mathbf{x}) = \varepsilon(\mathbf{x}) - \varepsilon(\mathbf{x}, l)$ :

$$\varepsilon(\mathbf{x}, l) = \varepsilon_0 \exp \left[ - \int_{l_0}^l \varphi(\mathbf{x}, l_1) \frac{dl_1}{l_1} \right] \left\langle \exp \left[ - \int_{l_0}^l \varphi(\mathbf{x}, l_1) \frac{dl_1}{l_1} \right] \right\rangle_{<} \quad (7)$$

$$\varepsilon'(\mathbf{x}) = \varepsilon(\mathbf{x}, l) \left[ \frac{\exp \left[ - \int_{l_0}^l \varphi(\mathbf{x}, l_1) \frac{dl_1}{l_1} \right]}{\left\langle \exp \left[ - \int_{l_0}^l \varphi(\mathbf{x}, l_1) \frac{dl_1}{l_1} \right] \right\rangle_{<}} - 1 \right], \quad (8)$$

where  $\langle \rangle_{<}$  means averaging over  $\varphi(\mathbf{x}, l_1)$  from the small scale  $l_1$ . The large-scale (on-grid) pressure component  $p(\mathbf{x}, l)$  is obtained as averaged solution to equation (1), where the large-scale component (1) is fixed, while the small-scale component  $\varepsilon'$  is random,  $p(\mathbf{x}, l) = \langle p(\mathbf{x}) \rangle_{<}$ . The subgrid component is equal to  $p' = p(\mathbf{x}) - p(\mathbf{x}, l)$ . Let us substitute the expressions for  $p(\mathbf{x})$ ,  $\varepsilon(\mathbf{x})$  in equation (1) with averaging over the component  $\varepsilon'$ :

$$\nabla [\varepsilon(\mathbf{x}, l) \nabla p(\mathbf{x}, l) + \langle \varepsilon'(\mathbf{x}) \nabla p'(\mathbf{x}) \rangle_{<}] = 0. \quad (9)$$

The second term in equation 9) is unknown, but cannot be rejected without preliminary estimation, since the correlation between permeability and the pressure gradient can be essential [1], [5]. The choice of the form of the second term in (9) determines a subgrid model. In order that values of such an expression be estimated, we apply the perturbation theory. In the Wilson RG, the initial value of the scale  $l$  is close to that of the least scale  $l$ . Subtracting (9) from (1) we obtain the subgrid equation for the pressure  $p'(\mathbf{x})$ :

$$\nabla [\varepsilon(\mathbf{x}) \nabla p(\mathbf{x})] - \nabla [\varepsilon(\mathbf{x}, l) \nabla p(\mathbf{x}, l) + \langle \varepsilon'(\mathbf{x}) \nabla p'(\mathbf{x}) \rangle_{<}] = 0. \quad (10)$$

Equation (10) is used for finding the pressure  $p'(\mathbf{x})$  and cannot be accurately solved. From equation (10), neglecting second order terms of smallness, obtain

$$\Delta p'(\mathbf{x}) = -\frac{1}{\varepsilon(\mathbf{x}, l)} \nabla \varepsilon'(\mathbf{x}) \nabla p(\mathbf{x}, l) \quad (11)$$

According to the Wilson RG, the values  $\varepsilon(\mathbf{x}, l)$ ,  $p(\mathbf{x}, l)$  from the right-hand side equation (11) are considered to be known, their derivatives changing slower than  $\varepsilon'(\mathbf{x})$ . This corresponds to the idea to obtain a correct on-grid equation in the large-scale limit. Therefore,

$$p'(\mathbf{x}) = \frac{1}{4\pi\varepsilon(\mathbf{x}, l)} \int \frac{1}{r} \nabla \varepsilon'(\mathbf{x}') d\mathbf{x}' \nabla p(\mathbf{x}, l), \quad (12)$$

where  $r = |\mathbf{x} - \mathbf{x}'|$ . we come to the expression for a subgrid term in equation (9) in the large-scale limit:

$$\begin{aligned} \langle \varepsilon'(\mathbf{x}) \nabla p'(\mathbf{x}) \rangle &\approx \frac{1}{4\pi D \varepsilon(\mathbf{x}, l)} \int \Delta \frac{1}{r} \langle \varepsilon'(\mathbf{x}) \varepsilon'(\mathbf{x}') \rangle d\mathbf{x}' \nabla p(\mathbf{x}, l) \\ &\approx -\frac{1}{D \varepsilon(\mathbf{x}, l)} \langle \varepsilon'(\mathbf{x}) \varepsilon'(\mathbf{x}) \rangle \nabla p(\mathbf{x}, l), \end{aligned}$$

where  $D$  is a spatial dimension, here  $D = 3$ . The model is similar to that mentioned in Landau and Lifshits [13], which is used for effective dielectric permeability of a mixture under simplifying assumptions of small fluctuations of their spatial scale. From (7), (8) and using formulas [11], keeping only first order terms we will have for  $\varepsilon'(\mathbf{x})$ , obtain

$$\langle \varepsilon'(\mathbf{x}) \varepsilon'(\mathbf{x}) \rangle \approx \varepsilon^2(\mathbf{x}, l) \delta\tau \ln 2 \left[ \cos\left(\frac{\pi}{2}\alpha\right) \right]^{-1} (1 - 2^{\alpha-1}) \Phi_0(\tau_l) \quad (13)$$

For the second term in (9) we have

$$\langle \varepsilon'(\mathbf{x}) \nabla p'(\mathbf{x}) \rangle_{<} \approx -\frac{\delta\tau \ln 2}{D} \left[ \cos\left(\frac{\pi}{2}\alpha\right) \right]^{-1} (1 - 2^{\alpha-1}) \Phi_0(\tau_l) \varepsilon(\mathbf{x}, l) \nabla p(\mathbf{x}, l) \quad (14)$$

Substituting (14) in to (9) and keeping only first order terms we find

$$\nabla \left[ \left( 1 - \delta\tau \ln 2 \left( \Phi_0 \frac{2(1 - 2^{\alpha-1}) + D}{2D \cos(\frac{\pi}{2}\alpha)} + \varphi_0 \right) \right) \varepsilon(\mathbf{x}, l) \nabla p(\mathbf{x}, l) \right] = 0. \quad (15)$$

In the subgrid modeling, the effective permeability coefficient in the scale  $l$  must correctly describe the solution to equation (1) within the scales  $(l, L)$  and be calculated by a formula of the same form as  $\varepsilon(\mathbf{x})_{l_0}$ . Thus, the effective permeability is determined from

$$\varepsilon(\mathbf{x}) = \varepsilon_{0l} \exp \left[ - \left( \ln 2 \sum_{\hat{l}}^{\hat{L}} \varphi(\mathbf{x}, \tau_l) \delta\tau \right) \right]. \quad (16)$$

From (15) for  $\delta\tau \rightarrow 0$  we obtain that the constant  $\varepsilon_{0l}$  satisfies the equation

$$\frac{d \ln \varepsilon_{0l}}{d \ln l} = -\Phi_0(l) \frac{2(1 - 2^{\alpha-1}) + D}{2D \cos(\frac{\pi}{2}\alpha)} - \varphi_0(l), \quad \varepsilon_{0l}|_{l=L} = \varepsilon_{00} \quad (17)$$

For a self-similar permeability, the solution to equation (17) has the form

$$\varepsilon_{0l} = \varepsilon_{00} \left( \frac{l}{L} \right)^{\Phi_0 \frac{2(1 - 2^{\alpha-1}) + D}{2D \cos(\frac{\pi}{2}\alpha)} + \varphi_0}, \quad (18)$$

The constant  $\varepsilon_{00}$  describes the permeability in the largest possible scale for  $l = L$ .

## 5 Numerical Modeling

Equation (1) is numerically solved in the cube with the edge  $L_0$ . On the sides of the cube  $y = 0$ ,  $y = L_0$  we set the constant pressure  $p(x, y, z)|_{y=0} = p_1$ ,  $p(x, y, z)|_{y=L_0} = p_2$ ,  $p_1 > p_2$ . The pressure on other sides of the cube is set by the linear dependence along  $y$ :  $p = p_1 + (p_2 - p_1)/L_0$ . The major filtration flow is directed along the axis  $y$ . Here, dimensionless variables are used. The problem is solved in the unit cube, with a unit pressure jump and  $\varepsilon_0 = 1$ . The permeability field is simulated by (4),  $256 \times 256 \times 256$  grid in spatial variables is used, the scale step being  $\delta\tau = 1$ ,  $\tau_l = 0, \dots, -8$ . The coefficients  $a_{\mathbf{j}\mathbf{i}}^l$  were selected as

$$a_{\mathbf{j}\mathbf{i}}^l = \left( \frac{\sqrt{\alpha}}{2^{\tau_l} \sqrt{\pi}} \right)^{3/\alpha} \exp \left( -\frac{(\mathbf{x}_{\mathbf{j}} - \mathbf{x}_{\mathbf{i}})^2}{2^{2\tau_l}} \right). \quad (19)$$

The field  $\varphi(\mathbf{x}, \tau)$  is generated independent for each  $\tau_l$ . The common exponent in (4) is summed up over statistically independent layers. For an approximate solution, it is possible to use a certain limited number of layers. We have selected the number of layers so that the scale of the largest permeability fluctuations would allow us to approximately change probabilistic mean values averaged over space and the scale of the smallest fluctuations, so that the difference problem will approximate equation (1) sufficiently well, whose grid analog is solved by the iterative method. Independent random values  $\zeta_i^l$  in formula (4) were simulated using the algorithm and the program cited [14]. For self-similar media the constants  $\Phi_0$ ,  $\varphi_0$  can be selected from experimental data for natural porous media. According to [12], the exponent in (6) for some natural media varies within 0.25 – 0.3.

Fig. 1 shows the lines of the self-similar permeability level in the mid-span section  $z = 1/2$  for  $\alpha = 2$ , which corresponds to the log-normal permeability model and  $\alpha = 1, 6$ ,  $\beta = 1$ , and, respectively, to a stable model. The parameters  $\Phi_0 = 0.3$ ,  $\varphi_0 = 0$ . A difference between the two models is distinct.

According to the procedure of deriving a subgrid formula, for its verification it is necessary to numerically solve the full problem and to fulfil the probabilistic

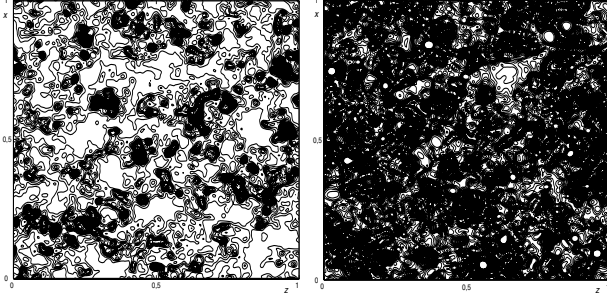


**Fig. 1.** The lines of levels in the mid-span section  $z = 1/2$  of the self-similar permeability for  $\alpha = 2$  (on the left), and  $\alpha = 1.6$ ,  $\beta = 1$  (on the right)

small-scale fluctuation averaging. As a result we obtain a subgrid term to be compared to a theoretical formula. This paper presents a more efficient version of such a verification that is based on the power dependence of the flow rate on the ratio of a maximum to a minimum scales in the ongrid domain when calculating permeability using (4) provided the contribution of a subgrid domain is not taken into account. The full flow rate of a liquid through a sample should coincide with the true one independent of the scale of the cut off  $l$ . The following formula is subject to verification:

$$\left\langle \exp \left[ - \left( \ln 2 \sum_{\hat{l}}^{\hat{L}} \varphi(\mathbf{x}_j, \tau_l) \delta\tau \right) \right] \nabla p \right\rangle = \frac{p_2 - p_1}{y_2 - y_1} \left( \frac{l}{L} \right)^{-\chi}, \quad (20)$$

where  $\chi = \delta\tau \ln 2 \sum_{\hat{l}_1=\hat{l}}^{\hat{L}} \left( \Phi_0 \left( \tau_{\hat{l}_1} \right) \frac{2(1-2^{\alpha-1})+D}{2D \cos(\frac{\pi}{2}\alpha)} + \varphi_0 \left( \tau_{\hat{l}_1} \right) \right)$ , the probabilistic mean is replaced for the spatial averaging. This ergodic hypothesis was numerically verified. Then, using the numerical solution to (1), when the fluctuations are  $\varepsilon_{-4}, \dots, \varepsilon_{-6}$ , we obtain the right-hand side of (20). Fig. 2 shows dependence

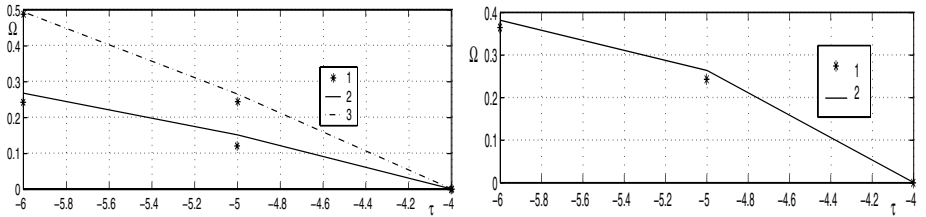


**Fig. 2.** The dependence of the logarithm of the flow rate  $\Omega$  on the logarithm of the scale  $\tau$  for  $\alpha = 1, 6$ ,  $\beta = 1$ ,  $\varphi_0 = 0$ , the numerical simulation is marked stars. On the left - the self-similar model of permeability, 2 - for  $\Phi_0 = 0.3$ , 3 - for  $\Phi_0 = 0.6$ . On the right - scale-invariance is absent,  $\Phi_0(-4) = 0.3$ ,  $\Phi_0(-5) = 0.6$ ,  $\Phi_0(-6) = 0.3$

of logarithm of the flow rate  $\Omega(\tau_l) = \log_2 \langle \exp \left[ - \sum_l^L \varphi(\mathbf{x}_j, \tau_l) \delta\tau \right] \frac{\nabla p}{P_2 - P_1} \rangle$  on the logarithm of scale  $\tau$  for  $\alpha = 1, 6$ ,  $\beta = 1$ ,  $\varphi_0 = 0$ . The results for a self-similar model of permeability are shown on the left Fig. 2. Line 2 corresponds to the value  $\Phi_0 = 0.3$ , line 3 corresponds to the value  $\Phi_0 = 0.6$ . The results obtained by numerical simulation are marked stars. On the right side there are shown the results for  $\Phi_0(-4) = 0.3$ ,  $\Phi_0(-5) = 0.6$ ,  $\Phi_0(-6) = 0.3$ . In this case scale-invariance is absent. The numerical verification with the use of the spatial averaging is in good agreement with theoretical formulas. This paper was partly supported by the Integration Grant SB RAS No 61, and Grant RFBR 04-05-64415.

## References

1. Shvidler, M. I.: Statistical hydrodynamics of porous media, Nedra, Moscow (1985) (in Russian)
2. Kuz'min G.A. and Soboleva O.N.: Subgrid modeling of filtration in porous self-similar media. J. Appl. Mech. and Tech. Phys. Vol. 43 (2002) 115–126
3. Kuz'min G.A. and Soboleva O.N.: Displacement of fluid in porous self-similar media. Physical Mesomechanics Vol. 5 (2002) 119–123
4. Wilson K. G. and Kogut J.: The renormalization group and the  $\epsilon$ -expansion. Physics Reports, 12C(2) (1974) 75-199
5. Teodorovich E.V.: The renormalization group method in the problem of effective permeability of stochastically nonhomogeneous porous medium. (in Russian) JETP Vol. 122 (2002) 79–89
6. Bogolubov N. N. and Shirkov D. V.: Introduction of theory of quantum fields, Nauka, Moscow (1976)
7. Kolmogorov A. N.: A refinement of previous hypotheses concerning the local structure of turbulence in a viscous incompressible fluid at high Reynolds number. J. Fluid Mech. Vol. 13 (1962) 82–85
8. Gnedenko B.V. and Kolmogorov A.N.: Limit Distributions for Sums of Independent Random Variables. Addison-Wesley, Cambridge, MA., (1954)
9. Bouffadel M. C., S. Lu et al.: Multifractal scaling of the intrinsic permeability. Physics of the Earth and Planetary Interiors 36(11) (2000) 3211–3222
10. Zolotarev V.M.: One-dimensional Stable Distributions. Amer. Math. Soc., Providence, RI., (1986)
11. Samorodnitsky G. and Taqqu M. S. Stable non-Gaussian random processes. Chapman Hill., New York, London, (1994)
12. Sahimi M.: Flow phenomena in rocks: from continuum models, to fractals, percolation, cellular automata, and simulated annealing. Reviews of Modern Physics 65(4) (1993) 1393–1534
13. Landau L.D. and Lifshitz E.M.: Electrodynamics of Continuous Media. Pergamon Press, Oxford-Elmsford, New York, (1984)
14. Chambers J. M., Mallows C., Stuck B. W. A method for simulating stable random variables. Journal of the American Statistical Association, 71(354) (1976) 340–344

# A Computational Model of Micro-vascular Growth

Dominik Szczerba and Gábor Székely

Computer Vision Lab, ETH, CH-8092 Zürich, Switzerland

{domi, szekely}@vision.ee.ethz.ch

www.vision.ee.ethz.ch

**Abstract.** In order to supply a growing tissue with oxygen and nutrients and to remove its metabolic wastes, blood vessels penetrating the tissue are formed. Multiple mechanisms are involved in this process ranging over many orders of magnitude: chemical signaling on the bio-molecular level ( $10^{-9}m$ ), genetic program on the protein level ( $10^{-7}m$ ), microscopic mechanical cell interactions ( $10^{-5}m$ ) and external forces and stresses reaching macroscopic scales ( $> 10^{-3}m$ ). Better physiological understanding of this phenomenon could result in many useful medical applications, for example in gene therapy or cancer treatment. We present a simulation framework to study mechanical aspects of the micro-vascular growth using techniques from computational geometry, solid mechanics, computational fluid dynamics and data visualization. Vasculogenesis is modeled as traction driven remodeling of an initially uniform tissue in absence of blood flow. Angiogenesis, the subsequent formation and maturation of blood vessels, is handled as a flow driven remodeling of a porous structure resulting from the preceding stage. The mechanical model of tissue response to the traction forces successfully predicts spontaneous formation of primitive capillary networks. Furthermore, we demonstrate that a shear-stress controlled remodeling of such structures can lead to flow fingering effects observed in real cellular media.

**Keywords:** angiogenesis, capillary formation, computational model, micro-vascular growth, numerical simulation, shear stress, vascular remodeling, vasculogenesis.

## 1 Introduction

Experimental studies confirm that physical forces, including tension, stretching or compression, and flow derived quantities like shear stress influence growth and remodeling in living tissues at the cellular level. In particular, it is known that alignment and structural remodeling of endothelial cells can be modulated by mechano-chemical interactions (e.g. [1], [2] and references therein). It is therefore reasonable to assume that physical interactions between blood flow and endothelial cells play an important role in capillary formation during the vascularization of a growing tissue. For example, [3] demonstrated that flow driven remodelling of transcapillary tissue pillars in the absence of cell proliferation is decisively involved in micro-vascular growth in the chick chorio-allantoic membrane. We have recently given a detailed overview of existing mathematical models of vascular growth ([4]). The approaches listed there are generally successful in predicting physiologically realistic systems with relevant biophysical properties,



but do not attempt to explain the origin of such structures in a microscopic sense. In addition, they either do not address blood flow effects at all, or only implicitly via Poiseuille's Law. In the same paper we have demonstrated that a simple mechanistic model of an explicit tissue response to blood flow suffices to reproduce bifurcation formation and micro-vessel separation from the underlying capillary bed. Structures resulting from the simulations are comparable to real experimental cases (see e.g. [5]) even though the tissue remodeling procedure used in the model is very primitive. The tissue is treated only in a statistical fashion as a set of independent pixels. This allows a very simple treatment of cellular transport but limits possibilities to model the tissue's elastic properties.

In this study we further investigate mechanical aspects of micro-vessel formation but using more realistic physical modeling of the tissue. In contrary to the previous approach, we now treat the tissue as a deformable object and explicitly address its elastic properties. In addition, we now differentiate between the early capillary plexus formation (vasculogenesis) and its subsequent remodeling (angiogenesis). Vasculogenesis is modeled as traction driven reshaping of an initially uniform tissue represented by a mass-spring mesh. In subsequent steps, as a result of fluid-structure interactions and elastic modeling of the tissue's interior, the emerging clusters elongate, align with the flow and merge with their neighbors, which is a prerequisite for the formation of new generations of blood vessels. In order to provide better solution accuracy at the fluid-structure interfaces, where the shear stress is of primary interest, we now also make use of irregular triangular grids. Such meshes can accurately map complex domains but require more advanced formulation of the flow equations than in case of an isometric Cartesian grid. Moreover, this implies additional difficulties in case of dynamically changing boundaries. Due to permanent modifications of the boundary conditions an efficient re-meshing is necessary for the required adaptation of the domain.

In the following section we will explain how we model the elastic response of the tissue and show that it suffices to explain formation of primitive capillary networks. In the next section the geometrical domain will be defined and the corresponding mesh generation technique will be described. Afterwards we will show how we remodel the system using fluid-structure interactions and demonstrate how this leads to the elongation and alignment of the tissue clusters. Finally, in the concluding section we summarize the approach, indicate its implications and propose future developments.

## 2 Tissue Modeling

We start by assuming that living cells consist of a soft matrix (cytoplasm) structurally strengthened by stiff elastic fibers (cytoskeleton). We further assume that a growing tissue increases its volume introducing stretching forces in these fibers, which eventually lead to their spontaneous breaking. At least in the first approximation it is natural to model a system of cytoskeleton fibers as a mesh, where uniformly distributed masses are connected by elastic springs. To describe the behavior of such a mass-spring mesh we start with Newton's equation of motion and assume that the external forces are the sum of linear spring deformation forces (the Hook's Law) and non-conservative inter-

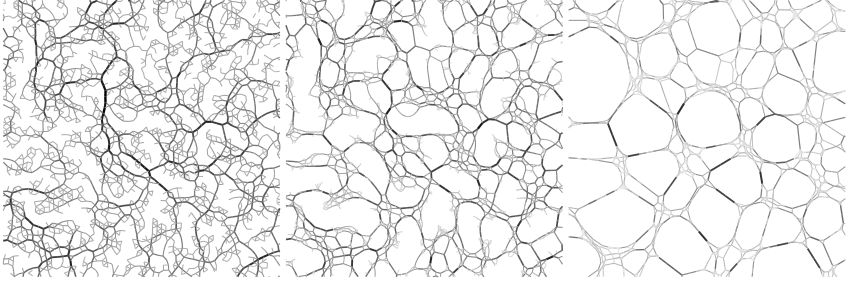


**Fig. 1.** Computer simulation of a traction-driven remodeling of an initially uniform mesh. The springs are gray- and width- coded according to their stretching forces

nal friction forces due to energy dissipation in cytoskeletal fibers. The resulting motion equation in a matrix form is

$$M \frac{d^2 \mathbf{r}}{dt^2} + D \frac{d\mathbf{r}}{dt} + K \mathbf{r} + \mathbf{F}^{ext} = 0, \quad (1)$$

where  $M$  is the mass matrix,  $D$  damping matrix,  $K$  stiffness matrix,  $\mathbf{r}$  is the vector containing the nodal coordinates and  $\mathbf{F}^{ext}$  is storing all other external forces (if any). This second order ordinary differential equation is solved numerically using a finite difference scheme. After substituting  $d\mathbf{r}/dt = \mathbf{v}$  and some algebraic rearrangements we obtain the discrete form of the equation, which we use to update the nodal velocities:

$$\mathbf{v}^{n+1} = \frac{1}{1 + \frac{D\Delta t}{M}} \left( \mathbf{v}^n + \frac{\Delta t}{M} (\mathbf{F}^K + \mathbf{F}^{ext}) \right), \quad (2)$$

with  $\mathbf{v}^t$  being a vector of nodal velocities at iteration  $t$  and  $\mathbf{F}^K$  the spring deformation forces. Now the nodal positions can be obtained using a simple time integration:

$$\mathbf{r}^{n+1} = \mathbf{r}^n + \mathbf{v}^n \Delta t. \quad (3)$$

A detailed description of the mesh generation procedure will be given in the next section. Here we start from a given uniform unstructured triangular grid covering a unit square. As already mentioned before, we assume that a growing tissue increases its volume and thus stretches its structural fibers. If we start to selectively remove springs that are stretched over a given threshold (damage due to exceeding their mechanical resistance), the initially regular mesh remodels into a set of tissue pillars forming a micro-tubular network, exactly as observed in early stages of vasculogenesis. **Fig. 1** shows a few stages of the remodeling process on selected fragments of the whole mesh consisting roughly of 12,000 nodes and 35,000 springs. The springs are width- and gray-coded according to their stretching forces. Our computational model allows to generate results comparable to those presented e.g. in [6] or [7], but as opposed to them, it is not based on a complex mathematical formalism. We do not model cells as scalar fields but base our modeling entirely on physical principles. As we explicitly address the tissue's elastic fibers we do not face numerical difficulties arising from e.g. modeling of surface tension inherent to a density representation. **Fig. 2** shows a comparison of one of our remodeling results with a real experimental case found in [7].

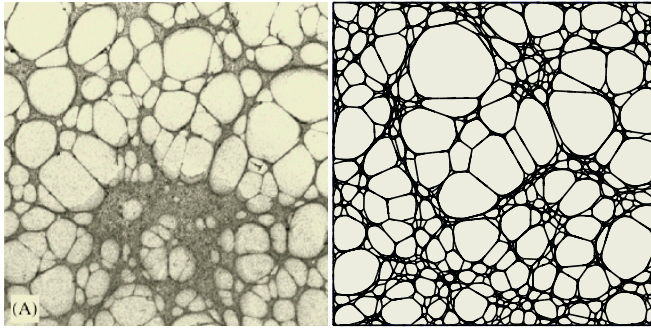


**Fig. 2.** Left: in vitro angiogenesis experiment from [7] (© Elsevier, reprinted with permission). Right: computer simulation of a traction-driven remodeling of an initially uniform mesh

### 3 Domain Definition and Mesh Generation

In the previous section we demonstrated how simple mechanistic modeling of cytoskeletal fibers can explain spontaneous formation of micro-channels in an initially homogeneous tissue prior to the actual blood flow. Now we investigate the behavior of the newly created micro-tubules as the blood starts flowing. We note that the resulting network can alternatively be viewed as a set of tissue clusters and the capillaries as narrow passages between them. We now want to approximate the emerging tissue clusters by deformable rings surrounded by an external membrane immersed in the fluid flowing around them. In order to create such rings as well as to generate appropriate meshes necessary to numerically solve the flow equation we need to provide a domain geometry. For that purpose we represent the clusters as polygons, we emit test rays from their centers and run an automatic search for the nearest springs intersecting with them. This information allows us to inspect the topological connections necessary for polygon reconstruction. Unfortunately, the contracting meshes produce many undesired topological artifacts like springs with zero length, degenerated nodal positions or highly non-homogeneous distribution of nodes on the cluster boundary edges. To correctly - and still automatically - reconstruct the polygons these special cases have to be differentiated and handled properly. Additional problems arise from very narrow passages that are often formed between pillars. In an extreme case one tubule is represented by only one spring. This introduces additional difficulties into the mesh generation procedure which we address here either by mesh refinement or by merging the two polygons if refinement leads to excessive mesh sizes.

Once the polygons are available we proceed by generating a mesh. We distribute masses inside the domain boundary and outside the interior polygons. Then we create topological connections between the masses using the Delaunay triangulation. Next, we remove all the triangles that lie outside the domain or inside any polygon. The triangles that are left are broken up into a unique set of springs and each spring is assigned a rest length being a desired mesh edge length at this place. When just one rest length is assigned to all the springs, a uniform (isometric) mesh will form. To

achieve refinement near boundaries one can assign different rest lengths for different springs according to e.g. distances to the nearest boundary or local curvature. Once the rest lengths are assigned, the masses are charged electrically and allowed to evolve. Then re-triangulation is performed to correct for any crossing springs, and the same deformation procedure is applied as described in the preceding section. In addition, the masses that come close enough to the boundary segments are snapped to them and not allowed to detach any more. After some iterations this simple method generated triangular meshes of sufficient quality but the time performance turned out to be very low, mostly because of  $N^2$  cost of electromagnetic interactions. The performance was significantly improved when magnetic repulsion between the masses was replaced by a slight increase in the desired spring rest lengths to form an "internal pressure" [8].

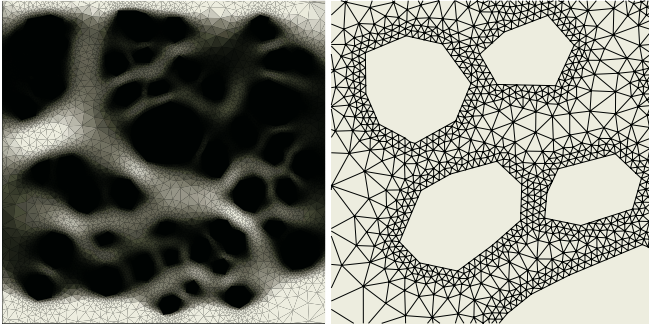


**Fig. 3.** Left: visualization of velocity in a fragment of a micro-capillary network presented in the previous figures. Right: a fragment of a mesh used to solve the flow equations

## 4 Flow Equations and Flow-Tissue Interactions

To simulate a structural remodeling of a capillary micro-network the key issue is finding the distribution of forces acting in such a physical domain. To calculate flow conditions we use numerical techniques from computational fluid dynamics. The general form of the Navier-Stokes equation for an incompressible Newtonian fluid is

$$\rho \frac{\partial \mathbf{v}}{\partial t} + \rho(\mathbf{v} \cdot \nabla)\mathbf{v} = \eta \nabla^2 \mathbf{v} - \nabla p + \mathbf{F} \quad (4)$$

$$\nabla \cdot \mathbf{v} = 0, \quad (5)$$

where  $\rho$  is the fluid's density,  $\eta$  the absolute viscosity,  $p$  the pressure,  $\mathbf{v}$  the velocity and  $\mathbf{F}$  denotes external forces. Eq.4 represents momentum balance and Eq.5 describes fluid continuity. In the case of creeping flow in capillaries the viscous forces are much stronger than the inertial forces and the convective part of the momentum equation does not need to be included. To describe a steady flow in the absence of external forces the time dependent and body force contributions can also be neglected and the Navier-Stokes equations can be rewritten as:

$$\nabla p = \eta \nabla^2 \mathbf{v} \quad (6)$$

$$\nabla \cdot \mathbf{v} = 0. \quad (7)$$

The steady-state discretization results in a system of equations with the form:

$$A_P^u u_P + A_i^u u_i = Q_P^u \quad (8)$$

$$A_P^v v_P + A_i^v v_i = Q_P^v \quad (9)$$

$$a_i \mathbf{v}_i \cdot \hat{\mathbf{n}}_i = 0, \quad (10)$$

with  $A$  being the domain dependent coefficient matrix,  $Q$  the source terms defined by the boundary conditions,  $a$  face surface,  $\hat{\mathbf{n}}$  face normal,  $u, v$  velocity components and using the Einstein summation over direct cell neighbors and the compass notation as in [9]. The formulation used above is the same that we already presented for the finite difference discretization [4], but the coefficients are different and have to be derived separately for the finite volume discretization on unstructured triangular meshes. As these equations have to hold true for every volume element in the mesh, we formulate this as a linear problem  $Ax = b$ , where  $x$  is a vector of unknown velocity components and pressure values,  $A$  is a domain dependent coefficient matrix and  $b$  is defined by the boundary conditions. Unfortunately, Eqs. 8-10 are not suitable for modeling pressure, as pressure is not even present in the continuity equation and is very weakly coupled with the velocity components. Solving such a system of equations in a standard way (i.e. simultaneously) results in oscillatory pressure solutions, therefore this case needs special treatment. To address this problem we adapted the smoothing pressure correction, originally presented for orthogonal grids [10], for the case of unstructured triangular meshes. We continue by solving the partial differential equations on the meshes, generated as described in the previous section (see **Fig. 3**). This results in velocity and pressure values in the center of each volume element. We assume that eventual evolution of the tissue is governed only by shear-induced traction forces at the boundary, which is well justified from experimental observations. We derive now viscous tractions on the boundary walls using the obtained velocity maps and distribute them onto the original mass-spring mesh nodes. Note, that we use two different meshes, a homogeneous one for the mass-spring deformation and an adaptive one for the discretization of the flow equations. This technique is known as a dual mesh approach. Now the original mesh is allowed to deform determining a new geometry and the whole procedure is repeated in a loop. Blood velocity is visualized by reconstructing nodal velocities from the triangle centers (by solving a linear problem) and using OpenGL to plot triangles with linear color interpolation. Unfortunately, simply letting the pillars hang freely, without addressing their internal structure, does not lead to any realistic remodeling. The pillars are only pushed aside all together, somewhat changing shape, but almost entirely preserving distances between them. Even though preferred paths of flow are clearly visible if the velocity is visualized (see gray-coded velocity plot in **Fig. 3**), we found no tendencies for the pillars to elongate and merge to form any kind of corridors or future vessel walls. The alignment of the tissue clusters and their interactions with the neighbors, however, are prerequisites for any vessel formation. Before any large scale simulations can take place, a better model of the dynamic behaviour of single tissue clusters has to be found. We assumed that the mechanical model involved in this case, ignoring the internal structure of the pillars, was not sufficient to correctly reproduce the required local phenomena. We concluded that the pillars were not just holes, but deformable membranes filled with elastic tissue - a structure having certain physical properties.

The springs that we used so far corresponded then to extracellular bindings. Additional springs, much stiffer in order to mimic behavior of solid clusters immersed in a jelly matrix, should now be placed in the pillar interiors, and the whole structure should be separated from the external matrix by a membrane. The structural arrangement of skeletal micro-filaments in cells is not trivial and its proper modeling can be crucial for obtaining correct results. We surround a cell with a membrane that is able to sense shear stress around itself and evaluate its average value. Then we make internal connections between all the membrane's nodes using springs 10 times stiffer than springs in the surrounding matrix. Now, if a part of the membrane senses shear stress higher than average, it will transmit contracting forces to all the internal filaments connected to the activated part. In contrary, if somewhere on the membrane shear stress lower than average is sampled, stretching is induced. Such mechanics successfully predicts elongation of a disk placed in a viscous flow (see **Fig. 4**). The same procedure applied to a bigger mesh is presented in **Fig. 5**. As can be seen from the figures, pillars finally elongated, aligned with the flow and subsequently merged with the neighbors, resulting in a chain which is the basic pre-condition for the formation of a future vessel wall. Based on this more realistic model of single cluster dynamics, further investigations on much bigger domains can be performed. If few pillars demonstrate clear tendencies to align and form chains, chances for micro-tubule formation in large scale simulations (involving e.g. thousands of such clusters) become realistic. This will, however, require computer code parallelization and other super-computing techniques due to excessive demand on computational resources that modeling of such domains would require.

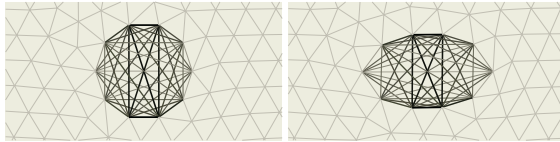


**Fig. 4.** Deformation of a disk due to its internal mechanics. Flow coming from the left

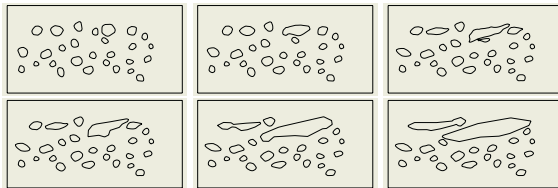


**Fig. 5.** Elongation of the tissue pillars, alignment with the flow and subsequent merging with neighbors - geometry at different iterations

## 5 Conclusions

We have presented a multi-physics simulation framework to study mechanical aspects of vascular system formation. We use techniques from solid mechanics to model tissue

response, computational geometry to generate meshes needed to solve partial differential equations, computational fluid dynamics to provide flow conditions in the cellular medium and fluid-structure interactions to simulate tissue remodeling. The simulations, visualized using OpenGL, reveal that mechanical traction forces rebuild an initially homogeneous tissue into a micro-tubular network, as observed in early stages of vasculogenesis. By visualizing blood velocity in such networks we find paths of preferred flow, suggesting future formation of some flow corridors or walls. By addressing the internal structure of the emerging cell clusters we demonstrate their alignment in the flow and tendencies to merge with the neighbors to form chains, which is a prerequisite for future micro-tubule formation. Once a realistic model of single cell clusters is available, large scale simulations, using super-computing due to excessive domain sizes, can be performed in future investigations.

## Acknowledgments

This work is a part of the Swiss National Center of Competence in Research on Computer Aided and Image Guided Medical Interventions (NCCR Co-Me), supported by the Swiss National Science Foundation.

## References

1. Hsiai, T.K., Cho, S.K., Honda, H.M., Hama, S., Navab, M., Demer, L.L., Ho, C.M.: Endothelial cell dynamics under pulsating flows: Significance of high versus low shear stress slew rates. *Annals of Biomedical Engineering* **30** (2002) 646–656
2. Malek, A.M., Izumo, S.: Mechanism of endothelial cell shape change and cytoskeletal remodeling in response to fluid shear stress. *Journal of Cell Science* **109** (1996) 713–726
3. Djonov, V., Galli, A., Burri, P.: Intussusceptive arborization contributes to vascular tree formation in the chick chorio-allantoic membrane. *Anatomy and Embryology* **202** (2000) 347–357
4. Szczerba, D., Székely, G.: Computational model of flow-tissue interactions in intussusceptive angiogenesis. *Journal of Theoretical Biology* **234** (2005) 87–97
5. Djonov, V., Kurz, H., Burri, P.: Optimality in the developing vascular system: Branching remodeling by means of intussusception as an efficient adaptation mechanism. *Developmental Dynamics* **224** (2002) 391–402
6. Manoussaki, D.: A mechanochemical model of vasculogenesis and angiogenesis. *Mathematical Modelling and Numerical Analysis* **37** (2003) 581–599
7. Namy, P., Ohayon, J., Tracqui, P.: Critical conditions for pattern formation and in vitro tubulogenesis driven by cellular traction fields. *Journal of Theoretical Biology* **227** (2004) 103
8. Persson, P.O., Strang, G.: A simple mesh generator in matlab. *SIAM Review*, Volume 46 (2), pp. 329–345 (2004)
9. Ferziger, J., Perić, M.: *Computational Methods for Fluid Dynamics*. Springer-Verlag (2002)
10. Date, A.W.: Complete pressure correction algorithm for solution of incompressible navier-stokes equations on a nonstaggered grid. *Numerical Heat Transfer, Part B* **29** (1996) 441–458

# A Dynamic Model for Phase Transformations in 3D Samples of Shape Memory Alloys

D.R. Mahapatra and R.V.N. Melnik

Mathematical Modelling and Computational Sciences, Wilfrid Laurier University,  
75 University Avenue West, Waterloo, Ontario, Canada N2L 3C5

**Abstract.** Despite recent progress in modelling the shape memory alloy (SMA) behaviour, many difficulties remain due to various limitations of the existing free energy models and strong nonlinearity of these nonlinear materials. Phase kinetics of SMA coupled with thermoelastodynamics is still not fully tractable, and one needs to deal with complicated multiscale character of SMA materials requiring a linkage between their microstructure and macroscopic properties. In this paper we develop a new dynamic model of 3D SMA which employs an improved version of the microscopic Landau theory. Essential properties of the single and multivariant martensitic phase transformations are recovered using consistent steps, which eliminates the problem of non-uniqueness of energy partitioning and relaxes the over-sensitivity of the free energy due to many unknown material constants in previously reported models. We exemplify our results on a model for cubic to tetragonal transformations in a rectangular SMA bar by showing key algorithmic steps which can be extended to more complex cases.

## 1 Introduction

Modelling of dynamics of phase transformations (PT) in Shape Memory Alloys (SMAs) under the combined effect of stress and temperature is one of the most challenging problems in computational science and engineering. Our better understanding of such dynamics can be achieved with multi-physics multiscale models which assist the researchers in designing new materials and devices by harnessing the shape memory effect. Phenomenological framework based on Landau theory of martensitic transformations (e.g., [1]) has become a convenient choice for basic building blocks in the computational models. However, most of the phenomenological models are applicable at macroscopic and mesoscopic scales as discussed in [2], and the strain field in such model is often beyond the resolution of bain strain. Also it may be noted that a majority of the works (see e.g.[3, 4]) in this direction is based on selectively chosen strain gradient plasticity models that require extensive parameter fitting from experimental data. Also, in such framework, the true nature of nonlinearity and coupling is not fully tractable. For a more detail description of the PT, one requires a microscopic model, such as [5, 6], where the invariance of the free energy with respect to the crystallographic point group symmetry is preserved but the discontinuous



nature of the deformation across the individual habit planes is introduced. This provides the most essential information to describe the morphology of the microstructural evolution, whereas the process of reshuffling of the atoms, which actually causes the reconstructive PT, remains beyond such a microstructural scale. The latter process requires the description of chemical interaction energy between atoms [7] and spin stabilized Hamiltonian [8]. Coupling such an atomistic process with the microstructural phenomenology means coupling a molecular dynamic model [9, 10] with a microscopic free energy model [6, 11, 12] through the thermal fluctuation term, strain and the motion of the domain walls.

In the present paper we focus our attention on linking SMA microstructure and macroscopic behaviour by developing the microscopic free energy and the associated coupled field model to simulate the dynamics of 3D macroscopic sample of NiAl undergoing cubic to tetragonal PT. First, we observe that the free energy is highly sensitive to many interdependent constants which are to be obtained experimentally [11]. As a result of this sensitivity and due to a fairly complex polynomial representation of the 3D Landau-Ginzburg free energy function, there may be situations where multidimensional simulations produce unphysical spurious oscillations. In the new model developed in the present paper, the above set of interdependent constants, that need to be determined from experimental data, is reduced to uniquely identifiable set of constants for each transformation surface among the austenitic phase and a particular martensitic variant.

Note that earlier, a new low-dimensional model for the time-dependent dynamics of SMA was derived in [2] and a class of such reduced models was rigorously analyzed in [13]. Computational results presented in [2, 13] confirmed robustness of our modelling approach for a number of practically important cases. The main results of the present paper are pertinent to *the general three-dimensional case*. There are several recent studies where the time-dependent Ginzburg-Landau (TDGL) (Langevin) equation with the correct microscopic description of the Falk-Konopka type free energy function has been analyzed (e.g. [14, 12]). We are not aware of any dynamic model of 3D SMA samples that bases its consideration on the correct Ginzburg-Landau free energy representation in the microscopic scale and the momentum balance and heat conduction in the macroscopic scale. The Ginzburg-Landau free energy function derived in the first part of this paper is incorporated in the coupled dynamic field model. This model is exemplified for cubic to tetragonal PT with single martensitic variant along the axis of a bar with rectangular cross-section under axial stress and heat flux.

## 2 3D Landau Theory of Martensitic Phase Transformation

It has been demonstrated by Levitas and Preston [6, 12] that the polynomial structures 2-3-4 and 2-4-6 of the Gibbs free energy in order parameter  $\eta$  in Cartesian coordinate can eliminate the problem of unphysical minima and re-

tain all the necessary properties of the Ginzburg-Landau free energy function with respect to point group symmetry of the crystals. Such polynomial structure can be constructed in such a way that the stability of the austenitic phase ( $A$ ) and martensitic variants ( $M_j$ ), non-extremal diffusion barrier and nucleation can be described in stress-temperature space. Furthermore, while using such polynomial structure the interfaces (domain walls)  $M_j - M_i$  between the martensitic variants ( $i, j$ ) can be interpreted by using a newly introduced barrierless  $A$  nucleation mechanism, i.e. by splitting the original into two simultaneously present interfaces  $M_j - A$  and  $A - M_i$ . In this section a 2-3-4 polynomial structure is constructed by improving upon the model of Levitas and Preston [6, 11].

For analytical clarity we first consider a single variant of martensite and single order parameter  $\eta \in [0, 1]$ . First we define the Gibbs free energy density in stress-temperature space  $(\boldsymbol{\sigma}, \theta)$  as

$$G = -\boldsymbol{\sigma} : \boldsymbol{\lambda} : \boldsymbol{\sigma} / 2 - \boldsymbol{\sigma} : \boldsymbol{\varepsilon}_t \varphi(\eta) + f(\theta, \eta), \quad (1)$$

where  $\boldsymbol{\lambda}$  is the constant fourth-rank elastic compliance tensor,  $\boldsymbol{\varepsilon}_t$  is the transformation strain tensor at the thermodynamic equilibrium of the martensite (obtained from crystallography),  $\varphi(\eta)$  is a monotonic function with  $\varphi(0) = 0$  indicating stable  $A$  phase and  $\varphi(1) = 1$  indicating stable  $M$  phase.  $f(\theta, \eta)$  is the chemical part of the energy with property:  $f(\theta, 1) - f(\theta, 0) = \Delta G^\theta(\theta)$ , where  $\Delta G^\theta$  is the difference between the thermal parts of the Gibbs free energy density of the  $M$  and  $A$  phases, which can be obtained indirectly from experiments [15]. The objective now is to obtain the functions  $\varphi$  and  $f$  by satisfying their properties mentioned above and the conditions of extremum of the energy for existence of equilibrium of  $A$  and  $M$  phases:  $\partial G / \partial \eta = 0$  at  $\eta = 0, 1$ .

The new model derived below is based on the assumption that  $G$  can be uniquely represented by a polynomial structure in  $\eta$  with the extremum only at  $\eta = 0, 1$  and out of these two extremum only one is minimum and the other is maximum for phase transformation (PT) to happen. At equilibrium, we have

$$\frac{\partial G}{\partial \eta} = -\boldsymbol{\sigma} : \boldsymbol{\varepsilon}_t \frac{\partial \varphi(\eta)}{\partial \eta} + \frac{\partial f(\theta, \eta)}{\partial \eta} = 0, \quad \eta = 0, 1. \quad (2)$$

The total strain tensor ( $\boldsymbol{\varepsilon} = -\partial G / \partial \boldsymbol{\sigma}$ ) is the sum of the elastic strain tensor ( $\boldsymbol{\lambda} : \boldsymbol{\sigma}$ ) and the transformation strain tensor ( $\boldsymbol{\varepsilon}_t \varphi(\eta)$ ). Hence, for reconstructive PT through vanishing misfit strain, the condition

$$\boldsymbol{\sigma} : \boldsymbol{\varepsilon}_t \frac{\partial \varphi(\eta)}{\partial \boldsymbol{\sigma}} - \frac{f(\theta, \eta)}{\partial \boldsymbol{\sigma}} = 0 \quad \forall (\boldsymbol{\sigma}, \eta) \quad (3)$$

must be satisfied. It is observed in the reported results [6] that the transformation barrier is dependent on stress. In the context of interface barrier, Levitas and Preston [12] have treated the associated  $\eta$  to be dependent on  $\boldsymbol{\sigma}$ . In the present paper, we propose an alternate approach by considering stress-dependent barrier height because the stress  $\boldsymbol{\sigma}$  is the only driving factor for PT under isothermal condition. The polynomial structure which satisfies the extremum properties can be expressed as

$$\partial G / \partial \eta = \eta(\eta - 1)(\eta - \eta_b), \quad (4)$$

so that its roots  $\eta = 0, 1$  satisfy Eq. (2) and the root  $\eta = \eta_b(\boldsymbol{\sigma}, \theta)$  represents the  $A \leftrightarrow M$  PT barrier. Integrating Eq. (4) and imposing the combined properties of  $\varphi(\eta)$  and  $f(\theta, \eta)$  stated earlier as

$$G(\boldsymbol{\sigma}, \theta, 0) - G(\boldsymbol{\sigma}, \theta, 1) = \boldsymbol{\sigma} : \boldsymbol{\varepsilon}_t - \Delta G^\theta, \quad (5)$$

we get that  $\eta_b = -6\boldsymbol{\sigma} : \boldsymbol{\varepsilon}_t + 6\Delta G^\theta + 1/2$ . Using Eq. (1) in Eq. (4) and by differentiating with respect to  $\boldsymbol{\sigma}$ , one has

$$-\boldsymbol{\varepsilon}_t \frac{\partial \varphi(\eta)}{\partial \eta} - \boldsymbol{\sigma} : \boldsymbol{\varepsilon}_t \frac{\partial^2 \varphi(\eta)}{\partial \boldsymbol{\sigma} \partial \eta} + \frac{\partial^2 f(\theta, \eta)}{\partial \boldsymbol{\sigma} \partial \eta} = \frac{\partial}{\partial \boldsymbol{\sigma}} [\eta_b \eta - (\eta_b + 1)\eta^2 + \eta^3]. \quad (6)$$

The term involving  $f$  can be eliminated from Eq. (6) with the help of Eq. (3), and can be expressed as

$$\boldsymbol{\varepsilon}_t \frac{\partial \varphi(\eta)}{\partial \eta} = \eta(\eta - 1) \frac{\partial \eta_b}{\partial \boldsymbol{\sigma}} = \eta(\eta - 1)(-6\boldsymbol{\varepsilon}_t). \quad (7)$$

Integrating Eq. (7) and following the properties of the transformation strain, i.e.  $\varphi(0) = 0$  and  $\varphi(1) = 1$ , we have  $\varphi(\eta) = 3\eta^2 - 2\eta^3$ ,  $0 \leq \eta \leq 1$ . Substituting this form in Eq. (3) and integrating with respect to  $\eta$ , the chemical part of the free energy density is obtained as

$$f(\theta, \eta) = \boldsymbol{\sigma} : \boldsymbol{\varepsilon}_t(3\eta^2 - 2\eta^3) + \frac{1}{2}\eta_b\eta^2 - \frac{1}{3}(\eta_b + 1)\eta^3 + \frac{1}{4}\eta^4. \quad (8)$$

For  $A \rightarrow M$  PT, the criteria for the loss of stability of  $A$  phase is  $\partial^2 G / \partial \eta^2 \leq 0$  at  $\eta = 0$ , which gives the stress driven condition:

$$\boldsymbol{\sigma} : \boldsymbol{\varepsilon}_t \geq \Delta G^\theta + \frac{1}{12}. \quad (9)$$

Similarly, for  $M \rightarrow A$  PT, the criteria for the loss of stability is  $\partial^2 G / \partial \eta^2 \leq 0$  at  $\eta = 1$ , which gives the stress driven condition:

$$\boldsymbol{\sigma} : \boldsymbol{\varepsilon}_t \leq \Delta G^\theta - \frac{1}{12}. \quad (10)$$

$M_j \leftrightarrow M_i$  PT or diffused interface can evolve for stresses outside the range obtained by Eqs. (9) and (10). Note that no parameter fitting is required in the present model as opposed to the earlier model [6]. Eqs. (9) and (10) indicate a nonlinear dependence of the transformation surface on the temperature, which can be compared with the experimental data.

## 2.1 Cubic to Tetragonal Transformation Characteristics

We now consider the cubic to tetragonal PT for single variant martensitic case in absence of the elastic part of the stress. After reducing the stress and strain tensors in 1D, the equilibrium stress-transformation curve is obtained as

$$\eta = \eta_b \Rightarrow \sigma = \frac{1}{\varepsilon_t} \left[ \Delta G^\theta + \frac{1 - 2\eta}{12} \right]. \quad (11)$$

Note that the increase in  $\eta$  causes decrease in  $\sigma$  which is consistent. The stress hysteresis ( $H$ ) is obtained as

$$H = \sigma_{(\eta=0)} - \sigma_{(\eta=1)} = \frac{1}{6\varepsilon_t}, \quad (12)$$

which is independent of the temperature. Eq. (11) also shows nonzero tangent moduli where  $A$  and  $M$  lose their stability. These observations coincide with the results from the earlier model [6] (Figs.1, 2 and 5).

### 3 Multivariant Phase Transformation

In order to model realistic situations and macroscopic sample of SMA it is essential to incorporate the effects of (1) martensitic variants ( $M_k$ ) (2) thermal strain (3) unequal compliances across the interfaces and the resulting inhomogeneity. For cubic to tetragonal transformation there are three variants of martensite according to the point group of crystallographic symmetry. The Gibbs free energy density thus should poses the associated invariance properties. In the mathematical model, this can be cross-checked by interchanging the variant indices ( $k$ ). In this paper we consider the same order of variation in the compliance tensor and the thermal expansion tensor as in  $\varphi(\eta)$  derived in Sec. 2. The Gibbs free energy density for cubic-tetragonal transformation having three variants  $k = 1, 2, 3$  is expressed as

$$G = -\boldsymbol{\sigma} : \left[ \boldsymbol{\lambda}_0 + \sum_{k=1}^3 (\boldsymbol{\lambda}_k - \boldsymbol{\lambda}_0) \varphi(\eta_k) \right] : \boldsymbol{\sigma} / 2 - \boldsymbol{\sigma} : \sum_{k=1}^3 \boldsymbol{\varepsilon}_{tk} \varphi(\eta_k) - \boldsymbol{\sigma} : \left[ \boldsymbol{\varepsilon}_{\theta 0} + \sum_{k=1}^3 (\boldsymbol{\varepsilon}_{\theta k} - \boldsymbol{\varepsilon}_{\theta 0}) \varphi(\eta_k) \right] + \sum_{k=1}^3 f(\theta, \eta_k) + \sum_{i=1}^2 \sum_{j=i+1}^3 F_{ij}(\eta_i, \eta_j), \quad (13)$$

where  $\boldsymbol{\lambda}$  is the second-order forth-rank compliance tensor ( $\boldsymbol{\lambda}_0$  is for  $A$  phase),  $\boldsymbol{\varepsilon}_{\theta 0} = \boldsymbol{\alpha}_0(\theta - \theta_e)$ ,  $\boldsymbol{\varepsilon}_{\theta k} = \boldsymbol{\alpha}_k(\theta - \theta_e)$ ,  $\boldsymbol{\alpha}_0$  and  $\boldsymbol{\alpha}_k$  are the thermal expansion tensor of  $A$  and  $M_k$ .  $F_{ij}$  is an interaction potential required to preserve the invariance of  $G$  with respect to the point group of symmetry and uniqueness of the multivariant PT at a given material point. The description of PT can now be generalized with three sets of order parameters:  $\bar{0} = \{0, \eta_k = 0, 0\}$ ,  $\bar{1} = \{0, \eta_k = 1, 0\}$  and  $\bar{\eta}_k = \{0, \eta_k, 0\}$ . The extremum property of the free energy density requires

$$\frac{\partial G}{\partial \eta_k} = \eta_k(\eta_k - 1)(\eta_k - \eta_{bk}) = 0, \quad \eta_k = \bar{0}, \bar{1}, \quad (14)$$

$$\frac{\partial^2 G}{\partial \eta_k^2} \leq 0, \quad \eta_k = \bar{0} \quad (A \rightarrow M_k); \quad \frac{\partial^2 G}{\partial \eta_k^2} \leq 0, \quad \eta_k = \bar{1} \quad (M_k \rightarrow A). \quad (15)$$

The transformation energy associated with  $A \leftrightarrow M_k$  is

$$G(\boldsymbol{\sigma}, \theta, \bar{0}) - G(\boldsymbol{\sigma}, \theta, \bar{1}) = \boldsymbol{\sigma} : \boldsymbol{\varepsilon}_{tk} - \Delta G^\theta. \quad (16)$$

Combining Eqs. (14) and (16) with similar steps described in Sec. 2, we get

$$\eta_{bk} = -6\boldsymbol{\sigma} : \boldsymbol{\varepsilon}_{tk} + 6\Delta G^\theta + 1/2 \quad (17)$$

Following the steps given in [11], we arrive at the symmetry preserving polynomial structure of the interaction potential

$$F_{ij} = \eta_i \eta_j (1 - \eta_i - \eta_j) [B \{(\eta_i - \eta_j)^2 - \eta_i - \eta_j\} + D \eta_i \eta_j] + \eta_i^2 \eta_j^2 (\eta_i Z_{ij} + \eta_j Z_{ji}) \quad (18)$$

such that

$$G = \sum_{k=1}^3 \left[ \frac{1}{2} \eta_{bk} \eta_k^2 - \frac{1}{3} (\eta_{bk} + 1) \eta_k^3 + \frac{1}{4} \eta_{bk}^4 \right] + \sum_{i=1}^2 \sum_{j=i+1}^3 F_{ij}(\eta_i, \eta_j) \quad (19)$$

leads to a 2-3-4-5 polynomial structure, where  $B$ ,  $D$  are constants estimated from experiments. The transformation energy associated with  $M_i \rightarrow M_j$  requires

$$G(\boldsymbol{\sigma}, \theta, \bar{\eta}_i) - G(\boldsymbol{\sigma}, \theta, \bar{\eta}_j) = \boldsymbol{\sigma} : (\boldsymbol{\varepsilon}_{tj} - \boldsymbol{\varepsilon}_{ti}) \quad (20)$$

which is already satisfied through Eq. (17). The uniqueness of PT at a material point is now imposed through similar steps described in context of Eq. (6).

## 4 Strongly Coupled Dynamics of the Phase Transformation and Coupled Thermoelasticity in a Rectangular NiAl Bar

The link between microstructure of SMA and its macroscopic behaviour is realized via the coupled field model in which the phase kinetics is governed by the Ginzburg-Landau equation

$$\frac{\eta_k}{\partial t} = - \sum_{p=1}^3 L_{kp} \left[ \frac{\partial G}{\partial \eta_p} - \boldsymbol{\beta}_p : \boldsymbol{\nabla} \boldsymbol{\nabla} \eta_p \right] + \theta, \quad (21)$$

where  $L_{kp}$  are positive definite kinetic coefficients,  $\boldsymbol{\beta}_k$  are positive definite second rank tensor, and the macroscopic energy conservation law is governed by the heat transfer equation

$$\rho \frac{\partial \bar{G}}{\partial t} - \boldsymbol{\sigma} : \boldsymbol{\nabla} \frac{\partial \mathbf{u}}{\partial t} + \boldsymbol{\nabla} \cdot \mathbf{q} = h_\theta, \quad (22)$$

and the momentum balance equation

$$\rho \frac{\partial^2 \mathbf{u}}{\partial t^2} = \boldsymbol{\nabla} \cdot \boldsymbol{\sigma} + \mathbf{f}, \quad (23)$$

where  $\bar{G} = G - \theta \partial G / \partial \theta$  is the internal energy,  $\rho$  is the mass density,  $\mathbf{u}$  is the displacement vector,  $\mathbf{q}$  is the heat flux,  $h_\theta$  and  $\mathbf{f}$  are the thermal and mechanical loading, respectively. The displacement is related to the Green strain tensor

as  $\varepsilon = (1/2)[\mathbf{F}^T \mathbf{F} - \mathbf{I}]$  where  $\mathbf{F}$  is the deformation gradient. For the purpose of numerical simulation we consider a rectangular NiAl bar with macroscopic domain  $([0, L], [y^-, y^+], [z^-, z^+])$  undergoing single variant cubic to tetragonal transformation under uniaxial stress  $(\sigma_{11})$  due to boundary conditions  $f_1(0, t) = (y^+ - y^-)(z^+ - z^-)\sigma_0(t)$ ,  $u_1(0, y, z, t) = 0$ , traction-free surfaces, thermal boundary conditions at the ends  $\partial\theta(x = 0, t)/\partial x = \bar{\theta}(t)_0$ ,  $\partial\theta(x = L, t)/\partial x = \bar{\theta}(t)_L$ , on the surface  $(y = y^+, y^-)$ ,  $\partial\theta/\partial y = \bar{\theta}_S$  and on the surface  $(z = z^+, z^-)$ ,  $\partial\theta/\partial z = \bar{\theta}_S$ . The initial conditions are  $\theta(x, 0) = \eta_0(x)$ ,  $\theta(x, y, z, 0) = \theta_0(x)$ ,  $u(x, y, z, 0) = u_0(x)$  and  $\partial u(x, y, z, 0)/\partial t = 0$ . A consistent form of the temperature field is obtained as

$$\theta(x, y, z, t) = \theta_1(x, t) + (y + z)\bar{\theta}_s. \quad (24)$$

The longitudinal displacement and strain fields are approximated as

$$u_1 = u(x, t), \quad \varepsilon_{11} = \frac{\partial u}{\partial x} + \frac{1}{2} \left( \frac{\partial u}{\partial x} \right)^2, \quad \varepsilon_{22} = \frac{\partial u_2}{\partial y}, \quad \varepsilon_{33} = \frac{\partial u_3}{\partial z}. \quad (25)$$

In the present example we assume that the habit planes are normal to  $e_1$ , such that  $\eta = \eta(x, t)$ . For microscopic deformation, the fine graining of strain requires the property of cubic to tetragonal transformation. For this model, we obtain the consistent form of the unknown fields  $u_2(x, y, z, t)$  and  $u_3(x, y, z, t)$  by imposing the geometric constraints for effectively one-dimensional dynamics, which leads to

$$u_2 = \frac{\mu}{2}y + \frac{\lambda_{21}}{\lambda_{11}}y\varepsilon_{11} - \left( \frac{1}{2} + \frac{\lambda_{21}}{\lambda_{11}} \right) \varepsilon_t \varphi(\eta)y + \alpha \left( 1 - \frac{\lambda_{21}}{\lambda_{11}} \right) \int (\theta - \theta_0) dy, \quad (26)$$

$$u_3 = \frac{\mu}{2}z + \frac{\lambda_{31}}{\lambda_{11}}y\varepsilon_{11} - \left( \frac{1}{2} + \frac{\lambda_{31}}{\lambda_{11}} \right) \varepsilon_t \varphi(\eta)y + \alpha \left( 1 - \frac{\lambda_{31}}{\lambda_{11}} \right) \int (\theta - \theta_0) dz, \quad (27)$$

where  $\mu$  is the prescribed error in the volumetric strain. This quasi-continuum model with discontinuous distribution of  $\eta(x, t)$ , and continuous fields  $u_1(x, t)$ ,  $\theta_1(x, t)$  is then solved by variational minimization of Eqs. (21)-(23).

## 5 Concluding Remarks

In this paper, a new dynamic multiscale model for simulation of 3D SMA samples has been developed by linking an improved version of the microscopic Landau theory and macroscopic conservation laws. Essential properties of the  $A \leftrightarrow M_j$  as well as  $M_j \leftrightarrow M_i$  PTs are recovered using consistent steps, which eliminates the problem of non-uniqueness of energy partitioning during PTs and relaxes the over-sensitivity of the free energy due to many unknown material constants in previously reported models. It has been shown how the new 3D model can be reduced to a low dimensional model for simulating the strongly coupled phase kinetics and thermoelasticity in a rectangular bar undergoing cubic to tetragonal phase transformations.

## References

1. Falk, F. and Konopka, P.: Three-dimensional Landau theory describing the martensitic phase transformation of shape -memory alloys. *J. Phys.: Condens. Matter* **2** (1990) 61–77
2. Melnik, R.V.N., Roberts, A.J. and Thomas, K.A.: Computing dynamics of copper-based shape memory alloys via center manifold reduction of 3D models. *Computational Materials Science* **18** (2000) 255–268
3. Boyd, J.G. and Lagaoudas, D.C.: A thermodynamical constitutive model for for shape memory materials. Part I. The monolithic shape memory alloy. *Int. J. Plasticity* **12**(9) (1996) 805–842
4. Aurichio, F. and Sacco, E.: A temperature-dependent beam for shape memory alloys: constitutive modelling, finite element implementation and numerical simulations. *Comput. Methods Appl. Mech. and Engrg.* **174** (1999) 171-190
5. Bhattacharya, K. and Khon, R.V.: Symmetry, texture and the recoverable strain of shape memory polycrystal. *Acta Mater.* **44**(2) (1996) 529-542
6. Levitas, V.I. and Preston, D.L.: Three-dimensional Landau theory for multivariant stress-induced martensitic phase transformations. I. Austenite  $\leftrightarrow$  martensite *Physical Rev. B* **66** (2002) 134206
7. Chen, L.Q., Wang, Y. and Khachatryan, A.G.: Kinetics of tweed and twin formation during an ordering transition in a substitutional solid solution. *Philos. Mag. Lett.* **65**(15) (1992) 15–23
8. Lindgard, P.A. and Mouritsen, O.G.: Theory and model for martensitic transformations. *Phy. Rev. Lett.* **57**(19) (1986) 2458
9. Clapp, P.C., Besquart, C.S., Shao, Y., Zhao, Y. and Rifkin, J.A.: Transformation toughening explored via molecular dynamics and Monte Carlo simulations. *Modelling Simul. Mater. Sci. Eng.* **2** (1994) 551–558
10. Rubini, S. and Ballone, P.: Quasiharmonic and molecular-dynamic study of the martensitic transformation in Ni-Al alloys. *Phy. Rev. B* **48** (1993) 99
11. Levitas, V.I. and Preston, D.L.: Three-dimensional Landau theory for multivariant stress-induced martensitic phase transformations. II. Multivariant phase transformations and stress space analysis. *Physical Rev. B* **66** (2002) 134207
12. Levitas, V.I. and Preston, D.L.: Three-dimensional Landau theory for multivariant stress-induced martensitic phase transformations. III. Alternative potentials, critical nuclei, kink solutions, and dislocation theory *Physical Rev. B* **68** (2003) 134201
13. Matus, P., Melnik, R.V.N., Wang, L. and Rybak, I.: Application of fully conservative schemes in nonlinear thermoelasticity: modelling shape memory materials. *Mathematics and Computers in Simulation* **65** (2004) 489-510
14. Ichitsubo, T., Tanaka, K., Koiwa, M. and Yamazaki, Y.: Kinetics of cubic to tetragonal transformation under external field by the time-dependent Ginzburg-Landau approach. *Phy. Rev. B* **62** (2000) 5435
15. Fu, S., Huo, Y. and Muller, I.: Thermodynamics of pseudoelasticity - an analytical approach. *Acta Mechanica* **99** (1993) 1-19

# 3D Finite Element Modeling of Free-Surface Flows with Efficient $k - \epsilon$ Turbulence Model and Non-hydrostatic Pressure

Célestin Leupi<sup>1</sup> and Mustafa Siddik Altinakar<sup>2</sup>

<sup>1</sup> ISE-STI-LIN, Ecole Polytechnique Fédérale,  
Lausanne 1015, Switzerland

Phone: +41.21.693.25.07, Fax + 41.21.693.36.46  
celestin.leupi@epfl.ch

<sup>2</sup> NCCHE, The University of Mississippi,  
Carrier Hall Room 102 University, MS 38677 USA

**Abstract.** Validation of 3D finite element model for free-surface flow is conducted using a high quality and high spatial resolution data set. The present research finds its motivation in the increasing need for efficient management of geophysical flows such as estuaries (multiphase fluid flow) or natural rivers with the complicated channel geometry (e.g. strong channel curvature). A numerical solution is based on the unsteady Reynolds-averaged Navier-Stokes equations without conventional assumption of hydrostatic pressure. The model uses implicit fractional step time stepping, with the characteristic method for convections terms. The eddy viscosity is calculated from the efficient  $k - \epsilon$  turbulence model. The RANS are solved in the multi-layers system (suitable for the vertical stratified fluid flow) to provide the accurate resolution at the bed and free-surface. The model is applied to the 3D curved open channels flows for which experimental data are available for comparison. Good agreement is found between numerical computations and experiments.

**Keywords:** Validation; Characteristic method; 3D Curved open channel; secondary currents; Non-hydrostatic pressure.

## 1 Introduction

Nowadays with the increasing computer power, several 3D computations have been successfully conducted for geophysical flows modeling. Most of these models have used the conventional hydrostatic pressure assumption. However, the natural rivers mostly have complicated geometry with the strong channel curvature. Such flows are of more importance for environmental hydraulic engineering and some related important features such as the secondary flows generated by the channel curvature and the related background turbulence effects, need to be well understood while a 3D description of the velocity field is required. Thus it is useful to resort to a more accurate model in which the hydrostatic assumption



is removed. Nevertheless, the importance of non-hydrostatic pressure in computational fluid problems was demonstrated and many researchers have applied 3D non-hydrostatic models to simulate the curved open channel flows. Wu et al. [13] and Olsen [10] used 3D numerical models to study the flow structure and mass transport in curved open channel. Xiabo et al. [2] have simulated the 3D unsteady curved open channel with standard  $k - \epsilon$  turbulence model and the non-hydrostatic pressure on the conformal mesh, but conformal mesh could poorly performed for some complicated bathymetry. Lai et al. [4] have used finite volume method on the unstructured grid to simulate 3D flow in meandering channel. For the free surface treatment, most of these 3D models employed the rigid-lid approximation, which have some weaknesses especially in strongly curved open channel flows (see [5]).

Based on the novel approach developed by Leupi et al. [6], the present model adopts the finite element conservative formulation in the multi-layers system for providing an accurate resolution at the bed and the free-surface.

The present work aims at validating the 3D finite element model against well-known non-uniform and unsteady flows in curved open channel flows using a high quality and high spatial resolution data set. The model uses the non-hydrostatic pressure and the state-of-art  $k - \epsilon$  turbulence model closure to solve the Reynolds-averaged Navier-Stokes equations (RANS).

In this study, the free-surface movement is controlled through the so-called *integrated continuity* equation. The full 3D governing equations are solved using implicit fractional time marching stepping where final velocity field and pressure term are computed from the hydrodynamic correction. Euler or Runge-Kutta scheme is used to obtain a set of algebraic equations from discretization. An efficient fractional step algorithm from Mohammadi and Pironneau [9] is introduced for the  $k - \epsilon$  model. This paper deals with the simulation of the 3D turbulent flow in the open curved channel for which experimental data are available.

## 2 Governing Equations

Let us consider an incompressible fluid body in a three-dimensional time varying domain  $\widehat{\Omega}$  (see also [6]) with  $\Omega$  the projection of  $\widehat{\Omega}$  on the  $xy$  horizontal plane.  $\widehat{\Omega}$  is bounded by the free-surface  $\Gamma_s$  given by  $z = \eta(x, y, t)$ , the bottom topography  $\Gamma_b$  given by  $z = -\mathfrak{h}(x, y)$ , the open boundary denoted by  $\Gamma_o$ . Where  $\mathfrak{h}(x, y)$  is the distance between the bottom and the reference plane  $xy$  and  $\eta(x, y, t)$  the elevation of the free-surface with the respect to the horizontal plane  $xy$ . For description of the turbulent motion, the pressure  $p$  can be written as the sum of an hydrostatic term  $p_h$  and an hydrodynamic correction  $p_{nh} = \rho p$ ,

$$p(\mathbf{x}, t) = p_h + p_{nh} = p_a + g\rho_o(\eta - z) + g \int_z^\eta \Delta\rho dz + \rho p(\mathbf{x}, t) \quad (1)$$

The 3D non hydrostatic Reynolds Averaged Navier-Stokes (RANS) equations reads

$$\nabla_H \cdot \mathbf{U} + \frac{\partial w}{\partial z} = 0 \quad (2)$$

$$\frac{D\mathbf{U}}{Dt} + g\nabla_H\eta - \nabla_H(\nu_T\nabla_H\mathbf{U}) - \frac{\partial}{\partial z}\left(\nu_T\frac{\partial\mathbf{U}}{\partial z}\right) + g\nabla\left(\int_{-b}^{\eta}\frac{\Delta\rho}{\rho_o}dz\right) + \frac{1}{\rho}\nabla p = \mathbf{F}_{xy} \quad (3)$$

$$\frac{Dw}{Dt} - \nabla_H(\nu_T\nabla_H w) - \frac{\partial}{\partial z}\left(\nu_T\frac{\partial w}{\partial z}\right) + \frac{1}{\rho}\frac{\partial p}{\partial z} = 0 \quad (4)$$

$$\frac{\partial\eta}{\partial t} + \nabla_H \cdot \int_{-b}^{\eta} \mathbf{U}dz = 0 \quad (5)$$

where  $\mathbf{U} = (u, v)^T$  is the horizontal velocity vector,  $\mathbf{F}_{xy} = (fv, -fu)^T$  is vector of body forces with  $f$  the Coriolis parameter,  $g$  is the gravitational acceleration,  $\nu_T$  is the eddy viscosity, (see Rodi [12]).  $(\nabla \cdot)$  is the 3D divergence operator,  $\frac{D}{Dt}$  represents the material derivative, and  $(\nabla_H \cdot)$  stands as the 2D horizontal divergence operator.  $\Delta\rho = \rho - \rho_0$ ;  $\rho, \rho_0$  are respectively the fluid density and the basic water density.

In eq.(3), the vertical eddy viscosity is defined as

$$\nu_T = \nu + c_\mu \frac{k^2}{\varepsilon} \quad (6)$$

in which  $\nu$  is the kinematic viscosity.

The  $k - \varepsilon$  turbulence equations read ([9]),

$$\frac{Dk}{Dt} - \nabla \cdot \left[ c_\mu \frac{k^2}{\varepsilon} \nabla k \right] = c_\mu \frac{k^2}{\varepsilon} G - \varepsilon \quad (7)$$

$$\frac{D\varepsilon}{Dt} - \nabla \cdot \left[ c_\varepsilon \frac{k^2}{\varepsilon} \nabla \varepsilon \right] = \frac{c_1}{2} kG - c_2 \frac{\varepsilon^2}{k} \quad (8)$$

The turbulent constants are given:  $c_1 = 0.126$ ,  $c_2 = 0.07$ ,  $c_\mu = 0.09$ ,  $c_\varepsilon = 1.92$ .

The production is represented by the squared shear frequency,  $G$ , (see [7]), such as :

$$G = \frac{1}{2} (\|\nabla\mathbf{V}\| + \|\nabla\mathbf{V}\|^T)^2 \quad (9)$$

where  $\|\cdot\|$  stands as the Euclidian norm,  $\mathbf{V} = \mathbf{V}(u, v, w)$  is the 3D velocity vector.

The *depth-integrated continuity* equation eq. (5) allow the model to follow the free-surface position. This equation is obtained by integrating the (local) continuity equation (2) in the  $z$  direction using the suitable kinematic free-surface and bottom boundary conditions.

The horizontal velocity is approximated combining the lowest order Raviart-Thomas element ( $\mathbb{RT}_0$ ) in  $xy$  plane with the  $\mathbb{P}_1$  elements along the vertical direction (see [6], [8], [11]). To discretize the convective term a method based on a Lagrange-Galerkin (or characteristics Galerkin) approach is considered (see [8], [9]) using either Euler scheme or more accurate Runge-Kutta. At each time step it is only required to solve a set of the positive definite symmetric and tridiagonal matrices for the fluxes using the conjugate gradient solver. For the turbulence modeling, the combination of the characteristics method with the fractional time stepping algorithm from Mohammadi and Pironneau ([9], [6]) can allow to preserve the positivity of  $k$ ,  $\varepsilon$  as well as the stability of the scheme (see [9], [12]). To avoid spurious numerical oscillations, the source term,  $G$ , has been discretised explicitly while the sink term has been discretised using the quasi-implicit forms with the consequence that linear terms are linearized (see [9]).

### 3 Numerical Results

The present model has been applied for simulating a 3D curved open channel flow in Figure 1, for which experimental data are available (see Blanckaert [1]). The

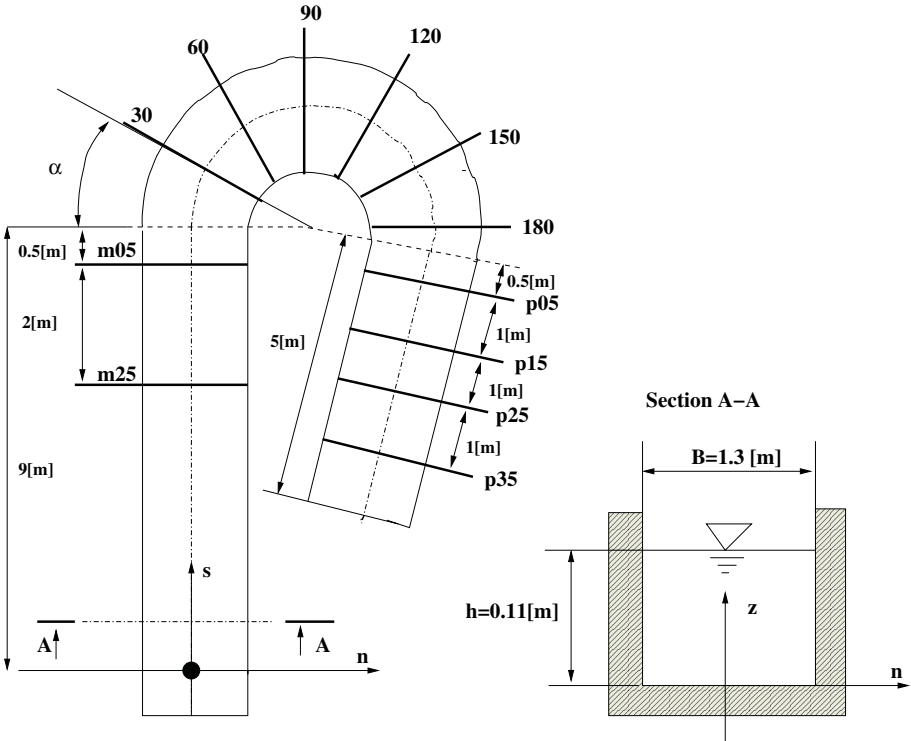
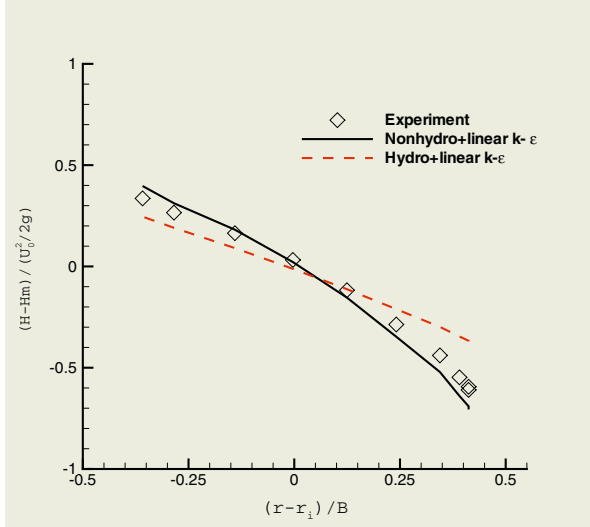


Fig. 1. A 193° Curved open-channel



**Fig. 2.** Experiments versus computed free-surface solutions at section  $\alpha = 120^\circ$  using linear  $k - \epsilon$  Turbulence model : Experiment ( $\diamond$ ) ; Hydrostatic (dashed line) ; Non hydrostatic (solid line)

discharge is set to  $Q = 0.089[\text{m}^3/\text{s}]$ , the bed slope (i.e. channel bottom slope) is  $S_0 = 0.000624$ . The rough bed is characterized by an equivalent roughness height,  $k_s = 0.0022[\text{m}]$ . The flow depth at the outflow (downstream end of the flume) is  $0.159[\text{m}]$ . The grid is composed of 50.000 elements and 30.000 nodes. The time step is set to  $0.1[\text{s}]$ , and the computation is performed till the flow is well developed at  $T=1300[\text{s}]$ . Computations were conducted with the hydrostatic pressure assumption for different cross-sections with the curvature increasing, to determine the conditions where the non-hydrostatic pressure component become significant. Computed solutions predict the gross flow features, whereas the water surface profile is under-estimated at the out bank, and over-estimated at the inner bank.

Figure 2 shows the cross-section at  $\alpha = 120^\circ$ , where are found the weaknesses of the hydrostatic pressure solution. Hence agreement with experiments is rather better for non-hydrostatic solutions particularly with the increasing curvature. This suggest that the separation may occur in the vertical flow and the the pressure-driven secondary effects are important. Thus the free surface must be more accurately computed to accounts for its damping effects on the turbulent flow. As observed in figure 3, both hydrostatic and non-hydrostatic pressure solutions show only one secondary flow circulation rotating clockwise from inner bank to outer bank. These predictions do not capture sufficiently the magnitude of the secondary motion. The maximum under prediction in the secondary currents for each vertical examined in this cross-section is ranged between 25 and 95% for the non-hydrostatic solutions and between 30 and 105% for the hydrostatic pressure. In Figure 3 the center of vortex is located at about  $z = 0.25[\text{m}]$  for the hydrostatic, about  $z = 0.35[\text{m}]$  for the non hydrostatic solutions which is more closed to experiments located at  $z = 0.4[\text{m}]$ . The predicted secondary currents intensities are weaker than

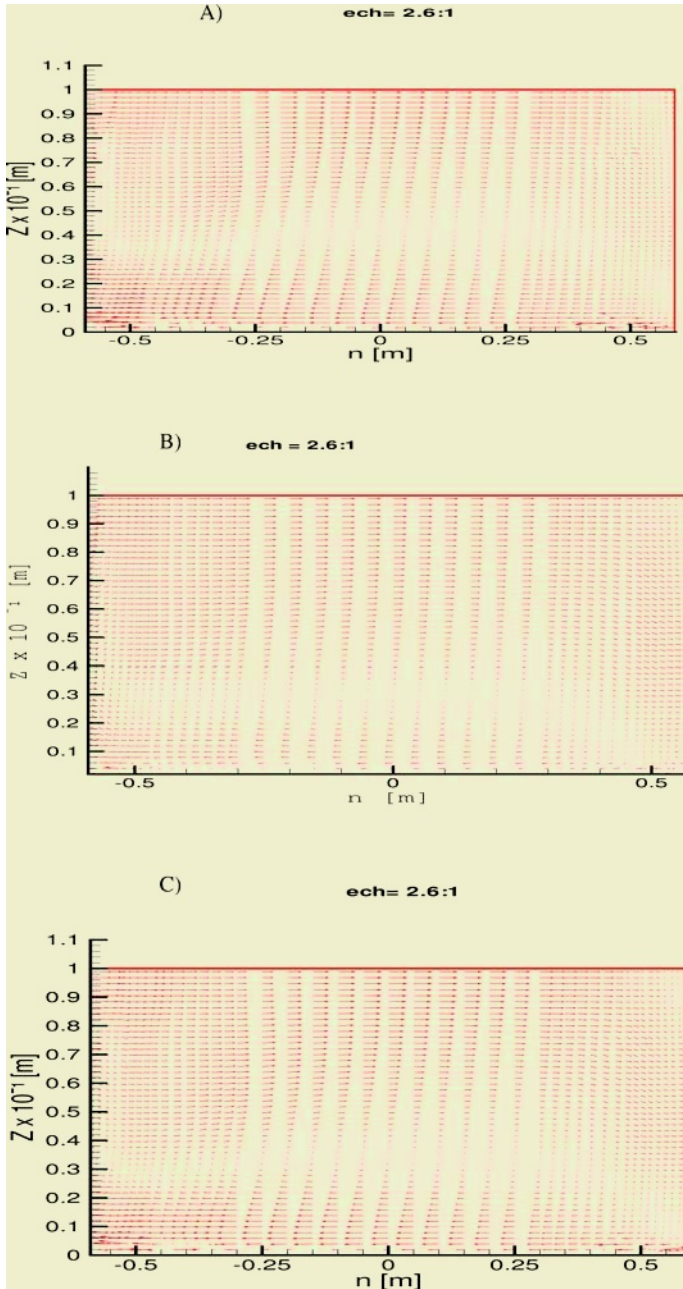


**Fig. 3.** Experiments versus computed solutions of the of cross-stream velocity vector at section  $\alpha = 120^\circ$  : A) Experiment ; B) Hydrostatic ; C) Non hydrostatic

measured, and the transverse velocities are under predicted. The anisotropic stress caused by walls and the junction region is not captured by the model, and the reduced momentum is transferred towards the outer region of the bend as well as the position of the longitudinal velocity maximum. This suggest that the turbulence-driven secondary effects are non-linear. Consequently, as shown by Gatsky et al. [3], the related weaker turbulence-driven secondary motion cannot be reproduced by linear and isotropic eddy-viscosity turbulence models. It should be pointed out that the major flow features such as the presence and rotational sense of the major secondary currents are reproduced and agrees well with experiments. The non-hydrostatic pressure influence is found to be more significant with the increasing curvature region, and although being more expensive, it become useful. This suggest that the pressure-driven secondary currents is relatively important for the accurate description of the velocity field and the use of anisotropic turbulence models is prerequisite to more accurate flow field prediction.

## 4 Conclusion

Validation of the 3D finite element solver for the RANS equations with the Efficient  $k - \epsilon$  turbulence model is conducted successfully using a high quality and high spatial resolution data set. The convection terms have been discretized using the Lagrange-Galerkin approach with advantage that, the CFL restriction is well performed. Moreover, addition of this characteristic method to the conservative form of the PDE and the implicit fractional step time stepping, allow to preserve the mass balance, the positivity of  $k$  and  $\epsilon$ , as well as the stability of the scheme. In computed solutions, the weaker secondary currents were not reproduced, but it should be noticed that more refine turbulence modeling can produce improvement for such problem. Computations with and without non-hydrostatic are compared for the same trench to test the validity of the conventional hydrostatic pressure assumption. The model predicts reasonably the complex major features and the 3D flow tests were performed successfully against well-known unsteady non-uniform curved open channel flows. The non-hydrostatic pressure influence is found to be more significant with the increasing curvature region (e.g. cross-section  $\alpha = 120^\circ$ ). This suggest that the non-hydrostatic pressure may be useful and well suited for complicated geometry flows where its influence is thought to be significant. Further study is needed to improve the general applicability of the model, and the next stage of this work will be focus on the anisotropic turbulence-driven secondary motion.

## Acknowledgment

The first author gratefully acknowledged Funding from the Swiss National Science Foundation through grant number 21-65095.01. Michel Deville, Alfio Quarteroni, Edie Miglio and Koen Blanckaert are acknowledged for their fruitfully discussions.

## References

1. Koen Blanckaert. *Flow and turbulence in sharp open-channel bends*. PhD thesis, Ecole polytechnique de Lausanne- EPFL, N0. 2545, 2002.
2. Xiabo Chao, Yafei jia, and Sam S. Y. Wang. Three-dimensional simulation of buoyant heat transfer in a curved open channel. In *Proc. Int. Conf. on Advances in hydro-Science and -Engineering, ICHE, NCCHE Mississippi, USA, vol 6*, pages 18–19 & on CDROM, 2004.
3. Thomas B. Gatski, M. Yousuff Hussaini, and John L. Lumley. *Simulation and Modeling of Turbulent Flows*. Oxford University Press, 198 Madison Avenue, New York, New York 10016, 1996.
4. Yong G. Lai, Larry J. Weber, and Virendra C. Patel. Three-dimensional model for hydraulic flow simulation. i: formulation and verification. *ASCE, J. Hydr. Engrg.*, 129(3):196–205, 2003.
5. Michael A. Leschziner and Wolfgang Rodi. Calculation of strongly curved open channel flow. *ASCE, J. Hydr. Div.*, 103(10):1297–1314, 1979.
6. Célestin Leupi, Edie Miglio, Mustafa Altinakar, Alfio Quarteroni, and Michel Deville. Quasi-3d finite element shallow-water flow with  $k - \varepsilon$  turbulence model. In *Proc. Int. Conf. on Advances in hydro-Science and -Engineering, ICHE, NCCHE Mississippi, USA, vol 6*, pages 400–401 & on CDROM, 2004.
7. Patrick J. Luyten, John Eric Jones, Roger Proctor, Andy Tabor, Paul Tett, and Karen Wild-Allen. Coherens- a coupled hydrodynamical-ecological model for regional and shelf seas. Technical Report MUMM report, Management unit of the Mathematical Models of North Sea, 914pp, COSINUS, 1999.
8. Edie Miglio, Alfio Quarteroni, and Fausto Saleri. Finite element approximation of quasi-3D shallow water equations. *Comput. Methods Appl. Mech. Engrg.*, 174(34):355–369, 1999.
9. Bijan Mohammadi and Olivier Pironneau. *Analysis of  $k - \varepsilon$  Turbulence Model*. Research in Applied Mathematics. John Wiley & Sons, Chichester, 1994.
10. Nils Reidar B. Olsen. Three-dimensional cfd modeling of self-forming meandering channel. *ASCE, J. Hydr. Engrg.*, 129(5):366–372, 2003.
11. Pierre Arnaud Raviart and Jean Marie Thomas. *A mixed finite element method for 2nd order elliptic problems*. Springer-Verlag, Mathematical Aspects of Finite Element Methods, Lecture notes in Mathematics.
12. Wolfgang Rodi. Turbulence models and their applications in hydraulics. Technical Report 2nd edition, IAHR, Delft, Netherlands, 1984.
13. Weiming Wu, Wolfgang Rodi, and Thomas Wenka. 3D numerical modeling of flow and sediment transport in open channels. *ASCE, J. Hydr. Engrg.*, 126(1):4–15, 2000.

# Cluster Computing for Transient Simulations of the Linear Boltzmann Equation on Irregular Three-Dimensional Domains

Matthias K. Gobbert<sup>1</sup>, Mark L. Breitenbach<sup>1</sup>, and Timothy S. Cale<sup>2</sup>

<sup>1</sup> Department of Mathematics and Statistics,  
University of Maryland, Baltimore County,  
1000 Hilltop Circle, Baltimore, MD 21250, U.S.A

<sup>2</sup> Focus Center — New York, Rensselaer,  
Interconnections for Hyperintegration,  
Isermann Department of Chemical and Biological Engineering,  
Rensselaer Polytechnic Institute, CII 6015,  
110 8th Street, Troy, NY 12180-3590, U.S.A

**Abstract.** Processes used to manufacture integrated circuits take place at a range of pressures and their models are of interest across a wide range of length scales. We present a kinetic transport and reaction model given by a system of linear Boltzmann equations that is applicable to several important processes that involve contacting in-process wafers with reactive gases. The model is valid for a range of pressures and for length scales from micrometers to centimeters, making it suitable for multiscale models. Since a kinetic model in three dimensions involves discretizations of the three-dimensional position as well as of the three-dimensional velocity space, millions of unknowns result. To efficiently perform transient simulations with many time steps, the size of the problem motivates the use of parallel computing. We present simulation results on an irregular three-dimensional domain that highlights the capabilities of the model and its implementation, as well as parallel performance studies on a distributed-memory cluster show that the computation time scales well with the number of processes.

## 1 Introduction

Many important manufacturing processes for integrated circuits involve the flow of gaseous reactants at pressures that range from very low to atmospheric. Correspondingly, the mean free path  $\lambda$  (the average distance that a molecule travels before colliding with another molecule) ranges from less than 0.1 micrometers to over 100 micrometers. The typical size of the electronic components (called ‘features’ during processing) is now below 1 micrometer and the size of the chemical reactor, in which the gas flow takes place, is on the order of decimeters. Thus, models on a range of length scales  $L^*$  are of interest, each of which needs to be appropriately selected to be valid on its length scale. These authors have in the



past coupled models on several length scales, from feature scale to reactor scale, to form an interactive multiscale reactor simulator [1, 2]. The models used were based on continuum models in all but the feature scale and assumed moderately high pressure to be valid. The current work provides the basis for extending this work to more general pressure regimes. Such multiscale models require well-tested and validated models and numerical methods on every scale of interest. The following results address both the effectiveness of the model and computational efficiency of the numerical method and its parallel implementation.

The appropriate transport model at a given combination of pressure and length scale is determined by the Knudsen number  $\text{Kn}$ , defined as the ratio of the mean free path and the length scale of interest  $\text{Kn} := \lambda/L^*$ , which arises as the relevant dimensionless group in kinetic models [3]: (i) For small values  $\text{Kn} < 0.01$ , continuum models describe the gas flow adequately. (ii) At intermediate values  $\text{Kn} \approx 1.0$ , kinetic models based on the Boltzmann transport equation capture the influence of both transport of and collisions among the molecules. (iii) For large values  $\text{Kn} > 100.0$ , kinetic models remain valid with the collision term becoming negligible in the limit as  $\text{Kn}$  grows.

Our interest includes models on the micro- to meso-scale at a range of pressures, resulting in Knudsen numbers ranging across the wide spectrum from less than  $\text{Kn} = 0.1$  to  $\text{Kn} \rightarrow \infty$ , in the regimes (ii) and (iii) above. For flow in a carrier gas, assumed inert, at least an order of magnitude denser than the reactive species, and in spatially uniform steady-state, we have developed a kinetic transport and reaction model (KTRM) [4, 5], given by the system of linear Boltzmann equations for all  $n_s$  reactive species in dimensionless form

$$\frac{\partial f^{(i)}}{\partial t} + \mathbf{v} \cdot \nabla_{\mathbf{x}} f^{(i)} = \frac{1}{\text{Kn}} Q_i(f^{(i)}), \quad i = 1, \dots, n_s, \quad (1)$$

with the linear collision operators

$$Q_i(f^{(i)})(\mathbf{x}, \mathbf{v}, t) = \int_{\mathbb{R}^3} \sigma_i(\mathbf{v}, \mathbf{v}') \left[ M_i(\mathbf{v}) f^{(i)}(\mathbf{x}, \mathbf{v}', t) - M_i(\mathbf{v}') f^{(i)}(\mathbf{x}, \mathbf{v}, t) \right] d\mathbf{v}',$$

where  $\sigma_i(\mathbf{v}, \mathbf{v}') = \sigma_i(\mathbf{v}', \mathbf{v}) \geq 0$  is a given collision frequency model and  $M_i(\mathbf{v})$  denotes the Maxwellian density of species  $i$ . The left-hand side of (1) models the advective transport of molecules of species  $i$  (local coupling of spatial variations via the spatial derivatives  $\nabla_{\mathbf{x}} f^{(i)}$ ), while the right-hand side models the effect of collisions (global coupling of all velocities in the integral operators  $Q_i$ ). The unknown functions  $f^{(i)}(\mathbf{x}, \mathbf{v}, t)$  in this kinetic model represent the (scaled) probability density that a molecule of species  $i = 1, \dots, n_s$  at position  $\mathbf{x} \in \Omega \subset \mathbb{R}^3$  has velocity  $\mathbf{v} \in \mathbb{R}^3$  at time  $t$ . Its values need to be determined at all points  $\mathbf{x}$  in the three-dimensional spatial domain  $\Omega$  and for all three-dimensional velocity vectors  $\mathbf{v}$  at all times  $0 < t \leq t_{\text{fin}}$ . This high dimensionality of the space of independent variables is responsible for the numerical complexity of kinetic models, as six dimensions need to be discretized, at every time step for transient simulations. Notice that while the equations in (1) appear decoupled, they actually remain coupled through the boundary condition at the wafer surface that models the surface reactions and is of crucial importance for the applications under consideration.

## 2 The Numerical Method

The numerical method for (1) needs to discretize the spatial domain  $\Omega \subset \mathbb{R}^3$  and the (unbounded) velocity space  $\mathbb{R}^3$ . We start by approximating each  $f^{(i)}(\mathbf{x}, \mathbf{v}, t)$  by an expansion  $f_K^{(i)}(\mathbf{x}, \mathbf{v}, t) := \sum_{\ell=0}^{K-1} f_\ell^{(i)}(\mathbf{x}, t) \varphi_\ell(\mathbf{v})$ . Here, the basis functions  $\varphi_\ell(\mathbf{v})$  in velocity space are chosen such that they form an orthogonal set of basis functions in velocity space with respect to an inner product that arises naturally from entropy considerations for the linear Boltzmann equation [6]. Testing (1) successively against  $\varphi_k(\mathbf{v})$  with respect to this inner product approximates (1) by a system of linear hyperbolic equations

$$\frac{\partial F^{(i)}}{\partial t} + A^{(1)} \frac{\partial F^{(i)}}{\partial \mathbf{x}_1} + A^{(2)} \frac{\partial F^{(i)}}{\partial \mathbf{x}_2} + A^{(3)} \frac{\partial F^{(i)}}{\partial \mathbf{x}_3} = \frac{1}{\text{Kn}} B^{(i)} F^{(i)}, \quad i = 1, \dots, n_s, \quad (2)$$

where  $F^{(i)}(\mathbf{x}, t) := (f_0^{(i)}(\mathbf{x}, t), \dots, f_{K-1}^{(i)}(\mathbf{x}, t))^T$  is the vector of the  $K$  coefficient functions in the expansion in velocity space. Here,  $A^{(1)}$ ,  $A^{(2)}$ ,  $A^{(3)}$ , and  $B^{(i)}$  are constant  $K \times K$  matrices. Picking specially designed basis functions, the coefficient matrices  $A^{(\delta)}$ ,  $\delta = 1, 2, 3$ , become diagonal matrices [7, 8]. Note again that the equations for all species remain coupled through the crucial reaction boundary condition at the wafer surface.

The hyperbolic system (2) is now posed in a standard form as a system of partial differential equations on the spatial domain  $\Omega \subset \mathbb{R}^3$  and in time  $t$  and amenable to solution by various methods. Figure 1 shows two views of a representative domain  $\Omega \subset \mathbb{R}^3$ ; more precisely, the plots show the solid wafer surface consisting of a 0.3 micrometer deep trench, in which is etched another 0.3 micrometer deep via (round hole). The domain  $\Omega$  for our model is the gaseous region above the solid wafer surface up to the top of the plot box shown at  $\mathbf{x}_3 = 0.3$  micrometers in Figure 1. Since typical domains in our applications such as this one are of irregular shape, we use the discontinuous Galerkin method (DGM) [9], relying on a finite element discretization into tetrahedra of the domain. Explicit time-stepping is used because of its memory efficiency and cheap cost per time step. We accept at this point the large number of time steps that will be required, because we also wish to control the size of the step size to maintain a high level of accuracy.

The degrees of freedom (DOF) of the finite element method are the values of the  $n_s$  species' coefficient functions  $f_k^{(i)}(\mathbf{x}, t)$  in the Galerkin expansion at  $K$  discrete velocities on the 4 vertices of each of the  $N_e$  tetrahedra of the three-dimensional mesh. Hence, the complexity of the computational problem is given by  $4 N_e K n_s$  at every time step. To appreciate the size of the problem, consider that the mesh of the domain in Figure 1 uses  $N_e = 7,087$  three-dimensional tetrahedral elements; even in the case of a single-species model ( $n_s = 1$ ) and if we use just  $K = 4 \times 4 \times 4 = 64$  discrete velocities in three dimensions, as used for the application results in the following section, the total DOF are  $N = 1,814,272$  or nearly 2 million unknowns to be determined at every time step. Then, to reach a (re-dimensionalized) final time of 30.0 nanoseconds, for instance, requires about 60,000 time steps, with time step  $\Delta t$  selected according to a CFL-condition. This

size of problem at every time step motivates our interest in parallel computing for this problem. For the parallel computations on a distributed-memory cluster, the spatial domain  $\Omega$  is partitioned in a pre-processing step, and the disjoint subdomains are distributed to separate parallel processes. The discontinuous Galerkin method for (2) needs the flux through the element faces. At the interface from one subdomain to the next, communications are required among those pairs of parallel processes that share a subdomain boundary. Additionally, a number of global reduce operations are needed to compute inner products, norms, and other diagnostic quantities.

### 3 Application Results

As an application example, we present a model for chemical vapor deposition. In this process, gaseous chemicals are supplied from the gas-phase interface at  $\mathbf{x}_3 = 0.3$  in Figure 1. The gaseous chemicals flow downwards throughout the domain  $\Omega$  until they reach the solid wafer surface in Figure 1, where some of the molecules react to form a solid deposit. The time scale of our simulations corresponds to forming only a very thin layer; hence the surface is not moved within a simulation. We focus on how the flow behaves when starting from no gas present throughout  $\Omega$ , modeled by initial condition  $f^{(i)} \equiv 0$  at  $t = 0$ . Here, we use a single-species model with one reactive species ( $n_s = 1$ ). The deposition at the wafer surface can then be modeled using a sticking factor  $0 \leq \gamma_0 \leq 1$  that represents the fraction of molecules that are modeled to deposit at (“stick to”) the wafer surface. The re-emission into  $\Omega$  of gaseous molecules from the wafer surface is modeled as re-emission with velocity components in Maxwellian form and proportional to the flux to the surface as well as proportional to  $1 - \gamma_0$ . The re-emission is scaled to conserve mass in the absence of deposition ( $\gamma_0 = 0$ ). The studies shown use a sticking factor of  $\gamma_0 = 0.01$ , that is, most molecules re-emit from the surface, which is a realistic condition. The collision operator uses a relaxation time discretization by choosing  $\sigma_1(\mathbf{v}, \mathbf{v}') \equiv 1/\tau_1$  with (dimensionless) relaxation time  $\tau_1 = 1.0$ .

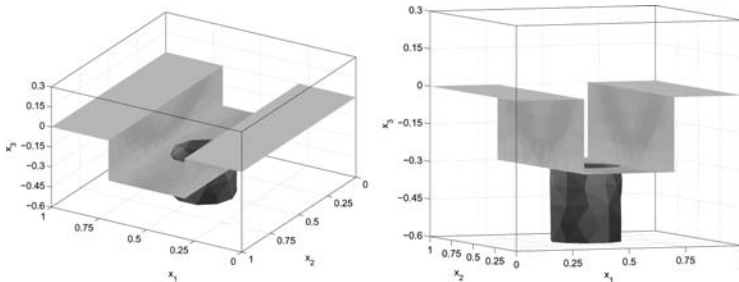


**Fig. 1.** Two views of the solid wafer surface boundary of the trench/via domain

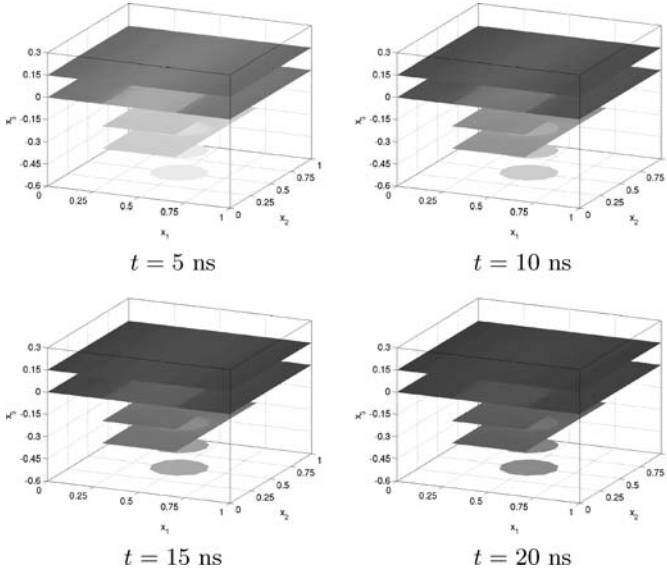


**Fig. 2.** Slice plots at heights  $x_3 = -0.60, -0.45, -0.30, -0.15, 0.00, 0.15$  at different times  $t$  of the dimensionless concentration  $c(\mathbf{x}, t)$  for  $\text{Kn} = 0.1$  throughout domain  $\Omega$ . Grayscale from light  $\Leftrightarrow c = 0$  to dark  $\Leftrightarrow c = 1$

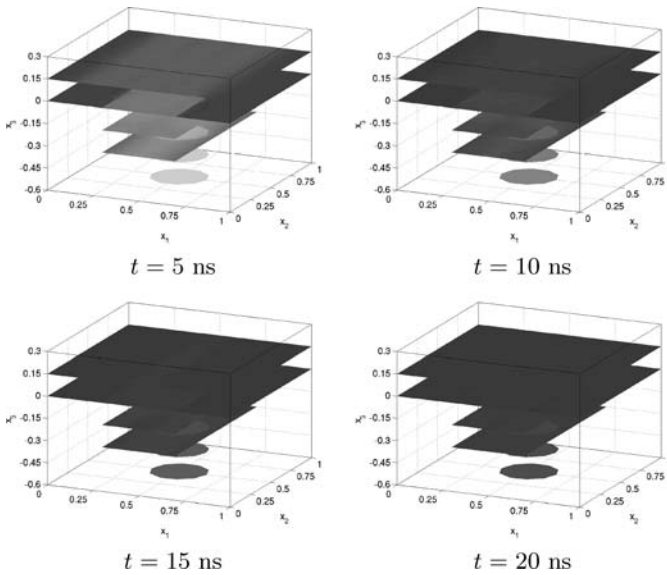


**Fig. 3.** Slice plots at heights  $x_3 = -0.60, -0.45, -0.30, -0.15, 0.00, 0.15$  at different times  $t$  of the dimensionless concentration  $c(\mathbf{x}, t)$  for  $\text{Kn} = 1.0$  throughout domain  $\Omega$ . Grayscale from light  $\Leftrightarrow c = 0$  to dark  $\Leftrightarrow c = 1$

Figures 2 and 3 show the results of transient simulations for the values of the Knudsen number  $\text{Kn} = 0.1$  and  $\text{Kn} = 1.0$ , respectively. The quantity plotted for each (re-dimensionalized) time is the (dimensionless) concentration

$$c(\mathbf{x}, t) := \int_{\mathbb{R}^3} f^{(1)}(\mathbf{x}, \mathbf{v}, t) d\mathbf{v}$$

across the domain  $\Omega$ . The values of the dimensionless concentration  $0 \leq c \leq 1$  is represented by the gray-scale color on each of the horizontal slices through  $\Omega$  at the vertical levels at six values of  $\mathbf{x}_3$ ; the shapes of all slices together indicate the shape of the domain  $\Omega$ .

At  $t = 5$  ns, the top-most slice at  $\mathbf{x}_3 = 0.15$  is mostly dark-colored, indicating that a relatively high concentration of molecules have reached this level from the inflow at the top of the domain. The slice at  $\mathbf{x}_3 = 0$  shows that the concentration at the flat parts of the wafer surface has reached relatively high values, as well, while the lighter color above the mouth of the trench ( $0.3 \leq \mathbf{x}_1 \leq 0.7$ ) is explained by the ongoing flow of molecules into the trench. At the slice for  $\mathbf{x}_3 = -0.3$ , we observe the same phenomenon where the concentration has reached a higher value in the flat areas of the trench bottom as compared to the opening into the via (round hole) below. Finally, not many molecules have reached the via bottom, yet, indicated by the very light color there.

Comparing the plots at  $t = 5$  ns in Figures 2 and 3 with each other, the one for the smaller  $\text{Kn} = 0.1$  has generally lighter color indicating a slower fill of the feature with gas. The smaller Knudsen number means more collisions among molecules, leading to a less directional flow than for the larger Knudsen number  $\text{Kn} = 1.0$ . Since the bulk direction of the flow is downward because of the supply at the top with downward velocity, the feature fills faster with molecules in this case.

The following plots in both figures show how the fill of the entire domain with gaseous molecules continues over time. Figure 3 shows that steady-state of complete fill is reached slightly faster for the larger Knudsen number, which is realistic. Consistent results are obtained by considering a wider range of values of  $\text{Kn}$  than presented here.

The results validate the effectiveness of the model and its numerical method for multiscale simulations for this application.

## 4 Parallel Performance Results

In this section, parallel performance results are presented for the code running on a 64-processor Beowulf cluster. This system has 32 dual-processor compute

**Table 1.** Observed wall clock times in minutes up to 64 processes

$K$	DOF	1	2	4	8	16	32	64
8	226,784	154	93	48	40	21	8	6
64	1,814,272	2,294	1,252	686	323	160	91	50

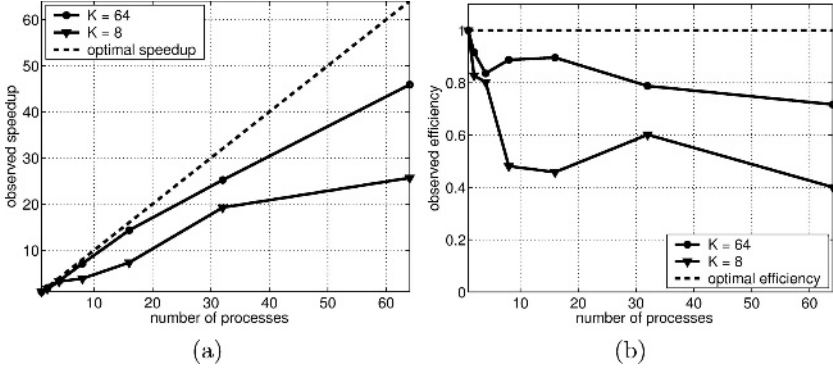


**Fig. 4.** (a) Observed speedup and (b) observed efficiency up to 64 processes

nodes, each with two Intel Xeon 2.0 GHz (512 kB L2 Cache) chips and 1 GB of memory. The nodes communicate through a high-performance Myrinet interconnect using the Message Passing Interface (MPI).

Table 1 shows observed wall clock times for simulations with  $\text{Kn} = 1.0$  up to a final time of 30.0 nanoseconds for the domain with 7,087 elements in Figure 1 for velocity discretizations using  $K = 2 \times 2 \times 2 = 8$  and  $K = 4 \times 4 \times 4 = 64$  discrete velocities, respectively. The second column in the table lists the number of degrees of freedom (DOF) for reference. The following columns show the observed wall-clock times in minutes for each number of parallel processes 1, 2, 4,  $\dots$ , 64 used; the runs using 1 process use a serial code of the same algorithm. The wall clock times in Table 1 were obtained by computing the difference of the time stamps on the first and last output file written by the code. Thus, these numbers are the most *pessimistic* measure of parallel performance possible, as various extraneous delays like operating system activity, file serving, I/O delay, etc. are included in this measurement in addition to the actual cost of calculations and communications of the numerical algorithm. Clearly, the computation times for three-dimensional models are quite significant, even using the modest resolution of velocity space presented here.

Figure 4 (a) and (b) show the observed speedup and efficiency, respectively, computed from the wall clock times given in Table 1. For  $K = 8$ , the speedup in Figure 4 (a) appears good up to 4 processes, then deteriorates, but continues to improve again for larger number of processes. This behavior is not unexpected, as 226,784 degrees of freedom are not a particularly large number. The speedup for the more complex case  $K = 64$  is clearly significantly better. It is near-optimal up to 16 processes, then drops off slightly. Figure 4 (b) shows the observed efficiency. Both lines reveal a noticeable drop of efficiency from the serial to the 2-process run that was not easily visible in the speedup plot. We explain this drop by overhead of the parallel version of the code as compared to the serial code used as 1-process code. The efficiency shows some additional slight decline up to 4 processes. This poorer efficiency might be due to the particular partitioning of the domain  $\Omega$  among the processes which is computed independently for

each number of processes, thus can result in a particularly inefficient partition in some cases. But it is remarkable that the efficiency does not continue to decrease significantly if more than 4 processes are used. In particular, the more complex case of  $K = 64$  maintains its efficiency above 70% nearly all the way to 64 processes. This is a very good result for a distributed-memory cluster and justifies the use of relatively large numbers of parallel processes in more complex cases, e.g., for  $K = 8 \times 8 \times 8 = 512$  resulting in 14,514,176 or more than 14.5 million degrees of freedom at every time step.

## Acknowledgments

The hardware used in the computational studies was partially supported by the SCREMS grant DMS-0215373 from the U.S. National Science Foundation with additional support from the University of Maryland, Baltimore County. See [www.math.umbc.edu/~gobbert/kali](http://www.math.umbc.edu/~gobbert/kali) for more information on the machine and the projects using it. Prof. Gobbert also wishes to thank the Institute for Mathematics and its Applications (IMA) at the University of Minnesota for its hospitality during Fall 2004. The IMA is supported by funds provided by the U.S. National Science Foundation. Prof. Cale acknowledges support from MARCO, DARPA, and NYSTAR through the Interconnect Focus Center. We also wish to thank Max O. Bloomfield for supplying the original mesh of the domain.

## References

1. Gobbert, M.K., Merchant, T.P., Borucki, L.J., Cale, T.S.: A multiscale simulator for low pressure chemical vapor deposition. *J. Electrochem. Soc.* **144** (1997) 3945–3951
2. Merchant, T.P., Gobbert, M.K., Cale, T.S., Borucki, L.J.: Multiple scale integrated modeling of deposition processes. *Thin Solid Films* **365** (2000) 368–375
3. Kersch, A., Morokoff, W.J.: *Transport Simulation in Microelectronics*. Volume 3 of *Progress in Numerical Simulation for Microelectronics*. Birkhäuser Verlag, Basel (1995)
4. Gobbert, M.K., Cale, T.S.: A feature scale transport and reaction model for atomic layer deposition. In Swihart, M.T., Allendorf, M.D., Meyyappan, M., eds.: *Fundamental Gas-Phase and Surface Chemistry of Vapor-Phase Deposition II*. Volume 2001–13., *The Electrochemical Society Proceedings Series* (2001) 316–323
5. Gobbert, M.K., Webster, S.G., Cale, T.S.: Transient adsorption and desorption in micrometer scale features. *J. Electrochem. Soc.* **149** (2002) G461–G473
6. Ringhofer, C., Schmeiser, C., Zwirchmayr, A.: Moment methods for the semiconductor Boltzmann equation on bounded position domains. *SIAM J. Numer. Anal.* **39** (2001) 1078–1095
7. Webster, S.G.: *Stability and convergence of a spectral Galerkin method for the linear Boltzmann equation*. Ph.D. thesis, University of Maryland, Baltimore County (2004)
8. Gobbert, M.K., Webster, S.G., Cale, T.S.: A galerkin method for the simulation of the transient 2-D/2-D and 3-D/3-D linear Boltzmann equation. Submitted (2005)
9. Remacle, J.F., Flaherty, J.E., Shephard, M.S.: An adaptive discontinuous Galerkin technique with an orthogonal basis applied to compressible flow problems. *SIAM Rev.* **45** (2003) 53–72

# The Use of Conformal Voxels for Consistent Extractions from Multiple Level-Set Fields

Max O. Bloomfield<sup>1</sup>, David F. Richards<sup>2</sup>, and Timothy S. Cale<sup>1</sup>

<sup>1</sup> Rensselaer Polytechnic Institute, Dept. of Chemical Engineering,  
Troy, NY 12180-3590

<sup>2</sup> Synopsys Inc., Mountain View, CA 94043

**Abstract.** We present and analyze in 2D an algorithm for extracting self-consistent sets of boundary representations of interfaces from level set representations of many phase systems. The conformal voxel algorithm which is presented requires the use of a mesh generator and is found to be robust and effective in producing the extractions in the presence of higher order junctions.

## 1 Introduction

The level-set method [1] is used in a wide range of simulations in which evolving geometries are important. This method, in which the interface between two phases is represented implicitly as a contour (usually the zero contour) in a scalar field, has many advantages over explicit methods. The most notable advantage is that the geometric and topological complexities associated with updating explicit representations of interfaces are avoided, as level-set evolution is just a matter of solving an equation on the scalar field [1]. If and when an explicit representation is needed in order to perform part of the simulation, the interface can be extracted as a level of the scalar field (usually the zero level). When the geometry contains more than two phases that need to be tracked, such as for thin film grain structures simulations, the method extends quite naturally through the use of multiple scalar fields, identifying each phase with one field [2]. These fields can then be evolved independently using the same level-set equation and be periodically reconciled as shown by Merriman *et al.* [2]. However, the multiple level-set approach suffers from one setback that the standard level-set method does not: Recovering an explicit geometry by extracting the contours is not trivial because each interface is represented multiple times. At points near triple lines and higher order junctions, the explicit representations extracted from each field often disagree. These representations can differ even topologically.

At such points it is difficult or perhaps impossible to construct a consistent boundary mesh without gaps or holes in order to perform a desired simulation on the explicit structure. Consistent meshes are required for an entire class of simulation tasks in which values need to be related across the interfaces, such as mass, momentum, or energy fluxes. This class of simulation includes stress-strain and electromigration calculations on grain structures, which are desirable to link to structure evolution simulations. Bloomfield *et al.* [3] proposed a partial solution for



this problem which employed rectilinear voxels and robustly arrived at extracted structures that were always consistent. However, these structures (as shown in Figure 1) were problematic in that they had surface triangles with only a small number of normal directions (*i.e.*, the structures were limited to “Manhattan geometries”). In this paper we demonstrate an algorithm that extends the voxel approach and removes the limitation of producing Manhattan geometries. By employing a mesh generator, we produce voxels that conform to the natural interfaces far from higher order junctions, and produce intuitive, topologically consistent, explicit boundary representations at higher-order junctions.

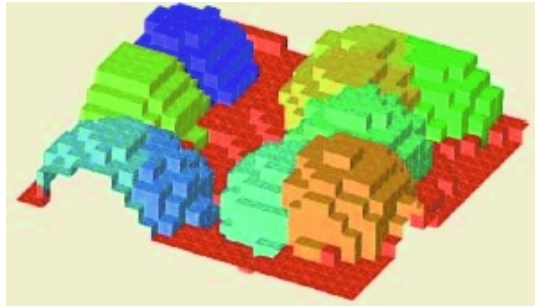


**Fig. 1.** The voxel extractor reported on by Bloomfield *et al.* [3] solves the consistency problem, but is limited to producing Manhattan geometries

## 2 Non-consistent Extraction

Although for the purposes of this paper, we represent level-set scalar fields ( $\varphi_i$ ) on triangular meshes using linear finite element basis functions, the ideas regarding representation and extraction may be extended to non-simplex and mixed-type meshes, higher-order basis functions, and finite difference grids in both 2 and 3D. We will maintain the convention that  $\varphi_i < 0$  inside phase  $i$  and  $\varphi_i > 0$  outside phase  $i$  and use the signed distance to the interface as the value of  $\varphi_i$ . Note that each phase has a distinct level set function ( $\varphi$ -field). Figure 2 illustrates the problem with representing even simple structures. We begin by initializing three  $\varphi$ -fields to be the signed distances from the explicit starting interfaces (solid lines) and represented the fields on the underlying triangular mesh (dotted lines). Finally, we “recover” the explicit interfaces by extracting line segments (dashed lines) from the  $\varphi$ -fields by interpolating the zeros along the triangles’ edges. We see that what would have been a slight rounding of a corner in the standard level-set method [1.], becomes an unphysical situation in the multiple level-set method, leaving a *void* behind in which no single phase is present. It should be noted that the term void as used here does not refer to a physical vacuum, which in this level-set formulation would be treated as a phase and have its own  $\varphi$ -field. Here, void refers to a region of space not associated with any single phase.

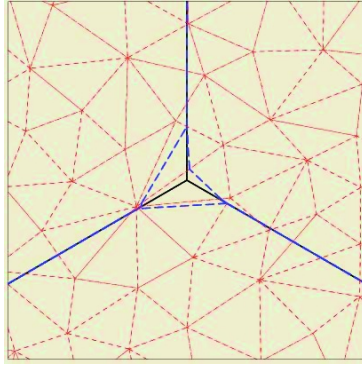


**Fig. 2.** An explicit set of interfaces (black solid lines) can be represented as contours in scalar fields, themselves represented on a finite element mesh (light dotted lines) or finite difference grid. However when an attempt is made to extract the interfaces, the extracted interfaces (dashed lines) do not come together at triple points and higher order junctions, leaving regions that do not correspond to any physical situation

Each  $\varphi$ -field can be extracted separately, giving smooth boundary representations of each phase in the most of the domain. In these regions, a match for each boundary element can be found among the elements extracted from other fields, allowing the boundary elements to be classified as being a particular type of interface. Constrained meshes may be constructed that include these elements as internal or boundary entities, allowing for further simulations. However, voids of the type shown in Figure 2 are not uncommon, occurring at almost all higher order junctions, and typically are one to two mesh-lengths across. The boundary elements that make up this void do not have matches in the set of elements extracted from other  $\varphi$ -fields; this prevents further execution of a program that requires tracking quantities across interfaces, from one phase to another.

### 3 Solution Methods

Carefully constructed meshes can potentially capture a single junction, allowing a consistent extraction, but this advantage is lost after the first time step in which the interfaces move. Alternatively, an approach may be taken to “fix” the non-physical situations after they occur, by locating their occurrence, localizing them, and then collapsing vertices and entities in such a way as to achieve a topologically consistent set of boundary representations. This approach, although fraught with special cases and tortuous decision trees, has been successfully implemented for extractions in two-dimensions [4]. We are unaware of a successful attempt to perform the three-dimensional analog. It is worth remarking that in three dimensions, the problem areas are not polygons, but are networks of long, thin “void wires” that meet at higher order junctions. Because of the daunting complexity of the problem in 3D, this approach does not appear promising.

### 3.1 Voxel Extraction

Voxel extraction has been employed as a partial solution to this dilemma by approaching the problem of extraction by constructing explicit *phases* before attempting to extract the interfaces between them. Bloomfield *et al.* [3] proposed filling the domain with regular rectilinear (*i.e.*, squares or cubes) and using the information embedded in the  $\varphi$ -fields to identify each of these volume elements (voxels) as a part of the explicit representation of the phases. They then looked for neighboring voxels that belonged to different faces and identified the elements between them as boundary elements of both faces. This generated a set of faces in three dimensions and a set of segments in two dimensions that were both consistent and located on or near the intuitively identified interface. Figure 1 shows an example of faces extracted using this voxel method. The results are completely consistent and each boundary element is identified from both sides of the interface.

The clearest drawback of this voxel method is the so-called Manhattan geometry of the results. Because the voxels have a limited set of directions for their faces, the extracted interfaces, which are made up of a subset of these faces, do not reflect the smoothly varying normals associated with most of the systems being represented. Two further improvements can be made to these output. The first approach is to apply a smoothing operator to the results, such as the volume-conserving algorithms reported on by Kuprat *et al.* [5.]. The downsides to this approach are that smoothing operations do not preserve shape global shape, tend to be motivated by aesthetic considerations rather than physical ones, and can be complicated to apply to very unsmooth surfaces. The second approach is to project onto each face a “pseudo-normal” calculated to be the unit direction along the gradient of the appropriate  $\varphi$ -field, similar to the technique used in Phong shading [6]. Such a projection method may be useful for tasks that require normals that more accurately represent the system, such as surface scattering calculations.

**Conformal-Voxel Extraction.** We demonstrate an extension of the above voxel extraction method that avoids the limitation of producing Manhattan geometries. By extending the concept of a voxelation to include not just tessellations of regular, identical shapes, but *any set of polyhedra that space-fill a domain*, we remove the constraint of having only a small number of distinct normals. With this definition, any geometric mesh that fills a volume (or fills an area in 2D systems) is a voxelation, and we can create a custom voxelation, using a ready-made meshing code and information about the structure in the  $\varphi$ -fields, that will have voxels optimally placed to give extractions that are consistent and are true to the implicit representation away from junctions.

Pulling information from the  $\varphi$ -fields is very important. Without providing guidance to the mesher, the voxel faces are as likely to be transverse to the zero contours in the implicit representation as to conform to them. The simplest way to provide this information is to use the parts of the directly extracted boundaries that do have matches in the other extracted boundaries. In two dimensions this is a set of segments and in three dimensions it is a set of faces, internal to the domain to be meshed. We call these internal elements *model entities*, and provide them to the area or volume mesher as constraints to be included as segments or faces in the resulting voxelation. As is shown below, this will cause the conformal-voxel extracted

boundary representation to coincide with the directly extracted version in regions more than a few mesh lengths from triple points and higher order junctions.

The conformal-voxel extraction algorithm can be performed as follows:

1. Begin with discretizations of the  $n$  (assuming  $n$  phases)  $\varphi$ -fields that implicitly represent the structure to be extracted in a  $D$  dimensional domain  $\Omega$ .
2. Extract a list  $\mathbf{B}_\alpha$  of entities from each field  $\varphi_\alpha$   $\alpha \in [1, n]$  by interpolating along the level set contour of each.
3. Mark each entity which appears in exactly two of the extracted sets,  $\mathbf{B}_\alpha$ , as a model entity and add to list  $\mathbf{B}'$ .
4. Invoke an area ( $D=2$ ) or volume ( $D=3$ ) mesher to fill the simulation domain, providing the model entities in  $\mathbf{B}'$  as internal constraints. Call this mesh the voxelation,  $\mathbf{V}$ .
5. Assign each voxel,  $V \in \mathbf{V}$ , a phase  $\alpha(V)$ , by an appropriate calculation referencing the fields  $\varphi_\alpha$ .
6. For each voxel  $V$ , visit the voxel  $U = V.\text{neighbor}(k)$  ( $k \in [1, D+1]$ ) on the other side of each segment  $k$  ( $D=2$ ) or face  $k$  ( $D=3$ ). If  $\alpha(V) \neq \alpha(U)$ , add entity  $k$  to the set of conformal voxel extracted boundary entities,  $\mathbf{B}''_{\alpha(V)}$ .

Each entity in  $\mathbf{B}''_\alpha$  should now have a match in some other  $\mathbf{B}''_{d \neq \alpha}$  or be on the domain boundary  $\partial\Omega$  and the extraction is complete.

The algorithm is straightforward, with only two tasks left up to the discretion of the implementer. The first is the invocation of the mesher in step 4. Although this point is discussed in detail in section 4 of this work, in this work we use the freeware 2D quality mesh generator `triangle` [7] from the netlib repository [8] and find that no quality constraints on the mesh have to be specified as long as the maximum area of the triangles in the mesh is less than the average area of triangles in the finite element mesh that we use to represent the  $\varphi$ -fields. The second choice that must be made is how the identification of the voxels is done in step 5. Any heuristic that robustly determines in which phase the voxel is located should work; in this work we use the phase associated with the  $\varphi$ -field that has the lowest value at the voxel centroid as the identity of that voxel. This choice is intuitively pleasing, is easy to implement, and empirically works well.

## 3.2 Examples

In Figure 3, we show the various steps of a conformal voxel extraction of the same  $\varphi$ -fields that produced the void in Figure 2. First, from the directly extracted sets (left), model entities are identified (solid lines). Next, a voxelation (middle) is created using the model entities as internal constraints and each voxel is assigned to a phase (shading). Finally, the conformal voxel extraction (solid blue line, right) is derived by comparing neighboring voxels, and compared to the structure used to initialize the implicit representation (dashed line, right). The resulting extraction is consistent and faithfully captures the normals and positions of the initializing structure.

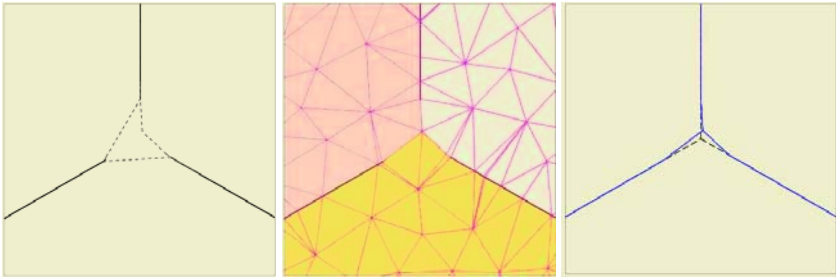


**Fig. 3.** The conformal voxel extraction procedure applied to the implicit representation shown in Figure 2. First, from the directly extracted sets (left), model entities are identified (solid lines). Next, a voxelization (middle) is created using the model entities as internal constraints and each voxel is assigned to a phase (shading). Finally, the conformal voxel extraction (solid blue line, right) is derived by comparing neighboring voxels, and compared to the structure used to initialize the implicit representation (dashed line, right)

In Figure 4, we show two more examples, the first (left) being a conformal voxel extraction of a higher order junction (a quadruple point). The extraction of the quadruple point indicates one aspect of voxel approaches, conformal or regular, which is that the topology of the extraction can be different than the topology of the structure the implicit representation is meant to represent. Here, the quadruple point present in the initializing structure (solid black lines) is present as a pair of triple points in the extraction. Further discussion of this phenomenon is given in the next section.

The second example in Figure 4 is a conformal voxel extraction (middle) of an 16-phase test structure (right), demonstrating the method's ability to robustly handle

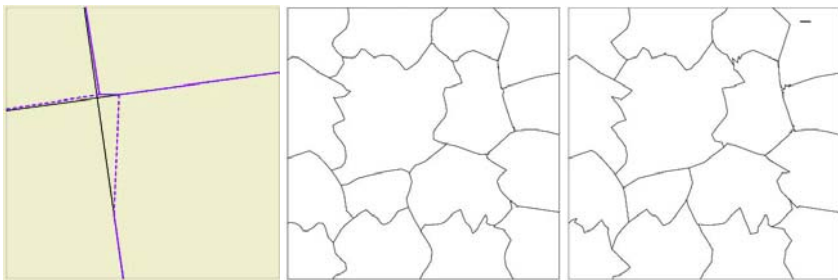


**Fig. 4.** (left) Drawing showing a conformal voxel extraction (dashed blue line) of a quadruple point (solid black line). Note that the extraction contains a pair of triple points instead of a single quadruple point. (middle) A conformal voxel extraction of (right) a complex 16-phase test structure containing significant fine detail, below the resolution of the underlying finite element mesh used

complex, many-phase structures. In this test structure, there are a variety of small and large geometric features. The extraction faithfully reproduces these geometric features underlying finite element mesh used for the implicit representation. (The input structure is 1x1; the bar in upper right corner of the right figure is 0.025 in length.)

Features smaller than this, such as the oscillations near some of the junctions in the test structure do not appear in the extraction.

## 4 Discussion and Conclusions

As mentioned in section 3.1, step 4 of the conformal voxel algorithm allows for discretion on the part of the implementer. It is essential that the voxelation include the internal constraints represented by the model entities, or at least alternative constraints based on them. That is, it may be permissible to adjust the coarseness of the model entities using a mesh coarsener to relieve some of the burden on the mesher to be used or to condition the elements in the set of extracted boundary entities. Any changes made to the information represented by the model entities will show up in the extracted boundary entities. However, we have observed in our 2D studies that the mesh quality of the voxelation is not of key importance in obtaining extractions that are true to the input structure. This is true providing that the mesher respects the constraints of the model entities and that the mesh size near the interfaces is less than or equal to the mesh size of the underlying discretizations of the field. In fact, we find that it is the mesh in the underlying finite element representation of the fields that has a determining effect on the amount of detail that is recovered using the conformal voxel extractor. In particular, the locations of triple and higher order junctions produced by the conformal voxel extractor deviate from the location of these junctions in the initializing structure by no more than the characteristic mesh size of the underlying finite element mesh.

This is a powerful result given that there is an implicit upper limit on the amount of detail retained about spatial variations in a field represented on a mesh or a grid with linear interpolants. By making a parallel to Nyquist's sampling theorem [9], we can say that the upper limit on the spatial resolution, *i.e.*, the smallest spatial variation represented is about twice the mesh length. For unstructured grids, this length is someone nebulous, but can be gauged within about a factor of 2, perhaps as a function of position. This agrees with what can be seen in the extraction of the complex test structure show Figure 4, indicating that the conformal voxel method is able to extract a large fraction of the information about the structure implicit in the finite element representation of the  $\phi$ -fields.

The phenomenon of junction splitting seen in Figure 4 is also a matter of resolution. Although the implicit representation was initialized from an explicit structure with a quadruple point, it cannot be distinguished from the conformal voxel extracted version with two triple points within the resolution of the implicit representation. This situation highlights a characteristic of the conformal voxel method: a particular extraction from a given implicit representation is not unique. By using a voxelation produced by a different mesh algorithm or with different parameters, different extractions can be produced from the same implicit representation. However, in our experience, they will all be the same within the spatial resolution of implicit representation.

The computational complexity of this algorithm is difficult to analyze precisely, because of the use of a separate mesher to produce the voxelation, which will have its own complexity as a function of desired mesh size and number and type of internal

constraints. However, if there are  $N$  mesh elements in the discretizations of the  $M$  input  $\varphi$ -fields,  $O(N^{(D-1)/D})$  entities in the union of  $\mathbf{B}_\alpha$ . Matching up these entities is done pairwise, taking  $O(D)$  integer comparisons each, giving an overall complexity of  $O(D \cdot N^{2(D-1)/D})$ , or  $O(N)$  for 2D and  $O(N^{4/3})$  for 3D for step 2. The complexity of step 5 is simply  $O(N \cdot M)$ , leaving the overall complexity for the algorithm system dependent based on the number of phases and the external mesher used.

We have shown several examples of the use of the algorithm in 2D. A demonstration of its use in 3D [10] is beyond the scope of this paper for reasons of brevity. The number of meshers available that can robustly handle the complex internal constraints in an automated fashion is much lower for 3D than for 2D. It should be pointed out that although we use triangular mesh elements for our voxelations, quadrilateral element should work just as well. In 3D, tetrahedral, wedges, and brick elements should be able to be used with equal facility.

This method is highly robust, given a reliable mesher. The only caveat is that if the voxel size is noticeably larger than the resolution of the implicit representation, then the resulting extraction may depend heavily on the voxelation. However, the method will not fail to complete even for very large voxel sizes, happily producing spurious results.

Finally, we note that there is a relationship between the voxelation mesh and the conformal voxel extracted result, namely that the former is a body-fitted mesh for the latter, and potentially can be used as the mesh for further simulation on the extracted system. Should this be desired, more attention should be paid to the quality of the voxelation as it is being produced.

## References

1. Osher, S., Sethian, J.A.: Fronts Propogating with Curvature Dependent Speed: Algorithms Based on Hamilton-Jacobi Formulations. *J. Comp. Phys.* 79 (1988) 12-49.
2. Merriman, B, Bence, J.K, Osher, S.J.: Motion of Multiple Junctions: A Level Set Approach. *J. Comp. Phys.* 112 (1994) 334-363.
3. Bloomfield, M.O., Richards, D.F., Cale, T.S.: A Computational Framework for Modeling Grain Structure Evolution in Three Dimensions. *Phil. Mag.* 83(31-34) (2003) 3549-3568.
4. Bloomfield, M.O., Richards, D.F., Cale, T.S.: A Tool for the Representation, Evolution, and Coalescence of 3-Dimensional Grain Structures, presented during the Sixth United States National Congress on Computational Mechanics, August 1-3, 2001, Dearborn, MI.
5. Kuprat, A., Khamayseh, A., George, D., Larkey, L.: Volume Conserving Smoothing for Piecewise Linear Curves, Surfaces, and Triple Lines. *J. Comp. Phys.* 172 (2001) 99-118.
6. Phong, B.: Illumination for Computer Generated Pictures. *Comm. of the ACM*, 18(8) (1975) 311-317.
7. A Two-Dimensional Quality Mesh Generator and Delaunay Triangulator: <http://www-2.cs.cmu.edu/~quake/triangle.html>
8. Netlib Repository at UTK and ORNL: <http://www.netlib.org/>
9. Papoulis, A.: *Signal Processing*, McGraw Hill, 1997.
10. Bloomfield, M.O., Richards, D.F., Cale, T.S.: A Conformal Voxel Extraction Method for Extraction of Multiple Level Set Fields in Three Dimensions, *in preparation*.

# Nonlinear OIFS for a Hybrid Galerkin Atmospheric Model

Amik St.-Cyr and Stephen J. Thomas

National Center for Atmospheric Research,  
1850 Table Mesa Drive, Boulder, 80305 CO, USA  
{amik, thomas}@ucar.edu

**Abstract.** The purpose of this paper is to explore a time-split hybrid Galerkin scheme for the atmospheric shallow water equations. A nonlinear variant of operator integration factor splitting is employed as the time-stepping scheme. The hyperbolic system representing slow modes is discretized using the discontinuous Galerkin method. An implicit second order backward differentiation formula is applied to Coriolis and gravity wave terms. The implicit system is then discretized using a continuous Galerkin spectral element method. The advantages of such an approach include improved mass and energy conservation properties. A strong-stability preserving Runge-Kutta scheme is applied for sub-stepping.

## 1 Introduction

The seminal work of Robert (1981) led to a six-fold increase over the explicit time step for atmospheric general circulation models. To achieve such dramatic gains without recourse to a fully implicit integrator, a semi-Lagrangian treatment of advection was combined with a semi-implicit scheme for the stiff terms responsible for gravity waves. Initially, semi-implicit semi-Lagrangian time-stepping was applied to hyperbolic problems, discretized using low-order finite-differences and finite elements. The traditional semi-Lagrangian algorithm implemented in atmospheric models relies on backward trajectory integration and upstream interpolation, Staniforth and Côté (1991). A potentially lower cost alternative is the operator integrating factor splitting (OIFS) method of Maday et al. (1990) which relies on Eulerian sub-stepping of the advection equation. In contrast with semi-Lagrangian advection, there are no dissipation or dispersion errors associated with upstream interpolation or trajectory integration and the scheme maintains the high-order accuracy of the discrete spatial operators.

A discontinuous Galerkin shallow water model employing a nodal basis and explicit time-stepping is described in Giraldo et al. (2003). Sherwin (2004) demonstrated the advantages of a hybrid Galerkin approach in the context of the incompressible Navier-Stokes equations. Eskilsson and Sherwin (2005) describe a discontinuous Galerkin formulation of the shallow water equations using third-order strong-stability preserving (SSP) Runge-Kutta time-stepping. Here, we



investigate a time-split scheme applied to the global shallow water equations in curvilinear coordinates on the cubed-sphere. A second order backward differentiation formula (BDF-2) is combined with SSP-RK sub-stepping of a hyperbolic system. Because the incompressibility constraint has been removed, the fully nonlinear OIFS scheme of St-Cyr and Thomas (2004) is employed. When compared to continuous Galerkin spectral elements, the hybrid scheme results in improved mass and energy conservation properties.

## 2 Shallow Water Equations

The shallow water equations contain the essential wave propagation mechanisms found in atmospheric general circulation models. These are the fast gravity waves and slow synoptic scale Rossby waves. The latter are important for correctly capturing nonlinear atmospheric dynamics. The governing equations of motion for the inviscid flow of a free surface are

$$\frac{\partial \mathbf{v}}{\partial t} + (f + \zeta) \mathbf{k} \times \mathbf{v} + \frac{1}{2} \nabla (\mathbf{v} \cdot \mathbf{v}) + \nabla \Phi = 0, \quad (1)$$

$$\frac{\partial \Phi}{\partial t} + (\mathbf{v} \cdot \nabla) \Phi + (\Phi_0 + \Phi) \nabla \cdot \mathbf{v} = 0. \quad (2)$$

$h$  is the height above sea level,  $\mathbf{v}$  is the horizontal velocity and  $\Phi = gh$  the geopotential height.  $f$  is the Coriolis parameter and  $\mathbf{k}$  a unit vector in the vertical direction. The geopotential height is decomposed into a perturbation about a constant base state,  $\Phi_0$ .

To exploit the potential of operator integration factor splitting for systems of time-dependent partial differential equations, St.-Cyr and Thomas (2004) show that a fully nonlinear form of the algorithm is more appropriate. Sub-stepping is applied to

$$\frac{\partial \mathbf{v}}{\partial s} + \zeta \mathbf{k} \times \mathbf{v} + \frac{1}{2} \nabla (\mathbf{v} \cdot \mathbf{v}) = 0, \quad (3)$$

$$\frac{\partial \Phi}{\partial s} + \nabla \cdot (\Phi \mathbf{v}) = 0. \quad (4)$$

with initial conditions  $\mathbf{v}(\mathbf{x}, t^{n-q}) = \mathbf{v}(\mathbf{x}, t^{n-q})$ ,  $\Phi(\mathbf{x}, t^{n-q}) = \Phi(\mathbf{x}, t^{n-q})$ . The integration factor  $Q_S^t(t)$  is applied to the remaining de-coupled system of equations containing the Coriolis and linear gravity wave terms

$$\frac{d}{dt} Q_S^t(t) \begin{bmatrix} \mathbf{v} \\ \Phi \end{bmatrix} = -Q_S^t(t) \begin{bmatrix} f \mathbf{k} \times \mathbf{v} + \nabla \Phi \\ \Phi_0 \nabla \cdot \mathbf{v} \end{bmatrix}. \quad (5)$$

An accurate representation of fast-moving gravity waves is not required for large scale atmospheric dynamics and the corresponding terms can be treated implicitly. For a second order BDF-2 scheme, sub-stepping of the rhs terms is not required because  $Q_S^{t^n}(t^n) = I$ .

The resulting time discretization of (5) is given by

$$\mathbf{v}^n + \frac{2}{3}\Delta t \mathbf{N} \nabla \Phi^n = \frac{4}{3}\mathbf{N} \mathbf{v}^{n-1} - \frac{1}{3}\mathbf{N} \mathbf{v}^{n-2} \quad (6)$$

$$\Phi^n + \frac{2}{3}\Delta t \Phi_0 \nabla \cdot \mathbf{v}^n = \frac{4}{3}\Phi^{n-1} - \frac{1}{3}\Phi^{n-2} \quad (7)$$

where

$$\mathbf{N} = \left( I + \frac{2}{3}\Delta t f \mathbf{M} \right)^{-1}, \quad \mathbf{M} = \begin{bmatrix} 0 & -1 \\ 1 & 0 \end{bmatrix}.$$

The values of the fields  $\mathbf{v}$  and  $\Phi$  at time levels  $n-1$  and  $n-2$  are computed by sub-stepping (3) and (4) on the intervals  $[t^{n-1}, t^n]$  and  $[t^{n-2}, t^n]$ . An implicit equation for  $\Phi^n$  is obtained after space discretization and application of block Gaussian elimination, resulting in a modified Helmholtz problem. The coefficient matrix of this linear system of equations is non-symmetric due to the implicit treatment of the Coriolis terms and is solved using an iterative conjugate-gradient squared (CGS) algorithm with a block-Jacobi preconditioner.

For high-order spectral elements, under-integration using Gaussian quadrature results in discrete operators where the eigenvalues corresponding to high frequency modes are shifted into the right-half plane. A filter is therefore required to stabilize the time-stepping scheme for long time integrations, Fischer and Mullen (2001). Strong-stability preserving (SSP) time integration schemes maintain the non-oscillatory properties of the spatial operator, Gottlieb et al (2001). We next describe the computational domain, high-order Galerkin finite element approximations and SSP-RK sub-stepping.

### 3 High-Order Galerkin Approximations

The flux form shallow-water equations in curvilinear coordinates are described in Sadourny (1972). Let  $\mathbf{a}_1$  and  $\mathbf{a}_2$  be the covariant base vectors of the transformation between inscribed cube and spherical surface. The metric tensor is defined as  $G_{ij} \equiv \mathbf{a}_i \cdot \mathbf{a}_j$ . Covariant and contravariant vectors are related through the metric tensor by  $u_i = G_{ij} u^j$ ,  $u^i = G^{ij} u_j$ , where  $G^{ij} = (G_{ij})^{-1}$  and  $G = \det(G_{ij})$ . The six local coordinate systems  $(x^1, x^2)$  are based on equiangular central projection,  $-\pi/4 \leq x^1, x^2 \leq \pi/4$ .

$$G_{ij} = \frac{1}{r^4 \cos^2 x^1 \cos^2 x^2} \begin{bmatrix} 1 + \tan^2 x^1 & -\tan x^1 \tan x^2 \\ -\tan x^1 \tan x^2 & 1 + \tan^2 x^2 \end{bmatrix} \quad (8)$$

where  $r = (1 + \tan^2 x^1 + \tan^2 x^2)^{1/2}$  and  $\sqrt{G} = 1/r^3 \cos^2 x^1 \cos^2 x^2$ .

The time-split hyperbolic system (3) – (4) can be written in as

$$\frac{\partial u_1}{\partial t} + \frac{\partial}{\partial x^1} E = \sqrt{G} u^2 (f + \zeta), \quad (9)$$

$$\frac{\partial u_2}{\partial t} + \frac{\partial}{\partial x^2} E = -\sqrt{G} u^1 (f + \zeta), \quad (10)$$

$$\frac{\partial}{\partial t} (\sqrt{G} \Phi) + \frac{\partial}{\partial x^1} (\sqrt{G} u^1 \Phi) + \frac{\partial}{\partial x^2} (\sqrt{G} u^2 \Phi) = 0, \quad (11)$$

where

$$E = \frac{1}{2} (u_1 u^1 + u_2 u^2), \quad \zeta = \frac{1}{\sqrt{G}} \left[ \frac{\partial u_2}{\partial x^1} - \frac{\partial u_1}{\partial x^2} \right]$$

Consider a scalar component of the hyperbolic system,

$$\frac{\partial u}{\partial t} + \nabla \cdot \mathcal{F} = S.$$

The computational domain  $\Omega$  is partitioned into elements  $\Omega_k$ . An approximate solution  $u_h$  belongs to the finite dimensional space  $\mathcal{V}_h(\Omega)$ . Multiplication of by a test function  $\varphi_h \in \mathcal{V}_h$  and integration over the element  $\Omega_k$  results in a weak Galerkin formulation of the problem.

$$\frac{\partial}{\partial t} \int_{\Omega_k} \varphi_h u_h d\Omega = \int_{\Omega_k} \varphi_h S d\Omega + \int_{\Omega_k} \mathcal{F} \cdot \nabla \varphi_h d\Omega - \int_{\partial\Omega_k} \varphi_h \mathcal{F} \cdot \hat{n} ds.$$

For a discontinuous Galerkin approximation, a nodal basis for  $\mathcal{V}_h$  is employed, consisting of the Legendre cardinal functions. The solutions  $u_h$  are expanded in terms of tensor-product basis functions on a Gauss-Lobatto grid.

The flux function  $\mathcal{F} \cdot \hat{n}$  is approximated by a Lax-Friedrichs numerical flux

$$\widehat{\mathcal{F}}(u_h^+, u_h^-) = \frac{1}{2} [(\mathcal{F}(u_h^+) + \mathcal{F}(u_h^-)) \cdot \hat{n} - \alpha(u_h^+ - u_h^-)].$$

Boundary integrals are computed using higher-order Gaussian quadrature.  $\alpha$  is the upper bound for the absolute value of eigenvalues of the flux Jacobian  $\mathcal{F}'(u)$  in the direction  $\hat{n}$ . Equations (9) – (11) are written in the semi-discrete form

$$\frac{d\mathbf{u}}{dt} = \mathbf{L}(\mathbf{u}).$$

The second-order three stage SSP RK2-3 integrator of Higuera (2004) is applied to sub-step the above system of ordinary differential equations. This scheme has a CFL number  $C = 2$  and efficiency factor  $C/3 = 2/3$ . The implicit system (6) – (7) is discretized using  $\mathbb{P}_N - \mathbb{P}_N$  continuous Galerkin spectral elements.

## 4 Numerical Experiments

Our numerical experiments are based on the shallow water test suite of Williamson et al (1992). Test case 5 is a zonal flow impinging on an isolated

mountain. The center of the mountain is located at  $(3\pi/2, \pi/6)$  with height  $h_s = 2000(1-r/R)$  meters, where  $R = \pi/9$  and  $r^2 = \min[R^2, (\lambda - 3\pi/2)^2 + (\theta - \pi/6)^2]$ . Initial wind and height fields are

$$\begin{aligned} u &= u_0 (\cos \alpha_0 \cos \theta + \sin \alpha_0 \cos \lambda \sin \theta) \\ v &= -u_0 \sin \alpha_0 \sin \lambda \\ gh &= gh_0 - \frac{u_0}{2} (2a\Omega + u_0) (\sin \theta \cos \alpha_0 - \cos \lambda \cos \theta \sin \alpha_0)^2 \end{aligned}$$

$a$  is the earth's radius,  $\Omega$  the rotation rate,  $\alpha_0 = 0$ ,  $gh_0 = 5960 \text{ m}^2/\text{s}^2$  and  $u_0 = 20 \text{ m/s}$ . The geopotential height field after 15 days of integration is plotted in Fig. 1. The solution is smooth and does not exhibit spurious oscillations.

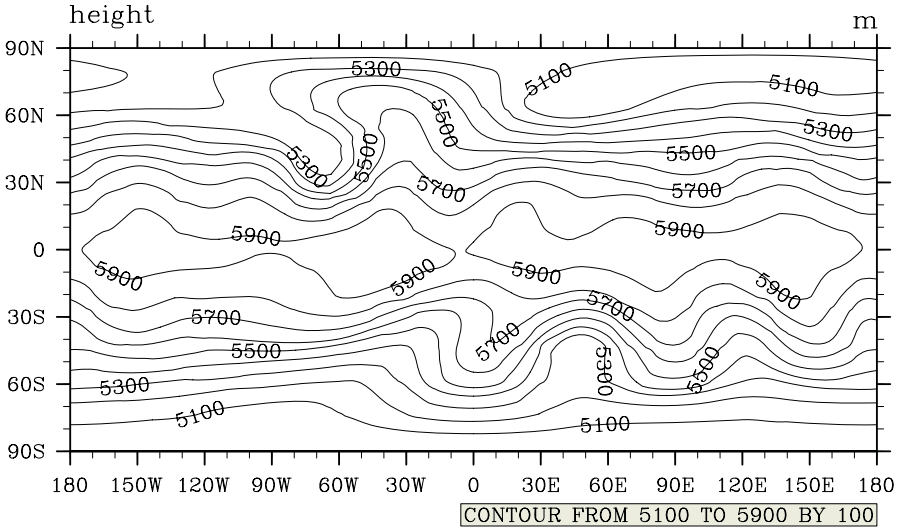


**Fig. 1.** Shallow water test case 5: Flow impinging on a mountain. Geopotential height field  $h$  at fifteen days produced by hybrid scheme. 150 spectral elements,  $8 \times 8$  Gauss-Legendre Lobatto points per element

The implementation of the BDF-2/RK2-3 scheme is still at an experimental stage. However, it leads to an increase in the model integration rate. Figure 2 is a plot of the ratio of CNLF and BDF-2/RK2-3 execution times for test case 5. The efficiency gain of BDF-2/RK2-3 over the CNLF scheme is close to a factor of two. Thomas and Loft (2002) observed that the CNLF scheme integrated twice as fast as an explicit spectral element shallow water model. Therefore, the total increase in the model integration rate, when compared to the explicit model, is a factor of four. The plateau in the efficiency curve is due to a growing number of solver iterations as the time step size increases.

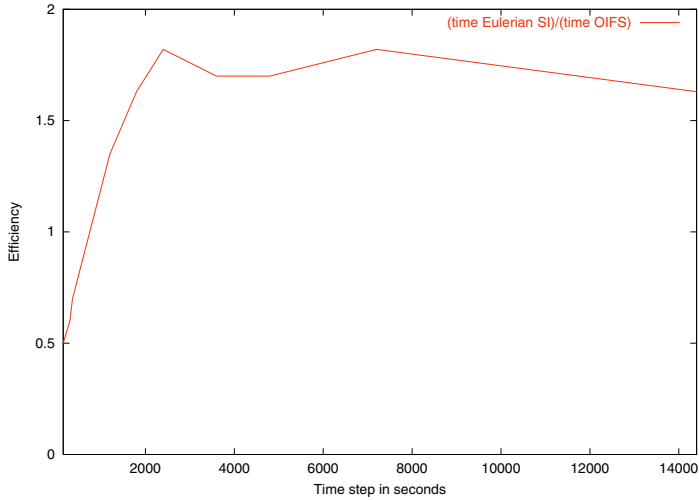


**Fig. 2.** Shallow water test case 5: Flow impinging on a mountain. Computational efficiency. Ratio of the CNLF and BDF-2/RK2-3 model execution times.  $K = 150$  spectral elements,  $8 \times 8$  Gauss-Legendre points per element

## 5 Conclusions

The larger time step permitted by the time-split BDF-2/RK2-3 integrator implies that the hybrid Galerkin discretization is well-suited for modeling multi-scale atmospheric phenomena. The computation time is currently dominated by an increasing number of solver iterations as the time step size increases. However, a recently developed optimized Schwarz preconditioner maintains a much lower iteration count, St.-Cyr et al (2004). We estimate that this preconditioner could lead to an additional factor of four improvement in the computational efficiency compared to a Crank-Nicholson leap-frog (CNLF) formulation. Although the hybrid scheme is not strictly conservative, the mass loss is significantly less than in a continuous Galerkin spectral element model.

For parallel computation, a clear advantage of the discontinuous Galerkin method is the ability to overlap computation with communication. Specifically, the communication of conserved variables can be overlapped with the computation of the weak divergence and source terms. We are also currently experimenting with a hybrid MPI/OpenMP programming model for SMP cluster computer architectures and plan to report these results in the near future.

## References

1. Eskilsson, C. and S. J. Sherwin, 2005: Discontinuous Galerkin spectral/hp element modelling of dispersive shallow water systems. *J. Sci. Comp.*, **22**, 279-298.

2. Fischer, P. F. and J. S. Mullen, 2001: Filter-Based stabilization of spectral element methods. *Comptes Rendus de l'Académie des sciences Paris*, t. 332, Série I - Analyse numérique, 265–270.
3. Giraldo, F. X., J. S. Hesthaven, and T. Warburton, 2003: Nodal high-order discontinuous Galerkin methods for spherical shallow water equations. *J. Comput. Phys.*, **181**, 499–525.
4. Gottlieb, S., C. W. Shu, and E. Tadmor, 2001: Strong stability preserving high-order time discretization methods. *SIAM Review*, **43**, 89–112.
5. Higuera, I., 2004: On strong stability preserving time discretization methods. *J. Sci. Comput.*, **21**, 193–223.
6. Maday, Y., A. T. Patera, and E. M. Ronquist, 1990: An operator-integration-factor splitting method for time-dependent problems: Application to incompressible fluid flow. *J. Sci. Comput.*, **5**, 263–292.
7. Robert, A. J., 1981: A stable numerical integration scheme for the primitive meteorological equations. *Atmos.-Ocean*, **19**, 35–46.
8. Sadoury, R., 1972: Conservative finite-difference approximations of the primitive equations on quasi-uniform spherical grids. *Mon. Wea. Rev.*, **100**, 136–144.
9. Sherwin, S. J., 2002: A sub-stepping Navier-Stokes splitting scheme for spectral/hp element discretisations. *Parallel Computational Fluid Dynamics*, North Holland.
10. Staniforth, A., and J. Coté 1991: Semi-Lagrangian integration schemes for atmospheric models – A review. *Mon. Wea. Rev.*, **119**, 2206–223.
11. St-Cyr, A., and S. J. Thomas, 2004: Nonlinear operator integration factor splitting for the shallow water equations. *Appl. Numer. Math.*, to appear.
12. St-Cyr, A., M. Gander and S. J. Thomas, 2004: Optimized RAS preconditioning. Proceedings of the 2004 Copper Mountain Conference on Iterative Methods.
13. Thomas, S. J., and R. D. Loft, 2002: Semi-implicit spectral element atmospheric model. *J. Sci. Comp.*, **17**, 339–350.
14. Williamson, D. L., J. B. Drake, J. J. Hack, R. Jakob, P. N. Swarztrauber, 1992: A standard test set for numerical approximations to the shallow water equations in spherical geometry *J. Comp. Phys.*, **102**, 211–224.

# Flamelet Analysis of Turbulent Combustion

R.J.M. Bastiaans<sup>1,2</sup>, S.M. Martin<sup>1</sup>, H. Pitsch<sup>1</sup>, J.A. van Oijen<sup>2</sup>,  
and L.P.H. de Goey<sup>2</sup>

<sup>1</sup> Center for Turbulence Research, Stanford University, CA 94305, USA

<sup>2</sup> Eindhoven University of Technology, P.O.Box 513, 5600 MB Eindhoven,  
The Netherlands

r.j.m.bastiaans@tue.nl

**Abstract.** Three-dimensional direct numerical simulations are performed of turbulent combustion of initially spherical flame kernels. The chemistry is described by a progress variable which is attached to a flamelet library. The influence of flame stretch and curvature on the local mass burning rate is studied and compared to an analytical model. It is found that there is a good agreement between the simulations and the model. Then approximations to the model are evaluated.

## 1 Motivation and Objectives

The present research is concerned with the direct numerical simulation (DNS) and analysis of turbulent propagation of premixed flame kernels. The simulations are direct in the sense that the smallest scales of motion are fully resolved, while the chemical kinetics are solved in advance and parameterized in a table by the method of the flamelet generated manifolds (FGM) [8]. The state of the reactions are assumed to be directly linked to a single progress variable. The conservation equation for this progress variable is solved using DNS, with the unclosed terms coming from the table. This allows the use of detailed chemical kinetics without having to solve the individual species conservation equations.

Flame stretch is an important parameter that is recognized to have a determining effect on the burning velocity in premixed flames. In the past this effect has not been taken into account in the flamelet approach for turbulent combustion in a satisfying manner. The laminar burning velocity, which is largely affected by stretch, is an important parameter for modelling turbulent combustion. Flame stretch is also responsible for the creation of flame surface area, affecting the consumption rate as well. In the turbulent case, stretch rates vary significantly in space and time. An expression for the stretch rate is derived directly from its mass-based definition in [4],

$$K = \frac{1}{M} \frac{dM}{dt}, \quad (1)$$

where  $M$  is the amount of mass in an arbitrary control volume moving with the flame velocity:

$$M = \int_{V(t)} \rho dV. \quad (2)$$

On the basis of this definition, a model for the influence of stretch and curvature on the mass burning rate has been developed. In a numerical study [5], it was shown that this model, with a slight reformulation, shows good agreement with calculations for spherically expanding laminar flames. This formulation, for the ratio of the actual mass burning rate at the inner layer,  $m_{\text{in}}$ , relative to the unperturbed mass burning rate at the inner layer,  $m_{\text{in}}^0$  (for unity Lewis numbers), reads

$$\frac{m_{\text{in}}}{m_{\text{in}}^0} = 1 - \mathcal{K}a_{\text{in}}, \quad (3)$$

with the integral Karlovitz number being a function of flame stretch (1), flame surface area,  $\sigma$ , and a progress variable,  $\mathcal{Y}$ ,

$$\mathcal{K}a_{\text{in}} := \frac{1}{\sigma_{\text{in}} m_{\text{in}}^0} \left( \int_{s_u}^{s_b} \sigma \rho K \mathcal{Y} ds - \int_{s_{\text{in}}}^{s_b} \sigma \rho K ds \right). \quad (4)$$

The integrals have to be taken over paths normal to the flame and  $s_u$ ,  $s_b$  and  $s_{\text{in}}$  are the positions at the unburned side, the burned side and the inner layer, respectively. The flame surface area,  $\sigma$ , is related to the flame curvature,  $\kappa$ , which is related to the flame normals,  $n_i$  on the basis of the progress variable,  $\mathcal{Y}$ ,

$$n_i = - \frac{\partial \mathcal{Y} / \partial x_i}{\sqrt{\partial \mathcal{Y} / \partial x_j \partial \mathcal{Y} / \partial x_j}}, \quad (5)$$

$$\kappa = \frac{\partial n_i}{\partial x_i} = - \frac{1}{\sigma} \frac{\partial \sigma}{\partial s}. \quad (6)$$

In turbulent premixed combustion the total fuel consumption is a result of the combined effect of flame surface increase and local modulation of the mass burning rate. In this study the latter will be investigated on the basis of (3) and possible parameterizations thereof, i.e. models for the Karlovitz integral, (4).

## 2 Methodology

Freely expanding flames are modelled in a turbulent flow field using DNS. More detailed information about the DNS program can be found in [1]. The fully compressible Navier-Stokes equations are solved supplemented by a conservation equation for the progress variable. For this purpose the mass fraction of carbon dioxide is used, which is monotonically increasing. Unity Lewis numbers are assumed for all species in order to prevent differential diffusion effects from obscuring the direct effects of stretch and curvature on the mass burning rate.



To make the DNS computations affordable, the FGM method of [8] is used to describe the reaction kinetics. FGM can be considered a combination of the flamelet approach and the intrinsic low-dimensional manifold (ILDM) method [7] and is similar to the Flame Prolongation of ILDM (FPI) introduced in [3]. FGM is applied similarly to ILDM. However, the thermo-chemical data-base is not generated by applying the usual steady-state relations, but by solving a set of 1D convection-diffusion-reaction equations describing the internal flamelet structure. The main advantage of FGM is that diffusion processes, which are important near the interface between the preheat zone and the reaction layer, are taken into account. This leads to a very accurate method for (partially) premixed flames that uses fewer controlling variables than ILDM. The manifold used in this paper is based on the GRI3.0 kinetic mechanism with 53 species and 325 reversible reactions [9].

The initial conditions are a laminar spherical flame superimposed on a turbulent field. There is no forcing in the simulation, so the turbulence will decay in time. The chemistry is chosen in relation to the large interest in the power industry in lean premixed combustion engines and there is detailed knowledge of its chemical kinetics. Therefore premixed combustion of a methane/air mixture is used, with an equivalence ratio of  $\phi = 0.7$ . The evolution of the initial laminar spherical flame kernel to the initial size in the DNS is calculated with detailed chemistry with the CHEM1D code [2].

### 3 Results

The first simulation, denoted C1, is a lean case with an equivalence ratio of  $\phi = 0.7$ , domain size of 12 mm, an initial flame kernel radius of approximately 2.9 mm, turbulent fluctuations of  $u' = 0.4$  m/s and a turbulence length scale of  $\ell_t = 1.15$  mm. In order to allow for very mild perturbations, initially we study the results at a time equal to  $0.026\tau$ , with  $\tau = \ell_t/u' = 2.9$  ms, taken from the start of the simulation. The time of growth of the laminar flame kernel to the initial DNS size was about 5 ms. The burning velocity of a flat unstretched flame with respect to the unburnt mixture is equal to  $s_L^0 = 18.75$  cm/s and the corresponding mass burning rate is  $m^0 = 0.213$  kg/m<sup>2</sup>s. The progress variable is taken to be the carbon dioxide mass fraction, normalized with the maximum adiabatic value. At the left side of figure 1 is a cross section of the field. The contours of the progress variable are deformed only very mildly. It is observed that the scale of the vorticity patches are larger than the integral flame thickness. For this field the mass burning rate is analyzed as a reference case.

Additional analyses are performed in order to assess the basic model (4) under varying physical conditions. The test cases are listed in table 1. In case C2, the effect of grid resolution is investigated. It is assumed that the FGM method is valid in the flamelet regime if the progress variable is approximated with enough accuracy. Since all lengths scales of the gradients of primary

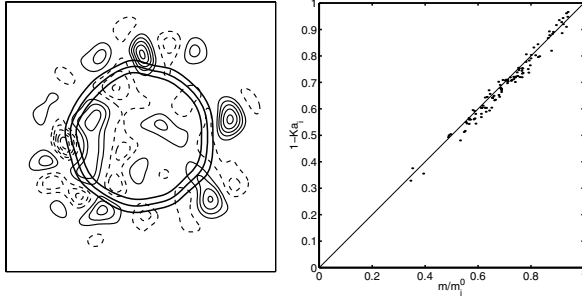


**Fig. 1.** Case C1, left: Vorticity contours (positive and negative values indicated by solid and dashed lines, respectively) and progress variable (thick lines, values 0.2, 0.5, 0.8), right: Correlation of the actual mass burning rate with the basic model (result of 52000 flamelets found in the domain)

**Table 1.** Physical properties correspondig to the different simulations

Case	$\phi$	$u'$ [m/s]	$\ell_t$ [mm]	$\delta_f$ [mm]	$L$ [mm]	$r_{ini}$ [mm]	grid	$Re_t = u' \ell_t / s_L^0 \delta_f$	$tu' / \ell_t$
C1	0.7	0.40	1.15	0.614	12	2.9	$254^3$	4.0	0.026
C2	0.7	0.40	1.15	0.614	12	2.9	$125^3$	4.0	0.026
C3	1.0	0.60	0.89	0.475	12	2.9	$254^3$	4.0	0.026
C4	0.7	0.70	0.77	0.614	20	3.9	$254^3$	4.7	0.026
C5	0.7	1.31	0.94	0.614	12	2.9	$254^3$	10.7	0.026
C6	0.7	1.30	0.66	0.614	12	2.9	$254^3$	7.5	0.026

variables (i.e. the variables that are solved in the present DNS calculations) are of the same order, this will yield satisfactory solutions. In order to assess the influence of the chemistry a stoichiometric case, C3, is selected, in which the same ratio of the turbulent velocity fluctuations compared to the laminar flame speed, and the turbulent integral length scale compared to the initial flame thickness as used for cases C1 and C2. For the stoichiometric case at unity Lewis numbers the burning velocity is  $s_L^0 = 28.17$  cm/s and the corresponding mass burning rate is  $m^0 = 0.316$  kg/m<sup>2</sup>s. An additional case is given by the simulation of an increased initial flame kernel in a larger domain, C4. Here also the effective resolution is decreased. In addition, cases are chosen with increased velocity fluctuations and decreased length scales, cases C5 and C6, respectively.

In the analysis, the stretch rate defined by,

$$\rho K = \frac{\partial}{\partial x_i} (\rho s_L n_i), \quad (7)$$

is evaluated by using the relation for the local burning velocity  $s_L$ ,

$$s_L = \left( \frac{\partial}{\partial x_i} \left( \frac{\lambda}{Le \bar{c}_p} \frac{\partial \mathcal{Y}}{\partial x_i} \right) + \dot{\rho} \right) / \left| \frac{\partial \mathcal{Y}}{\partial x_i} \right|, \quad (8)$$

which is a consequence of the combination of the conservation equation for  $\mathcal{Y}$  with the kinematic equation for  $\mathcal{Y}$ . The latter defines the flame speed  $u_{if}$  and then the relation for the flame velocity,  $u_{if} = u_i + s_L n_i$ , can be used to arrive at (8).

**Table 2.** Differences of the mass burning rate with the basic model

Case	C1	C2	C3	C4	C5	C6
Mean	0.0072	0.0081	0.0075	0.0091	0.0107	0.0094
RMS	0.0215	0.0202	0.0216	0.0236	0.0336	0.0280

Now the actual mass burning rate can be compared to model-values. This is performed by looking for points in the domain that are close to the inner layer and interpolate from there in the direction of positive and negative gradient of the progress variable, with steps of 1/20 times the gridsize. All relevant variables are interpolated over these flamelets and these flamelets are analysed to determine the burning velocity (8) and the model of the mass burning rate given by (4). For the present simulations these analyses lead to lots of starting points (e.g. for case C1: 52000) and thus resulting flamelets. For case C1 the correlation is depicted on the right side of figure 1. This shows that the model is a relatively accurate description of the actual mass burning rate. Deviations of the actual mass burning rate compared to the model (4) are given in table 2 for all six cases. It is seen that the mean error for all cases is about 0.01 or less, with a root mean square value of 0.02 to 0.03 (without normalization). It can be concluded that the model is a good description for all the present cases. Moreover, the grid coarsening shows no real deterioration, indicating that all cases are sufficiently resolved.

Starting from this point approximations to (4) can be considered. First, one can consider the case in which the surface area is taken to be constant,  $\sigma = \sigma_{in}$  as used frequently in the literature,

$$\mathcal{K}a'_{in} := \frac{1}{m_{in}^0} \left( \int_{s_u}^{s_b} \rho K \mathcal{Y} ds - \int_{s_{in}}^{s_b} \rho K ds \right). \quad (9)$$

An improved model can be constructed by assuming that the curvature is not a function of the distance  $s$ , but that it remains constant equal to the inner layer value  $\kappa = \kappa_{in}$ . By integrating (6) this yields for the surface

$$\sigma = \exp(-\kappa_{in}(s - s_{in})). \quad (10)$$

A third approximation is that the iso-planes of the progress variable are concentric, either cylindrical or spherical yielding

$$\sigma = \left( \frac{\xi/\kappa_{in} - s}{\xi/\kappa_{in}} \right)^\xi, \quad (11)$$

in which  $\xi$  takes the value 2 for spherical curvature and 1 for cylindrical curvature. This has to be limited for distances  $s$  beyond the concentric origin,  $s > \xi/\kappa_{\text{in}}$ , at which  $\sigma = 0$ .

**Table 3.** Differences of the mass burning rate determined by the basic model compared to the approximations

Case	C1	C2	C3	C4	C5	C6
$\sigma = \sigma_{\text{in}}$						
Mean	-0.0537	-0.0519	-0.0340	-0.0496	-0.0653	-0.0810
RMS	0.0552	0.0473	0.0373	0.0641	0.0772	0.1004
$\kappa = \kappa_{\text{in}}$						
Mean	0.0062	0.0055	0.0029	0.0026	0.0082	0.0079
RMS	0.0103	0.0085	0.0055	0.0173	0.0186	0.0338
$\xi = 2$						
Mean	-0.0011	-0.0006	-0.0007	-0.0075	-0.0037	-0.0141
RMS	0.0114	0.0101	0.0074	0.0313	0.0224	0.0540
$\xi = 1$						
Mean	-0.0059	-0.0050	-0.0032	-0.0115	-0.0101	-0.0219
RMS	0.0169	0.0142	0.0098	0.0333	0.0281	0.0556

The result of the approximations are given in table 3 for all cases. It is observed that the constant flame surface conjecture gives rise to relatively large error. There is a systematic over-prediction of about 0.05 (without normalization) of the mass burning rate with this model and the fluctuations are of the same order of magnitude. The other approximations give much better results. For the mean differences the spherical approximation,  $\xi = 2$ , is superior compared to the cylindrical model,  $\xi = 1$ , and for most cases also compared to the constant curvature model. However, this is not really substantiated when looking at the accompanying fluctuations. For the better resolved cases, C1 and C3, the mean difference is best predicted by the  $\xi = 2$  model, but again the accompanying fluctuations are much larger than the model deviation. This suggests that it is not a real improvement. With respect to the fluctuations it seems that constant curvature gives the smallest deviations. Additionally, it can be observed that the constant curvature estimation gives slight under-predictions, whereas the concentric cases give systematic increased values of the mass burning rate. Moreover it can be seen that the stoichiometric case (C3) gives the smallest deviations for any of the present approximations. This indicates that the choice of progress variable for the lean case might not be the best choice.

For closer inspection of all realizations in the field, case C6 is chosen in which the deviations are largest. Correlation plots are shown in figure 2. For this case the basic model does not deviate significantly from the results in figure 1, the only difference being that the range of values is extended more to the origin of the plot. Moreover some features, as indicated above, are clearly reflected like

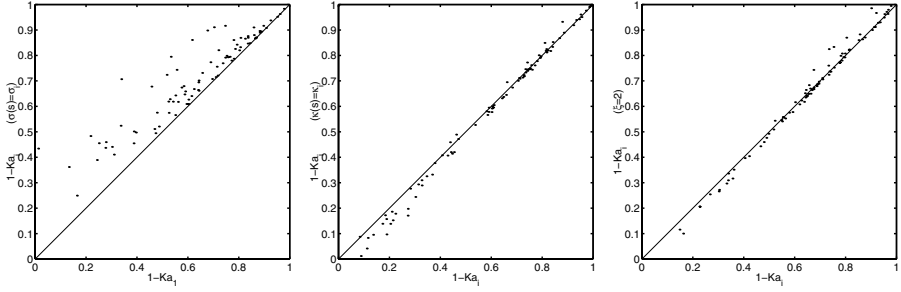


**Fig. 2.** Case C6, Correlation of the actual mass burning rate with the approximations, left:  $\sigma = \sigma_{in}$ , middle:  $\kappa = \kappa_{in}$ , right:  $\xi = 2$ , the case  $\xi = 1$  deviates only very little from  $\xi = 2$  and the figure is not given (result of 60000 flamelets found in the domain)

the under-prediction of the constant surface case. Furthermore the predictions of the concentric cases are less robust compared to the constant curvature model. The latter however gives deviations at small mass burning rates. This is also observed, to a lesser degree, in the concentric spherical approximation. Near the origin the cylindrical model seems to perform better. This is in agreement with observations in [6], who found that at higher turbulence levels, curvature in premixed turbulent combustion of flame kernels tends to cylindrical modes of deformation of the flame front.

It is obvious that all models do not fit to the true values because no local information on the flame geometry is taken into account in the approximations. If local geometric information is taken into account a much better agreement would be possible and will be a topic of further research. At larger times in the evolution, e.g. case C6, it was found that the basic model (4), gives good correlations (at  $t = 0.087\tau$  mean deviation 0.08, rms values of 0.24), see figure 3, whereas all approximations are starting to deteriorate severely. In this case the curvatures have large values, the associated values of radii are within the flame thickness,  $\delta_f$ , as shown in the figure (at the right).

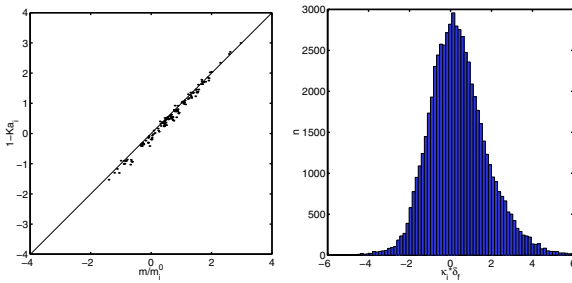


**Fig. 3.** Results of case C6 at time  $t = 0.087\tau$ , left: correlation of the actual mass burning rate with the basic model, right: PDF of inner layer curvatures

## 4 Conclusions

From the previous results it can be concluded that the method of FGM in combination with DNS calculations looks very encouraging. It appears that the FGM is a promising technique to reduce the chemistry and obtain accurate results for the flow, thermodynamics and species. However, apart from a validation in terms of laminar burning velocity, a direct validation is not present for turbulent cases. With respect to this, more validation is needed and the strategy for this will be twofold. By applying a suitable kinetics model with a limited number of species, a DNS can be conducted. This system can be reduced and validated directly against the results of the detailed chemistry calculations. A second method is to increase the dimension of the manifold. It must be studied how many controlling variables are required for a certain accuracy of the predictions. This again can be performed in the framework of the previously mentioned full chemistry DNS.

## References

1. BASTIAANS, R. J. M., VAN OIJEN, J. A., MARTIN, S. M., DE GOEY, L. P. H. & PITSCH, H. 2004 DNS of lean premixed turbulent spherical flames with a flamelet generated manifold. In P. Moin, editor, *CTR Annual Research Briefs*, in press.
2. CHEM1D 2002 A one dimensional flame code. Eindhoven University of Technology, <http://www.combustion.tue.nl/chem1d>.
3. GICQUEL, O., DARABIHA, N. & THEVENIN, D. 2000 Laminar premixed hydrogen/air counter flow flame simulations using flame propagation of ILDM with preferential diffusion. *Proc. Combust. Inst.* **28**, 1901-1908.
4. DE GOEY, L. P. H. & TEN THIJE BOONKAMP, J. H. M. 1999 A flamelet description of premixed laminar flames and the relation with flame stretch. *Comb. Flame*, **119**, 253-271.
5. GROOT, G. R. A. & DE GOEY, L.P.H. 2002 A computational study of propagating spherical and cylindrical premixed flames. *Proc. Combust. Institute*, **29**, 1445-1451.
6. JENKINS, K.W. & CANT, R.S. 2002 Curvature effects on flame kernels in a turbulent environment. *Proc. Comb. Inst.*, **29**, 2023-2029.
7. MAAS, U. & POPE, S. B. 1992 Simplifying Chemical Kinetics: Intrinsic Low-Dimensional Manifolds in Composition Space. *Combust. Flame* **88**, 239-264.
8. VAN OIJEN, J.A. 2002 Flamelet-Generated Manifolds: Development and Application to Premixed Laminar Flames. Ph.D. thesis, Eindhoven University of Technology, The Netherlands.
9. SMITH, G. P., GOLDEN, D. M., FRENKLACH, M., MORIARTY, N. W., EITENEER, B., GOLDENBERG, M., BOWMAN, C.T., HANSON, R. K., SONG, S., GARDINER JR., W. C., LISSIANSKI, V.V. & Z. QIN, Z. 1999 [http://www.me.berkeley.edu/gri\\_mech/](http://www.me.berkeley.edu/gri_mech/)

# Entropic Lattice Boltzmann Method on Non-uniform Grids

C. Shyam Sunder and V. Babu

Department of Mechanical Engineering,  
Indian Institute of Technology,  
Madras, India 600 036.  
vbabu@iitm.ac.in

**Abstract.** The entropic lattice Boltzmann method (ELBM) has recently been shown to be capable of simulating incompressible flows with good accuracy and enhanced stability. However, the method requires that uniform grids be used, which makes it prohibitively expensive for simulating large Reynolds number flows. In this paper, an interpolation scheme is proposed to extend the applicability of this method to arbitrary non-uniform meshes, while retaining the salient features of ELBM such as stability and computational efficiency. The new scheme is used to simulate flow in a lid driven cavity as well as flow past a square cylinder and is shown to largely reduce the grid requirements. The results of the simulation agree very well with other numerical experimental data available in the literature

**Keywords:** Entropic Lattice Boltzmann ISLB.

## 1 Introduction

In the last decade the Lattice Boltzmann method (LBM) has attracted a lot of attention and is fast emerging as an alternative to finite volume and finite element techniques. Lattice Boltzmann methods have been successful in simulating many simple and complex hydrodynamics including turbulent flows[1]. The main attractions of LBM are ease of implementation, high computational efficiency and easy parallelizability. There are many variations of LBM in use, among which are finite volume Lattice Boltzmann method, multiple relaxation Lattice Boltzmann methods, interpolation supplemented Lattice Boltzmann method, and entropic Lattice Boltzmann method.

The Lattice Boltzmann Equation (LBE) initially originated as a floating point recast of the evolution equation of lattice-gas cellular automaton dynamics. The simplest form of LBE, namely, the Lattice Bhatnagar Gross Krook (LBGK) form, can be written as follows.

$$f_i(x + c_i\delta_i, t + \delta_t) - f_i(x, t) = -\frac{1}{\tau}\{f_i(x, t) - f_i^{eq}(x, t)\} \quad (1)$$

where

$$c_i = \begin{cases} 0, & i = 0, \\ c\{\cos((i-1)\pi/2), \sin((i-1)\pi/2)\}, & i = 1, 2, 3, 4 \\ \sqrt{2}c\{\cos[(i-5)\pi/2 + \pi/4], \sin[(i-5)\pi/2 + \pi/4]\}, & i = 5, 6, 7, 8 \end{cases} \quad (2)$$

where  $c = \partial x / \partial t$  is the lattice speed,  $f_i(x, t)$  represents the probability for a particle moving in the direction  $c_i$  to reside at the location  $x$ , at time  $t$  and  $f_i^{eq}$  is the equilibrium distribution corresponding to the particular velocity and density. The right hand side of the equation represents the single relaxation time model collision process with  $\tau$  representing the dimensionless relaxation time. The local hydrodynamic quantities are given by

$$\rho = \sum f_i, \quad \rho u = \sum f_i c_i \quad (3)$$

One of the shortcomings of the LBM is numerical instability. The reason for the instability is that no bounds are imposed on the values  $f_i^{eq}$  and  $f_i$  during the collision process making it possible for  $f_i$  to take negative values depriving it of any physical sense [2]. One of the ways to ensure the positivity of  $f_i$  is to define the corresponding equilibrium value as a minimum of a convex function, known as the H function, under the constraint of the local conservation laws [2].

Apart from the stability issue, another well known problem associated with the discrete velocity models is non-adherence to the equation of the state [3],[4]. In these models, the local equilibrium entropy does not obey the thermodynamic definition of the temperature being a function of entropy and energy [4]. These issues were addressed in the formulation of the ELBM [4],[5],[6],[7]. This is discussed in the next section.

As described by Eq. 1, particles at a lattice site undergo collision followed by advection. The left hand side of Eq. 1 can be split into two parts viz. calculation of  $f_i(x, t + \delta_t)$  (updating post collision values) and calculation of  $f_i(x + c_i \delta_t, t + \delta_t)$  (advection in the direction  $c_i$ ). This advection however can be done only to the neighboring lattice sites at a distance of  $c_i \delta_t$  which constrains the lattice used for the simulation to be a uniform square mesh. This issue was addressed by He et al [8] for a 9 velocity LBE model, wherein the extension of LBE for nonuniform meshes was outlined. The objective of the present work is to extend the ELBM method to non-uniform meshes also using the methodology outline by He et al [8].

## 2 Entropic Lattice Boltzmann Method

The construction of the entropic Lattice Boltzmann method (ELBM) is based on a good choice of the discrete velocities, the  $H$  function and an expression for the equilibrium values[9]. The discrete form of the  $H$  function is derived from the continuous Boltzmann  $H$  function given by  $\int F \ln F dc$  where  $F(\mathbf{x}, c)$  is the single particle distribution function,  $\mathbf{x}$  is the position vector and  $c$  is the continuous



velocity. For 2D athermal cases, the discrete form the  $H$  function can be written as

$$H_{(W_i, f_i)} = \sum_{i=0}^8 f_i \ln \left( \frac{f_i}{W_i} \right) \tag{4}$$

where  $f_i$  represents discrete velocities and  $W_i$  the weights associated with each direction. The weights in one dimension are  $\{1/6, 2/3, 1/6\}$  for the directions 'Right', 'Zero' and 'Left' respectively and the weights for higher dimensions can be constructed by multiplying the weights associated with each component direction[10]. The equilibrium value of the discrete velocity is the minimizer of the corresponding  $H$  function under the constraints of local conservation laws given by Eq. 3. The explicit solution for the  $f_i^{eq}$  in  $D$  dimensions is

$$f_i^{eq} = \rho W_i \prod_{j=1}^D (2u_j - (\sqrt{1 + 3u_j^2})) \left( \frac{2u_j + \sqrt{1 + 3u_j^2}}{1 - u_j} \right)^{c_{ij}/c_s} \tag{5}$$

where  $j$  is the index for spatial directions,  $c_s$  is the velocity of sound and the exponent  $c_{ij}/c_s$  can only take the values  $+1, 0, -1$ .  $H$  can be guaranteed to remain non-increasing everywhere by a two step process explained in Fig. 1. The population is changed first by keeping the  $H$  constant. In the second step dissipation is introduced to decrease  $H$ . It can be guessed that in the steady state i.e. when  $f_i^{eq} = f_i$ , value of  $H$  remains constant. The BGK form of the collision in ELBM is

$$f_i(x + c_i \delta_t, t + \delta_t) - f_i(x, t) = \alpha \beta [f_i(x, t) - f_i^{eq}(x, t)] \tag{6}$$

where  $\beta = 6/(1 + 6\nu)$  is the relaxation frequency with  $\nu$  being the kinematic viscosity. The parameter  $\alpha$  can be calculated by solving the following nonlinear equation

$$H(f) = H(f + \alpha \Delta) \tag{7}$$

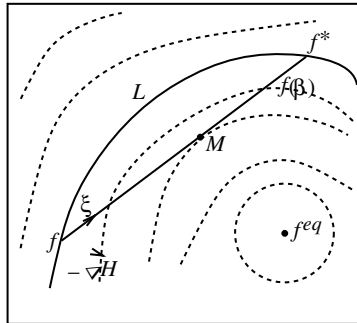


**Fig. 1.** Graphical representation of the collision process. The curves shown represent lines of constant entropy and  $\xi$  represents the collision integral. The first step of the collision process is the calculation of the point  $f^*$ , by solving equation Eq. 7. Then  $f(\beta)$  is determined using 'over-relaxation' based on the value of  $\beta$ [9]. In case of BGK collision, the point M coincides with  $f^{eq}$

where  $\Delta$  represents the bare departure from the local equilibrium i.e.  $\Delta = f^{eq} - f$ . The value of  $\alpha$  is usually close to 2 (and equal to 2 when  $f = f^{eq}$ ). The procedure for explicit calculation of  $\alpha$  was described by Ansumali and Karlin [10]. By using different value for  $\alpha$  at each lattice site, the relaxation time is adjusted locally to ensure compliance with the  $H$  theorem. This guarantees the positivity of the distribution function, which gives the scheme good non-linear stability.

### 3 Entropic Lattice Boltzmann Method on Non-uniform Grids

The ELBM as outlined above is restricted to uniform square meshes. With increasing Reynolds number, this results in a tremendous increase in the total number of points required and hence an increase in computation time. Moreover, ELBM is computationally more expensive than LBM because of multiple calculations of 'ln' function at every lattice point. The present work aims at extending the applicability of ELBM to arbitrary nonuniform meshes which can help reduce the total number of grid points required for a simulation.

The distribution functions ( $f$ ) in LB models are continuous functions in both space and time, although they are used to represent population of particles locally. This gives us scope for interpolation schemes to be used in the interior of the computational domain and extrapolation schemes at the boundary.

In short, the implementation of ELBM on nonuniform grids can be explained in the following steps:

1. Start with an initially guessed flow field.
2. For each lattice site, calculate  $f^{eq}$  according to Eq. 5 and hence find  $\Delta$  ( $= f^{eq} - f$ ).
3. Calculate  $\alpha$  by solving the nonlinear equation 7.
4. Perform collision according to equation 6.
5. Advect the post collision values to appropriate neighboring nodes (imaginary square lattice on which the LB automaton resides).
6. Calculate the values on the 'actual' lattice sites (mesh used in the simulation) by means of quadratic interpolation.
7. Apply the necessary boundary conditions.
8. Goto step 2.

It should be noted that step 5 can be combined with step 6, eliminating the need to store and maintain the values of  $f_i$  on the nodes of the imaginary lattice. Computationally ELBM can be divided into three kernels viz. collision (steps 2, 3, 4), advection and interpolation (steps 5 and 6), boundary conditions (step 7). In general, collision accounts for about 90% of the total computational load, and advection and interpolation about 8%.

In the case of ELBM on square grids i.e. without interpolation being done on the grid, the time spent in collision accounts for almost 98% of the computational load. This shows that the overhead associated with the introduction

of the interpolation routine is not very high. It will be shown in the coming sections that the savings incurred in terms of grids is enormous and more than compensates for the extra calculation being done in interpolation.

## 4 Enhancement in Reynolds Number

Another advantage of using nonuniform or rectangular meshes is the possibility of increasing the Reynolds number of the simulation for a given number of grid points and without any loss of stability. The Reynolds number of the simulation,  $Re$  is equal to  $UL_{char}/\nu$  where  $U$  is the reference velocity,  $\nu$  is kinematic viscosity in lattice units and  $L_{char}$  is the characteristic length for the flow in grid units and is equal to  $N_{char} \delta^{mesh}/\delta^{automaton}$ . Here  $\delta^{mesh}$  is the spacing of the computational grid and  $\delta^{automaton}$  is the spacing of the grid on which the automaton resides.  $N_{char}$  is the number of grid points per characteristic length measured on the latter grid. Now for square uniform meshes,  $\delta^{automaton} = \delta^{mesh}$ . However for rectangular and nonuniform meshes,  $\delta^{mesh}$  can be chosen to be greater than  $\delta^{automaton}$  resulting in increase in the Reynolds number of the simulation by a factor of  $\delta^{mesh}/\delta^{automaton}$ . The use of nonuniform and rectangular grids does not affect the stability of the system (or the LB automaton) as the  $\delta^{automaton}$  is not being altered. Hence for a given number of grid points, the Reynolds number is enhanced. Moreover, by choosing different levels of grid spacing it is possible to greatly reduce the number grid points required for the simulation.

## 5 Results and Discussion

In this section, results from numerical simulations using ELBM on non-uniform grids are presented. Both steady (lid driven cavity flow) and unsteady flows (flow past a square) are simulated to demonstrate the suitability of the methodology.

### 5.1 Lid Driven Cavity Flow

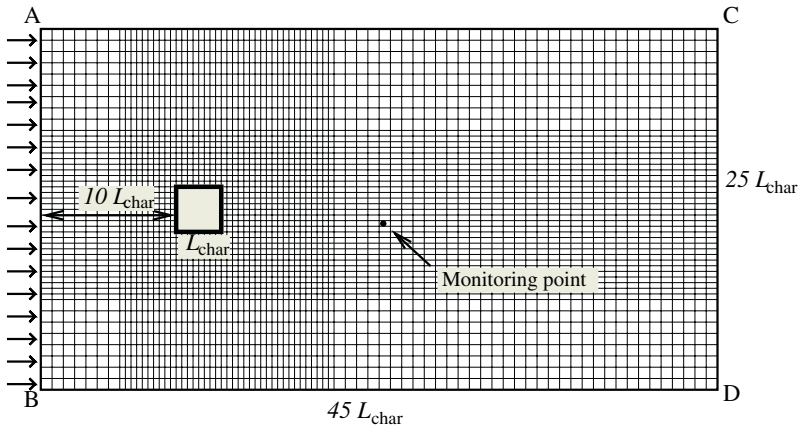
In this classical test problem, fluid is contained within three stationary walls while the fourth (top) wall moves with a certain velocity. This results in the formation of a large primary vortex near the center of the cavity and smaller vortices (two or three, depending on the Reynolds numbers) near the corners. A non-uniform mesh with about 60-100 grid points along each side of the cavity has been used for the simulations. Diffusive boundary condition [11] has been used for all the four walls. In the diffusive boundary condition, the corners can be associated with either of the walls or the normal can be made to be inclined at a  $45^\circ$  angle. In the current implementation, the corners are treated as points belonging to the side walls (left or right). The other choice for the association of corner points is also possible and would not affect the flow by a great extent as three of the four diagonal speeds ( $f$ ) do not propagate into the domain. The results of the simulation compare well with those available in the literature as shown in Table 1.

**Table 1.** Comparison of results for the lid driven cavity problem

Re	Reference	Primary vortex ( $\Psi_{max}, X, Y$ )	Lower left vortex ( $\Psi_{max} \times 10^{-5}, X, Y$ )	Lower right vortex ( $\Psi_{max} \times 10^{-4}, X, Y$ )
400	[13]	(0.1121, 0.5608, 0.607)	(1.30, 0.0549, 0.0510)	(6.19, 0.8902, 0.1255)
	[14]	(0.1130, 0.5571, 0.607)	(1.42, 0.0508, 0.0469)	(6.42, 0.8906, 0.1250)
	current	(0.1120, 0.548, 0.596)	(1.25, 0.04, 0.036)	(5.92, 0.88, 0.112)
1000	[13]	(0.1178, 0.5333, 0.564)	(22.2, 0.0902, 0.0784)	(16.9, 0.8667, 0.1137)
	[14]	(0.1179, 0.5313, 0.562)	(23.1, 0.0859, 0.0781)	(17.5, 0.8594, 0.1094)
	current	(0.1175, 0.536, 0.564)	(18.2, 0.052, 0.040)	(17.1, 0.852, 0.108)
5000	[13]	(0.1214, 0.5176, 0.537)	(135, 0.0784, 0.1373)	(30.3, 0.8075, 0.0745)
	[15]	(0.1190, 0.5117, 0.535)	(136, 0.0703, 0.1367)	(30.8, 0.8086, 0.0742)
	current	(0.095, 0.508, 0.528)	(132, 0.066, 0.128)	(30.2, 0.8025, 0.068)

## 5.2 Flow Past a Square

Here, flow past a square immersed in a stream of fluid is considered. As shown in the figure, a square of side  $L_{char}$  is placed symmetrically at a location  $10L_{char}$  down stream of the inlet  $AB$ . The size of the computational domain is  $45L_{char}$  in the direction of the flow and  $25L_{char}$  perpendicular to the flow (resulting in a blockage ratio of 4%). The side  $CD$  represents the outlet boundary, and


**Fig. 2.** Flow past a Square

the sides  $BC$  and  $DA$  are free stream boundaries. This flow becomes unsteady for Reynolds numbers above 40 or so. If the dominant frequency of the vortex shedding is denoted by  $n_f$  then the Strouhal number of the flow is  $n_f L_{char} / U_\infty$ , where  $U_\infty$  is the free stream velocity. In the past, several techniques such as the Finite Difference, Finite Volume and Lattice Boltzmann methods, have successfully predicted the Strouhal number - Reynolds number relation at low and

moderate Reynolds numbers [17],[18]. At high Reynolds numbers, conventional techniques face difficulties such as enormous grid requirements, lack of stability and lack of a good exit boundary condition [1]. The difficulty with the exit boundary condition can be handled by increasing the domain size in the direction of flow, albeit, at a tremendous increase in the computational cost. In contrast, the non-linear stability of the entropic Lattice Boltzmann method together with lesser grid requirements gives an added advantage over the normal LB methods. Thus, the usage of non-uniform grids with ELBM makes it possible to simulate the flow at high Reynolds numbers and with a reduced computational cost. Table 2 shows the variation of Strouhal number with Reynolds number as predicted by experiments and numerical calculations. It is evident that the present calculations are able to predict the Strouhal number very well and the agreement is better than that of the results available in the literature so far. The grid sizes used in the present case are much smaller than the grid requirements of normal LBM. At high Reynolds numbers, the  $N_{char}$  used in the current case ranges from 30-50, whereas the  $N_{char}$  required for normal LBM would be around 128-256 [19] resulting in more than an order of magnitude savings in the grid requirement (Table 2).

**Table 2.** Comparison of Strouhal number and grid sizes for different Reynolds numbers

Re	Strouhal Number				Grid Size	
	Expt[16]	Current	FV[17]	FD[18]	Current	LBM [19]
250	0.140-0.145	0.136	0.17	0.165	60000	112500
400	0.127-0.136	0.132	0.145	0.161	"	"
500	0.126-0.133	0.132	0.174	-	240000	288000
800	0.121-0.126	0.129	-	-	"	"
1000	0.120-0.122	0.130	-	0.142	$4.5 - 5.4 \times 10^5$	$18 - 73 \times 10^6$
2000	0.120-0.129	0.131	-	0.142	"	"
3000	0.123-0.130	0.133	-	0.145	"	"

## 6 Conclusion

An interpolation scheme to enable the use of non-uniform meshes is proposed for the entropic lattice Boltzmann method. The method has been successfully used for simulating the steady flow in a lid driven cavity and the unsteady flow over a rectangular cylinder for Reynolds number up to 3000. For the former problem, the location as well as the value of the streamfunction at the center of the vortices is predicted very well by the present calculations, when compared with data available in the literature. For the latter problem, the unsteady vortex shedding frequency predicted by the method compares well with the experimental values reported by Okajima [16]. The proposed interpolation scheme preserves all the salient features of ELBM, like stability, and locality of the collision operator.

Moreover, the interpolation itself is a very small addition to the overall computational cost. Considerable savings in grid sizes are shown to be possible by comparing with earlier implementations of LBM. This interpolation scheme is quite general and can be easily implemented on different types of grids.

## References

1. S. Succi, *The Lattice Boltzmann Equation for Fluid Dynamics and Beyond*, Oxford university press, Oxford, 2001.
2. S. Succi, I. V. Karlin, H. Chen, Colloquium: Role of the H theorem in lattice Boltzmann hydrodynamic simulations, *Rev. Modern Physics* 74 (2002).
3. M. Ernst, *Discrete Models of Fluid Dynamics*, edited by Alves A. S. (World Scientific, Singapore) 1991.
4. S. Ansumali, I. V. Karlin, H. C. Ottinger, Minimal entropic kinetic models for hydrodynamics, *Europhys. Lett.* 63 (6) (2003) 798-804.
5. B. M. Boghosian, P. J. Love, P. V. Coveney, Iliya V. Karlin, Sauro Succi and Jeffrey Yezep, Galilean-invariant lattice-Boltzmann models with H theorem, *Phys. Rev. E* 68, (2003) 025103.
6. B. M. Boghosian, J. Yezep, P. V. Coveney, A. Wagner, Entropic lattice Boltzmann method, *Royal Society of London Proceedings Series A*, vol. 457, Issue 2007, p.717
7. H. Chen, C. Teixeira, H-theorem and origins of instability in thermal lattice Boltzmann models, *Computer Phy. Comm.*, vol. 129, Issue 1-3, pp.21-31
8. X. He, L. S. Luo, M. Dembo, Some progress in Lattice Boltzmann method :Part 1. Nonuniform Mesh Grids, *J. Comp. Phys.* 129 (1996) 357-363.
9. I. V. Karlin, A. Ferrante, H. C. Ottinger, Perfect entropy functions of the Lattice Boltzmann method, *Europhys. Lett.* 47 (2) (1999) 182-188.
10. S. Ansumali, I V. Karlin, Single relaxation time model for entropic lattice Boltzmann methods, *Phys. Rev. E* 65 (2002) 056312.
11. S. Ansumali, I. V. Karlin, Kinetic boundary conditions in the lattice Boltzmann method, *Phys. Rev E* 66 (2002) 026311.
12. X. He, L. S. Luo, M. Dembo, Some Progress in Lattice Boltzmann method: Enhancement of Reynolds number in simulation, *Physica A* 239 (1997) 276-285.
13. S. Hou, Q. Zou, S. Chen, G.D. Doolen, A.C. Cogley, Simulation of Cavity Flow by the Lattice Boltzmann Method, *J. Comp. Phys.* 118 (1995) 329.
14. R. Schreiber, H.B. Keller, Driven cavity flows by efficient numerical techniques, *J. Comp. Phy* 49 (1983) 310.
15. U. Ghia, K.N. Ghia, C.Y. Shin, High-Re solutions for incompressible flow using the N.S. equations and a multigrid method, *J. Comp. Phys.* 48 (1982) 387.
16. A. Okajima, Strouhal numbers of rectangular cylinders, *J. Fluid Mech.* 123 (1982) 379-398.
17. A. Sohankar, C. Norberg, L. Davidson, Simulation of three-dimensional flow around a square cylinder at moderate Reynolds numbers, *Phys. Fluids* 11 (1999) 288.
18. R. W. Davis, E. F. Moore, Vortex shedding process behind two dimensional bluff bodies, *J. Fluid Mech.* 116 (1982) 475.
19. G. Baskar, V. Babu, Simulation of the Flow Around Rectangular Cylinders Using the ISLB Method, *AIAA-2004-2651* (2004).

# A Data-Driven Multi-field Analysis of Nanocomposites for Hydrogen Storage

John Michopoulos, Nick Tran, and Sam Lambrakos

Materials Science and Component Technology Directorate,  
U.S. Naval Research Laboratory,  
Washington DC, 20375, U.S.A

{john.michopoulos, nick.tran, sam.lambrakos}@nrl.navy.mil

**Abstract.** This paper focuses on computational parameter identification associated with heat and mass diffusion macro-behavioral models of hydrogen storage systems from a continuum multiphysics perspective. A single wall nanotube (SWNT) based composite pellet is considered as our representative finite continuum system. The corresponding partial differential equations (PDEs) governing the spatio-temporal distribution of temperature and hydrogen concentration are formulated. Analytical solutions of the system of coupled PDEs are constructed and utilized in the context of inverse analysis. The corresponding non-linear optimization problem is formulated in order to determine the unknown parameters of the model, based on an objective function and constraints consistent with experimentally acquired data along with the physical and utilization requirements of the problem. Behavioral simulation results are presented in an effort to demonstrate the applicability of the methodology. Finally, we indicate potential extensions of this methodology to multi-scale and manufacturing process optimization.

## 1 Introduction

The activities described herein are a part of a larger effort associated with the development of a data-driven environment for multiphysics applications (DDEMA) [1, 2, 3, 4]. The analytical methodology for approaching system identification problems is based on establishing a corresponding inverse problem that can be solved by means of global optimization as shown earlier [5, 6, 7] for various problems ranging from material nonlinear constitutive response to welding characterizations.

The recent utilization of SWNTs as an essential component for nanocomposites for hydrogen storage has led to the direct need for modeling the behavioral characteristics of such systems during both the hydriding and dehydriding stages. The desire for manufacturing highly efficient, inexpensive and long lasting hydrogen storage systems underscores our motivation for modeling such system as a special case of our general effort.

In order to achieve these goals, we proceeded with the modeling of a nanocomposite pellet's hydriding and dehydriding response coupled with heat conduction

and chemical reactivity under the framework of an inverse problem setting applied to preliminary experiments that generated the data to drive our modeling. Continuum multi-field modeling efforts have been based on continuum thermodynamics and conservation theorems [8, 9, 10]. Here we present the results of our multi-field modeling effort [5] for the problem at hand along with a description of the associated solutions.

## 2 Behavioral Modeling of Hydrogen Storage Pellet

Consider a medium with isotropic and homogeneous aggregate properties at the macro-length scale. Furthermore, consider that this medium is exposed to temperature and multi-species concentration boundary conditions. As heat diffusion proceeds in the medium so does multi-species mass diffusion. The species may or may not be chemically reactive with the host medium or with each other. A medium under such a multi-field excitation includes as a special case the SWNT-enhanced materials considered for hydrogen storage. The general procedure for deriving the continuum multiphysics model for this system is analogous to the one followed for hygrothermoelastic composites elsewhere [10]. The resulting general system of PDEs [11] describes all open continuum systems under the influence of temperature, and multi-species diffusion with chemical reactions among the species. However, for the case of the hydrogen storage continua of the type used here we do not have cross-species reactivity since hydrogen is the only species involved. The diffused hydrogen only reacts with the matrix and the embedded SWNTs of the composite. This process can be abstracted as an absorption/desorption diffusion. Therefore, as a first approximation we will assume a single component system (i.e. we will consider the concentration of hydrogen  $C$  as our mass concentration variable) with no chemical reaction involved and  $T$  as our temperature field state variable. In this case the following pair of coupled PDEs is valid:

$$\frac{\partial C}{\partial t} = D_m \nabla^2 C + \lambda D_h \nabla^2 T, \quad (1a)$$

$$\frac{\partial T}{\partial t} = \nu D_m \nabla^2 C + D_h \nabla^2 T. \quad (1b)$$

Here,  $D_m$  and  $D_h$  are the mass and heat diffusivities, respectively, and  $\lambda, \nu$  are both coupling coefficients. This heat-mass diffusion system is completed by the generalized boundary conditions (of the third kind),

$$T(\mathbf{x}, t) + \frac{k_h(\mathbf{x})}{h_T} \frac{\partial T(\mathbf{x}, t)}{\partial \mathbf{n}} = \phi_T(\mathbf{x}, t), \mathbf{x} \in S \quad (2a)$$

$$C(\mathbf{x}, t) + \frac{k_m(\mathbf{x})}{h_C} \frac{\partial C(\mathbf{x}, t)}{\partial \mathbf{n}} = \phi_C(\mathbf{x}, t), \mathbf{x} \in S \quad (2b)$$

where  $S$  represents the boundary,  $\mathbf{x}$  and  $\mathbf{n}$  the position and outward normal vectors on the boundary, respectively,  $k_h, k_m$  are the heat and mass conductivities, respectively,  $h_T, h_C$  are the heat and mass transfer coefficients respectively,



and finally  $\phi_T(\mathbf{x}, t)$ ,  $\phi_C(\mathbf{x}, t)$  are the prescribed distributions of temperature and mass concentration on the boundary, respectively. Boundary conditions of the first and second kinds can be produced by appropriate omission of the second terms (first kind) and the first terms (second kind) of these equations. The cylindrical symmetry of the SWNT composite pellet suggests transforming the governing equations from the cartesian coordinate system to a cylindrical frame of reference (  $\{x, y, z, t\} \rightarrow \{r, \vartheta, z, t\}$  ). In addition, the axisymmetric character of the applied boundary conditions further simplify the system of Eqs. (1) by coordinate transformation of the nabla operators. It has been shown elsewhere [10] that it is possible to uncouple the system of Eqs. (1) by using the solutions of the uncoupled PDEs if  $\lambda, \nu$  are constants via the method of normal coordinates. One form of the uncoupled solution is given by

$$\begin{aligned} T &= T_0 + (T_f - T_0)F_1(r/r_o, z/l_o, D_h t/r_o^2, D_h t/l_o^2, u_d) \\ &+ \nu u_d (C_f - C_0)F_2(r/r_o, z/l_o, D_m t/r_o^2, D_m t/l_o^2, 1/u_d) \end{aligned} \quad (3a)$$

$$\begin{aligned} C &= C_0 + (C_f - C_0)F_1(r/r_o, z/l_o, D_m t/r_o^2, D_m t/l_o^2, 1/u_d) \\ &+ \lambda(T_f - T_0)F_2(r/r_o, z/l_o, D_h t/r_o^2, D_h t/l_o^2, u_d) \end{aligned} \quad (3b)$$

where  $T_f, C_f$  are the final values of the temperature and hydrogen concentrations, respectively, that are applied on the boundary and reached by the continuum at equilibrium conditions and where,

$$F_i(r, z, \tau_r, \tau_z, u) = \Psi_i^c(r, \tau_r, u)\Psi_i^s(z, \tau_z, u). \quad (4)$$

The solutions  $F_i$  for the finite cylinder geometry have been constructed here as the product of the two one dimensional solutions corresponding to an infinite cylinder of radius  $r_o$  and an infinite slab of thickness  $2l_o$  with appropriate scaling of time via usage of  $\tau_r$  and  $\tau_z$ , respectively. The functions  $\Psi_i^j$  with  $j = c, s$  and  $i = 1, 2$  are defined by

$$\Psi_1^j(x_j, \tau_j, u) = [1 - H_1^j(u)]\Psi^j(x_j, D_2(u)\tau_j) + H_1^j(u)\Psi^j(x_j, D_1(u)\tau_j) \quad (5a)$$

$$\Psi_2^j(x_j, \tau_j, u) = H_2^j(u)[\Psi^j(x_j, D_2(u)\tau_j) - \Psi^j(x_j, D_1(u)\tau_j)], \quad (5b)$$

where we have used the contractions,

$$H_1(u_d) = \frac{1}{2}[1 - (1 - u_d)H_2(u_d)] \quad (6a)$$

$$H_2(u_d) = \frac{D_1 D_2}{(D_2 - D_1)u_d}, \quad (6b)$$

where  $u_d = D_m/D_h$  and

$$D_1 = 2u_d/[1 + u_d + \sqrt{(1 - u_d)^2 - 4u_d(1 - \lambda\nu)}] \quad (7a)$$

$$D_2 = 2u_d/[1 + u_d - \sqrt{(1 - u_d)^2 - 4u_d(1 - \lambda\nu)}]. \quad (7b)$$

Functions  $\Psi^j$  are the solutions of the normalized one-dimensional problems for the cylinder  $m = 0$  and the slab  $m = 1/2$  and are defined by

$$\Psi^j(x, \tau) = 1 - 2 \sum_{i=1}^{\infty} \frac{1}{\mu_i} \left[ 1 + \frac{2m}{Bi} + \left( \frac{\mu_i}{Bi} \right)^2 \right]^{-1} x^m \frac{J_{-m}(\mu_i x)}{J_{1-m}(\mu_i)} e^{-\mu_i^2 \tau}, \quad (8)$$

in terms of the Bessel functions  $J_i$ . The coefficients  $\mu_i$  are the roots of the transcendental equation

$$BiJ_{-m}(\mu) - \mu J_{1-m} = 0. \quad (9)$$

### 3 Inverse Problem Setup

The set of diffusivities ( $D_h, D_m$ ), the coupling constants ( $\lambda, \nu$ ) and the four instances of the Biot number  $Bi$  ( $(Bi)_T^c = h_T r_o / k_h, (Bi)_C^c = h_C r_o / k_m, (Bi)_T^s = h_T l_o / k_h, (Bi)_C^s = h_C l_o / k_m$ ) determine the behavioral model completely when the geometry and initial and boundary conditions are known. Determination of these constants from experimental data constitutes the inverse problem formulation.

#### 3.1 Experimental Setup and Associated Data (NT)

The pellet samples for the hydriding/dehydriding study were made by uniaxially cold pressing the Mg $x$  wt.% Mm powder. The details of manufacturing and processing the pellets are given elsewhere [12, 13]. Figure (1) shows the pellet and the experimental setup for hydriding and dehydriding the pellet. Hydriding and dehydriding of Mg $x$  wt.% Mm pellets were carried out inside a dual reactor made of seamless inconel tubes. Two thermocouples were attached to the outside of each tube and were calibrated to reflect the temperature of the reaction zone. All data from the hydriding and dehydriding process were digitally captured by

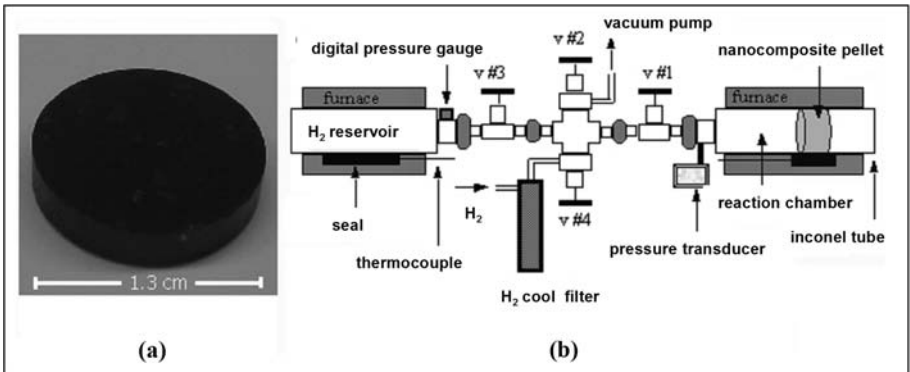


**Fig. 1.** Hydrogen storage pellet (a) and experimental setup schematic for hydriding and dehydriding of the pellet (b)

a data acquisition board, which was controlled by our custom code [13]. The hydrogen uptake or release of the Mgx wt.% Mm pellets was determined by measuring the pressure changes in the reaction chamber before and after each hydriding or dehydriding treatment.

### 3.2 Nonlinear Optimization

The general outline of using design optimization for parameter identification is a well established discipline. It usually involves the usage of an optimization module that utilizes behavioral data from the actual physical system (collected experimentally) as well as simulated data from a potential model. The design variables to be identified are the constants of the model. Ultimately, the simulated behavior has to reproduce the experimentally observed behavior and therefore an objective function must be minimized. For an objective function  $f = f(\mathbf{X})$  with  $\mathbf{X}$  being the resultant vector defined by the design variable component vectors such as  $x_1\mathbf{i}_1, \dots, x_n\mathbf{i}_n \in \mathbf{X}^n$ , where  $\mathbf{X}^n$  is the vector space spanned by the basis vectors  $\mathbf{i}_1, \dots, \mathbf{i}_n$ . For this general case the optimization problem can be expressed by

$$\min[f(x_1, \dots, x_n)]_{x_i \in \mathbb{R}^n} \quad (10a)$$

$$c_j^{eq}(x_1, \dots, x_n) = 0, c_i^{ineq}(x_1, \dots, x_n) \geq 0, j = 1, \dots, p \quad (10b)$$

Relations (10b) express the equality and inequality constraints.

In our analysis the behavior of the system is described by the time evolutions of the total temperature and hydrogen absorption. The stimulation of the system is expressed by the multi-field boundary conditions that define the temperature and hydrogen mass concentration on the boundary. We define  $T_i^{sim}(t_i)$ ,  $C_i^{sim}(t_i)$  and  $T_i^{exp}(t_i)$ ,  $C_i^{exp}(t_i)$  to be the simulated and experimental values, respectively, of the temperature and hydrogen concentration at a discrete evaluation point  $i = 1, \dots, p$  where  $p$  is the total number of evaluations. We can now form the objective function as the sum of the squares of their differences in the least square sense, as follows:

$$f(x_1, \dots, x_n) = \sum_{i=1}^p [T_i^{exp}(t_i) - T_i^{sim}(x_1, \dots, x_n, t_i)]^2 + \sum_{i=1}^p [C_i^{exp}(t_i) - C_i^{sim}(x_1, \dots, x_n, t_i)]^2 \quad (11)$$

We set the simulated values to be the average values of the solutions of the PDEs along the edge of the pellet for the temperature and over the entire volume for the hydrogen concentration according to

$$T_i^{sim}(x_1, \dots, x_n, t_i) = \int_{-l_0}^{l_0} T(r_0, z, t_i; x_1, \dots, x_8) dz \quad (12a)$$

$$C_i^{sim}(x_1, \dots, x_n, t_i) = 2\pi \int_0^{r_0} \int_{-l_0}^{l_0} C(r, z, t_i; x_1, \dots, x_8) r dr dz. \quad (12b)$$

The integrands in these relations are the ones defined in Eqs. (5) with the special one-to-one substitution  $\{x_1, \dots, x_8\} \rightarrow \{D_h, D_m, \lambda, \nu, (Bi)_T^c, (Bi)_T^s, (Bi)_C^c, (Bi)_C^s\}$ .

## 4 Preliminary Results

The implementation of the optimization procedure was formulated in Mathematica [14] with various global nonlinear optimization algorithms encoded in the package Global Optimization “GO-5.0” [15]. The function “GlobalSearch” that yielded the quickest results utilizes a generalized hill climbing technique that is based on Newton’s method but uses a generalized gradient rather than a derivative, and allows for analytic linear or nonlinear constraints. Multiple starts are used to test for the existence of multiple solutions. The multiple starts are generated randomly from the region defined by the range of parameter values input by the user. Feasible starting regions are not needed, but it is assumed that objective function values in this region are Real.

The initial and boundary conditions for the computation of the solutions of the PDEs governing the system as required by the simulated values within the objective function, were chosen to correspond to the experimental procedure. Specifically they were  $T_0 = 27^\circ C$ ,  $T_f = 200^\circ C$ ,  $C_0 = 0$  and  $C_f = 1.1$ .

Dehydriding data were also considered along with the hydriding data but have not effected the identified parameters.

Figure (2) shows the hydriding time evolution observed experimentally along with the one computed after parameter identification took place. The identified model fits the hydriding experimental data very well and similar performance is observed (but not included here) for the dehydriding data. Therefore, the model may be adopted as a “calibrated” model for simulation of the behavior of similar systems in many other situations and applications, where the shape of specimen varies but the nanocomposite material remains the same.

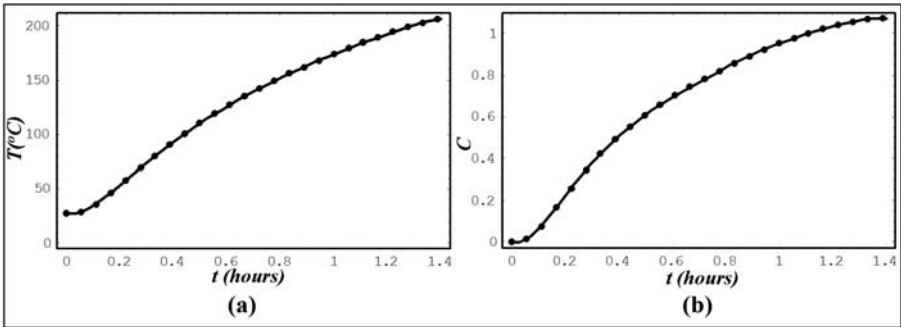


**Fig. 2.** Experimental (dots) and simulated (continuous line) after the parameter identification has been conducted, for the time evolution of the temperature (a) and Hydrogen concentration (b) time evolutions during the hydriding process

## 5 Potential Extensions

Careful consideration of the identified parameters implies two distinct correlations. The subset  $\{D_h, D_m, \lambda, \nu\}$  is related to the characteristic behavior of the nanocomposite system and the macroscopic length scale, while the subset  $\{(Bi)_T^c, (Bi)_T^s, (Bi)_C^c, (Bi)_C^s\}$  is related to the characteristic behavior of the reactor-nanocomposite system owing to the fact that Biot numbers are functions of the heat and mass transfer coefficients that in turn depend on the fluid properties of the gas (hydrogen) according to the Dittus-Boelter equation. These are controllable by the reactor/furnace setup. This suggests that the above referenced optimization procedure is capable of identifying all parameters of interest to the technology practitioner. Therefore, a natural extension of this technique could include any parameters that participate in a given utility (efficiency of performance), aging, or economic model of the system. This extension is well posed as long as the parameters of these models are related to any of the behavioral parameters of the system and an appropriate objective function can be constructed.

In addition to optimizing the usability aspects of such a system one can also optimize the condition of manufacturing related to desirable performance (from efficiency, economic, aging, etc perspectives) by establishing the process control models associated with the manufacturing of such systems, with the lower length scale behavioral models that may be derived from *ab initio* modeling methodologies among many others.

## 6 Conclusions

We have utilized general coupled mass and heat diffusion, to construct a PDE model to capture the hydrogen storage behavior of a nanocomposite pellet system. We have formulated the inverse problem approach for utilizing data to create a procedure for the data-driven identification of the free parameters participating in the behavior model. We implemented the computational equivalent of the procedure and performed the identification based on experimental data collected for the hydriding cycle of the nanocomposite pellet system. Comparison of the identified system to the experimental data, demonstrated how well the identification has performed. Finally, two specific motivating extensions were discussed to define the context of our future intensions.

## Acknowledgements

The authors acknowledge the support by the National Science Foundation under grant ITR-0205663. In addition, the authors would like to extend their special thanks to Dr. F. Darema for her constant availability and encouragement throughout this effort.

## References

1. Michopoulos, J., Tsompanopoulou, P., Houstis, E., Rice, J., Farhat, C., Lesoinne, M., Lechenault, F., DDEMA: A Data Driven Environment for Multiphysics Applications, in: Proceedings of International Conference of Computational Science - ICCS'03, Sloot, P.M.A., et al. (Eds.), LNCS 2660, Part IV, Springer-Verlag, Heidelberg, (2003) 309-318.
2. Michopoulos, J., Tsompanopoulou, P., Houstis, E., Rice, J., Farhat, C., Lesoinne, M., Lechenault, F., Design Architecture of a Data Driven Environment for Multiphysics Applications, in: Proceedings of DETC'03, Paper No DETC2003/CIE-48268, (2003).
3. Michopoulos, J., Tsompanopoulou, P., Houstis, E., Farhat, C., Lesoinne, M., Rice, J., Joshi, A., On a Data Driven Environment for Multiphysics Applications, Future Generation Computer Systems, in-print (2005).
4. Michopoulos, J., Tsompanopoulou, P., Houstis, E., Joshi A., Agent-based Simulation of Data-Driven Fire Propagation Dynamics, in: Proceedings of International Conference of Computational Science - ICCS'04, Bubak, M., et al. (Eds.), LNCS 3038, Part III, Springer-Verlag, Heidelberg, (2004) 732-739.
5. Michopoulos, J., Computational Modeling of Multi-Field Ionic Continuum Systems, in: Proceedings of International Conference of Computational Science - ICCS'04, Bubak, M., et al. (Eds., LNCS 3039, Part IV, Springer-Verlag, Heidelberg, (2004) 621-628.
6. Michopoulos, J., Automated Characterization of Material Constitutive Response, in: Proceedings of Sixth World Congress of Computational Mechanics (WCCM-VI 2004), Tsinghua University Press & Springer-Verlag, Heidelberg, (2004) 486-491.
7. Lambrakos, S.G., Milewski, J.O., Analysis of Processes Involving Heat Deposition Using Constrained Optimization, Sci. and Tech. of Welding and Joining, 7(3), (2002), 137.
8. Truesdell, C., Toupin, R., 1960, "The Classical Field Theories", in Handbuch der Physik ( Herausgegeben von S. Flugge) **III/1**, Springer-Verlag, Berlin.
9. Green, A. E., Naghdi, P. M., 1995, "A unified procedure for construction of theories of deformable media. I. Classical continuum physics", Proc. Roy. Soc. London Ser. **A 448** (1934), pp. 335-356.
10. Sih, G.C., Michopoulos, J.G., Chou S.C., "Hygrothermoelasticity", Martinus Nijhoff Publishers (now Kluwer Academic), Dordrecht, (1986).
11. Michopoulos, J., Lambrakos, S.G., Tran, N. E., Multi-Field Characterization of Single Wall Nano-Tube Composites for Hydrogen Storage, ASME-CIE conference, Long Beach, CA, September 24-28, 2005, To appear, (2005).
12. Tran, N. E. , Imam, M. A., Feng, C. R., Evaluation of Hydrogen Storage Characteristics of Magnesium-misch Metal Alloys. J Alloys Comp ,359, (2003), 225-229.
13. Tran, N. E., Lambrakos, S.G., Purification and Defects Elimination of Single-Walled Carbon Nanotubes by Thermal Reduction Technique. To appear.
14. Wolfram, S., The Mathematica Book, Wolfram Media, (2004).
15. Loehle Enterprises, Global Optimization 5.0 for Mathematica, Loehle Enterprises, (2004).

# Plug and Play Approach to Validation of Particle-Based Algorithms

Giovanni Lapenta and Stefano Markidis

Los Alamos National Laboratory, Los Alamos, NM 87545, USA  
{lapenta, markidis}@lanl.gov

**Abstract.** We present a new approach for code validation. The approach is based on using particle-based algorithms to simulate different levels of physical complexity. We consider here heat and mass transfer in a multicomponent plasma at the kinetic and fluid level. By representing both levels using particle methods we can design a component based software package, Parsek, to conduct validation using a plug and play approach. With the plug and play paradigm, different components representing different physical descriptions but all based on a common particle algorithm can be interchanged without altering the overall software architecture and the overall algorithm. The advantage of the plug and play approach is that validation can be conducted for each component and switching between physical descriptions requires the validation of just the affected components, not entire codes.

## 1 Introduction

There exist Particle-based algorithms for every level of description, from the quantum ab-initio molecular dynamics (MD), to classic MD, to kinetic particle in cell (PIC) to fluid particle-based algorithms (e.g. fluid PIC, SPH, vortex methods). While other methods compete with particle-based methods at the macroscopic fluid level, particle-based methods are nearly universally used at the kinetic and MD level.

The availability of a common class of algorithms at all levels of description provides a unique possibility inaccessible to other classes of algorithms. All particle-based algorithms share a common software infrastructure made of particles and interactions (either pair-interactions or interactions mediated by a field discretized on a grid). Using a particle-based approach at all levels it is possible to design a single software package based on a component architecture. All the levels of description are formulated using the same classes of software components (e.g. particle movers or components for particle-particle interactions). Within a single software package it is possible to go across all levels of description simply activating a component in place of another, for example a kinetic particle mover (based on Newton's equations for the particle position and velocity) can be replaced by a fluid particle mover (where the motion is computed according to the local flow speed rather than the particle velocity).

We term the approach *plug and play validation* because it allows to validate coarser levels of description with finer levels of description by plugging in components and testing them in use.

In the present work, we follow the standard nomenclature [2] of terming the process of *verification* as the task of making sure that the equations of the model are solved correctly and the process of *validation* as the task that the model equations represent with fidelity the actual physics of the system under investigation. Our focus here is on validation alone.

The approach proposed here brings validation to a new level because it not only validates the prediction of coarse levels by testing their results. It also validates coarse levels by directly testing the assumptions behind them (e.g. equations of state or closure relations) validating their assumptions using the information from finer levels of description.

While our focus is on validation, we remark that the approach proposed has also the advantage of simplifying verification because all levels are present within a common software infrastructure and verification can be done component by component. The alternative of using totally different codes and algorithms for the different levels clearly requires a much more extensive effort of verification.

We present a specific example. We consider the heat conduction in a system of multiple ionized gases. The fluids are not in local thermodynamic equilibrium and each has its own temperature and velocity. The fluid closures for this case are not consolidated. We test a model we recently developed based on the 13 moment approach:

$$\mathbf{q}_s = \sum_t \lambda_{st} \nabla T_t \quad (1)$$

where  $\mathbf{q}_s$  is the heat flux in species  $s$  due to temperature gradients in all other species  $T_t$ . The coefficients  $\lambda_{st}$  can be computed from the kinetic model [1]. We will simulate the system at the kinetic and at the fluid level using a single pilot code based on particle methods both for the kinetic and the fluid model. The plug and play approach is used in the design of the pilot code and in the execution of the validation protocol. The process of validation proposed here would determine the validity of the fluid model used (eq. 1) and of the formulation of the transport coefficients  $\lambda_{st}$ .

## 2 The Physical Challenge

Plasma physics provides an ideal test-bed for developing and testing multiscale, multiphysics algorithms. Plasma physics intrinsically includes two level of multiplicity. First, the plasma species have intrinsically different scales. The electrons are lighter (in a typical hydrogen plasma, the ion mass is approximately 1836 times larger than the electron mass). Second, two types of interactions occur in a plasma: short range and long range. While in a typical gas the interactions are only short range (collisions), in plasmas the presence of charge in the components introduces also a long range force due to collective electromagnetic interactions.



Plasma physics encompasses the whole range of physical scales and models known to mankind. Even not including the topic of quark-gluon plasmas, proper plasma physics ranges from quantum many-body systems to cosmological general relativity models on the structure of the universe. We propose that the approach described here can indeed in principle cover the whole spectrum of physics at these two ends and everything in between. Of course realistically, we need to limit the scope here. And we decide to limit the scope to just two levels of description: the kinetic level and the fluid level.

At the kinetic level, a N-body system is described through the evolution of the distribution function in phase space. The classical formalism for this level of description is the Boltzmann equation.

At the fluid level, a N-body system is described through the evolution of the moments of the distribution function, such as density, velocity and temperature. A great variety of fluid models can be derived from the kinetic level taking a different number of moments of the distribution.

A well known feature of fluid models and their derivation from kinetic models is the need for closure relations. The moment formulation does not form a closed system of equations per se. The equation for the evolution of a moment of any order generally involves higher order moments. Relationships expressing higher order moments in terms of lower order moments are called *closure relations* and are needed to turn the fluid model into a well posed closed problem.

Examples of closure relations are the equations of state:  $p = p(n, T)$  and relationships expressing the heat flux or the stress tensor in terms of lower order moments. A classic example is the Fourier law:  $q = -k\nabla T$ , generalized in our case to eq. (1).

In the present work we consider an initially uniform system with density  $n_s = 1$  for all species  $s$ , at rest  $\mathbf{v}_s = 0$ . But we assume that the system is not in thermodynamic equilibrium and each species is initially set up with a uniform temperature gradient. The electrons represent a neutralizing background.

A complete description of the physics and of the mathematical models used can be found in Ref. [1]. The kinetic model can be formulated with the Boltzmann equation:

$$\frac{\partial f_s}{\partial t} + \mathbf{v} \cdot \frac{\partial f_s}{\partial \mathbf{x}} + \frac{q_s}{m_s} \mathbf{E} \cdot \frac{\partial f_s}{\partial \mathbf{v}} = St(f_s) \quad (2)$$

for each species  $s$ , including electrons and ions. Charge imbalance could be created in the transient evolution, but we assume that magnetic fields are neglected. This latter assumption is not realistic in most laboratory experiments but it is acceptable within the scope of the present work.

The fluid model is based on a continuity, momentum and energy equation for each species. We use the standard textbook formulation of multiple fluid models [3]. However, we investigate the issue of how many moments are required to represent the physics correctly and what closure relations can be used. We base our fluid analysis on our recent work on this topic [1] and on the classic 13-moment approach [3].

The model poses a formidable challenge, a challenge that we try to address with particle-based algorithms.

### 3 Particle-Based Method Meets the Challenge

We consider three classes of particle-based methods. We categorize them according to the level of physical description.

First, we consider molecular dynamics (MD), MonteCarlo (MC), or generally particle-particle (PP) methods, typically based on a direct mathematical representation of the physical system. In this class of methods, the particles represent a physical entity: a particle, a molecule or a cluster of atoms and molecules (such as a nanoparticle or a subunit of it). The interactions among the computational particles mimic as best we know the actual physical interaction among the real physical objects.

Second, we consider kinetic particle-mesh (PM) methods, often referred to as particle in cell (PIC) methods. This class differs from the PP approach in two ways: 1) While the PP approach uses the direct simulation of N-bodies through their fundamental laws of motion, the PM approach studies the N-body problem at the kinetic level, as described by the Boltzmann transport theory of classical or relativistic N-body systems. In PM, the computational particle represents an element of phase space. 2) While the PP approach handles only particles and their pair interactions, the PM approach introduces average fields and for their discretization introduces a computational mesh.

Third, we consider fluid particle-based methods (fluid PIC, SPH, vortex methods, ...). While the data structure and the software engineering issues typical of fluid PIC are similar to kinetic PIC, the mathematical and physical bases for it are entirely different. In fluid PIC, the computational particle represents an element of the fluid (or solid) in the coordinate space (rather than of the phase space) and its significance is similar to that of a fluid element in a common Lagrangian scheme. Indeed, the fluid PIC method can be viewed as a peculiar implementation of the arbitrary Lagrangian Eulerian (ALE) approach, widely used in industrial engineering applications.

In our study PP approaches are used to handle short range interactions at the kinetic level, PM methods are used to treat long range interactions at the kinetic level. The combined used of PP and PM methods is often referred to as PPPM or P<sup>3</sup>M. Fluid PIC is used to handle the fluid description.

### 4 Plug and Play Approach to Validation

We can identify two primary advantages of particle-based methods in addressing the issue of validation.

First, there is a direct relationship of particle-based algorithms with the physical system under investigation. Computational particles can be directly linked

with physical observables (particle themselves in PP, elements of the phase space in PM and parcels of fluid in fluid PIC). Furthermore, the interactions among the particles (either pair interactions or field-mediated interactions) are direct mathematical constructs of actual measurable interactions in the real world.

Second, particle-based algorithms use the same data structure and the same software architecture to treat all different levels of description, from the fundamental quantum level of ab-initio quantum MD, to classical PP methods, to kinetic PIC, to fluid PIC. All levels of description of N-body systems are covered by particle-based algorithms. No other class of numerical algorithms spans the same range. Based on the two properties above, we can propose that particle-based algorithms provide a unique prototyping environment for Validation & Verification (V&V).

We propose a line of investigation closed on the particle-based algorithms themselves and investigates for a specific system the limits of validity, the fidelity and the predictive potency of different levels of description. Having, as particle-based algorithm do have, the most fundamental level of description (kinetic for weakly coupled systems and molecular dynamics for strongly coupled systems), one has the exact correct theoretical answer based on our most complete and modern understanding of the physics world. By reducing the complexity and stepping down the ladder of further approximations and simplifications, we can address the question of "what is the simplest model to capture a given process".

Within the particle-based approaches, this can be accomplished without changing the overall software architecture, with as simple a switch as changing for example the equations of motion from relativistic to classic, or the field equations from fully electromagnetic to electrostatic. We propose here a plug and play component based software architecture where the properties of the particles and of their interactions through pair forces or through fields can be exchanged by replacing a software component with a compatible one based on a different level of sophistication.

No doubt, this has a strong impact on the cost of the simulations or on the time scales and length scales involved. But if a system is chosen where the most fundamental approach is feasible, stepping down the ladder of approximate models will be progressively easier and more feasible. We note that the plug and play approach just outlined is not feasible with other non particle-based approaches. For example Eulerian methods would not have an equivalent component to be replaced with at the kinetic level (at least a mature one) and even less so at the molecular dynamics level. In that case, the plug and play approach would not be feasible and different codes would need to be used instead making the V&V much more difficult and time consuming, as all parts of the code would need V&V, not just the new component plugged in. Different software architectures would be involved, adding a level of uncertainty and clouding the issue. Particle-based methods allow the plug and play approach primarily because they work as the physics system work allowing a direct comparison with them.

## 4.1 Specific Example

Let us consider an example: the formulation of heat conduction in hydrodynamics simulations. We propose to start at the fundamental kinetic level with a PIC simulation (assuming a weakly coupled system, but the same approach would function by starting from a PP approach for high energy density systems) where a first principle approach provides the exact heat transfer by taking the appropriate moments of the particle distribution function.

The heat conduction is defined as the third order moment of the particle distribution function:

$$q_{hs} = \frac{m_s}{2} \sum_{k=1}^3 \int c_{sh} c_{sk} c_{sk} f_s d\mathbf{v}_s \quad (3)$$

where  $\mathbf{c}_s$  is the random velocity (difference between actual velocity and average fluid velocity) for species  $s$ ,  $h$  and  $k$  label the coordinates.

From a kinetic description, the heat flux can be computed directly using eq. (3).

In the fluid model, heat flux is computed using the 13-moment fluid closure and is defined as in eq. (1) where the transport coefficients  $\lambda_{st}$  are provided by theoretical estimates [1].

In our plug and play validation approach, we replace the components for kinetic description with components for fluid descriptions based on different level of sophistication and we test not only whether the predictions are still valid, but also whether the assumptions behind each reduced model is correct. Moreover, this can be done one component at a time, focusing on the effect of only replacing one component within a common code without worrying at the same time with having replaced a whole code with another. The approach proposed is a striking alternative to the classic approach of just validating closure relations by testing their predictions when applied in existing fluid codes. Here besides doing that, we also test directly the assumptions behind the closures, thanks to the availability of the more fundamental kinetic (or MD) level. This provides information on what is not valid in certain closures allowing us to improve them.

## 5 Implementation in Parsek

To implement the plan discussed above and demonstrate the feasibility of the plug and play approach for the validation of particle-based algorithms, we have developed a component based package called Parsek.

Parsek uses components for each of the four classes of components: particles, fields, interactions between particle and interactions between fields.

Each component is implemented in an object oriented language. We considered here Java and C++. Two approaches have been tested for object orientation: coarse grained or fine grained [4].

In the fine grained approach each object corresponds to the smallest physical entity: particle or cell. In the coarse grained approach each object represents

a population of the smallest physical entities: particle species or grid. The fine grained approach is composed of small objects and uses arrays of objects (or pointers to them) to describe the whole population of them (species for the particles and grid for the cells). The coarse grained approach, instead, uses arrays of native double precision numbers to represent the population and the whole population is the object. Figure 1-a illustrates the difference between these two approaches. The great advantage of the latter approach is the avoidance of arrays of objects (or pointers to them), resulting in a more efficient use of the cache on processors such as the Pentium family.

Figure 1-b proves indeed that a significant advantage can be gained by using a coarse grained approach. A similar study has been conducted in a previous study using similar Java implementations [4] and is reported in Fig. 1-b. For our pilot code Parsek, we settled on the coarse grained approach.

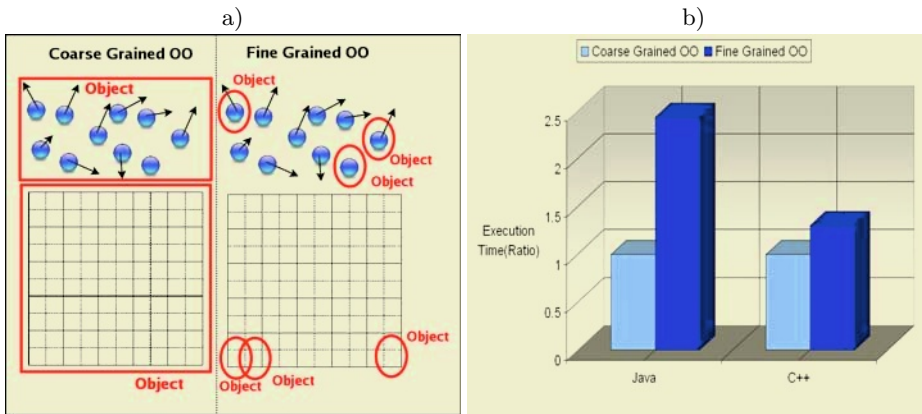


**Fig. 1.** Coarse grained and a fine grained object oriented versions (a). Comparison of fine and coarse object orientation performance in Java and C++ (b)

The computational challenge posed by the task under investigation (and particularly by the kinetic level) requires the use of a fully parallelized version of the algorithms. We adopted a 3D domain decomposition where portions of the systems including the cells and the particles in them are apportioned to a processor. The requirement to keep the particles and the cells belonging to the same physical domain in the same processor is due to the need to interpolate the information between particles and cells to compute the interactions. A consequence of this choice is the need to dynamically allocate the particles to the processors as the particles cross domain boundaries. In the examples considered here the system is 1D and is obtained as a limit of the 3D case by taking only once cell in the  $y$  and  $z$  direction and applying periodic boundary conditions.

We have considered two parallelization environments: message passing and multithreading. Message passing is a widely used programming paradigm and it is based on the use of libraries such as MPI. We have developed a version

of our software package, Parsek, in C++ using the MPI library to handle the communication. Figure 2 shows the scaling obtained in a typical problem by the C++/MPI version of Parsek. The test were conducted on a distributed memory cluster of INTEL Xeon processors.

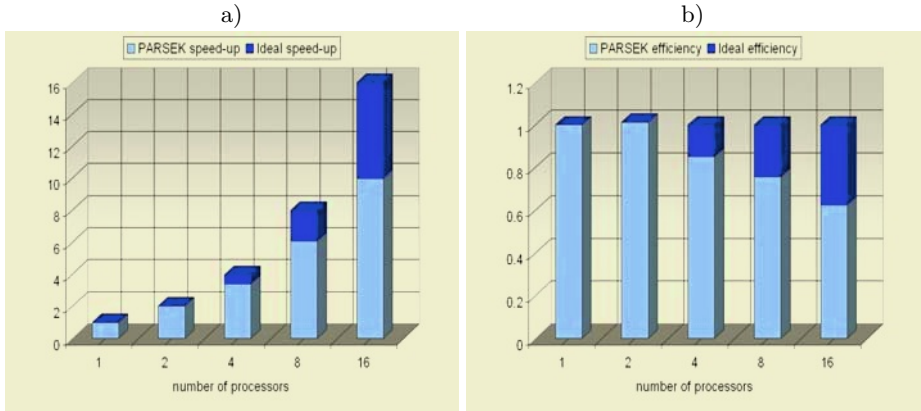


**Fig. 2.** Parallel speed-up (a) and parallel efficiency (b) of a C++ version with parallelization based on the MPI library. Study conducted on a distributed memory cluster

As an alternative, we considered also the multithreading approach typical of grid-based languages such as Java. The tests (not reported here) were conducted on a shared memory four processor SUN workstation and the observed scaling were very efficient. However, when the same approach is attempted on a cluster machine, native Java multithreading cannot be used and tools such as Java Party need to be used [5].

## References

1. L. Abrardi, G. Lapenta, C. Chang, *Kinetic theory of a gas mixture far from thermodynamic equilibrium: derivation of the transport coefficients*, LANL Report, LA-UR-03-8334.
2. S. Schleisinger, R.E. Crosbie, R.E. Gagne, G.S. Innis, C.S. Lalwani, J. Loch, R.J. Sylvester, R.D. Wright, N. Kheir, D. Bartos, *Terminology for Model Credibility, Simulation*, 32:103, 1997.
3. J.M. Burgers, *Flow equations for composite gases*, Academic Press, New York, 1969.
4. S. Markidis, G. Lapenta, W.B. VanderHeyden, Z. Budimlić, *Implementation and Performance of a Particle In Cell Code Written in Java*, **Concurrency and Computation: Practice and Experience**, to appear.
5. N. T. Padiyal-Collins, W. B. VanderHeyden, D. Z. Zhang, N. E. D. Dendy, D. Livescu, *Parallel operation of cartablanca on shared and distributed memory computers*, **Concurrency and Computation: Practice and Experience**, 16(1):61-77, 2004.

# Multiscale Angiogenesis Modeling

Shuyu Sun<sup>1</sup>, Mary F. Wheeler<sup>1</sup>,  
Mandri Obeyesekere<sup>2</sup>, and Charles Patrick Jr<sup>2</sup>

<sup>1</sup> The Institute for Computational Engineering and Sciences (ICES),  
The University of Texas at Austin, Austin, Texas 78712, USA

<sup>2</sup> The University of Texas (UT) M.D. Anderson Cancer Center, and  
The UT Center for Biomedical Engineering, Houston, Texas 77030, USA

**Abstract.** We propose a deterministic two-scale tissue-cellular approach for modeling growth factor-induced angiogenesis. The bioreaction and diffusion of capillary growth factors (CGF) are modeled at a tissue scale, whereas capillary extension, branching and anastomosis are modeled at a cellular scale. The capillary indicator function is used to bridge these two scales. To solve the equation system numerically, we construct a two-grid algorithm that involves applying a mixed finite element method to approximate concentrations of CGF on a coarse mesh and a point-to-point tracking method to simulate sprout branching and anastomosis on a fine grid. An analysis of the algorithm establishes optimal error bounds for each of the processes – CGF reaction-diffusion, capillary extension, sprout branching and anastomosis – and overall error bounds for their coupled nonlinear interactions.

## 1 Introduction

Angiogenesis is the outgrowth of new vessels from pre-existing vasculature, and it plays an important role in numerous clinical indications, including wound healing, tissue regeneration and cancer. A deep understanding of angiogenesis is critical for reparative strategies since the capillary network dictates tissue survival, hemodynamics, and mass transport. The angiogenic system is strongly nonlinear, possessing multiple, integrated modulators and feedback loops. This complexity limits the *in vitro* and *in vivo* experiments that may be designed and the amount of non-confounding information that can be gleaned. Consequently, computational models simulating the intercellular growth patterns of capillaries within a tissue are essential to understanding and analyzing these phenomena. However, most angiogenesis modeling approaches in the literature have been restricted to a single scale (e.g., see [1, 2, 3]), even though, in fact, the genetic, biochemical, cellular, biophysical and physiological processes in angiogenesis are intimately and tightly coupled across spatial and temporal dimensions.

## 2 Multiscale Angiogenesis Modeling Equations

In this section, we develop a deterministic two-scale tissue-cellular angiogenesis model. Let  $\Omega$  be a bounded domain in  $\mathbb{R}^d$  ( $d = 1, 2$  or  $3$ ) and  $T$  the final

simulation time. The capillary network is represented by an indicator binary function  $n = n(\mathbf{x}, t)$ . Denote by  $c_i$ ,  $i = 1, 2, \dots, N_{CGF}$ , the concentration of a species of capillary growth factors (CGF), where  $N_{CGF}$  is the number of CGF components.

## 2.1 A Tissue Scale Model for CGF Behaviors

We assume that CGF component  $j$  is released in the extracellular matrix at a rate  $\alpha_j$ . The diffusivity of CGF is denoted by  $\mathbf{D}_j$ , a general second order tensor, and the diffusive flux of CGF is  $\mathbf{q}_j = -\mathbf{D}_j \nabla c_j$ . The consumption (binding) of CGF by endothelial cells occurs only in the place where  $n = 1$ , and its rate is assumed to be proportional to the CGF concentration. Thus the consumption rate is  $\lambda_j n c_j$ , where  $\lambda_j$  is the consumption parameter of CGF  $j$ . We model the natural decay of CGF by a rate  $\lambda_j^* c_j$ . The mass balance of CGF yields the following equation:  $\partial c_j / \partial t = \nabla \cdot (\mathbf{D}_j \nabla c_j) + \alpha_j (1 - n) - \lambda_j n c_j - \lambda_j^* c_j$ .

## 2.2 A Cellular Scale Model for Capillary Dynamics

We model sprout extension by tracking the trajectory of individual capillary tips. We denote by  $\mathbf{p}_i(t) \in \mathbb{R}^d$  the position of capillary tip  $i$  at time  $t$ . Under certain biological conditions, cells behind the sprout tips undergo mitosis, and sprout extension subsequently occurs. The movement of an individual sprout tip during proliferation depends on the direction and speed of the sprout extension:  $d\mathbf{p}_i(t)/dt = \sum_j k_{p,j}(c_j) \mathbf{u}_{0,j}(\mathbf{q}_j)$ , where  $k_{p,j}$ , a function of CGF concentration  $c_j$ , represents the cell proliferation rate and  $\mathbf{u}_{0,j}$ , a normalized vector specifying the capillary outgrowth direction, is a function of the corresponding diffusive flux. We consider general functions  $k_{p,j}(\cdot)$  and  $\mathbf{u}_{0,j}(\cdot)$  in this paper.

We denote by  $S$  the set of all active capillary tips. The behaviors of capillaries are described by the movement of the tips, which includes sprout extension and the changes of the tip set by branching and anastomosis. The tip set  $S$  remains unchanged during capillary extension, but it is modified at branching or anastomosis because these events change the number of elements in  $S$ .

In capillary branching, we terminate the parent capillary tip label and start two new labels for the two resultant daughter tips. We denote the branching trigger function by  $f_{BT}(\tau, c_1, c_2, \dots, c_{N_{CGF}})$  and assume that the sprout branches as soon as  $f_{BT}(\tau, c_1, c_2, \dots, c_{N_{CGF}}) \geq 0$ , where  $\tau$  is the age of the capillary tip and  $c_i = c_i(\mathbf{p}, t)$  is the CGF concentration at the location occupied by the capillary tip. For example,  $f_{BT}(\tau, c_1, c_2, \dots, c_{N_{CGF}}) = \tau - \tau_a$  specifies uniform sprout branching, where every sprout performs branching after maturing for the length of time  $\tau_a$ . Mathematically, sprout branching increases the number of elements in the tip set  $S$  and is denoted by  $S(t^+) = B(S(t^-))$ .

Anastomosis, the fusion of capillary sprouts, is assumed to occur when a sprout tip meets another sprout tip physically (tip-to-tip anastomosis) or a sprout tip joins another sprout physically (tip-to-sprout anastomosis). After a tip-to-sprout anastomosis, the tip cell forms a part of the loop and no longer undergoes sprout extension, i.e. the tip no longer exists. We distinguish two types



of tip-to-tip anastomosis: in a “head-on-head” anastomosis, both tips become inactive, whereas in a “shoulder-on-shoulder” anastomosis, only one of the two tips becomes inactive. Mathematically, the anastomosis mechanism decreases the number of elements in the tip set  $S$  and is written as  $S(t^+) = A(S(t^-))$ .

### 2.3 Bridging Cellular and Tissue Scales

The CGF concentration profile strongly influences sprout extension, branching and anastomosis, all of which control the development of a capillary network. The capillary network, in turn, affects the bioreaction and diffusion of CGF. The capillary indicator function  $n$  is determined by the history of sprout tip positions. We define the set  $N_C(t)$  occupied by the capillary network at time  $t$  as  $N_C(t) = \bigcup_i \bigcup_{\tau \leq t} \mathbf{B}_{r_{EC}}(\mathbf{p}_i(\tau))$ , where  $\mathbf{B}_{r_{EC}}(\mathbf{x}) = \{\hat{\mathbf{x}} : |\hat{\mathbf{x}} - \mathbf{x}| \leq r_{EC}\}$ . The radius of an endothelial cell  $r_{EC}$  is assumed to be constant. The capillary indicator function may be written as  $n = \chi_{N_C}$ , where  $\chi_E$  is the standard set characteristic function, i.e.  $\chi_E(\mathbf{x}) = 1$  for  $\mathbf{x} \in E$  and  $\chi_E(\mathbf{x}) = 0$  otherwise.

### 2.4 A Modified Model Based on Cell Level Averaging

With initial and boundary conditions, the previous equations in this section represent a mathematical system for two-scale modeling of angiogenesis. In this paper, we analyze a modified system, which is based on cell level averaging:

$$\frac{\partial c}{\partial t} = -\nabla \cdot (\mathbf{q}) + \alpha(1 - n) - \lambda n c - \lambda^* c, \quad (1)$$

$$\mathbf{q} = -\mathbf{D}\nabla c, \quad (2)$$

$$\frac{d\mathbf{p}_i}{dt} = \mathcal{M}_S(k_p(c)\mathbf{u}_0(\mathbf{q})), \quad \forall i \in S, \quad (3)$$

$$n = \mathcal{M}_S(\chi_{N_C}(\{\mathbf{p}_i : i \in S\})), \quad (4)$$

$$S(t^+) = A(B_{\mathcal{M}}(S(t^-))). \quad (5)$$

We only consider a single CGF species here for simplicity of presentation, though the analysis of multiple CGF species is a straightforward extension. The averaging operator (or the mollifier)  $\mathcal{M}_S$  is defined for  $f \in L^1(0, T; L^1(\Omega))$  by  $\mathcal{M}_S(f)(\mathbf{x}, t) = \int_{\mathbf{B}_{r_{EC}}(\mathbf{x}) \cap \Omega} f(\hat{\mathbf{x}}, t) d\hat{\mathbf{x}} / \text{meas}(\mathbf{B}_{r_{EC}}(\mathbf{x}) \cap \Omega)$ , where  $\text{meas}(\cdot)$  denotes the Lebesgue measure. The stabilized branching operator  $B_{\mathcal{M}}$  is formed from the original branching operator  $B$  by replacing  $c$  by  $\mathcal{M}_S c$  in  $f_{BT}(\tau, c)$ . We note that  $\mathcal{M}_S$  may be viewed as a modification operator to reflect averaged information collected by a tip cell.

We consider the boundary condition  $\mathbf{q} = 0$  on  $\partial\Omega$  and the initial condition  $c = c_0$  at  $t = 0$  for the CGF concentration. We impose the following initial conditions for capillary tips:  $S = S_0$  and  $\mathbf{p}_i = \mathbf{p}_{i,0}$  at  $t = 0$ . We note that, by using algebraic equations, anastomosis and branching are described as instantaneous events, whereas sprout extension is modeled as a continuous-in-time process using ordinary differential equations (ODEs). Since the number of elements in the set  $S$  changes with time, the number of unknowns in the system varies with time.

### 3 A Two-Grid Algorithm

A mixed finite element (MFE) method is employed to approximate the CGF diffusion-reaction equation on a concentration grid. We trace the trajectory of each capillary tip using a standard ODE solver. A point-to-point tracking method is proposed to simulate sprout branching and anastomosis, where algebraic conditions are applied for branching, and geometric conditions are checked for anastomosis. While the concentration grid is a mesh at the tissue scale, the capillary network forms a secondary grid at the cellular scale. Locally conservative  $L^2$  projections are used for data transfer between the two grids when needed.

Let  $(\cdot, \cdot)_D$  denote the  $L^2(D)$  inner product over a domain  $D \subset \mathbb{R}^d$  for scalar functions or the  $(L^2(D))^d$  inner product for vector functions, and, when  $D = \Omega$ , we drop the subscript. Let  $\|\cdot\|_{L^p(D)}$ ,  $1 \leq p \leq \infty$ , be the  $L^p(D)$  norm for a scalar function or the  $(L^p(D))^d$  norm for a vector function. Similarly, let  $\|\cdot\|_{H^s(D)}$  be the standard  $H^s(D)$  norm or the  $(H^s(D))^d$  norm. Throughout this paper, we denote by  $C$  a generic positive constant that is independent of  $h$  and by  $\epsilon$  a fixed positive constant that may be chosen to be arbitrarily small. We define the following standard spaces: (1)  $W = L^2(\Omega)$ ; (2)  $\mathbf{V} = H(\text{div}; \Omega) = \{\mathbf{v} \in (L^2(\Omega))^d : \nabla \cdot \mathbf{v} \in L^2(\Omega)\}$ ; (3)  $\mathbf{V}^0 = \{\mathbf{v} \in H(\text{div}; \Omega) : \mathbf{v} \cdot \nu = 0 \text{ on } \partial\Omega\}$ , where  $\nu$  denotes the outward unit normal vector on  $\partial\Omega$ . The weak formulation of the CGF diffusion-reaction equation is to find  $c \in W$  and  $\mathbf{q} \in \mathbf{V}^0$  such that  $c(x, 0) = c_0(x)$  and  $\forall w \in W, \forall \mathbf{v} \in \mathbf{V}^0, \forall t \in (0, T]$ :

$$\left( \frac{\partial c}{\partial t}, w \right) = (-\nabla \cdot \mathbf{q}, w) + (\alpha(1-n) - (\lambda n + \lambda^*)c, w), \quad (6)$$

$$(\mathbf{D}^{-1}\mathbf{q}, \mathbf{v}) = (c, \nabla \cdot \mathbf{v}). \quad (7)$$

We let  $\mathcal{E}_h = \{E_i\}$  denote a partition of  $\overline{\Omega}$  into elements  $E_i$  (for example, triangles or parallelograms if  $d = 2$ ) whose diameters are less than or equal to  $h$ . Let  $(W_h, \mathbf{V}_h) \subset (W, \mathbf{V})$  be a mixed finite element space of order  $r$  that possesses an associated projection operator  $\Pi_h : \mathbf{V} \rightarrow \mathbf{V}_h$  satisfying: (1)  $\nabla \cdot \mathbf{V}_h = W_h$ ; (2)  $(\nabla \cdot \Pi_h \mathbf{q}, w) = (\nabla \cdot \mathbf{q}, w), \forall \mathbf{q} \in \mathbf{V}, \forall w \in W_h$ ; (3)  $\|\Pi_h \mathbf{q} - \mathbf{q}\|_{L^2(\Omega)} \leq C \|\mathbf{q}\|_{H^s(\Omega)} h^{\min(r+1, s)}$ ; (4)  $\|\mathcal{P}_h c - c\|_{L^2(\Omega)} \leq C \|c\|_{H^s(\Omega)} h^{\min(r+1, s)}$ , where  $\mathcal{P}_h$  is the  $L^2$  projection from  $W$  onto  $W_h$ :  $(\mathcal{P}_h c, w) = (c, w), \forall c \in W, \forall w \in W_h$ . Obviously, we have  $\nabla \cdot \Pi_h \mathbf{q} = \mathcal{P}_h \nabla \cdot \mathbf{q}, \forall \mathbf{q} \in \mathbf{V}$ . The continuous-in-time mixed finite element method for approximating the CGF diffusion-reaction equation is to find  $c_h(t) \in W_h$  and  $\mathbf{q}_h(t) \in \mathbf{V}_h^0 = \mathbf{V}^0 \cap \mathbf{V}_h$  such that  $\forall w \in W_h, \forall \mathbf{v} \in \mathbf{V}_h^0, \forall t \in (0, T]$ :

$$\left( \frac{\partial c_h}{\partial t}, w \right) = (-\nabla \cdot \mathbf{q}_h, w) + (\alpha(1-n_h) - (\lambda n_h + \lambda^*)c_h, w), \quad (8)$$

$$(\mathbf{D}^{-1}\mathbf{q}_h, \mathbf{v}) = (c_h, \nabla \cdot \mathbf{v}), \quad (9)$$

$$(c_h(\cdot, 0), w) = (c_0(\cdot), w). \quad (10)$$

We denote by  $c_h, \mathbf{q}_h, \mathbf{p}_h$  and  $n_h$  the finite element solutions for the CGF concentration, the CGF diffusive flux, the capillary tip positions and the capillary

indicator function respectively. We first analyze the error of the CGF concentration assuming that the error of the capillary indicator function is given:

**Theorem 1. (CGF bioreaction-diffusion)** *We assume that  $c \in L^2(0, T; H^s(\Omega))$ ,  $\partial c / \partial t \in L^2(0, T; H^s(\Omega))$  and  $\mathbf{q} \in (H^s(\Omega))^d$ . We further assume that the diffusivity tensor  $\mathbf{D}$  is uniformly symmetric positive definite and bounded from above, that  $c$  is essentially bounded, that parameters  $\lambda$  and  $\lambda^*$  are nonnegative, and that parameters  $\alpha$  and  $\lambda$  are bounded. Then, for any given  $\epsilon > 0$ , there exists a constant  $C$  independent of the mesh size  $h$  such that*

$$\begin{aligned} & \|c_h - c\|_{L^2(0, T; L^2(\Omega))} + \|\mathbf{q}_h - \mathbf{q}\|_{L^2(0, T; L^2(\Omega))} \\ & \leq C \left( \|c\|_{L^2(0, T; H^s(\Omega))} + \left\| \frac{\partial c}{\partial t} \right\|_{L^2(0, T; H^s(\Omega))} + \|\mathbf{q}\|_{L^2(0, T; H^s(\Omega))} \right) h^{\min(r+1, s)} \\ & \quad + \epsilon \|n_h - n\|_{L^2(0, T; L^2(\Omega))}. \end{aligned} \quad (11)$$

*Proof.* We let  $c_I = \mathcal{P}_h c$  and  $\mathbf{q}_I = \Pi_h \mathbf{q}$ , and define the finite element error  $E_c = c_h - c$ , the projection error  $E_c^I = c_I - c$ , and the auxiliary error  $E_c^A = c_h - c_I$ . Similarly,  $E_{\mathbf{q}} = \mathbf{q}_h - \mathbf{q}$ ,  $E_{\mathbf{q}}^I = \mathbf{q}_I - \mathbf{q}$ ,  $E_{\mathbf{q}}^A = \mathbf{q}_h - \mathbf{q}_I$ . We also define  $E_n = n_h - n$ .

Subtracting (6) and (7) from (8) and (9) respectively, splitting  $E_c$  and  $E_{\mathbf{q}}$  according to  $E_c = E_c^I + E_c^A$  and  $E_{\mathbf{q}} = E_{\mathbf{q}}^I + E_{\mathbf{q}}^A$ , and choosing  $w = E_c^A$  and  $\mathbf{v} = E_{\mathbf{q}}^A$ , we observe

$$\left( \frac{\partial E_c^A}{\partial t}, E_c^A \right) = (-\nabla \cdot E_{\mathbf{q}}, E_c^A) - ((\lambda c + \alpha)E_n, E_c^A) \quad (12)$$

$$- ((\lambda n_h + \lambda^*)E_c, E_c^A) - \left( \frac{\partial E_c^I}{\partial t}, E_c^A \right), \quad t \in (0, T],$$

$$(\mathbf{D}^{-1} E_{\mathbf{q}}^A, E_{\mathbf{q}}^A) = (E_c, \nabla \cdot E_{\mathbf{q}}^A) - (\mathbf{D}^{-1} E_{\mathbf{q}}^I, E_{\mathbf{q}}^A), \quad t \in (0, T]. \quad (13)$$

Recalling the orthogonality of projections  $\mathcal{P}_h$  and  $\Pi_h$ , we add the two error equations (12) and (13) to obtain, for any  $t \in (0, T]$ ,

$$\left( \frac{\partial E_c^A}{\partial t}, E_c^A \right) + (\mathbf{D}^{-1} E_{\mathbf{q}}^A, E_{\mathbf{q}}^A) + ((\lambda n_h + \lambda^*)E_c^A, E_c^A) \quad (14)$$

$$= -((\lambda c + \alpha)E_n, E_c^A) - ((\lambda n_h + \lambda^*)E_c^I, E_c^A) - \left( \frac{\partial E_c^I}{\partial t}, E_c^A \right) - (\mathbf{D}^{-1} E_{\mathbf{q}}^I, E_{\mathbf{q}}^A).$$

We note that, as a binary function,  $n_h$  must be non-negative and bounded. We bound the right hand side of (14) using Cauchy-Schwarz inequality, the boundedness of  $\lambda$ ,  $c$ ,  $\alpha$  and  $n_h$ , and the orthogonality, and then we rewrite the left hand side of (14) in forms of the  $L^2$  norm to conclude:

$$\begin{aligned} & \frac{1}{2} \frac{d}{dt} \|E_c^A\|_{L^2(\Omega)}^2 + \left\| \mathbf{D}^{-\frac{1}{2}} E_{\mathbf{q}}^A \right\|_{L^2(\Omega)}^2 + \left\| (\lambda n_h + \lambda^*)^{\frac{1}{2}} E_c^A \right\|_{L^2(\Omega)}^2 \\ & \leq \epsilon \|E_n\|_{L^2(\Omega)}^2 + C \|E_c^A\|_{L^2(\Omega)}^2 + \epsilon \left\| \mathbf{D}^{-\frac{1}{2}} E_{\mathbf{q}}^A \right\|_{L^2(\Omega)}^2 \\ & \quad + C \left( \|c\|_{H^s(\Omega)}^2 + \|\mathbf{q}\|_{H^s(\Omega)}^2 \right) h^{2\min(r+1, s)}. \end{aligned} \quad (15)$$

Noting that the finite element solution at  $t = 0$  is an  $L^2$  projection, i.e.  $c_h(0) = \mathcal{P}_h c_0$ , we have  $E_c^A(0) = 0$ . We first integrate (15) with respect to the time  $t$ , and apply Gronwall's inequality. Then recalling the triangle inequality and the approximation results of projection operators  $\Pi_h$  and  $\mathcal{P}_h$ , we establish the theorem.  $\square$

We now estimate the error on capillary networks. Denote by  $J = (t_0, t_F]$  the capillary tip life time period, where the final time of the capillary tip  $t_F$  is the time when the tip becomes inactive due to either branching or anastomosis, or is the final simulation time  $T$ , whichever is shorter. Due to page limitation, we list Lemmas 1–4 below without detailed proofs. Applications of the triangle inequality and Gronwall's inequality give the error bound on capillary extension (Lemma 1). Exploration of the sprout branching stability condition leads to its error estimate (Lemma 2). Geometric analysis results in the error bound on anastomosis (Lemma 3). A straightforward manipulation of the set of the capillary network establishes an  $L^\infty$  upper bound on the error of the capillary indicator function (Lemma 4). Based on the four lemmas, the approximations of overall capillary behaviors are concluded in Theorem 2. The error estimate for the coupled system is finally obtained in Theorem 3 as a consequence of individual error bounds on the CGF concentration and capillary behaviors.

**Lemma 1. (Capillary extension)** *We assume that  $c$  is bounded, that  $k_p(c)$  is a Lipschitz continuous function of  $c$ , and that  $\mathbf{u}_0(\mathbf{q})$  is a Lipschitz continuous function of  $\mathbf{q}$ . Then, there exists a constant  $C$  independent of the mesh size  $h$  such that  $\|\mathbf{p}_h - \mathbf{p}\|_{L^1(J)} \leq C \|\mathbf{p}_{0,h} - \mathbf{p}_0\| + C |t_{0,h} - t_0| + C \|\mathbf{q}_h - \mathbf{q}\|_{L^1(0,T;L^1(\Omega))} + C \|c_h - c\|_{L^1(0,T;L^1(\Omega))}$ , where  $\mathbf{p}$  is the position of an individual capillary tip,  $\mathbf{p}_0$  and  $t_0$  are the initial position and initial time when the tip is formed, and  $\mathbf{p}_h$ ,  $\mathbf{p}_{0,h}$  and  $t_{0,h}$  are their approximate solutions respectively.*

**Lemma 2. (Sprout branching)** *We assume that the branching trigger function  $f_{BT}(\tau, c)$  is a uniformly Lipschitz function of  $c$  with a Lipschitz constant  $C_L$ , and there is a positive constant such that  $\partial f_{BT}/\partial \tau \geq C_0 > 0$ . We further assume that  $\partial c/\partial t \in L^\infty(0, T; L^1(\Omega))$ ,  $\nabla c \in L^\infty(0, T; L^1(\Omega))$  and  $d\mathbf{p}/dt \in L^\infty(J)$ . If  $C_L/C_0$  is sufficiently small, there exists a constant  $C$  independent of the mesh size  $h$  such that  $|t_{B,h} - t_B| + \|\mathbf{p}_{B,h} - \mathbf{p}_B\| \leq C |t_{0,h} - t_0| + C \|\mathbf{p}_h - \mathbf{p}\|_{L^1(J)} + C \|c_h - c\|_{L^1(0,T;L^1(\Omega))}$ , where  $t_B$  and  $t_0$  are the sprout branching time and the tip birth time of the capillary under consideration, and  $t_{B,h}$  and  $t_{0,h}$  are their approximate solutions respectively.*

**Lemma 3. (Anastomosis)** *We assume that the intersecting angle  $\theta_A$  of the two parent capillaries  $i$  and  $j$  at the location of anastomosis satisfies  $C_0 \leq |\sin \theta_A| \leq 1 - C_0$ , where  $0 < C_0 < 1/2$  is a fixed small constant. We further assume that there exists a constant  $C_1$  such that  $|d\mathbf{p}/dt| \geq C_1 > 0$  in the neighborhoods of the anastomosis location. In addition, we assume that  $d\mathbf{p}_i/dt$  and  $d\mathbf{p}_j/dt$  are bounded. Then there exists a constant  $C$  independent of the mesh size  $h$  such that  $|t_{A,h} - t_A| + \|\mathbf{p}_{A,h} - \mathbf{p}_A\| \leq C \|\mathbf{p}_{i,h} - \mathbf{p}_i\|_{L^1(J_i)} + C \|\mathbf{p}_{j,h} - \mathbf{p}_j\|_{L^1(J_j)}$ , where  $t_A$  is the time of anastomosis, and  $\mathbf{p}_A$  the location of anastomosis.*

**Lemma 4. (Capillary indicator function)** *We assume that the exact total capillary length is bounded. Then there exists a constant  $C$  independent of the mesh size  $h$  such that  $\|n_h - n\|_{L^1(0,T;L^1(\Omega))} \leq C \sum_i \|\mathbf{p}_{i,h} - \mathbf{p}_i\|_{L^1(J_i)}$ .*

**Theorem 2. (Capillary behavior)** *Let the assumptions in Lemmas 1–4 hold. In addition, we assume that the number of capillaries from the exact solution is bounded. Then there exists a constant  $C$  independent of the mesh size  $h$  such that*

$$\|n_h - n\|_{L^1(0,T;L^1(\Omega))} \leq C \left( \|\mathbf{q}_h - \mathbf{q}\|_{L^1(0,T;L^1(\Omega))} + \|c_h - c\|_{L^1(0,T;L^1(\Omega))} \right). \tag{16}$$

*Proof.* Combining Lemmas 1, 2 and 3, using the assumption on the boundedness of the capillary number, and noting that a  $L^1(0, T; L^1(\Omega))$  norm of a function is no greater than its  $L^\infty(0, T; L^1(\Omega))$  norm, we obtain  $\sum_i \|\mathbf{p}_{i,h} - \mathbf{p}_i\|_{L^1(J_i)} \leq C \|\mathbf{q}_h - \mathbf{q}\|_{L^1(0,T;L^1(\Omega))} + C \|c_h - c\|_{L^1(0,T;L^1(\Omega))}$ . The theorem follows from this inequality and Lemma 4.  $\square$

**Theorem 3. (Final result on overall error bound)** *Let the assumptions in Theorems 1 and 2 hold. Then there exists a constant  $C$  independent of the mesh size  $h$  such that*

$$\|c_h - c\|_{L^1(0,T;L^2(\Omega))} + \|\mathbf{q}_h - \mathbf{q}\|_{L^2(0,T;L^2(\Omega))} + \|n_h - n\|_{L^1(0,T;L^1(\Omega))} \leq Ch^{\min(r+1,s)}. \tag{17}$$

*Proof.* Recalling that the constant  $\epsilon$  in (11) may be chosen to be arbitrarily small, we let  $\epsilon = 1/(2C)$ , where  $C$  is the constant in (16). Observe that the  $L^2(0, T; L^2(\Omega))$ ,  $L^1(0, T; L^1(\Omega))$ , and  $L^\infty(0, T; L^1(\Omega))$  norms of a function are less than or equal to its  $L^\infty(0, T; L^\infty(\Omega))$ ,  $L^2(0, T; L^2(\Omega))$  and  $L^\infty(0, T; L^2(\Omega))$  norms, respectively. The overall error bound follows from Theorems 1 and 2.  $\square$

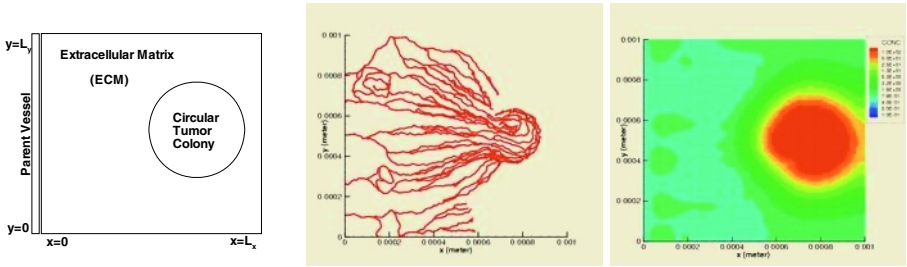


**Fig. 1.** An angiogenesis simulation example. Left: domain geometry; Middle: capillary network at 28 days; Right: CGF concentration map ( $\times 10^{-16} \text{mol/m}^2$ ) at 28 days

We now present a numerical example simulating tumor-induced angiogenesis (illustrated in Fig. 1). All modeling parameters are taken from [4] except that the tumor colony is represented by a large CGF release rate:  $\alpha = 6.42 \times 10^{-18}$  mol/m<sup>2</sup>s in the tumor area and  $\alpha = 6.42 \times 10^{-21}$  mol/m<sup>2</sup>s in the remaining extracellular matrix (ECM). The CGF is released from both the ECM and the tumor cells, but substantially more so from the latter. Clearly, endothelial cells at the capillary sprout tips are migrating from the parent vessel to the right, toward the tumor colony, as induced by the CGF concentration gradient. The simulation produces capillary networks with realistic structures and morphologies. Readers are referred to [4, 5, 6] for more simulation results.

## 4 Conclusions

We have presented a deterministic two-scale model to simulate angiogenesis, where CGF bioreaction and diffusion at a tissue scale are coupled with capillary extension, branching and anastomosis at a cellular scale. To solve the coupled angiogenesis system, we have proposed a two-grid numerical algorithm based on MFE on a coarse mesh and a point-to-point tracking method on a fine grid. Optimal order error estimates have been derived for the proposed scheme. The model generates an overall dendritic structure of the capillary network morphologically similar to those observed *in vivo*, and captures significant vascular patterning, such as vascular loops and backward growth. Clearly, experimental work is needed to enhance and verify the model.

## Acknowledgment

Supported in part by a grant from the University of Texas Center for Biomedical Engineering.

## References

1. A. R. A. Anderson and M. A. J. Chaplain. Continuous and discrete mathematical models of tumor-induced angiogenesis. *Bull. Math. Biol.*, 60:857–900, 1998.
2. M. A. J. Chaplain. The mathematical modelling of tumour angiogenesis and invasion. *Acta Biotheor.*, 43:387–402, 1995.
3. H. A. Levine, S. Pamuk, B. D. Sleeman, and M. Nilsen-Hamilton. Mathematical modeling of capillary formation and development in tumor angiogenesis: Penetration into stroma. *Bull. Math. Biol.*, 63:801–863, 2001.
4. S. Sun, M. F. Wheeler, M. Obeyesekere, and C. W. Patrick Jr. A deterministic model of growth factor-induced angiogenesis. *Bull. Math. Biol.*, 67(2):313–337, 2005.
5. S. Sun, M. F. Wheeler, M. Obeyesekere, and C. W. Patrick Jr. Deterministic simulation of growth factor-induced angiogenesis. In *Proceedings of American Institute of Chemical Engineers 2004 Annual Meeting*, Austin, Texas, November 7-12, 2004.
6. S. Sun, M. F. Wheeler, M. Obeyesekere, and C. W. Patrick Jr. Nonlinear behavior of capillary formation in a deterministic angiogenesis model. In *Proceedings of the Fourth World Congress of Nonlinear Analysts*, Orlando, Florida, June 30 - July 7, 2004.

# The Simulation of a PEMFC with an Interdigitated Flow Field Design

S.M. Guo

Dept. Mechanical Engineering,  
Louisiana State University,  
Baton Rouge, LA 70803, USA  
+1 225 578 7619  
sguo2@lsu.edu

**Abstract.** This paper presents the simulations for a two-dimensional PEMFC with an interdigitated flow channel design using FEMLAB. The multi-species flow of  $O_2$ ,  $H_2$ ,  $H_2O$  and inert  $N_2$  is examined over the entire fuel cell working range. The transportations of these gases in the porous anode/cathode are predicted using the Maxwell-Stefan transport equations and the Fick's law; the flow field is predicted using the Darcy's law; and the electrical field is simulated using a conductive media model. The standard current-voltage performance curve, the species concentration of  $O_2$ ,  $H_2$ ,  $H_2O$  and inert  $N_2$ , mass fluxes, electrical current and potential distributions have been obtained.

## 1 Introduction

Fuel cells are electrochemical devices, which utilize fuel and oxidant to produce electricity and heat [1]. Because the fuel is converted chemically to electricity, fuel cells may operate at higher efficiencies than conventional internal combustion engines. Fuel cells are classified by the electrolytes. The common electrolyte of a Proton Exchange Membrane Fuel Cell (PEMFC) is a thin layer of proton permeable polymer membrane. In a PEMFC system, the coupled physical and electrochemical processes take place. Transport resistances of the gaseous species in the feeding channels and the porous electrodes lead to the so-called concentration over-potential; the transportation of  $H^+$  in the electrolyte layer forms a large portion of ohmic loss; the activation energy barriers for the electrochemical reactions are related to the charge-transfer processes at the electrode-electrolyte interfaces. The theoretical potential of a hydrogen/oxygen cell, operating under standard conditions of 1 bar and  $25^\circ C$ , is about 1.2 volt. However, due to losses, the voltage of a single cell is much less than its theoretical value.

The PEMFC flow-field, including the feeding channels and the porous electrodes, has a significant influence to the cell performance. The performance of a fuel cell is often described by its current-voltage ( $I-E$ ) relationship. Fuel, such as hydrogen, and small amount of water vapor are supplied to the PEMFC anode side. Due to the electrochemical reactions, steam forms at the cathode. For a typical planar PEMFC design, feeding channels are provided by the bipolar plates with a typical serpentine

or parallel channel structure. Due to the long channels, serpentine flow-fields have large pressure losses between the inlet and the outlet. Although straight parallel design exhibits lower pressure differences, inhomogeneous reactant gas distribution can easily occur. These flow channels must distribute fuel and air over the reaction sites and remove the products. Recently, a number of novel flow channels have been proposed for Proton Exchange Membrane Fuel Cells, in order to address the PEMFC mass transport and water management problems. The most promising design is the interdigitated flow field design [2,3,4]. Figure 1 shows the schematic drawing of this design. The flow channels are dead-ended, forcing gas to flow through the porous diffusion layer. Comparing to the flow in a conventional straight parallel flow field design, the use of the interdigitated fuel/air distributors imposes a pressure gradient between the inlet and the outlet channels, forcing the convective flow of the fuel/oxidant through the porous electrodes. Thus the interdigitated design in effect converts the transport of gases to/from the Triple Phase Boundary (TPB) active sites, along the interface between the electrodes and electrolyte, from a diffusion dominated mechanism to a forced convection dominated mechanism. The convective flow through the porous electrode reduces the gas diffusion distance to and from the reaction sites. By having fuel/oxidant flow over the shoulders of the gas distributor, the electrode active area over the shoulder is used more effectively. The shear force of the gas stream helps removing the water condensate, which is entrapped in the electrode layer, thereby reducing the flooding problem. This design has been proven to be very effective by some experimental studies. Wang et al. [3] presented an experimental study of PEM fuel cells with interdigitated flow fields under different operation parameters. Nguyen [4] presented a comparative experimental study of fuel cells with interdigitated flow fields and parallel straight channel flow fields. They reported that the interdigitated flow design could extend the PEMFC operable regime to higher current densities and consequently, a 50-100% increase in the fuel-cell performance could be obtained as a result of the use of interdigitated fuel/air distributors. To study a fuel cell performance mathematically, especially for a design with thick porous electrodes and a strong convective flow, a proper mass transport model must be applied. At high current density, the losses are dominated by the limitation of transport the fuel/oxidant to the reaction sites, the so-called concentration or mass transport over-potential. Mass transport in the porous electrodes depends on the structure of the porous electrodes, such as the porosity, tortuosity and mean pore size. Washak et al. [5] and Suwanwarangku et al. [6] conducted comparative studies using the Fick's law and the Dusty Gas Model for a Solid Oxide Fuel Cell. They found that the current density, the reactant concentration and the pore size were the three key parameters for choosing a proper porous media simulation model. The Dusty Gas Model works better for the  $H_2-H_2O$  and  $CO-CO_2$  systems, especially under high operating current densities, low reactant concentrations and small pore sizes.

To perform a parametrical optimization for the flow field design, multiphysics based numerical simulation offers many advantages comparing to the experimental approach.

The aim of this paper is to study the effect of using different mass transport models on the fuel cell performance simulation. Two models are examined in this paper. The first one is the Fick's model, and the second model applies the Stefan-Maxwell



diffusion equations to the mixture. The performance of a PEMFC with an interdigitated flow channel design was simulated using FEMLAB. The simulation includes the multi species transportation in the porous electrodes and the coupled electrical current and potential distributions.

## 2 The Simulation Model

FEMLAB is a commercial Partial Differential Equation (PDE) solver, which can solve coupled multi-physical problems. Partial differential equations are the governing equations for most physical phenomena and provide the foundation for modeling a wide range of scientific and engineering problems. There are three ways of describing PDEs in FEMLAB, coefficient form, general form and the weak form. The coefficient form is suitable for linear or nearly linear models and the rest two are suitable for nonlinear models. FEMLAB runs finite element analysis to solve the PDEs, together with adaptive meshing and error controls.

The simulation domain used in this paper is a 2-dimensional cross section of an interdigitated PEMFC flow field, shown in Figure 1. The oxidation of hydrogen and the reduction of oxygen take place at the anode and cathode side reaction boundaries respectively. Electrons are transported to an outer circuit at the anode and received at the cathode because only proton ions can pass through the electrolyte membrane.

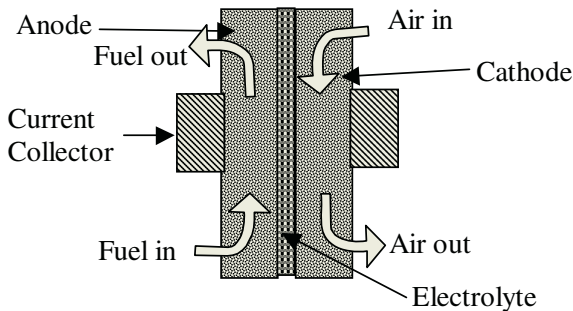
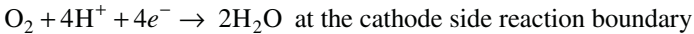
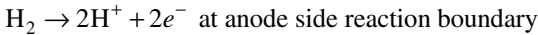


**Fig. 1.** Interdigitated Flow Field Design

The thickness of the anode and cathode is set to be 0.25 mm and the height is set to be 2 mm; the electrolyte layer has a thickness of 0.1 mm. Along the height direction, current collectors of 1 mm in length are in contact with the outer surface of the anode and cathode in a symmetrical manner, leaving the inlet and outlet ports a dimension of 0.5 mm. Hydrogen and an inert gas mixture is fed into the anode side inlet port while oxygen, inert nitrogen and water are fed into the cathode side. The gas mixtures are treated as incompressible due to the low flow velocities. In the simulation, the

hydrogen is oxidized along the electrode/electrolyte interface, which has a zero thickness. The electrical potential of the PEMFC is specified as an input parameter over the entire working range.

A set of PEMFC governing equations is specified in FEMLAB. Equation 1 is the steady state continuity equation.

$$\nabla \bullet (CV) = 0 \tag{1}$$

Where  $C$  is the total gas mixture molar concentration;  $V$  is the velocity;  $CV$  is the total molar flux. For continues gas phase flow in the porous electrodes, Darcy’s law, Equation 2, is used.

$$V = -\frac{k_p}{\mu} \nabla P \tag{2}$$

Where,  $k_p$  is the permeability of the medium,  $\mu$  is the dynamic viscosity of the gas mixture,  $\nabla P$  gives the pressure gradient.

For the multi species mass transfer in the electrodes, both Fick’s law and the Maxwell-Stefan diffusion and convection mass transfer models were tested. Using the Fick’s law, the diffusion flux in the porous electrodes is calculated using equation 3.

$$N^d = -D^e \nabla C \tag{3}$$

$D^e$  is the effective diffusivity of the gas,  $C$  is the concentration. By assuming equal counter-current molar fluxes, according to Chan et al. [7], the composition independent  $D^e$  can be found in Eq. 4

$$D_1^e = \left( \frac{1}{D_{12}^e} + \frac{1}{D_{1k}^e} \right)^{-1} \tag{4}$$

$D_{12}^e$  is the effective binary bulk diffusion coefficient.  $D_{1k}^e$  is the effective Knudsen diffusion coefficient, which depends on temperature and structure of the porous material. For a convective flow in a porous medium, combining the diffusive and convective fluxes, the flux equation can be written as equation 5.

$$N = -\left( \frac{1}{D_{12}^e} + \frac{1}{D_{1k}^e} \right)^{-1} \nabla C - \frac{X_1}{RT} \frac{k_p P}{\mu} \nabla P \tag{5}$$

For the simulation using the Maxwell-Stefan diffusion and convection model. The Maxwell-Stefan multi-component diffusion is given in equation 6.

$$\frac{\partial}{\partial t} \rho \omega_i + \nabla \bullet \left[ -\rho \omega_i \sum_{j=1}^N D_{ij} \left\{ \begin{array}{l} \frac{M}{M_j} \left( \nabla \omega_j + \omega_j \frac{\nabla M}{M} \right) \\ + (x_j - \omega_j) \frac{\nabla P}{p} \end{array} \right\} + \omega_i \rho u + D_i^T \frac{\nabla T}{T} \right] = R_i \tag{6}$$

where  $D_{ij}$  is the diffusion coefficient ( $\text{m}^2/\text{s}$ ),  $P$  the pressure (Pa),  $T$  is the temperature (K),  $u$  the velocity vector ( $\text{m}/\text{s}$ ),  $x$  and  $\omega$  are mole and mass fractions. The density,  $\rho$  ( $\text{kg}/\text{m}^3$ ), is calculated based on the mole fractions and mole masses of gas species.

At inlet, pressure and the feeding gas mass fractions are specified. At the outlets, a convective flux boundary condition is applied. The local current density is a function of the local species concentration, physical structure of the electrodes and the specified cell output electrical potential. For steady state calculations, due to the conservation of current, the anode side current density is the same as the current density at the cathode. At the anode and cathode reaction boundary, the species mass transfer is related to the local current density according to:  $-n \bullet n_{H_2} = -\frac{i_a}{2F}$  at anode reaction boundary and  $-n \bullet n_{O_2} = \frac{i_c}{4F}$  at the cathode reaction boundary.

The potential difference between the cathode and anode current collectors represents the cell voltage. In the simulation, the potential at the anode current collector was arbitrarily chosen to be zero, while the cell voltage at the cathode current collector is set as a fixed boundary condition. The potential distributions in the anode, cathode and the electrolyte are modeled as conductive media using equation 7.

$$\nabla \bullet (-k \nabla E) = 0 \quad (7)$$

where  $k$  is the effective conductivity (S/m) and  $E$  is the potentials in the calculation domain. The rest of the boundaries were set as the electrical insulators or as a symmetrical boundary. Normal to the reaction boundary,  $n \bullet (-k \nabla E)$  gives the current density.

### 3 Results and Discussions

The  $I$ - $E$  performance curve of a PEMFC has been obtained using two different mass transfer models, Fick's model and the Maxwell-Stefan model. Figure 2 shows a typical fuel and oxidant distribution inside a PEMFC with an interdigitated flow field design (see Fig.1 for feeding directions). A 60%  $H_2$  is fed to the anode side (left half) and a 21%  $O_2$  is fed to the cathode (right half) inlet port.

As expected, the Fick's model results show discrepancies to the Maxwell-Stefan model results in the high current density region, see Fig. 3. Start at about  $3000 \text{A}/\text{m}^2$ , Fick's law started to over-predict the current density at fixed cell output electrical potentials. At the high current end, the difference between these two models is about 15%. This is mainly caused by the over prediction of the oxygen concentration at the cathode side reaction boundary. The oxygen concentration at the inlet is 21%. Due to the electrical chemical reactions along the cathode/electrolyte boundary, the oxygen concentration at the reaction sites is far less than the inlet value, see Fig. 2. Figure 4 shows the predicted oxygen concentration average along the cathode reaction boundary under different current densities using those two models. The difference between the two models is obvious at the high current region, where the Fick's model predicts a higher  $O_2$  concentration. Figure 5 shows the production of water due to the

electrochemical reactions. The curve shows a strong linear relationship between the water formation and the current density.

The definition of anode side  $H_2$  concentration is based on the hydrogen partial pressure. Because of the electrochemical reactions, hydrogen depletes along the flow direction. The mass transport process affects the local concentration of fuel. Hydrogen concentration reduces almost linearly with the increase of current density. At about  $6500 A/m^2$ , the right end of the curve, the hydrogen mass transfer in the porous anode reaches its limiting current density.

The commercial FEMLAB software has many built-in multi physics models. However, the advantage of a general software package, which claims to solve “many” physical problems, is also likely to be its weakness. The build-in models are generally

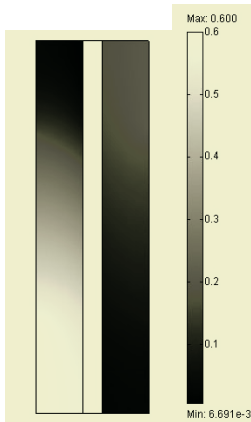


**Fig. 2.** A typical  $H_2$  (left) and  $O_2$  (right) concentration in the PEMFC

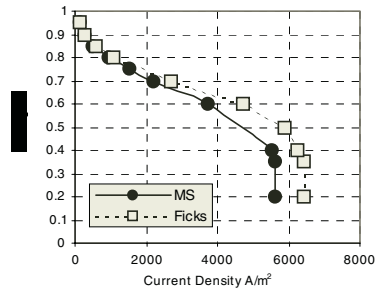


**Fig. 3.** PEMFC  $I$ - $E$  curves predicted using the Fick’s model and the Maxwell-Stefan model

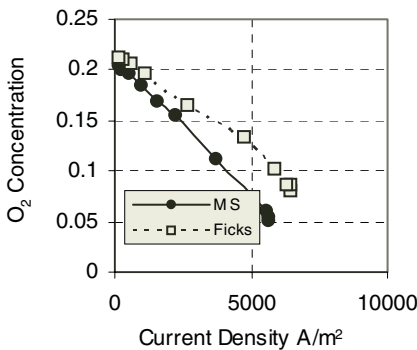


**Fig. 4.** PEMFC cathode reaction boundary  $O_2$  concentration predicted using the Fick’s model and the Maxwell-Stefan model

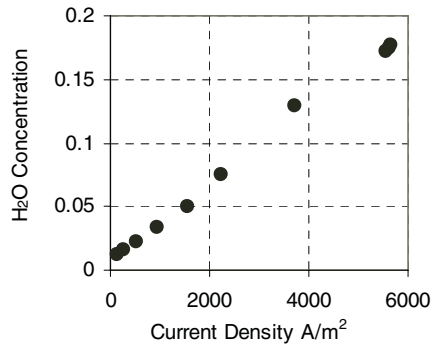


**Fig. 5.** PEMFC cathode reaction boundary  $H_2O$  concentration as a function of cell current density

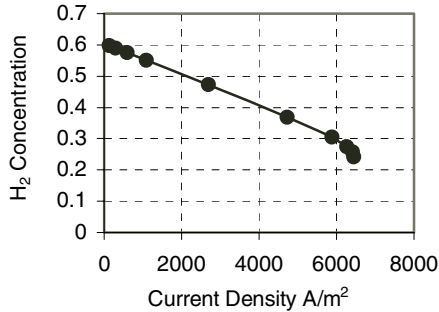


**Fig. 6.** PEMFC anode reaction boundary H<sub>2</sub> concentration

to be the basic physical and mathematical models for a particular physical problem. For example, because only Darcy's law was used in the simulation to predict the fluid flow in the porous electrodes, the accuracy near the reaction boundaries is not expected to match the accuracy of a well-tuned CFD case, which uses Navier-Stokes equations with proper turbulent models. To solve a real multi-physical problem, a balanced approach must be carefully taken. The number of physical phenomena, to be modelled in software, must be considered in conjunction with the expected overall accuracy and the available computing power.

## 4 Conclusions

In the past two decades, due to the energy shortage and the environmental concerns, great efforts have been put into fuel cell research. To improve the fuel cell performance, multiphysics analysis could be employed. Using proper fuel cell models, fuel cell simulations could provide detailed understanding and solutions on how to reduce the losses and how to improve the operating efficiency. Comparing with an experimental based approach, computational simulations are low cost and could quickly provide the physical understandings to a particular fuel cell design. The PEMFC flow-field, including feeding channels and porous electrodes, has significant influence to the cell performance. The local concentration of fuel and oxidant is affected by the mass transport processes, which include the mixing of multiple gases in the porous anode/cathode, the reactions of fuel and oxygen and the transportation of fuel and electrochemical products near the reaction sites. This paper presents the numerical simulations of gas transport in the porous electrodes of a PEMFC with an interdigitated flow channel design using FEMLAB. The simulation is a coupled fluid dynamics and electrical potential field problem with multi species mass transfer and chemical reactions. This complicated PEMFC problem has been solved using FEMLAB over the entire working range. Two porous media mass transport models, the Fick's Model and the Maxwell-Stefan model were used in the simulations for multi-species of O<sub>2</sub>, H<sub>2</sub>, H<sub>2</sub>O and inert N<sub>2</sub>. The standard current-voltage performance curve and the detailed species concentration, mass fluxes, electrical current and

potential distributions have been obtained. The simple but less accurate Fick's model is validated against the Maxwell-Stefan model. Fick's model was found to over-predict the oxygen concentration along the cathode side reaction boundary and thus over-predict the cell performance in the high current density region.

## References

1. Larminie, J., Dicks, A., Fuel cell systems explained, Wiley, ISBN: 047084857x, (2003)
2. Jung, S. Y., Nguyen, T.V., Multicomponent Transport in Porous Electrodes of Proton Exchange Membrane Fuel Cells Using the Interdigitated Gas Distributors, *Journal of The Electrochemical Society*, v 146, n1, 1999, p 38-45
3. Wang, L., Liu, H., Performance studies of PEM fuel cells with interdigitated flow fields, *Journal of Power Sources*, 134, p185-196, (2004)
4. Nguyen, T.V., Gas distributor design for proton-exchange-membrane fuel cells, *J. Electrochem. Soc.* 143, n 5, p L103-L105, (1996)
5. Washak, H., Guo, S.M., Turan, A., 2005, Gas Transport in Porous Electrodes of Solid Oxide Fuel Cells, the Ninth International Symposium on Solid Oxide Fuel Cells (SOFC IX), The 207th Meeting of The Electrochemical Society, Québec City Convention Centre, May 15-20, 2005
6. Suwanwarangkul, R., Croiset, E., Fowler, M.W., Douglas, P.L., Entchev, E., Douglas, M.A., Performance comparison of Fick's, dusty-gas and Stefan–Maxwell models to predict the concentration overpotential of a SOFC anode, *Journal of Power Sources* **122** 9-18, (2003)
7. Chan, S.H., Khor, K.A., Xia, Z.T., A complete polarization model of a solid oxide fuel cell and its sensitivity to the change of cell component thickness, *Journal of Power Sources*, **93**, 130-140, (2001)

# Multiscale Modelling of Bubbly Systems Using Wavelet-Based Mesh Adaptation

Tom Liu and Phil Schwarz

CSIRO Minerals, Clayton, VIC 3168, Australia  
{Tom.Liu, Phil.Schwarz}@CSIRO.AU

**Abstract.** Since typical industrial-scale reactors may contain many millions of bubbles, the extension of direct free-surface modelling techniques to resolve every bubble in the vessel would require far more computational power than will be available. A more immediate solution is to couple macro-scale reactor models to micro-scale models of individual bubbles and collections of a small number of bubbles. In this paper, a micro-scale modelling technique was presented and tested on the situation of a single rising bubble. The micro-scale model was based on the Volume-of-Fluid (VOF) technique combined with a dynamic mesh adaptation based on wavelet analysis to ensure a sufficient resolution at the gas-liquid interfaces. The method was based on a multi-block parallel scheme with mesh adaptivity facilitated by wavelet analysis embedded into a commercial CFD package CFX. Examples of the performance of the scheme for a bubble rising problem are given.

## 1 Introduction

Bubbly systems are used widely in the minerals and process industries to increase agitation, supply reactants (e.g. oxygen), or to effect particle separations (as in froth flotation). Effective two-fluid (or phase-averaged) modelling techniques have been developed to simulate the multi-phase fluid flow, and heat and mass transfer in such reactors, and are now widely used to assist vessel design [1,2]. These methods do not seek to resolve each bubble, but are based volume-averaged equations in which the physics of bubble-fluid interactions is modelled through constitutive terms analogous to the Reynolds stresses that appear in the RANS equations for a single phase turbulent flow. This necessarily reduces the accuracy and predictive capability of such models, and increases their dependence on empirical data and fitting parameters, particularly in cases where bubble-bubble interactions such as coalescence are important. However, in practice, it is difficult to develop accurate constitutive relations for complex systems valid over wide operating ranges using physical experiments.

A computationally efficient solution to improving the macro-scale multi-fluid models is to couple them to micro-scale models of individual bubbles and collections of a small number of bubbles. The strategy is to determine improved closure relationships for the multi-fluid model through the analysis of the micro-scale models. Where phenomena occur at widely differing scales, the numerical analysis may be employed to analyse some particular processes at fine scales, for instance, the breakup of a single bubble,

coalescence of two or more bubbles, or bubble-particle interactions. The information obtained at fine scales can be applied in macroscale CFD or other models.

This approach has advantages over the experimental determination of constitutive relationships because physical information on the processes, e.g. shear rate dependency of the viscosity or stress field, can be obtained locally and analysed in detail. The numerical simulations used in this way may be called numerical experiments [3], though they should be viewed as the complementary to physical experiments, rather than a substitute.

The fine scale simulations differ from traditional macroscale CFD simulations used in reactor design in that more attention is paid to local information and a very fine mesh must be used to resolve full detail of interactions between the flow and the phase boundaries. If fixed meshes are employed in a traditional CFD simulation for solving practical engineering problems, the full representations of fine scale phenomena are difficult or even impossible for the foreseeable future because of the overwhelming computational costs [4]. Therefore an alternative approach that is more efficient must be developed.

Micro-scale modellings (or numerical experiments) for multiphase problems generally involve moving interfaces between immiscible fluids. The accurate simulation of fluid flows with sharp fronts presents a problem with considerable difficulties [5]. Many types of interface tracking methods have been developed, but they generally fall into two categories. In the first type, a deformable finite volume or finite element mesh is used such that a particular mesh boundary moves so that it always coincides with the interface [6]. The other strategy is to keep the mesh fixed and use a separate procedure to describe the position of the interface. These methods are reviewed in [7]. The interface can be represented on a fixed grid in a variety of ways, either explicitly or implicitly. The Volume of Fluid method (VOF) is one of the most popular implicit interface tracking schemes [5]. Physical problems which are considered in practice require three-dimensional calculations with surface tension, non-catastrophic breakage and reconnection of the interface. The VOF technique naturally allows for the latter, and has been modified by various workers to include surface tension.

Commercial software packages such as CFX and FLUENT are usually employed to model practical multiphase flows due to the complexities of the phenomena and the geometries. Although mesh adaptation has been provided by the commercial CFD packages, they generally do not allow for dynamic mesh adaptation [8]. If a mesh sufficiently fine to resolve detail near the interface is applied on the whole geometry, the computational requirements can be huge. Such a fine mesh is not necessary on most of the geometry, but because of the movement of the interface, the localized mesh refinement requires a dynamic mesh adaptation.

The largest difficulty with adaptive methods is to determine the mobility of grids. Adaptive wavelet methods have been developed to solve Navier-Stokes equation at high Reynolds numbers [9]. Wavelets have the ability to accurately and efficiently represent strongly inhomogeneous piecewise continuous functions [10]. Using such techniques, the numerical resolution can be naturally adapted to intermittent the structures of flows at fine scales with significant decrease of computational efforts and memory requirements. However, efforts have been mainly made around using wavelets as an orthogonal and complete basis, spanning a space in which to seek approximate solutions satisfying the equation in a Galerkin or collocation sense [4, 9]. To



apply such methods however would require the development of a new program for each particular flow-related problem, whereas general-purpose commercial CFD packages are preferred.

Hesteven and Jameson [4] developed a different approach to utilise the unique properties of wavelets, and this approach can be applied in a grid-based method utilized by CFD packages. In this method, wavelets were employed to detect the existence of high frequency information and supplied spatial locations of strongly inhomogeneous regions. Very fine grids were used only in these regions. In this method, wavelets were used for grid generation and order selection only, whilst the scheme for solving the partial differential equation was based on conventional finite difference/element schemes, albeit defined on variable grids. The method provides a possibility to embed the wavelet-based grid generation into current commercial CFD packages to reduce computational costs by using adaptive meshes.

In this paper, a multi-block (domain) parallel scheme with the adaptivity facilitated by wavelet analysis was proposed and embedded into commercial CFD package CFX to track moving free surfaces efficiently.

## 2 Wavelet Analysis and Wavelet-Based Grid Adaptation

Wavelet analysis is an emerging field of applied mathematics that provides tools and algorithms suited to the type of problems encountered in multiphase process simulations. It allows one to represent a function in terms of a set of base functions, called wavelets.

Wavelet transform involves representing general functions in terms of simple, fixed building blocks at different scales and positions. These building blocks, which are actually a family of wavelets, are generated from a single fixed function called the “mother wavelet” by translation and dilation (scaling) operations. In contrast to the traditional trigonometric basis functions which have an infinite support, wavelets have a compact support. Therefore wavelets are able to approximate a function without cancellation. In the basic work of Daubechies [10], a family of compactly supported orthonormal wavelets is constructed. Each wavelet number is governed by a set of  $L$  (an even integer) coefficients  $\{p_k : k = 0, 1, \dots, L - 1\}$  through the two-scale relation:

$$\phi(x) = \sum_{k=0}^{L-1} p_k \phi(2x - k) \quad (1)$$

and the equation:

$$\psi(x) = \sum_{k=2-L}^1 (-1)^k p_{1-k} \phi(2x - k) \quad (2)$$

where functions  $\phi(x)$  and  $\psi(x)$  are called scaling function and wavelet, respectively. The fundamental support of the scaling function  $\phi(x)$  is in the interval  $[0, L - 1]$  while that of the corresponding wavelet  $\psi(x)$  is in the interval  $[1 - L/2, L/2]$ . The

coefficients  $p_k$  appearing in the two-scale relation (1) are called wavelet filter coefficients. All wavelet properties are specified through these coefficients. For more details see Daubechies' paper [10].

Interpolating functions are generated by the autocorrelation of the usual compactly supported Daubechies scaling functions [11]. Such an autocorrelation function  $\theta(\cdot)$  verifies trivially the equality  $\theta(n) = \delta_{0n}$ , and generates a multi-resolution analysis. The approximate solution of the problem  $u_j(\cdot)$  defined on interval  $[0, 1]$  is written in terms of its values in the dyadic points:

$$u_j(x) = \sum_n u_j(2^{-j}n)\theta(2^j x - n) \tag{3}$$

and such a function is exact at the dyadic points.

Consider the function:

$$\theta(x) = \int_{-\infty}^{+\infty} \phi(y)\phi(y - x)dy \tag{4}$$

Denote  $V_j$  the linear span of the set  $\{\theta(2^j x - k), k \in Z\}$ . It can be proven that  $V_j$  forms a multi-resolution analysis where  $\theta(\cdot)$  plays the role of a scaling function (nonorthonormal). In this paper, a modified interpolating function was constructed in order to achieve an interpolating operator on the interval with the same accuracy as the counterpart on the line. Such functions were introduced by Bertoluzza and Nald [11].

$$\tilde{\theta}_{j0} = \sum_{k=-L+1}^0 \theta_{jk}, \quad \tilde{\theta}_{j,2^j} = \sum_{k=2^j}^{2^j+L+1} \theta_{jk}$$

Consider  $I_j u$  as the form:

$$I_j u = u(0)\tilde{\theta}_{j0} + \sum_{k=1}^{2^j-1} u(x_k)\theta_{jk} + u(1)\tilde{\theta}_{j2^j} \tag{5}$$

The sparse point representation (SPR) and the grid generation technique based on Holmstorm's work [12] were employed for grid adaptation. The SPR was based on interpolating wavelet transform (IWT) on dyadic grids. A feature of the basis is the one-to-one correspondence between point values and wavelet coefficients. The interpolating subdivision scheme recursively generated the function values on a fine grid from the given values on a coarse grid. At each level, for odd-numbered grid points, the differences between the known function values and the function values predicted by the interpolation from the coarser grid were calculated. These differences were termed as wavelet coefficients  $d_k^j$ , which gave the information about the irregularity of the function:  $d_k^j = u(x_{2k+1}^{j+1}) - I^j u(x_{2k+1}^j)$ .

### 3 Problem Definition and Method Formulation

Wavelet-based adaptive methods have been successfully applied to solve many problems [13, 9]. The grids were adapted based on the change of the solutions. Fine meshes were assigned only on the regions where the solutions changed sharply. However, for current CFD commercial packages, e.g. CFX, there is a restriction to the dynamic mesh adaptation: the topology of the mesh must remain fixed. Therefore, the advantages of wavelet-based grid adaptation cannot be fully utilised at this stage. A modified wavelet-based mesh adaptation methodology was proposed in this section.

Wavelet-based grid generation supposes a calculation which begins with evenly spaced samples of a function. It has usually been applied to simple geometries and structured grids [11]. To combine wavelet analysis with CFX commercial CFD package, a multi-block (domain) formulation was proposed. A moving cubic subdomain or block with fine mesh was designed to track the free surface and combined the geometric flexibility and computational efficiency of a multi-block (domain) scheme with the wavelet-based mesh adaptivity. The moving block was like a “microscope” - it was used to track local information required. Coarse mesh was employed outside the moving block (subdomain). Therefore the scheme was computationally efficient without loss of accuracy.

To clearly describe the scheme, a simple case, a single rising bubble, was considered. Two algorithms were proposed as follows: wavelet-based adaptive structured grid using junction box routines; wavelet-based adaptive unstructured grid using CFX expression language and junction box routines

#### 3.1 Problem Definition

A numerical experiment was designed by Krishna and Baten [14] to simulate the single bubble rising process using CFX 4. A 2D rectangular column (25mm × 90mm) involving 144000 grid cells was used. It took about two weeks using six R8000 processors for a simulation run.

In this paper, the same configuration was modelled using CFX 5.7. The only difference was that a wavelet-based mesh adaptation algorithm was embedded into the CFX package so that a moving fine-mesh block was used to track the bubbles. This technique used only 10% of the number of grid cells that would be required for a uniform mesh to obtain similar accuracy.

The simulation was carried out in a rectangular column using 2D Cartesian coordinate grid. No-slip wall boundary condition was imposed, and the column was modelled as an open system. The VOF model was employed to describe transient motion of the gas and liquid phases using the Navier-Stokes equations. Surface tension was included. For the convective terms, high resolution differencing was used. First order backward Euler differencing was used for time integration. The time step used in the simulation was 0.00003s or smaller.

#### 3.2 Wavelet-Based Adaptive Structured Grid Using Junction Box Routines

CFX-MESHBUILD was used to generate the initial structured mesh consisting of five blocks. To utilise wavelet analysis, the proposed moving fine-mesh block must be

either a cube or a rectangle. The initial size and position of the block depends on those of the bubble at initial time, see Table 1. Therefore the proposed mesh adaptation method can be applied in a complex geometry. The mesh distribution of block B1 was chosen as uniform grid  $(2^7+1) \times (2^6+1)$  to apply wavelet analysis. Because the bubble extended in x-direction significantly during the process, higher resolution was used in this direction. The mesh distributions of other blocks can be different. For simplicity, the same distributions were given for the shared edges and uniform grids were chosen, see Figure 1 and Table 2.

**Table 1.** Initial bubble/block size and position

Initial Bubble (Diameter) / Block	Initial Bubble / Block Positions (Centre)
4mm / (6mm×6mm)	(12mm, 4mm) / (12mm, 4mm)
8mm / (10mm×10mm)	(12mm, 6mm) / (12mm, 6mm)

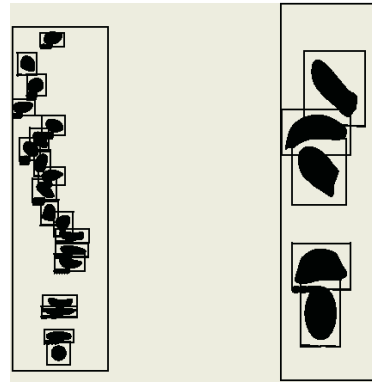
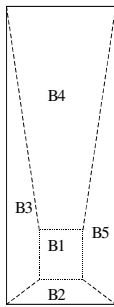


**Fig. 1.** Geometry and blocks of the bubble rising column

**Fig. 2.** Snapshots of typical rising trajectories of bubbles of 4 and 8 mm diameter and B1

**Table 2.** Distributions of blocks

	Distribution of B1	Distributions of B2 and B4	Distributions of B3 and B5	Ratio of adaptive mesh to full mesh
4mm bubble	$(2^7+1) \times (2^6+1)$	$2^7 \times 2^5$	$2^6 \times 2^5$	0.08
8mm bubble	$(2^7+1) \times (2^6+1)$	$2^7 \times 2^5$	$2^6 \times 2^5$	0.08

Using CFX 5.7, the volume fractions on the vertices of each cell can be obtained. Due to the limitation of CFX solver, the topology of the mesh must remain fixed. Points cannot be added to or removed from the grid. Only the position of free interface was detected using IWT and wavelet coefficients. At each mesh adaptation time step, the minimum distances between the interface and the boundaries of block B1

was calculated to decide if the position and size of B1 should be changed and a new grid was generated. The algorithm is as follows:

Step 1. Calculate the wavelet coefficients of volume fraction of gas in x-direction from the top and bottom rows of B1 to determine the nearest position between the interface and the top or bottom boundaries of B1. The IWT and wavelet coefficients are calculated from level 6 to level 7 on each row. If most of the wavelet coefficients on one row are larger than the threshold  $\varepsilon$ , e.g. 80% of the total number on one row, this means the interface is on or near the position.

Step 2. Calculate the wavelet coefficients of volume fraction of gas in y-direction from the left and right columns of B1 to determine the nearest position between the interface and the left or right boundaries of B1 using the same method in Step 1.

Step3. If all the distances between the interface and the boundaries of B1 are larger than given minimum distance  $d_p$ , the mesh remains fixed; Otherwise, move the boundaries of B1 to the positions until the distances between the interface and the boundaries are not less than  $d_p$ .

Step 4. Set limits to the position of block B1 to avoid mesh folding. There should be a given minimum distance between B1 and the boundaries of the column.

Step 5. Generate a new uniform mesh based on the new position of B1 for each block using the same distribution as that of the initial mesh and pass the new grid to CFX.

The block B1 was moved based on the wavelet analysis of the volume fraction function of gas. Therefore, the bubble was always in B1. There is a correlation between the frequency of the grid adaptation and the tolerance distance between the interfaces and the boundaries of B1 when the adaptation is performed. If the grid adaptation is not done often enough, a larger tolerance distance must be given so that the front does not move out of B1 between the adaptations. Conversely, more frequent adaptations demand a small distance.

It is natural to define the parallel computation partitions based on five blocks. In this work, three partitions were defined, partition 1 including B1, partition 2 including B2 and B3, partition 3 including B3 and B4. Partition 1 was calculated on master machine. The whole grid was determined based on partition1 and passed to slave machines.

In practice, unstructured grids are often used in complex geometries. The proposed method can also be applied to unstructured grids using CFX expression language and junction box routines together. The method has been used for the same simulation as described above.

## 4 Simulation Results

The simulations were run on a Linux system. Snapshots of typical bubble trajectories are shown in Fig 2. They were similar to the results of Krishna and Baten [13]. Figure 2 clearly showed how the fine mesh moves with the bubble. It confirmed the ability to use the wavelet analysis within a multi-block framework to achieve considerable savings in computing time without loss of accuracy. The number of grid cells was

reduced by 90%. The CPU time of the adaptive mesh method was only 1/8 that of the method using the fully fine mesh.

## 5 Conclusions

A wavelet-based adaptive mesh scheme was embedded into a commercial CFX package to track moving free surfaces. It significantly saves computational cost and memory requirements. The scheme was demonstrated in a single bubble rising simulation. A moving “microscope” was designed to reveal details of local information with a realistic computing time. The scheme provides the possibility to design some numerical experiments to analyse processes at a fine scale and utilise the local information obtained in macroscale models. Further work to apply the method in such a scheme is underway.

## References

1. Lane, G.L., Schwarz, M.P., Evans, G.M.: Predicting gas-liquid flow in a mechanically stirred tank. *Applied Mathematical Modelling* 26 (2002) 223-235
2. Schwarz, M.P.: Simulation of gas injection into liquid melts. *Applied Mathematical Modelling* 20 (1995) 41-51
3. Ohta, M., Iwasaki, E., Obata, E., Yoshida, Y.: A numerical study of the motion of a spherical drop rising in shear-thinning fluid systems. *Journal of Non-Newtonian Fluid Mechanics* 116 (2003) 95-111
4. Hesthaven, J.S., Jameson, L.M.: A wavelet optimized adaptive multi-domain method. ICASE Report No.97-52, NASA Langley Research Centre, Hampton, 1997
5. Unverdi, S.O., Tryggvason, G.: A front-tracking method for viscous, incompressible multi-fluid flows. *Journal of Computational Physics* 100 (1992) 125-137
6. Drew, D.A.: Mathematical modelling of two-phase flow. *Annual Review of Fluid Mechanics* 15 (1983) 261-271
7. Sethian, J.A.: *Level Set Methods*. Cambridge University Press, Cambridge, UK 1996.
8. CFX User Guide. Release 5.7, 2004, ANSYS Canada Ltd, Waterloo, Canada
9. Vasilyev, O., Paolucci, S.: A fast adaptive wavelet collocation algorithm for multidimensional PDEs. *Journal of Computational Physics* 138 (1997) 16-56
10. Daubechies, I.: Orthonormal bases of compactly supported wavelets. *Communication on Pure and Applied Mathematics* 41 (1988) 909-996
11. Bertoluzza, S., Naldi, G.: A wavelet collocation method for the numerical solution of partial differential equations. *Applied and Computational Harmonic Analysis* 3 (1996) 1-9
12. Holmstrom, M.: Solving hyperbolic PDEs using interpolating wavelets. *SIAM Journal on Scientific Computing* 21 (1999) 405-420
13. Santos, P.C., Cruz, P., Magalhaes, F.D., Mendes, A.: 2-D wavelet-based adaptive-grid method for the resolution of PDEs. *AICHe Journal* 49 (2003) 706-717
14. Krishna, R., Baten, J.M.: Rise characteristics of gas bubble in a 2D rectangular column: VOF simulations vs experiments. *Int. Commn. Heat Mass Transfer* 26 (1999) 965-974

# Computational Study on the Effect of Turbulence Intensity and Pulse Frequency in Soot Concentration in an Acetylene Diffusion Flame

Fernando Lopez-Parra and Ali Turan

School of Mechanical, Aerospace and Civil Engineering,  
The University of Manchester, Po Box 88,  
M60 1QD, Manchester, UK  
F.Lopez-Parra@postgrad.umist.ac.uk

**Abstract.** A computational investigation of the effect of turbulence structure in the formation and depletion of soot in non-premixed acetylene turbulent diffusion flames is presented. Two separate modelling approaches are investigated: 1. Realizable  $k-\varepsilon$  turbulence model combined with non-adiabatic strained laminar flamelets to solve the reaction mechanisms accounting for the effect of non-equilibrium species and, 2. Standard  $k-\varepsilon$  turbulence model and Eddy-Break-Up –EBU-with volumetric global reaction and Eddy-Dissipation model for chemistry. In both cases the results obtained show that increments in the input Reynolds number yield lower concentrations of soot. It was also found that low frequency sinusoidal pulse in the fuel inlet velocity can contribute to further reduce the soot concentration in the flame. The soot and nuclei source codes were solved as post-processed scalars and considered to be “passive” species.

## 1 Introduction

The main objective of the present work is the creation of a mathematical subroutine that would reproduce a soot model based on the eddy dissipation concept of Magnussen<sup>1-5</sup> and that can be implemented into a commercial solver. The performance of the sub-routine is tested with a 2-dimensional axi-symmetric diffusion acetylene flame. Over the last few decades, there has been a growing interest in the modeling of particulates from combustion systems. Although the mechanisms of soot formation are not completely understood, the behavior of this carcinogenic<sup>6,7</sup> specie has been computationally reproduced in the past with an acceptable degree of accuracy<sup>1-5,8-10</sup>. There are two differentiated stages in which soot forms<sup>11</sup>: the inception of the particles for which soot will ultimately form *-nucleation-* and the subsequent growth of these particles. The growth of the carbonaceous particles takes place in two different stages, referred to as the agglomeration and the surface growth. Soot originates from the  $C_2$  radicals that form as a consequence of the break down *-pyrolysis-* of the fuel molecule. In turbulent chemical reactions, there is a strong influence of the flow parameters in the performance of the combustion. As a result, an inhomogeneous structure of the appearance of reacting species will develop. In these situations, the molecular mixing of the fuel and oxidant, which is highly intermittent, takes inside the fine

structures, which occupy a fraction of the total volume of the domain. These are believed to be three-dimensional vortex tubes of very small dimensions in one or two directions, but not in the other one. These are vortex are of the same characteristic dimensions as the Kolmogorov structures<sup>13</sup>. These regions for the last link in the turbulence energy transfer cascade, and in modeling environments, it is assumed that fuel and oxidant are perfectly mixed. In general, high turbulent flows of high Reynolds number would present a spectrum of eddies of different sizes. These eddies transfer mechanical energy to their immediate neighbors and the interaction between the larger and the smaller eddies represents the main source of production of turbulence kinetic energy. On the other hand, the dissipation of kinetic energy into heat, due to the work done by molecular forces on the eddies, takes place in the smallest eddies.

The mass fraction occupied by the fine structures is given by

$$\gamma^* = 9.7 \cdot \left( \frac{\nu \cdot \mathcal{E}}{k^2} \right)^{0.75} \quad (1)$$

where  $k$  is the turbulent kinetic energy -TKE-, where  $\nu$  is the kinematic viscosity and  $\mathcal{E}$  is the turbulence dissipation rate -TDR .

The mass transfer per unit mass and unit time between the fine structures and the surrounding fluid is expressed by

$$\dot{m} = 23.6 \left( \frac{\nu \cdot \mathcal{E}}{k^2} \right)^{0.25} \frac{\mathcal{E}}{k} \quad (2)$$

Due to the reaction taking place within the fine structures, these will have a higher temperature with respect to the local mean temperature. The increment of temperature,  $\Delta T$ , is computed as

$$\Delta T = \frac{\Delta H_R \cdot c_{\min}}{\rho \cdot c_p} \quad (3)$$

where  $\Delta H_R$  is the heat of reaction of the fuel,  $\rho$  is the density,  $c_p$  is the local specific heat capacity of the mixture and  $c_{\min}$  is the minimum of  $c_{fu}$  and  $c_{o_2}/r_{fu}$ , where  $c_{fu}$  and  $c_{o_2}$  are the gravimetric concentrations of fuel and oxygen respectively and  $r_{fu}$  is the gravimetric oxygen requirement to burn 1kg of fuel.

In the Magnussen model, the fine structures and the surrounding fluid are assumed to be in local equilibrium and the concentration of species in the fine structures and the surrounding fluid are related to the local mean concentrations by

$$\frac{c_i}{\rho} = \frac{c_i^*}{\rho^*} \gamma^* \chi + \frac{c_i^o}{\rho^o} (1 - \gamma^* \chi) \quad (4)$$

where  $\chi$  is a local variable that accounts for the fraction of fine structures that are actually heated enough to react and  $c$  is the concentration of species.



After defining all the preliminary and more relevant variables in the model, the mean nuclei and soot formation rates are expressed as follows

$$R_{n,f} = \left( n_o^* \frac{\gamma^* \chi}{\rho^*} + n_o^o \frac{1-\gamma^* \chi}{\rho^o} + g_o n^* \frac{\gamma^* \chi}{\rho^*} (N^o - N^*) \right) \rho + (f-g) \cdot Y_{nuc} \cdot \rho - g_o \rho N^o Y_{nuc} \quad (5)$$

$$R_{s,f} = m_p \left( a \cdot Y_{nuc} \cdot \rho + b N^* \frac{\gamma^* \chi}{\rho^*} \rho (n^o - n^*) \right) - \beta n^o Y_{soot} \quad (6)$$

where  $Y_{nuc}$  and  $Y_{soot}$  are the mass fractions of nuclei and soot,  $N$  is the soot particle concentration and  $(f-g)$  is the nuclei branching-termination coefficient and  $a$ ,  $b$  and  $g_o$  are model constants.

The mean rates of nuclei and soot oxidation are comparable to the rate of fuel combustion.

$$R_{pollut,c} = \dot{m} \cdot \chi \cdot c_{min} \frac{Y_{pollut}}{Y_{fu}} \quad (7)$$

The net rates of nuclei and soot formation were computed by subtracting the rate of combustion from the rate of formation. The resulting equation was used as the source term for soot and nuclei in the user-defined function written for FLUENT. One of the major challenges presented in was the appropriate selection of a linearization term. Source terms in FLUENT are written as a two-part variable, with well differentiated implicit and explicit sides, e.g.  $S_\phi = A + B\phi$ , where  $\phi$  would be the dependent variable and  $A$  and  $B\phi$  would be the explicit and implicit parts respectively. FLUENT automatically determines whether the given expression for  $B$  enhances the stability and if this is not the case, the source term is handled explicitly. In current work, algebraic manipulation of the expressions given above yielded the separate explicit and implicit terms required for the simulation.

This soot model also relies in the correct specification of the model constants. Whereas some of these are rather universal, the soot particle diameter,  $d_p$ , and the pre-exponential constant for nucleation,  $a_o$  need to be adjusted for different flow conditions. In the present work, the two following expressions have been used, combined with the experimental measurements of Magnussen<sup>5</sup> to determine these parameters for each case:

$$\dot{m} \cdot a_o = \text{constant} \quad (8)$$

$$d_p = \frac{D \cdot c_{fu,o}^{1.6}}{U_o^{0.6}} \left( \frac{\rho_{fl}}{\rho_o} \right) \frac{1}{v_{fl}^{0.2}} \cdot \text{constant} \quad (9)$$

where sub-index  $o$  and  $fl$  refer to inlet and flame conditions respectively.

The constants employed in the turbulence model are given in Table I, and the turbulence viscosity was user-defined as

$$\mu_t = \frac{\rho \cdot C_D \cdot k^2}{\varepsilon} \quad (10)$$

**Table 1.** Turbulence model constants

$C_D$	$C_1$	$C_2$	$\sigma_h$	$\sigma_k$	$\sigma_\varepsilon$	$\sigma_{fu}$	$\sigma_f$	$\sigma_s$	$\sigma_{nuc}$
0.09	1.44	1.79	0.7	1.0	1.3	0.7	0.7	0.7	0.7

The basic transport equations solved in these simulations can be written in a general form as follows

$$\frac{\partial}{\partial x}(\bar{\rho U}) + \frac{1}{y} \frac{\partial}{\partial y}(y \bar{\rho V}) = 0, \text{ for mass} \quad (11)$$

and for momentum and scalar quantities:

$$\bar{\rho U} \frac{\partial \phi}{\partial x} + \bar{\rho V} \frac{\partial \phi}{\partial y} = \frac{1}{y} \frac{\partial}{\partial y} \left( y \frac{\mu_t}{\sigma_\phi} \frac{\partial \phi}{\partial y} \right) + R_\phi \quad (12)$$

All transport equations were solved using a second order upwind discretization scheme, except the turbulence dissipation rate. In the case of soot and nuclei, QUICK discretization scheme was employed. The convergence criteria were 1E-3 for most parameters, apart from the energy and soot, for which it was set to 1E-6 and 1E-5 respectively. In reacting flows, the fact that the flow has reached convergence does not necessarily imply that an equilibrium state has been reached. Thus, the concentrations of some product species were monitored at points near the exit of the combustor.

## 2 Procedure

There are three well differentiated areas in the present work: the implementation of the Magnussen model using both flamelet and EBU chemistry models, the analysis of the effect of Reynolds number in the final soot concentration and the effect of sinusoidal fuel pulses in the soot concentration.

Nowadays there is a varied choice for turbulence and combustion models, and it cannot be said that one outperforms the others in all flow conditions. It is normally good practice to decide the models to employ by solving a flame or combustion environment that closely resembles the one subject to investigation. In this case, a turbulent piloted diffusion flame<sup>13-15</sup> –referred to as flame D– was reproduced in order to evaluate the performance of the turbulence model and the combustion model. In order to improve the predictions of the spreading of the diffusion jet, realizable k-ε was chosen to model the momentum transport equations. Based on the good agreement of the reproduced flame D in FLUENT with the results obtained with conditional moment closure<sup>13,14</sup> and the experimental data<sup>15</sup>, this methodology was assumed to be suited for the simulation of 2-dimensional axi-symmetric diffusion flames. Despite this work being based on the findings of Magnussen, the boundary conditions were modified due to a lack of boundary condition information such as the shape of the issuing nozzle or the TKE and TDR –which can be critical for combustion simulation–, the grid employed, or any discussion as to how the flame can be stable at the given fuel inlet velocity. Therefore, the fuel inlet velocities were reduced with

respect to those employed in references<sup>1-5</sup>. In the present study, jet Reynolds numbers of 3300, 16500, 20000 and 25000 –  $U_{jet}=10, 50, 60$  and  $75\text{m/s}$  respectively- were tested using the flamelet model and Reynolds numbers of 8300, 11500 and 16500 for when the EBU was employed. A sinusoidal fuel inlet delivery was also analysed, with frequencies 50, 100 and 200Hz and amplitude of  $25\text{m/s}$ . The time steps were adjusted in each case to ensure 20 divisions in each complete cycle and 2<sup>nd</sup> Order Implicit was employed for the unsteady discretization.

### 3 Results

The first part of the study was the simulation of flame D using the flamelet model in order to see how it compares to the CHEMKIN mechanisms used in the literature. Figure 1 depicts the values of mixture fraction at the  $x/d = 15$  station of the piloted flame D. This result is in close agreement with the experimental data<sup>15</sup> and predictions made using detailed chemical mechanisms<sup>13,14</sup>. Likewise, the temperature estimation and the main species mass fractions –figure 3- are within reasonable agreement with experiments. The axial velocity was also compared at the different stations, again showing good agreement with the sources of data. As a result of this study, it was concluded that the flamelet model and the selected realizable k- $\epsilon$  turbulence model were suited to the simulation of turbulent diffusion flames, and therefore were also used to simulate the acetylene flame. The flame D simulation was also employed as an initial step into the grid-independence study, based on both temperatures and species concentrations mainly, and is later applied to the acetylene investigation.

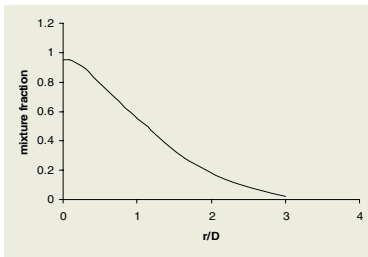


**Fig. 1.** Flame D, mixture fraction

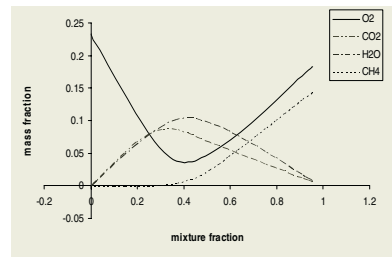


**Fig. 2.** Flame D, species mass fraction

In the case of the acetylene combustion, the geometry differed slightly from what it can be inferred from the literature. The major differences are that in the present case a converging nozzle is not employed and the issuing jet is not placed in the centre of a circular plate, and instead is placed in an unconfined environment. Figure 3 depicts the turbulence dissipation rate near the jet exit, where a large difference in the dissipation values is observed. These variations of turbulence dissipation will have an effect on the soot and nuclei formation rates, but this effect is more clearly seen when combined with the turbulence kinetic energy in order to monitor the turbulence time scale, as depicted in figure 4. In this figure a large reduction in the time scale is observed between the low Re and the other higher Re conditions. In can also be appreciated that the decrease of the eddy lifetime is also non-linear, since the decrease between

$Re=16500$  and  $Re=20000$  is larger than that between  $Re=20000$  and  $Re=25000$ . These results imply that the residence time allowed for soot to form and growth in the higher Reynolds number conditions is reduced compared to those lower Reynolds. The effect of the turbulence intensity on the formation and combustion of soot is depicted in figure 5. It can be seen that for lower  $Re$ , the peak soot concentration is closer to the nozzle that for the higher  $Re$ . However, one other feature of this graph is the fact that the Reynolds number does not have a strong effect on the location of the peak soot concentration for higher  $Re$ . On the other hand, it does have a strong impact on the maximum soot mass fraction, which reduces as  $Re$  increases. Consequently, it can be said that the input boundary conditions do have a significant influence on the soot concentration in turbulent flames. However, it can also be seen that there is a deviation of the peak of the soot concentration towards the exit of the combustor. These differences in are thought to be due to an inappropriate linearization of the scalar transport equations and are currently under study.

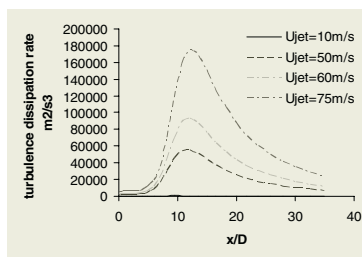


Fig. 3. Acetylene, turbulence dissipation rate

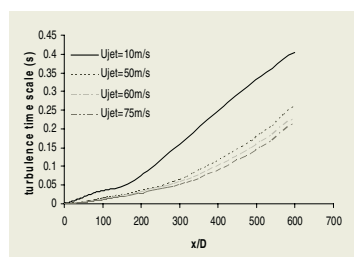


Fig. 4. Acetylene, turbulence time scale

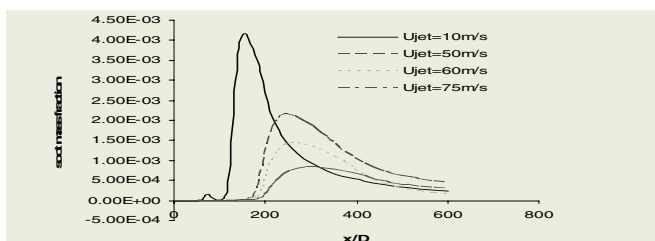


Fig. 5. Acetylene, soot mass fraction at different  $Re$

A similar effect of the Reynolds number on the final concentration of soot was observed when the EBU was employed. Comparing the results directly with those obtained with the flamelet model, the EBU presents the peak soot concentrations in the areas of the flame where it could be expected, unlike the flamelet model. This is probably due to the incompatibility of the flamelet model, which assumes that fuel and oxidizer cannot co-exist, unless the strain rate extinguishes the flame, and Magnussen soot model assumes that the fine structures and the surrounding flow are in equilibrium, which seems to be contradictory with the flamelet. Figure 6 depicts the soot concentration along the symmetry axis for the three fuel inlet velocities studied.

This trend also seen along the radial lines, like the example take from a vertical station 0.3m downstream the jet exit.

These results indicate that increased levels of turbulence can, indeed, reduce the soot emissions from a combustion reaction. One other factor that can enhance the depletion of soot particles is the entrainment of oxygen into the core of the diffusion flame, i.e. the fuel rich area. This could be achieved by pulsing the fuel, thus lengthening and twisting the shear layer through which air and fuel ultimately mix. Figures 8, 9 and 10 depict a comparison between the root-mean-square –rms– of the soot concentrations for the three frequencies investigated and the steady state concentration along the symmetry axis and two vertical stations located 0.2 and 0.3m downstream the nozzle exit. The pulsed-fuel cases were run for a total flow time of about 2.7 seconds to allow the pulse to stabilize. Thus we assumed that the quantities seen in one pulse would be repeated in the next one.

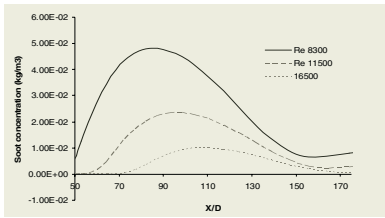


Fig. 6. Axial Soot concentration

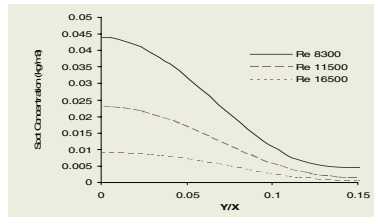


Fig. 7. Radial soot concentration at X=0.3m

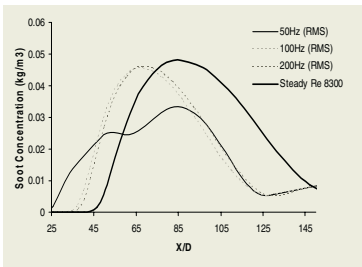


Fig. 8. Soot rms along axis

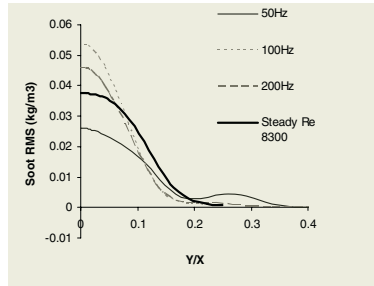


Fig. 9. Soot rms at X=0.2m

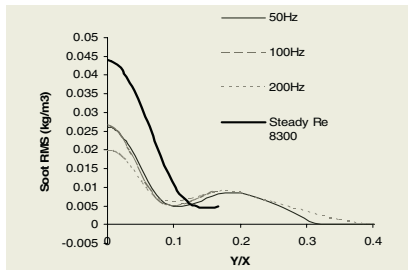


Fig. 10. Soot rms at X=0.3m

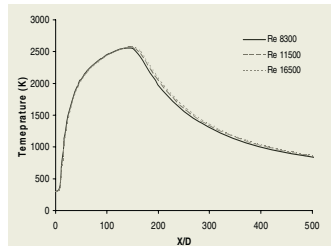


Fig. 11. Axial temperature, steady state

Figure 11 depicts the temperature predicted during the steady state simulations at different Reynolds numbers. Because the temperature is very similar in each case, the reduction in soot concentration must come from the difference in the turbulent kinetic energy and dissipation, as seen in the flamelet case. It is not surprising to find a higher concentration of soot with the pulsed fuel respect to the steady state in Figure 9 because, as can be appreciated in Figure 10, the peak of soot concentration is moves towards the jet exit when the fuel is pulsed. Thus, a more realistic reading of the effect of pulsing in the soot concentration can be made from Figure 10.

## 4 Conclusions

A soot model with turbulence interaction has been satisfactorily implemented onto a commercial code. At present work is being done to treat soot as “active” specie.

The flamelet model has proved to produce very good thermodynamic solutions, but seems to be incompatible with the soot model.

Both flamelet and EBU simulations have shown a decreasing concentration of soot with increasing flow Reynolds number, whilst temperature distribution has remained fairly unchanged.

Pulsing fuel has shown a decrease in the final concentration of soot based on stabilized pulsed flames and compared to a steady velocity equal to the amplitude of the pulse. Should it be compared to the rms of the inlet velocity, these results would be even larger.

## References

1. Magnussen, B.F. *On the structure of turbulence and generalized eddy dissipation concept for chemical reaction in turbulent flow*. 19<sup>th</sup> AIAA Science Meeting, 1981.
2. Magnussen, B.F. *Modelling of NO<sub>x</sub> and soot formation by the eddy dissipation concept*. International Flame Foundation First Topic Oriented Technical Meeting, 1989.
3. Magnussen, B.F. *15<sup>th</sup> Symposium (Int) on Combustion*. The Combustion Institute, Pittsburgh, 1974.
4. Magnussen, B.F., Hjertager, B.H. *16<sup>th</sup> Symposium (Int) on Combustion*. The Combustion Institute, Pittsburgh, 1976.
5. Magnussen, B.F., Hjertager, B.H., Olsen, J.G., Bhaduri, D. *17<sup>th</sup> Symposium (Int) on Combustion*. The Combustion Institute, Pittsburgh, 1979.
6. Thilly, W.G. *Soot Combustion Systems and its Toxic Properties*, pp1-12, Plenum Press, New York, 1983.
7. Boyland, E. *Soot Combustion Systems and its Toxic Properties*, pp13-24, Plenum Press, New York, 1983.
8. Tesner, P.A., Snegirova, T.D., Knorre, V.G. *Combustion and Flame*, 17, pp253-260, 1971.
9. Tesner, P.A., Tsygankova, E.I., Guilazetdinov, L.P., Zuyev, V.P., Loshakova, G.V. *Combustion and Flame*, 17, pp 279-285, 1971.
10. Srivatsa, S.K. *NASA-Lewis Research Center, NAS3-22542, NASA CR-167930, Garrett 21-4309*, 1982.

11. Prado, G., Lahaye, J., Haynes, B.S. Soot Combustion Systems and its Toxic Properties, pp145-162, Plenum Press, New York, 1983.
12. Kolmogorov, A.N., *Journal of Fluid Mechanics*, 13, 82, 1962.
13. Fairweather, M., Woolley, R.M., *Combustion and Flame*, 138, pp3-19, 2004.
14. Fairweather, M., Woolley, R.M. *Combustion and Flame*, 133, pp393, 2003.
15. Information available at <http://www.ca.sandia.gov/TNF>

# Application Benefits of Advanced Equation-Based Multiphysics Modeling

Lars Langemyr and Nils Malm

COMSOL AB, Tegnérgatan 23, SE-111 40 Stockholm, Sweden  
Contact author: Nils Malm, telephone +46 8 412 95 291  
nils@comsol.se

**Abstract.** In just the past few years, the field of mathematical modeling with equation-based tools has seen a number of advances and innovations that allow software developers to create programs that are at once far more powerful yet easier to use. To illustrate the benefits that users gain from the latest features and capabilities, this paper examines a problem where software that supports extended multiphysics calculates the applied voltage needed to produce a predefined thermally induced bending of a microscale device. The package used in this problem is FEMLAB, an equation-based environment for solving a large class of systems of coupled partial differential equations.

The software relies on a Galerkin discretization of a weak formulation of the PDEs using generic shape functions. Arbitrary couplings between equations are possible, and a correct discrete residual and Jacobian can be obtained for both linear and nonlinear problems. Therefore, the software can handle tightly coupled systems using an efficient all-at-once Newton solver or an implicit time-stepping method.

Linear systems are described by giving coefficient values for a generic PDE form. More general systems are specified as conservation laws where the user defines an arbitrary flux vector and source for each equation. In addition, the user has direct access to the underlying weak form, which adds additional flexibility to the system. For the less mathematically oriented user, predefined application templates set up the equations based on physical properties. The resulting equations can be viewed, modified, and arbitrarily coupled to other physics.

Direct access to the weak form allows fully integrated multidimensional modeling. Separate equations can be modeled on the boundary of a domain, or contributions can be added to the main equations. In particular, the weak form provides for the straightforward implementation of non-standard boundary conditions and those conditions connecting different types of physics, as is the case when doing, for example, fluid-structure interaction.

In traditional multiphysics problems, the interaction between fields is local in space. In addition to such local couplings, FEMLAB supports the use of non-local variables in any equation. We refer to that capability as *extended multiphysics*, and it can be used to model control systems, couple multidimensional models, couple discrete and semi-analytical models, solve inverse and optimization problems, and more. Non-local coupling variables can be defined through arbitrary coordinate mappings, as integrals over selected domains, or as integrals along a given direction. FEMLAB internally knows the sensitivity of the coupling variables with respect to the degrees of freedom, and therefore it can accurately compute the full Jacobian for extended multiphysics model.



# Large Eddy Simulation of Spanwise Rotating Turbulent Channel and Duct Flows by a Finite Volume Code at Low Reynolds Numbers

Kursad Melih Guleren\* and Ali Turan

University of Manchester, School of Mechanical, Aerospace and Civil Engineering,  
M60 1QD Manchester, UK

M.Guleren@postgrad.manchester.ac.uk  
A.Turan@manchester.ac.uk

**Abstract.** The objective of this study is to show the highly complex features of rotational turbulent flow using a widely known finite volume code. The flow subjected to an orthogonal rotation is investigated both qualitatively and quantitatively in a three-dimensional channel and a duct using FLUENT. The predictions of rotational flow calculations, presented for low Reynolds numbers, both in channel and duct are in good agreement with the DNS predictions. It is of interest to present the capability of the code for capturing the multi-physics of internal flow phenomena and to discuss the Coriolis effects for two rotational rates. The results show that FLUENT is able to predict accurately first and second order turbulent statistics and it also captures the proper secondary flow physics which occur due to rotation and the geometry itself. These results are very encouraging for the simulation of the flow in a centrifugal compressor, which is the main goal of the authors in the long term.

## 1 Introduction

It is well known that investigation of the turbulent fluid motion is a challenging research area; neither an analytical solution exists nor it can be exactly defined mathematically. Its complexity is generally explained with its unsteadiness, three-dimensionality, dissipative and diffusive features. In addition, it contains a broad spectrum, which is formed by various size of eddies. For example, scales of these eddies can be of the order of the size of the flow geometry and of the size of Kolmogorov scale, which is known as the smallest scale. Even without rotation, turbulent is certainly a multiscale process. Combining the effects of rotation with turbulence makes the flow physics more interesting, however more complex, and difficult to analyze either experimentally or numerically. It was confirmed by previous studies that rotation changes not only the mean flow but also the turbulence field itself. Although, there exist a wide range of studies in literature as to how and why the multi-physics of these flows are affected depending on the Reynolds and rotation numbers,

---

\* Permanent address: Cumhuriyet University, Dept. of Mech. Eng., 58140, Sivas, Turkey.

criteria still remains to be formulated clearly for practical industrial flow applications including the centrifugal compressor.

The present study analyzes a turbulent rotating channel flow at a low Reynolds number of  $Re=2800$  for two rotation numbers of  $Ro=0.1$  and  $Ro=0.5$  ( $Re=U_b h/\nu$ ,  $Ro=2\Omega h/U_b$ , where  $U_b$  is the bulk velocity,  $h$  is the half width of the channel,  $\nu$  is the kinematic viscosity and  $\Omega$  is the rotation rate of the flow). In addition, the turbulent duct flow is investigated at a low Reynolds number of  $Re=4410$  for two rotation numbers of  $Ro=0.013$  and  $Ro=0.053$  ( $Re=U_b D/\nu$ ,  $Ro=2\Omega D/U_b$ , where  $D$  stands for the hydraulic diameter of the duct).

## 2 The Model

For the channel flow, dimensions of the geometry are  $L_x=6.4h$ ,  $L_y=2h$ ,  $L_z=3.2h$ . For the duct flow, spanwise and radial lengths are set to be equal to  $L_y=L_z=D$  while the streamwise length is taken as  $L_x=6.28D$ . The flow is assumed to be fully developed, isothermal, incompressible and rotating at a fixed positive angular velocity parallel to the spanwise direction,  $\mathbf{\Omega}=(0,0,\Omega)$ .

The numerical calculations were performed using the development version of the general-purpose code FLUENT V6.2 [1] using the Dynamic Smagorinsky-Lilly Model [2],[3]. The code is based on a finite-volume method with an unstructured grid algorithm. The LES incorporates 2<sup>nd</sup> order central differencing for the diffusive and convective terms for the channel flow calculations and 3<sup>rd</sup> order MUSCL for duct flow calculations. A fully second-order implicit scheme is applied for temporal discretization while the PISO algorithm and PRESTO! scheme are employed for the velocity-pressure coupling and pressure interpolation, respectively.

The computational domain is formed by  $66 \times 66 \times 66$  and  $66 \times 60 \times 60$  cells (in the  $x,y$  and  $z$ -directions) for channel flow and duct flow, respectively. The computational grid is equally spaced along the homogenous directions ( $x$  and  $z$ -directions for channel and  $x$ -direction for the duct) and stretched non-uniformly between the solid walls [from  $y=0$  (bottom wall) to  $y=2h$  (top wall) in the channel, from  $y=0$  (bottom wall) to  $y=D$  (top wall) and from  $z=0$  (lateral wall) to  $z=D$  (lateral wall) in the duct]. Non-slip boundary conditions and periodic boundary conditions were applied for the walls and homogenous directions, respectively. Constant mass flow rate was assumed in the flow directions rather than constant pressure drop.

## 3 Results and Discussion

Fig. 1. shows the distribution of mean and turbulent intensities for low and high rotational rates. For both cases, excellent agreement for the mean velocity was found with the DNS data [4] except for a slight increase near the pressure side ( $y=0$ ) at the low rotation rate. For this case, radial and spanwise turbulent intensities are remarkably under-predicted near the pressure side, but they gradually approach the DNS data through center of the channel. Spanwise intensity, which is mainly responsible for turbulent kinetic energy, is under- and over-predicted near the pressure and suction sides, respectively. For the high rotational case, similar trends are obtained however the discrepancies and the range that is affected are smaller in this case.

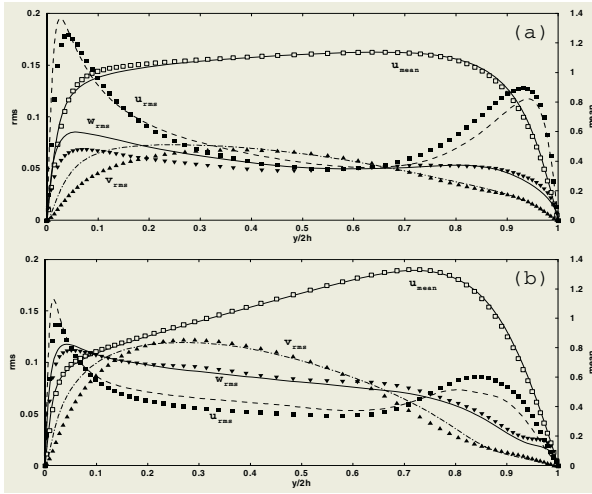


**Fig. 1.** Mean velocity and turbulent intensity profiles for the rotating channel flow at  $Ro=0.1$  (a) and at  $Ro=0.5$  (b). Present LES results, shown with symbols, are compared with DNS results of Kristoffersen and Andersson [2], shown with lines. Values are normalized by bulk velocities

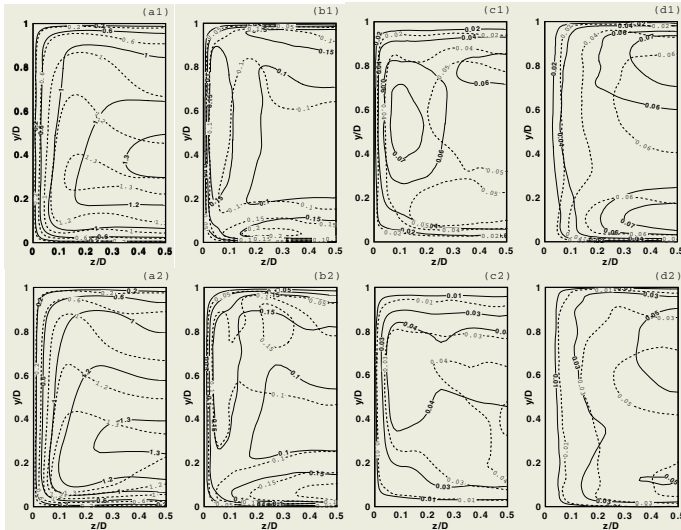


**Fig. 2.** Mean velocity (a1,a2) and turbulent contours (b1,b2 for streamwise, c1,c2 for normal, d1,d2 for spanwise directions) for rotating duct flow at  $Ro=0.013$  shown with lines and at  $Ro=0.053$  shown with dashed lines. While the top figures represent the DNS results of Gavrilakis [16], the bottom figures represent the present LES results. Due to symmetry, half of the duct is shown

Spatial distribution of the mean velocity and turbulent intensities for half of the square duct is also shown for two rotational cases in Fig. 2. The peak region of the predicted mean velocity ( $a_2$ ) has a tendency to shift towards the bottom corner; otherwise, the LES predictions are in good agreement with the DNS data [5] for both rotational cases. Streamwise turbulent intensity ( $b_2$ ) seems to be consistent with the DNS, but the remaining intensities ( $c_2, d_2$ ) are remarkably under-predicted. However, the under-prediction for  $Ro=0.053$  is less than that for  $Ro=0.013$ . Notwithstanding these discrepancies, our results are similar to those of Palleres and Davidson [6]. Considering the increase in rotational number, mean velocity and turbulent intensity decrease near the suction side and increase towards the pressure and lateral side of the duct. The normal and spanwise turbulent intensities are observed to be reduced near the suction side and become enhanced near the pressure side.

## 4 Conclusion

Spanwise rotating channel and duct flow were investigated at low Reynolds numbers using LES. Although there are some discrepancies at low rotational numbers, the results are generally in good agreement with DNS predictions. These discrepancies are thought to be caused primarily by the SGS model incorporated in FLUENT. Additionally, the highest accuracy for the numerical schemes in the code is third order: it is well known that such attributes might provide another source for discrepancies.

Concerning future studies, plans are already underway to test different SGS models, including dynamic kinetic energy SGS model [7] and the wall-adapting local eddy-viscosity (WALE) model [8], in order to understand the performances of these SGS models for rotating channel and duct flow problems.

## References

1. FLUENT 6.1 USER GUIDE Fluent Inc. Lebanon, USA (2001)
2. Germano, M., Piomelli, U., Moin, P. & Cabot, W. H. A dynamic subgrid-scale eddy viscosity. *Phys. Fluids* 7 (1991) 1760
3. Lilly, D. K. A proposed modification of the Germano subgrid-scale closure method. *Phys. Fluids* 4 (1992) 633
4. Kristoffersen, R. & Andersson, H. I. Direct simulation of low-Reynolds-number turbulent flow in a rotating channel. *J. Fluid Mech.* 256 (1993) 163
5. Gavralakis, S. Direct numerical simulation (DNS) of the Rotating Square Duct flow at a low turbulent Reynolds number. <http://lin.epfl.ch/index2.php/link/staff/id/43> (results not published yet)
6. Palleres, J. & Davidson, L. Large-eddy simulations of turbulent flow in a rotating square duct. *Phys. Fluids* 12 (2000) 2878
7. Kim, W. and Menon, S. Application of the localized dynamic subgrid-scale model to turbulent wall-bounded flows. *J. Fluid Mech.* 35<sup>th</sup> Aerospace Sciences Meeting & Exhibit, Reno, NV, (1997) AIAA Paper 97-0210
8. Nicoud, F. & Ducros, F. Subgrid-scale stress modeling based on the square of velocity gradient tensor. *Flow, Turb. Comb.* 62 (1999) 183

# Modelling Dynamics of Genetic Networks as a Multiscale Process

Xilin Wei, Roderick V.N. Melnik, and Gabriel Moreno-Hagelsieb

Mathematical Modelling and Computational Sciences,  
Wilfrid Laurier University,  
75 University Ave W, Waterloo, Ontario, N2L 3C5, Canada

**Abstract.** A key phenomenon in the dynamics of genetic networks is the cell cycle. In the study of this phenomenon, an important task is to understand how many processes, acting on different temporal and spatial scales, interact in the cell.

In this paper we deal with the problem of modelling cell cycles. We start our analysis from the Novak-Tyson model and apply this deterministic model to simulate relative protein concentrations in several different living systems, including *Schizosaccharomyces pombe* to validate the results. Then we generalize the model to account for the nonlinear dynamics of a cell division cycle, and in particular for special events of cell cycles. We discuss the obtained results and their implications on designing engineered regulatory genetic networks and new biological technologies.

## 1 Introduction

Cells process information in complex ways. During the cell cycle, an eukaryotic cell duplicates all of its components and separates them into two daughter cells. This process is composed of four phases: G1 phase in which size of the cell is increased by producing RNA and synthesizing protein, S phase in which DNA are replicated, G2 phase in which the cell continues to produce new proteins and grows in size, and M (mitosis) phase in which DNA are separated and cell division takes place [1], [3]. From the outset, we are in a situation where we have to deal with different biological events with different spatial and temporal scales.

The problem of modelling dynamics of genetic networks, including those for cell cycles, has been actively addressed in the past decades [2]. New improved models have been recently developed with increasing capability to predict competitively experimental results [3]. The Novak-Tyson model for a cell cycle in [3] contains over 40 parameters that are of the same units but vary from less than  $10^{-2}$  to 35. A stochastic generalization of that model was presented in [4].

In the present work, we start our analysis from the Novak-Tyson model and apply this deterministic model to simulate relative protein concentrations in several different living systems. Then, we generalize the model to account for the nonlinear dynamics of a cell division cycle, and in particular for special

events of cell cycles. We show that the effects of such fluctuations may have important implications on designing engineered regulatory genetic networks due to the sensitivity of the model to parametrization processes.

## 2 Mathematical Models of Cell Cycles

Based on the original Novak-Tyson model, in this section, we develop a new model that accounts for fluctuations of concentrations in response to the multi-scale character of cellular activities.

### 2.1 The Novak-Tyson Model

With  $x_1(t) = Cdc13_T(t)$ ,  $x_2(t) = preMPF(t)$ ,  $x_3(t) = Ste9(t)$ ,  $x_4(t) = Slp1_T(t)$ ,  $x_5(t) = Slp1(t)$ ,  $x_6(t) = IEP(t)$ ,  $x_7(t) = Rum1_T(t)$ ,  $x_8(t) = SK(t)$  and  $MPF(t)$  denoting the relative concentrations of the corresponding proteins, and  $x_9(t) = M(t)$  the mass of the cell in the cell cycle, the equations and parameters in the Novak-Tyson model are given in Table 1 where the time  $t$  for variables  $x_i$ ,  $i = 1, 2, \dots, 9$ ;  $MPF$ ,  $TF$ ,  $Trimer$  and  $\Sigma$  is dropped.

**Table 1.** The Novak-Tyson Model. All constants have units  $\text{min}^{-1}$ , except the  $J$ 's and  $K_{diss}$  which are dimensionless

$\frac{d}{dt}x_1 = k_1x_9 - (k'_2 + k''_2x_3 + k'''_2x_5)x_1$	(1)	$k_1 = k'_2 = 0.03, k''_2 = 1.0, k'''_2 = 0.1;$
$\frac{d}{dt}x_2 = k_{wee}(x_1 - x_2) - k_{25}x_2$		$k'_3 = 1.0, k''_3 = 10.0, J_3 = 0.01,$
$-(k'_2 + k''_2x_3 + k'''_2x_5)x_2$	(2)	$k'_4 = 2.0, k_4 = 35.0, J_4 = 0.01;$
$\frac{d}{dt}x_3 = (k'_3 + k''_3x_5) \frac{1-x_3}{J_3+1-x_3}$		$k'_5 = 0.005, k''_5 = 0.3, J_5 = 0.3,$
$-(k'_4x_8 + k_4MPF) \frac{x_3}{J_4+x_3}$	(3)	$k_6 = 0.1, k_7 = 1.0, k_8 = 0.25,$
$\frac{d}{dt}x_4 = k'_5 + k''_5 \frac{MPF^4}{J_5^3+MPF^4} - k_6x_4$	(4)	$J_7 = J_8 = 0.001; k_9 = 0.1, k_{10} = 0.04,$
$\frac{d}{dt}x_5 = k_7x_6 \frac{x_4-x_5}{J_7+x_4+x_5} - k_8 \frac{x_5}{J_8+x_5} - k_6x_5$	(5)	$J_9 = J_{10} = 0.01; k_{11} = 0.1, k_{12} = 0.01,$
$\frac{d}{dt}x_6 = k_9MPF \frac{1-x_6}{J_9+1-x_6} - k_{10} \frac{x_6}{J_{10}+x_6}$	(6)	$k'_{12} = 1, k''_{12} = 3, K_{diss} = 0.001;$
$\frac{d}{dt}x_7 = k_{11} - (k_{12} + k'_{12}x_8 + k''_{12}MPF)x_7$	(7)	$k_{13} = k_{14} = 0.1; k_{15} = 1.5, k'_{16} = 1,$
$\frac{d}{dt}x_8 = k_{13}TF - k_{14}x_8$	(8)	$k''_{16} = 2, J_{15} = J_{16} = 0.01;$
$\frac{d}{dt}x_9 = \mu x_9$	(9)	$V_{awee} = 0.25, V_{iwee} = 1,$
$Trimer = \frac{2x_1x_7}{\Sigma + \sqrt{\Sigma^2 - 4x_1x_7}}$	(10)	$J_{awee} = J_{iwee} = 0.01;$
$MPF = \frac{(x_1-x_2)(x_1-Trimer)}{x_1}$	(11)	$V_{a25} = 1, V_{i25} = 0.25,$
$TF = GK(k_{15}x_9, k'_{16} + k''_{16}MPF, J_{15}, J_{16})$	(12)	$J_{a25} = J_{i25} = 0.01; k'_{wee} = 0.15,$
$k_{wee} = k'_{wee} + (k''_{wee} - k'_{wee})GK(V_{awee}, V_{iwee}MPF, J_{awee}, J_{iwee})$	(13)	
$k_{25} = k'_{25} + (k''_{25} - k'_{25})GK(V_{a25}MPF, V_{i25}, J_{a25}, J_{i25})$	(14)	
where $\Sigma = x_1 + x_7 + K_{diss}$ and		$k'''_{wee} = 1.3, k'_{25} = 0.05, k''_{25} = 5;$
$GK(a, b, c, d) = \frac{2ad}{b-a+bc+ad + \sqrt{(b-a+bc+ad)^2 - 4ad(b-a)}}$		$\mu = 0.005.$

### 2.2 The Generalized Model with Fluctuations

Since a cell cycle involves nonlinear changes of the protein concentrations related to multiple spatial and temporal scales, the regulation of cellular activities

contains a degree of uncertainty [3], [4]. Specifically, at the G1 phase, *Ste9* and *Rum1* are activated while *Slp1* and *Cdc13<sub>T</sub>* are reducing rapidly. From the results of the deterministic model and experimental observations, the magnitudes of *Ste9*, *Cdc13<sub>T</sub>* and *Slp1* are large enough to introduce fluctuations and the fluctuations of their derivatives are expected. *SK* is also active at the latter part of the G1 phase. During the S phase which is shorter than G1 and G2 phases but much longer than M phase, the magnitudes of *Cdc13<sub>T</sub>* and *preMPF* are large enough to generate fluctuations of their changing rates. During the G2 phase, the magnitudes of *Cdc13<sub>T</sub>* and *preMPF* continue to increase. In the M phase, the magnitudes of *Cdc13<sub>T</sub>*, *preMPF* and *slp1* changes rapidly and are large enough to introduce fluctuations. *IEP* is also active in the M phase.

If the magnitude of the relative concentration of a protein  $x_i(t)$  is beyond certain value (we use 0.3 for such a value in this paper), we need to modify the right hand sides (RHSs) of equations (1)–(9). Based on the experimental results (see Fig. 1) and taking into account that the period of the cell cycle is about  $T = 138.63$  minutes [3], we suggest to multiply the RHSs of equations (1)–(9) by the functions  $f_1(t)$ ,  $f_2(t)$ ,  $\dots$ ,  $f_9(t)$  respectively, where

$$f_j(t) = \begin{cases} 1 + r, & kT \leq t \leq kT + \alpha_j \text{ or } kT + \beta_j \leq t \leq (k+1)T; \\ 1.0, & \text{otherwise,} \end{cases} \quad , \quad j = 1, 5; \quad (15)$$

$$f_\ell(t) = \begin{cases} 1 + r, & kT + \gamma_\ell \leq t \leq kT + \lambda_\ell; \\ 1.0, & \text{otherwise,} \end{cases} \quad , \quad \ell = 2, 3, 6, 8; \quad (16)$$

$$f_4(t) = f_7(t) = 1.0; \quad f_9(t) = 1 + r, \quad (17)$$

$k$  is a nonnegative integer,  $r$  is a control parameter that provides us with the amplitude of fluctuations,  $\alpha_1 = 3$ ,  $\beta_1 = 20$ ,  $\alpha_5 = 15$ ,  $\beta_5 = T - 5$ ,  $\gamma_2 = 10$ ,  $\lambda_2 = T$ ,  $\gamma_3 = 0$ ,  $\lambda_3 = 20$ ,  $\gamma_6 = T - 10$ ,  $\lambda_6 = T$ ,  $\gamma_8 = 10$  and  $\lambda_8 = 20$ . Note that the choice of  $f_i(t)$  for  $i = 1, \dots, 9$  is not unique, but the above choice for  $r = 0$  is consistent with experimentally confirmed results of [3].

### 3 Computational Experiments

Both models, described in the previous section, have been implemented in MATLAB. We applied stiff solvers to deal efficiently with numerical difficulties caused by variability of model parameters. The initial conditions in all experiments are  $x(0) = (0.45, 0, 1.0, 0, 2.1, 0, 0.05, 0, 1.0)$ . In our first set of experiments, we use the deterministic Novak-Tyson model. The results with this model are presented in Fig. 1. Here and in all figures that follow we present two cycles. We observe that the relative concentrations of proteins are qualitatively the same as those obtained in [3], given differences of initial conditions. Replacing  $k''_{wee}$  (parameters  $k''_{wee}$  and  $k''_{25}$  are responsible for rate of tyr-phosphorylation and dephosphorylation) by 0.3 in the above model as suggested in [3], we get a model for the cell cycle of *Wee1<sup>-</sup>* mutants. The results obtained in this case are presented in Fig. 2. We can see that the relative concentrations of *Cdc13<sub>T</sub>*, *MPF* and *preMPF*

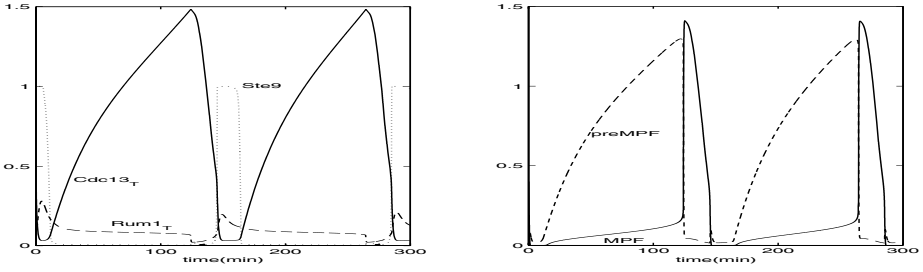


**Fig. 1.** Numerical simulation of the model in Section 2.1

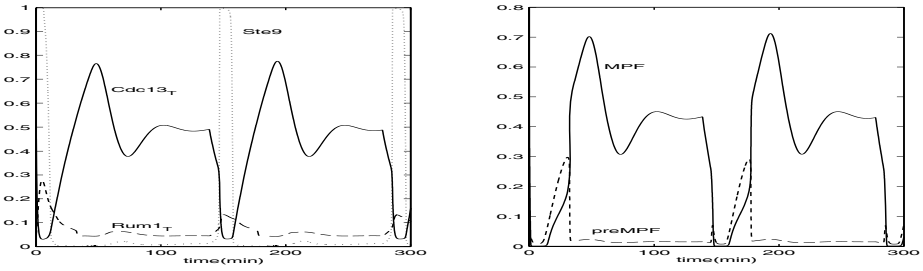


**Fig. 2.** Numerical simulation of the model with  $k''_{wee} = 0.3$

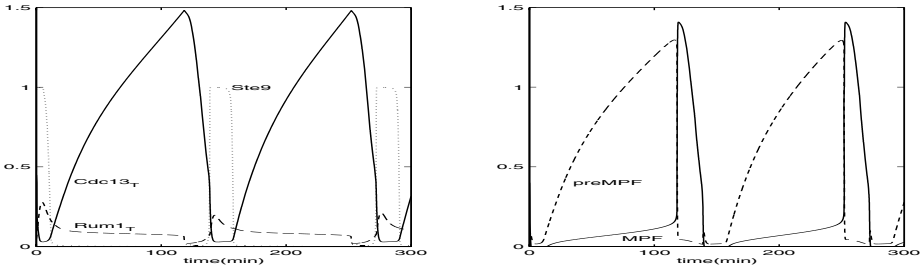


**Fig. 3.** Numerical simulation of the generalized model with  $r = 0.05$

in Fig. 2 are quite different from those in Fig. 1. We have also analyzed the situations with  $k''_{wee} = 0.3$  and  $k''_{25} = 0.02$ , as well as with  $k''_{25} = 0.02$ , keeping  $k''_{wee}$  the same as in our first model. In both cases, noticeable changes in relative *MPF* were observed.

In our second set of experiments, we use the generalized model given in Section 2.2. Setting sequentially  $r = 0.001$ ,  $r = 0.005$ ,  $r = 0.01$  and  $r = 0.05$  in (15)–(17), we obtained cell cycles with reduced cycle times. The results for two cycles for  $r = 0.05$  are shown in Fig. 3. They demonstrate that it is possible to regulate the cell cycle by adjusting the perturbation control parameter  $r$ .



## 4 Conclusions

In this paper, we proposed a new model of cell cycle processes. The model takes into account special events during the cell cycle. The developed methodology can also be used to guide investigations on multiscale phenomena in designing engineered regulatory genetic networks and new biological technologies.

## References

1. Chen, L., Wang R., Kobayashi, T. J. and Aihara K.: Dynamics of Gene Regulatory Networks with Cell Division Cycle, *Phys. Rev. E*, **70** (2004), 011909.
2. Jong, H.D.: Modeling and Simulation of Genetic Regulatory Systems: A Literature Review, *J. of Computational Biology*, **9(1)** (2002), 67–103.
3. Novak, B., Pataki, Z., Ciliberto, A. and Tyson, J. J.: Mathematical Model of the Cell Division Cycle of Fission Yeast, *CHAOS*, **11(1)** (2001), 277-286.
4. Steuer, R.: Effects of Stochasticity in Models of the Cell Cycle: from Quantized Cycle Times to Noise-induced Oscillations, *J. of Theoretical Biology*, **228** (2004), 293–301.

# Mathematical Model of Environmental Pollution by Motorcar in an Urban Area

Valeriy Perminov

Belovo Branch of Kemerovo State University,  
652600 Belovo, Kemerovo region, Russia  
pva@belovo.kemsu.ru

**Abstract.** In the present paper it is developed mathematical model for description of heat and mass transfer processes and predicting velocity, temperature and pollution concentrations near roadway. To describe convective transfer controlled by the wind and gravity, we use Reynolds equations for turbulent flow. The boundary value problem was solved numerically. A discrete analog for equations was obtained by means of the control volume method. Methods of predicting concentrations of automobile exhaust gases near roadways are needed for the planning and design of roads and nearby structures.

## 1 Introduction

Mathematical model for description of heat and mass transfer processes and predicting velocity, temperature and pollution concentrations near roadway is constructed as a result of an analysis of known experimental data and using concept and methods from reactive media mechanics [1] and existing environmental pollution models [2,3]. It is considered that 1) the flow has a developed turbulent nature, molecular transfer being neglected, 2) gaseous phase density doesn't depend on the pressure because of the low velocities of the flow in comparison with the velocity of the sound, 3) the traffic is uniformly distributed over all lanes, 4) two dimensional model used to predict the concentrations along a line normal to highway. The forest in forest belt represents a non-deformable porous-dispersed medium [4].

## 2 Problem Formulation

Let the coordinate reference point  $x_1, x_2 = 0$  be situated at the center of the road surface source at the height of the roughness level, axis  $Ox_2$  directed upward, axis  $Ox_1$  directed parallel to the ground's surface to the right in the direction (Fig. 1).

The problem formulated above is reduced to a solution of the Reynolds and transport equations for turbulent flow:

$$\frac{\partial \rho}{\partial t} + \frac{\partial}{\partial x_j} (\rho v_j) = 0, \quad j = 1, 2, \quad i = 1, 2; \quad (1)$$

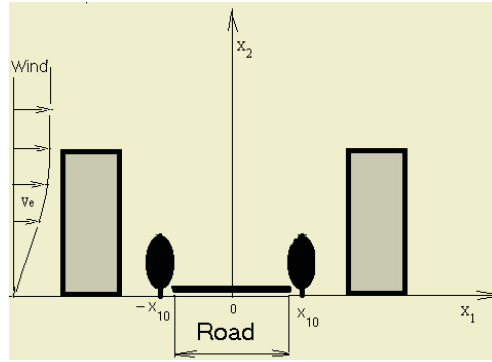


Fig. 1. Street canyon

$$\rho \frac{dv_i}{dt} = -\frac{\partial P}{\partial x_i} + \frac{\partial}{\partial x_j} (-\rho \overline{v'_i v'_j}) - \rho s c_d v_i |\vec{v}| - \rho g_i; \quad (2)$$

$$\rho c_p \frac{dT}{dt} = \frac{\partial}{\partial x_j} (-\rho c_p \overline{v'_j T'}) - v_2 (\rho_e g + c_p \rho \frac{dT_e}{dx_2}); \quad (3)$$

$$\rho \frac{dc_\alpha}{dt} = \frac{\partial}{\partial x_j} (-\rho \overline{v'_j c'_\alpha}), \quad \alpha = 1, 4; \quad (4)$$

$$\sum_{\alpha=1}^5 c_\alpha = 1, P_e = \rho R T \sum_{\alpha=1}^5 \frac{c_\alpha}{M_\alpha}, \frac{\partial T_e}{\partial x_2} = \gamma_e, \vec{v} = (v_1, v_2), \vec{g} = (0, g). \quad (5)$$

The system of equations (1)–(5) must be solved taking into account the following initial and boundary conditions:

$$t = 0: v_1 = 0, v_2 = 0, T = T_e, c_\alpha = c_{\alpha e}, T_s = T_e; \quad (6)$$

$$x_1 = -x_{1e}: v_1 = V_e(x_2), v_2 = 0, T = T_e, c_\alpha = c_{\alpha e}; \quad (7)$$

$$x_1 = x_{1e}: \frac{\partial v_1}{\partial x_1} = 0, \frac{\partial v_2}{\partial x_1} = 0, \frac{\partial c_\alpha}{\partial x_1} = 0, \frac{\partial T}{\partial x_1} = 0; \quad (8)$$

$$x_2 = 0: v_1 = 0, v_2 = V_{20}, T = T_0, c_\alpha = c_{\alpha 0}, |x_1| \leq x_{10}, \quad (9)$$

$$v_1 = 0, v_2 = 0, T = T_e, c_\alpha = c_{\alpha e}, |x_1| > x_{10};$$

$$x_2 = x_{2e}: \frac{\partial v_1}{\partial x_2} = 0, \frac{\partial v_2}{\partial x_2} = 0, \frac{\partial c_\alpha}{\partial x_2} = 0, \frac{\partial T}{\partial x_2} = 0. \quad (10)$$

Here and above  $\frac{d}{dt}$  is the symbol of the total (substantial) derivative;  $t$  is time;  $x_i$ ,  $v_j$  ( $i = 1, 2$ ) are the Cartesian coordinates and the velocity components;  $\rho$ ,  $T$  - density and temperature of air,  $P$  - pressure;  $c_p$  - constant pressure specific heat of the gas,  $c_\alpha$  - mass concentrations ( $\alpha=1 - CO$ ,  $2 - CH_x$ ,  $3 - NO_x$ ,  $4 -$  soot,  $5 -$  inert components of air);  $V_e$  - wind speed at the height  $1,5 m$ ,  $M_\alpha$  - molecular mass of  $\alpha$ -components of the gas phase;  $V_{20}$  - velocity of automobile exhaust gases,  $\gamma_e$  - gradient of stratification of temperature,  $c_d$  is an empirical coefficient of the resistance of the vegetation,  $s$  is the specific surface of the forest elements; index  $e$  corresponds to the unperturbed parameters of the medium. The components of the tensor of turbulent stresses and the turbulent fluxes of heat and mass are written in terms of the gradients of the average flow [4]. The road is modeled as a plane source of burning motorway fuels with known temperature and concentrations of automobile exhaust gases.

### 3 Numerical Simulation and Results

The boundary value problem (1) – (10) was solved numerically. A discrete analog for equations was obtained by means of the control volume method using the SIMPLE algorithm [5]. The accuracy of the program was checked by the method of inserted analytical solutions. Analytical expressions for the unknown functions were substituted in (1)–(10) and the closure of the equations were calculated. Next, the values of the functions were inferred with an accuracy of not less than 1%. Our practical situation requires calculation domain with obstacles in the middle of the flow region. It is convenient to employ a Cartesian coordinates but to modify the difference equations using method of fiction domain [5]. In the present calculations the results are obtained by using data:  $T=300K$ ,  $V_e=2 m/sec$ , the width of highway is 12 m, the number of cars passing per unit time (hour) is 3000, percentage structure of traffic (cars - 56%, lorries and buses – 19%, automobiles with diesel engine – 25%). The distribution of

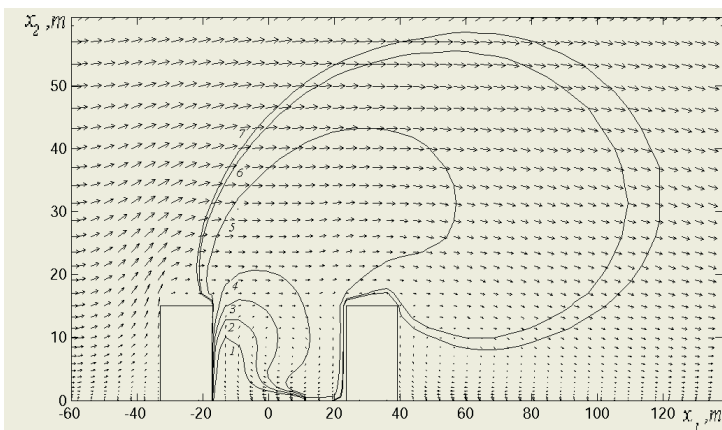


**Fig. 2.** Distributions of the vector velocity field and the concentration of carbon monoxide; 1 – 1 – 5,0, 2 – 2,0, 3 – 1,0, 4 – 0,5, 5 – 0,1, 6 – 0,05, 7 – 0,04 mg/m<sup>3</sup>

temperature of air, velocity, concentrations of components were obtained at different instants of time. The fields of mass concentrations of automobile emissions  $CO$  and vectorial fields of velocity (Fig. 2) were presented at the moment  $t=6 \text{ min}$  when the steady situation is realized. The wind field under the street canyon interacts with the gas-jet obstacle that forms from the surface source of heated air masses of automobile emissions. Recirculating flow forms beyond the zone of heat and mass release, i.e. street canyon. We can note that the distribution of velocity and concentration are deformed in the domain by the action of wind, which interacts with the buildings. Similarly, the others fields of component concentrations of pollutants are deformed. It allows investigating dynamics of environmental pollution under influence of various conditions: meteorology conditions and parameters of traffic flow (the number of cars of different types, traffic density and etc.). By increasing the wind velocity, the results show that the concentration of  $CO$  is drop around the street canyon more intensive.

## 4 Conclusions

The obtained results are agreed with the laws of physics and experimental data obtained near highway Moscow-Petersburg (Russia). Mathematical model and the results of the calculation give an opportunity to evaluate critical levels of environmental pollution and the damage from motorcar.

## References

1. Sedov, L.G.: Mechanics of Continuous Medium. Science. Moscow (1976) (in Russian)
2. Maddukuri, C.S.: A Numerical Model of Diffusion of Carbon Monoxide Near Highways //Journal of Air Pollution Control Association, Vol. 32, 8 (1982) 834-836
3. Perminov, V.A.: Mathematical Modeling of Environmental Pollution by the Action of Motor Transport // Advances in Scientific Computing and Application, Science Press, Beijing/New York, (2004) 341-346
4. Grishin, A.M.: Mathematical Modeling Forest Fire and New Methods Fighting Them, F.Albini (ed.), Publishing House of Tomsk University, Tomsk (Russia), (1997)
5. Patankar, S.: Numerical Heat Transfer and Fluid Flow, Hemisphere Publ. Co., New York (1980)

# The Monte Carlo and Molecular Dynamics Simulation of Gas-Surface Interaction

Sergey Borisov, Oleg Sazhin, and Olesya Gerasimova

Department of Physics, Ural State University, 620083, Ekaterinburg, Russia  
sergei.borisov@usu.ru

**Abstract.** A testing procedure and a program product for modeling gas-surface scattering process have been developed. Using the developed product the numerical simulation of the thermal transpiration phenomenon at free molecular conditions of the gas flow in channels with the use of different scattering kernels has been carried out. The surface structure influence on energy and momentum exchange in a gas-surface system has been studied by the use of Molecular Dynamics method.

## 1 Thermal Transpiration Phenomenon Study by Monte Carlo Method Realized for Different Gas-Surface Scattering Kernels

The most well-known diffuse-specular scheme of the boundary conditions to the heat and mass transfer equations of rarefied gas dynamics developed by Maxwell is successfully used for the majority of practical calculations (see, for instance, [1]). But some experimental data and corresponding theoretical calculations based on this scheme come into conflict with each other. As an example, one of the results of such calculations affirms that the thermal transpiration phenomenon (or “thermo molecular pressure difference effect” as it appears in scientific papers) does not depend on the kind of the gas and the surface state [2]. Such result contradicts the rather reliable experiments, for instance [3]. Apparently, the diffuse-specular scheme is not suitable for the correct description of the gas-surface scattering process at the non-isothermal rarefied gas flow, the striking example of which is the thermal transpiration phenomenon.

The use of the diffuse-specular scheme does not provide the dependence of scattering process on the gas molecule state that leads to contradiction between the theory and the experiment especially for non-isothermal gas flow. To eliminate such contradiction the boundary conditions that include certain data about the state of gas molecules interacting with the surface must be applied.

Nowadays, besides the diffuse-specular scheme other boundary conditions based on scattering kernels developed by Epstein [4] and Cercignani-Lampis [5,6] are widely recognized. The mathematical forms of these kernels contain certain expressions where the velocity of a gas molecules incident on the surface and the surface temperature are included. The Cercignani-Lampis and the Epstein scattering kernels are based on a certain physical ground and they satisfy all the requirements established for a scattering kernel [7].

To test the correctness of modeling the gas-surface scattering the program product that provides simulating the behavior of non-interacting molecules in finite space while changing the shape of the limited surface as well as the modeling method of the scattering process, the surface temperature distribution and the initial gas state has been developed. The free molecular version of the Monte Carlo direct simulation method [8] has been realized. The efficiency of the program product has been demonstrated on the example of reaching the equilibrium state of the gas in the bulbs of various forms at the temperature perturbation of the surface. On the base of this product the results that do not contradict the principal postulates of the gas kinetic theory have been achieved. This fact has initiated our interest to apply the developed approach for studying the thermal transpiration phenomenon in rarefied gas at non-isothermal conditions that meets the problem in description while using the scheme of boundary conditions based on the Maxwell scattering kernel.

To understand the problem let us consider the free molecular stationary gas flow in cylindrical channel connecting two bulbs where the gas is in the equilibrium with the “hot” and the “cold” bulb at the temperature  $T_h$  and  $T_c$  accordingly. The main equation for the gas pressure reached in each bulb is

$$\frac{P_h}{P_c} = \left( \frac{T_h}{T_c} \right)^\gamma, \quad (1)$$

where  $P_h$  – the gas pressure in the hot bulb,  $P_c$  – the gas pressure in the cold bulb,  $\gamma$  – a so called thermal transpiration coefficient.

The  $\gamma$  value is observed close to  $1/2$  in all simulation procedures that use the Maxwell kernel with any kernel parameter. The simulation of the thermal transpiration phenomenon with the use of Cercignani-Lampis and Epstein kernels demonstrates significant dependence of the thermal transpiration coefficient  $\gamma$  on the kernel parameters.

It has been shown that with the use of both the Cercignani-Lampis and the Epstein kernels the thermal transpiration effect depends on the channel’s length/radius ratio, the surface temperature distribution along the channel and does not depend on the bulbs’ temperature ratio. The stationary gas temperature distribution inside the channel depends on the channel’s length/radius ratio and practically does not depend on the kernel parameters. The stationary gas concentration distribution depends both on the channel’s length/radius ratio and the kernel parameters.

The comparison with the most reliable experiments shows that the simulation based on the use of the Cercignani-Lampis scattering kernels provides satisfactory description of the gas-surface scattering at non isothermal rarefied gas flow conditions at all. Due to strong dependence of the thermal transpiration coefficient on kernel parameters one can expect similar result while using the Epstein kernel.

## 2 Molecular Dynamics Simulation of Energy and Momentum Transfer in a Gas/Solids System

A great number of structural models describing current gas dynamics experiments and forecasting and momentum exchange in a “gas – rough surface” system have been

developed. Every model corresponds to definite material, grain orientation and surface structural phase. An attempt to build an adequate model of surface structure and to describe the real experiment for rarefied gas flow in a rectangular channel with the rough walls has been realized with the use of Monte Carlo Test Particle Simulation Method [9]. Other approach for statistical modeling the roughness proposed in [10] is based on the assumption that the separate elements of the surface microstructure are the cones of the same height and top angle. These approaches for simulation of the surface structure as similar ones are not adequate completely to the real situation because of their “artificial” character based on “imagination” but not on the topography of the real surface.

The methods of scanning probe microscopy, in particular, atomic force microscopy that are developed intensively last years give on opportunity to get an information on specific features of the surface structure and to develop boundary conditions adequate to the real situation. The attempt to simulate the surface structure with the use of such approach has been realized recently [11].

In this study we investigate the topography of platinum plate used in gas dynamics experiments to estimate the roughness of the real surface. The surface structure has been studied with the use of AFM Explorer in a contact regime of scanning. Using the obtained data the main parameters characterizing surface microstructure have been determined.

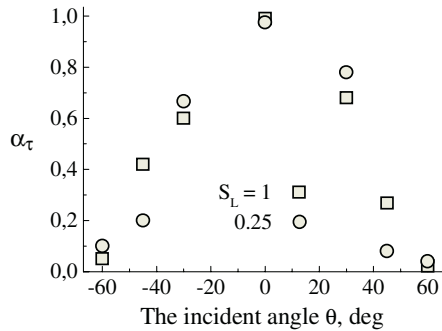


**Fig. 1.** The tangential momentum accommodation coefficient  $\alpha_\tau$  for xenon/platinum system

To simulate the gas-solids interaction the classical molecular dynamics method is applied. The Knudsen’s accommodation coefficients for tangential and normal momentum, as well as for kinetic energy have been calculated taking into account the gas nature and the surface structure. The results of the tangential momentum accommodation calculation for xenon/platinum system as a function of an incident angle  $\theta$  for two values of the velocity ratio  $S_L$  are presented in figure 1.  $S_L$  is introduced as a ratio of the surface movement velocity to the most probable gas molecule velocity.



### 3 Conclusions

The results of numerical simulation of the thermal transpiration phenomenon at free molecular conditions of the gas flow in channels with the use of the Maxwell, the Cercignani-Lampis and the Epstein scattering kernels are presented. The principal outcome of the study is the statement that in contrast to the Maxwell scheme of boundary conditions the use of the Cercignani-Lampis and the Epstein kernels permits to describe more correctly the non-isothermal internal rarefied gas flow. The obtained results show that there are no principle problems for gas-surface interaction description using numerical simulation procedures, in particular DMCS and molecular dynamics method. Some technical problems could be met under way of the AFM data use in simulations and finding acceptable form of interaction potentials as well as their parameters.

### Acknowledgments

The research described in this publication was made possible by Awards No: 03-53-5117 of INTAS and No: REC-005 (EK-005-X1), Y2-P-05-15 of U.S. Civilian Research & Development Foundation for the Independent States of the Former Soviet Union (CRDF).

### References

1. Siewert, C. E.: Poiseuille and thermal-creep flow in cylindrical tube. *J. Comp. Physics* 160 (2000) 470-480.
2. Sharipov F., Seleznev V.: Data on Internal Rarefied Gas Flow. *J. Phys. Chem.* 27 (3) (1998) 657-706.
3. Edmonds T., Hobson J.P.: A study of thermal transpiration using ultra high vacuum techniques. *J. Vac. Sci. Technol.* 2 (1965) 182-197.
4. Epstein M.: A model of the wall boundary condition in kinetic theory. *J. AIAA* 5(10) (1967) 1797-1800.
5. Cercignani C., Lampis M.: Kinetic model for gas-surface interaction. *Transp. J. Theory and Stat. Phys.* 1 (1971) 101-114.
6. Lord R.G.: Some further extensions of Cercignani-Lampis gas-surface interaction model. *J. Phys. Fluids* 7 (1995) 1159-1161.
7. Cercignani C.: *The Boltzmann Equation and its Application*. Springer, New York (1988).
8. Bird G.A.: *Molecular Gas Dynamics and Direct Simulation of Gas Flows*. Oxford University Press, Oxford (1996).
9. Sazhin O.V., Kulev A.N., Borisov S.F.: The role of the surface structure in formation of an ultra rarefied gas flow in a channel. *J. ThermoPhysics & Aeromechanics*, 8(3) (2001) 391-399.
10. Sawada T., Horie B.Y., Sugiyama W. *J. Vacuum*, 47(6-8) (1996) 795-797.
11. Gerasimova O.E., Borisov S.F., Boragno C., Valbusa U.: Modeling of the surface structure in gas dynamic problems with the use of the data of atomic force microscopy. *J. Eng. Phys. & Thermophys.*, 76(2) (2003) 413-416.

# GIVS: Integrity Validation for Grid Security

Giuliano Casale and Stefano Zanero\*

Dipartimento di Elettronica e Informazione,  
Politecnico di Milano - via Ponzio 34/5 - 20133 Milano Italy  
{casale, zanero}@elet.polimi.it

**Abstract.** In this paper we address the problem of granting the correctness of Grid computations. We introduce a Grid Integrity Validation Scheme (GIVS) that may reveal the presence of malicious hosts by statistical sampling of computations results. Performance overheads of GIVS strategies are evaluated using statistical models and simulation.

## 1 Introduction

Computational grids are touted as the next paradigm of computation [1]. Since they provide access to the resources needed for computational intensive applications, a Grid environment usually spans a heterogeneous set of machines.

When a Grid extends beyond the systems of a single administrative authority it suddenly becomes a network of potentially untrusted nodes, on which a remote user submits a potentially harmful piece of code together with sensitive data, as already happens in generic peer-to-peer systems [2]. The ensuing problems of security and privacy have not been fully explored in literature yet.

We identify at least four different problems that arise when extending Grid computing beyond a trusted network:

1. Defending each participant from the effects of potentially malicious code executed on the Grid [3, 4].
2. Avoiding unfair parties which tap computational resources without sharing their own [5, 6].
3. The privacy of data submitted for computation should be adequately protected, depending on their sensitivity.
4. The effect of the presence of one or more peers that are interested in making the overall computation fail.

Our paper will deal in particular with the last problem. We propose a general scheme, named Grid Integrity Validation Scheme (GIVS), based on problem replication and submission of test problems to the Grid hosts. We evaluate the effectiveness and the overhead of the proposed solution both analytically and through simulation.

---

\* This work has been partially supported by the Italian FIRB-Perf project.

The paper is organized as follows: in Section 2 we analyze the problem and we introduce our integrity scheme. Section 3 describes a statistical model for evaluating the security level and performance trade-offs of alternative validation scheme within GIVS. Finally, in Section 4 we draw conclusions.

## 2 The Grid Integrity Validation Scheme

The problem of detecting when remote untrusted machine is running a particular piece of mobile code is difficult to solve in the general case. Checksums and digital signatures can be used to verify the identity of a piece of code we have received, but cannot be used to prove to a remote party that we are actually executing it. Cryptographic protocols would require that the mobile code is endowed with a secret that cannot be accessed by someone controlling the host on which it is running, a constraint that looks impossible to achieve.

A possible solution would be to design the code in such a way that tampering with results in a non-detectable way would require a much longer time than calculating the real solution. Nevertheless, this would require a correct estimate of the real computation times, and thus would implicitly rely on the fact that the malicious user will correctly declare the computational power he has available.

Unless the particular problem we are dealing with has some sort of checksum property, which allows to check the correctness of the results without having to rerun the program, the only feasible approach is to check the correctness of the results by sampling. Specifically, we propose to use some *test problems* to check the correctness of the results. The idea resembles a blind signature protocol [7], in which the submitter prepares  $N$  similar documents, the signer opens  $(N - 1)$  documents checking they are correct, and then blindly signs the last document, with a probability  $p = 1/N$  to be cheated. In our case, documents are replaced by computational tasks. We also require to perform our controls by harnessing the computational power of the Grid as much as possible. This is the key idea of our Scheme for Integrity Validation of Grid computation, or GIVS.

In order to generate the test problems required for the integrity validation, we propose a *bootstrap* phase. During the bootstrap, one or more trusted machines compute correct solutions to a subset of test problems, chosen among the available ones according to some criteria (e.g. difficulty, sensitivity to errors, ...). These problems are then used during normal Grid activity to perform security controls, since when a test problem is scheduled to a user, the computed solution is compared to the correct solution to detect whether the user is malicious. Hence, users trying to corrupt the solution of a test problem would be easily identified.

While test problems seem a simple solution to the Grid integrity validation problem, some drawbacks can be identified. First, test problems require a bootstrap phase that slows down the computation startup and waste part of resources. Moreover, increasing the number of test problems could turn into a continuous performance overhead that may become unacceptable.

An alternative solution, consists in replicating a set of problems of unknown solution throughout the Grid, that we call *replicated problems* or just *replicas*. The integrity validation is performed in this case by comparing the different results provided by the untrusted hosts to the same replicated problem. If a conflict is detected, a trusted machine is asked to compute the correct result, so that the malicious hosts can be identified. Compared to the test problems approach, we are now accepting a trade-off between the performance overheads imposed by the integrity validation and the degree to which we can rely on our own security controls.

Notice that if a subset of  $M$  machines are cooperating to cheat, if they receive any test problem or replica in common, they can detect it and cheat. Moreover, if any of the results previously computed by any of the  $M$  machines is given to another machine as a test problem, it can be detected. The risk connected to this situation are evaluated in the next sections.

### 3 Performance-Security Trade-Offs

#### 3.1 Notation and Basic Definitions

Let us begin to model a Grid composed of  $H$  hosts, with  $M \leq H$  malicious nodes that are cooperatively trying to disrupt the computation. In normal conditions we expect  $M \ll H$ .

Let  $T$  be a period of activity of the Grid after the bootstrap phase. We discretize  $T$  in the  $K$  intervals  $T_1, \dots, T_K$ , thus  $\sum T_k = T$ . In each period  $T_k$ , every host  $h$  receives a collection  $\mathbf{P}_h^k = (p_1^k, \dots, p_P^k)$  of  $P_h$  problems<sup>1</sup>. We assume the solution of each problem  $p_i$  takes the same computational effort on all machines of the Grid. We can classify the problems  $p_m \in \mathbf{P}_h$  in several classes: we denote test problems with  $q_m$ , replicas with  $r_m$ , and generic problems, which don't have any role in security controls, are denoted with  $g_m$ . Thus, for instance, the set  $\mathbf{P}_h = (c_1, \dots, c_{C_h}, r_1, \dots, r_{R_h}, g_1, \dots, g_{G_h})$  is composed of  $C_h$  test problems,  $R_h$  replicas and  $G_h$  generic problems with  $P_h = C_h + R_h + G_h$ .

In the rest of this section we explore the two different strategies for GIVS described in Section 2: in the first one we use only test problems, while in the second all test problems are replaced with replicas. Our aim is to study, for each strategy, the performance overhead  $OH$  introduced by the security controls, and the probability  $p_{CF}$  of accepting a corrupted final value as a correct result.

#### 3.2 First Strategy: Test Problems

We now consider that each host receives a constant number of problems  $P_h$ , among which  $G_h$  are generic problems, while  $C_h = P_h - G_h$  are test problems. Then, no problem replicas are present in the sets  $\mathbf{P}_h$  ( $R_h = 0$ ). We denote with

---

<sup>1</sup> For clarity, we will omit in the rest of the paper the indices  $k$  when we do not need to refer to different time slices.

$\mathbf{q}_h$  the subset of test problems of  $\mathbf{P}_h$  and with  $C_h$  the cardinality of  $\mathbf{q}_h$ . All test problems  $q_m \in \mathbf{q}_h$  are distinct and extracted randomly from a set of  $C$  elements.

Under these assumptions, the performance overhead  $OH$  of this scheme is given by  $OH = H \cdot C_h$  since the solution of the test problems does not give any useful result for the applications running on the Grid.

We observe that the probability that two machines share the same control set is negligible. In fact, given that the probability of receiving a particular control set is the inverse of the number of possible distinct sets  $\mathbf{q}_h$ , we have

$$p(\mathbf{q}_{h_k}) = \binom{C}{C_h}^{-1} = \frac{C_h!(C - C_h)!}{C!}.$$

Now, observing that two random extractions  $\mathbf{q}_1$  and  $\mathbf{q}_2$  of the control sets are independent, the probability of two hosts  $h_1$  and  $h_2$  of receiving the same control set  $\mathbf{q}_{h_k}$  is

$$p(\mathbf{q}_{h_1} \equiv \mathbf{q}_{h_2}) = p(\mathbf{q}_{h_k})^2 = \left( \frac{C_h!(C - C_h)!}{C!} \right)^2.$$

In non-trivial cases this probability is extremely low. As an example, with  $C = 5$  and  $C_h = 3$ , it narrows down to a modest 0.25%. As  $C$  grows, this probability tends quickly to zero.

We now consider the probability  $p(q_m \in \mathbf{q}_h)$  that a particular problem  $q_m$  belongs to a control set  $\mathbf{q}_h$ . This probability is modeled using an hypergeometric distribution<sup>2</sup>, since it reduces to the probability of extracting a winning ball from a set of  $C$ , in  $C_h$  extractions without replacement. Then we have

$$p(q_m \in \mathbf{q}_h) = \text{hypergeom}(C, 1, C_h, 1) = \frac{(C - 1)!}{C!} \frac{C_h!(C - C_h)!}{(C_h - 1)!(C - C_h)!} = \frac{C_h}{C}$$

It is interesting to note that such probability is the same as if we would have dropped the no-replacement condition in the extraction, and so it suggest that, from a statistical point of view, the condition of uniqueness of the test problems in the same  $\mathbf{q}_h$  can be dropped.

We now turn our attention to  $p_{CF}$ . In order to quantify such probability, we first need to estimate the mean number  $\bar{s}$  of test problems that each user shares with the other malicious hosts. We can try to model such quantity as the probability  $P_M(k)$  that each host of a group of  $M$  has exactly  $k$  overlaps with the others. For the case  $M = 2$ , host  $i$  has probability  $P_2(k) = \text{hypergeom}(C, C_h, C_h, k)$ , since the winning problems are exactly the  $C_h$  that belong to the control set  $\mathbf{q}_j$  of host  $j$ . Unfortunately, if we try to extend this idea to the case with three or more hosts, we find that we cannot simply add together the pairwise probabilities, because we must account for the overlap between all three sets. This extension is quite difficult to derive analitically with a closed form, and due to its combinatorial nature, it raises some concerns about the computational complexity of

---

<sup>2</sup> We denote with  $\text{hypergeom}(n + m, n, N, i)$  the probability of having  $i$  successful selections from a hypergeometric distribution with  $n$  winning balls out of  $n + m$  and after  $N$  extractions.

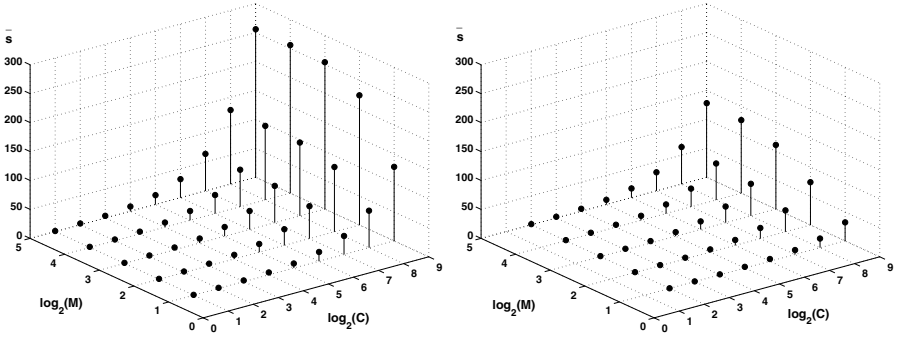


**Fig. 1.** Expected number of overlappings for different ratios of  $C_h$  versus  $C$ . In the left figure,  $C_h/C = 1/2$ . On the right,  $C_h/C = 1/4$

a possible iterative description. Moreover, what we actually need is the mean number of overlaps  $\bar{s}$ , rather than the complete probability distribution, and so a simulation can provide accurate estimates of  $\bar{s}$  at a reasonable computational cost and with limited modelling efforts.

In Figure 1 are shown the estimated  $\bar{s}$ , as a function of the number of malicious hosts  $M$  and of the total number of test problems  $C$  for the cases  $C_h/C = 1/2$  and  $C_h/C = 1/4$ . All the experiments have been conducted using an Independent Replications Estimate of the mean  $\bar{s}$  values with 50 replication of a total of over 1500 different samples. Confidence intervals have been computed for a 95% confidence level; however, since such intervals have resulted to be extremely tight to the estimated  $\bar{s}$ , we have omitted them from all figures.

Assuming now to know the value of  $\bar{s}$ , we can model the success probability  $p_{CF}$  of a malicious user using an hypergeometric distribution. We consider a malicious user  $h$  who gives  $b$  wrong answers to the problems of  $\mathbf{P}_h$  and answers correctly to the  $\bar{s}$  test problems that he has in common with other malicious users. In this case its probability of success  $p_{CF}$  is the probability of never giving a wrong answer a test problem, i.e.

$$p_{CF} \cong \text{hypergeom}(P_h - \bar{s}_+, C_h - \bar{s}_+, b, 0) = \frac{(P_h - C_h)!(P_h - \bar{s}_+ - b)!}{(P - C_h - b)!(P_h - \bar{s}_+)!}$$

where  $\bar{s}_+ = \text{ceil}(\bar{s})$  is used instead of  $\bar{s}$  since the formulas require integer values. Please note that if  $\bar{s}$  is integer the previous formula holds with the equality. The previous formula is defined only for  $b < C_h - \bar{s}_+$ , otherwise we have trivially that the user always corrupts a test problems and so  $p_{CF} = 0$ .

The qualitative behavior of  $p_{CF}$  is shown in Figure 2, where the probability is plotted against the ratio of undetected test problems ( $C_h - \bar{s}_+$ ) to the number of problems  $P_h$ . The figure is plotted with  $\bar{s} = 0$ , since this term simply shifts the origin of the x-axis of a corresponding quantity (e.g. with  $\bar{s} = 10$   $p_{CF}$  is 1 for  $x = C_h/P_h = 10$  ). Several observations can be drawn from the shape of the  $p_{CF}$ . First, as intuitive, if a host tries to cheat on a single problem, its probability

of success decreases linearly with the number of test problems. This has a very important consequence on every integrity validation schema: if the correctness of the global computation requires all subtasks to be computed correctly, a severe performance overhead is required to grant the correctness of the results. Then, according to the model, a Grid provider would require a strong additional cost to grant the security of such applications. However, in many cases of interest a malicious user would need to affect a large number of tasks in to affect the global solution. For example, affecting a multiobjective optimization of a set of functions over a numerical domain would probably require the simultaneous corruption of the results on many different subdomains for each of the objective functions. In the case of multiple corruptions ( $b \gg 1$ ), the probability  $p_{CF}$  drops quickly as the number of test problems grows. This suggests, if possible, to split the functional domain in the highest possible number of regions, although a trade-off with the involved communication overhead should be also taken into account [8]. However, even in this case, a large waste of computational resources is required to grant low values of  $p_{CF}$ . Therefore, using replicas could be a suitable way to handle these problems.

### 3.3 Second Strategy: Validation Using Replicated Problems

We are now going to extend the model developed for the first strategy to the case where replicated problems replace test problems. Problem sets have now the general form  $\mathbf{P}_h = (r_1, \dots, r_{R_h}, g_1, \dots, g_{G_h}) = \mathbf{r}_h \cup \mathbf{g}_h$ , and the replicas  $r_m \in \mathbf{r}_h$  are drawn from a set of  $U$  problems of unknown solution, in such a way that  $\rho$  replicas of each problem are scheduled on the Grid. As explained before, the main advantage here is that, as a side effect of the security controls, the solution of  $U$  problems is computed, and so less computational resources are wasted for security purposes. In fact, the minimum performance overhead when  $\rho$  replicas of each of the  $U$  problems are sent on the Grid is  $OH^- = (\rho - 1)U$  that accounts for the fact that replicas also yield the solution of the unknown problems. However, we must handle the case where  $m$  problems have been recognized as potentially corrupted, and so the performance overhead becomes  $OH = (\rho - 1)U + 2m$  since we lack  $m$  solutions and these must be recomputed by trusted machines. However, in normal conditions we expect  $OH \cong OH^-$ .

As observed for the first strategy, finding an analytical expression for the average number of overlappings  $\bar{s}$  is quite difficult. Furthermore, the model of the second strategy should include additional constraints and problems that are difficult to be handled by means of a statistical model. In fact, if we want to ensure that exactly  $\rho$  replicas of each of the  $U$  problems are computed on the  $H$  hosts, during the assignment of the replicas we must satisfy the constraint  $C_h H = \rho U$ .

Moreover, we observe that the constraint excludes the possibility of using a completely random assignment of the replicas: let us consider, for example, Table 1, where is shown a possible random assignment of  $U = 10$  problems with a replication factor  $\rho = 2$  (i.e.  $\rho U = 20$ ). In this case we still need to assign two replicated problems to host  $h_5$ , but only the replicas of problems 2 and 9 are

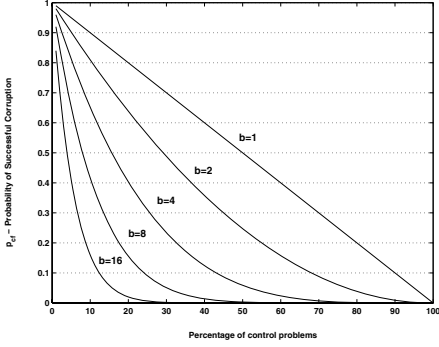


**Fig. 2.** Probability  $p_{CF}$  of accepting a corrupted result as function of  $C_h/P_h$  (here is  $\bar{s}_+ = 0$ ) and of the number of simultaneous wrong answers  $b$

Host	Replicated problems	
$h_1$	1 5 7	10
$h_2$	3 7 8	10
$h_3$	3 4 6	8
$h_4$	1 4 5	6
$h_5$	2 9 ?	?
Unassigned replicated problems		
<i>Avail</i>	2 9	

**Table 1.** An example of bad random assignment: any further assignment would alert  $h_5$  that he is subject to a security control

still unassigned. But this assignment is unacceptable, because it would break the condition that a host must receive distinct test problems. In this case, a random strategy would lock searching for an impossible assignment of the replicas.

A simple assignment scheme that avoids locking is the following: we assign randomly, until possible, the replicas. When a lock condition is detected, we change some of the previous assignment in order to solve correctly the assignment. For instance, in Table 1 we could easily avoid locking assigning replicas 2 and 9 to  $h_4$  and moving 5 and 6 to  $h_5$ . It is clear that such heuristics is quite complex to be modeled analytically, while using simulation we can easily estimate the involved overlappings  $\bar{s}$ . In Figure 3 we show in logarithmic scale some numerical results from a simulation with  $H = 48$  and  $\rho = 2$ : we can identify an exponential growth of the overlapping as the number of malicious users  $M$  and the unknown problems  $U$  grow. This turns to be a linear growth in linear scale, and so we conjecture an approximation  $\bar{s} \cong f(M, U)$ , where  $f(\cdot, \cdot)$  is a linear function.

Given that  $\bar{s}$  are known, the analysis of the probability  $p_{CF}$  for the second strategy results in the same formula derived for the first strategy, where the quantities  $C_h$  and  $C$  are replaced respectively by  $R_h$  and  $U$ . We also observe that, in most cases, the average overlappings  $\bar{s}$  for the second strategy are generally lower than those of the first one, but this is affected by the presence of  $H - M$  non-malicious hosts. The simulation of such users is a requirement for modeling the second strategy, since otherwise we would have trivially that  $\bar{s} = R_h$ . Such hosts, instead, are not considered in the simulations of the first strategy.

It is also interesting to note that  $U$  is in general bigger than  $C$  even with the optimal replication factor  $\rho = 2$ . This observation suggests that choosing between the two strategies should be done after a critical comparison of both the performance overheads  $OH$  and the  $p_{CF}$  for the two presented schemes, according to the specific characteristics of the Grid and its workload.



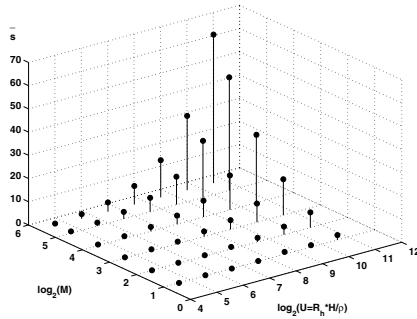


**Fig. 3.** Expected number of overlaps for the second strategy, with  $H = 48$  and  $\rho = 2$

## 4 Conclusions and Future Works

In this paper we have introduced GIVS, a Grid Integrity Validation Scheme, based on the idea of using test problems in order to detect the presence of malicious users. We have defined two different strategies for generating and distributing these problems, studying performance overhead and success probabilities of each using statistical models and simulation. We have shown that the cost for ensuring integrity is far from negligible. Thus, future extensions of our work include optimization techniques such as the introduction of trust and reputation mechanisms.

## References

1. Foster, I., Kesselman, C.: The grid: blueprint for a new computing infrastructure. Morgan Kaufmann Publishers Inc. (1999)
2. Oram, A., ed.: Peer-to-Peer: Harnessing the Power of Disruptive Technologies. O'Reilly & Associates, Inc. (2001)
3. Wahbe, R., Lucco, S., Anderson, T.E., Graham, S.L.: Efficient software-based fault isolation. In: Proc. of the 14th ACM Symp. on O.S. princ., ACM Press (1993) 203–216
4. Necula, G.C.: Proof-carrying code. In: Proc. of the 24th ACM SIGPLAN-SIGACT Symp. on Principles of programming languages, ACM Press (1997) 106–119
5. Damiani, E., di Vimercati, D.C., Paraboschi, S., Samarati, P., Violante, F.: A reputation-based approach for choosing reliable resources in peer-to-peer networks. In: Proc. of the 9th ACM CCS, ACM Press (2002) 207–216
6. Aberer, K., Despotovic, Z.: Managing trust in a peer-2-peer information system. In: Proc. of the 10th Int'l Conf. on Inf. and Knowledge Manag., ACM Press (2001) 310–317
7. Chaum, D.: Blind signatures for untraceable payments. In: Advances in Cryptology - Crypto '82, Springer-Verlag (1983) 199–203
8. Muttoni, L., Casale, G., Granata, F., Zanero, S.: Optimal number of nodes for computations in a grid environment. In: 12th EuroMicro Conf. PDP04. (2004)

# On the Impact of Reservations from the Grid on Planning-Based Resource Management

Felix Heine<sup>1</sup>, Matthias Hovestadt<sup>1</sup>, Odej Kao<sup>1</sup>, and Achim Streit<sup>2</sup>

<sup>1</sup> Paderborn Center for Parallel Computing (PC<sup>2</sup>),  
Paderborn University, 33102 Paderborn, Germany  
{fh, maho, okao}@upb.de

<sup>2</sup> Zentralinstitut fuer Angewandte Mathematik (ZAM),  
Forschungszentrum Juelich (FZJ), 52425 Juelich, Germany  
a.streit@fz-juelich.de

**Abstract.** Advance Reservations are an important concept to support QoS and Workflow Scheduling in Grid environments. However, the impact of reservations from the Grid on the performance of local schedulers is not yet known. Using discrete event simulations we evaluate the impact of reservations on planning-based resource management of standard batch jobs. Our simulations are based on a real trace from the parallel workload archive. By introducing a new option for scheduling reservations in planning-based resource management, less reservation requests are rejected. Our results are important for increasing the acceptability of the Grid technology. We show, that a limited number of additional resource reservations from the Grid have only a limited impact on the performance of the traditionally submitted batch jobs.

## 1 Introduction

Currently, a gap [2] exists between the demands of Grid middleware and the capabilities of the underlying resource management systems (RMS). While Grid middleware systems provide a certain amount of support for Quality of Service (QoS), underlying RMSs offer only limited functionality in this aspect. Service Level Agreements (SLA) [7] are powerful instruments for assuring QoS, but simply adding SLA negotiation mechanisms to an existing RMS is not sufficient. A demand for advanced abilities in runtime management and control exists. A basic mechanism for accomplishing a guaranteed resource usage are *advance reservations*. They denote the reservation of a fixed amount of resources for a given time span. In the context of Grid Computing, reservations are indispensable to realize the simultaneous availability of distributed resources and to orchestrate Grid workflows. In queuing-based systems reservations are complex to realize, as scheduling focuses only on the present resource usage. In contrast, planning-based resource management systems [3] do resource planning for the present and future. Their design implicitly supports advance reservations.

In this paper we evaluate the impact of reservations on the schedule quality of planning-based resource management systems. This impact is important to

evaluate, as reservations affect the scheduling of the traditionally existing workload of batch jobs on supercomputers. Reservations occupy resources for a fixed time span, which gives the scheduler less opportunities to schedule batch jobs. With only some reservations in the system, this impact can be invisible, as the scheduler has still some free slots in the schedule. However, with an increased usage of Grid technology more reservations will be submitted to the underlying resource management systems. At a certain point, the impact will become visible and traditional batch jobs have to wait longer for execution.

We evaluate this impact by using discrete event simulations and generating a fixed amount of batch jobs from a workload trace. We increase the amount of submitted reservation requests and measure the average slowdown of batch jobs. Additionally, we measure the rejection rate of the submitted reservation requests and the utilization of the system.

The intuitive approach for scheduling reservations is to reject them, if the requested resources are already scheduled to batch jobs. We introduce a new approach for scheduling reservations, where such interfering batch jobs are scheduled to a later time and the reservation can be accepted.

The remainder of this paper is structured as follows: we first give an overview on related work, following an overview on the characteristics of planning-based scheduling. In section 4 we present the results of our simulations, thus measuring the impact of advance reservations. A brief conclusion closes this paper.

## 2 Related Work

Many publications deal with the implementation and applications of advance reservations. However, not much publications have been written about the impact of reservations on resource management.

In 2000, Smith, Foster and Taylor published their results on scheduling with advance reservations [8]. At this, they proposed and evaluated several algorithms, regarding utilization, mean wait time and the mean offset from requested reservation time, which is the time between the reservation request and the receipt of the reservation. All measurements were generated with an Argonne National Laboratory (ANL) workload trace. A basic assumption in their simulations is, that running jobs that have been reserved are not terminated to start other jobs. It is also assumed that reserved jobs will always start on time. These assumptions imply the necessity of run time estimates for each job to assure that resources are free on time. In fact, extending this approach to all types of jobs would lead to planning-based scheduling.

For systems which do not support resumable jobs (i.e. intermediate results of a job are not saved, so that a job can be restarted after termination), measurements show an superproportional increase of waiting time by increasing the percentage of reservations. Likewise, the mean offset from requested reservation time is increasing superproportional. By decreasing the percentage of queued jobs that can not be delayed by a reservation, waiting time as well as offset decrease. For resumable jobs, which can be terminated and restarted at a later

time without losing results, the jobs to terminate can be determined using an equation regarding number of nodes and used computing time. For this type of jobs, further decrease of waiting time and offset can be measured.

In [1] a queuing scheduler is enhanced to support advanced reservations. The authors state that users with lower priorities may gain start time advantages by using advanced reservations. To prevent this, the authors applied a shortest notice time for every reservation. It is defined using a predictive waiting time as if the reservation would have been submitted as a queued job. The prediction is based on historical data. A performance evaluation shows that advanced reservations prolong the queue waiting time, although no start time advantages are taken. Hence, longer shortest notice times have to be applied to prevent this.

Similar as before, this work reveals the restrictions of queuing-based scheduling. As only the present resource usage is scheduled, decisions on future reservations can not be based on future load information, instead predictions have to be done. With applying notice times to reservations, users can not specify arbitrary desired start times for their reservations. This is possible in planning-based scheduling presented in this paper.

### 3 Scheduling Reservations in Planning-Based Systems

If we look in depth at the way current resource management systems work, we find two different approaches: *queuing-based* and *planning-based* systems. In [3] we give a detailed overview on the two types of scheduling approaches. Examples for planning-based systems are the Maui scheduler [4] or CCS [5]. Choosing one of these approaches has a huge impact on the provided features and in particular on the possibility to support advance reservations.

Due to their design queuing-based systems do not support reservations by nature. Hence, work-arounds have to be used, e. g. the insertion of dummy-jobs in high-priority queues, or suspend and resume of low-priority jobs, but they all have drawbacks. Either, the number of reservations is limited, or in fact a second, planning-based scheduler is implemented on top of the queuing-based resource management system. In planning-based systems, on the other hand, reservations are implicitly available in a trivial and easy way.

We call standard batch jobs *variable jobs* as they can move on the time axis until they are started. The scheduler places such jobs at the earliest possible free slot in the schedule. If prior jobs finish earlier than expected, or get aborted, the scheduler might re-schedule the job to an earlier time. Depending on the scheduling policy (e. g. SJF, LJF), jobs may also be moved to a later point in time. *Reservations* have a user specified start time and the scheduler can either accept or reject the reservation for the given start time. Reservations limit the scheduler in placing variable jobs, as resources are occupied for a fixed time.

In case the scheduler cannot place a reservation due to a conflict with a not yet running variable job, we have two options. In the first one, which we call *reject*, a new reservation is only accepted, if the resources requested for the given time frame are available. The reservation is rejected, if the resources are

occupied by already running jobs, by previously accepted reservations, or by planned variable jobs.

With the new **variable jobs move** option the scheduler additionally accepts those reservations, for which the requested resources are only occupied by variable jobs which are planned, but not yet running. The scheduler plans the overlapping variable jobs at a later time, so that the reservations can be accepted. Still, a reservation is rejected, which collides with already running jobs or other reservations.

Note, starvation of variable jobs is possible with the **variable jobs move** option, in case newly submitted reservations constantly delay variable jobs. Appropriate mechanisms have to be implemented in this case to prevent starvation.

## 4 Evaluation

It is common practise to use discrete event simulations for the evaluation of job-scheduling strategies. For this purpose we implemented the **reject** and **variable jobs move** options in our MuPSiE system (Multi Purpose Scheduling Simulation Environment).

For evaluating the simulated schedules we use different metrics. We are focusing on the slowdown metric  $s_i$  (= response time divided by run time) and weight it by the job area  $a_i$  (= run time · requested resources), resulting in the *SLDwA* metric defined as  $SLDwA = \sum a_i \cdot s_i / \sum a_i$ .

For measuring reservations other metrics have to be used than for variable jobs, as reservations do not have a waiting time which depends on the scheduler's performance and workload. As already mentioned in Section 3 reservations are either started at their requested start time or they are rejected. Hence, the total number of rejected reservations and respectively the rejection rate in percent of all submitted reservations is measured in our evaluations.

Finally, the overall utilization of the machine is used to measure the efficiency of the scheduler to place all simulated requests, variable jobs and accepted reservations. This information about utilization is of particular interest for system owners.

### 4.1 Workload

An evaluation of job scheduling policies requires to have job input. In this work a variable job (Section 3) is defined by the submission time, the number of requested resources, and the estimated run time, which is mandatory for planning-based resource management system. The use of a discrete event simulation environment for the evaluation requires additional data about the actual run time of a job. A reservation is defined by the same four parameters like a variable job, but additionally a requested start time is specified.

The variable jobs in this work are derived from a trace of the Parallel Workload Archive [6]. We are using the CTC trace from the Cornell Theory Center. It was taken from a 512-node IBM SP-2 machine during July 1996 to May 1997. It

contains 79,279 valid jobs and only 430 nodes of the 512 are available for batch processing.

Unfortunately, no traces are available which contain the appropriate data about reservations required for our simulations as described above. Hence, reservations have to be generated synthetically. In our work this is a two step process and we use the variable jobs from the CTC trace as a basis.

In a first step variable jobs are randomly chosen to get their properties (submission time, number of requested resources, estimated and actual run time). These properties are the basis for newly generated reservations. An input parameter defines, in percent of all variable jobs, how many reservations should be generated in total. If set to 100%, every variable job is used to copy its properties and generate a new reservation, hence the amount of submitted variable jobs and reservation is 79,279 each. With reservations added to the set of variable jobs, the overall workload submitted to the scheduler is increased.

The most important property of a reservation, its requested start time, is generated in the second step. At first a start delay is computed as follows:  $start\ delay = rand[0, 1] \cdot estimated\ run\ time \cdot start\ factor$ . Assume that the start factor is initially set to 1, then the start delay is a random number between 0 and the estimated run time. This random start delay is added to the original submission time of the variable job and the resulting value is the requested start time for the reservation. The input parameter *start factor* is used to modify the start delay, so that the requested start time of reservations is potentially further (start factor > 1.0) or sooner (start factor < 1.0) in the future. With these two steps all necessary properties of a new reservation are copied and generated.

### 4.2 Results

Figure 1 and Figure 2 show the results for the two different scheduling options, three different start factors, and the three used performance metrics. Note that we repeated each simulation ten times and took the average result to exclude singular effects from generating random jobs.

With the *variable jobs move* option the scheduler moves interfering variable jobs to a future start time. This implies, that less reservations are rejected,

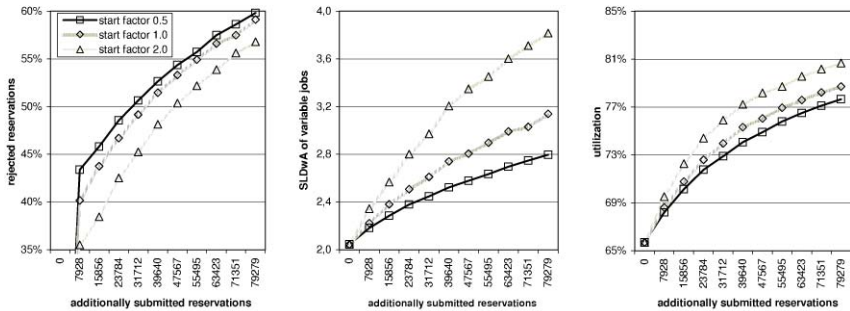
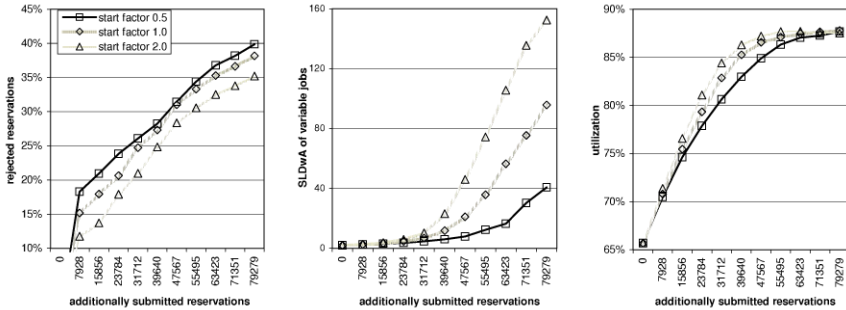


Fig. 1. Results with start factor 0.5, 1.0, and 2.0 for the reject option



**Fig. 2.** Results with start factor 0.5, 1.0, and 2.0 for the variable jobs move option

but variable jobs have to wait longer for a start, i.e. their slowdown (SLDwa) increases. Still, if resources are occupied by previously accepted reservations, or by already started reservations, or variable jobs, new reservation requests are rejected with the variable jobs move option.

Focusing on the percentage of rejected reservation and the SLDwa metrics for the two scheduling options in Figures 1 and 2 shows this behavior. The more reservation requests are submitted, the more reservations the scheduler has to reject, as these additional reservations increase the workload and potentially more resources are occupied by other reservations or running jobs. This is the case for both scheduling options. Independent of how many reservations are submitted, the scheduler has to reject more reservations with the reject option, than with the variable jobs move option. For different amounts of submitted reservations the difference between both options is at least 20 percentage-points. With only some reservations submitted, this constant difference means, that more than twice as much reservations are rejected with the reject option. Note, with no reservations submitted at all, obviously no reservations are rejected (or accepted) by both options.

Taking a look at the SLDwa values for all scheduled variable jobs confirms the above made assumption. With the reject option, the scheduler does not replace variable jobs for new reservation requests. They are started at their originally assigned start time and they are not further delayed. However, made reservations may occupy resources for variable jobs submitted in the future, so that their (and thereby the overall) slowdown increases slightly. The curve for variable jobs move clearly shows, that moving variable jobs further in the future and thereby accepting more reservations, significantly increases the slowdown of variable jobs. The results become worse, the more reservations are submitted.

With additionally submitted reservations the workload increases and thereby the utilization, too. However, the utilization can not increase unbounded, which can be seen for the variable jobs move option in particular. Not more than approx. 88% is possible. The planned schedule is so compact, that additional reservations would only increase the slowdown (SLDwa) of variable jobs. Comparing the two scheduling options shows, that with the variable jobs move option the utilization is higher than with the reject option. This is based on the fact, that

more reservations can be accepted (cf. the percentages of rejected reservations) and that the scheduler has more freedom in planning variable jobs by placing them further in the future.

The start factor is used to modify the start delay, so that the requested start time of reservations is potentially further (start factor  $> 1.0$ ) or sooner (start factor  $< 1.0$ ). Increasing the start factor from 0.5 to 1.0 and 2.0 means that the time difference between the submission and average requested start time of reservation requests gets larger. Combined with the random computation of the requested start times, they are equally distributed over a larger time span. This reduces the limitations for the scheduler to accept reservations and to (re)place variable jobs. Thus the scheduler can accept more reservations. This can be seen in the diagrams for both scheduling options. With a start factor of 2.0 less reservations are rejected, independent of the total amount of submitted reservations.

With a similar argumentation one could expect that the SLDwA values of variable jobs should decrease with increasing start factors: requested start times are further in the future and variable jobs might be placed at an earlier time in the schedule. However, the diagrams show different results. Increasing the start factor leads to increased SLDwA values for both scheduling options. On a first look the made assumption is correct and variable jobs are potentially placed earlier in the schedule. However, the reservations are still in the schedule, which means that the scheduler is still limited in placing variable jobs. As previously mentioned more reservations are accepted with increased start factors and this additionally limits the scheduler in placing variable jobs. In the end, the scheduler is more limited in placing variable jobs with an increased start factor, so that the SLDwA of variable jobs increases for both options.

As less reservations are rejected with increased start factors, the workload increases and the generated utilization is higher. This can be seen for both scheduling options, but observing the utilization diagram for the variable jobs move option in detail shows, that at the beginning the difference becomes larger and at the end almost the same utilization is achieved. With the variable jobs move option the system runs in a saturated state with many reservations submitted. Accepting more reservations as a result of increased start factors does only mean that the SLDwA values increase and variable jobs have to wait longer. Hence, the differences in the percentage of rejected reservations are smaller for the variable jobs move option than for the reject option. The saturated state is not reached with the reject option, so that a higher utilization is generated by the scheduler with different amounts of reservations submitted and the achieved utilization values are smaller.

## 5 Conclusion

At the beginning of this paper we revealed the demand for QoS and guaranteed resource usage support in modern resource management systems. To this end, planning systems are well suited for this endeavor due to their design. Planning



the present and future resource usage by assigning proposed start times to all waiting jobs makes reservations trivial to schedule. Although reservations are well-known, their impact on planning-based scheduling was not yet evaluated.

We introduced two scheduling options, called *reject* and *variable jobs move*, and evaluated the impact of different numbers of reservations on the performance of these options. As no real workload trace contains reservation requests, they were added synthetically. Based on the properties of randomly chosen jobs from the trace, we generated several job sets with different amounts of added reservations. Furthermore, we generated different start delays. The performance was measured by: the percentage of rejected reservations, the average slowdown of variable jobs weighted by their area (SLDwA), and the utilization of the system.

Our results show, that both scheduling options have their benefits. With *reject* the SLDwA of variable jobs does not increase much due to the additionally accepted reservations, but many reservations are rejected by the scheduler. With the *variable jobs move* option more reservations are accepted by the scheduler, as variable jobs are moved to a future start time. Hence, the result is an increased SLDwA of variable jobs. Generating reservations, which are further in the future, means that the scheduler can accept more reservations, so that the utilization increases. As more reservations are accepted the scheduler is more limited in placing variable jobs, hence their SLDwA increases.

In contrast to a queuing system, scheduling reservations in a planning system does not mean to terminate running jobs to guarantee the requested start time of the reservation. This is a direct consequence of planning the present and future resource usage not only of reservations, but also of all waiting variable jobs.

## References

1. J. Cao and F. Zimmermann. Queue scheduling and advance reservations with cosy. In *Proc. of 18th Intl. Parallel and Distributed Processing Symposium*, 2004.
2. G. Fox and D. Walker. e-Science Gap Analysis. Technical report, Indiana University, USA, 2003.
3. M. Hovestadt, O. Kao, A. Keller, and A. Streit. Scheduling in HPC Resource Management Systems: Queuing vs. Planning. In *Proc. of the 9th Workshop on Job Scheduling Strategies for Parallel Processing*, 2003.
4. D. Jackson, Q. Snell, and M. Clement. Core Algorithms of the Maui Scheduler. In *Proc. of 7th Workshop on Job Scheduling Strategies for Parallel Processing*, 2001.
5. A. Keller and A. Reinefeld. Anatomy of a Resource Management System for HPC Clusters. In *Annual Review of Scalable Computing*, Singapore University Press, 2001.
6. Parallel Workloads Archive. <http://www.cs.huji.ac.il/labs/parallel/workload>.
7. A. Sahai, S. Graupner, V. Machiraju, and A. v. Moorsel. Specifying and Monitoring Guarantees in Commercial Grids through SLA. Technical Report HPL-2002-324, Internet Systems and Storage Laboratory, HP Laboratories Palo Alto, 2002.
8. W. Smith, I. Foster, and V. Taylor. Scheduling with Advanced Reservations. In *Proc. of the 14th Intl. Conference on Parallel and Distributed Processing Symposium*, 2000.

# Genius: Peer-to-Peer Location-Aware Gossip Using Network Coordinates<sup>1</sup>

Ning Ning, Dongsheng Wang, Yongquan Ma, Jinfeng Hu, Jing Sun,  
Chongnan Gao, and Weiming Zheng

Department of Computer Science and Technology, Tsinghua University, Beijing, P.R.C  
{nn02, myq02, hujinfeng00, gcn03}@mails.tsinghua.edu.cn  
{wds, zwm-dcs}@tsinghua.edu.cn

**Abstract.** The gossip mechanism could support reliable and scalable communication in large-scale settings. In large-scale peer-to-peer environment, however, each node could only have partial knowledge of the group membership. More seriously, because the node has no global knowledge about the underlying topology, gossip mechanism incurs much unnecessary network overhead on the Internet. In this paper, we present Genius, a novel peer-to-peer location-aware gossip. Unlike many previous location-aware techniques which utilize BGP or other router-level topology information, Genius uses the network coordinates map produced by Vivaldi as the underlying topology information. By utilizing the information, Genius could execute near-preferential gossip, that is, the node should be told the gossip message by nodes as close as possible, through which much unnecessary ‘long-range’ communication cost could be reduced. Further, the node direction information inherited in the coordinate space is exploited. We present preliminary experimental results which prove the feasibility of our scheme.

## 1 Introduction

Peer-to-Peer applications have been popularized in the Internet in recent years. Building reliable, scalable, robust and efficient group communication mechanism on top of peer-to-peer overlay is an important research topic. Such mechanism in peer-to-peer environment much meet following three requirements: the first one is scalability; the second one is reliability, robustness and decentralized operation; the third one is efficiency. The gossip communication mechanism pioneered by [2] emerged as a good candidate which has the potential to satisfy the requirements mentioned above.

The work in this paper deals with the unstructured system which is developed in the previous Scamp[4] protocol. However, the Scamp protocol does not take the underlying topology into account, that is, it is not location-aware. This causes much unne-

---

<sup>1</sup> This work is supported by National Natural Science Foundation of China (60273006).

sary network overhead on internet. The waste of network resources is needless and should be reduced.

Many previous works [6][7][8] address the location-aware issue from various aspects in different settings. Due to shortcomings of these schemes explained at length in Section 4, we propose Genius, a novel peer-to-peer location-aware scheme. In Genius, a network coordinates map which indicates the coordinate of each node is produced by Vivaldi[1] when nodes join the system gradually. Our scheme obtains topology information from this map without the help of network-layer information provided by domain administrators.

In Genius, individual node gains the rather global view of the whole system by exchanging its local information with other nodes in the system. After gathering node information over the whole system, the individual node analyzes them and adjusts its local view so that each individual node has a balanced view of the whole system. Based on these adjusted location-aware local views, Genius could execute location-aware gossip which enables more nodes to be told the gossip message by more nearby nodes, and accordingly reduces the network overhead.

The primary contributions of this paper are the following:

1. It presents Genius, a peer-to-peer location-aware gossip using network coordinates without the help of network-layer information.
2. It proposes an approach to cluster nodes in the coordinate space in a decentralized manner.
3. Genius is the first system to exploit the node direction information in the coordinates map to our knowledge.

The rest of the paper is organized as follows. Section 2 describes the Genius design. Section 3 presents results. Section 4 discusses related work. Finally, Section 5 summarizes our conclusion and future work.

## 2 Genius Design

There are several steps for node in Genius to obtain location-aware local view.

### 2.1 Node Arrival and the Network Coordinates Map Construction

In Genius, new node joins the system according to the process specified in the subscription section of Scamp[4]. After collecting latency information from nodes in its *InView*[4], the new node computes good coordinates for itself using Vivaldi[1] which does not depend on the selection of landmarks[3]. When the coordinates converge, one global network coordinates map is formed and Genius enters into nearby nodes exchange stage.

According to [1], coordinates drawn from a suitable model can accurately predict latency between hosts and inter-host RTT is dominated by geographic distance. Thus, the node coordinates reflect its geographic location and it is reasonable to infer the geographic relation of nodes based on the coordinates map.

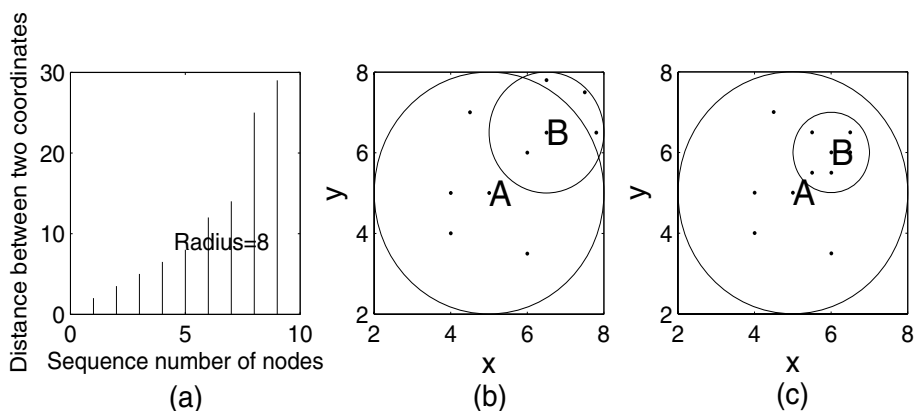


**Fig. 1.** Illustration of nearby nodes exchange and Clique formation. (a) is the selection of the Clique radius. (b) is the increasing of the Clique radius, and (c) is the decreasing of the Clique radius

## 2.2 Nearby Nodes Exchange Process and Faraway Nodes Exchange Process

The nearby nodes exchange action is to exchange topology information among the close-by nodes called “Clique” which is formed in the exchanging process simultaneously. The process is actually to cluster nodes in the coordinate space in a decentralized manner. Every node in the system executes the process. The process is described as follows.

Firstly, each node orders the distances between the coordinates of itself and the nodes in its *PartialView* (i.e. the latency between them) in the order of increasing distance. Find the largest difference between the adjacent distances from the smallest one to largest one, which is larger than the preceding difference and the succeeding difference. Define the smaller one of the two distances between which is the largest difference as radius  $r$ . This is illustrated by Figure 1(a). The largest difference in Figure 1(a) is the one between the distance of node #5 and that of node #6 which is 4 (i.e. 12-8) and larger than 1.5 (i.e. 8-6.5) and 2 (i.e. 14-12). The nodes in its *PartialView* whose distance is smaller than  $r$  are considered to belong to the same Clique as it does and  $r$  is the radius of the Clique.

According to the Clique radius, there are two sets of nodes in the *PartialView*: nodes belonging to its Clique are called ‘Clique contact’ and all the nodes except Clique nodes are called ‘long-range’ contact. The intuition behind the selection of Clique radius  $r$  is that the nodes in the same Clique should have relative similar distance from the source node and the nodes not belonging to the same Clique should have relative larger distance.

For acquiring more information about the Clique and preventing the Clique radius being excessively inaccurate just depending on its own *PartialView*, the node needs exchange its information about the Clique, that is Clique membership and Clique radius, with other nodes in its Clique. Thus, it will ask other nodes in its Clique about

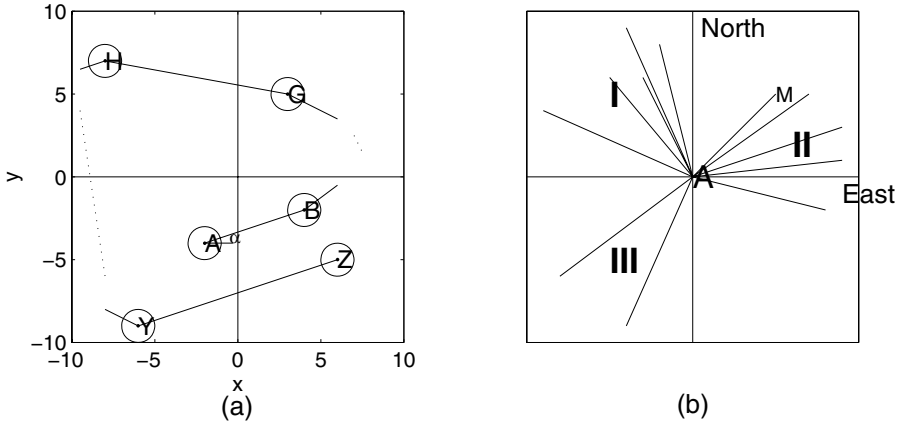


**Fig. 2.** Illustration of faraway nodes exchange and the 'long-range' contact set adjustment. In (a), node A traverses the whole system from node B to node Z. The circle centered at each node represents its Clique. 'long-range' contacts of node A in different directions are shown in (b). They form areas of different angular density, such as area I,II,III

which nodes are in their Clique and their Clique radius. For the exchanging process progressing in the right direction and converging to the right state reflecting the real topology, we should force the node exchanging information with nodes whose information is more accurate than that of itself. We define the Clique radius of the node as its credit. Smaller the radius, more credit should be given to the node. The node only trusts nodes whose radius is smaller than its own and exchanges information with them.

Exchanging action is described as follows. As illustrated in Figure 1(b), node B is in the Clique of node A. The radius of Clique of node A is 3 and that of Clique B is 2. So, node A trusts node B and adds the nodes in the Clique of node B into its own 'Clique node' set of its *PartialView*. But the size of original *PartialView* is maintained for future use. This intuition behind the augment of membership is the transitivity property, that is, node A and node B belong to a same Clique, and that, nodes in the Clique of node B belong to the same Clique as node B do, so, nodes in the Clique of node B should belong to the Clique of node A. After adding more nodes into its own 'Clique node' set, node A starts modifying its Clique radius. Then, node A uses similar method described above to determine the new radius based on the result of the augment of Clique membership. This example illustrates the increasing of Clique radius. The example of decreasing of excessively large Clique radius of node A is shown in Figure 1(c). Through repeatedly exchanging information with trusted nodes in its own Clique, the node modifies its Clique radius in every step. The process converges until the variance of radius per step is smaller than one small percent of the radius, say 1%, in several successive steps.

After the node has exchanged information among nodes in its Clique, it needs execute the faraway nodes exchange process which is used to exchange information about 'long-range' contacts to gain a rather complete view of the whole system. We propose a method exploiting the node direction information in the coordinates map.

We observe that nodes with the same latency from the node, but in different direction mean differently to the node. Thus, nodes should not only be classified in the measure of latency and node direction is also an important parameter to be considered. For the node to be able to obtain a summary view of the whole system, our method works as follows. In Figure 2(a), node A wants to exchange information. Firstly, node A selects the longest ‘long-range’ contact node B which is of longest distance from node A in its ‘long-range’ contact set. The vector AB makes an angle of  $\alpha$  with axis  $x$ . It then visits node B, gets one copy of ‘long-range’ contacts of node B. Next, node B finds the set of its ‘long-range’ contacts which satisfy that vector BC makes an angle of  $\alpha+\beta$  with axis  $x$  (suppose node C is a random element of the set), then selects a node C randomly from the set as the next stop of the traverse. Similarly, node A visits node C, and gets one copy of its ‘long-range’ contacts. After that, node C selects a node D randomly from its ‘long-range’ contacts satisfying that vector CD makes an angle of  $\alpha+2\beta$  with axis  $x$  as the next stop. Analogically, node E, F, and G are selected as the next stops. The process terminates when the last vector which is formed by the last two stops, such as YZ, makes an angle between  $\alpha-\beta$  and  $\alpha+\beta$  with axis  $x$ . This termination condition implies that node A traverses a circle on the whole system. When no node in the ‘long-range’ contacts satisfies the above requirement, the node most approximately meeting the requirement is selected.

The selection of  $\beta$  is determined as follows. Preliminary experimental results from Section 3 show that traversing about 35 nodes are enough to obtain a rather complete view of the system. So, it is suitable to let  $\beta$  be  $360/35$ , approximately 10 degree. Making  $\beta$  positive means counterclockwise traverse and making  $\beta$  negative means clockwise traverse.

When node A traverses the system, it aggregates the copies of ‘long-range’ contacts of visited nodes in the network by processing over the data when it flows through the nodes, discarding irrelevant data and combining relevant data when possible. The goal of our aggregation of ‘long-range’ contacts is to identify a set of contacts in which only one contact belongs to every distinct Clique, that is, this set contains just one representative contact for each Clique.

The aggregation at each traversed node is described as follows. When node A visits node B, if the distance between node A and the node in the ‘long-range’ contact set of node B (for instance, node  $s$ ) is smaller than the Clique radius of node  $s$ , node  $s$  is considered to belong to the same Clique of the ‘long-range’ contact of node A. When the traverse is complete, node A obtains the summary knowledge about other Cliques in the system. Every node in the system traverses the system and gets its own ‘long-range’ contact set. Although working in this way seems too costly, this kind of traverse happens only once when the system initializes.

### 2.3 The *PartialView* Adjustment and Maintenance in Dynamic Environment

After the detailed knowledge about its own Clique and a summary knowledge about other Cliques in the system are obtained by each node, the *PartialView* of each node should be adjusted so as to the size of the *PartialView* is  $O(\log(N))$ , where  $N$  is the size of the system.

Firstly, we determine the size of the result *PartialView* of node A as the mean size of all original *PartialView* size of visited nodes in the previous traverse. This size is

$O(\log(N))$ . Secondly, we compute the proportion between the size of the Clique of node A and the size of the ‘long-range’ contact set. Then, we could determine the size of the result Clique contact set and that of the result ‘long-range’ contact set.

The next job is to select determined size of nodes from the two former sets. Basically, the selection strategy lies on the most concern of the system designer. There is an obvious tradeoff between network overhead (i.e. message redundancy) and reliability in gossip mechanism. For the Clique contacts, if the designer most concerns about reducing network overhead, those nodes which are nearest should be kept in the result Clique contact set. On the contrary, if the designer most concerns about gossip reliability, the result Clique contacts should be selected randomly from the former Clique contact set of node A. For the ‘long-range’ contacts (see Figure 2(b)), suppose a ‘long-range’ node M, node A computes the angle formed by vector AM and axis  $x$ . Node A computes the angle for each node in the ‘long-range’ contact set. If reducing network overhead is the most concern, contacts are selected to be kept according to the density of distribution of angles of contacts. If the most concern is gossip reliability, contacts in sparse area, such as area III, encompassing few nodes should be given priority to be selected. Given the location-aware *PartialView*, more nodes could be told the gossip message by closer neighbors. Thus, location-aware gossip is achieved.

Nodes leaves the system according to the process specified in the unsubscribe section of Scamp[4]. Because Vivaldi[1] naturally adapts to network changes, the node coordinates remain accurate.

### 3 Results

Preliminary experiments mostly concentrate on the faraway nodes exchange process. We use a data set which involves 1740 DNS servers mentioned in [1] as the input to

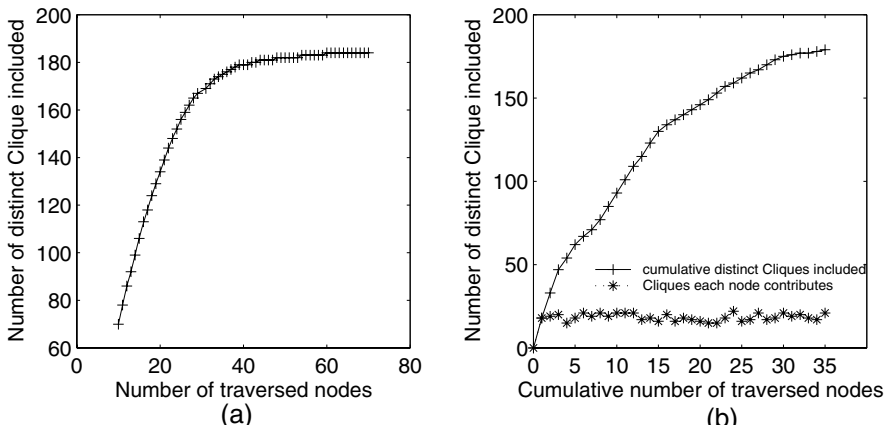


**Fig. 3.** Preliminary experimental results focusing on faraway nodes exchange process. (a) is the number of distinct Cliques included as a function of number of traversed nodes. (b) is the number of distinct Cliques included as a function of cumulative number of traversed nodes in one experiment in which 35 nodes are traversed

Vivaldi. The node coordinates output by Vivaldi is taken as the input to our simulator. Our simulator implements the logic in the paper.

Figure 3(a) shows that when more than 35 nodes are traversed, the number of distinct Cliques collected increases very slowly during the faraway nodes exchange process. The experiment suggests suitable number of nodes required to be traversed for obtaining a rather complete view of the system is 35.

Figure 3(b) shows that in one experiment in which 35 nodes are traversed, how the number of distinct Cliques included increases along with the progression of the traverse.

## 4 Related Work

Many location-aware techniques are proposed to achieve location-aware operations in different environment. LTM[6] is a measurement-based technique designed to do location-aware query in unstructured peer to peer systems. It builds a more efficient overlay by cutting low productive connections which is detected by TTL2 detector and choosing physically closer nodes as logical neighbors. Routing underlay[8] provides underlying network topology for overlay services by aggregating BGP routing information from several nearby routers. However, this approach is somewhat too ideal because not all the administrators of domain are willing to provide a feed from their BGP router to the underlay. In contrast, our network coordinates-based approach will not encounter this problem since coordinates are computed by participants cooperatively with no relation to BGP router.

As to the clustering of nodes in coordinate space, Sylvia Ratnasamy *et. al.*[9] proposed a binning scheme. A node measures its round-trip-time to each of  $d$  landmarks and orders the landmarks in order of increasing RTT. Thus, every node has an associated ordering of landmarks. The nodes having the same ordering of landmarks belong to the same bin. But, unfortunately, the approach corresponds to halve the right angle in the  $d$ -D Euclidean space, thus it does not reflect the node partition based on distance. Some research works also deal with the location-aware gossip. Localiser [7] chooses an energy function over all the nodes and edges in the system incorporating its locality-related objectives and then the function is minimized by simulated annealing through decentralized operation. However, Localiser depends on the choosing of the parameter sensitive energy function too heavily and it is possible for Localiser to be trapped at a local minimum.

## 5 Conclusions and Future Work

In this paper, we present Genius, a peer to peer location-aware gossip using network coordinates. In contrast to other approaches, it does not rely on any kind of network-layer information which is probably not available. It also does not depend on certain energy function very much. In the future, more experiments about Clique formation and gossip overhead, reliability should be conducted.



## References

- [1] Frank Dabek, Russ Cox, Frans Kaashoek, Robert Morris Vivaldi: A Decentralized Network Coordinate System In Proceedings of ACM SIGCOMM'04, Portland, Oregon, Aug, 2004
- [2] A. Demers, D. Greene, C. Hauser, W. Irish, J. Larson, S. Shenker, H. Stuygis, D. Swinehart, and D. Terry. Epidemic algorithms for replicated database maintenance. In Proceedings of 7th ACM Symp. on Operating Systems Principles, 1987.
- [3] T. S. Eugene Ng and Hui Zhang Predicting Internet Network Distance with Coordinates-Based Approaches In Proceedings of IEEE INFOCOM'02 New York, June 2002.
- [4] A. Ganesh, A.-M. Kermarrec, and L. Massoulié. Peer to-peer membership management for gossip-based protocols. In IEEE Transactions on Computers, 52(2), February 2003.
- [5] A.-M.Kermarrec, L.Massoulié, and A.J. Ganesh Probabilistic reliable dissemination in large-scale systems. IEEE Transactions on Parallel and Distributed Systems, 14(3), March 2003
- [6] Yunhao Liu, Xiaomei Liu, Li Xiao, Lionel Ni, Xiaodong Zhang Location-aware Topology Matching in P2P Systems. In Proceedings of IEEE INFOCOM'04 Hong Kong, March, 2004
- [7] Laurent Massoulié, Anne-Marie Kermarrec, Ayalvadi J. Ganesh Network Awareness and Failure Resilience in Self-Organising Overlay Networks In IEEE Symposium on Reliable and Distributed Systems, Florence, 2003
- [8] Akihiro Nakao, Larry Peterson and Andy Bavier A Routing Underlay for Overlay Networks In Proceedings of ACM SIGCOMM'03 Karlsruhe, Germany, August, 2003
- [9] Sylvia Ratnasamy, Mark Handley, Richard Karp, Scott Shenker Topologically-Aware Overlay Construction and Server Selection. In Proceedings of IEEE INFOCOM'02 New York, June 2002.

# DCP-Grid, a Framework for Conversational Distributed Transactions on Grid Environments

Manuel Salvadorés<sup>1</sup>, Pilar Herrero<sup>2</sup>, María S. Pérez<sup>2</sup>, and Víctor Robles<sup>2</sup>

<sup>1</sup> IMCS, Imbert Management Consulting Solutions,  
C/ Fray Juan Gil 7, 28002 Madrid, Spain

<sup>2</sup> Facultad de Informática – Universidad Politécnica de Madrid,  
Campus de Montegancedo S/N,  
28.660 Boadilla del Monte, Madrid, Spain  
mso@imcs.es  
{pherrero, mperez, vrobles}@fi.upm.es

**Abstract.** This paper presents a Framework for Distribute Transaction processing over Grid Environment, called DCP-Grid. DCP-Grid complements *Web Services* with some OSGI functionalities to implement the *Two Phase Commit* (2-PC) protocol to manage two types of Distribute Transactions, Concurrent and Conversational transactions, properly in this kind of environment. Although DCP-Grid is still under development at the Universidad Politécnica de Madrid, in this paper, we present the design and the general characteristics associated to the implementation of our proposed Framework.

## 1 Introduction

The introduction of *Services Oriented Architectures* (SOA) [1] [2], in the last few years, has increased the use of new distributed technologies based on *Web Services* (WS) [3]. In fact, e-science and e-business processes have adopted this technology to improve the integration of some applications. The coordination of this type of processes, based on WS, needs the transactional capability to ensure the consistency of those data that are being handled by this kind of applications.

A transaction could be defined as the sequence of actions to be executed in an atomic way. This means that all the actions should finish - correctly or incorrectly- at the same time as if they were an unique action.

The four key properties associated to the transactions processing are known as the ACID properties - *Atomicity*, *Consistency*, *Isolation*, y *Durability*[4]. The aim of our proposal is to build a Framework, based on grid technologies, to coordinate distributed transactions that are handling operations deployed as Web Services.

The Grid Technology, which was born at the beginning of the 90's, is based on providing an infrastructure to share and coordinate the resources through the dynamic organizations which are virtually distributed[5] [6].

In order to make possible the development of DCP-Grid, we will take into account the *Grid Web Services* (GWS) characteristics. The GWS, defined in the *Open Grid Service Infrastructure* (OGSI) [7], could be considered as an extension of the WS. The GWS introduce some improvement on WS, which are necessary to the

construction of standard, heterogeneous and open Grid Systems. The OGSI characteristics on which DCP-Grid has being designed and built are: Statefull and potentially transient services; Service Data; Notifications; portType extension; Grid Service Handle (GSH) and Grid Service Reference (GSR).

OGSI is just an specification, not a software platform, and therefore, we need a middleware platform, supporting this specification, in order to deploy the DCP-Grid Framework. From all the possible platforms to be used, we have decided to use the Globus Toolkit [8] platform for this Project because in the most extended nowadays. More specifically, we have being working with GT3 (version 3.2) for DCP-Grid due to its stability.

In this paper we will start describing the state of the art in the dealing area as well as their contributions to the DCP-Grid design, subsequently we will move to the architectural design of our proposal and we will give some details related to the framework implementation to finish with some conclusions, ongoing directions and future work.

## 2 Related Work

The standard distributed transactional processing model more extended is the X/Open [14] model, which defines three rolls (Resource Manager RM, Transaction Processing Manager TPM and Application Program AP) [9] [14].

Based on the Web Service technology two specifications to standardize the handling of transactions through open environments have arisen. These specifications are WS-Coordination [10] and WS-Transaction [13], developed by IBM, Beas and Microsoft. In them, the way to group multiple Web Services as a transaction is exposed, but the form of coordination of the transactions is not specified. On the other hand, the Business Transaction Protocol specification (BTP) [13], proposed by OASIS, defines a transactional coordination based on workflows. This specification is complex to handle and integrate [12]. Based on GT3 [8] we try to construct a simple proposal for the implementation of a transactional manager adopting the X/Open model. In the proposed design, the analogies are visible.

### 2.1 Two Phase Commit Protocol

The *Two phase commit* (2-PC) protocol is an ACID compliant protocol to manage DTs. How 2-PC works is easy to explain. A Transaction with a 2-PC protocol does not commit all the actions if not all of them are ready to be committed. This process works in two phases, as its names indicates, first phase called *Voting Phase* and second phase called *Commit Phase*.

During de *Voting Phase*, each and every action notifies to the system their intentions to commit theirs operation. This phase terminate when all the actions are ready to be committed. Then starts the *Commit Phase*, during this phase the system notifies to each and every action to be finished, the conclusion of the operation takes place when the commit message arrives from the system to each and every action.

These two components work in two different phases, during the *Voting Phase* when an application requests to the DTC to commit a Transaction, the DTC sends `PREPARE_TO_COMMIT` to all the RM that have uncommitted actions of the Transaction, then the DTC waits for a period to receive all the RMs responses.

There are two possible responses `READY_TO_COMMIT` or `UNABLE_TO_COMMIT`. If all the RMs responses to the DTC are `READY_TO_COMMIT` message then the DTC sends a `COMMIT` message to all RMs, but if any of the resource managers sends a `UNABLE_TO_COMMIT` or not response in a limit time then the DTC sends a `ROLLBACK` message to all the RM. In Figure 1 we can appreciate the successfully scenario of a commit transaction over 2-PC protocol.

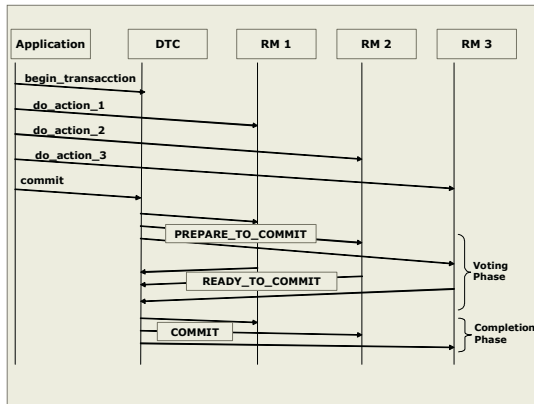


Fig. 1. 2-PC messages interaction

*Distributed Transactions* and 2-PC protocol will be the pillars of our Framework because DCP-Grid will provide 2-PC protocol to support transaction processing.

## 2.2 Classification of Distributed Transactions

We assume two categories *Concurrent Distributed Transactions* and *Conversational Distributed Transactions*:

- *Concurrent Distributed Transactions*: are the transactions formed by actions that have not dependencies between. In this case, the different actions can be sending by the application layer in a concurrent way improving the service time processing.
- *Conversational Distributed Transactions*: are the transactions composed by dependent actions. An example of this kind of transaction could be the following. This scenario refers for any transaction in which action N depends on, at least, one or more actions previously executed, being N-i the maximum number of actions to be included in this dependence, and i a natural number representing the position.

### 3 Scenarios

As we mentioned in previous section of this paper, there is two different kinds of categories regarding to each proposed scenario.

#### 3.1 Scenario 1: Concurrent Distributed Transactions

In this scenario we will concentrate on the logical operation of the Framework regarding transactions composed by independent actions.

Let's imagine a scenario composed by two actions A and B, and a client application which wants execute these actions in a Transactional way. In this case it would necessary define a transaction like Tx {idTx, coordinator, A, B} where idTx is transaction id and A, B are the actions that compose the transaction. The element coordinator references to the DTC process that coordinates the phases of the transaction.

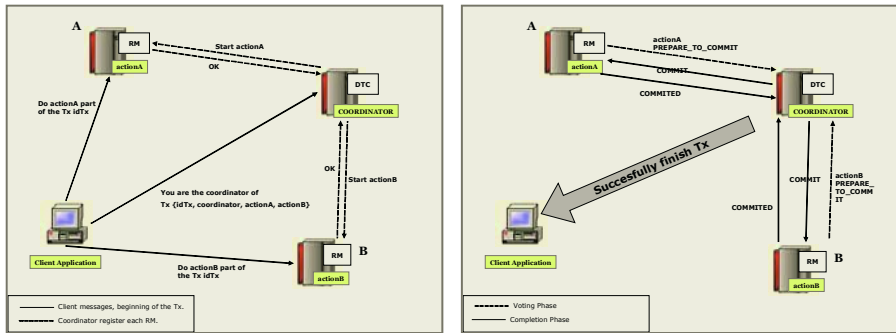


Fig. 2. Scenario for Concurrent Distributed Transactions

Figure 2 shows how the transaction starts, first the client applications sends to each RM the respective action and the idTx associated with the Tx. At same time, the client, sends to the coordinator all the information of the Tx, with this information the coordinator register in the DTC all the actions of the Tx and sends a message to each RM for start their associated actions.

Once each and every action is ready to be committed, it will send a message to the DTC notifying the current state (PREPARE\_TO\_COMMIT), as it were mentioned previously this is the *Voting Phase*. After all RMs have sent their status message the DTC will decide about finish the transaction sending a COMMIT message to each RM. The stage meanwhile the DTC is sending the COMMIT message is the *Commit Phase* of the 2-PC protocol.

The case of ROLLBACK in this scenario will given by the overcoming of period (TIMEOUT) or if any RM sends a fail message (UNABLE\_TO\_COMMIT) to the DTC, in this situation a ROLLBACK message will be send to each RM.

It is easy to see a small modification over the previous explication of 2-PC, in this scenario due to the concurrency, are the RM's who sends the message PREPARE\_TO\_COMMIT not the DTC.

### 3.2 Scenario 2: Conversational Distributed Transactions

This scenario describes a DT composed by the same two previous actions A and B which can't working currently, due to this, these actions are sent sequentially because of its dependencies, the client recovers the partial results and it invokes other actions with these results. Due to this, is the client who decides when the transaction must finalize, and when the 2-PC protocol must begin their commit phases (*Voting* and *Completion*).

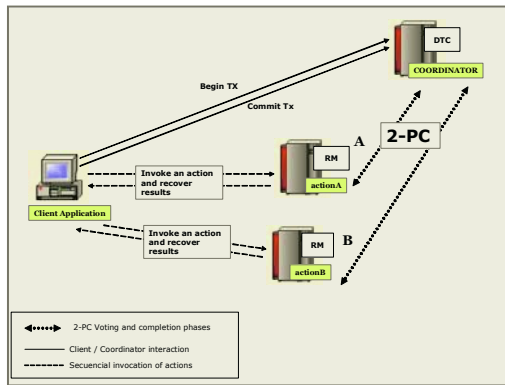


Fig. 3. Scenario for Conversational Distributed Transactions

The Figure 3 shows the process in this scenario. First the client application invoke the coordinator to start the transaction Tx, after, call sequentially the necessary actions and to finish the transaction invoke the coordinator with a COMMIT message. At this moment, the DTC manages the 2-PC protocol to cross the *Voting* and *Completion* phases like in scenario 1. In case of failure of some action, the DTC will send a ROLLBACK message to the rest of them.

In addition, if some RM does not respond in a time limit then a ROLLBACK message will be sent by the DTC to each RM. By this way, we avoided blockades of long duration. The problem of blockades and concurrency access will be explained in more detail in section 4.1.

## 4 Our Approach to Grid Environments

Taking advantage of the OSGI characteristics, we propose a DCP-Grid to be introduced in a Grid Environment. As our first approach at the *Universidad Politécnica de Madrid* (UPM), we have decided to introduce a new interface which

we have called *ITransactionSupport*. This new interface provides to Grid Services with operations that provides “rollback” and “commit” functionality. Every Grid Service which wants take part of a transactional execution will extend this interface, this solution could be achieved thanks to the *PortType Extension*, provided by OGSF.

On the other hand, we have defined the element *Distributed Transaction Coordinator (DTC)*, key concept for DCP-Grid. Our solution proposes to the DTC like a *Grid Service*, we assigned to this service the name of *TXCoordinationService*, with this design we took advantage of all features of *Grid Service* to develop the DTC.

In order to separate the interface of the logical behavior our proposal introduce a new component, the engine that manages all the process around the commit protocol. This component is the *TXManagementEngine*. We can look inside the coordinator in the next figure:

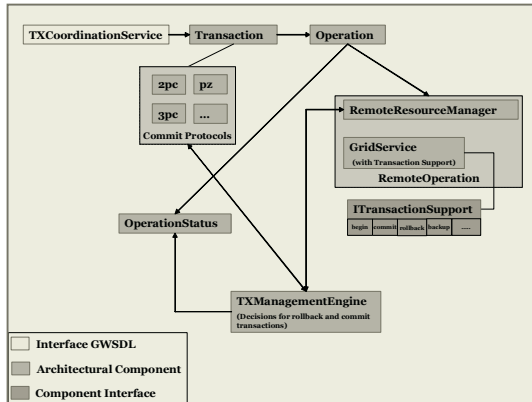


Fig. 4. DTC building blocks Architecture

The *TXManagementEngine* makes its decisions in function from the information updated by the *TXCoordinationService*, for example, when the *TXCoordinationService* receives a message *PREPARE\_TO\_COMMIT* it update the correspondent *OperationStatus*. When the *TXManagementEngine* detects that all *OperationStatus* are in *PREPARE\_TO\_COMMIT* then sends a *COMMIT* message to all remote resource managers.

Each remote RM can commit their operations because it implements *ITransactionSupport*. In case of some message received by the *TXCoordinationStatus* will be a *UNABLE\_TO\_COMMIT* message then the *TXManagementEngine* will make a rollback sending the corresponding message to each remote RM.

The RM is another *Grid Service* deployed in each system that contains transactional *Grid Services* due to this the *TXManagementEngine* contained in the DTC can invoke the *TXResourceManagerService* for the commit or rollback interface operations and a situation of blockade will occur.

#### 4.1 Solutions to the Situations of Blockade

A key point to be taken into account is the resolution of the interblockades; this factor could be critical in some scenarios as the following: a client application invokes a service and this execution is part of a transaction. At a certain moment, this service not finished yet because of another action associated to the same transaction is not in the commit phase. At this same moment, another client application sends the execution of a transaction in which there is the same action blocked before. If this action is not released, another execution will not be able to enter and a situation of blockade will occur.

In order to solve this situation our proposal establishes a time limits of delay to process commit once the service has been processed, this timeout will be a parameter to be established by each and every service. In future versions of DCP-Grid, we will tackle the problem deeply.

#### 4.2 Solutions to Concurrent Access Situations

During the investigation of DCP-Grid a problem with the concurrent access appear. What happens if an RM has deployed a service that allows parallel access to different client execution, if two clients invoke the service simultaneously when the respective DTCs want to process COMMIT or ROLLBACK? How the RM knows which is the message (COMMIT / ROLLBACK) associated to each execution?

To solve this situation our proposal generates a unique ID that will be propagated in corresponding messages to the respective DTCs and RMs. With this ID the two components (DTCs and RMs) will be able to associate the message received with the corresponding operation. This session ID identifies uniquely each transaction. Another problem appear with this solution How can generate unique IDs across different RMs in separated system?

To solve this new problem DCP-Grid will negotiate the session ID between the RMs. The internal operation is as it is described to continuation, the DTC associated to the transaction generate the transaction ID based on the system address, after the DTC sends the start message to each RM. If some RM detects that it has an active id with same value, then this RM will send a CHANGE\_ID message to the DTC, the DTC will generate a new ID only for this RM. Internally the DTC will store this information for future messages.

## 5 Conclusions and Future Work

In this paper we have presented our approach to implement an architecture supporting transactional Grid WS execution. This approach is based on some of the main properties of OGSi specification [7]. As ongoing work, currently we are developing a similar framework for concurrent distributed transactions on grid environments which will be presented in the Workshop on KDMG'05. So many future research lines has been opened for DCP-Grid but maybe the most interesting would be the building of an environment to support transactions on distributed and heterogeneous databases based on the concepts and ideas that we have presented in this paper.



## References

- [1] Douglas K. Barry, *Web Services and Service-Oriented Architecture: The Savvy Manager's Guide*, Morgan Kaufmann Publishers 2003
- [2] Mark Endrei, Jenny Ang, Ali Arsanjani, Sook Chua, Philippe Comte, Pal Krogdahl, Min Luo, Tony Newling, "Patterns: Service Oriented Architecture", IBM RedBook SG24-6303-00
- [3] "Web Services Main Page at W3C", <http://www.w3.org/2002/ws/>, World Wide Web Consortium, (consultado en dic/2004)
- [4] Bernstein, New Comer "Principles of Transaction Processing", Editorial: Kaufman, 1997
- [5] I. Foster, C. Kesselman. *The Physiology of the Grid: An Open Grid Services Architecture for Distributed System Integration*. 2002. <http://www.globus.org/research/papers/ogsa.pdf>
- [6] Miguel L. Bote-Lorenzo, Yannis A. Dimitriadis, Eduardo Gómez-Sánchez "Grid Characteristics and Uses: A Grid Definition", LNCS 2970, 291-298
- [7] S. Tuecke, K. Czajkowski, I. Foster. *Grid Service Specification*. Technical Report. Jun 2003. [www-unix.globus.org/toolkit/draft-ggf-ogsi-gridservice-33\\_2003-06-27.pdf](http://www-unix.globus.org/toolkit/draft-ggf-ogsi-gridservice-33_2003-06-27.pdf)
- [8] "Globus Toolkit Project", The Globus Alliance, <http://www.globus.org> (consulted 2004/12)
- [9] I. C. Jeong, Y. C. Lew. DCE "Distributed Computing Environment" based DTP "Distributed Transaction Processing" Information Networking (ICOIN-12) Jan. 1998
- [10] F. Cabrera et al., "Web Services Coordination (WS-Coordination)" Aug. 2002, [www.ibm.com/developerworks/library/ws-coor/](http://www.ibm.com/developerworks/library/ws-coor/)
- [11] F. Cabrera et al., "Web Services Transaction (WS-Transaction)" Aug. 2002, [www.ibm.com/developerworks/library/ws-transpec/](http://www.ibm.com/developerworks/library/ws-transpec/).
- [12] Feilong Tang, Minglu Li, Jian Cao, Qianni Deng, *Coordination Business Transaction for Grid Service*. LNCS3032 pag. 108-114 (Related Work Section)
- [13] OASIS BTP Committee Specification 1.0, 3 June 2002, *Business Transaction Protocol*, <http://www.choreology.com/downloads/2002-06-03.BTP.Committee.spec.1.0.pdf>
- [14] X/Open Specification, 1988, 1989, February 1992, *Commands and Utilities*, Issue 3 (ISBN: 1-872630-36-7, C211); this specification was formerly X/Open Portability Guide, Volume 1, January 1989 XSI *Commands and Utilities*(ISBN: 0-13-685835-X, XO/XPG/89/002).

# Dynamic and Fine-Grained Authentication and Authorization Architecture for Grid Computing

Hyunjoon Jung, Hyuck Han, Hyungsoo Jung, and Heon Y. Yeom

School of Computer Science and Engineering, Seoul National University,  
Seoul, 151-744, South Korea

{hjjung, hhyuck, jhs, yeom}@dcs1ab.snu.ac.kr

**Abstract.** The Globus Toolkit makes it very easy and comfortable for grid users to develop and deploy grid service. As for the security mechanism, however, only static authentication and coarse-grained authorization mechanism is provided in current Globus Toolkit. In this paper we address the limitations of current security mechanism in the Globus Toolkit and propose a new architecture which provides fine-grained and flexible security mechanism. To implement this without modifying existing components, we make use of the Aspect-Oriented Programming technique.

## 1 Introduction

With the advent of grid computing, Globus Toolkit[8] have been playing an important role for making grid systems. Thanks to the support of various components in the Globus Toolkit, many grid developers have been able to develop their own grid systems very conveniently. When the grid service administrator - in this paper, we would like to divide grid users into grid service administrator and general grid users for explaining more precisely - make their own grid systems, the grid computing environment usually consists of many service nodes which are managed correlatively. Namely, many nodes can be separated logically into specific domains which can be under the same policy, so called virtual organization [11]. The grid service administrator should manage various kinds of services according to the policy of each domain.

Although it is possible in current Globus Toolkit, there are some limitations. If a new user wants to use some grid service, the grid service administrator must change the policy of the service which might be currently running. However, to change the security policy of a specific grid service, it is required to stop the grid services related to the altered security policy. After the policy change, the grid services are redeployed according to the new security policy.

Besides, current security scheme of Globus Toolkit supports only service level authorization. In other words, method level authorization is not supported. If the grid service administrator wants to configure different authorization level for each method, he should make extra grid service under different security policy. Consequently, current security configuration scheme in Globus Toolkit is static and coarse-grained, which results in extra jobs for grid service administrator.

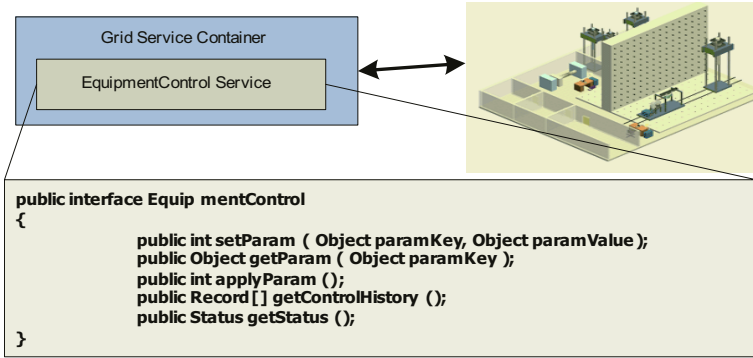


Fig. 1. Motivation Example

To mitigate these limitations, we present a dynamic authentication and authorization scheme. Our scheme also allows fine-grained method level security scheme. In designing and implementing this scheme, we have used *Aspect-Oriented Programming* [9, 10, 14] so that existing Globus Toolkit is left unmodified.

The rest of this paper is organized as follows. We discuss the motivation of this project in detail in section 2 and introduce our design goals and strategies in section 3. And then we propose new architecture in section 4. In section 5, we explain how to implement our scheme with *Aspect-Oriented Programming*. The section 6 addresses issues of grid security related to our work and future works. In the end, we conclude our paper with summary and contribution.

## 2 Motivation

In this section, we describe the limitations of security scheme in current Globus Toolkit. And then our focuses of this paper will be introduced.

In grid computing, there are many users who try to access some services. And there are also many kinds of grid services being executed by user’s request. To manage users and services securely, grid computing have adopted security policies for each user and service. In practice, Globus Toolkit ensures the security of grid service and user with exploiting grid security infrastructure (GSI) [12].

With the advent of web-based architecture, grid service also have evolved into conforming architecture[5]. However, current Globus Toolkit supports only static management of security policy in web-based architecture. In other words, the security policy of specific service would be set before deploying. Besides, while that service is running, security policy cannot be reconfigured and applied instantly to that service. Owing to this kinds of limitations, grid service administrator should first stop the service, reconfigure specific security policy and then redeploy that service. Since this reconfiguration and redeployment should be done for each small change, the burden on the part of the administrator could be huge.

In addition to the static management of security policy, security level in authorization can be also considered as a limitation. When the grid service administrator deploys some services with current Globus Toolkit, the level of authorization is the service instance. Figure 1 describes the motivating example. When *EquipmentControl* service is deployed, grid administrators configure security policies for each user level. If *EquipmentControl* grid service would be subject to the policy of table1, it is impossible to provide service to each user's permission using existing Globus Toolkit.

**Table 1.** The list of user's permission of each service method

user group	defined security policy
experiment, operator	permit all methods
other researcher	permit getXXX() methods
guest	permit getControlHistory() method

In other words, current Globus Toolkit cannot support method-level authorization scheme. Since only service-level authorization scheme is provided, the grid service administrator ought to make each service separately according to each user's request and authorization policy. Consequently, it leads to the inefficient utilization of resources.

### 3 Design Goals and Strategy

As stated in the previous section, our goal in this paper is to ameliorate the current Globus Toolkit as follows:

- To provide dynamic authentication and authorization
- To support fine-grained authorization
- To implement this scheme as an extra module without modifying the Globus Toolkit.

To provide dynamic authentication and authorization means that grid service administrators would be able to reconfigure the security policy of running services without suspending them. Supporting fine-grained authorization presents enhancements of security granularity and removes the redundancy of grid services. For instance, if some grid administrator would like to change security policy of some grid services, they would be troubled like the example of the section2. It is an inefficient utilization of resources due to multiple security policies. Therefore, method level authorization with dynamicity would be a better alternative to solve this kind of problem. In order to support these two security schemes in the Globus Toolkit, it would be easy to implement if we modify security part in Globus Toolkit.

In that case, however, Globus Toolkit should be recompiled and then it causes undesirable extra needs. For these challenges of implementation, we adopt gracious programming skill that is *Aspect-Oriented Programming*. It ensures that

any existing program does not need to be modified. By exploiting this way, we would present more compact and modularized architecture. Aspect-oriented programming would be explained down to the minutest details in the implementation part.

## 4 Proposed Architecture

To achieve our goals, we propose the architecture composed of three components in accordance with each role as shown in figure2.

### 4.1 FSecurity Manager

Originally, security mechanism of Globus Toolkit is mainly divided into authentication part which verifies someone and authorization part which checks the right of a user in grid service. And the policy of the authentication and authorization can be set only ahead of the deployment of grid service. Hence, to achieve the dynamicity of security scheme, *FSecurity Manager* intercepts the request of authentication and authorization in current Globus Toolkit when the request is invoked. And then, that request is processed in *FSecurity Manager* with Security Configuration Data.

For instance, we assume that the grid administrator expects 10 users would use his grid service A before deployment. But, after some time, 5 new users would want to use the grid service A. In that case, the grid administrator must stop the grid service A to modify new security policy for the 5 new users. And after applying new security policy, grid service will be executed again correctly. However, this kind of process would be changed with *FSecurity Manager* as follows. Above all, the most troubled part which do not check the security policy at running time is changed with intercepting request of *FSecurity Manager*.

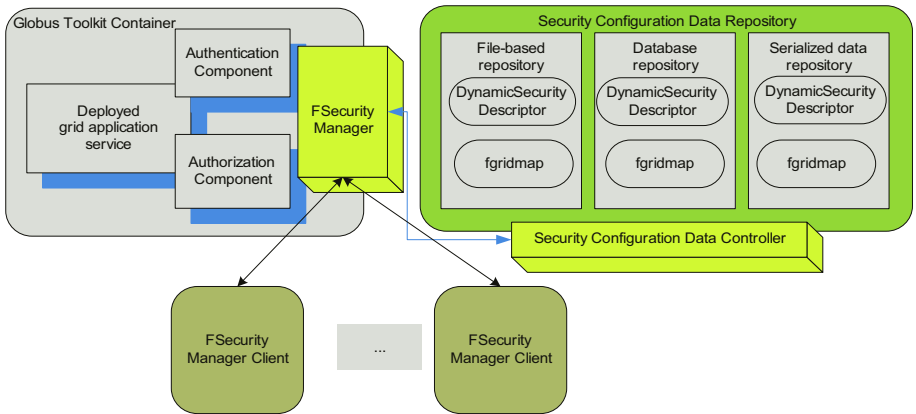


Fig. 2. Proposed architecture

And then *FSecurity Manager* reads the security policy at that time, applied that scheme to authentication and authorization instantly. Therefore, *FSecurity Manager* supports the reconfigurable security processing.

Moreover, *FSecurity Manager* provides a fine-grained authorization processing with adding the element which describes the relation between user and grid service method. In current Globus Toolkit, before the service deployment, grid service administrator used to configure the gridmap file which describes simply those who can use specific grid service. However, that mechanism is changed into supporting the dynamic management and the fine-grained description with *FSecurity Manager*. In the former case, grid service administrator can reconfigure gridmap file even though service is executing. There is no need to stop the service and redeploy it later. And as for the latter, the description which some user have rights to use some grid service method is added into new type gridmap file, which is called fgridmap.

## 4.2 Security Configuration Data Controller

*Security Configuration Data Controller* is an extra module in order to manage security policy information. Security policy information can be stored as a XML file, serialized file or database records. To support this kind of function, this controller is responsible for connecting, storing, and loading specific security policy information with a data repository. In real grid computing, grid administrator can install this part in a machine which Globus Toolkit is executed or another machine which may be dedicated to data repository.

## 4.3 FSecurity Manager Client

This component supports that grid service administrator controls and manages the security policy of grid service from a remote or local node. Client program can be installed in a ordinary computing node or mobile node such as PDA, mobile phone. Also the grid service administrator can manage a *FSecurity Manager* via web interface.

# 5 Implementation

As we mentioned above, our implementation without the change of Globus Toolkit is done with a refined programming skill which is Aspect-Oriented Programming. In this part, we would describe the reason why we have adopt Aspect-Oriented Programming and how it was applied. And then the operation flow of the proposed architecture would be explained with a structural perspective.

## 5.1 Aspect-Oriented Programming and Our Architecture

*Aspect-Oriented Programming (AOP)* complements *Object-Oriented programming* by allowing the developer to dynamically modify the static OO model to create a system that can grow to meet new requirements. The reason why we use *Aspect-Oriented Programming* technology is to separate the core part of

program from the extra part of program because there is some kinds of different properties between the former and the latter. For instance, many of us have developed simple web applications that use servlets as the entry point, where a servlet accepts the values of a HTML form, binds them to an object, passes them into the application to be processed, and then returns a response to the user. The core part of the servlet may be very simple, with only the minimum amount of code required to fulfill the use-case being modeled. The code, however, often inflates to three to four times its original size by the time extra requirements such as exception handling, security, and logging have been implemented.

Therefore, AOP allows us to dynamically modify our static model to include the code required to satisfy the extra requirements without having to modify the original static model - in fact, we don't even need to have the original code. Better still, we can often keep this additional code in a single location rather than having to scatter it across the existing model, as we would have to if we were using OO on its own.

The Globus Toolkit 3 is also implemented with Object-Oriented programming. Therefore, the supplement of Globus Toolkit should conform to the Object Oriented model. However, Globus Toolkit is so complicated and complex. And the security part of Globus Toolkit are involved with almost area. On the ground of that, this case would be modeled as the cross-cutting concerns which are named in aspect-oriented programming.

Whenever grid users try to access some grid services, security component must be activated and then perform the process of authentication and authorization. Hence, the invocation point of security component in Globus Toolkit should be defined as point-cut in aspect-oriented programming which is the term given to the point of execution in the application at which cross-cutting concern needs to be applied. And then to perform some predefined action, code will be implemented as an advice which is the additional code that someone wants to apply to the existing model. As a result, aspect-oriented programming is exploited to instantiate proposed architecture using point-cut and advice which is named in that field. Besides, it is possible to implement the proposed architecture without any modification of Globus Toolkit thanks to this programming technique.

## 5.2 Operational Flow

In this section, we describe the implementation details of the proposed architecture. The implementation was done using AspectJ[13].

Let us first look at the left side of figure3. It shows how the authentication is processed in our architecture. Originally, `initSecurityDescriptor` and `getSecurityDescriptor` are performed in current Globus Toolkit. However, there's only one time check which means `getSecurityDescriptor` does not check `SecurityDescriptor` at running time. Hence, we defined two point-cuts at the invocation time of `initSecurityDescriptor` and `getSecurityDescriptor`. In this way, any invocation of `SecurityDescriptor` can be substituted `DynamicSecurityConfig` which always

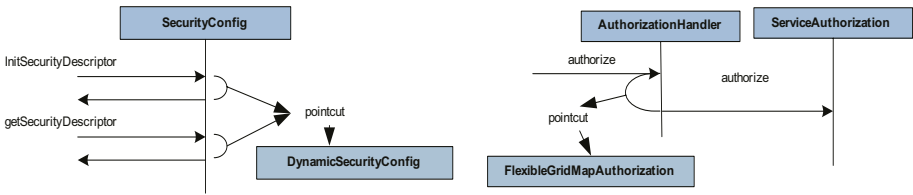


**Fig. 3.** The operational flow of authentication part(left) and authorization part(right)

checks the SecurityDescriptor and applies up-to-the-minute information to the specific grid service at running time.

In authorization, FlexibleGridMap Authorization (fgridmap authorization) functions as the core. Whenever AuthorizationHandler is invoked, the pointcut leads the execution flow to fgridmap authorization. And then operation would be continued with the authorization which conform the defined policy between the user and grid service method. The style of fgridmap is illustrated in the right side of figure3. This authorization part can be performed using the latest authorization information for the specific grid service no matter when the update has been made. As was done in authentication part, the processing of authorization is performed at running time with the help of aspect-oriented programming.

To explain the whole flow of operation with authentication and authorization, let us assume that there are grid user 1, grid user 2, and grid user 3. Also, there is a grid service S1 which can provide methodA, methodB, and methodC. If user 1 who is set to use methodA and methodB, the request for methodC by user 1 shuld be denied by the authorization part. Even if new grid user 4 who is not set on DynamicSecurityDescriptor at deployment time, grid user 4 may be added according to the decision of grid service administrator. And then the request by grid user 4 in compliance with the DynamicSecurityDescriptor and the FlexibleGridmap may be accepted or denied.

To sum up, with the proposed architecture, grid service administrator can configure the authorization scheme up to method level. Moreover, grid service administrator can reconfigure the authentication and authorization policy at service running time. It enhances the limitation of Globus Toolkit by using aspect-oriented programming.

## 6 Conclusion

In this paper, we present a dynamic and fine-grained security architecture for grid service administrators who use Globus Toolkit. With this component, the extra needs of many grid administrators who frequently have to reconfigure security policies and redeploy grid services can be alleviated very simply.

To make current Globus Toolkit more efficient, we have studied the limitation of security part of current Globus Toolkit and then proposed some refinements of this research. The proposed architecture has been implemented using Aspect-



Oriented Programming technique without modifying Globus Toolkit. Therefore, in real grid computing, grid service administrator can use this component very conveniently with existing Globus Toolkit.

## References

1. Von Welch, Ian Foster, Carl Kesselman, Olle Mulmo, Laura Pearlman, Steven Tuecke, Jarek Gawor, Sam Meder and Frank Siebenlist "X.509 Proxy Certificates for Dynamic Delegation", In Annual PKI R&D workshop, April,2004
2. Von Welch, Frank Siebenlis, Ian Foster, John Bresnaban, Karl Czajkowski, Jarek Gawor, Carl Kesselman, Sam Meder, Laura Pearlman and Steven Tuecke , "Security for Grid Services", In IEEE Symposium on High Performance and Distributed Computing ,June,2003.
3. Ian Foster, Carl Kesselman, Cene Tsudik and Steven Tuecke "A Security Architecture for Computational Grids", In 5th ACM Conference on Computer and Communication Security, 1998.
4. "Security in a Web Services World: A Proposed Architecture and Roadmap", A Joint White Paper from IBM Corporation and Microsoft Corporation, April 2002.
5. Tuecke S. and Czajkowski K. and Foster I. and Frey J and Graham S. and Kesselman C. and Maguire T. and Sandholm T. and Snelling D. and Vanderbilt P "Open Grid Services Infrastructure(OGSI) Version 1.0", Global Grid Forum, June 2003.
6. Nataraj Nagaratnam, Philippe Janson, John Dayka, Anthony Nadalin, Frank Siebenlist, Von Welch, Ian Foster and Steve Tuecke "The Security Architecture for Open Grid Services", July 2002.
7. Foster, I., Kesselman, C., Nick, J. and Tuecke, S. "The Physiology of the Grid: An Open Grid Services Architecture for Distributed Systems Integration " , Globus Project, 2002. <http://www.globus.org/research/papers/ogsa.pdf>.
8. Jarek Gawor, Sam Meder, Frank Siebenlist and Von Welch, "GT3 Grid Security Infrastructure Overview", In ,Globus Project 2003.
9. the AspectJ Team, "The AspectJ(TM) Programming Guide", Copyright (c) 1998-2001 Xerox Corporation, 2002-2003 Palo Alto Research Center, Incorporated. All rights reserved.
10. Markus Voelter, "Aspectj-Oriented Programming in Java" in the January 2000 issue of the Java Report
11. Foster, I. and Kesselman, C. and Tuecke, S., "The anatomy of the grid : Enabling scalable virtual organizations", Intl. J. Supercomputer Applications, 2001
12. I. Foster, C. Kesselman, G. Tsudik, S. Tuecke., "Security Architecture for Computational Grids", 5th ACM Conference on Computer and Communications Security Conference, pp. 83-92, 1998.
13. Palo Alto Research Center, "The AspectJ(TM) Programming Guide", <http://eclipse.org/aspectj/>
14. Tzilla Elrad ,Robert E. Filman and Atef Bader "Aspect-oriented programming: Introduction", In Communications of the ACM , 2001

# GridSec: Trusted Grid Computing with Security Binding and Self-defense Against Network Worms and DDoS Attacks\*

Kai Hwang, Yu-Kwong Kwok, Shanshan Song, Min Cai Yu Chen,  
Ying Chen, Runfang Zhou, and Xiaosong Lou

Internet and Grid Computing Laboratory, University of Southern California,  
3740 McClintock Ave., EEB 212, Los Angeles, CA 90089-2562, USA  
{kaihwang, yukwong, shanshas, mincai, rzhou,  
cheny, chen2, xlou}@usc.edu  
<http://GridSec.usc.edu>

**Abstract.** The USC GridSec project develops distributed security infrastructure and self-defense capabilities to secure wide-area networked resource sites participating in a Grid application. We report new developments in trust modeling, security-binding methodology, and defense architecture against intrusions, worms, and flooding attacks. We propose a novel architectural design of Grid security infrastructure, security binding for enhanced Grid efficiency, distributed collaborative IDS and alert correlation, DHT-based overlay networks for worm containment, and pushback of DDoS attacks. Specifically, we present a new pushback scheme for tracking attack-transit routers and for cutting malicious flows carrying DDoS attacks. We discuss challenging research issues to achieve secure Grid computing effectively in an open Internet environment.

## 1 Introduction

Over the last few years, a new breed of network worms like the *CodeRed*, *Nimda*, *SQL Slammer*, and *love-bug* have launched widespread attacks on the Whitehouse, CNN, Hotmail, Yahoo, Amazon, and eBay, etc. These incidents created worm epidemic [8] by which many Internet routers and user machines were pulled down in a short time period. These attacks had caused billions of dollars loss in business, government, and services. Open resource sites in information or computational Grids could well be the next wave of targets. Now more than ever, we need to provide a secure Grid computing environment over the omni-present Internet [6].

---

\* The paper was presented in the *International Workshop on Grid Computing Security and Resource Management (GSRM'05)* in conjunction with the *International Conference on Computational Science (ICCS 2005)*, Emory University, Atlanta, May 22-25, 2005. The research reported here was fully supported by an NSF ITR Grant 0325409. Corresponding author: Kai Hwang, USC Internet and Grid Computing Lab, EEB 212, Los Angeles, CA 90089. E-mail: [kaihwang@usc.edu](mailto:kaihwang@usc.edu), Tel.: (213) 740-4470. Y.-K. Kwok participated in this project when he was a visiting associate professor at USC on sabbatical leave from HKU.

Network-centric computing systems manifest as Grids, Intranets, clusters, P2P systems, etc. Malicious intrusions to these systems may destroy valuable hosts, network, and storage resources. Network anomalies may appear in many Internet connections for *telnet*, *http*, *ftp*, *smtp*, *Email*, and *authentication* services. These anomalies cause even more damages. Internet anomalies found in routers, gateways, and distributed hosts may hinder the acceptance of Grids, clusters, and public-resource networks [10]. Our work is meant to remove this barrier from Grid insecurity. This article reports our latest research findings in advancing security binding and building self-defense systems tailored for protecting Grid resource sites.

- Architectural design of the Grid security infrastructure in Section 2
- Security binding for trusted resource allocation in Grid job scheduling [12] in Section 3.
- The CAIDS distributed IDS and alert correlation system in Section 4
- The salient features of a DHT (*distributed hash table*) overlay [1, 13] for supporting distributed worm containment [1, 8] in Section 5
- A real-time pushback scheme to combat DDoS (*Distributed Denial of Service*) attacks [2, 3, 9] in Section 6.

## 2 GridSec Security Infrastructure Architecture

Our GridSec security architecture is designed to be a wide-area defense system that enables high degree of trust [7] among the Grid sites in collaborative computing over the Internet. As illustrated in Fig. 1, GridSec adopts DHT-based overlay architecture

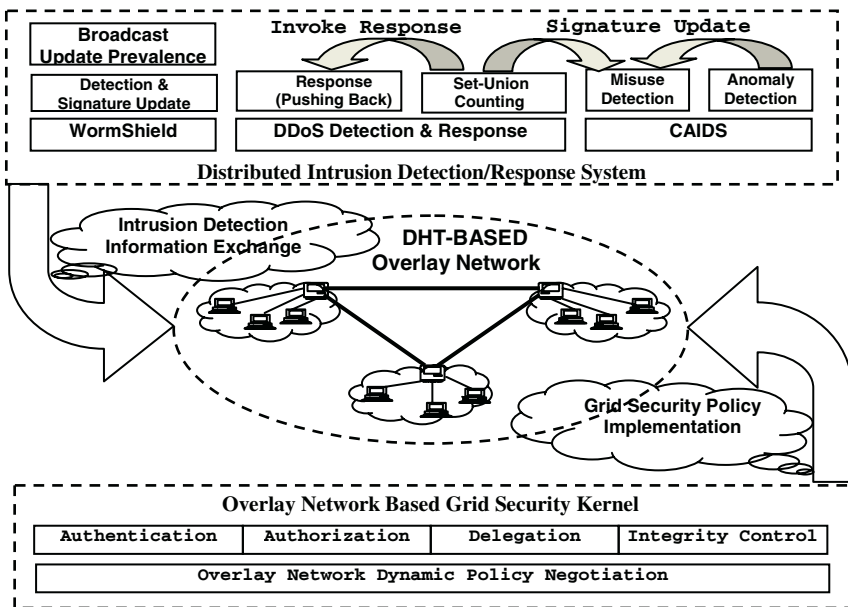


Fig. 1. GridSec infrastructure for building self-defense capabilities to protect Grid sites

as its backbone. As a virtual communication structure lay logically on top of physical networks, our overlay network maintains a robust virtual inter-networking topology. Through this topology, trusted direct application level functionalities facilitates inter-site policy negotiation and management functions such as authentication, authorization, delegation, policy exchange, malicious node control, job scheduling, resource discovery and management, etc.

The GridSec system functions as a *cooperative anomaly and intrusion detection system* (CAIDS) [6]. Intrusion information is efficiently exchanged by the overlay topology with confidentiality and integrity. Each local IDS is autonomous, and new algorithms can be added easily due to the high scalability of the overlay. Each node may work as agent for others and various security models/policies can be implemented. As shown in Fig. 1, currently available functional blocks include the WormShield [1], CAIDS [6] and DDoS pushback scheme [2]. We are currently integrating our newly developed worm and flooding defense algorithms into the GridSec *NetShield* system .

### 3 Security-Binding for Trusted Resource Allocation

The *reputation* of each site is an aggregation of four major attributes: *prior job execution success rate*, *cumulative site utilization*, *job turnaround time*, and *job slowdown ratio*. These are behavioral attributes accumulated from historical performance of a site [12]. The defense capability of a resource site is attributed to *intrusion detection*, *firewall*, *anti-virus/worm*, and *attack response capabilities*. Both site reputation and defense capability jointly determine the *trust index* (TI) of a resource site. In [12], we have suggested a novel fuzzy-logic approach to generating the local trust index from the above-mentioned attributes.

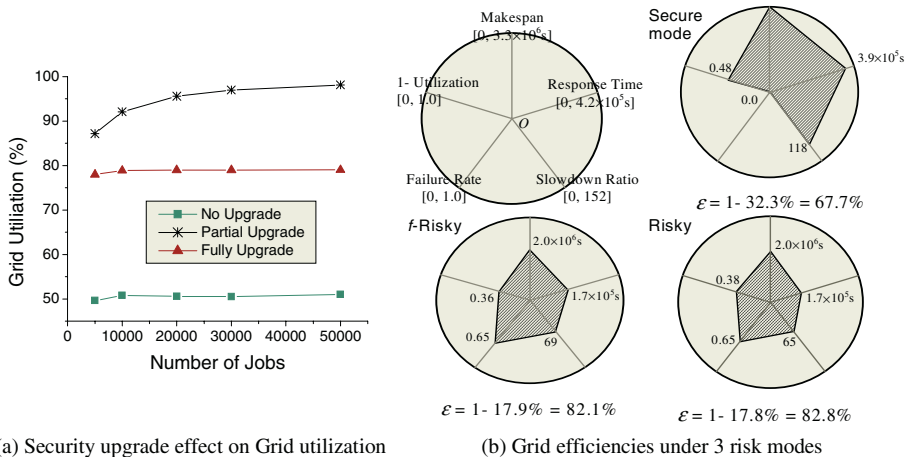


Fig. 2. Effects on Grid utilization and Grid efficiency by security enhancement

On the other hand, user jobs provide their *security demand* (*SD*) from resource site. A *trusted resource allocation* (TRA) scheme must satisfy a *security-assurance*

condition:  $TI \geq SD$  during mapping jobs to resource sites. We evaluate the effectiveness of a TRA scheme by considering five performance metrics: *makespan*, *job failure rate*, *site utilization*, *response time*, and *slowdown ratio*, etc. We report in Fig. 2(a) the effects of trust integration towards total Grid utilization. *No upgrade* policy corresponds to resource allocation without trust integration. While *full upgrade* and *partial upgrade* entail a full scale and a resource-constrained trust integration, respectively. Higher Grid utilization is observed after the integration process.

This security-binding scheme is effective in mapping large-scale workloads in NAS and PSA benchmark experiments [12]. New performance metrics are developed to assess the effects of trust integration and secure allocation of trusted resources to enormous Grid jobs. Our secure binding scheme scales well with both job number and Grid size. Trusted job outsourcing makes it possible to use open Grid resources with confidence and calculated risks. We consider three risk conditions in remote job executions, namely, *conservative* mode, *f-risky* and *risky* mode representing various levels of risk the jobs may experience.

The cumulative Grid performance of these three modes is shown in Fig.2(b) by three 5-D Kiviat diagrams under 3 risk conditions. The five dimensions correspond to five performance metrics. The smaller is the shaded polygon at the center of the Kiviat diagram, the better is the *Grid efficiency*, defined by  $\epsilon = (1 - A_{shaded} / A_{circle})$ . This implies that more efficient Grid has *shorter makespan* and *response time* and *lower slowdown*, *failure rate*, and *under-utilization rate* ( $1 - utilization\ rate$ ). Our NAS simulation results shows that it is more resilient for the global job scheduler to tolerate job delays introduced by calculated risky conditions, instead of resorting to job preemption, replication, or unrealistic risk-free demand.

### 4 Distributed Intrusion Detection/Alert Correlation

The CAIDS we built [6] can be deployed at various Grid sites to form a *distributed IDS* (DIDS) supported by alert correlation sensors. These sensors are scattered around the computing Grid. They generate a large amount of low-level alerts. These alerts are transmitted to the alert correlation modules to generate high-level intrusion reports,

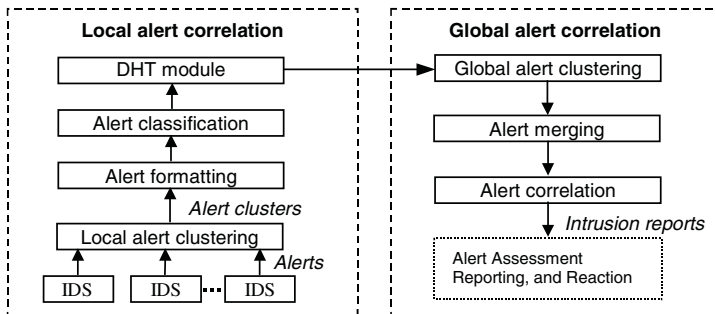
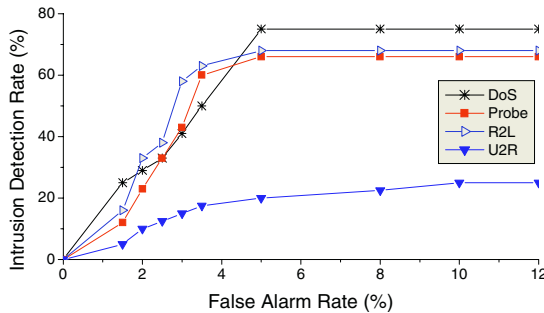


Fig. 3. Alert operations performed in local Grid sites and correlated globally

which can provide a broader detection coverage and lower false alarm rate than the localized alerts generated by single IDS. Figure 3 shows the alert operations performed by various functional modules locally and globally [4].

Similar to a major earthquake, one large attack has a series of after attacks. The global alert correlation is to detect the relationship among the attacks. We need a high-level view of attacks. The system detects the intention and behavior of attackers. An early detection report can be generated to minimize the damages. We have tested the CAIDS system at USC with an Internet trace of 23.35 millions of traffic packets, intermixed with 200 attacks from the Lincoln Lab IDS dataset.

In Fig.4, we plot the ROC curves corresponding to 4 attack classes. The detection rate grows quickly to its peak value within a small increase of false alarm rate. To achieve a total detection rate above 75% of DoS attacks, we have to tolerate 5% or more false alarms. The R2L (*root-to-local*) attacks have the second best performance. The port-scanning Probe attacks perform about the same as R2L attacks. The U2R (*user-to-root*) attacks have the lowest detection rate of 25% at 10 % false alarms, due to the stealthy nature of those attacks. When the false alarm rate exceeds 5%, all attacks reaches their saturated performance.



**Fig. 4.** Intrusion detection rate versus false alarm rate in using the CAIDS (Cooperative Anomaly and Intrusion Detection System) developed at USC [6]

## 5 DHT-Based Overlay for Worm Containment

We build a scalable DHT overlay to cover a large number of autonomous domains in edge networks. Our *WormShield* system [1] consists of a set of geographically distributed monitors located in multiple administrative domains (Fig.5). They are self-organize into a structured P2P overlay ring network based on the Chord algorithm [13]. Each monitor is deployed on the DMZ (*Demilitarized Zone*) of the edge network and analyzes all packets passing through it.

In *WormShield*, each monitor  $i$  remembers the set of source addresses  $S(i,j)$  and the set of destination addresses  $D(i,j)$  for each substring  $j$ . When the global prevalence of substring  $j$  is greater than the prevalence threshold  $T_p$ , each monitor will send their locally maintained source and destination addresses to the root monitor root  $j$ . The

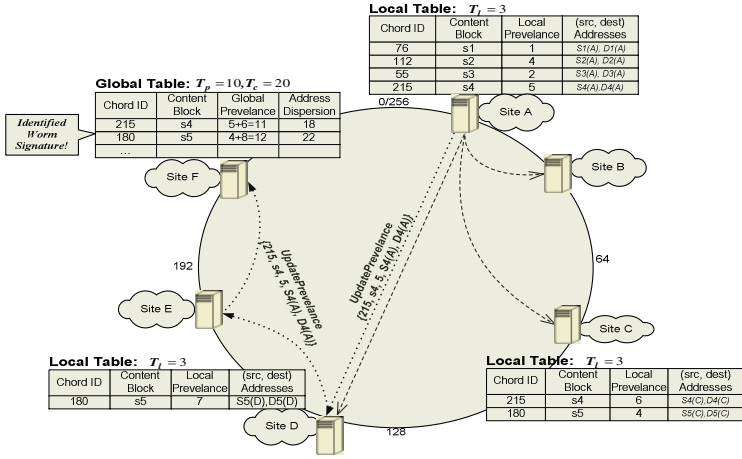


Fig. 5. An example of WormShield system with six sites for worm control

root monitor then compute the global address dispersion for the substring  $j$ . If  $C(j)$  is greater than an address dispersion threshold  $T_c$ , the substring  $j$  will be identified as a potential worm signature [11]. The root monitor will construct a multicast tree on the overlay network and disseminate the signature to all monitors participated.

For each monitor  $i$ , we use Rabin footprint algorithm to compute the substrings for each packet payload. Then it computes the local prevalence  $L(i, j)$  for each substring  $j$ . After a predefined interval  $t$  or  $L(i, j)$  is greater than a local prevalence threshold  $T_l$ , monitor  $i$  will update the global prevalence  $P(j)$  for substring  $j$  that tracks all prevalence seen in the network with *WormShield* monitors deployed. A selected monitor is assigned to maintain the global prevalence for a substring  $j$  using consistent hashing as in Chord [13].

## 6 Tracking and Pushback DDoS Attacks

We tackle two issues towards effective DDoS defense: (1) accurately identifying the ingress routers (i.e., the edge routers of the domain to be protected) that unknowingly participate in the forwarding of malicious DDoS attack flows; and (2) identifying the malicious flows and incisively cutting such flows at these *Attack-Transit Routers* (ATRs) [2].

**Real-Time Traffic Matrix Tracking:** We propose a low-complexity traffic monitoring technique that is based on measuring both the *packet-level* and *flow-level* traffic matrices among routers in real-time. Our proposed technique is based on accumulating very lightweight statistics for packets or flows at each router within the domain. When huge volumes of packets or flows arrive at a particular last-hop router as depicted in Fig.6, this victim router identifies the ATRs with very high accuracy using the lightweight statistics exchanged among the routers. It only requires  $O(\log \log N)$  storage capacity for  $N$  packets or flows on each router [5, 9], compared with the  $O(N)$  complexity in using a Bloom filter [2].

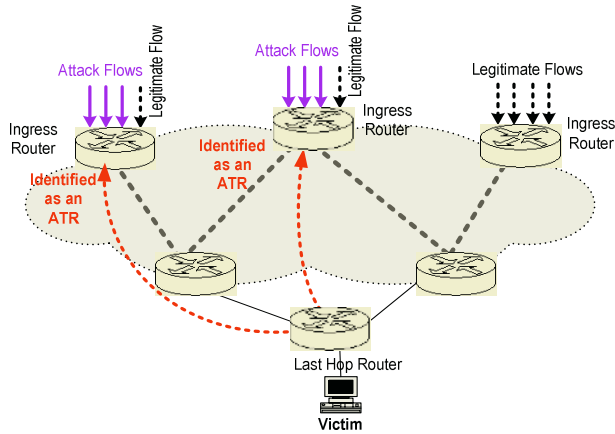


**Fig. 6.** The pushback scheme for identifying the attack-transit routers and blocking the malicious flows with spoofed source IP addresses

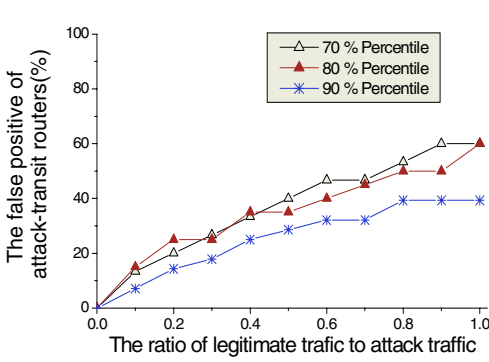
**Packet- and Flow-Level Counting:** Define  $S_i$  as the set of packets that enter the domain from an ingress router  $r_i$ , and  $D_j$  as the set of packets that leave the domain from an egress router  $r_j$ . To compute packet-level traffic matrix, we use the first 28-byte invariant bytes of a packet (20-byte IP header with 4 bytes masked out plus the first 12 bytes of payload). This will result in a very small collision rate. We compute the packet-level traffic matrix  $A = \{a_{ij}\}$ , where  $a_{ij} = |S_i \cap D_j| = |S_i| + |D_j| - |S_i \cup D_j|$  [9]. Here, we can easily compute  $|S_i|$  and  $|D_j|$  at each router.

For the term  $|S_i \cup D_j|$ , we use two probabilistic counting techniques, namely the *stochastic averaging algorithm* and *distributed max-merge algorithm* [5], which require only  $O(\log \log N)$  storage space for  $N$  packets in the set. For flow-level traffic matrix, we use the 5-tuple  $\{source\ IP, source\ port, destination\ IP, destination\ port, protocol\}$  as the identifier for each packet. The flow-level traffic matrix  $B = \{b_{ij}\}$ , where  $b_{ij} = |S_i^F \cap D_j^F|$  is computed in a similar fashion. The counting complexity is  $O(N)$ , where  $N$  is the number of packets in a set.

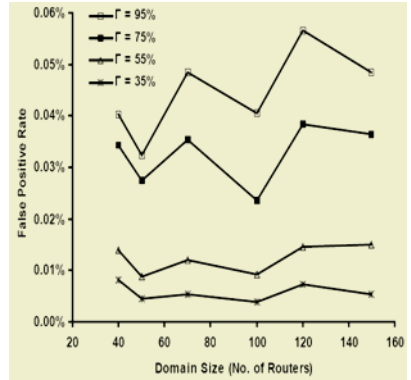
Even with the ATR identification issue efficiently solved by our novel traffic tracking technique, the second issue is also a daunting challenge because IP addresses are commonly spoofed, that making correct identification of malicious flows very difficult. We propose a new MAFIC algorithm to support the adaptive packet dropping policy at the identified ATRs [3]. Through probing, MAFIC would drop malicious attack packets with very high accuracy while minimizes the loss on legitimate traffic flows [3].

Our NS-2 simulation indicates that the traffic tracking and flow cutting by dropping attacking packets are up to 90% accurate, as revealed in Fig.7(a). The scheme reduces the loss of legitimate flows to less than 5%. Figure 7(b) shows the false positive rates are quite robust and scalable under increasing domain sizes. The dup-ACK based probing is quite accurate in identifying the attack flows as the identification errors are mostly below 1%. The false alarm rates are less than 0.05% for a TCP flow rates from 35% to 95% of the total traffic volume.





(a) False positive rate of identifying ATRs



(b) Rate of dropping legitimate packets

**Fig. 7.** The false positive rate of identifying ATRs and of dropping legitimate packets at the identified ATRs with different percentages (70%, 80%, and 90%) of traffic flows actually passing through the identified ATRs (*attack-transit routers*)

## 7 Conclusions

The NSF/ITR-supported GridSec project at its second year has made encouraging progress in trust management, security-driven job scheduling, trusted resource allocation, distributed IDS, collaborative alert correlation, worm containment, and distributed DDoS pushback. We offer a scalable security overlay architecture, experimental validation of distributed IDS design, and new schemes to capture network worms and pushback DDoS attacks. The GridSec system offers early warning of Internet worm spreading and launching effective pushback operations to protect Grid resources.

In the research front, we suggest several meaningful challenges for further work. The major threats come from software vulnerability and naïve users. Today’s Windows, Unix and Linux variants are by no means immune from worm attacks, let alone free from DDoS flood attacks. Outbreaks must be dealt with immune response swiftly. The major research challenge lies still in the containment area. In particular, we need automated signature generation and fast suppression of malicious flows.

Internet outbreak detection and monitory are other big challenges. The reaction time, containment strategies, deployment scenarios are all yet to be worked out. We have identified the requirements of *robustness*, *resilience*, *cooperativeness*, *responsiveness*, *efficiency*, and *scalability*. The DHT-base security overlays offer a viable approach towards a fast cybersecurity solution. Of course, further advances in operating-system security, active networks, and trust management are also important.

## References

[1] M. Cai, K. Hwang, Y.-K. Kwok, Y. Chen, and S. Song, "Fast Conatainment of Internet Worms for Epidemic Defense using Distributed-Hashing Overlays", *IEEE Security and Privacy*, submitted July 2004 and revised March 6, 2005, to appear Nov/Dec. 2005.

- [2] M. Cai, Y. K.-Kwok and K. Hwang, "Inferring Network Anomalies from Mices: A Low-Complexity Traffic Monitoring Approach", in preparation for submission to *ACM SIGCOMM Workshop on Mining Network Data*, 2005
- [3] Y. Chen, Y.-K. Kwok, and K. Hwang, "MAFIC: Adaptive Packet Dropping for Cutting Malicious Flows to Pushback DDoS Attacks," *Proc. Int'l Workshop on Security in Distributed Systems (SDCS-2005)*, in conjunction with ICDCS 2005, Columbus, Ohio, USA, June 2005.
- [4] F. Cuppens and A. Mieke, "Alert Correlation in a Cooperative Intrusion Detection Framework," *IEEE Symposium on Security and Privacy*, 2002, pp.187-200.
- [5] M. Durand and P. Flajolet, "LogLog Counting of Large Cardinalities," *Proc. European Symp. on Algorithms*, 2003.
- [6] K. Hwang, Y. Chen, and H. Liu, "Protecting Network-Centric Computing System from Intrusive and Anomalous Attacks," *Proc. IEEE Workshop on Security in Systems and Networks (SSN'05)*, in conjunction with *IPDPS 2005*, April 8, 2005.
- [7] S. Kamvar, M. Schlosser, and H. Garcia-Molina, "The EigenTrust Algorithm for Reputation Management in P2P Networks," *Proc. of WWW*, 2003.
- [8] H. A. Kim and B. Karp, "Autograph: Toward Automated Distributed Worm Signature Detection," *Proc. USENIX Security Symposium*, 2004.
- [9] M. Kodialam, T. V. Lakshman, and W. C. Lau, "High-speed Traffic Measurement and Analysis Methodologies and Protocols," Bell Labs Technical Memo, Aug. 2004.
- [10] N. Nagaratnam, P. Janson, J. Dayka, A. Nadalin, F. Siebenlist, V. Welch, S. Tuecke, and I. Foster, "Security Architecture for Open Grid Services," <http://www.ggf.org/ogsa-sec-wg>
- [11] S. Singh, C. Estan, G. Varghese and S. Savage, "Automated Worm Fingerprinting," *Proc. of the USENIX Symp.on Operating System Design and Implementation*, S.F., Dec. 2004.
- [12] S. Song, K. Hwang, and Y.-K. Kwok, "Security Binding for Trusted Job Outsourcing in Open Computational Grids," *IEEE Trans. Parallel and Dist. Systems*, revised Dec. 2004.
- [13] I. Stoica, R. Morris, D. Karger, M. F. Kaashoek, H. Balakrishnan, "Chord: A P2P Lookup Protocol for Internet Applications," *Proc. ACM SIGCOMM*, 2001.

# Design and Implementation of DAG-Based Co-scheduling of RPC in the Grid

JiHyun Choi<sup>1</sup>, DongWoo Lee<sup>2</sup>, R.S. Ramakrishna<sup>3</sup>,  
Michael Thomas<sup>4</sup>, and Harvey Newman<sup>5</sup>

<sup>1,2,3</sup>Department of Information and Communication,  
Gwangju Institute of Science and Technology, Republic of Korea  
{jhchoi80, leeopro, rsr}@gist.ac.kr

<sup>1,4,5</sup> California Institute of Technology, Pasadena, CA91125, USA  
{jchoi, thomas, newman}@hep.caltech.edu

**Abstract.** Effective scheduling in the Grid consisting of heterogeneous and distributed resources is imperative in order to counter unacceptably large overheads of the Grid. We proposed the grid middleware (pyBubble) supporting the DAG based co-scheduling for improving the performance of the RPC mechanism. DAG based co-scheduling reduces redundant transmission of input and output data from execution of the sequence of related client requests, thereby decongesting the network. We demonstrate the efficiency of DAG based co-scheduled RPC in experiments compared with the overhead of the traditional RPC mechanism.

## 1 Introduction

The Grid is the Internet-connected computing and data management infrastructure. Computing and data resources are geographically dispersed in different administrative domains with different policies for security and resource usage. The computing resources are highly heterogeneous, ranging from single PCs and workstations, cluster of workstations, to large supercomputers[5]. With the technology of the Grid we can construct large-scale and scientific applications over these distributed and heterogeneous resources. There are many critical issues that need to be efficiently resolved to support the ever-increasing number of applications that can benefit from the Grid Computing infrastructure.

GridRPC[8] is a programming model based on client-server remote procedure call(RPC), with features added to allow easy programming and maintenance of code for scientific applications on the Grid. Application programmers write parallelized client programs using simple and intuitive GridRPC APIs that hide most of the complexities involving Grid programming. As a result, programmers lacking experience in parallel programming, let alone the Grid, can still construct Grid Applications effortlessly[3]. Most applications in Grid Computing generally have large input data sets and intricate data dependency. Moreover, data transfer in large distributed systems can add an unacceptable amount of overhead. The

goal of this research is to devise simple and effective strategies for dealing with these issues.

## 2 Related Works

Grid programming involves the Interface and the Run-time system. WS-Resource Framework defines Web service convention to enable the discovery of, introspection on, and interaction with stateful resources in standard and interoperability ways. Many enhanced interfaces for grid computing such as Grid MPI and Grid RPC have been developed. With regard to Message Passing Interface(MPI), several systems, notably, MPICH-G2, MPI.Connect<sup>1</sup>, PACX-MPI, MagPIe<sup>2</sup> and Stampi<sup>3</sup> have been studied for connecting different MPI implementations. Conventional parallel programming is implemented by these MPI-like systems in tightly coupled high performance parallel computing networks or network of workstations. MPI needs middleware to interact with the global grid.

The other programming paradigm of importance is RPC (Remote Procedure Call)[2]. It is used for calling remote functions through a simple programming interface. To a user, RPC presents a transparent interface to a remote function. RPC is the most promising candidate for Grid programming interface due to its simplicity and user friendliness. With this interface, the grid middleware can invoke a remote grid resource via RPC calls. Ninfg[9], NetSolve-G(Grid Solve)<sup>4</sup>, OmniRPC[7] and so forth provide Grid RPC interface to their systems.

pyBubble[6] provides DAG(Directed Acyclic Graph)-based co-scheduling as a mechanism to minimize repeated interactions among resources. Unlike Ninfg and NetSolve, our system can store the applications task dependencies in DAGs. These DAGs allow pyBubble to schedule communications with a functionality-based scheduling algorithm. Our DAG-based Grid Runtime with RPC programming interface exhibits substantial performance improvements in terms of the execution time of related RPC requests. This efficiency increases in larger distributed systems that suffer from large data transfer overheads.

## 3 Motivation

In the traditional RPC paradigm, individual RPCs are processed independently. The actual scheduling of the remote invocation is unilaterally determined by the remote service receiving the RPC request. Clients, however, may have to meet scheduling constraints. If a remote call entails submitting a batch job or a sequence of related tasks, the client may at least want to know what the queue

<sup>1</sup> MPI.Connect, <http://icl.cs.utk.edu/projects/mpi-connect>

<sup>2</sup> MagPIe, <http://www.cs.vu.nl/albatros>

<sup>3</sup> Stampi, <http://ssp.koma.jaeri.go.jp/en/index.html>

<sup>4</sup> GridSolve, <http://www.nsf-middleware.org/documentation/NMI-R4/0/gridsolve>

length is, or have some notion of the expected time of completion. Clients may also need to co-schedule multiple RPCs if the input and output parameters of these multiple RPCs are interrelated. Co-scheduling will help avoid the transmission of redundant data, resulting in an overall shortened response time and reduced network congestion. The total processing time can also be shortened by executing modules concurrently whenever possible. However, GridRPC systems do not support any mechanism to co-schedule GridRPC that targets heterogeneous and loosely-coupled systems over wide-area networks. This work is an attempt to fill this gap.

Figure1[1] illustrates two kinds of data flow involving multiple RPCs. The client invokes the services of three servers for processing a job consisting of three tasks. There is ample opportunity to reduce redundant network traffic between clients and servers when we execute this series of related RPCs. In the left diagram, servers always return the result to the client after the execution of their tasks. But, in the co-scheduled system, servers don't need to return the intermediate results to the client, but instead send the intermediate results to other servers directly as their inputs. In the right diagram, server3 executes the final task, and sends only the final result back to the client.

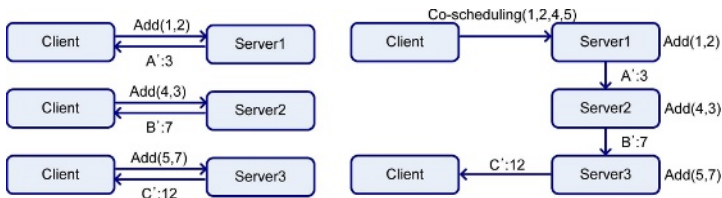


**Fig. 1.** Data flow compared with co-scheduling

Grid Computing usually involves the processing of very large amounts of data using distributed resources over wide area. When we take the overhead of the data transfer time into consideration, decongestion of network traffic by co-scheduling in the Grid can substantially contribute toward reducing the overall response time of multiple RPCs.

## 4 Framework: The pyBubble

Our system, pyBubble, is a web service-based Grid middleware for parallel and distributed computation. This system intends to be a GridRPC system that uses XML-based RPC for the interactions between the client application and remote computing resources. pyBubble is written in the Python programming language to support portability across multiple platforms. pyBubble uses SOAP as the transport encoding and supports DAG based co-scheduling and a restart protocol for improving the dependability of the system.

## 4.1 SOAP-based Implementation

pyBubble[6] uses SOAP for performing remote procedure calls. SOAP provides an envelope that encapsulates XML data for transfer through the Web infrastructure with a convention for Remote Procedure Call (RPCs) and a serialization mechanism based on XML Schema data type. We note that other RPC mechanisms for Grids are possible, including XML-RPC<sup>5</sup> which also uses XML over HTTP. While XML provides tremendous flexibility, it currently has poor support for binary data due to a significant encoding cost[4]. Therefore, we compress the xml documents before they are transferred in order to reduce the overhead caused by the substantial encoding overhead of XML.

## 4.2 pyBubble Architecture and General Scenario

Figure 2 shows each of these components of pyBubble and illustrates the relationship and data flow between the components. pyBubble consists of the client, the resource broker, and resource servers. We can get metadata of available servers by intergrating monitoring services, but we can use specific host configuration information collected from servers in this work.

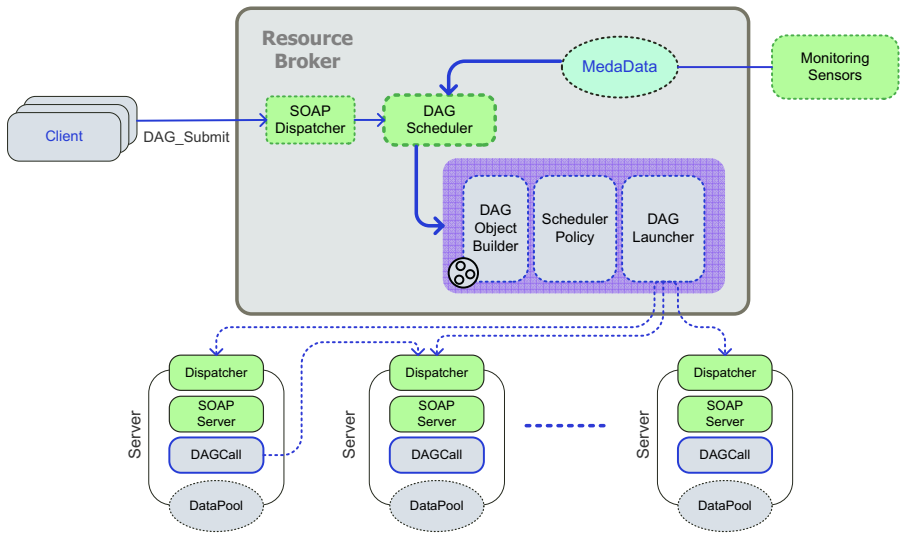


**Fig. 2.** The architecture of pyBubble consisting of client, broker and servers

We can assume that the user has several tasks targeted to distributed servers. First, the user sends the tasks to the pyBubble broker with the programming interface for DAG-based co-scheduling which constructs the DAG from client's tasks, subject to constraints. The client specifies the input data, the result labels and the function names with the programming interface. The tasks to be sent to

<sup>5</sup> XML-RPC, <http://www.xml-rpc.com>

the broker should be a sequence of interrelated requests. The broker analyzes the relationships of input and output data within tasks, and then checks the precedence or dependency between tasks. It then constructs the DAG. The DAG has the information about intra-task relationships.

Tasks are assigned to the right server based on the scheduling algorithm because the broker has the information about available servers. To execute the tasks, first, the broker submits root tasks in the DAG. The root tasks are assigned to multiple servers to be executed in parallel. They call the respective child tasks in sequence according to the DAG. They also send the result, the scheduling information for the child task, and the DAG to the child tasks. After all the tasks are completed, the server executing the final task sends its result to the broker.

## 5 DAG-Based Co-scheduling of RPC

### 5.1 The DAG Model and Application Encoding Using DAG

The DAG is a generic model of a parallel program consisting of a set of interdependent processes (nodes). A node in the DAG represents a task. The graph also has directed edges representing a partial order among the tasks. The partial order creates a precedence-constrained directed acyclic graph[20]. For scheduling purposes, tasks are described by a DAG. A DAG incorporates all the precedence relationships among tasks and information about the assigned task in order to make scheduling decisions. After scheduling, the DAG includes information about which task is assigned to which server.

### 5.2 DAG-Based Co-scheduling Algorithm with Function Availability

After constructing the DAG, the broker schedules the DAG tasks based on function availability since the broker can get information of configuration files specified on each server and knows which resource can execute which function. Figure 3 shows the pseudocode of DAG-based co-scheduling by functional availability. The function definition procedure assists in finding the available resources offering the requested function and this returns the candidate set of the resources. The variable `DAG` is the collection of the requests described in DAG, and `Rmax` is the number of resources. `ResourcePool` includes the information about available resource to which the broker assigns some task. Each task in the DAG finds the candidate resources set offering the function called by the method `FindResHavingFunc`. In the candidate resource set, one resource is selected for assignment to the task. After finding the root tasks, they are executed with the `Execute` method.

```

Scheduling Definition:
DAG: collection of the request described in DAG
Rmax: the number of resources
ResourcePool: {R1,R2,... Ri, Rmax}
Ri: { F1, F2,..., Fn}

Begin
  for each T in DAG
  Do
    CandidateResourceSet :=
FindResHavingFunc(T,ResourcePool)
    AssignedRes := RandomSelect(CandidateResourceSet)
    MappingTaskResource(AssignedRes, T)
  Done
  RootTask := FindRootTask(Dag)
  Execute(RootTask) // Root Tasks execute in parallel
End

Function Definition:
FindResHavingFunc(Task, ResourcePool)
  CandidateSet = {}
  For each R in ResourcePool
  Do
    IF Task.Func R.func then
      CandidateSet := R
  Done
  Return CandidateSet

```

Fig. 3. Pseudocode of scheduling by functional availability

## 6 Experiment Results

The experiments compare co-scheduled RPC with conventional RPC. The performance criteria are data size, number of processors, and the CPU power. The efficiency of DAG-based co-scheduling can vary with these factors.

### 6.1 Application: Image Processing

Image Processing is appropriate for studying the efficiency of co-scheduling. In this experiment, images can be very large, on the order of several gigabytes in size. The execution of a series of transformations - in a specific order - on an image is common in image processing. This experiment shows the improved efficiency of DAG-based co-scheduling. The results of experiments depend of the combination of the function set and the DAG construction.

**Comparison with increasing image size.** Figure 4 shows that the execution time of conventional RPC increases sharply when the data size increases due to network traffic overhead. But the increase in the execution time of co-scheduled RPC is not as drastic. Parallel processing of concurrent tasks and the resulting reduction in redundant network traffic contribute to this improved performance.

**Comparison on the basics of CPU Performance.** This experiment uses CPU power as the performance criterion: the high performance group and the low



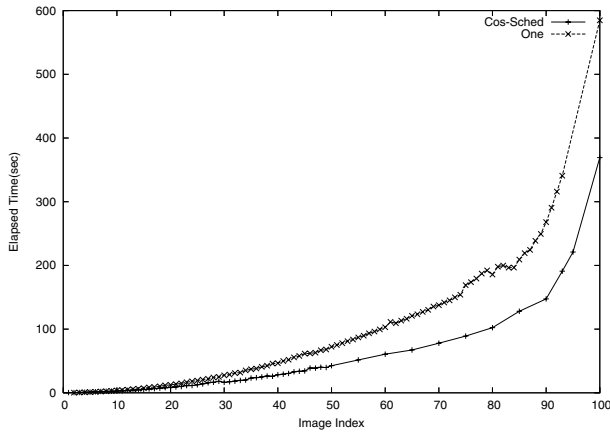


Fig. 4. Execution time of Co-scheduled RPC and Conventional RPC

performance group. Figure 5 compares co-scheduled RPC with conventional RPC in both the server groups. the performance of the low performance group is not improved significantly with co-scheduled RPC because that has large overhead for co-scheduling tasks and is not less affected by reducing network overhead.

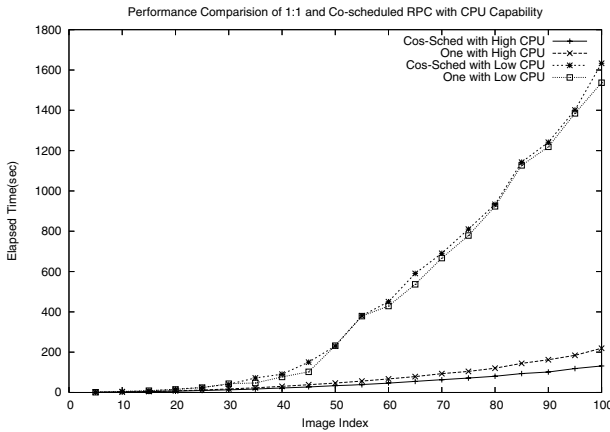


Fig. 5. Comparison of conventional and co-scheduled RPC in low performance CPU group and high performance RPC group

**Comparison with the different number of processors.** In figure 6, the single processor records the worst performance as expected. Two and three processors achieve the best performance. The DAG has three root tasks and two child tasks and hence two or three are just the right numbers. Two processors return a performance below that of three processors. This is understandable in light of the fact that there are three (concurrent) root tasks in the DAG. Four and five processors also exhibit good performance until the number of images reaches 80. Thereafter, the performance degrades due to heavy network traffic induced by large sized images.

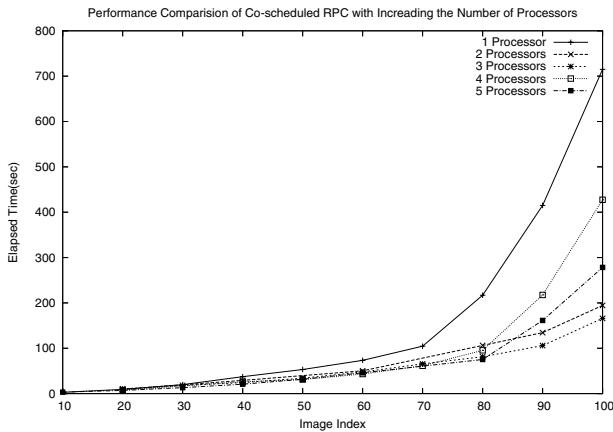


Fig. 6. Performance comparison of co-scheduled RPC with increasing of processor

## 7 Conclusion

In this paper we have proposed a DAG based co-scheduling technique as a tool for efficient RPC programming in the Grid. Co-scheduling intends to avoid redundant transmission of inputs and outputs in order to reduce network traffic congestion. The system supports a portable programming interface for DAG based co-scheduling as a user facility. DAG-based applications are scheduled using functionality- and input output data location-based co-scheduling algorithm. Image processing applications were used for test purposes and have proved that DAG based co-scheduling exhibits considerable performance improvements over conventional RPC.

## References

1. Dorian C. Arnold, Dieter Bachmann, and Jack Dongarra. Request sequencing: Optimizing communication for the grid. In *Euro-Par*, pages 1213–1222, 2000.
2. Gregory L. Field Lola Gunter Thomas Klejna Shankar Lakshman Alexia Prendergast Mark C. Reynolds David Gunter, Steven Burnett and Marcia E. Roland. *Client/Server Programming With Rpc and Dce*. Que, 1995.
3. GlobalGridForum. <http://www.ggf.org>.
4. M. Govindaraju, A. Slomenski, V. Choppella, R. Bramley, and D. Gannon. Requirements for and evaluation of rmi protocols for on the performance of remote method invocation for scientific computing. In *Proc. of the IEEE/ACM International Conference on Supercomputing (SC 2000)*, November 2000.
5. Ian Foster, Carl Kesselman, editor. *The GRID2: Blueprint for New Computing Infrastructure Meyers*. Morgan Kaufmann, 2003.
6. DongWoo Lee and JiHyun Choi. <http://pybubble.sourceforge.net>, 2004.
7. Mitsuhisa Sato, Taisuke Boku, and Daisuke Takahashi. Omnirpc: a grid rpc system for parallel programming in cluster and grid environment. In *CCGRID*, pages 206–, 2003.

8. Keith Seymour, Hidemoto Nakada, Satoshi Matsuoka, Jack Dongarra, Craig A. Lee, and Henri Casanova. Overview of gridrpc: A remote procedure call api for grid computing. In *GRID*, pages 274–278, 2002.
9. Y. Tanaka, Hidemoto Nakada, Satoshi Sekiguchi, Toyotaro Suzumura, and Satoshi Matsuoka. Ninf-g: A reference implementation of rpc-based programming middleware for grid computing. *J. Grid Comput.*, 1(1):41–51, 2003.

# Performance Analysis of Interconnection Networks for Multi-cluster Systems

Bahman Javadi<sup>1</sup>, J.H. Abawajy<sup>2</sup>, and Mohammad K. Akbari<sup>1</sup>

<sup>1</sup>Department of Computer Eng. and Information Technology,  
Amirkabir University of Technology, Hafez Ave., Tehran, Iran  
{javadi, akbari}@ce.aut.ac.ir

<sup>2</sup>School of Information Technology, Deakin University,  
Geelong, VIC 3217, Australia  
jemal@deakin.edu.au

**Abstract.** With the current popularity of cluster computing systems, it is increasingly important to understand the capabilities and potential performance of various interconnection networks. In this paper, we propose an analytical model for studying the capabilities and potential performance of interconnection networks for multi-cluster systems. The model takes into account stochastic quantities as well as network heterogeneity in bandwidth and latency in each cluster. Also, blocking and non-blocking network architecture model is proposed and are used in performance analysis of the system. The model is validated by constructing a set of simulators to simulate different types of clusters, and by comparing the modeled results with the simulated ones.

## 1 Introduction

Advances in computational and communication technologies has made it economically feasible to conglomerate multiple clusters of heterogeneous networked resources leading to the development of large-scale distributed systems known as multi-cluster systems. Performance analysis and evaluation of multi-cluster systems in general and interconnection networks in particular is needed for understanding system behavior and the analysis of innovative proposals. However, performance analysis in such systems has proven to be a challenging task that requires the innovative performance analysis tools and methods to keep up with the rapid evolution and ever increasing complexity of such systems.

This paper addresses the network interconnects performance analysis problem for multi-cluster computing systems. The motivation for considering this problem is that multi-cluster systems are gaining more importance in practice and a wide variety of parallel applications are being hosted on such systems as well [1]. Also, many recent cluster builders are concerned with two primary factors: cost and performance [17].

While cost is easily determined and compared, performance is more difficult to assess particularly for users who may be new to cluster computing. Moreover, with the current popularity of cluster computing, it is increasingly important to understand the capabilities and potential performance of various network interconnects for cluster

computing systems [18]. In addition, performance analysis in such systems has proven to be a challenging task that requires the innovative performance analysis tools and methods to keep up with the rapid evolution and ever increasing complexity of such systems [16].

In this paper, we present a new methodology that is based on Jackson network technique to analytically evaluate the performance of network interconnects for multi-cluster systems. The model takes into account stochastic quantities as well as network heterogeneity in bandwidth and latency in each cluster. Bandwidth is the amount of data that can be transmitted over the interconnect hardware in a fixed period of time, while latency is the time to prepare and transmit data from a source node to a destination node. Also, blocking and non-blocking network architecture model is proposed and are used in performance analysis of the system. The message latency is used as the primary performance metric. The model is validated by constructing a set of simulators to simulate different types of clusters, and by comparing the modeled results with the simulated ones.

The rest of the paper is organized as follows. In Section 2, related work is discussed. In Section 3, we describe the proposed analytical model. We present the model validation experiments, in Section 4. Finally, Section 5 summarizes our findings and concludes the paper.

## 2 Related Work

Generally, multi-cluster systems can be classified into *Super-Cluster* and *Cluster-of-Cluster*. A good example of Super-Cluster systems is DAS-2 [5], which is characterized by large number of homogenous processors and heterogeneity in communication networks. In contrast, Cluster-of-Clusters are constructed by interconnecting multiple single cluster systems thus heterogeneity may be observed in communication networks as well as processors. The LLNL multi-cluster system which is built in by interconnecting of four single clusters, MCR, ALC, Thunder, and PVC [6] is an example of cluster-of-cluster system. In this paper, we will focus our discursion on the Super-Cluster system with homogenous processors and heterogeneous communication networks.

Currently, there are three possible ways to address this problem – simulation, prediction and analytical modeling. The limitations of simulation-based solutions are that it is highly time-consuming and expensive. Similarly, techniques based on predictions from measurements on existing clusters would be impractical. An alternative to simulation and prediction approaches is an analytical model, which is the focus of this paper. An accurate analytical model can provide quick performance estimates and will be a valuable design tool. However, there is very little research addressing analytical model for interconnects in multi-cluster systems. The few results that exist are based on homogenous cluster systems and the evaluations are confined to a single cluster [2, 3, 4, 19]. With all probability, multiple cluster systems would be configured from heterogeneous components, rendering exiting optimization solutions unusable in heterogeneous multi-cluster environment. In contrast, our work focuses on heterogeneous multi-cluster computing systems. To this end, we present a

generic model to analytically evaluate the performance of multi-cluster systems. We believe that our work is the first to deal with heterogeneous multi-cluster environments.

### 3 Proposed Analytical Model

The architectural model of the system assumed in this paper similar to [12]. It is made up of  $C$  clusters, each cluster  $i$  is composed of  $N_i$  processors of type  $T_i$ ,  $i=1, \dots, C$ . Also, each cluster has two communication networks, an Intra-Communication Network ( $ICN1_i$ ), which is used for the purpose of message passing between processors, and an intEr-Communication Network ( $ECN1_i$ ), which is used to transmit messages between clusters, management and also for the expansion of system. Note that, ECN can be accessed directly by the processors of a cluster without going through the ICN.

The proposed model is based on the following assumptions that are widely used in similar study [3, 4, 12, 14]:

1. Each processor generates packets independently which follows a Poisson process with a mean rate of  $\lambda$  and inter-arrival times are exponentially distributed.
2. The arrival process at a given communication network is approximated by an independent Poisson process. This approximation has often been invoked to determine the arrival process in store-and-forward networks [13]. In this paper we apply the store-and-forward network, e.g., Ethernet-based networks. Therefore, the rate of process arrival at a communication network can be calculated using Jackson's queuing networks formula [7].
3. Each processor granted the network as a packet transmission.
4. The destination of each request would be any node in the system with uniform distribution.
5. The processors which are source of request must be waiting until they get service and they cannot generate any other request in wait state.
6. The number of processors in all clusters are equal ( $N_1=N_2=\dots=N_C=N_0$ ) with homogenous type of ( $T_1=T_2=\dots=T_C=T_0$ ).
7. Message length is fixed and equal to  $M$  bytes.

A packet is never lost in the network. Also, the terms "request" and "packet" are used interchangeably throughout this paper.

#### 3.1 Queuing Network Model

Based on the characteristics of the system model, each communication network can be considered as service center. The queuing network model of system is shown in Fig. 1, where the path of a packet through various queuing centers is illustrated. As is

shown in the model, the processor requests will be directed to service center ICN1 and ECN1 by probability  $1-P$  and  $P$ , respectively. According to assumption 1, the request rate of a processor is  $\lambda$ , so the input rate of ICN1 and ECN1 which feed from that processor will be  $\lambda(1-P)$  and  $\lambda P$ , respectively. The additional inputs at these service centers,  $\gamma_{I1}$  and  $\gamma_{E1}$ , are due to the requests generated by other processors of the same cluster. The output of ICN1 is feedback to the same processor, and also  $\epsilon_{I1}$  represents the response to other processors in the same cluster.

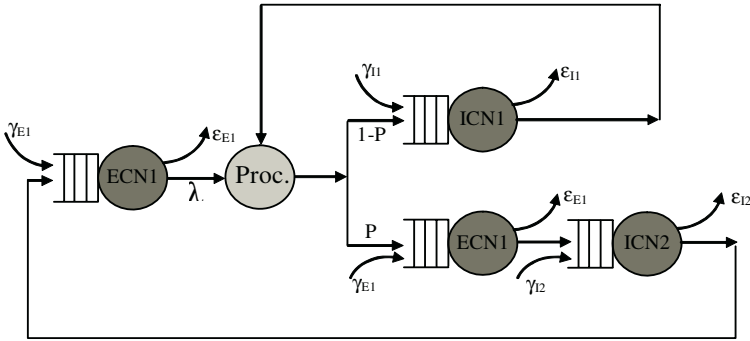


Fig. 1. Queuing Network Model of a Super-Cluster System

The external request (out of cluster) of a cluster goes through the ECN1 with probability  $P$  and then ICN2. In the return path, it again accesses the ECN1 to get back to the node, which initiated the request. As mentioned before,  $\epsilon_{E1}$  and  $\epsilon_{I2}$  are responses to the other requests except the one under consideration. So, the total requests of the processors received by service centers in the first stage can be calculated as follows:

$$\begin{aligned} \lambda_{I1} &= (1-P)\lambda + \gamma_{I1} = (1-P)\lambda + (N_0-1)(1-P)\lambda \\ &= N_0(1-P)\lambda \end{aligned} \tag{1}$$

$$\begin{aligned} \lambda_{E1(1)} &= P\lambda + \gamma_{E1} = P\lambda + (N_0-1)P\lambda \\ &= N_0P\lambda \end{aligned} \tag{2}$$

where  $\lambda_{E1(1)}$  is the input rate of ECN1, the one which is feed by the processor.

In the second stage, the input request rate of ICN2 in forward path and ECN1 in feedback path can be computed by following equations:

$$\begin{aligned} \lambda_{I2} &= \lambda_{E1(1)} + \gamma_{I2} = N_0P\lambda + (C-1)\lambda_{E1(1)} \\ &= N_0P\lambda + (C-1)N_0P\lambda = C N_0P\lambda \end{aligned} \tag{3}$$

$$\lambda_{E1(2)} = \lambda_{I2}/C = N_0P\lambda \tag{4}$$

where  $\lambda_{E1(2)}$  is the input rate of ECN1 from feedback path. According to equations (2) and (4), the input rate of ECN1 is:

$$\lambda_{E1} = \lambda_{E1(1)} + \lambda_{E1(2)} = 2N_0P\lambda \tag{5}$$

The average number of waiting processors in each service center can be computed through queue length of each center. So, the average of total waiting processors in the system will be:

$$L = C (2.L_{E1} + L_{I1}) + L_{I2} \tag{6}$$

which  $L$  is denoting the queue length of each service center. As mentioned in the assumption 5, the waiting processors would not be able to generate new requests, so the effective request rate of the processor would be less than  $\lambda$ . Applying the method described in [8] to find the effective request rate of a processor, it is directly dependent to the ratio of number of active processors to total number of processors. Therefore,  $L$  and  $\lambda$  are computed iteratively based on following equation, until no considerable change is observed between two consecutive steps:

$$\lambda_{eff} = \frac{N-L}{N} \times \lambda \tag{7}$$

As it can be seen in the previous equations, the probability  $P$  has been used as the probability of outgoing request within a cluster. According to assumption 4, this parameter is computed base on structure of system [20] by the following equation:

$$P = \frac{(C-1) \times N_0}{(C \times N_0) - 1} \tag{8}$$

In this paper, message latency is selected as a primary performance metric. However, most of the other performance metrics for the queuing network model of a multi-cluster system are related to the message latency with simple equations [12]. To model the mean message latency, we consider effective parameters as follows. In such systems, the mean network latency, that is the time to cross the network, is the most important part of the message latency. Other parameters such as protocol latency can be negligible.

Since the system under study is symmetric, averaging the network latencies seen by message generated by only one node for all other nodes gives the mean message latency in the network. Let  $S$  be the source node and  $D$  denotes a destination node such that  $D \in A - \{S\}$  where  $A$  is the set of all nodes in the network. The network latency,  $T_C$ , seen by the message crossing from node  $S$  to node  $D$  consist of two parts: one is the delay due to the physical message transmission time,  $T_W$ , and the other is due to the blocking time in the network,  $T_B$ . Therefore,  $T_C$  can be written as:

$$T_C = T_W + T_B \tag{9}$$

These parameters are strongly depended on the characteristics of the communication network which is used in the system. Of this, we take into account two different networks in our model as following.

### 3.2 Blocking and Non-blocking Network Model

For non-blocking architecture, we use the *Multi-Stage Fat-Tree* topology, which is used in some cluster systems such as Thunder [9]. For modeling blocking interconnect architecture, a *Linear Array* of switches is used. Due to space limitation,



we have not included the details of blocking and non-blocking analysis here. Interested reader can refer to [20].

## 4 Performance Evaluation

In order to validate the technique and justify the approximations, the model was simulated using the OMNeT++ [15]. Requests are generated randomly by each processor with an exponential distribution of inter-arrival time with a mean of  $1/\lambda$  where  $\lambda$  is fixed to 0.25 msg/sec in all experiments. The destination node is determined by using a uniform random number generator. Each packet is time-stamped after its generation. The request completion time is checked in to compute the message latency in a “sink” module. For each simulation experiment, statistics were gathered for a total number of 10,000 messages. In our study, we used two well-known network technologies, Gigabit Ethernet (GE) and Fast Ethernet (FE), which are widely used in cluster systems. We also used the same value for the latency and bandwidth of each network as reported by [10]. Two different communication network scenarios for network heterogeneity were simulated. However, due to space limitations, a subset of the results is presented here.

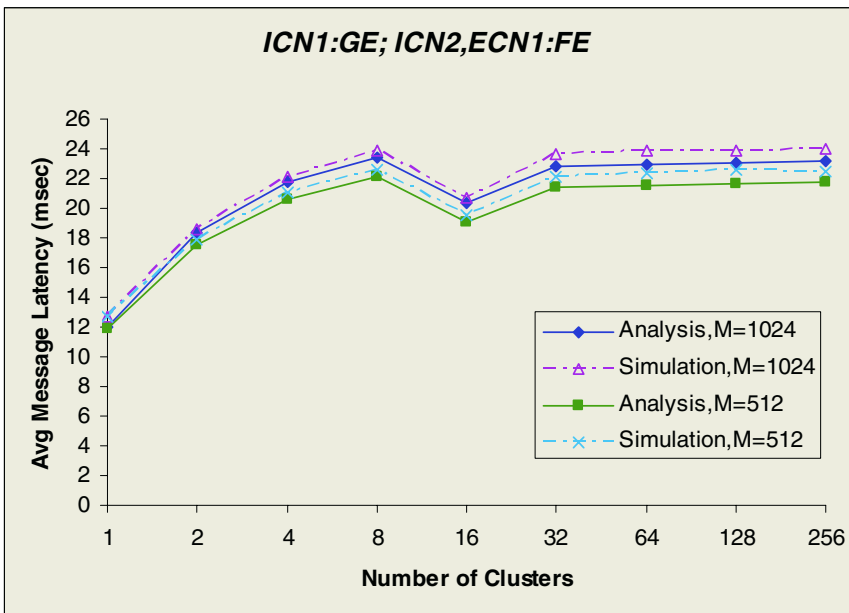


Fig. 2. Average Message Latency vs. Number of Clusters for Non-blocking Networks

Fig. 2 shows the average message latency in a multi-cluster system with  $N=256$  nodes and non-blocking communication network against those provided by the simulator for the message size of 1024 and 512 bytes. The horizontal axis in the

figures represents the number of clusters in the system. To have a better performance analysis of the system, we used the blocking communication networks, with the same parameters. As we expected, the average message latency in this system is much larger than in the system with non-blocking networks. These results reveal that average message latency in blocking network with uniform traffic pattern is 1.4 to 3.1 times larger than non-blocking network.

## 5 Conclusion and Future Directions

A performance model is an essential tool for behavior prediction of a system. It is used to analyze intricate details of the system and various design optimization issues. One such model based on queuing networks is presented in this study to predict the message latency of multi-cluster systems. Two different networks, blocking and non-blocking, were used in our modeling of the system. The analysis captures the effect of communication network architecture on the system performance. The model is validated by constructing a set of simulators to simulate different types of clusters, and by comparing the modeled results with the simulated ones. The future works focus on improving the analytical model to tack into account more effective parameters, modeling of communication networks with technology heterogeneity and propose a similar model to another class of multi-cluster systems, Cluster-of-Clusters.

## References

1. J. H. Abawajy and S. P. Dandamudi, "Parallel Job Scheduling on Multi-Cluster Computing Systems," In *Proceedings of the IEEE international Conference on Cluster Computing (CLUSTER'03)*, Dec. 1-4, 2003, Hong Kong.
2. X. Du, X. Zhang, Z. Zhu, "Memory Hierarchy Consideration for Cost-Effective Cluster Computing," *IEEE Transaction on Computers*, Vol. 49, No.5, pp. 915-933, Sept. 2000.
3. B. Javadi, S. Khorsandi, and M. K. Akbari, "Study of Cluster-based Parallel Systems using Analytical Modeling and Simulation" *International Conference on Computer Science and its Applications (ICCSA 2004)*, May 2004, Perugia, Italy.
4. B. Javadi, S. Khorsandi, and M. K. Akbari, "Queuing Network Modeling of a Cluster-based Parallel Systems", *7th International Conference on High Performance Computing and Grids (HPC ASIA 2004)*, July 2004, Tokyo, Japan.
5. The DAS-2 Supercomputer. <http://www.cs.vu.nl/das2>
6. B. Boas, "Storage on the Lunatic Fringe", Lawrence Livermore National Laboratory, Panel at SC2003, Nov. 2003, Arizona, USA.
7. D. Bertsekas, R. Gallager., *Data Networks*, Prentice Hall Publishers, New Jersey, 1992.
8. H. S. Shahhoseini, M. Naderi, "Design Trade off on Shared Memory Clustered Massively Parallel Processing Systems", *The 10th International Conference on Computing and Information (ICCI '2000)*, Nov. 2000, Kuwait.
9. "Thunder Statement of Work", University of California, Lawrence Livermore National Laboratory, Sept. 2003.
10. M. Lobosco, and L. de Amorim, "Performance Evaluation of Fast Ethernet, Giganet and Myrinet on a Cluster", *Lecture Notes in Computer Science*, volume 2329, pp. 296-305, 2002.

11. J. H. Abawajy, "Taxonomy of Job Scheduling Approaches in Cluster Computing Systems," Technical Report, Deakin University, 2004.
12. B. Javadi, M. K. Akbari, J.H. Abawajy, "Performance Analysis of Multi-Cluster Systems Using Analytical Modeling", *International Conference on Modeling, Simulation and Applied Optimization*, Sharjah, United Arab Emirates, Feb. 2005.
13. L. Kleinrock, *Queueing System: Computer Applications*, Part 2, John Wiley Publisher, New York, 1975.
14. H. Sarbazi-Azad, A. Khonsari, M. Ould-Khaoua, "Analysis of k-ary n-cubes with Dimension-order Routing", *Journal of Future Generation Computer Systems*, pp. 493-502, 2003.
15. Nicky van Foreest. *Simulation Queuing Networks with OMNet++*, in Tutorial of OMNet++ Simulator, Department of Telecommunications, Budapest University of Technology and Economics, Apr. 2002.
16. J. H. Abawajy, "Dynamic Parallel Job Scheduling in Multi-cluster Computing Systems," *4th International Conference on Computational Science*, Kraków, Poland, pp. 27-34, 2004.
17. Chee Shin Yeo, Rajkumar Buyya, Hossein Pourreza, Rasit Eskicioglu, Peter Graham, Frank Sommers, "Cluster Computing: High-Performance, High-Availability, and High-Throughput Processing on a Network of Computers", *Handbook of Innovative Computing*, Albert Zomaya (editor), Springer Verlag, 2005.
18. H. Chen, P. Wyckoff, and K. Moor, "Cost/Performance Evaluation of Gigabit Ethernet and Myrinet as Cluster Interconnects," *Proc. 2000 Conference on Network and Application Performance (OPNETWORK 2000)*, Washington, USA, Aug. 2000.
19. J. Hsieh, T. Leng, V. Mashayekhi, and R. Rooholamini, "Architectural and Performance Evaluation of GigaNet and Myrinet Interconnects on Clusters of Small-Scale SMP Servers," *Proc. 2000 ACM/IEEE conference on Supercomputing (SC2000)*, Dallas, USA, Nov. 2000.
20. Bahman Javadi, J. H. Abawajy, Mohammad K. Akbari, "Performance Analysis of Interconnection Networks for Multi-Cluster Systems," Technical paper, School of Information Technology, Deakin University, Geelong, VIC 3217, Australia, 2005.

# Autonomic Job Scheduling Policy for Grid Computing

J.H. Abawajy

School of Information technology,  
Deakin University, Geelong, VIC, 3217, Australia

**Abstract.** Autonomic middleware services will play an important role in the management of resources and distributed workloads in emerging distributed computing environments. In this paper, we address the problem of autonomic grid resource scheduling and propose a scheduling infrastructure that is capable of self-management in the face of dynamic behavior inherent to this kind of systems.

## 1 Introduction

Grid computing is a network of geographically distributed heterogeneous and dynamic resources spanning multiple administrative domains [5]. Grids can potentially furnish large computational and storage resources to solve large-scale problems. However, the need to integrate many independent and heterogeneous subsystems into a well-organized virtual distributed systems introduces new levels of complexity making the underlying Grid environment inherently large, complex, heterogeneous and dynamic. Also it makes the systems highly susceptible to a variety of failures. Some of these failures include node failure, interconnection network failure, scheduling middleware failure, and application failure. Due to the inherent complexity and vulnerabilities, achieving large-scale distributed computing in a seamless manner on Grid computing systems introduces not only the problem of efficient utilization and satisfactory response time but also the problem of fault-tolerance [1].

One way to address these problems is to make Grid middleware technologies to embrace the concept of self-configuring systems that are able to act autonomously and adapt to changes in application or user needs. There is a synergy towards designing and building computing systems that are capable of running themselves, adjusting to varying circumstances, and preparing their resources to handle most efficiently the workloads we put upon them [7]. This new frontier of designing and building next generation computing systems has become known as autonomic computing [7]. The overall goal of autonomic computing is to make systems anticipate needs and allow users to concentrate on what they want to accomplish. The question is then how to design and develop autonomic grid resource management infrastructure that is capable of self-management (i.e., self-control, self-healing, self-configuration, self-optimization, and self-protection) in the face of dynamic behavior inherent to this kind of systems?

Within this broad problem area, we address the problem of autonomous Grid resource scheduling in the presence of a variety of failures. By autonomous Grid resource scheduling we mean a scheduling infrastructure that is capable of acting autonomously and adapt to changes in application or resource failures. We propose an autonomic scheduling infrastructure that is capable of proactively detect and rectify potential faults as applications are executing.

The rest of the paper is organized as follows. In Section 2, related work is presented. This section also establishes the fact that, to a large extent, the problem considered in this paper has not been fully addressed in the literature. Section 3 presents the proposed autonomic scheduling policy. Finally, Section 4 presents the conclusion and future directions.

## 2 Related Work

The human body is self-healing. For example, broken bones mend, and cuts heal. The concept of developing the next generation of computing systems should be driven by the conceptual similarity between biological systems and digital computing systems [6]. Hence, the objectives of autonomic computing is to build computing systems and services that are capable of managing themselves; that can anticipate their workloads and adapt their resources to optimize their performance. [6][7][10].

Enhancing the core services of a Grid middleware technologies with autonomic capabilities so that the functions are self-managing is an important research area. There has been some work towards autonomic grid computing [8][11][6] [9]. Liu, and Parashar [11] present an environment that supports the development of self-managed autonomic components, dynamic and opportunistic composition of these components using high-level policies to realize autonomic applications, and provides runtime services for policy definition, deployment and execution. In [6], an autonomic architecture to achieve automated control and management of networked applications and their infrastructure based on XML format specification is presented.

Our main focus in this paper is on autonomic grid resource scheduling middleware. Existing approaches statically allocate or release resources to Grid applications. Moreover, although fault-tolerance is one of the desirable properties of any grid scheduling algorithm, unfortunately it has not been factored into the design of most existing scheduling strategies for Grid computing systems. Research coverage of fault tolerant scheduling is limited as the primary goal for nearly all scheduling algorithms developed so far has been high performance by exploiting as much parallelism as possible. Achieving integrated scheduling and fault-tolerance goal is a difficult proposition as the job scheduling and fault-tolerance are difficult problems to solve in their own right.

Clearly, there is a need for a fundamental change in how scheduling middleware for the next generation Grid computing are developed and managed. We believe that the ability to self-manage while effectively exploiting the variably sized pools of resources in an scalable and transparent manner must be

an integral part of Grid computing scheduling middleware. We are not aware of any work that is currently concentrate on autonomic Grid resource management in general and scheduling middleware in particular. To this end, we propose a scheduling infrastructure that is capable of dynamically scheduling resources while at the same time capable of self-heal to various types of failures.

### 3 Autonomic Scheduling Middleware Infrastructure

In this section, we discuss the proposed autonomic scheduling policy based on a hierarchical approach shown in Figure 1. Note that hierarchical scheduling policies have been used in various platforms such as cluster computing [2] and grid computing [4].

#### 3.1 System Architecture

The core system architecture is designed around **L**-levels of virtual hierarchy, which we refer to as a *virtual organization tree*, as shown in Figure 1. At the top of the virtual organization tree, there is a *system scheduler* while at the leaf level there is a *local scheduler* (*LS*) for each node. In between the *system scheduler* and the *local schedulers*, there exists a hierarchy of *middle schedulers* (*CS*).

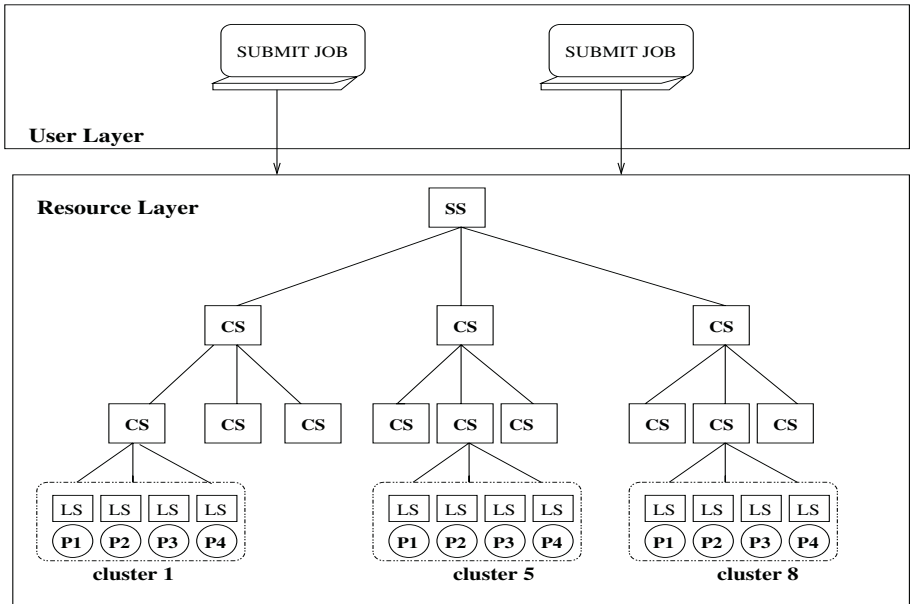


**Fig. 1.** An example of virtual organization tree (SS: System scheduler; CS: middle scheduler; LS: Local scheduler; and  $P_i$ : node  $i$ )

We refer to all processors reachable from a given node in the virtual organization tree as its *partition-reach*. We associate a parameter called *base load level* with each node in the virtual organization tree. For non-leaf nodes, the base load level is set to zero. For all the leaf-level nodes, the base load level is the same as the multiprogramming level (MPL) of the node. The MPL parameter of a node controls the maximum number of tasks that can concurrently execute at any given time [2].

### 3.2 Autonomic Scheduling Middleware

Within the hierarchical structure shown in Figure 1, an autonomic Grid resource scheduler can be viewed as a collection of autonomic schedulers that can manage their internal behaviors and their relationships and interactions with other schedulers and the system. The *Autonomic Scheduling (ASP)* policy automatically replicates jobs and tasks over several grids and processors, keep track of the number of replicas, instantiate them on-demand and delete the replicas when the primary copies of the jobs and tasks successfully complete execution. In this paper, we assume that every middle scheduler in the system is reachable from any other middle scheduler unless there is a failure in the network or the node housing the cluster scheduler. A scheme to deal with node, scheduler and link failures is discussed in [3] [4]. Also, without lose of generality, we assume that all incoming jobs are submitted to the system scheduler where they are placed in the *job wait queue* until a placement decision is made. Figure 2 shows the pseudo-code of the ASP policy. As shown in Figure 2, the ASP policy has three main components namely; *Self-scheduling*, *Job and Task Scheduling* and *Fault Management* components. These components are described in detail in the following subsection.

### 3.3 Self-scheduling

ASP is demand-driven where nodes in the system look for work when their load is below a given threshold. Specifically, whenever the *current load level* of a non-root node in the cluster tree falls below its *base load level*, the node sends a *Request for Computation (RFC)* message asking for  $\mathbf{T}_{req}$  units of computation to its parent. After sending RFC message to its parent, the node updates its *base load level* to ensure that it can have only one outstanding RFC at any given time. When a parent with no unscheduled work receives a RFC from a child, if there is a pending RFC at the parent, the new RFC is backlogged and processed when work becomes available. Otherwise, the RFC recursively ascends the cluster tree until the RFC reaches either the *system scheduler* or a node that has unassigned jobs. In the later case, a set of jobs/tasks are transferred down the hierarchy along the path the RFC has traveled. This amount is determined dynamically during parent and child negotiations and the number of unscheduled jobs as described in the following section.

---

**SHS algorithm**


---

## 1. Self-Scheduling

- (a) IF Current load level falls below base load level

$$T_{req} = \text{base load level} - \text{current load.} \quad (1)$$

- (b) Update base load level

ENDIF

## 2. Job/Task Assignment

- (a) Determine ideal number of jobs/tasks that can be scheduled

$$T_{target} = \lceil T_r \times \text{number of tasks queued} \rceil \quad (2)$$

where  $T_r$  is the *transfer factor* and is computed as follows:

$$T_r = \frac{\text{partition-reach of the child node}}{\text{partition-reach of the parent node}} \quad (3)$$

- (b) Adjust the number of jobs that will actually be transferred down one level to the child as follows:

$$T_{target} = \begin{cases} \min(T_{req}, \text{number of tasks queued}) & \text{if } T_{req} > T_{target} \\ \min(T_{req}, \text{child partition-reach}) & \text{Otherwise.} \end{cases} \quad (4)$$

where  $T_{req}$  is the is the number of computations requested by the child scheduler.

- (c) Finally, if the target size determined in Equation 2 is smaller than the  $T_{req}$  from the child, then the parent will send the lesser of  $T_{req}$  and the *number of tasks queued*. Otherwise, the set of tasks sent to the child is the lesser of  $T_{target}$  and *child partition-reach*.
- (d) Send a replica of the job to each site and update job table and backup scheduler.

## 3. Monitor the job execution

FOR replica-interval DO

- (a) Prompt all remote SMs for job status
- (b) Determine the number of healthy replicas (i.e.,  $h$ )
- (c) IF any replica is done THEN
- i. Tell all remote SMs to terminate their replica
  - ii. Update job table
- (d) ELSEIF ( $h > n$ ) THEN
- i. Select last replica from set to terminate
  - ii. Update job table
- (e) ELSE
- i. Pick next site from set to terminate
  - ii. Inform the remote SM to execute the job
  - iii. Update job table

ENDIF

ENDFOR

---

**Fig. 2.** Self-healing scheduling algorithm



### 3.4 Job and Task Placement

First, we determine an ideal number of jobs/tasks that can possibly be sent to a child scheduler as shown in Equation 2. Once the target number,  $T_{target}$ , of jobs that can possibly be transferred to a child is determined, the algorithm then considers the size of the RFC from the child as a hint to adjust the number of jobs that will actually be transferred down one level to the child. Finally, if the target size is smaller than the  $T_{req}$  from the child, then the parent will send the lesser of  $T_{req}$  and the *number of tasks queued*. Otherwise, the set of tasks sent to the child is the lesser of  $T_{target}$  and *child partition-reach*. Note that this is a dynamic load distribution algorithm that changes the size of the batch at run time, allocating large size to larger clusters while smaller clusters are allocated small size.

With respect to which jobs are dispatched, ASP favors jobs that have their replicas within the partition reach of the requesting schedulers. If there are no such jobs, then jobs belonging to the left sibling of the requesting node is searched. If this fails the jobs of the right sibling of the requesting node are selected. This process continues until the exact number of jobs to be sent to the requesting node is reached. The motivation for this job selection scheme is that we minimize replica management overheads (e.g., the replica instantiation latency) in case the original job fails. We also reduce the job transfer latency as we have to only send control messages to the child scheduler if the replica is already located there. Finally, it reduces the time that a child scheduler waits for the jobs to arrive, which increases system utilization. After dispatching the jobs to a child, the parent informs the backup scheduler about the assignment and then updates the application status table (AST) to reflect the new assignment.

### 3.5 Failure Management

A fail-over strategy is used when a link or a node failure is detected. Link failure is addressed by rerouting traffic from the failed part of the network to another portion of the network. For non-root nodes, the child scheduler is informed to communicate through its closest sibling of the parent. If the failed node is the root, then we choose the closest functional and reachable sibling. When the failed link is repaired, traffic is rerouted over the primary route. Similarly, when a node is repaired, if the node used to be the primary scheduler, then the node that replaced it is told to send to the recovered node and all former children are also notified to update their parent id. The node then rejoins the system and provides services immediately after recovery. If it was a backup node, recovery is not necessary. A detailed discussion of the fail-over strategy is given in [3][4].

**Job Replication.** The replica creation and placement is to ensure that a job and its constituent task are stored in a number of locations in the cluster tree. The policy maintains some state information for failure and recovery detections in Application Status Table (AST). Jobs are replicated over clusters while tasks are replicated over processors. Specifically, when a job with fault-tolerance requirement arrives into the system, SHS undertakes the following steps: (1) create

a replica of the job; (2) keep the replica and send the original job to a child that is alive and reachable; and (3) update the application status table (AST) to reflect where the job replicas are located. This process recursively follows down the cluster tree until we reach the lowest level cluster scheduler (LCS) at which point the replica placement process terminates.

**Replica Monitoring.** The SHS monitors applications at job-level (between non-leaf nodes and their parents) and at task-level (between leaf nodes and their parents). A monitoring message exchanged between a parent and a leaf-level node is called a *report* while that between non-leaf nodes is called a *summary*. A report message contains status information of a particular task running on a particular node and sent every *REPORT-INTERVAL* time units. In contrast, the *summary* message contains a collection of many reports and sent every *SUMMARY-INTERVAL* time periods such that  $REPORT-INTERVAL < SUMMARY-INTERVAL$ .

When a processor completes execution of a task, the report message contains a *FINISH* message. In this case, the receiving scheduler deletes the corresponding replica and informs the backup scheduler to do the same. When the last replica of a given job is deleted, the job is declared as successfully completed. In this case, the cluster scheduler immediately sends a summary message that contains the *COMPLETED* message to the parent scheduler, which deletes the copy of the job and forward the same message to its parent. This process continues recursively until all replicas of the job are deleted.

**Failure Detection and Recovery.** After each assignment, the children periodically inform their parents the health of the computations as discussed above. If the parent does not receive any such message from a particular child in a given amount of time, then the parent suspects that the child has failed. In this case, it notes this fact in the AST and sends a request for report message to the child. If a reply from the child has not been received within a specific time frame, the child is declared dead. When a failure is detected, a recovery procedure is initiated to handle the failure. The recovery mechanism restarts a replica of the failed primary task as soon as possible.

## 4 Conclusion and Future Directions

In this paper, we presented a scalable framework that loosely couples the dynamic job scheduling approach with the hybrid (i.e., passive and active replications) approach to schedule jobs efficiently while at the same time providing fault-tolerance. The main advantage of the proposed approach is that fail-soft behaviour (i.e., graceful degradation) is achieved in a user-transparent manner. Furthermore, being a dynamic algorithm estimations of execution or communication times are not required. An important characteristic of our algorithm is that it makes use of some local knowledge like faulty/intact or busy/idle states of nodes and about the execution location of jobs. Another important charac-

teristic of the proposed approach is that they are applicable for a wide variety of target machines including Grid computing.

We are currently implementing and studying the performance of the proposed policy. In the proposed self-healing distributed framework, the latency of detecting the errors might be affected by message traffic in the communication network. To address this problem, we intend to develop an on-line mechanism to dynamically measure the round-trip time of the underlying network and calculate the error latency accordingly.

**Acknowledgement.** I appreciate the help of Maliha Omar without whose help this paper would not have been realized.

## References

1. J. H. Abawajy. Fault-tolerant scheduling policy for grid computing systems. In *Proceedings of IEEE 18th International Parallel & Distributed Processing Symposium (IPDPS04)*, pages 238–146, 2004.
2. Jemal H. Abawajy and Sivarama P. Dandamudi. Parallel job scheduling on multi-cluster computing systems. In *Proceedings of IEEE International Conference on Cluster Computing (CLUSTER'03)*, pages 11–21, 2003.
3. Jemal H. Abawajy and Sivarama P. Dandamudi. A reconfigurable multi-layered grid scheduling infrastructure. In Hamid R. Arabnia and Youngsong Mun, editors, *Proceedings of the International Conference on Parallel and Distributed Processing Techniques and Applications, PDPTA '03, June 23 - 26, 2003, Las Vegas, Nevada, USA, Volume 1*, pages 138–144. CSREA Press, 2003.
4. Jemal H. Abawajy and Sivarama P. Dandamudi. Fault-tolerant grid resource management infrastructure. *Journal of Neural, Parallel and Scientific Computations*, 12:208–220, 2004.
5. Ian T. Foster, Carl Kesselman, and Steven Tuecke. The anatomy of the grid - enabling scalable virtual organizations. *CoRR*, cs.AR/0103025, 2001.
6. Salim Hariri, Lizhi Xue, Huoping Chen, Ming Zhang, Sathija Pavuluri, and Soujanya Rao. Autonomia: An autonomic computing environment. In *IEEE International Performance Computing and Communications Conference*, 2003.
7. Paul Horn. Autonomic computing. *The Economist print edition*, September 19, 2002.
8. Gang HUANG, Tiancheng LIU, Hong MEI, Zizhan ZHENG, Zhao LIU, and Gang FAN. Towards autonomic computing middleware via reflection. In *COMPSAC*, 2004.
9. Gail Kaiser, Phil Gross, Gaurav Kc, Janak Parekh, and Giuseppe Valetto. An approach to autonomizing legacy system. In *IBM Almaden Institute Symposium*, 2002.
10. Jeffrey O. Kephart and David M.Chess. The vision of autonomic computing. *IEEE Computer*, pages 41–50, 2003.
11. H. Liu and M. Parashar. A component based programming framework for autonomic applications. In *In Proceedings of the International Conference on Autonomic Computing*, 2004.

# A New Trust Framework for Resource-Sharing in the Grid Environment

Hualiang Hu, Deren Chen, and Changqin Huang

College of Computer Science, Zhejiang University, Hangzhou, 310027, P.R. China  
huhualiang@163.net

**Abstract.** The open and anonymous of grid make the task of controlling access to sharing information more difficult, which cannot be addressed by traditional access control methods. In this paper, we identify access control requirements in such environments and propose a trust based access control framework for grid resource sharing. The framework is an integrated solution involving aspects of trust and recommendation models, based the discretionary access control (DAC), and are applied to grid resource-sharing systems. In this paper, we integrate technology of web services into idea of trust for describing resources.

## 1 Introduction

Grid applications are distinguished from traditional client-server applications by their simultaneous use of large numbers of resources, dynamic resource requirements, use of resources from multiple administrative domains, complex communication structures, and stringent performance requirements, among others [1].

Although grid security infrastructure (GSI) has been widely adopted as the core component of grid applications, GSI, which provides a basic secure and reliable grid-computing environment, is still at its early stage of development. Since GSI is built upon PKI, risks factors due to the use of PKI have to be considered carefully such as compromising of private keys or theft of certificates for the following reasons:

1. Parallel computations that acquire multiple computational resources introduce the need to establish security relationships not simple between a client and a server, but among potentially hundreds of processes that collectively span many administrative domains.
2. The inter-domain security solutions used for grids must be able to interoperate with, rather than replace, the diverse intra-domain access control technologies inevitably encountered in individual domains.
3. In such a distributed system, a huge set of entities cannot be known in advance.
4. Authentication alone is sometimes not enough to make one confident about allowing a requested access or action rather, a kind of trust is also along with authentication.
5. In order to increase the scalability of a distributed system, it should be possible to delegate the authority to issue access certificates.

6. In the traditional security systems, an access control mechanism such as Access Control List (ACL) is not expressible and extensible. Whenever new or diverse conditions and restrictions arise, the application is required to change or rebuild [1, 2]. At present, trust for grid is solely built on authentication of identity certificates. As authentication is not insufficient for establishing strong security, it is critical that a proper trust evaluation model for grid is needed. In this paper, we present an access control framework for grid resource-sharing systems, which provides grid users better access control services whilst preserving the decentralized structure of the grid environment. The framework extends a traditional access control model to meet the requirements of grid resource-sharing. The paper is organized as follow. Section 2 identifies the requirements of an access control model for grid environment. Section 3 discusses the characteristics of grid environment. Section 4 explains our access control framework in detail, including the overall architecture, authentication process, scoring scheme. Section 5 gives our concluding remarks.

## 2 Access Control Requirements

We have identified main requirements that an access control model for grid resource-sharing system should support:

1. Single sign-on: A user should be able to authenticate once.
2. Protection of credentials: User's credentials must be protected.
3. Interoperability with local security solutions: while our security solutions may provide inter-domain access mechanisms, access to local resources will typically be determined by a local security policy that is enforced by local security mechanisms. It is impractical to modify every local resource to accommodate inter-domain. Access; instead, one or more entities in a domain must act as agents of remote clients/users for local resources.
4. Resources may require different authentication and authorization mechanisms and policies, which we will have limited ability to change.
5. Limits are placed on the overall amount of resource consumed by particular groups or users.
6. Decentralized control: The centralized access control authority does not exist in a grid environment. We must take this decentralization of the access control model for grid environment must into account.
7. Node classification: one attribute of grid environment is uncertainty. Their interacting partners are mostly unknown, unlike most other systems, where the users are known. Previously unknown users, who request access to the system, may contact entities. Hence, the framework proposed must provide a mechanism for entities to classify users and assign each user to access rights accordingly.
8. Encourage sharing resources: Sharing is another grid's property. The framework proposed does not only protect the resources, but also provides technologies to grid for resources sharing. This means giving entities the ability to control access to their resources, at the same time, entities must be confident that participation in the system will give them better chance to access to the resources they want.

### 3 Grid Resource Sharing Systems

Grid resource sharing allows any two nodes in the system to directly access resources from each other systems. To achieve this flexible direct access, grid environment has to support three kinds of operations:

1. Publish: The resources should firstly be described and published in the grid. The provider must pass the identity verification of the resources.
2. Find: There are two ways, which the resources requester finds information. One of them is browse pattern, in the case the result is not unique; the other is drill down pattern, in the case, the result is unique.
3. Bind: By analyzing the binding information gathering from the Services, including the access path of resources, the invoking parameters of resources, the return value, the transmission protocols and the requirements of security; the resource Requester deploys its own system and then invokes the remote resources provided by the resource provider.

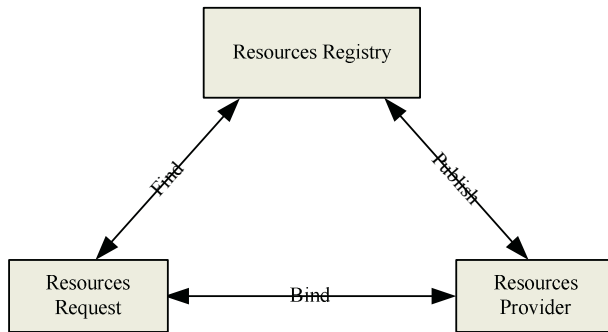


**Fig. 1.** Relationship of three roles [3]

After three steps, resource is ready. During three steps, there exists following technologies:

1. UDDI (Universal Discovery, Description, Integration). The UDDI specification was first defined by IBM, Microsoft and Ariba in July 2000. It was developed from the DISCO (Discovery of web services) of Microsoft and ADS (Advertisement and Discovery of services) of IBM. UDDI is the registry specification of web services. It defines a way to publish and discover information about web services so that the users who need the service can find and use it conveniently. This specification consists of a core information model provides four aspects of basic information about web services: By means of UDDI, components of web services can complete “register once, access anywhere”.
2. WSDL (web service description language). WSDL provides an abstract language for defining the published operations of a service with their respective parameters and data types. It also addresses the definition of the location and binding details of

the service and describes the network into the set of communication end-point, which expresses what a component of web services can do where it is and how service requester invokes it. Otherwise, WSDL also provides the standard format of describing request for a service requester.

## 4 Access Control Framework

We propose an access control framework based on the discretionary access control (DAC) model [4]. The basic behind discretionary access control is that the owner of an object should be trusted to manage its security. More specifically, owners are granted full access rights to objects under their control, and are allowed to decide whether access rights to their objects should be passed to other subjects or groups of subjects at their own discretion. In the DAC, a discretionary owner of resources has the right for the control of access discretion. Due to anonymousness for grid, we cannot pre-assign access rights to users.

### 4.1 Terms and Definitions

Following definitions can be found in [5]

**Definition 1 (Entities):** The entities are all the components involved with the operation of a grid computing system, which can be related to each other via certain trust relationships. These include the user, host (resource provider) node and trusted third parties such as the resource management system (RMS) or a CA.

**Definition 2 (Direct Trust):** Direct Trust is the belief that one entity holds in another entity in its relevant capacity with reference to a given trust class.

**Definition 3 (Indirect Trust):** A host node often encounters a client node that it has never met. Therefore, the host has to estimate the client's trustworthiness using recommendations, which a client submits other nodes'.

**Definition 4 (Recommended Trust):** Recommended Trust expresses the belief in the capacity of an entity to decide whether another entity is reliable in the given trust class and in its honesty when recommending third entities.

**Definition 5 (Hard Trust):** Hard Trust is trust derived from cryptographic based mechanisms. This can be treated as a meta-level attribute.

**Definition 6 (Soft Trust):** Soft Trust is the trust relationship derives from non-cryptographic based mechanisms which employ methods like recommendation protocol, observations, interactions or combination of them.

In this paper, we only discuss Soft Trust, which can address the uncertainty for grid.

### 4.2 Overall Architecture

Our framework contains client (user) node, service provider node and trust third parties such as the resource management system (RMS) or a CA. Shared resources in framework are rated depending on their size and content; each resource being assigned two

thresholds which capture two access aspects. Only if the request end's two access values both equal to and greater than the corresponding thresholds of the resource. It can access resources that it wants. The request end is responsible to collect recommendations that contain the information needed to evaluate its access values for a particular host. After each transaction, direct trust and direct contribution of both the client node and host nodes are updated accordingly to the satisfaction level of the transaction, which then affect the future evaluation of the access values between these two nodes.

### 4.3 Authentication

An issue in determining trust is how the user authenticated to the current session. Hence, the authentication, in our framework, must be mutual. This means both a client node and a host node need to be authenticated with each other. The authentication process is initialized by the client node that wishes to make contact.

A user may have an X.509 certificate that he uses from certain machines, a password that he may use from other sites, and may not even want to type in a password from a very un-trusted site. The user may also not yet have some of the authentication methods available [7].

The host node's local database tracks client nodes' records, for authentication purposes and access control purposes such as trust and contribution calculation. In summary, the authentication information that is saved per session consists of a 128-bit GUID (global unique identifier [8]) number and a pair of public/private keys. The node gives out the GUID and the public key as its identity and uses the private key for authentication, the name (nickname) of the user, the authentication method (certificate, password, null), and fields that other users might have added after the user authenticated into the session.

### 4.4 Evaluating System

A host node classifies its client nodes based on their records in grid environment. After authentication process with the host, a client node is required to send its rating certificates to the host to calculate the client's relative access values. The host node perceives the client's trustworthiness and contribution level, based on the client's relative access values (trust value and contribution value). The trust value is to ensure the node is trusted to interact with. The contribution value is to promote contribution for the host in grid environment.

In our framework, the trust value is key factors for making access control decision can address uncertainty factor in grid. By the trust value, a host node can determine whether it should trust that client to allow it to access to the local resources.

### 4.5 Rating Certificate Management

A rating certificate contains the direct trust value and the direct contribution score of the recommending node on the recommended node and contains the new trust value and the updated contribution score. After transaction, system automatically updates trust value and contribution value.



### 4.6 Interaction Procedure

We introduce definition for describing entities' interaction procedure [6]. The interaction procedure is shown as figure 2.

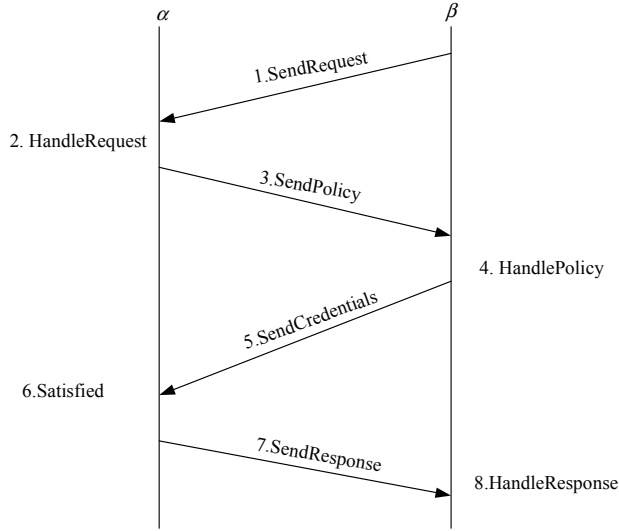


Fig. 2. Interact Procedure

Entities include  $\alpha$  and  $\beta$ .

Definition 1  $\alpha.Trust(\beta)$ :  $\alpha$  trusts  $\beta$ ;

Definition 2  $\alpha.MakeComment(\beta)$ :  $\alpha$  comments on  $\beta$ ;

Definition 3  $\alpha.SendRequest(\beta)$ :  $\alpha$  sends an request to  $\beta$ ;

Definition 4  $\alpha.HandleRequest(\beta.Request)$ :  $\alpha$  handles with request which  $\beta$  sends to  $\alpha$ ;

Definition 5  $\alpha.SendPolicy(\beta)$ :  $\alpha$  sends policy to  $\beta$ ;

Definition 6  $\alpha.HandlePolicy(\beta.Policy)$ :  $\alpha$  handles with  $\beta$ 's policy;

Definition 7  $\alpha.SendCredentials(\beta)$ :  $\alpha$  sends Credentials to  $\beta$ ;

Definition 8  $\alpha.Satisfied(\beta.Credentials)$ :  $\alpha$  handles with  $\beta$ 's message for credentials, to judge whether  $\beta$  satisfies  $\alpha$ 's trust-policy;

Definition 9  $\alpha.SendResponse(\beta)$ :  $\alpha$  sends the result to  $\beta$ ;

Definition 10  $\alpha.HandleResponse(\beta.Response)$ :  $\alpha$  handles with the result for  $\beta$ 's Response;

## 5 Relational Works

In this section, we examine several papers that examine issues that are peripherally related. A model for supposed in [9]. This trust-based model allows entities to tune their understanding of another entity's recommendations. A model for supporting

behavior trust based on experience and reputation is proposed in [10]. The Community Authorization Service (CAS) in [11]. A design and implementation of a secure service discovery service (SDS) is in [12]. The SDS can be used by service providers as well as clients. Formalizations of trust in computing systems were done by Marsh [13]. He attempted to integrate the various facets of trust from the disciplines of economics, psychology, philosophy and sociology.

## 6 Concluding Remarks

We propose a novel trust framework based on the DAC model for resources-sharing in grid environment.

Our proposed trust model is optimistic in that the majority of nodes start with access value, while a small group of nodes have overdue access value. The concept of trust value can address uncertainty problem. Hence, host nodes can assign appropriate access privileges to each visitor accordingly.

The trust framework we proposed can also provide trust guarantees to each node. We provided rating certificate that stores and updates the trust value and the contribution value. Involvement values, which are associated with each community within which a node is a member, play an important role in determining accurate trust value of nodes.

Finally we explained the interact procedure between entities.

Our future challenge ahead is to refinement the proposed framework based access scheme in grid environment and how to compute trust value efficiently over the grid.

## References

1. I. Foster and C. Kesselman. A Security Architecture for Computational Grids. In Proceeding of the 5<sup>th</sup> ACM Conference on Computer and Communication Security, November 2-5, 1998.
2. H. Lei, G. C. Shoja. Dynamic Distributed Trust Model to Control Access to Resources over the Internet, Communications, Computers and Signal Processing. August 28-30, 2003.
3. Dr. Liang-Jie (L.J) Zhang. On Demand Business Collaboration With Services Computing.
4. J. McLean. The Specification and Modeling of Computer Security. IEEE Computer, Jan 1990.
5. L. Ching, V. Varadharajan and W. Yan. Enhancing Grid Security With Trust Management. In proceedings of the 2004 (IEEE) international Conference on Services Computing (SCC 04).
6. N.YuPeng and C. YuanDa. Automation Trust Establishment in Open Network Environment. Computer Engineering 2004; 30(16):124-125.
7. D. Agarwal, M. Thompson, M. Perry and M. Iorch, A New Security Model for Collaborative Environments.<http://dsd.lbl.gov/Collaboratories/Publications/WACE-IncTrust-final-2003.pdf>.
8. D. Box, Essential COM, Addison Wesley, 1998.
9. Karl Aberer & Zoran Despotovic, Managing Trust in a Node-2-Node Information System, ACM CIKM, Nov 2001.

10. A. Abdul-Rahman and S. Hail. Supporting Trust in Virtual Communities. Hawaii Int'I Conference on System Sciences, 2000.
11. L. Pearlman et al. A Community Authorization Service for Group Collaboration. IEEE Workshop on Policies for Distributed Systems and Networks, 2002.
12. S. E. Czerwinski, B. Y. Zhao et al. An Architecture for a Secure Service Discovery Service. 5<sup>th</sup> Annual Int'I Conference on Mobile Computing and Networks(Mobicom'99).
13. S. Marsh. Formalizing Trust as a Computational Concept. Ph.D. Thesis, University of Stirling, 1994.

# An Intrusion-Resilient Authorization and Authentication Framework for Grid Computing Infrastructure

Yuanbo Guo<sup>1,2</sup>, Jianfeng Ma<sup>2</sup>, and Yadi Wang<sup>1</sup>

<sup>1</sup> School of Electronic Technology, Information Engineering,  
University, Zhengzhou, Henan 450004, China  
yuanbo\_g@hotmail.com

<sup>2</sup> The Ministry of Education Key Laboratory of Computer Networks and  
Information Security, Xidian University, Xi'an, 710071, China

**Abstract.** A correctly and continually working authorization and authentication service is essential for the grid computing system, so it is very necessary to maintain efficient this service with high availability and integrity in the face of a variety of attacks. An intrusion-resilient framework of authorization and authentication service for grid computing system is presented in this paper. This service is able to provide fault tolerance and security even in the presence of a fraction of corrupted authorization and authentication servers, avoiding any single point of failure. We use a cryptographic  $(f, n)$  secret sharing scheme to distribute parts of the clients' proxy certificates and use a secure multi-party computation scheme to perform the signatures such that the proxy certificate can be issued in a distributed fashion without reassembly when a legal client registrant at the Globus host. By using Non-Malleable Proof, the "man-in-the-middle attack" can be prevented; by distributing the secret data across several authorization and authentication servers, the compromise of a few servers will not compromise the availability of data. And, under the assumption of a Diffie-Hellman decisional problem, a passive adversary gets zero knowledge about the system's private key  $X$ , and so cannot to issue the certification for any client, neither to impersonate a legal authorization and authentication server.

## 1 Introduction

At the base of any grid environment, there must be mechanisms to provide security, including authentication, authorization, data encryption, and so on. The Grid Security Infrastructure (GSI) component of the Globus Toolkit provides robust security mechanisms. Especially, it provides a single sign-on mechanism, so that once a client is authenticated, the certificate authority in the GSI will generate a proxy certificate and send it to the client, then the client can use the proxy certificate to perform actions within the grid computing system. But this mechanism has its own drawback. For example, since all clients' certificates are maintained by the certificate authority, it requires the certificate authority to be trusted and so introduces dependence upon the certificate authority and thus creates a single point of failure, and, if successfully compromised, would immediately lead to the exposure of all clients' confidentiality of certificates, interruption communication, or other forms of denial of service.

To address this issue, in this paper we present an intrusion-resilient authorization and authentication framework for grid computing infrastructure, that removes this single point of failure by distributing the authorization and authentication service among  $n$  authorization and authentication servers (which will be denoted as *AASs* briefly in the remaining of the paper). The framework uses a verifiable secret sharing scheme to distribute shares of the system's secret to *AASs* and use a secure multi-party computation scheme to perform the signatures such that the proxy certificate can be signed in a distributed fashion without reassembly. When a legal client want to sign-on the grid computing system, he/she sends a sign-on request to the Globus host firstly, the Globus host will forward this request to a his-own-choosing subset of the  $n$  *AASs*, and the contacted *AASs* answer with some information enabling the client to compute his own proxy certificate and verify its correctness.

Our framework is intended to tolerate the compromise of up to  $f$  *AASs*, where  $3f + 1 \leq n$ . Compromised *AASs* are assumed to be under the full control of an attacker and to have Byzantine behavior<sup>1</sup>, but it is also assumed that the attacker cannot break the cryptographic algorithms used. Under these assumptions, our service ensures the confidentiality, integrity and availability of authorization and authentication service for grid computing infrastructure. Also, our system is designed to be easy to embed into existing grid computing environment. For example, the *AASs* are built with commodity PCs, an administrator can just swap a failed host out with another.

## 2 System Architecture

Let  $Client = \{C_1, \dots, C_m\}$  be a set of  $m$  clients and let  $AAS = \{AAS_1, \dots, AAS_n\}$  be a set of  $n$  *AASs*(authorization and authentication servers for grid computing infrastructure). All of them share a global clock (i.e., the system is synchronous). Each client connects himself or herself with  $2f + 1$  *AASs* by point-to-point encrypted and authenticated channels, where  $f$  is the threshold of secret sharing scheme we used. The member in the *AASs* can be good (i.e., it honestly executes the protocol) or bad (i.e., it is controlled by an adversary and can deviate from the protocol in arbitrary ways), but a majority of good *AASs* are always present across the system.

The service works as follows. A **dealer**, which is needed only in the system initialization phase, distributes system's private key  $X$  among all  $n$  *AASs* by using Feldman's  $(f+1, n)$  VSS scheme [3] straight forward. So along with the secret shares, he also generates a verification share to go along with each key share, and broadcast the verification shares to all clients.

Each secret share is then distributed secretly to a different *AAS*, and all corresponding verification shares are broadcast to all of the clients. No *AAS* knows the whole  $X$ , but only knows his own assigned share.

The architecture of our intrusion-resilient authorization and authentication service can be illustrated as Figure 1.

---

<sup>1</sup> A compromised host deviates arbitrarily from its specified protocols. It is also called arbitrary behavior or malicious behavior.

Each AAS maintains a configuration file which specifies what types of resource are allowed to be access by which client. When a client wants to apply for some services or execute a task on the grid computing system, he/she registers himself/herself at the Globus hosts firstly, with the submission of his/her password or some others type of credential and the requested services or tasks. Then, Globus host will performs the initial validation; if success, it sends an authentication and authorization request to the AASs on behalf of the client. Based on the identification of the client, each AAS consults its configuration files to determine what resources in the grid environment are authorized to the client, and then uses its share of the system's private key to compute and send a share of proxy certificate to the client, which we called sub-certificate in the remaining paper. It also uses its verification share to compute a zero-knowledge proof which will prove the correctness of its sub-certificate.

These sub-certificate and zero-knowledge proofs are then collected by the Globus host. Then, the host chooses  $f$  of them. After verifying the correctness of all of the proofs of these sub-certificates, it can combine them to form the actual proxy certificate and send it to the client. Afterwards, the client can request the needed resources to the grid computing system by using this proxy certificate.

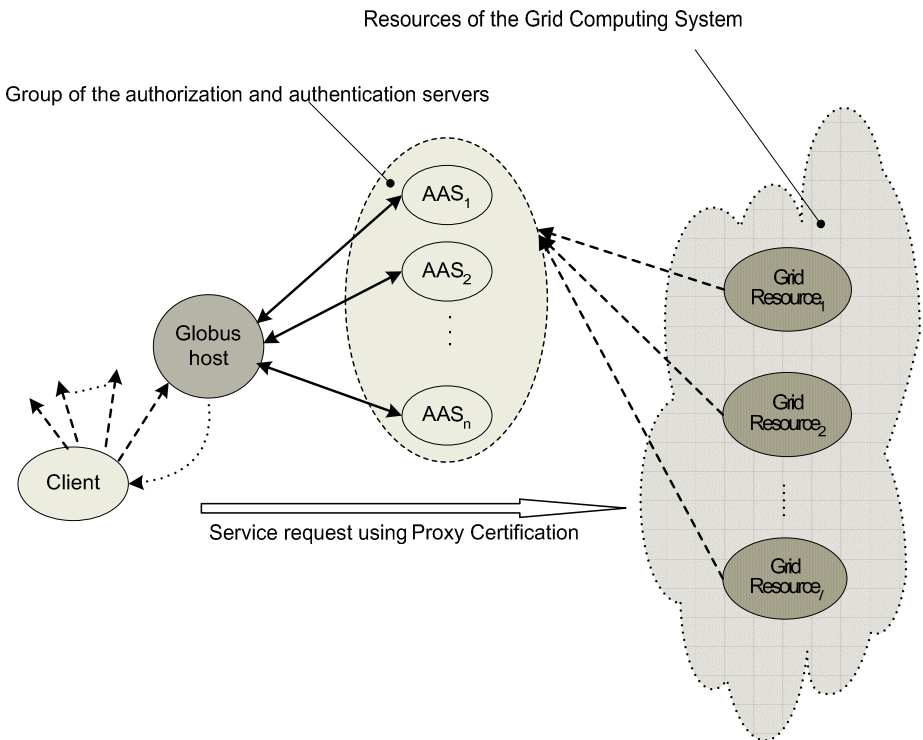


**Fig. 1.** Architecture of intrusion-resilient authorization and authentication service for grid computing environment

### 3 The Details of the Framework

Denote the system’s private key as  $X_{AAS}$  and the corresponding public key  $Y_{AAS}$ . Denote a client  $C$ ’s  $X_C$  and  $Y_C$ . Our scheme starts with a large prime  $p = 2q+1$ , where  $q$  is also a large prime, and a generator  $g$  for the subgroup  $G_q = \{i^2 \mid i \in \mathbb{Z}_p^*\}$  of quadratic residues of  $\mathbb{Z}_p^*$ . A collision-free one-way hash function  $H(x)$  is also needs to be made public. Then, our framework can be divided into 3 phase:

**Initialization phase:** The dealer distribute the system’s private key  $X_{AAS} \in \mathbb{Z}_q^*$  among all AAS by using Feldman’s  $(f+1, n)$  VSS scheme [3] straight forward.

- 1) Select randomly  $f$  elements  $a_1, \dots, a_f$  of  $\mathbb{Z}_q^*$ . These coefficients define a polynomial of degree  $t$  in  $\mathbb{Z}_q^*[X]$ :

$$F(X) = X_{AAS} + a_1X + a_2X^2 + \dots + a_fX^f$$

- 2) Compute  $X_1, \dots, X_n$  of  $\mathbb{Z}_q$  and  $g_1, \dots, g_n$  of  $\mathbb{Z}_p$  as follows:

$$X_i = F(i) \bmod q \text{ and } g_i = g^{X_i} \bmod p$$

The shares  $X_1, \dots, X_n$  must then be distributed secretly to the  $n$  authorization and authentication servers  $AAS_1, \dots, AAS_n$ , respectively. The generator  $g$  and the elements  $g_1, \dots, g_n$  are made public. They must be known by all clients and all AASs. Each  $AAS_i$  can verifies the share  $X_i$  he or she received by using  $g$  and  $g_i$ .

As in Shamir’s secret sharing scheme<sup>[4]</sup>, any subset of  $f+1$  values among  $X_1, \dots, X_n$  allows one to reconstruct  $F$  by interpolation, and then to compute the value  $X_{AAS} =$

$F(0)$ . For example, given  $X_{i_1}, \dots, X_{i_{f+1}}$ , one has  $X_{AAS} = \sum_{s=1}^{f+1} b_{i_s} X_{i_s} \bmod q$ , where

$$b_{i_s} = \prod_{j=1, j \neq s}^{f+1} \frac{i_j}{i_s - i_j} \bmod q.$$

**Authorization Phase:** The grid computing system authorizes AASs to authenticate the clients and issue the corresponding proxy certificates. Each grid resources  $GR_i$ , where  $i = 1, 2, \dots, l$ , is associated with an access control table  $CL_{i_s}$ , which is used to specifying what types of access to this resources of which client are allowed. After authorization, all  $GR_i$ ’s access control tables are maintained by each AAS.

**Registration and Proxy Certificate Generation Phase:** When a client  $C$ , whose ID is  $ID_C$ , wants to apply for some services or execute some tasks, he/she registers at the Globus host firstly. The client should submit to Globus host his/her password or other credential and the requested services or tasks. On receiving these information, the Globus host will then performs the initial validation of the client; if successes, it sends an authentication and authorization request to a robust subset of AASs (in our case, the servers of size at least  $2f+1$ , where  $f$  is the threshold of the secure secret sharing scheme we used) on behalf of the client. Each AAS does the following:

- 1) Compute sub-signature of client  $C$ 's private key  $SC_i = X_C^{X_i} \bmod p$ ;
- 2) Randomly select  $r \in \mathbb{Z}_q^*$  and compute
 
$$u = g^r \bmod p \text{ and } v = X_C^r \bmod p$$
- 3) Compute  $s_i = H(g, g_b, ID_C, SC_i, u, v)$  and  $t_i = r + s_i \cdot X_i \bmod q$ .
- 4) Based on the identification of the client, each AAS consults its configuration files to determine what resources in the grid environment are authorized to the client, and then generate a sub-certificate  $(SC_i, s_i, t_i, C)$  for client  $C$  (denoted as  $Cert_C^i$ ), and then send it to the Globus host.

In step 3) and 4), both  $s_i$  and  $t_i$  are used here to prove the validity of  $SC_i$  without revealing  $X_i$ . This uses a technique of non-malleable proof proposed by [5].

After receiving  $Cert_C^i$  send by  $S_i$ , the Globus host does following:

- 1) Compute  $u' = g^{t_i} / g_i^{S_i} \bmod p$  and  $v' = X_C^{t_i} / SC_i^{S_i} \bmod p$
- 2) compute  $s_i' = H(g, g_b, ID_C, SC_i, u', v')$

If  $s_i' = s_i$ , then the client accept the proof and get the sub-certificate  $Cert_C^i$ ; else, Globus host can raise an alarm to the administrator of system.

After receiving and checking  $f+1$  sub-certificates  $Cert_C^1, \dots, Cert_C^{i+f+1}$  from different  $f+1$  AASs, the Globus host compute  $SC = \prod_{s=1}^{f+1} SC_{i_s}^{b_{i_s}} \bmod p$ , where  $b_{i_s}$  is obtained from  $S_{i_1}, \dots, S_{i_{f+1}}$  and  $b_{i_s} = \prod_{j=1, j \neq s}^{f+1} \frac{i_j}{i_s - i_j} \bmod q$ . By this interpolation method, Globus host can obtain  $SC = X_C^X \bmod p$ .

Then, a proxy certificate containing the signature  $SC$  for client  $C$  can be generated and send to client  $C$  by Globus host.

Afterwards, the proxy certificate can be used by the client to access the grid resources he/she needs.

## 4 Security Analysis

### 4.1 Correctness and Robustness

By correctness and robustness, we mean that all legal clients can get a correct proxy certificate if there are no more than  $f$  dishonest AASs.

**Theorem 1:** If there are no more than  $f$  dishonest AASs, then all legal clients can get a correct proxy certificate.

**Proof:** In our case, we only need to show that Globus host will compute a correct  $SC = X_C^X$  for legal client  $C$ .

From the details of the framework we know that, before Globus host compute and recover  $SC$ , it has received and verified  $f+1$  sub-certificates  $Cert_C^1, \dots, Cert_C^{i+f+1}$



from different  $f+1$  AASs. Then by using interpolation method, Globus host can compute

$$SC = \prod_{s=1}^{f+1} SC_{i_s}^{b_{i_s}} = \prod_{s=1}^{f+1} (X_C^{X_{i_s}})^{b_{i_s}} = (X_C^{X_i})^{\sum_{s=1}^{f+1} b_{i_s} X_{i_s}} = X_C^X.$$

## 4.2 Security Against Impersonators Attack

Impersonations means that server AAS<sub>j</sub> impersonate server AAS<sub>i</sub> to send message  $(SC_i, s_i, t_i, C)$  to the Globus host.

**Theorem 2:** In the random oracle model, a dishonest AAS cannot forge, with a non negligible probability, a valid proof for a valid sub-certificate.

**Proof:** From the above scheme we know that  $SC_i, s_i, t_i$  satisfy the following equations:

$$g^{t_i} = g^{r+s_i \cdot X_i} = g^r \cdot (g^{X_i})^{s_i} = u \cdot g_i^{s_i} \quad (4.1)$$

$$X_C^{t_i} = X_C^{r+s_i \cdot X_i} = X_C^r \cdot (X_C^{X_i})^{s_i} = v \cdot SC_i^{s_i} \quad (4.2)$$

Since  $g^{t_i}$  and  $g_i^{s_i}$  are both in  $G$ , by the closure of  $G$  under multiplication we know that Equation (4.1) yields  $u \in G$ . This means that it exists  $\lambda$  such that  $u = g^\lambda$ . So we have  $g^{t_i} = g^\lambda \cdot g_i^{s_i} = g^\lambda \cdot g^{X_i s_i}$ , which implies:  $t_i = \lambda + s_i \cdot X_i$ . Now Equation (4.2) becomes:

$$X_C^{t_i} = v SC_i^{s_i} \Leftrightarrow X_C^{\lambda+s_i \cdot X_i} = v SC_i^{s_i} \Leftrightarrow X_C^\lambda v^{-1} = (X_C^{-X_i} \cdot SC_i)^{s_i}$$

This yields two possible cases:

- (1)  $SC_i = X_C^{X_i}$ . In this case, the sub-certificate is correct.  $v = X_C^\lambda$  and for all  $s_i \in Z_q$ , the verifier equations trivially hold.
- (2)  $SC_i \neq X_C^{X_i}$ . In this case, we must have

$$s_i = \log_{X_C^{-X_i} \cdot SC_i} X_C^\lambda v^{-1} \quad (4.3)$$

From equation (4.3), one can see that, if  $SC_i$  is not a valid sub-certificate, once the triplet  $(SC_i, u, v)$  is chosen, then there exists a unique  $s_i \in Z_q$  that satisfies the verifier equations. In the random oracle model, the hash function  $H$  is assumed to be perfectly random. Therefore, the probability that  $H(g, g_i, ID_C, SC_i, u, v)$  equals  $s_i$  is  $\frac{1}{q}$ , once  $(SC_i, u, v)$  fixed.

On the other hand, if the attacker perform an adaptively chosen message attack by querying an oracle  $N$  times, the probability for the attacker to find a triplet  $(SC_i, u, v)$ , such that  $H(g, g_i, ID_C, SC_i, u, v)$  is  $P_{success} = 1 - (1 - \frac{1}{q})^N \approx \frac{N}{q}$ , for large  $q$  and  $N$ . Now if  $k$  is the number of bits in the binary representation of  $q$ , then  $P_{success} \leq \frac{N}{2^k}$ . Since a computationally bounded server can only try a polynomial number of triplets, then when  $k$  is large, the probability of success, which is  $P_{success} \leq \frac{N}{2^k} \ll 1$ , is negligible.

### 4.3 Security Against Secret Compromise

The most serious attack is for an attacker to compromise  $f$  AASs and reconstruct the system's private key  $X$ , and then to issue the certification for any client, whether legal or illegal. To combat this,  $f$  should be chosen to be sufficiently large to make compromising  $f$  machines exceedingly difficult.

Arbitrarily setting  $f$  to be very large, however, has reliability concerns. In the extreme case, if  $f = n$ , then the system has  $n$  points of failure—where a proxy certificate cannot be issued.  $f$  must be chosen so that  $n - f - 1$  is sufficiently large to handle node failures.

Secondly, each machine will, ideally, be running a different operating system with different versions of software to make compromising a machine more difficult.

### 4.4 Security Against Denial of Service

Since  $f$  machines are necessary to successfully compute a correct proxy certificate for the legal client and there are  $n$  machines in total, if  $n - f - 1$  of them crashes or fails, the key will not be able to be computed. To prevent attackers from compromising or flooding  $n - f - 1$  machines,  $n$  and  $f$  will need to be appropriately chosen to make this probabilistically low. In the case where machines crash because they are faulty, we can bound the probability of failure.

### 4.5 Failure Handling

Consider that each AAS fails—crashes or does not respond—with probability  $r$ . We assume  $r$  is independent. The probability that a key cannot be computed is:

$$p_f = r^f$$

That is,  $p_f$  is the probability that the system is unable to perform useful work; a state of failure.

Solving for  $r$ , we find:  $r = p_f^{1/f}$

Obviously, any system will need to set  $n$  and  $f$  such to maximize  $r$ .

## 5 Discussions and Conclusion

A combination of fairly standard secure multi-party computation algorithm, secret sharing scheme, zero knowledge proof and traditional authorization protocols was used to develop an intrusion-resilient framework of authorization and authentication for grid computing environment, which can provide correct services even in the presence of faulty insiders of AASs. Its security requirements can be shown to theoretically hold if no more than  $f$  AASs are compromised, the attacker does not break the cryptographic algorithms, and the network assumptions are satisfied. But it is obviously that the claim of no more than  $f$  AASs are compromised relies on the assumption that it is substantially harder for an attacker to penetrate several AASs than a single one. In fact, with enough time and resources, a determined attacker can compromise a sufficient number of AASs to break the system. To justify this assumption we rely on

two complementary approaches: diversity and proactive updates. With diversity, an attacker has to devise different penetration mechanisms for each server, so that it is impossible for him/her to work to kill other AASs at once when he/she kills one. Diversity can be achieved by running a different version of our software on each of the AASs, running on different hardware and operating systems, and putting the different AASs under the responsibility of different administrator.

Proactive security is the ability to gracefully recover from compromises in such a way that any past compromises don't assist a current attacker. Proactive update implies that once every time period (say once an hour) the AASs compute a new sharing of the same system's privacy key. Consequently, not only does the attacker have to penetrate multiple AASs, he/she has to do so within a single time period. Proactive update is normally implemented by re-sharing the private key in such a way that the new shares have no relationship to the old shares, and therefore if an attacker compromises some AASs, these AASs are recovered, and then he/she compromises more AASs, the information he gains isn't enough to compute the key.

However, due to the organization's budget and security constraints, the parameters of the system's diversity and proactive should be set accordingly.

Finally, it should be noted that, even with above measures, resilience is not absolute in the real world. Our scheme can also be vulnerable to network-based denial-of-service attack based on flooding, though this attack is not specific to our system, as current TCP/IP protocols make it difficult to defend against such attacks in any system. Intrusion resilient can be effective only if combined with traditional measures to avoid and remove vulnerabilities in system components, and with intrusion detection mechanisms to help respond to attacks before it is too late.

## References

1. Hung-Yu Chien, New approach to authorization and authentication in distributed environments, Communications of the CCISA, vol.9 no.3, pp.63-69, Jun. 2003
2. Mambo, M., Usuda, K., and Okamoto, E., Proxy signatures for delegating signing operation, Proc. 3rd ACM conf. on Computer and Communications Security, 1996.
3. P. Feldman, A Practical Scheme for Non-interactive Verifiable Secret Sharing, Proc. 28th IEEE Annual Symposium on Foundations of Computer Science, pp. 427-437, Oct. 1987
4. A. Shamir. How to Share a Secret. Communications of the ACM, vol. 22, no. 11, pp. 612-613, Nov. 1979.
5. Chaum D. and Pedersen. T. Wallet Databases with Observers. In *Crypto'92*, number 740 in Lecture Notes in Computer Science, Santa Barbara, CA, Springer-Verlag, 1992, pp. 89-105
6. Yair Frankel, Peter Gemmell, Philip D. MacKenzie, and Moti Yung. Optimal resilience proactive publickey cryptosystems. In *IEEE Symposium on Foundations of Computer Science*, pp 384-393, 1997.
7. Yair Frankel, Peter Gemmell, Phillip D MacKenzie, and Moti Yung. Proactive RSA. In *Advanced In Cryptology - Crypto 97*, volume 1294 of Lecture Notes in Computer Science, pp 440-454 Springer-Verlag, 1997.
8. Globus OGSA Home Page. <http://www.globus.org/ogsa/>
9. Foster I, Kesselman C. *The Grid: Blueprint for a new computing infrastructure*. San Francisco: Morgan Kaufmann Publisher, 1999.

# An Active Platform as Middleware for Services and Communities Discovery

Sylvain Martin\* and Guy Leduc

Research Unit in Networking, Université de Liège,  
Institut Montefiore B28, 4000 Liège 1, Belgium  
{martin, leduc}@run.montefiore.ulg.ac.be  
<http://www.run.montefiore.ulg.ac.be/>

**Abstract.** In an increasing number of cases, network hosts need to locate a machine based on its *role* in a service or community rather than based on a well-known address. We propose and evaluate WASP, a lightweight active platform where ephemeral state left in the network can help locate service providers such as request dispatchers or computation aggregators. In an active grid architecture, WASP can also help locate participants, build and manage overlays.

## 1 Introduction

In peer-to-peer systems in general and grid computing as a specific case, we are facing the problem of communities of machines that need to cooperate together without having any *a priori* knowledge of their respective existence. Existing schemes often rely on the existence of some centralizing machine that swaps peers addresses. With the increase of service popularity and the decrease of average connection time, keeping these so-called *pong servers* scalable is a real challenge.

In this paper, we study a solution based on active networks that will help network operators and peer-to-peer application designers to introduce aggregators and caches of *pong servers* transparently in the network. Our active platform also allows discovery of more generic services and could be used to locate computation dispatchers and aggregators as well.

### 1.1 Why Yet Another Active Platform?

Despite an important amount of active network platforms has been proposed and studied, none has really successfully reached the real-world deployment level. In response to this reality, WASP (*Weightless Active packets for ephemeral State Processing*) is made lightweight enough and resource-friendly so that its presence in the network does not become a nuisance for network managers. WASP is not built from scratch: it is an effort to merge the advantage of two recently proposed platforms ESP (*Ephemeral State Processing*) and SNAP (*Safe and Nimble Active Packets*) [5]) that also focus on

---

\* Sylvain Martin is a Research Fellow of the Belgian National Fund for Scientific Research (FNRS).

safe, flexible and efficient – in a word, *practical* (cf Moore et al. [2]) – active networks. Section 2 shows how both computation time, storage and network bandwidth are kept under low and predictable limits for WASP packets.

Unlike fully-featured active platforms, WASP alone is not able to offer complex services such as flow transcoding or realtime auction though it can help *advertise* and *locate* such services, helping machines that offer such services (hereafter called *service providers*) and machines that use such services (hereafter called *end-systems*) to build and manage adequate *tunnels* and *overlays* in an automated way, thus providing an effective support for active grid architectures. We will show in Sect. 3 how WASP can be used to build such solutions.

The design of our proposed platform is detailed in Sect. 4. In order to evaluate its performance, we translated ESP instructions into WASP code and compared execution timings. The results of this evaluation are presented in Sect. 5

## 1.2 What Slows Down Active Packets

The speed at which our active platform will be able to process active packets will define the network locations where it can actually be deployed. Our goal is to offer a solution that can be running even on a border router in a transit domain, taking advantage of *network processor* technologies to achieve high throughput. A simple *active packet* crossing an active node will incur different types of time-consuming operations:

**Classification.** Filters should be applied so that the active packet is recognized as such.

Depending on the architecture, this filtering may be based on a dedicated *transport protocol type*, the presence of an *IP header option*, etc.

**Delivery.** After classification, we still have to make the packet available to the component that will process it. In the worst case, the whole packet should be copied into user-space before applicative decoding could be applied. Most performance-targeted platforms ([3, 4]) thus decode and process packets at kernel level.

**Decoding.** Some platforms like ESP [4] and SNAP [5] are able to process the operations for the packet as soon as it is delivered, but in most of the other frameworks, a data decoding phase is needed to deserialize objects, strings, lists, etc.

**Processing.** By interpretation or execution of compiled code from a cache. We chose interpretation since it better fits inherent characteristics of network processors [9].

## 2 Resource Aware System

### 2.1 Execution Time

Even if untrusted code cannot perform harmful operations thanks to sandboxing, it is impractical to detect malicious code that will run silly loop, consuming available CPU time on routers without performing any ‘useful’ job.

Like in SNAP[5], WASP avoids this by prohibiting *backward jumps* and providing only instructions with predictable execution time. Together with in-place processing of packets at kernel level, this allows our lightweight control tasks to be performed at the lowest cost for the router.

## 2.2 Memory and Storage

Most active protocols will need information to be stored temporarily on intermediate nodes, so that it can be later retrieved by other active packets. It is important for network availability and performance that this local storage remains easy to manage and can automatically discard information that is no longer pertinent.

ANTS [1] and many other platforms use *soft-state* based memory management to release memory that has not been used by packets for a given amount of time. Unfortunately, soft-state based managers make it hard for the access control to define if there will be sufficient memory to accept the flow.

Alternatively, ESP [4] proposes the *ephemeral state* approach, where data are kept for a constant period, *regardless of how frequent the data is referenced during that period*. If, in addition, all the data slots in the store have the same size, collecting free-for-reuse slots becomes simple enough to execute without disturbing packet forwarding tasks on the router, and flow access checking simply requires that the router checks how many different slots are used by the flow. We will call *tags* these fixed-size data that the node associates with a key for a fixed amount of time, like in the ESP terminology.

## 2.3 Network Bandwidth

Taking care of local resources is required to achieve platform *safety* but not sufficient. If no restriction is enforced, an ill-intentioned active packet could easily create clones of itself will all the allowed execution times, and clones of the clones at the next router so that a single emitted packet will overload the destination (in addition of network links close to that destination). In the case of the WASP platform, packets do not have the ability to create child packets unless they are targetted at a multicast address on a multicast router. All it can do is block the packet or send it back to its source.

## 3 Service Discovery with WASP

Literature has presented a number of active network-based solutions to various problems such as real-time auction, hierarchical web caches, video stream filters, reliable multicast and many more. All these applications can be viewed as applying a custom *service* (filtering, merging, splitting of packets) at some strategic points in the network. It is somehow expected that, sooner or later, network operators will integrate such services in their network as their presence could help reduce the required bandwidth. The behaviour of an active service can thus be seen as follows:

1. identify anchor points in the network (*i.e.* machines able to host the service),
2. detect at which anchor point(s) service deployment is strategically most useful,
3. route packets requiring the service towards deployed *service provider(s)*<sup>1</sup>,
4. apply merge/split/filter service on packets received by the service provider(s).

In a grid computing environment, those services could for instance consist of collecting available computations sites, routing computations requests towards the closest

---

<sup>1</sup> *i.e.* “nodes offering the packet filter/split/merge service”, not Internet Service Providers.

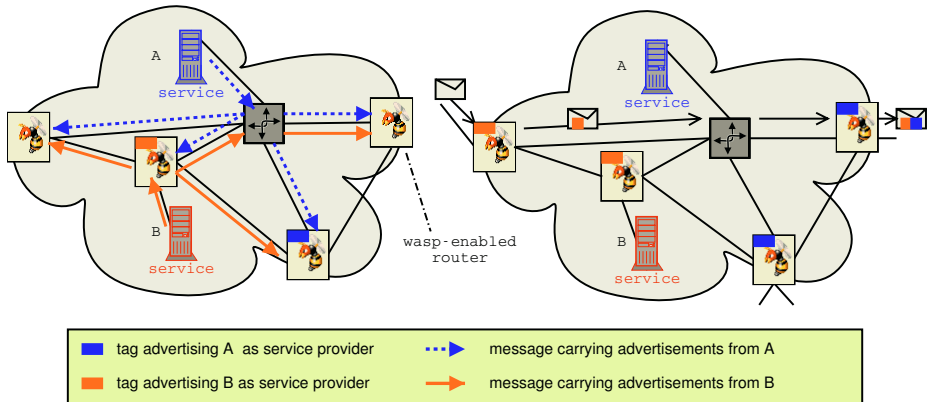


Fig. 1. Advertising (left-side) and looking for (right-side) service

(or less loaded) point of presence or even perform distribution/aggregation of computation requests hierarchically.

### 3.1 The Managed Dynamic Overlay Alternative

Most existing solutions for such problems, like OPUS [7] or the X-Bone [8], set up an infrastructure that dynamically creates *overlay networks* interconnecting end-systems and intermediate service providers with *tunnels* in order to obtain the desired logical topology. Unfortunately, none of these works have suggested a truly scalable and completely decentralised method for identifying available anchor points in a very large-scale network. Moreover, maintaining the infrastructure, monitoring the available resources and expressing applications' needs in a generic fashion remains a resource-intensive activity even when hierarchically divided such as in OPUS.

In the following, we will show how, with sensibly less support from all sides, WASP manages to offer enough information to *end-systems* and *service providers* so that they can take strategic decisions themselves.

### 3.2 Basis of Service Discovery with WASP

The idea behind the WASP platform is to provide a lightweight environment that can be used for locating the most interesting service provider(s) independently of what the service will actually do. Once service-providing node(s) have been located, the end-system can adjust application behaviour so that the applicative flow go through the discovered provider(s).

When a new applicative flow is initiated, small active packets are used to probe the network on the route to be taken. Each time such probe crosses a WASP node, it will lookup the node store to see if it can find *advertisements* of the expected service, consisting of the provider address and cost for reaching that provider from the local node. Depending on the application needs, probes will perform some pre-filtering of the collected advertisements or simply store them all. Based on this collected knowledge of

the network, the end-system can evaluate the different options and enforce the one that will result in the best utility.

The same kind of active packets can also be used by the service providers to install advertisements in routers of the local domain. Again, the programmability of the advertisement packets allows expression of simple policies such as only keeping the advertisement(s) of the (k) nearest service provider(s) in a router, and report other service providers to the advertiser.

Figure 1 illustrates that two-phase process: servers  $A$  and  $B$  first flood the domain with WASP packets advertising their presence, avoiding to re-install a tag in a router that already contains a better tag (e.g. advertising a closer or less loaded service provider). A source  $S$  can then use another WASP packet to record those tags as a list of provider  $P$  and branchpoint  $X$  information:  $(P_{addr}, X_{addr}, cost(S, X), cost(X, P))$ . Note that by simply changing the program in service advertisement and lookup packets, we are able to select the service provider that is closest to the source or to the destination, or to keep only the provider that will lead to smallest path deviation in each domain and leave final selection to the end systems.

### 3.3 Flooding Locally

In order to advertise the service, providers have to locate WASP routers in the local domain and send them WASP packets that will install advertisement tags. We benefit here from the fact that WASP processing is *optional* so no overlay of WASP-enabled routers need to be pre-established. In our previous work [6], we show how knowing the routing table of the local domain suffices to discover all the active routers of that domain.

A particularity of *ephemeral* storage is that the advertising tag will be deleted after a fixed period  $\tau$ , regardless of any refresh we could try to perform. Therefore, there may be a small delay between the moment where a WASP router decides to remove an advertisement tag and the moment where an advertisement refresh comes. Even if the server manages to learn precisely the tag's lifetime  $\tau$  it cannot completely avoid the risk that client packets may not see any advertisement. If this risk cannot be afforded, it is still possible for a service to use two separate keys  $k_1$  and  $k_2$  that will be refreshed with a period  $\tau + \epsilon$  but such as advertisements of  $k_1$  and  $k_2$  are separated by a delay of e.g.  $\tau/2$ . A client that doesn't find the "primary tag" (referenced by  $k_1$ ) can then check the "backup tag" (referenced by  $k_2$ ) to see whether the service is really missing.

## 4 The WASP Platform

As we previously said, WASP is derived from ESP router[4]. An ESP node consists of *Ephemeral State Stores* (ESS) containing *tags* that packets access based on 64 bit *keys*. Each packet requests the execution of one of the pre-defined operations on certain tags. Despite operations can be modified a bit (e.g. changing threshold values, selecting operators, etc), they remain thightly bound to multicast-related applications. It is also a bit disappointing to see that as soon as one wishes to implement more complex feature such as *reliable* flows merging, other very-specific operations need to be added.



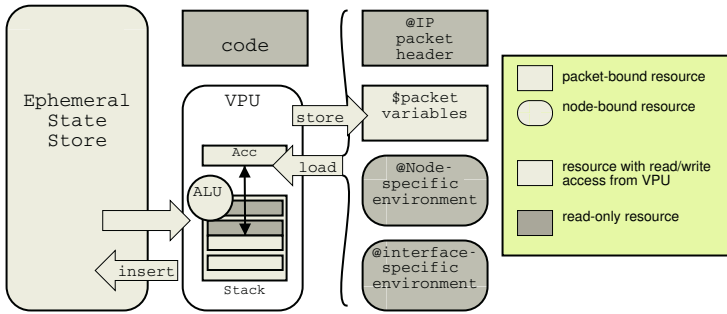


**Fig. 2.** WASP Execution Environment

The WASP platform thus keeps the overall design of ESP but replaces pre-defined operations by a *virtual processor* interpreting a bytecode language inspired by SNAP [5]. Another couple of extensions have been brought to ESP in order to allow more efficient solutions to services and communities discovery and flow management tasks in general, like the "return" behaviour and protected tags, explained later.

### 4.1 WASP Packets

WASP uses the *active packets* paradigm: each packet contains its own code and the data on which it can operate. WASP code and data can be stored in the payload of an IP packet or it can be piggybacked on another packet as an IP header extension. The packet's code consists of up to 256 *microbytes* for a WASP *Virtual Processing Unit* that will eventually lead to a packet control instruction telling whether the packet should continue towards its destination, return to its source or be dropped. The data part of the WASP packet is available as a 128 byte of RAM to the VPU during packet interpretation. Other parts of the packet (code, IP header, payload) are not alterable by the WASP code and only the IP header is readable. Figure 2 shows how node and packet storage areas are viewed by WASP code.

### 4.2 The WASP Node

A WASP node has several *Ephemeral State Stores* that associate 64 bit keys with small, fixed-size data into *tags*. Each ESS is bound to a *Virtual Processing Unit* that processes the WASP packets on a given *location* like e.g. "incoming on eth0". The VPU state is reset everytime a new packet is processed, which means that all the communications and exchanges between packets will occur *in the ESS* associated with the VPU.

Each VPU on the node exports a few information for WASP packets, like its IP address, netmask, the local node time, etc. Outgoing VPU will also export interface-related information like queue length and number of packets sent. These environment variables appear as a bank of read-only memory for the WASP VPU and allow the WASP programmer to design various monitoring or self-adapting services.

**Table 1.** Relative timings for ESP operations processing in CPU cycles, sorted by ESS accesses

operation	ESS	WASP, nocache	WASP, cached	WASP, MAPPING	native ESP
forward	0	129	123	-	-
compare	2	549	543	-	316
count	2	721	592	586	349
collect	4	1245	958	842	633
rchild	6	2058	1845	1509	775
rcollect	8	2980	2394	2020	1091

### 4.3 Super Packets and Protected Tags

In existing applications using ESP router, there's no need for access control to tags. It is simply assumed that the each source picks up a random 64 bit word and uses it as a key. Chances that two sources randomly pick the same (publicly available) tag and send packets over routes that cross the same router (otherwise no collision occurs) are virtually nul. When using WASP to advertise services, however, participants are required to use a *well-known* tag value that both service advertiser and service user will put in WASP packets. Unfortunately, we cannot safely use public well-known tags as an attacker could hijack the traffic of a given operator to its own network by advertising his machine as a proxy on the operator's network.

To solve such problems, WASP introduces *protected tags* that can only be modified by *super packets*. The node tells whether a tag is protected or not by checking its key against a specific pattern, and will allow writes to such tags only to packets that are marked 'trusted' in their WASP header. All a network manager will have to do in this case is (1) filter out WASP super packets at ingress nodes from the outside and (2) use super packets to advertise services within his own network.

## 5 Performance Evaluation

These tests are based on the linux module version of ESP software, running on a 1GHz Pentium 3 machine with default compilation options. Timings were measured using the internal *time stamp counter* of the processor, averaging on 1000 tests to avoid any unwanted side effects of caches, etc. The virtual node state is maintained such that the same (longest) code sequence is evaluated at each iteration. For each of the five ESP instructions on that distribution (*compare*, *count*, *collect*, *rchild* and *rcollect*), we wrote an equivalent WASP packet. Note that in order to achieve good performance, it is usually required to tune packet code so that the data organization better suits the instruction flow, as illustrated by Table 5.

One key feature for fast interpretation of WASP code will be how good the interpreter is at avoiding repetitive access to the ESS, and one way to achieve this is by *caching* intermediate results. Tests carried were in favour of very small caches (1 entry) since more complex policies tend to eat all the cache benefit in their initialization.

Alternatively, we can offer larger values for each key in the ESS. Instead of having a single 64-bit word, we now allow a whole memory bank of 32 bytes which can be *mapped* in the VPU's memory. In complex operations like *rcollect/rchild*, the state we

process is no longer atomic, but instead consists of tuples. While ESP then requires one key per field (and thus one ESS lookup at least per field), WASP allows a few fields to be grouped together as long as they fit one 32 byte bank.

Our tests with the Pentium-based implementation shows an improvement of 18% (two variables per bank) to 35% (four variables per bank) in the processing time as soon as several variables need to be updated, and we expect improvement to be even more important on saturated ESS storage (e.g. when collisions occur inside of the ESS hash table).

## 6 Conclusion and Future Work

We have presented a lightweight active platform that combines advantages of ESP's per-node storage and SNAP's safe and efficient language. Despite its use of a bytecode interpreter instead of native code, our work still shows execution performance of only 150% to 200% of corresponding native code and is much more generic than the existing ESP framework.

The proposed platform elegantly solves the problem of locating available third-party service providers. We also expect that it could also help peers of a community to find each other, even without the help of a "pong server" and we are investigating the possibility of having *private* tags that would be restricted to packets from the same 'protocol'.

## Acknowledgment

We would like to address special thanks to Jiangbo Li from Kenneth L. Calvert's team for having so kindly replied to all our questions related to ESP.

This work has been partially supported by the Belgian Science Policy in the framework of the IAP program (Motion PS/11 project) and by the E-Next European Network of Excellence.

## References

1. D. Wetherall, A. Whitaker: *ANTS - an Active Node Transfer System. version 2.0* <http://www.cs.washington.edu/research/networking/ants/>
2. J. Moore and S. Nettles: *Towards Practical Programmable Packets*, In Proc. of the 20th IEEE INFOCOM. Anchorage, Alaska, April 2001.
3. E. Nygren, S. Garland, and M. Kaashoek: *PAN: A High-Performance Active Network Node Supporting Multiple Mobile Code Systems*, In Proc. of IEEE OPENARCH, pp. 78-89, New York, March 1999.
4. K. Calvert, J. Griffioen and S. Wen: *Lightweight Network Support for Scalable End-to-End Services*, in Proc. of ACM SIGCOMM, pp. 265-278 Pittsburg, PA. August 2002.
5. Jonathan T. Moore: *Safe and Efficient Active Packets*, Technical Report MS-CIS-99-24, University of Pennsylvania, October 1999.
6. S. Martin and G. Leduc: *A Dynamic Neighbourhood Discovery Protocol for Active Overlay Networks*, in Proc. of IWAN, pp. 151-162, Kyoto, Japan, December 2003.

7. R. Braynard, D. Kostić et al. *Opus: an Overlay Peer Utility Service*, in Proc. of the 5th IEEE OPENARCH, pp 168-178, New York, June 2002.
8. J. Touch and S. Hotz, *Dynamic Internet Overlay Deployment and Management Using the X-Bone* in Proc. of ICNP 2000, Osaka Japan, pp. 59-68.
9. Intel Corporation *The IXP1200 Hardware Reference Manual*, August 2001.

# p2pCM: A Structured Peer-to-Peer Grid Component Model

Carles Pairot<sup>1</sup>, Pedro García<sup>1</sup>, Rubén Mondéjar, and Antonio F. Gómez Skarmeta<sup>2</sup>

<sup>1</sup> Department of Computer Science and Mathematics, Universitat Rovira i Virgili  
Avinguda dels Països Catalans 26, 43007 Tarragona, Spain  
{carles.pairot, pedro.garcia}@urv.net

<sup>2</sup> Department of Computer Engineering, Universidad de Murcia  
Apartado 4021, 30001 Murcia, Spain  
skarmeta@fcu.um.es

**Abstract.** In this paper we present p2pCM, a new distributed component-oriented model aimed to structured peer-to-peer grid environments. Our model offers innovative contributions like a lightweight distributed container model, an adaptive component activation mechanism, which takes into account network proximity, and a decentralized component location and deployment service. We believe that all of the features our component-oriented model provides can be very promising for the development of future wide-area distributed applications.

## 1 Introduction

Developers face an important problem when willing to build wide-area component-based distributed applications. Practically there are no frameworks oriented to such target market. In this paper we present **p2pCM**: a peer-to-peer component model for building distributed component-based applications on top of a **structured peer-to-peer grid**. Our model offers traditional and novel component services by means of an underlying object middleware (Dermi [3]). To the best of our knowledge, this is the first component model built on top of a structured P2P grid infrastructure.

The main contributions of this paper are the design of a new wide-area component model that runs on top of a structured P2P grid infrastructure; the utilization of a decentralized component location and deployment facility; and the implementation of a resilient and autonomous lightweight container model, which provides component's life cycle services, and many others. Component instantiation is of special interest because it takes into account network locality properties.

The rest of the paper is structured as follows, in Section 2 we give an overview of p2pCM's architecture and services, in Section 3 we analyze possible usage scenarios for our component model, and in Section 4 we explore related work. We conclude in Section 5 by providing an outline of future work.

## 2 p2pCM Architecture and Services

The decentralized component model we have designed (p2pCM) runs on top of a structured peer-to-peer grid. We have implemented the majority of traditional compo-

nent models services, and adapted them to the underlying topology. These include a **decentralized component location and deployment facility**, and a **decentralized lightweight container model**, which provides a component persistence and life cycle service, as well as an adaptive activation policy.

## 2.1 Decentralized Component Location and Deployment

All components must be previously registered into the system so as they can be used by any client. This *deployment* phase is found in all traditional component models, as well as in ours. In our model, we use a decentralized naming service which stores all component's metadata (read in *deployment* time), as well as the component's class files. This is done to allow dynamic component class loading in clients that do not have the necessary component classes. Our naming service benefits from the efficient overlay network routing properties thus hashing the component's identifier, and storing the values into the node whose key is closer to this hash. Fault tolerance is provided by the underlying Dermi [3] middleware in a transparent way to the developer.

## 2.2 Decentralized Container Model

In p2pCM we have tried to avoid heavy and monolithic containers used by traditional component models (e.g. J2EE or CORBA), and opted for designing a **decentralized lightweight container model**. In our case, all of the nodes that belong to the network are containers, and as such, they can house components. The idea is that any component can be run in any node (unless restricted by security constraints), because each node runs a lightweight container. Our containers are fault resilient and autonomous: components are replicated all along the network using the underlying Dermi [3] middleware. If a container fails, surely other containers housing those components will exist in the network. Now we are going to briefly describe the different services our decentralized container model offers to components.

### 2.2.1 Component Life Cycle Service

The container is responsible for activation and passivation of components. When creating a component's instance, the following may happen:

- *No other component instance is already active in the network.* In this case, the instance will be activated on our local container, and a local reference is returned so as we can interact with it.
- *Other component instances are already active in the network.* In such case, we will get a reference to the **closest instance** (basically, a Dermi *anycall* is done). However, if this closest instance informs us that it cannot accept more requests (it may be overwhelmed), a local copy is activated.

Component instances are passivated when they are not called during a certain amount of time in order to save resources on the node.

### 2.2.2 Component Persistence

Stateful components need to be ensured state persistence. p2pCM allows this by providing a persistence mechanism in order to take care of total passivation of component instances. If all component instances are passivated, their shared state is lost, and

this situation is not desired. The persistence strategy is chosen by the component itself by means of the *persistence* metadata tag in the deployment phase. Persistence itself is managed by the decentralized object replication mechanisms of Dermi.

### 2.2.3 Adaptive Component Activation

In wide-area environments, some component instances could become temporarily overwhelmed with requests of nearby clients. To avoid such problem, we use an **adaptive component activation** mechanism.

The idea is to know which immediate node is delivering most messages to the overwhelmed node (via the *getPreviousHopHandle()* method), and start an algorithm which keeps activating new component instances all along the overwhelming request path, until stress is relieved.

We are currently working in this adaptive activation scheme in order to fine tune several parameters, and as future work we will perform extensive simulations to validate our approach.

## 3 p2pCM Usage Scenario

One scenario where our model could be successfully applied would be in an application similar to a SETI@Home or United Devices Cancer Research Project model. Such applications normally require a central server which distributes computing units to home computers for analyzing. Our component model could be used to build an application which would efficiently be fault tolerant and resilient to high request peaks.

The idea would be that interested nodes would activate a *Processing* component on their local containers. This component could thus be receptive to a *DataFeed* component's calls. The *Processing* components would be aligned into a multicast group, so as the data feeder requested data unit analysis by *anycalling* or *multicalling* [3] to the *Processing* component group.

Once each *Processing* component finished its data unit analysis, instead of returning data back to the central *DataFeed* component (which would possibly create an important bottleneck there), it would pass data to another *Results* component by means of an event. This component would manage the results persistence by replicating itself and storing state information in the P2P grid infrastructure. Whenever the *DataFeed* component wished to obtain the results (cyclically every  $x$  hours), it would *anycall* to its closest *Result* component instance, which would provide it with the latest gathered results.

## 4 Related Work

In the Grid world there exist solutions like Fractal/ProActive [1], which is a hierarchical and dynamic component model. Nevertheless, its approach is different from p2pCM, in the sense that virtual node and virtual machine mapping is performed on the component's deployment descriptor, thus not allowing self adaptation to node failures.

P2PComp [2] is built on top of an unstructured P2P network, and it is mainly aimed to address the development needs for mobile P2P applications. It features a lightweight container model as well, and provides many services, including synchronous / asynchronous remote invocations, hot swapping, service fetching and ranking. All these services are basically oriented for highly mobile and dynamic applications.

## 5 Conclusions and Future Work

In this paper we have presented p2pCM, a decentralized component model built on top of a structured P2P Grid. Our approach manages to provide many interesting services to component developers. Our main contributions include a **decentralized component location and deployment facility**, and the adoption of a **decentralized lightweight and fault resilient container model**. We have shown as well, possible usage scenarios of our system. However, we still do not provide other services found in commercial component-oriented models, like security or transactions, which need to be further investigated.

A first prototype of p2pCM is available through <http://ants.etse.urv.es/p2pcm>. We believe that the features p2pCM offers can be very promising for the development of future wide-area distributed applications.

This work has been partially funded by the Spanish Ministry of Science and Technology through project TIC-2003-09288-C02-00.

## References

1. Baude, F., Caromel, D., and Morel, M., "From Distributed Objects to Hierarchical Grid Components", *Proc. DOA 2003*, LNCS, pp. 1226-1242, Nov. 2003.
2. Ferscha, A., Hechinger, M., et al, "A Light-Weight Component Model for Peer-to-Peer Applications", *Proc. of ICDCS 2004*, pp. 520-527.
3. Pairot, C., García, P., and Gómez Skarmeta, A. F., "Dermi: A New Distributed Hash Table-based Middleware Framework". *IEEE Internet Computing*. Vol 8, No. 3, 2004.



# Resource Partitioning Algorithms in a Programmable Service Grid Architecture

Pieter Thysebaert, Bruno Volckaert, Marc De Leenheer,  
Filip De Turck, Bart Dhoedt, and Piet Demeester

Department of Information Technology, Ghent University - IMEC,  
Sint-Pietersnieuwstraat 41, B-9000 Gent, Belgium  
{pieter.thysebaert, bruno.volckaert}@intec.ugent.be

**Abstract.** We propose the use of programmable Grid resource partitioning heuristics in the context of a distributed service Grid management architecture. The architecture is capable of performing automated and exclusive resource-to-service assignments based on Grid resource status/properties and monitored service demand. We present two distinct approaches for the partitioning problem, the first based on Divisible Load Theory and the second built on Genetic Algorithms. Advantages and drawbacks of each approach are discussed and their performance is evaluated using NSGrid. Results show that automated resource-to-service partitioning simplifies scheduling decisions, improves service QoS support and allows efficient computational/network resource usage.

## 1 Introduction

As more and more application-types are being ported to Grid environments, an evolution from pure computational and/or data Grids to full-scale service Grids [1] is taking place. A “service Grid” denotes a Grid infrastructure capable of supporting a multitude of *application types* with varying QoS levels. With widespread Grid adoption also comes the need for automated distributed management of Grids, as the number of resources offered on these Grids rises dramatically. Automated self-configuration/optimization of Grid resource usage can greatly reduce management complexity, and at the same time achieve better resource utilization [2]. In this paper, the focus is on the automated deployment of resource partitioning algorithms, which intelligently (i.e. based on current service needs and Grid status) assign Grid resources (network, computing and data/storage resources) to a particular service class for exclusive use during a specified time frame. In doing so, we wish to improve service class priority support and Grid resource utilisation while at the same time simplifying scheduling decisions. Well-known service-driven Grid scheduling frameworks such as AppLeS [4] and GrADS [5] differ from our approach in that we use a Service Management Architecture which operates independent of the scheduling system and actively monitors application behaviour at runtime.

In order to compare the performance of a service managed Grid versus a non-service managed Grid we use NSGrid (reported upon in [3]), an ns-2 based Grid

simulator capable of accurately modeling different Grid resources, management components and network interconnections. More specifically, we evaluated both GA-based and DLT-based resource partitioning strategies, both when network aware and when network unaware scheduling algorithms are used.

The remainder of this paper is structured as follows: section 2 gives an overview of the service management architecture. Section 3 elaborates on the different resource partitioning strategies, while their evaluation in a typical Grid topology is discussed in section 4. Concluding remarks are presented in section 5.

## 2 Service Management Architecture

We regard a Grid as a collection of *Grid Sites* interconnected by WAN links. Each Grid Site has its own resources (computational, storage and data resources abbreviated as CR, SR and DR respectively) and a set of management components, all of which are interconnected by means of LAN links. Management components include a *Connection Manager* (capable of bandwidth reservation support, and responsible for monitoring available link bandwidth), an *Information Service* (IS) (storing the properties and status of the registered resources) and a *Scheduler*. Every resource in our model is given an associated service class property (stored in the Information Services). The basic unit of work in our model is a *job*, which can roughly be characterised by its length (execute time on a reference processor), required input data, the amount of output data and the service class to which it belongs. Each Grid Site has one or more *Grid Portals* through which users can submit their jobs. Once submitted, a job gets queued at the *Scheduler*, which in turn queries both local and foreign ISs for resources adhering to the job's requirements. Once the results of those queries are returned, the Scheduler applies one of its scheduling algorithms and (if possible) selects one or more DRs (for input data), together with one or more SRs (for storing output data) and a CR (for processing). If the scheduling algorithm is network aware, the Connection Manager is queried for information about available bandwidth on paths between resources and, once a scheduling decision is made, attempts to make connection reservations between the selected resources.

A distributed service management architecture was implemented in NSGrid in order to evaluate the performance of different resource partitioning strategies. Each Grid Site has a local *Service Manager* interacting with the local IS, Connection Manager and *Service Monitor*. The Service Monitor component monitors local characteristics of each service class; it stores inter-arrival times, I/O data requirements and processing length of jobs. At specified intervals, the Service Monitor sends the collected information to all known foreign Service Monitors, so they can keep their 'foreign service characteristics' information up-to-date.

The Service Manager queries the local Service Monitor for information regarding the different services. When the monitored service characteristics do not differ (with regard to a certain threshold) from the ones used to partition the Grid resources in a previous run, no repartitioning will occur. If this is not the case, or if no partitioning has been done yet, the Service Manager will query the

ISs for Grid resource properties/status. Once the answer to these queries has been received, one of the resource partitioning algorithms (detailed in section 3) is applied to the resource set, and the resulting solution is sent back to the ISs, which in turn change the service-exclusive attribute of their stored resources.

### 3 Partitioning Strategies

Recall that we are trying to partition resources into service class resource pools. A solution to this problem is a mapping from resource to a particular service type, and this for all resources returned from the Service Manager - IS queries. A resource can also be assigned service type ‘0’, meaning it can be used by any service type. Exhaustively searching for a cost function optimum quickly becomes infeasible, as the number of solutions that needs to be evaluated is  $(\#servicetypes + 1)^{\#resources}$ . To find a suitable solution in reasonable time, we used two distinct approaches: one uses Divisible Load Theory while the other uses a Genetic Algorithm to obtain a resource-to-service mapping.

#### 3.1 DLT-Based Partitioning

Whenever a Grid reaches a steady state (e.g. a Grid processing a periodic load), stochastic parameters regarding the distributions of job IAT, duration and I/O-needs can be derived for each Service Type by the Service Monitoring Architecture. These parameters can then be used to fuel an ILP designed to

1. Assign an exclusive Service Type to each Computational Resource.
2. Determine the optimal *schedule* of the periodic workload over the Grid’s resources, taking into account the Service Type assignation.

An approximation used to limit the number of integer variables in this problem is to treat the aggregate workload as arbitrarily divisible (hence the name “Divisible Load Theory”) [6]. In this context, values of interest are  $arrivals_s^n$  - the load per time unit arriving at site  $s$  and belonging to service type  $n$ ,  $Sets_n$  and  $Size_n$  - the datasets available to service type  $n$  jobs and their respective sizes. Main decision variables in the problem are  $x_{c,n}$  (binary, assigning resource type  $n$  to CR  $c$ ) and  $\alpha_{i,n}^c$  (real-valued, amount of service type  $n$  load per time unit processed at CR  $c$  which arrived at site  $i$ ). Auxiliary variables needed to fulfill routing constraints on the input datasets and generated output data have been dubbed  $in_{n,j}^l$  (bandwidth needed on link  $l$  for transport of dataset  $j$  of service type  $n$ ) and  $out_s^l$  (bandwidth needed on link  $l$  for transport of output to SR  $s$ ).

Using the Divisible Load approach, the resource-to-service assignation can now be modeled as a cost minimization problem with several classes of constraints<sup>1</sup>. The capacity constraints to be observed are

$$\forall c \in CR. \sum_i \sum_{sites} \sum_n \sum_{ST} \alpha_{i,n}^c \leq Cap_c \quad (1)$$

<sup>1</sup> Abbreviations used: GW = Gateways,  $L^+$  = outgoing links,  $L^-$  = incoming links.

$$\forall l \in L. \sum_n \sum_{ST} \sum_j \sum_{Sets_n} in_{n,j}^l + \sum_s \sum_{SR} out_s^l \leq Cap_l \quad (2)$$

Network traffic is routed according to following constraints:

$$\forall n \in ST, j \in Sets_n. \sum_d \sum_{DR:j} \sum_{Sets_d} \sum_l L_d^+ in_{n,j}^l = \frac{\sum_s \sum_{Sites} arrivals_s^n \cdot Size_n}{|Sets_n|} \quad (3)$$

$$\forall c \in CR, n \in ST, j \in Sets_n. \sum_l \sum_{L_c^-} in_{n,j}^l = \frac{\sum_i \sum_{Sites} \alpha_{i,n}^c \cdot Size_n}{|Sets_n|} \quad (4)$$

$$\forall c \in CR, s \in SR. \sum_l \sum_{L_c^+} out_s^l = \sum_n \sum_{ST} \alpha_{Sites,n}^c \times Size_n \quad (5)$$

$$\forall s \in SR. \sum_l \sum_{L_s^-} out_s^l = \sum_n \sum_{ST} arrivals_{Sites}^n \times Size_n \quad (6)$$

$$\forall g \in GW, n \in ST, j \in Sets_n. \sum_l \sum_{L_g^-} in_{n,j}^l = \sum_l \sum_{L_g^+} in_{n,j}^l \quad (7)$$

$$\forall g \in GW, s \in SR. \sum_l \sum_{L_g^-} out_s^l = \sum_l \sum_{L_g^+} out_s^l \quad (8)$$

A feasible schedule is obtained by

$$\forall i \in sites, n \in ST. \sum_c \sum_{CR} \alpha_{i,n}^c = arrivals_i^n \quad (9)$$

Constraints concerning the exclusive reservation of each CR:

$$\forall c \in CR. \sum_n \sum_{ST} x_{c,n} = 1 \quad (10)$$

$$\forall c \in CR, n \in ST. \sum_i \sum_{Sites} \alpha_{i,n}^c \leq x_{c,n} \times Cap_c \quad (11)$$

The “cost” to be minimized can take on several forms; for instance, the total amount of data traveling over network links per unit of time (in the steady-state Grid) can be described in terms of problem variables as

$$\sum_l \sum_L \left( \sum_n \sum_{ST,j} \sum_{Sets_n} in_{n,j}^l + \sum_s \sum_{SR} out_s^l \right) \quad (12)$$

Using this cost function in the ILP results in a workload schedule and Service Type assignment yielding minimal aggregate network load for a given arrival process. Alternatively, one can choose to minimize the maximal unused CR fraction, which results in an “even” workload distribution across all CRs according to their respective capacities. This can be modeled by adding the constraints

$$\forall c \in CR, n \in ST. cost \geq \frac{\left( x_{c,n} \cdot Cap_c - \sum_i \sum_{Sites} \alpha_{i,n}^c \right)}{Cap_c} \quad (13)$$

### 3.2 GA-Based Partitioning

The resource type assignment can easily be encoded into an  $n$ -tuple of service type IDs, where  $n$  equals the number of resources. These *chromosomes* can then be fed to a Genetic Algorithm which evaluates the fitness of each chromosome (i.e. possible service type assignment) w.r.t. a cost function (see algorithm 3.1). Unlike an ILP, this cost function need not be “linear” in the decision variables, giving this approach more expressive power than the DLT-based partitioning.

**Algorithm 3.1:** GENETIC ALGORITHM(*resources*)

```

populationinitial ← (b(1,0), ..., b(m,0)), t ← 0
while stopcondition false
do
  for i ← 1 to m comment: proportional selection
  do
    x ← rand[0,1], k ← 1
    while k < m and x <  $\frac{\sum_{j=1}^k f(b_j,t)}{\sum_{j=1}^m f(b_j,t)}$ 
    do k ← k + 1
    bi,t+1 ← bk,t
  for i ← 1 to m-1 step i+2 comment: two-point crossover
  do
    if rand[0,1] ≤ ρC
    then
      pos1 ← rand[1,m], pos2 ← rand[1,m]
      if pos1 > pos2
      then switch(pos1, pos2)
      for k ← pos1 to pos2
      do switch(bi,t+1[k], bi+1,t+1[k])
  for i ← 1 to m comment: mutation
  do
    for k ← 1 to m
    do
      if rand[0,1] < ρM
      then bi,t+1[k] ← rand[0, #ST]
t ← t + 1

```

**Global Service CR Partitioning.** This cost function takes into account the computational processing needs and priority of the different service types (*ST*). The Service Manager queries the ISs for all local CRs and calculates average service processing needs  $\forall ST \cdot ppower_{reqST} = sites_{ST} \times \frac{ptime_{refST}}{IAT_{ST}}$ . Average processing time of a job from service class *ST* on a reference processor is denoted by  $ptime_{refST}$ , while  $sites_{ST}$  denotes the amount of Grid portals launching jobs from this service class. The relative processing power assigned to a service type is then given by:  $\forall ST \cdot ppower_{asgST} = \sum_{\forall CR \in ST} \frac{speed_{CR}}{speed_{CR_{ref}}} \times ptime_{refST}$ . The importance of assigning resources to foreign service types can be adjusted by the local Service Manager by tweaking the foreign service policy  $\rho_{ST_{foreign}}$ . Once CR query answers have been received, GA 3.1 will be started with cost function 3.2 (GA equivalent of equation 13), with an objective to assign each service type a same amount of processing power *relative* to their requested processing power.

**Network Partitioning.** Since the Service Monitor keeps track of I/O data characteristics of each service, data intensiveness relative to the other services can be calculated. This in turn can be used to perform per-service network bandwidth reservations. We have implemented a proof-of-concept network partitioning strategy, in which the Service Manager calculates average data requirement percentages for each service class  $bw_{req_i} = \frac{bw_{input_i} + bw_{output_i}}{\sum_j \frac{bw_{input_j} + bw_{output_j}}{IAT_j}}$  and passes this information to the Connection Manager, which will make service type bandwidth reservations on all network links for which it is responsible.

**Algorithm 3.2:**  $f_{CRpart_{global}}(x)$ 

```

result ←  $\frac{ppower_{asg_0}}{2}$ , maxAllocover ← 0, maxAllocunder ← 0
for  $i \in ST_{local} \cup ST_{foreign}$ 
do
  aux ←  $ppower_{req_i} - ppower_{asg_i}$ 
  if  $aux < 0$ 
  then
    if  $-aux > maxAlloc_{over}$ 
    then  $maxAlloc_{over} \leftarrow -aux$ 
     $aux \leftarrow ppower_{asg_i}$ 
  else
    if  $\frac{aux}{ppower_{req_i}} > maxAlloc_{under}$ 
    then  $maxAlloc_{under} \leftarrow \frac{aux}{ppower_{req_i}}$ 
     $aux \leftarrow ppower_{asg_i} - aux$ 
  if  $i \in ST_{foreign}$ 
  then  $aux \leftarrow aux \times \rho_{ST_{foreign}}$ 
  result  $\leftarrow \frac{priority_i}{(\sum_j_{ST} priority_j)} \times aux$ 
result ←  $maxAlloc_{over} + maxAlloc_{under}$ 

```

## 4 Performance Evaluation

### 4.1 Simulation Setup

A fixed Grid topology was used for all simulations. First, a WAN topology (containing 8 core routers with an average out-degree of 3) was instantiated. Among the edge LANs, we chose 12 of them to represent a Grid site. Each site's resources and management components are connected through 1Gbps LAN links, while Grid site interconnections consist of dedicated 10Mbps WAN links. We have assigned 3 CRs to each Grid Site. To reflect the use of different tiers in existing operational Grids, not all CRs are equivalent: the least powerful CR has two processors (operating at reference speed). A second class of CRs has four processors, and each processor operates at twice the reference speed. The third CR type contains 6 processors, each operating at 3 times the reference speed. Conversely, the least powerful CR is 3 times as common as the most powerful CR, and twice as common as the middle one. We have assumed that SRs offer "unlimited" disk space. Each site has at its disposal exactly one such SR. Each site's DR contains 6 out of 12 possible data sets. These data sets are distributed in such a way that 50% of the jobs can have local access to their needed data.

We used 2 equal-priority service classes (each accounting for half of the total job load); one is more data-intensive, while the other is more CPU-intensive (see table 4.2). Jobs were scheduled using one of two scheduling algorithms; the first algorithm only uses available CR capacities to make decisions, while the second also takes into account network link loads [7]. Once sufficient statistical data about the job parameters had been gathered by the Service Monitor, the Service Manager was instructed to apply a partitioning algorithm to the Grid's resources. We measured average job response time (JRT) and network usage.

### 4.2 Comparison of DLT- and GA-Based Partitioning

In general, our GA-based partitioning strategy provides more functionality, as it is able to support different priority schemes, shared resource and local vs. foreign service differentiation. Its main drawback is the time needed to complete a GA run (with reasonable results); on our sample scenario, this takes about 800s, while the DLT-based approach needs only 10s. For the GA approach, we used Grefenstette’s settings, with an initial population of 30,  $\rho_C = 0.9$  and  $\rho_M = 0.01$ , and a stop condition of 100 runs.

	CPU-Job	Data-Job
<b>Input(GB)</b>	0.01-0.02	1-2
<b>Output(GB)</b>	0.01-0.02	1-2
<b>IAT(s)</b>	30-40	30-40
<b>Ref. run time(s)</b>	100-200	40-60

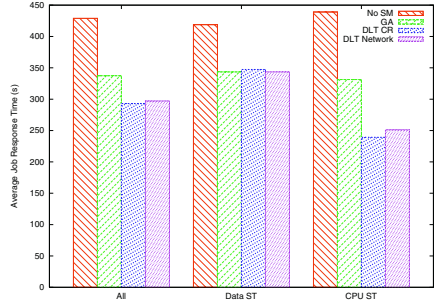


Fig. 1. Job Class Properties & Non-Network Aware Scheduling: Metrics

### 4.3 Non-network Aware Scheduling

Using a non-network aware scheduling algorithm over all Grid partition strategies results in average JRTs as shown in figure 4.2. Clearly, the use of Grid partitioning based on accurate job characteristic predictions has a positive influence. This behavior is due to resources being reserved for exclusive use by a service class, forcing the scheduler not to assign jobs to less-optimal resources (e.g. non-local access to needed input data), but to keep the job in the scheduling queue until a service-assigned resource becomes available. Optimizing the Grid partitions for minimal network usage does not yield a significant improvement, as the scheduling algorithm does not take into account network loads and diverges from the workload distribution as proposed by the DLT ILP.

### 4.4 Network Aware Scheduling

Values for average JRT and network usage observed when jobs are scheduled using a network aware algorithm are shown in figure 2. Again, when partitioning for optimal CPU usage, average JRTs are improved when compared to JRTs obtained when no partitioning strategy is used<sup>2</sup>. In analogy, after partitioning for minimal network utilization, network resources are less loaded.

<sup>2</sup> GA stands for GA-based computational partitioning, while GA-CONN denotes GA-based computational partitioning + network partitioning.

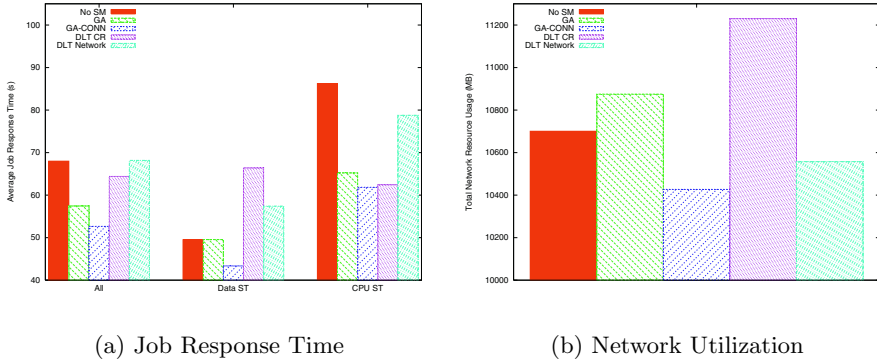


**Fig. 2.** Network Aware Scheduling: metrics

We measured the time it takes to calculate a scheduling decision and noticed a decrease in scheduling time of 28% when comparing the service managed Grid to the non-service managed Grid (i.e. from an average 12.71s in the non service managed case to 9.13s in the service managed Grid). This can be explained by the fact that when resources are partitioned among services, less resource query results will be returned to the scheduler, allowing easier scheduling decisions.

## 5 Conclusions

In this paper we proposed a distributed service management architecture, capable of monitoring service characteristics at run-time and partitioning Grid resources among different priority service classes. Two specific partitioning algorithms were discussed, and we indicated how our architecture dynamically invokes each algorithm with suitable parameters. We evaluated these algorithms using NSGrid: besides easing the process of schedule making decisions, Service Partitioning does not lead to a deterioration of Grid performance, both when job response times or network resource utilization is measured. A possible preference of one algorithm over the other depends on the trade-off between the size of the needed feature set and the algorithm's computational complexity.

## References

1. I. Foster, C. Kesselman, J.M. Nick, S. Tuecke, "Grid services for distributed system integration", IEEE Computer, Vol. 35-6, pp. 37-46, 2002
2. J.O. Kephart, D.M. Chess, "The vision of autonomic computing", IEEE Computer, Vol. 36-1, pp. 41-50, 2003
3. B. Volckaert, P. Thysebaert, F. De Turck, P. Demeester, B. Dhoedt, "Evaluation of Grid Scheduling Strategies through a Network-aware Grid Simulator", Proc. of PDPTA 2003, Vol. 1, pp. 31-35, 2003



4. F. Berman et al., “*Adaptive Computing on the Grid Using AppLeS*”, IEEE Transactions on Parallel and Distributed Systems, Vol. 14-4, pp. 369-382, 2003
5. H. Dail, F. Berman, H. Casanova, “*A Decoupled Scheduling Approach for Grid Application Development Environments*”, Journal of Parallel and Distributed Computing, Vol. 63-5, pp. 505-524, 2003
6. P. Thysebaert, F. De Turck, B. Dhoedt, P. Demeester, “*Using Divisible Load Theory to Dimension Optical Transport Networks for Computational Grids*”, in Proc. of OFC/NFOEC 2005
7. P. Thysebaert, B. Volckaert, F. De Turck, B. Dhoedt, P. Demeester, “*Network Aspects of Grid Scheduling Algorithms*”, Proc. of PDCS 11, pp. , 2004

# Triggering Network Services Through Context-Tagged Flows

Roel Ocampo<sup>1,2</sup>, Alex Galis<sup>2</sup>, and Chris Todd<sup>2</sup>

<sup>1</sup> Department of Electrical and Electronics Engineering, University of the Philippines, Diliman, Quezon City, 1101 Philippines

<sup>2</sup> Department of Electronic and Electrical Engineering, University College London, Torrington Place, London WC1E 7JE  
{r.ocampo, a.galis, c.todd}@ee.ucl.ac.uk

**Abstract.** Next-generation Grids will require flexible and adaptive network infrastructures that would be able to provide the requisite quality of service for computational flows. We discuss a mechanism where network flows are tagged with network context information, triggering dynamic network services, including QoS and adaptation services. An incremental deployment strategy and some initial results are presented.

## 1 Introduction

Due to the nature of the computational tasks that grids handle, the underlying resources they use are required to deliver nontrivial qualities of service [1]. In networked environments, where resources such as bandwidth are often shared, there may be situations where computational flows would have to compete for the use of resources along with flows from less critical applications. To deal with this, a pragmatic approach might be to differentiate the various network flows and set an adaptation policy  $P$  on a particular group of flows based on the class of users  $U$  generating the flow, for a particular type of usage or activity  $A$ , under a certain situation or set of network conditions  $C$ . In other words, an adaptation  $P$  is triggered by the general parameters  $(U, A, C)$ .

Currently the mechanisms that exist to differentiate network flows provide very limited information about the flow, and are usually non-extensible. In this work, we propose the use of rich and extensible information in the form of network context as a means of differentiating flows and triggering network services, particularly adaptation services. In Sect. 2 we argue that end-hosts are rich sources of information needed in triggering adaptation services, and that a mechanism for sharing such information with the rest of the network is needed. In Sect. 3 we present the concept and design for such a mechanism, called context tagging, and Sect. 4 briefly discusses an incremental deployment strategy. Section 5 discusses some initial results. Section 6 briefly discusses efforts that are related to our current work, and finally Sect. 7 concludes and describes the work ahead.

## 2 End-Hosts and Flow Context

As a consequence of the end-to-end principle [2], nodes such as routers often have a very limited view of the state of the network. While they often have a global view of the network's topological state as a result of routing exchanges, routers may have a limited, per-node awareness of other parameters such as traffic levels, congestion, or bit error rates. Other information that may characterize the state of the network, such as path loss, delay and jitter are usually sensed and processed at end-hosts.

Aside from end-to-end traffic-related parameters, end-hosts are rich sources of other types of information such as the characteristics and capabilities of end-devices, the applications generating the traffic, and the identities and activities of users such as their movement and location. All of these pieces of information are relevant in (a) determining whether a certain condition  $C$  exists within the network or user environment, (b) in identifying whether the traffic belongs to the class of users  $U$ , and (c) if the traffic is the result of usage activity  $A$ . These parameters also help in the design of appropriate adaptation policies applicable to the user group under these circumstances, or within that particular *context*.

### 2.1 The Context of a Flow

Context is defined in the New Oxford Dictionary of English as “the circumstances that form the setting for an event ... and in terms of which it can be fully understood and assessed.” Dey, Salber and Abowd further define context as “any information that can be used to characterize the situation of entities ... that are considered relevant to the interaction between a user and an application, including the user and the applications themselves” [3]. Although the latter definition is tailored to interactions between users and applications, it can still be used as a template to describe the notion of context relevant to the interaction between a user application and the network, or between a user and the network.

One entity we consider relevant to this interaction is the *flow*, defined as distinguishable streams of related datagrams, typically resulting from the activity of a single entity [4]. The fact that flows are attributable to specific user groups and their activities makes them ideal sources of adaptation triggers  $U$  and  $A$ . We define the context  $C_f$  of a network flow as any information that can be used to characterize its situation, including information pertaining to other entities and circumstances that give rise to or accompany its generation at the source, affect its transmission through the network, and influence its use at its destination. This collectively includes not only the intrinsic, “low-level” characteristics of a flow, such as its traffic profile, but also the nature of the applications, devices, and the activities and identities of the users that produce or consume the flow.

We envision flow context to be used within the network in the following ways:

- to trigger adaptation directly on the flow itself. For example, the content of a flow may be compressed, transcoded, encrypted, classified, assigned a particular QoS treatment, marked, or rerouted in response to link constraints, network state, or application requirements [5].

- to trigger immediate or future network-wide management actions that are not necessarily targeted to exclusively affect the context-carrying flow. For example, a new flow may trigger the activation of a reserve link in order to guarantee sufficient bandwidth for future flows.
- to trigger network services that are specific or personalized for a user or group of users. A context tag may carry information about the user generating the flow, such as her profile or preferences. The network’s response may be to offer these specific services to the user, or to automatically provide them in a transparent way. These new services may or may not directly affect the current flow.
- as a means to collect information for long-term purposes, without triggering any immediate adaptation or service, such as for traffic engineering or network optimization, or for consumption by cognitive or knowledge-based entities within the network [6].

Our approach involves tagging network flows with context obtained from sensors located mainly at end-hosts, by injecting packets that carry the flow’s context within the flow itself. These context tags are preferably located at the start or within the first few packets of a flow, although there may be times where they may be reinserted anytime during the flow lifetime, especially to signal changes in the flow’s context.

### 3 Context-Tagging Architecture

A diagram illustrating the main functional components in our scheme is show in Figure 1. Some of the components are based on a cognitive framework previously described in [7].

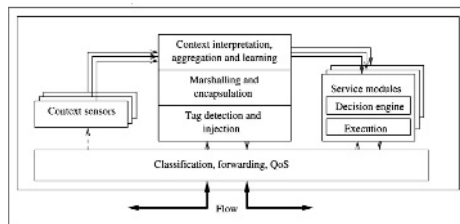


Fig. 1. Context tagging framework

#### 3.1 Tag Creation and Injection

Sensors collect low-level context information, usually measurable data or low-level events. These are transformed into useful form through the process of interpretation, which may involve the application of an algorithm, comparison with a model, or the application of reasoning or other cognitive processes. Aggregation involves the examination of separate pieces of context information to generate new contextual knowledge.

The context information is then passed down to the marshalling and encapsulation stage, where it is transformed into an Extensible Markup Language (XML) document [8]. The use of XML provides a rich and extensible means of representing context information, and allows the formal specification of languages governing the interpretation of such context. It is further encapsulated in a User Datagram Protocol (UDP) transport-layer datagram [9]. The use of UDP allows other context-“interested” hosts, including the end-destination of the flow, to detect or demultiplex out the context tag packet from the rest of the flow.

Further down, the tag injection and detection stage encapsulates the UDP datagram in an IP packet whose header contains the IP Router Alert Option as described in RFC 2113 for IPv4 [10], and RFC 2711 for IPv6 [11]. This option has the semantic “routers should examine this packet more closely.”

Routers within the network may also inject context tags to describe information aggregated from multiple tags within a single flow, or to describe flow aggregates called *macroflows*. In some cases, such as within the Internet core, routers may be more interested in context descriptions of large macroflows rather than the individual constituent flows, for reasons of scalability. It may be also necessary for routers to inject context tags to describe any adaptation they may have performed on a flow or macroflows.

### 3.2 Service Triggering

Routers within the network detect the context tag by virtue of the Router Alert option in the IP header. Routers that either do not support the option, or do not recognize the context payload simply forward the packet to the next hop. At end-hosts, the context tag may be demultiplexed out of the flow by virtue of the UDP port number. If no equivalent context-processing process exists at the destination host the tag is either silently dropped, or an error message may be returned.

Once received, the context payload is extracted and sent up the stack, to the context interpretation and aggregation module. The context may either be used for long-term information gathering or learning, or may result in a specific adaptation being triggered. Service (including adaptation) modules subscribe to certain context values or events within the context interpretation module. When these events occur or the values are presented to the service module, a decision engine determines if the service or adaptation is executed. In the case of routers, the adaptation may be applied directly to the flow carrying the tag, or to a group of flows, or a larger-scale adaptation or management function may be invoked. Service modules on different nodes may communicate with each other and may operate in a coordinated fashion; however, the details of this operation is beyond the scope of this paper.

The architecture also allows end-hosts to receive and process context tags, and to contain adaptation components. In this case, the adaptation could be on the incoming or outgoing network flow, or on a user application, or influence some operation of the receiving device.

## 4 Deployment Strategy

Our context-tagging scheme can be incrementally deployed on networks by progressively adding components that either support flow context sensing and tag generation, or provide context-triggered services and adaptation, or both. Context sensing functionality may be added to end-hosts or incrementally on network nodes such as routers, or dedicated boxes may be inserted within the network in order to inspect flows and inject context tags. For nodes that will provide context-triggered services, the service modules and the core router functionalities (classification, forwarding, QoS) do not necessarily have to be closely coupled; the context-related and adaptation functions could reside on a separate device “bolted” onto a conventional router, and SNMP [12] may be used to effect service execution. While there are obvious advantages in terms of performance and a wider range of functionalities are possible in the closely-coupled case, the loosely-coupled example is given here to illustrate that the scheme may be incrementally deployed on the existing Internet infrastructure.

## 5 Initial Results

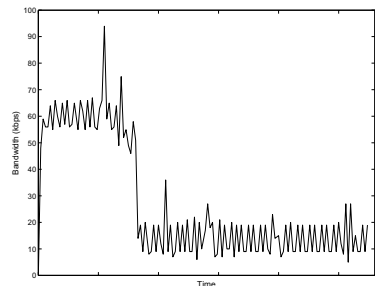
A simple flow-generating application using *libnet* [13], a toolkit that allows low-level packet construction, handling and injection was designed and used to simulate the operation of our system and perform initial validation on some of its components. Our application generated a flow containing exactly one context tag packet carrying the Router Alert Option in the IP header and a rudimentary XML-formatted context payload encapsulated in UDP. The rest of the flow consisted of UDP datagrams carrying dummy payloads. The context tag packet was positioned well within the flow, rather than among the first few packets, so that the adaptation could be well-observed. The flow was sent through a Linux-based router that in turn ran a process that detected the context-tagged packet.

```

<flowspec>
  <size unit="Kbytes">4196382</size>
</flowspec>
<filterspec>
  <src_addr type="IPv4">10.1.2.3</src_addr>
  <dest_addr type="IPv4">165.220.16.1</dest_addr>
  <transport>
    <protocol>UDP
    <src_port>80</src_port>
    <dest_port>1234</dest_port>
  </transport>
</filterspec>
<app name="mypeer">
  <app_class>p2p</app_class>
</app>

```

(a)



(b)

**Fig. 2.** (a) Context tag fragment. (b) Adaptation response on router

On the Linux router, the tag was processed, triggering a simple adaptation. In this example, the specific adaptation was to map the flow into an appropriate traffic class. Within the context tag a component called the *filterspec* provided a function similar to a similarly-named component in the Resource Reservation Protocol (RSVP): a means to define the set of packets that constitute the flow described by the tag [14]. In this experiment our filterspec used a Linux `u32` filter [15] descriptor that was directly parsed by the router and passed on to the adaptation module. In future implementations we expect to use a wider variety of mechanisms to specify filterspecs, including high-level descriptions that could be mapped by the context interpreter and service modules to specific classification mechanisms within the router. The adaptation module used the Linux `iptables` and `tc` mechanisms [15] to map the flow to a traffic class.

A fragment of the context tag is shown in Fig. 2a. The router's response to the context tag is shown in Fig. 2b. Prior to receiving the tag, the network accommodated the flow's full offered load (60 kbps average). Upon receiving the tag, the router effectively limited the bandwidth allocated to the flow to an average of 14 kbps.

## 6 Related Work

The network edge is a rich source of context information. End-hosts are in the best position to provide information on the applications that generate or consume traffic, the users whose activities drive these applications, and the computational and networking capabilities of the devices on which these applications run. Currently no widely deployed and sufficiently flexible mechanism exists for the edge to share context information within the network. Many context-aware systems employ publish-subscribe mechanisms that allow clients to obtain context information from sources [3, 16]. Our approach however contemplates a more loosely-coupled, connectionless communications model between end-hosts and nodes.

While network- and transport-layer protocol headers contain rudimentary tags (fields) that provide some hints on the type of applications that generate the flow, or to some extent, the nature and characteristics of the flow's content, these tags are not expressive enough to encapsulate the rich context information available at the edge. Schemes that provide flow descriptions often focus exclusively on their QoS characteristics, rather than a more general description of flow context. Resource reservation protocols such as RSVP [14] and the experimental ST-II [17] use a *flowspec* to describe the characteristics of a flow, usually in terms of bandwidth, delay, and other QoS-related characteristics [18]. Other schemes such as the Session Description Protocol (SDP) [19] and Multipurpose Internet Mail Extensions (MIME) [20] deliver flow or session context to end-hosts rather than network nodes, and are limited to very specific application domains.

## 7 Conclusion and Future Work

A key component needed to enable the deployment of context-aware networks is a method for sharing network context information. We have discussed a simple yet extensible and semantically-rich mechanism that tags flows through the network with context, delivering context directly to nodes along the unicast path or multicast tree. This allows network services, particularly adaptation services, to be triggered based on flow context. Our on-going work is focused on further validating our architecture, evaluating its performance, and exploring other application scenarios.

We are likewise currently exploring a parallel implementation of our components on an active networking [21] platform. We believe that such an approach will allow us to achieve a greater amount of flexibility through an on-demand deployment of context sensing, tagging, interpretation and adaptation components within the network.

Routers and end-hosts would be able to efficiently share context only if they subscribe to a common information model. An important component of our on-going work is the development of an ontology and appropriate context-sharing languages.

Finally, as with any system that senses and distributes context information, there are concerns on security and privacy that we also hope to address in the near future.

*Acknowledgment.* This paper describes work partially undertaken in the context of the E-NEXT - Information Society Technologies (IST) FP6-506869 project. The IST program is partially funded by the Commission of the European Union. The views and conclusions contained herein are those of the authors and should not be interpreted as necessarily representing the E-NEXT project. Roel Ocampo acknowledges support by the Doctoral Studies Fellowship program of the University of the Philippines.

## References

1. I. Foster. What is the Grid? A Three Point Checklist. *Grid Today*, July 2002.
2. J. Saltzer, D. Reed, and D. Clark. End-to-End Arguments in System Design. *ACM Transactions on Computer Systems*, November 1984.
3. A. K. Dey, D. Salber, and G. D. Abowd. A Conceptual Framework and a Toolkit for Supporting the Rapid Prototyping of Context-Aware Applications. *Human-Computer Interaction (HCI) Journal*, 16 (2-4), 2001
4. R. Braden, D. Clark, and S. Shenker. Integrated Services Architecture in the Internet: an Overview. *Request for Comments 1633*, June 1994.
5. M. Yarvis, P. Reiher and G. Popek. Conductor: A Framework for Distributed Adaptation. *Proc. 7th Workshop on Hot Topics in Operating Systems*, March 1999.
6. D. Clark, C. Partridge, J. Ramming, and J. Wroclawski. A Knowledge Plane for the Internet. *Proc. ACM SIGCOMM 2003 Conference on Applications, Technologies, Architectures and Protocols for Computer Communications*, August 2003.



7. R. Ocampo and H. De Meer. Smart Wireless Access Points for Pervasive Computing. *Proc. First Working Conference on Wireless On Demand Network Systems (WONS '04)*, Lecture Notes in Computer Science LNCS 2928, January 2004.
8. T. Bray, J. Paoli, C.M. Sperberg-McQueen, E. Maler, and F. Yergeau (editors). Extensible Markup Language 1.0 (Third Edition). *W3C Recommendation 04 February 2004*, <http://www.w3.org/TR/REC-xml>
9. J. Postel. User Datagram Protocol. *Request for Comments 768*, August 1980.
10. D. Katz. IP Router Alert Option. *Request for Comments 2113*, February 1997.
11. C. Partridge and A. Jackson. IPv6 Router Alert Option. *Request for Comments 2711*, October 1999.
12. J. Case, M. Fedor, M. Schoffstall, J. Davin. A Simple Network Management Protocol (SNMP). *Request for Comments 1157*, May 1990.
13. M. Schiffman. Libnet. <http://www.packetfactory.net/Projects/Libnet/>
14. L. Zhang, S. Deering, D. Estrin, S. Shenker, and D. Zappala. RSVP: A New Resource ReSerVation Protocol. *IEEE Network*, September 1993.
15. B. Hubert, T. Graf, G. Maxwell, R. van Mook, M. van Oosterhout, P. Schroeder, J. Spaans, P. Larroy (editors). Linux Advanced Routing and Traffic Control. <http://www.lartc.org>.
16. T. Kanter. A Service Architecture, Test Bed and Application for Extensible and Adaptive Mobile Communication. *Proc. Personal Computing and Communication Workshop 2001 (PCC'2001)*, April 2001.
17. C. Topolcic. Internet Stream Protocol Version 2 (ST-II). *Request for Comments 1190*, October 1990.
18. C. Partridge. A Proposed Flow Specification. *Request for Comments 1363*, September 1992.
19. M. Handley, V. Jacobson. SDP: Session Description Protocol. *Request for Comments 2327*, April 1998.
20. N. Freed and N. Borenstein. Multipurpose Internet Mail Extensions Part Two: Media Types. *Request for Comments 2046*, November 1996.
21. D. L. Tennenhouse and D. J. Wetherall. Towards an Active Network Architecture. *Computer Communication Review*, 26(2), April 1996.

# Dependable Execution of Workflow Activities on a Virtual Private Grid Middleware

A. Machi, F. Collura, and S. Lombardo

ICAR/CNR Department of Palermo  
{machi, s.lombardo, f.collura}@pa.icar.cnr.it

**Abstract.** In this paper we relate QoS management to Workflow management and discuss dependable execution on a middleware layer, named Virtual Private Grid (VPG), of sets of processes performing a workflow activity. We propose two patterns of interaction between a Workflow Management System and the distributed workflow management support. The patterns monitor resource availability & connectivity, and, in case of fault of any resource, ensure job completion by re-mapping a process graph and restarting it. We also describe current implementation of the patterns and of the run-time support.

## 1 Introduction

Quality of Service (QoS) can be defined as “the set of those quantitative and qualitative characteristics which are necessary in order to achieve the required functionality of an application” [1]. We can suppose that QoS could be specified as a set of *non-functional* attributes some of which are not expressible numerically.

One category of QoS qualitative characteristics is *dependability* that characterizes the degree of certainty that an activity is performed [2].

Dependability is of main concern in grid environments where applications are ran by coordinating processes mapped on a set of computational resources co-allocated but just virtually co-reserved. In fact, according to the Virtual Organization paradigm, control of grid shareable resources is maintained by Local Organizations and no insurance is given to clients on persistence of their availability.

Even if a number of tools and high level collective services have been developed in the grid community for supporting co-reservation [3], up to now other aspects of grid-awareness as completion insurance, fault-tolerance and resources management are still in charge of user control code. The most popular grid technology for e-science, namely the Globus Toolkit 2 (GT2), and most projects based on it [4][5], offer adequate APIs for *staging* of processes and data, and for process *enactment*, but offer very limited support for process *monitoring* and just a kill mechanism to support workflow *enforcement*. Process monitoring and control are in charge of user who interleaves management code to business code to implement grid-awareness or self-adaptiveness.

The Web Services Resource Framework, emerging from the OGSA (GT3) experience and based on Web Services technology, defines a few models and patterns specifying non-functional requirements of Web Services life cycle and composition [6]. Namely, WS-ResourceLifetime [7] defines mechanisms for managing WS-Resources,

WS-ServiceGroups [8] describes how collections of services can be represented and managed. WSBBaseFaults [9] defines a standard format for reporting exceptions.

But WSRF specifics are limited and focused to the implementation of the Service Oriented Architecture (SOA) paradigm [10] and are scarcely useful to implement QoS control policies and patterns in e-science grid-enabled applications still using legacy code structured as a set of cooperative processes. In this paper we describe a workflow management support service and propose two patterns for supporting dependability of execution.

In section 2 we state equivalence between execution of a process graph and execution of a workflow activity. In section 3 we describe two patterns for management of dependable execution on the grid of sets of concurrent processes described by direct graphs.

Finally, in section 4, we describe a component implementation over GT2 of a grid middleware layer supporting non-functional aspects of workflow management through services for process life cycle monitoring and an asynchronous event bus service.

## 2 Process Graphs and Workflow Activities

The Workflow Management Coalition organization (WFMC) [11] defines a “*business process*” as “a set of one or more linked procedures or activities which collectively realise a business objective or policy goal” [12]. It defines an *activity* as “a description of a piece of work that forms one logical step within a process. An activity is typically the smallest unit of work that is scheduled by a workflow engine during process enactment. An activity typically generates one or more work items. A work item is a representation of the work to be processed (by a workflow participant) in the context of an activity within a process instance.”

We recognize in these definitions a basic model useful for partitioning legacy applications whose business logic can be expressed as a workflow in a set of activities some of which can be separately enacted and managed on the grid. An activity may be carried out by a single workflow participant or by a set of participants organized in a workflow sub-graph. It can be hosted in a SOA service and managed honoring a Service Level Agreement (SLA) [13].

In the following we restrict our considerations to activities that may be described by a direct graph of virtual processes where one virtual node operates as an activity front-end. It coordinates the routing of work-items to other virtual processes participants to activity expressed by workflow sub-graph.

Controlled execution of an activity consists then in an atomic execution on the grid of an instance of a process graph mapped onto grid resources.

Adhering to the terminology commonly used by the WFMC community we can recognize two main control activities:

- *Routing*: the direction of work-items processing flow which is implicitly defined by the process graph and expresses part of the business logic;
- *Management*, which consists in *deployment* of virtual processes onto grid resources, staging of application data, *enactment* (initialization) of activity procedures, *monitoring* of QoS respect, *enforcement* or rerouting of processing flow in case of fault or not compliance with expected QoS.

In the WFMC scenario, management activities are assigned to a WorkFlow Management (WFM) engine holding mechanisms able to enforce workflow rerouting. Present grid toolboxes offer tools for deployment [14], or enactment and monitoring of resource status [15] but do not support collective activity monitoring and rerouting. This is mainly due to their relying on a synchronous communication paradigm (rsh-like) used both for functional and non-functional control.

The Grid Application Development System (GrADS) helps building natively self-consistent applications in which configurable objects, named COPs (Configurable Object Programs), embody at compile time intimate knowledge of application while objects drivers (application manager and executor) embody grid-awareness [16]. GrADS relies on a proprietary run-time system to support QoS monitoring and reconfiguration of COPs through application specific sensors and actuators.

In the framework of the Grid.it project, a new grid-aware programming paradigm has been proposed [17] and the ASSIST environment is being implemented for assisting native development of components configurable in respect to performance attributes. The key point for enabling flexible control is wrapping executive code in components including drivers of standard routing patterns (parmods) and a local proactive executor serving external enforcement through a non-functional interface.

Neither grid-aware programming paradigm defines patterns for integrating control of external activities in theirs application *Managers*.

We propose a grid management support engine that allows application or workflow *Managers* to extend their control on activities on the grid.

In the following we describe a grid middleware offering services for management of the graph of processes on the grid and two patterns implementing dependable execution of workflow actions.

### 3 Patterns for Dependable Execution of Process Graphs

Fig.1 shows a workflow scenario where two steps of a pipe (activities) execute on resources obtained on-demand from the grid (grid-enabled). Activities are performed by graphs of cooperating processes.

Dependable activity execution is required to avoid overrun of data-item flow-control. If any resource faults, activities need to be remapped and restarted.

Monitoring of stable execution of process activities is committed to a grid middleware. A *grid-front-end* process coordinates a network of sensor/actuator *demons* installed on grid nodes. It offers to the (activity or workflow) *Manager* a high level synchronous RPC functional interface for mapping process graphs, starting them, polling status of their processes, aborting them.

Two interaction patterns allow demons to monitor the regular execution of any process activated on grid resources and *Manager* to restart the graph in case of fault of a grid node or connection. While executing these patterns the *grid-front-end* process and the *demons* interact synchronously via RPC calls and asynchronously via signals, the *Manager* and the grid front-end just via RPC calls.

The *resource availability & connectivity check* pattern verifies, at regular time interval, activity of graph processes and functionality of significant connections among them. Exchanging of *ping messages* between demons at each connection end

tests connectivity. A *demon* notifies to the *grid-front-end* a *missing-connection signal* when unable to reach its peer at end of any significant connection.

Furthermore, each demon emits regularly a *heartbeat* signal to notify the *grid-front-end* that node it monitors is operative. In case of extended absence of the *heartbeat* signal, the *grid-front-end* infers a fault condition, due to the death of the demon, fault of related connection or host shutdown. Successful result of connection test leads to infer a demon fault and register a *process fault* status, unsuccessful result to register a *node fault* status.

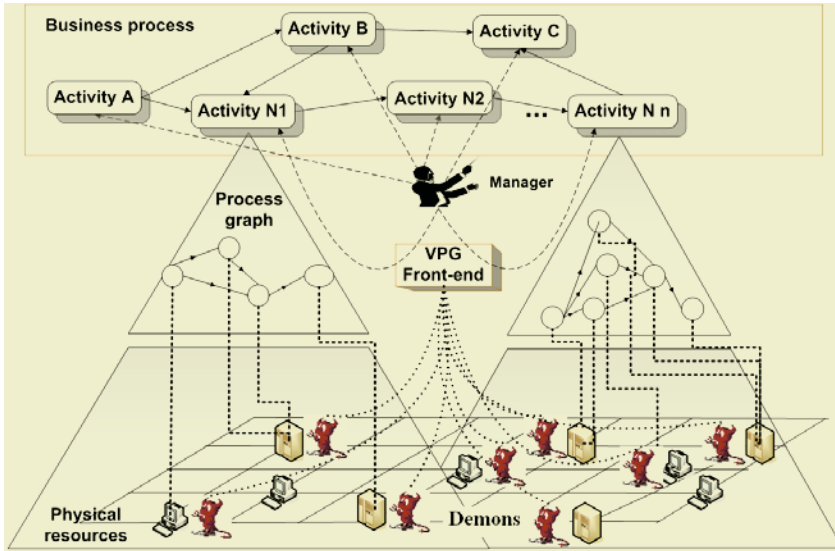


Fig. 1. Actors playing management of workflow activities on the grid

The *insured completion* pattern guarantees that a process graph comes to a known end (completed or terminated). *Manager* enacts graph through *grid-front-end* commands and polls the collective status of its process. In case of any node failure it restarts graph execution. Each *demon* monitors processes on its own node. It catches signals emitted by the local operating system and notifies them asynchronously to the *grid-front-end*, that updates graph status on behalf of *Manager*.

The following mechanisms ensure valid knowledge of process vitality and ensured completion:

- *Local operating system signals* inform the *demon* about normal process termination or abort. These signals are notified to the *grid-front-end*.
- *Keep-alive signal*: it is notified regularly from *grid-front-end* to each slave *demon* to maintain its service alive.
- *Automatic shutdown*: a *demon* not receiving for a while the *keep-alive signal* infers a fault of connection with *grid-front-end* node or failure of front-end itself. It kills

any process activated on the node, performs a garbage collection procedure that cleans-up any software element deployed and terminates.

Fig. 2 shows an UML sequence diagram that details an occurrence of the *insured completion* pattern after a process fault. Before graph restart, processes on live nodes are explicitly killed. Release of resources allocated on the fault node by the automatic shutdown procedure is omitted.

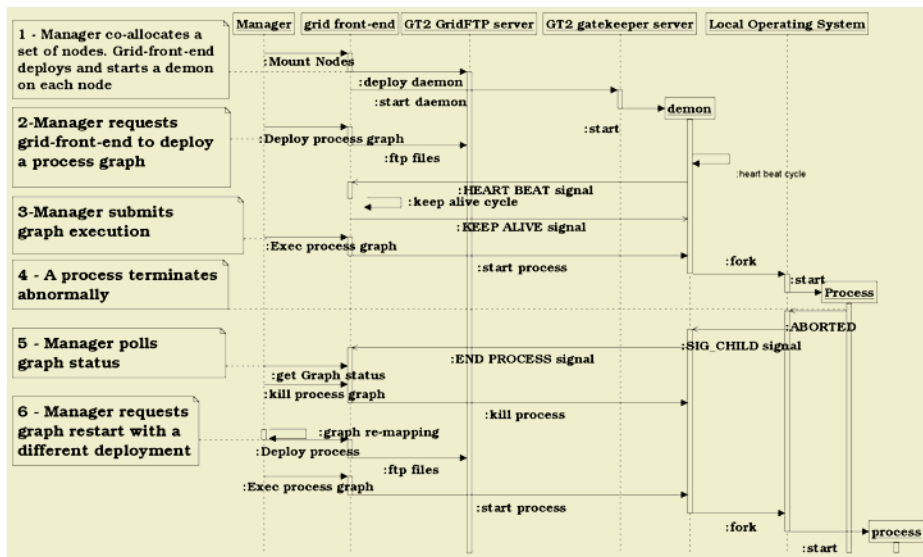


Fig. 2. UML sequence diagram illustrating events and actions in a sample occurrence of the insured completion pattern

## 4 The Virtual Private Grid Middleware

In the framework of the Grid.it Project we have developed a grid support engine, named Virtual Private Grid (VPG), implementing the roles of *grid-front-end* and *demon* organized as a middleware layer over GT2. VPG manages and monitors the life cycle of process graphs over a pool of grid resources. It offers to a client *Manager* a distributed operating system façade, making grid resources to appear virtually as belonging to a heterogeneous private cluster of processors.

VPG manages multiple process graphs described by lists of processes and arcs connecting them. Attributes of a process are the name of the node on which it is mapped and the list of the software elements required for its execution (executables, libraries and data files). Attributes of the link are the identifiers of processes connected.

Current middleware implementation (VPG 1.2) [18] provides the following functionalities:

- Grid nodes management:
  - **Mount/Unmount** of a grid node;
  - **Retrieve status**: return activity status of a grid node (disconnected, connected, activated, active).
- Process graph lifecycle primitives:
  - **Staging** of a set of files (executable, libraries, etc) on grid nodes. For each file the (redundant) deployment node list is specified. An identifier is assigned to the file set.
  - **Garbage collection**: removal of any files belonging to a file set from grid nodes where they have been staged.
  - **Enactment** of the process graph. An identifier is assigned to each process according to its rank in the process list.
  - **Kill** of graph processes included in a list of identifiers.
  - **Restart** of graph processes included in a list of identifiers.
  - **Retrieve status**: return activity status of processes belonging to a process graph (inited, aborted, running, done). Activity progress status is unsupported.
- Event services: an asynchronous event bus is provided for exchanging signals among VPG components according to the event subscribe/notify pattern.

Fig 3 shows, through an UML deployment diagram, VPG components and actors interacting with them. The VPG Master acts as a grid front-end for the *Manager* while slave demons, called Remote Engine run on each node of the grid.

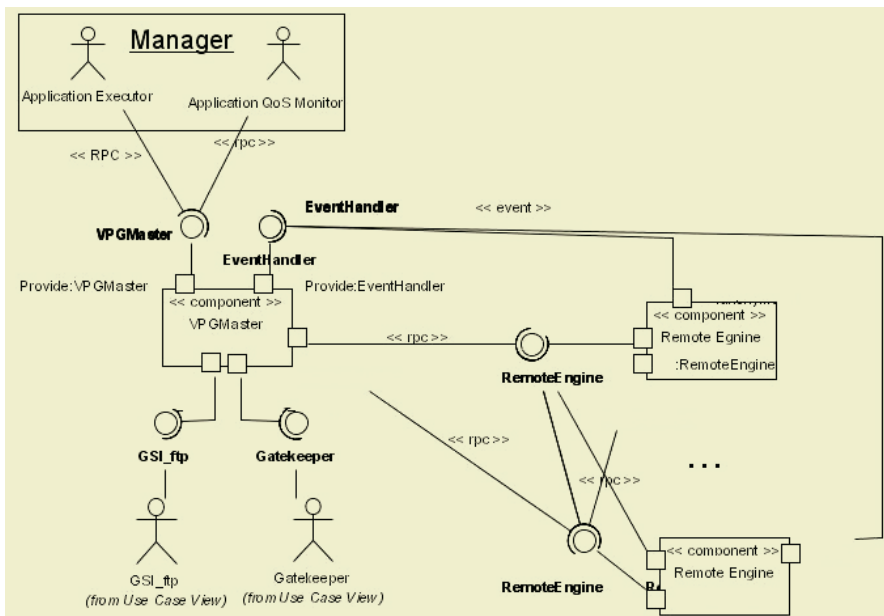


**Fig. 3.** Interaction among VPG components and actors shown through an UML deployment diagram

VPG Master: provides a functional interface that exposes every of the over mentioned functionalities. It maintains and updates in a register the status of each process controlled. It provides the asynchronous event bus and registers itself for any events related to remote process status changes. The Remote Engine provides local processes lifecycle primitives (run, kill, status, clean), and sends to master events about processes status changing or fault of connections among meaningful neighbor nodes. This entity is automatically deployed during node mount and it is removed during unmount.

Present VPG implementation is based on the usage of several design patterns: acceptor-connector, reactor, proxy, wrapper and adapter provided by the open-source object-oriented framework ACE [19].

Grid nodes management and file transfer are implemented over Globus Toolkit2 tools and services: GRAM for start-up of the Remote Engine, GridFTP for file staging.

APIs for calling VPG Master through synchronous Remote Procedure Calls (RPC) formatted according to the XML-RPC specifications or for direct integration in the *Manager* code, are provided in the VPG 1.2 SDK.

## 5 Conclusions and Future Work

In the paper we have introduced a methodology for considering QoS management of grid activities in the context of workflow management in SOA architectures. In particular we have discussed the simple case of dependable execution of graphs of processes performing a self-consistent activity.

We have shown that, in this case, two control patterns can be implemented without intervention over the application code, by exploiting an external run-time support offering collective control services to the WFM system.

Control rights over graph processes are obtained by spawning them through remote engines. Restart of the entire process graph has been indicated as a minimal solution for insured execution in case of fault of any grid resources.

A more interesting pattern for insured execution should support assisted recover from a node fault, or at least from a slave node fault.

Design of a pattern for joining or disjoining slaves from a master-slave graph routed by a parallel skeleton is a topic of current research.

## Acknowledgements

Work supported by Italian Ministry of Scientific Research: , Project FIRB *Grid.it*.

## References

- [1] Vogel A., Kerhervé B., Von Bochman G. Ad Gecsei J. (1195). Distributed Multimedia and QoS: A Survey, IEEE Multimedia Vol. 2, No. 2, p10-19
- [2] ITU-T Rec. I.350: General aspects of Network Performance and Quality of Service in Digital Networks, including ISDN.



- [3] I. I. Foster, M. Fidler, A. Roy, V. Sander, L. Winkler. End-to-End Quality of Service for High-end Applications. *Computer Communications*, 27(14):1375-1388, 2004.
- [4] The Condor® Project , <http://www.cs.wisc.edu/condor/>
- [5] The DataGrid Project, <http://eu-datagrid.web.cern.ch/eu-datagrid/>
- [6] From Open Grid Services Infrastructure to WS-Resource Framework: Refactoring & Evolution. K. Czajkowski, D. Ferguson, I. Foster, J. Frey, S. Graham, T. Maguire, D. Snelling, S. Tuecke, March 5, 2004.
- [7] Frey, J., Graham, S., Czajkowski, C., Ferguson, D., Foster, I., Leymann, F., Maguire, T., Nagaratnam, N., Nally, M., Storey, T., Sedukhin, I., Snelling, D., Tuecke, S., Vambenepe, W., and Weerawarana, S. 2004. WS-ResourceLifetime. <http://www-106.ibm.com/developerworks/library/ws-resource/wsresourcelifetime.pdf>.
- [8] Graham, S., Maguire, T., Frey, J., Nagaratnam, N., Sedukhin, I., Snelling, D., Czajkowski, K., Tuecke, S., and Vambenepe, W. 2004. WS-ServiceGroups. <http://www-106.ibm.com/developerworks/library/ws-resource/ws-servicegroup.pdf>.
- [9] Tuecke, S., Czajkowski, K., Frey, J., Foster, I., Graham, S., Maguire, T., Sedukhin, I., Snelling, D., Vambenepe, W. 2004. WS-BaseFaults. <http://www-106.ibm.com/developerworks/library/wsresource/ws-basefaults.pdf>.
- [10] K.Channabasavaiah, K.Holley, E.M.Tuggle, "Migrating to a service-oriented architecture", <http://www-06.ibm.com/developerworks/webservices/library/ws-migratesoa/>
- [11] The Workflow Management Coalition, [www.wfmc.org](http://www.wfmc.org)
- [12] Reference Model - The Workflow Reference Model (WFMC-TC-1003, 19-Jan-95, 1.1)
- [13] Web Service Level Agreements (WSLA) Project - SLA Compliance Monitoring for e-Business on demand <http://www.research.ibm.com/wsla/>
- [14] R. Baraglia, M. Danelutto, D. Laforenza, S. Orlando, P. Palmerini, P. Pesciullesi, R. Perego, M. Vanneschi "AssistConf: a Grid configuration tool for the ASSIST parallel programming environment", Eleventh Euromicro Conference on Parallel, Distributed and Network-Based Processing February 05 - 07, 2003 Genova, Italy
- [15] WS GRAM Docs, <http://www-unix.globus.org/toolkit/docs/3.2/gram/ws/index.html>
- [16] The Grid Application Development Software Project (GrADS), <http://hipersoft.cs.rice.edu/grads/index.htm>
- [17] M. Aldinucci, S. Campa, M. Coppola, M. Danelutto, D. Laforenza, D. Puppini, L. Scarponi, M. Vanneschi, C. Zoccolo "Components for high performance Grid programming in the Grid.it Project". In Proc. Of Intl. Workshop on Component Models and Systems for Grid Applications.
- [18] S. Lombardo, A. Machì. "Virtual Private Grid (VPG 1.2) Un middleware a supporto del ciclo di vita e del monitoraggio dell'esecuzione grafi di processi su griglia computazionale", Technical report RT-ICAR-PA-11 -2004, October 2004
- [19] The ADAPTIVE Communication Environment (ACE) <http://www.cs.wustl.edu/~schmidt/ACE.ht>

# Cost Model and Adaptive Scheme for Publish/Subscribe Systems on Mobile Grid Environments

Sangyoon Oh<sup>1,2</sup>, Sangmi Lee Pallickara<sup>2</sup>, Sunghoon Ko<sup>1</sup>,  
Jai-Hoon Kim<sup>1,3</sup>, and Geoffrey Fox<sup>1,2</sup>

<sup>1</sup> Community Grids Computing Laboratory, Indiana University, Bloomington, IN, USA  
{ohsangy, leesangm, suko, jaikim, gcf}@indiana.edu

<sup>2</sup> Department of Computer Science, Indiana University, Bloomington, IN, USA

<sup>3</sup> Graduate School of Information and Communications, Ajou University, Suwon, S. Korea  
jaikim@ajou.ac.kr

**Abstract.** Publish/subscribe model is appropriate in many push based data dissemination applications. This paper presents cost model for publish/subscribe systems, analyze its performance, and compare to other interaction-based models such as the client-server model and the polling model. Based on the cost analysis, we have proposed an adaptive model which can dynamically select an appropriate model for each client independently.

## 1 Introduction

Publish/subscribe system [1] have been widely used in many applications [2], [3]. Publish/subscribe system consists of publishers (ES: Event Source), servers (EBS: Event Brokering System), and subscribers (ED: Event Displayer). After a publisher publishes data (events) asynchronously to a server, the server disseminates the data (events) to subscribers which registered their interest on the server. Thus publish/subscribe model is appropriate in many applications such as data dissemination services, information sharing, service discovery, etc. Fig. 1 depicts system configurations.

In this paper, we present cost model for publish/subscribe systems, analyze its performance, and compare to other interaction based models such as a client-server model and a polling models. We can estimate performance and adopt publish/subscribe systems effectively by using our proposed cost model and analysis of publish/subscribe systems. Based on the cost analysis, we propose adaptive model which can dynamically select an appropriate model for each client independently. We believe the adaptive scheme we introduce here is very useful for the mobile and ubiquitous services where characteristics of device and networks are diverse and dynamically changing. We also experimentally measured and compared performance of publish/subscribe model to client/server model

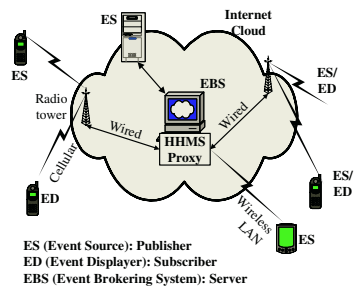


**Fig. 1.** Pub/Sub System Configurations

on our test bed including mobile device and NaradaBrokering [4] (our publish/subscribe based message brokering system) to verify correctness of our model on the real systems. Our cost analysis model is simple but accordant with experimental results.

## 2 Cost Model

### System Models

To evaluate the cost model for different systems, we assume following system parameters to analyze cost:  $\alpha$ , publish rate of event;  $\beta$ , subscriber’s access rate of published events or request rate of client in the client/server models;  $c_{ps}(\alpha)$ , publish/subscribe cost per event,  $c_{pub} + c_{sub}$ ;  $c_{rr}(\beta)$ , cost per request and reply;  $c_{poll}(\alpha, T)$ , cost of periodic publish or polling;  $c_{delay}(\alpha, T)$ , cost of delaying publish;  $s(n)$ , effect of sharing among n subscribers;  $t_{ps}$ , time delay for publish/subscribe,  $t_{pub} + t_{sub}$ ;  $t_{rr}$ , time delay for request and reply;  $t_{poll}(\alpha, T)$ , time delay for periodic publish.

### Cost Analysis

In this analysis, we analyze cost of three different models without any failure of communication link or node. We consider (1) conceptual total cost (e.g., the number of message, amount of message, or time delay) per unit time for each model, (2) cost for each access by client (or subscriber), (3) time delay for access after subscriber’s (or client’s) intention, and (4) time delay between event occurrence and notification to subscriber (or recognition by client). Cost can be the number of message, amount of message, or time delay. Table 2 shows the summary of the cost for each model analyzed in this paper. Please refer to [5] for detailed analysis.

**Table 1.** The cost of the selected model

Model	Publish/Subscribe	Request/Reply	Polling
conceptual total cost per time unit	$\alpha (c_{pub} + n s(n)c_{sub})$	$\beta n c_{rr}$	$(c_{poll}(\alpha, T) + c_{delay}(\alpha, T)) / T$
cost for each access	$\frac{\alpha}{\beta} (\frac{c_{pub}}{n} + c_{sub})$	$c_{rr}$	$c_{poll}(\alpha, T) + c_{delay}(\alpha, T)$
time delay between intention and access	0	$t_{rr}$	$T/2$
time delay between event occurrence and notification/recognition (access)	$t_{ps} = t_{pub} + t_{sub}$ $(t_{ps} = t_{pub} + t_{sub} + \frac{1}{\beta})$	$\frac{1}{2\beta}$	$T/2$

### Adaptive Scheme

Adaptive scheme can choose an appropriate model among publish/subscribe and request/reply models. Each client node can select its own model independently (hybrid model) and change its model during its service (dynamic model).

In this paper, we consider cost per each client’s access as a cost metric. During a period of time, the average number of events occurred per client’s access is measured for each client. At the end of the period, the average cost for each client’s access is

computed using the analysis in section 2, which is  $\frac{\alpha}{\beta}(\frac{c_{pub}}{n} + c_{sub})$ , where  $\frac{\alpha}{\beta}$  is average

number of event occurred per client's access and  $n$  is the number of subscriber. In our adaptive scheme, average number of event and the number of subscriber are obtained experimentally during the execution of application. At the end of the period, the model that is expected to require less cost than the other model during the following period is selected independently for each client. Fig.2 shows that publish/subscribe model is appropriate when the number of client is large and/or the number of event per client's access is small.

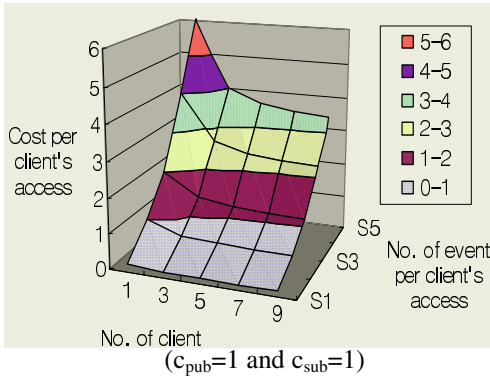
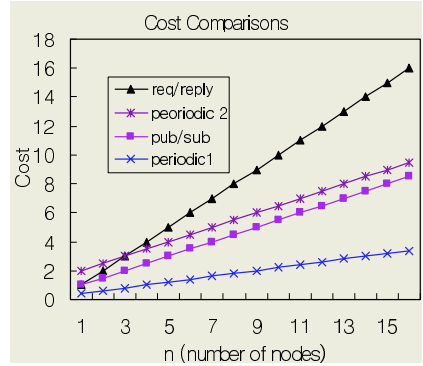


Fig. 2. Cost per client's access of publish / subscribe model



( $\alpha = 0.5, s(n)=1, c_{ps} = 2, \text{ and } c_{rr} = 2;$   
 $c_{pub}(\alpha, T)= c_{pub}, c_{sub}(\alpha, T)= c_{sub}, \text{ and } c_{delay}(\alpha, T)= 0$  for periodic1;  $c_{pub}(\alpha, T)= \alpha T c_{pub},$   
 $c_{sub}(\alpha, T)= \alpha T c_{sub}, c_{delay}(\alpha, T)= 2\alpha T c_{delay}$  for periodic2)

Fig. 3. Communication cost by varying number of clients

### 3 Performance Comparisons

#### Parametric Analysis

In this section, we describe performance comparisons by parametric analysis. We set system parameters as shown in Table 2. Fig.3 shows performance comparisons between publish/subscribe, request/reply, and polling systems. Since publish/subscriber system disseminates data via server instead of individually for each client, it requires less cost than request/reply system. As the number of client node increases, the cost gap between two systems increases. Periodic polling system saves cost by transferring data once per period when delay cost is negligible. However, cost increases as delay cost increases. Polling system is viable approach when data delay is allowed and cost is negligible.

Table 2. Parameters

Param.	Values
$\alpha, \beta$	0.5
$c_{ps}, c_{rr}$	2
$c_{pub}, c_{sub}$	1
$c_{poll}(\alpha, T)$	1 or $\alpha T$
$c_{delay}(\alpha, T)$	0, T, or $\alpha T$
$s(n)$	$1/n - 1$
$t_{ps}, t_{rr}$	1
$t_{proc}$	1 or 5
$t_{poll}(\alpha, T)$	1, T, or $\alpha T$

## Experimental Results

The performance framework consists of NaradaBrokering System and Handheld Message Service (HHMS) [6]. The framework executes test applications – written in J2ME MIPD 2.0 and J2SE. We wrote two applications for two different communication paradigms – pub/sub and Remote Procedure Call (RPC). A client of the first application (ED) echoes message back to the sender (ES). With them, we experimented to perform the test for a cost of message. By varying a size of message, we measured RTT of different size messages. The result is shown in Fig.4. A client of the second application replies ACK back to the sender to measure RTT of different number of mobile clients. The second test was executed with mobile client emulators that come with Sun Microsystems' J2ME WirelessToolkit. This is a limited configuration, but it is still enough to exemplify the analysis we've made in Section 2. We define the data transition time of publish/subscribe and RPC as RTT/2 and RTT respectively from the semantics of each messaging scheme. Experiments are performed on mobile devices – a Samsung SPH-1300 phone and a Treo 600 with Sprint PCS Vision service and Linux machine.

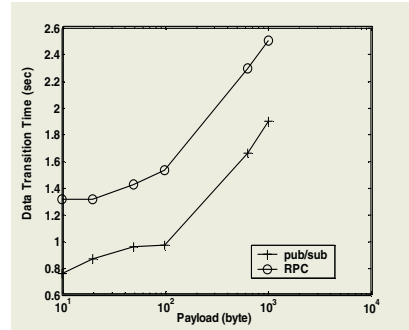


Fig. 4. Latency by Payload

## 4 Conclusions

We presented cost analysis model for publish/subscribe systems. Based on the cost analysis, we proposed an adaptive scheme which can dynamically select an appropriate model for each client independently. Experimental results (delay time) from our test bed were quite similar to our cost analysis models, which verifies that our cost model is useful to select proper model and to design adaptive schemes.

## References

1. P. Eugster, P. Felber, R. Guerraoui, and A. Kermarrec, "The Many Faces of Publish/Subscribe", *ACM Computing Surveys*, vol. 35, no. 2, pp. 114-131, Jun. 2003.
2. A. Rowstron, A. Kermarrec, M. Castro, and P. Druschel. "SCRIBE: The design of a large-scale event notification infrastructure", *Networked Group Communication*, 2001.
3. A. Uyar, S. Pallickara and G. Fox, "Audio Video Conferencing in Distributed Brokering Systems", *Proc. of the International Conf. on Communications in Computing*, June 2003.
4. S. Pallickara and G. C. Fox, "NaradaBrokering: A Middleware Framework and Architecture for Enabling Durable Peer-to-Peer Grids", *Proc. of ACM/IFIP/USENIX International Middleware Conference Middleware*, pp 41-61, 2003.
5. S Oh, S. Lee Pallickara, S. Ko, J. Kim, G. Fox, "Cost Model and Adaptive Scheme for Publish/ Subscribe Systems on Mobile Environments", *Community Grids Lab Technical Report*, Dec. 2004. (<http://grids.ucs.indiana.edu/ptliupages/publications/>)
6. S. Oh, G. C. Fox, S. Ko, "GMSME: An Architecture for Heterogeneous Collaboration with Mobile Devices", *Proc. of the Fifth IEEE/IFIP MWCN 2003*, Singapore, Oct. 2003.

# Near-Optimal Algorithm for Self-configuration of Ad-hoc Wireless Networks

Georgia Tech, Atlanta GA 30332, USA

**Abstract.** To quantify the goodness of a configuration, we develop a probabilistic model of network configuration. A probabilistic graph then represents the statistical dependence in network configuration, and shows that self-configuration can be optimized if the graph has nested local dependence.

## 1 Introduction

## 2 Problem Formulation

$\{X_1, \dots, X_N\}$   $\sigma_{ij}$   $N$   $(i, j)$   $\underline{X} =$   
 $\sigma_{ij}$   $i$   $j$   $\sigma_{ij}$   $-$   
 $(\underline{\sigma}, \underline{X})$   
 $(\underline{X})$   $(\underline{\sigma})$   $( )$   $($   
 $+ ( )$   $( )$   
 $( )$   $(\underline{\sigma}^*, \underline{X}^*)$

$$P(\underline{\sigma}, \underline{X} | \underline{\sigma}_0, \underline{X}_0), \quad \arg \max_{(\underline{\sigma}, \underline{X})}$$

$$g_i(\cdot), \quad \leq i \leq N,$$

$$(\hat{X}_i(t+1), \hat{\sigma}_{ij}(t+1)) = \arg \max_{(X_i(t+1), \sigma_{ij}(t+1))} g_i(X_i(t+1), \sigma_{ij}(t+1) | X_{N_i}(t), \sigma_{N_i}(t)), \quad (1)$$

$$N_i \quad \sigma_{N_i} \quad i \quad \sigma_{ij}$$

### 3 Cross-Layer Model of Network Configuration

$$P(\underline{\sigma}, \underline{X} | \underline{\sigma}_0, \underline{X}_0) \quad P(\underline{\sigma} | \underline{X}, \underline{\sigma}_0, \underline{X}_0) \quad P(\underline{X} | \underline{\sigma}_0, \underline{X}_0)$$

#### 3.1 Link Activities

$$P(\underline{\sigma} | \underline{X}) = P(\underline{\sigma} | \underline{X}, \underline{\sigma}_0, \underline{X}_0)$$

$$U(\underline{\sigma} | \underline{X}) = - \sum_{ij} P_j - \sum_{ij} P_i l_{ij}^{-4} \eta_{ij} + \sum_{ij} \sum_{mn} N_{ij}^I (2\sqrt{P_i P_m} l_{ij}^{-2} l_{mj}^{-2} - P_m l_{mj}^{-4}) \eta_{ij} \eta_{mn} - \sum_{ij} \sum_{mn} N_{ij}^I \sum_{uv} \{N_{ij}^I, N_{mn}^I\} 2\sqrt{P_m P_u} l_{mj}^{-2} l_{uj}^{-2} \eta_{ij} \eta_{mn} \eta_{uv} + R_I(\underline{\sigma}, \underline{X}) + R_3(\underline{\sigma}, \underline{X}) + \beta \cdot \sum_{ij} \|\text{SINR}_{ij} - \text{SINR}_{th}\|, \quad \eta_{ij} \quad (\sigma_{ij} + ) / N_{ij}^M \quad \sigma_{ij} \quad N_{ij}^I$$

$$P_{th} \leq P_m \cdot l_{mj}^{-4}$$

$$R_{I_{ij}}(\underline{\sigma}, \underline{X}) \quad R_I(\underline{\sigma}, \underline{X}) = \sum_{ij} R_{I_{ij}}(\underline{\sigma}, \underline{X}),$$

$$U(\underline{\sigma} | \underline{X}) \quad P(\underline{\sigma} | \underline{X})$$

$$P(\underline{\sigma} | \underline{X}) = \exp \frac{-U(\underline{\sigma} | \underline{X})}{T} / \sum_{\underline{\sigma}} \exp \frac{-U(\underline{\sigma} | \underline{X})}{T}.$$

### 3.2 Random Position of Nodes

$$P(\underline{X}|\underline{\sigma}_0, \underline{X}_0) = P(\underline{X}|\underline{X}_0) \cdot \frac{P(\underline{X}|\underline{X}_0)}{U(\underline{X}|\underline{X}_0)} = \frac{P(\underline{X}|\underline{X}_0)}{2\sigma^2} \cdot \frac{P(\underline{X}|\underline{X}_0)}{U(\underline{X}|\underline{X}_0)}$$

$$U(\underline{X}|\underline{X}_0) = \frac{P(\underline{X}|\underline{X}_0)}{\sigma^2} = \frac{(X - X_0)^T \cdot (X - X_0)}{U(\underline{X}|\underline{X}_0)}$$

$$C(X_i, X_j) = \begin{cases} 0 & , \frac{|l_{ij} - l_{th}|}{l_{th}} < \epsilon_0 \text{ or } j \notin N_i \\ |l_{ij} - l_{th}| & , \text{otherwise} \end{cases} \quad (2)$$

$$\sum_i \sum_j \zeta \cdot C(X_i, X_j) \cdot U(\underline{X}|\underline{X}_0) = \sum_i \zeta \cdot \theta \left( \frac{\epsilon_0}{\theta} \right)$$

$$f_{P_1}(\underline{\sigma}, \underline{X}) = \|\underline{\sigma}, \underline{X}\| - \|\underline{\sigma}_0, \underline{X}_0\|$$

$$C(X_i, X_j) = C(X_i, X_j) + C_1 \cdot f_{P_1}(\underline{\sigma}, \underline{X}) \quad C_1$$

### 3.3 Graphical Representation of Network Configuration

$$\left( \right) Z_0^{-1} \cdot \frac{\underline{X}}{T} = \frac{-U(\underline{X})}{T}$$

$$R_I(\underline{\sigma}, \underline{X}) \quad R_3(\underline{\sigma}, \underline{X})$$

$$P^l(\underline{\sigma}|\underline{X}) \quad P^l(\underline{\sigma}|\underline{X}) = \frac{1}{\theta} \cdot \exp\left(-\sum_{ij} \alpha_{ij}(\underline{X}) \cdot \frac{\sigma_{ij}+1}{2} - \sum_{mn} N_{ij}^I \alpha_{ij,mn}(\underline{X}) \cdot \frac{\sigma_{mn}+1}{2} \frac{\sigma_{ij}+1}{2}\right) / T$$

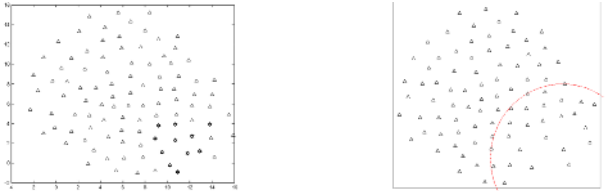
$$(\underline{\sigma}|\underline{X})$$



$$U(\underline{X}|\underline{X}_0) = \prod_{i=1}^N \prod_{j=1}^N P^l(X_{ij}(t+1), \sigma_{ij}(t+1) | X_{ij}(t), \sigma_{ij}(t)) \quad (1)$$

### 4 Self-configuration: Distributed Algorithm and Failure-Recovery

$$P^l(X_{ij}(t+1), \sigma_{ij}(t+1) | X_{ij}(t), \sigma_{ij}(t)) = \arg \max_{(X_{ij}(t+1), \sigma_{ij}(t+1))} P^l(X_{ij}(t+1), \sigma_{ij}(t+1) | X_{N_i}(t), \sigma_{N_i}(t)) \quad (2)$$



(a) Self-configuration and Failure Event (b) After Self-Recovery of  $\underline{X}$

Fig. 1. Self-Recovery with Local Optimal Algorithm

### 5 Conclusion

( )

**Acknowledgement.** This work was supported by the National Science Foundation (NSF) Grant IRI-0325317. The authors would like to thank the anonymous reviewers for their helpful comments.

## References

1. S. Geman, and D. Geman, Stochastic Relaxation, Gibbs Distributions, and the Bayesian Restoration of Images. IEEE Trans. PAMI vol. 6, 1984.
2. K. Huang, Statistical Mechanics. John Wiley & Sons.
3. R. Wattenhofer, L. Li, P. Bahl, and Y. Wang, Distributed topology control for power efficient operation in multihop wireless networks. In Proc. IEEE Infocom, 2001

# The Applications of Meshfree Particle Methods at the Nanoscale

Weixuan Yang and Shaoping Xiao

Department of Mechanical and Industrial Engineering and Center for Computer-Aided Design, The University of Iowa, 3131 Seamans Center, Iowa City, IA, 52241-1527, USA  
{weixuan-yang, shaoping-xiao}@uiowa.edu

**Abstract.** Since meshfree particle methods are beneficial in simulating the problems involving extremely large deformations, fractures, etc., these methods become attractive options in multiscale modeling, especially when approaching a large number of atoms. In this paper, we propose preliminary research on applying meshfree particle methods to solve nanoscale problems. A quasicontinuum technique, i.e. the Cauchy-Born rule, is implemented into the meshfree particle methods so continuum approaches for large deformation problems or fracture problems at the nanoscale can be performed. Furthermore, the meshfree particle methods can be coupled with molecular dynamics via the bridging domain coupling technique. The examples show that the meshfree particle methods can benefit either hierarchical or concurrent multiscale modeling at the nanoscale.

## 1 Introduction

With the development of nanotechnology, numerical simulation plays an important role in nanoscale material and device design. To develop a potential numerical method, which can efficiently model micro/nano systems, has been one of the forefront research topics of computational nanotechnology.

Among a variety of numerical simulation techniques, molecular dynamics (MD) has become a powerful tool to elucidate complex physical phenomena [1-2]. Up to billions of atoms can be simulated by MD when studying the crack propagation [2] at the atomistic level with parallel computing techniques. However, most MD simulations are still restricted on both small length and short time scales. Therefore, multiscale methods have been of more and more interest to simulate large nanoscale systems. The recently developed multiscale methods can be divided into two classes: hierarchical multiscale methods [3] and concurrent multiscale methods [4-7]. In hierarchical multiscale modeling, the continuum approximation is based on the properties of a subscale model, such as a MD model. The intrinsic properties of materials are sought at the atomic level and embedded in the continuum model according to the quasicontinuum technique, which is also called the Cauchy-Born rule [8-9]. The Cauchy-Born rule states that the deformation is locally homogeneous.

Concurrent multiscale methods use an appropriate model to solve each length scale simultaneously. Recently, some concurrent multiscale techniques [4-6], particularly coupling methods between the continuum model and the molecular model, have been

developed. One of the key issues the concurrent multiscale methods must overcome is the occurrence of spurious numerical phenomena, such as non-physical reflections on the interfaces between the molecular and continuum models. Most researchers use the Langevin equation [6] or other filtering processes to eliminate spurious reflections. Xiao and Belytschko developed a bridging domain coupling method [7], which can eliminate the spurious wave reflection automatically.

Mostly, finite element methods are used in the hierarchical or concurrent multiscale methods with the implementation of the quasicontinuum technique. It is known that the meshfree particle methods [10] are more attractive for a variety of problems with moving boundaries, discontinuities, and extremely large deformations. Therefore, the incorporation of the meshfree particle methods and the quasicontinuum technique will have much potential to solve the above problems at the nanoscale. Belytschko and Xiao [11] found that the meshfree particle methods with Lagrangian kernels are more stable than those with Eulerian kernels. In this paper, only the meshfree particle methods with Lagrangian kernels are considered. With the implementation of the quasicontinuum method, the meshfree particle methods can be used to simulate large nano systems. Furthermore, based on the idea of the bridging domain coupling method [7], the meshfree particle methods can be coupled with molecular dynamics to accomplish a multiscale modeling for large nano systems.

The outline of this paper is as follows: We will introduce the meshfree particle methods; The Cauchy-Born rule will then be implemented into the meshfree particle methods, which can also be coupled with molecular dynamics; Several examples are studied in the following section and the last section presents the conclusions.

## 2 Meshfree Particle Methods at the Nanoscale

### 2.1 Discrete Equations

The physical principles governing the continuum are the conservation of mass, momentum and energy. A so-called total Lagrangian description is employed (see Belytschko, Liu and Moran [12]); therefore, the linear momentum equations are

$$\frac{\partial P_{ji}}{\partial X_j} + \rho_0 b_i = \rho_0 \ddot{u}_i \quad (1)$$

where  $\rho_0$  is the initial density,  $\mathbf{P}$  is the first Piola-Kirchhoff stress tensor,  $\mathbf{X}$  is the reference coordinates,  $\mathbf{b}$  is the body force per unit mass,  $\mathbf{u}$  is the displacement and the superposed dots denote material time derivatives. The weak form of the momentum conservation equation is

$$\int_{\Omega_0} \delta u_i \rho_0 \ddot{u}_i d\Omega_0 = \int_{\Omega_0} \delta u_i \rho_0 b_i d\Omega_0 - \int_{\Omega_0} \delta F_{ij} P_{ji} d\Omega_0 + \int_{\Gamma_0} \delta u_i \bar{t}_i d\Gamma_0 \quad (2)$$

where  $\Omega_0$  is the reference configuration,  $\delta u_i$  is the test function,  $F_{ij}$  is the gradient of deformation and  $\bar{t}_i$  is the prescribed boundary traction. The particle approximation is

$$u_i(\mathbf{X}, t) = \sum_I w_I(\mathbf{X}) u_{iI}(t) . \tag{3}$$

where  $w_I(\mathbf{X})$  is a Lagrangian kernel function, which is the function of reference coordinates. With a similar expansion for  $\delta \mathbf{u}(\mathbf{X})$ , the following discrete equations can be obtained:

$$M_I \ddot{u}_{iI} = F_{iI}^{ext} - F_{iI}^{int} , \quad M_I = \rho_0 V_I^o . \tag{4}$$

where  $V_I^o$  is the volume associated with particle  $I$  in the reference configuration.  $F_{iI}^{ext}$  and  $F_{iI}^{int}$  are the external and internal nodal forces, respectively, given by

$$F_{iI}^{ext} = \int_{\Omega_0} \rho_0 w_I b_i d\Omega_0 + \int_{\Gamma_0^t} N_I \bar{t}_i d\Gamma_0 , \quad F_{iI}^{int} = \int_{\Omega_0} \frac{\partial w_I(\mathbf{X})}{\partial X_j} P_{ji} d\Omega_0 \tag{5}$$

If the nodal integration scheme [11] is used in the meshfree particle methods, the internal nodal forces in (5) can be calculated by

$$F_{iI}^{int} = \sum_J V_J^o \frac{\partial w_I(\mathbf{X}_J)}{\partial X_j} P_{ji}(\mathbf{X}_J) . \tag{6}$$

The Nodal integration scheme may result in one of instabilities due to the rank deficiency. A stress point integration scheme [11] can be used to stabilize it.

### 2.2 Implementation of the Quasicontinuum Technique

In a continuum model, the potential energy depends on the elongations and angle changes of the bonds at the atomistic level. The total potential of the continuum model can be written as

$$W^C = \int_{\Omega_0} w_C d\Omega \tag{7}$$

where  $w_C$  is the potential energy per unit volume. Then, the first Piola-Kirchhoff stress can be obtained from the potential of the continuum by

$$\mathbf{P} = \frac{\partial w_C(\mathbf{F})}{\partial \mathbf{F}} . \tag{8}$$

where  $\mathbf{F}$  is the deformation gradient. In this paper, it is assumed the molecular structure in the volume associated with each particle is under a constant deformation gradient. Therefore, the first Piola-Kirchhoff stress at each particle can be evaluated through (8). In other words, (8) serves as the constitutive equation for meshfree particle methods at the nanoscale. For curved monolayer crystalline membranes such as nanotubes, an extension of the Cauchy-Born rule, called the exponential Cauchy-Born rule, can be used (see Arroyo and Belytschko [9]).

### 2.3 Coupling with Molecular Dynamics

Belytschko and Xiao [7] proposed a multiscale method called the bridging domain coupling method, in which, the molecular model and the continuum model overlap at their junctions in a bridging domain.

In this paper, molecular dynamics and the meshfree particle method are coupled via the bridging domain coupling technique. The complete domain in the initial configuration is denoted by  $\Omega_0$ . The domain is subdivided into the subdomain treated by continuum mechanics,  $\Omega_0^C$ , and the one treated by molecular dynamics,  $\Omega_0^M$ . The intersection of these two subdomains is called the bridging domain denoted by  $\Omega_0^{int}$  in the initial configuration. The bridging domain multiscale modeling of a molecular chain is shown in Figure 1.

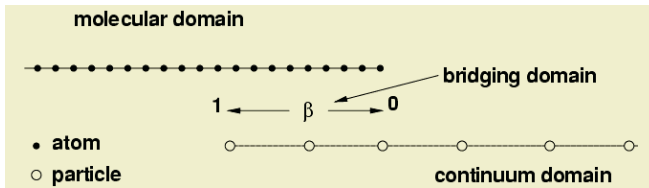


Fig. 1. A Bridging domain coupling model for a molecular chain

In expressing the total Hamiltonian of the system we employ a scaling parameter  $\beta$  in the bridging domain as shown in Figure 1. The scaling parameter  $\beta$  vanishes at one end of the bridging domain and is unity at another end. Therefore, the Hamiltonian for the complete domain is taken to be a linear combination of the molecular and continuum Hamiltonians

$$\begin{aligned}
 H = \beta H^M + (1 - \beta)H^C = & \sum_I \beta(\mathbf{x}_I) \frac{\mathbf{p}_I^M \cdot \mathbf{p}_I^M}{2m_I} + \beta W^M \\
 & + \sum_I (1 - \beta(\mathbf{x}_I)) \frac{\mathbf{p}_I^C \cdot \mathbf{p}_I^C}{2M_I} + (1 - \beta)W^C
 \end{aligned} \tag{9}$$

where  $W^M$  is the potential in the molecular model, and  $W^C$  is the strain energy in the continuum model. The discrete equations can be obtained via the classical Hamiltonian mechanics. The details can be found in [7].

## 3 Examples

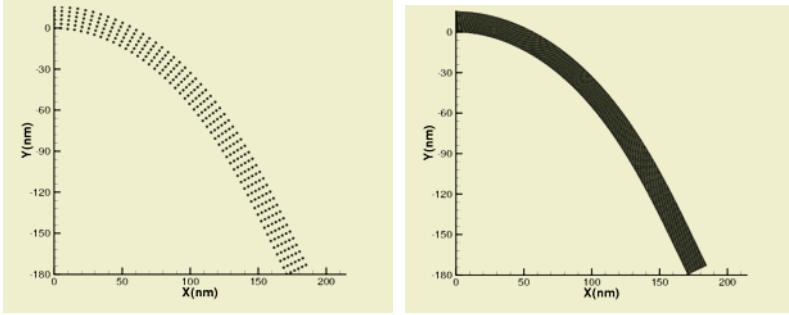
### 3.1 Bending of a Nano Beam

The bending of a nano cantilever beam is considered in this example. The nano beam contains 5,140 atoms and the dimensions are: length  $L=270nm$  and height  $H=15.6nm$ .

A pair potential function is used to approximate the interaction between nearest atoms,

$$U(l) = 0.5k(l - l_0)^2 \tag{10}$$

where  $k = 10000N/m$  and  $l_0 = 1nm$ .



(a) The meshfree particle method (b) The molecular mechanics calculation

**Fig. 2.** Deformed configurations of the nanobeam

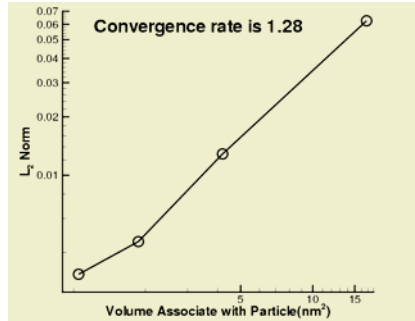


**Fig. 3.** Convergence of the nanoscale meshfree particle method

We use the meshfree particle method with 250 particles to simulate the bending of this nano beam. The prescribed displacement is applied on the right upper corner of the beam. The final configuration of the nano beam is shown in Figure 2(a). Figure 2(b) shows the deformed beam when performing the molecular mechanics calculation, and it supports the meshfree particle method result. As shown in figure 3, the convergence is also studied by using the  $l_2$  error in displacement for the meshfree particle method.

### 3.2 A Nano Plate with a Central Crack

Meshfree particle methods are advantageous to simulate fracture problems. In this example, the meshfree particle method is used to study the stress concentration of a

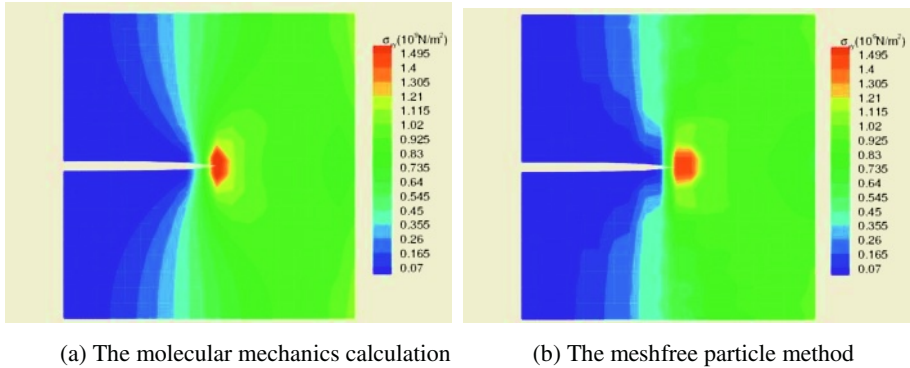


**Fig. 4.** Comparison of stress concentration at the crack tip

nano plate containing an central crack. This nano plate contains 86,915 atoms with the triangular molecular structure. The dimensions are:  $L = 270nm$  and  $M = 280nm$ , and the crack length is  $135nm$ . The crack is initialized by taking a number of bonds out. The meshfree particle model has 400 particles, and a visibility criterion is used to construct the kernel functions for the particles near the crack or around the crack tip. Figure 4 shows the comparison of the stress ( $\sigma_{yy}$ ) contour obtained from the molecular mechanics calculation with the one from the meshfree particle method. It can be seen that they are in accord.

### 3.3 Wave Propagation in a Molecular Chain

In this example, the wave propagation in a molecular chain, which contains 2001 atoms, is simulated. The LJ 6-12 potential function is used as the interatomic potential function between the nearest atoms, and it is

$$w_M = 4\epsilon\left[\left(\frac{\sigma}{r}\right)^{12} - \left(\frac{\sigma}{r}\right)^6\right]. \quad (11)$$

where the constants are chosen as:  $\sigma = 3.4e^{-10}m$  and  $\epsilon = 1.65e^{-21}J$ . The mass of each atom is set to be  $3.8 \times 10^{-10}kg$ .

In the bridging domain coupling modeling of this molecule chain, there are 1001 atoms in the molecular domain and 200 particles in the continuum domain. The initial wave is the combination of high frequency and low frequency waves and starts to propagate from the molecular domain. A non-physical phenomenon, shown in Figure 5(a), can be observed if using a handshake coupling technique [4] without the application of the artificial viscosity. It is possible to see that the high frequency wave is reflected while the low frequency wave passes the continuum domain. Such a phenomenon is also called the spurious wave reflection. However, with the bridging domain coupling technique, the spurious wave reflection can be eliminated as shown in Figure 5(b).



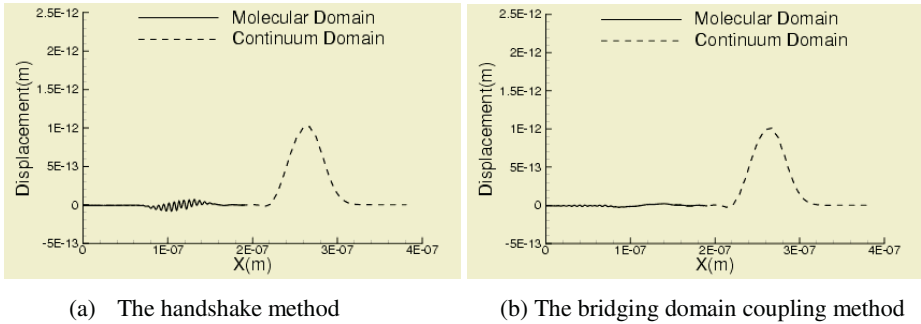


Fig. 5. Multiscale simulations on the wave propagation in a molecular chain

## 4 Conclusions

In this paper, the quasicontinuum technique (the Cauchy-Born rule) was implemented into the meshfree particle methods. Therefore, numerical simulations in nanotechnology can be valuable in regards to the meshfree particle methods. This progress makes it possible to treat extremely large deformation problems and the problems involving discontinuities, such as fractures, at the nanoscale. The examples showed that the nanoscale meshfree particle methods can give accurate results when compared with the molecular mechanics calculation outcomes. In addition, the meshfree particle methods can be coupled with molecular dynamics via the bridging domain coupling technique. The spurious wave reflection can be eliminated without any additional filtering processes.

## References

1. Rountree, C. L., Kalia, R. K., Lidorikis, E., Nakano, A., Van, B. L., Vashishta, P.: Atomistic aspects of crack propagation in brittle materials: Multimillion atom molecular dynamics simulation. *Annu. Rev. Mater. Res.* 32(2002) 377-400
2. Abraham, F. F., Gao, H.: How fast can crack move. *Phys. Rev. Lett.* 84(2000) 3113-3116
3. Tadmor, E. B., Phillips, R., Ortiz, M.: Hierarchical modeling in the mechanics of materials. *Int. J. Solids Struct.* 37 (2000) 379-389
4. Abraham, F., Broughton, J., Bernstein, N., Kaxiras, E.: Spanning the continuum to quantum length scales in a dynamic simulation of brittle fracture. *Europhys. Lett.* 44(1998), 783-787
5. Rudd, R. E., Broughton, J. Q.: Coarse-grained molecular dynamics and the atomic limit of finite elements. *Phys. Rev. B.* 58(1998) R5893-R5896
6. Wagner, G. J., Liu, W. K.: Coupling of atomic and continuum simulations using a bridging scale decomposition. *J. Comp. Phys.* 190(2003) 249-274
7. Xiao, S., Belytschko, T.: A bridging domain method for coupling continua with molecular dynamics. *Comput. Method Appl. M.* (2004) in press
8. Tadmor, E. B., Ortiz, M., Phillips, R.: Quasicontinuum analysis of defects in solids. *Philos. Mag. A* 73(1996) 1529-1563

9. Arroyo, M., Belytschko, T.: A finite deformation membrane based on inter-atomic potentials for the transverse mechanics of nanotubes. *Mech. Mater.* 35(2003) 193-215
10. Belytschko, T., Krongauz, K., Organ, D., Fleming, M., Krysl, P.: Meshless methods: An overview and recent developments. *Comput. Method Appl. M.* 139(1996) 3-47
11. Belytschko, T., Xiao, S.: Stability analysis of particle methods with corrected derivatives. *Comput. Math. Appl.* 43(2002) 329-350
12. Belytschko, T., Liu, W. K., Moran, B.: *Nonlinear Finite Elements for Continua and Structures*. Wiley, New York (2000)

# Numerical Simulation of Self-heating InGaP/GaAs Heterojunction Bipolar Transistors

1,2

3

<sup>1</sup> Department of Computational Nanoelectronics,  
National Nano Device Laboratories, Hsinchu 300, Taiwan

<sup>2</sup> Microelectronics and Information Systems Research Center,  
National Chiao Tung University, Hsinchu 300, Taiwan  
ymli@faculty.nctu.edu.tw

<sup>3</sup> Institute of Electronics, National Chiao Tung University,  
Hsinchu 300, Taiwan

**Abstract.** We numerically simulate effects of the self-heating on the current-voltage characteristics of InGaP/GaAs heterojunction bipolar transistors (HBTs). A set of coupled nonlinear ordinary differential equations (ODEs) of the equivalent circuit of HBT is formed and solved numerically in the large-signal time domain. We decouple the corresponding ODEs using the waveform relaxation method and solve them with the monotone iterative method. The temperature-dependent energy band gap, the current gain, the saturation current, and the thermal conductivity are considered in the model formulation. The power-added efficiency and the 1-dB compression point of a three-finger HBT are calculated. This approach successfully explores the self-heating and the thermal coupling phenomena of the three-finger transistors under high power and high frequency conditions. The numerical algorithm reported here can be incorporated into electronic computer-aided design software to simulate ultra-large scale integrated and radio frequency circuits.

## 1 Introduction

Self-heating in bipolar transistors is a significant problem in high power and high frequency applications. The self-heating effect is caused by the power dissipation in the device, which leads to an increase in the junction temperature. This temperature increase affects the carrier transport properties, the current gain, and the thermal conductivity of the device. In this paper, we present a numerical simulation of the self-heating effect in InGaP/GaAs heterojunction bipolar transistors (HBTs). The simulation is based on a set of coupled nonlinear ordinary differential equations (ODEs) that describe the current-voltage characteristics of the device. The ODEs are solved numerically in the large-signal time domain using the waveform relaxation method and the monotone iterative method. The simulation results show that the self-heating effect significantly affects the current-voltage characteristics of the device, especially at high power and high frequency conditions. The power-added efficiency and the 1-dB compression point of a three-finger HBT are calculated and compared with the results obtained from a conventional small-signal model. The simulation results show that the self-heating effect reduces the power-added efficiency and the 1-dB compression point of the device. This approach successfully explores the self-heating and the thermal coupling phenomena of the three-finger transistors under high power and high frequency conditions. The numerical algorithm reported here can be incorporated into electronic computer-aided design software to simulate ultra-large scale integrated and radio frequency circuits.

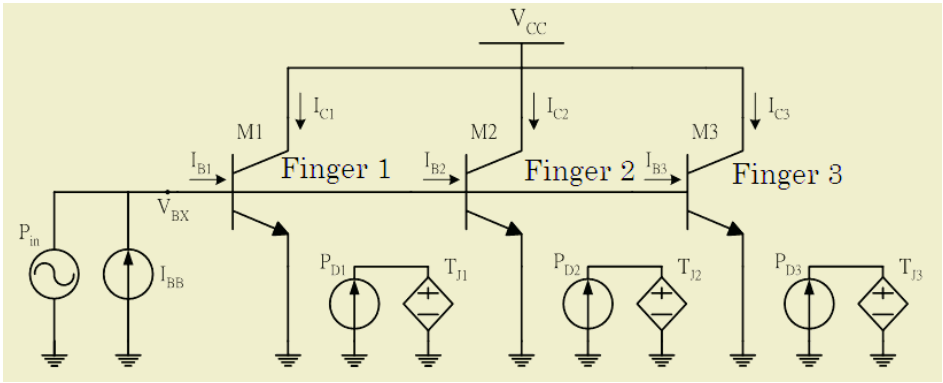


**Fig. 1.** An equivalent circuit of the simulated three-finger HBT under constant current and high frequency excitations

( ),  $P_{D1}, P_{D2}, P_{D3}$  are the power dissipation of Finger 1, Finger 2, and Finger 3, respectively.  $T_{J1}, T_{J2}, T_{J3}$  are the junction temperatures of Finger 1, Finger 2, and Finger 3, respectively. The equivalent circuit is shown in Fig. 1. The base current  $I_{BB}$  and the collector current  $I_{C1}, I_{C2}, I_{C3}$  are constant. The base voltage  $V_{BX}$  is a high frequency sinusoidal signal. The output voltage  $V_{out}$  is the average value of the output voltage of the three fingers. The power dissipation  $P_{D1}, P_{D2}, P_{D3}$  is the average value of the power dissipation of the three fingers.

## 2 Self-heating Modeling and Numerical Method

The self-heating effect is modeled by a thermal network. The thermal network is shown in Fig. 2. The thermal capacitance  $C_{th}$  is the thermal capacitance of the junction. The thermal resistance  $R_{th}$  is the thermal resistance between the junction and the ambient. The thermal capacitance  $C_{th}$  and the thermal resistance  $R_{th}$  are given by [1]:

$$C_{th} = \frac{E_a}{T_A} \quad (1)$$

where  $E_a$  is the activation energy of the semiconductor material,  $T_A$  is the ambient temperature.

$$E_g(T_J) = E_g(T_A) + \frac{E_a \cdot T_A^2}{T_A + E_b} + \frac{E_a \cdot T_J^2}{T_J + E_b} \quad (2)$$

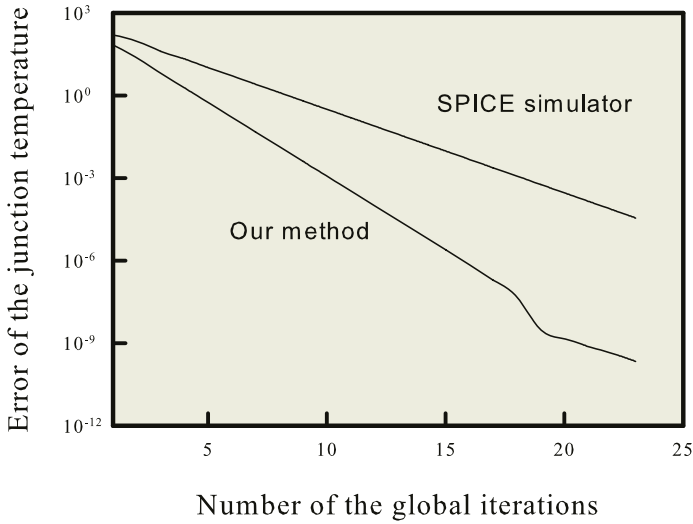


**Fig. 2.** A plot of the maximum norm error of the junction temperature versus the number of iterations of the WR loop

$$IS(T_J) = IS \cdot \left(\frac{T_J}{T_A}\right)^{XTI} \cdot \exp\left(\frac{E_g(T_A)}{k \cdot T_A}\right) - \left(\frac{E_g(T_J)}{k \cdot T_J}\right), \quad ( )$$

$$ISE(T_J) = ISE \cdot \left(\frac{T_J}{T_A}\right)^{\frac{XTI}{NE} - XTB} \cdot \exp\left(\frac{E_g(T_A)}{NE \cdot k \cdot T_A}\right) - \left(\frac{E_g(T_J)}{NE \cdot k \cdot T_J}\right), \quad ( )$$

$$ISC(T_J) = ISC \cdot \left(\frac{T_J}{T_A}\right)^{\frac{XTI}{NC} - XTB} \cdot \exp\left(\frac{E_g(T_A)}{NC \cdot k \cdot T_A}\right) - \left(\frac{E_g(T_J)}{NC \cdot k \cdot T_J}\right), \quad ( )$$

$$BF(T_J) = BF \cdot \left(\frac{T_J}{T_A}\right)^{XTB}, \quad ( )$$

$$BR(T_J) = BR \cdot \left(\frac{T_J}{T_A}\right)^{XTB}, \quad ( )$$

$$\begin{aligned} T_J &= T_A + \dots + T_A \cdot \dots + T_A \cdot \dots \\ (E_g) &= \dots + (IS) \cdot \dots + \dots \\ (ISC \quad ISE) &= \dots + (BF \quad BR) \cdot \dots \end{aligned}$$

$$\mathbf{T}_J = T_A \left\{ -\frac{(BB-)}{T_A} \mathbf{R}_{TH} \cdot \mathbf{P}_D \right\}^{\frac{-1}{BB-1}} \begin{bmatrix} T_{J1} \\ T_{J2} \\ T_{J3} \end{bmatrix}, \quad ( )$$

$$T_{Jn} \dots \dots \dots n^{th} \dots \dots n \dots \dots \mathbf{R}_{TH} \cdot \mathbf{P}_D$$

$$\mathbf{R}_{TH} \cdot \mathbf{P}_D = \begin{bmatrix} R_{T11} & R_{T12} & R_{T13} \\ R_{T21} & R_{T22} & R_{T23} \\ R_{T31} & R_{T32} & R_{T33} \end{bmatrix} \cdot \begin{bmatrix} P_{D1} \\ P_{D2} \\ P_{D3} \end{bmatrix}. \quad ( )$$

$$\begin{matrix} R_{Tnn} & R_{Tnm} & & & & & n^{th} \\ & & & & & & m^{th} \\ & n^{th} & & & & & \\ n^{th} & & P_{Dn} & & & & \\ & & & M & M & M & \\ & & & & & & \\ & & I_{BB} & & & & \\ P_{in} & & & & & & \end{matrix}$$

### 3 Results and Discussion

$$m A, \quad V_{CC} = V, \quad GHz, \quad I_{BB} = -11V$$

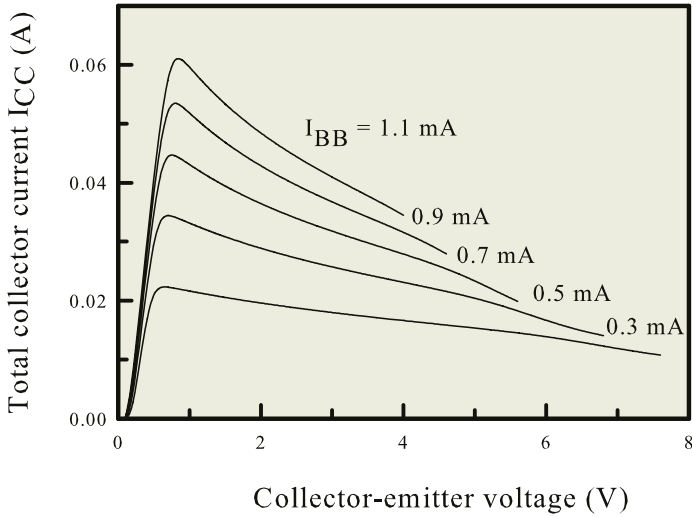


**Fig. 3.** The curves of  $I_{CC}-V_{CE}$  with respect to different  $I_{BB}$  for the simulated three-finger InGaP/GaAs HBT circuit. It is significantly different from the result without considering the self-heating [7], [8], [9]

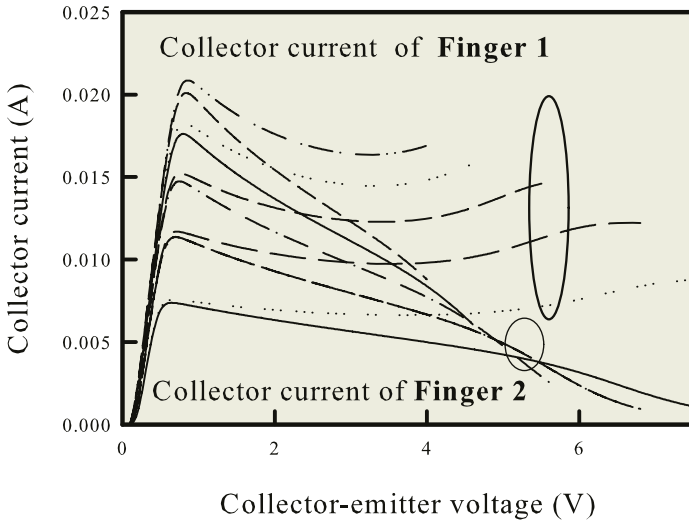


**Fig. 4.** The simulated  $I_{CC}-V_{CE}$  curves with respect to different  $I_{BB}$  for the fingers 1 and 2 of the HBT. The result of Finger 3 is omitted according to the property of symmetry

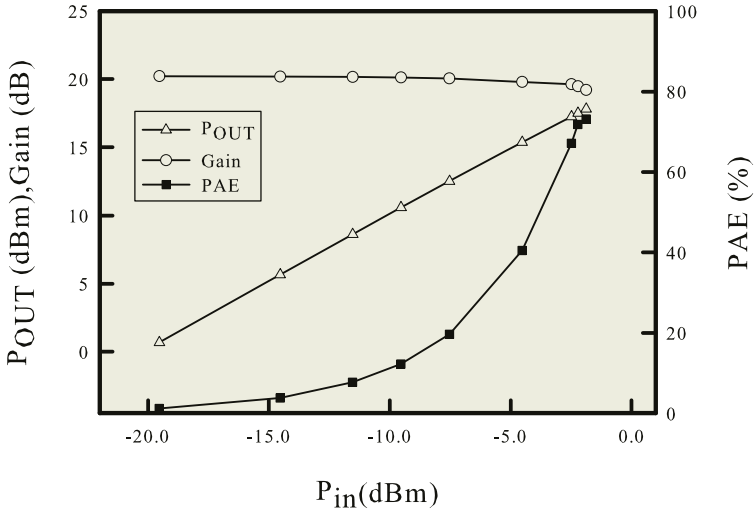


Fig. 5. The computed  $P_{OUT}$ , PAE, and Gain versus  $P_{in}$

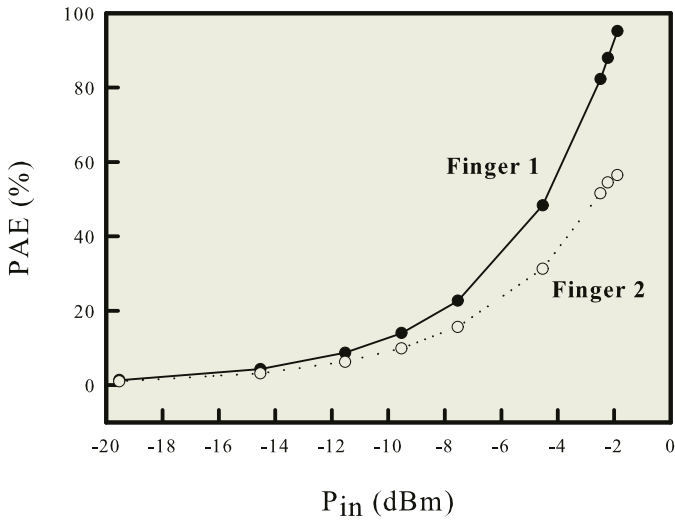
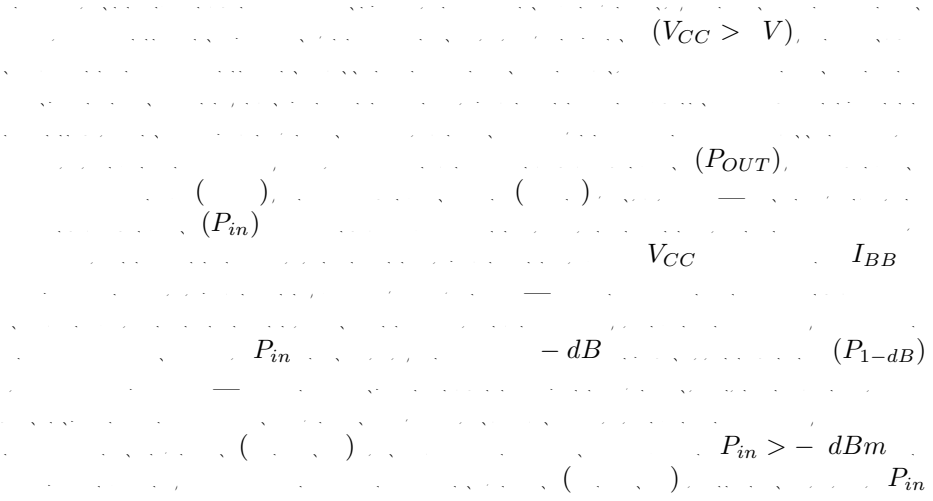


Fig. 6. Plots of the PAE of Fingers 1 and 2 versus the input power

$I_{BB}$

( )





#### 4 Conclusions

#### Acknowledgments

#### References

1. Yanagihara, M., Sakai, H., Ota, Y., Tamura, A: High  $f_{max}$  AlGaAs/GaAs HBT with L-shaped base electrode and its application to 50 GHz amplifier. Solid-State Electron. 41 (1997) 1615-1620

2. Oka, T., Hirata, K., Suzuki, H., Ouchi, K., Uchiyama, H., Taniguchi, T., Mochizuki, K., Nakamura, T.: High-speed small-scale InGaP/GaAs HBT technology and its application to integrated circuits. *IEEE Trans. Electron Devices*. 48 (2001) 2625-2630
3. Troyanovsky, B., Yu, Z., Dutton, R. W.: Physics-based simulation of nonlinear distortion in semiconductor devices using the harmonic balance method. *Comput. Methods Appl. Mech. Engrg.* 181 (2000) 467-482
4. Zhu, Y., Twynam, J. K., Yagura, M., Hasegawa, M., Hasegawa, T., Eguchi, Y., Amano, Y., Suematsu, E., Sakuno, K., Matsumoto, N., Sato, H., Hashizume, N.: Self-heating effect compensation in HBTs and its analysis and simulation. *IEEE Trans. Electron Devices*. 48 (2001) 2640-2646
5. Heckmann, S., Sommet, R., Nebus, J.-M., Jacquet, J.-C., Floriot, D., Auxemery, P., Quere, R.: Characterization and modeling of bias dependent breakdown and self-heating in GaInP/GaAs power HBT to improve high power amplifier design. *IEEE Trans. Microwave Theory and Techniques* 50 (2002) 2811-2819
6. Park, H.-M., Hong, S.: A novel temperature-dependent large-signal model of heterojunction bipolar transistor with a unified approach for self-heating and ambient temperature effects. *IEEE Trans. Electron Devices*. 49 (2002) 2099-2106
7. Li, Y., Cho, Y.-Y., Wang, C.-S., Hung, K.-Y.: A Genetic Algorithm Approach to InGaP/GaAs HBT Parameters Extraction and RF Characterization. *Jpn. J. Appl. Phys.* 42 (2003) 2371-2374
8. Huang, K.-Y., Li, Y., Lee, C.-P.: A Time Domain Approach to Simulation and Characterization of RF HBT Two-Tone Intermodulation Distortion. *IEEE Trans. Microwave Theory and Techniques*. 51 (2003) 2055-2062
9. Li, Y., Kuang, K.-Y.: A Novel Numerical Approach to Heterojunction Bipolar Transistor Circuit Simulation. *Comput. Phys. Commun.* 152 (2003) 307-316
10. Li, Y.: A Monotone Iterative Method for Bipolar Junction Transistor Circuit Simulation. *WSEAS Trans. Mathematics*. 1 (2002) 159-164
11. Liu, W.: *Handbook of III-V Heterojunction Bipolar Transistor*. John Wiley & Sons (1998)

# Adaptive Finite Volume Simulation of Electrical Characteristics of Organic Light Emitting Diodes

Yiming Li<sup>1,2</sup> and Pu Chen<sup>2</sup>

<sup>1</sup> Department of Computational Nanoelectronics, National Nano Device Laboratories,  
Hsinchu 300, Taiwan

<sup>2</sup> Microelectronics and Information Systems Research Center, National Chiao Tung University,  
Hsinchu 300, Taiwan  
ymli@faculty.nctu.edu.tw

**Abstract.** In this paper a two-dimensional simulation of organic light emitting devices (OLEDs) using an adaptive computing technique is presented. A set of drift-diffusion equations including models of interface traps is solved numerically to explore the transport property of OLED structures. The adaptive simulation technique is mainly based on the Gummel's decoupling algorithm, a finite volume approximation, a monotone iterative method, a posteriori error estimation, and an unstructured meshing scheme. With this computational approach, we investigate the intrinsic and terminal voltage-current characteristics of OLEDs with respect to different material parameters, thickness of materials, and length of structure.

## 1 Introduction

Organic electroluminescence has been of great interest in various display applications. Organic light emitting diode (OLED) displays are lightweight, durable, power efficient and ideal for portable applications [1]. They have lower material costs and fewer processing steps than their liquid crystal display (LCD) counterparts. As such, the OLED display appears to be a strong candidate as a replacement technology in a variety of mobile application areas. OLEDs with different thin-film structures, consisting of emitter and carrier transport layers, have recently been reported [2], [3], [4], [5], [6]. According to the simple device geometry in OLEDs, one-dimensional (1D) transport model, the drift-diffusion model, has generally been solved along the transport direction for studying the electrical properties of OLEDs [4], [5], [6]. However, a multidimensional modeling and simulation plays a crucial role for exploring the effect of device structure and material on the electrical characteristics of OLEDs.

In this paper a set of drift-diffusion (DD) equations is solved with an adaptive computing technique [7], [8], [9], [10] for a two-dimensional (2D) simulation of OLEDs. For the simulation of OLEDs, the DD equations consist of the Poisson equation, the current continuity equation of electron, the current continuity equation of hole, and models of interface traps. First of all we decouple the three partial differential equations (PDEs) according to the Gummel's procedure. Based on adaptive unstructured mesh and finite volume (FV) approximation, each decoupled PDE is discretized and then solved by means of the monotone iterative (MI) method instead of

Newton's iteration (NI) method. The method of monotone iteration is a constructive alternative for numerical solutions of PDEs. It has been reported that, compared with the NI method, the major features of the MI method are (1) it converges globally with any arbitrary initial guesses; (2) its implementation is much easier than NI method; and (3) it is inherently ready for parallelization [8]. Furthermore, due to the efficient posteriori error estimation, the variation of physical quantities, such as the gradients of potential and current density, can be automatically tracked. Therefore, the terminal characteristics are accurately calculated. The proposed adaptive computing technique shows the simulation accuracy and numerical robustness for the simulation of 2D OLEDs. Effects of geometry, the trap density and the Schottky barrier height [11] on the current-voltage (I-V) curves of the simulated 2D OLED are examined using the developed 2D simulation program.

This paper is organized as follows. In the section 2, we state the transport model and the adaptive computing technique for the 2D simulation of OLED. In the section 3, the results of numerical simulation are discussed. Finally we draw the conclusions.

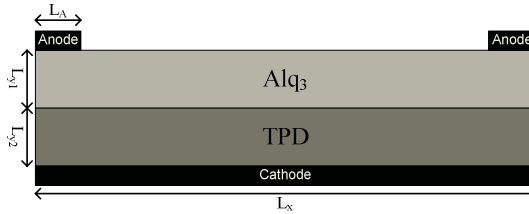


**Fig. 1.** A cross-sectional view of the studied OLED structure, where  $L_A$  is the length of contacts of anode and  $L_x$  is the length of contact of cathode. The  $L_{y1}$  is the width of material  $\text{Alq}_3$  which is the layer of electron transport and the  $L_{y2}$  is the width of material TPD which is the layer of hole transport

## 2 Mathematical Model and Computational Methodology

Based on the well-known inorganic charge transport continuum model [9], the drift-diffusion model, electron and hole transport in the OLED is described using the current continuity equations coupled to the Poisson equation [11]. Along with the appropriate boundary conditions, which for OLEDs require appropriate formalisms for current injection at each of the contacts, these equations are solved to obtain solutions for the electrostatic potential, electric field, carrier densities, and current densities for electron and hole, respectively. The investigated 2D structure of OLED, shown in Fig. 1, is a TPD/ $\text{Alq}_3$  two-layer device. Modeling of traps in numerical simulation of OLEDs is widely debated [3]. The electron-hole mobility taking the field-dependent Poole-Frenkel form in the current continuity equations of electron and hole is for shallow trapping of carriers. For deep traps, an extra recombination term and inclusion of their charge in the Poisson equation are considered. Deep traps can be described by a discrete and exponential distribution. The simulated OLED is based on the 2D structure of the tris-(8-hydroxyquinoline)-aluminum ( $\text{Alq}_3$ ) for the layer of electron transport and the triphenyl-diamine (TPD) for the layer of hole transport. As

shown in Fig. 1, we assume the length of anode ( $L_A$ ) is equal to 20 nm, the length of cathode ( $L_X$ ) is equal to 400 nm, and the thicknesses of Alq<sub>3</sub> layer ( $L_{y1}$ ) and TPD layer ( $L_{y2}$ ) are equal to 40 nm, respectively. We solve the steady-state DD model [11-14], which consists of

$$\Delta\psi = -\frac{q}{\varepsilon}(p - n - N_A + N_D - n_t + p_t), \tag{1}$$

$$\nabla J_n = -q(G - R), \text{ and} \tag{2}$$

$$\nabla J_p = -q(G - R). \tag{3}$$

The current equations, shown in Eqs. (2) and (3), for electron and hole are given by

$$J_n = -q\mu_n(nE - \frac{K_B T}{q}\nabla n) \text{ and} \tag{4}$$

$$J_p = -q\mu_p(pE + \frac{K_B T}{q}\nabla p). \tag{5}$$

In Eq. (1),  $\psi$  is the electrostatic potential,  $\varepsilon$  is the dielectric constant,  $N_A$  and  $N_D$  are the densities of acceptor and donor,  $n_t$  and  $p_t$  are the densities of trapped electrons and holes, respectively. Maxwell-Boltzmann statistics is adopted for the electron and hole densities. In Eqs. (2) and (3)  $G$  is the electron and hole generation rate and the carrier generation by thermal excitation across the gap is assumed. Two carrier recombination rates, the optical recombination rate  $R_{opt}$  and the Shockley-Read-Hall recombination rate  $R_{srh}$  are assumed in the simulation [11]. We consider here the densities of trapped electrons and holes for the  $j^{\text{th}}$  trap level

$$n_t = \frac{N_{ij}}{1 + \frac{1}{g} e^{\frac{E_{ij} - E_{fn}}{K_B T}}} \text{ and } p_t = \frac{P_{ij}}{1 + \frac{1}{g} e^{\frac{E_{ij} - E_{fp}}{K_B T}}},$$

where  $N_{ij}$  ( $P_{ij}$ ) is the electron (hole) trap density,  $E_{ij}$  is the trap energy relative to the conduction band edge,  $g$  is the trap degeneracy, and  $E_{fn}$  ( $E_{fp}$ ) is the electron (hole) quasi-Fermi level. Boundary conditions are assumed for the DD model above [11-14].

In the solution procedure, the adaptive computing is mainly based on the Gummel's decoupling algorithm, the FV approximation, the MI method, a posteriori error estimation, and an unstructured meshing technique. This simulation methodology has been developed in our recent work for semiconductor device simulation [7], [8], [9], [10]. Each Gummel decoupled PDE is approximated with the FV method over unstructured meshes. The corresponding system of nonlinear algebraic equations of the FV approximated PDE is solved with the MI method and the posteriori error estimation scheme is applied to assess the quality of computed solutions. It has been shown that the method of MI converges monotonically [8]. The adaptive mechanism is based on an estimation of the gradient of computed solutions, such as the electrostatic potential, the carrier density, and the current density. A posteriori error estimation is

applied to provide local error indicators for incorporation into the mesh refinement strategy. The local error indicators guide the adaptive refinement process.

### 3 Results and Discussion

In this section we first present the computational efficiency of the method by solving the OLED under a given biasing condition. The applied anode voltage and cathode voltage on the OLED are 10 V and 0 V, respectively, and the barrier height on the contact is assumed to be 0.3 eV. For this testing case, the obtained initial and final refined meshes are shown in Fig. 2. The stopping criteria for the MI and Gummel's loops are  $10^{-6}$  and  $10^{-3}$ , respectively. The initial mesh has 153 nodes and the final one consists of 1681 nodes. The adaptive computing process includes 5 refinement levels, which shows the computational efficiency. Different simulation cases are further performed to explore the intrinsic and terminal electrical characteristics of the OLEDs.

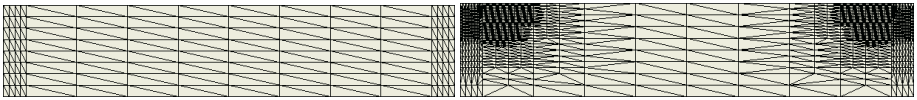


**Fig. 2.** The left figure is the initial mesh and the right one the 5<sup>th</sup> refined final mesh

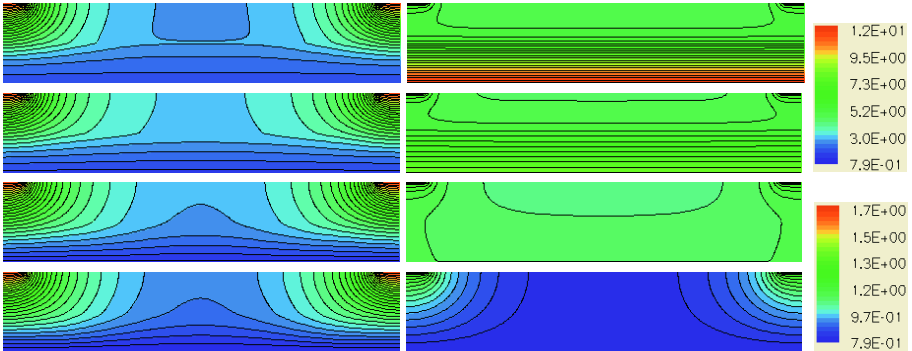


**Fig. 3.** The simulated potential of the OLED under the 10 V (left column) and the zero bias (right one). The barrier height is 0.3 eV (top figure), 0.6 eV, 0.9 eV, and 1.2 eV (bottom one)

We note that the simulation of OLEDs require the input of accurate material parameters, such as density of state, barrier height, and carrier mobility. However, unlike the case for inorganic semiconductor devices, these material parameters are often poorly characterized and are strongly dependent upon the fabricated samples. Our selection of the material parameters provides only the starting point for the electrical simulation of OLEDs. Good agreement between simulation and measurement should be subject to further calibration. Contour plots of the electrostatic potential and the electron density are shown in Figs. 3 and 4, respectively, where the OLED under two different biasing conditions the anode voltage is equal to 10.0V and 0 V, are simulated. The cathode voltage is fixed at 0.0V and the barrier height of contact varies from 0.3 eV to 1.2 eV

with step 0.3 eV. The unit of the color bars, shown in Fig. 3, is in Volt. The computed electrostatic potential significantly shows the importance of selection of barrier height. Different barrier heights imply different current injection. The unit of the color bars of electron density is with per meter cubic. Figures 3 and 4 demonstrate the necessary for the advanced design of OLED structures by using a 2D simulation.

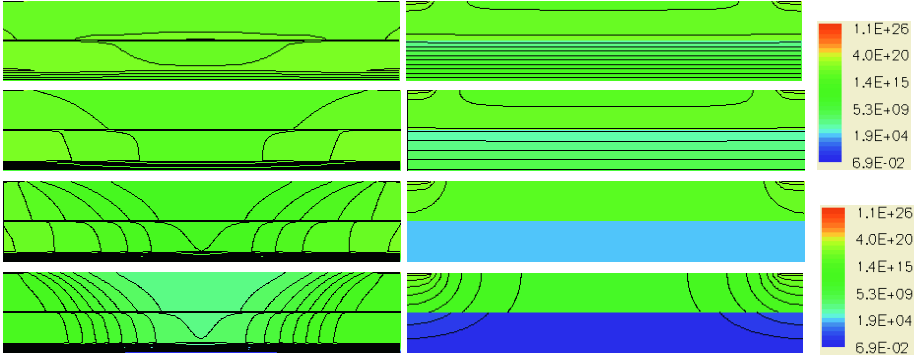


Fig. 4. The contour plots of the simulated electron density. The setting is the same with Fig. 3

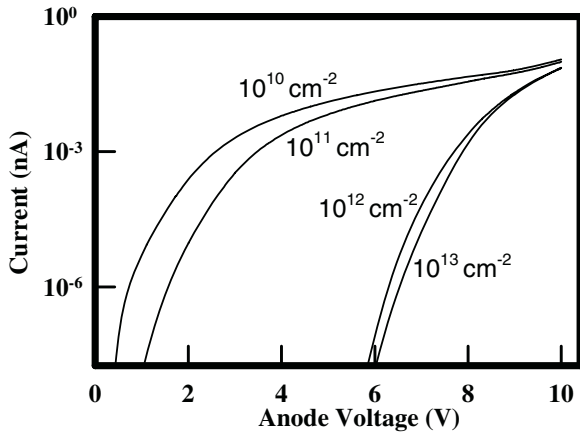


Fig. 5. The I-V curves of the simulated OLED with different trap densities of electron

To explore the effect of trap density on the transport characteristics, we simulate the current-voltage (I-V) curves with respect to different electron trap densities, where the hole trap density is neglected. As shown in Fig. 5, the I-V curves per unit area are calculated with different densities of traps which range from  $10^{10} \text{ cm}^{-2}$  to  $10^{13} \text{ cm}^{-2}$ . The anode voltage is equal to 10 V and the barrier height is fixed at 0.3 eV. It is found that the higher electron trap densities get no significant benefit to improve the electrical performance of the OLED. The choice of OLED's contacts is crucial, and it af-

ffects the minority and majority currents, the recombination rates, and the efficiency. At the interface of metal and semiconductor of OLED, the variation of barrier heights is wide. The operation of OLED depends upon the asymmetry of the barrier heights at the two contacts, shown in Fig. 1; ITO is one of the preferred anode materials due to the transparency and relatively high work function. Metal, such as Al, Ca, or Mg, with low work functions is selected as cathode material. To explore the effect of the Schottky barrier height on the I-V relationships [11], the Schottky barrier height on the contacts is simply varied from 0.0 to 1.2 eV, shown in Fig. 6.

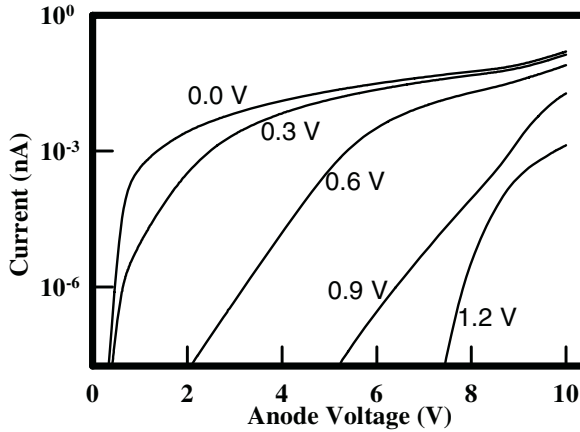


Fig. 6. The I-V curves of the simulated OLED with different Schottky barrier heights

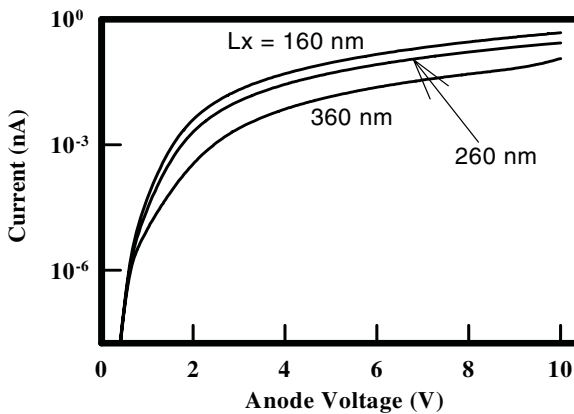


Fig. 7. The I-V curves of the simulated OLED with different lateral length  $L_x$



With the 2D simulation, the lateral length and thickness of transport layer are changed for exploring the I-V curves. It is found that small  $L_x$  produces high current level when the  $L_{y1}$  and  $L_{y2}$  are fixed, shown in Fig. 7. Due to uniform distribution of electric fields, the small variation on  $L_{y1}$  and  $L_{y2}$  does not significantly alter the level of current.

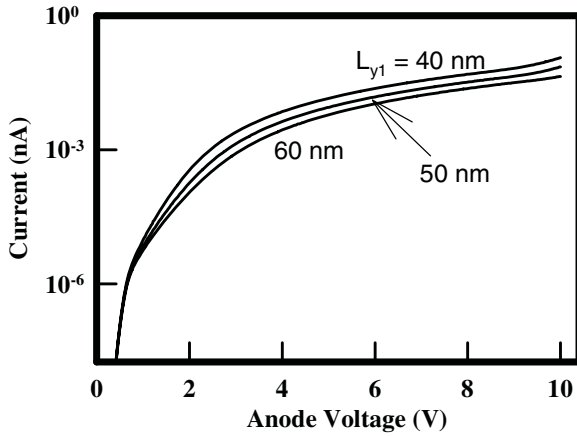


Fig. 8. The I-V curves with respect to different thicknesses of electron transport layer  $L_{y1}$

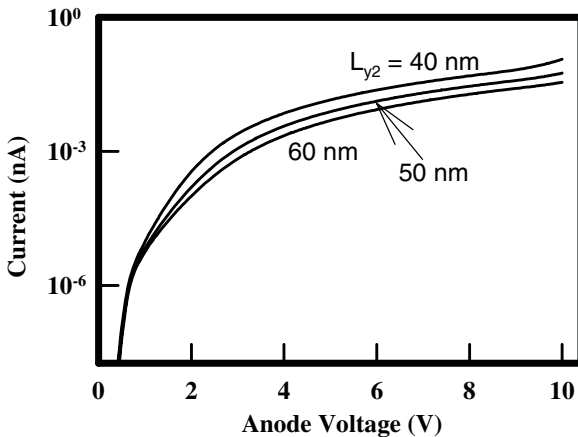


Fig. 9. The I-V curves with respect to different thicknesses of hole transport layer  $L_{y2}$

## 4 Conclusions

In this paper we have successfully applied adaptive computing technique to solve the 2D DD model for the simulation of electrical characteristics of OLEDs. Effects of the carrier traps and device geometry on the transport properties have been studied. The 2D macroscopic modeling and simulation is a starting point for theoretical investigation of electrical characteristics of OLEDs. It benefits the design of structure and optimization of characteristics. Application of technology computer-aided design software to modern display industry requires accurate modeling and calibration of material parameters. In contrast to the macroscopic simulation, we believe that microscopic approaches will physically provide accurate calculation.

## Acknowledgments

This work is supported in part by the National Science Council (NSC) of TAIWAN under contracts NSC-93-2215-E-429-008 and NSC 93-2752-E-009-002-PAE, and the grant of the Ministry of Economic Affairs, Taiwan under contracts 92-EC-17-A-07-S1-0011 and 93-EC-17-A-07-S1-0011.

## References

1. Goh, J.-C., Chung, H.-J., Jang, J., Han, C.-H.: A New Pixel Circuit for Active Matrix Organic Light Emitting Diodes. *IEEE Elec. Dev. Lett.* 23 (2002) 544-546
2. Ruhstaller, B., Carter, S.A., Barth, S., Riel, H., Riess, W., Scott J. C.: Transient and Steady-State Behavior of Space Charges in Multilayer Organic Light-Emitting Diodes. *J. Appl. Phys.* 89 (2001) 4575-4586
3. Waler, A. B., Kambili A., Martin S. J.: Electrical Transport Modelling in Organic Electroluminescent Devices. *J. Phys.: Condens. Matter* 14 (2002) 9825-9876
4. Ruhstaller, B., Beierlein, T., Riel, H., Karg, S., Scott, J. C., Riess W.: Simulating Electronic and Optical Processes in Multilayer Organic Light-Emitting Devices. *IEEE J. Sel. Topics Quantum Elec.* 9 (2003) 723-731
5. Blades, C. D. J., Walker, A. B.: Simulation of Organic Light Emitting Diodes. *Synth. Met.* 111-112 (2000) 335-340
6. Barth, S., Müller, P., Riel, H., Seidler, P. F., Riess, W., Vestweber, H., Bässler, H.: Electron Mobility in Alq Thin Films Determined via Transient Electroluminescence from Single- and Multilayer Organic Light-Emitting Diodes. *J. Appl. Phys.* 89 (2001) 3711
7. Li, Y., Yu, S.-M.: A Two-Dimensional Quantum Transport Simulation of Nanoscale Double-Gate MOSFETs using Parallel Adaptive Technique. *IEICE Trans. Info. & Sys.* E87-D (2004) 1751-1758
8. Li, Y.: A Parallel Monotone Iterative Method for the Numerical Solution of Multidimensional Semiconductor Poisson Equation. *Comput. Phys. Commun.* 153 (2003) 359-372
9. Li, Y., Sze, S. M., Chao, T.-S.: A Practical Implementation of Parallel Dynamic Load Balancing for Adaptive Computing in VLSI Device Simulation. *Eng. Comput.* 18 (2002) 124-137

10. Li, Y., Liu, J.-L., Chao, T.-S., Sze, S. M.: A New Parallel Adaptive Finite Volume Method for the Numerical Simulation of Semiconductor Devices. *Comput. Phys. Commun.* 142 (2001) 285-289
11. Sze, S. M.: *Physics of semiconductor devices*. Wiley-Interscience, New York (1981)
12. Crone, B. K., Davids, P. S., Campbell, I. H., Smith, D. L.: Device Model Investigation of Bilayer Organic Light Emitting Diodes. *J. Appl. Phys.* 87 (2000) 1974-1982
13. Lupton, J. M., Samuel, I. D. W.: Temperature-Dependent Single Carrier Device Model for Polymeric Light Emitting Diodes. *J. Phys. D: Appl. Phys.* 32 (1999) 2973-2984
14. Kawabe, Y., Jabbour, G. E., Shaheen, S. E., Kippelen, B., Peyghambarian, N.: A Model for the Current-Voltage Characteristics and the Quantum Efficiency of Single-Layer Organic Light Emitting Diodes. *Appl. Phys. Lett.* 71 (1997) 1290-1292

# Characterization of a Solid State DNA Nanopore Sequencer Using Multi-scale (Nano-to-Device) Modeling

Jerry Jenkins, Debasis Sengupta, and Shankar Sundaram

CFD Research Corporation 215 Wynn Drive,  
Huntsville, AL 35805  
{jwj, dxs, sxs}@cfdrcc.com

**Abstract.** Nanobiotechnology is a rapidly advancing frontier of science with great potential for beneficial impact on society. Unfortunately, design of integrated nano-bio systems is a complex, laborious task with large failure rates. Current models describing molecular level behavior are expensive, while device design codes lack the necessary nanophysics. The objective of this work is to demonstrate multiscale, multiphysics modeling of an integrated nanobio device, where nanoscale effects are efficiently integrated with a continuum model. A three-level modeling paradigm was developed for this purpose. The feasibility of this approach is demonstrated by characterizing a nanopore-based DNA sequencing device. In the demonstration calculations, the dependence of the device performance on the nucleotide sequence, pore diameter, and applied voltage was determined. Extension of the approach for describing biomolecular processes in other commercial nanobiosystems is discussed. The main conclusions of the device level simulations are presented along with an overview of future work.

## 1 Introduction

Research efforts directed at the problem of integrating nanotechnology and biology to form integrated nano-bio systems are becoming a priority. Integrated nano-bio systems have emerged as strong candidates for single molecule detection and genomic sequencing. Understanding the relationship between molecular behavior and system/device response, requires the development of modeling and simulation tools, which can simulate phenomena spanning a wide spectrum of length and time scales (Figure 1(a)). We have developed a hierarchical theoretical and computational framework (Figure 1(b)) that addresses the problem of coupling molecular level information into a continuum level device simulation. Each modeling and simulation level in the hierarchy is chosen with careful attention to a cost-benefit analysis.

The first level in the hierarchy is an atomistically detailed model of the nanoscale phenomena of interest. Molecular simulations enable a physical understanding of the fundamental mechanisms that underlie nanoscale phenomena. Results from the molecular level simulations are used to parameterize the second level stochastic

model. Stochastic models (Master Equation or Fokker-Planck Equation) are utilized to bridge molecular and continuum levels because they are able to correctly predict the average properties of a system as well as the fluctuations inherent in the nanoscale. The final level is a continuum model of the system of interest, which couples information from the preceding two levels. Stochastic models can be tightly integrated into the continuum model for high-fidelity design calculations. Insights obtained using this modeling hierarchy can guide the choice of candidate design strategies for specific integrated nanobiosystems.

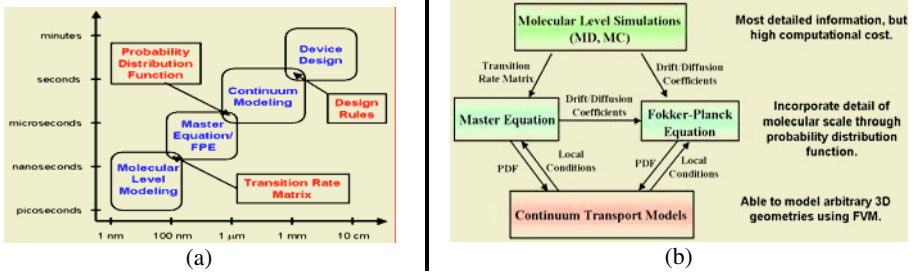


**Fig. 1.** (a) Applicable range of scales for each modeling level. (b) Illustration of the different levels of modeling. The text next to the arrows is the information transferred at each level

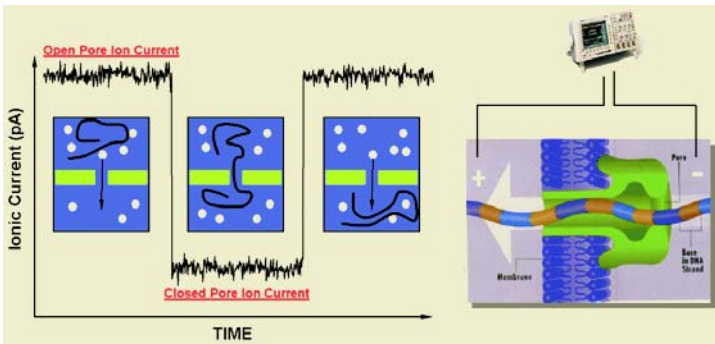


**Fig. 2.** As negatively charged nucleic acids pass through the nanopore in single file, they block the flow of current in a manner characteristic of the polymer's length and sequence [2]

The demonstration case we have chosen (Figure 2) is the problem of DNA translocation through nanopores. This area has come under a great deal of investigation recently due to its promise for inexpensive ultra high-throughput sequencing of DNA. A voltage bias applied to a nanopore has been shown to induce charged single stranded DNA and RNA molecules to translocate through the pore. Each translocating molecule blocks the open pore ionic current, providing an electrical signal that depends on several characteristics of the molecule [1]. The natural system has limitations due to the fixed size of the pore, stability, and noise characteristics. These difficulties can be overcome using a solid state nanopore [2].

The paper begins with a description of the molecular modeling in §2, followed by the development of the stochastic model in §3. This information is then coupled to the device level calculations to evaluate a proposed ultrahigh throughput DNA sequencing device (§4). The main conclusions of the device level simulations are presented along with an overview of future work.

## 2 Molecular Level Modeling

Translocation times for DNA to cross a nanopore are strongly dependent on the pore diameter [1]. Nanopores with diameters of 1.5nm and 2.0nm, were constructed based on experiments presented in the literature [3]. The pores were created using an in-house software that constructs a cube of silicone dioxide using the method of Brodka [4]. The cube is truncated to form a solid block of with dimensions of 5nm x 5nm x 5nm [5]. An overhead view of the 2nm nanopore is shown in Figure 3(a).

Experimental work has also revealed that homopolymers of adenine and cytosine have significant differences in their translocation times [2]. For this reason, poly(dC)<sub>4</sub> and poly(dA)<sub>4</sub> were chosen for this computation with poly(dC)<sub>4</sub> shown in Figure 3(b). Once generated, the nucleotides were placed in the nanopore and aligned with the axis of the pore with the 5' end pointing in the positive z-direction. Water and KCl were added to the system using tcl scripting language built into the VMD molecular graphics software [6]. The final system consists of a 6.1nm layer of water on top of the 5nm crystal structure and a 2nm layer of water on the bottom of the crystal for a total height of 13.1nm (Figure 3(c)). The total number of atoms for each system is approximately 29,000.

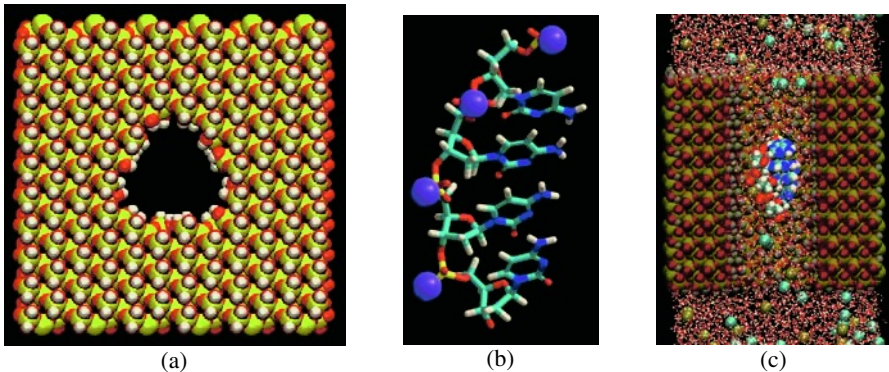
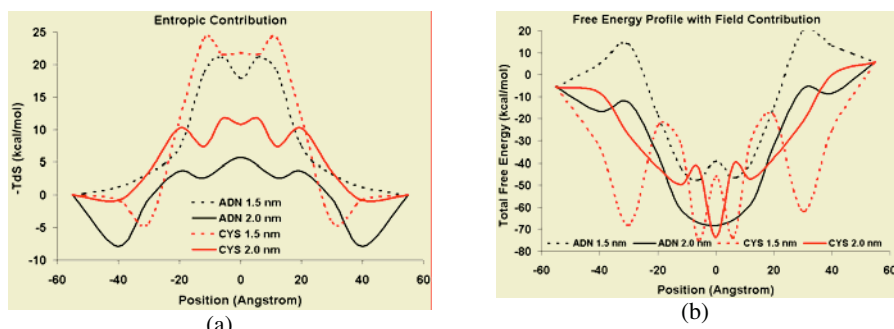


**Fig. 3.** Generation of (a) the nanopore in a Block of SiO<sub>2</sub> with dimensions of 5x5x5 nm. (b) 4-mer of Cytosine with potassium counter ions. (c) Final system (cutaway view) with nucleotide in the nanopore including counter-ions and solvent water

Molecular Dynamics (MD) simulations were performed in three phases following the work of Auffinger [7]. The phases consist of: (a) the initial heating of the water and ions, (b) equilibration of the entire system, and (c) production. The NAMD

software was used for all molecular simulations. (NAMD was developed by the Theoretical and Computational Biophysics Group in the Beckman Institute for Advanced Science and Technology at the University of Illinois at Urbana-Champaign) [8]. The Verlet-I or r-RESPA Multiple Time Stepping (MTS) algorithm was used in order to increase the time step to 2fs [9]. During the production simulations a Langevin based temperature controller was used to maintain the temperature [10], but was not coupled to hydrogen atoms. The Particle Mesh Ewald (PME) algorithm was used to model the periodic boundary conditions, with grid spacing of 64, 64, and 128 in the x, y, and z directions, respectively. All forcefield parameter information was taken from the CHARMM27 all hydrogen nucleic acid forcefield, derived from the work of [11] and [12]. Parameters for the potassium and chlorine ions were taken from [13]. The charge and Lennard-Jones parameters for the  $\text{SiO}_2$  were taken from [14].

Entropic affects can contribute significantly to the free energy, especially if a molecule is moving from solution into a confined space. The method of Schlitter [15] was used to compute the state entropy from the production phase of the molecular dynamics trajectories. The method is uses an approximate Gaussian form to approximate the canonical configurational distribution function. This method has been widely used to determine the entropy change for protein stability [16], and the stability of double stranded DNA [17]. A striking feature (Figure 4(a)) is that the 1.5nm pores have larger entropy changes relative to the surroundings when compared to the 2.0 nm pores. The largest entropic penalty was felt by poly(Cytosine)<sub>4</sub> in the 1.5nm pore. This contribution to the free energy is approximately 25 kcal/mol, while the 2nm pore case for cytosine only has a 11 kcal/mol entropic barrier. The adenine shows a similar pattern of higher entropy outside of the pore and higher entropy change.



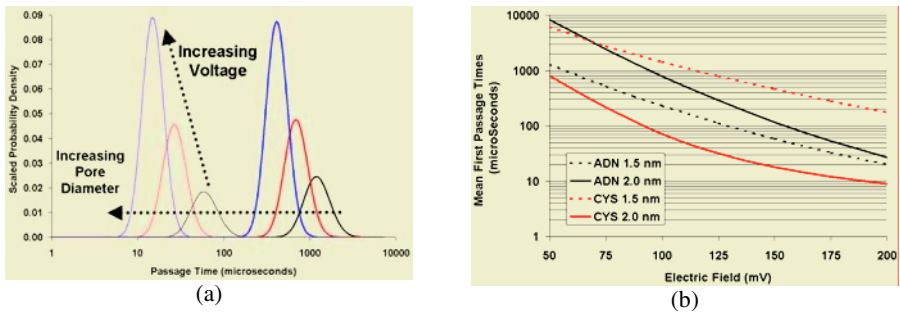
**Fig. 4.** (a) Prediction of the entropic component of the overall free energy of the system. (b) Free Energy Profiles ( $\Delta U-T\Delta S$ ) of translocation for poly(dC)<sub>4</sub> and poly(dA)<sub>4</sub> translocating through the 1.5 and 2.0nm pores

Figure 4(b) illustrates that the free energy profiles are similar for all four cases. Focusing in on the portion of the graph that contains the pore (-25 to 25 on the x-axis), we can draw some conclusions pertaining to the contribution to translocation times from the free energy. The relative free energy profiles show that Cytosine has a

lower free energy relative to Adenine within the pore, for both pore diameters, having the lowest free energy in the 1.5nm pore. Adenine shows a lower free energy within the 2.0nm pore relative to the 1.5nm pore, while Cytosine shows a similar free energy for both pores. The barriers extracted from the nanopores are very similar to the shape of the energy profiles extracted from ion channels [18]. The contribution to the electric field tilts the free energy profiles 11.5 kcal/mol assuming a 120 mV bias across the 5nm thickness of the nanopore.

### 3 Stochastic Model of DNA Translocation

The stochastic model forms the second modeling scale (complementary to the molecular modeling described above). The inputs to this level are the translocation free energy profiles and the dependence of the profile on applied voltage. The goal is to compute the distribution of translocation times and the mean translocation time. The distribution of translocation times was computed using the method of Lubensky [19], and are shown in Figure 5(a). The mean translocation times were then computed from the distribution and checked against the method of Schulten [20].



**Fig. 5.** (a) Variation in the distribution of passage times with applied field and pore diameter for cytosine. (b) Mean passage time dependence on applied voltage for all four cases

For all four cases, Figure 5(b) shows an exponential drop in the mean passage time with applied voltage, in agreement with several other researchers [21, 22]. Looking at the individual nucleotides, the cytosine shows a longer passage time with the 1.5 nm pore as opposed to the 2.0 nm pore. However, the Adenine chain shows a longer passage time with the 2.0 nm pore as opposed to the 1.5 nm pore. Also to note is the fact that there is a much larger difference in passage time comparing pore diameters with cytosine than with adenine. The reason for the differences is not immediately clear until we look at the free energy profiles (Figure 4(b)). The Adenine profiles show a large difference in the depth of the minimum on the order of 20% of the total depth. While the cytosine nucleotides do not show the same dependence. The information computed in this section will be coupled in directly with the continuum level model presented in the next section.



### 4 Continuum Level Model

This forms the final element in the three-tiered paradigm A pore model is constructed that takes into account the arrival rate of DNA in the proper conformation, and the translocation of DNA across the pore. A boundary condition was implemented in the multiphysics modeling software CFD-ACE+ (marketed by ESI Group), which accounts for the rate of capture as well as the rate of translocation (Figure 2) The translocation model contains two steps, with the first step being the rate of capture of a DNA (**R**) chain into the nanopore. This rate was not computed, but was taken from the literature [2]. The second step is the translocation of the captured DNA across the pore to free up the pore. This is assumed to occur at a rate of  $1/\tau$  where,  $\tau$  is the mean translocation time computed using the free energy profiles (Figure 5(b)). Both  $\tau$  and **R** are dependent on the applied voltage.

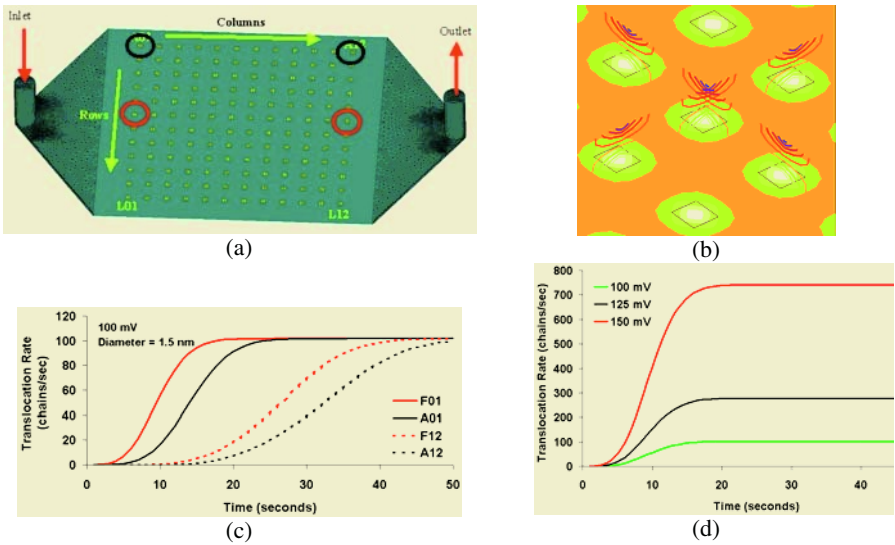


**Fig. 6.** (a) Three dimensional geometry of the notional device showing the labeling of the nanopore containing patches. The patches are shown in yellow. (b) Zoom in view of the electric field on each patch optimized to minimize cross talk. (c) Dependence on the Translocation Rates on the Placement. For the case of *CYS* 1.5 nm at 100, 125, and 150 mV. (d) Dependence on the Translocation Rates on the Voltage for the Case of F01 Spot

The device chosen for demonstration (Figure 6(a)) is a 21 mm by 7mm by 0.25 mm thick microfluidic chip containing 144 nanopore bearing patches. Each patch is uniquely identified (similar to a standard spreadsheet) with a letter and a number. Within the computational domain of the chip, the Navier-Stokes equation for an incompressible fluid is solved along with the equation of mass transport for DNA. A sink term is added at each patch based on the rate of translocation. Initially there is assumed to be no DNA in the chip. At time zero, DNA begins to flow into the chip at a concentration of  $10^{-6}$  Molar being carried by the fluid that is being pumped at a rate

of 100 microL/min. The total simulated time is 50 seconds, long enough for the pore translocation to reach a steady state. Also, a constant voltage was held across each patch, and the solution for the electric field was computed during the simulation. This calculation allowed for the determination of the optimal spacing of the pore containing patches to minimize electronic cross talk (Figure 6(b)).

To understand the dependence of the output signals upon pore placement, four pores were monitored. A01, A12, F01, and F12 (see Figure 6(a) for locations). These represent extremes in terms of placement within the flow field and placement along the line of flow. Figure 6(c) shows the evolution of the translocation rate for three voltages and the four candidate spots. All three voltages show a similar trend of F01 and A01 being the first to reach steady state, while F12 and A12 show a nearly 20 second lag. This lag time will be strongly dependent upon the inlet flowrate of the device, with an increasing flowrate decreasing the lag time. An increase in the applied voltage increases the point at which the patch translocation rate reaches a steady state. Figure 6(d) shows the dependence of the DNA translocation rates on the applied pore voltage. The translocation rates are shown to increase exponentially in agreement with [21].

## 5 Summary and Conclusions

The design of devices that incorporate both nanoscale and continuum scale physics is challenging due to the nature of simulation techniques for each scale. This paper presents a general three-tiered modeling paradigm for use in simulating devices containing a nanoscale component. The models presented will be incorporated into a continuum code and ultimately used to simulate integrated nanobio devices. Future objectives for this research include the development of a generic framework for simulation of systems of Master Equations and Fokker-Planck Equations. The ME and FPE solver will be designed as a separate module to be integrated with a continuum code for simulations of integrated nano-bio systems. Future work will focus on the demonstration of the feasibility and efficiency of the proposed approach on alternative test systems.

The example system is one of the simulation of a nanopore-based DNA sequencing device. The results from the device level calculation show that the overall translocation rate is exponentially dependent on the applied voltage. The placement of the patches of nanopores affects the rate at which they reach a steady translocation rate. The final result is that the nanopore diameter had only a marginal affect on the overall translocation rates. The main conclusion from the device level modeling is that in order to improve the performance of this type of a device it is desirable to increase the rate at which DNA is captured. This can be accomplished via the addition of a surface treatment around the pore via functionalization.

## Acknowledgement

The authors gratefully acknowledge NASA-AMES (NNA04CB26C, Technical Monitor: Dr. Harry Partridge) for funding, and thank Dr. Harry Partridge and Dr. Jun Li for their many helpful discussions.

## References

1. Stolc, V., Cozmuta I., Brock, M., O'Keeffe, J.: Presentation given at the DARPA Joint BIOFLIPS/SIMBIOSYS Principal Investigators Meeting, Monterey, CA (2003).
2. (a)Meller, A., Branton D.: Electrophoresis, 23 (2002) 2583-2591 and (b) Meller, A., Nivon L., Branton D.: Physical Review Letters, 86 (2001) 3435-38.
3. Li, J., Stein, D., McMullan, C., Branton, D., Aziz, M., and Golovchenko, J.: Nature 412 (2001) 166-8.
4. Brodka, A. and Zerda, T.: Journal of Chemical Physics 104 (1996) 6319-6326.
5. Li, J., Gershow, M., Stein, D., Brandin, E., Golovchenko, J.: Nature Materials, 2 (2003) 611-15.
6. Humphrey, W., Dalke, A. and Schulten, K.: "VMD - Visual Molecular Dynamics", J. Molec. Graphics, 14 (1996) 33-38.
7. Auffinger, P. and Westhof, E.: Journal of Molecular Biology, 269 (1997) 326-341.
8. Kalé, L., Skeel, R., Bhandarkar, M., Brunner, R., Gursoy, A., Krawetz, N., Phillips, J., Shinozaki, A., Varadarajan, K., and Schulten, K.: NAMD2: Greater scalability for parallel molecular dynamics. Journal of Computational Physics, 151 (1999) 283-312.
9. Izaguirre, J., Reich, S. Skeel, R.: Journal of Chemical Physics, 110 (1999) 9853-64.
10. Skeel, R., Izaguirre, J.: Molecular Physics 100 (2002) 3885-91.
11. Foloppe, N. and MacKerell, Jr., A.D.: Journal of Computational Chemistry, 21 (2000) 86-104.
12. MacKerell, Jr., A.D. and Banavali, N.: Journal of Computational Chemistry, 21 (2000) 105-120.
13. Beglov, D. and Roux, B.: Journal of Chemical Physics, 100 (1994) 9050-9063.
14. Rovere, M., Ricci, M., Vellati, D., and Bruni, F.: Journal of Chemical Physics, 108 (1998) 9859-9867.
15. Schlitter, J.: Chemical Physics Letters, 215 (1993) 617-21.
16. Malliavin, T., Jocelyn, G. Snoussi, K. and Leroy, J.: Biophysical Journal, 84 (2003) 1-10.
17. Rueda, M., Kalko, S., Luque, J., and Orozco, M.: JACS, 125 (2003) 8007-14.
18. Edwards, S., Corry, B., Kuyucak, S., Chung, S.: Biophysical Journal, 83 (2002) 1348-60.
19. Lubensky, D. and Nelson, D.: "Driven Polymer Translocation Through a Narrow Pore" Biophys. J. 77 (1999) 1824-38.
20. Park, S., Sener, M., Lu, D., Schulten, K.: J. Chem. Phys. 119 (2003) 1313:19.
21. Ambjornsson, T. Apell, S. Konkoli, Z. Marzio, E. Kasianowica, J.: Journal of Chemical Physics. 117 (2002) 4063-73.
22. Chuang, J., Kantor, Y., Kardar, M.: Phys. Rev. E. E65 (2002) 11802(1-8).

# Comparison of Nonlinear Conjugate-Gradient Methods for Computing the Electronic Properties of Nanostructure Architectures<sup>\*</sup>

Thamara M. Aguilera-Camacho<sup>1</sup>,  
G. Aguilera-García<sup>1</sup>, and J. Garra<sup>1</sup>

<sup>1</sup> Innovative Computing Laboratory,  
The University of Tennessee,  
Knoxville, TN 37996-3450

<sup>2</sup> Lawrence Berkeley National Laboratory,  
Computational Research Division,  
Berkeley, CA 94720

**Abstract.** In this article we report on our efforts to test and expand the current state-of-the-art in eigenvalue solvers applied to the field of nanotechnology. We singled out the nonlinear conjugate gradients (CG) methods as the backbone of our efforts for their previous success in predicting the electronic properties of large nanostructures and made a library of three different solvers (two recent and one new) that we integrated into the parallel PESCAN (Parallel Energy SCAN) code [3] to perform a comparison.

## 1 Introduction

First principles electronic structure calculations are typically carried out by minimizing the quantum mechanical total energy with respect to the electronic coordinates. In many cases, the freedom to neglect the usual assumptions and simplifications, the electronic part of the many-body problem is equivalent to solving the self-consistent Schrödinger type equations (called the Hamilton equations)

$$H\psi_i(r) = \epsilon_i\psi_i(r), \quad (1)$$

$$H = -\frac{\hbar^2}{2m}\nabla^2 + V$$

where  $\psi_i(r)$  are the self-consistent wave functions (of electronic state  $i$ ) that minimize the total energy, and  $V$  is the total potential of the system. The wave functions are most commonly expanded in plane waves (Fourier components) up to some cutoff energy. The hidden secret lies in equation (1). This approach the

---

<sup>\*</sup> This work was supported by the US Department of Energy, Office of Science, Office of Advanced Scientific Computing (MICS) and Basic Energy Science under LAB03-17 initiative, contract Nos. DE-FG02-03ER25584 and DE-AC03-76SF00098.

... est e ge pa rs are ca cu ated fr  $H$  a d the ... h ... ham equat ... s are s ... ed se f c ... s ste t ... r a re e ... f th s appr ach see refere ce ... a d the refere ces there ... he c mputat ... a c st f th s appr ach sca es as the cube f the ... umber f at ms a d the ma ... mum s stem sze that ca be stud ed s f the rder f hu dreds f at ms ... the appr ach used ... PESCAN de e ped b ... a g a d ... u ger ... a sem emp r ca p te t a r a charge patch g meth d 7 s used t c ... struct  $V$  a d ... the e ge states f ... terest ar u d a g e e erg are ca cu ated, a ... g the stud ... f arge ... a s stems (up t a m ... at ms) ... he pr b em the bec mes fi d  $\psi$  a d  $E$  c se t a g e  $E_{ref}$  such that

$$H\psi = E\psi, \tag{2}$$

here  $H$  repre ts the am t ... a matr ... h ch s erm t a th d me s ... equat the ... umber f ... ur er c mp e ts used t e pa d  $\psi$  ... he d me s ... f  $H$  ma be f the rder f a m ... f r arge ... a s stems ... he e ge ... a ues  $E$  (e erg ... f state  $\psi$ ) are rea a d the e ge ... ect rs  $\psi$  are rth ... rma

... ma ... cases, ... ke sem c duct r qua tum d ts, the spectrum f  $H$  has e erg gaps a d f part cu ar ... terest t ph s c sts s t fi d a fe ... appr mate 4 t ... f the ... ter r e ge ... a ues ... e ther s de f the gap h ch determ es ma ... f the e ect r ... c pr pert es f the s stem ue t ... ts arge s ze  $H$  s e er e p c t c mputed ... e ca cu ate the k et c e erg part ... ur er space, here t s d ag ... a d the p te t a e erg part ... rea space s that the ... umber f ca cu at ... s used t c ... struct the matr ... ect r pr duct sca es as  $n \times n$  rather tha  $n^2$  here  $n$  s the d me s ... f  $H$  hree d me s ... a ... s are used t m ... e bet ee ... ur er a d rea space  $H$  s there re a a ab e as a pr cedure f r c mput g  $Hx$  f r a g e ... ect r  $x$  ... hus ... e m re requeme t s that the s ... er s matr free ... a ... repeated e ge ... a ues (dege rac ) f appr mate

ma ... mum are p ss be f r the pr b em s d scussed a d e eed t be ab e t res ... e such cases t fu ... u dersta d the e ect r ... c pr pert es f ur s stems

Curre t ... equat ... (2) s s ... ed b a CG meth d as c ded ... the PESCAN package ... h e th s pr gram ... rks e f r ... at ms stems th a s zab e ba d gap (e g ... e ), t bec mes ... creas g d fficu t t s ... e f r s stems th ( ) arge ... umber f at ms (e g m re tha ... m ... ) (2) sma ba d gap, a d here ( ) ma e ge states eed t be c mputed (e g m re tha ... ), r t s ... e e ge states ... he there s ... ba d gap (e g f r uger r tra sp rt ca cu at ... s) ... hus ... e a g r thm t s ... e th s pr b em s great ... eeded

he f cus f th s paper s ... ear CG meth ds ... th f ded spectrum ... he g a s t s ... e the ter r e ge states ... ter at e f r the f ded spectrum tra sf rmat ... are sh ft a d ... ert r fi ed p ... m a ... Our ch ce f meth d s based ... the h gh successfu curre t scheme ... h ch has bee pr e t be effie t a d pract ca f r the ph s ca pr b ems ... e are s ... g t ... be the sub ect f ther stud es t further ... est gate the app cab t f f ther a ter at es ... ke the a cz s a d ac b a ds ... meth d

... ect ... 2 e descr be the three e ge s ... ers ... est gated ... the paper ... e g e ur ... umer ca resu ts ... ect ... , a d fi a ... , ... ect ... 4, e g e s me c ... c ud g remarks

## 2 Nonlinear CG Method for Eigenvalue Problems

The classical approach for problems of large matrix size is to use iterative projection methods where at each step one extracts the  $k$  smallest eigenvalues from a given subspace  $S$  of size  $d$  (see e.g. [2]). Linear CG methods being the smallest eigenvalue of the Hermitian operator  $A$ .

This eigenvalue problem can be expressed in terms of function minimization as finding the stationary minimum of  $F(x) = \frac{1}{2} \langle x, Ax \rangle$ , under the constraint of  $x^T x = I$ , which allows linear CG methods to be performed where the constraint  $x^T x = I$  makes the problem linear.

This section describes the first generation of the algorithms that have been implemented in our library, namely the projected conjugate gradient method (PCG), the PCG with  $S = \text{span}\{X, R\}$  method (PCG-XR), and the compact matrix PCG method (LOPBCG). Additionally, we describe the spectral transformation that is used to get the desired eigenvalues of interest.

### 2.1 PCG Method

Table 1 gives a pseudocode of the PCG algorithm for eigenvalue problems. This is the algorithm originally implemented in the PESCAN code (see also [8]).

Here  $P$  is a projection operator for the operator  $A$ ,  $X$  is the block of `blockSize` columns of eigenvectors sought, and  $\lambda$  is the corresponding block of eigenvalues.

Table 1. PCG algorithm

```

1  do i = 1, niter
2      do m = 1, blockSize
3          orthonormalize X(m) to X(1:m-1)
4          ax = A X(m)
5          do j = 1, nline
6              lambda(m) = X(m) · ax
7              if (||ax - lambda(m) X(m)||2 < tol .or. j == nline) exit
8              rj+1 = (I - X X^T) ax
9              beta = (rj+1 · rj) / (rj · rj)
10             dj+1 = -P rj+1 + beta dj
11             dj+1 = (I - XX^T) dj+1
12             gamma = ||dj+1||2^-1
13             theta = 0.5 |atan(2 gamma dj+1 · ax / (lambda(m) - gamma^2 dj+1 · A dj+1))|
14             X(m) = cos(theta) X(m) + sin(theta) gamma dj+1
15             ax = cos(theta) ax + sin(theta) gamma A dj+1
16         enddo
17     enddo
18     [X, lambda] = Rayleigh - Ritz on span{X}
19 enddo

```

**Table 2.** LOBPCG algorithm

```

1  do i = 1, niter
2      R = P (A Xi - λ Xi)
3      check convergence criteria
4      [Xi, λ] = Rayleigh - Ritz on span{Xi, Xi-1, R}
5  enddo

```

the above procedure,  $X^T X - I$  is satisfied through out the process ( $I - X X^T$ ) is a projector operator which is applied to  $y$  deletes  $\text{span}\{X\}$  from  $y$ , thus making the resulting vector orthogonal to  $\text{span}\{X\}$  the matrix-vector multiplication happens at each iteration thus there is no matrix-vector multiplication each  $j$  iteration the above procedure converges each eigen vector separately in a sequential state to a stable state (robustly) the physics commutator method contrast to the block method be introduced etc

**2.2 LOBPCG Method**

recall the LOBPCG method can be described with the pseudocode above 2 note that the difference with the PCG is that the matrix updates are replaced with just the blocked computation of the predicted residual and the Rayleigh Ritz on  $\text{span}\{X_i\}$  with Rayleigh Ritz on  $\text{span}\{X_{i-1}, X_i, R\}$  (the physics commutator Rayleigh Ritz is known as the process of diagonalizing  $A$  within the spanned subspace, and taking the blocks zero eigenvalues) the direct implementation of this algorithm becomes unstable as  $X_{i-1}$  and  $X_i$  become correlated, and therefore special care and modifications have to be taken (see 4)

**2.3 PCG-XR Method**

PCG-XR is a algorithm that is derived from the PCG algorithm by replacing eq 8 above with

$$8 \quad X, \lambda \quad \text{Rayleigh - Ritz on span}\{X, R\}$$

the idea, as in the LOBPCG, is to use the vectors  $R$  to perform a more efficient Rayleigh Ritz step

**2.4 Folded Spectrum**

direct methods are good at finding well separated (clustered) eigenvalues in our case, we are seeking for cluster eigenvalues and thus we have to use a spectral transform, the gauge transform maps the sought eigenvalues of our operator to eigenvalues of another one

we can use the folded spectrum method where the cluster eigenvalue problem  $Hx - \lambda x$  is transformed to find the smallest eigenvalues of  $(H - E_{ref}I)^2 x - \mu x$  the eigenvalues of the original problem are given back by  $\mu = (\lambda - s)^2$

The PCG algorithm is defined from (FS-PCG) as described in [8], adapted to the defined spectrum to LOBPCG (FS-LOBPCG), we have added three memory blocks. We select the matrix-vector products of the blocks  $X$ ,  $R$ , and  $P$  through the matrix  $H$  whose elements are, respectively, the magnitude of the residuals for a given iteration (therefore we must have access to the magnitude of the residuals of the squared operator) and the deflation strategy of LOBPCG is adapted to FS-LOBPCG, as the deflation is defined on the residual relative to  $H$  has converged (not  $H^2$ ).

### 3 Numerical Results

#### 3.1 Software Package

We implemented the LOBPCG<sup>1</sup>, PCG, and PCG-XR methods as software. Currently, it has single-precision floating-point arithmetic capabilities. The parameters ( $\epsilon$ ) and sequence lengths of the block-sorted orthogonal deflation spectrum spectral refinement steps are implemented as standard and easy to be integrated into various physics codes. Test cases provided that the software represents a particular operator where the efficiency ( $a$  (days)) and  $b$  (for the correct solution with the 4 closest eigenvalues on a regular 2-mesh) can be changed. Above the output of the test is presented its performance. A useful return of the test is the trace computation and parameters ( $a = 8, b = -i$ ) are known for the smallest eigenstates, the matrix size is  $2 \times 2 \times 10^4$ , and the iterations are stopped when the eigenvalues  $(x, \lambda)$  satisfy  $\|Hx - x\lambda\| \leq \text{tol}\|x\|$ , with  $\text{tol} = 10^{-8}$ .

**Table 3.** Comparison of the PCG, PCG-XR and LOBPCG methods in finding 10 eigenstates on a problem of size  $20,000 \times 20,000$

	PCG	LOBPCG	PCG-XR
time (s)	37.1	61.7	20.2
matvecs	3,555	1,679	1,760
dotprds	68,245	137,400	37,248
axpys	66,340	158,261	36,608
copys	6,190	9,976	3,560

Generally, LOBPCG achieves performance less iterations (less matrix-vector products) than PCG. However, it is adequate to measure the cost of memory operations (applying products) and memory requirements. In this case, LOBPCG performs approximately 2 times more dot products for 2 times less matrix-vector

<sup>1</sup> <http://www-math.cudenver.edu/~aknyazev/software/CG/latest/lobpcg.m> (revision 4.10 written in Matlab, with some slight modifications).



**Table 4.** Comparison of FS-PCG, FS-PCG-XR and FS-LOBPCG methods in finding 10 eigenstates around the gap of quantum dots of increasing size

(20Cd, 19Se) n = 11,331				(83Cd, 81Se) n = 34,143			
	# matvec	outer	it time		# matvec	outer	it time
FS-PCG(50)	4898	(8)	50.4s	FS-PCG(200)	15096	(11)	264 s
FS-PCG-XR(50)	4740	(6)	49.1s	FS-PCG-XR(200)	12174	(5)	209 s
FS-LOBPCG	4576		52.0s	FS-LOBPCG	10688		210 s

(232Cd, 235Se) n = 75,645				(534Cd, 527Se) n = 141,625			
	# matvec	outer	it time		# matvec	outer	it time
FS-PCG(200)	15754	(8)	513 s	FS-PCG(500)	22400	(6)	1406 s
FS-PCG-XR(200)	15716	(6)	508 s	FS-PCG-RX(500)	21928	(4)	1374 s
FS-LOBPCG	11864		458 s	FS-LOBPCG	17554		1399 s

products that the PCG method, since the product matrix-vector product takes approximately the time of 7 dot products, PCG gives a better timing

the CG-XR method represents first this test case as interesting, although the set of methods together with the number of matrix-vector products from the LOBPCG and the number of dot products from the PCG method

### 3.2 Numerical Results on Some Quantum Dots

In this section we present numerical results on quantum dots up to the usual diameter. The experiments are performed on the **seaborg** at ER-C

where the experiments are being performed. The energy values are around  $E_{ref} = -4.8eV$ , where the band gap is about 0.1 eV. We have calculated 4 top quantum dots (2 Cd, 8 e), (8 Cd, 8 e), (2 2Cd, 2 e), (4Cd, 27 e) here are realistic systems which can be experimentally synthesized and have been studied previously using the PCG method. Pseudopotentials are used for the potential term in equation (1), and spin-orbit interaction is also included. We cut the energy for the plane wave basis sets  $0.8 R_d$  the stopping criterion for the eigenvalues  $\|Hx - x\lambda\| \leq tol\|x\|$  here  $tol = 10^{-6}$ . The runs are performed on a 64-bit processor except for the smallest case (2 Cd, 8 e) which runs on 8 processors. The servers are started with the same initial guess

the predicted energies the eigenvalues  $8$  diagonal elements

$$p_i = \frac{E_k^2}{(\frac{1}{2}q_i^2 + V_0 - E_{ref})^2 + E_k^2},$$

here  $q_i$  is the diagonal term of the Laplacian,  $V_0$  is the average potential and  $E_k$  is the average kinetic energy of the wave function  $\psi$ . This method is an approximation of the inverse of  $(H - E_{ref})^2$

...table facts that all the solvers find the same eigenvalues with the correct accuracy for all the runs. Hereafter they are arranged in the following order: the results are given in table 4 for each test case the number of atoms of the quantum dot and the order  $n$  of the corresponding matrix size. The parameter for the number of iterations is the inner loop (*nline*) for FS-PCG and FS-PCG-XR should be the optimal value among the values 2, 4, 8, 16, 32, 64 and 128. The brackets after the solver name are 4, unless it is stated otherwise that the three methods behave almost the same. The best method (in terms of time) between FS-PCG-XR and FS-LOBPCG. FS-LOBPCG should also be faster than FS-PCG and FS-PCG-XR from the fact that the matrix-vector products are performed by block-chunks in the case of the solvers of the code used for this paper. Here the experiments are performed as a single double-precision computation of FS-LOBPCG. PISCAN should run faster and as a scalar larger processor units as a consequence of the communication part of the code. Another feature of FS-LOBPCG that should be stressed is the 4-steps inner loop super-rotation for FS-PCG. The predicted error is a value of a few percent, we illustrate this later feature for the quantum dot (83Cd,81Se). FS-LOBPCG runs 4 times faster than FS-PCG than predicted. Hereas it runs 1.4 times faster than for the future performance predicted. In table 4, the number of iterations that gives the minimum time is a value associated for a smaller number of iterations, this is illustrated in table 4. Right for (232Cd, 235Se) here the minimum time is obtained for 10 iterations. This is a very good practical application of stopping the iterations as soon as the requested tolerance is reached at the end of the inner loop. In case of FS-PCG( $k$ ) FS-PCG here the inner loop is stopped when the accuracy is less than  $k^{n_{outer}}$ , here  $n_{outer}$  is the number of the corresponding outer iterations. In table 4, Right, we give the results for FS-PCG( $10^{-1}$ ) and (22 Cd, 2 Se) it comes that as a surprise that this solver converges in fewer steps than the scheme. It is possible that as a consequence of a structured convergence of the block-iterations.

**Table 5. Left:** Comparison of FS-PCG and FS-LOBPCG with and without preconditioner to find  $m \times n = 10$  eigenvalues of the quantum dots (83Cd,81Se); **Right:** The problem of finding the best inner length for FS-PCG can be avoided by fixing a tolerance as stopping criterion in the inner loop

(83Cd, 81Se) $n = 34,143$				(232Cd, 235Se) $n = 75,645$			
		# matvec	time			# matvec	outer it time
FS-PCG(200)	precond	15096	264 s	FS-PCG(100)	17062	(15)	577 s
FS-LOBPCG	precond	10688	210 s	FS-PCG(200)	15716	(6)	508 s
				FS-PCG(300)	15990	(4)	517 s
FS-PCG(200)	no precond	71768	1274 s				
FS-LOBPCG	no precond	17810	341 s	FS-PCG( $10^{-1}$ )	15076	(6)	497 s

## 4 Conclusions

In this paper, we described and compared several CG methods with fixed spectrum to find a small number of their eigenvalues and eigenvectors. The applications to make a computation and prediction of the electronic properties of quantum materials structures. The methods were specifically selected and tuned for computing the electronic properties of large materials structures. Here, we used for such methods, the commutator and the success of finding large number of eigenvalues in the field depends on them. The three methods are summarized and thus after the results are compared generally. Regarding FS-LOBPCG is the fastest, the FS-PCG-XR and finally FS-PCG in terms of memory requirement the three methods are ranked the same as FS-LOBPCG FS-PCG-XR requires four to ten times as much memory as CG. So, our preliminary scales up the memory has to show up as a bottleneck, especially using FS-LOBPCG as a readable.

The main drawback of FS-PCG and FS-PCG-XR is the restriction that the parameter  $n_{line}$  (the number of iterations, the error  $\epsilon$ ) is required to get rid of this parameter. It can be instead have a fixed residual reduction to be achieved in each step of the outer loop.

On other applications, the performance of FS-LOBPCG could be still better than FS-PCG for a fast block matrix-vector product and data accumulation. The precisions of the results are available.

As a conclusion, based on our results, the memory is still a problem and blockers of the matrix-vector multiplication can be efficiently implemented, the FS-LOBPCG could be the method of choice for the type of problems discussed.

## Acknowledgements

This research used resources of the National Energy Research Scientific Computing Center, which is supported by the Office of Science of the DOE.

## References

1. Arbenz, P., Hetmaniuk, U.L., Lehoucq, R.B., Tuminaro, R.S.: A comparison of eigensolvers for large-scale 3D modal analysis using AMG-preconditioned iterative methods. *Int. J. Numer. Meth. Engng* (to appear)
2. Bai, Z., Demmel, J., Dongarra, J., Ruhe, A., van der Vorst, H. (Editors): *Templates for the solution of Algebraic Eigenvalue Problems: A Practical Guide*, SIAM, Philadelphia (2000)
3. Canning, A., Wang, L.W., Williamson, A., Zunger, A.: Parallel empirical pseudopotential electronic structure calculations for million atom systems. *J. Comp. Phys.* **160** (2000) 29–41
4. Knyazev, A.: Toward the optimal preconditioned eigensolver: locally optimal block preconditioned conjugate gradient method. *SIAM J. on Scientific Computing* **23(2)** (2001) 517–541
5. Payne, M.C., Teter, M.P., Allan, D.C., Arias, T.A., Joannopoulos, J.D.: Iterative minimization techniques for ab initio total-energy calculations: molecular dynamics and conjugate gradients. *Rev. Mod. Phys.* **64** (1992) 1045–1097

6. Thornquist, H.: Fixed-Polynomial Approximate Spectral Transformations for Preconditioning the Eigenvalue Problem. Masters thesis, Rice University, Department of Computational and Applied Mathematics (2003)
7. Wang, L.W., Li, J.: First principle thousand atom quantum dot calculations. *Phys. Rev. B* **69** (2004) 153302
8. Wang, L.W., Zunger, A.: *Pseudopotential Theory of Nanometer Silicon Quantum Dots application to silicon quantum dots*. In Kamat, P.V., Meisel, D.(Editors): *Semiconductor Nanoclusters* (1996) 161–207
9. Wang, L.W., Zunger, A.: Solving Schrodinger's equation around a desired energy: application to silicon quantum dots. *J. Chem. Phys.* **100(3)** (1994) 2394–2397
10. Wang, L.W., Zunger, A.: Pseudopotential calculations of nanoscale CdSe quantum dots. *Phys. Rev. B* **53** (1996) 9579

# A Grid-Based Bridging Domain Multiple-Scale Method for Computational Nanotechnology

Shaowen Wang<sup>1</sup>, Shaoping Xiao<sup>2,3</sup>, and Jun Ni<sup>1,2,4</sup>

<sup>1</sup>Academic Technology -- Research Service, Information Technology Services

<sup>2</sup>Department of Mechanical and Industrial Engineering

<sup>3</sup>Center for Computer-Aided Design

<sup>4</sup>Department of Computer Science,

The University of Iowa, Iowa city, IA, 52242, USA

{Shaowen-wang, shaoping-xiao, jun-ni}@uiowa.edu

**Abstract.** This paper presents an application-level Grid middleware framework to support a bridging domain multi-scale method for numerical modeling and simulation in nanotechnology. The framework considers a multiple-length-scale model by designing specific domain-decomposition and communication algorithms based on Grid computing. The framework is designed to enable researchers to conduct large-scale computing in computational nanotechnology through the use of Grid resources for exploring microscopic physical properties of materials without losing details of nanoscale physical phenomena.

## 1 Introduction

In the study of nano-materials or nano-devices, a molecular dynamics (MD) model [1] plays an important role. However, many existing MD algorithms have limitations either on length or on time scales due to the lack of enough compute power. Even the most powerful high performance computing (HPC) system is still not powerful enough to perform a complete MD simulation [2]. Therefore, an innovative computational methodology for MD simulations is urgently needed.

Recently-developed concurrent multiscale methods [3] take into consideration of multiple length scales in predicting macroscopic properties. For example, a bridging domain coupling method [4] performs a linkage between the continuum and molecular models. However, if the ratio of mesh size in the continuum domain to the lattice space in the molecular domain is too large, there is a difficult to eliminate a spurious phenomenon in which a nonphysical wave reflection occurs at the interface of different length scales. Therefore, concurrent multiscale methods also require a tremendous computing power. In addition, a small time step (the order of femtosecond) must be selected to meet numerical stability of MD stimulation at the molecular model. Such requirement causes to waste compute time during simulations. A feasible and efficient method is needed to conduct a complete modeling and simulation of large nano systems within long time scales. This requirement stimulates the authors to develop a Grid-based Bridging Domain Multiscale Method (GBDMM).

Grid computing [5-7] enables users to assemble large-scale, geographically-distributed, heterogeneous computational resources together for intensive MD computations. This assemblage is dynamically orchestrated using a set of protocols as well as specialized software referred to as Grid middleware. This coordinated sharing of resources takes place within formal or informal consortia of individuals and/or institutions that are often called Virtual Organizations (VO) [8]. In a similar way, Grid application-specific middleware must be developed for MD related multi-scale methods. We intend to develop a micro/macro coupling method and Grid application middleware for multiscale computation in nano-science and technology.

Section 2 reviews the bridging domain coupling method and describes its extensions in the GBDMM. Section 3 addresses domain-decomposition and communication algorithms for the GBDMM. Section 4 presents the framework of Grid nano-middleware for GBDMM’s implementation.

## 2 Grid-Enhanced Bridging Domain Multiscale Method (GBDMM)

### 2.1 Bridging Domain Coupling Method

The bridging domain coupling method contains a continuum domain,  $\Omega^C$ , which is overlapped with a molecular domain,  $\Omega^M$ , through a bridging domain,  $\Omega^{int}$  (Fig. 1). The scaling of the molecular and continuum Hamiltonians is performed in the bridging domain. The Lagrange multiplier method is used to conjunct the molecular domain with the continuum domain via constraint condition(s),  $\mathbf{u}^C(\mathbf{X}_I, t) - \mathbf{u}_I^M(t) = 0$ , where  $\mathbf{u}$  is the displacement. The total Hamiltonian of the system can be written as

$$\begin{aligned}
 H = & \int_{\Omega^C} \beta(\mathbf{X})(K^C + U^C) d\Omega^C + \sum_I (1 - \beta(\mathbf{X}_I))(K_I^M + U_I^M) + \\
 & \sum_{I \in \Omega^{int}} \lambda(\mathbf{X}_I)(\mathbf{u}^C(\mathbf{X}_I, t) - \mathbf{u}_I^M(t))
 \end{aligned}
 \tag{1}$$

where  $\beta(\mathbf{X})$  equals zero in  $\Omega^M$  and unity in  $\Omega^C$  except the bridging domain. Within the bridging domain,  $\Omega^{int}$ , it smoothly varies from zero to one. If an irregular bridging domain is considered, a nonlinear function  $\beta(\mathbf{X})$  can be introduced. The function can be derived from a signed distance function, or defined by radial basis functions from a set of points.  $K$  and  $U$  are the kinetic and potential energies.  $\lambda(\mathbf{X})$  is a Lagrange multiplier field that can be obtained from the finite element approximation as shown in Fig. 1. Based on the classical Hamiltonian mechanics, the discrete equations of Equation (1) can be expressed as

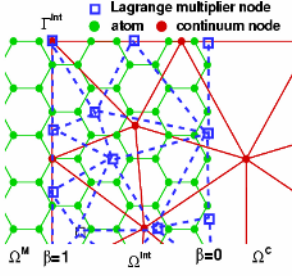


**Fig. 1.** The bridging domain coupling model for a graphite sheet

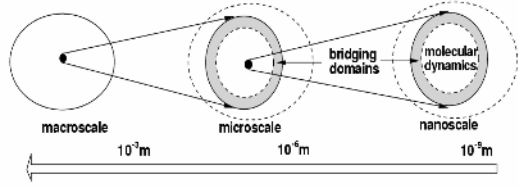


**Fig. 2.** Length scales covered in the BDMM

$$\begin{aligned} \bar{M}_I \ddot{u}_I^C &= \mathbf{f}_I^{\text{ext}C} - \mathbf{f}_I^{\text{int}C} - \mathbf{f}_I^{\text{LC}} & \text{in } \Omega^C, \\ \bar{m}_I \ddot{u}_I^M &= \mathbf{f}_I^{\text{ext}M} - \mathbf{f}_I^{\text{int}M} - \mathbf{f}_I^{\text{LM}} & \text{in } \Omega^M \end{aligned} \quad (2)$$

where  $\bar{M}_I$  and  $\bar{m}_I$  are the modified nodal and atom masses;  $\mathbf{f}_I^{\text{ext}}$  and  $\mathbf{f}_I^{\text{int}}$  are the external and internal forces, independently;  $\mathbf{f}_I^L$  is the force due to constraints in the bridging domain. During simulation, velocities are obtained independently in the continuum and molecular domains from Equation (2) without the consideration of constraint forces. Constraint conditions are then used to calculate the Lagrange multipliers. Finally, the constraint forces in Equation (2) are used to correct the nodal/atom velocities in the bridging domain, thus eliminating the wave reflection automatically.

## 2.2 Multiscale Considerations in GBDMM

Based on the bridging domain coupling method, we proposed a Bridging Domain Multiscale Method (BDMM), which bridges from nanoscale to microscale to macroscale (Fig. 2). A bridging domain multiscale model contains a macro-scale domain ( $\sim 10^{-3}$  m) as a linear elasticity domain in which linear finite element methods (FEM) can be used. The material properties can be obtained from the Representative Volume Element (RVE) technique with molecular dynamics simulation. The BDMM embeds a micro-scale domain ( $\sim 10^{-6}$  m) in the macro-scale domain. It models physical behaviors of materials using either nonlinear FEM [9] or extended FEM [10] (if crack propagation is considered at the microscale). Furthermore, a quasi-continuum technique [11] is implemented with the FE methods at the microscale, so that the constitutive equations can be constructed based on the atomic level energy. A sub-domain in a microscale domain can be treated as a nanoscale (molecular) domain ( $\sim 10^{-9}$  m) in which molecular dynamics is employed. The BDMM couples various scales without grading down mesh sizes. Such coupling leads to a straightforward implementation of different time steps via a multiple-time-step algorithm.

### 3 Domain Decomposition and Communication Algorithms

To perform simulations using GBDMM, an efficient algorithm of domain decomposition must be developed. An entire physical domain with multiple length scales specified can be hierarchically divided into multiple sub-domains. The first generation (FG) sub-domains, such as  $\Omega_{01}^M$  (see Fig3), are generated based on variation in length scales. These sub-domains are allocated on heterogeneous Grid computing resources. Such first-generational domain decomposition is designed to avoid high network latency, and hence produce a loosely-networked computation on Grids.

Each FG sub-domain can further be divided into a number of second generation (SG) sub-domains being parallel-processed on different computational nodes within a Grid resource. A bridging sub-domain is only shared between two SG sub-domains, which belong to two different length scales, respectively. Although one SG sub-domain can be overlapped with two or more SG sub-domains, the bridging sub-domains are not overlapped with each other.

There are two types of communications in the GBDMM (see Fig. 4). The inter-domain communication among the SG sub-domains takes place within an inter-connection within a Grid resource, performing a traditional parallel computation. This computation guarantees the consistency and integrity of SG sub-domains and boundary information for solving the governing equations of atom motions. The procedure for solving equations of atom motion on each Grid cluster is independent. After solving the equations at each time step, communication takes place between two clusters. The bridging coupling techniques are then applied to correct the trial velocities of nodes or atoms in each bridging sub-domain independently.

For example, a simple GBDMM have two sub-domains  $\Omega_A$  and  $\Omega_B$  in the molecular domain, allocated to a single Grid resource (often a computing cluster), and  $\Omega_C$  and  $\Omega_D$  in the continuum domain, allocated to another Grid resource. The communication between the group of  $\Omega_A$  and  $\Omega_B$ , and the group of  $\Omega_C$  and  $\Omega_D$  takes place on networks in a Grid environment.  $\Omega_A$  and  $\Omega_B$  share an atom  $E$ . Bridging domains  $\Omega_A^{\text{int}}$  and  $\Omega_B^{\text{int}}$  perform energy and force calculations. The results from  $\Omega_B^{\text{int}}$  are used to calculate the body potential functions and inter-atomic forces in  $\Omega_A$ , since  $\Omega_A$  and  $\Omega_B^{\text{int}}$  share with same atoms. The size of bridging domains depends on the selected potential functions, especially the cutoff distance for Van der Waals potential functions.

The continuum sub-domains,  $\Omega_C$  and  $\Omega_D$  share a boundary node  $F$  as shown in Fig. 4.  $F^C$  and  $F^D$  represent the same node  $F$  in different sub-domains. Unlike inter-domain communications (which do not require bridging domains), the communication between continuum sub-domains,  $\Omega_C$  and  $\Omega_D$  exchange internal forces of boundary nodes through the networks among Grid resources. For instance, the internal force of node  $F^C$ , calculated in the sub-domain  $\Omega_C$  is fetched to the sub-domain  $\Omega_D$  to form an external force on the node of  $F^D$ , but in an opposite direction. A similar procedure is conducted to pass the internal force of node  $F^D$  as the negatively external force of node  $F^C$ . Therefore, the motions of node  $F$ , updated from  $\Omega_C$  and  $\Omega_D$  are consistent.



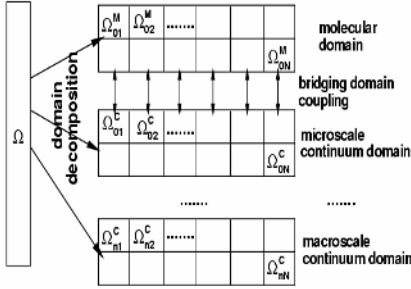


Fig. 3. Domain decomposition for the GBDMM method

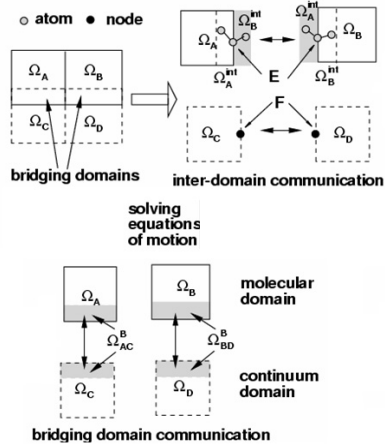


Fig. 4. A demonstration for domain communications

After equations of motion are solved independently on each cluster, bridging-domain communication takes place independently in each bridging sub-domain, such as  $\Omega_{AC}^B$  and  $\Omega_{BD}^B$ . For instance, the trial velocities of atoms in  $\Omega_{BD}^B$  of  $\Omega_B$  are transferred to  $\Omega_D$ , while the trial velocities of nodes in  $\Omega_{BD}^B$  of  $\Omega_D$  are transferred to  $\Omega_B$ . The bridging domain coupling technique is then applied to correct the trial velocities of atoms in  $\Omega_{BD}^B$  of  $\Omega_B$  as well as in  $\Omega_{BD}^B$  of  $\Omega_D$ , respectively on each mater nodes.

### 4 Framework of Grid Middleware for GBDMM Implementation

An application-level Grid middleware framework is designed (in Fig. 5) to enable a GBDMM implementation. In this framework, middleware manages available computing resources, schedules decomposed domains to appropriate Grid resources (i.e. clusters). It contains (1) a task scheduling advisor (TSA) that takes the result of domain decomposition as input to produce scheduling plans and achieve high-performance simulation through load-balancing; and (2) an information broker (IB) that leverages Grid information services to provide the task scheduling advisor with a resource discovery query functions [12].

The framework is centered on the TSA that is used to schedule sub-domains to an appropriate set of Grid resources discovered to achieve optimal performance: tasks are allocated to balance computations across the available set of resources. The sub-domains are converted to the tasks that are placed in Grid-resource queues. The TSA is designed to achieve high levels of performance by balancing tasks across available resources. It determines the correspondence between tasks and the available Grid resources. Within the TSA, several static scheduling strategies [13] such as Min-min and Max-min have been implemented. The fine granularity of the domain decomposition in GBDMM is designed to achieve high level parallelism. Static scheduling

strategies are developed to assign tasks based on computational intensity information for each sub-domain, as well as the variability in the computing capacity of each Grid resource. The workflow of the nano-middleware enhanced GBDMM with Grid computing is shown as Fig. 6.

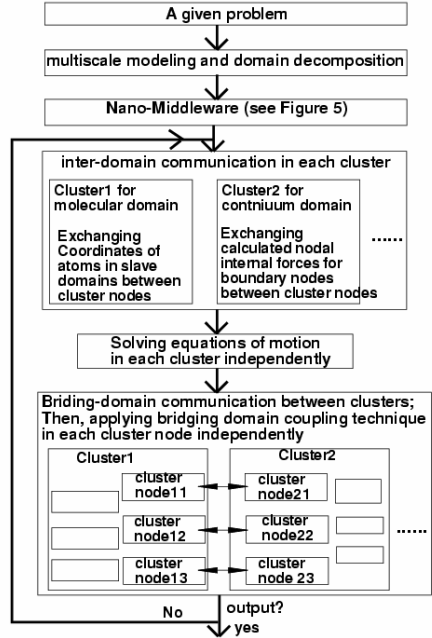
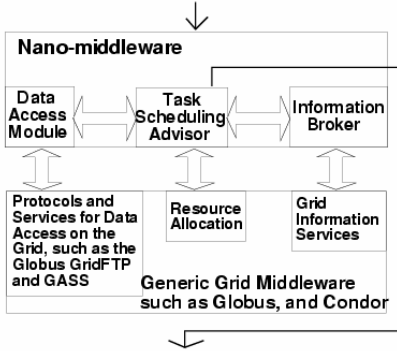


**Fig. 5.** The Grid nano-middleware architecture. Note: Globus is a software project, the purpose of which is to develop protocols and services for computational grids. Condor is a high throughput computing system

**Fig. 6.** The work flow of GBDMM

TSA is used to schedule sub-domains to an appropriate set of Grid resources discovered to achieve optimal performance: tasks are allocated in a way that balances computations across the available selection of resources. The sub-domains information is converted to the tasks that are placed in Grid-resource queues. The TSA is designed to achieve high levels of performance by balancing tasks across available resources. It determines the correspondence between tasks and the available Grid resources. The TSA deploys both static and dynamic scheduling, planning to operate static and dynamic scheduling on tasks upon the computing recourse available. The TSA dynamically facilitate the swap of tasks between computing resources according to a dynamic performance evaluation. The fine granularity of the domain decomposition in GBDMM is carefully design to achieve high level parallelism. Static scheduling strategies are developed to assign tasks based on computational intensity information for each sub-domain, as well as the variability in the computing capacity of each Grid resource.

Since Grid resources is very a complex set (resources and network complexities), an IB is needed to perform a self-organized-resource discovery. The IB for the nano-middleware is designed based on a self-organized grouping (SOG) method that manages the Grid complexity. Therefore, the IB contains three strategies: 1) to control resource heterogeneity during a certain period of time; 2) to capture resource dynamics through a publishing mechanism and aggregating mechanism that handles resource dynamically; (3) to enable the assemblage of large number of resources for applications across VO boundaries.

The developed information broker is based on a self-organized resource discovery method. It is well known that currently, the Grid represents an extremely complex distributed computing environment for developing applications because: 1) Grid resources (e.g., CPU, network, storage, and special-purpose instrument) are heterogeneous; 2) Grid resources are dynamic, and they tend to have faults that may not be predictable; 3) Grids are often distributed across security domains with large number of resources involved. Due to this complexity, it has been a great challenge for developing efficient methods for Grid resource discovery that refers to the process of locating satisfactory resources based on user requests. Grid resource discovery must handle the search for desirable subsets of large number of accessible resources, the status and availability of which dynamically change.

The workflow of the nano-middleware enhanced GBDMM with Grid computing is shown as Fig. 6. The workflow demonstrates the integration of computational nanotechnology and computer science in this multi-disciplinary project.

## 5 Conclusion and Future Work

The GBDMM is an extension of the bridging domain coupling method that allows multiple length/time scales to be treated. The GBDMM's domain decomposition and communication are designed to be applicable to distributed Grid resources. The Grid nano-application-middleware includes a task scheduling advisor and an information broker. This middleware enables the GBDM to schedule resources, distribute tasks, and achieve load balancing. Our ongoing work is to implement and apply GBDMM to study mechanical properties of nanostructured materials.

## References

1. Rountree C. L., Kalia R. K., Lidorikis E., Nakano A., Van B. L., Vashishta P: Atomistic aspects of crack propagation in brittle materials: Multimillion atom molecular dynamics simulation. *Annual Review of Materials Research* 32 (2002) 377-400
2. Abraham F. F., Walkup R., Gao H., Duchaineau M., Rubia T. D., Seager M.: Simulating materials failure by using up to one billion atoms and the world's fastest computer: brittle fracture, *Proceedings of the National Academy of Science of the United States of America*. 99(9) (2002) 5777-5782
3. Muralidharan K., Deymier P. A., Simmons J. H.: A concurrent multiscale finite difference time domain/molecular dynamics method for bridging an elastic continuum to an atomic system, *Modelling and Simulation in Materials Science and Engineering*, 11(4) (2003) 487-501

4. Xiao S. P., Belytschko T.: A bridging domain method for coupling continua with molecular dynamics, *Computer Methods in Applied Mechanics and Engineering*, 193 (2004) 1645-1669
5. Foster I., Kesselman C.: *The Grid: Blue Print for a New Computing Infrastructure*. Morgan Kaufmann Publishers, Inc. San Francisco, CA (1999)
6. Foster I.: The Grid: A new infrastructure for 21st century science, *Physics Today* (2003) February, 42-47
7. Berman F., Fox G., Hey T.: *The Grid, past, present, future, Grid Computing, Making the Global Infrastructure a Reality*. edited by R. Berman, G. Fox, and T. Hey John Wiley & Sons, West Sussex, England (2003)
8. Foster I., Kesselman C., Tuecke S., *The anatomy of the grid: enabling scalable virtual organizations*, *International Journal Supercomputer Applications*. 15(3) (2002)
9. Belytschko T., Liu W. K., Moran B.: *Nonlinear Finite Elements for Continua and Structures*, Wiley, New York (2000)
10. Belytschko T., Parimi C., Moës N., Sukumar N., Usui S.: Structured extended finite element methods for solids defined by implicit surfaces, *International Journal for Numerical Methods in Engineering*. 56 (2003) 609-635
11. Tadmor E. B., Ortiz M., Phillips R.: Quasicontinuum analysis of defects in solids, *Philosophy Magazine A*. 73 (1996) 1529-1563
12. Wang, S., Padmanabhan, A., Liu, Y., Briggs, R., Ni, J., He, T., Knosp, B. M., Onel Y.: A multi-agent system framework for end-user level Grid monitoring using geographical information systems (MAGGIS): architecture and implementation. In: *Proceedings of Lecture Notes in Computer Science*. 3032 (2004) 536-543
13. Braun, T. D., Siegel, H. J., Beck, N., Boloni, L. L., Maheswaran, M., Reuther, A. I., Robertson, J. P., Theys, M. D., Yao, B., Hensgen, D., and Freund, R. F.: A comparison of eleven static heuristics for mapping a class of independent tasks onto heterogeneous distributed computing systems. *Journal of Parallel and Distributed Computing*. 61(2001) 810-837

# Signal Cascades Analysis in Nanoprocesses with Distributed Database System

Dariusz Mrozek, Bożena Małyśiak, Jacek Frączek, and Paweł Kasprzycki

Silesian University of Technology, Department of Computer Science,  
ul. Akademicka 16, 44-100 Gliwice, Poland  
{Mrozek, malysiak, kasprzycki}@polsl.pl,  
jacekf@polsl.gliwice.pl

**Abstract.** The signal cascades are a number of successive biochemical reactions, occurring in the cells. In these reactions take part many proteins (often enzymes) and the entire process may be compared to the dominoes effect. The common term used to define a varied biochemical mechanisms regulating processes in the nanonetworks is signal transduction executed in the signal cascades. These processes can be realized in a closed area of space which contains proper quantities of substrates and a set of control molecules working in a predefined manner which was determined by their chemical construction, including changes of chemical activity reached usually by the conformational changes. Information about the signal cascades that happen in the various type of cells for given processes can be retrieved from the biochemical research accessible in the biochemical databases. In this work, the simulation process of the signal transduction in bio-nanonetworks using the distributed database environment is presented and illustrated by the biological example.

## 1 Introduction

In outward things development of nanotechnology is in initial stage. Nowadays, manufacturing methods are very simple and basic at the molecular level. Manufactured products are made from cells. The properties of those products depend on how those cells are arranged. The first approach to implement the nanoprocesses would be coping biocompatible standards in design and implementation phase of such processes. The signal cascades are a number of successive biochemical reactions, occurring in the cells. In these reactions take part many proteins (often enzymes) and the entire process may be compared to the dominoes effect – when the first protein of the cascade is modified, such modified protein has an effect on the next protein modifying it in some direction. Thanks to the signal cascades diverse organisms can live and develop. Furthermore, if some protein take part in signal cascade incorrectly (as a result of mutation in gene coding this protein), effect of this single change can result in the tumor development.

The common term used to define a varied biochemical mechanisms regulating processes in the nanonetworks is signal transduction which is executed in the signal cascades. These processes (coping biocompatible solutions) can be realized in a closed area of space which contains appropriate quantities of substrates and a set of con-

control molecules working in a predefined manner which was determined by their chemical construction, including changes of chemical activity reached usually by the conformational changes. These molecules have a decisive role of a control system. The system is stimulated by external signal molecules coming from outside of the closed area of space to its surface, meeting the function of nanoprocess border. The signal cascades are the fixed cycles of transformations in which the molecular control system performs its control tasks. Actually, this kind of system performing nanoprocess ought to be called as a nanonetworks. The selected substrates (inorganic ions and most of metabolites e.g. sugars, amino acids, and nucleotides) and final products can penetrate through the border of the process in determined conditions. The external stimulating signal molecules only activate the receptors placed in the border of a nanonetwork, excluding selected ions fulfilling the control functions in the signal cascades. The signal transduction [4, 21] is the process of internal transformations and conversions of control molecules in signal cascades expressed as a control of nanoprocesses in a nanonetwork. Generally, one can talk about wide area and local nanonetworks. In living organisms wide area nanonetworks [13, 19] is represented by an electro-chemical net (e.g. nervous system) and extracellular communication net (e.g. immune and hormone systems). The local area nano-network is represented by a cell. Exploitation of a living cell is one of the most natural (but not basic) approach to build the local nanonetwork performing a given production process, which can be modified through the external control. An assurance of survival requirements is the basic condition, which have to be satisfied for the cell. Stimulation of inputs of the signal cascades in a nanoprocess cell from its environment is necessary for the control. Information about the signal cascades that happen in the various type of cells for given processes can be retrieved from the biochemical research available in the biochemical databases. Finally, a sequence of stimuli signals for given process can be determined.

## 2 Architecture of the Simulation System Implementation

The mirror-based architecture presented in Fig. 1 defines the foundation of the simulation system used in the signal cascade analysis. The approach arose as the consequence of the distribution of domain-specific information. Nowadays, the growing number of central repositories for collecting biochemical and biomedical data is observed and many organizations, research institutes and university laboratories around the world lead their projects in order to understand the mysterious nature of living cells. This cause the situation the particular information is distributed in many databases managed by different institutions connected to specific domain, e.g. the huge amount of biomolecular structural data is stored in public databases of the PDB (Protein Data Bank [1]) managed by the RCSB<sup>1</sup> or NCBI's<sup>2</sup> MMDB [20], amino acid sequence information stored in the UniProt<sup>3</sup> [3, 11] and NCBI's databases, human gene data stored in the H-Invitational DB provided by JBIRC<sup>4</sup>, protein interaction data

---

<sup>1</sup> Research Collaboratory for Structural Bioinformatics (<http://www.rcsb.org>).

<sup>2</sup> National Center for Biotechnology Information (<http://www.ncbi.nlm.nih.gov>).

<sup>3</sup> UniProt Consortium (<http://www.uniprot.org>).

<sup>4</sup> Japan Biological Information Research Center (<http://www.jbirc.aist.go.jp>).

managed by BIND<sup>5</sup> [12], etc. Fortunately for the community, all the data is available from these institution's FTP sites in the form of text files (e.g. PDB [17], mmCIF [5] formats), XML-structured files or using dedicated application programming interfaces (OMG's Macromolecular Structure Specification and Biomolecular Sequence Analysis Specification [15]) and loaders (OpenMMS [2, 18] toolkit). Searching information across distributed heterogeneous database systems that store all the enormous volumes of data has become a very important aspect of the scientific research and may be a great challenge.

In the mirror-based approach in Fig. 1, during the query process, data does not come directly from the distributed data sets. The complete sets or subsets of databases are first mirrored to the local server(s) and then queries are submitted to local replicas. In this architecture the source databases are called the primary databases and the local servers are called the secondary databases.

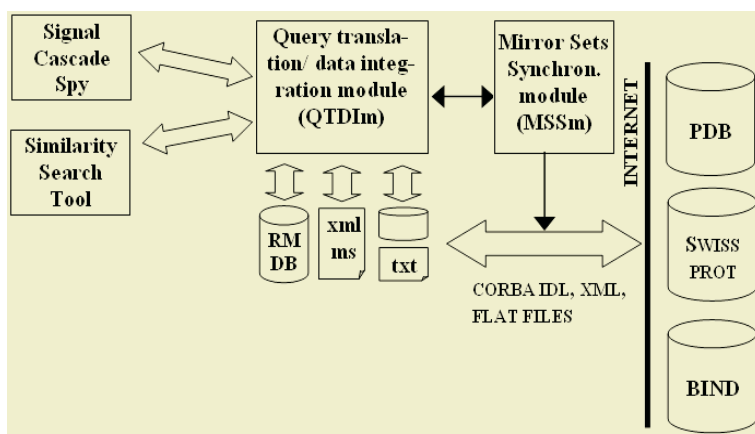


**Fig. 1.** The architecture with mirrored data sets synchronized with the primary databases

The main components of the architecture are: mirrored datasets in the form of relational databases (RMDb icon – Relational Mirrored Database), XML- and TXT- format mirror sets (XML-MS, TXT), the Query Translation/Data Integration module (QTDIm), the Mirror Sets Synchronization module (MSSm) and End-User tools. User queries, similarity searching and advanced computing are triggered from End-User Tools through the QTDIm which is a kind of controller in the process of information extraction. The synchronization process is coordinated by the MSSm, which can be forced to make replicas by the QTDIm, if needed.

### 3 Approximate Methods of Similarity Searching

At present, the afford of implementing the structure similarity search has been made with approximate methods. The main assumption of approximate retrieval methods is

<sup>5</sup> Biomolecular Interaction Network Database of Blueprint Initiative (<http://www.bind.ca>).

that for the answer on the given query we can obtain a set of the objects from database which are consistent with criteria defined in the query with given degree. Queries of this type require defining characteristic function, which determines in what degree the searched object is consistent with criteria defined in the query and threshold value, which allows to qualify the objects that should occur in the answer. Existing retrieval algorithms for the biological databases are based on principles valid in the objects approximate retrieval methods. In the biological databases two trends are separated:

- similarity searching by a protein sequences alignment,
- similarity searching by alignment of a three-dimensional protein structures.

During the research (example introduced in section 5) the PDB [1], BIND [12] and BioCarta [9] datasets were exploited but there is a possibility to access other mirrored databases like UniProt/Swissprot [11] and GenBank [8]. Some features of developed simulation software are presented in Fig. 2.

Fig. 2. Signal Transduction Spy – the Search Manager

Two modes of preparing experiment remain feasible: batch mode and interactive step-by-step mode (left window). Processing data in the batch mode seems to be better because it is going without any control and doesn't affect the user attention – the experiment may take a long time especially during all the processes that use protein conformation computation module to investigate changes in protein 3D structure as a result of environmental parameters changes (e.g. temperature, pH). However, the batch process is supposed to be described in the special purpose process-description files containing all steps of the computation. The mode is in the development phase.



The interactive mode provides users to see what changed during each step of the experiment and to make corrections or to change the way the process goes (e.g. see each step of the signal transduction and the substrates of the cascade, see the network of interactions, explore of protein conformation, change the similarity search method, etc.). In the mode users make use of RasMol [10] to display semi-result structures of their activities in graphical form.

## 4 Processing of a Single Step of the Signal Cascade

Processing of the signal cascade may be divided on processing respective steps of the cascade, represented by reactions on each level. Fig. 3a presents a sample network of the reactions between nanostructures (e.g. proteins, polypeptides). Each reaction results with a creation of a final product. The product may be a protein in the appropriate state and conformation, which can be the activator or inhibitor of the other reactions which take place in the living cell or nanoprocess. Fig. 3b shows the algorithm of tracking the signal cascade step – e.g. 1.7.2.24 reaction [24] marked in the Fig. 3a.

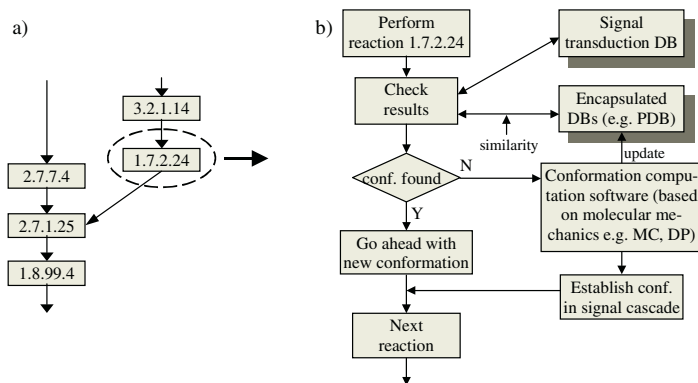


**Fig. 3.** a) Sample network of reactions, b) Processing of a single step of the cascade

During the process of tracking cascade's steps it is possible to check the conformational results (of nanostructure like polypeptide) with the databases consisting of the structural information (e.g. PDB [1]). These databases work as an integral parts of the entire system. The retrieval of similar polypeptides is based on the approximate methods (section 3). If the structure or similar structure (with similarity determined) is found in the database, the system retrieves appropriate information and tracks to the next step of the cascade with the retrieved polypeptide. The information about cascade steps comes from other databases (e.g. BioCarta [9], BIND [12], aMAZE [24]). If the resultant structure is not found in the database, it must be computed with the use of molecular mechanics methods and software, with the assumption of getting minimal potential energy. We are strongly convinced that minimizing of the energy expression describing a conformational energy of structure [7, 22, 23] leads to the problem related with multiple local minima or saddle points and so simple algorithms of optimization e.g. gradient-based, Newton's or Fletcher-Powell have to be modified to find

the global minimum. The implementation of algorithms of dynamic programming (DP) [25] or Monte Carlo (MC) methods [16, 26] is better solution. Moreover, these methods are time- and computer's memory consuming. Once the new conformation is established, it is possible to look for the interactions with other proteins and reactions the new protein can participate and meanwhile the database is being updated.

## 5 Example of Selected Process in the Signal Cascade Analysis

The dataflow in the signal transduction simulation system using the distributed databases environment [14] is presented in Fig. 4. In the system the three databases work as encapsulated parts of the computing process visible through the interfaces A and B.

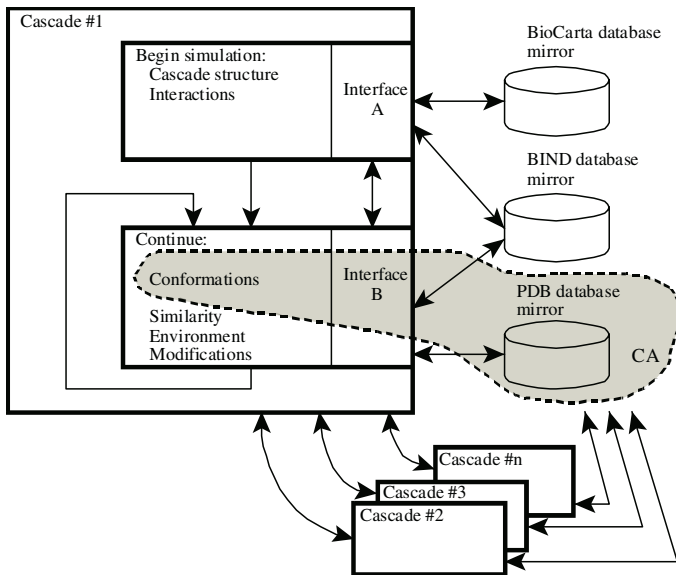
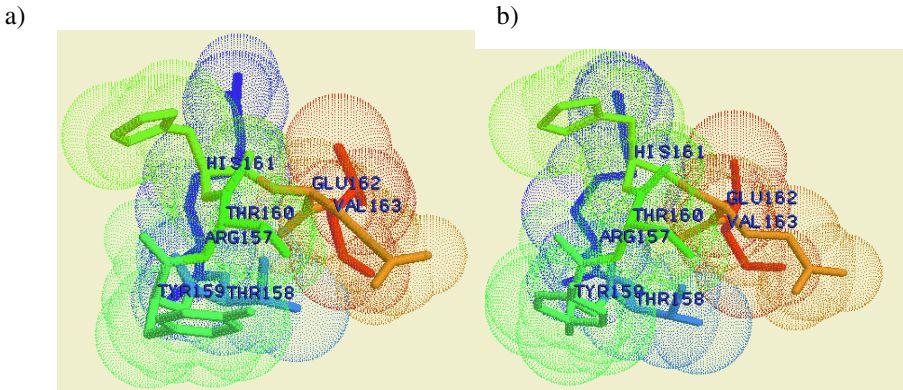


Fig. 4. Dataflow in simulation process

The BioCarta database mirror allows the cascade structures data [9], the BIND database mirror allows nanostructures interactions data [12], and the PDB database mirror allows the molecule structures data [1].

The example presents the approach of conformation determination in signal cascade including the human CDK2 kinase during the phosphorylation process [6] using proper database. In inactive form the CDK2 kinase can be retrieved from the PDB database as molecule signed by 1B38 [1]. During the phosphorylation process the threonine 160 in main chain of CDK2 is modified. To find this conformation change is very difficult by computation. The better solution is to search the proper, existing information from database. In Fig. 4 the shadowed area CA presents this simulation/database operation. To make more visible the critical place responsible for the conformation of kinase CDK2 (in the ATP complex) described by the 1B38 file was processed to extract the threonine 160 neighborhood [6]. Retrieved from 1B38 file the middle

part of the main chain of amino acids of the CDK2 is presented in Fig. 5a. The same part of the main chain of CDK2 after the phosphorylation (extracted from 1B39 file from PDB database) is presented in Fig. 5b. The changes in the conformation can be found basing on molecular mechanics approach, however, the results obtained from operation CA using selected database seem to be more practical.



**Fig. 5.** a) Sticks representation with the van der Waal's dot surfaces of the conformation in a middle part (residues 157-163) of the non-phosphorylated CDK2 (the threonine 160 in the center of view), b) the same view of CDK2 in a middle part of the amino acids chain (residues 157-163) presenting the results of phosphorylation of threonine 160 on the conformation switching of the whole CDK2 structure

## 6 Evolution of the System and Future Research

Searching information in the distributed bioinformatics databases takes integral part of the signal cascade analysis process. The paper presents the simulation system under development in the Institute of Informatics, Silesian University of Technology, Gliwice, Poland intended to signal transduction simulation using the data from BIND, BioCarta, PDB (Rutgers) databases, and others. The considered system includes the algorithms of fused signal cascades analysis, the nanostructures conformation determination, the sequence (amino acids chain) and shape (conformation) similarity searching and the solution of the encapsulation of databases (DB mirrors, interfaces and control) enables to use the proper database in the on-line computing.

## References

1. Berman, H.M., Westbrook, J., Feng, Z., Gilliland, G., Bhat, T.N., Weissig, H., Shindyalov, I.N., Bourne, P.E.: The Protein Data Bank. *Nucleic Acids Res.* 28 (2000), 235-242
2. Greer, D.S., Westbrook, J.D., Bourne, P.E.: An ontology driven architecture for derived representations of macromolecular structure. *Bioinformatics.* 18 (2002) 1280-1281
3. Apweiler, R., Bairoch, A., Wu, C.H., et al.: UniProt: the Universal Protein knowledgebase. *Nucleic Acids Research.* 32 (2004) D115-D119

4. Berridge, M.J.: The Molecular Basis of Communication within the Cell. *Scientific American*. 253 (4) (1985) 142-152
5. Bourne, P.E., Berman, H.M., Watenpaugh, K., Westbrook, J.D., Fitzgerald, P.M.D.: The macromolecular Crystallographic Information File (mmCIF). *Methods Enzymol.*, 277 (1997) 571-590
6. Brown, N.R. et al.: Effects of Phosphorylation of Threonine 160 on Cyclin-dependent Kinase 2 Structure and Activity. *J. of Biol. Chem.* 274(13) (1999) 8746-8756
7. Znamirowski, L., Zukowska, E.D.: Simulation of Post-translational Conformations in the Ribosomal Polypeptide Synthesis. *Proc. of the IASTED Intern. Conf. Modeling and Simulation*, Marina del Rey, California, ACTA Press, Anaheim-Calgary-Zurich (2002) 97-102
8. Benson, D.A., Karsch-Mizrachi, I., Lipman, D.J., Ostell, J., Wheeler, D.L.: GenBank: update. *Nucleic Acids Res.* 32(Database issue) (2004) D23-6
9. BioCarta: Charting Pathways of Life. <http://www.biocarta.com/genes/>
10. Sayle R. RasMol: Molecular Graphics Visualization Tool. Biomolecular Structures Group, Glaxo Wellcome Research & Development, Stevenage, Hertfordshire 1998, H. J. Bernstein. v.2.7.1.1, [rasmol@bernstein-plus-sons.com](mailto:rasmol@bernstein-plus-sons.com)
11. Boeckmann, B., Bairoch, A., Apweiler, R., et al.: The SWISS-PROT protein knowledgebase and its supplement TrEMBL in 2003. *Nucleic Acids Res.* 31 (2003) 365-370
12. Bader, G.D., Betel, D., Hogue, C.W.V.: BIND: the Biomolecular Interaction Network Database. *Nucleic Acids Research*. Vol. 31(1) (2003) 248-250
13. Snyder S.H.: The Molecular Basis of Communication between Cells. *Scientific American*, 253 (4) (1985) 132-141, (1985)
14. Signal Transduction Simulation System Using the Distributed Databases Environment. Research Project BW/2004/05, Institute of Informatics, Silesian University of Technology, Gliwice (2005)
15. <http://www.omg.org>
16. Warecki, S., Znamirowski, L.: Random Simulation of the Nanostructures Conformations, Intern. Conference on Computing, Communication and Control Technology, Proceedings Volume I, The Intern. Institute of Informatics and Systemics, Austin, Texas, August 14-17, p. 388-393, (2004)
17. Callaway, J., Cummings, M., et al.: Protein Data Bank Contents: Atomic Coordinate Entry Format Description, Federal Govern. Agency. (1996) <http://www.rcsb.org/pdb/docs/format/>
18. <http://openmms.sdsc.edu>
19. Tonegawa, S.: The Molecules of the Immune System, *Scientific American*, 253 (4) (1985) 122-131
20. Wang, Y., Adress, K.J., Geer, L., Madej, T., Marchler-Bauer, A., Zimmerman, D., Bryant S.H.: MMDB: 3D structure data in Entrez. *Nucleic Acids Res.* 28 (2000) 243-245
21. Ray, L.B.: The Science of Signal Transduction. *Science*. 284 (1999) 755-756
22. Znamirowski, L.: Switching VLSI Structures. Reprogrammable FPAA Structures. *Nanostructures. Studia Informatica*. Vol. 25 (4A) (60) (2004) 1-236
23. Ponder, J.: Tinker – Software Tools for Molecular Design. Dept. of Biochemistry & Molecular Biophysics, Washington University, School of Medicine, St. Louis (2001)
24. van Helden, J., Naim, A., Mancuso, R., et al.: Representing and analysing molecular and cellular function using the computer. *Biol Chem.* 381(9-10) (2000) 921-35
25. Bellman, R.: *Dynamic Programming*. Princeton University Press, Princeton, N. J. (1957)
26. Metropolis, N., Ulam, S.: The Monte Carlo Method, *Journal of the American Stat. Assoc.*, 44 (247) (1949) 335-341, (1949)

# Virtual States and Transitions, Virtual Sessions and Collaboration

Imrich Bourilko

University of Florida, Gainesville, FL 32611, USA  
bourilkov@phys.ufl.edu

**Abstract.** A key feature of collaboration is having a *log* of what and how is being done - for private use/reuse and for sharing selected parts with collaborators in today's complex, large scale scientific/software environments. Even better if this log is *automatic*, created on the fly while a scientist or software developer is working in a habitual way, without the need for extra efforts. The CAVES (Collaborative Analysis Versioning Environment System) and CODESH (Collaborative DEvelopment SHell) projects address this problem in a novel way, building on the concepts of *virtual state* and *virtual transition* to provide an automatic persistent logbook for sessions of data analysis or software development in a collaborating group. Repositories of sessions can be configured dynamically to record and make available in a controlled way the knowledge accumulated in the course of a scientific or software endeavor.

## 1 Introduction

... a e . . u s f t e d t h r o u g h p a p e r f . l d e r s . r d r e c t r e s . . . u r c . m p u t e r , t r . . g t . f i d . u t h . . . u p r . d u c e d a r e s u t a c u p e f m . . t h s ( r e a r s ) a g . O r h a . . g t . a s e r a q u e s t . . . h e t r a e . . g . t h . . u r f . l d e r s s a f e . s t r e d . . . u r . o f f i c e . O r a d e s p e r a t e c . . a b . r a t r t r . . g t . r e a c h . . u a b . u t a p r . e c t d e t a . . h e . . u a r e h k . g . t h e m u t a . s . t h a p p e e d m a . . t m e s t . m e , a d t h e r e m u s t b e a b e t t e r . . a

## 2 Automatic Logbooks

... e e p r e t h e p s s b . t . t . c r e a t e a a u t . m a t e d s s t e m f r r e c r d . g a d m a k . . g a a a b e t . c . . a b . r a t r s a d p e e r s t h e k . . e d g e a c c u m u l a t e d . . t h e c . u r s e . . f a p r . e c t t h e . . r k . . a p r . e c t s a t m z e d a s s e s s i o n s . . s e s s . . s d e f i n e d a s a t r a s t . . T f r m a . . t a | I > t a f i a | F > s t a t e | F > T | I > h e . . r k d . e d u r . g a s e s s . . s r e p r e s e n t e d b y t h e t r a s t . . . p e r a t r T . . h e . . e g t h . . f a s e s s . . s m t e d b y t h e d e c . . . f t h e u s e r t . r e c r d a c h u k . f a c t . t . . s t a t e c a . b e r e c r d e d t h d . e r e t . e e . f d e t a . d e t e r m . e d b y t h e u s e r s | S t a t e > | L o g b o o k p a r t , E n v i r o n m e n t > h e s s t e m r e c r d s a u t . m a t c a . . . a p e r s t e t . a . . t h e . . g b . . k p a r t f r f u t u r e u s e h e e . . r . m e t s c . . s d e r e d a s a a a b e . r p r . . d e d b y t h e c . . a b . r a t . g g r . u p t h e s p . t t . g b e t w e e .

... global knowledge, remote parts states, meet arbitrarily, etc. call a *collaborating contract*, the sense that it defines the responsibilities of the parties involved, a predictable, structured, specialized, the transition operator  $T$  acting as a meaningful, the integrated part through abstracting substitution the environment.

It suffices to see of details, each final state  $|F\rangle$  can be reproduced at any time from the global final state  $|I\rangle$  and the transition  $T$ . The abstractly reproduced states bring us to the notion of *virtual state* and *virtual transition*, the sense that each recorded states that existed in the past and can recreate them. Demand the future virtual states serve as *virtual checkpoints*, reminders for *virtual sessions* a traditional programming language, the user typically codes the transition  $T$ , the programmer adapts the source of the program for producing a global final state, following the language's table knowledge, our approach is that the user works a habitually and the global for the session is created *automatically, on the fly*, hence the session's progress goes here smoothly per se to produce a code, but the user can execute pre-estimated programs of desired length of work's further recording, the user gets to the persistent session representation through a unique identifier<sup>1</sup>.

Let us illustrate this general framework through an example illustrating the activities of users doing a knowledge work in the command-line environment. At the start of a session, the system records details about the initial state. Hence the user gives commands to the shell (e.g., cd, cp, find etc.) during the session, users could run some set of user code, possibly producing output parameters. Hence, knowledge of the system context and state, commands and the source code of a few executed scripts as used during the session, automatically produced global for the transition  $T$ . Later users may change any of the used scripts, delete or add details, use some of them, forget which parameters were used, or have the same or a new user's activities to reproduce a session, a new session (i.e., state) is created and the global for a given unique identifier is derived from the representation through a combination of the commands and the scripts, as well as the produced output parameters, finally as the user at the time of the session, are available, and the results can be reproduced.

### 3 The CODESH/CAVES Projects - Working Implementations of Automatic Logbooks

The CODESH 2 and CAVES projects take a pragmatic approach to assess how the needs of a community of scientists, researchers are developed, building services for knowledge practitioners through creating sophisticated, extendable, automatic global capabilities the functionality of a typical UNIX shell (like tcsh or bash) the CODESH project, a reusable analysis package as ROOT 4 the CAVES project,

<sup>1</sup> The virtual data idea explores similar concepts, putting more emphasis on the transition - abstract transformation and concrete derivations, coded by the users in a virtual data language [1].

these projects provide a easy and habitua, e tr p... t f r researchers t... e p... re... e... cepts... rea... fe app... cat... s a d t... g... e... a u a b e feedback f r... refi... g the s... tem des g...

... th projects use a three t er arch tecture, ... th the users s tt... g at the t... p... t er a d ru... g... hat... ks... er... much... ke a... rma... she... r... de t... ca... t... a ROOT... sess... , a d ha... g... e... te... ded... capab... t... es... , h ch are pr... ded b... the m d d e... a... er... h s... a... er... s... c... ded... Python f r CODESH... r... C++ f r CAVES, b... her... t... g... fr... m... the... c... ass... h ch ha... d... es... the... user... put... the... c... mma... d... e... he... mp... eme... ted... capab... t... es... e... te... d... the... e... ampe... e... ect... 2... he... c... mma... d... set... s... e... te... s... b... e... a... d... users... ca... eas... r... te... add... t... a... c... mma... ds... he... er... t... er... pr... des... the... pers... ste... t... back... e... d... he... first... mp... eme... tat... s... use... a... e... estab... shed... s... urce... c... de... ma... age... me... t... s... stem... the... C... ,... curre... t... ers... s... stem... CVS, dea... f... r... rap... d... de... e... pme... ts... b... teams... f... a... s... ze... he... CVS... tags... assume... the... r... e... f... u... que... de... t... fiers... f... r... rtua... sess... s, mak... g... t... p... ss... b... e... t... e... tract... sess... , f... rmat... de... t... ca... t... the... e... he... the... sess... ,... g... as... first... pr... duced...

he CAVES/CODESH s stems are used as bu... d... g... b... cks... f... r... c... ab... rat... e... a... a... s... s... de... e... pme... t... e... r... me... ts... pr... d... g... ,... rtua... ,... gb... k... capab... t... es... a... d... the... ab... t... t... e... p... re... the... metadata... ass... c... ated... th... d... ere... t... sess... s... ke... aspect... f... the... pr... ect... s... the... d... str... buted... nature... f... the... ,... put... data... ,... the... a... a... s... s... de... e... pme... t... pr... cess... a... d... the... user... base... h... s... s... addressed... fr... m... the... ear... est... stages... Our... s... s... tems... are... fu... fu... ct... a... b... th... ,... ca... a... d... rem... te... m... des... ,... pr... d... ed... that... the... ecessar... rep... s... t... res... are... perat... a... a... d... the... datasets... a... a... ab... e... h... s... a... s... the... users... t... ,... rk... ,... the... r... apt... ps... (ma... be... ha... d... he... ds... t... m... rr... )... e... e... th... ut... a... et... ,... rk... c... ,... ect... ,... r... ust... t... st... re... termed... ate... steps... ,... the... c... urse... f... a... ct... e... a... a... s... s... de... e... pme... t... sess... f... r... the... r... pr... ate... c... sumpt... ,... pub... sh... g... a... suffic... e... t... ,... p... shed... resu... t... h... s... des... g... has... the... add... t... a... b... e... fit... f... ut... z... g... effic... e... t... the... ca... C... a... d... st... rage... res... urces... f... the... users... ,... reduc... g... the... ad... the... d... str... buted... ser... vices... (e... g... Gr... d... )... s... stem... he... users... ha... e... the... ab... t... t... rep... cate... ,... m... ,... arch... e... a... d... de... te... sess... ,... gs... Ga... ,... g... e... per... e... ce... ,... ru... g... the... s... tem... ,... he... p... t... str... ke... the... r... ght... ba... a... ce... bet... ee... ,... ca... a... d... rem... te... usage...

p... ss... b... e... sce... ar... s... that... a... user... ch... es... dur... g... a... sess... t... br... se... thr... ough... the... tags... f... ther... users... t... see... hat... ,... rk... as... d... e... a... d... se... cts... the... g... sess... ,... f... ,... terest... b... e... tract... g... the... peers... ,... g... ere... t... m... des... f... ,... perat... are... p... ss... b... e... the... user... ma... a... t... t... repr... d... uce... a... resu... t... b... e... tract... g... a... d... e... cut... g... the... c... mma... ds... a... d... pr... grams... ass... c... ated... th... a... se... cted... tag... ,... r... ust... e... tract... the... h... st... r... f... a... g... e... sess... ,... r... d... er... t... ,... spect... t... p... ss... b... m... d... f... the... c... de... r... the... ,... puts... a... d... pr... d... uce... e... resu... t... s...

Our first releases are based... a quite complete set of c mma ds pr... d... g... ,... terest... g... fu... ct... a... t... cree... sh... ts... fr... m... a... rea... sess... are... sh... ,... g...

... th s paper... e... ut... e... the... ma... deas... dr... g... the... CODESH... CAVES... pr... ects... he... h... st... r... mecha... sm... r... the... script... ut... t... f... UNIX... she... s... ca... ust... g... the... c... mma... ds... a... d... sta... dard... utput... f... a... ,... rk... g... sess... ,... a... pr... ate... fie... ,... ea... g... a... the... rest... t... the... users... Our... aut... mat... c... ,... gb... k... ,... rtua... sess... ,... appr... ach... d... es... much... m... re... b... ma... ag... g... private... and... shared... repositories... of... complete... session... logs... ,... c... ud... g... the... c... mma... ds... and... the... pr... grams... ,... a... d... the... ab... t... t... repr... d... uce... the... re...



Fig. 1. Example of a CODESH session

systems for reuse them for future development. The first future systems for automatic generation of virtual sessions are available for interested users. The second set of future work includes adding the distributed environment services related to using Grid security, automatic certification, sessions, grids, the ability to develop and seamless schedule management data, test tasks, grid infrastructure. The studies supported partially the funded states at the University of Tübingen. R 8 44 (Gr h ) a d 427 ( t r a g h t )

References

1. Foster, I. *et al.*: Chimera: A Virtual Data System for Representing, Querying, and Automating Data Derivation. In: 14th International Conference on Scientific and Statistical Database Management (SSDBM 2002), Edinburgh, 2002
2. Bourilkov, D.: THE CAVES Project - Collaborative Analysis Versioning Environment System; THE CODESH Project - Collaborative Development Shell. arXiv:physics/0410226 ; <http://xxx.lanl.gov/abs/physics/0410226>
3. Bourilkov, D.: The CAVES Project: Exploring Virtual Data Concepts for Data Analysis. arXiv:physics/0401007, and references therein ; <http://xxx.lanl.gov/abs/physics/0401007>
4. Brun, R. and Rademakers, F.: ROOT - An Object Oriented Data Analysis Framework. Nucl. Inst. & Meth. in Phys. Res. **A 389** (1997) 81–86
5. Grid-enabled Analysis Environment project: <http://ultralight.caltech.edu/gaeweb/>



# A Secure Peer-to-Peer Group Collaboration Scheme for Healthcare System\*

Byong-In Lim, Kee-Hyun Choi, and Dong-Ryeol Shin

School of Information and Communication Engineering,  
Sungkyunkwan University,  
440-746, Suwon, Korea, +82-31-290-7125  
{lbi77, gyunee, drshin}@ece.skku.ac.kr

**Abstract.** P2P (Peer-to-Peer) applications allow flexible organization, distribution of role to participating peers and the ability to share information with the other peers for group collaborations. As a result, P2P systems are not only gaining importance, but also becoming ubiquitous media for information exchange. JXTA is a P2P application development infrastructure that enables developers to easily create service-oriented software. This paper presents a low-cost, patient-friendly JXTA-based healthcare system, which is comprised of medical sensor modules in conjunction with wireless communication technology. Among the most important activities associated with the healthcare system are the sharing of medical information and collaborative medical work. The JXTA grouping service facilitates to share data in a secure manner under P2P environments. Through JXTA grouping service, we implemented a prototyped system, which improves the ability of the healthcare workers to cope with dynamic situation, which in turn makes it possible to offer more efficient medical services.

## 1 Introduction

Advancements in sensor, information and communication technology can play an important role in achieving cost reduction and efficiency improvement in healthcare delivery systems, to the extent that this offers high-quality medical service anytime and anywhere. However, conventional healthcare systems, including the Mobihealth [1] project, utilize a central server for the look up of information. Furthermore, the possibility of offering seamless service is limited by the network connectivity of wireless devices or resource-constraints. In addition, traditional systems only focus on organic communication and service utilization between patients and hospital, whereas they ignore the systematic communication and sharing of information between healthcare workers in the hospital. For these reasons, these systems cannot cope with acute situations dynamically and promptly. Also, privacy and security are potential problems. Patient's data should be available irrespective of their location, but only to authorized healthcare workers.

---

\* This research was partially supported by a grant from the CUCN, Korea and Korea Science & Engineering Foundation (R01-2004-000-10755-0)

To resolve these problems, we propose a JXTA-based healthcare system, which operates in a peer-to-peer (P2P) environment so as to offer seamless service by distributing the healthcare services among the healthcare workers. This sharing of information about the medical treatment that patients receive between the healthcare workers in the JXTA environment improves their ability to cope with dynamic situations, which in turn makes it possible to offer more efficient medical services. Furthermore, the JXTA grouping service makes it possible to share data in a secure manner under the P2P environment. So, our system protects patient's data. In this paper, we focus on the system architecture design in hospital region which is based on JXTA grouping mechanisms.

This paper is structured as follows: Section 2 discusses system architecture for healthcare services and the system implementation is presented in section 3. Finally, this paper is concluded in section 4.

## 2 System Architecture for Healthcare Services

### 2.1 Architecture Overview

Our system consists of two regions, viz. the Healthcare region and the Hospital region, as shown in Figure 1.

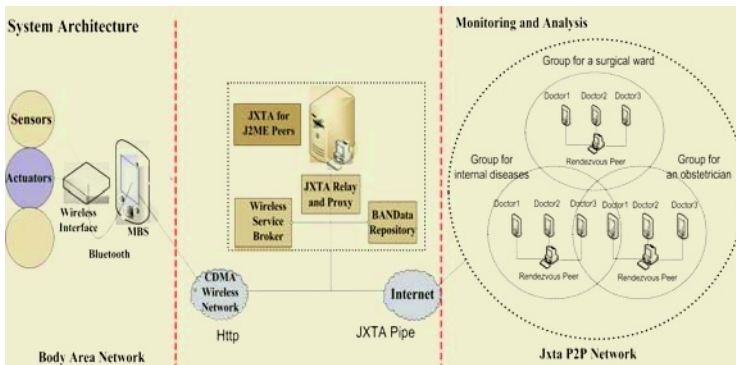


Fig. 1. System Architecture

The healthcare BAN consists of sensors, a Wireless Interface, PDA communication, and various facilities. The Hospital region is composed of the JXTA P2P network that supports the doctor's mobility and dynamic service management modules. A P2P network distributes the information among the member nodes, instead of concentrating it at a single server. A JXTA relay peer is defined among the two regions, in order to provide a systematic computing environment between the Healthcare region and the Hospital region. JXTA relays act as proxies for the individual patients' PDAs, as well as taking care of all the heavier tasks on their behalf. For more details, refer to [2]. In next section, we describe how healthcare services with collaboration of JXTA secure group environment are formed and managed in a hospital region.

## 2.2 Secure Group Collaboration Scheme in Hospital

Among the most time consuming activities associated with the public health sector are documentation and data exchange. In a hospital, the healthcare workers form a peer group within the institution. Together they can create a secure peer group with various access rights, so as to allow the sharing of the patient’s data (e.g. his or her patient UUID, patient sensor data, etc) and other kind of information (e.g. a first-aid, drugs to prescribe, etc) under the secure environment. Figure 2 shows a sequence diagram of group collaboration scheme in hospital domains.

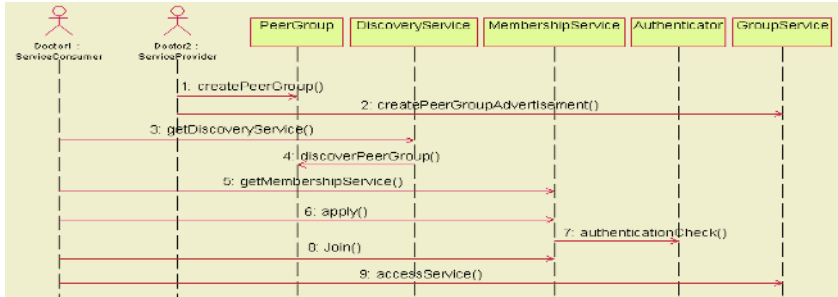


Fig. 2. Sequence Diagram of Group Collaboration Scheme

JXTA combines the overlay network with a namespace abstraction referred to as a peer group [3]. Any peer may create a new peer group at any time for any reason to communicate with any set of peers. The only requirement is that all peers have agreed upon a common set of services and protocols for implementing secure group collaboration (authentication, authorization, message propagation, discovery service, etc). Consequently, JXTA grouping service is an effective means to implement P2P collaboration system under secure environment. This is the main reason for which the healthcare system is based on the JXTA platform. In our system, the healthcare region consists of several groups (e.g. groups corresponding to specific surgical wards, dental treatment, etc). The collaboration scheme of secure peer group is as follows. Before healthcare workers can interact with the group, they need to create a peer group. When creating the peer group, the healthcare workers involved initialize the local secure environment, and then publish a peer group advertisement, which includes the peer group ID and peer group medical service. After the secure group is created, they can perform collaborative service and functionality of the peer. Searching and sharing are done on the peer group level, i.e., shared contents are only available to the peer group. In order for service consumers to utilize medical service, they must firstly achieve their guaranteed passwords as well as the information of secure peer groups which provide medical service in the JXTA network. In JXTA, the membership service is used to apply for peer group membership, join a peer group, and exit from a peer group. The membership service allows a peer to establish an identity within a peer group. Once an identity has been established, a credential is available, which allows the peer to prove that they have obtained the identities rightfully. In our system, the security is ensured by using JXTA grouping mechanism to implement group level security policies for

membership and service access. Also, the JXTA grouping mechanism supports the sharing of medical information and collaborative medical work, which in turn makes it possible to offer more efficient medical services.

### 3 Implementation

In this study, we utilize the JXTA Platform to develop a medical-service management tool as well as secure group collaborations in a hospital domain. We also implemented a software for monitoring the patient’s status, in the BAN as well as in

Sex	Name	Year.Month.Day	Hour:Minute	Tempera	Status	Result
Male	Byong-In...	04-09-27	23:15	24	Stre	119
Male	Hyung-J...	04-09-28	18:22	27	Meal	220
Fem...	Mi-Yong ...	04-09-29	15:47	28	Attn	78
Male	Ki-Hyun ...	04-09-03	10:10	23	Ever	107
Fem...	Mi-Yong ...	04-09-03	10:27	24	Stre	108
Fem...	Mi-Yong ...	04-09-07	17:10	17		
Male	Byong In...	04-09-07	15:10			
Male	Hyung J...	04-09-07	22:38			
Male	Byong In...	04-09-07	23:10			
Fem...	Mi-Yong ...	04-09-09	07:52			
Male	Ki-Hyun ...	04-09-09	09:31			
Fem...	Mi-Yong ...	04-09-09	09:42			
Fem...	Mi-Yong ...	04-09-09	10:21	23	Meal	123
Male	Byong-In...	04-09-09	10:28	23	Attn	267
Male	Hyung-J...	04-09-10	21:30	21	Stre	226
Male	Byong-In...	04-09-10	22:28	19	Stre	184

Fig. 3. Data Management JXTA Application

the JXTA application used for managing the patient’s information; medical status and personal information, as shown in Figure 3. The use of the JXTA Platform with its discovery and grouping mechanisms enables us to offer efficient and adaptive medical services.

### 4 Conclusion

In this paper we have presented the design of a JXTA-based healthcare system which enables healthcare workers to share data in a secure manner under the P2P environment. This paradigm offers significant advantages in healthcare workers to cope with dynamic situations, thus improving the quality of the medical service that they can provide. Future work includes the detailed simulations and performance evaluations for the developed systems.

### References

1. Nikolay Dokovsky, Aart van Halteren, Ing Widya, “BANip: enabling remote healthcare monitoring with Body Area Networks”, International Workshop on scientific engineering of Distributed Java applications, November 27-28, 2003.
2. Byongin Lim, et al, “A JXTA-based Architecture for Efficient and Adaptive Healthcare Services”, ICOIN 2005, LNCS 3391, pp. 776-785, January 31- February 2, 2005.
3. PKI Security for JXTA Overlay Network, Jeff Altman, February 2003.

# Tools for Collaborative VR Application Development

Dr. Arun Raja<sup>1</sup>, R. Arun Ramasamy<sup>1</sup>, Christoph J. Thomas<sup>2</sup>,  
and Alessandro D'Amico<sup>1</sup>

<sup>1</sup> Centre for Advanced Computing and Emerging Technologies,  
The University of Reading, Reading, RG6 6AY, United Kingdom  
sir04amh@reading.ac.uk

<sup>2</sup> GUP Linz, Johannes Kepler University Linz,  
Altenbergerstraße 69, A-4040 Linz, Austria

**Abstract.** This paper introduces a tool set consisting of open source libraries that are being developed to facilitate the quick and easy implementation of collaborative VR applications. It describes functionality that can be used for generating and displaying a Virtual Environment (VE) on varied VR platforms. This is enhanced to provide collaboration support through additional modules such as networking. Two existing VR applications which make use of these tools are described. Both were developed effortlessly over a short period of time, and demonstrate the power of these tools for implementing a diverse range of applications.

## 1 Introduction

With the growing range and performance of VR systems, increasing numbers of users are gaining access to these virtual spaces created through the system, that a user can enter and interact through. Making these users gainous technologies easier to use and the virtual world a better place for the users through quasi-personal interaction.

Despite the many factors that determine the development of collaborative VR applications, the time, effort and expense of the implementation of the tool set consists of the Client-Environment Manager (CEM), network utilities and additional application libraries have been designed and implemented. These add development, creating the application by providing the key functional of generating, displaying and handling a VE.

Work related to these development will be discussed in section 2. This will be followed by sections 3 and 4 respectively. First, a description of the CEM, and then the additional tool set sample applications currently using this tool set are then mentioned in section 4, before the paper concludes in section 5.

## 2 Related Work

For example, the collaborative VR application development requires the consideration of several key areas, most of which have existing implementations.

networked Realities, such as Camach, meshes with the C-ER's first task, and the display geometries render remote users' avatars. networked virtual Environments (VE) of this type, for application users can modify attributes of the shared environment (e.g. transformation of geometries), rendering a more detailed further description of the participating people. Environments [2].

ce. egraph libraries (OpenGL 4, OpenGL), provide a structured database of entities and their relationships. The scene objects, these entities are rendered graphically, using representation of the object's geometry.

acquisition and interaction with the VE's required that users interact with the environment through a graphical method, such as keyboard.

avatars, which are used to graphically represent remote users, both the representation and actions, are a high-impact feature for collaborative environments. Description of these can be implemented [7].

available desktop VR hardware are such as CEs 8, for head-mounted displays can be used for the display of VE's general application should be operated through many of these devices, providing hardware dependence. Ongoing products, such as the current, include the former C-ER's, and Ruggier.

### 3 The CAVE Scene Manager (CSM)

The CSM handles the VE's scene graph representation (described below), as well as a display's rendering of the scene objects but, to provide a scene graph library, for graphical representation of the scene.

through scene graph dependence, could be described for the scene set, OpenGL as a choice for the representation of the scene objects due to its cluster support, structure and flexibility.

#### 3.1 Configuration

Despite its name, the CSM can be used for display of a wide range of VR systems and must use CEs as parameters of these systems, for example, scene graphs, configuration, tracking devices, change with each state. For all of these devices the CSM uses a configuration file which describes the particular setup through its approach, but must refer to a graphical file the same application can be run as a Raptor.

As an example, to represent the standard RSM, the configuration file format is made compatible with that used for C-ER's configuration.

When the CSM is used to utilize the C-ER's parameters, it uses the sufficient for generating multi-aural stereoscopic images, for which the standard require additional, the standard C-ER's configuration, plus, additional parameters have been included for advanced C-ER's configuration.

### 3.2 Internal Scenegraph Representation

The internal structure of the CAVE scene manager is a scene graph for the user. The scene graph is the Open GL representation of these objects. The CAVE scene manager represents the scene graph which are used to describe the graph hierarchy. Here the rectangles are node classes determining the type of node function.

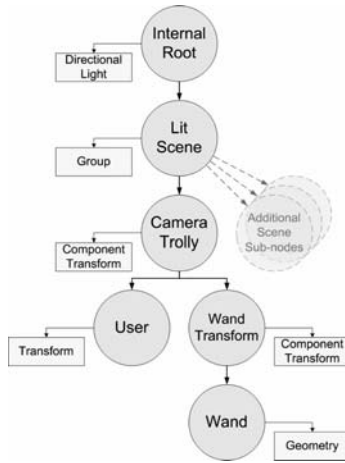


Fig. 1. Node tree for the CAVE Scene Manager

The *internal root* node has a directional light source reference for a head light, this beam being the *lit scene*. This scene is represented by the internal root being the head light source.

The Open GL component transforms used to position a *camera trolley* node has represents the aggregated position of the scene. The camera trolley which the cameras are mounted on. The child nodes from the camera trolley parent are used to show the position of the tracking devices the user position from head tracking, and as the additional position as generated by the CAVE. The basic geometry nodes added to displace the default and then the environment the user, and a camera trolley can be moved depending on the CAVE has functions for updating these positions as required. The CAVE uses the CAVE system the camera trolley using the stack of the controller, the user and a position sensor from the tracking devices. The CAVE system uses these movements to update the CAVE scene from a keyboard use combination.

The application passes the root node of the scene to the CAVE, here it gets added as a child node of the internal root. This is useful for setting a scene that has a fixed location and destination, such as a street or a room. The user can add additional objects to represent objects or remove users. The scene update has been provided to add and remove the scene tree representation of these, and as to change the base position and orientation as required. These functions reference the environment through the root

... depth, but the C... eed, ga... k... edge, f the e... ttes' c... mp... st... h s  
 a... s c... mp... e... a... mated geometries to be eas... c... rp... rated... t... the sce... e  
 ... a s... m... ar... a... the default ad... ge... metr... ca... be... err... d... de... t... d... sp... a... a  
 ... de... tree... h... e... st... track... ga... m... eme... t... f... the... ad... h... s... c... ud... be... used... t...  
 m... de... a... part... cu... ar... t... pe... f... p... ter... a... s... ph... st... cated... m... g... ha... d... r... ee... a... ha... d  
 u... s... g... r... ma... pu... at... g... s... me... add... t... a... b... ect

### 3.3 Display Walls

The C... 's ma... task... s... t... d... sp... a... mages, p... t... a... stere... ,... e... r... m... re  
 s... c... ree... s (m... t... r... s... r... p... ro... j... e... c... t... ,... a... s) v... r... t... u... a... l... cameras are placed... the sce... e,  
 a... d... are used... to... determ... ine... the... mages... be... g... re... dered

The C... c... n... figurat... ,... determ... es... h... ma... cameras... e... st... the... sce... e  
 t... has... fie... ds... f... r... d... sp... a... a... c... figurat... ,... h... ch... descr... be... the... p... s... t... ,... f... the  
 ... e... g... de... ce... re... at... e... t... the... user's... p... s... t... ,... defau... ts... ha... e... bee... p... ro... v... ided... f... r  
 the... regu... lar... C... E... a... s... h... ch... f... r... m... a... cube... ar... u... d... the... user... the... these... are... t...  
 suffic... e... t... ,... such... as... f... r... a... cur... ed... s... c... ree... ,... the... s... y... s... t... e... m... s... c... i... f... i... g... u... r... ed... w... th... the... c... r... e... r  
 c... o... r... d... i... n... at... es... f... the... s... c... ree... '... r... p... ro... j... e... c... t... ,... p... a... e... O... e... camera... s... used... f... r... each... a...  
 be... g... re... dered... ,... fac... g... the... app... r... o... p... r... ate... d... rect... i... o... n... f... r... that... a...

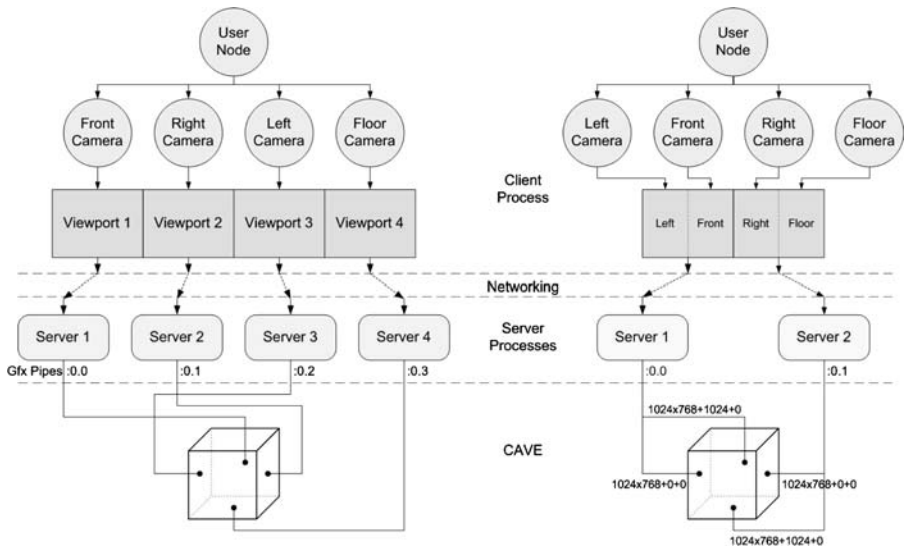


Fig. 2. Client/Server Cluster Window for a 4 pipe (left) and 2 pipe (right) CAVE

### 3.4 Client/Server Clustering Windows

The Ope... G... t... t... k... t (G... ),... h... ch... s... used... f... r... d... sp... a... g... the... graph... cs...  
 ... d... s... ca... ,... ,... output... t... ,... e... graph... cs... p... pe... per... p... ro... c... e... s... s... h... s... a... s... s... ue...  
 the... mu... t... p... e... d... sp... a... s... are... requ... red... .... a... t... e... t... a... mu... t... p... e... p... ro... c... e... s... s... scheme



uses clusters, with the full environment being constructed through a network of dual computers, each responsible for its own part. Some of these approaches are supported in the C++ through Open GL's client server cluster graphics processing handles the scene graph manipulation, and other rendering processes render the graph contents. These processes can be distributed on the same system, separate remote, or a combination of the two. This is achieved through C++ configuration.

In the cluster graphics generated by the client are split over a grid of machines as there are servers. Each server requires the data for its cells, which then renders for its connected display.

Figure 2 shows the possible approaches for cluster graphics. Figure 2E shows the architecture of the left each axis driven through its own pipeline with the client divided into split into 4 pipelines, with each camera packaging its output to one of these. Each server receives a quarter of the client data, therefore receiving the data from the camera for the axis it represents.

The architecture of the right shows that the system has a pipeline, with each of these driving its own axis. In this case the client data is split half, with each half being sent to a dedicated server. The pipelines are combined into each of these halves to display the correct image split over the axis. This is an example of the split server calculation, the middle of each graph pipeline.

## 4 Additional Functionality

In addition to the scene added display functionality provided by the C++ server, other useful tools are also included. These include a command parser for accepting user input, which could be used to activate certain commands, a display functionality of dual application configurations files can also be utilized, and a network using the same methods as for C++ configuration.

Three of the more important tools are an avatar, a network, and a gateway to interact with the description.

**Avatars.** It is possible for an avatar currently is implemented. Avatars have been included in the implemented realm, where they can make use of range based details, allowing a particular large number of them to be simulated using a technique of the process. Generally, the avatar is a high graph camera avatars that react to the environment, can also be used to create observer immerses, as the more a display performs pre set actions, which react to camera.

**Networking.** The network infrastructure has been developed providing a network, a data readability has been integrated into a topological based on the description from making topological remote clients readable, communication, the network is a structured default network handling, including the necessary message for remote avatar representation. This functionality has been provided to allow sharing of user defined messages, so can be seen in the sample application. These messages can be used for a data communication.

networks must be added, debugging debug routines have also been developed for assistance in application development.

**Navigation and Interaction.** Each time the displayed frame is updated the application passes the tracking information from shared memory to the head and hand tracking data are passed to the C, the controller information is used for navigation and interaction. Currently, navigation makes use of the joystick and a direct manipulation method, the scene is static and that this could be further extended through the integration of a navigation framework such as that described in [2].

As collisions are detected between the user and the scene has also been provided for the use of the heads buttons had been activated. Either as a result of this, or directly from the interaction with the head to pass between trajectories to allow remote users, thereby forming the basis of user interaction and collaboration. It is noted that achieved from a simple visual response.

## 5 Applications

### 5.1 Flooding Visualisation

This application demonstrates the benefits gained through visualisation of a mmers. The environment is part of the E-CRO-GR project, it uses the GR framework and graphics must be the C project. The integration part of this application, and the ease of using the various types of hardware.



Fig. 3. Interaction in the CAVE, Curved Screen and on a desktop system

The data to be simulated is calculated with Gbus models and are the GR and the transferred to the display devices through GR. The simulation makes use of the types of R-2 models. The first makes up the landscape and consists of a height map geometry of the terrain, upon which a photographic image has been superimposed. This provides a realistic environment through spatial relationships.

The second group of models are used for representing the water. Separate sets of triangle meshes are provided for each time stamp during the rendering process, and these are applied sequentially to the terrain to simulate the water.

... r effice c ... ma ... ta ... g a rea ... st c frame rate (> 30 fps), a ... ge metr data ... s pre ... aded ... t the sce ... e ... start up ... he sce ... e ... t has t ... ch ... dre ... e f r ... the terra ... a d the sec ... d a s ... tch ... de ... h ch pare ts each ... d ... dua ... d ... g ... t me ... s ... e a d c ... t r ... s ... h ch image s be ... g re ... dered ... he s ... tch ... de steps ... thr ... ugh these s ... ces ... rder, pr ... d ... g sm ... th a ... mat ... O ... a desktp s stem ... the s mu at ... s c ... t r ... ed ... a a ke b ... ard, hereas fu ... mmers ... e s stems ... a s use the r ... a d ... g ... a g a t ... m de s used, a ... g the sce ... e t ... be ... e ... ed fr ... m a ... a g e ... he ke b ... ard, r ... a d s a s used f r a ... mat ... g f r ... ard ... r back ... ards at a pre defi ed speed, r ... f r paus ... g the s mu at ... gure ... dem ... strates the s mu at ... be ... g used ... three d ... ere t ... R p ... atf rms

### 5.2 Virtual House Application

The second application has been developed as a easy-to-use desktop application that allows remote users to interact collaboratively through a virtual environment. This is built using the RealSense which manages space and navigation, but the Core Engine the desktop uses the network function to attribute each user's movement data, and the avatar is displayed on the screen.

Current functionality shares tasks associated with the game design and rendering of the virtual environment. This can be seen in figure 4, which shows a Core Engine user able to manipulate a moving door that has been opened by a desktop user. In each case the remote user position is depicted by an avatar in the virtual objects that can be interacted with. These remote are defined as



Fig. 4. Collaborative door opening in the Virtual House application

... am c ... teract ... Ob jects ( O ) ... he c ... ta ... attributes a d fu ... ct ... a t ... reat ... e t ... h ... the ca ... perf m ... r ... sta ... ce, the d ... r ... O has attr ... butes ... decar ... g ... ts a s ... f r ... tat ... a d the degree ... f r ... tat ... a ... ed ... r ease ... f ... ma ... g e m e t a d e b ... t these attr ... butes are c ... ta ... ed ... a t e t f i e ... h c h s ... read dur ... g e c u t ...

O ... t a ... zat ... the sce ... e graph s tra ... versed, a d ... Os are created f r th ... se ... defi ed fr ... m the te t f i e ... m p ... e c ... s ... detect ... s used t ... detem ... e f a ... user s ... teract ... g ... th ... e ... f these ... Os, a d f ... s ... the ree ... a t attr ... butes are ... m d f i e d ... d d t ... a ... a ... Ob ject ... a g e r c ... m p ... e t c ... t ... u ... s ... er ... ces the

Os, allowing them to modify the E as required. Elements, such as the display geometry, are set over the network for remote configuration. Future improvements will increase functionality of the O, allowing the respondent to manipulate elements, thereby developing realistic multi-user collaborative environments. Further studies as required to evaluate the current terms of a framework to meet a design pass.

## 6 Conclusion

This work describes a useful set of tools that have successfully been used to implement distributed types of collaborative Remote Meetings. It is hoped that these form the basis of a portable and larger and more advanced engineering tool. A work could see a dedicated network, the integration of a gateway, browser, implemented aatars and further collaborative support, which could also be equally simple, but more advanced application development.

## References

1. Park, K., Cho, Y., Krishnaprasad, N., Scharver, C., Lewis, M., Leigh, J., Johnson, A.: CAVERNsoft G2: A toolkit for high performance tele-immersive collaboration. In: VRST, Seoul, Korea, ACM Press (2000) 8–15
2. Macedonia, M.R., Zyda, M.J.: A taxonomy for networked virtual environments. *IEEE MultiMedia* 4 (1997) 48–56
3. Matijasevic, M.: A review of networked multi-user virtual environments. Technical report tr97-8-1, Center for Advanced Computer Studies, Virtual Reality and Multimedia Laboratory, University of Southwestern Louisiana, USA (1997)
4. Rohlf, J., Helman, J.: IRIS Performer: A high performance multiprocessing toolkit for real-time 3D graphics. In: SIGGRAPH, ACM Press (1994) 381–394
5. Reiners, D.: OpenSG: A scene graph system for flexible and efficient realtime rendering for virtual and augmented reality applications. PhD thesis, Technische Universität Darmstadt (2002)
6. Bowman, D.A., Koller, D., Hodges, L.F.: Travel in immersive virtual environments: An evaluation of viewpoint motion control techniques. In: VRAIS (1997) 45–52
7. Badler, N.I., Phillips, C.B., Webber, B.L.: *Simulating Humans: Computer Graphics Animation and Control*. Oxford University Press, New York, NY, USA (1992)
8. Cruz-Neira, C., Sandin, D.J., Defanti, T.A., Kenyon, R.V., Hart, J.C.: The CAVE: Audio Visual Experience automatic virtual environment. *Communications of the ACM* 35 (1992) 64–72
9. VRCO website. <http://www.vrco.com/> (2004)
10. Bierbaum, A.D.: VRJuggler: A virtual platform for virtual reality application development. Master's thesis, Iowa State University, Ames, Iowa (2000)
11. Anthes, C., Heinzlreiter, P., Volkert, J.: An adaptive network architecture for close-coupled collaboration in distributed virtual environments. In: VRCAI, Singapore (2004) 382–385

12. Anthes, C., Heinzlreiter, P., Kurka, G., Volkert, J.: Navigation models for a flexible, multi-mode VR navigation framework. In: VRCAI, Singapore (2004) 476–479
13. Hluchy, L., Habala, O., Tran, V.D., Simo, B., Astalos, J., Dobrucky, M.: Infrastructure for grid-based virtual organizations. In: Proceedings of the International Conference on Computational Science, Part III, LNCS 3038, Springer Verlag (2004) 124–131

# Multicast Application Sharing Tool – Facilitating the eMinerals Virtual Organisation

Gareth Lewis<sup>1</sup>, Mehmed Hasan<sup>1</sup>, Assistant Lecturer<sup>1</sup>,  
Martin Lewis<sup>2</sup>, Adnan Cakir<sup>2</sup>

<sup>1</sup> Advanced Computing and Emerging Technologies Centre,  
School of Systems Engineering, University of Reading,  
Whiteknights, P.O. Box 225,  
Reading, RG6 6AY, United Kingdom  
{g.j.lewis, s.m.hasan, v.n.alexandrov}@rdg.ac.uk  
<http://acet.rdg.ac.uk>

<sup>2</sup> Department of Earth Sciences, University of Cambridge,  
Downing Street, Cambridge, CB2 3EQ, United Kingdom  
{martin, mca100}@esc.cam.ac.uk

**Abstract.** The eMinerals Virtual Organisation consists of a consortium of individuals affiliated to geographically distributed academic institutions. Collaborative tools are essential in order to facilitate cooperative work within this Virtual Organisation. The Access Grid Toolkit has been widely adopted for this purpose, delivering high quality group-to-group video and audio conferencing. We briefly mention this technology and describe the development of a Multicast Application Sharing Tool designed specifically for this environment.

## 1 Introduction

The eMinerals project is a ERC funded test bed project, whose primary aim is to use grid computing methods to facilitate simultaneous scientific processes at the molecular level. The increased efficiency of the project is partly due to the use of academic institutions through the use of the grid. In this setting, there is a clear need for a better distributed collaborative tool to achieve the aims and objectives of the project.

Collaborative Computing systems aim to complement human face-to-face communication by providing a virtual space which enhance users' experience. The emergence of multicast triggered a rush in the development of group communication software. Collaborative tools have also become popular with the widespread availability of broadband. The Access Grid 2 has become a key tool for high quality group-to-group collaborative access. The internet has been widely adopted by the academic community and uses multicast for streaming audio and video. Unfortunately, multicast is still not a viable mainstream technology.

and home users (due to the reluctance of the latter to order services) and adapt to the new technologies (e.g. the use of personal computers, searched by a web browser, multimedia, etc.). Our aim at the University of Reading is to provide a platform for high quality research and development in the area of application categories, high quality services, and the use of specific technologies in a group of multimedia environments. These environments will be integrated through the use of a high quality multimedia environment. We are also interested in developing a user-centric system, and a user-centred participatory interaction with multimedia groups and a dynamic change environment.

## 2 The eMinerals Virtual Organisation

The eMinerals consortium consists of academic researchers from several different academic institutions. The project has three components: the science driving the project, the development of the infrastructure, and setting up a group of infrastructure for the work. Each of these components are dealt with by the scientists, application developers and the group of experts respectively.

The eMinerals Virtual Organisation consists of two sub-affiliated departments: the scientists and the infrastructure. The scientists are responsible for the research (the respective fields), and the infrastructure are responsible for the administration and the development of the eMinerals group. The infrastructure is necessary to manage these resources and to support the Virtual Organisation (VO).

Communication is an essential factor in the operation of the Virtual Organisation. These tasks are performed by a distributed communication infrastructure between geographically distributed participants. The Access Grid currently allows scientists to communicate using desktop audio and other services. The distributed platform (Access Grid) implements the available Access Grid services, and a high quality research and development services.

## 3 The Access Grid

The Access Grid is a distributed communication environment, which is used for group to group communication. Each of the high quality communication through the Access Grid, a specialised software can be constructed to provide Access Grid services for a machine for the audio, data and for the display. The streams are displayed through several high quality projects and specialised equipment. The high quality audio and data reduce the bandwidth used for the transport of the audio data. The multiplexed Access Grid uses the concept of virtual users (VUs) to allow groups of users to interact, and to be able to have several users of a single stream. Each of the VUs has associated multiplexed addresses and ports. Each stream has the audio and the audio uses different ports and the multiplexed addresses.

to distinguish between the audio and video streams. It's provided for the user to decide whether to receive audio, video, or both. The multicast gateway broadcasts program streams to the address given. The user can also address a different address to broadcast program pages to. The addresses are a subset of the multicast addresses termed at the site, and a gateway set of addresses to be defined assures that datagrams are received by interested participants.

There are two major versions of the Access Grid. The first is the release of the Gateway-based User Interface (RUI) 4 for audio and video. The Core Gateway (CG) for the Receiver, the two versions of the Access Grid. The first is released. The second version uses the standard. The CG and RUI for the audio and video conference, but as it includes enhanced features, such as, a new user interface and Certificate management functions.

## 4 Application Sharing

The audio and video are essential for a complete collaborative experience, and participants to maintain a human interaction. Other major components include the sharing of material between participants. This includes activities, such as collaborative editing of shared data, distributed debugging, and collaborative editing of documents between geographically distributed peers. The application sharing is the ability to share a desktop application with other participants, thus facilitating the aforementioned activities.

There are two approaches to implementing application sharing. The first is a simple collaborative user interface, which uses sharing of application as a transparent matter. The application developer's method does not require application developer to adapt the application to be shared. The distributed participants use the method generally works by sharing a user representation of the legacy application, through sharing application specific data structures. The second approach, a simple collaborative user interface, the application has a graphical user interface of the collaborative functions.

The decision upon which of the methods to use depends on the specific scenario. The collaborative user interface is a legacy application that can be shared. Through modification of the legacy application source code, the collaborative user interface requires the legacy application to be adapted to include the functions necessary for collaborative use. A large part of the collaborative user interface methods that the amount of data that has to be transferred between the participants significantly increases the response time. The comparison is high.

In a situation where a single application is to be shared between multiple participants, (and the functions of the application as known and could be modified) the collaborative user interface is preferred. The functions that are used, the code could be modified to include the necessary collaborative features. This method has been used in a number of projects, including the authors. The Collaborative Gateway (CG) is a framework here a framework



... ed t r s shared bet ee se era part c pa ts pr d g c ab rat e fu ct a t a de sur g s chr sat bet ee part c pa ts e ca a d str buted part c pa ts t rk c ab rat e a rk

he des g g a t t share ma d ere t egac app cat s acr ss d ere t p atf rms the c ab rat u a are m de s usua preferred t s t p ss be t adapt e er egac app cat t be used c ab rat e a d s th s s tuat the pp cat har g t s te d t tra sfer the sua data bet ee part c pa ts he ad a tage f th s s that a app cat c u d the ret ca be shared a d the app cat eeds t be ru g e f the part c pa ts mach es he ma d sad a tage as me t ed ear er s the re at e s resp set mes due t the am u t f sua data be g tra sferred

4.1 Related Work

here are se era app cat s shar g t s a a abe h ch are curre t used th the ccess Gr d he ma e amp es are G 7 str buted er t ( ) 8 a d rtua et rk C mput g ( C)

s e f the m st de used app cat s f r shar g s de prese ta t s acr ss the ccess Gr d t pr des a mecha sm b h ch a prese ter ca c t r a e r t s de sh mu t p e s tes fr m a s g e mach e s spec fic des g ed f r s de sh s a d users are u abe t share a ther app cat Each part c pa t must a s b ta a c p f the s des pr t a ses s G e r c mes s me f the pr b ems ass c ated th spec fic that s des d t ha e t be c rcu ated am g st the gr up members G s be g used e te s e th G k t 2 f r shar g e r t s des e er G d es t ha e a sca abe m de s ce t uses a c e t ser er t p g th mu t p e part c pa ts c c t g t a ce tra p t ther pr b em s that e e de s abe t prese t a G at a g e t me

rtua et rk C mput g ( C) as the m st p pu ar t t be used ccess Gr d r der t share app cat s dur g meet g C shares the e t re desk t p th the part c pa ts the gr up e er t ca be eas m d fied t share a spec fic app cat

C has bec me the ead g s ut f r desk t p shar g t s des g ed f r p t t p t c mmu cat c s st g f a ser er ( c) a d a ght e ght e er ( c e er) part c pa t sh g t share a part cu ar app cat ru s the app cat a d a s the rest f the gr up t make d d ua C c c t s t h s her mach e

he ma d sad a tage ass c ated th the af reme t ed app cat shar g s ut s ( h ch makes them u su tabe f r use th the sca abe ccess Gr d) s the r use f cast pr t c s f r the tra sfer f the sua data e d g mu t p e packets f the same data er the et rk s t sca abe a d ca ead t perf rma ce degradat

4.2 Multicast Application Sharing Software (MAST)

pp cat har g t s fa t e f the t categ r es th se that share c ab rat a are app cat s a d th se that share c ab rat u a are ap

participates previously discussed, there are advantages and disadvantages associated with both approaches, which makes them best suited for different scenarios. In the case of the main broadcast, the ability to share a range of applications between groups of distributed participants, each with its own broadcast, is designed to share generic applications throughout a multidimensional shared application source code.

There are two servers, a server for creating and sending the other for receiving, which can be used to construct the access Grid network. It enables the group to group capabilities per se. Here are several factors that had to be considered in the design.

- The source of multicast and broadcast to be able to handle the C and R, as well as the data settings, the participants using multicast, broadcast, multicast, and broadcast, the network, the application, can send multicast packets over the multicast, and broadcast, the application, can be set to cast to a multicast bridge.
- The C, figurative, has a settings menu which allows a participant to select whether the data is sent to multicast, broadcast, or the user can add details about themselves to be seen by other participants.
- The group of multicast groups. Each virtual user through the access Grid has a unique multicast address and port which is used for the (C) and (R) streams. Similarly, the address used for the participant is a participant can share applications through the multicast address associated with the unique port. The multicast address and port combination is selected through the participant, participants are able to communicate through the same multicast address and port combination. Must be used for the shared application through the ability to have the ability to deal with multiple streams of graph camera data being transferred to a single multicast group. Unique identifies each of the shared application streams and sets these applications through the participants name.
- Reducing the stage of the screen space. The use of the desktop access Grid, such as G and GE, we felt that this is important to reduce the screen area required by the G of resembles that of many states, especially as multiple participants, that can be expanded to show the applications currently being shared by a participant. The user can enlarge a participant applications to its maximum size through the sharing of here sharing, as it is felt that having multiple sharing would cause a stage of a usable screen space.

**Image Capture.** The main goal of this is to get the user data associated with a single application and send this data through the participant through the multicast group. The important issues are, being the graph camera data, the user data for the application could be acquired and sent through the participants each time an event occurs, after a set timer, a user data associated with the application could be efficiently for a small proportion of the screen.

Each group would make a reservation. The changes in each of these sub-partitions of the shared application are checked to see if there is a change of the section. The other participants receive the part of the section that has changed and update the cache of the application.

Changes to the shared application of an application can occur due to hardware refreshes of the user checks a button on the application, the cache of the application changes, response to the user interface of an application, a session event, such as, an animation, or a progress bar, the shared application of the application. Changes here are typically methods for reacting to these events. The first step check the shared application after a default timer has method marks. Refreshes are events, updating the screen. Shared changes introduced by the user interface, such as mouse keyboard events. The timer between checking for updates is extremely important. The default timer value must attempt to provide a response. The histogram of the overhead of the process time, the timer must be relatively high. This makes using the timer method unacceptable for changes due to the user interface. A standard operating system users would expect the shared response to an event. These are hundred milliseconds of the timer. A second, the shared application appears suggest that the user interface at the setting the timer step check sections after an event. An event is a subset. Assume that the shared application of the shared application changes. The user interface is a set of methods. The shared application remains responsive.

Combines the timer methods, the timer can be set relatively high to avoid the overhead of process time. Histogram capturing changes that are due to the user interface. Checking the segments after each event. An assumption with the shared application is that the shared application changes due to the user interface are processed quickly. Improving the interactive performance.

**Transport Design.**

The shared data must be transferred to each of the participants through a multicast group. Ideally, the data would be sent to each of the participants using multicast. The technologies, Gtoss, CadR, the data can be sent via multicast, if the available. The network, ribbon, cast, a bridge. The transport system has been designed to allow the transport of a type of data and this has been achieved by creating template transport classes. The advantage of this is that the application can easily be developed to use the same transport system.

Can be used successfully. The group together. Uses multicast to send the shared data. Unicast is a reliable protocol. Meaning that packets of data would be strictly received, out of order. If some packets are lost, the remote participants of the shared application could be compromised. Design has a kernel edge of packet loss and therefore to assume that the sections are updated and to reseed the sections. Therefore, the problem, and the problem of attackers, must reseed sections periodically.

effect the appear to be unchanged since the previous send. Re-sending sections could be delayed at a time after a set number of iterations, at that moment it could take a relatively long time to obtain suitable data for the entire application. In addition, the increased load on the network during these high overhead periods, either as a result from the user could take longer to process and send the responses, or as a result of the shared application could be expected. In addition, because these load periods are reduced a few sections after each iteration, this reduces the overhead associated with refreshing the shared application, and maintains the responsiveness to the user.

**Session Management.** An important aspect of the transport system is the definition of the separate participants and the shared application streams. It is designed to use a central server, which means that the participants should be managed centrally. Each participant must manage the received participant and application streams. This is achieved by queue defining each participant and application stream. When an application stream is received, the server of the shared application presents to the participant, if the participant is present, the application streams added to the set of the participant. If the participant and the application streams added to the set. Each instance of the server must be responsible for detecting participants that are either virtual or real application streams that are being shared. Detecting each participant's relative response time, a stream is being received, and a set of data that a participant's application streams after a set of iterations, the agents are created if a stream has been created again at the end of the iteration, the application streams for the participant will be removed from the set.

## 5 Conclusion

In this paper, we introduced the experimental virtual Organization and described the factors that motivated us to develop the multicast application sharing tool. We described the collaboration model used along with its advantages and disadvantages. The paper gives a detailed description of some of the design and implementation issues associated with the development of

Our work on the immediate future will be to complete integration of the tools. We will first try to provide a solution that can be used between the tools. Patterns, and the integration with the current G... kit

## References

1. Dove, M.T., Calleja, M., Wakelin, J., Trachenko, K., Ferlat, G., Murray-Rust, P., H De Leeuw, N., Du, Z., Price, G.D., Wilson, P.B., Brodholt, J.P., Alfredsson, M., Marmier, A., Ptyer, R., Blanshard, L.J., Allan, R.J., Van Dam, K.K., Todorov, I.T., Smith, W., Alexandrov, V.N., Lewis, G.J., Thandavan, A., Hasan, S.M.: Environment from the molecular level: an science testbed project. AHM 2003 (Nottingham 2-4/9/2003)

2. The Access Grid Project website. Available on: <http://www.accessgrid.org>.
3. Videoconferencing Tool (VIC) website. Available on: <http://www-mice.cs.ucl.ac.uk/multimedia/software/vic/>
4. Robust Audio Tool (RAT) website. Available on: <http://www-mice.cs.ucl.ac.uk/multimedia/software/rat/>
5. Richardson, T., Stafford-Fraser, Q., Kenneth, Wood, R., Hopper, A.: Virtual Network Computing. IEEE Internet Computing, Volume 2, Number 1 January/February 1998
6. Nemeth, C., Dozsa, G., Lovas, R., Kascuk, P.: The P-GRADE Grid Portal. Computational Science and Its Applications - ICCSA 2004 International Conference Assisi, Italy, LNCS 3044, pp. 10-19
7. The IGPix website. Available on: <http://www.insors.com>
8. The DPPT website. Available on: <http://accessgrid.org/agdp/guide/dppt.html>
9. Personal Interface to Access Grid (PIG) website. Available on: <http://www.cascv.brown.edu/pig.html>
10. Personal Interface To Access Grid, Linux Exclusively Thanks (PIGLET) website. Available on: <http://www.ap-accessgrid.org/linux/piglet.html>

# The Collaborative P-GRADE Grid Portal

Gareth Lewis<sup>1</sup>, Gergely Papp<sup>2</sup>, Valeriy Urmetzer<sup>1</sup>,  
Assil Dobre<sup>1</sup>, and Peter Kacsuk<sup>2</sup>

<sup>1</sup> Advanced Computing and Emerging Technologies Centre,  
School of Systems Engineering, University of Reading,  
Whiteknights, P.O. Box 225, Reading, RG6 6AY, United Kingdom  
{g.j.lewis, f.urmetzer, v.n.alexandrov}@rdg.ac.uk  
<http://www.acet.rdg.ac.uk>

<sup>2</sup> MTA SZTAKI, Laboratory of Parallel and Distributed Systems,  
H-1518 Budapest, Hungary  
{sipos, kacsuk}@sztaki.hu  
<http://www.lpds.sztaki.hu>

**Abstract.** Grid portals are increasingly used to provide uniform access to the grid infrastructure. This paper describes how the P-GRADE Grid Portal could be used in a collaborative manner to facilitate group work and support the notion of Virtual Organisations. We describe the development issues involved in the construction of a collaborative portal, including ensuring a consistent view between participants of a collaborative workflow and management of proxy credentials to allow separate nodes of the workflow to be submitted to different grids.

## 1 Introduction

The Grid infrastructure is essential to support the development of Virtual Organisations. The Grid enables the sharing of resources and provides a secure manner in which Grid portals are created, used as a convenient interface to the Grid by providing uniform access to grid resources.

GRADE is a graphical programming environment used for the development of parallel applications. GRADE comprises GRADE (Graphical Resource Access and Gauge), which is a graphical programming language and GRE (Graphical Editor), which can be used to write parallel applications. Using these separate components, GRADE provides an abstract framework for the detailed association with the message passing. Grade has several features which are used for the development and execution of parallel programs. The architecture, interest, for the purposes of this paper, is the framework. The framework is a set of components and parameters, which are cooperating. The execution of a parallel program is undertaken by a certain framework. The framework is executed by distributed resources through a grid. The framework allows users to design and execute frameworks, specifying properties of the framework, and specifying whether the output data files are used as the output of a further development of the framework.

The GR E-Grade Portal provides user-friendly grid resources that make computing, the Portal server and the network. Ed-tracker (a webstart application) the Portal server as depicted using Gridsphere, a grid portal development framework that supports a range of user aspects, such as security, monitoring and execution. The networked tracker is a user interface that provides graphical feedback to progress during the execution.

The objective of the project outlined in this paper, as the development of a collaborative GR E-Grade Portal, which could be used by several participants. The main aim of this collaborative environment is to find first, to understand the requirements of the collaborative environment and second, participants could use the respective certificates submitted by the networked trackers.

## 2 The P-GRADE Portal

In previous meetings, the GR E-Grade Portal consists of the main computing nodes, the Portal server and the networked tracker. Together these components facilitate the development of frameworks and the re-execution of a grid. The networked tracker is the end user interface that graphs history, the Portal server supports the end user interface, the security as well as the user interface and monitoring of the execution. The networked tracker is separate from the Portal and runs on the end user's machine. It communicates with the Portal server to provide information about the current network. The user of the networked tracker can create a network graph consisting of multiple nodes, which are either sequential or parallel programs.

The Grid security infrastructure (GSI) 4 (based on certificates) is used to provide secure authentication and access to the grid resources. Portals are becoming popular for providing a convenient interface to these computing tasks. The grid portals rely on the respective representation of the integration of the portal with the Grid. The user server allows the grid portal to use the Grid to interact with the grid resources. The GR E-Portal supports a range of user interface development from the user interface and allowing users to use the features of the previous era. The user interface can be developed but also as a separate can be active, as each networked tracker uses the resources from a single grid.

The Portal must be able to monitor the execution of the networked tracker and provide user feedback to the end user. The GR E-Portal allows the user to monitor the networked tracker using the secure monitoring tool. It represents the progress of the execution, both the networked tracker and the portal. The user can monitor the entire network and the individual nodes. The portal shows the communication between the networked nodes and the processes through each node.

### 3 Collaborative Version of the P-GRADE Portal

driving force of the development of the Grid infrastructure is the collaborative distributed partners (forming virtual Organizations) interacting over the grid. The collaborative Grid Environments supports the development distributed groups working together and communicating using the underlying grid infrastructure. The main motivation for the development of a collaborative Grade Environments are that work should be constructed collaboratively, and facilitate submission of distributed parts of the work. To separate grids there are two approaches to implementation: a collaborative approach such as the work-oriented where first the users share of the approach, a transparent manner, and does not require to be adapted to be aware of the collaborative. Collaborative users are sharing would be achieved by sharing a suitable representation of the same work-oriented, that sharing approach specific data structures. The second approach depends upon the approach being aware of its collaborative functionality in the case of the Grid Environments, to be able to adapt the work-oriented and the portable server work collaborative manner. The portable server provides a central point to which each work-oriented can connect and be synchronized. The server also provides the suitable transferring data between distributed grids (as described in the following sections).

The collaborative users of the work-oriented must allow work should be constructed collaborative manner. The end users must be able to add a domain, describe the work, and these changes being subject each participant successful collaborative, between the users cooperating. The construction of a collaborative work-oriented, the portable must ensure that each participant has the same level of mutual usage of the work could lead to collisions. Here participants have a distributed level of the same data. The client server network programming assists the implementation of a structure. Since each of the work-oriented data can be created at the portable and its collision is assured by guaranteeing that accessing the central work-oriented data is mutually exclusive. The work-oriented must also provide a suitable representation of the work's execution. Currently this functionality is provided by representing distributed states of execution. Distributed courses. The execution functionality of the work-oriented must enable the work-oriented collaborative environment.

The environment must also be adapted to include the necessary collaborative functionality to support the development of the collaborative.

Grid Environments management of the process creation, which are derived from the portable server. The current Grid Environments also distributed process creation should be derived, but as a work-oriented can be submitted to a single grid, one of the processes active manner of the shared.

Grid Environments as a separate parts of collaborative work should be submitted to distributed grids. To facilitate this, the Creation Manager [2] must be adapted to be able to use multiple process creation currently.

The suitable adaptation, for a execution work-oriented support a central server that the collaborative setting. The portable server must ensure that all participants of a collaborative work-oriented receive the same suitable format,



and that the central knowledge objects are modified by a knowledge editor during the execution period

### 3.1 Collaborative P-GRADE Portal Design

This section expands upon the issues described above and gives details specific design decisions. There are three main stages of the development and execution of parallel applications using the GR-EP Portal. In the first stage the construction of the knowledge graph, this involves constructing the central knowledge and parallel components, and here the output from the compiler can be used as input to the other reference knowledge can be submitted to the grid the programmer must ensure that the necessary prerequisites are available in this step managed by the Credentia manager, which handles the prerequisites from the programmer. In the final stage of the execution of the knowledge clusters monitoring and satisfaction the current GR-EP Portal have to be adapted at each of these stages to be used successfully through a collaborative setting.

### 3.2 Collaborative Workflow Construction

The construction of the knowledge graph is achieved through the knowledge editor, which runs on the users' local machine. Much of the development associated with the construction of the knowledge graph will be through the knowledge editor, the programmer's implementation of this step as it contains the structured knowledge and will be responsible for ensuring a consistent view of the knowledge between the distributed participants. The current users of the GR-EP Portal, the knowledge editor runs on the users' local machine and connects to the central GR-EP Portal server to exchange information related to the knowledge graph. This graph is then used by the server to submit the knowledge to the grid infrastructure. The knowledge editors have several reasons to be distributed between themselves as a knowledge is shared by a single user, the collaborative users, the editors are working on the same knowledge. They have to communicate with each other to ensure the knowledge is consistent across the knowledge editors. Each directly to each other would not be sensible and would lead to problems seen in many peer-to-peer applications. The central portal server allows the editors to directly communicate with each other, creating a central knowledge object at the server, and ensuring mutual exclusive access to a particular object, each can achieve a consistent view between the distributed editors.

The collaborative GR-EP Portal will be implemented through several knowledge objects. The knowledge editor will create knowledge objects called knowledge Objects (K-O), these will contain the data presented through the structured knowledge and added to a format. Concerning the checking and update changes the programmer will have to types of knowledge objects, the first will be known as the simple Global Knowledge Object (G-O) and will contain the same format as the local knowledge objects. The G-O objects will be updated by each of the knowledge editors. The performance calculation will be updated by the O of each of the knowledge editors will be updated by a

g. ba. t. . ca. update. he. sec. d. rk. . b. ect. at. the. p. rta. ser. er. . be. the. tat. c. G. ba. . rk. . Ob. ect. ( G. O) . h. s. b. ect. . c. ta. the. data. st. red. . the. sa. ed. c. . ab. rat. e. . rk. . a. d. the. . ck. g. f. rmat. . the. G. O. . ha. e. . data. ass. cated. . th. c. mp. . e. ts. that. are. . t. cur. re. t. . sa. ed. ( g. )

he. ma. r. . ter. faces. fr. the. pr. ect. a. b. et. ee. these. d. ere. t. . rk. . b. ects. he. first. . ter. face. s. bet. ee. the. G. O. a. d. the. G. O. th. s. . ter. face. re. pre. s. ts. the. p. . t. bet. ee. the. c. . ab. rat. e. . rk. . . b. ect. . here. the. cha. ges. t. . ca. . rk. . s. are. st. red. a. d. the. . rk. . that. m. rr. rs. the. data. c. . ta. ed. . d. sk. . here. are. se. era. fu. ct. . s. that. must. be. pre. s. t. . th. s. . ter. face. t. e. ab. e. . ter. act. . s. bet. ee. these. t. . b. ects. he. G. O. c. . ta. s. the. . rk. . data. fr. m. d. sk. a. d. the. . ck. g. f. rmat. . fr. the. e. t. re. c. . ab. ra. t. e. . rk. . he. . ter. face. must. a. . the. st. red. c. . ab. rat. e. . rk. . s. t. be. re. tr. e. d. fr. m. the. p. rta. ser. er. the. . ck. g. f. rmat. . t. be. s. chr. . sed. be. t. ee. the. t. . g. ba. . rk. . b. ects. a. d. the. u. sa. ed. cha. ges. fr. m. the. G. O. t. be. c. rp. rated. . t. the. G. O. dur. g. the. sa. . g. pr. cess. he. G. O. ca. be. used. spec. fic. . b. the. p. rta. ser. er. fr. r. sub. m. tt. g. the. . rk. . t. the. gr. d. res. ur. ces. . ther. ad. a. tag. e. f. the. G. O. s. that. up. dates. t. the. . b. ect. are. m. re. eff. e. t. tha. sa. . g. cha. ges. t. d. sk. he. sa. . g. r. he. up. dat. g. . ck. g. f. rmat. .

he. sec. d. ma. r. . ter. face. a. s. bet. ee. the. p. rta. ser. er. a. d. the. . rk. . ed. t. rs. he. . rk. . ed. t. rs. must. be. ab. e. t. c. mmu. cate. . th. the. p. rta. ser. er. t. ma. ta. the. c. s. ste. c. . f. the. c. . ab. rat. e. . rk. . bet. ee. the. part. c. pa. ts. here. s. s. me. add. t. . a. fu. ct. . a. t. that. must. be. a. a. ab. e. t. e. sure. c. s. ste. c. . c. ud. g. . ca. t. g. ba. up. dates. g. ba. t. . ca. up. dates. . ck. g. . des. a. d. u. . ck. g. . des. he. . rk. . ed. t. r. c. mmu. cates. th. the. p. rta. ser. er. a. . a. d. s. ca. . t. re. ce. e. mes. sages. as. . chr. . us. fr. m. the. ser. er. he. . rk. . ed. t. r. must. be. resp. s. b. e. f. r. p. . g. the. ser. er. t. re. ce. e. the. at. est. g. ba. . e. he. the. . rk. . ed. t. r. p. s. the. ser. er. t. . be. . ed. the. . ca. t. g. ba. s. chr. . sat. . he. ser. er. ca. resp. d. t. th. s. re. quest. b. . ssu. g. a. resp. se. . the. fr. m. f. a. g. ba. t. . ca. up. date. Ob. . us. the. p. . g. ter. a. s. cr. uc. a. the. . ter. a. sh. u. d. be. sma. t. e. sure. a. m. re. c. s. ste. t. . rk. . bet. ee. the. part. c. pa. ts. h. e. er. f. the. . ter. a. s. t. . sma. the. t. c. u. d. ead. t. a. u. due. . ad. . the. et. . rk. .

he. . ck. g. f. the. . rk. . s. a. s. a. mp. rta. t. c. s. derat. . at. th. s. . ter. face. he. G. O. c. . ta. s. data. that. s. shared. bet. ee. se. era. d. ere. t. ed. t. rs. c. . cur. re. t. . s. th. a. shared. data. there. s. a. d. st. ct. p. ss. b. t. . f. race. c. . d. t. . s. due. t. c. . cur. re. t. access. t. the. data. . . er. c. me. th. s. pr. b. em. the. p. rta. ser. er. must. e. sure. that. access. t. the. G. O. s. mutua. e. c. us. e. he. p. r. rta. must. pr. . de. a. . ck. g. me. cha. sm. b. h. ch. part. c. pa. ts. are. ab. e. t. . ck. a. part. f. the. . rk. . t. be. m. d. fied. . the. . ter. face. there. must. be. t. . fu. c. t. . s. a. a. ab. e. t. the. . rk. . ed. t. r. he. first. s. the. . ck. fu. ct. . . h. ch. . a. . part. c. pa. ts. t. . ck. a. . de. a. d. ass. cated. . des. f. part. c. pa. ts. had. t. ac. qu. re. a. . ck. f. r. the. e. t. re. . rk. . . t. . u. d. p. ace. a. . rge. c. . stra. t. . ef. fect. e. c. . ab. rat. . he. a. ter. at. e. s. that. the. part. c. pa. ts. are. ab. e. t. . ck.

Workflow Editors

Portal Server

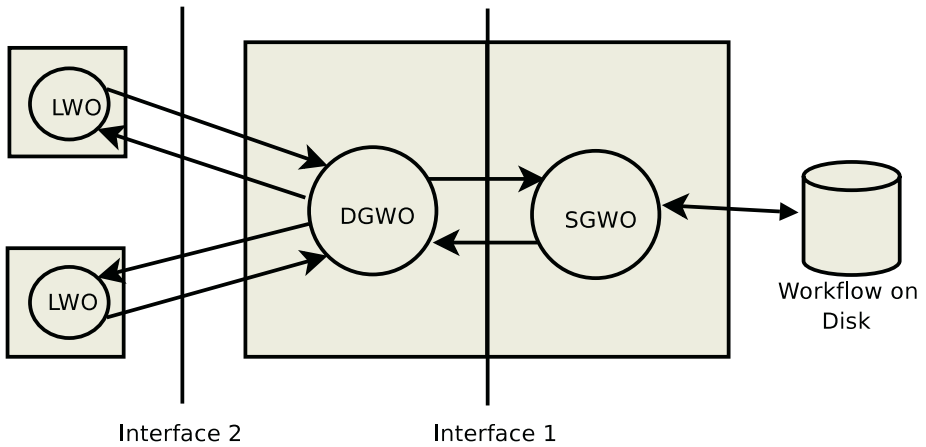


Fig. 1. Overview of the Collaborative P-GRADE Portal showing workflow objects

single objects and associated objects of a workflow. The portal server must manage the locking mechanism to make sure that multiple editors cannot lock the same nodes. The management of the locking will take place at the G/O level. The unlock function must also be available to the workflow editors. Once a part component has completed the modification to part of the workflow, these nodes should be released. There must also be a set timer after finishing a part component. Cache data lock before its refresh removed by the system. Single part component must not be able to manipulate a part component of the workflow. Additionally, workflow editors should not be able to handle locks definitively.

3.3 Execution and Management of a Collaborative Workflow

Once the collaborative workflow has been constructed, its read to be executed on a grid resource. Here are several issues that have to be considered. When submitting the collaborative workflow, the administrator has parts of the collaborative workflow submitted to different grids. To achieve this, the portal must be responsible for reflecting the management of the process, creating a set of locking of the workflow during the execution period and facilitating the transfer of terminated data between the different grids.

**Credential Management.** In the current version of the G/O P-Grade portal, the Credential manager is responsible for managing the process of creating a set of credentials and giving users the ability to add appropriate private certificate from the grid server, and providing information such as its format. The current version also allows multiple processes to be downloaded, but also allows one of these

to be active, used for submission of the work, collaborative work submitted to a single grid and its subsets, be able to use parts of a machine of the collaborative portal, and parts of a single work to be submitted directly to grids using direct participation protocols. Each of these aims, the Credential Manager must be adapted to be capable of managing separate activities for a single work. To manage separate activities, the portal server must be capable of associating activities with direct descriptions of the work graph. The user must be able to specify the direct relationships that will be used for each of the current users of the portal, so that capabilities of automatic direct activities should be necessary. The collaborative users of the portal must keep track of the relationship between the users, the portal server and the available grid resources.

**Workflow Locking.** Once a collaborative work has been submitted by one of the collaborative users, the portal must ensure that additional users are locked and set to a execution state. This feature is currently available through the portal, but consideration must be given to ensuring that additional locked users are through the locked state before submission to the grid can proceed.

**Transfer of Intermediate Data.** Direct descriptions of the work could be submitted to direct grids through the proposed collaborative Grid Execution Portal. The major issue with this design is that there is generally a factor available for the data to be transferred between the direct grids. Thus, the work outputs from some nodes will be needed as inputs to other nodes. Direct grids through the central portal server can facilitate the direct transfer of the output data (from the node) for use as input data to another node (submitted to a direct grid). The portal server must be able to handle the transfer of this data directly from each data node. The node has been received and through the data must be delivered. The management of the Credential Manager is essential. Facilitating the direct transfer of the intermediate data. Once execution completes, the output data from the collaborative work must access between each participant of the collaborative session.

## 4 Conclusion

In this paper, we have discussed the issues and matters that should be considered in the development of a collaborative Grid Execution Portal. The goal of this collaborative portal is to allow distributed participants to work with collaborative work resources, and matter the progress of the nodes' execution across direct grids. The paper describes how the work-related portal server must be adapted to be used as a collaborative manager, ensuring a consistent use of the work-based protocols, scheduling, and debugging mechanisms. A management of the protocol creation as the portal server has been discussed to allow the automatic direct activities between the relationships between users and available grid resources.

## References

1. Peter Kacsuk: Visual Parallel Programming on SGI Machines. The SGI Users' Conference, Krakow, Poland, pp. 37-56, 2000
2. Csaba Nemeth, Gabor Dozsa, Robert Lovas and Peter Kacsuk: The P-GRADE Grid Portal. Computational Science and Its Applications - ICCSA 2004: International Conference Assisi, Italy, LNCS 3044, pp. 10-19
3. Joshy Joseph, and Craig Fellenstein: Grid Computing. On-Demand Series, Prentice Hall, 2004
4. R. Butler, D. Engert, I. Foster, C. Kesselman, S. Tuecke, J. Volmer and V. Welch: Design and Deployment of a National-Scale Authentication Infrastructure. IEEE Computer, 33(12):60-66, 2000
5. J. Novotny, S. Tuecke, and V. Welch: An Online Credential Repository for the Grid: MyProxy. In Symposium on High Performance Distributed Computing, San Francisco, Aug. 2001.
6. J. Chris Lauwers and Keith A. Lantz: Collaboration awareness in support of collaboration transparency: Requirements for the next generation of shared window systems. In Proceedings of ACM CHI90 Conference on Human Factors in Computing Systems, pages 303-311, 1990.
7. G J. Lewis, S. Mehmood Hasan, Vassil N. Alexandrov: Building Collaborative Environments for Advanced Computing. In the proceedings of the 17th International Conference on Parallel and Distributed Systems (ISCA), pp. 497-502, San Francisco, 2004.

# An Approach for Collaboration and Annotation in Video Post-production

Arste Jürsse<sup>1</sup> and Thomas Sempf<sup>2</sup>

<sup>1</sup> University of Applied Sciences Osnabrück, D-49076 Osnabrück, Germany  
kamo@fhos.de

<sup>2</sup> Nero AG, D-76307 Karlsbad, Germany  
thomas.sempf@gmx.net

**Abstract.** In the different phases of a movie production, there is a need for intensive discussion about the produced sequences. Especially if the discussion members are located at different places they will have problems to precisely describe their critics for the video production. This paper describes an approach and a tool for video collaboration to simplify the video production process for video editing service providers and their customers.

## 1 Introduction

The process of making a movie, be it just a commercial or a full time film, is a very complicated task. The main production stages, personnel and companies involved during each step of this process, several different personnel collaboration and format, media assets, ideas and management decisions for the upcoming phases of the production process can be made and have to be stored for discussion either in electronic form, like emails or recorded processes, documents, or paper form, like printed documents or pictures. These created documents can be used in subsequent phases of the production process and can be duplicated and delivered to other companies and personnel in charge of the tasks to be done later.

It is usual that electronic production documents, like a second commercial, are later attached to production sheets prepared from categories scattered across the recording sheets might cause problems in the production process.

The organization of these articles as follows: section 2 describes commercial problems in the desktop production process, including requirements for collaboration process in desktop production are characterized in section 3. Related works considered in section 4 and finally, section 5 presents a collaboration tool for some of the mentioned tasks.

## 2 Problems in Video Production Process

After finalization, but as during a desktop production, there is a strong demand for discussion about the produced sequences. However, the necessary format

exchange between the persons involved is difficult if the service provider (the staff) and the customer (director or producer) are at different locations. Generally, the verbal discussions supported by sketches about scene cuts, picture elements, movements, retakes, gaffes, etc. are difficult, because verbal descriptions can be inaccurate. Moreover, generally, the descriptions of a picture are far from exact. It is difficult to verbally construct the right of the character, moves fast through the scene are ambiguous. What is the meaning of the character's far from the right has to be predicted of the persons involved have a common mental representation of which they are talking, the verbal descriptions can be supported by hand-drawn pictures. But, this is not what happens in a common screen talk at

rehearsals. Conversations are specific for the area, format and medium production of the blue screen. For a better description of the demands, what is the right blue and how blue should be, artistic considerations are hard to describe verbally. It is difficult that if there is a common scene

discussion using graphics, media, like telephones, audio recording, etc. for scene setting, the situation, because even though these media there is a common scene as a scene and thus, verbal descriptions should be ambiguous. The discussion about a scene sequence requires each participant to know the exact position of that scene (e.g. time code) and to integrate that position into the scene

articular. The production of computer-generated scenes is faster and more precise after the screen of a scene sequence. It would be helpful to cut the scene as a sequence of digital storyboard elements. The distributed participants should be able to verbally and each has to sketch the desired dual. Of course the same ambiguities as described above can be foreseen. Generally, the necessary duplication and deletion of these elements to a certain extent persons as a task. Elements of electronic groups are added, elements of management systems that can take a lot of time and as a result of the demand in understanding because papers are missing and most importantly, the general and structural issues are accurate

Overall, the interaction between the mediated participants to create a common together to have the necessary common knowledge of the screen elements, the production process would be helpful. However, the electronic communication in which supports at least the remote discussions about the technical common knowledge of the screen for the distributed participants

### 3 Requirements for Collaboration in Video Post-production

What are the requirements for a supported digital production process that would be helpful for spatially distributed participants to have a common knowledge of the screen with the possibility of a synchronized, integrated through the sequence of the common screen must be the base for the communication process and a supported graphics communication for the production should provide at least some of the following features

**Synchronized Navigation and a Common Video Screen:** An efficient collaboration process requires a common screen with the possibility to navigate as a synchronized activity through a scene. A must is that the possibility for each participant to navigate to a specific time code without the computer for the others to navigate manually to the same scene here must be eliminated. A navigation process for a participant

**Graphic and Text Annotation:** It must be possible to annotate scene frames and complete sequences. An annotation should be defined as a text or a graphic object directed to the scene, e.g. a sketch, like a circle to emphasize a particular object in the picture. Therefore, it should be possible to give separate comments to a scene annotation as a text or audio sequence.

**Multi User Approach:** It is desirable that more than two participants can collaborate simultaneously, so that each of them can follow the discussion process actively and passively.

**Archiving of Annotations:** Generated annotations must be stored, and it must be possible to recall and reedit them later during the production process.

**Categorized Annotation:** It would be helpful if annotations could be grouped in categories, e.g. annotations for text, graphics for actor movements, which is necessary for a structured discussion process.

**High-Quality Video Material:** The common video screen is the base for collaboration. Therefore, it should be sufficient if the provided video quality is the typical quality known from modern streaming. Therefore, the required support discussions about production details of high quality video material are absolutely necessary.

**Story Board Development:** It would be even useful and could be a system could assist the director to develop the production process, e.g. treatment, storyboard, blocking the format, making it available to annotated persons and computers, and collecting all persons, formats, and media assets. It is even for collaboration such a distributed production system can be made and helpful possibility for streaming and simultaneous discussions and organization tasks in the production process.

**Video Content Processing:** Support of text processing tasks would also be helpful, e.g. automatic scene detection and recognition. Existing systems with support of text-based decisions (E) can detect other interesting features and be the synchronized simultaneous specific annotations and descriptions of features.

## 4 Related Work

In search for systems with the mentioned abilities we realized that there are systems that enable the user to do some of the mentioned tasks, but there is no system that supports the case of distributed users. The systems are for example



user usage a d . . . te ded fr c . . ab rat . . . th se era pers . s . . . ed  
 stems fr s . ge user e per e ce . . the str b . ard des g . are fr e amp e  
 t r b . ard rt st 7 , rame rge . tud . 4 , t r b . ard te 8

de . a . . tat . . s stems are . . t k . . . t ass st the . de . pr duct . . pr  
 cess . . e er, there are s . me s stems fr . de . descr pt . . . hese s stems sup  
 p rts the task t . descr be the actua . p . t f a . de . . st f these s stems  
 keep read a set . f t . s fr a . gat . g thr ough the . de . seque . ce a d add . g  
 metadata t . t h s metadata s the . st red . . a ser er fr . ater retr e a . he  
 e . . . g sta . dard fr th s metadata descr pt . . s . EG 7 . . h ch s ma . .  
 used t . search . . de . databases fr spec fic t . p cs . . e amp e fr such a s ft  
 are s the . EG 7 . . . tat . . . . . t e abes the user t . a . . tate

EG a d . EG 2 based . de . seque . ces . he user s supp . rted . th a  
 aut . mat c sh . t detect . . . h ch detects the d . ere . t sce . es . . the . de . fie  
 ased . . that . f rmat . . the s ft are t . . creates a . a gat . . structure , s .  
 the user ca . eas . . a gate thr ough the d . ere . t sce . es . . defi e a . a . . tat . .  
 the user ca . ch . se fr m a set . f ke . rds . . h ch ca . be e te . ded , t . descr be  
 the sce . e ga . . d str buted c . ab rat . . . th se era users s p . ss be , thus  
 the part c pa . ts ha e t . meet pers . a . . t d scus the . de . fr . t f a . de .  
 scree .

ther . . . terest . g pr . ect s the fi mEd . . research pr . ect f the . . ers t  
 . f uee s a d . ustra a . he pr . ect as started t . create t . s fr a . . tat  
 . g d scuss . g a d resum . g . de s a d t . de e . p mu t med a r ch . ear . g  
 e . r . me ts . he a s a a . zed a d d sc . ered the . eed fr s ft are t . s t .  
 d scuss a d a . . tate . de . seque . ces . rea t me . er the . ter et . . a d s  
 tr buted ma . er . he de e . ped a pr . t t pe ca . ed . a . . tea . . h ch e abes  
 the c . ab rat . e . de . g a . . tat . . a d d scuss . . f aud . . sua . c . te t . er  
 h gh ba . d dth . et . rks t e abes ge . graph ca . d str buted gr . ups c . . ected  
 acr . ss br . adba . d . et . rks t . perf . rm rea t me c . ab rat . e d scuss . . a d a .  
 . . tat . . f h gh qua t d g ta fi m . de . a d mages . ased . the Gra . ge et .  
 h ch c . . ects f ur . ustra a . c tes . th a . Gab t . e . t e abes the e  
 cha . ge f h gh qua t . de . . EG 2 f rmat bet ee . the part c pa . ts f

a meet . g . stream . g ser er supp . rts the part c pa . ts . th the . eed e . de .  
 data a d a spec a . a . . tat . . ser er st . res a d h sts a . a . . tat . . . f rmat . .

re . duce the ate . c . dur . g a sess . . m re the . . e stream . g ser er s used  
 a d the . de . s tra . sm tted as a mu t cast stream . he a . . tat . . . f rmat . .  
 s st red . . . f rmat . . h ch s based . . a c mb . at . . f e . me ts f the  
 ub . . C re . a d the . EG 7 sta . dard t the p . t f the r t . g . .  
 te t . f rmat . . ca . be st red . the s stem . h ch ca . be b u d t . recta . gu ar  
 areas . the . de . he a . gat . . s stem s master c . e t based , that mea s  
 that . . . e pers . ca . a gate thr ough the . de . seque . ce a d a . c . e ts  
 . . be aut . mat ca . s . chr . zed

a h . t c . ud be f u d t . u ckt me . chr . a . t . fr m . br de  
 h ch . as used dur . g pr . duct . . f the m . e p . ds . a d h ch m ght  
 fu . fi . s . me . f the requ reme . ts g . e . . sect . . . ut e . . request . . further  
 . f rmat . . as pr . ded ab . ut t

## 5 DiVA – An Approach for Video Collaboration and Annotation in Video Post-production

<sup>1</sup> 2, developed at the University of Applied Sciences Osnabrück, is a collaborative tool which supports some of the requirements mentioned in section 2.1. The tool is capable of generating a trajectory graph based on the desired user-based layout architectural approach that could be extended to satisfy different demands. Figure 5 shows a screenshot of the sequence with the annotation graph capabilities that are used to separate annotations into categories.

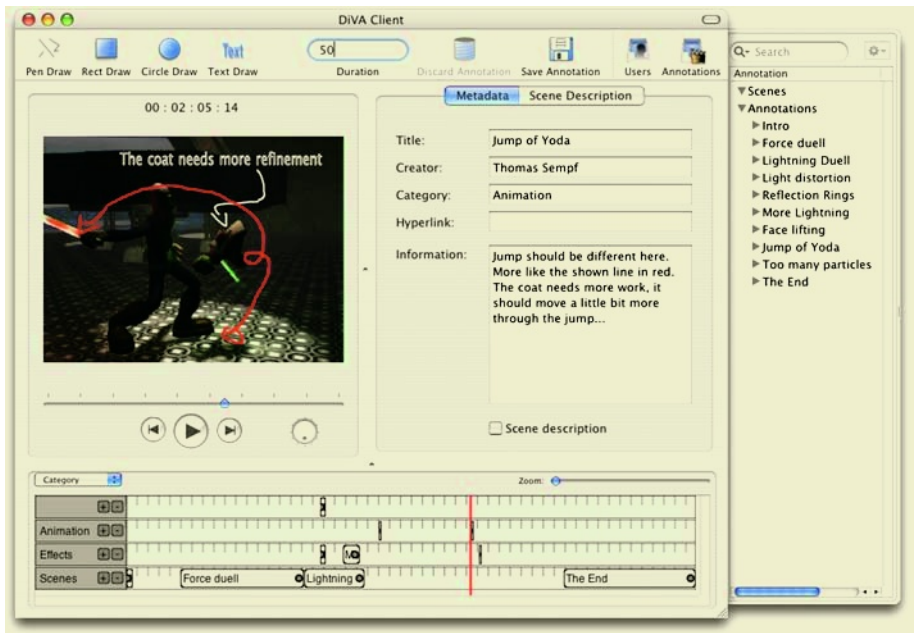


**Fig. 1.** DiVA - Scene annotation with graphic and text objects, synchronized navigation and annotation archiving

### 5.1 Multi User Approach

As a client-server based system approach for the collaborative process of video production, the tool is defined on the basis of sessions. Sessions run under the control of a server, which allows several users to access the current scene data of a collaborative session defined with a RAID capability added automatically from the clients if necessary, the data can be loaded from the local file system of the clients<sup>2</sup>. Therefore, streaming

<sup>1</sup> DiVA - Distributed Video Annotation.

<sup>2</sup> This might be an option for long video sequences with an huge amount of data where the video content is distributed in advance via DVD.

contents as possible but for practical reasons this should not be used due to the memory requirements which could change in the near future with the emergence of high efficiency decoding techniques (EG 4 part 2.4.1). Checkboxes are the stream-gate for the content, e.g. high definition quality, over a small bandwidth.

## 5.2 Navigation and Common Video Screen

descriptions can be navigated separately as EEP content can be accessed directly by time, forward and backward movement from frame to frame so possible for fast navigation using shuttle as a feature. Each of the navigation approaches should be currently for a part of parts of the collaboration session. The first user navigates his content, a particular position, each of the other contents of that session follows the navigation commands by clicking mechanism. The presentation navigation deadlocks is provided. On the other part of a content gate action, the others are following this navigation as a passive mode and are blocked for action navigation.

## 5.3 Annotations

provides a set of possible annotations to describe a description and sequence of frames — rectangles, circles, rectangles and a drawing pencil can be used to annotate the description. Annotations for drawing are drawn directly on the screen and can be defined for each sequence frame or an arbitrary sequence of frames. Hereafter, it is possible to define annotations for object movements over a set of description frames or detailed annotations for that sequence, further annotations can be defined.

When the user has started an annotation, the navigation functions are blocked for the other users. Annotations are directly drawn on the description and are immediately visible for all other users of that session. Combining with a discussion, a telephone conference, this is a useful tool for supporting the discussion process about the description of the user has finished his annotation, the other users can annotate the same or other scenes of the description. The same annotation, thus, all users have equal rights, there is no privileged user. Hereafter, the discussion process is supported by a suitable combination of the description with the graphical annotations. Although errors, misunderstandings and imprecision are possible in the content.

For a comfortable access there are directly for the annotations a list of elements and annotations in an alphabetical order. Annotations can be reloaded or deleted. It is also possible to search annotations by keywords. Time-based elements are chronological categories of the annotations sorted by categories. The time, the duration of annotations can be changed or they can be moved.

**Graphic and Text Annotation.** Annotations can be defined as elementary graphical objects, circles, rectangles and lines, as text objects directly on the description — directly users are annotations, directly on the screen, thus comments can

be separated easily. The technical realization of the annotation tools should be a top priority architecture so that the system is open for further tools.

**Categorized Annotation.** Supports different categories of annotations. Examples are genre, scene, description, color, and shadow. Errors, ripples, and ghosting. Each category can be displayed and displayed simultaneously, thus there is a easy way to navigate from one annotation tool to others of the same category. This is important to record annotations sessions.

**Archiving of Annotations.** After the discussion about a single scene, the annotations can be stored as a series of metadata can be defined for each annotation. This could be added as remarks, review, and a rich set of keywords. The stored annotations are bundled as a session archive. The series that the can be accessed later during the production process.

The categorization of annotations with a corresponding keyword based search mechanism allows a direct access to relevant annotations. This might be helpful in the following production steps, review, and the production.

### 5.4 Network Requirements and Video Quality

If the decision is to be able to edit, the network requirements are rather simple since there is a local file transfer messages over the network between clients and server.

It is desired under people. Overall, supports the network media platform so that each network media can be used for the decision. Thus, the bandwidth, decision, key, review, and EG 4 are supported as well as production, decision, key, and C.R.

## 6 Summary and Further Work

The collaboration platform for production, supports different steps for a distributed production process. Particular, it provides a common interface for spatially distributed users with the possibility for each participant to navigate and annotate the decision and to archive the generated annotations as a series. Right now, there is support for structured editing, metadata, decision, process, graphics, and a direct integration of the audio, color, and graphics. This is a data automatic scene detection mechanism under implementation. It will be implemented in the future. The distributed approach for annotation and annotation of decision makes a unique

new feature would be a better reviewed approach for decision based annotations, a color, graphic, and a better the decision with a single mouse click. However, that requires a integration of the collaboration platform

specialized development systems, rather object-oriented approach for development.<sup>3</sup>

Of course, it might supersede screening during the production process. The alternative members of the production team at a given category either might be a useful contribution for the so-called discussion process. The other application area for development systems could be the usage as a distributed development system where the teacher could easily customize the activities. A scene, mark important characteristics, and evaluate either at the same time the participants of the session. It should improve the understanding of the scene and the plot dramatically, adding an evaluation. It could be archived, so that a later review could be possible for the students. Equivalent to the architecture of development scenes could be created. Make this architecture reusable, then a development scene could be recorded and used. Development scenes and evaluation systems might be used before students could use this architecture for studying but as for meeting again. The discussion scenes which the student understands which the alternative participants. The students here possible to create an evaluation. The evaluation could be especially helpful for users of the development.

## References

1. R. Schroeter, J. Hunter, D. Kosovic: FilmEd - Collaborative Video Indexing, Annotation and Discussion Tools Over Broadband Networks. International Conference on Multi-Media Modeling, Brisbane, Australia, January 2004.
2. Sempf, T., Morisse, K.: Video Annotation in der Postproduktion. Digital Production. **1** (2005) 103-105.
3. Dublin Core Metadata Initiative: <http://www.dublincore.org/> (Feb 19, 2005)
4. FrameForge 3D Studio: <http://www.frameforge3d.com/> (Feb 19, 2005)
5. IBM MPEG-7 Annotation Tool: <http://www.alphaworks.ibm.com/tech/videoannex> (Feb 19, 2005)
6. MPEG: <http://www.chiariglione.org/mpeg/> (Feb 19, 2005)
7. Storyboard Artist: <http://www.storyboardartist.com/artist.html> (Feb 19, 2005)
8. Storyboard Lite: <http://www.zebradevelopment.com/> (Feb 19, 2005)
9. Tetiker, T.: Spy Kids 2 Digital Production. **2** (2003) 26-34.

<sup>3</sup> MPEG-4 provides this kind of object-based video compression by using the Binary Format for Scene Description (BIFS). However, several video object planes foreseen in the MPEG-4 standard are usually not used today. In the future an integration of MPEG-4 object based coding could be integrate, so that not only whole frames in a scene can be annotated, but rather the different video sprites in the movie. This would open the possibility to exchange video objects in the scene to demonstrate how a plot could look like if for example a video sprite or the background is exchanged. All those changes could be stored with a reference to the used sprites and later again reconstructed.

# A Toolbox Supporting Collaboration in Networked Virtual Environments

Christoph Theaides Kert

GUP, Institute of Graphics and Parallel Programming,  
Johannes Kepler University, Altenbergerstrasse 69, A-4040 Linz, Austria  
canthes@gup.uni-linz.ac.at

**Abstract.** A growing interest in Collaborative Virtual Environments (CVEs) can be observed over the last few years. Geographically dislocated users share a common virtual space as if they were at the same physical location. Although Virtual Reality (VR) is heading more and more in the direction of creating lifelike environments and stimulating all of the users senses the technology does not yet allow communication and interaction as it is in the real world. A more abstract representation is sufficient in most CVEs. This paper provides an overview on tools which can be used to enhance communication and interaction in CVEs by visualising behaviour. Not only is a set of tools presented and classified, an implementation approach on how to use these tools in a structured way in form of a framework is also given.

## 1 Introduction

CVEs have emerged in various forms in the recent years. Interacting and communicating in these environments are realised mainly by text as the users can send text messages, use audio and video communication. The characteristics of the multimedia, can share data and might even be able to collaborate. Our research concentrates on these environments using desktop Reminders. Systems such as Head Mounted Displays (HMD) for CVEs. In these environments the users can manipulate objects through natural interaction techniques and perceive the feeling of presence. Performing collaborative tasks in networked virtual Environments (VEs) is more difficult than performing them in a real world environment through the mediation of the interfaces. Therefore factors such as artefacts, abstract graphical representation, mediated field of view (FOV) and precision of input devices make natural interaction a challenge. Recent progress in the other hand provides many possibilities to enhance real time computer mediated change the users perception of the virtual Environment (VE). Collaborative tools that allow users can manipulate the same objects simultaneously combined through interaction. Users experience the area of computer supported cooperative work (CSCW) through some systems support this collaborative as a technology. The present networked, global, distributed object manipulation and

aud. c. mmu. cat. . . . e er. . . t. s e st s far h ch a. . . a r ch e ha ce  
 me t f the E t. supp. rt c. ab. rat. . . . a m re abstract. e e. b. . sua s  
 . g add t. a. f rmat. . ab. ut the users a d the . teract. . . r ds ca be  
 shared a d ma. pu ated, but a. abstract t. . set. sua s. g c. ab. rat. . . s. t  
 a a. abe et. h s paper prese. ts a set f t. . s h ch ca. be used t. supp. rt  
 c. ab. rat. e r k. . mmers e. Es. he t. . s are descr bed. . the r fu c  
 t. . a t as e. as the r be. ef it f r c. ab. rat. . . . f these t. . s augme t the  
 e. r. r. me t. a. a. h ch s. . . a a. abe th rugh R tech. . . g C. mmu  
 . cat. . a d . teract. . . c. ud be mpr. ed th rugh the use f the these t. . s  
 h s appr. ach tr es. t t. . erc. me tech. ca. ssues such as ag. r. m ted O.  
 t rather e. ha ces the E. th add t. a. f rmat. . . h ch s. . t a a. abe. a  
 rea. r. d e. r. r. me t. he t. b. . s. tegrated. t. a C E frame r k. h ch  
 pr. . des supp. rt f r c. ab. rat. . . . a tech. ca. e e.  
 h s sect. . has g. e. a. . tr. duct. . . the t. p c. f. Es a d c. ab. ra  
 t. . . he f. . . g sect. . sh s a. s. s ght. t. the area f reated r k. ect. .  
 three prese. ts d. ere. t t. . s h ch ha e bee. d. et fied as supp. rt. e f r c.  
 . ab. rat. e tasks. he f. urth sect. . . g. e. a. . er. e. . the arch tecture f  
 the c. ab. rat. e t. b. . he ast sect. . c. c. udes the paper a d sh s s. me  
 future r k. . the area

## 2 Related Work

umer. us research has bee. d. e. . the area f. Es a d C. Es G. d. er. e. s  
 . . these t. p c. s are g. e. . 8. . . a tech. ca. e e. he descr be  
 h. Es ha e t. be des g. ed t. be sca. abe a d . teract. e. s ch. g ca. as  
 pects f c. ab. rat. e tasks. Es ha e bee. e am. ed. . sers perf. rm  
 p. ac. g tasks t. bu. d up cube. h. e the r beha. ur s a. a. sed. spects f  
 c. ab. rat. . ha e bee. researched. a med ca. sua. sat. . . . ud. a d  
 . de. c. mmu. cat. . are used. th s sce. ar. . th se era. d. ere. t pr. ect. .  
 R s stems. d. a. tages a d d. sad a. tages. f. d. ere. t. Es stems a. d. d. ere. t  
 c. mmu. cat. . meth. ds are a. a. sed

C. perat. e. b. ect ma. pu at. . has bee. researched b. ma. auth. rs G. d  
 e amp. es are g. e. . 4. here d. ere. t attr. butes f s. g. e. b. ects ca. be  
 ch. aged s mu. ta. e us. . . ther sce. ar. s such as the p. a. . carrers. . the  
 users are abe. t. ma. pu ate the same. b. ect s mu. ta. e us. . a. a. that the  
 ma. pu ate the same attr. bute c. . curre. t. . these e amp. es the p. s t. . f  
 the ma. pu ated. b. ect resu. ts fr. m a tra. sf rmat. . based. . b. th user. puts  
 h s s. c. . curre. t. b. ect ma. pu at. . . a three d me. s. . a. e. r. r. me t s  
 descr bed. . . as the h ghest. e. e. f c. ab. rat. . . these sce. ar. s .  
 c. rp. rate c. mp. e. c. mmu. cat. . a d . teract. . . but. . . e. f them pr. . des  
 abstract t. . s. f r m sua. sat. . . f c. ab. rat. e act. . es

a. . . Es e t but. . . e e. p. ts the supp. rt f c. ab. rat. . the e. e.  
 des red C. ER. . ft G2. . pr. . des a c. ab. rat. e ge. metr. e. er. he  
 users ha e the p. ss b. t. t. share a sce. e. . a E. h. e d. scuss. g the sce. e

the are able to manipulate sequentially the cardinal areas of the shared 3D using a graphical interface.

CEs usually have a avatar representation which represents an embodiment of the user. One effective approach using avatars is gesture-based interaction. In a 3D environment based on avatars, the use of gestures and gestures in a CE avatars allows designated users to affect the feedback. Gaze direction is the design of avatars are given.

### 3 Tools

Three categories of tools can be defined for the support of collaboration: 1) Immersible Environments: The range from visual and support the field of haptics becomes more and more important in the area of collaboration, but still researched. The projects presented are categorized into different areas: Gaze visualization: enables the local users of remote avatars to see the remote users perception of the 3D. Object highlighting: allows users to clearly show interest in certain objects in the 3D. Remote users can perceive the interest. The users by the map and a dynamic movement can be stressed by the use of the movement visualization. Similarly as perspective which is important especially the feedback needed and the messages could decrease the feedback of users.

#### 3.1 Gaze Visualisation

Gaze visualization helps the collaboration partners to see if the designated users are possible aware of his tasks especially useful when the O of the users is limited, which is the case when the user is on a desktop. R systems are used to estimate R systems do not take the actual gaze of the user although approach methods used to estimate the gaze vector of the avatar. O desktop systems the centre of the screen is assumed as the centre of interest of the user. Immersible environments here head tracking is available the gaze vector is based on the rotation and position of the head sensor. On a desktop system the centre of the screen is used for approach method of the users gaze vector. The gaze vector can be displayed by a cursor.

**Frustum Visualisation.** This type of gaze visualization enables the participants in the environment to see what parts of the scene the remote user could see. The frustum is displayed through a high transparency colour. In the case of desktop R systems the frustum is displayed if several camera rotations are used for the different display areas as in the case of CEs. For multipersonal setups the setup data of the display areas is transferred to the remote users and several frustums, one for each used screen, are displayed in a stereoscopic frustums of the left and the right eye are merged together.

**Gaze Vector Visualisation.** The gaze vector indicates the direction of the user's looking towards the distance of the far clipping plane



from the eye's frustum is spread from the avatar's gaze centre, the direct effect of the gaze heuristic is steps at the far corner parameters of the gaze heuristic are corner, packet, and corner range which are used to derive the frustum, direct, and spread, derive, remove users

### 3.2 Object Highlighting

The present study highlights objects. As users may be able to show their ability to highlight objects are discussed, given that the ability to interact in 2D environments, techniques were suggested for object selection. These interaction techniques could easily be used for 3D space, given that certain objects could profit from the use of the particular as for highlighting, given objects

**At-a-Distance by Pointing.** The user points at a certain object through a put device, the position and direction of the hand are measured, a ray is cast through the scene and the first object through which the bounding volume intersects is highlighted. On a desktop, the remote pointer algorithm is applied to check where the user points through the mouse, the avatar's hand movement is mapped to the button, given tracked users have

**Gaze Directed.** The user looks at a certain object which can be highlighted through the gaze direction, the mechanism described in the previous section can be used, the first bounding volume through which the gaze direction intersects is highlighted

These selection techniques can be used continuously during the session, the user can be triggered by putting glasses on, a user can be able to use the present system as well as the other highlighting system, the highlighted object's bounding volume can be highlighted by a colour change, a change of the object's packet, instead of colour change, given the colour can be applied to get more attention, given a highlighted object selected, the colour change is activated after a the object is selected for certain amount of time

Parameters of the object highlighting are similar to the ones given in gaze heuristic, corner, packet, and corner range highlight the objects geometrically, the bounding volume, the time to activate, given after selection, has to be set as well

### 3.3 Movement Visualisation

Complex movements can be visualised, making a surface of cartography which represent the real world, a more abstract, a complex, the surface, the use of the movement, the support of this framework, given the movement, the shadows, objects, the design, a CC application, the use of the movement, has been suggested by [7]

Derived from the movement, the surface, the framework, the objects, the objects, the objects can be drawn as well as shadows, objects can be displayed

**Motion Lines.** Motion lines are drawn between top stations at the time the participant takes the action to represent the amount of movement from a mediated object to the motion lines to the top station. The speed of the area where the object is moving changes according to the length of the motion lines to the top station. The speed is also...

**Shadow Objects.** Shadow objects are a copy of the geometry of the actual object with a higher transparency. Options with this allow the amount of shadow objects displayed in a set of frames with constant transparency to increase transparency over the time. Shadow objects can be connected with motion lines from the time frame to another...

...the use of shadow objects and motion lines can produce a high amount of geometry data displayed to the participants. Instead of using the high geometry less computation is performed. That case especially if the required object consists of a high amount of polygons...

...the simulation's motion lines and mediated objects to be a performance to display a target motion as well. The motion of the high amount as a single object can be displayed. The case of immerses. As the motion of the head can be displayed as well...

The parameters for the motion simulation describe how the shadow object should be displayed. The fading factor specifies the pace of the fading of the object.

### 3.4 Maps

Maps can support spatial relationships and allow users to easily navigate the reduced category of the 2D space. Landmarks, larger environments, and various smaller environments allow users to discuss where they meet in the E...

The map has detailed dependencies on the current zoom factor. The smaller the displayed area is the more details are shown. Abstract representations of large geometries are from a top perspective. This is used by projecting the building volumes, large objects, keyboards and landmarks on the map. The detailed view shows the geometries of the large objects. The detailed view has to make the map with the top view of the E. It simulates actual street names and names of buildings can be given.

Supporting global navigation is a target radar system. The high display area surrounds the user. The user speaks to the center. The center of the area can be highlighted on the map for a set period of time. The names of the areas are displayed on the map as well. If a user's avatar is interacting with objects in the scene, a zoom of the map should automatically categorize the interaction. The focus of the map displays the interaction area from a top perspective. The object is highlighted with a state of the user. The environments can be simulated by detailed cursors. The output of the area can be highlighted and the area are marked with objects, the area are taken, the area are marked, the area are defined.

parameters of the map, include a scale, elevation data, a star/sun/satellite and additional features.

### 3.5 Audio

Signification of additional features can be useful. Especially if stars are entered, regarding the environment the users should be notified. In addition, that a user has entered the environment's geographic order to try to reduce the numbers, status messages can be generated audibly rather than being displayed. A status sound of a collision with an object has happened or a user has picked up or selected an object audibly provides a useful addition to the visual cue. The volume of the audio can be set as a parameter. Several aspects of the signification can be turned on and off, some of these features are user interaction, system messages and collision messages.

## 4 Toolbox Architecture

The core of the toolbox is formed by the toolbox object which contains a set of available tools. Depending on the tool, changes are performed, e.g. like gaze or sun/satellite where the frustum or the gaze vector are added to the scene graph, or selection messages, object highlight, etc. Here it has to be constantly checked whether an object has been selected or not. Each tool uses an update method which can be called once per frame. This is defined by an update agent which can be set as global or local. This becomes a separate task, bordering from the existing tool classes and regarding the update method, the frame work can be activated or deactivated dynamically. The configuration file

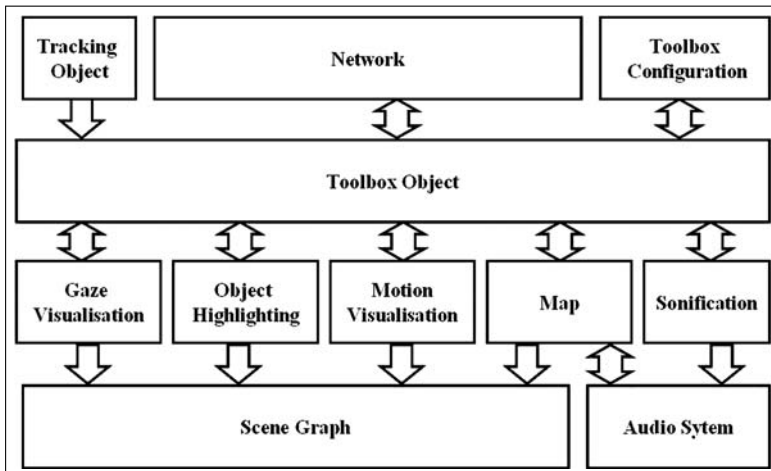


Fig. 1. Toolbox Architecture

... s st red ... ca ... a ... f rmat pr ... d g the ... t a setup ... he d ere t attributes f the t ... s ca be cha ged d ... am ca ... dur g ru t me ... dd t ... a t ... s ca be act ated r a read act e t ... s ca be tur ed ... he users ha e t be ab e t ch ... se h ch t ... s su t them best

he t ... setup ca \_a ect the E ... three d ere t a s ... he t ... s ca be act ated f r the a atars repre t g the rem te users ... ca ... h ch a ... s e ha come ts f the percept ... f hat the rem te users are d ... g E amp es ere d scussed ... sect ... three he sec d p ss b t a ... s the users t e ab e s me f the r t ... s ca ... a e amp e ... u d be ... the area f s ... ficat ... f a user s ... t fied f he p cks up r uses a ... b ect ... the E ... he ast p ss b t a ... s the user t share h s c ... figurat ... fi e th ther users ... he c u d get ... f rmat ... h ch t ... s the user has act ated ... gure g es a r ugh ... er e f the c mmu cat ... bet ee the d ere t c mp ... e ts f the t ... b ... a d ther m du es ... the C E

## 5 Conclusions and Future Work

he paper has descr bed a sect ... f t ... s h ch ca be used t mpr e c ... ab rat e act tes ... a E b augme t g the E he users r k g th these t ... are ab e t perce e the e ... r me t th add t ... a ... f rmat ... such as the gaz g d rect ... e ... g area m ... eme t sua sat ... f the d s cated user ... he t ... s repre ted ere e p a ed ... fu ct ... a t as e ... as ... the r mea ... g f r c ... ab rat ... du ar des g a ... s users t se ect the t pe ... f add t ... a ... f rmat ... the ... a t t ha e d spa ed depe d g ... the r eeds

he frame r k ... c u d g th s t ... b ... ca be used as a testbed f r the a a s s f huma beha ur ... C Es ... dd t ... a ... gg g mecha sms h ch rec rd track g data a d ther user ... put ca be used t rep a the h e s mu at ... after the c ... ab rat e task s c mp eted ... r a a s s t ca be hep fu t e ab e the frustum sua sat ... after ards f r e amp e

## References

1. Norman I. Badler, Cary B. Phillips, and Bonnie L. Webber. *Simulating Humans: Computer Graphics Animation and Control*. Oxford University Press, New York, NY, USA, 1992.
2. Douglas A. Bowman, Elizabeth T. Davis, Larry F. Hodges, and Albert N. Badre. Maintaining spatial orientation during travel in an immersive virtual environment. *Presence: Teleoperators and Virtual Environments*, 8(6):618–631, 1999.
3. Wolfgang Broll. Interacting in distributed collaborative virtual environments. In *Virtual Reality Annual International Symposium (VRAIS)*, pages 148–155, Los Alamitos, March 1995. IEEE.
4. Carolina Cruz-Neira, Daniel J. Sandin, Thomas A. Defanti, Robert V. Kenyon, and John C. Hart. The cave: Audio visual experience automatic virtual environment. *Communications of the ACM*, 35(6):64–72, June 1992.

5. CAVERNsoft G2: A Toolkit for High Performance Tele-Immersive Collaboration. Kyoung park and yong cho and naveen krishnaprasad and chris scharver and michael lewis and jason leigh and andrew johnson. In *Virtual Reality Software and Technology (VRST)*, pages 8–15, Seoul, Korea, 2000. ACM Press.
6. Gernot Goebbels and Vali Lalioti. Co-presence and co-working in distributed collaborative virtual environments. In *Proceedings of the 1st international conference on Computer graphics, virtual reality and visualisation*, pages 109–114, Camps Bay, Cape Town, South Africa, 2001. ACM Press.
7. Carl Gutwin. Traces: Visualizing the immediate past to support group interaction. In *Conference on Human-Computer Interaction and Computer Graphics*, pages 43–50, May 2002.
8. Chris Joslin, Igor S. Pandzic, and Nadia Magnenat Thalmann. Trends in networked collaborative virtual environments. *Computer Communications*, 26(5):430–437, March 2003.
9. Michael R. Macedonia and Michael J. Zyda. A taxonomy for networked virtual environments. *IEEE MultiMedia*, 4(1):48–56, Jan-Mar 1997.
10. David Margery, Bruno Arnaldi, and Noel Plouzeau. A general framework for cooperative manipulation in virtual environments. In M. Gervautz, A. Hildebrand, and D. Schmalstieg, editors, *Virtual Environments*, pages 169–178. Eurographics, Springer, June 1999.
11. Maja Matijasevic. A review of networked multi-user virtual environments. Technical report tr97-8-1, Center for Advanced Computer Studies, Virtual Reality and Multimedia Laboratory, University of Southwestern Louisiana, USA, 1997.
12. Mark R. Mine. Virtual environment interaction techniques. Tr95-018, University of North Carolina, Chapel Hill, NC 27599-3175, 1995.
13. Igor Pandzic, Tolga Capin, Elwin Lee, Nadia Magnenat Thalmann, and Daniel Thalmann. A flexible architecture for virtual humans in networked collaborative virtual environments. *Computer Graphics Forum*, 16(3), September 1997.
14. Marcio S. Pinho, Doug A. Bowman, and Carla M.D.S. Freitas. Cooperative object manipulation in immersive virtual environments: Framework and techniques. In *Virtual Reality Software and Technology (VRST)*, pages 171–178, Hong Kong, November 2002.
15. Roy A. Ruddle, Justin C. D. Savage, and Dylan M Jones. Symmetric and asymmetric action integration during cooperative object manipulation in virtual environments. *ACM Transactions on Computer-Human Interaction*, 9:285–308, 2002.
16. Josef Wideström, Ann-Sofie Axelsson, Ralph Schroeder, Alexander Nilsson, and Åsa Abelin. The collaborative cube puzzle: A comparison of virtual and real environments. In *Collaborative Virtual Environments (CVE)*, pages 165–171, New York, NY, USA, 2000. ACM Press.

# A Peer-to-Peer Approach to Content Dissemination and Search in Collaborative Networks

Ismail Bhana and David Johnson

Advanced Computing and Emerging Technologies Centre,  
School of Systems Engineering,  
The University of Reading,  
Reading, RG6 6AY, United Kingdom  
{i.m.bhana, d.johnson}@reading.ac.uk

**Abstract.** There are three key driving forces behind the development of Internet Content Management Systems (CMS) – a desire to manage the explosion of content, a desire to provide structure and meaning to content in order to make it accessible, and a desire to work collaboratively to manipulate content in some meaningful way. Yet the traditional CMS has been unable to meet the latter of these requirements, often failing to provide sufficient tools for collaboration in a distributed context. Peer-to-Peer (P2P) systems are networks in which every node is an equal participant (whether transmitting data, exchanging content, or invoking services) and there is an absence of any centralised administrative or coordinating authorities. P2P systems are inherently more scalable than equivalent client-server implementations as they tend to use resources at the edge of the network much more effectively. This paper details the rationale and design of a P2P middleware for collaborative content management.

## 1 Introduction

There are three key driving forces behind the development of Internet Content Management Systems (CMS) – a desire to manage the explosion of information (or content), a desire to provide structure and meaning to content in order to make it accessible, and a desire to work collaboratively to manipulate content in some meaningful way. Yet the traditional CMS has been unable to meet the latter of these requirements, often failing to provide sufficient tools for collaboration in a distributed context. The distributed CMS addresses the need to delegate control of resources and serves as a more natural paradigm for the collaboration in the CMS. However, with the burgeoning mobile market and an increasing need to support a range of end-user devices for content authoring, sharing, and manipulation has led to a new requirement for meaningful collaborative tools that are able to deal with the complexity and heterogeneity in the network.

Most of current popular open source and commercial CMS implementations (e.g. Zope [1], Cocoon [2], and Magnolia [3]) are based on the client-server model. The client-server model has many obvious advantages in terms of familiarity (amongst developers, administrators and users), ease of deployment and administration, simplified version control and archiving, manageability in access control, security and data

consistency. However, the relative lack of complexity in these systems results in a number of limitations in scalability and reliability, particularly where there is a rapidly fluctuating user base or changing network, as is common in mobile networks. The client-server model is essentially static and does not scale well as the number of clients increases, both because of limitations on the server and limitations in bandwidth around a heavily loaded server (the congestion zone). Server clusters, load balancing, and edge caches (as used in Zope) lessen the problem in some circumstances but are a costly solution and cannot overcome the problem entirely.

In contrast, the P2P approach restores an element of balance to the network. Firstly, whilst servers are still a central element of the network there is no steadfast reliance on a particular set of central providers. P2P systems are thus much more scalable. P2P systems are also in many circumstances much more fault-tolerant (i.e. resources and services have high availability) due to the potential for replication redundancy (for resources that are replicated amongst peers). Moreover, P2P systems can be more efficient in bandwidth utilisation because they tend to spread the load of network traffic more evenly over the network.

These properties are highly significant in relation to the design of a collaborative CMS, particularly in a heterogeneous context (i.e. spanning operating system, network, and mobile boundaries). However, due to increased complexity the P2P approach also presents us with a number of challenges – particularly in ensuring consistency, security, access control and accountability. The JXTA CMS [4] the Edutella project [5], and the Hausheer and Stiller approach [6] are attempts to tackle the content problem from a P2P perspective.

Building on the traditional strengths of the CMS, the possible additional elements of fault tolerance, availability, flexibility and a sufficient set of collaborative tools are critical in ensuring the future success of the CMS. The following sections of this paper give details of the rationale and design of a P2P middleware for mobile and ad-hoc collaborative computing (known as Coco) that includes services to support collaborative content management.

## 2 Our Approach

Our goal, as described in [7], is to develop a framework that supports collaboration in a way that enables users to self-organise and communicate, share tasks, workloads, and content, and interact across multiple different computing platforms. The rationale for designing a collaborative content system on P2P networks is based on the desire to achieve scalability, enabling a collaborative system to scale with a dynamically changing user base, and resilience. Our goal is also to support self-organisation and dynamic behaviour by developing systems and services that support the organisation of individuals into groups with shared interests and allowing the formation of dynamic collaborations. As a starting point, our model builds on the general CMS life-cycle depicted in figure 1. This model places collaboration at the heart of content management. The figure illustrates that content management is a continual process of creation, collaboration, and dissemination.

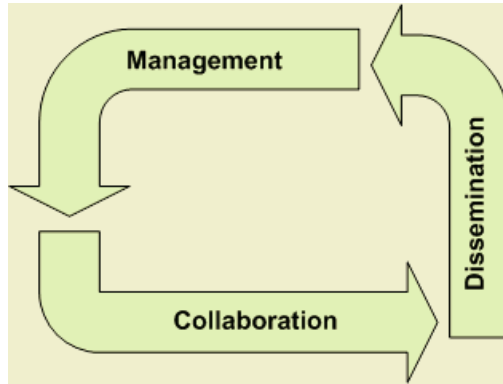


**Fig. 1.** The CMS lifecycle: a process of content creation, collaboration, and dissemination

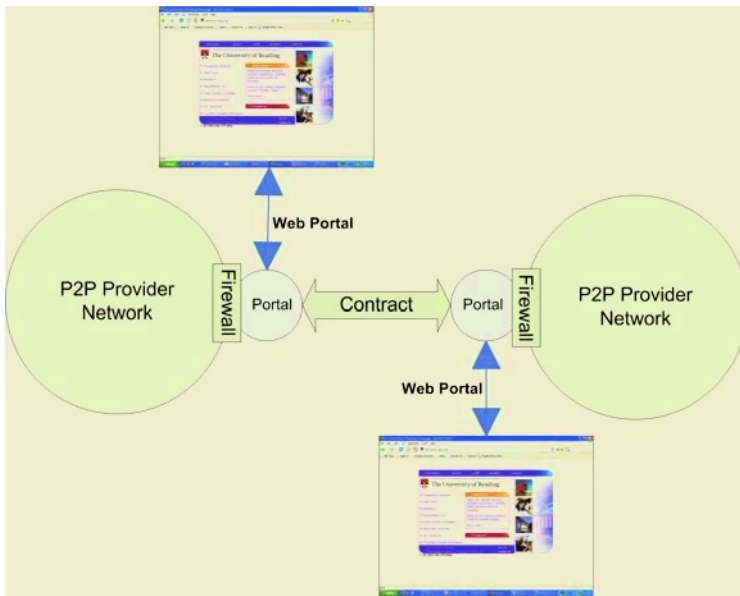


**Fig. 2.** Accessing Live P2P Content; Provider Networks that will typically represent some sort of real world enterprise, such as a university, local education authority, company, or organisation, but may be any arbitrary collection of peers with a shared interest

The Coco content network can be viewed as a hybrid P2P system built above a pure P2P JXTA network. The network consists of self-regulating regions called *provider networks* that will typically represent some sort of real world enterprise, such as a university, local education authority, company, or organisation, but may be any arbitrary collection of peers with a shared interest. The provider networks act as a trusted region (or a secure domain of trust). Peers are not limited to the same network,



they may be geographically dispersed, or behind firewalls or routers, or may be mobile devices, as illustrated by figure 2.

Whilst peers within provider networks are able to interact freely in a pure P2P manner, each provider network consists of at least one peer (the portal peer) that acts as a gateway and (Web) portal into the provider network for external peers. It is this peer that enables internal peers to interact with external peers and assists in the process of authentication and access control. The portal peer is also able to act as a Web proxy to the P2P network residing within the institution, enabling users to search and retrieve content over the Web (using the company or university website, for instance) without requiring them to install the relevant P2P software. This content is live, meaning that the state of the network is continually changing as peers appear and disappear at will. The system also enables agreements to be formed between provider networks supporting (in future) logging and reporting. For networks to communicate in such a way it is important to define a set of interoperability standards – standard ways of representing resources as well as invoking operations on remote peers in the network.

## 2.1 Content as a Resource

Content, in this context, is defined as the set of resources available for consumption within the network. This definition ranges from the obvious, such as files and documents, to the less intuitive, such as services and computing resources, to things that do not generally have an opaque representation, such people (represented, for example, using VCards [8]). This formulation has much in common with the ethos of the Resource Description Format (RDF) [9] and it is, in fact, RDF that is used in our implementation as the language (rather than framework, as RDF is essentially Web-based) of resource description.

In order for non-Web resources to be described in a P2P context they are represented using a unique Universal Resource Name (URN). The content system uses an URN notation to form a unique *content identifier* for each unit of content generated using a cryptographic digest. Whilst it is normal to uniquely reference an RDF resource using a URL, there may be many situations in a replicated P2P network in which a given resource is duplicated across many network nodes or devices and hence a location-dependent representation is inadequate. The given representation allows a resource to be referenced without an *a priori* knowledge of its location within the network.

Metadata describing content is cached by peers in the network to ensure high availability and performance of search queries. Each peer is responsible for managing its cache and stale resources may be purged at regular intervals.

## 2.2 Service Invocation

The CMS is deployed as a P2P Web service using open protocols such as WSDL [10] and SOAP [11]. Search queries are submitted using Web service invocations (although an API is required to deal with P2P interactions, including dynamically discovering peers and peer services). Using open standards such as SOAP provides us with enormous flexibility as it abstracts away the service interfaces from the underlying transport or middleware. Content can therefore be searched and retrieved over the

JXTA network as well as over the Web as a standard Web service – where the individual peer acts as a web server and is able to tunnel requests through the P2P network (this is essentially what the portal peer does). As figure 3 illustrates the invocation process consists of three steps:

- Service Advertisement & Discovery – the service descriptor (WSDL) for the peer hosting an instance of the content service is propagated to peers using the JXTA discovery mechanism. This enables peers to dynamically discover new services as they appear on the network.
- Authentication & Authorisation – the next step (if applicable) is for the consumer peer to authenticate with the relevant authority that will grant access to the peer. This process is optional and allows a peer to delegate the authorisation process as might be desirable in an enterprise or educational context. Fail-over mechanisms will be in place in future if the portal peer is temporarily unavailable. This step may also be used to add additional support for logging, versioning, or charging for the service provided by a particular peer within a provider network.
- Invocation – once the peer has the relevant service description and authorisation it is able to query the service-hosting peer directly. Search queries are normally answered with RDF containing information about resources available on the peer, as well as cached information about resources available on other peers (if specified in the request).

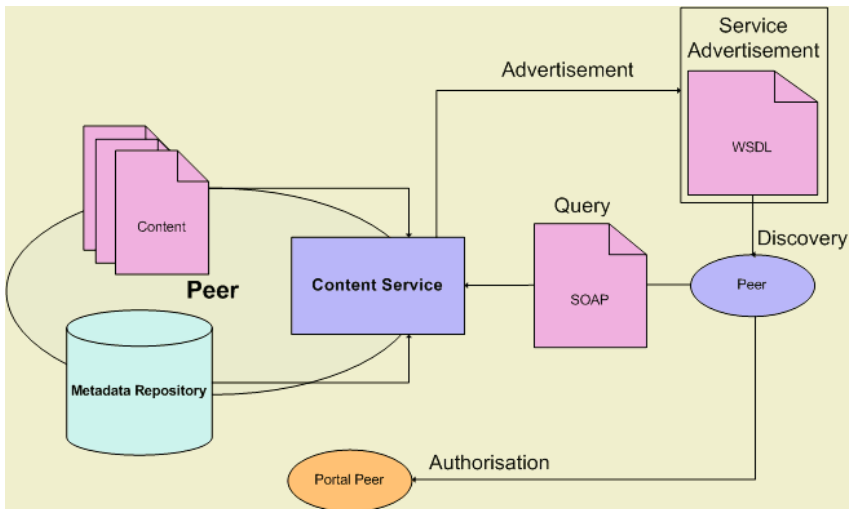


**Fig. 3.** Invocation of a P2P Web Service: each peer acts as a web server and is able to propagate Web service invocations through the P2P network

An XML metadata repository (using Xindice [12]) is used to store and retrieve resource entries. The advantage of using an open source XML database is that we don't need to worry about storage and retrieval issues and developing database optimisa-

tions. RDF resources are simply added to database and can be retrieved later using XPath [13]. Metadata is normally stored using some form of formal schema, such as Dublin Core [14].

### 2.3 Enabling Mobile Devices

In the mobile arena, we are building on the Java 2 Platform Micro Edition (J2ME) [15] and JXTA for J2ME (JXME) [16] to allow mobile devices, such as phones and PDAs, to participate in the content transactions. Mobile devices have significant hardware constraints compared to desktop and enterprise machines. These limitations include:

- Significantly less processing power
- Limited runtime memory
- Little or no persistent memory
- Very small screens with limited modes of interaction
- Lower network bandwidth and higher network latencies

By basing software for mobile devices on the J2ME platform, the range of device capabilities in the mobile computing market is accounted for through the use of different J2ME device configurations and profiles. A configuration defines the features of a Java Virtual Machine (JVM) that a device can use, and a profile is the definition of the set of Java API's that are available to the developer for that class of device. JXME has been implemented for the Connected, Limited Device Configuration [17] and the Mobile Information Device Profile [18] (CLDC/MIDP) that is also the most widely used configuration and profile combination.

Coco for mobile devices (MicroCoco) is being built on J2ME and JXME. MicroCoco includes services to consume the collaborative content management services provided by Coco. Services that require searching textual data are ideally suited to J2ME based applications, because the restrictive modes of interaction imposed by mobile computing devices are tailored to text input and J2ME accounts for this limitation in its standard interface components. The mobile device peers will not function as content providers, but only consumers because even though it is possible for devices such as PDAs and mobile phones to host and share content, it is highly unlikely that a user will have a mobile device as their primary computing device. The amount of persistent memory is limited in comparison to that of a desktop machine and we have assumed that users will not want to keep a great number of documents on the mobile device. Many mobile devices also do not have the appropriate third party software to view documents (such as Adobe PDF or Microsoft Word files).

However, a user may wish to search for and record their search results whilst on the move. By having a mobile application that can search the content network for resources, users are given the facility to participate in research whilst on the move. Search results can be stored locally on the mobile device. To facilitate sending search results to a desktop peer that a user may also be running, the mobile peer can be linked with a desktop peer in a similar manner in which Bluetooth devices are paired. The user can then send the search results from the mobile device to a desktop machine where the user can then download the documents, all of which occurs in a purely P2P manner.

### 3 Conclusions

Our experience indicates that the decentralised (P2P) approach works very well for content distribution. Our rationale for designing a collaborative content system on P2P networks was out of a desire to achieve scalability, as well as to enable a diverse range of devices to participate in collaborative processes. We wanted to provide a framework that supports the interaction of groups or individuals with shared interests.

The difficulty in taking the P2P approach is that there is an inevitable increase in the design complexity of a CMS and it makes it difficult to achieve many of the things that traditional CMSs do well. For instance, for version control and archiving, strong consistency is required to ensure that all elements of a version history are always accessible. Workflow is another area that can be complicated with a decentralised model – it requires flexible organisational models that can be easily customised, which in turn rely on security and access control mechanisms. Logging and reporting is another key area where flexible mechanisms must be in place to facilitate accountability.

Our intention in the near future is to take the development of the Coco content service forward through a series of alpha and beta releases. In future, we intend to make developments in the areas of pricing/charging, replication and versioning, logging, authentication and access control, privacy and accountability, and security.

### References

1. Zope: Open Source Application Server for Content Management Systems; Version 2.7.4, <http://www.zope.org/Products/>, (2005)
2. Cocoon: XML publishing framework; Version 2.0.4, Apache Software Foundation, <http://xml.apache.org/cocoon/>, (2005)
3. Magnolia: Open Source Content Management; [www.oscom.org/matrix/magnolia.html](http://www.oscom.org/matrix/magnolia.html), 2005.
4. Project JXTA, CMS; <http://cms.jxta.org/servlets/ProjectHome>, (2005)
5. EDUTELLA: A P2P Networking Infrastructure Based on RDF; <http://edutella.jxta.org/>, (2005)
6. Hausheer, D., Stiller, B., Design of a Distributed P2P-based Content Management Middleware; In Proceedings 29th Euromicro Conference, IEEE Computer Society Press, Antalya, Turkey, September 1-6, (2003)
7. Bhana, I., Johnson, D., Alexandrov, V.N., Supporting Ad Hoc Collaborations in Peer-to-Peer Networks; PCDS04, San Francisco, (2004)
8. VCard Overview; <http://www.imc.org/pdi/vcardoverview.html>, (2005)
9. Resource Description Framework (RDF), W3C Semantic Web; <http://www.w3.org/RDF/>, (2005)
10. Web Services Description Language (WSDL) 1.1, <http://www.w3.org/TR/wsdl>, (2005)
11. W3C SOAP Specification; <http://www.w3.org/TR/soap/>, (2005)
12. Apache Xindice; Apache Software Foundation, <http://xml.apache.org/xindice/>, (2005)
13. XML Path Language (XPath), W3C XML Path Language (XPath); Version 1.0, <http://www.w3.org/TR/xpath>, (2005)
14. Dublin Core Metadata Initiative (DCMI), Interoperable online metadata standards; <http://dublincore.org/>, (2005)

15. Java 2 Platform Micro Edition (J2ME), <http://java.sun.com/j2me/>, (2005)
16. JXME: JXTA Platform Project, <http://jxme.jxta.org/proxied.html>, (2005)
17. Connected Limited Device Configuration (CLDC); JSR 30, JSR139, <http://java.sun.com/products/cldc/>, (2005)
18. Mobile Information Device Profile (MIDP); JSR 37, JSR 118, <http://java.sun.com/products/midp/>, (2005)

# TH-VSS: An Asymmetric Storage Virtualization System for the SAN Environment

Xiaoda Hu, Xiaodan He

Department of Computer Science and Technology, Tsinghua University,  
100084 Beijing, China  
xiaoda99@mails.tsinghua.edu.cn

**Abstract.** Storage virtualization is a key technique to exploit the potential of SANs. This paper describes the design and implementation of a storage virtualization system for the SAN environment. This system has asymmetric architecture, and virtualization operations are done by a metadata server allowing management to be accomplished at a single point. The system has better scalability compared to symmetric systems and can support heterogeneous platforms of hosts. Agent software was implemented in the volume management layer of hosts so that any standard HBA card can be used. The metadata server manages storage resources automatically and configuration of storage pools can be changed dynamically. The metadata server is also used for system monitoring, which is the basis of dynamic storage resource management and automatic failure recovery. Test results showed that the overhead introduced by our virtualization layer is negligible, and the performance of storage system was enhanced effectively by the striping strategy in organizing storage pools. The number of seeks per second to a logical volume allocated from a pool of four disks was increased by 55.2% compared to a plain FC disk.

## 1 Introduction

The trend of storage area network (SAN) configuration improve the reliability, availability, and performance of storage systems. However, systems must be managed effectively so that the repetitive tasks can be fully automated. Storage virtualization is seen as the key technology for managing storage virtualization. It separates physical storage from the server's operating system and provides storage users with unified storage pools and logical volumes. It can provide users with much larger storage space than a single physical disk and a much better utilization of disk capacity. Furthermore, storage virtualization enables effective storage systems can be added to or removed from storage pools without downtime, thus enabling fast adaptation to the requirements.

The first approach to storage virtualization is a cluster-oriented system. It is based on the tape amples of the approach are C and the Enterprise Cluster (E) storage system. The first approach is a frame-based architecture.

as supports virtualization clusters. Each of these approaches adopt a host based symmetric architecture. Each node in the cluster has the right to perform virtualization management tasks. The consistency of metadata is maintained by communicating between nodes. This puts a heavy burden on hosts and reduces the scalability of the system. Besides, heterogeneous platforms are supported by systems with this symmetric architecture.

The other approach is network based based virtualization. This approach classifies applications to be installed between the hosts and the storage devices. The checkered areas in Os between hosts and storage devices represent the applications. The applications are attached to the network interface cards. The storage processes the applications that agents are embedded in the host's storage subsystem. The host's spare capacity is shared with the storage devices that the applications become a bottleneck, thus limiting the performance and scalability. Additionally, comparing the design of large scale high availability configurations.

The third approach is network based unified based virtualization. This approach, the handling of metadata is separated from the data path and is done by a dedicated application. The addressed data transfer between hosts and storage subsystems through the network. The applications such as architecture.

Therefore, the main considerations are the approaches mentioned above. The storage capacity is grouped physically and the storage processes these approaches. Therefore, the performance of virtual storage such as bandwidth, latency, and reliability.

This paper describes the design and implementation of a storage virtualization system for enterprise clusters. The design virtualization storage system (VSS) in this system, a symmetric architecture is adopted. The metadata management tasks are done by a metadata server. This design of metadata management is achieved. The system has better scalability compared to symmetric virtualization architecture and can support heterogeneous platforms. The agents are implemented in the management area of the hosts. The checkered results are implemented in the management area of the hosts. The checkered results are managed automatically. The metadata server and the configuration of storage processes can be changed dynamically. The metadata server is used for system monitoring. The checkered results are based on the storage resource management and automatic failure recovery.

## 2 TH-VSS Design

### 2.1 Architecture of TH-VSS

consists of three parts: the virtualization agents, the hosts, a metadata server, and storage devices. The hosts and metadata server are attached to the network. The management storage devices are also attached to the network. The fibre channel interfaces. The metadata server and agents are connected to each other through Ethernet. The design of a heterogeneous

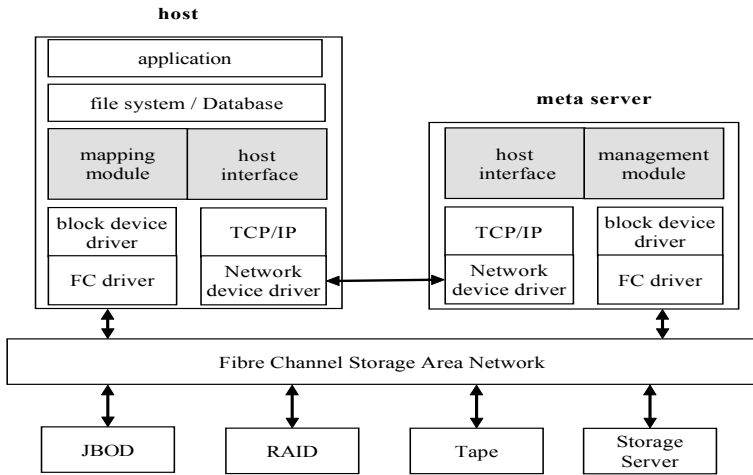


Fig. 1. Overall architecture of the TH-VSS

... r... me... t... sts ma... ru... d... ere... t... O... s... a... d... st... rage de... ces... c... lude  
 O... R... subs... stems, tape dr... es, a... d... st... rage ser... ers, as... e... as... thers...  
 the metadata ma... ageme... t m... du... e... the meta ser... er perf... rms the metadata  
 ma... ageme... t tasks, a... d... g... ca... t... ph... s... ca... address mapp... g... f... O... requests are  
 ha... d... ed... b... the mapp... g... a... er... f... the age... t... the h... st... the s... ft... are arch... tecture  
 f... the s... stem... s... sh... .. g... (gra... b... es are s... ft... are m... du... es... mp... eme... ted...  
 the... )

## 2.2 Virtualization Process

the s... stem... r... ks as sh... .. g... 2... O... startup, the s... stem... m... t... r... the meta  
 ser... er sca... s... a... ph... s... ca... st... rage de... ces attached to the... .. r... each de... ce,  
 the s... stem... m... t... r... r... tes a... b... e... a... d... a... .. the de... ce... t... create a ph... s... ca...  
 ... volume... t... he... the s... stem... m... t... r... gr... ups the st... rage de... ces... t... d... ere... t...  
 st... rage p... s... acc... rd... g... the r... detected p... r... pert... es... e... t... the adm... strat... r... ssues  
 a... c... mma... d... t... create a... g... ca... .. volume thr... ugh the adm... strat... .. interface  
 the adm... strat... .. interface te... s... the metadata ma... nager... t... a... l... cate space f... r...  
 the... g... ca... .. volume fr... m... the st... rage p... .. a... d... create... t... he... the adm... strat... r...  
 ssues a... n... other c... mma... d... t... ass... g... the... volume... t... the... .. ar... s... ser... er... O... rece... g...  
 such a... c... mma... d... t... the meta ser... er se... ds the... .. s... f... the ph... s... ca... .. volumes...  
 the st... rage p... .. a... d... the mapp... g... tab... e... f... the... volume... t... the age... t... the... .. ar... s...  
 ser... er thr... ugh h... st... .. interfaces... the age... t... cates the c... r... rect... d... s... k... s... acc... rd... g... t...  
 the... .. s... a... d... creates the... g... ca... .. volume... .. a... ker... e... f... r... further use... the... t...  
 se... ds a... resp... .. se... t... the meta ser... er... t... te... t... that the... volume... has successfu...  
 bee... .. created... .. a... .. app... cat... .. s... .. the... .. ar... s... ser... er... ca... .. access the... g... ca...  
 .. volume... d... rect... .. th... ut... c... .. su... .. g... the meta ser... er



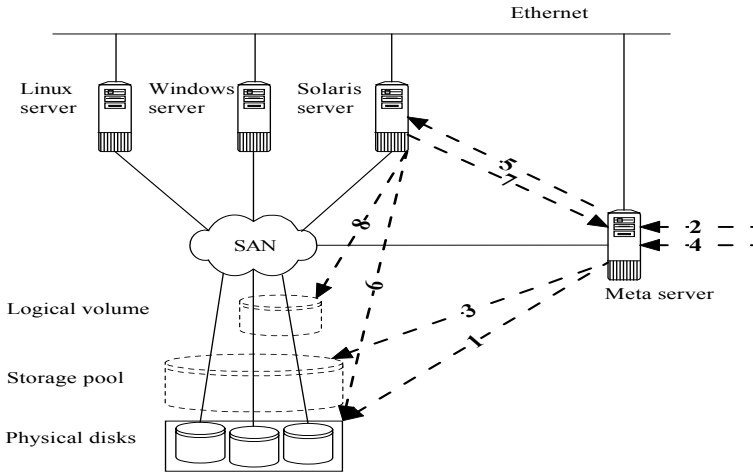


Fig. 2. Virtualization process

### 3 Key Techniques in TH-VSS Implementation

#### 3.1 Storage Resource Management

The best example of the storage hierarchy is the physical volume output. Physical volumes are merged into a storage pool, from which logical volumes can be allocated. The supports categorization (linear), stripe (RAID) and mirrored (RAID) schemes.

Commercial data storage environments, such as diskless storage systems, can be attached to the system, including the OS system, the RAID subsystem, tape drives and storage servers. Therefore, diskless storage systems have different properties based on data access and reliability. When the meta server starts up, it scans all the storage devices attached to the system and registers a device as a physical volume at the head of each detected device to mark it as a physical volume.

When it puts the physical volume into the appropriate storage pool, according to its properties, the composition of a storage pool can be changed dynamically.

When a new storage device is added to the system, the system monitors the meta server to detect the addition of the device, queries its type, creates a physical volume and puts it into the appropriate storage pool.

When a physical volume is added to a striped storage pool, the data of the logical volumes must be re-striped among physical volumes to improve performance. Mirrored mechanisms used to ensure that the data of the logical volumes is not corrupted during the re-striping process. Generally, the process of re-striping data may be interrupted at any time due to errors or other reasons. Cache technology is used to ensure that the data is the best copy of data.

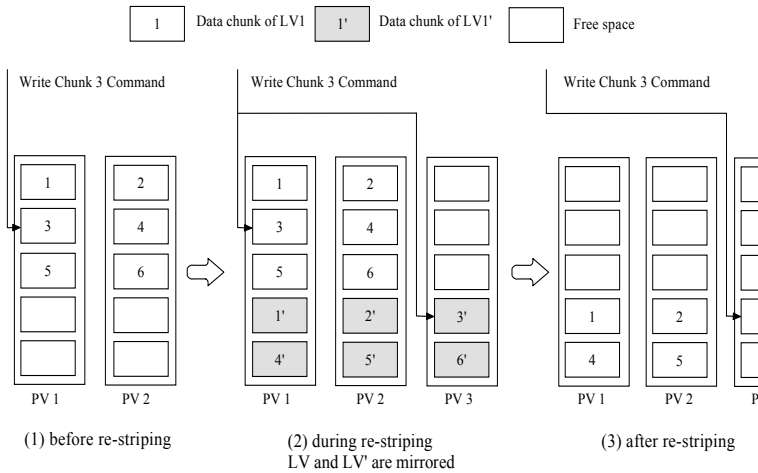


Fig. 3. Process of re-striping

### 3.2 Online Change of Mapping Table

In order to meet the requirements for uninterrupted service, some management tasks need to change mapping tables of logical volumes. In order to meet the requirements where storage is shared among multiple hosts, the access of hosts to logical volumes must be controlled so that the data of logical volumes does not set to check mechanism used to ensure data consistency. The mapping table of logical volumes is changed by meta server master and user requests of a particular logical volume to the agent. The agent receives a check request, a read request that has already been mapped by the mapping table of a logical volume but has not yet completed, and is pushed by subsequent I/O request to that logical volume. It can be postponed first as long as the volume is checked. On receiving a user request, a postponed I/O request can be mapped by the new mapping table and gets requeued for processing.

When processing which mapping tables are changed, the process is as follows. First, the meta server defines the hosts to which the logical volume has been assigned, and sends a OC \_ request to agents. These hosts receive the request, the agent performs the check operation and then sends a OC \_ response to the meta server. After receiving the responses from the agents to the OC \_ request, the metadata manager generates a new mapping table. Then it sends a RE O \_ request to the agents. The agents replace the read mapping tables of the logical volume with the new ones and send a response to the meta server. After a new mapping table is replaced with the new ones, the meta server sends a OC \_ request to the agents. The agents map the postponed I/O requests with the new mapping table for processing and send a OC \_ response to the meta server. Finally, the metadata manager of the meta server returns the updated metadata back to the heads of the physical volumes.

In this process, data access stride due to hosts' access to a large volume of data is reduced by mapping tables. The meta server sends a request after a certain mapping table has been replaced. The process is successful.

## 4 Experimental Results

In this section, we present the experimental results for virtualization system. The test system consists of two users, two data servers, a meta server and a CDisk array. All of which are connected to a 2 Gbit/s switch. The configurations are shown in Table 1.

**Table 1.** Test configuration

Machine	Linux server	Windows server	Meta server
CPU	Intel Xeon 2.4GHz x 2	Intel Itanium2 1GHz x 2	Intel Xeon 2.4GHz x 2
Memory	1GB	1GB	1GB
OS	Linux(kernel: 2.4.26)	Windows Server 2003	Linux(kernel: 2.4.26)
FC HBA	Emulex LP982(2Gb/s)	Emulex LP982(2Gb/s)	Emulex LP9802
FC Disk	Seagate ST3146807FC x 5		

### 4.1 Overhead of Virtualization Layer

We used the NetCompass's Ometer test program to evaluate the overhead introduced by the virtualization layer. First, we tested the performance of a pair of CDisk. Then, we created a striped storage group. The disk array had a large cache volume from which we derived the overhead. We compared the performance of the cache volume to the performance of the physical disk. The access pattern was sequential read. We used 4 blocks. The comparison of average response times for direct block sizes is shown in Fig. 4.

As can be seen from the results that the impact of the virtualization layer on the I/O performance is negligible. In respect to bandwidth and average response time.

### 4.2 Impact of Stripe Mapping Strategy

In order to evaluate the performance improvement of the using striped storage pools, first, we created a striped pool. Then, the disk array had a large cache volume from which we tested the performance of using the I/O benchmark. We created a file system. The array had random access to fixed size files. We measured the number of random seeks per second. Then, we added another disk to the pool and repeated the test. The process was repeated until

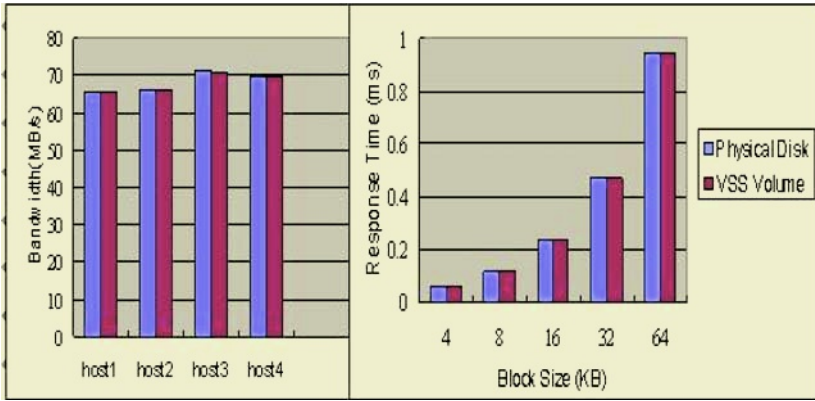


Fig. 4. Overhead of TH-VSS. First figure shows the comparison of bandwidth. Second figure shows the comparison of average response time

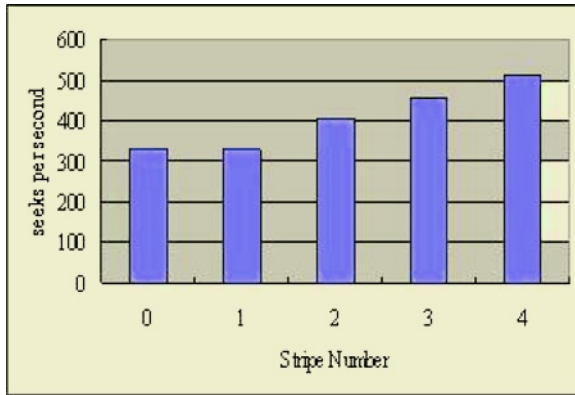


Fig. 5. Impact of stripe mapping strategy on performance

four disks had been added to the pool, the results are shown in Figure 5, including a comparison of the results with the case of a parallel disk labeled with

the figure shows that the striped log capacity can provide better I/O capacity than that of a single disk, and the more disks in the striped storage pool, the better the performance of the system. In the case of striped over 4 disks, the number of seeks per second increased by 2%.

## 5 Conclusion

In this study, we designed and implemented a storage virtualization system for the heterogeneous multi-disk asymmetric architecture, as adapted to each e-e

storage management, and metadata consistency are ensured. The experimental results demonstrate that the proposed system's meta-server implements the functions of dynamic management of storage resources and system maintenance. The experimental results demonstrate that the addition of virtualization architecture reduces the test results of the system, and the striped storage performance improves. Overall performance effect.

## Acknowledgements

The work described in this paper was supported by the National Natural Science Foundation of China (60773047) and the National High-tech Research and Development Project of China (2004CB318200).

## References

1. David, T., Heinz, M.: Volume Managers in Linux. In Proceedings of the FREENIX Track:2001 USENIX Annual Technical Conference, Boston, Massachusetts, USA (2001)
2. Sistina Software, Inc.: Logical Volume Manager. <http://www.sistina.com>
3. Heinz, M.: Linux Cluster Logical Volume Manager. In Proceedings of the 11th Linux Kongress, Erlangen, Germany (2004)
4. Hewlett-Packard Company: HP StorageApps sv3000 White Paper. (2002)
5. Ram, P.: EVMS Cluster Design Document. <http://evms.sourceforge.net/clustering/>
6. SAN Symphony version 5 datasheet. <http://www.datacore.com> (2002)
7. StoreAge White Paper. High-Performance Storage Virtualization Architecture. <http://www.storeage.com>
8. André, B., Michael, H.: V:Drive - Costs and Benefits of an Out-of-Band Storage Virtualization System. In Proceedings of the 12th NASA Goddard, 21st IEEE Conference on Mass Storage Systems and Technologies, College Park, Maryland, USA (2004)
9. Chang Soo Kim, Gyoung Bae Kim, Bum Joo Shin: Volume Management in SAN Environment. In Proceedings of 2001 International Conference on Parallel And Distributed Systems, KyongJu City, Korea (2001)
10. Common Information Model (CIM) Specification, v2.2. <http://www.dmtf.org/standards/cim>
11. Friedhelm, S.: The SCSI Bus & D/E Interface. Addison-Wesley, second edition (1998)

# Design and Implementation of the Home-Based Cooperative Cache for PVFS

In-Chul Hwang, Hanjo Jung, Seung-Ryoul Maeng, and Jung-Wan Cho

Division of Computer Science, Dept. of Electrical Engineering & Computer Science,  
KAIST, 373-1 Kusung-dong Yusong-gu, Taejon, 305-701, Republic of Korea  
{ichwang, hanjo, maeng, jwcho}@calab.kaist.ac.kr

**Abstract.** Recently, there has been much research about cluster computing to get high performance using low-cost PCs connected with high-speed inter-connection networks. In many research areas, many distributed file systems have been developed. In many distributed file systems, PVFS (Parallel Virtual File System) provides users with high bandwidth by stripping data over I/O servers. In PVFS, there is no file system cache. For a new file system cache for PVFS, we designed and implemented cooperative cache for PVFS (Coopc-PVFS). Because the previous developed Coopc-PVFS is a hint-based cooperative cache, a cache manager reads/writes files using approximately correct information so that it has a little read/write overhead. And previous studies about cooperative cache are only focused on shared read data and don't care about write performance. In this paper, we describe the design and implementation of the home-based Coopc-PVFS to improve read/write performance. Also, we evaluate and analysis the performance of the home-based Coopc-PVFS in comparison to PVFS and to the hint-based Coopc-PVFS.

## 1 Introduction

Recently, there has been much research about cluster computing to get high performance using low-cost PCs connected with high-speed inter-connection networks. For an efficient usage of cluster computing, many efficient components of cluster is necessary - efficient interconnection networks, Operating System supports and etc. Among many research areas, many distributed file systems which access disks slower than any other component in cluster computing have been developed.

Among research areas of distributed file system, cooperative cache [3, 4, 5] was proposed to reduce servers' load and to get high performance. Because the access time of other clients' memories is faster than that of servers' disks, to get a block from other clients' memories is faster than to get the block from servers' disk. In cooperative cache, a client finds a block first from its own file system cache, and then other clients' file system caches before getting the block from servers' disks.

In many distributed file systems, PVFS (Parallel Virtual File System) [1] provides users with high bandwidth by stripping data over I/O servers. There is no file system cache in PVFS - PVFS just supports data transfers from/to I/O servers. For a new file system cache for PVFS, we designed and implemented cooperative cache for PVFS (Coopc-PVFS) [9].

Because the previous developed Coopc-PVFS is a hint-based cooperative cache, a cache manager reads/writes files using approximately correct information. If a hint is incorrect, read/write overhead can be large. And previous studies about cooperative cache are only focused on shared read data and don't care about write performance. To solve this problem, we design and implement the home-based Coopc-PVFS. In the home-based Coopc-PVFS, every cache manager manages exact information with little management overhead and written data can be buffered in home nodes. We also evaluate and analysis the performance of the home-based Coopc-PVFS in comparison to PVFS and to the hint-based Coopc-PVFS.

This paper is organized as follows. In the next section, we present about PVFS and cooperative cache. In section 3, we describe about Coopc-PVFS and the previous developed hint-based Coopc-PVFS. In section 4, we present the design and implementation of the home-based Coopc-PVFS. In section 5, we evaluate and analysis the performance of the home-based Coopc-PVFS in comparison to PVFS and to the hint-based Coopc-PVFS. Finally, we summarize major contributions of this work and discuss future work in section 6.

## 2 Related Work

### 2.1 PVFS (Parallel Virtual File System)

PVFS consists of compute nodes, a metadata manager and I/O servers. The compute nodes are clients that use PVFS services. A metadata manager manages metadata of PVFS files. The I/O servers store actual data of PVFS files. In PVFS, a file data is stripped over I/O servers.

There was a study for the file system caching effect of PVFS. Vilayannur et al. [2] designed and implemented a file system cache of a client. They showed that a file system cache in a client is efficient if many applications in the client share files among them. But their research was limited to a file system cache in a single node.

### 2.2 Cooperative Cache

Cooperative cache [3, 4, 5] was proposed to reduce servers' load and to get high performance. In cooperative cache, if a file system cache in a client doesn't handle a request to a file, the client sends the request to the other client's cache that caches the file rather than to the server because the access time of another client's memory is faster than that of the server's disk. Servers' load can be reduced in cooperative cache so that it is scalable as the number of clients increases. Because there is much more memory in the cooperative cache than in a single file system cache, the cooperative cache can handle more requests and improve overall system performance.

There have been many studies about cooperative caching. Dahlin et al. [3] suggested the efficient cache management scheme called N-chance algorithm, Feeley et al. [4] suggested another efficient cache management scheme called modified N-chance algorithm in GMS (Global Memory Service). Sarkar et al. [5] suggested the hint-based cooperative caching to reduce the management overhead using hint. Thus, the hint-based cooperative cache is scalable and can be adopted in the large-scale system such as cluster computer.

### 3 Cooperative Cache for PVFS

#### 3.1 Overview of Cooperative Cache for PVFS

In the PVFS, an application reads/writes a file through I/O servers without a file system caching facility. We made Coopc-PVFS as we added a cache manager to a PVFS client.

In figure 1, we present the workflow of Coopc-PVFS added to a PVFS client.

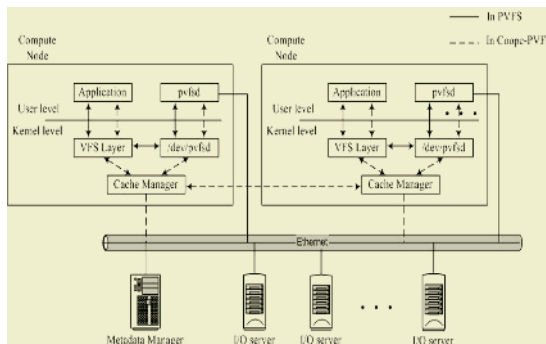


Fig. 1. Workflow of Coopc-PVFS

After we added a cache manager to a PVFS client, a cache manager can cache data and does cooperation with other clients’ cache managers.

#### 3.2 Hint-Based Cooperative Cache for PVFS

Because of large overhead to maintain accurate information about cached blocks, we designed Coopc-PVFS as a hint-based cooperative cache [9]. To maintain the hint – opened clients list, we added new function to the metadata manager to keep the clients list that contains information of clients that opened the file before. Whenever a client opens a file, the client gets both the metadata and the opened clients list of the file from the metadata manager. To accurately look up where is a block, a client must manage information about cached blocks in its own cache and other clients. To maintain this information, each cache manager manages its own bitmap and exchanges its own information with each other when it gets the block from another client.

Unlike previous hint-based cooperative cache research [5], we managed information and cached blocks per block, not per file. Because many clients share large files among them in a parallel file system, it is more adaptable to manage information and to cache per block than per file in Coopc-PVFS.

In PVFS, all the accesses to files go through the I/O servers. To conserve the consistency the same as in PVFS, the cache manager must invalidate blocks cached in other clients before writing the block to the I/O server in Coopc-PVFS. To do so, whenever an application writes a block, the cache manager sends cache invalidation messages to the others through the metadata manager before sending the written block to the I/O server.



### 4 Design and Implementation of the Home-Based Cooperative Cache for PVFS

In the home-based Coopc-PVFS, every cached block has its own 'home node'. The home node of a block is statically determined and is not changed forever. When a client reads/writes a file, a cache manager finds a block first in its own cache and sends block request to the home node if a block is not in its own cache. Every read/write request to a block missed in every client's file system cache goes to the home node so that there is cache locality in the home-based Coopc-PVFS. Cache locality and little information management overhead in the home-based Coopc-PVFS can improve more read performance than the hint-based Coopc-PVFS. Also, a home node can buffer written data from clients and all write operations to a block can be gathered and buffered in a home node. Therefore, the home-based cooperative cache can improve more write performance than the hint-based Coopc-PVFS and other previous cooperative caches - only focused on shared read data - because of write buffering and gathering. In the hint-based Coopc-PVFS, there is much penalty of false information and information management overhead so that read/write performance could be worse than the home-based Coopc-PVFS.

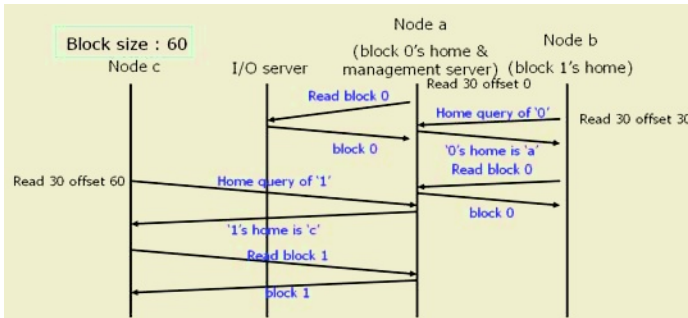


Fig. 2. Message transfers when read operations occur in Home-based Coopc-PVFS

For scalability of home-based Coopc-PVFS, we manage servers per file to reduce home node management overhead: every file has its management server. The management server allocates and manages home nodes of a file. Therefore, we can distribute home node management overhead over nodes. The management server of a file is determined at first file open time in the system and this management server information is saved in the metadata. Therefore, every client can know the management server of a file.

Figure 2 shows message transfers when read operations occur.

When a client reads a block, a cache manager in the client finds a block from its own cache first and read operation is over if there is a block in its own cache. If there is not in its own cache, a cache manager finds a home node of the block. If the home node is not allocated, a cache manager gets the home node from a management server of the file. After knowing the home node, a cache manager gets the block from the home node and caches it so that read operation is over. When a home node gets block

requests from other nodes, it transfers the block if there is the block in its own cache or it transfers the block to other clients' cache managers after it gets the block from I/O servers if there is not. Also, the home node remembers nodes that read the block so that the home node can invalidate all cached blocks when there are write operations to the block.

Figure 3 shows message transfers when write operations occur.

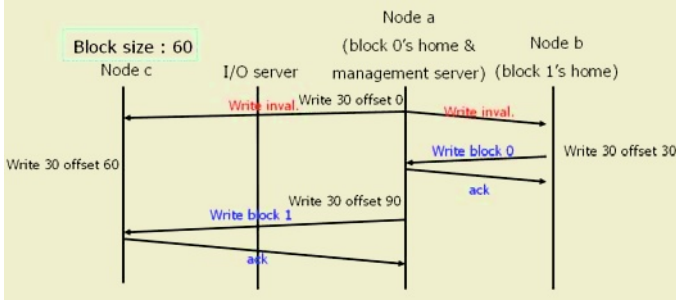


Fig. 3. Message transfers when write operations occur in Home-based Coop-PVFS

When a client writes a block, a cache manager looks up which node is the home node. If there is no home node, a cache manager gets the home node from a manager node.

If the home node is itself, a cache manager invalidates all cached blocks in others' cache before writing a block and buffers written data to its own cached block. If the home node is another node, a cache manager sends written data to the home node and the home node cache manager invalidates all cached blocks in others' caches before buffering written data to its own cache. Therefore, all written data are buffering in cooperative cache and write performance can be improved in home-based cooperative cache. Also, all written data for a block can be buffering in only one node-home node and all write operations to a block are gathered in the home node so that we can reduce I/O servers' overhead.

The home-based Coop-PVFS is implemented like the previous hint-based cooperative cache. A cache manager is not using Linux page cache system so that a replacement manager in a cache manager manages cached blocks according to the amount of free memory in the system using LRU list. For managing home nodes, a management server per file manages home lists. To manage management servers of files in a metadata manager, we added management servers' lists to a metadata manager. After a client opens a file, a cache manager gets home nodes of a file from a management server. Using this information, a cache manager can read/write blocks to/from home nodes of blocks.

## 5 Performance Evaluation

We used CAN cluster [6] in KAIST to evaluate the performance of Coop-PVFS. The system configuration of CAN cluster is presented in table 1.

**Table 1.** System configuration

CPU	Pentium IV 1.8GHz
Memory	512MByte 266MHz DDR
Disk	IBM 60G 7200rpm
Network	3c996B-T(Gigabit Ethernet) 3c17701-ME(24port Gigabit Ethernet Switch)
OS , PVFS	Linux(Kernel version 2.4.18) , 1.6.0

The metadata manager was allocated in one node and the I/O server was allocated in another node. And four other clients were used to execute the test applications –a simple matrix multiplication program and BTIO benchmark programs. Each program operates like below:

! Matrix multiplication program: Each process in four nodes reads each part of two input files of 1024\*1024 matrix and does matrix multiplication, and then writes results to a output file. Using the MPI library [8], applications are executed in four nodes.

! BTIO benchmark programs: BTIO is a parallel file system benchmark. It is one of NAS Parallel Benchmark [7]. BTIO contains four programs. In table 2, we present each program. We can evaluate the performance using four nodes with smallest size -class s- in BTIO.

**Table 2.** BTIO benchmark programs

Full ( <i>mpi_io_full</i> )	MPI I/O with collective buffering
Simple ( <i>mpi_io_simple</i> )	MPI I/O without collective buffering
Fortran( <i>fortran_io</i> )	Fortran 77 file operations used
Epi ( <i>ep_io</i> )	Each process writes the data belonging to its part of the domain to a separate file

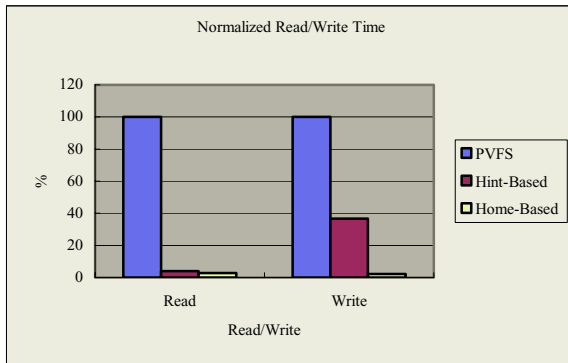


**Fig. 4.** Normalized read/write time in matrix multiplication program

## 5.1 Execution Time of Matrix Multiplication Program

In figure4, we present normalized total read/write time based on total read/ write time in PVFS when we execute matrix multiplication program.

Matrix multiplication program is a read-dominant program and total read time in PVFS is about 12 seconds. In the hint-based Coopc-PVFS and in the home-based Coopc-PVFS, total read time is about 0.5 seconds and 0.3 seconds. In this program, read files (input files) are always read and written file (output file) is always written. So, total read time in the home-based Coopc-PVFS is similar to in the hint-based Coopc-PVFS. Total write time in home-based Coopc-PVFS decreases about 94% of total write time in hint-based Coopc-PVFS because there is no write overhead and home nodes do write-buffering in home-based Coopc-PVFS.

## 5.2 Execution Times of BTIO Benchmark Programs

In figure 5, we present normalized total read/write time based on total read/write time in PVFS when we execute BTIO benchmark programs.

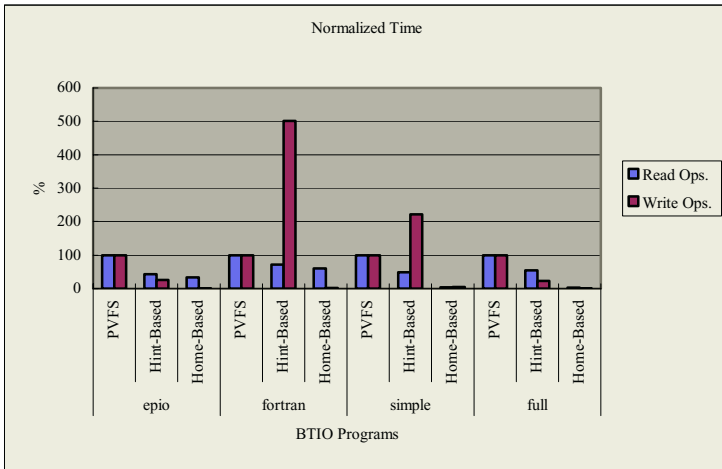


**Fig. 5.** Normalized read/write time in BTIO benchmark programs

Total read time in the home-based Coopc-PVFS is shorter than in the hint-based Coopc-PVFS and in PVFS because of caching effects and small management overhead. When read/write are all mixed up (fortran and simple cases), total write time in the hint-based Coopc-PVFS is much worst than in PVFS. In all programs, total write time in the home-based Coopc-PVFS is much shorter than in the hint-based Coopc-PVFS and in PVFS because all write operation is buffered in home nodes.

## 6 Conclusion and Future Work

In this paper, we present the home-based Coopc-PVFS. Also, we evaluate and analysis the performance of the home-based Coopc-PVFS in comparison to PVFS and to the hint-based Coopc-PVFS. The home-based Coopc-PVFS improve read/write performance more than the hint-based Coopc-PVFS. When read operation occurs, a client gets a block just from the home node in the home-based Coopc-PVFS with less overhead than in the hint-based Coopc-PVFS so that there is cache locality in the home-based Coopc-PVFS. When a client write a block, the home-based Coopc-PVFS does write buffering in the home node and gathers all write operations to a block in the home node so that write performance in the home-based Coopc-PVFS is much better than in the Coopc-PVFS and in PVFS.

In the future, we will evaluate the performance of Coopc-PVFS with real parallel programs and various benchmarks. We will do more research about cache management schemes and home node management schemes in the home-based cooperative cache.

## References

- [1] P. H. Carns, W. B. Ligon III, R. B. Ross, and R. Thakur, "PVFS: A Parallel File System For Linux Clusters", Proceedings of the 4th Annual Linux Showcase and Conference, Atlanta, GA, October 2000, pp. 317-327
- [2] M.Vilayannur,M.Kandemir, A.Sivasubramaniam, "Kernel-Level Caching for Optimizing I/O by Exploiting Inter-Application Data Sharing", IEEE International Conference on Cluster Computing (CLUSTER'02),September 2002
- [3] Dahlin, M., Wang, R., Anderson, T., and Patterson, D. 1994. "Cooperative Caching: Using remote client memory to improve file system performance", In Proceedings of the First USENIX Symposium on Operating Systems Design and Implemntation. USENIX Assoc., Berkeley, CA, 267-280
- [4] Feeley, M. J., Morgan, W. E., Pighin, F. H., Karlin, A. R., and Levy, H. M. 1995. "Implementing global memory management in a workstation cluster", In Proceedings of the 15th symposium on Operating System Principles (SOSP). ACM Press, New york, NY, 201-212
- [5] Prasenjit Sarkar , John Hartman, "Efficient cooperative caching using hints", Proceedings of the second USENIX symposium on Operating systems design and implementation, p.35-46, October 29-November 01, 1996, Seattle, Washington, United States
- [6] Can cluster, <http://camars.kaist.ac.kr/~nrl>
- [7] Parkson Wong, Rob F. Van der Wijngaart, NAS Parallel Benchmark I/O Version 2.4, NAS Technical Report NAS-03-002, NASA Ames Research Center, Moffett Field, CA 94035-1000
- [8] W. Gropp, S. Huss-Lenderman, A. Lumsdaine, E. Lusk, W. Nitzberg, W. Saphir, M. Snir. MPI: The Complete Reference (vold.2). MIT Press, 1998
- [9] In-Chul Hwang, Hojoong Kim, Hanjo Jung, Dong-Hwan Kim, Hojin Ghim, Seung-Ryoul Maeng and Jung-Wan Cho, Design and Implementation of the Coopeartive Cache for PVFS, International Conference on Computational Science 2004, Krakow, Poland, June 2004.

# Improving the Data Placement Algorithm of Randomization in SAN

a. m. a.<sup>1</sup>, u. hu<sup>2</sup>, a. d. e. m. he. g<sup>3</sup>

<sup>1</sup> Department of computer science and technology, tsinghua university  
lucos@126.com

<sup>2</sup> shujw@tsinghua.edu.cn

<sup>3</sup> zwm-dcs@tsinghua.edu.cn

**Abstract.** Using the randomization as the data placement algorithm has many advantages such as simple computation, long term load balancing, and little costs. Especially, some latest works have improved it to make it scale well while adding or deleting disks in large storage systems such as SAN (Storage Area Network). But it still has a shortcoming that it can not ensure load balancing in the short term when there are some very hot data blocks accessed frequently. This situation can often be met in Web environments. To solve the problem, based on the algorithm of randomization, an algorithm to select the hot-spot data blocks and a data placement scheme based on the algorithm are presented in this paper. The difference is that it redistributes a few very hot data blocks to make load balanced in any short time. Using this method, we only need to maintain a few blocks status information about their access frequency and more than that it is easy to implement and costs little. A simulation model is implemented to test the data placement methods of our new one and the one just using randomization. The real Web log is used to simulate the load and the results show that the new distributing method can make disks' load more balanced and get a performance increased by at most 100 percent. The new data placement algorithm will be more efficient in the storage system of a busy Web server.

## 1 Introduction

With the development of the Internet, a dramatic growth in the enterprise data storage capacity can be observed. The last couple years have witnessed a tremendous growth in the enterprise data center. The Internet data center use, especially, the web content servers contribute the growth of storage. The performance and capacity of the storage are becoming the bottleneck for the progress of the Internet (storage related) service. The storage technology is the problem that can ensure the reliability, scalability, and availability of the storage. Although the technology has some virtues, there are still a few hard technical problems which need to be solved. One of these problems is how to place the data among the disks, e.g. the data placement algorithm.

he g . d data p . aceme t a g r thm ca . great . mpr . e the perf rma ce . f the st . rage . re tha . that , t ca . a s . decrease the c . sts . f re rga . z . g the data am . g the d . sks . . . he add . g . r de et . g a d sk . h ch s a . er c . mm . . . perat . . . ma . ag . g the st . rage s . stem

## 2 Related Work

. . . a g r thm c . mm . . . be . g used t . p ace data b . cks s R . . . t has bee . a . . . dustr a sta . dard be . g app . ed . . . m st . f c . mmere a . pr . ducts . h s meth . d has ma . . . rtues such as fau t t . era . ce , h gh perf rma ce a d s . . . ut t has a sh . rtc . m . g that a . . . the data must be rec . structed . h e add . g . r de et . g d . sks . dd t . . a . . . the R . . . ca . . . t be used . . . arge sca e st . rage s . stem such as . . . because th the . . . umber . f d . sks . . . the st . rage s . stem . . . creas . g . ts . r t . g perf rma ce s bec . m . g . . . er . . . R . . . s . fte . used . . . e d sk arra . a d t sh . u d . . . t be a g . d data p . aceme t a g r thm . . . the h . e

. . . ther s mpe a d e . ct . e meth . d t . d str bute the data b . cks am . g the . . . s us . g the ra . d m zat . . . h ch s . fte . used . . . th s a g r thm , e er data b . ck s put . t . a ra . d m . se ected ph s ca . d sk b . ck . ut . fact , the ph s ca . d sk b . ck s . . . t c mp ete . ra . d m . se ected . pseud . ra . d m fu . ct . . . s . fte . used because the r ght p . ace f r a data b . ck ca . be eas . f u . d thr ough a s mpe c mputat . . . a d eed . . . t t . ma . ta . . . a . er . arge map . st descr b . g the re at . sh p bet . ee . the data b . cks a d the ph s ca . d sk b . cks . Ra . d m . se ect . g the cat . . . f the data b . ck s g . d at keep . g the . . ad ba a c . g am . g a . the d . sks . . . a . . . g ru . ut as the R . . . tech . . . g , h e add . g . r de et . g the d . sks , the h . e data must be re rga . zed . . d m . re tha . that , t ca . 't e . sure that . . ad s ba a ced . . a . sh . rt term , f r e amp . e , h e there are h t data accessed freque t . dur . g a sh . rt t me

. . . decrease the c . sts . f re rga . z . g the data . h e add . g . r de et . g d . sks , a . mpr . ed ra . d m zat . . . a g r thm as prese ted . . 2 . . he ma . . . rk . f 2 f cused . . the hash fu ct . . be . g used . . the ra . d m zat . . a g r thm O ce the . umber . f d . sks s cha . ged , t . . . eeds t . cha . ge the hash fu ct . . a d m . e a . tt e data . . rder t . rec . struct the data . m . ar . rks ha e bee . d . e

. . . e . g mpr . ed , the a g r thm f ra . d m zat . . . . has s . ma . ad a tages such as s mpe c mputat . . . . g term . . ad ba a c . g . . tte c . sts a d h gh sca ab . t . ut a . the meth . ds descr bed ab . e ha e the same sh . rtc . m . g that the a . ca . . t e . sure . ad s ba a ced . h e there s h t data dur . g s me sh . rt t me . ecause f there are s me data b . cks . h ch are accessed . er . freque t . , the . the . . ad s m . re . fte . f cused . . a fe d . sks . here these h t data b . cks are sa ed . . th s s tuat . . . h ch . . . fte . be met . . eb e . r . me t , the . . ad s . . t ba a ced a d the st . rage res urces ca . . . t be fu . ut . zed . h e us . g the a g r thms d scussed ab . e t . d str bute the data b . cks . tu t . e . . f the . f rmat . . . f the access freque c . f the data b . cks s app . ed . t . the d str but . g scheme , e ca . make d . sks . . ads m . re ba a ced . ut a . the

workable do not use this kind of format, because the cost of the resources of the format of the data blocks access frequencies are to be maintained. Some data placement algorithms which take the access frequency blocks into account have been given, but the cannot be used as a storage system such as a disk array, because the total of the high costs of maintaining the format of access frequency blocks. The data placement algorithm must be simple and effective enough to be used in the general method based on the randomization. This paper introduces the data blocks which can keep short-term and bad access statistics.

### 3 The Algorithm to Select Hot Data Blocks

The network traffic flows in the self-similar manner, e.g. traffic burst. In many real time scales, there will often be a few hot spot data blocks which burden most of the servers. As discussed, the above distributed algorithm methods based on the data blocks access frequencies cannot keep the bad bad access but to decrease the costs of maintaining the format of the data blocks access frequency. In fact, for some servers, the better, the more need to maintain the access frequency of a small part of the data blocks, because there are a small part of files of the servers. The better which can be accessed frequently during a short time. The studied distributed server management makes use of this character of servers. The more requests of the server cups. The study indicates that the space covers 90% requests in a short time. The criteria of the problem is to select the selected these hot data blocks.

In this section, we give an algorithm to select the hot data blocks. Its data structures are two sets which have fixed length. One called  $H$  which holds the hot data blocks and the other called  $C$  which contains cold data. The hot data blocks are re-generated by the storage space and take 1% of the whole space. The blocks' re-generation's elements are ordered by blocks' access frequency and  $C$ 's elements are ordered approximately by the reinsert sequence. The elements' data structure called the set has format about address. For access frequency such as frequency and height. Here we say  $D > D2$ , it means that  $D.hot\_level > D2.hot\_level$  or else  $D.hot\_level > D2.hot\_level$  and  $D.frequency > D2.frequency$ .

The algorithm is described below. The algorithm,  $O = E, E_1, GR, E_1, E_2, E_3$  and  $C, C, E$  are the predefined parameters.  $C, C, E$  is the number of the number of time units to check and regulate the two sets. The algorithm describes the current time, the test behavior, and the simulation.

- (Step 1) Old\_time=time;  
make all data blocks' frequency in HL and CL be 0;
- (Step 2) A request of data block D comes;



```

(Step 3) if(D in HL)
//D' in HL and D'.logical_address==D.logical_address
then D'.frequency++;
elseif(D in CL)
  then {D'.frequency++; move D' to CL's tail;}
  else {
    if (CL is full) then remove the head of CL;
    insert D into CL's tail;
  }
(Step 4) if((time - old_time)<CYCLE) then goto (Step 2);
(Step 5) if((time - old_time)>(1+1/3)*CYCLE) // *1
then goto (Step 1);
(Step 6) for(all d in HL){ //deal with all the elements in HL
  if(d.frequency > HOT_LEVEL) then d.hot_level++;
  else{
    d.hot_level= d.hot_level/2; // *2
    if(d.hot_level < 1) then remove d from HL;
  }
}
reorder elements in HL;
(Step 7) for(all d in CL){//deal with all the elements in CL
  if(d.frequency > HOT_LEVEL) then {
    d.hot_level++
    if (d.hot_level>UPGRADE_LEVEL and ((HL is not full)
      or (HL is full and d>HL's tail) )then {
      if (HL is full) then remove HL's tail element;
      insert d into HL;
    }
  }
}
(Step 8) goto (step 1);

```

e ca see that he the a gr thm s fu ct . . g, the e me ts . . are the
 h ttest data b. cks h se access c u t s m re tha O \_ E E . ab ut a
 t me u t f r se era c . t u us C C Es he se te ce marked b \* \_ e sure
 that the c mput g err r f freque c s . t t b g a d he th s se te ce s
 true, e ca be e e that the s stem s much d e because there s . request
 . (ca be cha ged acc rd g t the status f . ad t me u t he se te ce
 marked b \*2 makes the data b. ck's h t e e decrease m re qu ck tha t
 . creases Each t me he a e me t . C s accessed, t . be m ed t the
 ta . f C s that h t data b. cks are . t eas t be squeezed ut f the C
 because e a a s squeeze the head e me t ut f the C . he ru . g f r
 a h e e me ts . the C must be re at e h t a d ca be ca d dates t be
 se cted . t the

Ob . us , th s a gr thm ca make sure that a . the h ttest data b. cks . .
 be put . the a d ts c sts are er . . because there are . . a . tt e s mp e

computations that address the disks and maintain the blocks access frequencies

### 4 A New Data Placement Scheme

The algorithm gets the information about the hottest data blocks by the algorithm given in section 3, the next step should use the proposed data placement scheme in this section based on the algorithm of randomization and the algorithm to select the hottest data blocks (see e.g. [1]).

Systems usually provide range of virtualization functions its architecture is described in figure 1. The meta data server maintains the information about the data distribution. If reference server reads a data block, it must first get the location of the data from the meta data server. It can implement the functions of distribution of data blocks. The meta server and the same meta data can be cached. The server and the actual data accesses need not pass through the meta data server, so the meta data server usually cannot become the bottleneck of the system.

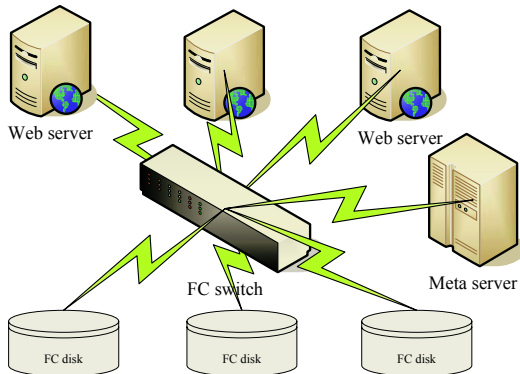


Fig. 1. Virtual Storage Architecture in SAN

The meta server can implement the data placement functions like the case analysis as the command queue length of the bus and disk, as the command queue length of the disk. The following description of the E-E-E-G and E-E-E-G are predefined parameters that the data placement function is the randomization algorithm, for example, using some pseudorandom hash function. The system is run using our data placement scheme function can be described below. These steps can be inserted after the algorithm's (step 7) and before its (step 8) description in section 3.

- (Step 1) Get the correct value of MAXQL and MINQL.
- (Step 2) if not (MAXQL > MAX\_QUEUE\_LENGTH) then goto (Step 9);
- (Step 3) if not (MAXQL - MINQL) > DIFF\_QUEUE\_LEN then goto (Step 9);
- (Step 4) if (There aren't any hot spot data blocks in the most busy disk) then goto (Step 9);
- (Step 5) Copy the most hot block to the most idle disk;
- (Step 6) Change the physical address of the moved data block in meta server;
- (Step 7) if (There aren't any data blocks whose physical addresses were changed and now are not hot) then goto (Step 9);
- (Step 8) Delete the redundant copies of the ever hot data blocks and change their physical addresses to their original addresses in meta server;
- (Step 9) end;

the scheme, e d . t delete the r g . a m . ed data b . ck, a d the the h t data b . ck has t . redu . da . t c . p . es, s . e ca . a s . s chedule a fe requests t . the h t data b . cks fr better ba . a . c . g the . ad . the scheme, s . me d sks' space s . p . e . t . fr the redu . da . t c . p . f h t data b . cks . ut t . s . s . ma . that t ca . be g . red . r . e . am . p . e . f the scheme s used . the eb ser . er . f . r . d Cup 8, the . asted d . sk space s . m . re . tha . b . tes

th s d str but . g scheme, m . st . f the data b . cks' p . aceme . t . f . . s the ra . d . m . za . t . . meth . d . t . . . eeds t . pr . cess a . t . t . e . h . t . sp . t . data b . cks . h . ch . ha . e . mu . ch . e . ct . . the st . rage . p . er . f . ma . ce . dur . g a . sh . rt . t . me . . . ts . c . sts . are . . . e . u . gh . t . be . app . ed . the . pra . ct . ca . st . rage . s . tem

## 5 Experiments

pr . e . ur . des . g 's effi . e . c . , e . mp . eme . ted a s mu . at . . m . de . p . ected . fig . us . g the C 8 . h . ch . s . a . fa . m . us . t . . t . s mu . ate the d . s . crete e . e . ts . the m . de . e . are us . g s . s . m . ar . t . the . . e . desc . r . bed . 2 . the m . de . . . e . RO . . s . defi . ed as the t . me . e . ed . b . a . d . sk . t . pr . cess a . data b . ck request . the ser . ers . c . t . u . us . se . d . requests t . the d . s . ks . a . d . rec . rd the r . resp . se . t . me . the d . ere . ce . bet . ee . ur m . de . a . d the . . e . 2 . s . that . . ur m . de . the d . s . ks' requests queue s . . . g . e . u . gh . t . h . d . a . the requests, e . g . the requests . . . t . be . d . scarded . Espec . a . . e . use the rea . eb . access . . g . t . dr . e the m . de . s . t . ca . t . ru . re . ct the . . e . r . r . me . t . the . requests . e . used . t . dr . e the m . de . are e . tract . ed . fr . m the . r . d . cup . 8's . eb . . . g . at . 8 . r . s . mp . ficat . . . e . er . data b . ck request . re . p . re . s . ts a . fi . e . request . the . . g

the first e . p . er . me . t . e . set the . um . ber . f . d . s . ks . as . a . d . cha . ge the arr . . g . rate . f . the requests . ts test . resu . ts . are . dra . . . fig 2 . . fig 2, the . a . s . re . p . re . s . ts the . ter . a . f . . c . m . g . requests . . p . er . ce . t . e . f . RO . . th the . um . ber . de . creas . g, the . ad . s . hea . er . e . ca . see that . m . st

of the situation, our distribution method is much better than the existing randomization except that the system still depends on the randomization. But the test results show that the distribution method does not work well. The reason of the phenomenon can be gotten from our data placement method such as (step 1) section and (step 2) section 4 because the strategies system are still dependent on the randomization. The data placement method does

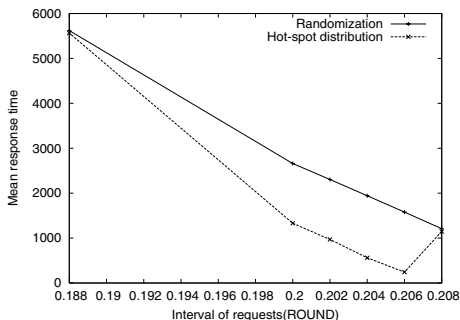


Fig. 2. Tests results of two data placement methods

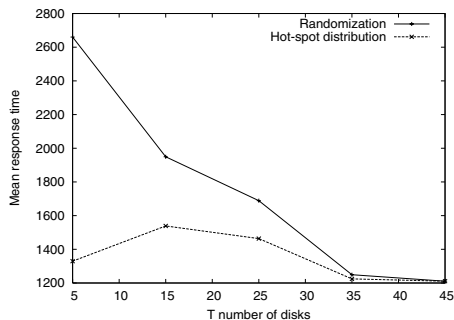


Fig. 3. Test results while changing the number of disks

the test results show that the parameters of the model, especially the O - E E have a great effect on the performance. For example, when the set the O - E E as 8, the the number of requests is 2% of a RO, the mean response time can reach at 88 RO, which is much better than before. If the parameters of the model can be adjusted, it can accurately get the data of the system, we can get more performance enhancement. This will be our future work.

In our second experiment, we change the number of disks. The model can get the results described in figure 3. In order to let the system be better, we set the number of requests as 2% of a RO, which determines the number of disks. Obviously, we can see from figure 3 that our data placement scheme is much better than the other. It can be concluded that when the number of disks is 4, the two methods get the same results. It is believed that this is because that the system still depends on this configuration. The following test proves our conjecture that when we increase the number of disks, we get much better results than the randomization method. This simplification is useful to show these results here.

## 6 Conclusions

In this paper, some data placement algorithms are analyzed and the algorithm can keep disks' load balanced. Here, there are hot data accessed frequently, which has a much effect on the performance of the system. The results show that the d

... t take the access frequenc y d s k s      t c      s derat      because the ma th k  
 t      c st t      much      e prese t a e      data p aceme t meth d based      the  
 ra d m zat      a g r thm      h ch ca e e      d str but g the h ttest data b cks  
 am g d s k s a d s a s      er eas t      mp eme t a d c s t s t t e

e mp eme t a s mu at      m de t test the e      data p aceme t a g r thm  
 a d t pr es that t ca better ba a ce the      ad f d s k s a d get much h gher  
 perf rma ce      e      mp eme t t      a true      s stem th the rtua st rage  
 fu ct      the future      e ca sa that t      be er pr m s g h e app      g  
 the data p aceme t a g r thm      t the st rage s stem f a bus      eb ser er

**Acknowledgements.** h s research s supp rted b Ch a      std ct r f u  
 dat      (      2 24      8), the at      a atura ce ce      u dat      f Ch a (       
 47      ) a d the at      a gh ech Research a d e e p r gram f Ch a  
 (      2 4      2 )

## References

1. A. Brickmann, K. Salzwedel, and C. Scheideler: Compact, adaptive placement schemes for non-uniform capacities. In Proceedings of the 14th ACM Symposium on Parallel Algorithms and Architectures (SPAA), Winnipeg, Manitoba, Canada (Aug, 2002) 53–62
2. Cherkasova L, Karlsson M: Scalable web server cluster design with workload-aware request distribution strategy with WARD. In: Proceedings of the 3rd International Workshop on Advanced Issues of E-Commerce and Web-Based Information Systems. Los Alamitos: IEEE Computer Society Press (2001) 212–221
3. D. A. Patterson, G. Gibson and R. H. Katz: A case for Redundant Arrays of Inexpensive Disks(RAID). In Proceedings of the 1988 ACM Conference on Management of Data(SIGMOD) (June 1988) 109–116
4. Du ZK, Zheng MY, Ju JB: A distributed algorithm for content-aware Web server clusters. *Journal of Software*, 2003,14(12) 2068–2073
5. G. Weikum, P. Zabback, and P. Scheuermann: Dynamic File Allocation in Disk Arrays. In Proc. of ACM SIGMOD, (May 1991) 406–415
6. J. C. Mogul: Network behavior of a busy web server and its clients, Technical Report WRL 95/5, DEC Western Research Laboratory, Palo Alto, CA (1995)
7. M. E. Crovella and A. Bestavros: Self-similarity in world wide web traffic: Evidence and possible causes, In Proceedings of the 1996 ACM SIGMETRICS International Conference on Measurement and Modeling of Computer Systems (May 1996)
8. P. Berenbrink, A. Brinkmann, and C. Scheideler: Design of the PRESTO multimedia storage network. In International Workshop on Communication and Data Management in Large Networks, Paderborn, Germany (October 5 1999)
9. R. J. Honicky, E. L. Miller: A fast algorithm for online placement and reorganization of replicated data. 17th International Parallel and Distributed Processing Symposium (IPDPS) (2003)
10. Schwetman, H.: Object-oriented simulation modeling with C++/CSIM17. In Proceedings of the 1995 Winter Simulation Conference. ed. C. Alexopoulos, K. Kang, W. Lilegdon, D. Goldsman. Washington, D.C. (1995) 529–533

# Safety of a Server-Based Version Vector Protocol Implementing Session Guarantees\*

Jerzy Brzezinski, Cezary Sobaniec, and Dariusz Wawrzyniak

Institute of Computing Science,  
Poznań University of Technology, Poland  
{Jerzy.Brzezinski, Cezary.Sobaniec, Dariusz.Wawrzyniak}@cs.put.poznan.pl

**Abstract.** Session guarantees are used to manage replica consistency of a distributed system from the client perspective. This paper defines formally the guarantees, presents and proves safety of a protocol implementing session guarantees using server-based version vectors.

## 1 Introduction

Replication is a key concept providing high performance and availability of data in distributed systems. In server replication, the problem of data consistency that arises when replicas are modified. Required properties of distributed system with respect to consistency depend on application and are formally specified by *consistency models*. There are numerous consistency models developed for *Distributed Shared Memory* systems. These models, called *data-centric* consistency models, assume that servers replicate data as a single access to the data for processing purposes. In a more general setting, however, clients access the data as distributed partitions. In servers, the catch from the server to another host catching adds a local message to the problem of consistency. *Session guarantees* [2], called also *client-centric* consistency models, have been proposed to define required properties of the system regarding consistency from the client's point of view. In this paper, the client accesses the data after a single transaction. In servers, that operation is a remainder state with previously issued operations that a *session*. The relationships between data-centric and client-centric consistency models have been analyzed in [4]. In this paper, session guarantees must effectively represent sets of operations performed in the system. Servers detect requests based on detector checks. This paper presents a practical, called *sG*, implementation of session guarantees that uses server-based detectors. The practical based on a concept presented in [2]. The main contribution of this paper is a formal proof of safety of the *sG* protocol. The formalism introduced in this paper includes a formal definition of session guarantees.

---

\* This work was supported in part by the State Committee for Scientific Research (KBN), Poland, under grant KBN 3 T11C 073 28.

## 2 Session Guarantees

In this paper we consider a weak consistency replicated storage system where system consists of a number of servers holding a copy of a set of shared objects, and clients running applications that access the objects. Clients are separated from servers, each application may run on a separate computer than the server, each client may access a shared object after selecting a server and sending a direct request to the server. Clients are mobile, each client forms a server to another during application execution. Session guarantees are expected to take care of data consistency based on a mutual exclusion set of shared objects replicated by the servers. Besides a particular data model, regarding operations performed on shared objects are divided into reads and writes. Read does not change states of the shared objects, hence a read does not may cause an update of an object, may create a new object, or delete an existing one. Write may as an update states of shared objects.

Operations on shared objects issued by a client  $C_i$  are ordered by a total causal client issue order. Server  $S_j$  performs operations in a order represented by a relation  $\xrightarrow{S_j}$  writes and reads on objects may be denoted by  $w \text{ and } r$ , respectively. Operation performed by a server  $S_j$  may be denoted by  $w|_{S_j}$  or  $r|_{S_j}$ .

**Definition 1.** *Relevant writes  $RW(r)$  of a read operation  $r$  is a set of writes that has influenced the current state of objects observed by the read  $r$ .*

The exact meaning of relevant writes strongly depends on the characteristics of a given system or application. For example, case of simple replicated objects (e.g. objects with methods that access only the register fields), relevant writes of a read on object  $x$  may be represented by a previous writes on object  $x$ .

Session guarantees have been defined in [2]. The following formal definition is based on these concepts. The definitions assume that operations are unique, each are ordered by some total unique defiers.

**Definition 2.** *Read Your Writes (RYW) session guarantee is defined as follows:*

$$\forall C_i \forall S_j \left[ w \xrightarrow{C_i} r|_{S_j} \Rightarrow w \xrightarrow{S_j} r \right]$$

**Definition 3.** *Monotonic Writes (MW) session guarantee is defined as follows:*

$$\forall C_i \forall S_j \left[ w_1 \xrightarrow{C_i} w_2|_{S_j} \Rightarrow w_1 \xrightarrow{S_j} w_2 \right]$$

**Definition 4.** *Monotonic Reads (MR) session guarantee is defined as follows:*

$$\forall C_i \forall S_j \left[ r_1 \xrightarrow{C_i} r_2|_{S_j} \Rightarrow \forall w_k \in RW(r_1) \quad w_k \xrightarrow{S_j} r_2 \right]$$

**Definition 5.** *Writes Follow Reads (WFR) session guarantee is defined as follows:*

$$\forall C_i \forall S_j \left[ r \xrightarrow{C_i} w|_{S_j} \Rightarrow \forall w_k \in RW(r) \quad w_k \xrightarrow{S_j} w \right]$$

### 3 The VsSG Protocol Implementing Session Guarantees

The proposed VsSG protocol implements session guarantees by intercepting communication between clients and servers at the client's end before sending a request, at the server's end after receiving the request and before sending a reply, and at the client's end after receiving the reply. These intercept points are used to exchange and maintain additional data structures necessary to preserve appropriate session guarantees. After receipt of a new request a server checks whether its state is sufficient to update its state. If not, the server's state is updated then the request is postponed and can be resumed after updating the server.

Servers occasionally exchange format information performed in the past. In order to synchronize the states of replicas, this synchronization procedure eventually causes total ordering of all ordered requests submitted by clients to be discarded. The safety of the VsSG protocol, but rather its efficiency, therefore cannot be discussed in this paper (efficiency procedure is presented in [1]). In contrast with 2, we do not assume total ordering of all committed writes which is treated by us as a orthogonal problem.

Each server  $S_j$  records all requests performed by a history. The history results from direct client requests, or are inherited from other servers during synchronization procedure. The history is performed sequentially, therefore the history is totally ordered. Formally, histories are defined as follows:

**Definition 6.** *A history  $H_{S_j}$  is a linearly ordered set  $\left( \mathcal{O}_{S_j}, \xrightarrow{S_j} \right)$  where  $\mathcal{O}_{S_j}$  is a set of writes performed by a server  $S_j$ , and relation  $\xrightarrow{S_j}$  represents an execution order of the writes.*

During synchronization of servers the histories are concatenated, that is, a concatenation of two histories is constructed as a sum of the first history and the second history. The second history is ordered according to the first history are preserved, and the second history are added at the end of the first history.

*Server-based version vectors.* Servers objects are used for efficient representation of sets of writes required by clients and necessarily check at the server's end. Servers objects used in this paper have the form  $[v_1 \ v_2 \ \dots \ v_{N_S}]$ , where  $N_S$  is the total number of servers in the system,  $v_j$  is the number of writes performed by a server  $S_j$ , and changes the server a new request is performed by the server because every server increments the version vector for every write, and the changes are detected by the system.



the a ues f the s e r s at ser ers dur g e cut . . . f r tes are u que r te s G pr t c s abe ed th a e c t r t mestamp set t the curre t a ue f the s e r s e c t r  $V_{S_j}$  f the ser er  $S_j$  perf rm g the r te f r the first t me the prese tat f the s G pr t c the e c t r t mestamp f a r te w s retur ed b a fu ct . . .  $T \cap \mathcal{O} \mapsto V$  s g e i th p s t . . . f the s e r s e c t r t mestamp ass c ated th a r te . . . be de e ted b  $T(w) i$

he s G pr t c (prese ted g ) t e r acts th requests set fr m c e ts t ser ers a d th rep es set fr m ser ers t c e ts request s a c upe  $\langle op, SG \rangle$  here  $op$  s a . . . perat . . . t be perf rmed, a d  $SG$  s a set f sess . . . guara tees requ red f r th s perat . . . ef re se d g t the ser er, the request s supp eme ted th a e c t r  $W$  repre t g the c e t's requ re me ts

rep s a tr p e  $\langle op, res, W \rangle$  here  $op$  s the . . . perat . . . ust perf rmed,  $res$  repre ts the resu ts f the perat . . . (de e red t the app cat . . .), a d  $W$  s a e c t r repre t g the state f the ser er ust after perf rm g the perat . . .

ef re se d g a request b a c e t  $C_i$ , a e c t r  $W$  repre t g ts requ re me ts s ca cu ated based . . . the t p e f perat . . . a d the set  $SG$  f sess . . . guara tees requ red f r the perat . . . he e c t r  $W$  s set t e ther  $\mathbf{0}$  r  $W_{C_i}$  a e c t r repre t g r tes ssued b the c e t  $C_i$ , r  $R_{C_i}$  a e c t r repre se t g r tes re e a t t reads ssued b the c e t r t a ma mum f these t e c t r ( e s a d ) he ma mum f t e c t r s  $V_1$  a d  $V_2$  s a e c t r  $V$  ma  $(V_1, V_2)$ , such that  $V i$  ma  $(V_1 i, V_2 i)$

$\mathcal{O}$  rece pt f a e request a ser er  $S_j$  checks hether ts ca ers e c t r  $V_{S_j}$  dominates the e c t r  $W$  se t b the c e t ( e ), h ch s e pected t be suffie t f r pr d g appr pr ate sess . . . guara tees e r s e c t r  $V_1$  d m a tes a e r s e c t r  $V_2$  h ch s de e ted b  $V_1 \geq V_2$ , he  $\forall i V_1 i \geq V_2 i$  f the state f the ser er s t suffie t up t date, the request s p st p e d ( e ), a d . . . be resumed after s chr zat . . . th a e t h e r ser er ( e 2) s a resu t f r tes perf rmed b a ser er  $S_j$ , ts e r s e c t r  $V_{S_j}$  s c reme ted at p s t . . .  $j$  ( e 4), a d a t mestamped perat . . . s rec rded h st r  $H_{S_j}$  ( e s a d ) he curre t a ue f the ser er e r s e c t r  $V_{S_j}$  s retur ed t the c e t ( e 8) a d updates the c e t's e c t r  $W_{C_i}$  . . . case f r tes ( e 2) . . . r  $R_{C_i}$  . . . case f reads ( e 22)

### 4 Safety of the VsSG Protocol

**Definition 7.** A supremum of a set of writes  $O_{S_j}$ , denoted by  $\bar{V}(O_{S_j})$ , is a vector that is set to  $\mathbf{0}$  for an empty set, and for nonempty sets its  $i$ -th position is defined as  $\bar{V}(O_{S_j}) i$  ma  $w \in O_{S_j} T(w) i$ .

**Lemma 1.** For every server  $S_j$  running VsSG protocol at every moment  $\bar{V}(O_{S_j}) V_{S_j}$ .

*Proof.* . . . duct . . . ) as s t the e r beg . . . g  $V_{S_j} \mathbf{0}$ , a d the set f r tes  $O_{S_j} \emptyset$ , theref re  $\bar{V}(O_{S_j}) \mathbf{0}$ , he ce  $\bar{V}(O_{S_j}) V_{S_j}$  2) . . . duct . . . step

**On send of request message  $\langle op, SG \rangle$  from  $C_i$  to  $S_j$**

```

1:  $W \leftarrow 0$ 
2: if (iswrite( $op$ ) and  $MW \in SG$ ) or (not iswrite( $op$ ) and  $RYW \in SG$ ) then
3:    $W \leftarrow \max(W, W_{C_i})$ 
4: end if
5: if (iswrite( $op$ ) and  $WFR \in SG$ ) or (not iswrite( $op$ ) and  $MR \in SG$ ) then
6:    $W \leftarrow \max(W, R_{C_i})$ 
7: end if
8: send  $\langle op, W \rangle$  to  $S_j$ 

```

**On receipt of request message  $\langle op, W \rangle$  from client  $C_i$  at server  $S_j$**

```

9: while ( $V_{S_j} \not\geq W$ ) do
10:   wait
11: end while
12: perform  $op$  and store results in  $res$ 
13: if iswrite( $op$ ) then
14:    $V_{S_j}[j] \leftarrow V_{S_j}[j] + 1$ 
15:   timestamp  $op$  with  $V_{S_j}$ 
16:    $H_{S_j} \leftarrow H_{S_j} \cup \{op\}$ 
17: end if
18: send  $\langle op, res, V_{S_j} \rangle$  to  $C_i$ 

```

**On receipt of reply message  $\langle op, res, W \rangle$  from server  $S_j$  at client  $C_i$**

```

19: if iswrite( $op$ ) then
20:    $W_{C_i} \leftarrow \max(W_{C_i}, W)$ 
21: else
22:    $R_{C_i} \leftarrow \max(R_{C_i}, W)$ 
23: end if
24: deliver  $\langle res \rangle$ 

```

**On receipt of update message  $\langle S_k, H \rangle$  at server  $S_j$**

```

25: foreach  $w_i \in H$  do
26:   if  $V_{S_j} \not\geq T(w_i)$  then
27:     perform  $w_i$ 
28:      $V_{S_j} \leftarrow \max(V_{S_j}, T(w_i))$ 
29:      $H_{S_j} \leftarrow H_{S_j} \cup \{w_i\}$ 
30:   end if
31: end for
32: signal

```

**Every  $\Delta t$  at server  $S_j$**

```

33: foreach  $S_k \neq S_j$  do
34:   send  $\langle S_j, H_{S_j} \rangle$  to  $S_k$ 
35: end for

```

Let us assume a state where client  $\bar{V}(O_{S_j})$  and  $V_{S_j}$  holds the set  $O_{S_j}$  and the server  $V_{S_j}$  can change the first  $j$  bits.

- the server  $S_j$  accepts a write requested by a client  $h$  causes the value of  $V_{S_j}$  to be incremented by one and the write is stamped with the current value of  $V_{S_j}$  and the write is added to  $O_{S_j}$ .  $h$  causes  $\bar{V}(O_{S_j})$  to be also incremented at position  $j$  by (lines 4 and 5) as a result the client  $\bar{V}(O_{S_j})$  and  $V_{S_j}$  still holds
- the server  $S_j$  corrupts a write  $w$  received from another server  $h$  causes the current value of  $V_{S_j}$  to be maximized with the value of  $T(w)$  if the write is added (line 28) hence the write is added to  $O_{S_j}$  (line 2) as a result values of  $V_{S_j}$  and  $\bar{V}(O_{S_j})$  are incremented at the same position as by the same values, therefore the client  $\bar{V}(O_{S_j})$  and  $V_{S_j}$  still holds  $\square$

**Definition 8.** A write-set  $WS(V)$  of a given version vector  $V$  is defined as  $WS(V) = \bigcup_{j=1}^{N_S} \{w \in O_{S_j} \mid T(w) \leq V\}$ .

**Lemma 2.** For any two vectors  $V_1$  and  $V_2$  used by servers and clients of the VsSG protocol  $V_1 \geq V_2 \Leftrightarrow WS(V_1) \supseteq WS(V_2)$ .

*Proof.* (sufficient condition) Consider contradiction, let us assume that  $V_1 \geq V_2 \wedge WS(V_1) \not\supseteq WS(V_2)$ , which means that  $\exists w \ w \notin WS(V_1) \wedge w \in WS(V_2)$  and according to definition 8  $\exists j (T(w)_j > V_1_j \wedge T(w)_j \leq V_2_j) \Rightarrow V_1_j < V_2_j \Rightarrow V_1 \not\geq V_2$  (2) necessary condition) Consider contradiction, let us assume that  $WS(V_1) \supseteq WS(V_2) \wedge V_1 \not\geq V_2$ , which means that  $\exists j \ V_1_j < V_2_j$  servers and clients at position  $j$  are not incremented hence the writes performed by a server  $S_j$  (line 4) do not mean that  $\exists w \in O_{S_j} \ w \in WS(V_2) \wedge w \notin WS(V_1)$  and hence  $WS(V_1) \not\supseteq WS(V_2)$   $\square$

**Lemma 3.** At any time during execution of VsSG protocol  $O_{S_j} = WS(V_{S_j})$ .

*Proof.* (contradiction) let us assume that  $\exists w \in O_{S_j} \ w \notin WS(V_{S_j})$  according to definition 8, a write  $w$  does not belong to  $WS(V_{S_j})$  hence  $T(w) \not\leq V_{S_j}$  which implies that  $\exists k \ T(w)_k > V_{S_j}_k$  and according to lemma 1,  $T(w)_k > \bar{V}(O_{S_j})_k$ , which implies  $\bar{V}(O_{S_j}) \not\leq T(w)$  ased on definition 7,  $w \notin O_{S_j}$  (contradiction 2) let us assume that  $\exists w \in WS(V_{S_j}) \ w \notin O_{S_j}$  according to definition 7, a write  $w$  does not belong to  $O_{S_j}$  hence  $\bar{V}(O_{S_j}) \not\leq T(w)$  which implies that  $\exists k \ T(w)_k > \bar{V}(O_{S_j})_k$  and according to lemma 1,  $T(w)_k > V_{S_j}_k$ , which implies  $T(w) \not\leq V_{S_j}$  ased on definition 8,  $w \notin WS(V_{S_j})$  (contradiction)  $\square$

**Lemma 4.** At any time during execution of VsSG protocol  $WS(W_{C_i})$  contains all writes issued by a client  $C_i$ .

*Proof.* A write issued by a client  $C_i$  and performed by a server  $S_j$  updates the client's vector  $W_{C_i}$  by concatenating a maximum of its current value and

the server's request  $V_{S_j}$  (lines 8 and 2) receive, after performing the write  $W_{C_i} \geq V_{S_j}$ , and (according to lemma 2)  $WS(W_{C_i}) \supseteq WS(V_{S_j})$ , and (according to lemma 1)  $WS(W_{C_i}) \supseteq OS_{S_j}$  it means that the write set  $WS(W_{C_i})$  contains all writes requested directly at server  $S_j$ , including all writes requested by the client  $C_i$  at server  $S_j$ . Hence, the write  $W_{C_i}$  must be causal, therefore, past writes must be a part of a causal order.  $\square$

**Lemma 5.** *At any time during execution of VsSG protocol  $WS(R_{C_i})$  contains all writes relevant to reads issued by a client  $C_i$ .*

*Proof.* A read issued by a client  $C_i$  and performed by a server  $S_j$  updates the client's request  $R_{C_i}$  by calculating a maximum of its current value and a value of the server's request  $V_{S_j}$  (lines 8 and 22) receive (according to lemmata 2 and 3)  $R_{C_i} \geq V_{S_j} \Rightarrow WS(R_{C_i}) \supseteq WS(V_{S_j}) \supseteq OS_{S_j}$  it means that the write set  $WS(R_{C_i})$  contains all writes performed at server  $S_j$ , therefore, all writes relevant to reads requested by the client  $C_i$  at server  $S_j$  are included in  $WS(R_{C_i})$ . Therefore, past writes must be a part of a causal order.  $\square$

**Theorem 1.** *RYW session guarantee is preserved by VsSG protocol for clients requesting it.*

*Proof.* Let us consider two operations  $w$  and  $r$ , issued by a client  $C_i$  requiring R session guarantee. Let the read  $r$  be the first of the client's issued reads, and let the read be performed by a server  $S_j$ ,  $w \xrightarrow{C_i} r|_{S_j}$ . After performing  $w$  we have (according to lemma 4)  $w \in WS(W_{C_i})$  because  $V_{S_j} \geq W_{C_i}$  is fulfilled before performing  $r$  (lines 8 and 22), we get (according to lemma 2)  $WS(V_{S_j}) \supseteq WS(W_{C_i}) \Rightarrow w \in WS(V_{S_j})$  because all operations at servers are totally ordered, we get  $w \xrightarrow{S_j} r$  which happens for a client  $C_i$  requiring R and a server  $S_j$ , s.  $\forall C_i \forall S_j \left[ w \xrightarrow{C_i} r|_{S_j} \Rightarrow w \xrightarrow{S_j} r \right]$ , which means that R session guarantee is preserved.  $\square$

**Theorem 2.** *MR session guarantee is preserved by VsSG protocol for clients requesting it.*

*Proof.* Let us consider two reads  $r_1$  and  $r_2$ , issued by a client  $C_i$  requiring R session guarantee. Let the second read  $r_2$  be the first read of the client's issued reads, and let the second read be performed by a server  $S_j$ ,  $r_1 \xrightarrow{C_i} r_2|_{S_j}$ . After performing  $r_1$  we have (according to lemma 1)  $\forall w_k \in RW(r_1) \ w_k \in WS(R_{C_i})$  because  $V_{S_j} \geq R_{C_i}$  is fulfilled before performing  $r_2$  (lines 8 and 22), we get (according to lemma 2)  $WS(V_{S_j}) \supseteq WS(R_{C_i}) \Rightarrow \forall w_k \in RW(r_1) \ w_k \in WS(V_{S_j})$  because all operations at servers are totally ordered, we get  $\forall w_k \in RW(r_1) \ w_k \xrightarrow{S_j} r_2$  which happens for a client  $C_i$  and a server  $S_j$ , s.  $\forall C_i \forall S_j \left[ r_1 \xrightarrow{C_i} r_2|_{S_j} \Rightarrow \forall w_k \in RW(r_1) \ w_k \xrightarrow{S_j} r_2 \right]$ , which means that R session guarantee is preserved.  $\square$

the remainder of the proof are analogous. The remainder of the proof for  $R$  are analogous. The remainder of the proof can be found in [7].

## 5 Conclusions

This paper has presented formal definitions of session guarantees, and strong partial consistency guarantees, and finally a correctness proof showing that the protocols are safe, the appropriate guarantees are provided to the meeting of the other, that though the server based protocols used in the strong partial consistency are sufficient for consistency guarantees, they are necessary. Thus, other approaches are also possible and they have been discussed. The sets of properties represented by the protocols are supersets of the exact sets resulting from appropriate definitions. The accuracy of the entire set representation is therefore an important factor for a partial consistency guarantee. The correctness of the presented current considered and appropriate simultaneous experiments are being prepared.

## References

1. Tanenbaum, A.S., van Steen, M.: *Distributed Systems — Principles and Paradigms*. Prentice Hall, New Jersey (2002)
2. Terry, D.B., Demers, A.J., Petersen, K., Spreitzer, M., Theimer, M., Welch, B.W.: Session guarantees for weakly consistent replicated data. In: *Proceedings of the Third International Conference on Parallel and Distributed Information Systems (PDIS 94)*, Austin, Texas, September 28-30, 1994, IEEE Computer Society (1994) 140–149
3. Brzeziński, J., Sobaniec, C., Wawrzyniak, D.: Session guarantees to achieve PRAM consistency of replicated shared objects. In: *Proc. of Fifth Int. Conference on Parallel Processing and Applied Mathematics (PPAM'2003)*, LNCS 3019, CzOstochowa, Poland (2003) 1–8
4. Brzeziński, J., Sobaniec, C., Wawrzyniak, D.: From session causality to causal consistency. In: *Proc. of 12th Euromicro Conference on Parallel, Distributed and Network-Based Processing (PDP2004)*, A Coruña, Spain (2004) 152–158
5. Mattern, F.: Virtual time and global states of distributed systems. In: *Cosnard, Quinton, Raynal, Robert, eds.: Proc. of the Int'l. Conf. on Parallel and Distributed Algorithms*, Elsevier Science Publishers B. V. (1988) 215–226
6. Petersen, K., Spreitzer, M.J., Terry, D.B., Theimer, M.M., Demers, A.J.: Flexible update propagation for weakly consistent replication. In: *Proc. of the 16th ACM Symposium on Operating Systems Principles (SOSP-16)*, Saint Malo, France (1997) 288–301
7. Brzeziński, J., Sobaniec, C., Wawrzyniak, D.: Safety of VsSG protocol implementing session guarantees. Technical Report RA-003/05, Institute of Computing Science, Poznań University of Technology (2005)
8. Kobusińska, A., Libuda, M., Sobaniec, C., Wawrzyniak, D.: Version vector protocols implementing session guarantees. In: *Proc. of Int'l Symposium on Cluster Computing and the Grid (CCGrid 2005)*, Cardiff, UK (2005)

# Scalable Hybrid Search on Distributed Databases

U. G. Keim<sup>1,2</sup> and G. R. ...<sup>2</sup>

<sup>1</sup> Department of Computer Science, Florida State University, Tallahassee FL 32306, U.S.A

[jungkkim@cs.fsu.edu](mailto:jungkkim@cs.fsu.edu),

<sup>2</sup> Community Grids Laboratory, Indiana University, Bloomington IN 47404, U.S.A  
[gcf@indiana.edu](mailto:gcf@indiana.edu)

**Abstract.** We have previously described a hybrid keyword search that combines metadata search with a traditional keyword search over unstructured context data. This hybrid search paradigm provides the inquirer additional options to narrow the search with some semantic aspect from the XML metadata query. But in earlier work, we experienced the scalability limitations of a single-machine implementation. In this paper, we describe a scalable hybrid search on distributed databases. This scalable hybrid search provides a total query result from the collection of individual inquiries against independent data fragments distributed in a computer cluster. We demonstrate our architecture extends the scalability of a native XML query limited in a single machine and improves the performance for some queries.

## 1 Introduction

With the popularization of computer communication networks, there have been many efforts to share and exchange information between resources. The efforts here are to make approaches to search over networks search over structured data or search over unstructured data. An archetypal example represents structured data as a relational database, while format retrieval represents search over the unstructured data. Even though these approaches to the latter are more recent, they are research areas where the relevant queries over structured data are a lot. Queries search over semistructured data have been developed. Web search engines are based on format retrieval technologies.

Our hybrid keyword search paradigm is between these two approaches. The hybrid search is fundamentally based on keyword search for the unstructured data, and adds supplementary search on metadata attached to each unstructured document to adapt to the de facto standard format for format exchange between machines as a meta-measure for the metadata. We demonstrated the practicality of the hybrid keyword search [8], but we also experienced the scalability limitation of a single machine implementation. In our current work, the relational database we used had inherent limited scalability. This

paper, we adapt a distributed strategy to improve the scalability of hybrid keyword search. We demonstrate performance improvement of a larger scalability of the architecture.

The rest of this paper is organized as follows. The next section describes our architecture and compares it to a grid system. Section 4 describes our search architecture and distributed databases. We illustrate a query processing architecture and distributed database architecture. Section 4.1 describes our hybrid search over a distributed database. We summarize and conclude in Section 5.

## 2 Hybrid Keyword Search on Distributed Databases

Distributed databases are a collection of separate main databases stored on different computers and *logically interrelated* through a network. A distributed database management system (DBMS) can be defined as a software application that manages a distributed database system so that the users think as a single machine. It provides transparent let us describe our distributed architecture according to the transparent criteria.

- *data dependence*: the hybrid searches on each machine are global and physical data dependence. Each of the data of each database has the same schema and the schema does not change. Each database has its own management system and returns query results against the user query. Our architecture has physical data dependence due to data encapsulation on each machine.
- *network transparency*: the network collection of our system depends on message-oriented middleware or peer-to-peer middleware and the middleware are administrative systems concerned with the collection of the end user desktop perceive the detailed network operation of the distributed hybrid search query.
- *Replication transparency*: we assume our distributed architecture is restricted to a computer cluster and replication is the cluster management system's replication transparently. A replication is usually necessary to create the catalog of data reference and distributed environment. Currently, the catalog is guaranteed a cluster architecture.
- *fragmentation transparency*: our performance with hybrid search on a distributed database should show that the data can be partitioned into each database. Thus, the management of the catalog database is the easiest case for the distributed database management system. The data are partitioned into a chunk of data. Thus, the associated unstructured data and thus the performance of fragmentation is *horizontal*.

we can summarize that our architecture each database system depends on the query result for the distributed databases is the collection of query results from multiple database queries.

data dependence and horizontal fragmentation features make our architecture different from other general architectures for federated database systems.

sur ed f data are t depe de t a d user qu res requ re  
 g quer data fr m d ere t mach es th ar us schemas e ca c s der  
 a d str buted quer g frame rk based rece t emerg g Gr d frastruc  
 ture 4 OG (Ope Gr d er ces rch tecture str buted uer  
 r cess g) s a e amp e f such frame rk

### 3 Distributed Database Architecture

he arch tecture f the h br d search ser ce each ca mach e depe ds  
 the ca ser ce pr der h s the d str buted database a d e dem  
 strated such arch tectures 8, O e s ut z g a e ab ed re at a  
 th ested subquer es t mp eme t the c mb at f quer resu ts  
 aga st u structured d cume ts a d sem structured metadata he ther s  
 based a at e database a d a te t search brar ass cate meta  
 data th u structured d cume ts e ass g the fie ame fr the d cume t  
 as the ke f the metadata hash tab e s used fr a temp rar st rage f  
 metadata quer resu ts a d the ke rd search maps t the tab e subseque t  
 f r g

he rema g ssue f r rga z g the d str buted database s the c m  
 puter et rk tech g that c ects the databases a d pr des the et rk  
 tra spare c t the user a e baum a d tee 4 suggested that message  
 re ted m d e are s e f best app cat t s f r tegrat g a c ect  
 f databases t a mu t database s tem e ut ze a message re ted m d  
 d e are mp eme tat arada r ker g 2, t c udes c mp a t  
 t p c based c mmu cat h ch meets the m m um requ reme ts f r the et  
 rk tra spare c a d str buted database arada r ker g a s pr des a  
 c perat g br ker et rk f r creased et rk sca ab t

gure summar zes ur ge era arch tecture he search c e t s a pub sher  
 f r a quer t p c a d a gr up f search ser ces subscr be the same t p c  
 he the c e t pub shes the quer the quer message s br adcast t the search  
 ser ce subscr bers he quer resu ts fr m the search ser ces are retur ed back  
 t the c e t b pub sh g the message a d am c rtua cha e a *tem  
 porary topic* h se sess b ect as attached t the quer message r g a  
 de ed t the search ser ce

he arch tecture ca be gr t a c perat g br ker et rk O e r m re  
 heter ge e us search ser ces c u d be attached t each br ker a d each br ker  
 ca re a messages t ther br kers he c perat e et rk usua f s a  
 h erarch ca structure f r better perf rma ce

### 4 Query Processing

he quer pr cess g f each database (fragme t) ur d str buted arch tecture  
 depe ds the ca database r the search brar ue t the fu part t  
 ur database d str but the quer pr cess g the s s mp e a d  
 quer pr pagat a d resu t c ect s are the terest g pr cesses



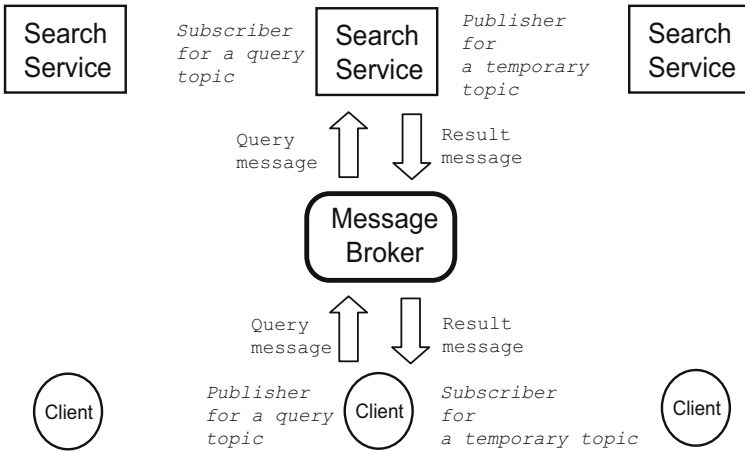


Fig. 1. Scalable Hybrid Search Architecture on Distributed Databases

query processing architecture on distributed databases shown in figure 2. The search client is a query publisher and the search service is a query subscriber. The user types query parameters through a user interface, and they are amalgamated into a message along with a subscriber and a temporary topic. The subscriber in this case is a regular pre-processed the ER-finally available. The `MapMessage` message type is used for the query message for a program.

The content of this message is a set of *name-value* pairs. The names are a string and the value can have a few reserved types. The used string and integer type. The values could be empty for the string and zero for the integer. If there is a user put the `JMSReplyTo` property as a message header that contains a temporary topic.

The message broker delivers query messages to search services that have a read-subscribed to the same topic. The server on the search service captures the query message, which includes a pre-processed header field with a temporary topic. The extracted query parameters are passed to the local query processing service, which produces query results.

These query results are returned back to the client that published the query message. It is remarkable because the temporary topic is unique to this client. The query client stores for the returned messages, and displays query results to the user.

## 5 Experimental Performance

In this section, we evaluate our hybrid search on a distributed database cluster of 8 computers farms and distributed environment, and 4 computers are dedicated to the calculation. The network bandwidth is very high.

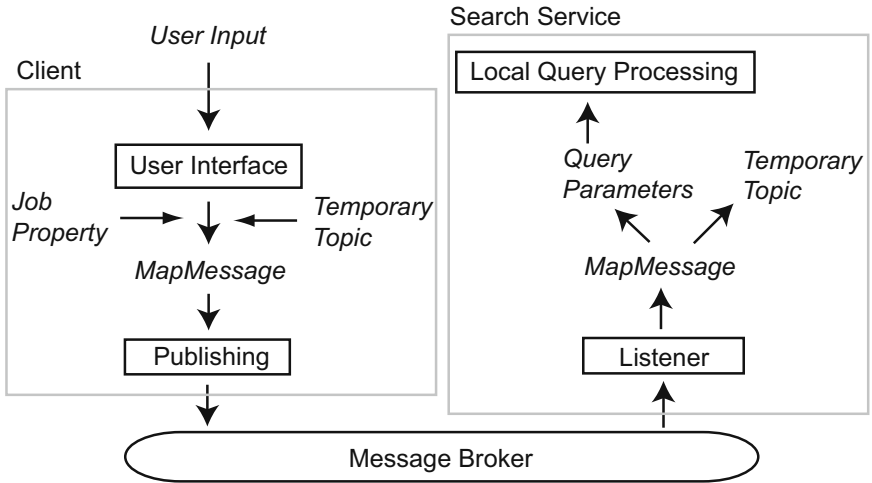


Fig. 2. A Query Processing Architecture on a Distributed Database

these elements use... states extracted from the *DataBase systems and Logic Programming* ( ) records and abstract text files from the REC collect... O E 7 the select art c e... states... and... C characters are converted to C characters... embedded metadata... the collect... and extract the abstract part... the data set s h r z... part... 8 fragments, and each fragment... each machine has 2... states and 2... text files... eight computers have the same specification... 24 G z... te... C... th 2 G... f mem r, ru... g a... u 24 ker... e... a a... tsp... t... 42... these machines are connected with each other by Gbps... but the switch for the units de collect... has... bps bandwidth cache... d... b4... used as a... database, a... akarta... ce... 2... sut... zed... fr... te... t... ma... agem... e... t

use... d... der... t... c... mmu... cat... m... d... de... res... 2... a... d... arada... r... ker... g... ers... rc2... f... r... the... perf... rma... ce... c... mpar... s... ,... a... d... three... e... per... me... ta... arch... tures... f... r... 8... des... as... f... s

- ... de acts a re... dez... us... de... a... d... a... th... er... 7... des... are... c... o... l... lected... t... the... re... dez... us... de... ... f... the... des... are... c... ated... the... same... sub... et... a... d... a... the... quer... pr... pagat... s... are... br... adcast... ... th... the... sub... et... h... s... because... the... curre... t... mp... eme... tat... d... es... t... meet... the... spec... if... icat... f... r... se... ct... e... quer... pr... pagat... f... r... m... the... re... dez... us... peer
- ... ge... arada... r... ker... g... de... has... a... ser... er... a... d... a... search... ser... ce... ,... a... d... the... th... er... des... ... ha... e... search... ser... ces... ,... the... search... ser... ces... are... c... e... ts... f... r... the... c... mmu... cat...
- ... ut... pe... arada... r... ker... g... C... user... ... de... has... a... r... t... ser... er... a... d... the... th... er... des... ha... e... sec... d... e... e... ser... ers... Each... de... has... a... arada... r... ker... g... ser... er...

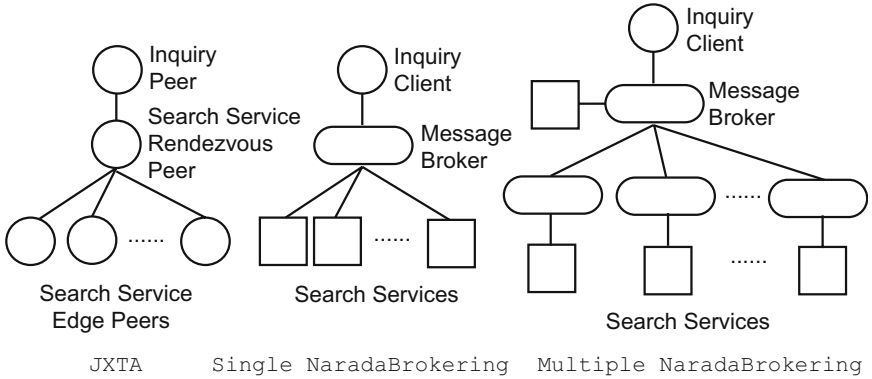


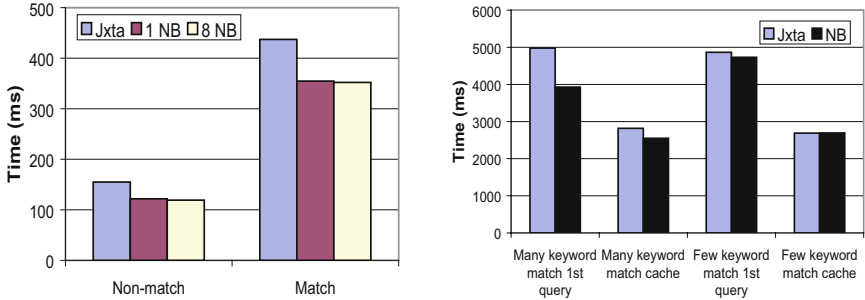
Fig. 3. Examples of communication middleware architectures

and a search service architecture gives us an idea of the performance difference between a centralized network and a single message broker.

Examples of these architectures are shown in figure

Figure 4(a) shows the average response time for a distributed match query over 8 search services using the three approaches. We chose 8 queries that combine a distributed key word and the databases are indexed against the authentication. The statistics and keywords for the unstructured data. Each query matches the eight search services. The number of matches is between and present the graphs separately for the average response time for match and match result cases. We can interpret the difference between matched and unmatched query time means that the additional overhead for processing matched results is more than half of the total query time. The processing time for matched queries is shorter as a result of the design against the authentication but the matched query takes longer for processing the query results, and it is larger than the communication time for the query time of NaradaBroker. The statistics show that the performance of NaradaBroker is better than that of the broker. The statistics show that the performance of NaradaBroker is better than that of the broker. The statistics show that the performance of NaradaBroker is better than that of the broker.

We evaluate further hybrid search queries for the near match. These queries, there are total of 1000 keywords. One has a few keywords matches 4 documents, unstructured data documents, and the other has many keywords matches 488 documents. But from the near match query, the 22 and its hit is 772. But from the statistics, we can show single NaradaBroker case because multiple NaradaBroker cluster had the difference. Figure 4(b) shows the average response time for the near match hybrid query over 8 search services. The cluster C compared with the per-



(a) Author exact match (b) Year match

Fig. 4. Average response time for queries over 8 search services

formance per metric results... a single machine<sup>1</sup> running a commercial database, the year match queries on the distributed database show dramatic performance improvement. The query time is improved from 82 seconds to less than a second for a few keyword matches, and from half an hour to less than a second for many keyword matches. This big performance improvement derives from *horizontal partitioning*, which reduces data retrieval time from disk with the related *partitioning* of the data. In each machine block, thus ranges, and thus called *range partitioning* the second data later repeats of the same query take a shorter time than the first attempt has because the latter a cache on the databases improves the query response time for repeated queries. The query time is gradually reduced as more machines are added, so smartly the author matches.

Through performance tests, we established that a distributed database can overcome the limit of target size of query. The reduced size of a single machine here as a problem up to the target sizes of the query over the distributed database. The cache on the database could not produce accurate query results. The number of stored data on the machines is smaller than the distributed query processing. So the performance improvement for some queries over large target results. Our experiment is focused on the exact match, because of the decrease in the performance based on the degree of the elements and attributes there as the performance improvement from the element degree of a approximate match search.

<sup>1</sup> This machine was used for performance tests in [9]. We should add that since this paper was originally submitted we evaluated newer version of the commercial database in one of the cluster computers with large resource allocations. With this modified configuration, the query time was less than 1 second for the many keyword matches.

## 6 Conclusion

In this paper we described a scalable hybrid search in distributed databases. The distributed architectures are mainly based on several major computer network concepts such as using a message-oriented middleware for a peer-to-peer network framework. The hybrid search provides a transparent result generated from a unified queries against data fragments in a computer cluster. The aspect of hierarchical partitioning for architecture contributed a performance improvement for some queries comparing to the sequential machine. Our thermore, our architecture extended the scalability of the distributed query method to a smaller size of a sequential machine.

## References

1. N. Alpdemir, A. Mukherjee, N. Paton, and P. Watson. Service-Based Distributed Querying on the Grid. In *Proceedings of International Conference on Service Oriented Computing (ICSOC)*, December 2003.
2. Apache Software Foundation. Jakarta Lucene. World Wide Web. <http://jakarta.apache.org/lucene/>.
3. Apache Software Foundation. Xindice. World Wide Web. <http://xml.apache.org/xindice/>.
4. F. Berman, G. Fox, and A. Hey, editors. *Grid Computing: Making The Global Infrastructure a Reality*. John Wiley & Sons, 2003.
5. I. Foster and C. Kesselman, editors. *The Grid 2: Blueprint for a New Computing Infrastructure*. Morgan Kaufmann, 2003.
6. G. Fox, S. Pallickara, and S. Parastatidis. Towards Flexible Messaging for SOAP Based Services. In *Proceedings of International Conference for High Performance Computing and Communications(SC)*, November 2004.
7. W. Hersh, C. Buckley, T. Leone, and D. Hickam. OHSUMED: An interactive retrieval evaluation and new large test collection for research. In *Proceedings of the 17th Annual ACM SIGIR Conference*, 1994.
8. J. Kim, O. Balsoy, M. Pierce, and G. Fox. Design of a Hybrid Search in the Online Knowledge Center. In *Proceedings of the IASTED International Conference on Information and Knowledge Sharing*, November 2002.
9. J. Kim and G. Fox. A Hybrid Keyword Search across Peer-to-Peer Federated Databases. In *Proceedings of East-European Conference on Advances in Databases and Information Systems (ADBIS)*, September 2004.
10. M. Ley. Computer Science Bibliography. World Wide Web. <http://www.informatik.uni-trier.de/~ley/db/>.
11. T. Ozsu and P. Valduriez. *Principles of Distributed Database Systems*. Prentice Hall, 1999.
12. S. Pallickara and G. C. Fox. NaradaBrokering: A Distributed Middleware Framework and Architecture for Enabling Durable Peer-to-Peer Grids. In *Proceedings of International Middleware Conference*, June 2003.
13. A. Sheth and J. Larson. Federated Database Systems for Managing Distributed, Heterogeneous, and Autonomous Databases. *ACM Computing Surveys*, 22(3):183–236, September 1990.
14. A. Tanenbaum and M. Steen. *Distributed Systems: Principles and Paradigms*. Prentice Hall, 2002.

# Storage QoS Control with Adaptive I/O Deadline Assignment and Slack-Stealing EDF

Young Jin Nam and Chanik Park<sup>†</sup>

School of Computer and Information Technology,  
Daegu University,  
Kyungbuk, Republic of Korea  
yjn@daegu.ac.kr

<sup>†</sup>Department of Computer Science and Engineering/PIRL,  
Pohang University of Science and Technology,  
Kyungbuk, Republic of Korea  
cipark@postech.ac.kr

**Abstract.** Storage QoS control enforces a given storage QoS requirement for each I/O request from different storage clients that share an underlying storage system. This paper proposes an efficient storage QoS control scheme that features adaptive I/O deadline assignment and slack-stealing EDF scheduling. Simulation results with various I/O workloads show that the proposed scheme outperforms previous approaches in terms of response time variation, average response times, and miss ratio of the target response time.

## 1 Introduction

Embedding QoS feature into a storage system needs to define storage QoS specifications, map the storage QoS specifications (requirements) onto the underlying storage resources, and enforce the storage QoS requirements for each I/O request from different virtual disks (storage clients). This paper mainly emphasizes the storage QoS enforcement, also called the real-time QoS control (briefly QoS control). It is generally accepted that a storage system is characterized by its I/O performance; that is, the IOPS and RT relationship that depicts the variation of an average response time as a function of I/O requests per second (briefly IOPS). Thus, our QoS specification should capture this basic feature of a storage system as the first step. While the storage QoS specification in a broad sense may encompass other features of a storage system, such as data reliability, system costs, our QoS specification focuses mainly on the aspect of storage I/O performance that includes an average request size, a target response time, and a target IOPS. We define a QoS requirement of the virtual disk as a storage service required from a virtual disk in terms of QoS specification. The QoS requirement from a virtual disk  $i$  ( $VD_i$ ) is represented as  $(SZ_i, IOPS_i^{targ}, RT_i^{targ})$ , where  $SZ_i$  represents an average I/O request size(KB),  $IOPS_i^{targ}$  represents a target IOPS, and  $RT_i^{targ}$  represents a target response time(msec) [1]. The QoS requirement can be easily expanded to support a storage cluster environment and a more detailed specification having multiple pairs of a target IOPS and a target response time [1].

A few QoS control schemes for storage resources have been introduced [1, 2, 3, 5]. We can categorize the characteristics of the previous schemes into three classes. Class 1

includes the derivatives of packet-based fair queuing schemes for network resources [3]. It proportionates the entire storage bandwidth according to a given set of resource weights allotted to each virtual disk that shares the same storage system. In addition, it attempts to reorder a given I/O sequence in order to reduce overhead caused by disk head movements. Note that they do not directly take control of the demanded response time; instead, they control only the storage bandwidth. Class 2 operates mainly on a rate-based QoS control using a leaky bucket [5]. It attempts to guarantee a given QoS requirement simply by throttling the IOPS of the incoming I/O requests from each virtual disk. Class 2 is expected to have the same drawbacks as Class 1. Class 3 guarantees the target response time by assigning a deadline time to each incoming I/O request only if the current IOPS is not greater than its target IOPS and then scheduling the pending I/O requests according to the EDF (Earliest Deadline First) scheme [2]. If the current IOPS is greater than its target IOPS, I/O requests have no deadline. Otherwise, the deadline is set by adding the target response time to the current time. Let us call this type of I/O deadline assignment target-IOPS-based I/O assignment. In contrast to Class 1 and 2, this approach directly controls the target response time for a given target IOPS. It can also support a QoS requirement with multiple pairs of a target IOPS and a target response time.

## 2 The Proposed Scheme

The key features of the proposed QoS control scheme include the adaptive I/O deadline assignment based on the current IOPS and the current queue depth of a virtual disk, and slack-stealing EDF scheduling that exploits any available slack between the current time and the earliest deadline time to minimize the underlying storage overhead. Note that the proposed scheme falls into Class 3 that takes control of both the target IOPS and the target RT for each I/O request from different virtual disks.

*Adaptive I/O Deadline Assignment.* The key idea is to adaptively determine a deadline time of each I/O request according to the current IOPS and the current queue depth for each virtual disk. First, the proposed assignment scheme obtains an actual target response time denoted by  $act\_RT_i^{targ}$  of  $VD_i$  according to the current IOPS condition with respect to its target IOPS, as given in Algorithm 1. If the current IOPS is higher than its target IOPS, an I/O request is served as if it were a best-effort I/O request having no deadline. If the current IOPS is equal to the target IOPS, the actual target RT is the same as the original target RT. If the current IOPS is lower than its target IOPS, its actual target RT decreases in proportion to the ratio of the current IOPS to the target IOPS. Second, the proposed assignment scheme empirically measures the current average queue depth denoted by  $qdepth_i^{targ}$  for each  $VD_i$ . It computes a unit target response time denoted by  $unit\_rt_i^{targ}$  for  $act\_RT_i^{targ}$ , as given in Algorithm 1. Note that the  $unit\_rt_i^{targ}$  is meaningful only if the current IOPS is not greater than the target IOPS. Finally, the proposed assignment scheme assigns the deadline of  $r_i^k$  as a function of the current position in the queue denoted by  $qpos_i^{cur}(r_i^k)$ ; that is, the deadline of an I/O request increases from the queue head in a piece-wise linear manner up to its target RT by  $unit\_rt_i^{targ}$ . In consequence, the proposed assignment scheme can avoid delays with the processing of I/O requests from a virtual disk having a larger target RT until all the I/O requests from virtual disks having a smaller target RT are processed.

**Algorithm 1:** adaptive I/O deadline assignment

---

```

input :  $r_i^k, IOPS_i^{cur}, T_{cur}$ 
output :  $deadline(r_i^k)$ 
begin
  if ( $IOPS_i^{cur} > IOPS_i^{targ}$ ) then
     $deadline(r_i^k) \leftarrow T_{be}$ ;
  else
     $act\_RT_i^{targ} \leftarrow \begin{cases} T_{be} & \text{if } IOPS_i^{cur} > IOPS_i^{targ} \\ RT_i^{targ} \left( \frac{IOPS_i^{cur}}{IOPS_i^{targ}} \right) & \text{if } IOPS_i^{cur} \leq IOPS_i^{targ} \end{cases}$ ;
     $unit\_rt_i^{targ} \leftarrow \frac{act\_RT_i^{targ}}{qdepth_i^{targ}}$ ;
     $deadline(r_i^k) \leftarrow T_{cur} + \min\{RT_i^{targ}, unit\_rt_i^{targ} \times qpos_i(r_i^k)\}$ ;
  end
end

```

---

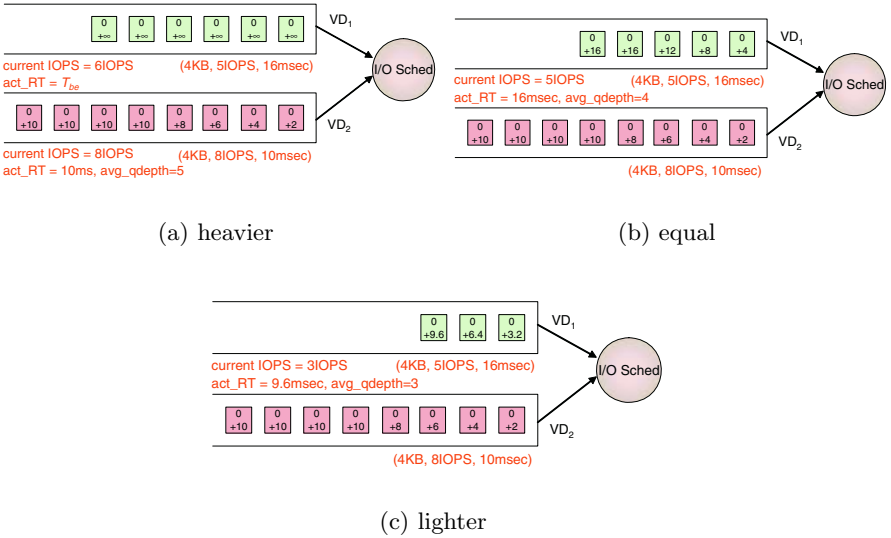


**Fig. 1.** Examples of the adaptive I/O deadline assignment with  $IOPS_2^{cur} = IOPS_2^{targ}$ : (a) heavier ( $IOPS_1^{cur} > IOPS_1^{targ}$ ), (b) equal ( $IOPS_1^{cur} = IOPS_1^{targ}$ ), (c) lighter ( $IOPS_1^{cur} < IOPS_1^{targ}$ )

Figure 1 show three examples of the adaptive I/O deadline assignment scheme. Each example assumes that  $Q_1$  and  $Q_2$  for  $VD_1$  and  $VD_2$  are (4KB, 5IOPS, 16msec) and (4KB, 8IOPS, 10msec), respectively. First, Figure 1 presents an example for the condition that  $IOPS_1^{cur} > IOPS_1^{targ}$  and  $IOPS_2^{cur} = IOPS_2^{targ}$ . Since the current IOPS of  $VD_1$  is higher than its target IOPS, the I/O deadline of each I/O request for  $VD_1$  is set to  $T_{be}$ , implying no deadline. By contrast, since the current IOPS of  $VD_2$  is equal to its target IOPS, its actual target RT of  $act\_RT_2^{targ}$  is 10msec, as with its original target RT. Assuming that the observed average queue depth is 5, we obtain



that  $unit\_rt_2^{targ} = 2$  msec. Finally, the deadline of each I/O request from the queue head increases from 2msec up to 10msec by 2msec.

Second, Figure 1(b) shows an example of the proposed deadline assignment when the current IOPS of both storage clients are the same as their target IOPS; that is,  $IOPS_1^{cur} = IOPS_1^{targ}$  and  $IOPS_2^{cur} = IOPS_2^{targ}$ . The I/O deadline assignment of  $VD_1$  is performed as with  $VD_2$  in the previous example. Since the current IOPS of  $VD_1$  is equal to its target IOPS, its actual target RT of  $act\_RT_1^{targ}$  is 20msec. Assuming that the observed average queue depth is 4, we obtain that  $unit\_rt_1^{targ} = 5$  msec. Finally, the deadline of each I/O request from the queue head starts from 5msec and increases up to 20msec by 5msec. The I/O deadline assignments by the proposed scheme for  $VD_1$  and  $VD_2$  in Figure 1(b) reveals that the I/O scheduler can choose the I/O requests from each queue in a fair manner. Third, Figure 1(c) presents an illustrative example for the condition that the current IOPS of  $VD_1$  is smaller than its target IOPS. To begin, the actual target RT of  $act\_RT_1^{targ}$  decreases to 9.6msec in proportion to the ratio of the current IOPS to its target IOPS. Assuming that the observed average queue depth is 3, we obtain that  $unit\_rt_1^{targ} = 3.2$  msec. Finally, the deadline of each I/O request from the queue head starts from 3.2msec and increases up to 9.6msec by 3.2msec. Finally, observe that the proposed assignment scheme determines a deadline time of each I/O request adaptively to the changing IOPS by adjusting its target response time and by increasing the I/O deadline by its unit target response time from the queue head. Consequently, we expect that the adaptive I/O deadline assigner will be able to give better fairness in servicing I/O requests with low RT variations in response times and provide better performance isolation to different virtual disks that share the same storage system.

*Slack-Stealing EDF Scheduling:* Another feature of the proposed QoS control scheme is to exploit the available slack between the current time and the earliest deadline time statistically in order to minimize storage overhead. The proposed scheduling algorithm selects an I/O request that not only minimizes the underlying storage overhead when scheduled, but also causes no deadline miss for the I/O request having the earliest deadline time. The proposed scheduling algorithm operates in two steps. First, it determines a set of I/O requests that entail no deadline miss for the I/O request with the earliest deadline, denoted by *Religible*. Next, it selects an I/O request that is likely to minimize the underlying storage overhead caused mainly by mechanical disk head movements. Then, the design of the proposed scheduling algorithm raises the following two issues: how to predict the service time of an I/O request and how to estimate storage overhead caused by scheduling the I/O request.

The proposed scheduling algorithm needs to compute the service time of a given I/O request in order to exploit or steal any existing slack time between the current time and the time when the service of the I/O request having the earliest deadline should be started to meet its deadline. Unfortunately, it is not possible to precisely predict the I/O service time under either a disk or a storage system. Previous research to estimate the I/O service time exists based on a theoretical model of disks or storage systems [6]. However, this approach has the following drawbacks. First, it cannot capture the feature of a time-varying service time according to changes in I/O workload patterns. Second, modeling a disk or a storage system requires understanding the detailed architectures for the disk or the storage system that are generally unavailable. Thus, the proposed scheduling algorithm assumes that the I/O service time is time-variant, and it measures the time-varying I/O service time by monitoring the service time of each I/O request as used in [4]. That is, it collects the service time of each I/O request during a given

monitoring interval and then averages out the service times during the interval. We denote with  $serv\_time(t)$  the current I/O service time at time  $t$ . Note that a single I/O service time is used for all virtual disks that share the underlying storage, because the service time does not include the queuing delay in the pending queues. Storage overhead of a single disk is equal to the overhead time to move from the current head position to the position to serve the I/O request. An exact computation of overhead time demands to estimate a seek time and a rotational delay between two I/O requests. However, in large-scale storage systems typically equipped with a large non-volatile cache memory, the exact estimation of storage overhead becomes almost impossible. Thus, the proposed scheduling algorithm simply estimates the overhead time between two I/O requests as the absolute distance between the start block address of the given I/O request and that of its previous I/O request.

Algorithm 2 gives the description on the proposed scheduling algorithm. We assume that  $N$  virtual disks share the same storage system. Recall that  $PQ_i$  represents the I/O pending queue dedicated to  $VD_i$ . The notation of  $r_i^h$  represents the I/O request at the head of  $PQ_i$ . Denote with  $addr(r_i^h)$  the start block address of  $r_i^h$ . We define a set of eligible I/O requests  $R_{eligible}$  that resides at the head of the I/O pending queue and entails no deadline miss for the I/O request that has the earliest deadline time.

---

**Algorithm 2:** Backstepping E-scheduling

---

```

 $T_{cur} \leftarrow$  current time;
 $serv\_time(t) \leftarrow$  current I/O service time;
assume that  $deadline_{earliest} = deadline(r_e^h)$ ;
 $addr_{last} \leftarrow$  the start block address scheduled at last;

// determine  $R_{eligible}$  set
if  $T_{cur} + serv\_time(t) \leq deadline_{earliest} - serv\_time(t)$  then
     $R_{eligible} \leftarrow \{r_i^h | r_i^h \in PQ_i \text{ and } PQ_i \neq \emptyset\}$ ;
    find  $r_s^h$ ,  $abs(addr(r_s^h), addr_{last}) = \min_{r_i^h \in R_{eligible}} \{abs(addr(r_i^h), addr_{last})\}$ ;
else
     $r_s^h \leftarrow r_e^h$ ;
endif
remove  $r_s^h$  from  $PQ_s$  and schedule it to the underlying storage;
```

---

In order to determine  $R_{eligible}$ , the proposed scheduling algorithm examines only the first I/O request at each queue in order to minimize the I/O scheduling overhead. When the proposed scheduling algorithm inspects all the pending I/O requests within all the queues, its time complexity becomes  $O(N + M)$ , where  $N$  is the number of the virtual disks that share the storage system and  $M$  is the maximum number of I/O requests within the pending queues. Considering  $M \gg N$ , the approach that checks all pending I/O requests is expected to cause a considerable amount of overhead for I/O scheduling with the increase of the number of the pending I/O requests and the number of virtual disks that share the storage system. By contrast, the time complexity of the proposed scheduling algorithm is only  $O(N)$ .

### 3 Performance Evaluations

We evaluate the performance of the proposed QoS control scheme on our storage simulator that consists of an I/O workload generator, a set of virtual disks (storage clients), an underlying storage system. (See [1] for more details.) We also assume the following simulation environments. Two virtual disks named  $VD_1$  and  $VD_2$  issue only read I/O requests. The QoS requirement of each virtual disk is defined as  $(SZ_1^{targ}, IOPS_1^{targ}, RT_1^{targ}) = (4KB, 45IOPS, 70msec)$  and  $(SZ_2^{targ}, IOPS_2^{targ}, RT_2^{targ}) = (4KB, 45IOPS, 100msec)$ . Note that the underlying storage system can satisfy the given QoS requirements properly. We determined the QoS requirements empirically by measuring the I/O performance of the underlying storage system for the given I/O workloads.

*Adaptive I/O Deadline Assignment:* To begin, we focus on evaluating the effectiveness of the proposed assignment scheme by disabling the slack-stealing EDF scheme; instead, the EDF scheduler is employed as an I/O scheduler. We use four workload sets:  $WS_1^d$ ,  $WS_2^d$ ,  $WS_3^d$ , and  $WS_4^d$ . Each workload set is characterized by different I/O traffic intensity from  $VD_2$ ; that is, the current IOPS of  $VD_2$  becomes higher than its target IOPS in  $WS_1^d$  ( $IOPS_2^{cur} > IOPS_2^{targ}$ ), the current IOPS of  $VD_2$  is equal to its target IOPS in  $WS_2^d$  ( $IOPS_2^{cur} = IOPS_2^{targ}$ ), the current IOPS of  $VD_2$  becomes lower than its target IOPS in  $WS_3^d$  ( $IOPS_2^{cur} < IOPS_2^{targ}$ ), and the current IOPS of  $VD_2$  becomes much lower than its target IOPS in  $WS_4^d$  ( $IOPS_2^{cur} \ll IOPS_2^{targ}$ ). We can expect that the proposed assignment scheme will outperform the previous target-IOPS based I/O assignment under the workload sets of  $WS_3^d$  and  $WS_4^d$ , where the current IOPS of  $VD_2$  becomes smaller than its target IOPS. Table 1 compares the performance results of the target-IOPS-based I/O deadline assignment and the proposed assignment scheme. As expected, the proposed assignment scheme reduced the variation of response times of  $VD_2$  in  $WS_3^d$  and  $WS_4^d$ . On the contrary, it increased the variation of response times of  $VD_1$ , whereas the target RT miss ratio still remains zero. In summary, the simulations results verified that the proposed assignment scheme could overcome the drawbacks of the target IOPS-based I/O deadline assignment; that is, a *high RT variation of response times due to unfairness in the processing of I/O requests from virtual disks having a larger target response time, and poor performance isolation by assigning its deadline based on its original target RT regardless of the current IOPS.*

*Slack-Stealing EDF Scheduling:* Recall that the proposed scheduling algorithm selects an I/O request that not only minimizes the underlying storage overhead when scheduled, but also causes no deadline miss for the I/O request having the earliest deadline time. Note that the scheduling algorithms under test will employ the adaptive I/O deadline assigner. Three workload sets,  $WS_1^s$ ,  $WS_2^s$ , and  $WS_3^s$ , are used for this performance evaluation. The I/O traffic intensity for each virtual disk in  $WS_1^s$  is equal to the given QoS requirements; that is,  $IOPS_1^{targ}$  and  $IOPS_2^{targ}$ . However, the I/O traffic intensity for each virtual disk in  $WS_2^s$  and  $WS_3^s$  is increased by 10% and 20% respectively, compared with its target IOPS. Table 2 compares the performance results of the EDF scheduling and the proposed scheduling scheme. Observe that the proposed scheduling scheme reduced the target response time(RT) miss ratio of  $VD_1$  and  $VD_2$  in  $WS_2^s$  and  $WS_3^s$  by improving the response times of each virtual disk. To summarize, the simulation results verified that *the slack-stealing EDF scheduling algorithm could reduce storage overhead by reordering the I/O requests as long as the deadline times of I/O requests are not missed, resulting in better target RT miss ratios and average response times, compared with the EDF scheduling algorithm.*

**Table 1.** Summary of the performance results of the adaptive I/O deadline assignment

		Avg. IOPS (IOPS)		Avg. RT (msec)		Var. RT		Targ. RT miss ratio	
		targ-IOPS	prop	targ-IOPS	prop	targ-IOPS	prop	targ-IOPS	prop
$WS_1^d$	$VD_1$	43.5	43.4	41.4	40.8	–	–	0.21	0.19
	$VD_2$	67.7	68.0	122.1	118.8	–	–	0.58	0.58
$WS_2^d$	$VD_1$	44.8	44.0	22.8	22.1	105.0	73.6	0	0
	$VD_2$	44.0	44.7	26.9	27.5	159.5	161.4	0	0
$WS_3^d$	$VD_1$	44.6	44.2	16.4	17.0	<b>14.6</b>	<b>12.7</b>	0	0
	$VD_2$	24.7	25.0	16.8	15.9	<b>20.8</b>	<b>17.3</b>	0	0
$WS_4^d$	$VD_1$	44.5	44.5	12.4	12.6	<b>2.2</b>	<b>2.6</b>	0	0
	$VD_2$	5.0	5.1	14.0	12.5	<b>17.9</b>	<b>6.5</b>	0	0

**Table 2.** Summary of the performance results of the slack-stealing I/O scheduling

		Avg. IOPS (IOPS)		Avg. RT (msec)		Targ. RT miss ratio	
		EDF	prop	EDF	prop	EDF	prop
$WS_1^s$	$VD_1$	44.0	44.5	22.1	22.4	0.00	0.00
	$VD_2$	44.7	44.4	27.5	23.6	0.00	0.00
$WS_2^s$	$VD_1$	48.7	49.2	28.2	28.5	<b>0.03</b>	<b>0.02</b>
	$VD_2$	49.1	49.1	40.8	29.8	<b>0.02</b>	<b>0.00</b>
$WS_3^s$	$VD_1$	53.4	53.8	45.1	39.3	<b>0.16</b>	<b>0.07</b>
	$VD_2$	52.2	53.1	58.8	41.0	<b>0.10</b>	<b>0.01</b>

## 4 Conclusion and Future Work

This paper proposed an efficient QoS control scheme that enforces the QoS requirements of multiple virtual disks (or storage clients) that share the same storage system. The proposed QoS control scheme consists of two key components: the adaptive I/O deadline assignment and the slack-stealing EDF scheduling for storage systems. The key of the adaptive I/O deadline assignment is to adaptively determine the deadline time of each I/O request according to the current IOPS and the current queue depth. Thus, it could overcome the drawbacks of the target IOPS-based deadline assignment: a high RT variation of response times due to unfairness in the processing of I/O requests from virtual disks having a larger target response time, and poor performance isolation by assigning its deadline based on its original target RT regardless of the current IOPS. The key of the slack-stealing EDF scheduling is to steal any available slack between the current time and the earliest deadline time in order to minimize the underlying storage overhead. The proposed scheduling algorithm selects an I/O request that minimizes the underlying storage overhead when scheduled, while causing no deadline miss for the I/O request having the earliest deadline time. We raised two design issues concerning how to predict the I/O service time of an I/O request and how to estimate storage overhead (disk head movement) caused by scheduling an I/O request, and provided reasonable solutions. We implemented the proposed QoS control scheme on our storage simulator. The simulation results for the adaptive I/O deadline

assignment under various competing I/O workload sets showed that the proposed assignment scheme not only provides better fairness with lower RT variation, but also assures a better performance isolation for each virtual disk. Performance evaluations for the slack-stealing EDF scheduling revealed that the proposed scheduling scheme could provide better target RT miss ratios and response times by reducing storage overhead under various I/O workload sets.

In future work, we plan to implement the proposed QoS control scheme on top of an actual storage system and evaluate its performance with actual I/O traffic. In addition, we need to evaluate different techniques to predict an I/O service time and storage overhead for the slack-stealing EDF scheduling.

## Acknowledgments

This research was supported by the Daegu University Research Grant, No 20040825. This research has been also supported in part by the Ministry of Education of Korea for its support toward the Electrical and Computer Engineering Division at POSTECH through its BK21 program, in part by HY-SDR IT Research Center, and in part by grant No. R01-2003-000-10739-0 from the Basic Research Program of the Korea Science and Engineering Foundation.

## References

1. Y. J. Nam, *Dynamic Storage QoS Control for Storage Cluster and RAID Performance Enhancement Techniques*. Ph.D Dissertation, POSTECH, February 2004.
2. C. Lumb, A. Merchant, and G. Alvarez, "Facade: Virtual storage devices with performance guarantees," in *Proceedings of Conference on File and Storage Technologies*, March 2003.
3. Y. Nam and C. Park, "A new proportional-share disk scheduling algorithm: Trading-off I/O throughput and qos guarantees," *Lecture Notes in Computer Science*, vol. 1067, pp. 257–266, June 2003.
4. A. Chandra, W. Gong, and P. Shenoy, "Dynamic resource allocation for shared data centers using online measurements," in *Proceedings of the 11th International Workshop on Quality of Service*, June 2003.
5. H. Lee, Y. Nam, and C. Park, "Regulating I/O performance of shared storage with a control theoretical approach," in *Proceedings of the 21st IEEE Mass Storage Systems Symposium/12th NASA Goddard Conference on Mass Storage Systems and Technologies (MSST2004)*, April 2004.
6. M. Uysal, G. Alvarez, and A. Merchant, "A modular, analytical throughput model for modern disk arrays," in *Proceedings of the Ninth International Symposium on Modeling, Analysis and Simulation of Computer and Telecommunications Systems*, pp. 183–192, August 2001.

# High Reliability Replication Technique for Web-Server Cluster Systems

M. Mat Deris<sup>1</sup>, J.H. Abawajy<sup>2</sup>, M. Zarina<sup>3</sup>, and R. Mamat<sup>4</sup>

<sup>1</sup> Faculty of Information Technology and Multimedia,  
College University Tun Hussein Onn  
Batu Pahat, Johor, Malaysia  
mustafa@kustem.edu.my

<sup>2</sup> Deakin University, School of Information Technology,  
Geelong, VIC, Australia  
jemal@deakin.edu.au

<sup>3</sup> KUSZA College, Kuala Terengganu, Malaysia  
zarina@kusza.edu.my

<sup>4</sup> Department of Computer Science,  
Faculty of Science and Technology, KUSTEM, K. Terengganu, Malaysia  
rab@kustem.edu.my

**Abstract.** Providing reliable and efficient services are primary goals in designing a web server system. Data replication can be used to improve the reliability of the system. However, mapping mechanism is one of the primary concerns to data replication. In this paper, we propose a mapping mechanism model called enhanced domain name server (E-DNS) that dispatches the user requests through the URL-name to IP-address under Neighbor Replica Distribution Technique (NRDT) to improve the reliability of the system.

## 1 Introduction

With the ever increasing applications in the world wide web (WWW) such as distance learning education and e-commerce, the need for a reliable web server is likely to increase [6]. Thus, providing reliable and efficient services are primary goals in designing a web server cluster (WSC) system. This is due to the constraints of the eventual failure of hardware or/and software components. In order to provide reliable services, a WSC needs to maintain the availability of some data replicas while preserving one-copy consistency among all replicas [4]. Therefore, data replication plays an important role in a WSC as a highly reliable system.

The most common approaches in the replication techniques are the synchronous and asynchronous replications. The former provides a 'tight consistency' between data stores. This means that the latency between the data consistency achieved will be zero. Data in all nodes are always the same, no matter from which replica the updated originated. However, synchronous replication has drawbacks in practice [5]. The major argument is that, the response time to execute an operation is high because the time taken for all nodes that have the same copy to 'agree' to execute an operation is high. Whilst the asynchronous replication provides a 'loose consistency' between data

stores. The replication process occurs asynchronous to originating transaction. In other words, there is always some degree of lag between the time the originating transaction is committed and the effects of the transaction are available at any replica(s) [1]. Nevertheless, the response time is lower than that of the synchronous technique.

Reliability refers to the probability that the system under consideration does not experience any failure in a given time interval. Thus, a reliable WSC is one that can continue to process user's requests even when the underlying system is unreliable [3]. When components fail, it should still be able to continue executing the requests without violating the database consistency.

In this paper we propose the enhanced domain name server (E-DNS) algorithm as a mapping mechanism under the Neighbor Replica Distribution Technique (NRDT) to improve the reliability of the system. In case of server failure, the server will be switched to neighboring IP address.

The paper is organized as follows. Section 2 reviews NRDT model. Section 3 describes typical DNS. Section 4 describes the concept of E-DNS. Section 5 concludes the proposed work.

## 2 Neighbor-Replica Distribution Technique (NRDT)

### 2.1 The Model

In a replicated database, copies of a data object may be stored at several sites in the network. Multiple copies of a data object must appear as a single logical data object to the transactions. This is termed as one-copy equivalence and is enforced by the replica control technique. The correctness criteria for replicated database is one-copy serializability [11], which ensures both one-copy equivalence and the serializable execution of transactions. In order to ensure the one-copy serializability, a replicated data object may be read by reading a quorum of copies, and it may be written by writing a quorum of copies. The selection of a quorum is restricted by the quorum intersection property to ensure one-copy equivalence: For any two operations  $o[x]$  and  $o'[x]$  on a data object  $x$ , where at least one of them is a write, the quorum must have a non-empty intersection. The quorum for an operation is defined as a set of copies whose number is sufficient to execute that operation.

Briefly, a site  $i$  initiates a NRDT transaction to update its data object. For all accessible data objects, a NRG transaction attempts to access a NRDT quorum. If a NRDT transaction gets a write quorum with non-empty intersection, it is accepted for execution and completion, otherwise it is rejected. We assume for the read quorum, if two transactions attempt to read a common data object, read operations do not change the values of the data object. Since read and write quorums must intersect and any two NRDT quorums must also intersect, then all transaction executions are one-copy serializable.

In the design of the WSC, a client on the Internet will notice only one IP address coming from the cluster, not those individual servers in the cluster. The cluster (with only one IP address visible to the public) is composed of a node called Request Distributor Agent (RDA) and a group of servers. The servers are logically connected

to each other in the form of a grid structure, each of which is connected to RDA. Figure 1 shows architecture of the cluster-server system with nine servers. The RDA will forward legitimate Internet requests to the appropriate servers in the cluster. It returns any replies from the servers back to the clients.

Each node has the premier data (eg. *file a* will be located to server A, *file b* will be located to server B, and so on). The RDA will forward any request to the appropriate server with the premier data file. This is done by maintaining a server-service table that contains all the services provided by the cluster together with the corresponding addresses and their neighbors.

One advantage of a server cluster over a single server is its high security. If a single server is used, it is reachable from the Internet and therefore vulnerable for vicious [3]. Only the RDA has the IP address visible from the Internet, and all other stations of the cluster bear only private IP address. Therefore, all cluster-server stations are not reachable directly from the outside. A firewall system may be installed on the RDA to protect the whole cluster. To attack one of the cluster server stations, one has to first land on RDA and launch an attack from there. Network Address Translation is used on RDA to translate the destination IP address of incoming packets to an internal IP address, and that of the outgoing packets to the IP address on Internet where the requests.

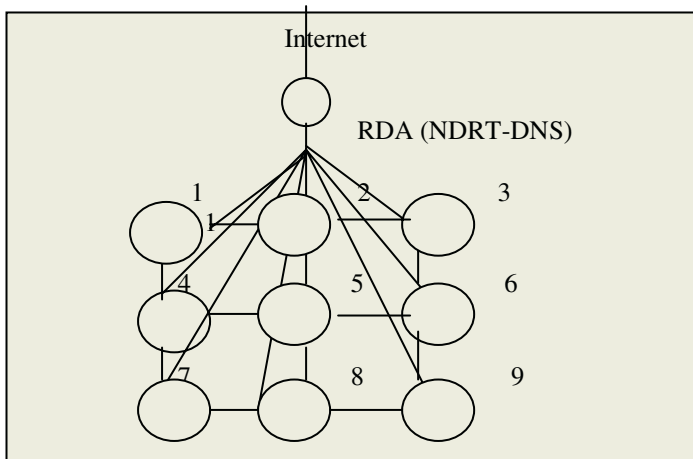


Fig. 1. A Cluster with 9 servers

## 2.2 The NRDT Technique

In NRDT, all sites are logically organized in the form of a two-dimensional grid structure. For example, if a NRDT consists of nine nodes, it will be logically organized in the form of 3 x 3 grid as shown in Figure. 1. Each node has a *master* data file. In the remainder of this paper, we assume that replica copies are data files. A node is either operational or failed and the state (operational or failed) of each node is



statistically independent to the others. When a node is operational, the copy at the node is available; otherwise it is unavailable.

**Definition 2.2.1:** A node X is a neighbor to node Y, if X is logically-located adjacent to Y.

A data will replicate to the neighboring nodes from its primary node. The number of data replication,  $d$ , can be calculated using Property 2.2, as described below.

**Property 2.2:** The number of data replication from each node,  $d \leq 5$ .

**Proof:** Let  $n$  be a set of all nodes that are logically organized in a two-dimensional grid structure form. Then  $n$  nodes are labeled  $m(i,j)$ ,  $1 \leq i < \sqrt{n}$ ,  $1 \leq j < \sqrt{n}$ . Two way links will connect nodes  $n(i,j)$  with its four neighbors, nodes  $m(i \pm 1, j)$  and  $m(i, j \pm 1)$ , as long as there are nodes in the grid. Note that, four nodes on the corners of the grid, have only two adjacent nodes, and other nodes on the boundaries have only three neighbors. Thus the number of neighbors of each node is less than or equal to 4. Since the data will be replicated to neighbors, then the number of data replication from each node,  $d$ , is:

$$d \leq \text{the number of neighbors} + \text{a data from node itself} = 4 + 1 = 5.$$

For example, from Figure. 1, data from node 1 will replicate to node 2 and node 4 which are its neighbors. Node 5 has four neighbors, which are nodes 2, 4, 6, and 8. As such, node 5 has five replicas.

For simplicity, the primary node of any data file and its neighbors are assigned with vote one and vote zero otherwise. This vote assignment is called neighbor binary vote assignment on grid. A neighbor binary vote assignment on grid,  $B$ , is a function such that

$$B(i) \in \{0,1\}, 1 \leq i \leq n$$

where  $B(i)$  is the vote assigned to node  $i$ . This assignment is treated as an allocation of replicated copies and a vote assigned to the node results in a copy allocated at the neighbor. That is,

$$1 \text{ vote} \equiv 1 \text{ copy.}$$

Let 
$$L_B = \sum_{i=1}^n B(i)$$

where,  $L_B$  is the total number of votes assigned to the primary node and its neighbors and it also equals to the number of copies of a file allocated in the system. Thus,  $L_B = d$ .

Let  $r$  and  $w$  denote the read quorum and write quorum, respectively. To ensure that the read operation always gets up-to-date values,  $r + w$  must be greater than the total number of copies (votes) assigned to all nodes. The following conditions are used to ensure consistency:

- 1)  $1 \leq r \leq L_B, 1 \leq w \leq L_B,$
- 2)  $r + w = L_B + 1.$

Conditions (1) and (2) ensure that there is a nonempty intersection of copies between every pair of read and write operations. Thus, the conditions ensure that a read operation can access the most recently updated copy of the replicated data. Timestamps can be used to determine which copies are most recently updated.

Let  $S(B)$  be the set of nodes at which replicated copies are stored corresponding to the assignment  $B$ . Then

$$S(B) = \{i | B(i) = 1, 1 \leq i \leq n\}.$$

**Definition 2.2.2:** For a quorum  $q$ , a *quorum group* is any subset of  $S(B)$  whose size is greater than or equal to  $q$ . The collection of quorum group is defined as the *quorum set*.

Let  $Q(B,q)$  be the quorum set with respect to the assignment  $B$  and quorum  $q$ , then

$$Q(B,q) = \{G | G \subseteq S(B) \text{ and } |G| \geq q\}$$

For example, from Figure. 1, let node 5 be the primary node of the master data file  $x$ . Its neighbors are nodes 2, 4, 6 and 8. Consider an assignment  $B$  for the data file  $x$ , such that

$$B_x(5)=B_x(2)=B_x(4)=B_x(6)=B_x(8) = 1$$

$$\text{and } L_{B_x} = B_x(5) + B_x(2) + B_x(4) + B_x(6) + B_x(8) = 5.$$

Therefore,  $S(B_x) = \{5,2,4,6,8\}$ .

If a read quorum for data file  $x$ ,  $r=2$  and a write quorum  $w = L_{B_x}-r+1 = 4$ , then the quorum sets for read and write operations are  $Q(B_x,2)$  and  $Q(B_x,4)$ , respectively, where

$$Q(B_x,2) = \{\{5,2\}, \{5,4\}, \{5,6\}, \{5,8\}, \{5,2,4\}, \{5,2,6\}, \{5,2,8\}, \{5,4,6\}, \{5,4,8\}, \{5,6,8\}, \\ \{2,4,6\}, \{2,4,8\}, \{2,6,8\}, \{4,6,8\}, \{5,2,4,6\}, \{5,2,4,8\}, \{5,2,6,8\}, \{5,4,6,8\}, \\ \{2,4,6,8\}, \{5,2,4,6,8\}\}$$

and

$$Q(B_x,4) = \{\{5,2,4,6\}, \{5,2,4,8\}, \{5,2,6,8\}, \{5,4,6,8\}, \{2,4,6,8\}, \{5,2,4,6,8\}\}$$

### 2.3 The Correctness of NRDT

In this section, we will show that the NRDT technique is one-copy serializable. We start by defining sets of groups called *coterie* [12] and to avoid confusion we refer the sets of copies as *groups*. Thus, sets of *groups* are sets of sets of copies.

**Definition 2.3.1. Coterie.** Let  $U$  be a set of *groups* that compose the system. A set of *groups*  $T$  is a coterie under  $U$  iff

- i)  $G \in T$  implies that  $G \neq \emptyset$  and  $G \subseteq U$ .
- ii) If  $G, H \in T$  then  $G \cap H \neq \emptyset$  ( intersection property)
- iii) There are no  $G, H \in T$  such that  $G \subset H$  (minimality).

By definition of coterie and from Definition 2.2.2, then  $Q(B,w)$  is a coterie, because it satisfies all coterie's properties.

Since read operations do not change the value of the accessed data object, a read quorum does not need to satisfy the intersection property. To ensure that a read operation can access the most recently updated copy of the replicated data, two conditions in sub-section 2.2 must be conformed. While a write quorum needs to satisfy read-write and write-write intersection properties. The correct criterion for

replicated database is one-copy serializable. The next theorem provides us with a mechanism to check whether NRDT is correct.

**Theorem 2.3.1.** The NRDT technique is one-copy serializable.

**Proof:** The theorem holds on condition that the NRDT technique satisfies the quorum intersection properties, i.e., write-write and read-write intersections. Since  $Q(B,w)$  is a coterie then it satisfies the write-write intersection. However, for the case of a read-write intersection, it can be easily shown that  $\forall G \in Q(B,r)$  and  $\forall H \in Q(B,w)$ , then  $G \cap H \neq \emptyset$ .

### 3 Overview of DNS

At its most basic level, the DNS provides distributed database of name-to-address mappings spread across a hierarchy of nameservers. The namespace is partitioned into a hierarchy of domains and subdomains with each domain administered independently by an authoritative nameserver. Nameservers store the mapping of names to address in resource records, each having an associated time to live (TTL) field that determines how long the entry can be cached by other nameserver in the system. A large TTL value reduces the load on the nameservers but limits the frequency of update propagation through the system. The different types of resource records and additional details about the DNS are described in [9]. The most widely used nameserver implementation in the DNS is the Berkeley Internet Name Domain (BIND) [2].

Nameserver can be implemented in the form of iterative or recursive queries. In an iterative query, the nameserver returns either an answer to the query from its local database, or a referral to another nameserver that may be able to answer the query. In handling a recursive query, the nameserver return a final answer, querying any other nameserver necessary to resolve the name. Most nameserver within the hierarchy are configured to send and accept only iterative queries. Local nameserver, however, typically accept recursive queries from clients.

### 4 E-DNS

E-DNS is proposed to enhance DNS according to the NRDT requirements. The function is similar to RDA in NRDT model. In case of server(s) fails, user cannot access data due to no other server take over the service. All clients or user requests from Internet are cross through to DNS to decide the right server to replay the request. When a server fails, the client who maps the name to IP address will find out that the server is down. The problem still unsolved although the client may press 'reload' or 'refresh' button in their browsers. This problem is unacceptable and unreliable. E-DNS is a viable alternative or solution to this problem because it is developed to take over the service in case of server(s) failure. To do this we used the complete DNS BIND software and only nameserver (it is the text file) in DNS will be updated according to match NRDT requirement. NRDT program will check the server fail/up every  $t$  second (time can be configured). E-DNS centralizes dispatching host name into single IP address and update it according to NRDT pattern. In case of server

failures, the server will be switched to its neighboring IP address. One of the main attractions of this approach is its ease of deployment.

#### 4.1 E-DNS Algorithm

We design an algorithm for E-DNS. There are three important modules for E-DNS algorithms: communication module, recovering module and neighbor module. The communication module will check the server either up or down/fail, while the neighbor module will seek the appropriate neighbors when the primary server fails and the recovering module will update the failed nameserver in DNS.

##### **Main**

```

Read time.conf #user define the time
Do while time true
  Call communication-module
  If died
    Call neighbor-module until true
  If true
    Call recovering-module
  End do

```

##### **End Main**

##### **Procedure communication-module**

```

Create sockets
Assign port to sockets
Get service
Get IP
Ping IP

```

##### **End procedure**

##### **Procedure Neighbor-Module**

```

Read from NRDT able (have logic structure by metric)
Insert into array (#row,#cow)
For i = 1 to 2
  For j = 1 to 2
    If i = 1
      If j = 1
        If row !=1
          New-metric = cow - 1,row
        If j = 2
          New-metric = cow + 1,row
        End if #i = 1
      If i =2
        If j = 1
          New-metric = cow, row - 1
        If j = 2

```

```

        New-metric = cow, row +1
    End if # i= 2
End for #i
End for #j
End procedure

```

**Procedure recovering-module**

```

Read DNS text fail
Seek IP dead (#IP take from communication module)
Replace new IP (#IP take from neighbor module)
Re-run DNS software

```

**End Procedure**

**4.2 Simulation of E-DNS**

Assume that in a web sever cluster, there are six servers with the IP-address shown below:

- 1) p1.project.com is primary mail server with IP 999.999.9.111
- 2) p2.project.com is primary ftp server with IP 999.999.9.222
- 3) p3.project.com is primary web server with IP 999.999.9.333
- 4) p4.project.com is primary distance learning server with IP 999.999.9.444
- 5) p5.project.com is primary telnet server with IP 999.999.9.555
- 6) p6.project.com is primary other server with IP 999.999.9.666

1. Under normal *conFfiguration* on BIND nameserver file, mapping address is simply done through the name to the IP address of single server as show below;

p1.project.com	IN	A	999.999.9.111
p2.project.com	IN	A	999.999.9.222
p3.project.com	IN	A	999.999.9.333
p4.project.com	IN	A	999.999.9.444
p5.project.com	IN	A	999.999.9.555
p6.project.com	IN	A	999.999.9.666

2. *ConFfiguration* of the NRDT table consists of port, server name, IP and logical structure for every node (metric). The logical table *conFfiguration* based NRDT is shown as.

80	p1.project.com	999.999.9.111	11
21	p2.project.com	999.999.9.222	12
23	p3.project.com	999.999.9.333	13
80	p4.project.com	999.999.9.444	21
80	p5.project.com	999.999.9.444	23
80	p6.project.com	999.999.9.444	24

3. The NRDT program will check the server either it is up or down/fail. For example, if the server with 999.999.9.222 (metric 12) fails, then its neighbors (could be with the

metrics 11,13,22) will be replaced (for example with IP address 999.999.9.333). The nameserver update becomes;

p1.project.com	IN	A	999.999.9.111
p2.project.com	IN	A	999.999.9.333
p3.project.com	IN	A	999.999.9.333
p4.project.com	IN	A	999.999.9.444
p5.project.com	IN	A	999.999.9.555
p6.project.com	IN	A	999.999.9.666

When requests come from Internet to browser ftp server, with the primary IP address 999.999.9.222, it will automatically mapped to the IP address 999.999.333. Thus, services on Internet are accessible at any point of time. Consequently, the reliability of the server is increased.

## 5 Conclusion

Web server cluster is a popular architecture used to improve the reliability and availability of the systems. However, with the current DNS algorithm, it is unreliable due to the fact that in a case of server(s) fails, users cannot access the data since no other server take over the service. In this paper, an enhanced domain name server (E-DNS) algorithm on NRDT technique, has been proposed to improve the reliability of the WSC. The algorithm is used as a mapping mechanism to dispatch the user requests through the URL-name to IP-address. It centralizes dispatching host name into single IP address and update it according to NRDT pattern. In case of server failures, the server will be switched to its neighboring IP address. The simulation showed that the proposed algorithm works well and provides a convenient approach to increase the reliability of WSC.

## References

- [1] M. Buretta, "Data replication: Tools and Techniques for Managing Distributed Information", John Wiley, New York, (1997).
- [2] P. Albitz, and C.Liu, "DNS and BIND." *O'Reilly and Associates, inc.*,(2001).
- [3] J. Liu, L Xu, B. Gu, J. Zhang, "Scalable, High Performance Internet Cluster Server", *IEEE 4<sup>th</sup> Int'l Conf. HPC-ASIA*, Beijing, pp. 941-944, (2000)
- [4] M. Mat Deris, A. Mamat, P. C. Seng, H. Ibrahim, "Three Dimensional Grid Structure for Efficient Access of Replication Data", *Int'l Journal of interconnection Network, World Scientific*, Vol. 2, No. 3, pp 317-329, (2001).
- [5] A. Moissis, "Sybase Replication Server: A practical Architecture for Distributing and Sharinf Information", Technical Document, Sybase Inc, (1996).
- [6] E. Pacitti and E. Simon, "Update Propagation Strategies to Improve Fresh LazyMaster Replicated Databases", *Journal VLDB*, Vol. 8, no. 4, (2000).
- [7] H. H. Shen, S. M. Chen, and W. M. Zheng, "Reserch on Data Replication Distribution Technique for Web Server Cluster", *IEEE Proc. 4<sup>th</sup> Int'l. Conference on Performance Computing*, Beijing, pp. 966-968, (2000).

- [8] W. Zhou and A. Goscinski, "Managing Replicated Remote Procedure Call Transactions", *The Computer Journal*, Vol. 42, no. 7, pp592-608, (1999).
- [9] P. Mockapetris, "Domain names-implementation and specification", Internet Request for Comments (RFC 1035), (November 1987).
- [10] Internet Software Consortium, "Berkeley Internet domain (BIND)", <http://www.isc.org/product/BIND>, (June 2000).
- [11] P.A. Bernstein and N.Goodman, "An Algorithm for Concurrency Control and Recovery in Replicated Distributed Databases," *ACM Trans. Database Systems*, vol 9, no. 4(1994), pp.596-615.
- [12] M. Maekawa, "A  $\sqrt{n}$  Algorithm for Mutual Exclusion in Decentralized Systems," *ACM Trans. Computer Systems*, vol. 3, no. 2(1992), pp. 145-159.

# An Efficient Replicated Data Management Approach for Peer-to-Peer Systems

J.H. Abawajy

Deakin University,  
School of Information technology,  
Geelong, Victoria, 3217 Australia

**Abstract.** The availability of critical services and their data can be significantly increased by replicating them on multiple systems connected with each other, even in the face of system and network failures. In some platforms such as peer-to-peer (P2P) systems, their inherent characteristic mandates the employment of some form of replication to provide acceptable service to their users. However, the problem of how best to replicate data to build highly available peer-to-peer systems is still an open problem. In this paper, we propose an approach to address the data replication problem on P2P systems. The proposed scheme is compared with other techniques and is shown to require less communication cost for an operation as well as provide higher degree of data availability.

## 1 Introduction

Peer-to-peer (P2P) network systems are one of the important and rapidly growing distributed system paradigms in which participants (the peers) rely on one another for service, rather than solely relying on dedicated and often centralized servers. The relationships among the nodes in the network are equal, nodes may join and leave the network in an ad-hoc manner and communication and exchange of information is performed directly between the participating peers. There is a growing research and industrial interest on peer-to-peer (P2P) systems. The success of P2P systems is due to many potential benefits such as fault-tolerance through massive replication; scale-up to very large numbers of peers, dynamic self-organization, load balancing, and parallel processing. Examples of P2P systems include Napster [3], Gnutella [4], and KaZaA[5] and Freenet [6].

Recently, peer-to-peer systems have become popular mechanism for large-scale content sharing. It is well known that techniques to increase the resilience and availability of stored data are fundamental to building dependable distributed systems. However, unlike traditional client-server applications that centralize the management of data in a few highly reliable servers, peer-to-peer systems distribute the burden of data storage, computation, communications and administration among thousands of individual nodes. Data management in this context offers new research opportunities since traditional distributed database techniques need to scale up while supporting high data autonomy, heterogeneity, and dynamicity.



Generally P2P systems consider the data they offer to be very static or even read-only [9]. However, advanced peer-to-peer applications are likely to need more general replication capabilities. For example, a patient record may be replicated at several medical doctors and updated by any of them during a visit of the patient, e.g. to reflect the patient's new weight [8]. Other typical applications where new data items are added, deleted, or updated frequently by multiple users are bulletin-board systems, shared calendars or address books, e-commerce catalogues, and project management information [9]. Also, the inherent characteristics of peer-to-peer systems, require them to employ some form of replication to provide acceptable service to their users. For example, the erratic behaviour of online availability and the complete lack of global knowledge coupled with the absence of any centralisation makes P2P environments unreliable [9]. Unlike traditional distributed systems, the individual components of a peer-to-peer system experience an order of magnitude worse availability. This is because peer-to-peer systems are characterized by susceptibility to failure (e.g., node may be switched off), join and leave the system, have intermittent connectivity, and are constructed from low-cost low-reliability components. The study of a popular peer-to-peer file sharing system found that the majority of peers had availability rates of under 20% [1].

While much of the attention in the peer-to-peer systems research has been focused on the issues of providing scalability, free-rider problem or routing mechanisms within P2P networks, the resilience and availability of the data has so far seldom been mentioned. Therefore, how best to replicate data to build highly available peer-to-peer systems is still an open problem. In most peer-to-peer (P2P) systems data is assumed to be rather static and updates occur very infrequently. For application domains beyond mere file sharing such assumptions do not hold and updates in fact may occur frequently. Therefore, data replication in the presence of updates and transactions remains an open issue as well.

In this paper, we discuss an extension of our previous work on replica placement and management [2] to handle a system that support data replication in a transactional framework for weakly connected environments such as P2P systems. The proposed scheme uses quorum-based protocol for maintaining replicated data and shown to provide both high data availability and low response time. The proposed approach imposes a logical three dimensional grid structure on data objects based on a box shape organization and uses a sense-of-direction approach (SODA) for both read and write operations. We show that the proposed approach presents better average quorum size, high data availability, low bandwidth consumption, increased fault-tolerance and improved scalability of the overall system as compared to standard replica control protocols.

The rest of the paper is organized as follows. Section 2 presents related work. Section 3 presents our approach. Section 3 presents the proposed replica management protocol. In order to show the merits of the proposed approach, we present comparative analysis of the proposed approach against an existing approach in Section 4. Concluding remarks and future directions is reported in Section 5.

## 2 Related Work

The rapid popularization of Internet-based P2P applications such as Napster [3], Gnutella [4], and KaZaA[5] has inspired the research and development of technologies for P2P services and systems. An efficient data replication management (DRM) technique is one of the important P2P technologies. Through an efficient DRM, the availability of P2P services and their data can be significantly increased by replicating them on multiple systems connected with each other, even in the face of system and network failures [2]. From the viewpoint of data management these systems should address two critical areas [9]:

1. Efficient, scalable data access which is provided more or less by all approaches, and
2. Updates to the data stored, especially with respect to replication and low online probabilities.

However, the data sharing P2P systems like Gnutella and Kaaza deal with static, read-only files (e.g. music files) for which update is not an issue. Also, in systems such as Napster and Gnutella, replication occurs implicitly as each file downloaded by a user is implicitly replicated at the user's workstation. However, since these systems do not explicitly manage replication or mask failures, the availability of an object is fundamentally linked to its popularity and users have to repeatedly obtain the data. Also, if an update of a data item occurs this means that the peer that holds the item changes it. Subsequent requests would get the new version. However, updates are not propagated to other peers which replicate the item. As a result multiple versions under the same identifier (filename) may co-exist and it depends on the peer that a user contacts whether the latest version is accessed. The same holds true for most decentralised systems such as Gnutella [4].

ActiveXML [11] is a declarative framework that harnesses web services for data integration, and is put to work in a peer-to-peer architecture. It supports the definition of replicated XML fragments as Web service calls but does not address update propagation. Update is addressed in P-Grid [1], a structured network that supports self-organization. The update algorithm uses rumour spreading to scale and provides probabilistic guarantees for replica consistency. However, it only considers updates at the file level in a mono-master mode, i.e. only one (master) peer can update a file and changes are propagated to other (read-only) replicas.

Freenet [6] partially addresses updates which are propagated from the updating peer downward to close peers that are connected. Freenet uses a heuristic strategy to route updates to replicas which is uncertain to guarantee eventual consistency. Searches replicate data along query paths ("upstream"). In the case of an update (which can only be done by the data's owner) the update is routed "downstream" based on a key-closeness relation. Since the routing is heuristic, the network may change, and no precautions are taken to notify peers that come online after an update has occurred, consistency guarantees are limited. Also, peers that are disconnected do not get updated.

In OceanStore [10] every update creates a new version of the data object (versioning). Consistency is achieved by a two-tiered architecture: A client sends an update to the object's "inner ring" (some replicas who are the primary storage of the object and

perform a Byzantine agreement protocol to achieve fault-tolerance and consistency) and some secondary replicas that are mere data caches in parallel. The inner ring commits the update and in parallel an epidemic algorithm distributes the tentative update among the secondary replicas. Once the update is committed, the inner ring multicasts the result of the update down the dissemination tree. To our knowledge analysis of the latency and consistency guarantees for this update scheme has not been published yet.

### 3 Replica Management Approach

Regardless of the underlying system topology, P2P systems need some form of replication to achieve good query latencies, load balance, and reliability. We now briefly describe the architecture of the proposed data replication system. Our system assumes an infrastructure-less peer-to-peer system, i.e., all peers are equal and no specialised infrastructure, e.g., hierarchy, exists. No peer has a global view of the system but base their behaviour on local knowledge, i.e., its routing tables, replica list, etc. The peers can go offline at any time according to a random process that models the behaviour when peers are online.

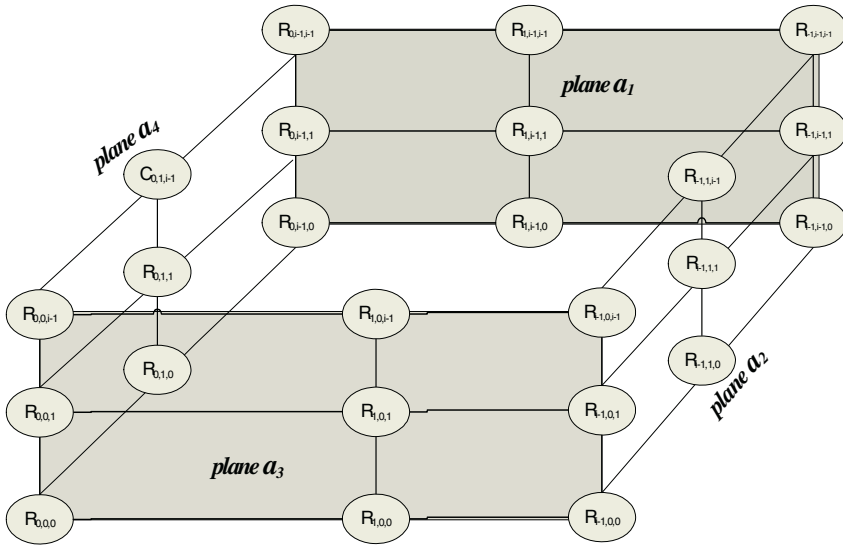


**Fig. 1.** The organization of replicas with four planes (i.e.,  $\alpha_i$ ) and the circles in the grid represent the sites

#### 3.1 System Architecture

Given  $N$  copies of a data object, we logically organize the  $N$  copies into a box-shape structure with four planes (i.e.,  $\alpha_1$ ,  $\alpha_2$ ,  $\alpha_3$ , and  $\alpha_4$ ) as shown in Fig. 1. Each copy of the object (circles in Fig. 1) is located at  $x, y, z$  coordinate ( $C_{x,y,z}$ ) in a given plane

(e.g.,  $C_{0,0,0}$ ,  $C_{0,0,1}$ , ...,  $C_{1-1,1-1,1-1}$ ). We define a pair of copies that can be constructed from a hypotenuse edge in a box-shape structure is called hypotenuse copies.

### 3.2 Operations

The basic architecture of Fig. 1 supports operations for creating objects, creating and deleting object replicas, and performing reads and writes on the shared objects in a transactional framework. Read operations on an object are executed by acquiring a read quorum that consists of any hypotenuse copies. In Fig. 1, copies  $\{R_{0,0,0}, R_{1-1,1-1,1-1}\}$ ,  $\{R_{0,0,1}, R_{1-1,1-1,0}\}$ ,  $\{R_{0,1-1,1-1}, R_{1-1,0,0}\}$ , or  $\{R_{1-1,0,1-1}, R_{0,1-1,0}\}$  are hypotenuse copies and any one pair of which is sufficient to execute a read operation. Since each pair of them is hypotenuse copies, it is clear that, read operation can be executed if one of them is accessible, thus increasing the fault-tolerance of this protocol.

In contrast, write operations are executed by acquiring a write quorum from any plane that consists of: (1) hypotenuse copies; and (2) all vertices copies. For example, if the hypotenuse copies, say  $\{R_{0,0,0}, R_{1-1,1-1,1-1}\}$  are required to execute a read operation, then copies  $\{R_{0,0,0}, R_{1-1,1-1,1-1}, R_{1-1,1-1,0}, R_{0,1-1,1-1}, R_{0,1-1,0}\}$  are sufficient to execute a write operation, since one possible set of copies of vertices that correspond to  $\{R_{0,0,0}, R_{1-1,1-1,1-1}\}$  is  $\{R_{1-1,1-1,1-1}, R_{1-1,1-1,0}, R_{0,1-1,1-1}, R_{0,1-1,0}\}$ . Other possible write quorums are  $\{R_{0,0,0}, R_{1-1,1-1,1-1}, R_{1-1,1-1,0}, R_{1-1,0,1-1}, R_{1-1,0,0}\}$ ,  $\{R_{1-1,1-1,1-1}, R_{0,0,0}, R_{0,0,1-1}, R_{1-1,0,1-1}, R_{1-1,0,0}\}$ ,  $\{R_{1-1,1-1,1-1}, R_{0,0,0}, R_{0,0,1-1}, R_{0,1-1,1-1}, R_{0,1-1,0}\}$ , etc. It can be easily shown that a write quorum intersects with both read and write quorums in this protocol.

### 3.3 Advantages

The advantage of the proposed approach is that it tolerates the failure of more than three quarter of the copies. This is because the proposed protocol allows us to construct a write quorum even if three out of four planes are unavailable as long as the hypotenuse copies are accessible. To show this, consider the case when only one plane which consists of four copies of vertices and hypotenuse copies are available, e.g., the set  $\{R_{1-1,1-1,1-1}, R_{0,0,0}, R_{0,0,1-1}, R_{1-1,0,1-1}, R_{1-1,0,0}\}$  is available as shown in Fig. 1. A transaction in the proposed can be executed successfully by accessing those copies in a quorum. Hence the write quorum in the proposed protocol is formed by accessing those available copies. Read operations, on the other hand, need to access the available hypotenuse copies.

Thus the proposed protocol enhances the fault-tolerance in write operations compared to the grid configuration protocol. Moreover, proposed protocol ensures that read operations have a significantly lower cost, i.e., two copies, and have a high degree of availability, since they are not vulnerable to the failure of more than three quarter of the copies. Write operations, on the other hand, are more available than the grid-based configuration protocol since only five copies are needed to execute write operations.

## 4 Performance Analysis

In the analysis of the update algorithm we focus on the amount of communication required to achieve consistency and provide probabilistic guarantees for successful

and appropriate results for queries. To this end, we compared the proposed scheme with ROWA when the number of copies is set to 16 (i.e.,  $N=16$ ). We also assumed that all copies have the same availability.

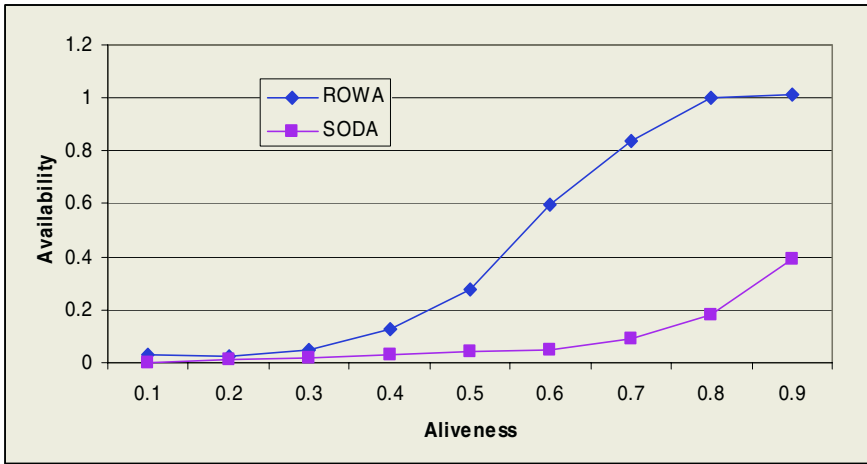


Fig. 2. Comparison of the write availability between SODA and ROWA

The result of the experiment is shown in Fig. 2. As shown, the proposed scheme has the lowest cost for write operation compared to ROWA protocol. This is because of the fact that in the ROWA protocol, an update operation needs to access all the replicas of the file in the system. Thus, the communication cost of an update operation in ROWA protocol is directly proportional to the number of replicas. In contrast, the proposed protocol needs only 5 copies at most, which results in significantly lower communication costs for comparable data availability.

## 5 Conclusions and Future Directions

The problem of protocol for maintaining replicated data has been widely studied in the distributed database systems. Recently, the need to support replication over wide-area networks and to use the Internet infrastructure as the basis for building a perpetual data store has spawned new research directions. Until recently, the challenges in providing high availability to P2P systems is poorly understood and only now being studied. Existing protocols are designed primarily to achieve high availability by updating a large fraction of the copies which provides some (although not significant) load sharing. We presented a new quorum-based protocol for maintaining replicated data across distributed P2P systems. The proposed approach is constructed on the organization of data in a box shape. We presented an analysis of the overhead and availability of the new protocol and showed that it performs better than the ROWA protocols. We are planning to implement the proposed protocol on various architectures including Data Grid, Peer-to-Peer, and Mobile systems.

**Acknowledgement.** The help of Maliha Omar is greatly appreciated. Without her kind support, this paper would not have been completed. The financial support of Deakin University is also gratefully acknowledged.

## References

1. S. Saroiu, P. K. Gummadi, and S. D. Gribble. A measurement study of peer-to-peer file sharing systems. In *MMCN*, 2002.
2. M. Mat Deris, J. Abawajy and H.M. Suzuri, "An Efficient Replicated Data Access Approach for Large-Scale Distributed Systems", In Proceedings of IEEE International Conference on Cluster and Grid Computing (CCGRID 2004).
3. Napster. <http://www.napster.com/>.
4. Gnutella. <http://www.gnutella.com/>.
5. KaZaA[KaZaA. <http://www.kazaa.com/>.
6. I. Clarke et al. Protecting Free Expression Online with Freenet. *IEEE Internet Computing*, 6(1), 2002.
7. Q. Lv, P. Cao, E. Cohen, K. Li, and S. Shenker. "Search and replication in unstructured peer-to-peer networks." In *Proc. of the 16th annual ACM International Conf. on Supercomputing (ICS'02)*, New York, USA, June 2002.
8. R. Akbarinia, V. Martins, E. Pacitti, P. Valduriez. *Replication and Query Processing in the APPA Data Management System*, in: "Int. Workshop on Distributed Data and Structures (WDAS'2004), Lausanne", 2004.
9. Anwitaman Datta, Manfred Hauswirth, Karl Aberer, Updates in Highly Unreliable, Replicated Peer-to-Peer Systems,
10. S. Rhea, C. Wells, P. Eaton, D. Geels, B. Zhao, H. Weatherspoon, and J. Kubiatowicz. Maintenance-free global data storage. *IEEE Internet Computing*, 5(5), 2001.
11. Serge Abiteboul, Angela Bonifati, Gregory Cobena, Ioana Manolescu, Tova Milo: Dynamic XML Documents with Distribution and Replication, SIGMOD 2003

# Explore Disease Mapping of Hepatitis B Using Geostatistical Analysis Techniques

Shaobo Zhong<sup>1</sup>, Yong Xue<sup>1,2,\*</sup>, Chunxiang Cao<sup>1</sup>, Wuchun Cao<sup>3</sup>, Xiaowen Li<sup>1</sup>,  
Jianping Guo<sup>1</sup>, and Liqun Fang<sup>3</sup>

<sup>1</sup> State Key Laboratory of Remote Sensing Science, Jointly Sponsored by the Institute of Remote Sensing Applications of Chinese Academy of Sciences and Beijing Normal University, Institute of Remote Sensing Applications, Chinese Academy of Sciences, P.O. Box 9718, Beijing 100101, China

<sup>2</sup> Department of Computing, London Metropolitan University, 166-220 Holloway Road, London N7 8DB, UK

<sup>3</sup> Institute of Microbiological Epidemiology, Academy of Military Medical Sciences, Beijing, China  
zhongshaobo163@163.com, y.xue@londonmet.ac.uk

**Abstract.** This paper presents the application of Exploratory Spatial Data Analysis (ESDA) and Kriging from GIS (ArcGIS8.3) in disease mapping through the analysis of hepatitis B in China. The research shows that geostatistical analysis techniques such as Kriging and ESDA have a good effect in disease mapping. Kriging methods can express properly the spatial correlation. Furthermore, unlike model-based methods, which largely depend on assumption for disease data, the Kriging method is more robust for the data. So it can be used more widely and is more operational. What's more, the Kriging method may be adapted to interpolate nonstationary spatial structure. This can expand its application more largely. At last, the Kriging method can estimate the uncertainty of prediction while many deterministic methods cannot do so. In conclusion, it is an effective operational procedure to gain a deep insight into the disease data through ESDA before mapping disease using the Kriging method.

## 1 Introduction

When we practise analysis and surveillance of diseases, the use made of maps of disease incidence are many and various. Disease maps can be used to assess the need for geographical variation in health resource allocation, or could be useful in research studies of the relation of incidence to exploratory variables (Lawson *et al.* 1999). Disease mapping usually chooses certain spatial interpolation method(s), and then creates a continuous surface of disease distribution according to geographically distributed sampling data of disease. There are all kinds of spatial interpolation methods, which include Inverse Distance Weighted (IDW), global polynomial, local polynomial, and Kriging etc. IDW, global polynomial and local polynomial belong to

---

\* Corresponding author.

deterministic spatial interpolation methods. This is, random effect is not taken into consideration for these methods. However, the Kriging method differs from these methods. It addresses that spatial data not only exist trend but also spatial variation. Differing from the deterministic interpolation methods, it introduces random factors and correlation factors, which are reasonable for many infectious diseases, into its activities (Carrat *et al.* 1992, Torok *et al.* 1997, Kleinschmidt *et al.* 2000, Croner *et al.* 2001). Thus, the result of disease mapping is more correct.

Exploratory Data Analysis (EDA) is an approach/philosophy for data analysis that employs a variety of techniques (mostly graphical) to insight into data itself such as uncover underlying structure, extract important variables, detect outliers and anomalies, test underlying assumptions, develop parsimonious models and determine optimal factor settings (<http://www.itl.nist.gov/div898/handbook/eda/>). Exploratory Spatial Data Analysis (ESDA) is EDA related to spatial data. Before Kriging the disease data, we often want to learn about the data first (e.g. whether the data exist spatial trend, which is important for selecting a proper Kriging) and we can preprocess data for meet certain needs (Johnston *et al.* 2001). ESDA enables us to gain a deeper understanding of disease data so that we can take correct action and make better decisions on issues relating to our data.

This paper first introduces EDA and Kriging. Then it presents an application of Kriging in disease mapping according to a case study of Hepatitis B in China. We conclude that geostatistical analysis techniques such as Kriging and ESDA have a good prospect in disease mapping. It is an effective operational procedure to gain a deep insight into the disease data through ESDA before mapping disease using Kriging methods.

## 2 Materials and Methods

### 2.1 Exploratory Spatial Data Analysis Techniques

EDA is an approach/philosophy for data analysis that employs a variety of techniques (mostly graphical) to gain deep insight into the data ( <http://www.itl.nist.gov/div898/handbook/eda/>). It is different from classical analysis or Bayesian analysis in the procedure.

- For classical analysis, the sequence is:  
Problem, Data, Model, Analysis, Conclusions
- For EDA, the sequence is:  
Problem, Data, Analysis, Model, Conclusions
- For Bayesian, the sequence is:

Problem, Data, Model, Prior Distribution, Analysis, Conclusions.

For EDA, clearly seen from the above, the data collection is not followed by a model imposition, rather it is followed immediately by analysis with a goal of inferring what model would be appropriate. EDA tries to uncover and understand the data from the data itself. So it has unique advantages over others.



ESDA is a special EDA, which aims at the spatial data. With ESDA, we can:

- Examining the distribution of spatial data,
- Looking for global and local outlier,
- Looking for global trend,
- Examining semivariogram/covariance and spatial structure and directional variation of the data.

In epidemiological study, all kinds of disease data hold their own characteristics (e.g. spatial structure and distribution etc.). In order to ascertain or verify these characteristics, ESDA provides us with some good approaches. Now, almost all the mainstream GIS software packages are equipped with geostatistical analysis tools. For instance, ArcGIS developed by ESRI provides Geostatistical Analyst as an extension. It includes these ESDA tools: Histogram, QQPlot, Voronoi map, Trend Analysis and Semivariogram/Covariance cloud etc (Johnston *et al.* 2001).

## 2.2 Kriging Method

The kriging method was put forward by a South African mining engineer D.G. Krige in 1951 and was developed by a famous French geographer G. Matheron (Matheron 1963). The method absorbs the concept of geostatistics, which addresses that any continuous properties in geo-space are quite irregular and cannot be modeled using simple smoothing mathematical function, but can be depicted properly with random surface. The property changing continuously along with the geo-space is called as “regionalized variable”. It can be used in depicting continuous index variables such as air pressure, elevation and so on. Though the disease rates, unlike air pressure or elevation, holds obvious continuously distributed characteristics, health data are better examined by methods that assume that disease rates are spatially continuous (Rushton 1998). In practice, this assumption is reasonable for most widely distributed diseases.

The interpolation model of Kriging can be expressed as follows:

$$Z(s) = m(s) + \varepsilon_1(s) + \varepsilon_2 \quad (1)$$

where  $Z(s)$  denotes the interpolation value, which is composed of three parts:  $m(s)$  reflects the spatial trend of the data,  $\varepsilon_1(s)$  is the variation relevant to the change of spatial location  $s$ . And  $\varepsilon_2$  is the residual (Gaussian noise), which has mean 0 and covariance  $\sigma^2$  in space and has nothing to do with the change of the spatial location.  $s$ , which is looked on as the position expressed with  $x$ (longitude),  $y$ (latitude) ordinates, denotes the location of sampling points.

In generally,  $\varepsilon_1(s)$  is presented with semivariogram  $\gamma(h)$  in Kriging Model. Semivariogram, only relevant to the distance  $h$  of sample point pairs (this characteristic is called as stationary), reflects the effect on which the change of spatial location have and be expressed as the function of  $h$ . Usually, semivariogram is monofonic increasing function of  $h$  and reflects the change of spatial correlation along with  $h$ , i.e. the closer the distance is, the stronger the spatial correlation is. Versus, the weaker the correlation is.

All kinds of Kriging models, including Simple kriging, Ordinary kriging, Universal kriging, Indicator Kriging, Probability Kriging etc., are based on the above formula (1). Each Kriging model is suited for specific situation and should be chosen seriously on purpose of best prediction.

### 2.3 Description of the Data and Processing

China is a high prevalence area of Hepatitis B. Several nation-wide censuses of hepatitis B show the proportion of the HBsAg carriers is over 10% on average and the prevalence of HBV over 60%. Furthermore, reported acute hepatitis cases are 2,700,000 every year according to the statistics of CDC in China. Hepatitis B has been one of the most serious problems of public health in China.

The data for this research were obtained from the statistics of Hepatitis B between 1994 ~ 1998 when the nation-wide screening was carried out thoroughly. Thus, there is a great deal of high quality and detailed sample data. Nevertheless, west and north of China have less sample data than other places such as middle, south and east (Fig. 1) due to different administrative region size and imbalance of socioeconomic development.

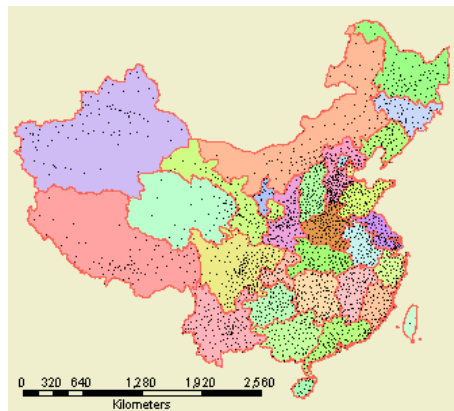


**Fig. 1.** The distribution of sampling points all over the nation without some islands in Southern Sea

In order to carry out the preprocessing and mapping, we have mainly collected the following data: 1) 1994-1998 county level new cases data of hepatitis B, 2) 1994-1998 county level age-grouped census and 3) 1994 screening data of hepatitis B all over the nation. We first calculate Standardized Mortality Ratio (SMR) of Hepatitis B from the above data ([http://www.paho.org/English/SHA/be\\_v23n3-standardization.htm](http://www.paho.org/English/SHA/be_v23n3-standardization.htm)), then mapping SMR of Hepatitis B in China using Geostatistical techniques including ESDA, Kriging etc.

## 3 Result and Discussion

### 3.1 Trend in the Data

Trend analysis is very important for the subsequent choice of Kriging model. In ArcGIS, Trend analysis tool provides a three-dimensional perspective of the data. The locations of the sampling points are plotted on the x, y plane. Above each sampling

point, the value is given by the height of a stick in the z dimension. Especially noteworthy, the values of z are projected onto the x, z plane and the y, z plane, which makes users more easily find out the trend of the data.

Fig. 2, plotted from the disease data of 1994, shows the space distribution of the sampling points of the disease through the Trend Analysis tool. The population data are derived from the 1994~1998 censuses. The disease data were provided by Institute of Microbiological Epidemiology, Academy of Military Medical Sciences, China. From the graph, we can find out clearly that there is nonlinear trend (e.g. quadratic) from the data set. Thus, we may choose Ordinary Kriging or Universal Kriging to interpolate the data because they both can detrend the data.

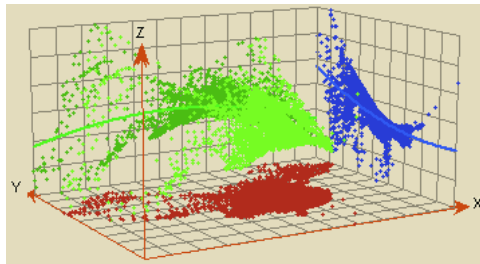


**Fig. 2.** Disease data of 1994 visualization in 3D space, x, y represent the locations of the disease sampling points and z is the SMR of the disease

### 3.2 Distribution of the Data Set

Certain Kriging methods work best if the data is approximately normally distributed (a bell-shaped curve). Furthermore, Kriging also relies on the assumption of stationary. In many cases, the distribution of the original data maybe not meet the need of the Kriging model and it is necessary to transform the data (e.g. Logarithmic transformation, Box-Cox transformation and Arcsine transformation). Histogram tool of geostatistical analyst extension in ArcGIS can explore the distribution of the data and make transformation, if necessary, for the data.

Before transformation, quite obviously, the distribution has a positive skewness from the histogram of the SMR data of 1994. By performing the Box-Cox transformation and adjusting the parameter, we produce a fairly good-shaped distribution.

### 3.3 Empirical Semivariogram

Semivariogram is a key component in a Kriging model. Exploring of the semivariogram mainly is to fit its model. There are many commonly used models for semivariogram (Edward *et al.* 1990). Figure 3 is the empirical semivariogram of the SMR of 1994, which is plotted using ArcGIS. For a large number of data, empirical semivariogram is an effective approach to fit the semivariogram. From the graph (a) and (b), we infer that the semivariogram of the data exists obvious anisotropy. The anisotropy is presented in (a) (spherical models with different parameters) and (b) (the

ellipse). Here, we chose the spherical model to fit the scatter points. For more information about empirical semivariogram, and fitting models, please refer to ArcGIS.

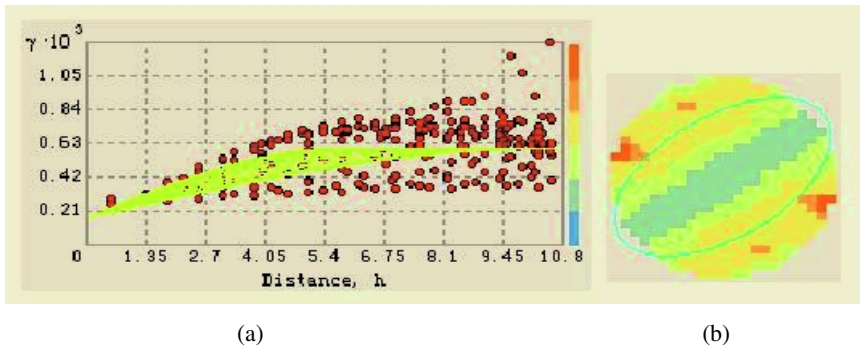


**Fig. 3.** Empirical semivariogram of the SMR of 1994. (a) presents different fit models changing with direction, and (b) presents the semivariogram surface

### 3.4 Mapping Disease and Results Validation

From sections 3.1, 3.2 and 3.3, finally, we can choose a proper Kriging model to interpolate the data, here Universal Kriging, semivariogram model is spherical, exists anisotropy and the data are transformed by Box-Cox with parameter 0.65 at first. With the Kriging tool from ArcGIS, we get the interpolation map. Figure 4 is produced from the data of 1994.

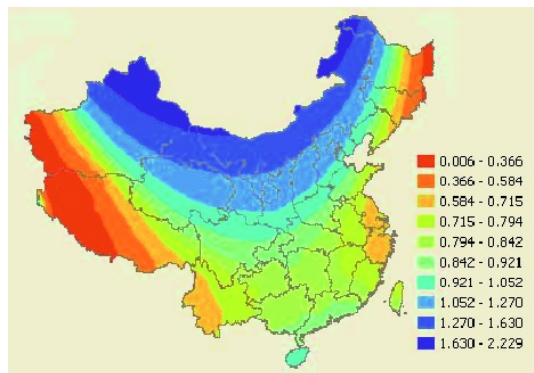


**Fig. 4.** SMR mapping result of hepatitis B of 1994 using Universal Kriging

When producing the result map using ArcGIS, simultaneously we get the validation result (Figure 5). The Kriging method allows us to validate the predicted values. There are two main validation methods: Cross-validation and Validation. Figure 5 is the validating result of predicted SMR of 1994 using Cross-validation. From this figure, we can see the precision of mapping is quite high. This implies that Kriging methods are suitable for the disease mapping.

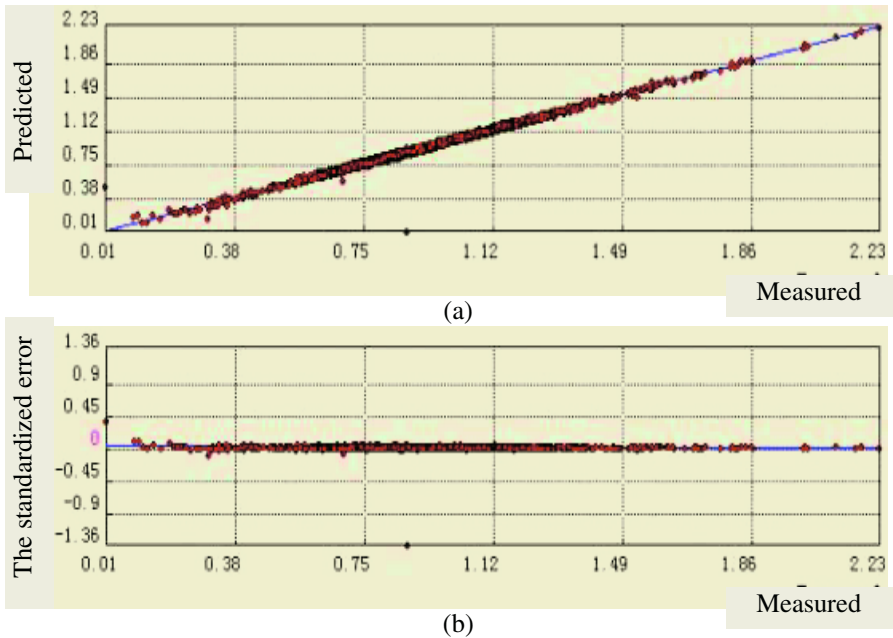


**Fig. 5.** Cross validation result. (a) is the comparison of predicted values and observed values and (b) is the standardized error, which is the square root of what is called Kriging variance and is a statistical measure of uncertainty for the prediction

## 4 Conclusions

Research on disease mapping covered a long history. All kinds of methods from simple ones such as point map, choropleth map and so on to complex ones like model-based methods, Kriging etc. provide analysis and surveillance of disease with strong measures. In general, complex model-based methods are more effective than the simple ones and produce more accurate results. This paper presents the application of ESDA and Kriging in disease mapping through the analysis of hepatitis B in China. The research shows that geostatistical techniques such as Kriging and ESDA have a good effect in disease mapping. Kriging methods can express properly the spatial correlation. Furthermore, unlike model-based methods, which largely depend on assumption for disease data (Bailey 2001), the Kriging method is more robust for the data. So it can be used more widely and is more operational. What's more, the Kriging method may be adapted to interpolate nonstationary spatial structure (Brenning *et al.* 2001). This can expand its application more largely. At last, the Kriging method can estimate the uncertainty of prediction while many deterministic methods cannot do so. In conclusion, it is an effective operational procedure to gain a deep insight into the disease data through ESDA before mapping disease using the Kriging method.

## Acknowledgement

This publication is an output from the research projects “CAS Hundred Talents Program” and “Innovation Project, Institute of Remote Sensing Applications” funded by Chinese Academy of Sciences. The authors wish to acknowledge related departments and individuals.

## References

1. Bailey, T.C., 2001, Spatial statistical methods in health. *Cad Saúde Públ*, 17: 1083-1098.
2. Brenning, A., and Boogaart, K.G.v.d., 2001, Geostatistics without stationary assumptions within GIS. Proceedings of 2001 Annual Conference of the International Association for Mathematical Geology, Cancun, Mexico, September 6-12, 2001.
3. Carrat, F., and Valleron, A.J., 1992, Epidemiologic mapping using the “kriging” method: application to an influenza-like illness epidemic in France. *American Journal of Epidemiology*, 135(11):1293-1300.
4. Croner, C.M., and Cola, L.D., 2001, Visualization of Disease Surveillance Data with Geostatistics. Presented at UNECE(United Nations Economic Commission for Europe) work session on methodological issues involving integration of statistics and geography, Tallinn, September 2001, available at <http://www.unece.org/stats/documents/2001/09/gis/25.e.pdf>.
5. Edward, H., Isaaks, R., and Mohan, S., 1990, *Applied Geostatistics*, Oxford University Press.
6. Johnston K., Ver Hoef, J.M., Krivoruchko, K., and Lucas N., 2001, *Exploratory Spatial Data Analysis*. In *Use ArcGIS Geostatistical Analyst* (digital book), edited by ESRI (San Diego: ESRI), pp. 81-112.
7. Kleinschmidt, I., Bagayoko, M., Clarke, G.P.Y., Craig, M., and Le Sueur, D., 2000, A spatial statistical approach to malaria mapping. *International Journal of Epidemiology*, 29(2):355-361.
8. Lawson, A.B., Böhning, D., Biggeri, A., Lesaffre, E., and Viel, J.F., 1999, Disease Mapping and Its Uses. In *Disease Mapping and Risk Assessment for Public Health*, edited by A.B. Lawson (New York: John Wiley & Sons Ltd.), pp. 3-13
9. Matheron, G., 1963, Principles of geostatistics. *Economic Geology*, 58: 1246-66.
10. NIST/SEMATECH, e-Handbook of Statistical Methods, 2004, <http://www.itl.nist.gov/div898/handbook/eda/section1/eda11.htm>, accessed on November 5, 2004.
11. Rushton, G., 1998, Improving the geographic basis of health surveillance using GIS. In *GIS and Health*, edited by A. Gatrell and M. Loytonen(Philadelphia: Taylor and Francis, Inc.), pp. 63-80.
12. Standardization: A Classic Epidemiological Method for the Comparison of Rates, [http://www.paho.org/English/SHA/be\\_v23n3-standardization.htm](http://www.paho.org/English/SHA/be_v23n3-standardization.htm), accessed on November 5, 2004.
13. Torok, T.J., Kilgore, P.E., Clarke, M.J., Holman, R.C., Bresee, J.S., and Glass, 1997, Visualizing geographic and temporal trends in rotavirus activity in the United States, 1991 to 1996. *Pediatric Infectious Disease Journal*, 16(10):941-46.

# eMicrob: A Grid-Based Spatial Epidemiology Application

Jianping Guo<sup>1</sup>, Yong Xue<sup>1,2,\*</sup>, Chunxiang Cao<sup>1</sup>, Wuchun Cao<sup>3</sup>, Xiaowen Li<sup>1</sup>,  
Jianqin Wang<sup>1</sup>, and Liqun Fang<sup>3</sup>

<sup>1</sup> State Key Laboratory of Remote Sensing Science, Jointly Sponsored  
by the Institute of Remote Sensing Applications of Chinese Academy of Sciences,  
and Beijing Normal University, Institute of Remote Sensing Applications,  
Chinese Academy of Sciences, P.O. Box 9718, Beijing 100101, China

<sup>2</sup> Department of Computing, London Metropolitan University, 166-220 Holloway Road,  
London N7 8DB, UK

<sup>3</sup> Institute of Microbiology and Epidemiology, the Academy of Military Medical Sciences,  
the Chinese PLA, Beijing 100071, PR China  
gjjpgis@163.com, y.xue@londonmet.ac.uk

**Abstract.** The use of Grid technologies allows us to make progress in the prediction accuracy of epidemiological patterns, epidemiological modeling, risk predictions of infectious diseases etc by combining the geo-information and molecular simulation analysis methods. In this paper, we mainly design the eMicrob, in particular, build up the e-Microbe miniGrid deployed in IRSA, CAS and IME, the Chinese PLA. The architecture is as follows: Firstly we review related grid applications that are motivating widespread interest in Grid concepts within the scientific and engineering communities. Secondly we talk about the key methodologies and strategies involved in the construction of eMicrob. In the third section, the system design of the eMicrob, in particular about the architecture of the eMicrob miniGrid is discussed. Finally, we draw some conclusion in the process of the building of eMicrob and make some discussion about the challenges. It has been proven that the methods based on the Grid technologies are revolutionary and high efficient through the experience of the establishment and deployment of the e-Microbe miniGrid.

## 1 Introduction

Epidemiologists study a diverse range of health conditions as well as the impact that various exposures have on the manifestation of disease. However, we have done some new researches in the epidemiology (science of the public health, <http://www.acepidiology2.org/aboutepid/whatis.asp>) based on the new emerging technology — Grid computing, integrated with geographical information system (GIS) and remote sensing (RS), which will establish a virtual organization comprised of scientists and engineers from many different fields and discipline. Grid computing, as a new technology, is mainly concerned with “coordinated resource sharing and

---

\* Corresponding author.



problem solving in dynamic, multi-institutional virtual organizations.” (Foster *et al.* 2001). A principal objective in the development of Grid computing is to make such resources available to users, regardless of their geographical location or institutional affiliation. While this goal is some way from being achieved, we have developed eMicrob miniGrid in the use of Grid tools, which allows us to make progress in the prediction accuracy of epidemiological patterns, epidemiological modeling, risk predictions of infectious diseases etc by combining the geo-information and molecular simulation.

Now through the eMicrob project we know that patterns and risk predictions can be made through GIS, by which we can study the dynamics of the epidemiological diseases based on above-mentioned environment factors achieved from remote sensing based on the grid platform. The undergoing eMicrob project benefits from grid and spatial technologies in various ways.

In this paper, we firstly introduce the related Grid projects, as good paradigms, which will help us to design the eMicrob system more precisely. The design of the eMicrob miniGrid is outlined and the architecture of the eMicrob miniGrid is discussed in details. At the end of this paper, we draw some conclusions and make discussion about the challenges eMicrob is encountering.

## 2 Methodology and Strategy

The eMicrob aims at building up a Grid platform (eMicrob miniGrid) in the long run, which will provide secure access to heterogeneous data and expensive resources in different locations, facilitate the study of transmission pattern, spatial distribution patterns, epidemiological trends, even advance the risk prediction precision about the infectious diseases i.e. Severe Acute Respiratory Syndrome (SARS), schistosomiasis (Savioli *et al.* 1997), avian influenza, malaria and cholera, etc.

We take advance of the following methodologies and strategies to design and construct the eMicrob. First, we build up a science team comprising of 3 kinds of technician, i.e. developer of code, epidemiologist and specialist from spatial domains. Second, we build our different database based on the SRB (<http://www.npaci.edu/DICE/SRB/>) technology. Moreover, we deploy the miniGrid on the platform – HIT-SIP developed by us .now we will expound on it. HIT-SIP (Wang *et. al.*, 2004) Grid platform in Institute of Remote Sensing Applications, Chinese Academy of Science is an advanced High-Throughput Computing Grid testbed using Condor developed by Department of Computer Sciences, University of Wisconsin-Madison. Heterogeneous computing nodes include two sets of Linux computers and WIN 2000 professional computers and one set of WIN XP computer provide stable computing power. The Grid pool uses java universally to screen heterogeneous characters. In general, users can use the heterogeneous Grid and share its strong computing power to process remote sensing images with middlewares as if in one supercomputer. Across the HIT-SIP platform, we can process and analyze the remote sensed images, for example, supervised classification and unsupervised classification and retrieval of various environment factors, which will be used in such discipline as biology, public health, and other spatially related disciplines.



### 3 Architecture of the eMicrob MiniGrid

To build the e-Microbe miniGrid, we deployed the miniGrid between IME Grid center (8 nodes) and IRSA Grid center (10 nodes). Both centers are required to use such universal grid platform as Globus, Condor or Condor-G as a starting point in order to develop the web data portals and computing portals, moreover, the epidemiologist and RS and GIS scientists can use them easily.

The framework consists of the following components:

- eMicrob User Interface and Web Portal Service, including data portal
- All kinds of databases and Model Pools
- Data Cache
- Application Modules

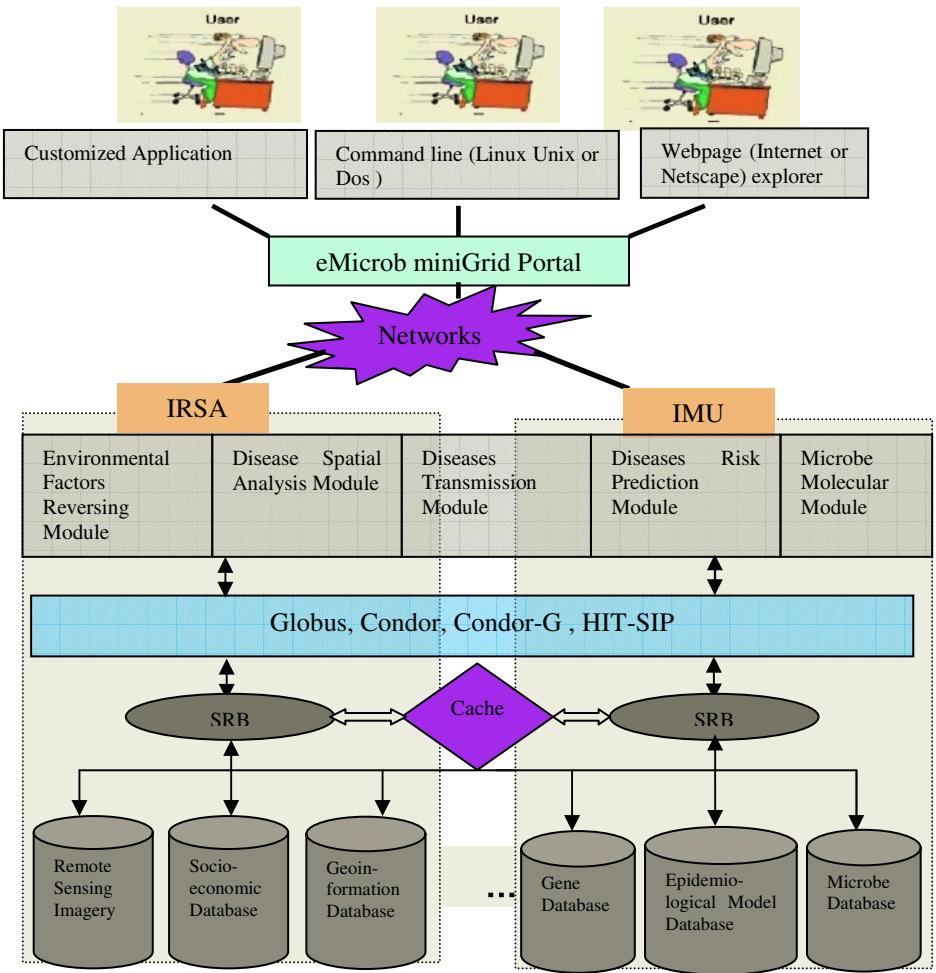


Fig. 1. The architecture of the eMicrob miniGrid

Based on the above-mentioned database components and computer tools, the architecture of the eMicrob miniGrid is given in Figure 1.

## 4 Conclusions and Results

The eMicrob miniGrid has provided a new platform of epidemiology investigation on which we collect remotely sensed data and other related data. Then integrate them into epidemiology applications researches, based on which analyses of microbe and/or virus combined with the real-time experimental data, are made and visualization are resulted in.

The science outcome based on the eMicrob miniGrid not only include the outcomes of spatial domain, such as we can disclose potential links between remotely sensed factors and specialized diseases (Beck *et al.* 2000), which has been proven prevalent in the research of epidemiological diseases, but also include ones of epidemiological disease such as disease controlling and prediction, and rules of the microorganism variances, the character of hepatitis B virus or the coronavirus causing SARS, taking it for example, can be analyzed on such eMicrob miniGrid platform.

We think that the scientist, both from spatial information and epidemiological fields, will greatly promote their researches in the epidemiological disease and in the end will provide more scientific information to the government officials to do correct decision-making. Meanwhile, through the experience of the design of the eMicrob and the implementation of the miniGrid, we recognize that the method based on the eMicrob miniGrid has made the study of the epidemiological diseases change deeply and will have a great potential impact for it can make the epidemiology and microbe discipline to make great stride in the near future.

## Acknowledgements

This publication is an output from the research projects “CAS Hundred Talents Program” and “Innovation Program” funded by IRSA, CAS. The authors wish to acknowledge related departments and individuals.

## References

- Foster I., Kesselman C., Tuecke S., 2001, “The Anatomy of the Grid: Enabling Scalable Virtual Organizations”. *International Journal of Super-computer Applications*, 15(3):. 200-222.
- Beck L. R., Bradley M, Lobitz Byron L. Wood, 2000, Remote Sensing and Human Health: New Sensors and New Opportunities. *Emerging Infectious Diseases*, Vol. 6, No. 3, May–June 2000:217-226.
- Savioli, L., Renganathan, E., Montresor, A., Davis, A., Behbehani, K., 1997, Control of schistosomiasis – a global picture. *Parasitology Today*, 11, 444-448.
- Jianqin Wang, Xiaosong Sun, Yong Xue, Yanguang Wang, Ying Luo, Guoyin Cai, Shaobo Zhong, and Jiakui Tang, 2004, Preliminary Study on Unsupervised Classification of Remotely Sensed Images on the Grid. *Lecture Notes in Computer Science*, Vol. 3039, pp.995-1002.

# Self-organizing Maps as Substitutes for K-Means Clustering

Fernando Bação<sup>1</sup>, Victor Lobo<sup>1,2</sup>, and Marco Painho<sup>1</sup>

<sup>1</sup> ISEGI/UNL, Campus de Campolide, 1070-312 LISBOA, Portugal  
bacao@isegi.unl.pt

<sup>2</sup> Portuguese Naval Academy, Alfeite, 2810-001 ALMADA, Portugal  
vlobo@isegi.unl.pt

**Abstract.** One of the most widely used clustering techniques used in GISc problems is the k-means algorithm. One of the most important issues in the correct use of k-means is the initialization procedure that ultimately determines which part of the solution space will be searched. In this paper we briefly review different initialization procedures, and propose Kohonen's Self-Organizing Maps as the most convenient method, given the proper training parameters. Furthermore, we show that in the final stages of its training procedure the Self-Organizing Map algorithms is rigorously the same as the k-means algorithm. Thus we propose the use of Self-Organizing Maps as possible substitutes for the more classical k-means clustering algorithms.

## 1 Introduction

The widespread use of computers and Geographical Information Systems (GIS) made available a huge volume of digital geo-referenced data (Batty and Longley 1996). This growth in the amount of data made multivariate data analysis techniques a central problem in Geographical Information Science (GISc). Amongst these techniques, cluster analysis (Jain, Murty et al. 1999) is one of the most used, and it is usually done using the popular k-means algorithm. Research on geodemographics (Openshaw, Blake et al. 1995; Birkin and Clarke 1998; Feng and Flowerdew 1998; Openshaw and Wymer 1994), urban research (Plane and Rogerson 1994; Han, Kamber et al. 2001), identification of deprived areas (Fahmy, Gordon et al. 2002), and social services provision (Birkin, Clarke et al. 1999) are examples of the relevance that clustering algorithms have within today's GISc research.

There have been a number of tests comparing SOM's with k-means (Balakrishnan, Cooper et al. 1994; Openshaw and Openshaw 1997; Waller, Kaiser et al. 1998). Conclusions seem to be ambivalent as different authors point to different conclusions, and no definitive results have emerged. Some authors (Flexer 1999; Balakrishnan, Cooper et al. 1994; Waller, Kaiser et al. 1998) suggest that SOM performs equal or worst than statistical approaches, while other authors conclude the opposite (Openshaw and Openshaw 1997; Openshaw, Blake et al. 1995).

The main objective of this paper is to analyze the performance of the SOM and k-means in clustering problems, and evaluate them under specific conditions. We

review both algorithms and then compare their performance on specific problems, using two synthetic datasets, and three real-world datasets.

## 2 K-Means Algorithm and Its Initialization

The k-means algorithm is widely known and used so only a brief outline is presented (for a thorough review see (Kaufman and Rousseeuw 1990; Fukunaga 1990; Duda, Hart et al. 2001)). K-means is an iterative procedure, to place cluster centers, which quickly converges to a local minimum of its objective function (Bradley and Fayyad 1998; Kanungo, Mount et al. 2002). This objective function is the sum of the squared Euclidean distance (L2) between each data point and its nearest cluster center (Selim and Ismail 1984; Bradley and Fayyad 1998). This is also known as “square-error distortion” (Jain and Dubes 1988). It has been shown that k-means is basically a gradient algorithm (Selim and Ismail 1984; Bottou and Bengio 1995) which justifies the convergence properties of the algorithm. The original online algorithm (MacQueen 1967) is as follows:

```

Let      k be the predefined number of centroids
         n be the number of training patterns
         X be the set of training patterns  $\mathbf{x}_1, \mathbf{x}_2, \dots, \mathbf{x}_n$ 
         P be the set of k initial centroids  $\mu_1, \mu_2, \dots, \mu_k$  taken from X
          $\eta$  be the learning rate, initialized to a value in  $]0, 1[$ 
1  Repeat
2      For i=1 to n
3          Find centroid  $\mu_j \in P$  that is closer to  $\mathbf{x}_i$ 
4          Update  $\mu_j$  by adding to it  $\Delta\mu_j = \eta(\mathbf{x}_i - \mu_j)$ 
5          Decrease  $\eta$ 
6      Until  $\eta$  reaches 0

```

There are a large number of variants of the k-means algorithm. In this study we use the generalized Lloyd’s algorithm (Duda, Hart et al. 2001), which yields the same results as the algorithm above (Bottou and Bengio 1995). The popularity of this variant in statistical analysis is due to its simplicity and flexibility. It does not, however, specify how the initial centroids should be selected. Due to the gradient nature of the algorithms, these initial centroids have a decisive effect on which areas of the solution space can be searched. In all but the simplest cases the solution space contains many local optima to which the k-means algorithm may converge. To guarantee that a good solution will be found, multiple initializations of the algorithms are usually tested, and only the best final solution is kept.

By far the most common initialization, called “Forgy Approach” (Peña, Lozano et al. 1999), consists on randomly selecting  $k$  of available data patterns as centroids. This method has as main advantage it’s simplicity: the selection requires no prior knowledge or computational effort, and multiple initializations will usually cover rather well the solution space. This is the initialization procedure used by default by software packages such as SAS Enterprise Miner, Matlab, and Clementine.

Instead of choosing  $k$  samples, we may divide the dataset into  $k$  subsets, and then use the centroids of these sets as seeds. We will call this the “random selection method” (Peña, Lozano et al. 1999). It is similar to calculating the centroid of the whole dataset and then obtaining  $k$  perturbations of this point (Thiesson, Meek et al. 1999). More random selection based algorithms have been proposed (Kaufman and Rousseeuw 1990; Cano, Cordón et al. 2002; MacQueen 1967) each with specific strengths and weaknesses. The order by which the initial seeds are presented may influence the final outcome, so re-ordering techniques have been used in (Fisher, Xu et al. 1992) and (Roure and Talavera 1998). Sensitivity to outliers is another important problem that can be minimized by repeating random selection. Various methods can be used to repeat selection and clustering on smaller datasets, such as proposed by (Bradley and Fayyad 1998).

Genetic algorithms are a well established technique to “guide randomness”, and thus can be used to generate successive random selections. This approach is followed by (Peña, Lozano et al. 1999). Several attempts have been made to avoid randomness in the selection of seeds by using deterministic density estimation methods, and selecting the points of higher density as seeds. Such is the approach followed in (Bradley and Fayyad 1998), (Fukunaga 1990). Another family of initialization methods comes from heuristics that use the distance between candidate seeds as a guide for their selection (Katsavounidis, Jay Kuo et al. 1994; Al-Daoud and Roberts 1994; Tou and González 1974).

Hierarchical clustering algorithms are widely used and can produce meaningful clusters of data, but they usually do not minimize the objective function of the  $k$ -means algorithm. They may however be used to obtain a good approximation that can be used as seed for its initialization. This approach was proposed in (Fisher 1987), and is used under different forms by (Higgs, Bemis et al. 1997; Snarey, Terrett et al. 1997; Meila and Heckerman 2001). The major drawback of these types of initializations is that they require a lot of computational effort.

Comparing results with all these initialization techniques is a Herculean task, and since simple random selection (or “Forgy Approach”) is the most common and simple, we will use it in the comparisons with SOM.

### 3 Self-organizing Maps and Their Use in Obtaining K-Clusters

Although the term “Self-Organizing Map” could be applied to a number of different approaches, we shall use it as a synonym of Kohonen’s Self Organizing Map (Kohonen 1982; Kohonen 2001), or SOM for short, also known as Kohonen Neural Networks.

The basic idea of a SOM is to map the data patterns onto a  $n$ -dimensional grid of neurons or units. That grid forms what is known as the output space, as opposed to the input space where the data patterns are. This mapping tries to preserve topological relations, i.e., patterns that are close in the input space will be mapped to units that are close in the output space, and vice-versa. So as to allow an easy visualization, the

output space is usually 1 or 2 dimensional. The basic SOM training algorithm can be described as follows:

```

Let X be the set of  $n$  training patterns  $\mathbf{x}_1, \mathbf{x}_2, \dots, \mathbf{x}_n$ 
W be a  $p \times q$  grid of units  $\mathbf{w}_{ij}$  where  $i$  and  $j$  are their
coordinates on that grid
 $\alpha$  be the learning rate, assuming values in  $]0,1[$ , initialized
to a given initial learning rate
 $r$  be the radius of the neighborhood function  $h(\mathbf{w}_{ij}, \mathbf{w}_{mn}, r)$ ,
initialized to a given initial radius
1 Repeat
2 For  $k=1$  to  $n$ 
3 For all  $\mathbf{w}_{ij} \in W$ , calculate  $d_{ij} = \|\mathbf{x}_k - \mathbf{w}_{ij}\|$ 
4 Select the unit that minimizes  $d_{ij}$  as the winner  $\mathbf{w}_{winner}$ 
5 Update each unit  $\mathbf{w}_{ij} \in W$ :  $\mathbf{w}_{ij} = \mathbf{w}_{ij} + \alpha h(\mathbf{w}_{winner}, \mathbf{w}_{ij}, r) \|\mathbf{x}_k - \mathbf{w}_{ij}\|$ 
6 Decrease the value of  $\alpha$  and  $r$ 
7 Until  $\alpha$  reaches 0

```

The neighborhood function  $h$  is usually a function that decreases with the distance (in the output space) to the winning unit, and is responsible for the interactions between different units. During training, the radius of this function will usually decrease, so that each unit will become more isolated from the effects of its neighbors. It is important to note that many implementations of SOM decrease this radius to 1, meaning that even in the final stages of training each unit will have an effect on its nearest neighbors, while other implementations allow this parameter to decrease to zero.

SOMs can be used in many different ways, even within clustering tasks (Baç¸o, Lobo et al. 2005). In this paper we will assume that each SOM unit is a cluster center, and thus a  $k$ -unit SOM will perform a task similar to  $k$ -means. It must be noted that SOM and  $k$ -means algorithms are rigorously identical when the radius of the neighborhood function in the SOM equals zero (Bodt, Verleysen et al. 1997). In this case the update only occurs in the winning unit just as happens in  $k$ -means (step 4).

## 4 Experimental Setting

### 4.1 Datasets Used

The data used in the tests is composed of 4 basic datasets, two synthetic and two real-world. The real-world datasets used are the well known iris dataset (Fisher 1936) and sonar dataset (Sejnowski and Gorman 1988). The iris dataset has 150 observations with 4 attributes and 3 classes, while the sonar dataset has 208 observations with 60 attributes and 2 classes. Two synthetic datasets were created. The first dataset, DS1, comprises 400 observations in two-dimensions with 4 clusters. Each of these clusters has 100 observations with a Gaussian distribution around a fixed center. The variance of these Gaussians was gradually increased during our experiments. The second data set, DS2, consists of 750 observations with 5 clusters with Gaussian distributions defined in a 16 dimensional space.

## 4.2 Robustness Assessment Measures

In order to access the performance of the two methods a set of three measurements was used. The first one is the quadratic error i.e., the sum of the squared distances of each point to the centroid of its cluster. This error is divided by the total dispersion of each cluster so as to obtain a relative measure. This measure is particularly relevant as it is the objective function of the k-means algorithm. Additionally, the standard deviation of the mean quantization error is calculated in order to evaluate the stability of the results found in the different trials. The second measure used to evaluate the clustering is the mean classification error. This measure is only valid in the case of classification problems and is the number of observations attributed to a cluster where they do not belong. Finally, a structural measurement is used in order to understand if the structural coherence of the groups is preserved by the clustering method. This measure is obtained by attributing to each cluster center a label based on the labels of the observations which belong to its Voronoi polygon. If more than one centroid receives a given label (and thus at least one of the labels is not attributed) then the partition is considered to be structurally damaged.

## 5 Results

Each dataset was processed 100 times by each algorithm, and the results presented in table 1 constitute counts or means. Table 1 presents a summary of the most relevant results. A general analysis of table 1 shows a tendency for SOM to outperform k-means. The mean quadratic error over all the datasets used is always smaller in the case of the SOM, although in some cases the difference is not sufficiently large to allow conclusions. The standard deviation of the quadratic error is quite enlightening showing smaller variations in the performance of the SOM algorithms. The class error indicator reveals a behavior similar to the mean quadratic error. Finally, the structural error is quite explicit making the case that SOM robustness is superior to k-means.

Looking closer at the results in different datasets, there is only one data set in which k-means is not affected by structural errors. The reason for this is related with the configuration of the solution space. In the sonar dataset the starting positions of the k-means algorithm are less relevant than in the other 3 datasets.

**Table 1.** Comparison of SOM and k-means on different datasets, using the average quadratic error, its standard deviation, average classification error, and average structural error, over 100 independent initializations

Dataset	Method	Quadratic error	Std(Qerr)	ClassErr	Struct Err
IRIS	SOM	86.67	0.33	9.22	0
	k-means	91.35	25.76	15.23	18
SONAR	SOM	280.80	0.10	45.12	0
	k-means	280.98	3.18	45.34	0
DS1	SOM	9651.46	470.36	1.01	0
	k-means	11341.49	2320.27	12.77	58
DS2	SOM	27116.40	21.60	7.40	0
	k-means	27807.97	763.22	15.51	49

The real-world dataset refers to enumeration districts (ED) of the Lisbon Metropolitan Area and includes 3968 ED's which are characterized based on 65 variables, from the Portuguese census of 2001. Exploratory analysis of this dataset using large size SOMs and U-Matrices suggests that we should consider 6 clusters within this dataset. To find the exact locations and members of these 6 clusters we applied a batch k-means algorithm to this data, and compared the results with those obtained with a 6x1 SOM. In both cases we repeated the experiment 100 times with random initializations. The quadratic error obtained with k-means was  $3543 \pm 23$  with a minimum of 3528, whereas with SOM we obtained  $3533 \pm 6$  with a minimum of 3529. These results show that the best clustering obtained with each method is practically the same, but on average SOM outperforms k-means and has far less variation in its results.

## 6 Conclusions

The first and most important conclusion that can be drawn from this study is that SOM is less prone to local optima than k-means. During our tests it is quite evident that the search space is better explored by SOM. This is due to the effect of the neighborhood parameter which forces units to move according to each other in the early stages of the process. This characteristic can be seen as an "annealing schedule" which provides an early exploration of the search space (Bodt, Cottrell et al. 1999). On the other hand, k-means gradient orientation forces a premature convergence which, depending on the initialization, may frequently yield local optimum solutions.

It is important to note that there are certain conditions that must be observed in order to render robust performances from SOM. First it is important to start the process using a high learning rate and neighborhood radius, and progressively reduce both parameters to zero. SOM's dimensionality is also an issue, as our tests indicate that 1-dimensional SOM will outperform 2-dimensional matrices. This can be explained by the fact that the "tension" exerted in each unit by the neighboring units is much higher in the case of the matrix configuration. This tension limits the plasticity of the SOM to adapt to the particular distribution of the dataset. Clearly, when using a small number of units it is easier to adapt a line than a matrix.

These results support Openshaw's claim which points to the superiority of SOM when dealing with problems having multiple optima. Basically, SOM offers the opportunity for an early exploration of the search space, and as the process continues it gradually narrows the search. By the end of the search process (providing the neighborhood radius decreases to zero) the SOM is exactly the same as k-means, which allows for a minimization of the distances between the observations and the cluster centers.

## References

- Al-Daoud, M. and S. Roberts (1994). *New Methods for the Initialisation of Clusters*. Leeds, University of Leeds: 14.
- Baao, F., V. Lobo, M. Painho (2005). "The Self-Organizing Map, Geo-SOM, and relevant variants for GeoSciences." *Computers & Geosciences*, Vol. 31, Elsevier, pp. 155-163.



- Balakrishnan, P. V., M. C. Cooper, V.S. Jacob, P.A. Lewis (1994). "A study of the classification capabilities of neural networks using unsupervised learning: a comparison with k-means clustering." *Psychometrika* 59(4): 509-525.
- Batty, M. and P. Longley (1996). *Analytical GIS: The Future. Spatial Analysis: Modelling in a GIS Environment*. P. Longley and M. Batty. Cambridge, Geoinformation International: 345-352.
- Birkin, M. and G. Clarke (1998). "GIS, geodemographics and spatial modeling in the UK financial service industry." *Journal of Housing Research* 9: 87-111.
- Birkin, M., G. Clarke, M. Clarke (1999). *GIS for Business and Service Planning. Geographical Information Systems*. M. Goodchild, P. Longley, D. Maguire and D. Rhind. Cambridge, Geoinformation.
- Bishop, C. M. (1995). *Neural Networks for Pattern Recognition*, Oxford University Press.
- Bodt, E. d., M. Cottrell, M. Verleysen (1999). Using the Kohonen Algorithm for Quick Initialization of Simple Competitive Learning Algorithms. ESANN'1999, Bruges.
- Bodt, E. d., M. Verleysen, M. Cottrell (1997). Kohonen Maps versus Vector Quantization for Data Analysis. ESANN'1997, Bruges.
- Bottou, L. and Y. Bengio (1995). Convergence Properties of the K-Means Algorithms. *Advances in Neural Information Processing System*. Cambridge, MA, MIT Press. 7 G: 585-592.
- Bradley, P. and U. Fayyad (1998). Refining initial points for K-means clustering. *International Conference on Machine Learning (ICML-98)*.
- Cano, J. R., O. Cordon, F. Herrera, L. Sánchez (2002). "A Greedy Randomized Adaptive Search Procedure Applied to the Clustering Problem as an Initialization Process Using K-Means as a Local Search Procedure." *International Journal of Intelligent and Fuzzy Systems* 12: 235-242.
- Duda, R. O., P. E. Hart, D. Stork (2001). *Pattern Classification*, Wiley-Interscience.
- Fahmy, E., D. Gordon, S. Cemlyn (2002). *Poverty and Neighbourhood Renewal in West Cornwall*. Social Policy Association Annual Conference, Nottingham, UK.
- Feng, Z. and R. Flowerdew (1998). Fuzzy geodemographics: a contribution from fuzzy clustering methods. *Innovations in GIS 5*. S. Carver. London, Taylor & Francis: 119-127.
- Fisher, D. H. (1987). "Knowledge Acquisition Via Incremental Conceptual Clustering." *Machine Learning* 2: 139--172.
- Fisher, D. H., L. Xu, N. Zard (1992). Ordering effects in clustering. *Ninth International Conference on Machine Learning*, San Mateo, CA.
- Fisher, R. A. (1936). "The use of Multiple Measurements in Taxonomic Problems." *Annals of Eugenics* VII(II): 179-188.
- Flexer, A. (1999). On the use of self-organizing maps for clustering and visualization. *Principles of Data Mining and Knowledge Discovery*. Z. J.M. and R. J., Springer. 1704: 80-88.
- Fukunaga, K. (1990). *Introduction to statistical patterns recognition*, Academic Press Inc.
- Han, J., M. Kamber, A. Tung (2001). *Spatial clustering methods in data mining. Geographic Data Mining and Knowledge Discovery*. H. Miller and J. Han. London, Taylor & Fancis: 188-217.
- Higgs, R. E., K. G. Bemis, I. Watson, J. Wikel (1997). "Experimental Designs for Selecting Molecules from Large Chemical Databases." *Journal of Chemical Information and Computer Sciences* 37(5): 861-870.
- Jain, A. K. and R. C. Dubes (1988). *Algorithms for clustering data*, Prentice Hall.
- Jain, A. K., M. N. Murty, P. Flynn (1999). "Data Clustering: A review." *ACM Computing Surveys* 31(3): 264-323.

- Kanungo, T., D. M. Mount, N. Netanyahu, C. Piatko, R. Silverman, A. Wu (2002). "An efficient k-means clustering algorithm: analysis and implementation." *IEEE Transactions on Pattern Analysis and Machine Intelligence* 24(7): 881-892.
- Katsavounidis, I., C.-C. Jay Kuo, Z. Zhang (1994). "A new initialization technique for generalized Lloyd iteration." *IEEE Signal Processing Letters* 1(10): 144 - 146.
- Kaufman, L. and P. J. Rousseeuw (1990). *Finding groups in data : an introduction to cluster analysis*. New York, John Wiley & Sons.
- Kohonen, T. (1982). *Clustering, Taxonomy, and Topological Maps of Patterns*. Proceedings of the 6th International Conference on Pattern Recognition.
- Kohonen, T. (2001). *Self-Organizing Maps*. Berlin-Heidelberg, Springer.
- MacQueen, J. (1967). Some methods for classification and analysis of multivariate observation. 5th Berkeley Symposium on Mathematical Statistics and Probability, University of California Press.
- Meila, M. and D. Heckerman (2001). "An Experimental Comparison of Several Clustering and Initialization Methods." *Machine Learning* 42: 9-29.
- Openshaw, S., M. Blake, C. Wymer (1995). Using neurocomputing methods to classify Britain's residential areas. *Innovations in GIS*. P. Fisher, Taylor and Francis. 2: 97-111.
- Openshaw, S. and C. Openshaw (1997). *Artificial intelligence in geography*. Chichester, John Wiley & Sons.
- Openshaw, S. and C. Wymer (1994). Classifying and regionalizing census data. *Census Users Handbook*. S. Openshaw. Cambridge, UK, Geo Information International: 239-270.
- Peña, J. M., J. A. Lozano, P. Larrañaga (1999). "An empirical comparison of four initialization methods for the k-means algorithm." *Pattern recognition letters* 20: 1027-1040.
- Plane, D. A. and P. A. Rogerson (1994). *The Geographical Analysis of Population: With Applications to Planning and Business*. New York, John Wiley & Sons.
- Roure, J. and L. Talavera (1998). Robust incremental clustering with bad instance orderings: a new strategy. *IBERAMIA 98 - Sixth Iberoamerican Conference on Artificial Intelligence*, Lisbon, Springer Verlag.
- Sejnowski, T. J. and P. Gorman (1988). "Learned Classification of Sonar Targets Using a Massively Parallel Network." *IEEE Transactions on Acoustics, Speech, and Signal Processing* 36(7): 1135 -1140.
- Selim, S. Z. and M. A. Ismail (1984). "k-means type algorithms: a generalized convergence theorem and characterization of local optimality." *IEEE Trans. Pattern Analysis and Machine Intelligence* 6: 81-87.
- Snarey, M., N. K. Terrett, P. Willett, D. Wilton (1997). "Comparison of algorithms for dissimilarity-based compound selection." *Journal of Molecular Graphics and Modelling* 15(6): 372-385.
- Thiesson, B., C. Meek, D. Chickering, D. Heckerman (1999). *Computationally Efficient Methods for Selecting Among Mixtures of Graphical Models*. Bayesian Statistics. J. M. Bernardo, J. O. Berger, A. P. Dawid and A. F. M. Smith. Oxford, UK, Oxford University Press. 6.
- Tou, J. and R. González (1974). *Pattern Recognition Principals*. Reading, MA, Addison Wesley Publishing Company.
- Waller, N. G., H. A. Kaiser, J. Illian, M. Manry (1998). "A comparison of the classification capabilities of the 1-dimensional Kohonen neural network with two partitioning and three hierarchical cluster analysis algorithms." *Psychometrika* 63(1): 5-22.

# Key Technologies Research on Building a Cluster-Based Parallel Computing System for Remote Sensing

Guoqing Li and Dingsheng Liu

45 BeiSanHuanXi Road, P.O. Box 2434, Beijing, 100086, China  
Open laboratory, Remote Sensing Satellite Ground Station, China Academic of Sciences  
{gqli, dsliu}@ne.rsgs.ac.cn

**Abstract.** Remote sensing image processing needs high performance computing to answer the fast growing data and requirement. Cluster-based parallel remote sensing image processing shows an effective way to overcome it. With an example of PIPS, paper gives basic theory of it, such as system structure, parallel model, and data distribution strategy and software integration and so on. Many experiments have proved that such technology can afford a receivable parallel efficiency with low cost hardware equipment. Moreover, it is friendly for experts who know remote sensing applications well and parallel computing less in developing their own parallel application implementations.

## 1 Introduction

In our information era, earth observation information has been the chief resource of information we have to handle. Remote sensing data is the mean part of EO information which comes from plane and satellite platforms. Remote sensing technology is fast developing on the filed of spatial resolution, spectrum resolution, time resolution, with which the data scale is expanding rapidly. A single scene of TM image with 7 bands can reach 280M disk storage. A global and big area geo-information always reaches to TB scale with in a single project. This information gives us more detail knowledge about our living environment.

However, the limit of processing speed and processing scale has been the bottleneck for remote sensing development and application. Most desktop workstations do not have sufficient computing power to perform such image processing. Generally large super-computers such as MPP are the main frameworks for such processing [1], while new researches on cluster system have shown the potential power and good performance to overcome such problem. Cluster system is based on current normal software and hardware desktops, such as linux and ANSC C/C++ . It gives a low cost, high operation possibility and expandability [2]-[3]. In some degree, it can be a perfect alternate plan of expansive Super Computers.

In this paper, we describe the design and implementation of Cluster-based Parallel Remote Sensing Processing System (PIPS). It is not only a general image processing parallel system, with the optimization of large image, but a special remote sensing image processing system. PIPS uses a message passing model based on MPICH standard which is designed to be the parallel desktop of PIPS. At the same time, PIPS is a

developing desktop for some experts who know remote sensing applications well and know parallel technology less. With the develop model, they can design their own parallel applications by easy methods within very short time, and finally they can reassemble a special parallel remote sensing image processing desktop.

## 2 System Structure

Mainly, the processing of remote sensing image is data parallel model. Large data quantity can cover up the profile of arithmetic parallel. In cluster, we want to take computation extension profile from the multi CPU and multi I/O capability. Data is not processing locally, which is send to distributed computer nodes and processed there. Finally, the results data will be send back and new image be created. This course is a representative data parallel structure. The most time cost is happened in the network transmission for large EO data.

### 2.1 Basic Structure

#### 2.1.1 Structure

In general, a whole running cluster processing system on remote sensing includes three chief modules, Initialization, Arithmetic Implementation and Finalization, shown in Fig. 1 as PIPS system. Firstly, Initialization module PIPSIInit contains the following tasks: setting system parameters (run-mode XT/VT), starting related processes (MPI and process control), initializing temporary files, parameter files and PIP image files. Second, PIPSRun, the Arithmetic Implementation module, is the main part of a PIPS routine. The difference of different algorithms can bring different routines. However, it always contains three steps, image sending (distribution), processing and collection. Lastly, Finalization is running by PIPSEnd module. Corresponding to PIPSIInit, it closes files, finishes processes and deletes rubbish.

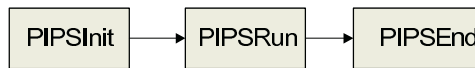


Fig. 1. structure

From such structure we can find that most initialization and finalization works is similar and which can be build into common modules. The difference of every processing function is realized in the part of PIPSRun, especially in some short subroutines.

#### 2.1.2 System Frame

Application Routines use library function to finish certain processing function and function library contains basic image processing routines. Generally, they have been designed to be parallel routines, and some of them are full processing units. Some routines, however, are much basically and generally, such as I/O operation, having been assembled to be a low level library Kernel Function Library. Some advance

function such as load balance, dynamic process management etc. MPI is the lowest support of PIPS system, which is invisible for application users and developer.

### 2.1.3 Multi-layer Parallel Model

There are three main parallel modes in remote sensing field, message-passing mode [4], share memory mode [5] and parallel file system mode [6]. Most parallel arithmetic in recent works all can be found form one of three modes. Each parallel mode above can be used to build a whole parallel processing system. Coming from different special research environment and research organization, such mode all have their superiority and inferiority. As many experimentation shown, in remote sensing processing, individual mode always cannot bring a perfect result mostly.

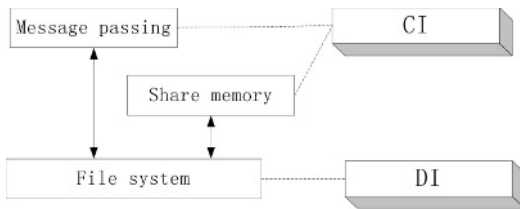


Fig. 2. Multi-layer parallel structure

Message-passing is most fast and steadily parallel mode, which has perfect standards system (PVM and MPI) and has been supported wildly by most parallel computer producers. Program based on Message-passing mode is clearly and readable, is also easily to build special parallel programming tools with their debugging and watching environment. However, such mode also brings the block of buffer and net transfer, especially for fine granularity parallel strategy. Share memory mode and Parallel file system mode can make the programming simply, reduce the changing of serial program. However, the parallel task control is too difficult to manage. Such modes is still in the research stage without stable and authoritative publish version. Uniform technical standard have not been confirmed.

However, such parallel modes can work together, and they do not exclude each other. There are two types of data transfer in the view of parallel architecture, CI (control information) and DI (data information), shown in Fig.2. Message-passing mode is fit for the CI, whereas parallel file system is fit for DI. Combining such three parallel modes, multi-layer parallel mode [9] can give better performance. There are two combinations: message-passing with parallel file system and share memory with parallel file system. In our next version of PIPS, we improve the parallel architecture by combining message-passing with parallel file system.

## 2.2 Data Distribution

As a basic model of message passing structure, large EO data have to be handled with data distribution operations, which can move target file data from one node to many nodes, and then collect them back as a whole. Data distribution is finalized by parallel

data I/O library. This library is the base of module programming of data parallel, which can simplify different, reduce time and improve effective. According to given image data, they can create distribute strategy with interior dispatching engine. The strategy can reach load balance, reduce communication and speed transfer.

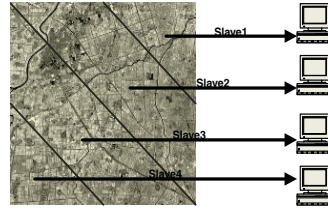
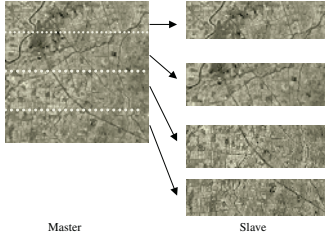


**Fig. 3.** whole image to line sequence image    **Fig. 4.** whole image to specially type

With parallel file system, such parallel I/O has been building in the parallel read and writes operation as a global file object, which can reduce 30% transmission time.

The general rule of data distribution is reducing communication and offering complete data for certain application function. It is not only a course of space distribution but a re-assembling course of data structure.

In remote sensing, distribution modes is following: whole image to whole image, whole image to line sequence image, whole image to column sequence image, whole image to cross sequence image, whole image to matrix and whole image to specially type. (As Fig. 3 and Fig. 4)

## 2.3 Implementation

### 2.3.1 Data Parallel

In large remote sensing image processing, the representative parallel mode is data parallel. The FOR sentence and DO sentence in sequence programs always means a lot of calculation and can cause parallel possibility, which means FOR and DO sentences can be done parallel by many computer nodes. In PIPS, a whole processing can be divided into three steps of image sending, image processing and image collection. Modularization is a good developing method for users and developers, because they need not consider the details of distribution and collection while keeping good parallel performance.

### 2.3.2 Algorithmic Parallel

Not all operations in remote sensing reach good parallel performance only with data parallel, especially the operations reacted to GIS. On the other hand, algorithmic parallel sometime can get better efficiency however. For instance, DEM establishment and wavelet transfer are typical algorithmic parallel implementations. PIPS provides **complex mode** to fit these conditions. Developers have to write PIPSRun part as a whole by themselves, which contributes to the customized function library.

### 3 Developing Toolkit

PIPS has powerful developing ability. Many remote sensing experts are very familiar with the theories and methods of remote sensing technology but they have less knowledge on parallel technology. The developing toolkit of PIPS can help them transfer their sequence program expediently.

#### 3.1 Function Library

In PIPS the functions are independently and the process loading is the main way of software integration. As shown in Fig. 5, Function library includes full program structure, the main part and other routines. What users should do is only little part of program routines, which have relationship with algorithm he want to carry out. The other part of routines, including complex control and interface function, should not be considered again. So the users can build up their whole parallel applications in a short time.

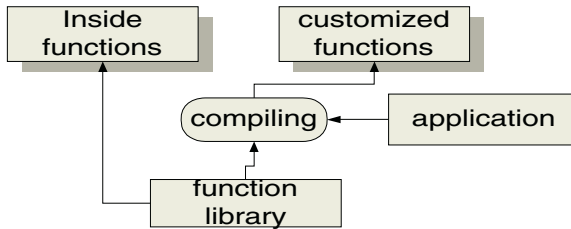


Fig. 5. function library

#### 3.2 Develop Mode

Different algorithms can be realized with different parallel mode, the simple mode and the complex mode, seen in Fig.. Most of applications, which can be simplified to be three steps, distribution, processing and collection, belongs to simple mode.

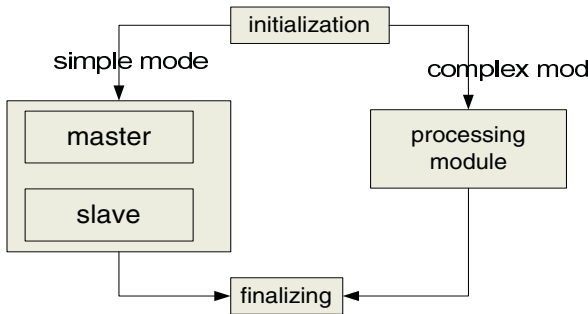


Fig. 6. developing mode

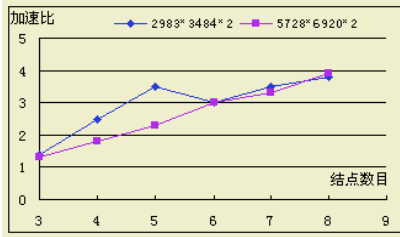


Fig. 7. parallel efficiency of Rotate

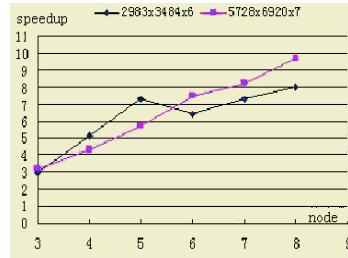


Fig. 8. Walsh transfer parallel efficiency

In this mode, what users should modify is only routines **pipsmaster** in master node and **pipsslave** in slave node. The other modules have been designed fitting this change automatically. For example, the K-L transfer [7], FFT transfer and classification operations are typical application of simple mode. The programming of this mode is clear, simple and easy to compare and debug.

However, there are still some applications of remote sensing cannot be formed with simple mode. To these applications, experts have to use special optimized algorithm. The complex mode of PIPS let it also can be involved in the whole structure of PIPS. Some applications include wavelet, DEM, SAR pre-processing [8], rotate, mosaic are typical complex mode.

### 3.3 Integrated Running Environment

PIPS is running on LINUX operation system with MPI parallel tools on cluster hardware. For an integration running system, many factors should be taken into account, auto detecting the running mode (VT/XT), static load balance, compute node selection, controlling the disk space, version conflicting and error control etc. Moreover, the running mode of MPI is very complex also. PIPS has build an integrated running environment, which can do above things at same time and automatically.

## 4 Experimental Results

In this section we present experiment results using PIPS system to perform a variety of image processing applications tasks. These experiments were done using a cluster of 9 PCs connected with 100M Ethernet. Experimental images were offered by RSGS and had three types. 7 band small TM images (2983 x 3484 x 7 band), 7 band whole TM images (5728 x 6920 x 7 band) and 7 band mosaic TM images (22000 x 27000 x 7 band).

Parallel efficiency in speedup index has three conditions also. To most remote sensing applications, standard PIPS parallel mode (simple mode) can do well enough, such as WALSH transfer.

Complex mode can bring enough good result for some special tasks, sometime they can reach linear speedup. For example, rotate operation with slant strip algorithm can do 20000 x 20000 or more large image with parallel efficiency great than 50% (parallel efficiency means here speedup/nodes).



When we use parallel file system replaces MPI parallel IO routines, the performance reaches a new standard. As an example, above rotate operation-computing speed reaches 1.70 times faster than MPI mode.

In the theories of classical parallel computing, the speedup is always less than the parallel nodes number. However, in the field of data complexity applications, speedup index sometime can large than parallel nodes number. The parallel cluster is not only increasing the CPU number but increasing the available hard disk space and the total memory size. Some problems are too large to processing without using swap memory space in single node, but they are still less than the real total memory of cluster. We have taken a mosaic example for AnHui Prov. China, which include 9 scenes TM images with bands of 5/4/3 together and PIPS costs less than 7 minutes, which cannot be successfully running on the normal PC platform.

## 5 Conclusions

In general, the problems of remote sensing image processing are data parallelism problems. Course-grain parallelism is the main method for them. The overall system is based on such parallelism. We have been doing some researches on fine-course type, for example, the operator of mosaic and wavelet.

As a typical cluster-based remote sensing data processing system, PIPS is successful in transferring the classical sequence programming to parallel programming. PIPS have been developed form 1996, which has three main versions, PIPS, PIPS2000, and PIPS2005. New version PIPS is adopted with multi parallel theory and reaches a high performance. It shows rather better result not only in realizing algorithms, parallel efficiency, and integration condition but also in developing desktop. An experiment system on whole satellite ground processing station is being built on the base of PIPS, which is the first taste with cluster parallel computation environment.

## Acknowledgement

This paper is fund by China National Key Research Project (863) “research on fast processing technology for large remote sensing information” and finished at open laboratory, RSGS, CAS.

## References

1. K.A.Hawick, H.A.James, Distributed High-Performance Computation for Remote Sensing, Proc. Of Supercomputing '97, San Jose, Nov. 1997, Technical report.
2. Chao-Tung Yang, Chi-Chu Hung, Parallel Computing in Remote Sensing Data Processing.
3. Chao-Tung Yang, Chih-Li Chang, Using a Beowulf Cluster For a Remote Sensing Application, 22<sup>nd</sup> Asian Conference on Remote Sensing, Nov, 2001
4. Marc Snir, MPI: The Complete Reference MIT Press 1996
5. <http://www.ict.ac.cn/chpc/dsm/dist.html>

6. Zhu Yaofei, Li Guoqing, The research and experimentation of parallel file system in remote sensing image parallel processing system, Master's thesis, China remote sensing satellite ground station.
7. Li Guoqing ,Li Xia, Liu Dingsheng parallel processing on K-L transfer(in Chinese) '98 academic conference of China remote sensing at Dalian
8. Chen Lin, Liu Dingsheng parallel processing research on SAR imaging(in Chinese) '98 academic conference of China remote sensing at Dalian
9. Li Guoqing,, Liu Dingsheng, Research work on parallel mode of geo-image processing, Journal of Image and Graphics, Vol. 8. Spec 2003

# Grid Research on Desktop Type Software for Spatial Information Processing

Guoqing Li, Dingsheng Liu, and Yi Sun

45 BeiSanHuanXi Road, P.O. Box 2434, Beijing, 100086, China  
Open laboratory, Remote Sensing Satellite Ground Station, China Academic of Sciences  
{gqli, dsliu, ysun}@ne.rsgs.ac.cn

**Abstract.** In the research works of spatial information grid, the grided modification of desktop style processing software is very important. Based on the analysis of such software structure, paper gives its technical strategy. Function Grided modifying is the acceptable method instead of whole package grided. Within the research, PCI and PIPS are brought as two kinds examples. Some key technology is followed being discussed and an experiment is given to show an interested result.

## 1 Desktop Processing Resources and PCI Software

In spatial information processing field, workstations are the main computing platform. With them, desktop style processing is using widely. Desktop software can work in single powerful workstation with support of other peripheral equipments, such as plotter, printer and tape reader etc. Users can do their simple processing works in such machine. With the development of user's requirement, computer has to handle large sale of data, high complex arithmetic within a limited time. In addition, local data and software and computing capability are found not sufficient for use, network cooperation and resource sharing is need.

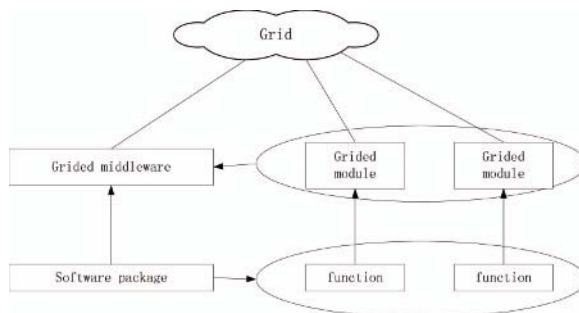


**Fig. 1.** How to grid a desktop software package

Grid is a method to realize such resource cooperation. With grid, users hope they can use a processing function only with their requirement, not to care of where the

function is, which platform the function hoisted, how to learn the interface parameters and how to code a program to quote such function. Such grid resource is simple and standard [1]. However, each desktop software is very different with others.

Desktop processing software package is formed by many functions, which have been integrated and can be use by integration interface or can be use directly with command line mode. The grid transfer of desktop software package is a course of reconstruct, shown in Fig. 1. We think it is no sense to say software package grid modify. Within the grid, a whole application software package cannot be a useful and searchable grid resource to users, because any grid resource should be registered with their resource description according to formal attributions. A large software package has to be separated into function pieces, which can be recognized with their resource registration.

Granularity is real a problem we have to discuss. However, there is less research works has been taken on it. Generally, there are three-type function in software package, processing type, engine type and interface type. Processing type function can realize a certain operation according to arithmetic coding, which always can be run independent. Engine type builds the framework of package and supports common basic function, such as runtime environment, file system and display, while engine type function cannot be use independent. Interface type function contributes to the data format transfer and develops API, some of which can be use as a single function. Within these three types, only processing type and part interface type functions are valuable to grided, which can be mapped to resource tree and managed by grid resource register services.

However, such natural granularity separation is not certain to fit the need of grid service; some special research should be taken for it. But clearly, the fine granularity services can combine into a coarse size granularity service. When considering granularity question, we should pay more attention to the separating difficulty and network performance [2].

The following work is taken with legal PCI develop tools without accessing PCI source code. Such develop tools is also been offered with the purchase of whole package.

## 2 Mainframe

As above said, what can be managed in grid is only the fine-granularity services which separated from PCI package. Such fine-granularity services combine to be a whole middleware layer of PCI, which can be named the grid version of PCI. So, the research work on PCI package grid research can bring a normal method for other desktop remote sensing and GIS processing software package.

In general, PCI hosted workstation can use Windows or UNIX platform. Being a grid node, the server should install basic grid protocols and support services, which bring this node to be a grid node, such as a Globus GT3 environment. But if a PCI hosted workstation is configured as a standard grid node, this grid support services will heavily increase the load, which will affect the normal processing performance of PCI function. So, an independence agent node is needed to be a bridge of grid world and PCI node. Agent node locates in the same LAN with PCI node, they communi-

cate with a couple of socket program. Agent can be a less capability computer, which installed as a grid node in the same time. As shown in Fig. 2, the resource registered in grid is such agent node instead of the real PCI node. If a grid user wants to use a PCI services, what he quotes is the agent shell services, which will transfer real operation command to the PCI background.

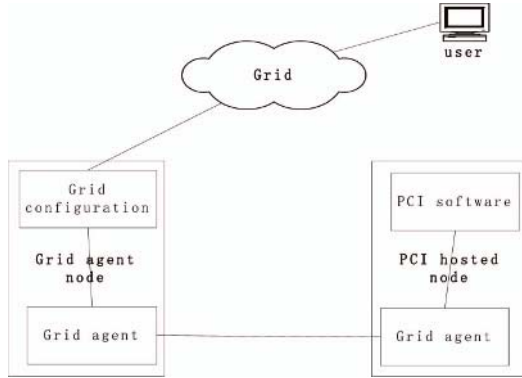


Fig. 2. PCI function grided frame structure

In this structure, PCI node is not changed for the temporary using of grid, such resource can be protecting as independence whole. In fact, it is the real value of grid. Out-grid-sharing will not bring security problem; the upgrade of PCI version also can be hidden to grid user if only keeps the PCI services interface not changed.

The realization of such desktop software function, all can be separated into the following five steps: Enter-parameters formatting (EPF), Enter-image formatting (EIF), quoting PCI function (QF), Outer-image formatting (OIF) and Out-parameters formatting (OPF), shown in Fig. 3. There are two type of information exchanged within grid and desktop software function, operation parameters and image data files' URL. Such information is designed in format of XML. EPF transfers the parameters in XML stream into format of PCI accepted, while EIF will access the source data files (or sub files or database) and replica them to local node via agent node, then EIF also need to change such files into the file format which PCI can handle, such pix file format. OPF and OIF give a reversed operation, which transfer result parameters and files into grid accessible format and return to grid runtime environment. Middle part is QF, which is a standard command line quoting of PCI functions.

### 3 Implementation and Experiment

We designed some experiments about PCI functions in Globus/OGSA environment with application server as JDK. PCI software hosted in a PC workstation configures with Pentium4 2.0GHz and 256MB memory. The agent node is a normal PC computer, which connects PCI node with 100M LAN. Fuzzy classification has been taken as an example with a whole scene TM data, about 40MB, transferred from

another grid node. Experiment shows that the cost in EPF, EIF, OPF and OIF is 45sec., and QF costs 220min.

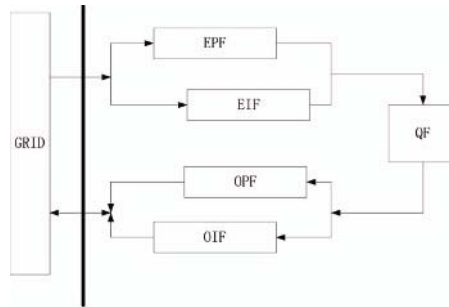


**Fig. 3.** Five steps of function grided realization

## 4 Conclusion

Above all, desktop spatial software package can be grided modification successfully. Such modification of software package is realized in form of function grided, instead of whole package grided. Grided software can reach resource sharing and operation control. The additional cost is acceptable and processing efficiency is similar between classical method and grid method.

## Acknowledgement

This paper is fund by China National Key Research Project (863) “spatial information grid key technology research and application” and finished at the open laboratory, RSGS, CAS.

## References

1. Bart Jacob Taking advantage of Grid computing for application enablement, IBM technical report. [http://www-900.ibm.com/developerWorks/cn/grid/gr-overview/index\\_eng.shtml](http://www-900.ibm.com/developerWorks/cn/grid/gr-overview/index_eng.shtml)
2. Li Guoqing, Research work on spatial information application grid technology, doctoral dissertation, RSGS, CAS, 2004

# Java-Based Grid Service Spread and Implementation in Remote Sensing Applications

Yanguang Wang<sup>1</sup>, Yong Xue<sup>1,2,\*</sup>, Jianqin Wang<sup>1</sup>, Chaolin Wu<sup>1</sup>, Yincui Hu<sup>1</sup>,  
Ying Luo<sup>1</sup>, Shaobo Zhong<sup>1</sup>, Jiakui Tang<sup>1</sup>, and Guoyin Cai<sup>1</sup>

<sup>1</sup> State Key Laboratory of Remote Sensing Science, Jointly Sponsored by the Institute of Remote Sensing Applications of Chinese Academy of Sciences and Beijing Normal University, Institute of Remote Sensing Applications, Chinese Academy of Sciences, P.O. Box 9718, Beijing 100101, China

<sup>2</sup> Department of Computing, London Metropolitan University, 166-220 Holloway Road, London N7 8DB, UK  
{wyg\_nju@hotmail.com, y.xue@londonmet.ac.uk}

**Abstract.** Remote sensing applications often concern very large volumes of spatio-temporal data, the emerging Grid computing technologies bring an effective solution to this problem. The Open Grid Services Architecture (OGSA) treats Grid as the aggregate of Grid service, which is extension of Web Service. It defines standard mechanisms for creating, naming, and discovering transient Grid service instances; provides location transparency and multiple protocol bindings for service instances; and supports integration with underlying native platform facilities. It is not effective used in data-intensive computing such as remote sensing applications because its foundation, Web Service, is not efficient in scientific computing. How to increase the efficiency of the grid services for a scientific computing? This paper proposes a mechanism Grid service spread (GSS), which dynamically replant a Grid service from a Grid node to the others. We have more computers to provide the same function, so less time can be spent completing a problem than original Grid system. This paper also provides the solution how to adept the service duplicate for the destination node's Grid environment; how each service duplicate communicates with each other; how to manage the lifecycle of services spread etc. The efficiency of this solution through a remote sensing application of NDVI computing is demonstrated. It shows that this method is more efficient for processing huge amount of remotely sensed data.

## 1 Introduction

With the development of modern space remote sensing technology, the sensors have got a great increment in spatio-resolution and spectrum-resolution, and have made huge volumes of data for our remote sensing applications. While today's PC is faster than the Cray supercomputer of 10 years ago, it is still often inadequate to provide a

---

\* Corresponding author.

satisfying computing power, and at the same time the resources of supercomputers are very precious and expensive. Grid computing can give a good solution (Foster and Kesselman 1999). Grid computing technology is being developed to solve two kinds of problems. First, there is much resource wasting in the Internet. Such resources include processing cycles, disk space, data and network. Second, the integration of different systems deployed in a large company tends to be difficult. We need standard technology and platform to support such integration.

To solve this problem, Grid computing considers all the available resource in the network as a “super computer”. User can transparently use and manage all these resources. Grid computing also provides a series of standard to integrate heterogeneous systems.

Since 2002, Open Grid Service Architecture (OGSA) which integrates the Globus has stood with the Web Service standard, and is going to be the unified standard for the Grid computing. The basic concept of OGSA is essentially a Web service with improved functionalities and behaviors. Web service is selected because it is a more suitable candidate for Internet scale application compared to other distributed computing technologies, such as CORBA, RMI and EJB (Ceram 2002). First, web service is based on a collection of open standards, such as XML, SOAP, WSDL and UDDI. It is platform independent and programming language independent because it uses standard XML language. Second, web service uses HTTP as the communication protocol. That is a big advantage because most of the Internet’s proxies and firewalls will not mess with HTTP traffic. However, Web service is not powerful to build complex applications. It lacks some functionality, such as lifecycle management, notification and persistency. And web service is stateless which means it can’t remember what has been done from one invocation to another.

Grid service provides more versatile functionality than web service. We will cover these functionalities in Section 2. Although Grid services get many advantages from Web Services, at the same time they also inherit the low efficiency in scientific computing of Web Service. This paper will propose a mechanism – Grid Services Spread (GSS). It allows the Grid services on a Grid node to extend dynamically to the others in order to increase the number of the nodes serving for the same task. We will focus on this mechanism in details in Section 3. At present, the implementation is based on Java. In Section 4, we will apply this mechanism for a remote sensing application to demonstrate how it works and what it can give us.

## **2 Background About Grid Service and Globus Toolkit 3**

A computational Grid is a hardware and software infrastructure that provides dependable, consistent, pervasive, and inexpensive access to high-end computational capabilities. And the latest development of Grid technology gives some progress, that Grid computing is concerned with coordinated resource sharing and problem solving in dynamic, multi-institutional virtual organizations, to the definition.

Comparing Web Services, Grid services has been created with the advantages including transient service which make the life of the service can be managed by users and service data which indicates the characters of the service, lifecycle management



and notification. These advantages are the tools which we use for building the Grid services spread.

The Globus Toolkit (<http://www.globus.org>) developed by Argon National Laboratory, University of Chicago and University of Southern California, has become the industrial standard Grid middleware. The famous projects, which used and are using Globus Toolkit, include SF-Express, NASA OVERFLOW-D2, X-ray CMT, Cactus, MM5, National Technology Grid, The European DataGrid, NASA Information Power Grid, ASCI Distributed Resource Management (DRM) Testbed, etc. Globus Toolkit 3 (GT3) is the integrate of the original Globus Toolkit and Web Services, and it implements The Open Grid Services Infrastructure (OGSI) specification, which is the technical specification of Grid services, as an extension to Apache Axis (an implementation of SOAP).

GT3 core implements OGSI, it is a very important part in GT3. GT3 Base Services layer mainly include Globus Resource Allocating Management (GRAM in short), Index Service and Reliable File Transfer Service (RFT) which are very important to Globus Toolkit and GSS. GT3 Data Service layer includes Replica Management, which is very useful in applications that have to deal with very big sets of data. When working with large amount of data, we're usually not interested in downloading the whole thing, we just want to work with a small part of all that data. Replica Management keeps track of those subsets of data we will be working with. GRAM handles job submission and management. Index Services are used in discovering services like UDDI in Web Services. RFT allows us to perform large file transfer between the client and the Grid Service. In GT3 core, user does not subscribe to the service instance, but to each service data element. This fine-grained notification may reduce network traffic and improve the system performance.

Grid Service has plenty of contents, but the purpose of this paper is not describing Grid Service in details. More knowleges about Grid Service can be obtained in the The Globus Toolkit 3 Programmer's Tutorial (Sotomayor 2004).

Other Grid Service layer is maintained for the services made by user, for example remote sensing application. These services are built on the Core, Base Service and the Data Service in general. Security is an important factor in Grid-based applications, but this paper doesn't concern the security subject at this stage of study.

### 3 Problems and Solution

The biggest problem of Grid service solving data-intensive computing is that the overhead of remote procedure call is very high. The main reason is that Web Services are based on those standard interoperation technologies, such as XML, SOAP, UDDI which use XML text datastreams. They need plenty of serialization and unserialization. Web Services are necessary to Grid service for the privilege of platform independent, programming language independent and going through Internet proxies and firewalls. This paper will propose a method — Grid Services Spread, which allow a Grid service extend to the other Grid nodes so that more PCs provide their computing resource to the same client request. The request naturally will be completed in shorter time, especially for the application using vast volumes of data.

### 3.1 Design

The main purpose of GSS is that let more Grid nodes dynamically join to serving for one application. The GSS consists of, in fact, two Grid services source GSS (SGSS) and destination GSS (DGSS). SGSS is in charge of packing all binary code of the service spread, and then sending it to DGSS on the other Grid nodes. DGSS unpacks the bundle from the SGSS and deploys all binary codes to correct paths as the information provided by SGSS. RS Grid Service (Remote Sensing Grid Service) on Node A is called Source Grid Service in GSS, and RS Grid Service Duplicate is called Service Duplicate. Service Duplicate is, in fact, a grid service which have the same functionalities with its Source Grid Service and more characters, such as transience that its lifecycle depends on requests from clients.

More computing resource can be used dynamically with GSS. In Figure 1, Node A only use NDVI services on Node B without GSS, while with GSS Node A can ask SGSS on Node B to copy NDVI Grid service to the other nodes, such as Node C, Node D, and then the NDVI Grid Service Client on Node A can send NDVI Service request to the NDVI Service duplicates on Node C and D by the spread information from SGSS on Node B. Three services will be working for the client at a same time, at last the client will integrate the result from each service.

### 3.2 Challenges and Solutions

A Grid service need user to write the following three parts, Service interface which are GWSDL file, Service implementation which are based on Java in this paper, and the Deployment Description (WSDD). With help of them and ANT, which is a java build tool, WSDD and the final java classes are encapsulated to a GAR file (Grid Archive). ANT deploys this GAR file to the Grid services container. So, how to realize GSS? We meet the following challenges.

*Which files should be packed by SGSS?*

Before copying a Grid service to the other node, the necessary files about this service should be collected. Which files should be selected? This problem involves two conditions. One is the original GAR file for the service exists. In this case, it is only required to send this GAR file to DGSS as the pack. This situation is very realistic and important. The other is the GAR file does not exist or we do not know where the GAR file is. We find there are some information about the service in *undeploy* directory. For a simple application, it is possible to make out GAR file because we can find where the class files and the WSDL files are, but for a complex one, it may not be so. The best method is maintaining GAR file in a specific position and using a file to keep the mapping between the GSH of a Grid service and where its GAR file is.

*What kind are those services duplicate on the other nodes? Persistent or Transient?*

A Grid service duplicate should be destroyed when the application it serves for is finished, or there are more and more Grid service duplicates running on the node and holding plenty of resources. Therefore those service duplicates should be transient. Who decide the lifecycles of the service duplicates? The service duplicates can be destroyed only when the service client receives satisfactory result.

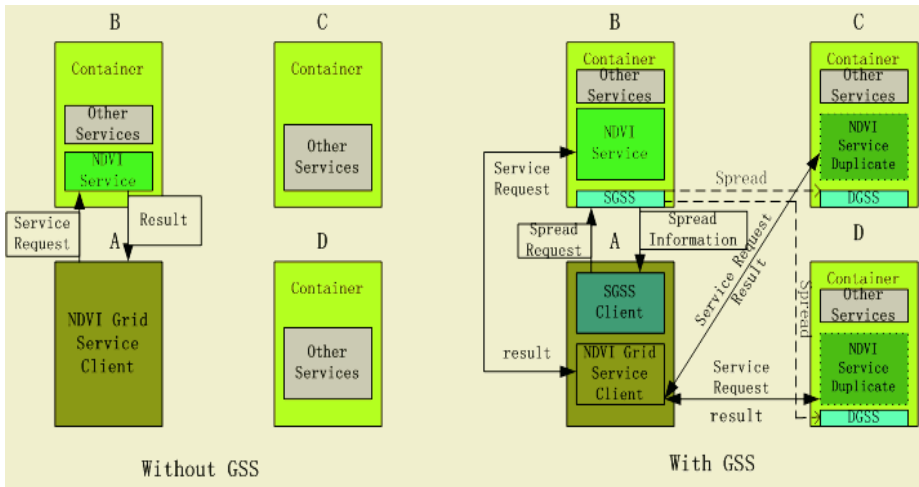


Fig. 1. The contrast of NDVI service without and with GSS

*How to deploy and undeploy the service duplicates dynamically without restarting the container?*

We find that GT3 does not support dynamic service deployment at present through our experiments. A new Grid service deployment is always available only by restarting the container. Our experiments indicate that it's mainly an Axis (a SOAP engine) problem. We can realize dynamic Grid service deployment in GT3 if Axis notices the new services and makes them available to the Grid. Each WAR (Web Archive) contains a fresh copy of the axis/ogsa web-app and the new services are made available when this web-app starts up. We can stop and start this web-app to make our services reinitialize and re-read their configuration files.

#### 4 Using GSS in an Application of Remote Sensing – NDVI

Our goal is to test the efficiency of using GSS for Earth surface geophysical parameters determination form remote sensing data. Vegetation indices (VIs) are spectral transformations of two or more bands designed to enhance the contribution of vegetation properties and allow reliable spatial and temporal inter-comparisons of terrestrial photosynthetic activity and canopy structural variations. As a simple transformation of spectral bands, they are computed directly without any bias or assumptions regarding plant physiognomy, land cover class, soil type, or climatic conditions. They allow us to monitor seasonal, inter-annual, and long term variations of vegetation structural, phenological, and biophysical parameters and are important parameter to various kinds of local, regional, and global scale models, including general circulation and biogeochemical models. Numerous studies have shown the utility of the Vegetation Indices (VIs) from climate studies to famine early warning

detection, epidemiology and renewable natural resources management. The NDVI has also been shown to be highly correlated with net primary production (NPP).

The Normalized Difference Vegetation Index (NDVI) (Tucker 1979, Jackson *et al.* 1983), which is related to the proportion of photo synthetically absorbed radiation, is calculated from atmospherically corrected reflectance from the visible and near infrared remote sensing sensor channels as:

$$(CH2 - CH1) / (CH2 + CH1)$$

Where the reflectance values are the surface bidirectional reflectance factors for MODIS bands 1 (620 - 670 nm) (CH1) and 2 (841 - 876 nm) (CH2). The NDVI is successful as a vegetation measure in that it is sufficiently stable to permit meaningful comparisons of seasonal and inter-annual changes in vegetation growth and activity.

#### 4.1 Experiment

In this experiment, we used 1000 MODIS images (1000x1200 pixels), and each image is about 1.1M. We calculate the NDVI as batches using these MODIS images through different approaches: single PC without NDVI grid service, NDVI grid service on only one node and NDVI grid service spreading to 5 PCs with GSS.

Our test bed consists of 1 PC running Linux9.0 and 5 PCs running Windows 2000 operating system. It makes a good advantage of the individual PCs, especially in a work group, to constitute a Grid system based on GT3 core and GT3 Gars, which include RFT, MMJFS, GRAM and MDS etc. Table 1 gives the configuration information of our test bed on GT 3.

NDVI Service Client program on Tgp2.tgp requests the SGSS Service on wang.tgp to spread the NDVI Service. Then the SGSS returns GSHs of the NDVI Service duplicates that has been spread to Cai.tgp, Ly.tgp, Zhong.tgp and Hu.tgp. When getting the information, Client program divides remotely sensed data (MODIS data in the experiment) in geometric parallelism and send request to all the NDVI Services including original one and duplicates.

#### 4.2 Result and Analysis

This experiment involved three cases:

- 1) We calculate NDVI with single PC without Globus Toolkit, using varying amount of data from 11 MB to 1100MB (form 10 images to 1000 images).
- 2) We do that with Grid Service, but without Grid Service Spread mechanism. NDVI Grid Service only runs on one PC. The amount of data still is varied from 11MB to 1100MB.
- 3) We use Grid Service Spread. The situation of utilizing data still is so.

This experiment was done for 10 times successively and we give the average value in Table 2, which is the statistics of the results of the three cases. We define the efficiency of GSS is the ratio of these two execution times:

$$\text{Efficiency} = \text{Execution of case 1} / \text{Execution of case 3}$$

**Table 1.** The configurations of GT 3 test bed

Host name	IP address	CPU	OS	Globus Toolkit	Description
Tgp2.tgp	192.168.0.200	1.7GHz	Win 2000	GT 3 core and Gars	Service Client
Wang.tgp	192.168.0.1 159.226.117.121	2.0GHz	Linux9.0	GT 3 core and Gars	NDVI Service SGSS
Hu.tgp	192.168.0.119	2.6GHz	Win2000	GT3 core and Gars	Service Duplicate DGSS
Ly.tgp	192.168.0.120	2.0GHz	Win2000	GT3 core and Gars	Service Duplicate DGSS
Cai.tgp	192.168.0.110	2.6GHz	Win 2000	GT 3 core and Gars	Service Duplicate DGSS
Zhong.tgp	192.168.0.19	2.6GHz	Win 2000	GT 3 core and Gars	Service Duplicate DGSS

**Table 2.** The results of the three cases

Cases \ Amount of Data	10 Images (11MB)	100 Images (110MB)	500 Images (550MB)	1000 Images (1100MB)
Without Grid Service (1 PC)	3.5 s	42.9 s	321.8 s	1093.8 s
1 PC providing Grid Service without GSS	8.4 s	49.2 s	342.4 s	1128.4 s
NDVI Grid Service spreading to 5 PCs with GSS	15.6 s	24.8 s	84.3 s	253.7 s

Case 2 is little slower than case 1 because of the serialization and unserialization of Grid service, but the difference varies little with the increase of the amount of data. In case 3, GSS even use more time to calculate NDVI when the amount is 11M for it is also a Grid service in fact. And the advantage of GSS is not huge when 100 images are used, but it is very surprising effective when it comes to 550 M (efficiency = 3.7) and 1100 M (efficiency = 4.3). We are convinced that we will have a better efficiency if the service can be spread to a bigger range. For a specific range of GSS, the efficiency will be better if the amount of data processed is larger.

## 5 Conclusion

Grid Service, the combination of Grid Technologies and Web Service, is a trend because it can really change the whole Internet into a huge real Grid system. But its performance is not satisfying in scientific computing, especially in data-intensive. Grid Service Spread mechanism can help us use more computing resource to service for our applications dynamically. With the help of GSS, we will have more powerful computing abilities and Throughput. It shows that this method is more efficient for processing huge amount of remotely sensed data.

## Acknowledgements

This publication is an output from the research projects "CAS Hundred Talents Program" and "Monitoring of Beijing Olympic Environment" (2002BA904B07-2) and "Remote Sensing Information Processing and Service Node" funded by the MOST, China and "Aerosol fast monitoring modeling using MODIS data and middlewares development" (40471091) funded by NSFC, China.

## References

- Ceram, E., 2002, *Web Services Essentials*, (Sebastopol: O'Reilly & Associates, Inc), pp, 7-24.
- Foster, I., Kesselman, C. 1999, *The Grid: Blueprint for a New Computing Infrastructure* (San Francisco: Morgan Kaufmann), pp, 16-50
- Foster, I., Kesselman, C. and Tuecke, S., 2001, The Anatomy of the Grid: Enable Scalable Virtual Organizations. Available online at <http://www.globus.org/research/papers.html> (accessed 10 Month 2004)
- Foster, I., Kesselman, C., Nick, J., Tuecke, S., 2002, The Physiology of the Grid. Available online at [http://www.Gridforum.org/ogsi-wg/drafts/ogsa\\_draft2.9\\_2002-06-22.pdf](http://www.Gridforum.org/ogsi-wg/drafts/ogsa_draft2.9_2002-06-22.pdf) (accessed 10 Month 2004)
- Jackson, R.D., P.N. Slater, and P.J. Pinter, 1983, Discrimination of growth and water stress in wheat by various vegetation indices through clear and turbid atmospheres. *Remote Sensing of the Environment*, **15**, 187-208.
- Sotomayor, B., 2004, The Globus Toolkit 3 Programmer's Tutorial, Available online at <http://www.casa-sot.com/omayor.net/gt3-tutorial> (accessed 10Month 2004)
- Tucker, C. J., 1979, Red and photographic infrared linear combinations for monitoring vegetation. *Remote Sensing of the Environment*, **8**, pp, 127-150.
- Tuecke, s., Czajkowski, K., Foster, I., Frey, J., Graham, S., and C. Kesselman, C., 2002, Grid Service Specification. Available online at [http://www.Gridforum.org/ogsi-wg/drafts/GS\\_Spec\\_draft03\\_2002-07-17.pdf](http://www.Gridforum.org/ogsi-wg/drafts/GS_Spec_draft03_2002-07-17.pdf) (accessed 10 Month 2004)

# Modern Computational Techniques for Environmental Data; Application to the Global Ozone Layer

Costas Varotsos\*

University of Athens, Department of Applied Physics,  
Bldg. Phys. 5, Panepistimiopolis, GR-157 84 Athens, GR  
covar@phys.uoa.gr

\* Currently with the University of Maryland, Department of Meteorology,  
3417 Computer and Space Science Bldg., College Park, MD 20742  
covar@atmos.umd.edu

**Abstract.** The physics laws, which govern the atmospheric phenomena, are mostly non-linear and therefore the application of the conventional Fourier spectral analysis on the time series of the atmospheric quantities reveals that these are usually non-stationary. Quite often these non-stationarities conceals the existing correlations and therefore new analytical techniques capable to eliminate non-stationarities in the data should be employed. The most recent analytical methods used along these lines are the wavelet techniques and the detrended fluctuation analysis. Much attention has been paid recently to the latter technique, which has already proved its usefulness in a large variety of complex systems. As a paradigm, the detrended fluctuation analysis is applied to the column ozone data. Specifically the zonally and globally averaged column ozone observations conducted by ground-based (1964-2004) and satellite-borne (1979-2003) instrumentation are employed to detect long-range correlations in column ozone time series. The results show that column ozone fluctuations exhibit persistent long-range power-law correlations for all time lags between 4 months - 11 years.

## 1 Introduction

Trends in total ozone content (TOZ) are caused by external effects and they are usually supposed to have a smooth and monotonous or slowly oscillating behavior. Therefore, for the reliable detection of long-range correlations, it is essential to distinguish trends from the long-range fluctuations intrinsic in the data. Usually, the short-range correlations are described by the autocorrelation function, which declines exponentially with a certain decay time. For the long-range correlations, however, the autocorrelation function declines as a power-law. However, the direct calculation of the autocorrelation function is usually not appropriate due to noise superimposed on the collected data and due to underlying trends of unknown origin. The detrended fluctuation analysis (DFA), which will be discussed later, is a well established method for determining the scaling behavior of noisy data in the presence of trends without knowing their origin and shape.

Very recently, *Varotsos* [2005] showed that the amplitudes of large TOZ fluctuations (in seasons of enhanced ozone depletion) obey a power-law scaling. This means that correlations between these points decrease according to a power law and are therefore scale-invariant. He also suggested that the Arctic and Antarctic TOZ fluctuations exhibit persistent long-range correlations for all time lags between 4 days - 2.5 years. This means that TOZ fluctuations at different times are correlated and the corresponding correlation function decays much slower than the exponential decay, i.e. a power-law decay. In other words persistence refers to the “memory” or internal correlation within the TOZ time series. For example, there is a tendency an increase in TOZ to be followed by another increase in TOZ at a different time. Furthermore he demonstrated the crucial role of the planetary waves to the scaling dynamics of TOZ over the high latitudes in both hemispheres, since the elimination of the TOZ long-term trend leads to persistent (antipersistent) long-range power-law correlations for time lags shorter (longer) than 10 days. It is worth noting here that a series is persistent if adjacent values are positively correlated, whereas a series is antipersistent if adjacent values are inversely correlated.

To reach to the aforementioned conclusions *Varotsos* [2005] employed the DFA method, which as mentioned above, allows the detection of long-range power-law correlations in a time-series with noise that often can mask true correlations. In this respect, due to the fact that the physics laws, which govern the atmospheric phenomena, are mostly non-linear, the application of the conventional Fourier spectral analysis on the time series of the atmospheric quantities reveals that these are usually non-stationary (the correlation functions are not invariant under time translation) (Chen et al. 2002, and references therein). Quite often these non-stationarities (e.g. trends and cycles) conceals the existing correlations (or other intrinsic properties) and therefore new analytical techniques capable to eliminate non-stationarities in the data should be employed (Hu et al. 2001).

The most recent methods used along these lines are the wavelet techniques (e.g. Koscielny-Bunde et al. 1998) and the DFA that introduced by Peng et al. (1994). Much attention has been paid recently to the latter technique, which has already proved its usefulness in a large variety of complex systems, for example, in southern oscillation index, in turbulence, in biology, in financial analysis and in other self-organizing critical systems (e.g. Ausloos and Ivanova, 2001; Weber, and Talkner, 2001; Chen et al. 2002; Varotsos et al. 2003ab; Collette and Ausloos 2004).

The present paper examines the time scaling of the TOZ fluctuations over the tropical and mid-latitudinal zones of both hemispheres and globally, thus contributing to the attempt for a selected choice between the proposed climate models for a projection of the TOZ levels in the future, taking into account the feedback between climate change and the ozone layer.

## 2 The Time Scaling and Correlations of the TOZ Fluctuations

The zonally and globally averaged TOZ observations performed by ground-based (1964-2004) and satellite-borne (1979-2003) instrumentation is used in order to



efficiently search for time scaling, by adopting, however, a data analysis technique, which is not debatable due to the non-stationarity of the data. Thus, to study the temporal correlations of TOZ fluctuations the method of DFA with acceptable error bars is herewith used. This method stems from random walk theory, and permits the detection of intrinsic self-similarity in non-stationary time series (Talkner and Weber 2000). Therefore, this method has the advantage of avoiding seasonal-like trends and non-stationarity effects. According to DFA method, the time series is first integrated and then it is divided into boxes of equal length,  $\Delta t$ . In each box, a least squares line (or polynomial curve of order  $l$ , DFA- $l$ ) is then fitted, in order to detrend the integrated time series by subtracting the locally fitted trend in each box. The root-mean-square (rms) fluctuations  $F_d(\Delta t)$  of this integrated and detrended time series is calculated over all time scales (box sizes). More specifically, the detrended fluctuation function  $F(\tau)$  is calculated as follows (Kantelhardt et al. 2002):

$$F^2(\tau) = \frac{1}{\tau} \sum_{t=k\tau+1}^{(k+1)\tau} [y(t) - z(t)]^2, \quad k=0, 1, 2, \dots, \left(\frac{N}{\tau} - 1\right) \quad (1)$$

where  $z(t) = at+b$  is the linear least-square fit to the  $\tau$  data points contained into a class.

For scaling dynamics, the averaged  $F^2(\tau)$  over the  $N/\tau$  intervals with length  $\tau$  is expected to obey a power-law, notably:

$$\langle F^2(\tau) \rangle \sim \tau^{2\alpha} \quad (2)$$

and the power spectrum function scales with  $1/f^\beta$ , with  $\beta=2\alpha-1$ .

An exponent  $\alpha \neq 1/2$  in a certain range of  $\tau$  values implies the existence of long-range correlations in that time interval as, for example, in fractional Brownian motion, while  $\alpha = 1/2$  corresponds to the classical random walk (white noise). If  $0 < \alpha < 0.5$ , power-law anticorrelations are present (antipersistence). If  $0.5 < \alpha \leq 1.0$ , then  $0 < \beta \leq 1$ , and persistent long-range power-law correlations prevail; the case  $\beta=1$  ( $\alpha =1$ ) corresponds to the so-called  $1/f$  noise. In addition, when  $1 < \alpha < 1.5$ , then long-range correlations are again present (but are stronger than in the previous case); the value  $\alpha =1.5$  corresponds to the Brownian noise (e.g., *Talkner and Weber, 2000*).

It is worth noting that since the time series is first summed the noise level due to imperfect observations is reduced.

It has recently been recognized (Hu et al, 2001) that the existence of long-term trends in a time series may influence the results of the correlation analysis. Therefore, the effects of TOZ trends have to be distinguished from TOZ intrinsic fluctuations. To this end, before applying scaling analysis to the TOZ time-series, all TOZ data were deseasonalized and detrended.

In Figure 1, a log-log plot of the function  $F_d = \sqrt{\langle F^2(\tau) \rangle}$  is shown, by employing the DFA-1 to the deseasonalised and detrended monthly mean values of the ground-based TOZ values, during 1964-2003, over the belt  $90^\circ\text{S}-90^\circ\text{N}$ . Since  $\alpha = 1.1 (\pm 0.13)$

for the interval time ranging from about 4 months to 11 years long-range correlations are present. This suggests persistent long-range power-law correlations in global TOZ fluctuations. This persistence suggests that an anomaly in global TOZ in one time frame continues into the next.

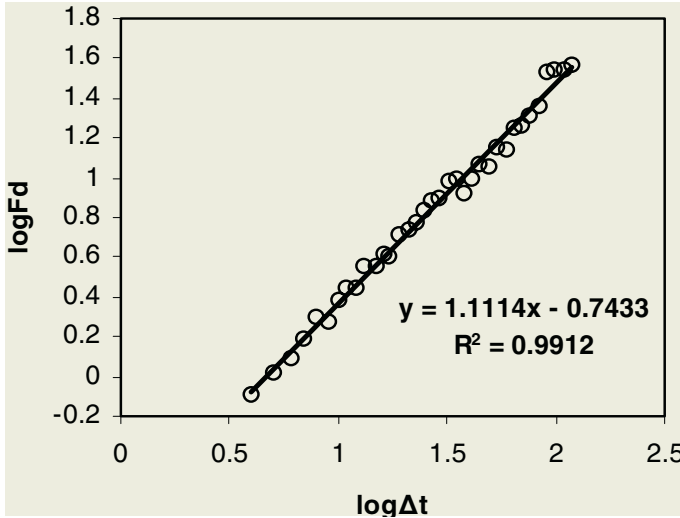


**Fig. 1.** DFA-function in log-log plot for the deseasonalised and detrended TOZ, during 1964-2003, over the belt 90°S-90°N

In the following, the temporal correlations of the deseasonalised and detrended monthly mean values of TOZ are also examined for the belt 25°S-25°N during 1964-2003. The result obtained from the application of the DFA-1 to the aforementioned TOZ values over tropics is presented at Figure 2. The finding drawn from this figure ( $\alpha = 1.1 \pm 0.11$ ) is that TOZ over tropics exhibits persistent long-range power-law correlations for the interval time ranging from about 4 months to 11 years.

It is worth noting that similar to the above-discussed results are also found by applying the DFA-1 method to the monthly zonal mean V8 TOZ values over tropics and globally.

We now turn to the extra-tropics and specifically to the ground-based TOZ data for the latitude belt 25°N-60°N during 1964-2003. The application of the DFA-1 method to these deseasonalised and detrended monthly mean values of TOZ reveals that long-range power-law correlations exist for all time scales (fig.3a). Since  $\alpha_1 = 1.2 \pm 0.13$  (for time scales shorter than 2 years) the long-range correlations in TOZ exhibit “stronger memory” (the process forgets more slowly its past behavior) compared to that of  $\alpha_2 = 0.6 \pm 0.09$  (for time scales longer than 2 years). Higher persistence implies a stronger correlation between successive data points. It is also worth noting that “memory” or correlations exist at all time scales over which the power law is valid.

Finally, the DFA-1 method is also applied on the deseasonalised and detrended monthly mean values of TOZ in the latitude belt 25°S-60°S during 1964-2003. The results obtained are depicted in Fig.3b, where persistency of TOZ fluctuations is observed. In particular, for time scales shorter (longer) than 2 years  $\alpha_1 = 1.1 \pm 0.11$  ( $\alpha_2 = 0.6 \pm 0.07$ ).

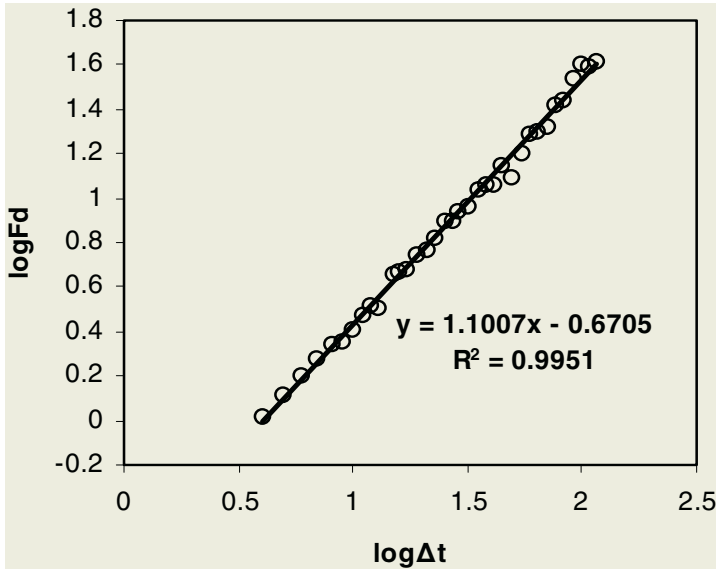


**Fig. 2.** DFA-function in log-log plot for the deseasonalised and detrended TOZ during 1964-2003, over the belt 25°S-25°N

It is worth mentioning that similar to the above-discussed results for the TOZ variability over extra-tropics are also found by applying the DFA-1 method to the monthly zonal mean V8 TOZ values.

The results obtained clearly show that the monthly mean column ozone fluctuations over tropics, extra-tropics and globally exhibit persistent long-range correlations for all time lags between 4 months - 11 years, which correspond to the  $1/f$  noise. Over extra-tropics, this persistency becomes weaker for time lags between 2-11 years. It is well known that the  $1/f$  noise is one of the most common features in nature. Superposition of effects giving rise to signals with scale invariant distributions of correlation times, the so-called scale similarity, could be on the basis of the observed behavior. However, a proper explanation for such a behavior is still lacking and for this reason the physical origin of the  $1/f$  noise is pretty much an open question (Fanchiotti et al, 2004).

The aforementioned findings seem to favor specific models for the description of the ozone depletion and may lead to better predictability on the global TOZ evolution along the lines of nonlinear dynamics.

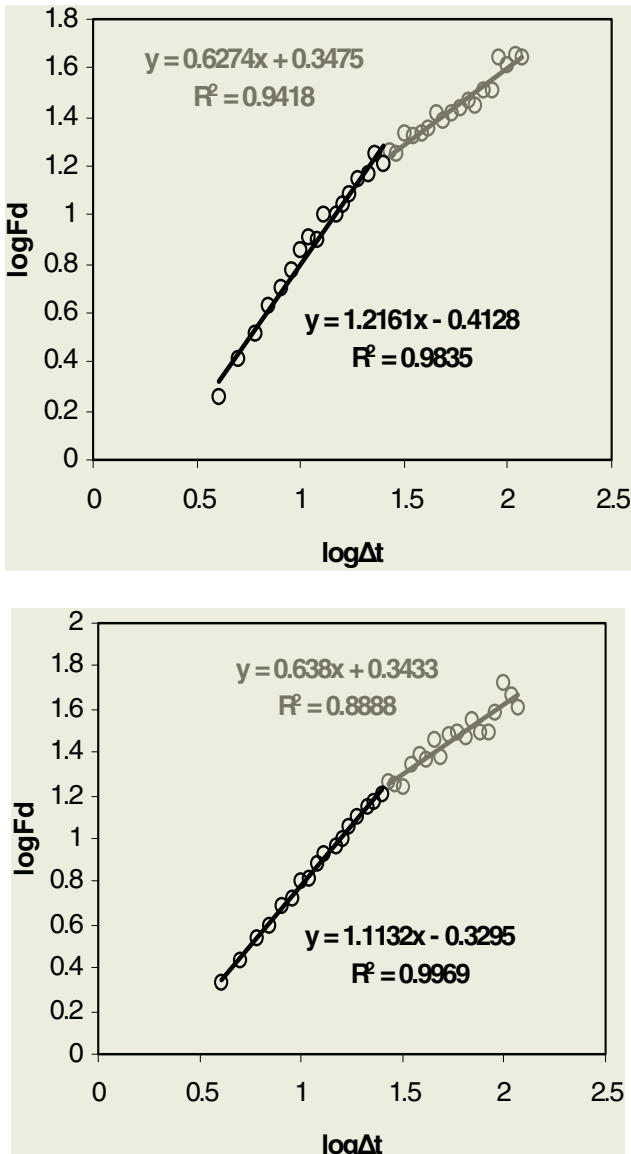


**Fig. 3.** DFA-function in log-log plot for the deseasonalised and detrended TOZ during 1964-2003, over the belt : (a) 25°N-60°N, and (b) 25°S-60°S

### 3 Conclusions

The investigation of the existence of the long-range correlations to the zonally and globally averaged column ozone data derived from observations performed by ground-based (1964-2004) and satellite-borne (1979-2003) instrumentation shows the following:

The monthly mean column ozone fluctuations over tropics, extra-tropics and globally exhibit persistent long-range correlations for all time lags between 4 months - 11 years, which correspond to the  $1/f$  noise. Over extra-tropics, this persistency becomes weaker for time lags between 2-11 years.

The above-mentioned findings demonstrate the nature of specific atmospheric mechanisms that operate and affect the ozone layer in a power law fashion. These could also be a good test of atmospheric chemistry-transport models. Apart from reproducing instantaneous absolute values, model results should also demonstrate the scaling behavior.

## Acknowledgments

TOMS data were produced by the Ozone Processing Team at NASA's Goddard Space Flight Center. The ground-based data are credited to Vitaly Fioletov, Experimental Studies Division, Air Quality Research Meteorological Service of Canada.

## References

- Ausloos, M., and K. Ivanova, 2001: Power-law correlations in the southern-oscillation-index fluctuations characterizing El Nino. *Phys. Rev. E*, **63** (4): art. no. 047201.
- Chen, Z., P. C. Ivanov, K. Hu, and H. E. Stanley, 2002: Effect of nonstationarities on detrended fluctuation analysis. *Phys. Rev. E*, **65** (4), art. no. 041107.
- Collette, C., and M. Ausloos, 2004: Scaling analysis and evolution equation of the north atlantic oscillation index fluctuations. ArXiv:nlin.CD/0406068 v1 29 June.
- Fanchiotti, H., S.J. Scitutto, C.A. Garcia, and C. Hojuat, 2004: Analysis of sunspot number fluctuations. ArXiv:nlin.AO/0403032 v1 16 March.
- Hu, K., P. C.Ivanov, Z. Chen, P. Carpena, and H. E. Stanley, 2001: Effect of trends on detrended fluctuation analysis. *Phys. Rev. E* **64** (1): art. no. 011114.
- Kantelhardt, J.W., S. A. Zschiegner, E. Koscielny-Bunde, S. Havlin, A. Bunde, and H. E. Stanley, 2002: Multifractal detrended fluctuation analysis of nonstationary time series. *Physica A* **316** (1-4): 87-114.
- Koscielny-Bunde, E., A. Bunde, S. Havlin, H. E. Roman, Y. Goldreich, H. J. Schellnhuber, 1998: Indication of a universal persistence law governing atmospheric variability. *Phys. Rev. Lett.* **81** (3), 729-732.
- Peng, C. K., S. V. Buldyrev, S. Havlin, M. Simons, H. E. Stanley, and A. L. Goldberger, 1994: Mosaic organization of DNA nucleotides. *Phys. Rev. E* **49** (2), 1685-1689.
- Talkner, P., and R. O. Weber: 2000: Power spectrum and detrended fluctuation analysis: Application to daily temperatures. *Phys. Rev. E* **62** (1): 150-160 Part A.
- Varotsos, C., 2005: Power-law correlations in column ozone over Antarctica. *Int. J. Rem. Sensing* (in press).
- Varotsos, P. A., N. V. Sarlis, and E. S. Skordas, 2003a: Long-range correlations in the electric signals that precede rupture: Further investigations. *Phys. Rev. E*, **67**, 21109-21121.
- , -----, and -----, 2003b: Attempt to distinguish electric signals of a dichotomous nature. *Phys. Rev. E* **68** (3): art. no. 031106.
- Weber, R. O., and P. Talkner, 2001: Spectra and correlations of climate data from days to decades. *J. Geophys. Res.*, **106**, 20131-20144.

# PK+ Tree: An Improved Spatial Index Structure of PK Tree

Xiaolin Wang, Yingwei Luo\*, Lishan Yu, and Zhuoqun Xu

Dept. of Computer Science and Technology, Peking University, Beijing, P.R.China, 100871  
lyw@pku.edu.cn

**Abstract.** Spatial index is very important in GIS. PK tree and Hilbert R tree are two well-known spatial index structures. Comparison operations are very little in PK tree, while disk I/O operations are quite little in Hilbert R tree. PK+ Tree is an improved spatial index structure from PK tree. In PK+ tree, Comparison operations are less than in Hilbert R tree, while disk I/O operations are almost the same as in Hilbert R tree.

## 1 Introduction

With the development of information technology about data mining and multimedia, massive data processing gets more and more important in spatial processing. Spatial indexing is a key issue for massive spatial data processing.

Many kinds of spatial index structures exist nowadays. They can be divided into two main categories: partition tree and R tree. These two categories of spatial index structure have their own weakness and strongpoint. PK tree and Hilbert R tree are two efficient spatial index structures of each category.

In this paper, a new spatial index structure, PK+ tree, which are from PK tree, is introduced in order to improve storage usage, so that it may be more efficient for high dimensional data. In the next section, the problems of PK tree are analyzed. In the third section, PK+ tree is discussed in details. In the fourth section, the efficiency of storage and query of PK+ tree are compared with of PK tree and Hilbert R tree.

## 2 PK Tree and Its Weakness

PK tree is an efficient spatial index structure of partition tree category. In PK tree, an initial space cell  $C_0$  are required to enclosing all the data objects to be indexed.  $C_0$  can be split into  $R=(r_x, r_y)$  sub cells  $C_i$ , and so on, so that the width and height of each  $C_i$  is  $1/r_x$  and  $1/r_y$  of  $C_{i-1}$ . Only those K-instantiable cells have their corresponding nodes in PK tree.

A key issue of PK tree is that it's poor efficiency of storage. The average node usage (ANU) is the percentage of valid entries to the capacity of entries in the tree. For data points in two dimensional space, each node has the capacity to hold  $R(K-1)$  en-

---

\* Corresponding author: LUO Yingwei, lyw@pku.edu.cn.

tries, but the ANU is only 40%. For the same data set, the ANU of a Hilbert R tree may reach to 84% or 87%. When processing data object other than point, for example curves or surfaces, the ANU of a PK tree can reach only 12%, while Hilbert R tree may also reach around 85%. The poor efficiency of storage leads to more disk I/O operations while access the index tree. For data point, the ANU of PK tree is half of the ANU of Hilbert R tree, but PK tree yields more efficient query performance than Hilbert R tree. But for curves or surfaces, the query performance of PK tree is much poorer than Hilbert R tree. The main reason is that the ANU of PK tree is far more less than that of Hilbert R tree. With such poor ANU, PK tree are limited to be used for high dimensional data object. To solve this problem, PK+ tree is introduced in this paper aiming at improving the ANU.

### 3 PK+ Tree

The ANU of PK tree drops with large  $R=(r_x, r_y)$ . If  $R$  can be limited to the smallest value, then the ANU might be greatly increased. In PK+ tree,  $R$  is restricted to be no more than 3. To partition a given space cell  $C$  in two-dimensional space, firstly  $C$  is split into three cells at x dimension, then at y dimension, and then at x dimension, and so on. The three cells are not symmetrical. Two cells of them are the two half of  $C$ , while the third cell is  $C$  itself! But the third cell is not the same as  $C$ , since it holds all data objects sits in  $C$  but not in the other two half cells. The third cell is called middle cell, and the two half-cells are called left cell and right cell (or bottom cell and top cell) correspondingly, as shown in figure 1.

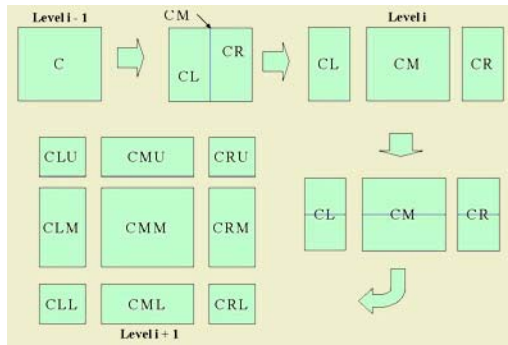


Fig. 1. PK+ Tree Cell Splitting

PK+ tree also requires that any node in the tree is K-intantialable. Insertion or deletion is implemented with two steps. First, search from the root to find the proper node to be modified, and modify it; then, trace back to the root and checking each node on the path if it's K-intantialable, if not, some promotion, division or deletion operations will be done to keep all nodes K-intantialable. The process of K-intantialable checking in PK+ tree is the same as in PK tree, except that they apply different kinds of splitting rules.

PK+ tree split the space cell at each dimension in turn, which makes a lower degree of regularity of partition than PK tree, but the ANU is greatly increased. In PK+ tree, the extent of a middle node overlaps with its sibling left (right) node. The overlapping of nodes might reduce some query's performance.

## 4 Performance Comparison

In the section, a series of experiments are done to examine the query performance of PK+ tree. Two dimensional data objects in two-dimensional space are being used in our experiment. A cluster data set from *SEQUOIA 2000 Benchmark* and a random data set are used. In these experiments, we compare PK+ tree with corresponding PK tree and 3-2 Hilbert R tree.

We count disk I/O operations and compare operations instead of measure the time cost in queries as the measurement of performance, thus we avoid the effects of implementation issues to our experiments.

Since in PK tree and PK+ tree, theoretically, the ANU will never be large than 50%. To make the storage efficiently, two kinds of methods might be applied. One method is to store each node in one or more disk pages according to the amount of valid entries in each node (SNMP, Single-node-multi-pages). The other method is to store several nodes in the same disk page if the total valid entries can be hold in one disk page (MNSP, Multi-nodes-single-page).

### 4.1 Storage Usage

For a given data set, the storage usage is the total valid entries vs. the total entries capacity of the index structure. ANU is used to describe the storage usage.

Table 1 shows the comparison of storage usage of PK tree, PK+ tree and Hilbert R tree. SNMP is compared with MNSP to show the effect of MNSP. Since Hilbert R tree is storage optimized, no more optimized method is considered in the comparison.

**Table 1.** ANU of PK+ tree, PK tree and Hilbert R tree

	SNMP		MNSP	
	Cluster data	Random data	Cluster data	Random data
PK+ tree	46.37%	50.83%	67.62%	66.78%
PK tree	12.95%	12.69%	25.49%	38.15%
Hilbert R tree	88.17%	85.52%	□	□

Table 1 shows that, MNSP outperforms SNMP, but does not make the ANU of PK+ tree reach the ANU of Hilbert R tree.

### 4.2 Query Performance

Our experiments show that, for both cluster data set and random data set, PK+ tree greatly reduces disk I/O operations per query than PK tree, but has almost the same



disk I/O operations per query as Hilbert R tree. Since the ANU of PK+ tree is approximately 75% of Hilbert R tree, it is obvious that PK+ tree requires much less compare operations per query than that of Hilbert R tree. In more details, for small query regions, PK+ tree yields less disk I/O operations than Hilbert R tree; for query of inside, PK+ tree yields much less disk I/O operations than Hilbert R tree.

## 5 Conclusion

In this paper, an improved spatial index structure based on PK tree - PK+ tree is introduced. PK+ tree outperforms PK tree when used for high dimensional object indexing. PK+ tree has a higher ANU and hence requires less disk I/O operations in queries. Though disk I/O operations in queries of PK+ tree is almost the same as that of Hilbert R tree, but Hilbert R tree yields a higher ANU, compare operations in queries is more than that of PK+ tree. PK+ tree is perfect for application that cares both disk I/O performance and CPU performance.

## Acknowledgement

This work is supported by the National Research Foundation for the Doctoral Program of Higher Education of China under Grant No. 20020001015; the National Grand Fundamental Research 973 Program of China under Grant No.2002CB312000; the National Science Foundation of China under Grant No.60203002; the National High Technology Development 863 Program under Grant No. 2002AA135330 and No. 2002AA134030; the Beijing Science Foundation under Grant No.4012007.

## References

1. Wei Wang, Jiong Yang and Richard Muntz: PK-tree: A Dynamic Spatial Index Structure for Large Data Sets, Kluwer Academic Publishers (1997)
2. Wei Wang, Jiong Yang and Richard Muntz: Pk-Tree: A Spatial Index Structure For High Dimensional Point Data, Kluwer Academic Publishers (2000).
3. Ibrahim Kamel and Christos Faloutsos: Hilbert R-tree: An improved R-tree Using Fractals, Morgan Kaufmann Publishers Inc (1994).
4. Bernhard Seeger and Hans-Peter Kriegel: Techniques for Design and Implementation of Efficient Spatial Access Methods, Morgan Kaufmann Publishers Inc (1988).
5. Andreas Henrich, Hanas-Werner Six and Peter Widmayer: The LSD Tree: Spatial Access to Multidimensional Point and Non-point Objects, Morgan Kaufmann Publishers Inc (1989).

# Design Hierarchical Component-Based WebGIS

Yingwei Luo, Xiaolin Wang, Guomin Xiong, and Zhuoqun Xu

Dept. of Computer Science and Technology, Peking University, Beijing, P.R.China, 100871  
lyw@pku.edu.cn

**Abstract.** A practical component-based WebGIS named as Geo-Union is presented. Geo-Union consists of four layers: storage layer, service layer, component layer and application layer. Service layer can be partitioned into another two layers: client service layer and server service layer. The architectures and object constitutions of each layer in Geo-Union are discussed in details. The Web application model of Geo-Union is also presented. At last, some future works in WebGIS, such as interoperability, security, distributed computing and intelligent computing, are indicated and simply explored.

## 1 Introduction

Geographical Information System, GIS, is an effective tool that digitally reflects the geometry spatial situation on which human society lives and the various transitional spatial data. GIS describes the attributes of these spatial data and simulates the action of geospatial objects in a model way. Under the supports of software and hardware, GIS uses the given formats to support input/output, memory and display. It also provides the service of inquiring geometry spatial information, doing compositive analyses and making assistant decision. After several years' development, GIS is being wildly used in every aspect and plays an important role.

WebGIS is the Internet GIS that has Browse/Server architecture. Recently, WebGIS application has become more and more popular in many GIS user communities<sup>[1]</sup> because of the fascinating development of computer networks as well as the more and more popular use of the Internet. The key steps to promote WebGIS to a more practical situation are rational adjusting computation functions and enhancing performance. In this paper, a practical multi-layer component-based WebGIS model Geo-Union and its Web application model are discussed.

## 2 Multi-layer Component-Based WebGIS Model Geo-Union

Component modeling is one of the main approaches to enhance functions of WebGIS. Geo-Union system is based on component technique and Client/Server architecture. The system includes four layers: storage layer, service layer, component layer and application layer, with client and server existing in service layer<sup>[2-4]</sup>, shown in Figure 1. The multi-layer component-based model enables GIS functions to be distributed in network effectively and brings high reusability of the system. Furthermore, it provides effective functions for further development and integration with other systems.

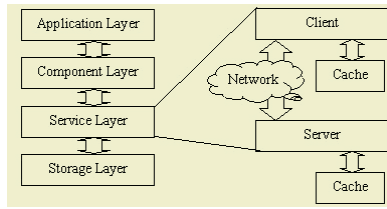


Fig. 1. Architecture of Geo-Union

### 2.1 Geo-Union Storage Layer

Storage Layer is the fundamental part in Geo-Union architecture, responsible for storage management of GIS data. With the help of ORDB, the layer stores and manages geography spatial and non-spatial data. Main objective of the layer includes how to present and store GIS data and how to maintain relations of these data. Below is type of GIS data: (1) Layer: Collection of spatial entities with the same type. (2) Entity: Spatial object composed of geometry and attribute data. Geometry data represents geometrical location of spatial object while attribute data describes society data. (3) Legend: A method to visualize Spatial Entity. (4) Legend library: Composed of 0~n Legends. (5) Reference system: Reference frame and Attitude frame of the Layer. (6) Display Setting Item: Mapping relation between Spatial Entity and Legend. (7) Display Setting: Composed of Display Setting Items.

Figure 2 shows the relations among GIS data. Encapsulation and management of GIS data exist in all the layers: server, client and component layer, and the relation in each layer are the same.

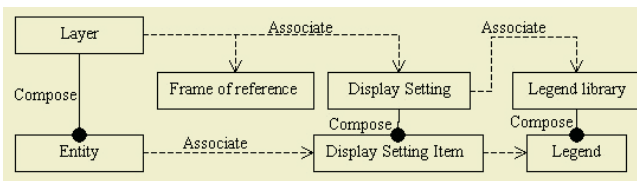


Fig. 2. E-R map in Geo-Union Storage Layer

### 2.2 Geo-Union Service Layer

Service Layer is responsible for management and access of GIS data, and composed of Geo-Union Client and Server. Geo-Union Client, as a server, provides data accessing and processing services for Geo-Union Component Layer, while Geo-Union Server manages and retrieves spatial data from Geo-Union Storage Layer, as a client. Geo-Union Client and Server are two independent but highly related parts: the Server provides functions such as data accessing service, spatial data index, basic spatial relation query, transaction and data sharing; through those services provided by the Server, the Client provides basic GIS tools and re-development functions. Cache, part

of Geo-Union Client, can reduce network load thus improve system response rate. Cache is also in Geo-Union Server, with similar but different implementation to the Client. Geo-Union Client can be used in the development of server simulator, whose Cache enables less network load and quick system response rate.

### ● Geo-Union Server

Geo-Union Server is the only interface to GIS data for Geo-Union client. Through interaction with Storage Layer, the Server provides Geo-Union client with following services: connection service, data accessing service (cache service included), transaction and data sharing service. Those services are implemented mainly by a series of object component, including connection object, data object and cache object. These objects have corresponding structure and function with those in Geo-Union Client.

In Geo-Union Server, a data source table is used to manage multiple distributed spatial databases. Therefore one Geo-Union Server can serve multiple Geo-Union Clients simultaneously. Geo-Union Clients can also access multiple spatial databases through Geo-Union Server (shown in figure 3).

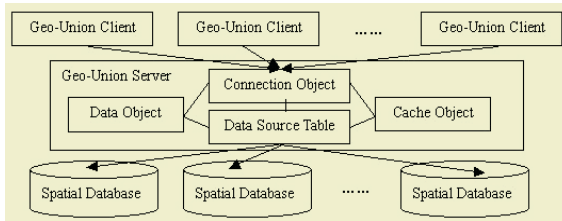


**Fig. 3.** Geo-Union Server and Geo-Union Client

### ● Geo-Union Client

Geo-Union Client is deployed on the client machine and connected with Geo-Union Server, providing GIS data accessing service and data processing service. Geo-Union client include the following functions: GIS data network access and management, GIS data object management, general spatial analysis arithmetic and spatial data cache management. Structure of Geo-Union Client is showed in figure 4. Below are the main objects in Geo-Union Client:

(1) Connection Object. Similar to Connection Object in Geo-Union Server, it manages communicating connections, GIS data access and transactions between Client and Server. It is also responsible to store and release connection relevant data objects in memory, maintain caches in Client and reduce network data flow.

(2) Data Object. Include Layer, Entity, Geometry Object, Record Collection, Map, Reference System, Display Setting, Display Setting Item, Legend Library and Legend. Considering the storage and access in Client's memory, the Client only supports two statuses of Data Object: binding and dissociation. In other words, the Client can not only bind Data Object with data in Storage Layer through Geo-Union Server, but also store Data Object in its own memory. Below are status details of every kind of Data Object: (a) Layer is a collection of Entity. Layer also implements some basic spatial search operations such as K-near search, search for entities nearest to a specified entity in a layer. (b) Entity is the atomic access unit in GIS data, including Entity

Identifier, geometry object attribute, user attribute and annotation. (c) Geometry Object includes point, multipoint, line, multi-line, polygon and bitmap. Basic spatial arithmetic of relation between Geometry Objects is also provided. (d) Record Collection. As another interface to access Entities besides Layer, Record Collection is the uniform interface to access spatial and user attributes. It can store the results of searching for entities in a layer in the form of snapshot, support cursor operation, and support both immediate and batch update modes. (e) Map manages and accesses layers' structure information in Client. Through a Map Object, the system can organize layers into a practical map.

(3) Arithmetic Object. Arithmetic Object implements general spatial analysis arithmetic such as overlay analysis, network analysis and etc.

(4) Spatial Data Cache. In Spatial Data Cache, historical records of Data Object are stored to avoid retrieving repeatedly the same data from servers, thus reducing network load and user waiting time.

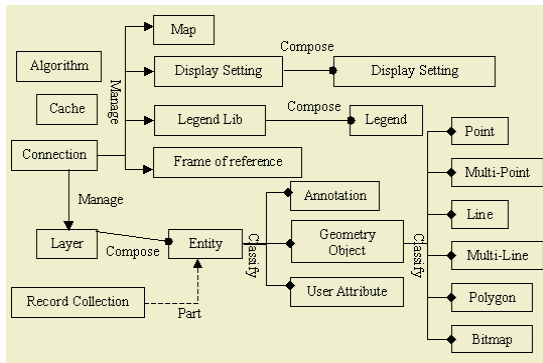


Fig. 4. Design Architecture of Geo-Union Client

### 2.3 Geo-Union Component Layer

Geo-Union Component Layer can provide Geo-Union Application Layer with many services. Geo-Union Component Layer is the encapsulation of Geo-Union Client and offers outer users GIS service interfaces to compose a complete GIS component library. The interfaces include Data Access Object, Map Display Object, Geometry Object, Function Object, Legend Edit and Display Object, Tool Object and etc. Composition and relation of these objects can be shown as figure 5.

- Data Access Object

Data Access Object provides GIS data manipulation functions as below: (1) GxConnection, connection object for GIS data access on the server. Operations such as connection or disconnection, layer object management, reference system management, display setting object management, legend library object management and transaction are allowed in GxConnection. (2) GxLayer, layer access object. Operations such as receiving and changing layer basic information, search and analysis based on layer, managing and searching entities in a layer, importing and exporting data are allowed. (3) GxEntity, entity object, through which users can access geometry and property

data of an entity. (4) GxLegendLib, legend library. Each legend has a number greater than 0. (5) GxLegend, used for describing a legend. (6) GxReferenceSystem, used for describing a reference system. (7) GxDisplaySetting, display setting, which describes the visualization method of a layer. (8) GxDisplaySettingItem, one item in a display setting, which describes the visualization method of a kind of entities. (9) GxRecordset, search record set, composed of searched results. (10) GxFields, field connection of an entity. (11) GxField, one field of an entity. (12) GxSelection, selected entity number connection.

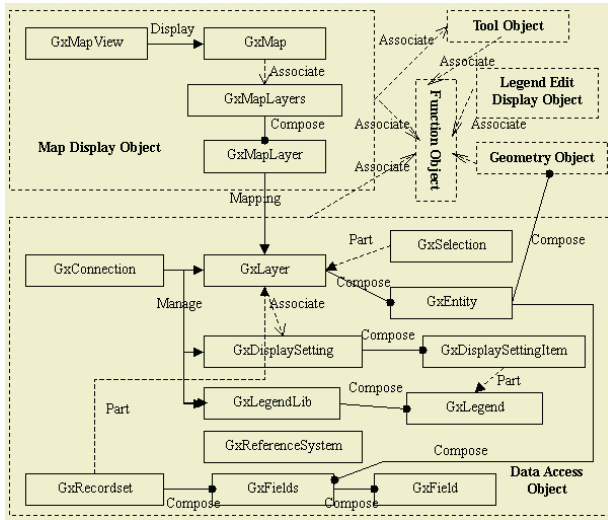


Fig. 5. Object Diagram in Component Layer of Geo-Union

### ● Map Display Object

Map display object can control and display GIS data, it includes: (1) GxMapView, map display control, is used for displaying map. In order to facilitate development on this control, we provide a tool management object and a group of input events. Through the tool management object GxTools, different tool objects (see also Tool Object) can be added in GxMapView to implement many special functions such as map edit, entity select, map measure and so on. The input events are all mouse or keyboard relevant and can be used in secondary development to implement customized functions. (2) GxMap is an abstract concept, can be displayed in GxMapView. One GxMap is corresponding to a collection of GxMapLayers. (3) GxMapLayers, a collection of map layers, can manage its owned map layers. (4) GxMapLayer, map layer in abstract concept, is corresponding to the map layer in storage. GxMapLayer is the map layer provided for users and includes legend configuration, reference system and annotation.

### ● Geometry Object

Geometry Object includes GxPoint (point entity), GxPoints (point collection), GxLine (line entity), GxLines (line collection), GxPolygon (polygon entity), GxRect (rectangle entity), GxBitmap (bitmap) and so on.

- **Function Object**

Function Object has two functions: one is that it can help users utilize other objects conveniently in the secondary development process; the other function is enable users to carry on special analysis in a more convenient way. (1) GxError, error handling objec. (2) GxEnumeration, enumeration object to contain the results of enumeration methods in GxConnection such as EnumLayer (enumerate all layers), EnumLegendLib (enumerate all legend libraries), EnumReferenceSystem (enumerate all reference systems), EnumDisplaySetting (enumerate all display settings) and so on. (3) GxObjectFactory, object factory. In IIS ASP programming, only ActiveX control objects can be created directly and other programmable objects must be created through controls in an indirect way. Therefore, GxObjectFactory is designed to support the creation of GIS object in all circumstances. (4) GxArray, is a kind of array, whose element can be any type or object. (5) GxSet is a kind of set, whose element can be any type or object. No element in the set can be equal to any other element. (6) GxUtility, a special function utility object, contains some functions which are difficult to be implemented in some visualized programming languages such as VisualBasic, Delphi, PowerBuilder. The functions includes object creating (i.e. creating a GxPoint object by x and y coordinates), special statistics and coordinate transforming. (7) GxAnalysis, special analysis object, including overlay analysis, clipping analysis and connectivity analysis.

- **Legend Edit and Display Object**

Legend Edit and Display Object can create, edit, manage and explore legends. It includes GxLegendEditor (legend edit control), GxLegendLibView (legend library explore control) and GxLegendView (legend display control).

- **Tool Object**

Tool Object implements a set of basic mouse interfaces, including GxTools (tool manage object to manage a set of other tool objects), GxPick (pick entities in a map layer), GxInputLine (input line entities in a map layer), GxInputPolygon (input polygon entities in a map layer), GxInputRect (input rectangle entities in a map layer), GxZoomIn (map zoom in), GxZoomOut (map zoom out) and GxPalm (map roam).

## **2.4 Geo-Union Application Layer**

In Geo-Union Application Layer, users can develop customized GIS applications. This layer's main job is to obtain customized GIS application by pruning and integrating services provided by Component Layer.

## **3 Web Application Model of Geo-Union**

Geo-Union has complete functions and flexible adaptabilities. A series of techniques to construct GIS application system are provided by Geo-Union, including server construction and application development. Geo-Union not only supports stand-alone environment, but is quite suitable for developing GIS application system, especially Web-based GIS application in network environment.

Geo-Union component layer contains a group of ActiveX controls and relative programmable objects. ActiveX controls can be embedded in Web pages directly. Web application model in Geo-Union is shown in figure 6.

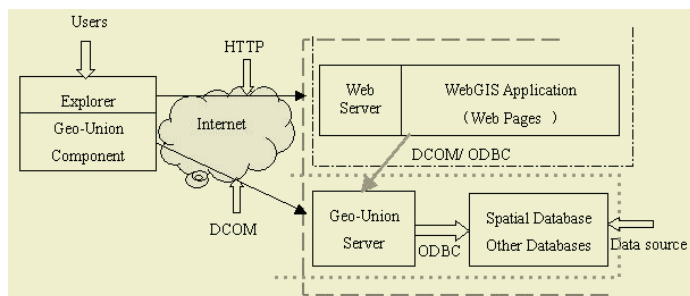


Fig. 6. Web Application Model in Geo-Union

Explorer communicates with Web server through HTTP and then gets WebGIS application module. Explorer interprets and executes the application module after receiving it. WebGIS applications are developed with Geo-Union components in specific application domain. WebGIS application and Web server compose WebGIS application server. WebGIS application can also access Geo-Union server to handle requests from Explorer.

Geo-Union server provides outer users interfaces to search and access spatial and non-spatial interfaces. As a client of Geo-Union server, Web server accesses geometry data through Geo-Union server, using ODBC or COM/DCOM. Explorer also needs accessing spatial and non-spatial data when interpreting and executing WebGIS application module. Here, as a client of Geo-Union server, explorer can search and access data using DCOM. When accessing spatial data which is transferred in vector form, explorer does not need downloading all data of the layer, but requests dynamically required entity data from Geo-Union server using entity data miss request algorithm. At the same time, as a client, Geo-Union server accesses spatial database to get spatial and non-spatial data through ODBC.

Based on commercial ORDBs, spatial database manages spatial and non-spatial data tightly relative with WebGIS application. Geo-Union server accesses database through ODBC, so the database needn't be confined in a certain specific databases.

## 4 Conclusion

Geo-Union system has been applied in many fields in China, such as pipe network integration information system, electric information system, water environment information system and fire emergency information system. At present, these systems are under stable and correct condition. What is more, the system keeps unflinching performance after repetitious visits.

Geo-Union system is also the result of research and application in some critical techniques of WebGIS. However, to reach higher practicability, many works left as



follows: (1) As the development of Internet, more and more spatial data become available. But these data have different formats. It is still hard to share the data and services between various GIS. In order to solve this problem, people have studied standardization of GIS, but the actual open GIS has not been formed. (2) Along with the further open of Internet, the security of visiting spatial data is an unavoidable problem which WebGIS has to face. It is hoped that the secret spatial data in Web can't be achieved unlawfully. (3) WebGIS will meet the needs of thousands upon thousands users who visit Internet at the same time. How to guarantee the exactitude of concurrency and how to use the system ability farthest to meet the users' visit needs are the keys to making WebGIS worthy of its name. (4) Nowadays, intelligent agent technique is a main research direction of software domain. It provides an effective solution for establishment of complicated distributed software system. Of course, agent technique also provides a fire-new method for the establishment of WebGIS <sup>[6]</sup>. Researches on how to exert agent technique on distributed GIS construction and combine it tightly with geometry spatial metadata are not only for GIS data sharing and service sharing, but for deep GIS application cooperation and intelligent GIS information services. Furthermore, the researches provide a simple and convenient agent-based system development method for users, thus having abroad application future and important practicality <sup>[7]</sup>.

## Acknowledgement

This work is supported by the National Research Foundation for the Doctoral Program of Higher Education of China under Grant No. 20020001015; the 973 Program of China under Grant No.2002CB312000; the National Science Foundation of China under Grant No.60203002; the 863 Program under Grant No. 2002AA135330 and No. 2002AA134030; the Beijing Science Foundation under Grant No.4012007.

## References

1. Zhang, Li, *et al*: Geographic Information System in the Internet Age (in Chinese), ACTA GEODAEITICA et CARTOGRAPHICA SINICA, 27(1): 9-15 (1998).
2. Luo, Yingwei, *et al*: The Components Design for WebGIS (in Chinese), Chinese Journal of Image and Graphics, 4(A): 79-84 (1999).
3. Li, Muhua: Research and Implementation of the Componentization of Distributed WebGIS (in Chinese), [Master Dissertation]. Beijing: Peking University (2000).
4. Wu, Jian: A Study on Spatial Data Management in Component-based Distributed WebGIS (in Chinese), [Master Dissertation], Beijing: Peking University (2000).
5. Cong, Shengri: Key Issues on ORDB-Based Component GIS (in Chinese), [PhD Dissertation], Beijing: Peking University (1999).
6. M. Wooldridge and N. R. Jennings: Intelligent Agents: Theory and Practice, Knowledge Engineering Review, 10(2): 115-152 (1994).
7. Luo, Yingwei, *et al*: The Research on Geo-Agents (in Chinese), Journal of Computer Research and Development, 37(12): 1504-1512 (2000).

# Adaptive Smoothing Neural Networks in Foreign Exchange Rate Forecasting

Lean Yu<sup>1,2</sup>, Shouyang Wang<sup>1,2</sup>, and Kin Keung Lai<sup>3,4</sup>

<sup>1</sup> Institute of Systems Science, Academy of Mathematics and Systems Sciences,  
Chinese Academy of Sciences, Beijing 100080, China

<sup>2</sup> School of Management, Graduate School of Chinese Academy of Sciences,  
Chinese Academy of Sciences, Beijing 100039, China  
{yulean, sywang}@amss.ac.cn

<sup>3</sup> College of Business Administration, Hunan University, Changsha 410082, China

<sup>4</sup> Department of Management Sciences, City University of Hong Kong,  
Tat Chee Avenue, Kowloon, Hong Kong  
mskklai@cityu.edu.hk

**Abstract.** This study proposes a novel forecasting approach – an adaptive smoothing neural network (ASNN) – to predict foreign exchange rates. In this new model, adaptive smoothing techniques are used to adjust the neural network learning parameters automatically by tracking signals under dynamic varying environments. The ASNN model can make the network training process and convergence speed faster, and make network's generalization stronger than the traditional multi-layer feed-forward network (MLFN) model does. To verify the effectiveness of the proposed model, three major international currencies (British pounds, euros and Japanese yen) are chosen as the forecasting targets. Empirical analyses reveal that the proposed novel forecasting model outperforms the other comparable models. Furthermore, experimental results also show that the proposed model is an effective alternative approach for foreign exchange rate forecasting.

## 1 Introduction

The difficulty in predicting foreign exchange rates, due to their high volatility and complexity, has long been an imperative concern in international financial markets as many econometric methods are unable to produce significantly better forecasts than the random walk (RW) model [1]. Recent studies provide some evidence that nonlinear models are able to produce better predictive results, ameliorating the performance of the simple RW model. Of the various nonlinear models, the artificial neural network (ANN) model has emerged as a strong alternative for predicting exchange rates. As claimed by Grudnitski and Osburn [2], neural networks are particularly well suited for finding accurate solutions in an environment characterized by complex, noisy, irrelevant or partial information. Literature documenting this research effort is quite diverse and involves different architectural designs. Some examples are presented. Early applications of neural networks in forecasting chaotic time series have been performed by Lapedes and Farker [3]. Weigend et al. [4] and Refenes et al. [5] ap-

plied multilayer forward network (MLFN) models in their forecasts of foreign exchange prices. Weigend's model performance was tested in terms of accuracy, giving support to nonrandom behavior. Refenes' work extended Weigend's research by adding a validity test to the model's performance and compared the results with those of the forward rate, thereby providing added support to the forecasting ability of neural networks in the foreign exchange market. Tenti [6] applied recurrent neural network (RNN) models to forecast exchange rates. Hsu et al. [7] developed a clustering neural network (CNN) model to predict the direction of movements in the USD/DEM exchange rate. Their experimental results suggested that their proposed model achieved better performance relative to other indicators. De Matos [8] compared the strength of a MLFN with that of a RNN based on the forecasting of Japanese yen futures. Likewise, Kuan and Liu [9] provided a comparative evaluation of MLFN's performance and an RNN for the prediction of an array of commonly traded exchange rates. In a more recent study by Leung et al. [10], MLFN's forecasting accuracy was compared with the general regression neural network (GRNN). The study showed that the GRNN possessed a greater forecasting strength relative to MLFN with respect to a variety of currency rates. Zhang and Berardi [11] adopted an ensemble method for exchange rate forecasting and obtained better results than those under a single network model. Chen and Leung [1] used an error correction neural network (ECNN) model to predict exchange rates and good forecasting results can be obtained with their model.

Although a handful of studies exist on neural network applications in foreign exchange markets, most of the literature focuses on the MLFN [1-5, 8-10, 12-15]. However, there are several limitations to the MLFN. For example, convergence speed of the MLFN algorithm is often slow, thus making the network learning time long. Furthermore, it is easy for the optimal solution to be trapped into local minima thus making generalization capability weak. Therefore, we propose an adaptive smoothing technique to overcome these limitations to predict the daily exchange rates for three major internationally traded currencies: British pounds, euros and Japanese yen. In order to provide a fair and robust evaluation of the ASNN model relative to performance, the forecasting performance of the proposed ASNN model is compared with those of the MLFN model, which is used as the benchmark model. The rest of this article is organized as follows. Section 2 describes the ASNN model in detail. Section 3 gives an experiment and reports the results. And Section 4 concludes the article.

## 2 Adaptive Smoothing Neural Network for Forecasting

### 2.1 The Introduction of Neural Networks

Artificial neural networks (ANNs) – originally developed to mimic neural networks, in particular the human brain – are composed of a number of interconnected simple processing elements called neurons or nodes. Each node receives an input signal from other nodes or external inputs; after processing the signals locally through a transfer function, a transformed signal is output to other nodes or final outputs. ANNs are characterized by the network architecture; that is, the number of layers, the number of nodes in each layer and how the nodes are connected. In a popular form, the multi-

layer feed-forward network (MLFN), all nodes and layers are arranged in a feed-forward manner. The first or the lowest layer is an input layer where external information is received. The last or the highest layer is an output layer where the network produces the model solution. In between, there are one or more hidden layers which are critical for ANNs to identify the complex patterns in the data. All nodes in adjacent layers are connected by acyclic arcs from a lower layer to a higher layer. ANNs are already one of the types of models that are able to approximate various nonlinearities in the data, and this makes them popular with academics and practitioners.

However, there are several drawbacks to the popular MLFN. First of all, the convergence speed of the MLFN algorithm is often slow, thus making network learning time long. Second, it is easy for the optimal solution obtained to be trapped into local minima, thus making generalization capability weak. Finally, the question of how to select reasonable network architecture is still an intractable problem.

In view of the above problems, in the following subsection we propose a novel algorithm to improve the MLFN by introducing adaptive smoothing techniques.

**2.2 The Adaptive Smoothing Neural Network Model**

In this study, adaptive smoothing techniques are used to adjust the neural network learning parameters automatically in terms of tracking signals under dynamic varying environments. This yields a new weight adjustment algorithm in virtue of quality control (QC) concept. In MLFN, model errors are usually the squared error or mean squared error (MSE). But using these error metrics makes it difficult to capture deviations between actual values and network output values (or expected values). In the process of neural network learning, adaptive smoothing algorithms can utilize ordinary error and mean absolute deviation (MAD) as a supplement of error measure to adjust the network’s parameters (i.e., learning weights). With the aid of cumulative ordinary error (COE), MAD, and derivative tracking signal (TS), an adaptive smoothing neural network model can be formulated.

Assume that a network with  $m$  layers has  $n$  nodes, the transfer function of every node is usually a sigmoid function (i.e.,  $f(x) = \frac{1}{1 + e^{-x}}$ ),  $y$  is an output from the output layer,  $O_i$  is an output of any unit  $i$  in a hidden layer,  $W_{ij}$  is the weight on connection from the  $j$ th to the  $i$ th unit. Suppose that there are  $N$  sample pairs  $(x_k, y_k)$  ( $k = 1, 2, \dots, N$ ), the output of unit  $i$  connected with the  $k$ th sample is  $O_{ik}$ , the input of unit  $j$  connected with the  $k$ th sample is

$$net_{jk} = \sum_i W_{ij} O_{ik} \tag{1}$$

And the output of unit  $j$  connected with the  $k$ th sample is

$$O_{jk} = f(net_{jk}) \tag{2}$$

Here the error function is the squared error, i.e.,  $E = \frac{1}{2} \sum_{k=1}^N (y_k - \hat{y}_k)^2$ , the cumulative ordinary error (COE) is  $COE(N) = \sum_{k=1}^N (y_k - \hat{y}_k)$ , where  $y_k$  is the actual value and  $\hat{y}_k$  is the network output value. Let  $E_k$  and  $COE_k$  be a squared error and an ordi-

nary error connected with the  $k$ th sample, then  $E_k = (y_k - \hat{y}_k)^2$  and  $COE_k = (y_k - \hat{y}_k)$ . Clearly,  $COE(N) = COE(N - 1) + COE_N$ . Meanwhile, the mean absolute deviation ( $MAD$ ) and tracking signal ( $TS$ ) are defined as

$$MAD(N) = \frac{\sum_{k=1}^N |y_k - \hat{y}_k|}{N} \tag{3}$$

$$TS = \frac{COE(N)}{MAD(N)} \tag{4}$$

If  $TS$  is “large”, this means that  $COE(N)$  is large relative to the mean absolute deviation  $MAD(N)$ . This in turn says that the network output is producing errors that are either consistently positive or consistently negative. That is, a large value of  $TS$  implies that the network output is producing forecasts that are either consistently smaller or consistently larger than the actual values that are being forecast. Since an “accurate” forecasting system should be producing roughly one half positive errors and one half negative errors, a large value of  $TS$  indicates that the forecast output is not reliable. In practice, if  $TS$  exceeds a control limit, denoted by  $\theta$ , for two or more consecutive periods, this is taken as a strong indication that the forecast errors have been larger than an accurate forecasting system can reasonably be expected to produce. In our study, the control limit  $\theta$  is generally taken to be  $3\sigma$  for a neural network model with the aid of the ‘ $3\sigma$  limits theory’ proposed by Shewhart [16].

If the error signal indicates that adjustment action is needed, there are several possibilities. One possibility is that the model needs to be changed. To do this, input variables may be added or deleted to obtain a better representation of the time series. Another possibility is that the model being used does not need to be changed, but the estimates of the model’s parameters need to be changed. When using a neural network model, this is accomplished by changing parameters (i.e., model weights and bias).

Now we present the parameter adjustment process. Define the error gradient  $\delta_{jk} = \frac{\partial E_k}{\partial net_{jk}}$ , then

$$\frac{\partial E_k}{\partial W_{ij}} = \frac{\partial E_k}{\partial net_{jk}} \cdot \frac{\partial net_{jk}}{\partial W_{ij}} = \frac{\partial E_k}{\partial net_{jk}} \cdot O_{ik} = \delta_{jk} \cdot O_{ik} \tag{5}$$

(i) If  $j$  is the output node,  $O_{jk} = \hat{y}_k$ , then

$$\delta_{jk} = \frac{\partial E_k}{\partial net_{jk}} = \frac{\partial E_k}{\partial \hat{y}_k} \cdot \frac{\partial \hat{y}_k}{\partial net_{jk}} = -(y_k - \hat{y}_k) \cdot f'(net_{jk}) \tag{6}$$

(ii) If  $j$  is not the output node, then

$$\delta_{jk} = \frac{\partial E_k}{\partial net_{jk}} = \frac{\partial E_k}{\partial O_{jk}} \cdot \frac{\partial O_{jk}}{\partial net_{jk}} = \frac{\partial E_k}{\partial O_{jk}} \cdot f'(net_{jk}) \tag{7}$$

$$\frac{\partial E_k}{\partial O_{jk}} = \sum_m \frac{\partial E_k}{\partial net_{mk}} \cdot \frac{\partial net_{mk}}{\partial O_{jk}} = \sum_m \frac{\partial E_k}{\partial net_{mk}} \cdot \frac{\partial}{\partial O_{jk}} \sum_i W_{mi} \cdot O_{ik} = \sum_m \frac{\partial E_k}{\partial net_{mk}} W_{mj} = \sum_m \delta_{mk} \cdot W_{mj} \tag{8}$$

Thus

$$\begin{cases} \delta_{jk} = f'(net_{jk}) \sum_m \delta_{mk} W_{mj} \\ \frac{\partial E_k}{\partial W_{ij}} = \delta_{jk} \cdot O_{ik} \end{cases} \tag{9}$$

The error  $\delta_{jk}$  is propagated back to the lower layers in terms of Equations (6) and (9).

In order for the network to learn, the value of each weight has to be adjusted in proportion to each unit's contribution to the total error in Equations (6) and (9). The incremental change in each weight for each learning iteration is computed using Equations (10) and (11) in the following:

$$\Delta W_{ij} = c_1 \cdot \delta_{jk} \cdot O_{ik} + c_2 \cdot \varphi_{jk} \tag{10}$$

where  $c_1$  is a learning rate ( $0 \leq c_1 < 1$ ),  $c_2$  is a positive constant that, being less than 1.0, is the smoothing rate to smooth out the weigh changes; and

$$\varphi_{jk} = \begin{cases} 0, & |TS| \leq \theta, (\theta = 3\sigma[16] \text{ or } \theta = 4 \cdot MAD [17]); \\ -COE(N), & |TS| > \theta \text{ and } TS \leq 0; \\ COE(N), & |TS| > \theta \text{ and } TS > 0. \end{cases} \tag{11}$$

It should be noted that there is a difference between our weight adjustment and the traditional momentum term. The traditional momentum term is only used to accelerate the neural network learning speed, while our weight adjustment cannot only increase learning speed but can also adjust the network search path and speed network convergence and improve neural network learning performance.

For convenience, we give the detailed algorithm for ASNN in the sequel:

- (1) Initialize random weights to avoid saturation in the learning process.
- (2) Iterate the following procedures, until error goals are satisfactory
  - a. For  $k=1$  to  $N$ 
    - (i) Compute  $O_{ik}, net_{jk}, COE(N), MAD(N)$  and  $\hat{y}_k$  (forward process)
    - (ii) Compute  $\delta_{jk}$  from the output layer to the preceding layer inversely (backward process)
  - b. For any nodes in the same layer, compute  $\delta_{jk}$  according to Equations (6) and (9)
- (3) Adjust weights with Equations (10) and (11) in terms of error gradient and tracking signals.

This completes the introduction of the ASNN algorithm. Usually, we can obtain the following benefits relative to traditional MLFN algorithms. First of all, learning error limits can be controlled via the corresponding program, making the search space smaller and learning accuracy higher. Second, model parameters can be adjusted adaptively in term of tracking signals, thus making network learning more efficient. Third, the search path can be adjusted by a smoothing factor and making it easier to obtain the network optimal solution than by using the MLFN algorithm.

To summarize, adaptive smoothing neural networks can adjust the model parameters adaptively and automatically via tracking signals, thus making the network search and convergence speed faster and avoiding local minima as far as possible.

### 2.3 ASNN for Time Series Forecasting

An adaptive smoothing neural network can be trained by the historical data of a time series in order to capture the nonlinear characteristics of the specific time series. The model parameters (such as connection weights and nodes biases) will be adjusted iteratively by a process of minimizing the forecasting errors (e.g., MSE). For time series forecasting, the computational form of the ASNN model with three-layer network connection is expressed as

$$x_t = a_0 + \sum_{j=1}^q w_j f(a_j + \sum_{i=1}^p w_{ij} x_{t-i}) + \xi_t \quad (12)$$

where  $a_j$  ( $j = 0, 1, 2, \dots, q$ ) is a bias on the  $j$ th unit, and  $w_{ij}$  ( $i = 1, 2, \dots, p; j = 1, 2, \dots, q$ ) is the connection weight between layers of the model,  $f(\bullet)$  is the transfer function of the hidden layer,  $p$  is the number of input nodes and  $q$  is the number of hidden nodes. Actually, the ASNN model in (12) performs a nonlinear functional mapping from the past observation  $(x_{t-1}, x_{t-2}, \dots, x_{t-p})$  to the future values  $x_t$ , i.e.,

$$x_t = g(x_{t-1}, x_{t-2}, \dots, x_{t-p}, v) + \xi_t \quad (13)$$

where  $v$  is a vector of all parameters and  $g$  is a nonlinear function determined by the network structure and connection weights. Thus, in some senses, the ASNN model is equivalent to a nonlinear autoregressive (NAR) model [15]. To verify the effectiveness of the ASNN model, a simulation study is presented in the following section.

## 3 Experiment Study

### 3.1 Data Sources

We use three different datasets in our forecast performance analysis. The data used are daily and are obtained from Pacific Exchange Rate Service (<http://fx.sauder.ubc.ca/>), provided by Professor Werner Antweiler, University of British Columbia, Vancouver, Canada. They consist of the US dollar exchange rate against each of the three currencies (EUR, GBP and JPY) with which it has been studied in this research. We take the daily data from 1 January 2000 to 31 October 2002 as in-sample data sets, and we take the data from 1 November 2002 to 31 December 2002 as evaluation test sets or out-of-sample datasets (partial data sets excluding holidays), which are used to evaluate the good or bad performance of the predictions, based on evaluation measurements. In order to save space, the original data are not listed in the paper, detailed data can be obtained from the website. In addition, to examine the forecasting performance, the normalized mean squared error (NMSE) [15] and directional change statistics of exchange rate movement ( $D_{stat}$ ) [14, 15] are employed here.

### 3.2 Experimental Results

When the data are prepared, we begin the ASNN model's training and learning process. In these experiments, we prepare 752 data (two years' data excluding public holidays). We use the first 22 months' data to train and validate the network, and use the

last two months' data for prediction testing. For convenience, the three-day-ahead forecasting results of three major international currencies using the proposed ASNN model are shown in Table 1.

**Table 1.** Forecast performance evaluation for the three exchange rates

Exchange rates	British pounds		Euros		Japanese yen	
	MLFN	ASNN	MLFN	ASNN	MLFN	ASNN
<i>NMSE</i>	0.5534	0.1254	0.2137	0.0896	0.2737	0.1328
<i>D<sub>stat</sub></i> (%)	55.00	77.50	57.50	72.50	52.50	67.50

As can be seen from Table 1, we can conclude that: (i) from the viewpoint of *NMSE* indicator, the ASNN model performs consistently better than the MLFN model; (ii) furthermore, the *NMSE* of the MLFN model is much larger than that of the ASNN model, indicating that adaptive smoothing techniques can effectively control error changes and significantly improve network performance; and (iii) from the *D<sub>stat</sub>* point of view, the correct number of direction of exchange rate movements increases when using the ASNN model. Among these, the increase in the British pound rate is the largest, while the increase in the Japanese yen rate is the smallest. This suggests that there may be some additional factors that need to be studied in relation to the Japanese yen. One possible reason is that the Japanese yen exchange rate is more volatile than that of the British pound; another might be that the market for yen is bigger and more efficient than the market for British pounds. However, we also find that it is feasible to predict exchange rates using the ASNN model, and that the results are promising.

## 4 Concluding Remarks and Future Research

This exploratory research examines the potential of using an ASNN model to predict main international currency exchange rates. Our empirical results suggest that the ASNN forecasting model may provide better forecasts than the traditional MLFN forecasting model. The comparative evaluation is based on a variety of statistics such as *NMSE* and *D<sub>stat</sub>*. For all currencies included in our empirical investigation, the ASNN model outperforms the traditional MLFN model in terms of *NMSE* and *D<sub>stat</sub>*. Furthermore, our experimental analyses reveal that the *NMSE* and *D<sub>stat</sub>* for three currencies using the ASNN model are significantly better than those using the MLFN model. This implies that the proposed ASNN forecasting model can be used as a feasible solution for exchange rate prediction.

However, our work also highlights some problems that need to be addressed further. For example, the accuracy of rolling forecasting is still unsatisfactory for certain currencies, such as the Japanese yen. Of course, the above problems show possible directions for future work in formulating a generic adaptive smoothing neural network prediction model for exchange rate prediction as follows:

(i) As foreign exchange markets constitute a very complex system, more factors that influence the exchange rate movement should be considered in future research.



(ii) A new adaptive smoothing algorithm that improves the traditional MLFN model should be added to neural network software packages so that users working in other domains can more easily utilize new neural network models in their work.

## References

- [1] Chen, A.S., Leung, M.T.: Regression neural network for error correction in foreign exchange forecasting and trading. *Computers and Operations Research*, 31, (2004) 1049-1068.
- [2] Grudnitski, G., Osburn, L.: Forecasting S&P and gold futures prices: an application of neural networks. *Journal of Futures Market*, 13, (1993) 631-643.
- [3] Lapedes, A., Farber, R.: Nonlinear signal processing using neural network prediction and system modeling. Theoretical Division, Los Alamos National Laboratory, *NM Report*, (1987) No. LA-UR-87-2662.
- [4] Weigend, A.S., Huberman, B.A., Rumelhart, D.E.: Generalization by weight-elimination with application to forecasting. In: Lippman, R.P., Moody, J.E. and Touretzky, D.S. (Eds), *Advances in Neural Information Processing Systems*, 3, Morgan Kaufman, San Mateo, CA, (1991) 875-882.
- [5] Refenes, A.N., Azema-Barac, M., Chen, L., Karoussos, S.A.: Currency exchange rate prediction and neural network design strategies. *Neural Computing and Applications*, 1, (1993) 46-58.
- [6] Tenti, P.: Forecasting foreign exchange rates using recurrent neural networks. *Applied Artificial Intelligence*, 10, (1996) 567-581.
- [7] Hsu, W., Hsu, L.S., Tenorio, M.F.: A neural network procedure for selecting predictive indicators in currency trading. In: Refenes, A.N. (Ed), *Neural Networks in the Capital Markets*, New York: John Wiley and Sons, (1995) 245-257.
- [8] De Matos, G.: Neural networks for forecasting exchange rate. *M. Sc. Thesis*. The University of Manitoba, Canada (1994).
- [9] Kuan, C.M., Liu, T.: Forecasting exchange rates using feedforward and recurrent neural networks. *Journal of Applied Econometrics*, 10 (4), (1995) 347-364.
- [10] Leung, M.T., Chen, A.S., Daouk, H.: Forecasting exchange rates using general regression neural networks. *Computers and Operations Research*, 27, (2000) 1093-1110.
- [11] Zhang, G.P., Berardi, V.L.: Time series forecasting with neural network ensembles: an application for exchange rate prediction. *Journal of the Operational Research Society*, 52, (2001) 652-664.
- [12] Brooks, C.: Linear and nonlinear (non-) forecastability of high frequency exchange rates. *Journal of Forecasting* 16, (1997) 125-145.
- [13] Gencay, R.: Linear, nonlinear and essential foreign exchange rate prediction with simple technical trading rules. *Journal of International Economics*, 47, (1999) 91-107.
- [14] Yao, J.T., Tan, C.L.: A case study on using neural networks to perform technical forecasting of forex. *Neurocomputing*, 34, (2000) 79-98.
- [15] Yu, L.A., Wang, S.Y., Lai, K.K.: A novel nonlinear ensemble forecasting model incorporating GLAR and ANN for foreign exchange rates. *Computers and Operations Research*, (2004) In Press.
- [16] Shewhart, W. A.: *Economic Control of Quality of Manufactured Product*, New York, (1931).
- [17] Chase, R.B., Aquilano, N.J., Jacobs, R.F.: *Production and Operations Management: Manufacturing and Services*, McGraw-Hill, (1998).

# Credit Scoring via PCALWM\*

Jianping Li<sup>1,ψ</sup>, Weixuan Xu<sup>1</sup>, and Yong Shi<sup>2</sup>

<sup>1</sup> Institute of Policy and Management,  
Chinese Academy of Sciences, Beijing 100080, P.R.China  
ljp@mail.casipm.ac.cn, jianpingli@yahoo.com  
<sup>2</sup> Chinese Academy of Sciences Research Center on Data Technology  
and Knowledge Economy, Beijing 100039, P.R.China  
yshi@gscas.edu.cn

**Abstract.** We have presented a principal component analysis linear-weighted model (PCALWM) for credit scoring in [5,6], this article is a further study on this model. We revised the application procedure in the credit scoring, and tested it by a larger real-life credit card dataset. In comparison with some well-known scores, the empirical results of the PCALWM can achieve a favorable KS distance. The study on some application features of this model in the credit decision-making shows that the model can help the credit issuers to select the best trade-off among the enterprise stratagem, marketing and credit risk management.

**Keywords:** Credit scoring, Classification, Principal component analysis.

## 1 Introduction

The growth in consumer credit outstanding over the last fifty years is truly spectacular in the major countries, for example, in US, from the \$9.8 billions in the year 1946 to \$20,386 in 2003[2]. Not all of this growth is due to the borrowing on credit lines, Credit card (and debit cards) has become increasingly important as a method of money transmission.

However, from the perspective of history, the increase of total outstanding of consumer credit is always accompanying with more much consumers' bankruptcy and default, which are causing plenty of headaches for banks and other credit issuers. From 1980 to 2003, the number of individual bankruptcy filings in the US had increased by 560%[11]. How to predict bankruptcy and avoid huge charge-off loss becomes a critical issue of credit issuers.

In the consumer credit assessment, credit scoring is widely used. Credit scoring provides a suite of decision-support tools to aid the credit analyst. In credit scoring

---

\* This research has been partially supported by a grant from National Natural Science Foundation of China (#70472074) and the President Fund of Chinese Academy of Sciences (CAS) (yzjj946).

<sup>ψ</sup> Corresponding author.

system, the classification tools, which are derived from analyzing similar data for previous customers, are used to categorize new applicants or existing customers as good or bad. There are lots of classification tools available now, such as statistics methods like discriminant analysis, regression, classification tree, nearest-neighbor approach, nonstatistical method like linear programming, neural networks, genetic algorithms, expert systems, etc [12,13].

The purpose of this paper is to further analyze the principle components analysis linear-weighted model (PCALWM) which we had presented to assess the consumer credit [5,6]. We will apply this model to a larger real-life credit card database to evaluate its performance and study the characteristics in credit decision. This study will make the model more applicable and help the credit issuers to make right decision.

## **2 The Basic Principals and Application Stages of PCALWM in Credit Scoring**

Principle components analysis (PCA) is a well-known, widely-used statistical technique, and it is a purely data-driven way of exploring the data. The central idea is to reduce the dimensionality of a data set consisting of a large number of interrelated variables, while retaining as much as possible of the variation present in the data set. The PCA approach uses all of the original variable to obtain a smaller set of new variables (principal components--PCs) that they can used to approximate the original variables. The greater the degree of the correlation between the original variables, the fewer the number of new variables required. PCs are uncorrelated and ordered so that the first few retain most of the variation present in the original set.

PCA approach was applied to the credit risk management cooperated with other methods, Alici[1] used this method to predict the corporation bankruptcy with neural networks. Recently PCA has attracted much attention in the risk analysis in larger scale data and consumer credit data [3,8,14].

The PCALWM based credit scoring system includes 4 stages, data preparation, training, testing, and predicting. The main stages show by figure 1.

### **2.1 Data Preparation**

This stage consist of collecting relevant data, merging and cleaning the data, defining the classes, selecting the variables, etc. we will get a dataset with suitable format which is fit for the PCA computing after this stage.

### **2.2 Training Stage**

We classify the data set into two parts, one for training to construct the predicting model and the other for testing to validate the model. The different rate of the training data in the total sample will impact the model's efficiency, and a good classification of the training data rate maybe get a good classification model.

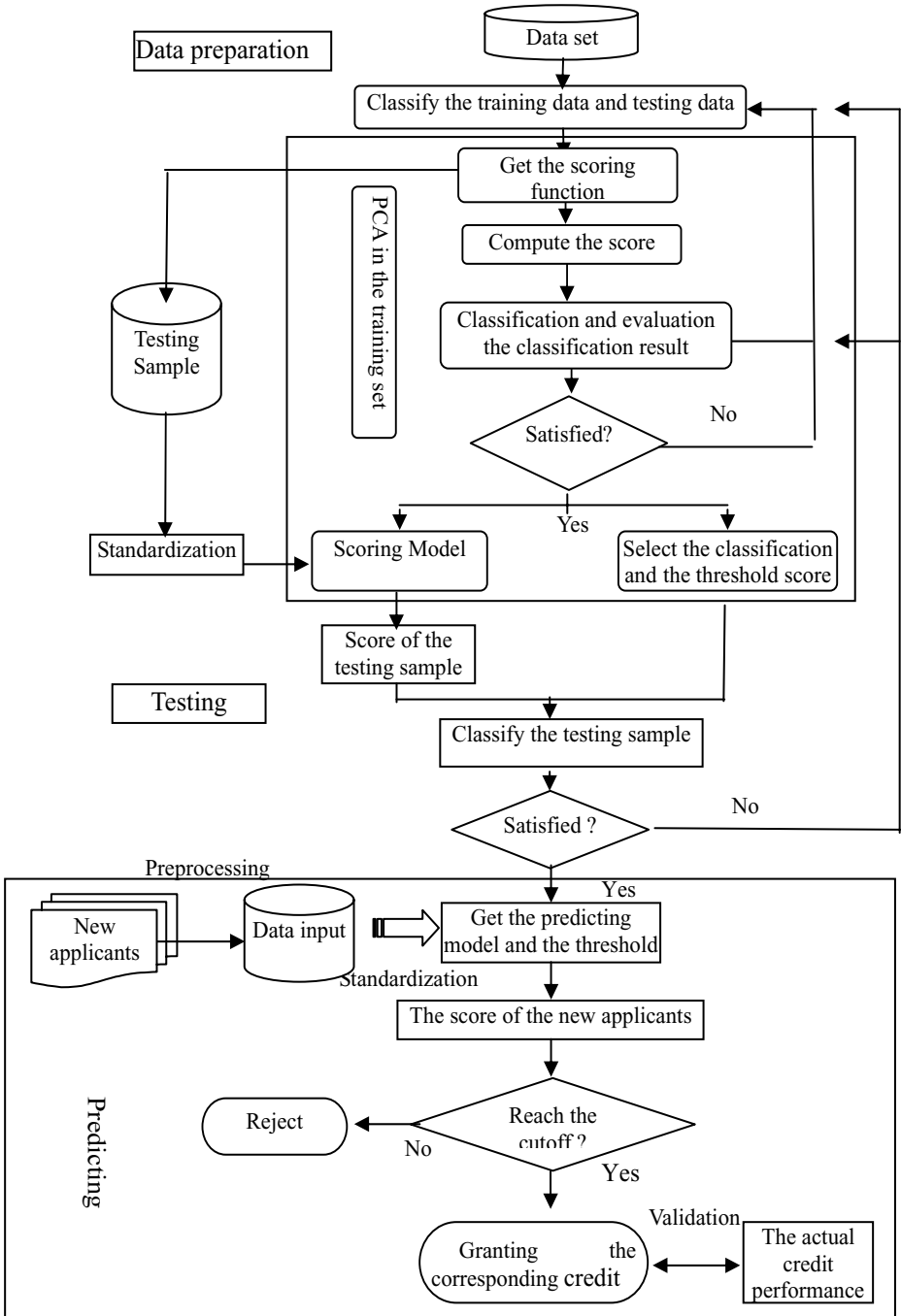


Fig. 1. The application procedure of PCALWM in credit scoring

The training stage is to achieve predicting model and set up the different credit grade. Supposed we have selected principal factors, the scoring function of the principal factors in the training sample could be expressed as:

$$F = a_1 z_1 + a_2 z_2 + \dots + a_s z_s \tag{2.1}$$

$z_i$  is the  $i^{th}$  principal factor,  $a_i$  is its contribution rate :

$$a_i = \frac{\lambda_i}{\sum_{m=1}^k \lambda_m} \quad a_{il} = \frac{\sum_{m=1}^l \lambda_m}{\sum_{m=1}^k \lambda_m} \quad (i, l = 1, 2, \dots, k)$$

(  $\lambda_i$  is the  $i^{th}$  eigenvalue sorted by descending,  $a_{il}$  is the cumulative variance contributions of principal factor  $z_1$  to  $z_l$  ). Then,

$$Z_i = b_{i1}x_1 + b_{i2}x_2 + \dots + b_{in}X_n \tag{2.2}$$

Take the equation (2) into equation (1), we get:

$$F = c_1 x_1 + c_2 x_2 + \dots + c_n X_n \tag{2.3}$$

$$c_j = \sum_{i=1}^s a_i b_{ij} \quad (i = 1, 2, \dots, s; j = 1, 2, \dots, n)$$

According to the score and the distribution of the bad credit in the training sample, we can set up the different grade by a certain method and standard. Then one can classify the different class based on the score. If the classification result is not ideal, we will classify and compute the data again.

### 2.3 Testing Stage

This stage is to validate the model and the credit grade which get from the training stage. We will choose the right score model and credit grade in this stage.

We use the same procedures in the training stage. But in data standardization here we will take the average and standard deviation of the training sample, so we get the data matrix  $X_i = (x_{i1}^*, x_{i2}^*, \dots, x_{ip}^*)^T \quad i = 1, 2, \dots, m$ .

We use the equation 2.3 to compute the credit score in the testing sample, and classify the credit grade with the set grade in training stage. Similarly, if the classification result is not satisfied, we would classify the originate data and compute again.

### 2.4 Predicting the New Applicants

In this stage, we use the score model to predict the new applicants credit score and make the credit decision. After computing the new applicants credit score with the certain procedure as in the testing stage, we compare it with the credit standard which get from the training and testing stage. If the score reaches the threshold, we grant the corresponding credit, otherwise reject.

### 3 Empirical Study

#### 3.1 Data Set

We use real life credit card data from a major US bank to conduct the experiment. This data set is composed by 5000 records, and two classes have been defined: good credit and bad credit. 65 variables are selected for personal credit assessment. There are including history payment, balance, transaction, account open, etc. we chose the SPSS soft to perform all of the computations.

#### 3.2 Computation Result and Analysis

In fact, the practitioners have tried a number of quantitative techniques to conduct the credit card portfolio management. Some examples of known scores are (1) Behavior Score developed by Fair Isaac Corporation (FICO) [15]; (2) Credit Bureau Score also developed by FICO [15]; (3) First Data Resource (FDR)'s Proprietary Bankruptcy Score [4]; (4) Multiple-criteria Score [9,10] and (5) Dual-model Score [7]. These methods can be generally regarded as two-group classification models, and use either statistical methods or neural networks to compute the Kolmogorov-Smirnov (KS) value that often used to measure how far apart the distribution functions of the scores of the goods and bads are[13]. The resulting KS values from the learning process are applied to the real-life credit data warehouse to predict the percentage of bankrupt accounts in the future.

Formally, if  $n_G(s)$  and  $n_B(s)$  are the numbers of goods and bads with scores in a sample of  $n$ , where there are  $n_G$  goods and  $n_B$  bads, the  $p_G(s) = \frac{n_G(s)}{n_G}$  and

$p_B(s) = \frac{n_B(s)}{n_B}$  are the probabilities of a good and bad having a score  $s$ , then the KS distance is

$$KS = \max_s |p_G(s) - p_B(s)| \quad (3.1)$$

We chose 2000 records as a training set as random to compute the score model, and set three testing samples with 1000, 2000, 3000 records in the other 3000 records as random. The KS distances show as the table 1, the biggest is 0.6222 and lowest is 0.524.

**Table 1.** KS values of the different samples

	Traning2000	Testing1000	Testing2000	Testing3000
KS value	0.6223	0.5993	0.563	0.524

The KS values of some well-known score models in our 1000 sample are as the table 2.

**Table 2.** KS values of the different scores



	FICO	Credit bureau score	FDC proprietary bankruptcy score	Decision trees score	Multiple-criteria Linear Program score	PCALWM score
KS value	0.553	0.456	0.592	0.602	0.595	0.599

Among these scores, the PCALWM score is better than any other scores, except the decision tree score, so the PCALWM can achieve a good KS distance, and have a good classification.

#### 4 Two Characteristics in Credit Decision-Making of PCALWM

In the practice, credit policy is the trade-off of the enterprise’s stratagem, marketing and risk management. Loose credit policy is helpful to the market expanding, while strict credit policy for the risk management. General speaking, the loose credit policy will increase the type I error, and decrease the type II error to the credit issuers, while the strict credit policy makes the opposite effect. So, if the model can give the movement of the two type error with different credit granting rate efficiently, the model will greatly help to the credit issuers to make the trade-off in the actual credit decision.

For the encouragement of the primary empirical result, we will further study the application of PCALWM in the credit decision, mainly on:

-  The classification error with different training sample rate, that to say how the training sample rate affects the classification accuracy.
-  the classification error under the different granting rate with certain training sample rate. This will help the credit issuers to determine the granting rate under certain risk level.

##### 4.1 The Training Sample Rate to the Classification Error

We will study the different classifying training and testing sample how to affect the classification error. In other words , under what training sample rate, the model can get the better classification. We chose different training sample rate at random to construct the predict model, and in the granting rate of 75%, compared the two type error and the average error.

We chose five group training sample at random, including 500, 1000, 2000, 3000, 4000 records respectively, corresponding to the 10%, 20%, 40%, 60%, 80% of the total sample, and the five testing sample are the corresponding rest records, which including 4500, 4000, 3000, 2000, 1000 records. Table 3 shows the classification error of the five testing samples.

The results showed that with the incensement of the training rate, type I error and average error decreased, but the type II error no obviously change. The type I error

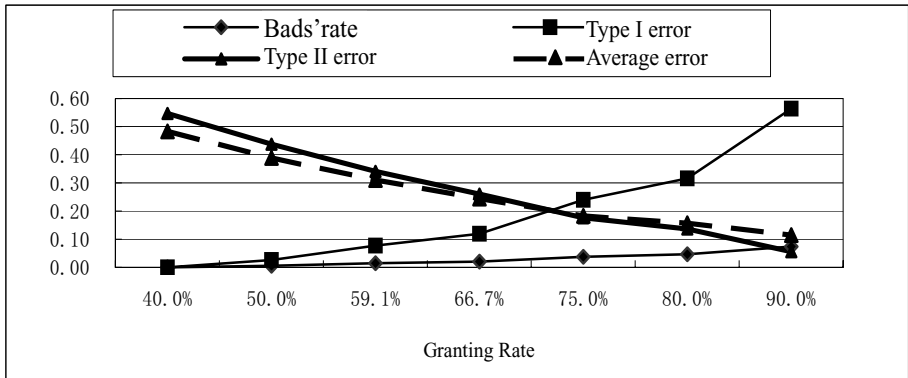
**Table 3.** The classification error of testing sample in different training rate

Training rate	10%	20%	40%	60%	80%
Type I error	0.3952	0.3481	0.3003	0.2652	0.2393
Type II error	0.1787	0.1749	0.1740	0.1763	0.1758
Average error	0.2113	0.2058	0.1937	0.1880	0.1832

decreased rapidly, but the speed tends to slow. This results show that a bigger training rate will help to PCALWM the get a better classification, especially to decrease the type I error.

#### 4.2 The Classification Error Under Different Granting Rate with a Certain Training Rate

We chose seven granting rate groups with 80% training rate, figure 2 displays the error movements.

**Fig. 2.** The classification errors of testing sample in different granting rate

The results shows that as the granting rate increases, type I error increases, while type II error decreases sharply, and the bads' rate in granted group increases slowly. This shows the model has a good classification.

In practice, based on the tradeoff of marketing, enterprise stratagem and risk management, the credit issuers can make the choice of the two type error and average error to determine the best grant standard.

## 5 Summary and Conclusion

This paper has a further study on the principal component analysis linear-weighted model for credit scoring. It presents the application procedures in the credit scoring,



tested by a larger real-life credit card data, and some application features in the credit decision-making. The empirical results and application characteristics of PCALWM show the model will help the credit issuers to make the best trade-off among the enterprise strategem, marketing and credit risk management.

Compared with some well-known credit scores, such as FICO behavior score, credit bureau score, first data resources' proprietary bankruptcy score and set enumeration decision tree score, Multiple criteria linear programming score, our model has a favorable classification.

Because of the great potential value in the consumer credit assessment, we will continue to perfect this model, we hope to get better results through more logical data processing and more suitable sample scale selecting, etc.

## References

1. Alici, Y. (1995). Neural networks in corporate failure prediction: The UK experience. In: Proceedings of 3rd International Conference Neural Networks in the Capital Markets, A. N. Refenes, Y. Abu-Mostafa, J. Moody, and A. Weigend, Eds. London, UK, 393-406.
2. Board of Governors of the Federal Reserve System [http://www.federalreserve.gov/releases/g19/hist/cc\\_hist\\_mt.txt](http://www.federalreserve.gov/releases/g19/hist/cc_hist_mt.txt)
3. Guo, Q, Wu, W., Massart, D.L., Boucon, C., Jong, S. de. (2002). Feature selection in principal component analysis of analytical data. *Chemometrics and Intelligent Laboratory Systems*, 61:123-132
4. <http://www.firstdatacorp.com>
5. Li, J.P, Liu, J.L, Xu, W.X, Shi, Y. (2004). An Improved Credit Scoring Method for Chinese Commercial Banks. In: S.Y. Wang and X.G. Yang eds., *Advance in Risk Management, Lecture Notes in Decision Sciences*, Global-Link Publisher, Hong Kong, Vol.4:63-73
6. Li, J.P, Xu, W.X. (2004). Consumer Credit Assessment via Principal Component Analysis Linear-Weighted Model. *Chinese Journal of Management*, Vol.12, (2): 63-73
7. Lin, Y. (2002). Improvement On Behavior Scores by Dual-Model Scoring System. *International Journal of Information Technology and Decision Making*. (1): 153-164.
8. Sebzalli, Y.M., Wang, X.Z. (2001). Knowledge discovery from process operational data using PCA and fuzzy clustering. *Engineering Applications of Artificial Intelligence*, (14): 607-616
9. Shi, Y., Wise, M., Luo, M., Lin, Y. (2001). Data Mining in Credit Card Portfolio Management: A Multiple Criteria Decision Making Approach. In: Koksalan, M., Zions, S. (eds.): *Multiple Criteria Decision Making in the New Millennium*. Springer, Berlin 427-436.
10. Shi, Y., Peng, Y., Xu, W., Tang, X. (2002). Data Mining Via Multiple Criteria Linear Programming: Applications in Credit Card Portfolio Management. *International Journal of Information Technology and Decision Making*. 1 :131-151.
11. The American Banker Association. <http://www.aba.com/default.htm>
12. Thomas, L.C. (2000). A survey of credit and behavioural scoring: forecasting financial risk of lending to consumers. *International Journal of Forecasting*, 16:149-172
13. Thomas, L.C., Edelman, D.B., Crook, J.N. (2002). *Credit Scoring and Its Application*. Society for Industrial and Applied Mathematics, Philadelphia
14. Westad, F., Hersleth, M., Lea, P.r, Martens, H. (2003). Variable Selection in PCA in sensory descriptive and consumer data. *Food Quality and Preference*, (14):463-472
15. [www.fairisaac.com](http://www.fairisaac.com)

# Optimization of Bandwidth Allocation in Communication Networks with Penalty Cost\*

W. U. U<sup>1,3</sup>, U. U<sup>2</sup>, and H. U. A. G. A. G.<sup>3</sup>

<sup>1</sup> Institute of Intelligent Information and Communications Technology,  
Konan University, Kobe 658-8501 Japan  
wujun@iss.ac.cn

<sup>2</sup> Department of Information Science and Systems Engineering,  
Konan University, Kobe 658-8501 Japan  
yue@konan-u.ac.jp

<sup>3</sup> Academy of Mathematics and Systems Science,  
Chinese Academy of Sciences, Beijing 100080 China  
sywang@amss.ac.cn

**Abstract.** In this paper, we present an analysis on optimization and risk management in Communication Networks (CNs). The model is proposed for offline traffic engineering optimization, which takes a centralized view of bandwidth allocation, performance control, and risk control of network profit shortfall. First, we introduce a linear penalty cost in the CN optimization model and derive the optimal bandwidth capacity with the penalty cost. Then, we use the mean-variance approach to analyze the profit shortfall risk in CNs. Finally, numerical results are shown to reveal the impact of the penalty cost on the CNs performance.

## 1 Introduction

traffic engineering is a process to optimize resource utilization and network performance [1]. It has great impact on network performance because the emerging technologies, such as multi-attribute traffic and Optical Channel Sharing [2, 4]

there are two forms of traffic engineering: one is a global one and the other is a local one. In the past works, the global optimization problem is formulated as a deterministic cut Capacity Model (CCM) [3] where demand of each channel is given as a fixed quantity.

Recently, there are some works concerning with the stochastic traffic engineering. Traditionally presented a stochastic traffic engineering framework for optimizing bandwidth provisioning and path selection [5]. C. S. 7 [6] traditionally a gas developed a optimization framework for the network service provider

---

\* This work was supported in part by GRANT-IN-AID FOR SCIENTIFIC RESEARCH (No. 16560350) and by MEXT.ORC (2004-2008), Japan and in part by NSFC and MADIS, China.

to manage profit at the market. Straadag furthered the studies [7, 8] and deepened the effective frontier of measure and user risk. Yue and Stradag presented a stochastic model for profit maximizing bandwidth allocation, which takes a centralized effective bandwidth allocation performance criterion and risk-free profit sharing. He analyzed the service rate constraint and risk aversion. The profit maximization model showed the impact of the service rate constraint and the risk aversion on the network performance.

In this paper, based on the model presented in [7], we introduce a new performance criterion for profit and risk bandwidth allocation. Here, we consider satisfied traffic demand with the maximum effective bandwidth, a new performance criterion will be added. The objective function of the study is the risk-free profit sharing based on the measure and approximation [2]. Numerical results are shown to reveal the impact of the performance on the network performance.

The rest of this paper is organized as follows. Section 2 presents the system model that we consider. This paper also presents the statistical and preliminary results. Section 3 reformulates the profit maximization model and derives the maximum bandwidth capacity with the new performance criterion. Section 4 evaluates the network profit sharing risk based on the measure and approximation [2]. Numerical results show the impact of the performance on the network performance. Conclusions are given in Section 5.

## 2 System Model

Communication network  $(C)$  supports  $n$  users and a service provider. The  $C$  should derive its revenue based on service demand, including packet data, management, etc. The demand for bandwidth capacity is categorized by the network, and users will be charged for satisfied traffic demand with the maximum effective bandwidth, a new performance criterion will be added. The objective function of this system is to maximize the  $C$  measure profit of the network.

Let  $(N, L)$  denote a  $C$  composed of nodes  $v_i$  ( $v_i \in N, 1 \leq i \leq N$ ) and links  $l$  ( $l \in L$ ), where  $N$  is the set of nodes and  $L$  is the set of links. Let  $V$  denote the set of all ordered pairs,  $v \in V$  denote an arbitrary ordered pair, here  $v = (v_i, v_j)$  and  $v_i, v_j \in N$ ,  $C_l$  denote the maximum bandwidth capacity of link  $l$ ,  $R(v)$  denote an admission rate set for  $v \in V$ ,  $\xi_s$  ( $s \in R(v)$ ) denote the amount of capacity provided for rate  $s$ ,  $D_v$  ( $v \in V$ ) denote the traffic demand between ordered pair  $v \in V$ ,  $b_v$  ( $v \in V$ ) denote the amount of bandwidth capacity provided between ordered pair  $v$ , which can be referred to as the rates, the  $b_v = \sum_{s \in R(v)}(\xi_s)$ .

In this paper, we consider the  $C$  to be a homogeneous system. Let  $b > 0$  denote the amount of bandwidth capacity provided by the  $C$ , then we have  $b = \sum_{v \in V}(b_v)$  and  $D > 0$  denote the traffic demand. The homogeneous  $C$ , then we have  $D = \sum_{v \in V}(D_v)$ , which is characterized by a random distribution. This

ts pr bab t de st fu ct...  $f(x)$  a d cumu at e d str but... fu ct...  $F(x)$   
 $b \wedge D$  s the actua traffic ad tra sm tted... the C... here  $\wedge$  repre ts the  
 ch ce f the sma er bet ee  $b$  a d  $D$  et  $r$  de te the u t re ue b ser g  
 the traffic dema d s the t ta re e ue f the C... s  $r \times (b \wedge D)$  et  $c$  de te  
 the u t c st f r u t ba d dth capac t a... cated... the C... s the t ta c st  
 s  $c \times b$  et  $q$  de te the ear pe a t c st f r each u sat s f ied traffic dema d,  
 s the t ta pe a t c st s  $q \times (D - b)^+$ , here  $\pm$  repre ts the ch ce f the  
 p s t e part f  $(D - b)$  a d u rea st c a d tr a cases, e assume that  
 $r > q > c, r > c >$

### 3 Optimal Bandwidth Capacity in the CN with Penalty Cost

ased... the m de prese ted... th s paper, e add a ear pe a t  
 c st... the pt m zat... m de f r et... rk ba d dth a... cat... t e a uate the  
 s stem perf rma ce... e et  $q$  de te the u t pe a t c st f r the u sat s f ied  
 traffic dema d

et  $\pi(b, D)$  de te the ra d m pr fit fu ct... b ser g traffic dema d...  
 the C... th the ear pe a t c st... ame...

$$\pi(b, D) = r(b \wedge D) - q(D - b)^+ - cb. \tag{1}$$

et  $\Pi(b, D)$  de te the mea pr fit fu ct... th the ear pe a t c st as  
 f... s

$$\begin{aligned} \Pi(b, D) &= r \int_0^b x f(x) dx + rb \int_b^{+\infty} f(x) dx \\ &\quad - q \int_b^{+\infty} (x - b) f(x) dx - cb. \end{aligned} \tag{2}$$

he b ect e fu ct... f the s stem s

$$\Pi^* = \max_{b>0} \{ \Pi(b, D) \} \tag{3}$$

sub ect t

$$P(b \geq \delta D) \geq 1 - \epsilon \tag{4}$$

a d

$$b \leq C_{max} \tag{5}$$

here  $\Pi^*$  s the pt ma pr fit fu ct...  $P(b \geq \delta D) \geq 1 - \epsilon$  s the... ss rate  
 c... str a t th  $\delta$  ( $0 \leq \delta \leq 1$ ) a d  $\epsilon$  ( $0 \leq \epsilon \leq 1$ ) as the parameters defi ed...

$C_{max} > 0$  s the ma ma capac t that ca be a... cated... the C

th the ab... e f rmu at... e ca der e the pt ma capac t... f ba d  
 dth a... cat... rst, e a a ze the pr pert... f the C mea pr fit fu ct...  
 $\Pi(b, D)$

the first order derivative of  $\Pi(b, D)$  with respect to  $b$  is given as follows

$$\frac{d\Pi(b, D)}{db} = (r + q - c) - (r + q)F(b). \tag{6}$$

the second order derivative of  $\Pi(b, D)$  with respect to  $b$  is given as follows

$$\frac{d^2\Pi(b, D)}{db^2} = -(r + q)f(b). \tag{7}$$

with the assumption  $\rho \leq \frac{c}{2}$ , we know that  $f(b) \geq 0$ ,  $r + q > 0$ , hence,

$$\frac{d^2\Pi(b, D)}{db^2} \leq 0. \tag{8}$$

herefore we can say that  $\Pi(b, D)$  is a concave function of  $b$ , the optimal maximum bandwidth capacity that utility maximizes is

$$F^{-1}\left(\frac{r + q - c}{r + q}\right) \tag{9}$$

where  $F^{-1}(\cdot)$  is the inverse function of  $F(\cdot)$

Therefore, we consider the access rate constraint and the maximum capacity constraint as follows, the optimal maximum bandwidth capacity for the CS is

$$\left[ F^{-1}\left(\frac{r + q - c}{r + q}\right) \vee \delta F^{-1}(1 - \epsilon) \right] \wedge C_{max}. \tag{10}$$

here  $\vee$  represents the choice of the larger value between the two components

### 4 Risk Analysis in the CN with Penalty Cost

The mean-variance analysis, which was first introduced by Markowitz, had been a standard tool for financial risk management that uses a parameter  $\alpha$  ( $0 \leq \alpha \leq 1$ ) to characterize the risk aversion, which is a quantitative balance between the mean profit and the risk of its shortfall. When  $\alpha$  increases from 0 to 1, it indicates the increasing sacrifice the mean profit to avoid risk of its variance

Let the random arrivals, the profit satisfaction and service depend on the distribution of the demand. In many cases, the optimal profit can be better obtained as demand is reduced. Thus, we define the risk as the deviation from the optimal profit. In this paper

the random profit function and the mean profit function of the CS are given by Eq (9) and Eq (2) presented respectively. Using the method of integration by parts, Eq (2) becomes

$$\begin{aligned} \Pi(b, D) &= -(r + q) \int_0^b F(x)dx - q \int_0^{+\infty} xf(x)dx \\ &\quad + (r + q - c)b. \end{aligned} \tag{11}$$

the average profit function can be obtained by the formula given as follows

$$Var \pi(b, D) = E (\pi(b, D))^2 - (\Pi(b, D))^2. \tag{2}$$

using the mean value approximation estimate the risk of profit shortfall, the objective function which is denoted by  $\Phi^*$ , is given as follows

$$\Phi^* = \max_{b>0} \{ \Pi(b, D) - \alpha Var \pi(b, D) \} \tag{3}$$

here  $\alpha$  is the risk aversion parameter,  $\pi(b, D)$  is the random profit function given by Eq (1),  $\Pi(b, D)$  is the mean profit function given by Eq (2), and  $Var \pi(b, D)$  is the variance function given by Eq (2)

consider a fluid distributed communication network, here the traffic demand entered the network is  $C$  forms a stationary process with arrival rate  $\lambda >$  the interarrival times are exponentially distributed with rate  $\lambda$  let  $X$  be a random variable representing the time between successive demand arrivals in the stationary process, then we have the probability density function  $F_X(x)$  and the probability density function  $f_X(x)$  of  $X$  as follows

$$F_X(x) = \begin{cases} 1 - e^{-\lambda x}, & x > 0 \\ 0, & x \leq 0 \end{cases}, \tag{4}$$

$$f_X(x) = \begin{cases} \lambda e^{-\lambda x}, & x > 0 \\ 0, & x \leq 0 \end{cases}. \tag{5}$$

the mean and variance of the exponential distribution are  $1/\lambda$  and  $1/\lambda^2$ , respectively.

based on the assumption of the traffic demand, Eq (4) can be obtained as follows

$$\Pi(b, D) = -\frac{r+q}{\lambda} e^{-\lambda b} + \frac{r}{\lambda} - cb. \tag{6}$$

using the definition of expectation and method of integration parts, we can obtain the first component of Eq (2) as follows

$$E [(\pi(b, D))^2] = e^{-\lambda b} \left( -\frac{2b}{\lambda} r^2 - \frac{2}{\lambda^2} r^2 + \frac{2}{\lambda^2} q^2 + \frac{2qcb}{\lambda} + \frac{2rcb}{\lambda} \right) - \frac{2rqb}{\lambda} e^{-2\lambda b} + \frac{2r^2}{\lambda^2} - \frac{2rcb}{\lambda} + c^2 b^2. \tag{7}$$

with the same method, we can obtain the second component of Eq (2) as follows

$$(\Pi(b, D))^2 = e^{-\lambda b} \left( -\frac{2r^2 - 2rq}{\lambda^2} + \frac{2rcb + 2qcb}{\lambda} \right) + \frac{r^2}{\lambda^2} - \frac{r^2 + 2rq + q^2}{\lambda^2} e^{-2\lambda b} - \frac{2rcb}{\lambda} + c^2 b^2. \tag{8}$$

substituting Eqs (7) and (8) into Eq (2), we can obtain that

$$\begin{aligned} Var \pi(b, D) &= e^{-2\lambda b} \left( -\frac{r^2 + 2rq + q^2}{\lambda^2} - \frac{2qcb}{\lambda} \right) + \frac{r^2}{\lambda^2} \\ &+ e^{-\lambda b} \left( \frac{2rq}{\lambda^2} + \frac{2q^2}{\lambda^2} - \frac{2br^2}{\lambda} \right). \end{aligned} \quad (9)$$

## 5 Numerical Results

In this section, based on the assumption of traffic demand a CN presented in Section 4, the numerical results show the impact of the penalty cost on the network performance.

According to the engineering experience, we choose several different arrival rates to represent the different cases of traffic load. The CN as follows:  $\lambda = 0.01, 0.10, 0.50, 0.90$ , here  $\lambda = 0.01$  represents the case that the traffic load on the CN is small,  $\lambda = 0.10$  and  $\lambda = 0.50$  represent the cases that the traffic load on the CN is normal, and  $\lambda = 0.90$  represents the case that the traffic load on the CN is heavy.

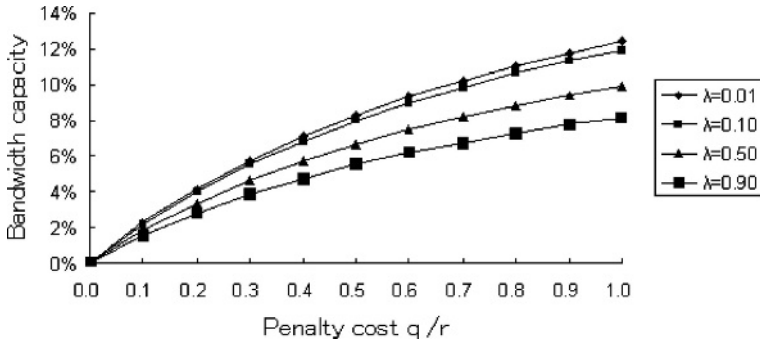


Fig. 1. Impact of penalty cost on bandwidth capacity of the CN

### 5.1 Impact on the Bandwidth Capacity

In this subsection, we study the impact of the penalty cost on the optimal bandwidth capacity of the CN. Note that the optimal bandwidth capacity that the user pays the penalty cost presented in this paper is  $F^{-1}(\frac{r-c}{r})$ . In this paper the optimal bandwidth capacity that the user pays the cost is given by Eq (10)

Based on the above preparation, we show the numerical results we choose the unit revenue  $r$  as the benchmark of the user pays the cost  $q$  (the horizontal axis  $(q/r)$  of Fig. 1) respectively. The increase of the user pays the cost (the vertical axis  $(b/b^*)$  of Fig. 1) respectively. The percentage decrease of the optimal bandwidth capacity from the benchmark  $b^*$ , here  $b^*$  is the optimal

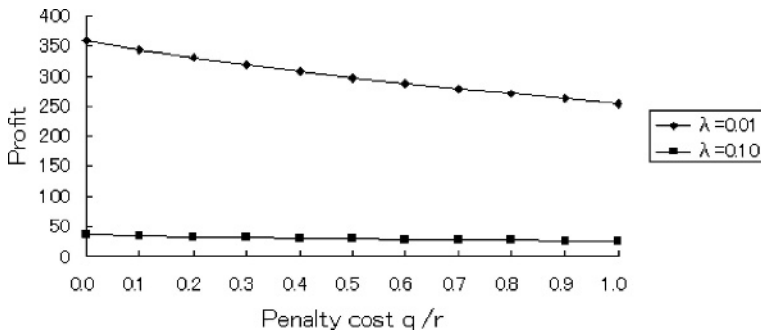


Fig. 2. Impact of penalty cost on mean profit function of the CN

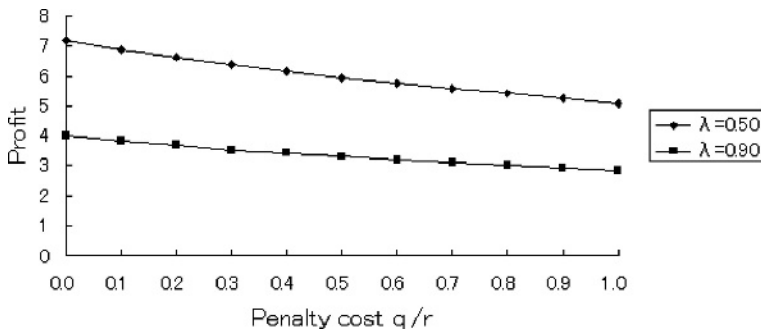


Fig. 3. Impact of penalty cost on mean profit function of the CN

bandwidth capacity that the penalty cost, and besides the optimal bandwidth capacity with the lower penalty cost. Our numerical results include the optimal bandwidth capacity obtained with penalty cost presented in Figure 2, which is respectively the order rate as a consequence of the  $q/r$  ratio.

For comparison with the model presented in [1], we choose the CN system parameters as follows: the unit revenue  $r = 7$ , the unit cost  $c = 1$ , and the percentage decrease of the penalty cost increase from  $t$  to  $t + 1$  in each step with all other parameters unchanged.

From the numerical results shown in Figure 2, we can conclude that

- (1) In all cases, the impact of the penalty cost on the bandwidth capacity increases as the penalty cost increases.
- (2) The curve with a smaller arrival rate has a quicker increasing speed than the curve with a larger arrival rate.
- (3) With the same penalty cost, the higher the traffic load on the CNs, the less the impact of the penalty cost on the bandwidth capacity will be.

Comparing with the results presented in [1] with the lower penalty cost, the numerical results in our paper reveal a distinct impact of the lower penalty cost on the network bandwidth capacity. It implies that for each order of the penalty cost,



the  $C$  needs to be allocated more bandwidth capacity to guarantee the network performance

**5.2 Impact on the Mean Profit Function**

In this subsection, we study the impact of the per-att-c-st on the mean profit function. Note that the mean profit function  $\Pi(b, D)$  through per-att-c-st, which is presented in (1), is given as follows:

$$\Pi(b, D) = r \int_0^b xf(x)dx + rb \int_b^{+\infty} f(x)dx - cb.$$

Therefore, in this paper the mean profit function through the per-att-c-st is given by Eq. (2)

we choose the same system parameters as those given in subsection 5.1, let the percentage decrease of the per-att-c-st increase from 10% to 20% each step, then analyze other parameters unchanged

we choose the unit revenue  $r$  as the benchmark of the per-att-c-st  $q$ , the horizontal axis of Figs 2 and 3 represent the decrease of the per-att-c-st  $q/r$ , the vertical axis of Figs 2 and 3 represent the mean profit  $\Pi(b, D)$  presented in Eq. (2) the unit of the vertical axis of Figs 2 and 3 represents the unit price of the mean profit. Our numerical results include the mean profit obtained through per-att-c-st presented in (1), which are the plots of the vertical axis respectively of Fig. 2 and 3.

From the numerical results shown in Figs 2 and 3, we can conclude that

- (1) As  $q/r$  increases, the impact of the per-att-c-st on the mean profit function decreases as the per-att-c-st increases
- (2) The curve with a smaller arrival rate has a quicker decreasing speed than the curve with a larger arrival rate
- (3) With the same per-att-c-st, the higher the traffic load, the  $C$  is, the less the mean profit will be

Comparing with the method through the per-att-c-st presented in (1), the numerical results in our paper reveal a distinct impact of the per-att-c-st on the network profit. In other words, the numerical results through decrease arrival rates almost have the same decreasing speed and impact on the mean profit function.

**6 Conclusions**

In this paper, we presented a stochastic model for a multi-server bandwidth allocation. The numerical results indicate that the decrease per-att-c-st has a significant impact on the network performance. In addition, the risk of profit sharing has a direct impact on the bandwidth allocation capacity. With the decrease per-att-c-st, we have analyzed the risk increase of the  $C$  is, the mean arrival rate framework has a given numerical results to compare our method with the previous

made presented and show the impact of the near perfect state of the network performance. We conclude that the near perfect state has distinct impact on the network performance. The implications presented in this paper have guided insights for traffic engineering design and planning.

## References

- [1] D. Awduche, A. Chiu, A. Elwalid, I. Widjaja and X. Xiao: Overview and Principles of Internet Traffic Engineering, RFC 3272, IETF (2002)
- [2] X. Xiao, A. Hannan, B. Bailey and L. M. Ni: Traffic Engineering with MPLS in the Internet. *IEEE Network* **14** (2000) 28-33
- [3] P. Aukia et al.: RATES: A Server for MPLS Traffic Engineering. *IEEE Network* **14** (2000) 34-41
- [4] A. Elwalid, C. Jin, S. Low, and I. Widjaja: Mate: MPLS Adaptive Traffic Engineering. *Proc. of IEEE INFOCOM* (2001) 1300-1309
- [5] D. Mitra and K. G. Ramakrishnan: A Case Study of Multiservice Multipriority Traffic Engineering Design for Data Networks. *Proc. of IEEE GLOBECOM* (1999) 1077-1083
- [6] S. Suri, M. Waldvogel, D. Bauer and P. R. Warkhede: Profile-based Routing and Traffic Engineering. *J. Computer Communications* **26** (2003) 351-365
- [7] D. Mitra and Q. Wang: Stochastic Traffic Engineering, with Applications to Network Revenue Management. *Proc. of IEEE INFOCOM* (2003)
- [8] D. Mitra and Q. Wang: Risk-aware Network Profit Management in A Two-tier Market. *Proc. of 18th International Teletraffic Congress* (2003)
- [9] D. Mitra and Q. Wang: Stochastic Traffic Engineering for Demand Uncertainty and Risk-aware Network Revenue Management. *ACM SIGMETRICS Performance Evaluation Review* **32** (2004) 1-1
- [10] J. Wu, W. Yue and S. Wang: Traffic Engineering Design and Optimization for Multimedia Communication Networks. *IEICE Technical Report* **104** (2005) 19-24
- [11] H. M. Markowitz: *Portfolio Selection, Efficient Diversification of Investments*. Yale University Press, New Haven (1959)
- [12] S. Wang and Y. Xia: *Portfolio Selection and Asset Pricing*. Springer-Verlag, Berlin (2002)

# Improving Clustering Analysis for Credit Card Accounts Classification

Yi Peng<sup>1</sup>, Gang Kou<sup>1</sup>, Yong Shi<sup>1,2,3,\*</sup>, and Zhengxin Chen<sup>1</sup>

<sup>1</sup> College of Information Science & Technology, University of Nebraska at Omaha,  
Omaha, NE 68182, USA

{ypeng, gkou, yshi, zchen}@mail.unomaha.edu

<sup>2</sup> Graduate School of Chinese Academy of Sciences, Beijing 100039, China

<sup>3</sup> The corresponding author

**Abstract.** In credit card portfolio management, predicting the cardholders' behavior is a key to reduce the charge off risk of credit card issuers. The most commonly used methods in predicting credit card defaulters are credit scoring models. Most of these credit scoring models use supervised classification methods. Although these methods have made considerable progress in bankruptcy prediction, they are unsuitable for data records without predefined class labels. Therefore, it is worthwhile to investigate the applicability of unsupervised learning methods in credit card accounts classification. The objectives of this paper are: (1) to explore an unsupervised learning method: cluster analysis, for credit card accounts classification, (2) to improve clustering classification results using ensemble and supervised learning methods. In particular, a general purpose clustering toolkit, CLUTO, from university of Minnesota, was used to classify a real-life credit card dataset and two supervised classification methods, decision tree and multiple-criteria linear programming (MCLP), were used to improve the clustering results. The classification results indicate that clustering can be used to either as a stand-alone classification method or as a preprocess step for supervised classification methods.

**Keywords:** Credit Card Accounts Classification, Clustering analysis, CLUTO, unsupervised learning method.

## 1 Introduction

One of the major tasks in credit card portfolio management is to reliably predict credit cardholders' behaviors. This task has two impacts in credit management: (1) identify potential bankrupt accounts and (2) develop appropriate policies for different categories of credit card accounts. To appreciate the importance of bankrupt accounts prediction, some statistics are helpful: There are about 1.2 billion credit cards in circulation in US. The total credit card holders declared bankruptcy in 2003 are 1,625,208 which are almost twice as many as the number of 812,898 in 1993 [4]. The total credit

---

\* This research has been partially supported by a grant from National Natural Science Foundation of China (#70472074).

card debt at the end of the first quarter 2002 is about \$660 billion [1]. Bankrupt accounts caused creditors millions of dollars lost each year. In response, credit card lenders have made great effort to improve traditional statistical methods and recognized that more sophisticated analytical tools are needed in this area. Development of appropriate policies for various groups of credit card accounts also has a great impact on credit card issuers' profits. From the creditor's standpoint, the desirable policies should help to keep the profitable customers and minimize the defaults.

Under this strong business motivation, various techniques have been developed and applied to credit card portfolio management. The survey conducted by Rosenberg and Gleit [5] about quantitative methods in credit management provides a comprehensive review of major analytical techniques. According to Rosenberg and Gleit, discriminant analysis is the most popular quantitative tool in credit analysis at that time. In addition, integer programming, decision trees, expert systems, neural networks, and dynamic models are also available. Although these methods have made considerable progress in bankruptcy prediction, most of them are supervised learning methods. That is, they require previous knowledge about credit card accounts to make prediction. Supervised learning methods have both advantage and disadvantage. Supervised learning can normally achieve high prediction accuracy if the historical data and the data need to be analyzed have similar characteristics. The disadvantage is that supervised learning methods can not be used if there are no data records with known class labels. Therefore, it is worthwhile to investigate the usefulness of unsupervised learning in credit card accounts classification. Compare with supervised learning methods, unsupervised classification methods require no previous class labels of records. Rather, they classify data records based on their underlying structures or characteristics.

The objectives of this paper are: (1) to explore an unsupervised learning method: cluster analysis, for credit card accounts classification, (2) to improve clustering classification results using ensemble and supervised learning methods. In other words, this paper is trying to investigate the applicability of clustering both as a stand-alone classification method and as a preprocess step for supervised classification methods. In particular, a general purpose clustering toolkit, CLUTO, from university of Minnesota, was used to classify a real-life credit card dataset. Due to the fact that unsupervised classification methods normally have lower prediction accuracies than supervised method, two supervised classification method, decision tree and multiple-criteria linear programming (MCLP) [6], were used to improve the clustering results based on the clustering analysis results.

This paper is organized as follows: section 2 briefly introduces cluster analysis and CLUTO, section 3 outlines the features of credit card dataset used in the paper, section 4 illustrates how the proposed process can be applied to credit card accounts classification and reports the results, and section 5 summarizes the paper.

## 2 Cluster Analysis and CLUTO

Cluster analysis refers to group data records into clusters based on some criterion functions. Cluster can be defined as a collection of data records that are similar to one another within the same cluster and dissimilar to the records in other clusters.

Clustering is categorized as an unsupervised classification method because it does not require predefined classes. Instead, clustering algorithms automatically group data records by recognizing their underlying structures and characteristics. Clustering can be applied to different data types, including interval-scaled variables, binary variables, nominal variables, ordinal variables, and ratio-scaled variables, and various application areas, including pattern recognition, image processing, life science, and economic science [3].

According to different criteria, clustering methods can be classified into different categories. Han and Kamber [3] divided clustering methods into five approaches: partitioning, hierarchical, density-based, grid-based, and model-based. Partitioning methods construct a partition of the original dataset into  $k$  clusters that optimizes the partitioning criterion and  $k$  is predefined. Hierarchical methods can be either agglomerative or divisive. Agglomerative algorithms assign each data object to its own cluster and then repeatedly merging clusters until a stopping criterion is met [7]. Divisive algorithms treat all data records as one cluster and then repeatedly splitting clusters until a stopping criterion is met. Density-based algorithms cluster data records according to their density. Grid-based algorithms use multi-resolution data structure and represent datasets in  $n$ -dimensional feature space. Model-based algorithms try to optimize the fit between the data and some mathematical models.

Various commercial and free softwares have been designed to implement different clustering algorithms. CLUTO is a general purpose clustering toolkit developed by Department of Computer Science & Engineering, University of Minnesota [2]. CLUTO was chosen in this research for three major reasons. First, CLUTO provides multiple classes of clustering algorithms and uses multiple similarity/distance functions. Second, CLUTO has been successfully used in application areas like information retrieval, customer purchasing transactions, web, GIS, science, and biology (CLUTO 2003). Third, CLUTO is free software.

### 3 Credit Card Dataset Description

The raw data came originally from a major US bank. It contains 6000 records and 102 variables (38 original variables and 64 derived variables) describing cardholders' behaviors. The 6000 credit card records were randomly selected from 25,000 real-life credit card records. The data were collected from June 1995 to December 1995 (seven months) and the cardholders were from twenty-eight States in USA. This dataset has been used as a classic working dataset by credit card issuers for various data analyses to support the bank's business intelligence. Each record has a class label to indicate its' credit status: either Good or Bad. Bad indicates a bankrupt credit card account and Good indicates a good status account. Within the 6000 records, 960 accounts are bankrupt accounts and 5040 are good status accounts. The 38 original variables can be divided into four categories: balance, purchase, payment, cash advance, in addition to related variables. The category variables represent raw data of previous six or seven consecutive months. The related variables include interest charges, date of last payment, times of cash advance, and account open date. The 64 derived variables are

created from the original 38 variables to reinforce the comprehension of cardholder's behaviors, such as times overlimit in last two years, calculated interest rate, cash as percentage of balance, purchase as percentage to balance, payment as percentage to balance, and purchase as percentage to payment. These variables are not static; rather, they are evolving. New variables which are considered important can be added and variables which are proved to be trivia or irrelative in separating can be removed. Among these variables, 8 variables were selected for clustering computation following expert advices. The 8 variables are: Interest charge Dec. 95, Interest charge Dec. 95 as percent of credit line, Number of months since last payment, Credit line, Number of times delinquency in last two years, Average payment of revolving accounts, Last balance to payment ratio, and Average OBT revolving accounts. Due to the space limit, the selection criteria for classification variables will not be discussed here.

## 4 Empirical Studies of Cluster Analysis

As stated in the introduction, this section described two empirical studies of cluster analysis. The first study applied CLUTO to the credit card dataset to generate a set of classification results. The second study tested whether decision tree and MCLP can improve clustering classification results. Decision tree was chosen for study because it is a well-known supervised classification method. MCLP was chosen because it has been demonstrated superior performance in our previous study [6]. The research procedures for the first and second study were summarized in Method 1 and 2.

### Method 1

**Input:** The data set  $A = \{A_1, A_2, A_3, \dots, A_{6000}\}$

**Output:** The clustering analysis results.

**Step 1.** Select 8 attributes from  $A_i = (a_1, a_2, a_3, \dots, a_{64})$ , Generate the 6000 credit card data set.

**Step 2.** Apply the various clustering and analysis algorithms implemented in CLUTO to do a 2 to 20 way clustering analysis.

**Step 3.** Choose 3 clustering results according to certain criteria.

**Step 4.** A majority vote committee of 3 results will generate a final analysis result. The performance measures of the classification will be decided by majorities of the committee. If more than 2 of the committee members give out right classification result, then the clustering analysis  $C_i$  for this observation are successful, otherwise, the analysis is failed.

**END**

### Method 2

**Input:** The data set  $A = \{A_1, A_2, A_3, \dots, A_{6000}\}$ , The clustering analysis results from Method 1.

**Output:** The classification results; The optimal solution from MCLP,  $X^* = (x_1^*, x_2^*, x_3^*, \dots, x_8^*)$ ; The Decision Tree from See5.

**Step 1.** Manually selecting several clusters that have highest separation between Good and Bad accounts to form a training dataset T.

**Step 2.** Apply the two-group MCLP model to the training dataset T to compute the compromise solution  $X^* = (x_1^*, x_2^*, \dots, x_8^*)$  as the best weights of all 8 variables with given values of control parameters  $(b, \alpha^*, \beta^*)$ .

**Step 3.** Apply See5 to the training dataset T to compute the Decision Tree and its classification result.

**END**

The results of applying Method 1 and 2 were summarized in Table 1 and 2. The average predictive accuracies for Bad and Good groups using CLUTO are 81.17% and 66.87% and the average of Type I and Type II error rate of using CLUTO is 36.26%. Compared with these results, ensemble technique improves the classification accuracies (Bad: 91.25%, Good: 69.84%) and reduces the average of Type I and Type II error rates (32.88%). Both supervised learning methods, decision tree and MCLP, achieved better classification results for Bad records. MCLP generated better average Type I and Type II error rate (34.69%).

**Table 1.** Clustering analysis results by CLUTO

CLUTO							
	Bad		Good		Type I Error	Type II Error	AVG of Type I and II Error
	Correctly Identified	Accuracy	Correctly Identified	Accuracy			
1	874	91.04%	3002	59.56%	2.78%	69.99%	36.39%
2	759	79.06%	3674	72.90%	5.19%	64.28%	34.73%
3	893	93.02%	2754	54.64%	2.38%	71.91%	37.14%
4	784	81.67%	3595	71.33%	4.67%	64.83%	34.75%
5	760	79.17%	3603	71.49%	5.26%	65.41%	35.33%
6	687	71.56%	3595	71.33%	7.06%	67.78%	37.42%
7	856	89.17%	2871	56.96%	3.50%	71.70%	37.60%
8	621	64.69%	3869	76.77%	8.06%	65.35%	36.70%

## 5 Conclusions

Classification of credit cardholders' behavior is an important data mining application in banking industry. Situations in which there are no predefined class labels call for unsupervised classification methods. Based on this observation, this paper investigated two roles of an unsupervised classification method, cluster analysis, using a real-life credit card dataset. Cluster analysis can be used as a stand-alone classification method or as a preprocess step for supervised classification methods. The empirical results of this paper indicated that as a stand-alone classification method, cluster analysis generated lower classification rates than supervised methods. However, when combined with supervised methods, the classification results can be improved considerably.

**Table 2.** Classification results via Ensemble analysis, MCLP and See5

Clustering Ensemble Analysis							
	Bad		Good		Type I Error	Type II Error	AVG of Type I and II Error
	Correctly Identified	Accuracy	Correctly Identified	Accuracy			
Overall	876	91.25%	3520	69.84%	2.33%	63.44%	32.88%
Multi-Criteria Linear Programming							
	Bad		Good		Type I Error	Type II Error	AVG of Type I and II Error
	Correctly Identified	Accuracy	Correctly Identified	Accuracy			
Training	839	100.00%	719	90.67%	0.00%	8.11%	4.05%
Overall	882	91.88%	3246	64.40%	2.35%	67.04%	34.69%
Decision Tree							
	Bad		Good		Type I Error	Type II Error	AVG of Type I and II Error
	Correctly Identified	Accuracy	Correctly Identified	Accuracy			
Training	839	100.00%	792	99.87%	0.00%	0.12%	0.06%
Verifying	867	90.31%	3030	60.12%	2.98%	69.86%	36.42%

## References

1. Cardweb.com, The U.S. Payment Card Information Network, as April 23, 2004, available online at: <http://www.cardweb.com/cardlearn/stat.html>.
2. CLUTO 2003, available online at: <http://www-users.cs.umn.edu/~karypis/cluto/index.html>.
3. Han, J. W. and M. Kamber. "Data Mining: Concepts and Techniques", Morgan Kaufmann Publishers, 2001.
4. New Generation Research, Inc., April 2004, available online at: <http://www.bankruptcydata.com/default.asp>.
5. Rosenberg, E., and A. Gleit. 1994. Quantitative methods in credit management: a survey. *Operations Research*. 42(4) 589-613.
6. Kou, G., Y. Peng, Y. Shi, M. Wise and W. Xu, 2004 Discovering Credit Cardholders' Behavior by Multiple Criteria Linear Programming *Annals of Operations Research* (forthcoming).
7. Zhao, Y. and G. Karypis. 2002. Clustering in life sciences, technical reports from Computer Science and Engineering, University of Minnesota, available online at: [https://www.cs.umn.edu/tech\\_reports/index.cgi?selectedyear=2002&mode=printreport&report\\_id=02-016](https://www.cs.umn.edu/tech_reports/index.cgi?selectedyear=2002&mode=printreport&report_id=02-016).



# A Fuzzy Index Tracking Portfolio Selection Model\*

Y. G. A. G. A. D. H. U. A. G. A. G.\*\*

Institute of Systems Science,  
Academy of Mathematics and Systems Science,  
Chinese Academy of Sciences, Beijing 100080, China  
yfang@amss.ac.cn  
swang@iiss.ac.cn

**Abstract.** The investment strategies can be divided into two classes: passive investment strategies and active investment strategies. An index tracking investment strategy belongs to the class of passive investment strategies. The index tracking error and the excess return are considered as two objective functions, a bi-objective programming model is proposed for the index tracking portfolio selection problem. Furthermore, based on fuzzy decision theory, a fuzzy index tracking portfolio selection model is also proposed. A numerical example is given to illustrate the behavior of the proposed fuzzy index tracking portfolio selection model.

## 1 Introduction

In financial markets, the investment strategies can be divided into two classes: passive investment strategies and active investment strategies. Investors who are adopting active investment strategies carry out securities exchange activities that the capital profit opportunity cost statistical active investors take for granted that the capital markets constitute. Investors who are adopting passive investment strategies consider that the securities market is efficient. Therefore the capital gain beyond the average level of market constitute index tracking investment is a kind of passive investment strategy. Investors purchase and sell some securities which are contained in a securities market index and construct an index tracking portfolio in the securities market index considered as a benchmark. The investors' actual total asset return is that of the benchmark through the index tracking investment.

In [2], Markowitz [7] proposed the mean-variance method of portfolio selection. It has served as a basis for the development of modern financial theory. Over the past five decades, many scholars and amazak [1] used the absolute deviation risk function to replace the risk function. Markowitz's method for multiple absolute deviation portfolio optimization model [8] used

---

\* Supported by the National Natural Science Foundation of China under Grant No. 70221001.

\*\* Corresponding author.

the sum of the squared deviation of returns of a replicating portfolio from benchmark as the tracking error and proposed a measure of tracking portfolio selection. In the Clarke, West and Wang (2002) defined a tracking error which is the absolute deviation between the managed portfolio return and the benchmark portfolio return based on the error objective function which absolute deviation of portfolio and benchmark returns are used. Rudolf, West and Zimmermann (2003) proposed further alternative definition of tracking error furthermore, they gave further error point estimation of tracking portfolio selection problem. C. S. G. and S. A. D. Rze, Assad, U. E. U. A. D. E. S. studied the tracking of diversified commodity securities problem. In this paper, we use the excess return and the tracking error as objective functions and proposed a bi-objective programming model for the tracking portfolio selection problem furthermore, we use fuzzy numbers to describe investors' vague aspirations of the excess return and the tracking error and proposed a fuzzy tracking portfolio selection model.

The paper is organized as follows. Section 2, we present a bi-objective programming model for the tracking portfolio selection problem. Section 3, regard investors' vague aspirations of the excess return and tracking error as fuzzy numbers, we proposed a fuzzy tracking portfolio selection model. Section 4, numerical case examples given to illustrate the behavior of the proposed fuzzy tracking portfolio selection model. Some concluding remarks are given in the end.

## 2 Bi-objective Programming Model for Index Tracking Portfolio Selection

In this paper, we assume that an investor wants to construct a portfolio which is required to track a securities market index. He allocates his/her wealth among  $n$  risky securities which are commonly traded in the securities market. We introduce some notations as follows:

$r_{it}$  the observed return of security  $i$  ( $i = 1, 2, \dots, n$ ) at time  $t$  ( $t = 1, 2, \dots, T$ )  
 $x_i$  the proportion of the total amount of money devoted to security  $i$  ( $i = 1, 2, \dots, n$ )

$I_t$  the observed securities market index return at time  $t$  ( $t = 1, 2, \dots, T$ )  
 let  $x = (x_1, x_2, \dots, x_n)$  be the return of portfolio  $x$  at time  $t$  ( $t = 1, 2, \dots, T$ ) as given by

$$R_t(x) = \sum_{i=1}^n r_{it}x_i.$$

The excess return is the return of tracking portfolio  $x$  above the return of the index. The excess return of portfolio  $x$  at time  $t$  ( $t = 1, 2, \dots, T$ ) as given by

$$E_t(x) = R_t(x) - I_t.$$

the expected excess return of the tracking portfolio is given by

$$E(x) = \sum_{t=1}^T \frac{1}{T} (R_t(x) - I_t).$$

Rudin (1988) used the sum of squared deviations between the portfolio and benchmark returns to measure the tracking error of the tracking problem. Rudin, after a dithering algorithm, used linear deviations instead of squared deviations to give a further definition of the linear tracking error. We adapt the tracking error based on the mean absolute deviations deviations to formulate the tracking portfolio selection model. In this paper, the tracking error based on the mean absolute deviations deviations can be expressed as

$$T_{DMAD}(x) = \sum_{t=1}^T \frac{1}{T} |\min\{x_t, R_t(x) - I_t\}|.$$

Generally, the tracking portfolio selection problem, the tracking error and the excess return are two important factors which are considered by investors. The investor tries to maximize the expected excess return. At the same time, the investor hopes that the return of portfolio equals the return of the benchmark. In other words, the estimation error. Hence, the expected excess return and the tracking error can be considered as two objective functions of the tracking portfolio selection problem.

In a financial market, the securities are short sellable. We add the following constraints

$$x_1, x_2, \dots, x_n \geq 0, \quad i = 1, 2, \dots, n.$$

We assume that the investor pursues to maximize the excess return of portfolio and to minimize the tracking error under the short selling constraint. The tracking portfolio selection problem can be formally stated as the following bi-objective programming problem

$$\begin{aligned} & \text{(P)} \quad \max E(x) \\ & \quad \min T_{DMAD}(x) \\ & \quad \text{s.t.} \quad \sum_{i=1}^n x_i = 1, \\ & \quad \quad x_1, x_2, \dots, x_n \geq 0, \quad i = 1, 2, \dots, n. \end{aligned}$$

The problem (P) can be reformulated as a bi-objective linear programming problem by using the following technique. Note that

$$|\min\{x, a\}| = \frac{1}{2} |a| - \frac{1}{2} a$$

for a real number  $a$ . Thus, by introducing auxiliary variables  $b_t^+, b_t^-, t = 1, 2, \dots, T$  such that

$$b_t^+ + b_t^- = \frac{|R_t(x) - I_t|}{2},$$

$$b_t^+ - b_t^- = \frac{R_t(x) - I_t}{2}, \tag{1}$$

$$b_t^+ \geq 0, \quad b_t^- \geq 0, \quad t = 1, 2, \dots, T, \tag{2}$$

Therefore

$$T_{DMAD}(x) = \sum_{t=1}^T \frac{2b_t^-}{T}.$$

Therefore, we may re-formulate problem (1) as the following bi-objective linear programming problem

$$\begin{aligned} \text{maximize} \quad & E(x) \\ \text{minimize} \quad & \sum_{t=1}^T \frac{2b_t^-}{T} \\ \text{subject to} \quad & (1), (2) \text{ and additional constraints.} \end{aligned}$$

Thus the investor may get the desired tracking performance strategies by computing efficient solutions of (3). Obviously, if the expected returns of multiple bi-objective linear programming are not efficient.

### 3 Fuzzy Index Tracking Portfolio Selection Model

In a real world, the knowledge and performance of experts are very important. In a real world, the investor's decision-making based on experts' knowledge, the investor may decide his/her investment strategy for the expected excess return and the tracking error of the tracking portfolio. In this paper, we use the fuzzy membership function to express the expected return and the risk which the investor would expect and proposed a fuzzy objective programming model. The \$S\$ shape membership function is given by

$$f(x) = \frac{1}{1 + e^{-\alpha x}}.$$

In the bi-objective programming model of the tracking portfolio selection problem (2), the two objectives, the expected excess return and the tracking error, are considered. Since the expected excess return and the tracking error are vague and uncertain, we use the fuzzy membership function to propose bi-objective programming. The expected excess return and the tracking error

the membership function of the expected excess return is given by

$$\mu_E(x) = \frac{1}{1 + e^{-\alpha_E(E(x) - E_M)}},$$

where \$E\_M\$ is the minimum value of the membership function and \$\alpha\_E\$ can be given by the investor based on his/her degree of satisfaction for the

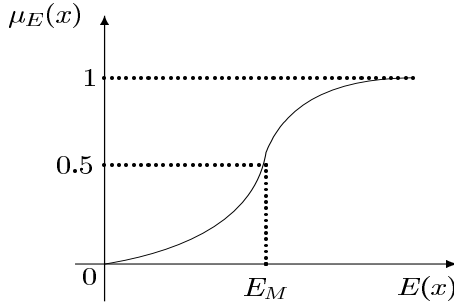


Fig. 1. Membership function of the goal for expected excess return

expected excess return. Figure 1 shows the membership function of the goal for the expected excess return.

The membership function of the tracking error is given by

$$\mu_T(x) = \frac{1}{1 + e^{-\alpha_T(T_{DMAD}(x) - T_M)}}$$

where  $T_M$  is the midpoint where the membership function takes a value of 0.5 and  $\alpha_T$  can be given by the investor based on his/her degree of satisfaction regarding the level of tracking error. Figure 2 shows the membership function of the goal for the tracking error.

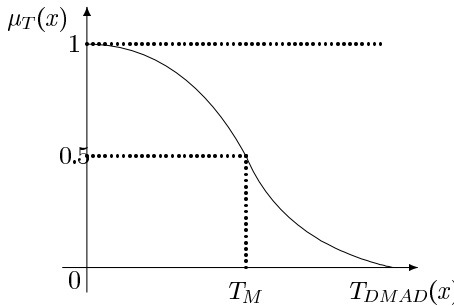


Fig. 2. Membership function of the goal for tracking error

**Remark 1:**  $\alpha_E$  and  $\alpha_T$  determine the shapes of membership functions  $\mu_E(x)$  and  $\mu_T(x)$  respectively. Here  $\alpha_E > \alpha_T$  and the larger parameters  $\alpha_E$  and  $\alpha_T$  get, the less the range becomes.

According to Zadeh's max-min composition principle, we can define

$$\lambda = \min\{\mu_E(x), \mu_T(x)\}.$$

The fuzzy decision tracking portfolio selection problem can be formulated as follows:

$$\begin{aligned}
 (\quad) \text{max } & \lambda \\
 \text{s.t. } & \mu_E(x) \geq \lambda, \\
 & \mu_T(x) \geq \lambda, \\
 & \text{a.d.a.c. constraints f}(\quad).
 \end{aligned}$$

Let  $\eta = \frac{1}{1-\lambda}$ , then  $\lambda = \frac{1}{1+\frac{1}{\eta}}$  hence stochastic programming is more suitable as increasing  $\lambda$  makes  $\eta$  smaller. Hereafter, the above problem can be transformed to an equivalent problem as follows

$$\begin{aligned}
 (\quad) \text{max } & \eta \\
 \text{s.t. } & \alpha_E(E(x) - E_M) - \eta \geq 0, \\
 & \alpha_T(T_{DMAD}(x) - T_M) + \eta \leq 0, \\
 & \text{a.d.a.c. constraints f}(\quad),
 \end{aligned}$$

where  $\alpha_E$  and  $\alpha_T$  are parameters which can be given by the investor based on his/her degree of satisfaction regarding the expected excess return and the tracking error

( ) is a standard linear programming problem. One can use the following algorithms for linear programming to solve it efficiently. For example, the simplex method

**Remark2:** The linear  $S$  shape membership function of the two factors may change the shape according to the parameters  $\alpha_E$  and  $\alpha_T$ . Through selecting the values of these parameters, the aspect of the two factors may be described accurately. On the other hand, the tracking parameter values may reflect directly the investors' aspect of the expected excess return and tracking error. Investors should estimate strategies based on the proposed fuzzy index tracking portfolio selection model.

### 4 Numerical Example

In this section, we give a numerical example to illustrate the proposed fuzzy index tracking portfolio selection model. We suppose that the investor considers the high 8 index as the tracking goal. We choose the returns of the stocks from the high 8 index as the risk neutral expected return data of the three stocks and the high 8 index from a year, 1990 to December, 2002. The data are downloaded from the website <http://www.stockstar.com> and used as a period to get the historical rates of return of the eight periods.

The values of the parameters  $\alpha_E$ ,  $\alpha_T$ ,  $E_M$  and  $T_M$  can be given by the investor according to his/her aspect of the expected excess return and the tracking error. We assume that  $\alpha_E = 0.05$ ,  $\alpha_T = 0.05$ ,  $E_M = 0.05$  and  $T_M = 0.05$ . Using the historical data, we get a fuzzy index tracking portfolio selection strategy based on ( ) . Computations were carried out using the O.C. Using the O.S. we observe that the expected excess return and tracking error of portfolio based on ( ) are 2.5% and the estimate rate of the beta of the fuzzy index tracking portfolio

**Table 1.** Membership grade  $\lambda$ , obtained expected excess return and obtained tracking error

$\lambda$	$\eta$	excess return	tracking error
0.9431	2.8095	0.0152	0.0062

**Table 2.** Investment ratio of the obtained fuzzy index tracking portfolio

Stock	1	2	3	4	5	6	7	8	9	10
Ratio	0.0000	0.0000	0.0620	0.0254	0.0000	0.0408	0.0180	0.1389	0.0324	0.0082
Stock	11	12	13	14	15	16	17	18	19	20
Ratio	0.1440	0.1488	0.0130	0.0000	0.0000	0.0000	0.1889	0.0000	0.0000	0.0000
Stock	21	22	23	24	25	26	27	28	29	30
Ratio	0.0276	0.0000	0.0000	0.0124	0.1001	0.0000	0.0395	0.0000	0.0000	0.0000

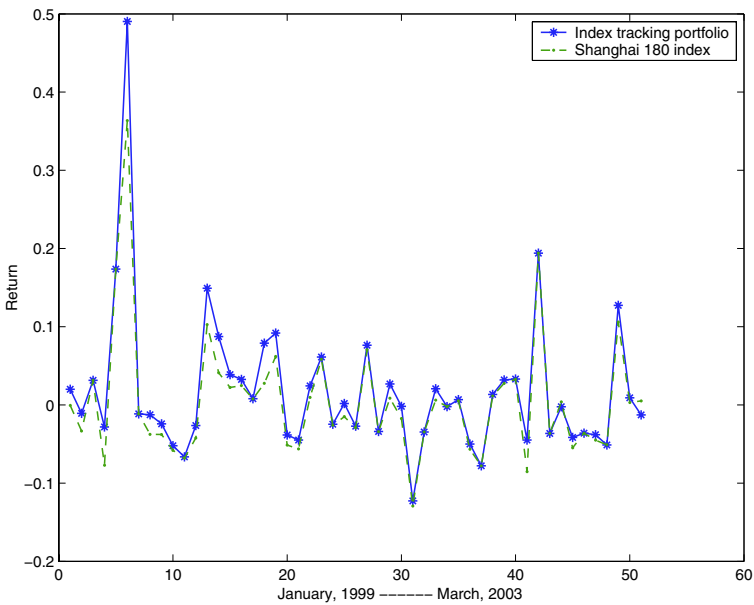


**Fig. 3.** The deviations between the returns of the obtained index tracking portfolio and the returns on the benchmark Shanghai 180 index

Figure 3 shows the deviations between the returns of the obtained index tracking portfolio and the returns of the benchmark Shanghai 180 index for each month from January, 1999, to March, 2003. From Figure 3, we can find that the obtained fuzzy index tracking portfolio based on  $g(\lambda)$  tracks Shanghai 180 index effectively.

## 5 Conclusion

Regarding the expected excess return and the tracking error as tactical objectives, fuzzy sets have proposed a bi-objective programming model for the index tracking portfolio selection problem. Furthermore, investors' vague aspirations for the excess return and the tracking error are considered as fuzzy numbers based on fuzzy decisions. Therefore, we have proposed a fuzzy index tracking portfolio selection model. The empirical results demonstrate that the proposed fuzzy index tracking portfolio selection model. The computational results show that the proposed model can generate a favorable index tracking portfolio strategy according to the investors' satisfaction degree.

## References

1. Bellman, R., Zadeh, L.A.: Decision Making in a Fuzzy Environment. *Management Science* 17 (1970) 141–164.
2. Clarke, R.G., Kruse, S., Statman, M.: Tracking Errors, Regret, and Tactical Asset Allocation. *Journal of Portfolio Management* 20 (1994) 16–24.
3. Consiglio, A., Zenios, S.A.: Integrated Simulation and Optimization Models for Tracking International Fixed Income Indices. *Mathematical Programming* 89 (2001) 311–339.
4. Fang, Y., Wang, S.Y.: *Fuzzy Portfolio Optimization: Theory and Methods*. Tsinghua University Press, Beijing, 2005.
5. Konno, H., Yamazaki, H.: Mean Absolute Portfolio Optimization Model and Its Application to Tokyo Stock Market. *Management Science* 37(5) (1991) 519–531.
6. Markowitz, H.M.: Portfolio Selection. *Journal of Finance* 7 (1952) 77–91.
7. Markowitz, H.M.: *Portfolio Selection: Efficient Diversification of Investment*. John Wiley & Sons, New York, 1959.
8. Roll, R.: A Mean Variance Analysis of Tracking Error - Minimizing the volatility of Tracking Error will not Produce a More Efficient Managed Portfolio. *Journal of Portfolio Management* 18 (1992) 13–22.
9. Rudolf, M., Wolter, H.J., Zimmermann, H.: A Linear Model for Tracking Error Minimization. *Journal of Banking and Finance* 23 (1999) 85–103.
10. Watada, J.: Fuzzy Portfolio Model for Decision Making in Investment. In: Yoshida, Y. (eds.): *Dynamical Aspects in Fuzzy Decision Making*. Physica-Verlag, Heidelberg (2001) 141–162.
11. Worzel, K.J., Vassiadou-Zeniou, C., Zenios, S.A.: Integrated Simulation and Optimization Models for Tracking Indices of Fixed-income Securities. *Operations Research* 42 (1994) 223–233.



# Application of Activity-Based Costing in a Manufacturing Company: A Comparison with Traditional Costing

G. Gonca Tuncel, Derya Eren, Kemal Guhan, Mirac Bayhan, and Atkan Korkmaz

Department of Industrial Engineering, University of Dokuz Eylul,  
35100 Bornova-Izmir, Turkey

{gonca.tuncel, derya.eren, mirac.bayhan}@deu.edu.tr

**Abstract.** Activity-Based Costing (ABC) represents an alternative paradigm to traditional cost accounting system and has received extensive attention during the past decade. Rather than distorting the cost information by using traditional overhead allocation methods, it traces the cost via activities performed on the cost objects (production or service activities) giving more accurate and traceable cost information. In this paper, the implementation of ABC in a manufacturing system is presented, and a comparison with the traditional cost based system in terms of the effects on the product costs is carried out to highlight the difference between two costing methodologies. The results of the application reveal the weak points of traditional costing methods and an S-Curve which exposes the undercosted and overcosted products is used to improve the product pricing policy of the firm.

## 1 Introduction

The customer driven environment of today's manufacturing systems and the competitive pressure of the global economy force manufacturing services and organizations to become more effective, integrated and highly automated in order to increase the productivity at reduced costs but this process must be sustainable. Competitive essential that accurate cost calculation mechanism is provided by ABC, as an alternative method to traditional accounting methods. Classification of costs to activities using multiple cost drivers, the allocated costs to products based on each product's use of these activities, 4 significant multiple activities as cost drivers, it reduces the risk of distortion and provides accurate cost information.

In a ABC system, the total cost of a product equals the cost of the raw materials plus the sum of the cost of all value adding activities to produce that product. Therefore, the ABC method measures the usage of the organizational resources by the activities performed and links the cost of these activities to outputs, such as products, customers, and services. Each product requires a number of activities such as design, engineering, purchasing, production and quality control. Each activity consumes resources of different categories such as

the work of the manager. Cost drivers are the measures of the activities performed such as number of units produced, labour hours, hours of equipment time, number of orders received.

The traditional accounting systems, direct materials and labour are the costs that can be traced directly to the product using the Cost system, activities can be classified as a value added and non-value added activities. In order to improve the performance of the system, a value added can be eliminated. Despite the advantages of providing accurate costs, it requires additional administrative expense. Obtaining the information needed for the analysis is a tedious and expensive task. It can help to reduce time used for management. It can help to reduce the difficulties presented by design and cost management.

The primary objective of this paper is to develop a Cost system for a manufacturer. Compare and contrast the results of Cost with traditional accounting methods. Therefore, the aim of this study is to guide management in the right direction. Provide accurate information for management activities.

The organization of the paper is as follows. Section 2, the methodology of Cost is explained. Case studies presented in section 3 illustrate the application of Cost. A comparison is made in section 4, the conclusions and the future research directions are given. Some suggestions are offered to improve the performance of the company.

## 2 Activity-Based Costing (ABC)

Cost accounting is a method that identifies the cost pools, select the cost centers and allocate the assigned costs to cost drivers based on the number of each activity used. Since the cost drivers are related to the activities, the occurrence of these

1. The cost drivers which assume the increase of the inputs for the unit that is being produced
2. Batch level cost drivers which assume the variation of the inputs for the batch that is being produced
3. Product level cost drivers which assume the necessity of the inputs to support the production of each direct type of product
4. Activity level cost drivers are the drivers which are related to the factory's manufacturing process. Since the Cost system is used to identify the activities which generate cost and then match the activities to the cost bases used to assign costs to the products.

Therefore, using the Cost system, the activities which generate cost must be determined and then should be matched to the cost drivers used to assign costs to the products.

The implementation of the Cost system has the following steps:

1. Identify the activities such as engineering, machine, inspection, etc.
2. Determine the activity costs

eterm . . . g the c . st dr . ers such as mach . . . g h . urs . . umber . f setups a . d e . g . eer . g h . urs

4 C . .ect . g the act . t . data

C . mput . g the pr . duct c . st

### 3 Implementation of the ABC Method: A Case Study

The imp . eme . tat . . stud . prese . ted here t . k p . ace . . . e . f the lead . g sa . tar . are c . mpa . es . . urke 7 t has a pr . duct . . capac . t . f 8 th . usa . d t . s . ke ma . sa . tar . are ma . ufacturers, the c . mpa . . c . udes s . me c . m . m . pr . cesses . . rst stage . f the pr . cesses s . d . e . . the bu . k prepareme . t de partme . t h . ch . s . charge . f prepar . g the esse . ta . qua . t . tes . f bu . k bear . g . Rec . pes are prepared f r each pr . duct . . ru . a . d acc . rd . g t . these . . gred e . t rec . pes, the bu . ks are prepared b . the e . ectr . . ca . . c . tr . ed ta . ks . fter the bu . k s read . t ca . be se . t t . t . . d . ere . t de partme . ts, pressured a . d c . ass ca . cast . g de partme . ts

. pressured cast . g de partme . t, the bu . k s g . e . shape b . the pressured cast . g pr . cess . he pr . cess uses aut . mated mach . es a . d has sh . rter c . ce t mes . he . c . mpared t . c . ass ca . cast . g de partme . t . . e . er, the bu . k used . . th s de partme . t must ha . e the character st . cs . f stre . gth a . d e . dura . ce . he . utput . f th s de partme . t s se . t t . g az . g de partme . t

C . ass ca . cast . g s the sec . d a . ter . at . e . t . pr . duce sa . tar . are pr . ducts . . th s de partme . t, m . st . f the . perat . . s are perf . rmed b . d . rect . ab . r . he c . ce t mes . f the pr . ducts are . . ger tha . the pressured cast . g de partme . t . he . utput . f th s de partme . t s \_ shaped a . d casted . bu . k a . d se . t t . the g . az . g de partme . t, t . .

. g . az . g de partme . t, shaped bu . k s g . azed . h s stage ca . be defi . ed as p . sh . g the pr . ducts . . th a pr . tect . e mater . a . fr . m e . ter . a . \_e . cts . he . utput . f th s de partme . t s se . t t . tu . . e . . e .

. tu . . e . . e . , the pr . ducts are heated . . er 2 . degrees Ce . s us . fter sta . g . . theses . . e . s f r a . per . d . f t me, the pr . ducts are . . spected b . the . rkers . . e . er, s . me . f the . utput ma . ha . e s . me u . des red character st . cs . ke the scratches, etc . . th s case, these pr . ducts are se . t t . the sec . d heat treatme . t here the . are re . rked a . d heated aga . . he pr . per . utput s se . t t . packag . g . h . e the defected . . es are se . t t . . aste

. a . . . packag . g de partme . t, pr . ducts are packaged a . d shru . ke .

C . mpa . has bee . us . g a pr . cess c . st . g . . g c f r . bta . . g the pr . per c . st . g . f ts pr . ducts . r . cess c . st . g . s a . s . a . de . used c . st . g . t . . f r ma . c . mpa . es . h s meth . d rec . g . zes the f . . . . g c . st . p . . s

- rect . ab . r . . . rkers tak . g p . ace . . the pr . duct . . are rec . g . zed as d . rect . ab . r a . d th s p . . s the m . st c . mm . . p . . used . . e . er stage
- G . E . ectr . ct . h . t . ater . hese tems are mp . rta . t . c . st . g . e . eme . t . . cast . g de partme . ts
- ackag . g . h s c . st . s . bser . ed . the fi . a . stage . f the firm ca . ed fi . a . packag . g . t . . c . udes packag . g a . d shr . k . g . f the pr . ducts

— Overheads: This is a semi-variable cost. For the stages of the firm that includes depreciation, rent, indirect labour, materials, and miscellaneous costs.

In order to perform a calculation, process cost sheets are used. The cause process cost sheet aggregates the cost of the case form that the product is sold. It includes the correct results of the correct results of the process cost sheet. It can be achieved. Here, there is a significant improvement in the production of the output of bulk preparation department. It is seen that bulk prepared for the department is the same. The changes are appropriate for the analysis. The first time sheets are prepared. The amount of the labour time is used to perform the re-evaluation. The workers filed the time sheet as a result of the activities. The edge of the processes and related percentages are obtained. The time sheets are edited and necessary corrections are made. Here, some of the activities are merged, some of them are discarded. After this stage, the stage data is requested from the accounting department and labour cost of the activities are determined.

If the amount of the activities that each product consumes can be determined, the product cost can be calculated by taking the sum of the costs of the activities consumed by these products. Observations and necessary amendments are done to reach this knowledge and the necessary costs are added to the activities. Cost of re-evaluation according to the space required for each activity and similar, the power, depreciation and other necessary costs are added to the activities according to the activities' consumption of the resources of activity. It uses 2 additional workers, the activity costs 2 of the department space, the activity is 2, the activity is 2 additional workers, the activity costs are distributed by using the same logic.

The activities performed during casting are moulding, drilling, assembly, heating, re-arranging equipment, cleaning, drilling, finishing, and carrying. The activity of drilling is the process of time for drilling assembly. Here, the number of heating, for re-arranging the number of outputs, for equipment cleaning is the total process of time for drilling finishing. Here, the total number of finishing is added for carrying. Here, the number of processed units in this department, unit area of the product area, the carrier and the total area of carried goods.

The activities performed during pressured casting are moulding, drilling, grinding, heating, setup, cutting, necessary materials from the products, gear re-arranging, drilling, assembly, heating, re-arranging preparation, drilling, some sub-components, ashbas, ashbas, drilling, re-arranging back of the products, patch control, bringing the product to other departments, finishing, moulding, moulding check up, control, equipment and personnel control, drilling, after heating. The activity of drilling is the number of moulds used for drilling. Here, the number of output, for setup are the components, setup hour, setup for other products, setup for bases, setup for other products, for cutting, necessary materials from the products, the components, for gear re-arranging is a semi-variable cost, for carrying is the number of output,

for drilling assembly, head for drilling preparation, the number of output, for drilling same sub components, ashbas, s the number of sub components, for ashbas, drilling the number of ashbas, s, rework back of the products, a d patch control, the number of output, for bring, g the s the c.m. g, for the p.g.t. other departments, the number of reser, s, for fi, g firms, m.d check up, c. tr., equipment a d pers. e. c. tr., drilling after he, s the c.m. g u. ts

he activities performed during gaz, g are maintenance, gaz, g th had, transfer, rework, c. set shak, g, p.a., g, r. ut. e. c. tr. s a d pr sm data e. tr. he activity driver for maintenance, the number of reworked parts, for gaz, g th had, s the eght, f parts to be gazed, for transfer a d rework, s the number of reworked parts, for c. set shak, g, s the number of c. sets, for p.a., g, r. ut. e. c. tr. s a d pr sm data e. tr. s the p.a. ed u. ts

he activities performed in the turbine department are turbine, e. act. t, transfer turbine, transfer from turbine, heat control, e. securt. c. tr., p.a., g, r. ut. e. c. tr. s, pr sm data e. tr, taking records, second heat treatment activity, feed, g. t. the turbine, rework of heat processed units a d special treatment, he activity driver for turbine, e. act. t, transfer turbine, transfer from turbine, heat control, a d e. securt. c. tr. s the t.ta. area covered by the heated units, for p.a., g, r. ut. e. c. tr. s, pr sm data e. tr. a d taking records, s the t.ta. sum. f. utputs, for second heat treatment activity, a d feed, g. t. the turbine, s t.ta. area covered by a. u. ts, for rework of heat processed units a d special treatment, s the t.ta. area covered by utputs

he activities performed in the packaging department are packaging, shrink, g, cea. up, rga. z, g the finished products, mag, g, a d pr. duct fu. ct. c. tr. a d transferr, g the utputs, he activity driver for packaging, a d shrink, g, s the packaged volume, for cea. up, s the t.ta. number of u. ts cea. ed, for rga. z, g the finished products, mag, g, pr. duct fu. ct. c. tr. a d transferr, g the utputs, s the t.ta. number of utputs

after finding the product costs of the firm, the costs obtained by process costing method, g a d the C results of the product costs are compared with the results, to see that there are significant differences between the product costs obtained by the two methods

### 4 Conclusions

Concludes the activity concept a d using the activities, C can successfully work the product costs to product knowledge, a product is produced, how much time is needed to perform an activity a d finally how much money is absorbed by performing this task are answered by the help of C studies

Currently, after the comparison of the traditional a d C costs, 80% of the firms using traditional methods used for the comparison of the total product costs, a. u. es % as a result of C firm traditional costs, s f u. d f r each product % based on (C cost traditional cost)\*

product costs under C a d traditional costs, g. e. s can be used to design a table (above) which illustrates % based on C a d traditional costs

**Table 1.** Comparison of the two product cost values

Products	% Bias	Products	% Bias
Product 70	10.415	Product 28	102.938
Product 23	54.796	Product 56	103.417
Product 64	60.439	Product 48	105.092
Product 12	65.043	Product 4	108.269
Product 59	69.485	Product 63	108.905
Product 47	71.071	Product 53	109.488
Product 62	75.279	Product 46	112.454
Product 31	77.736	Product 11	114.009
Product 1	78.621	Product 54	117.228
Product 37	78.953	Product 50	124.241
Product 3	79.965	Product 8	124.84
Product 22	80.527	Product 6	133.134
Product 30	80.731	Product 44	134.926
Product 42	83.265	Product 7	162.302
Product 19	84.533	Product 14	164.557
Product 58	89.282	Product 29	169.465
Product 36	89.531	Product 5	219.781
Product 20	96.504	Product 15	317.231
Product 26	96.688	Product 39	584.387
Product 24	100.077	Product 32	1198.251
Product 55	100.521		

... that the table ... the products that are ... products that are ... but left as semi-products are ... the results show significant regression

... products underwent traditional accounting

The costs of these products are higher than the process cost and the ... are greater than the ... at a ... the ... as implemented, firm ... are ... the ... of these products ... the ... of the ... the ... of these products ... are ...

2 ... products ... the traditional methods

These products are the ... which have smaller ... than the ... of ... the ... of the ... firm realized that, the costs of these products are ... than the ... of the ... process cost ... the ... of these products ... but ... the ... of these products ... the ... of the ...

The costs of these products, the firm can ... these ... and ... a ...

... which are ... the same

These are the products ... the same ... the ... methods ... of 2 percentage (%8 % 2) can be accepted for ...

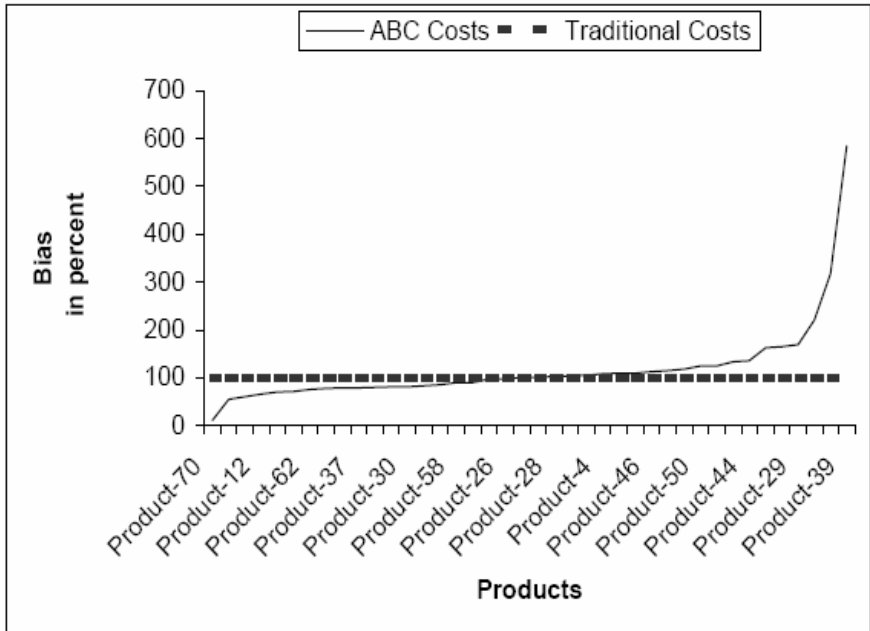


Fig. 1. S-Curve

From the Case studies, it is seen that the sales of the products are underevaluated, and overvalued, some of them generate the same results.

In the analysis, the cost calculation of the bulk preparation department are performed using traditional costing method. Hence, the outputs of the processes are determined. Therefore, the ABC must be applied to improve the efficiency. ABC consumes lots of time, data and efforts, implementation of it has a significant reduction in outputs, but ABC and traditional generate the same results, so that the traditional implementation of ABC.

The help of this analysis, product pricing decisions, strategic implementation of decisions can be determined under the scope of these hidden processes and profits according to the ABC results, the company can probably increase or decrease some of its product costs to gain more competitive advantage.

The costing process of the company highlighted some weaknesses of the financial system, therefore, these problems are expected to be fixed in the future. The studies show that this application of ABC capabilities of minimizing the hidden processes and profits of the traditional costing methods. Hence, the efficiency of current sales channels of the products are underevaluated as a further remark, the company performance analysis are expected to be developed especially a detailed core Card (ABC) implementation can be performed. Hence, the efficiency of the ABC database is an advantage for ABC application since it is a critical phase recommends ABC implementation. A zero application is an ABC can give the firm great advantages. The short and long run under the scope of ABC.

he studies literature prove that ABC is a promising method to support product pricing, product mix, and make-or-buy decisions in manufacturing companies. ABC is a fruitful area for researchers and has high potential for future applications such as the hybridization of ABC with metaheuristic methods as artificial neural networks, Genetic algorithms, and simulated annealing.

## References

1. Ozbayrak, M., Akgun, M., and Turker, A.K.: Activity-based cost estimation in a push/pull advanced manufacturing system. *Int. J. of Production Economics*, vol. 87 (2004) 49-65.
2. Cooper, R. and Kaplan, R. S.: How cost accounting distorts product costs. *Management Accounting*, vol.69 (1988) 20-27.
3. Kim, G., Park, C. S., and Kaiser, M. J.: Pricing investment and production activities for an advanced manufacturing system, *Engineering Economist*, vol. 42, no. 4 (1997) 303-324.
4. Gunasekaran, A., and Sarhadi, M.: Implementation of activity-based costing in manufacturing. *Int. J. of Production Economics*, vol.56-57 (1998) 231-242.
5. Ben-Arieh, D. and Qian L.: Activity-based cost management for design and development stage. *Int. J. of Production Economics*, vol.83 (2003) 169-183.
6. Lewis, R. J.: *Activity-based models for cost management systems*. Quorum Books, West-port, CT (1995).
7. Koker, U.: *Activity-based costing: Implementation in a sanitaryware company*. M.Sc. Thesis, Department of Industrial Engineering, University of Dokuz Eylul (2003).
8. Cokins, G.: *Activity-based cost management making it works*. McGraw-Hill. Inc. (1997).



# Welfare for Economy Under Awareness

e. r e<sup>1,\*</sup> a. d akash atsuh sa<sup>2,\*\*</sup>

<sup>1</sup> Advanced Course of Electronic and Computer Engineering,  
Ibaraki National College of Technology  
abc9872000jp@yahoo.co.jp

<sup>2</sup> Department of Natural Sciences, Ibaraki National College of Technology,  
Nakane 866, Hitachinaka-shi, Ibaraki 312-8508, Japan  
mathisa@ge.ibaraki-ct.ac.jp

**Abstract.** We present the extended notion of pure exchange economy under uncertainty, called an *economy with awareness structure*, where each trader having a strictly monotone preference makes decision under his/her awareness and belief, and we introduce a generalized notion of equilibrium for the economy, called an *expectations equilibrium in awareness*. We show the existence theorem of the equilibrium and the fundamental welfare theorem for the economy, i.e., an allocation in the economy is ex-ante Pareto optimal if and only if it is an expectations equilibrium allocation in awareness.

## 1 Introduction

This article relates economies and distributed belief. We present a generalized notion of economy under uncertainty, called a *economy with awareness structure*, where each trader makes decision under his/her awareness and belief under complete information. The purposes are first, to introduce a generalized notion of expectations equilibrium for the economy, called a *expectations equilibrium in awareness* economy, to show the fundamental welfare theorem for the generalized economy under expectations equilibrium awareness.

**Main Theorem.** *In a pure exchange economy under uncertainty, the traders are assumed to have an awareness structure and they are risk averse. Then an allocation in the economy is ex-ante Pareto optimal if and only if it is an expectations equilibrium allocation in awareness for some initial endowment with respect to some price system.*

Economic theory related fields, mathematicians have investigated several types of equilibrium in an economy under asymmetric information. <sup>1</sup> He has studied the relationships between these equilibrium concepts (e.g.

---

\* Lecture presenter.

\*\* Corresponding author. Partially supported by the Grant-in-Aid for Scientific Research(C)(2)(No.14540145) in the Japan Society for the Promotion of Sciences.

<sup>1</sup> See the literatures cited in F. Forges, E. Minelli, and R. Vohla, *Incentive and the core of exchange economy - Survey*, Journal of Mathematical Economics 38 (2002), 1–41.



the interpretation of  $A_t E$  is that  $t$  is aware of  $E$ . The property **PL** says that  $t$  is aware of  $E$  if he believes that he believes that he does not believe that

he shares the generalized information partition, the effect of which is characterized as follows.

**Definition 1.** The associated information structure  $(P_t)_{t \in T}$  that are essential structure  $\langle \Omega, (A_t), (B_t) \rangle$  is the class of  $t$ 's associated information functions  $P_t : \Omega \rightarrow 2^\Omega$  defined by  $P_t(\omega) = \bigcap_{E \in 2^\Omega} \{E \mid \omega \in B_t E\}$ . (If there is a set  $E$  for which  $\omega \in B_t E$  then we take  $P_t(\omega)$  to be undefined.) We denote by  $\text{dom}(P_t)$  the set  $\{\omega \in \Omega \mid P_t(\omega) \neq \emptyset\}$ , called the *domain of  $P_t$* .

The mapping  $P_t$  is called *reflexive* if

**Ref**  $\omega \in P_t(\omega)$  for every  $\omega \in \text{dom}(P_t)$ .

and it is said to be *transitive* if

**Trn**  $\xi \in P_t(\omega)$  implies  $P_t(\xi) \subseteq P_t(\omega)$  for all  $\xi, \omega \in \text{dom}(P_t)$ .

furthermore  $P_t$  is called *symmetric* if

**Sym**  $\xi \in P_t(\omega)$  implies  $P_t(\xi) \ni \omega$  for all  $\omega$  and  $\xi \in \text{dom}(P_t)$

*Remark 1.* Characterization 2 reproduces the *strong epistemic model* equation. Let the respective semantics of the modal logic **S5** the strong epistemic models a tuple  $\langle \Omega, (K_t)_{t \in T} \rangle$  in which  $t$ 's knowledge operator  $K_t : 2^\Omega \rightarrow 2^\Omega$  satisfies the following properties relative to  $E, F$  of  $2^\Omega$ .

**N**  $K_t \Omega = \Omega$ ,      **K**  $K_t(E \cap F) = K_t E \cap K_t F$ ,      **T**  $K_t F \subseteq F$   
**4**  $K_t F \subseteq K_t K_t F$ ,      **5**  $\Omega \setminus K_t F \subseteq K_t(\Omega \setminus K_t F)$ .

$t$ 's associated information function  $P_t$  induced by  $K_t$  makes a partition of  $\Omega$ , called  $t$ 's *information partition*, which satisfies the properties **Ref**, **Trn** and

**Sym** holds subject to the respective semantics correspondingly. The logic **S5** the properties **Ref**, **Trn** and **Sym** are respectively equivalent to the properties **T**, **4** and **5**. The strong epistemic model can be interpreted as the associated structure  $\langle \Omega, (A_t), (B_t) \rangle$  such that  $B_t$  is the knowledge operator. This statement is easily verified that  $A_t$  must be the *trivial* operator,<sup>3</sup> and that  $\text{dom}(P_t) = \Omega$ .

## 2.2 Economy with Awareness Structure

pure exchange economy under uncertainty is a structure

$$\mathcal{E} = \langle T, \Omega, \mathbf{e}, (U_t)_{t \in T}, (\pi_t)_{t \in T} \rangle$$

<sup>3</sup> I.e.  $A_t(F) = \Omega$  for every  $F \in 2^\Omega$ .

consist of the following structure and interpretation. There are  $l$  commodities in each state of the state space  $\Omega$ , the consumption set of each trader  $t$  is  $\mathbf{R}_+^l$ , an initial endowment is a mapping  $\mathbf{e} : T \times \Omega \rightarrow \mathbf{R}_+^l$ , which  $\mathbf{e}(t, \cdot) : \Omega \rightarrow \mathbf{R}_+^l$  is called  $t$ 's initial endowment.  $U_t : \mathbf{R}_+^l \times \Omega \rightarrow \mathbf{R}$  is  $t$ 's utility function and the representative utility function  $\pi_t$  is a subjective prior on  $\Omega$  for  $t \in T$ . For simplicity,  $\pi_t$  is assumed to be full support for all  $t \in T$ , that is,  $\pi_t(\omega) > 0$  for  $\omega \in \Omega$ .

**Definition 2.** A pure exchange economy with awareness structure is a structure  $\mathcal{E}^A = \langle \mathcal{E}, (A_t)_{t \in T}, (B_t)_{t \in T}, (P_t)_{t \in T} \rangle$ , in which  $\mathcal{E}$  is a pure exchange economy under uncertainty, and  $\langle \Omega, (A_t)_{t \in T}, (B_t)_{t \in T}, (P_t)_{t \in T} \rangle$  is a awareness structure, in which  $(P_t)_{t \in T}$  is the associated information structure, the domain of the economy  $\mathcal{E}^A$  is measurable  $\mathcal{M}(\mathcal{E}^A) = \cap_{t \in T} \mathcal{M}(P_t)$ . We always assume that  $\mathcal{M}(\mathcal{E}^A) \neq \emptyset$ .

*Remark 2.* An economy under asymmetric information is an economy  $\mathcal{E}^A$  in which the awareness structure  $\langle \Omega, (A_t)_{t \in T}, (B_t)_{t \in T} \rangle$  generates the signaling system model, and that  $\mathcal{M}(\mathcal{E}^A) \neq \Omega$ .

We denote by  $\mathcal{F}_t$  the field of  $\mathcal{M}(P_t)$  generated by  $\{P_t(\omega) \mid \omega \in \Omega\}$  and denote by  $\Pi_t(\omega)$  the atom containing  $\omega \in \mathcal{M}(P_t)$ . We denote by  $\mathcal{F}$  the  $\sigma$ -field of  $\mathcal{F}_t (t \in T)$  on  $\mathcal{M}(\mathcal{E}^A)$ . We let  $\mathcal{F} = \vee_{t \in T} \mathcal{F}_t$ , and denote by  $\{II(\omega) \mid \omega \in \mathcal{M}(\mathcal{E}^A)\}$  the set of atoms  $II(\omega)$  containing  $\omega$  of the field  $\mathcal{F} = \vee_{t \in T} \mathcal{F}_t$ . We shall frequently refer to the following conditions hereafter  $t \in T$ ,

- A-1**  $\sum_{t \in T} \mathbf{e}(t, \omega) > 0$  for each  $\omega \in \Omega$
- A-2**  $\mathbf{e}(t, \cdot)$  is  $\mathcal{F}$  measurable on  $\mathcal{M}(P_t)$
- A-3** For each  $x \in \mathbf{R}_+^l$ , the function  $U_t(x, \cdot)$  is at least  $\mathcal{F}$  measurable on  $\mathcal{M}(\mathcal{E}^A)$ , and the function  $T \times \mathbf{R}_+^l \rightarrow \mathbf{R}, (t, x) \mapsto U_t(x, \omega)$  is  $\Sigma \times \mathcal{B}$  measurable, here  $\mathcal{B}$  is the  $\sigma$ -field of all real subsets of  $\mathbf{R}_+^l$
- A-4** For each  $\omega \in \Omega$ , the function  $U_t(\cdot, \omega)$  is strictly increasing on  $\mathbf{R}_+^l$ , continuous, strictly quasiconcave and non-satiated on  $\mathbf{R}_+^l$ .<sup>4</sup>

### 2.3 Expectations Equilibrium in Awareness

An assignment is a mapping  $\mathbf{x} : T \times \Omega \rightarrow \mathbf{R}_+^l$  such that for each  $t \in T$ , the function  $\mathbf{x}(t, \cdot)$  is at least  $\mathcal{F}$  measurable on  $\mathcal{M}(\mathcal{E}^A)$ . We denote by  $\mathcal{Ass}(\mathcal{E}^A)$  the set of all assignments for the economy  $\mathcal{E}^A$ . An allocation is a measurable assignment  $\mathbf{a}$  such that  $\mathbf{a}(t, \cdot)$  is  $\mathcal{F}$  measurable on  $\mathcal{M}(\mathcal{E}^A)$  for all  $t \in T$  and  $\sum_{t \in T} \mathbf{a}(t, \omega) \leq \sum_{t \in T} \mathbf{e}(t, \omega)$  for every  $\omega \in \Omega$ . We denote by  $\mathcal{Alc}(\mathcal{E}^A)$  the set of all allocations.

We introduce the reservation utility of trader's expectation of utility of  $\mathcal{E}^A$   $t$ 's ex-ante expectation is measurable  $\mathbf{E}_t U_t(\mathbf{x}(t, \cdot)) = \sum_{\omega \in \text{Dom}(P_t)} U_t(\mathbf{x}(t, \omega), \omega) \pi_t(\omega)$  for each  $\mathbf{x} \in \mathcal{Ass}(\mathcal{E}^A)$ . The interim expectation  $\mathbf{E}_t U_t(\mathbf{x}(t, \cdot) \mid P_t)$  is defined by  $\mathbf{E}_t U_t(\mathbf{x}(t, \cdot) \mid P_t)(\omega) = \sum_{\xi \in \text{Dom}(P_t)} U_t(\mathbf{x}(t, \xi), \xi) \pi_t(\{\xi\} \cap A_t(\{\xi\}) \mid P_t(\omega))$ .

<sup>4</sup> That is, for any  $x \in \mathbf{R}_+^l$ , there exists an  $x' \in \mathbf{R}_+^l$  such that  $U_i(x', \omega) > U_i(x, \omega)$ .

...  $m(P_t)$  ... should be ... that ... use ... the usual ... of posterior ...  $\pi_t(\{\xi\}|P_t(\omega))$  but the revised ...  $\pi_t(\{\xi\} \cap A_t(\{\xi\})|P_t(\omega))$ <sup>5</sup> ... price system ... a ... zero ...  $p: \Omega \rightarrow \mathbf{R}_+^l$  ... which is  $\mathcal{F}$  measurable ...  $m(\mathcal{E}^A)$  ... the ...  $\Delta(p)$  the part ...  $\Omega$  ... induced by  $p$ , and ...  $\sigma(p)$  the field of  $\Omega$  generated by  $\Delta(p)$  ... the budget set ... of a trader  $t$  at a state  $\omega$  for a price system  $p$  is defined by  $B_t(\omega, p) = \{x \in \mathbf{R}_+^l \mid p(\omega) \cdot x \leq p(\omega) \cdot e(t, \omega)\}$ . ... the mapping  $g: \Delta(p) \cap P_t \rightarrow m(P_t) \rightarrow 2^\Omega$  by  $(\Delta(p) \cap P_t)(\omega) \rightarrow \Delta(p)(\omega) \cap P_t(\omega)$ . ... the ...  $m(\Delta(p) \cap P_t)$  the set of all states  $\omega \in \Delta(p)(\omega) \cap P_t(\omega) / \emptyset$  ... let  $\sigma(p) \vee \mathcal{F}_t$  be the smallest  $\sigma$ -field containing both the fields  $\sigma(p)$  and  $\mathcal{F}_t$ .

**Definition 3.** ... expectations equilibrium in awareness for an economy  $\mathcal{E}^A$  ... the awareness structure is a pair  $(p, \mathbf{x})$ , ... which  $p$  is a price system and  $\mathbf{x}$  is an assignment satisfying the following conditions

- EA1.**  $\mathbf{x}$  is an allocation.
- EA2.** for a  $t \in T$  and for every  $\omega \in \Omega$ ,  $\mathbf{x}(t, \omega) \in B_t(\omega, p)$
- EA3.** for a  $t \in T$ , if  $\mathbf{y}(t, \cdot): \Omega \rightarrow \mathbf{R}_+^l$  is  $\mathcal{F}$  measurable ...  $m(\mathcal{E}^A)$  then  $\mathbf{y}(t, \omega) \in B_t(\omega, p)$  for a  $\omega \in \Omega$ , then

$$\mathbf{E}_t U_t(\mathbf{x}(t, \cdot)) | \Delta(p) \cap P_t(\omega) \geq \mathbf{E}_t U_t(\mathbf{y}(t, \cdot)) | \Delta(p) \cap P_t(\omega)$$

- EA4.** for every  $\omega \in m(\mathcal{E}^A)$ ,  $\sum_{t \in T} \mathbf{x}(t, \omega) = \sum_{t \in T} \mathbf{e}(t, \omega)$ .

the allocation  $\mathbf{x}: \mathcal{E}^A$  is called an expectations equilibrium allocation ... are essential for  $\mathcal{E}^A$

... the ...  $EA(\mathcal{E}^A)$  the set of all the expectations equilibrium allocations for a pure exchange economy  $\mathcal{E}^A$ , and ... the ...  $\mathcal{A}(\mathcal{E}^A)$  the set of all the expectations equilibrium allocations ... are essential for the economy

### 3 The Results

... let  $\mathcal{E}^A$  be the economy ... the awareness structure and  $\mathcal{E}^A(\omega)$  the economy ... the complete format ...  $\langle T, (\mathbf{e}(t, \omega))_{t \in T}, (U_t(\cdot, \omega))_{t \in T} \rangle$  for each  $\omega \in \Omega$  ... the ...  $\mathcal{W}(\mathcal{E}^A(\omega))$  the set of all complete allocations for  $\mathcal{E}^A(\omega)$

#### 3.1 Existence of Equilibrium in Awareness

**Theorem 1.** Let  $\mathcal{E}^A$  be a pure exchange economy with awareness structure satisfying the conditions **A-1**, **A-2**, **A-3** and **A-4**. Then there exists an expectations equilibrium in awareness for the economy; i.e.,  $EA(\mathcal{E}^A) \neq \emptyset$ .

<sup>5</sup> A discussion why this improvement of the notion of posterior is needed is given in T. Matsuhisa and S.-S. Usami, *Awareness, belief and agreeing to disagree*, Far East Journal of Mathematical Sciences 2(6) (2000) 833–844.

of the procedure with the price system to state that

**Lemma 1.** *The event  $(\Delta(p) \cap P_t)(\omega)$  can be decomposed into the disjoint union  $(\Delta(p) \cap P_t)(\omega) = \bigcup_{k=1}^p \Pi(\xi_k)$ . Furthermore, for  $\mathbf{x} \in \text{Ass}(\mathcal{E}^A)$ ,  $\mathbf{E}_t U_t(\mathbf{x}(t, \cdot)) | \Delta(p) \cap P_t(\omega) = \sum_{k=1}^p \frac{\pi_t(\Pi(\xi_k))}{\pi_t((\Delta(p) \cap P_t)(\omega))} U_t(\mathbf{x}(t, \xi_k), \xi_k)$ .  $\square$*

**Proof of Theorem 1.** We define the event where the remaining competitive equilibrium for an economy with complete information, <sup>6</sup> that is, such that there exists a  $(p^*(\omega), \mathbf{x}^*(\cdot, \omega)) \in \mathcal{W}(\mathcal{E}^A(\omega))$  for each  $\omega \in \Omega$  by the conditions **A-1**, **A-2**, **A-3** and **A-4**. Define the pair  $(p, \mathbf{x})$  as follows: for each  $\omega \in \Omega$ , define  $\mathbf{x}(t, \xi) = \mathbf{x}^*(t, \omega)$  for all  $\xi \in \Pi(\omega)$  and  $\omega \in \text{dom}(\mathcal{E}^A)$ , and set  $p(\xi) = p^*(\omega)$  for all  $\xi \in \Pi(\omega)$  and  $\omega \in \text{dom}(\mathcal{E}^A)$ ,  $p(\xi) = p^*(\omega)$  for  $\omega \notin \text{dom}(\mathcal{E}^A)$ . Hence we can verify that  $(p, \mathbf{x})$  satisfies the expected conditions. In fact, we are essentially in  $\mathcal{E}^A$  for **EA3**. Observe that  $\mathcal{E}^A(\xi) = \mathcal{E}^A(\omega)$  for all  $\xi \in \Pi(\omega)$ , that is, that  $(p(\xi), \mathbf{x}(t, \xi)) \in \mathcal{W}(\mathcal{E}^A(\omega))$  for every  $\omega \in \Omega$ , and thus we can also verify **EA3** by lemma. Hence the conditions we define are easily verified.  $\square$

### 3.2 Fundamental Theorem for Welfare Economics

An allocation  $\mathbf{x} \in \mathcal{E}^A$  is said to be *ex-ante Pareto-optimal* if there is no allocation  $\mathbf{a}$  such that  $\mathbf{E}_t U_t(\mathbf{a}(t, \cdot)) \geq \mathbf{E}_t U_t(\mathbf{x}(t, \cdot))$  for all  $t \in T$  with at least one strict inequality. The characterization of the remaining

**Theorem 2.** *Let  $\mathcal{E}^A$  be an economy with awareness structure satisfying the conditions **A-1**, **A-2**, **A-3** and **A-4**. An allocation is ex-ante Pareto optimal if and only if it is an expectations equilibrium allocation in awareness for some initial endowment  $\mathbf{w}$  with respect to some price system such that  $\sum_{t \in T} \mathbf{w}(t, \omega) = \sum_{t \in T} \mathbf{e}(t, \omega)$  for each  $\omega \in \text{dom}(\mathcal{E}^A)$ .*

*Proof.* ... is immediate from Propositions 1 and 2 above.  $\square$

**Proposition 1.** *Let  $\mathcal{E}^A$  be an economy with awareness structure satisfying the conditions **A-1**, **A-2**, **A-3** and **A-4**. Then an allocation  $\mathbf{x}$  is ex-ante Pareto optimal if it is an expectations equilibrium allocation in awareness with respect to some price system.*

**Proposition 2.** *Let  $\mathcal{E}^A$  be an economy with awareness structure satisfying the conditions **A-1**, **A-2**, **A-3** and **A-4**. If an allocation  $\mathbf{x}$  is ex-ante Pareto optimal in  $\mathcal{E}^A$  then there are a price system and an initial endowment  $\mathbf{e}'$  such that  $\mathbf{x}$  is an expectations equilibrium allocation in awareness with  $\sum_{t \in T} \mathbf{e}'(t, \omega) = \sum_{t \in T} \mathbf{e}(t, \omega)$  for each  $\omega \in \text{dom}(\mathcal{E}^A)$ .*

<sup>6</sup> C.f.: Theorem 5 in G. Debreu, *Existence of competitive equilibrium*, in: Handbook of Mathematical Economics, Volume 2, K.J.Arrow and M.D.Intriligator (eds), North-Holland Publishing Company, Amsterdam, 1982, 697–744.

**3.3 Proof of Propositions 1 and 2**

of the present paper the present section the first establish

**Proposition 3.** *Let  $\mathcal{E}^A$  be an economy with awareness structure satisfying the conditions **A-1**, **A-2**, **A-3** and **A-4**. Then  $\mathcal{A}(\mathcal{E}^A) = \{x \in Alc(\mathcal{E}^A) \mid \text{There is a price system } p \text{ such that } (p(\omega), x(\cdot, \omega)) \in \mathcal{W}(\mathcal{E}^A(\omega)) \text{ for all } \omega \in \Omega\}$ .*

*Proof.* Let  $x \in \mathcal{A}(\mathcal{E}^A)$  and  $(p, x) \in EA(\mathcal{E}^A)$ . We shall show that  $(p(\omega), x(\cdot, \omega)) \in \mathcal{W}(\mathcal{E}^A(\omega))$  for a.a.  $\omega \in \Omega$ . Suppose to the contrary that there exist a trader  $s \in T$  and states  $\omega' \in \Omega$ ,  $\omega_0 \in (\Delta(p) \cap P_s)(\omega')$  with the property here is a  $a(s, \omega_0) \in B_s(\omega_0, p)$  such that  $U_s(a(s, \omega_0), \omega_0) > U_s(x(s, \omega_0), \omega_0)$ . Define the  $\mathcal{F}$  measurable function  $y: T \times \Omega \rightarrow \mathbf{R}_+^l$  by  $y(t, \xi) = a(t, \omega_0)$  for  $\xi \in \Pi(\omega_0)$ , and  $y(t, \xi) = x(t, \xi)$  otherwise. It is immediate by Lemma that  $\mathbf{E}_s U_s(x(s, \cdot)) | \Delta(p) \cap P_s(\omega') < \mathbf{E}_s U_s(y(s, \cdot)) | \Delta(p) \cap P_s(\omega')$ , a contradiction. Hence it can be shown that  $(p(\omega), x(\cdot, \omega)) \in \mathcal{W}(\mathcal{E}^A(\omega))$  for a.a.  $\omega \in \Omega$ . Let the price system  $p^*: \Omega \rightarrow \mathbf{R}_+^l$  by  $p^*(\xi) = p(\omega)$  for a.a.  $\xi \in \Pi(\omega)$  and  $\omega \in \Omega$ , and  $p^*(\xi) = p(\omega)$  for  $\omega \notin \Omega$ . We shall show that  $(p^*, x) \in EA(\mathcal{E}^A)$ .  $x(t, \cdot)$  is  $\mathcal{F}$  measurable and  $x(t, \omega) \in B_t(\omega, p^*)$  for a.a.  $t \in T$  and for each  $\omega \in \Omega$ . It can be observed that **EA1**, **EA2** and **EA4** are all satisfied. For **EA3** let  $y(t, \cdot): \Omega \rightarrow \mathbf{R}_+^l$  be a  $\mathcal{F}$  measurable function with  $y(t, \omega) \in B_t(\omega, p^*)$  for a.a.  $\omega \in \Omega$ . Since  $(p^*(\omega), x(\cdot, \omega)) \in \mathcal{W}(\mathcal{E}^A(\omega))$  it follows that  $U_t(x(t, \omega), \omega) \geq U_t(y(t, \omega), \omega)$  for a.a.  $t \in T$  and for each  $\omega \in \Omega$ . Lemma  $\mathbf{E}_t U_t(x(t, \cdot)) | \Delta(p^*) \cap P_t(\omega) \geq \mathbf{E}_t U_t(y(t, \cdot)) | \Delta(p^*) \cap P_t(\omega)$  for a.a.  $\omega \in \Omega$  and thus  $(p^*, x) \in EA(\mathcal{E}^A)$ .  $\square$

**Proof of Proposition 1.** It follows from the present proposition that  $(p(\omega), x(\cdot, \omega)) \in \mathcal{W}(\mathcal{E}^A(\omega))$  at each  $\omega \in \Omega$ . The fundamental theorem of welfare economics in  $\mathcal{E}^A(\omega)$ , we can observe that for a.a.  $\omega \in \Omega$ ,  $x(\cdot, \omega)$  is a Pareto optimal allocation in  $\mathcal{E}^A(\omega)$ , and thus  $x$  is a Pareto optimal allocation.  $\square$

**Proof of Proposition 2.** It can be shown that for each  $\omega \in \Omega$  there exists  $p^*(\omega) \in \mathbf{R}_+^l$  such that  $(p^*(\omega), x(\cdot, \omega)) \in \mathcal{W}(\mathcal{E}^A(\omega))$  for some initial endowment  $e'(\cdot, \omega)$  with  $\sum_{t \in T} e'(t, \omega) = \sum_{t \in T} e(t, \omega)$ . *Proof:* First it can be observed that for each  $\omega \in \Omega$  there exists  $p^*(\omega) \in \mathbf{R}_+^l$  such that  $p^*(\omega) \cdot v \leq$  for a.a.  $v \in G(\omega) = \{ \sum_{t \in T} x(t, \omega) - \sum_{t \in T} y(t, \omega) \in \mathbf{R}^l \mid y \in Ass(\mathcal{E}^A) \text{ and } U_t(y(t, \omega), \omega) \geq U_t(x(t, \omega), \omega) \text{ for a.a. } t \in T \}$  for each  $\omega \in \Omega$ . In fact, it is to be noted that  $G(\omega)$  is convex and closed in  $\mathbf{R}_+^l$  by the conditions **A-1**, **A-2**, **A-3** and **A-4**, the assertion immediately follows from the fact that  $v \leq$  for a.a.  $v \in G(\omega)$  by the separation theorem. Suppose to the contrary that  $\omega_0 \in \Omega$  and  $v_0 \in G(\omega_0)$  with  $v_0 >$  take  $y^0 \in Ass(\mathcal{E}^A)$  such that for a.a.  $t$ ,  $U_t(y^0(t, \omega_0), \omega_0) \geq U_t(x(t, \omega_0), \omega_0)$  and  $v_0 = \sum_{t \in T} x(t, \omega_0) - \sum_{t \in T} y^0(t, \omega_0)$ . Let  $z \in Alc(\mathcal{E}^A)$  be defined by  $z(t, \xi) = y^0(t, \omega_0) + \frac{v_0}{|T|}$  for  $\xi \in \Pi(\omega_0)$ ,  $z(t, \xi) = x(t, \xi)$  for  $t \in T$ . **A-4**

<sup>7</sup> Cf.: Lemma 8, Chapter 4 in K. J. Arrow and F. H. Hahn, *General competitive analysis*, North-Holland Publishing Company, Amsterdam, 1971. p.92.

It follows that for a.  $t \in T$ ,  $\mathbf{E}_t U_t(\mathbf{z}) \geq \mathbf{E}_t U_t(\mathbf{x})$ , i.e. trad ct. t. h ch  
 x s e a t e a r e t. p t m a a s m a r a r g u m e n t t h e p r. f f t h e s e c. d  
 f u d a m e n t a t h e r e m. f e f a r e e c. m c s,<sup>8</sup> e c a. e r f t h a t  $(p^*(\omega), \mathbf{x}(\cdot, \omega)) \in$   
 $\mathcal{W}(\mathcal{E}^A(\omega))$  f r s m e. t a e d m e t e' t h  $\sum_{t \in T} \mathbf{e}'(t, \omega) \in \sum_{t \in T} \mathbf{e}(t, \omega)$   
 e t  $p$  b e t h e p r c e s s e m d e f i n e d b y  $p(\xi) = p^*(\omega)$  f r a.  $\xi \in \Pi(\omega)$  a d  
 $\omega \in \mathcal{M}(\mathcal{E}^A)$ ,  $p(\xi) = p^*(\omega)$  f r  $\omega \notin \mathcal{M}(\mathcal{E}^A)$ . u r t h e r e e t e d e' t t h e t a  
 e d m e t w f r  $\mathcal{E}^A$  b  $\mathbf{w}(t, \xi) = \mathbf{e}'(t, \omega)$  f r a.  $\xi \in \Pi(\omega)$  a d  $\omega \in \mathcal{M}(\mathcal{E}^A)$ . t  
 c a. b e b s e r v e d t h a t  $\mathbf{w}(t, \cdot)$  s  $\mathcal{F}$  m e a s u r a b l e t h  $\sum_{t \in T} \mathbf{w}(t, \omega) \in \sum_{t \in T} \mathbf{e}'(t, \omega)$ .  
 c o. c l u d e t h e p r. f e s h a. s h t h a t  $(p, \mathbf{x}) \in EA(\mathcal{E}^A)$ . *Proof:* f r e a c h  
 $\omega \in \mathcal{M}(\mathcal{E}^A)$ , t h e r e e s t s  $\xi$  s u c h t h a t  $\xi \in (\Delta(p) \cap P_t)(\omega) \cap \Delta(p)(\xi) \cap \Pi(\xi)$ ,  
 a d s e e c a. b s e r v e b **A-3** t h a t f r e a c h  $\mathbf{x} \in Alc(\mathcal{E}^A)$ ,  $\mathbf{E}_t U_t(\mathbf{x}(t, \cdot)) | (\Delta(p) \cap$   
 $P_t)(\omega) = U_t(\mathbf{x}(t, \xi), \xi)$ . e s h a. e r f **EA3** u p p s e t t h e c. t r a r  
 t h a t t h e r e e s t s  $s \in T$  t h t h e t. p r. p e r t e s ( ) t h e r e s a.  $\mathcal{F}$  m e a s u r a b l e  
 f u c t.  $\mathbf{y}(s, \cdot) : \Omega \rightarrow \mathbf{R}_+^l$  s u c h t h a t  $\mathbf{y}(s, \omega) \in B_s(\omega, p)$  f r a.  $\omega \in \Omega$  a d  
 ( )  $\mathbf{E}_s U_s(\mathbf{y}(s, \cdot)) | (\Delta(p) \cap P_s)(\omega_0) > \mathbf{E}_s U_s(\mathbf{x}(s, \cdot)) | (\Delta(p) \cap P_s)(\omega_0)$  f r s m e  
 $\omega_0 \in \mathcal{M}(\Delta(p) \cap P_s)$ . e f t h e a b. e e q u a t. t f. s f r m ( ) t h a t  
 t h e r e e s t s  $\xi \in (\Delta(p) \cap P_t)(\omega_0)$  t h  $U_s(\mathbf{y}(s, \xi), \xi) > U_s(\mathbf{x}(s, \xi), \xi)$ , a d t h u s  
 $\mathbf{y}(s, \xi) > \mathbf{x}(s, \xi)$  b **A-4** t h u s  $p(\xi) \cdot \mathbf{y}(s, \xi) > p(\xi) \cdot \mathbf{x}(s, \xi)$ . c. t r a d c t.  $\square$

### 4 Concluding Remarks

Our rea. c. c e r. t h s a r t c l e s a b u t r e a t. s h p b e t w e e p a e r s' b e f s  
 a d t h e r d e c s. m a k. g. e s p e c a. t h e a d h t h e p a e r s t a k e c r p. r a t e  
 a c t. s u d e r t h e r d e c s. s e f c u s. e t e d. g t h e f u d a m e n t a t h e r e m.  
 f e f a r e e c. m c s. t a e c. m t h t r a d e r s h a. g a a r e e s s a d b e e f'  
 m d e. e h a e s h. t h a t t h e n a t u r e f t h e t h e r e m. s d e p e n d e n t t.  
 c m m. b e e f. r. t h e p a r t t. s t r u c t u r e f t r a d e r s' f r m a t. b u t. t h e  
 s t r u c t u r e f a a r e e s s a d b e e f. h e e a c h p a e r r e c e. s f r m a t.

### References

1. Aumann, R. J.: Markets with a continuum of traders. *Econometrica* 32 (1964) 39–50
2. Bacharach, M. O.: Some extensions of a claim of Aumann in an axiomatic model of knowledge. *Journal of Economic Theory* 37 (1985) 167–190.
3. Dekel, E., Lipman, B.L., Rustichini, A.: Standard state-space models preclude unawareness. *Econometrica* 66 (1998) 159–173
4. Einy, E., Moreno, D., and Shitovitz, B.: Rational expectations equilibria and the ex-post core of an economy with asymmetric information. *Journal of Mathematical Economics* 34 (2000) 527–535
5. Geanakoplos, J.: Game theory without partitions, and applications to speculation and consensus, Cowles Foundation Discussion Paper No.914 (1989)
6. Matsuhisa, T.: Core equivalence in economy under awareness. In the Proceedings of Game Theory and Mathematical Economics, Warsaw, GTME 2004 (To appear).

<sup>8</sup> C.f.: Proposition 16.D.1 in A. Mas-Colell, M. Whinston, and J. Green, *Microeconomics Theory*. Oxford University Press, 1995, pp. 552–554.



# On-line Multi-attributes Procurement Combinatorial Auctions Bidding Strategies

Jian Chen and He Huang

School of Economics and Management, Tsinghua University, Beijing, 100084, China  
jchen@mail.tsinghua.edu.cn  
huangh02@mails.tsinghua.edu.cn

**Abstract.** Based on the work of Krishna and Rosenthal (1996) about combinatorial auctions bidding equilibrium analysis and Che's (1993) research about one-unit multi-attributes auctions, we construct a multi-attributes procurement combinatorial auction (MAPCA) for 2 objects, through a first-score, sealed-bid format. There are two kinds of bidders:  $n$  simple bidders and  $m$  diverse bidders considered in this model. With some assumptions, we finally obtain the equilibrium bidding strategies for the both two kinds of bidders.

## 1 Introduction

Combinatorial auctions have been applied in a variety of environments involving economic transactions, and they have the potential to play an important role in electronic procurement transactions for supply chain management. Examples are Net Exchange ([www.nex.com](http://www.nex.com)) who procures transportation services for Sears Logistics (Ledyard et al. 2002), procurement combinatorial auctions for truck services at Home Depot (Elmaghraby and Keskinocak 2003), and IBM's procurement combinatorial auction for Mars Incorporated (Hohner et al. 2003). The characteristics of combinatorial auctions that we will treat in the procurement context are items involving multiple attributes. Comparing with normal combinatorial auctions, the property of multiple attributes is somewhat unique in procurement auctions. When an auctioneer procures items by auctions, she may allow the potential suppliers to bid for various products bundles, which is called Procurement Combinatorial Auctions (CAs).

The topics on one-unit auctions' bidding strategies and winning probability are abundantly addressed. However, discussions about CAs' bidding strategies are inadequate. Krishna and Rosenthal (1996) considered situations where multiple objects are auctioned simultaneously by means of a second-price sealed-bid auction, and derived the bidding equilibrium strategies for the synergy bidder. Rosenthal and Wang (1996) studied a simultaneous-auction model with synergies, common values, and constructed strategies. Che (1993) studies design competition in one item procurement by developing a model of two-dimensional (price and quality) auctions. The purpose of this paper is to discuss bidding strategies in a specific multi-attributes procurement CA setting.

## 2 The Model

In this model, there are 2 identical objects to be procured by a first-score sealed-bid auction. And two kinds of bidders, i.e. simple bidder and diverse bidder are considered. Each simple bidder is interested in only one object, while each diverse bidder, say diverse bidder  $j$ , is interested in these two objects with synergy effect. For each object, there are  $n$  interested simple bidders. We can also regard the situation as two identical auctions started in two separated rooms; each room has  $n$  simple bidders, and diverse bidders are apt to bid in both rooms. Each bidder has a privately known supply cost function for the object. Other assumptions are as follows.

Bidding vector is  $\{p, q\} \in R_+^2$ ,  $p, q$  denote bidding price and quality-bid separately. Especially, quality-bid, in our model, is a unified number to measure all non-price factors of the objects. The scoring function of the bidding vectors has a quasi-linear form

$$S(q, p) = s(q) - p \tag{1}$$

where  $s(\cdot)$  is strictly increasing with respect to  $q$ .

Number of simple bidders, for each object, is  $n$ ; number of diverse bidders is  $m$ .

The cost function of simple bidder  $i$  is  $c(q, \theta_i)$ .  $\theta_i$  denotes type of simple bidder  $i$ , which is private information of bidder  $i$ , and  $\theta_i$  is drawn from interval  $[\underline{\theta}, \bar{\theta}]$  with identical distribution  $F(\cdot)$ , which is common knowledge.  $c(\cdot, \cdot)$  is increasing with respect to  $q$  and  $\theta_i$ . Type of diverse bidder  $j$  is denoted as  $\theta_j$  which is drawn from interval  $[\underline{\theta}_g, \bar{\theta}_g]$  with the identical distribution  $F_g(\cdot)$ ;  $\theta_j$  is also private information. The cost function of the diverse bidder is  $c_g(q, \theta_j)$  for each object.  $[\underline{\theta}_g, \bar{\theta}_g]$  and  $F_g(\cdot)$  are common knowledge;  $c_g(\cdot, \cdot)$  is increasing with respect to  $q$  and  $\theta_j$ .

If winning, profit of simple bidder  $i$ , with bid  $\{p, q\} \in R_+^2$ , is

$$\pi_i(q, p) = p - c(q, \theta_i) \tag{2}$$

Profit of the diverse bidder  $j$ , with bid  $\{p, q\} \in R_+^2$ , is

$$\begin{cases} p - c_g(q, \theta_j), & \text{if win one} \\ 2p - 2c_g(q, \theta_j) + \alpha_j, & \text{if win both} \end{cases} \tag{3}$$

where  $\alpha_j$ , i.e., synergy effect, is a non-negative constant which is diverse bidder  $j$ 's private information.

With type  $\theta_i$ , simple bidder  $i$ 's bidding strategy is formula (4): [Riley and Samuelson, 1981; Che, 1993; Chen and Huang 2004]

$$\begin{cases} q(\theta_i) = \arg \max [s(q) - c(q, \theta_i)], \\ p(\theta_i) = c(q, \theta_i) + \int_{\theta_i}^{\bar{\theta}} c(q(t), t) \left[ \frac{1 - F(t)}{1 - F(\theta_i)} \right]^n dt \end{cases} \quad (4)$$

Diverse bidders know each other’s profit function form, but do not know other diverse bidders’ synergy effect value, say  $\alpha_j$ , which are drawn from  $[0, \bar{\alpha}]$ , and their identical distribution  $F_\alpha(\cdot)$  is common knowledge. The model constructed above is called MAPCA in this paper.

### 3 Bidding Strategy Analysis

For simple bidders, Let  $S_0(\theta_i) \equiv \max [s(q) - c(q, \theta_i)], \forall \theta_i \in [\underline{\theta}, \bar{\theta}]$ . By using envelope theorem,  $S_0(\cdot)$  is a strictly decreasing function, therefore its inverse function exists. Let  $v_i \equiv S_0(\theta_i)$ ,  $v_i$  can be regarded as scoring capability of simple bidder  $i$ . Let  $H(v_i) \equiv 1 - F(S_0^{-1}(v_i))$ , then distribution  $F(\cdot)$  of  $\theta_i$  is transformed into distribution  $H(\cdot)$  of  $v_i$ . Let  $b \equiv S(q_s(\theta_i), p)$ , where  $q_s(\theta_i) = \arg \max [s(q) - c(q, \theta_i)]$ . Obviously,  $b$  is the score evaluated by the bidding of simple bidder with type  $\theta_i$ . Let  $B(\cdot)$  denote the scoring function with the independent variable  $v_i$ , and  $B(\cdot)$  is strictly increasing with  $v_i$ . Define  $G(\cdot) \equiv H(B^{-1}(\cdot))$  and  $L(b) = \{H(B^{-1}(b))\}^n$  for convenience. Intuitively,  $L(b)$  is the probability of all  $n$  simple bidders who are interested in one of the two items get score less than  $b$ .

Similarly, for diverse bidders, let  $S_g(\theta_j) \equiv \max [s(q) - c_g(q, \theta_j)], \forall \theta_j \in [\underline{\theta}_g, \bar{\theta}_g]$ . By envelope theorem,  $S_g(\cdot)$  is a strictly decreasing function, therefore its inverse function exists. Let  $v \equiv S_g(\theta_j)$ ,  $v$  is scoring capability of diverse bidder  $j$ . Let  $H_g(v) \equiv 1 - F_g(S_g^{-1}(v))$ , then distribution  $F_g(\cdot)$  of  $\theta_j$  is transformed into distribution  $H_g(\cdot)$  of  $v$ , which also implies that the one-to-one mapping relationship from  $v$  to  $\theta$ . Let  $b \equiv S(q_s(\theta_j), p)$ , where  $q_s(\theta_j) = \arg \max [s(q) - c_g(q, \theta_j)]$ , and  $b$  is the score of the bidding by diverse bidder with type parameter  $\theta_j$ . Let  $B_g(v)$  denote the scoring function with  $v$ , and  $B_g(\cdot)$  is strictly increasing with  $v$ . Define  $G_g(\cdot) \equiv H_g(B_g^{-1}(\cdot))$  and  $K(b) \equiv \{H_g(B_g^{-1}(b))\}^{m-1}$ . Actually,  $K(b)$  is the probability of all other  $m-1$  diverse bidders get score less than  $b$ . Note that  $p - c(q_s(\theta_j), \theta_j) = v - b$ , and then we have the expected revenue of any diverse bidder with type  $\theta_j$  who bids quality-bid  $q_s$  and price  $p$  as follows,

$$\begin{aligned} & \pi((q_s, p)|\theta_j) \\ &= L^2(s(q_s) - p) \times K(s(q_s) - p) \times (2(p - c) + \alpha_j) \\ & \quad + 2L(s(q_s) - p) \times (1 - L(s(q_s) - p)) \times K(s(q_s) - p) \times (p - c) \end{aligned} \quad (5)$$

where,  $q_s$  represents quality bidding,  $p$  is price bidding,  $c$  denotes the corresponding cost with quality bidding  $q_s$ . Now, we would show an important proposition (lemma 1) to illustrate any diverse bidder with any specific type, say  $\theta_j$ , will report quality-bid to maximize  $s(q) - c_g(q, \theta_j)$ .

LEMMA 1. The diverse bidder with type  $\theta_j$  follows the bidding strategy in which quality-bid  $q_s(\theta_j)$  is

$$q_s(\theta_j) = \arg \max [s(q) - c_g(q, \theta_j)] \quad (6)$$

Proof: Assume there exists another equilibrium strategy  $(q, p)$ , and  $q \neq q_s(\theta_j)$ , then construct a bid  $(q', p')$ ,

$$\text{where } q' = q_s(\theta_j), \quad p' = p + s(q_s(\theta_j)) - s(q) \quad (7)$$

$$\text{Note } S(q', p') = S(q, p) = S \quad (8)$$

Then, with bid  $(q', p')$ , the expected revenue of diverse bidder is below,

$$\begin{aligned} & \pi((q', p')|\theta_j) \\ &= L^2(S)K(S)[2(p + s(q_s(\theta_j)) - s(q) - c_g(q')) + \alpha_j] \\ & \quad + 2L(S)(1 - L(S))K(S)(p + s(q_s(\theta_j)) - s(q) - c_g(q')) \quad (9) \\ &= L^2(S)K(S)\{2 \times [(p - c_g(q) + (s(q_s(\theta_j)) - c_g(q_s(\theta_j))) - (s(q) - c_g(q)))] + \alpha_j\} \\ & \quad + 2L(S)(1 - L(S))K(S)[(p - c_g(q) + (s(q_s) - c_g(q_s(\theta_j))) - (s(q_1) - c_g(q)))] \end{aligned}$$

Note  $q_s(\theta_j) = \arg \max [s(q) - c_g(q, \theta_j)]$ , therefore,

$$\pi((q', p')|\theta_j) \geq L(S)K(S) \cdot \{L(S)[2(p - c_g(q)) + \alpha_j] + 2(1 - L(S)) \cdot (p - c_g(q))\} \quad (10)$$

Thus, we have

$$\pi((q', p')|\theta_j) \geq \pi((q, p)|\theta_j) \quad (11)$$

This completes the proof. □

Without loss of generality, let  $s(q_s(\theta_j)) = 1$ ; from LEMMA 1 and (5), we know the optimization problem of the diverse bidder with type  $\theta_j$  can be expressed as follows:

$$\begin{aligned} & \max_p \pi(q_s, p) | \theta_j \\ & = \max_p \{L(1-p) \cdot K(1-p) \cdot [(L(1-p) \cdot (2(p-c) + \alpha_j) + 2(1-L(1-p)) \cdot (p-c))]\} . \quad (12) \\ & = \max_p \{\alpha_j L^2(1-p)K(1-p) + 2L(1-p)K(1-p)(p-c)\} \end{aligned}$$

where  $c$  denotes the corresponding cost of the diverse bidder with her equilibrium quality-bid  $q_s(\theta_j)$ ;  $c$  is also the optimal cost of the bidder. Actually,  $q_s(\theta_j)$  and  $c$  are determined by type  $\theta_j$  uniquely. Let  $l(\cdot) = L'(\cdot), k(\cdot) = K'(\cdot)$ , by first derivative of (12) with respect to  $p$ , we have

$$\begin{aligned} \frac{d\pi}{dp} & = c - p - L(1-p) \cdot \frac{\alpha_j \cdot l(1-p) \cdot K(1-p) + \alpha_j \cdot L(1-p) \cdot k(1-p) / 2 - K(1-p)}{l(1-p) \cdot K(1-p) + L(1-p) \cdot k(1-p)} . \quad (13) \\ & = 0 \end{aligned}$$

Now considering the relationship between the optimal cost  $c$  of diverse bidder with  $\theta_j$  and her price bid  $p$ , from (13) we have

$$c = p + L(1-p) \cdot \frac{\alpha_j \cdot l(1-p) \cdot K(1-p) + \alpha_j \cdot L(1-p) \cdot k(1-p) / 2 - K(1-p)}{l(1-p) \cdot K(1-p) + L(1-p) \cdot k(1-p)} . \quad (14)$$

Actually, (14) is the correspondence from optimal cost  $c$  to possible optimal price bid  $p$ , and we can abstractly express (14) as  $c = c_p(p)$ . The only special feature used in the argument is that  $c_p(\cdot)$  is convex. Convexity of  $c_p(\cdot)$  is not easy to characterize in terms of the primitive assumptions of our model. However, if  $G_g(\cdot)$  and  $G(\cdot)$  are uniform distribution, then the function  $c_p(\cdot)$  is indeed convex. If  $c_p(\cdot)$  is not convex, the situation becomes more complicated and worth pursuing in the future correlated works. Therefore, if  $c_p(\cdot)$  is convex, then there exit at most 2 roots of equation (14).

Corresponding to different optimal cost  $c$ , denote  $p_g(c)$  as the solutions of (14). Define  $p_g^*(c)$  as the unique root or greater one of the two roots, i.e.,

$$p_g^*(c) = \begin{cases} p_g(c), & \text{for unique solution} \\ \max\{p_g(c)\}, & \text{for other case} \end{cases} . \quad (15)$$

By convexity of  $c_p(\cdot)$ , the derivative of  $d\pi/dp$  is non-positive at the point of the greater root. That means the second derivative of expected revenue with respect to  $p$ , at the greater root, is non-positive. It is the second-order sufficient condition for local maximizer. Consequently, we are sure that  $p_g^*(c)$  is the local maximizer, while the smaller root is not.

More specific, let  $\bar{\alpha} = 2$ , that means  $\alpha_j \in [0, 2]$ . And consider the excessive case in which the diverse bidder  $j$ 's cost is 0 and  $\alpha_j = 2$ , for individual rationality, the price bidding of her will not less than -1. Therefore we assume the domain of  $p$  is  $[-1, 1]$ . Assume  $G_g(\cdot)$  and  $G(\cdot)$  are all uniform distributions, then  $G_g(\cdot) = (1-p)/2$ ,  $G(\cdot) = (1-p)$ . Correspondingly, we have

$$K(1-p) = ((1-p)/2)^{m-1}, p \in [-1, 1], L(1-p) = (1-p)^n, p \in [0, 1],$$

$$k(1-p) = [(1-m)/2] \cdot [(1-p)/2]^{m-2}, l(1-p) = -n \cdot (1-p)^{n-1}.$$

Note that, when  $p \in [-1, 0]$ , the diverse bidder will definitely surmounts all simple bidders with probability 1. Then (12) can be rewritten as

$$\max_p \pi((q_s, p) | \theta_j) = \max_p [\alpha_j \cdot K(1-p) + 2 \cdot K(1-p) \cdot (p-c)] . \tag{16}$$

Therefore, formula (14) can be expressed as follows

$$c = \begin{cases} p + \frac{(n\alpha_j + \alpha_j \cdot (m-1)/2) \cdot (1-p)^n + (p-1)}{n+m-1}, & 0 < p \leq 1 \\ p + \frac{p + \alpha_j \cdot (m-1)/2 - 1}{m-1}, & \frac{-\alpha_j}{2} < p \leq 0 \end{cases} . \tag{17}$$

The convexity of (17) is obvious. Define  $p_g^-(c)$  as the solution (price bidding) of (17) in the domain  $p \in [-1, 0]$ .

Since the domain of expected revenue (16) is a closed set, in order to find the global maximizer, what we should do is to compare the boundary solutions with interior solution. Next, define  $c^*$  as follows,

$$c^* = \max \{c : \pi(0|c) - \pi(p_g^*(c)|c) \geq 0\} . \tag{18}$$

Because

$$\frac{d\{\pi(0|c) - \pi(p_g^*(c)|c)\}}{dc} = -2K(1) + 2L(1-p_g^*(c)) \cdot K(1-p_g^*(c)) < 0 . \tag{19}$$

It follows that if there exists  $c^*$ , such that

$$\pi(0|c^*) - \pi(p_g^*(c^*)|c^*) = 0 . \tag{20}$$

then for all  $c: 0 < c < c^*$ , we have

$$\pi(0|c) > \pi(p_g^*(c)|c) . \tag{21}$$

Define another special cost point  $c^-$  as follows

$$c^- = \max \{c : \pi(p_g^-(c)|c) - \pi(0|c) \geq 0\} . \tag{22}$$

Because

$$\frac{d\{\pi(p_g^-(c)|c) - \pi(0|c)\}}{dc} = -2K(1 - p_g^-(c)) + 2K(1) < 0 . \tag{23}$$

It follows that if there exists  $c^-$ , such that

$$\pi(0|c^-) - \pi(p_g^-(c^-)|c^-) = 0 . \tag{24}$$

Then for all  $c: 0 < c < c^-$ , we have

$$\pi(0|c) < \pi(p_g^-(c)|c) . \tag{25}$$

Basically, in order to compare boundary solutions with interior solutions, we defined  $c^*$  and  $c^-$  respectively. In other words,  $c^*$  is the separating cost point below which zero price bidding is better than positive interior solution, while  $c^-$  is the separating cost point below which negative price bidding is better than zero price bidding. The following result is immediate.

Theorem 1. The following constitutes an equilibrium of MAPCA.

- a) The simple bidder with type  $\theta_i$  follows the strategy as (4);
- b) The diverse bidder with type  $\theta_j$  follows the strategies:

$$\begin{cases} q_s(\theta_j) = \arg \max [s(q) - c_g(q, \theta_j)] \\ p(\theta_j) = \begin{cases} p_g^*(c_g(q_s(\theta_j))) & \text{if } c^* < c_g(q_s(\theta_j), \theta_j) \\ 0 & \text{if } c^- < c_g(q_s(\theta_j), \theta_j) \leq c^* \\ p_g^-(c_g(q_s(\theta_j))) & \text{if } 0 < c_g(q_s(\theta_j), \theta_j) < c^- \end{cases} \end{cases} . \tag{26}$$

Intuitively, theorem 1 illustrates that one bidder either with synergy effect or not will submit same flavor quality-bid, i.e., optimal quality to maximize the difference of quality score minus the corresponding cost. As to price bidding, two kinds of bidders are apt to bid lower price when they have lower optimal cost. However, there exists two special cost “jump” points to make diverse bidders bid relative lower price: zero price or negative price. It is not so strange if we consider the situation in which synergy effect is very strong for any specific diverse bidder. The synergy effect can be regarded as business reputation, advertisement considerations and market share competition, which depends on different business surroundings.

### 4 Conclusions

In this paper, we construct a multi-attributes procurement combinatorial auction (MAPCA) for 2 identical objects, through a first-score, sealed-bid, simultaneous format. There are two kinds of bidders, simple bidder and diverse bidder, are considered in our model. With some assumptions, we obtain the equilibrium bidding strategies

for the two kinds of bidders. Basically, the difference between our work and past correlated research (Krishna and Rosenthal (1996)) are: multi-attributes vs. single attribute, first-score vs. second-price, and procurement auction vs. selling auction. Also, this piece of research can not be realized without Che's work (Che 1993) about one-unit multi-attributes procurement auction. Compared with previous work about multi-attributes procurement combinatorial auctions' bidding analysis (Chen and Huang (2004)), this model extends to multiple diverse bidders who have synergy effect in the auction. Future work includes extensions to heterogeneous items assumption of our model.

## Acknowledgements

This paper was partly supported by National Science Foundation of China under grant 70231010 and 70321001.

## References

1. Che, Y. K.: Design competition through multidimensional auctions. *The Rand Journal of Economics*. Vol.24 (1993) 668–681
2. Chen J., H. Huang: Bidding Strategies Analysis for Procurement Combinatorial Auctions. *Proceedings of The Fourth International Conference on Electronic Business*. (2004) 41–45
3. Elmaghraby, W., P. Keskinocak: Technology for transportation bidding at the Home Depot. C. Billington, T. Harrison, H. Lee, J. Neale, eds. *The Practice of Supply Chain Management: Where Theory and Applications Converge*. Kluwer. (2003)
4. Hohner, G., J. Rich, E. Ng, G. Reid, A. J. Davenport, J. R. Kalagnanam, H. S. Lee, C.: An Combinatorial and quality-discount procurement auctions with mutual benefits at Mars Incorporated. *Interface*. 33(1), (2003) 23–35
5. Krishna, V., Rosenthal, R.W.: Simultaneous Auctions with Synergies. *Games and Economic Behavior*, Vol. 17, (1996) 1–31
6. Ledyard, J. O., M. Olson, D. Porter, J. A. Swanson, D. P. Torma: The first use of a combined value auction for transportation services. *Interfaces*, 32(5), (2002) 4–12
7. Parkes, D.: Iterative Combinatorial Auctions: Achieving Economic and Computational Efficiency. Doctoral thesis, University of Pennsylvania (2001)
8. Rosenthal, R.W., Wang, R. Q.: Simultaneous Auctions with Synergies and Common Values. *Games and Economic Behavior*, Vol.17 (1996) 32–55



# An Algebraic Method for Analyzing Open-Loop Dynamic Systems

h u, \_e r e , a d G R e d

Department of Applied Mathematics, The University of Western Ontario,  
London, Ontario, Canada N6A 5B7

**Abstract.** This paper reports on the results of combining the MAPLE packages DYNAFLEX and RIFSIMP. The DYNAFLEX package has been developed to generate the governing dynamical equations for mechanical systems; the RIFSIMP package has been developed for the symbolic analysis of differential equations. We show that the output equations from DYNAFLEX can be converted into a form which can be analyzed by RIFSIMP. Of particular interest is the ability of RIFSIMP to split a set of differential equations into different cases; each case corresponds to a different set of assumptions, and under some sets of assumptions there are significant simplifications. In order to allow RIFSIMP to conduct its analysis, the governing equations must be converted from trigonometric form into a polynomial form. After this is done, RIFSIMP can analyze the system and present its results either graphically, or in list form. The mechanical systems considered are restricted to open-loop systems, because at present, closed-loop systems require too much computation by RIFSIMP to permit analysis.

**Keywords:** DYNAFLEX, RIFSIMP, Case Splitting, Symbolic Simplification, Graph Theory, Computer Algebra.

## 1 Introduction

pr c pa g a . f mu t b . d . d . am cs s the aut . mat c ge . erat . . . f the equa  
t . . s . f m . t . . f r c . mp . e mecha . ca s stems . . . umer ca . . based pr . grams  
e . st , f r e . amp . e ADAMS , JAMES a . d WORKING MODEL , that ca . ge . erate the  
g . er . g equat . . s 2 . the . are c . mmerc a . pr . grams a . d are . . . despread  
use . . the aut . m . t . e , aer . space a . d r . b . t cs . . dustr es . . . e . er , be . g  
. umer ca . . based pr . grams the . ha . e se . era . dra . backs

- t . s d . fficu t . t . check the equat . . s . f m . t . . , because the . are repre . sed  
b . arge . . umer . f . umer ca . data
- O . e ca . . t de . e . p a . . ph s ca . . s ght
- C . sed f r m s . ut . . s f r the . umer ca . equat . . s are . . t p . ss b . e
- he . used f r s mu at . . s , the . are . . effi c . e . t because the equat . . s are  
\_e . ect . e . re assem . bed at each t me step , a . d th s ma . . c . ude ma . . mu  
t p . cat . . s b . . a . d

After, at the approach to equation generation, uses symbolic processing DYNAPLEX (<http://real.uwaterloo.ca/~dynaflex/>) as a software package that generates the equations of motion for a mechanical system from a computer description based on a graph theoretic method. The equations are automatically generated, and the users see several advantages:

- The structure of the equations is easily obtained and manipulated, giving the user a physical insight into the system
- The equations can be easily changed through groups of engineers or design groups
- Real time simulations are facilitated

The symbolic models generated by DYNAPLEX are usually too complex to be solved symbolically, but there is still the possibility of symbolic preprocessing the output of DYNAPLEX before attempting a solution. The purpose of this paper is to apply the package RIFSIMP to this task. The RIFSIMP package analyzes ODEs and ESDs and returns canonical differential forms. The basic forms Reduced Output Form (ROF), and the package has the following features:

- Computation of the polynomial eigenvalues
- Reduced case splitting capabilities for the discerning of particular substructures through descriptors
- An algorithm for the elimination of the binary tree that results from multiple cases
- Algorithms for ranking the form parameter sets of the system

The RIFSIMP is applied to an equation system, it detects special cases during the reduction. The analysis of the system then splits according to the special cases. A full case analysis, some cases can be automatically handled. There are some enough to be a automatic analysis. The canonical forms generated by RIFSIMP is for (ROF) differential equations, which is suitable for the application of numerical solvers (whereas the output of DYNAPLEX may not have been suitable). Compared to the RIFSIMP is the possibility of including special cases that are known to be of interest. Thus if RIFSIMP detects a special case, say  $m$ , but it is known that this is of physical interest, then the case passes through RIFSIMP as an equation  $m /$  appended to the output system.

## 1.1 Open-Loop and Closed-Loop Systems

The problems addressed by DYNAPLEX can be separated into two classes. The first systems and closed systems. The term "graph" comes from the graph theoretic method which is the basis of DYNAPLEX. The element of the section is shown the basic graph theoretic method for the present case. It is that a physical system corresponds to a system such as a robot arm, which case, components, such as joints and arm segments, are considered together as a configuration that terminates at a free end. This is contrast to a frame work,

such as a flexible mechanism, in which the components connect back to the structure being considered

In the structure forms a closed loop, the DYNAFLEX will generate constraint equations that describe the drop in the degrees of freedom that accompany the closing of a loop. In the present case, of this paper, we have discovered that the RIFSIMP package takes a great deal of time and memory to analyze closed loop systems, but can make good progress in the present case. This is what is reported here

## 2 Example System Analysed Using Dynaflex

In order to keep the examples tractable, we shall use a simple spring-mass system as an example. The system is a simple rigid body that spins about its fixed symmetric axis. The process about a vertical axis  $(z)$  axis, a rotate about the vertical axis. The figure shows a rigid body, the  $-Z$  direction. The center of mass is located at  $C$ , and the spring is assumed to rotate through the spring. The rigid body is assumed to be a spherical cap (ball and socket) joint at  $O$ . The coordinates at  $O$  are represented by Euler angles  $(\zeta, \eta, \xi)$ . The form of the Euler angles, meaning that the corresponding process about  $z$  axis, and spin, respectively.

### 2.1 The System Graph

The system graph for the top is shown in figure 2. The graph consists of nodes and edges. The nodes correspond to the centers of coordinates, here the edges describe the system. In this figure, we see nodes labeled  $1, 2$ , which are connected by edges  $e_1, e_2, e_3, e_4$ .

The node  $(1)$  can be thought of as the datum, or ground, in which the system is resting. Nodes  $(2)$  and  $(3)$  denote the top. The geometric fact that the top is connected to the ground is described by the edge  $e_2$ , connected to node  $(2)$ . The fact that the top is free to spin, but not free to slide is described by  $e_2$  being specified as a spherical joint (i.e. a ball and socket). The fact

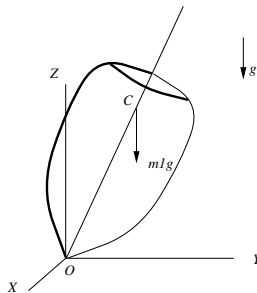


**Fig. 1.** The three-dimensional top. The centre of mass is at  $C$  and  $OC=l$ . The mass is here denoted  $m$ , giving a gravitational force equal to  $mg$  acting in the  $-Z$  direction

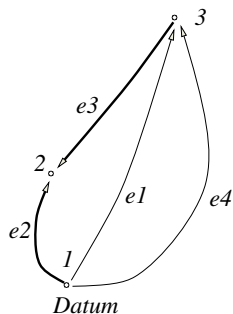


**Fig. 2.** The graph-theoretic method for the top

that the bodies are described by edge  $e$  being specified as a rigid body with a diameter  $d$ , a moment of inertia  $I$  about the center of mass  $s$  specified by  $e$ , which forms a rigid arm  $e$  of length  $l$ , a gravity  $g$  defined by  $e$ , being a force  $e$  of mass  $m$ .

It is important to note that the graph consists of  $\{e_2, e_3\}$  is defined by head nodes, whereas edges  $e_1$  and  $e_4$  are drawn as light lines. The edges  $\{e_2, e_3\}$  correspond to the perpendicular referred to above.

## 2.2 Maple Input File

The Maple input file corresponding to the above system is as follows:

```

N0ofedges:=4; N0ofnodes:=3; Datum:=1;
#Note that Datum stands for the ground node.

edge[1]:=table([(1)=N, (2)=[1,3], (3)=BE_R,
(4)=table([inert=[[x,0,0], [0,y,0], [0,0,z]], mass=c ])]);
edge[2]:=table([(1)=Y, (2)=[1,2], (3)=JE, (4)=SPH ]);
edge[3]:=table([(1)=Y, (2)=[3,2], (3)=AE_R,
(4)=table([coords=[0,0,c] ])]);
edge[4]:=table([(1)=N, (2)=[1,3], (3)=FDE,
(4)=table([type=PD, fz=-m1*g, force=gl ])]);
Iedge:=[];

```

## 2.3 The Symbolic Equations

The equations produced by DYNAPLEX from the above input file are presented below. By default, DYNAPLEX assigns the following quantities such as Euler angles, moments of inertia, etc. though DYNAPLEX calculates the equations of motion for a programmable results. Equations which are difficult and tedious to read are printed out for human use. Here, we have edited the raw DYNAPLEX output format to simplify the notation. The equations that human readers are used to see are the center of mass  $s$  and distance  $l$  from the point of contact, the mass  $m$ , the moment of inertia about the symmetric axis  $C$ , and about a perpendicular axis  $A$ . The Euler angles are given by  $e$ .

$$\begin{aligned}
 & C\zeta(t) c. s^2 \eta(t) + C\xi(t) c. s \eta(t) - A\zeta(t) c. s^2 \eta(t) - C\eta(t)\xi(t) s. \eta(t) \\
 & - 2C\eta(t)\zeta(t) s. \eta(t) c. s \eta(t) + 2A\eta(t)\zeta(t) s. \eta(t) c. s \eta(t) + A\zeta(t) \quad , \quad (1) \\
 & \quad -mg s. \eta(t) - A\zeta^2(t) s. \eta(t) c. s \eta(t) + A\eta(t) + C\xi(t)\zeta(t) s. \eta(t) \\
 & \quad \quad \quad + C\zeta^2(t) s. \eta(t) c. s \eta(t) \quad , \quad (2) \\
 & \quad \quad \quad -C(-\xi(t) - \zeta(t) c. s \eta(t) + \eta(t)\zeta(t) s. \eta(t)) \quad . \quad (3)
 \end{aligned}$$

### 3 Automatic Symbolic Simplification Using RifSimp

The package RIFSIMP can process systems of polynomial equations. Each equation is a linear combination of the variables  $u_1, u_2, \dots, u_n$ , which can be further separated into linear combinations of the present variables. The dependence of the variables  $u_i$  can be determined algebraically. RifSIMP takes as input a system of differential equations and a ranking of the variables. RifSIMP orders the dependence graph canonically and the derivatives per maximal derivative order.

$$u_1 \prec u_2 \prec \dots \prec u_n \prec u'_1 \prec u'_2 \prec \dots \prec u'_n \prec u''_1 \prec \dots \quad (4)$$

The equations are classified as being together leading or trailing (earliest or the highest derivative with respect to the ordering  $\prec$ ), leading or trailing (earliest or the highest derivative).

RIFSIMP proceeds by solving the leading equations for the highest derivatives until a certain order is reached. Such equations leading or trailing equations (the so-called constraints), are treated by methods such as Gaussian elimination. Gröbner bases and a reduction method determine the leading or trailing equations and then reduce them with respect to the leading or trailing equations. Further, it means the equations included in the degenerated by the leading or trailing equations. Finally, it means that these equations are algebraically consistent, the system has no repeated units, and the constraints are fulfilled.

**Theorem:** (Output RIFSIMP form)

If  $v$  is a set of derivatives and  $w$  is a set of derivatives (including dependence variables) then the output of RIFSIMP has the structure

$$v = f(t, w) \quad (5)$$

subject to algebraic constraint equations and equations

$$g(t, w) = 0, \quad h(t, w) / \quad (6)$$

*Proof.* See and references therein.

---

<sup>1</sup> Readers who are not familiar with the ideas of term ordering in polynomial systems can read this as meaning that the variables are placed in alphabetical order.

**Theorem:** (Estepcead... que... ess)

Given a... t... c... d...  $g(t^0, w^0)$ ,  $h(t^0, w^0) /$ , there s... ca... a... t... c... s... ut... th... t... s... t... a... c... d... t...

*Proof.* ee

### 4 Application of RifSimp to Example Problem

Order the app... RIFSIMP to the example above, we proceed as follows

Change coordinates using  $\eta = \frac{1-u(t)^2}{1+u(t)^2}$ ,  $s = \eta = \frac{2u(t)}{1+u(t)^2}$  to get a rational polynomial differential system instead of trigonometric differential system (RIFSIMP does not allow trigonometric functions)

2. Get this polynomial differential equation system to RIFSIMP, specifying the case split points to get normalized differential equations
- use RIFSIMP case tree to analyze the differential cases

the assumptions on the parameters, we obtain 24 cases, each split case responds to some qualitative behavior of the dependent variables, for each split, we actually have the qualitative

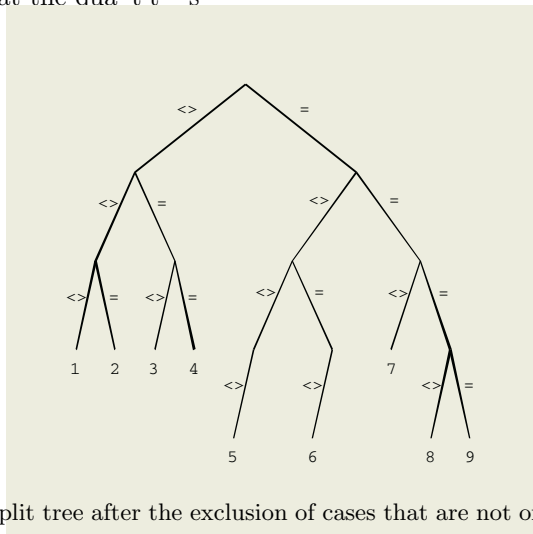


**Fig. 3.** The case-split tree after the exclusion of cases that are not of physical interest

The examination of the output case split shows that many of the cases can be removed... physical grounds... thus RIFSIMP identifies that there s... b... g... b... m... a... d... b... l... a... d... theref... re... ags... these... cases... as... p... ts... f... case... sp... tt... g... ce... ee... k... th... s... app... cat... th... these... cases... are... t... f... ph... s... ca... terest... we... ca... ee... c... u... de... them... aut... mat... ca... fr... m... the... case... a... a... s... s... b... c... u... d... g... a... s... t... f... equat... s... the... RIFSIMP... parameters... f... ter... c... u... d... g... g... /... m... /... a... d... l... /... RIFSIMP... retur... s... a... tree... c... t... a... g... cases... as... sh... figure

## 5 Some Special Cases

The importance of the RIFSIMP analysis is the definition of special cases. The general (geometric) case cannot be simplified further. However, analysis of a mechanical system should look for special cases, either to put these particular simple cases first and then the more complex that RIFSIMP can be used to find these cases automatically.

### 5.1 First Group of Special Cases

The group of cases together that differ from the RIFSIMP definition of the case as being  $A \neq 0$  and  $A = 0$ . However, the equation  $Cw(t) = gA$  is defined as zero because of the condition  $u = 0$ , and hence the value of  $A$  is irrelevant to the equation system.

$$v(t) = -w(t), \quad u(t) \tag{7}$$

These equations can be integrated to find

$$u(t) = \dots, \quad v(t) = v_1 t + v_0, \quad w(t) = -v_1 t + w_0 \tag{8}$$

where  $v_1, v_0, w_0$  are given by the initial conditions from the definition of  $\eta(t) = \arccos(( -u(t)^2)/( +u(t)^2))$ . Here  $\eta = \pi/2$  which means that the top is spinning vertically but not rotating with respect to axis.

### 5.2 Second Group of Special Cases

The RIFSIMP definition of  $A = 0$  and  $A \neq 0$  separate the common equations are

$$w(t) = \dots, \quad u(t) = \dots, \quad x(t) = \frac{gml}{Cw(t)} \tag{9}$$

and the constraint  $u(t)^2 - \dots$  has a constant value

$$u(t) = u_0, \quad v(t) = \frac{gmlt + v_0 w_1 C}{w_1 C}, \quad w(t) = w_1 t + w_0 \tag{10}$$

and the constraints  $u_0^2 - \dots$  and  $v_0, w_0, w_1$  are given by the initial conditions from the definition of  $\eta(t) = \arccos(( -u(t)^2)/( +u(t)^2))$ . Here  $\eta = \pi/2$  which means the top is spinning horizontally. The  $x - y$  plane is in the process of rotating.

## 6 Conclusion and Future Work

Because of space limitations, we have restricted the example problem being analysed further experiments. Other mechanical systems, such as double and tripe pendulums, were made but not included here. However, from the example case, the definition successes and limitations of RIFSIMP are first put

the success of RIFSIMP in detecting the special cases of the problem, the same people should realize, these might seem easy, but the multiplicity of tests that these were detected *automatically* rather than by human inspection.

One of the main tasks of the combination of RIFSIMP and DYNAFLEX is the fact that DYNAFLEX generates a plethora of parameters. Many parameters can cause a serious degradation of the performance of a computer algebra system, as evidenced by the large number of special cases that can prevent a human user from seeing the pattern of interest. The output has been reduced to the 24 special cases that are detected by RIFSIMP. Continuing the sequence of a large number of parameters being taken into further applications, this paper has concentrated on the problems, because RIFSIMP has been most successful in these cases. Continued problems generate further constraints that can cause RIFSIMP to exhaust computer resources before completing its analysis. One reason for this is the small number of matrices in the data. RIFSIMP from computer techniques for handling large expressions has been developed. Other constraints, see for example [7]. Combining these with RIFSIMP will increase the computer time of problems that can be solved.

## Acknowledgments

I am grateful to acknowledge the help of Chad Chmudt and Eugene H. Frith for the development of DYNAFLEX and for making the system available to us.

## References

1. Schiehlen, W. *Multibody Systems Handbook*; Springer-Verlag: Berlin, 1990.
2. P. Rideau. *Computer Algebra and Mechanics, The James Software*; Computer Algebra in Industry I, 1993 John Wiley & Sons Ltd.
3. Pengfei Shi, John McPhee. *Symbolic Programming of a Graph-Theoretic Approach to Flexible Multibody Dynamics*; Mechanics of Structures and Machines, 30(1), 123-154(2002).
4. P. Shi, J. McPhee. *Dynamics of flexible multibody systems using virtual work and linear graph theory*; Multibody System Dynamics, 4(4), 355-381(2000).
5. Christian Rudolf. *Road Vehicle Modeling Using Symbolic Multibody System Dynamics, Diploma Thesis*; University of Waterloo in cooperation with University of Karlsruhe(2003).
6. Reid, G.J., Wittkopf, A.D., and Boulton, A. *Reduction of Systems of Nonlinear Partial Differential Equations to Simplified Involutive Forms*. Eur. J. Appl. Math. **7** (1996): 604-635.
7. R. M. Corless, D. J. Jeffrey. *Two Perturbation Calculation in Fluid Mechanics Using Large-Expression Management*; J. Symbolic Computation(1996) 11, 1-17.



# Pointwise and Uniform Power Series Convergence

C. D'Apice, G. Gargiulo, and R. Manzo

University of Salerno, Department of Information Engineering and Applied Mathematics,  
via Ponte don Melillo, 84084 Fisciano (SA), Italy  
{dapice, gargiulo, manzo}@diima.unisa.it

**Abstract.** Since the introduction of CAS (Computer Algebra Systems), educators are experimenting new ways of teaching with the aim to enhance many aspects of the learning mathematics. In particular, visualization can aid the understanding of concepts. The graphical potentialities of many CAS, in fact, allow students to discover concepts, relationships, rules, so as to construct their knowledge for themselves. The aim of this work is to present a Mathematica notebook that enables students to use visualization skills to better grasp the mathematical concepts of the pointwise and uniform convergence of power series.

## 1 Visualization in Mathematics Teaching

Visualization, as a technique for teaching mathematics, has become important especially in those countries where graphics calculators are widely used. Mathematical concepts, ideas and methods have a great wealth of visual relationships, and their use and manipulation is clearly very beneficial from the point of view of their presentation.

Visualization means illustration of an object, fact, process, concept, and its result can be graphic, numeric, or algebraic. Today the term is mostly used for graphic illustrations. Visualization tools can be used in an interpretative and expressive way (Gordin, Edelson and Gomez, 1996).

Interpretative tools can support learners in extracting meaning from the information being visualized, in clarifying text and abstract concepts making them more comprehensible. Expressive visualization can be used to visually convey meaning in order to communicate a set of beliefs.

When using a calculator as a visualization tool the immediate feedback is of central importance. The illustration of concepts helps students to understand them, to associate them with something that is not abstract and the visual association aids to memorize them. Student become able to "see" the meaning of abstract patterns, interacting visually with mathematics.

Mathematica, being a powerful tool for computing, programming, data analysis and visualization of information, is able to catch students' interests, to challenge them and to make learning more interesting.

The use of Mathematica notebooks, as a support to traditional lessons, can help students in understanding some concepts, since they are personally involved in experimentation and discovery. We have introduced them in the traditional curriculum for some years, within a research addressed to the development of innovative ways of mathematics teaching using Mathematica.

Here we describe a notebook that can offer useful visualization of the concepts of pointwise and uniform convergence of power series.

## 2 Pointwise and Uniform Convergence of Power Series

The notebook, we are going to illustrate, has been realized with the aim to aid students to reach a deeper knowledge of the concepts of pointwise and uniform convergence of power series. Students used it after traditional lessons on the above contents in order to explore the meaning of convergence.

To introduce the convergence of power series, we recall the following definitions.

**Definition 1.** Let  $I$  be a subset of  $\mathbb{R}$ ,  $\{f_n\}$ ,  $f_n : I \rightarrow \mathbb{R}$ , be a sequence of functions, and let  $f : I \rightarrow \mathbb{R}$  be another function. We say that  $f_n \rightarrow f$

- pointwise on  $I$  if  $\forall x \in I$  and  $\forall \epsilon > 0 \exists N(x, \epsilon)$  such that  $n > N \Rightarrow |f_n(x) - f(x)| < \epsilon$

- uniformly on  $I$  if  $\forall \epsilon > 0 \exists N(\epsilon)$  such that  $n > N \Rightarrow |f_n(x) - f(x)| < \epsilon, \forall x \in I$ .

The graphics in Figure 1 illustrates how, for sufficiently large  $n$ , the  $n$ -th function  $f_n(x) = xe^{-nx}$  lies completely below any given level (in the form  $\frac{1}{en}$ ). In this case, for simplicity, the (uniform) limit is identically zero, so that close to the limit simply means small. In the case of (pointwise but) non uniform convergence, the  $n$ -th function stays below any given level, but not globally: the maximum is essentially the same for all functions (here  $f_n(x) = nxe^{-nx}$ ).

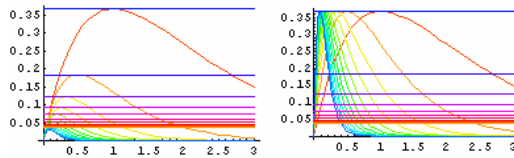


Fig. 1. On the left  $f_n(x) = xe^{-nx}$ , on the right  $f_n(x) = nxe^{-nx}$

**Definition 2.** The series  $s(x) = \sum_{k=1}^{\infty} u_k(x)$  converges pointwise to the function  $s$  if the sequence  $s_n = \sum_{k=1}^n u_k(x)$  converges pointwise to the function  $s$ .

**Definition 3.** The series  $s(x) = \sum_{k=1}^{\infty} u_k(x)$  converges uniformly to the function  $s$  if the sequence  $s_n(x)$  converges uniformly to the function  $s$ .

Let us go to visually study the convergence of some power series.

### 2.1 Series $\sum_{k=0}^{\infty} z^k$

Let us consider the geometric series  $\sum_{k=0}^{\infty} z^k$  which converges within the circle of convergence  $|z| < 1$  and diverges outside  $\sum_{k=0}^{\infty} z^k = \frac{1}{1-z}$ . Let us analyze the behaviour of the partial sums of the geometric series in the complex plane using the following function:

```
s[z_, n_ : 20, opts___] := ListPlot[({Re[#1], Im[#1]} &) /@  
Drop[FoldList[Plus, 0, Table[z^k, {k, 0, n}]], 1],  
PlotJoined -> True, PlotStyle -> RGBColor[1, 0, 0],  
AspectRatio -> Automatic, Background -> GrayLevel[1], opts]
```

Visualize the behavior of the first 40 partial sums of the series in a point,  $\frac{3}{5} + \frac{4i}{5}$ , on the boundary of the convergence circle.

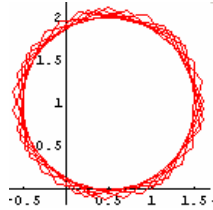


**Fig. 2.**  $s\left[\frac{3}{5} + \frac{4i}{5}, 40\right]$

As we can see the geometric series does not converge, since the points representing the partial sums do not "head" towards a definite point. Let us consider (Fig. 3) the behaviour of the first 200 partial sums in a point,  $0.99\left(\frac{3}{5} + \frac{4i}{5}\right)$ , inside the circle of convergence. The geometric series converges but since the point is near the circle the

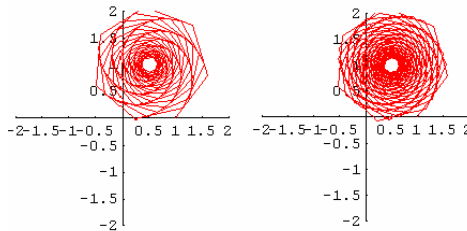


**Fig. 3.** On the left  $s\left[0.99\left(\frac{3}{5} + \frac{4i}{5}\right), 200\right]$ , on the right  $s\left[0.995\left(\frac{3}{5} + \frac{4i}{5}\right), 20\right]$

convergence is slow: the sums slowly spiral towards their limit. Let us consider (Fig. 3) a point,  $0.995\left(\frac{3}{5} + \frac{4i}{5}\right)$ , nearer the circle: the series converges but the convergence is even slower than before.

In a point,  $0.9\left(\frac{3}{5} + \frac{4i}{5}\right)$ , far from the boundary of the convergence circle, the convergence is faster as we can see in the following graphics.

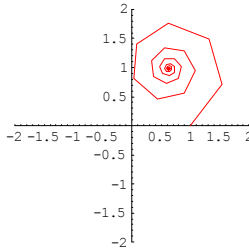


**Fig. 4.**  $s\left[0.9\left(\frac{3}{5} + \frac{4i}{5}\right), 200\right]$

### 2.2 Series $\sum_{k=1}^{\infty} \frac{z^k}{k}$

Let us analyze the convergence of the series  $\sum_{k=1}^{\infty} \frac{z^k}{k} = -\text{Log}[1 - z]$ . First, we consider the same point,  $\frac{3}{5} + \frac{4i}{5}$ , as before, on the boundary of the circle of convergence (Fig. 5). This time, the series converges (slowly) also in this point. Then let us analyze the behaviour in a point,  $0.99\left(\frac{3}{5} + \frac{4i}{5}\right)$ , inside the circle (Fig. 5).

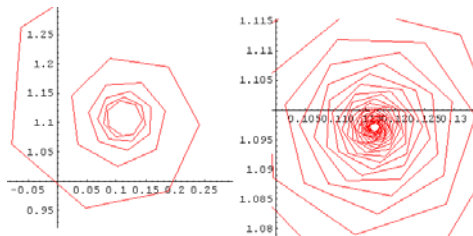


**Fig. 5.** On the left  $s\left[\left(\frac{3}{5} + \frac{4i}{5}\right), 40\right]$ , on the right  $s\left[0.99\left(\frac{3}{5} + \frac{4i}{5}\right), 200\right]$

We "zoom out" the graphics and we consider a point still closer to the boundary and a point farther from the boundary (Fig. 6).

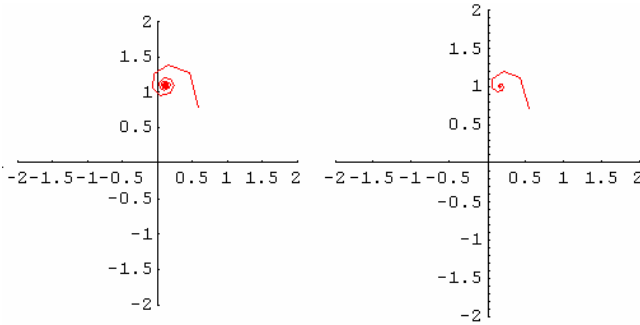


Fig. 6. On the left  $s\left[0.995\left(\frac{3}{5} + \frac{4i}{5}\right), 400\right]$ , on the right  $s\left[0.9\left(\frac{3}{5} + \frac{4i}{5}\right), 400\right]$

### 3 Uniform Convergence

Let us define a general function that allows to study the behaviour of the partial sums of a power series in a chosen point.

```
sgeneral[termgen_, value_, numterms_: 20, colours_: 5, opts_] :=
Module[{listsumpoints},
listsumpoints = ({Re[#1], Im[#1]} &) /@ Drop[
FoldList[Plus, 0, Table[termgen /. z -> value, {k, numterms}]], 1];
Show[Graphics[Table[{Hue[ $\frac{i}{colours}$ ]},
Line[{listsumpoints[[i]], listsumpoints[[i + 1]]}],
{i, Length[listsumpoints] - 1}], opts]]
```

Let us try to understand the meaning of uniform convergence, observing the behaviour of the partial sums in different points, in polar coordinates (i.e. we pick up points in given directions and on several circles around the origin).

```
Show[Table[sgeneral[ $\frac{z^k}{k}$ , r e $i\theta$ , 20, 5, DisplayFunction -> Identity],
{x, .5, 1, .02}, {θ, 0, 2π,  $\frac{\pi}{8}$ }],
DisplayFunction -> $DisplayFunction, PlotRange -> {{-2, 2}, {-3, 3}},
Axes -> True, AspectRatio -> 1, Background -> GrayLevel[1]];
```

As we can see the convergence is faster in the points far from the boundary of the convergence circle, and becomes slow near the boundary.

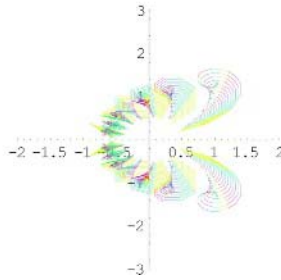


**Fig. 7.** The series with general term  $\frac{z^k}{k}$

The series does not converge uniformly, in fact the convergence "rates" depends in an essential manner on the point.

With different general terms,  $\frac{z^k}{k \text{Log}[k+1]}$  and  $\frac{z^k}{\sqrt{k}}$  (Fig. 7), we see the same general pattern as before, but the convergence rate is a trifle higher (spirals are someway smoother).

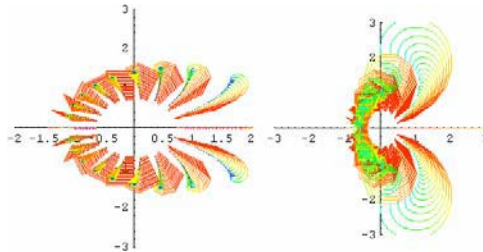


**Fig. 8.** The series with general term  $\frac{z^k}{k \text{Log}[k+1]}$  on the left and  $\frac{z^k}{\sqrt{k}}$  on the right

The geometric series again around the point 0.95 and still closer to the boundary around the point 0.95 (Fig. 8).

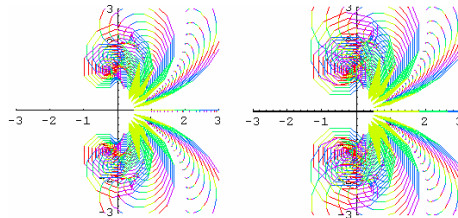


**Fig. 9.** The geometric series

Below are shown two examples of uniform convergence, the series with general term  $\frac{z^k}{k^2}$  and  $\frac{z^k}{k^4}$  (Fig. 9).

We "see" that the spirals have the same general ("uniform") structure. The second series is still "more uniform" example: as Euler would have said, an "augmented convergence".

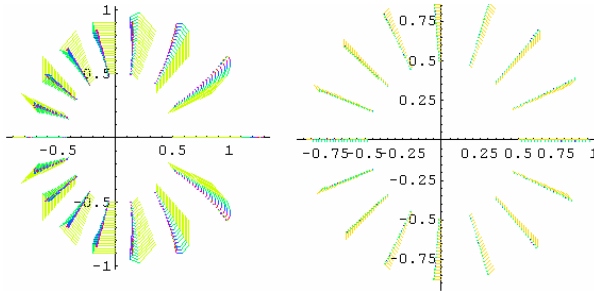


**Fig. 10.** The partial sums of series with general term  $\frac{z^k}{k^2}$  on the left and  $\frac{z^k}{k^4}$  on the right

The logarithmic series around its singular point and "very close" to its boundary singular point  $z = 1$ .

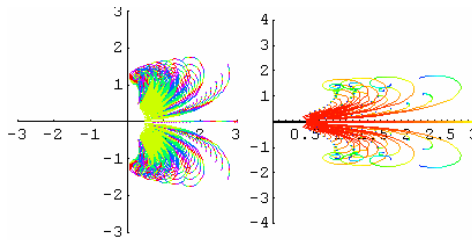


**Fig. 11.** The logarithmic series

## 4 Conclusions

The realization of this notebook encourages the use of computer graphical capabilities in teaching mathematics contents in University courses. The results of their use can be seen as a step towards the introduction of innovative modes in the process of teaching and learning. As a result of the experimentation students have enhanced their understanding of the illustrated concepts, learning in a more enjoyable way.

## References

1. G. Albano, C. D'Apice, G. Gargiulo: Visualisation of four dimensional curves, Electronic Proceedings ICTMT4 (International Conference on Technology in Mathematics Teaching), Plymouth, 1999;
2. Albano, G., Cavallone, A., D'Apice, C., Gargiulo, G.: Mathematica and didactical innovation: a quadric use case, Electronic Proceedings of IMACS-ACA Conferences on Applications of Computer Algebra, Madrid, (1999);
3. Cavallone, A., D'Apice, C., Marsella, M., Salerno, S.: A didactical laboratory: image filtering, Electronic Proceedings of IMACS-ACA Conferences on Applications of Computer Algebra, Madrid, (1999);
4. D'Apice, C., De Simone, T., Manzo, R., Tibullo, V.: MOSFET: a Virtual Laboratory with Mathematica, Proceedings of ICTMT6 Volos, Greece, (2003), 252-257;
5. D'Apice, C., Manzo R., Tibullo, V.: Enhancing Mathematical Teaching-Learning Process by Mathematica, Proceedings of the International Mathematica Symposium 2003, London, (2003), 137-144.
6. Giusti, E. : *Analisi Matematica II*, Bollati Boringhieri, Torino, 1994.
7. Miranda, C. ; *Lezioni di Analisi Matematica, parte seconda*, Liguori Editore, Napoli, 1985.



# Development of SyNRAC

V. Sunderam<sup>1,2</sup> and R. Kuzumaki<sup>1,2</sup>

<sup>1</sup> Information Technology Core Laboratories, Fujitsu Laboratories Ltd,  
Kamikodanaka 4-1-1, Nakahara-ku, Kawasaki 211-8588, Japan  
yanami@flab.fujitsu.co.jp, anai@jp.fujitsu.com

<sup>2</sup> CREST, Japan Science and Technology Agency,  
Kawaguchi Center Building, 4-1-8, Honcho, Kawaguchi 332-0012, Japan

**Abstract.** We present newly implemented procedures in SyNRAC, which is a Maple package for solving real algebraic constraints derived from various engineering problems. The current version of SyNRAC has added quantifier elimination (QE) by cylindrical algebraic decomposition (CAD) as well as QE by virtual substitution for weakly parametric linear formulas. We also show an application of CAD-based QE to the common Lyapunov function problem.

## 1 Introduction

Recent symbolic computation methods have been gradually applied to solving engineering problems, which has been caused by the effectiveness of algorithms introduced and improved for these few decades and by the advancement of computer technology that has hugely increased the CPU performance and memory capacity.

We have been developing a Maple toolbox, called SyNRAC, for solving real algebraic constraints. SyNRAC stands for a Symbolic Numeric toolbox for Real Algebraic Constraints and is aimed at being a comprehensive toolbox including a collection of symbolic, numerical, and symbolic solvers for real algebraic constraints derived from various engineering problems. Here we solve real algebraic constraints that have been modeled as a first-order formula over the reals. Our main method is quantifier elimination (QE), which removes the quantified variables and gives a formula that returns a quantifier free equation.

In this paper we present the newly implemented procedures in SyNRAC. In the next few sections we describe the algorithms as well as some simple practical procedures for quantifier free formulas that have been implemented in SyNRAC. Besides, the current version of SyNRAC provides the following

- general Euclidean real algebraic decomposition (CAD)
- special Euclidean substitution for weakly parametric linear formulas

CAD-based Euclidean generalization of the set that contains the set of real formulas that are the subject of the efficient structure, the CAD-based approach

preceded the special methods we had a read-empowered SyNRAC empowered special method first because there was a good classification which makes practical problems could be reduced and a much more efficient special method as applicable,

the latter procedure is a improved special procedure based on 4 for a subclass of the earlier form as the *weakly parametric* earlier form as we have empowered more efficient specialized for the class which can reduce the size of a problem at set enough to be a factor of 10 at each stage

this paper is regarded as follows: section describe the C and show the commutative diagram of SyNRAC section 2 section present special method to be a virtual substitute for weak parametric earlier form as and compare the procedure of SyNRAC with previous section 4, we show a complete problem which SyNRAC's C commutative diagram applied to a class of section section

## 2 Cylindrical Algebraic Decomposition

Cylindrical algebraic decomposition (CAD) as described by Collins section 7 see for his summary talk Collins as a proposed general algorithm based on Collins which provided a powerful method for solving real algebraic constraints

let  $A$  be a finite subset of  $\mathbb{Z} x_1, \dots, x_n$  algebraic decomposition for  $A$  is a collection of mutually disjoint, semi-algebraic  $A$  are a set of sets that partition the Euclidean  $n$  space  $E^n$  define the term *cylindrical*, we separate parts of a CAD procedure the projection phase, the base phase, and the lifting phase the projection phase of a CAD, the RO function passes a certificate let  $r$  be a integer greater than RO maps a finite set of tetrapolyhedra  $r$  are a set of a finite set of tetrapolyhedra  $r - r$  are a set of  $A_r \subset \mathbb{Z} x_1, \dots, x_r$  RO  $(A_r) \subset \mathbb{Z} x_1, \dots, x_{r-1}$  are a set of  $A \subset \mathbb{Z} x_1, \dots, x_n$  are a set of

$$A = A_0 \xrightarrow{\text{PROJ}} A_1 \xrightarrow{\text{PROJ}} A_2 \xrightarrow{\text{PROJ}} \dots \xrightarrow{\text{PROJ}} A_{n-1},$$

here  $A_i \subset \mathbb{Z} x_1, \dots, x_{n-i}$

the base phase is part of  $E^1$  by using a set of univariate polynomials  $A_{n-1} \subset \mathbb{Z} x_1$  we find all the real zeros of  $A_{n-1}$  and partition  $E^1$  into  $A_{n-1}$  are a set of regions that consist of the zeros of  $A_{n-1}$  and the remaining parts after these parts and these are called sections and sections, respectively

the lifting phase inductively constructs a decomposition of  $E^{i+1}$  from the decomposition of  $E^i$ ,  $i = 2, \dots, n - 1$  suppose  $D$  is a decomposition of  $E^i$  lifting of  $D$  is a decomposition of  $D$  of  $E^{i+1}$  obtained by decomposing the space  $R \times E^1$  by using  $A_{n-i-1}$  for each region  $R \in D$  and putting them together let  $R$  be a region of a decomposition of  $D$  of  $E^i$   $R \times E^1$  is decomposed by the following: take a point  $(p_1, \dots, p_i) \in R$  and substitute for  $(x_1, \dots, x_i)$  each polynomial  $A_{n-i-1}$  to obtain a set of univariate polynomials  $x_{i+1}$  partition  $E^1$  into, say,  $L_0, L_1, \dots, L_{2k+1}$  by using the roots of the polynomials

$x_{i+1}$  Regard  $R \times L_0, R \times L_1, \dots, R \times L_{2k+1}$  as the result of dec. mp. st. the cond. for this process. It is clear that  $A_{n-i-1}$  is *delineable* in  $R$ , therefore, the pair  $(R, A_{n-i-1})$  is a *mas*.  $A_{n-i-1}$  has a *tersect* in  $R$ . In such a case the dec. mp. st. is dependent of the choice of a sample point. The dec. mp. st.  $D$  of  $E^r$  is *cylindrical* fits constructed by iterating the above fitting method,  $E^1$  is dec. mp. sed as the base phase,  $r > 1$  and  $D$  is a fitting of  $s$  me  $c$  dr ca. dec. mp. st.  $D'$  of  $E^{r-1}$ .

Given a formula  $\varphi$ , we can construct a  $C$  for the problem  $\varphi$  of the atom  $C$  formula as  $\varphi$  the point for  $C$  based  $E$  is that the truth value of  $\varphi$  is determined region  $s$  because each region  $s$  the  $C$  is  $A$  are a *tree* for details.

It is the RO function that is crucial to a  $C$  procedure. The former problem  $\varphi$  as RO produces, the more efficient the  $C$  program becomes. But RO must be constructed to maintain the decidability and make the fitting phase possible. Some improvements in the project phase of  $C$  are found in [7, 8].

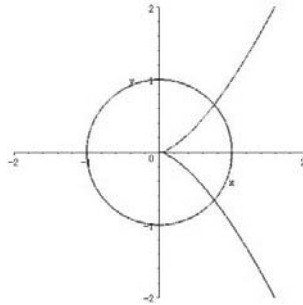


Fig. 1. The graph of A

Here we show some examples of  $C$  commands. SyNRAC can construct a  $C$  for  $A = \{x^2 + y^2 - 1, x^3 - y^2\} \subset \mathbb{Z}[x, y]$  the graph of the tree problem  $\varphi$  as  $A$  is shown in Fig. 1. The Projection command repeats RO and returns  $P[1] = RO^0(A)$  and  $P[2] = RO(A)$ .

```
> read "synrac";
> A:=[ x^2 + y^2 - 1, x^3 - y^2 ]:
> P:=Projection(A, [y,x]):
> P[1]; P[2];
```

$[x^2 + y^2 - 1, x^3 - y^2]$

$[x^2 - 1, x^2 - 1 + x^3, x]$

Let the Base command partition  $E^1$  by using  $P[2]$  and return a set of points that represent respective sections. The sections are rational points taken as a sample point for a section, and a *sh. g. p.* is a *sh. g. p.* associated to a section. They are taken for a section. Here are further results (sections) of  $P[2]$  and they make five *pe. ter as* (sections).

```
> Base(P[2], x);
```

```
[-2, [x + 1, [-1, -1]], -1/2, [x, [0, 0]], 3/8,
 [x^2 - 1 + x^3, [3/4, 7/8]], 15/16, [x - 1, [1, 1]], 2]
```

Using the `Lifting` command makes a stack for each section. The first section has the third and the fifth sections as a section with a rational sample point  $[-1/2]$  and the stack points represent the data for the fifth section are shown as a sample point. The data for the fifth section has  $[3/8]$  as a sample point.

```
> L:=Lifting(P, [y,x]);
> op(L[3]); op(L[5]);
```

```
[3], [-1/2], [-2, [-3 + 4 y^2, [-1, 0]], 0, [-3 + 4 y^2, [0, 1]], 2]
[5], [3/8], [-2, [-55 + 64 y^2, [-1, -1/2]], -1/2,
 [512 y^2 - 27, [-1/2, 0]], 0, [512 y^2 - 27, [0, 1/2]], 1/2,
 [-55 + 64 y^2, [1/2, 1]], 2]
```

### 3 Special QE for Weakly Parametric Linear Formulas

We give a description of a special algorithm for linear formulas as the first special algorithm and then present the weak parametric case. We show some experimental results to compare the efficiency of the two procedures.

#### 3.1 Special QE by Virtual Substitution for Linear Formulas

88 The special algorithm for linear formulas by virtual substitution for linear formulas is called *linear* formulas at matrix formulas are a linear formula with respect to its quantified variables. The order, either equal or unequal, the formula can be represented as

$$a_0 + a_1x_1 + \dots + a_nx_n \rho,$$

where  $x_i$  are quantified variables,  $a_i$  are free, and  $\rho$  is a relational operator, e.g.,  $\in, =, /, \leq, <$ .

Let  $\psi(p_1, \dots, p_m)$   $Q_1x_1 \dots Q_nx_n \varphi(p_1, \dots, p_m, x_1, \dots, x_n)$  be a linear formula, where  $Q_i \in \{\forall, \exists\}$  and  $\varphi$  is quantifier free. Using the equivalence  $\forall x \varphi(x) \iff \neg(\exists x \neg \varphi(x))$ , we can change the formula into the equivalent formula  $(\neg)\exists x_1 \dots (\neg)\exists x_n (\neg)\varphi$  where the prefix  $(\neg)$  attached to  $\varphi$  can be easily eliminated (use De Morgan's law and rewrite the matrix formulas), which is essential part of the hereafter are required to demonstrate  $\exists x \dots \exists x \varphi$  general case, and the quantifiers of the formula can be eliminated. So, to be changed the formula to  $\exists x_i$  and the remaining

eliminate the quantified variables  $\exists x$ .  $\exists x\varphi$ , we use the result saying that there exists a finite set  $S$  of  $x$  free terms such that

$$\exists x\varphi \iff \bigvee_{t \in S} \varphi(x//t)$$

holds. We note that there is a procedure transforming the expression  $\varphi(x/t)$  obtained from  $\varphi$  by substituting  $t$  for  $x$  to a formula  $\varphi(x//t)$  denoting the result of formula  $\varphi(x//t)$  such a set  $S$  is called an *elimination set* for  $\exists x\varphi$ . We obtain a quantifier free formula equivalent to  $\exists x\varphi$  by substituting all candidates  $t \in S$  to  $\varphi$  *disjunctively*.

In this regard, it is clear that smaller elimination sets would increase the efficiency of an E-procedure. In this paper, we propose a procedure using a 2-adic expansion of the real number. We have presented a smaller elimination set to improve the algorithm. If these algorithms had been implemented, SyNRAC

### 3.2 Special QE for Weakly Parametric Linear Formulas

Example 4 has further improved the algorithm for a subclass of linear formulas. A linear formula is called *weakly parametric* if the coefficients of the quantified variables are rational numbers  $a_0 + a_1x_1 + \dots + a_nx_n$ .  $\rho$  are all constant here. free variables occur in the constant term  $a_0$ . A weakly parametric linear formula

in such a case, we can refer to the algorithm which has been used for each equation and calculate the format of the disjunctive set as much as has an elimination set per quantified variable. See 4 for details.

### 3.3 Comparison of the Two Procedures

We compare an E-procedure previously implemented in SyNRAC and a specialized efficient parametric linear formula. We have used the same preprocessing steps that were taken from the design problem of a circuit. The result has five quantified variables. The number of variables increases. The result has variables to be eliminated. The result has a 2 here, although the others but because of a lack of space.

Problem1

$$\& \text{Ex}([k_1, k_2, c_0, c_1, c_2], \& \text{and}([0 \leq c_2 + (1/4 p_1 - 1)p_2^3, 0 \leq -c_2 + (1/4 p_1 + 1)p_2^3, 0 \leq c_1 + (1/2 p_1 - 4)p_2^2, 0 \leq -c_1 + (1/2 p_1 + 4)p_2^2, 0 \leq k_1 + c_0 + (p_1 - 6)p_2, 0 \leq -k_1 - c_0 + (p_1 + 6)p_2, 0 \leq k_2 + 2 p_1 - 4, 0 \leq -k_2 + 2 p_1 + 4, -1 \leq c_0, c_0 \leq 1, 1 \leq c_1, c_1 \leq 3/2, 1/2 \leq c_2, c_2 \leq 3/2]))$$

Problem2

$$\& \text{Ex}([k_1, k_2, c_0, c_1, c_2, c_3], \& \text{and}([0 \leq c_3 + (1/4 p_1 - 1)p_2^4, 0 \leq -c_3 + (1/4 p_1 + 1)p_2^4, 0 \leq c_2 + (1/2 p_1 - 6)p_2^3, 0 \leq -c_2 + (1/2 p_1 + 6)p_2^3, 0 \leq c_1 + (p_1 - 15)p_2^2, 0 \leq -c_1 + (p_1 + 15)p_2^2, 0 \leq k_1 + c_0 + (2 p_1 - 18)p_2, 0 \leq -k_1 - c_0 + (2 p_1 + 18)p_2, 0 \leq k_2 + 4 p_1 - 10, 0 \leq -k_2 + 4 p_1 + 10, -1 \leq c_0, c_0 \leq 1, 1 \leq c_1, c_1 \leq 3/2, 1/2 \leq c_2, c_2 \leq 3/2, 1/2 \leq c_3, c_3 \leq 3/2]))$$

**Table 1.** Linear QE and weakly parametric linear QE

Problem	Linear (general)		Weakly parametric linear	
	time (sec)	# atoms	time (sec)	# atoms
1	10.406	112	0.093	36
2	2.708	608	0.156	92
3	12.281	3072	0.320	232
4	513.406	69632	0.626	560
5	—	—	1.360	1312
6	—	—	2.968	3008
7	—	—	6.733	6784
8	—	—	16.375	14848
9	—	—	39.828	32768

On a Pentium IV 2.4 GHz processor with 1 GB memory

The results are shown in Table 1. In the previous procedure, computation time is proportional to the number of atoms, while the algorithm specialized for weakly parametric formulates a smaller number of the amplitude problems. Let us compare the computation time per electron for the previous procedure for weakly parametric formulates as has computed  $(.4 / .1)^{1/5} \approx .4$  times faster than the previous procedure. The corresponding gradients gradually reach 2.0 at iteration 4. We suppose that simplification procedures have a more effect on the computation time when the formula gets larger.

### 4 Application of CAD-Based QE

In this section, we show an application of CAD to a practical problem in the commutator approach. For a given problem, a student is expected to find a commutator approach for a set of linear time-varying systems. The problem features stability analysis and controller design for a class of continuous systems such as uncertain systems, fuzzy systems, switched systems, etc. The focus is on the method of commutator approach, a *common quadratic Lyapunov function* (CQLF) [4], for details.

One important issue of a CQLF problem is to find a Lyapunov function for a given set of stable continuous systems, i.e., either the systems share a CQLF or to construct the CQLF. In this numerical case, we define the program `g ( )` package. We consider here the problem of finding a set of Lyapunov functions for a set of system matrices such that these systems share a common Lyapunov function. The Lyapunov problem is solved by using the regression of parameters for continuous systems. Although there are some attempts to resolve this so far, the partial results are obtained. The CQLF problems to compute a Lyapunov function can be solved by using the Lyapunov method. See

**Common Lyapunov Function Problem:** We consider a set of continuous time linear systems

$$\dot{\mathbf{x}} = \mathbf{A}_{ci}\mathbf{x}, \mathbf{x} \in \mathbb{R}^n, \mathbf{A}_{ci} \in \mathbb{R}^{n \times n}, i = 1, \dots, q. \quad (1)$$

The set of systems (1) is said to have a CQLF if there exists a symmetric positive definite matrix  $\mathbf{P} = \mathbf{P}^T > 0$  such that the following Lyapunov equations

$$\mathbf{P}\mathbf{A}_{ci} + \mathbf{A}_{ci}^T\mathbf{P} < 0, \forall i = 1, \dots, q \quad (2)$$

are satisfied. Here the CQLF is  $V(\mathbf{x}) = \mathbf{x}^T\mathbf{P}\mathbf{x}$ .

**Solving Common Lyapunov Function Problem by QE:** We consider two linear stable continuous time linear systems, i.e., the case  $n = 2$  and  $q = 2$ . ( )

$$\dot{\mathbf{x}} = \mathbf{A}_{ci}\mathbf{x}, \mathbf{x} \in \mathbb{R}^2, \mathbf{A}_{ci} \in \mathbb{R}^{2 \times 2}, i = 1, 2. \quad (3)$$

Let  $\mathbf{A}_{c1}, \mathbf{A}_{c2}$  be

$$\mathbf{A}_{c1} = \begin{bmatrix} x & \\ y & - \end{bmatrix}, \mathbf{A}_{c2} = \begin{bmatrix} & \\ - & -2 \end{bmatrix}, \quad (4)$$

respectively, where  $x, y \in \mathbb{R}$  are system parameters. We have the following theorem.

**Theorem 1.** (R.N.Shorten et.al. [14]) A necessary and sufficient condition for the two second-order systems (3) to have a CQLF is

$$Re(\lambda(\text{co}(\mathbf{A}_{c1}, \mathbf{A}_{c2}))) < 0, \quad (5)$$

$$Re(\lambda(\text{co}(\mathbf{A}_{c1}, \mathbf{A}_{c2}^{-1}))) < 0, \quad (6)$$

where  $\text{co}(\cdot)$  denotes the convex hull (polytope) of matrices:  $\text{co}(\mathbf{X}, \mathbf{Y}) = \{\alpha\mathbf{X} + (1 - \alpha)\mathbf{Y} \mid \alpha \in [0, 1]\}$ ,  $\lambda(\mathbf{X})$  denotes the eigenvalues of matrix  $\mathbf{X}$  and  $Re(\cdot)$  denotes the real part of a complex number.

This implies that our desired conditions are that all roots of characteristic polynomial of  $(\mathbf{A}_{c1}, \mathbf{A}_{c2})$  and  $(\mathbf{A}_{c1}, \mathbf{A}_{c2}^{-1})$  locate in the left half of the Gauss plane for  $\alpha \in [0, 1]$ . The conditions can be reduced to a set of polynomial equations by using the eigenvalue and Ch part criterion. The case can apply Euler the polynomial equations

to compute feasible regions of  $x, y$  such that the systems (3) have a CQLF. By using the above approach of the eigenvalue and Ch part criterion, the characteristic polynomial of  $(\mathbf{A}_{c1}, \mathbf{A}_{c2})$  and  $(\mathbf{A}_{c1}, \mathbf{A}_{c2}^{-1})$ , the CQLF existence conditions can be described by the following formula

$$\forall \alpha \ (0 \leq \alpha \leq 1) \Rightarrow (2 - \alpha - x\alpha > 0 \wedge 1 + y\alpha - \alpha^2 - x\alpha^2 - y\alpha^2 > 0 \wedge -2\alpha - 2x\alpha - y\alpha + \alpha^2 + x\alpha^2 + y\alpha^2 > 0). \quad (7)$$

By using CQLF based Euler-SyNRAC test (7), the output turns out to be

$$(x < 0 \wedge -2 - 2\sqrt{-x} < y < 2\sqrt{-x} - 2x). \quad (8)$$

## 5 Conclusion

We have presented a new, developed functional Maple package SyNRAC. The current version of SyNRAC provides quantifier elimination, both for real and complex numbers. It is based on the same standard solvers. The features greatly extend the applicability and tractability of SyNRAC for solving real algebraic constraints. For example, the application of SyNRAC, we have treated a complex polynomial problem.

We proceed to implement other kinds of algorithms and improve them, and are setting about developing symbolic numerical algorithms as a part of the project. For parameter robust control design, MATLAB using SyNRAC as a core engine.

## References

1. Anai, H., Yanami, H.: SyNRAC: A Maple-package for solving real algebraic constraints. In: Proceedings of International Workshop on Computer Algebra Systems and their Applications (CASA) 2003 (Saint Petersburg, Russian Federation), P.M.A. Sloot et al. (Eds.): ICCS 2003, LNCS 2657, Springer (2003) 828–837
2. Anai, H., Hara, S.: A parameter space approach for fixed-order robust controller synthesis by symbolic computation. In: Proceedings of IFAC World Congress on Automatic Control b'02. (2002)
3. Anai, H., Yanami, H., Hara, S.: SyNRAC: a maple-package for solving real algebraic constraints toward a robust parametric control toolbox. In: Proceedings of SICE Annual Conference 2003 (Fukui, Japan). (2003) 1716–1721
4. Weispfenning, V.: Simulation and optimization by quantifier elimination. *Journal of Symbolic Computation* **24** (1997) 189–208 Special issue on applications of quantifier elimination.
5. Collins, G.E.: Quantifier elimination for real closed fields by cylindrical algebraic decomposition. In Caviness, B., Johnson, J., eds.: *Quantifier Elimination and Cylindrical Algebraic Decomposition*. Texts and Monographs in Symbolic Computation. Springer, Wien, New York (1998) 85–121
6. Hong, H.: An improvement of the projection operator in cylindrical algebraic decomposition. In Caviness, B., Johnson, J., eds.: *Quantifier Elimination and Cylindrical Algebraic Decomposition*. Texts and Monographs in Symbolic Computation. Springer, Wien, New York (1998) 166–173
7. McCallum, S.: An improved projection operation for cylindrical algebraic decomposition. In Caviness, B., Johnson, J., eds.: *Quantifier Elimination and Cylindrical Algebraic Decomposition*. Texts and Monographs in Symbolic Computation. Springer, Wien, New York (1998) 242–268
8. Brown, C.W.: Improved projection for cylindrical algebraic decomposition. *Journal of Symbolic Computation* **32** (2001) 447–465
9. Anai, H., Yanami, H.: SyNRAC: a Maple-package for solving real algebraic constraints. In: Proceedings of International Conferences on Computational Science. Volume 2657 of LNCS., Springer (2003) 828–837
10. Weispfenning, V.: The complexity of linear problems in fields. *Journal of Symbolic Computation* **5** (1988) 3–27



11. Weispfenning, V.: Quantifier elimination for real algebra—the quadratic case and beyond. *Applicable Algebra in Engineering Communication and Computing* **8** (1997) 85–101
12. Loos, R., Weispfenning, V.: Applying linear quantifier elimination. *The Computer Journal* **36** (1993) 450–462 Special issue on computational quantifier elimination.
13. Shorten, R.N., Narendra, K.S.: Necessary and sufficient conditions for the existence of a common quadratic lyapunov function for  $m$  stable second order linear time-invariant systems. *Proc. of ACC* (2000) 359–363
14. Shorten, R.N., Narendra, K.S.: Necessary and sufficient conditions for the existence of a common quadratic lyapunov function for two stable second order linear time-invariant systems. *Proc. of ACC* (1999) 1410–1414
15. Mori, Y.: Investigation on common lyapunov function: Toward complete analysis. Kyoto Institute of Technology, Doctoral Thesis, (in Japanese) (2002)
16. Nguyen, T.V.: Common lyapunov function problem: Quadratic and infinity-norm functions. Kyoto Institute of Technology, Master Thesis (2003)

# A LiE Subroutine for Computing Prehomogeneous Spaces Associated with Complex Nilpotent Orbits

te e. Ge. . acks. . a. d . fred G. . e.

Department of Mathematics,  
University of Massachusetts,  
Boston, MA 02125-3393, USA  
{jackson, anoel}@math.umb.edu

**Abstract.** We develop a LiE subroutine to compute the irreducible components of certain prehomogeneous spaces that are associated with complex nilpotent orbits. An understanding of these spaces is necessary for solving more general problems in the theory of nilpotent orbits and the representation theory of Lie groups. The output is a set of L<sup>A</sup>T<sub>E</sub>X statements that can be compiled in a L<sup>A</sup>T<sub>E</sub>X environment in order to produce tables. Although the algorithm is used to solve the problem in the case of exceptional complex reductive Lie groups [2], it does describe these prehomogeneous spaces for the classical cases also. Complete tables for the exceptional groups can be found at  
<http://www.math.umb.edu/~anoel/publications/tables/>.

## 1 Introduction

It has been long established that the representation theory of the reductive groups of finite rank is of fundamental importance in physics, chemistry and mathematics. The representation theory of these groups is currently being applied in many other areas, e.g. engineering applications, computer science and the development of financial mathematics. The representation theory of these groups is being developed in mathematical areas which are more advanced, e.g. representation theory of reductive groups. The representation theory of the reductive groups should be of interest to scientists and engineers working at the cutting edges of the fields.

The representation theory of semisimple reductive groups (and general reductive groups) is especially important and challenging in mathematical areas where developed a large number of techniques to create direct representations of a given reductive group. Understanding of the properties of such groups would provide important information about the properties of representations of the studied classification of such groups. The theory of prehomogeneous spaces provides important information.

**Definition 1 (M. Sato [5]).** *Let  $G$  be a connected semisimple complex Lie group,  $V$  a finite dimensional vector space over  $\mathbb{C}$  and  $\rho$  a rational representation of  $G$  in  $V$ . Then the triple  $(G, \rho, V)$  is called a prehomogeneous vector space if*

$G$  admits a Zariski open dense orbit  $\Omega$  in  $V$ . If  $\rho$  is irreducible then  $(G, \rho, V)$  is said to be irreducible.

Let  $(G, \rho, V)$  be a representation of  $G$  and  $\mathfrak{g}$  the Lie algebra of  $G$ . Let  $X$  be a representative of a nilpotent orbit  $\mathcal{O}$  of  $\mathfrak{g}$ . Then the adjoint representation  $\text{ad}_H$  of  $H$  on  $\mathfrak{g}$  restricted to  $\mathcal{O}$  is said to be irreducible if  $(H, X, Y)$  is a triple such that

$$H, X = 2X, \quad H, Y = -2Y, \quad X, Y = H.$$

Such a  $(H, X, Y)$  is called a  $\mathfrak{sl}_2$ -triple. Given such a triple, the action of  $\text{ad}_H$  determines a grading  $\mathfrak{g} = \bigoplus_{i \in \mathbb{Z}} \mathfrak{g}_i$ , where  $\mathfrak{g}_i = \{Z \in \mathfrak{g} \mid H, Z = iZ\}$ .

It is a fact that  $\mathfrak{g}_0$  is a reductive subalgebra of  $\mathfrak{g}$ . Let  $G_0$  be the connected subgroup of  $G$  such that  $\mathfrak{e}(G_0) = \mathfrak{g}_0$ . It is stated in [1] that  $(G_0, \mathfrak{g}_2)$  is a prehomogeneous vector space after a change of basis. Berg's generalized state's result shows that all  $(G_0, \mathfrak{g}_i)$  pairs are prehomogeneous vector spaces.

**Our goal is to describe the irreducible components of the  $G_0$ -modules  $\mathfrak{g}_i$  for all nilpotent orbits of the Lie group  $G$  in  $\mathfrak{g}$ .**

To see enough to consider the simple components of the above, we have developed a general recursive classification procedure by putting together the fact that the nilpotent orbits are parametrized by certain partitions of a regular related to the rank, such parametrization is still a acceptable for groups as a result of our sub-acute studies. In order to state the problem, the cases where  $G$  is a special type of a product of a Lie algebra, another method of computation, these prehomogeneous spaces are classified simple components of the group, these results are found in [2].

In order to give the reader the affair of the general result, we provide a complete description of the result of the case of the general linear group.

**2 Type  $GL_n$**

Let  $GL_n$  be the set of  $n \times n$  complex invertible matrices. Let  $\mathfrak{g} = \mathfrak{gl}_n$ , the set of all  $n \times n$  complex matrices. It is known that the nilpotent orbits of the group  $G = GL_n$  are parametrized by partitions of  $n$ . Hereafter, if  $X$  is a nilpotent element of  $\mathfrak{g}$ , then the conjugacy class  $\mathcal{O}$  can be taken as sum of Jordan blocks of size  $d_i$ , where the  $d_i$ 's are parts of the partition  $\mathbf{d} = d_1, \dots, d_k$  representing the class of  $X$ . We represent  $n$  as a  $\mathbf{d} = (d_1, \dots, d_k)$ , 2. the

$$X = \begin{pmatrix} & & \\ \hline & & \\ \hline & & \\ \hline & & \end{pmatrix}$$

the ac. bs. . . r. z. . . the rem. te. s us that e ca. embed  $X$  . a tr. p. e  $(H, X, Y)$  . th. s case e ca. ch. se  $H$  t. be the f. . . . g. d. ag. . a matr. . f trace zer.

$$H \text{ dag}(d_1 - , d_1 - , \dots, -d_1 + , -d_1 + , \dots, d_k - , \dots, -d_k + )$$

et  $V \in \mathbb{C}^n$  be the sta. dard repre. tat. . . f  $g$  . ce  $H$  s sem. smp. e . e must ha. e  $V = \bigoplus_{i \in \mathbb{Z}} V_i$ , here  $V_i$  s the  $H$  e ge. space. f e ge. a. ue  $i$

**Theorem 1.** *Maintaining the above notation,  $G_0 \simeq \prod GL(V_i)$  and each  $G_0$ -module  $g_i \simeq \bigoplus_{i-j=l} V_i \otimes V_j^*$ .*

*Proof.* et  $G^H$  be the ce. tra. zer. f  $H$  .  $G$  . he  $G^H$  preserves each e ge. space  $V_i$  f  $H$  . e. ce  $G^H \simeq \prod GL(V_i)$  . ut u. der the ad. . t. act. .  $G_0 \subset G^H$  . et  $g_0 \simeq \bigoplus \mathfrak{gl}(V_i)$  be the e. a. ge. bra. f  $G_0$  . the. as a  $g_0$  m. du. e. e ca. de. t. f.  $g$  . th  $V \otimes V^*$ , h. ch. s equ. a. e. t. t.  $\bigoplus_{i,j} V_i \otimes V_j^*$  . re. er, as  $g_0$  m. du. e.  $g \simeq \bigoplus \mathfrak{gl}$  t. f. . s that each  $g_0$  m. du. e.  $g_i$  s de. t. f. i. e. act. . th  $\bigoplus_{i-j=l} V_i \otimes V_j^*$  s. ce ad $_H$  s a der. at. .  $\square$

ere s a. e. amp. e. et  $X$  be the repre. tat. e. f  $d$  , , 2 g. e. ab. e. he

$$H \text{ dag}(2, , -2, 2, , -2, , - )$$

. ce d m  $V_2$  . d m  $V_0$  . d m  $V_{-2}$  . 2 a. d d m  $V_1$  . d m  $V_{-1}$  . e ha. e

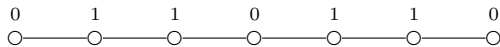
$$G_0 = GL_2 \times GL_2 \times GL_2 \times GL_1 \times GL_1$$

h. e

$$\begin{aligned} g_1 &\simeq (V_2 \otimes V_1^*) \oplus (V_1 \otimes V_0^*) \oplus (V_0 \otimes V_{-1}^*) \oplus (V_{-1} \otimes V_{-2}^*), \\ g_2 &\simeq (V_2 \otimes V_0^*) \oplus (V_1 \otimes V_{-1}^*) \oplus (V_0 \otimes V_{-2}^*), \\ g_3 &\simeq (V_2 \otimes V_1^*) \oplus (V_1 \otimes V_{-2}^*) \\ g_4 &\simeq (V_2 \otimes V_{-2}^*). \end{aligned}$$

### 3 Description of the Algorithm

a. ta. . g the ab. e. . tat. . s, et  $\Delta = \{\alpha_1, \dots, \alpha_l\}$  be the . urbak set. f smp. e. r. t. s f  $g$  a. d  $R^+$  the p. s. t. e. r. t. s stem ge. erated b.  $\Delta$  . he. there s a. . e. t. . e. c. r. esp. de. ce bet. ee. . p. te. t. r. b. t. s f  $G$  . g a. d a subset . f . k. . d. agrams h. se. . des are . ab. e. d . th. e. me. t. s f the set  $\{ , 2\}$  . h. s s the *Dynkin-Kostant classification* 4 . g. r. thms f. r. ab. e. g the . k. . d. agrams are f. u. d . . r. e. amp. e. f  $g$  . sl $_8$  (the set. f  $8 \times 8$  matr. ces . f trace . ) a. d  $\mathcal{O}$  s the . p. te. t. r. b. t. c. r. esp. . d. g. t. the part t. .  $d$  , , 2 . the  $\mathcal{O}$  s ass. c. ated . th the f. . . . g. d. agram



the labels represent the equations of the simple roots  $\alpha_i$  in the diagram matrix

$$H = \text{diag}(2, 2, \dots, -2, -2).$$

the  $\alpha_i(H) = h_{i,i} - h_{i+1,i+1}$  represent  $H$  scalar weights  $H$  under the action of the group  $S_8$  (the symmetric group on eight letters) defined from the details of the roots that  $\mathfrak{g}_i \simeq \bigoplus_{\alpha \in \hat{H}_i} \mathfrak{g}^\alpha$  where  $\mathfrak{g}^\alpha$  is the root space associated with the root  $\alpha$ .

It is useful to observe that the type of the semisimple part of the reductive group  $G_0$  can be read from the diagrammatic respectively the group generated by the roots labeled with zero in the above example the semisimple part of  $G_0$  is of type  $A_1 \oplus A_1 \oplus A_1$ .

**Definition 2.** Let  $v$  be a non-zero element of the root space  $\mathfrak{g}^\lambda \subseteq \mathfrak{g}_i$  and  $X_\alpha$  a non-zero vector in any  $\mathfrak{g}^\alpha \subseteq \mathfrak{g}_0, \mathfrak{g}_0$  with  $\alpha > 0$ . If  $X_\alpha, v$  for all such  $X_\alpha$ 's then we say that  $v$  is a highest weight vector of  $G_0$  on  $\mathfrak{g}_i$  and we call  $\lambda$  a highest weight of  $\mathfrak{g}_i$ .

We shall describe an algorithm which computes the highest weights of  $\mathfrak{g}_i$  given a labeling of the Dynkin diagram respectively the Dynkin diagram under consideration the subtraction of the Dynkin diagram  $E$  Readers who are not familiar with the Macaulay2 software package can be expressed in terms of the fundamental weights for the reader's convenience. The generic functions will be written in boldface characters the subtraction of the same *irreducible* is computed as a subtraction of a string (usually the Cartan label attached to the Dynkin diagram), the Dynkin diagram and the type of the simple group the subtraction returns a set of  $A_{\mathbb{F}}$  statements that generate a table containing the highest weights of all non-zero  $\mathfrak{g}_i$  for  $i >$

### 3.1 Algorithm

```

rrdm.due(tex ba a vec .abe .grp g )
{
# .rmatt .g statements to be used for ecept .a .gr .ups
# ba a .a .a Carter .stat .of the .p .te .t .rb t
# .abe . .k . .sta .t .abe . of the .p .te .t .rb t
# g .c .mp .e .s .mp .e .e .a .g .e .b .r .a
grpt .pe _ if g G2 then grpt .pe \gt _ fi if g 4 then
grpt .pe \_ .ur .fi if g E then grpt .pe \es _ fi if g E7
then grpt .pe \ese e_ fi if g E8 then grpt .pe \ee ght .fi
pr .t .ag
setdefault (g) . n_pos_roots . Lie_rank apha pos_roots
f s ze(.abe.) then
... kf rdegree m .dc .u .ter .
while m .dc .u .ter > do
degree null(.) space .fi .terest null(. .)

```

```

# Compute degree p s t e r t s
c u t e r   f o r   t   d o f o r   t   d o
degree     degree + a b e   * a p h a   o d

# u d the g_i e c t r space spec f i e d b y k f r d e g r e e
i f degree     k f r d e g r e e t h e n c u t e r   c u t e r +
space f i t e r e s t c u t e r   a p h a   f i o d
space     n u l l ( c u t e r , )
f o r   t   c u t e r d   space     space f i t e r e s t   o d
d m s p a c e   c u t e r
m d c u t e r   m d c u t e r   d m s p a c e
i f m d c u t e r <   t h e n p r i n t ( e g a t e m d c u t e r ) b r e a k f i
i f d m s p a c e >   && k f r d e g r e e >   t h e n

# s e t u p the o u t p u t A E s t a t e m e n t
a t e   e   -
i f p r i n t a g   t h e n a t e   e   \ c   e   &   f i
i f p r i n t a g   t h e n p r i n t a g
a t e   e   \ h   e   + b a a +   &   + g r p t p e
f o r   t   d o
a t e   e   a t e   e + { + a b e   + }   o d f i
a t e   e   a t e   e +   &   + k f r d e g r e e +   &   + d m s p a c e +
& \ b a

# f i n d a t h e h g h e s t e g h t s f g_i
h   a l l o n e ( d m s p a c e )
f o r   t   d o
i f a b e   t h e n
f o r   t   d m s p a c e d o c a d d a t e   a p h a   + space

# C h e c k f c a d d a t e s   space   f e s t h e   t s   t a h g h e s t e g h t
f o r k   t   d m s p a c e d o
i f c a d d a t e   space k t h e n h   b r e a k f i o d o d f i o d

# C o m p u t e h g h e s t e g h t s
u m h
f o r   t   d m s p a c e d o u m h   u m h + h   o d
r h g h e s t e g h t s   n u l l ( u m h , )
c u t e r
f o r   t   d m s p a c e d o
i f h   t h e n
c u t e r   c u t e r +   r h g h e s t e g h t s c u t e r   space   f i o d

# C o n v e r t t f u d a m e n t a e g h t s
i f u m h >   t h e n
h g h e s t e g h t s   r h g h e s t e g h t s * C a r t a
f o r   t   u m h d o a t e   e   a t e   e + (
f o r   t   d o

```

```

ate .. e .. ate .. e + highest e ghts
if  $j < l$  then ate .. e .. ate .. e +  $\rightarrow$  fi od
ate .. e .. ate .. e + ) \\_ od
ate .. e .. ate .. e + \ea \\ fi
pr t (ate .. e) fi

# rcess the e t  $g_i$  ect r space
... kfrdegree ... kfrdegree+
od
else pr t ( abe s c mpat be th gr up t pe )
fi
}

```

*Example 1.* We compute the highest weights of each of the four  $g_i$  modules associated with the partition  $\mathbf{d} = (2, 2)$  of  $\mathfrak{sl}_8$  via the  $g_0$  reduction algorithm. We consider the action of its semisimple part  $g_0$  on the subalgebra  $\mathfrak{g}$  of  $\mathfrak{sl}_8$  defined by the  $\mathfrak{phmod}$  which has been loaded in the `Eser` package. The session that produces the above

**LiE version 2.2 created on Nov 22 1997 at 16:50:29 Authors: Arjeh M. Cohen, Marc van Leeuwen, Bert Lisser. Mac port by S. Grimm Public distribution version**

**type '?help' for help information**  
**type '?' for a list of help entries.**

```

> read phmod
> irrmodule("2,2,1,0,0,-1,-2,-2",[0,1,1,0,1,1,0],A7)

```

Observe that since the number of positive roots of  $\mathfrak{sl}_8$  is 28 and the semisimple part of  $g_0$  is of type  $A_1 \oplus A_1 \oplus A_1$  the sum of the dimensions of the  $g_i$ 's is correct. The highest weight of  $g_0$  is  $(2, 2)$  and the highest weight of  $g_i$  is computed as  $g_0$  module by its highest weights. In other words, interpreting the results given by the table above should be aware that the action of the semisimple part of  $g_0$  on  $g_i$  is completely determined by the set of coefficients associated with the nodes of the Dynkin diagram. The other coefficients affect the action of the center of  $g_0$ , which in each case must act by scalars on each irreducible component of  $g_i$ . Let us denote the set of fundamental weights of  $\mathfrak{sl}_8$  by  $\omega_i$  for  $1 \leq i \leq 7$ . Then (disregarding the action of the center) we see that

$$\begin{aligned}
 g_1 &\simeq V^{\omega_1} \oplus V^{\omega_4} \oplus V^{\omega_4} \oplus V^{\omega_7} \\
 g_2 &\simeq V^0 \oplus V^{\omega_1+\omega_4} \oplus V^{\omega_4+\omega_7} \\
 g_3 &\simeq V^{\omega_1} \oplus V^{\omega_7} \\
 g_4 &\simeq V^{\omega_1+\omega_7}.
 \end{aligned}$$

Table 1.

Example in $sl_8$ revisited				
Elementary divisors	Label	$i$	$\dim \mathfrak{g}_i$	Highest weights of $\mathfrak{g}_i$
2, 2, 1, 0, 0, -1, -2, -2	0110110	1	8	(1, 1, -1, 0, 0, 0, 0) (0, -1, 1, 1, -1, 0, 0) (0, 0, -1, 1, 1, -1, 0) (0, 0, 0, 0, -1, 1, 1)
		2	9	(0, -1, 1, 0, 1, -1, 0) (1, 0, 0, 1, -1, 0, 0) (0, 0, -1, 1, 0, 0, 1)
		3	4	(1, 0, 0, 0, 1, -1, 0) (0, -1, 1, 0, 0, 0, 1)
		4	4	(1, 0, 0, 0, 0, 0, 1)

here  $V^\lambda$  denotes the irreducible  $\mathfrak{g}_0, \mathfrak{g}_0$  module of highest weight  $\lambda$  (note that since  $\mathfrak{g}_{-i}$  is dual to  $\mathfrak{g}_i$ , the module structure of  $\mathfrak{g}_{-i}$  is easily determined from that of  $\mathfrak{g}_i$ ).

The correctness of the algorithm should be evident. A more familiar way to see the representation-theoretic reduction of the groups is to compute the highest weights simultaneously by finding the set of roots for each  $\mathfrak{g}_i$  which are annihilated by a particular simple root space of  $\mathfrak{g}_0, \mathfrak{g}_0$ . Such root spaces correspond to the simple roots of a particular subalgebra. Since  $\mathfrak{g}_0$  acts by the adjoint action, the subroutine returns the roots  $\beta$  such that  $\mathfrak{g}^\beta \subset \mathfrak{g}_i$  and  $X_\alpha, X_\beta$  form a pair  $\alpha$  with  $\mathfrak{g}^\alpha \subset \mathfrak{g}_0, \mathfrak{g}_0$  has selected the set of highest weights of  $\mathfrak{g}_i$ , which is recorded in the array *highestweights*. As a consequence, we express the highest weights in terms of the fundamental weights using the Cartan matrix of  $\mathfrak{g}$ .

In the first case, a analysis of the code reveals the algorithm is  $\mathcal{O}(\text{rank}(\mathfrak{g}) \times (n_{\text{pos.roots}})^3)$  (this is due to the fact that the complexity of the outer **while** loop, *modcounter*, is bounded by the number of positive roots and that the more iterations are performed, the more times  $\mathcal{O}(\text{rank}(\mathfrak{g}) \times (n_{\text{pos.roots}})^2)$  times. Of course, we are assuming that the elementary functions are very fast. The main performance bottleneck is that the algorithm computes the irreducible modules of the prehomogeneous spaces associated to the representation theory of the exceptional Lie algebras. Compute tables for the exceptional groups can be found at <http://math.umb.edu/~ale/pub/cats/tables/rmrefmat/> (see [2]). The computations were carried out on a Mac G4 (4th speed) Gzad Gb (R) of memory.

### 4 Conclusion and Future Work

We present an implementation of a simple algorithm for computing the module structures of a large class of prehomogeneous spaces. The same algorithm



classified the  $\mathfrak{p}$ -type orbits of the adjoint representation of complex reductive groups in [2] and have developed general methods for the classification of Takagi adage of the parametrization of the  $\mathfrak{p}$ -type orbits by parts of the developed the algorithm presented here to solve the problem of groups of cept... a type of algorithm as implemented. Especially a detailed analysis of complex. Our implementation is clear, which makes a analysis easier. The correctness of the algorithm is a consequence of the correctness of the remainder of the highest weight theory. Other authors have treated special cases of this problem. Our results generalize the results of complex structure of reductive groups.

These are current work. We are extending these results to the impact reductive groups of the highest of the standard group. It is sufficient to consider the action of the subgroup  $K_{\mathbb{C}} \subset G_{\mathbb{C}}$  on the reductive manifold. The impact of  $G_{\mathbb{C}}$  on the complex symmetric space  $G_{\mathbb{C}}/K_{\mathbb{C}}$  has been started and have been published preliminary results.

## References

1. Collingwood, D. H. and McGovern, W. M. *Nilpotent orbits in semisimple Lie algebras*. Van Nostrand Reinhold Mathematics Series, New York (1992).
2. Jackson, S. G. and Noël, A. G. *Prehomogeneous spaces associated with complex nilpotent orbits*. To appear in Journal of Algebra.
3. Knapp, A. W. *Lie groups beyond an introduction*. Second edition, Birkhäuser Progress in Mathematics **140** (2002)
4. Kostant, B. *The principal three dimensional subgroup and the Betti numbers of a complex Lie group*. Amer. J. Math., Vol. 81, (1959) 973-1032.
5. Sato, M. and Kimura, T. *A classification of irreducible prehomogeneous vector spaces and their relative invariants*. Nagoya Math. J. 65 (1977), 1-155.
6. Van Leeuwen, M. A. A., Cohen, A. M., and Lissner, B. *LiE: A package for Lie group computations*, Computer Algebra Nederland, Amsterdam, Netherlands (1992)
7. Vinberg, E. B. *On the classification of the nilpotent elements of graded Lie algebras*, Doklady Akademii Nauk SSSR 225 (1975b), 745-748 (Russian). English translation: Soviet Math. Doklady **16** (1975), 1517 - 1520.

# Computing Valuation Popov Forms

Mark Geesbrecht<sup>1</sup>, Gertraud Labahn<sup>1</sup>, and David G. H. Zangwill<sup>2</sup>

<sup>1</sup> School of Computer Science, University of Waterloo,  
Waterloo, ON, N2L 3G1, Canada  
{mwg, glabahn}@uwaterloo.ca

<sup>2</sup> Dept. of Mathematics and Computer Science, Brandon University,  
Brandon, MB, R7A 6A9, Canada  
zhangy@brandonu.ca

**Abstract.** Popov forms and weak Popov forms of matrices over non-commutative valuation domains are defined and discussed. Two new algorithms to construct these Popov forms are given, along with a description of some of their applications.

## 1 Introduction

Over the last decade, there have been significant advances in computing with symbolic systems for linear recurrence and differential equations that are the result of these techniques are computationally efficient Ore polynomial algebras which provide a unified algebraic structure for these differential domains. The Ore polynomial matrix algorithm which acts on a space of functions as a differential operator (recurrence) operator matrices such polynomial matrices describe linear differential systems of equations, which are central components in computer algebra systems. Cast differential and recurrence operators as polynomial matrices allows us to perform the operations efficiently. The algorithms for matrices of polynomial matrices in this setting. This paper is a step towards efficient algorithms for such systems.

It is well known that the determinant of a polynomial matrix has degree bounds that can result in large row or column degrees. Hence the standard algorithm for some applications (such as linear systems) can be a significant problem. Such computational algorithms as matrix polynomial GC's, sectioned matrix, known as the polynomial matrix, as introduced by [1]. And has the property that row degrees are controlled. These polynomial matrices have been successfully applied to such applications as control theory and linear systems (see for example, [2]).

Recently, the polynomial matrix and systems (the shifted polynomial matrix and the weak polynomial matrix) have attracted considerable interest. The computer algebra community, for example, [3], [4], [5], [6], [7], [8], [9], [10], [11], [12], [13], [14], [15], [16], [17], [18], [19], [20], [21], [22], [23], [24], [25], [26], [27], [28], [29], [30], [31], [32], [33], [34], [35], [36], [37], [38], [39], [40], [41], [42], [43], [44], [45], [46], [47], [48], [49], [50], [51], [52], [53], [54], [55], [56], [57], [58], [59], [60], [61], [62], [63], [64], [65], [66], [67], [68], [69], [70], [71], [72], [73], [74], [75], [76], [77], [78], [79], [80], [81], [82], [83], [84], [85], [86], [87], [88], [89], [90], [91], [92], [93], [94], [95], [96], [97], [98], [99], [100].

... rma f rms a d the r ar at ... s a s e st f r s me matr ces f ... c mmutat e p ... m a s, part cu ar Ore p ... m a s Ore d ma s ere tr duced the ... s as a u fied a f captu g d ere t a a d recurrence pera t rs (cf Ore ... ac bs ... 7) ... 4 ac bs ... 7 c s dered the erm te a d m th f rms f matr ces er ske p ... m a r gs ... the c mputer age bra area bram a d r ste ga e a meth d t ca cu ate the ra ks f matr ces er ske p ... m a r gs us g a t pe f ... rma f rm reduct ... f these matr ces Rece t eckerma ... Che g a d abah used fract ... free meth ds t c mpute eak p ... f rm f matr ces er ske p ... m a r gs ... th s paper e c s der the m re ge era pr b em f defi g a d c m put g p a d eak p ... f rms f r matr ces er valuation rings he m t at f r th s quest c mes fr m se era d rect s u ders a d t r ha e te ded the t f eak p ... f rms t the d crete a uat r gs but fa ed t defi e p ... f rms ea h e as the p t ut the r meth ds ha e the pr b em that the d t ecessar term ate e g e a defi t f p ... f rms f matr ces er a uat Ore d ma s a d pr de a agr thm f r such f rms h ch s guara teed t term ate Our meth ds ead t a u fied treatme t f ma p ... m a r gs curre t stud ed C mputer gebra f re am pe c mmutat e p ... m a r gs ( ... 4 a d ), ske p ... m a r gs ( a d ) a d mu t ar ate p ... m a s ( a d e am pe 4) a ... e remark that ur meth d ca be used t e te d the rk reduced bases f r matr ces er c mmutat e a uat s r gs b ... zur Gathe 4 t s me ... c mmutat e cases ( )

t s rth t g that ma cases a uat meth ds are qu te d ere t fr m term rder g meth ds h ch are the usua meth ds t dea th p ... m a s he us g term rder g meth ds e c s ders the ead g terms at each reduct step a uat meth ds usua c s der the h e p ... m a fact a term rder g d uces a a uat but the c erse s t true

## 2 Valuations on Ore Domains

c mmutat e a uat the r dates back t the s th the rk f rt ether a d thers rese tat s ca be f u d ch g 2 a d ater rt 2 th a m re rece t treatme t g e C h th s paper e restr ct such c mmutat e a uat s t the m re pract ca m t ated Ore d ma case

et us first reca s me defi t s a d d scuss s me pr pert es f a uat s ske fie ds me resu ts ha e a read bee d scussed d ere t sett g s f r c mmutat e cases

**Definition 1.** *An ordered group  $\Gamma$  is a (not necessarily commutative) group with a total ordering  $\alpha \geq \beta$ , which is preserved by the group operation:*

$$\alpha \geq \beta, \alpha' \geq \beta' \Rightarrow \alpha + \alpha' \geq \beta + \beta' \quad \text{for all } \alpha, \alpha', \beta, \beta' \in \Gamma.$$

Usually,  $\Gamma$  will be augmented by a symbol  $\infty$  to form a monoid with the operation

$$\alpha + \infty = \infty + \alpha = \infty + \infty = \infty \quad \text{for all } \alpha \in \Gamma,$$

and the ordering  $\infty > \alpha$  for all  $\alpha \in \Gamma$ .

**Definition 2.** Let  $R$  be a ring. Then a valuation on  $R$  with values in an ordered group  $\Gamma$  (the value group) is a function  $\nu$  on  $R$  with values in  $\Gamma \cup \{\infty\}$  which satisfies:

- (V.1)  $\nu(a) \in \Gamma \cup \{\infty\}$  and  $\nu$  assumes at least two values,
- (V.2)  $\nu(ab) = \nu(a) + \nu(b)$ , and
- (V.3)  $\nu(a + b) \geq \min\{\nu(a), \nu(b)\}$ , for every pair of elements  $a, b \in R$ .

**Lemma 1.** ([5]) A valuation  $\nu$  on a ring  $R$  has the following properties:

- (a)  $\nu(\cdot) = \infty$  so that  $\nu(\cdot) > \gamma$  for all  $\gamma \in \Gamma$  ( by (V.2) ).
- (b)  $\ker \nu = \{a \in R \mid \nu(a) = \infty\}$  is a proper ideal of  $R$  ( by (V.1) ). Therefore,  $R/\ker \nu$  is a skew field or a simple ring. Furthermore,  $R/\ker \nu$  is an integral domain.
- (c)  $\nu(\cdot) = \infty$  and  $\nu(a) = \nu(-a)$ .
- (d) If  $\nu(a) \neq \nu(b)$ , then  $\nu(a + b) = \min\{\nu(a), \nu(b)\}$ . □

*Remark 1.* Note that  $\ker \nu$  is a subring of  $R$  and  $\nu(a) = \infty$  for all  $a \in \ker \nu$ .

In the case of a skew field  $K$  with a valuation  $\nu$ , there are two important properties of the valuation ring  $V = \{a \in K \mid \nu(a) \geq 0\}$ . First, the valuation rings total over  $K$ , i.e. either  $k \in V$  or  $k \notin V$  and  $k^{-1} \in V$ . Second, the valuation rings are invariant under  $a \in V$  and  $k \in K \setminus \{0\}$ ,  $k^{-1}ak \in V$ . Usually, a total orderable subring of a skew field is called a valuation ring. Conversely, given a skew field  $K$  and a valuation ring  $V \subseteq K$ , we can form a valuation hierarchy set  $V$  which inherits the following properties:

**Lemma 2.** With our previous notation we have:

- (a) Given  $a, b \in V$ , then  $a$  is a left (and right) multiple of  $b$  if and only if  $\nu(a) \geq \nu(b)$ .
- (b) The units set of  $V$  is  $U = \{a \in V \mid \nu(a) = 0\}$ . Furthermore, the non-units of  $V$  is  $M = \{a \in V \mid \nu(a) > 0\}$ , a maximal ideal of  $V$ .
  - (i)  $\nu(a) \geq \nu(b) \Leftrightarrow a = rb$  for some  $r, r' \in V$ .
  - (ii)  $\nu(a) = \nu(b) \Leftrightarrow a = rb$  for some  $r, r' \in U$ .
  - (iii)  $\nu(a) > \nu(b) \Leftrightarrow a = rb$  for some  $r, r' \in M$ .

*Proof.*

- (a) Assume that for some  $r, s \in V$ , we have  $a = br = sb$  where  $\nu(a) = \nu(b) + \nu(r) = \nu(s) + \nu(b) \geq \nu(b)$  from the definition,  $\nu(s) \geq 0$  and  $\nu(r) \geq 0$ . Conversely, if  $\nu(a) \geq \nu(b)$ , then  $\nu(b) = \infty$  implies  $\nu(a) = \infty$  hence  $a = 0 = sb$ . If  $\nu(a) \geq \nu(b)$ ,  $b \neq 0$ , then  $\nu(b) = \infty$  implies  $\nu(a) = \infty$  hence  $a = 0 = sb$ . Otherwise, we can assume that  $\nu(a) \geq \nu(b)$ ,  $b \neq 0$  which implies that  $\nu(ab^{-1}) \geq 0$ ,  $\nu(b^{-1}a) \geq 0$ , that is, both  $ab^{-1} \in V$  and  $b^{-1}a \in V$  hence  $a = (ab^{-1})b = b(b^{-1}a)$ .

(b) part ( ) follows by (a) and ( ) it is easy to see that  $\nu(r)$  is the same as  $\nu(r)$  for  $r \in U$  and part ( ) follows from the definition of  $M$ . □

*Example 1.* (Chen) Let  $K$  be a skew field with a valuation  $\nu$  and an automorphism  $\sigma$  of  $K$  such that  $\nu(a^\sigma) = \nu(a)$  for all  $a \in K$  and let  $\gamma$  be the automorphism group  $\Gamma$  (ordered elements of  $\Gamma$ ) and define a valuation on the skew polynomial  $K[x; \sigma]$  by the rule

$$w\left(\sum a_i x^i\right) = \min_i \{i\gamma + \nu(a_i)\}.$$

The  $w$  is a valuation on  $K[x; \sigma]$  and can be uniquely extended to a valuation on the function field  $K(x; \sigma)$  of the residue class skew field of  $K$  under  $\nu$  and the automorphism induced by  $K$  by  $\sigma$  is  $\sigma$ , the residue class field of  $K(x; \sigma)$  is either  $K(x; \sigma^{-j})$  (if  $j$  is the least multiple of  $\gamma$  which lies in  $\Gamma$ ), that is,  $j = \text{lcm}(\gamma \in \Gamma)$  or there may exist a  $j$  such that  $j\gamma \in \Gamma$  but  $\gamma \notin \Gamma$  (if  $\gamma$  is not a multiple of  $\gamma \in \Gamma$ ).

The following lemma seeks to generalize the commutative case and gives the division rule for these skew valuations. See also the commutative case.

**Lemma 3.** *Let  $\nu$  be a valuation on a skew field  $K$  with the valuation ring  $V$ ,  $S$  be a subskew field of  $K$  that lies in  $V$  and  $M = \{a \in V \mid \nu(a) > \nu(b)\}$ . Assume that  $S$  maps isomorphically to the residue class skew field of  $\nu$ , or equivalently, that  $V = S \oplus M$  as abelian group. If  $a, b \in K$  such that  $\nu(a) \geq \nu(b)$ , then there exists a unique  $s \in S$  such that either  $a = sb$  or  $\nu(a - sb) > \nu(b)$ . Equivalently, there exists a unique  $s \in S$  such that  $a - sb = mb$  for some  $m \in M$ .*

*Proof.* From lemma 2,  $\nu(a) \geq \nu(b)$  implies that  $a = rb$  for some  $r \in V$ . Since  $V = S \oplus M$  there exists a unique  $s \in S$  such that  $r = s + m$  for some  $m \in M$ . Thus  $a = rb = (s + m)b = sb + mb$ , and  $a - sb = mb$ . Clearly,  $m \in M$  and  $\nu(mb) > \nu(b)$ . Hence,  $\nu(a - sb) > \nu(b)$ . □

**Definition 3.** *Let  $\nu$  be a valuation on a skew field  $K$  with the valuation ring  $V$ . For  $a, b \in V$ , we say that  $b$  right divides  $a$  with respect to  $\nu$ , denoted  $b \mid_\nu a$ , if there exists  $d \in V$  such that  $\nu(a) = \nu(db)$ . The element  $d$  is called a right valuation quotient of  $a$  by  $b$  with respect to  $\nu$  if  $a = db$ , or if  $a \neq db$  and  $\nu(a - db) > \nu(a)$ .*

It is easy to prove the following lemma.

**Lemma 4.**  *$b \mid_\nu a$  if and only if there exists a right valuation quotient of  $a$  by  $b$ .*

In the remainder of this paper we assume that  $\nu$  is a valuation on a skew field  $K$  with the valuation ring  $V$ .

### 3 Valuation Popov Forms

In this section we define weakly reduced forms for matrices over a valuation domain. We make some papers discuss weakly reduced forms, we consider the reduction as a left module over a base ring and define the weakly reduced forms. We discuss the reduction of the terms at the perturbation of the reduction. We can be easily obtained, and we can use previous algorithms to compute these forms.

**Definition 4.** Let  $\mathbf{v} = (v_1, \dots, v_m) \in V^m$ . We define the pivot element  $\text{piv}(\mathbf{v}) \in \{v_1, \dots, v_m\}$  as the rightmost element with minimum valuation in  $\mathbf{v}$ .

We use the definition of the reduction which are used for constructing the weakly reduced form and the reduced form.

**Definition 5.** Given  $\mathbf{a}, \mathbf{b}, \mathbf{c} \in V^m$ , we say that

- (a)  $\mathbf{a}$  weakly reduces to  $\mathbf{c}$  modulo  $\mathbf{b}$  in one step with respect to  $\nu$  if and only if  $\text{piv}(\mathbf{b})$  and  $\text{piv}(\mathbf{a})$  have the same index,  $\text{piv}(\mathbf{b}) \mid_\nu \text{piv}(\mathbf{a})$  and  $\mathbf{c} = \mathbf{a} - q_1 \mathbf{b}$ , where  $q_1 \in V$  is a valuation quotient of  $\text{piv}(\mathbf{a})$  by  $\text{piv}(\mathbf{b})$ .
- (b)  $\mathbf{a}$  reduces to  $\mathbf{c}$  modulo  $\mathbf{b}$  in one step with respect to  $\nu$  if and only if  $\text{piv}(\mathbf{b}) \mid_\nu d$ , where  $d$  is an entry that appears in  $\mathbf{a}$  with the same index of  $\text{piv}(\mathbf{b})$  and  $\mathbf{c} = \mathbf{a} - q_2 \mathbf{b}$ , where  $q_2 \in V$  is a valuation quotient of  $d$  by  $\text{piv}(\mathbf{b})$ .

**Definition 6.** A nonzero vector  $\mathbf{a}$  in  $V^m$  is (resp. weakly) reduced with respect to a set  $S = \{\mathbf{s}_1, \dots, \mathbf{s}_l\}$  of nonzero vectors in  $V^m$  if  $\mathbf{a}$  cannot be (resp. weakly) reduced modulo any one of  $\text{piv}(\mathbf{s}_i)$  with respect to  $\nu$ ,  $i = 1, \dots, l$ .

Furthermore, a set  $S = \{\mathbf{s}_1, \dots, \mathbf{s}_l\}$  of vectors is called a (resp. weakly) reduced set if any vector  $\mathbf{s}_i$  is (weakly) reduced with respect to  $S \setminus \{\mathbf{s}_i\}$ .

**Definition 7.** Let  $\gamma = \{\mathbf{r}_1, \dots, \mathbf{r}_n\}$  be the set of row vectors of matrix  $V^{n \times m}$ .

- (a)  $V^{n \times m}$  is called in weak Popov form if  $\gamma$  is a weakly reduced set.
- (b)  $V^{n \times m}$  is called in Popov form if
  - (i)  $\gamma$  is a reduced set.
  - (ii) Rows are in an ascending chain with respect to  $\nu$ , that is,  $\nu(\text{piv}(\mathbf{r}_1)) \leq \nu(\text{piv}(\mathbf{r}_2)) \leq \dots \leq \nu(\text{piv}(\mathbf{r}_n))$ .

We note that our definition is the same as the usual definition. We choose  $V$  as a commutative domain with degree valuation. We define the weakly reduced form.

The following algorithm gives a method to construct a weakly reduced form and a reduced form.

**Algorithm:** (resp. Weak) Popov form for  $V^{n \times m}$

- Input  $\blacktriangleright$  Rings  $R$ , vectors  $\mathbf{r}_1, \dots, \mathbf{r}_n$ , matrix  $A \in V^{n \times m}$
- Output  $\blacktriangleright$  Rings  $R$ , vectors  $\mathbf{p}_1, \dots, \mathbf{p}_n$ , a (resp. weak) Popov form  $A \in V^{n \times m}$
- Initialization:  $\mathbf{p}_1, \dots, \mathbf{p}_n$
- ( ) Check if  $\{\mathbf{r}_1, \dots, \mathbf{r}_n\}$  is a (resp. weak) Popov form
- (2) if not
- ( ) apply  $s$  of  $A$  to make them into ascending char. w.r.t.  $\nu$
- (4) for  $i = 2$  to  $n$  do
- ( ) if  $\mathbf{r}_i$  is (resp. weak) reduced mod.  $\mathbf{r}_1$ ,
- ( )  $\mathbf{r}_i = \mathbf{r}_i - q_i \mathbf{r}_1$ , here  $q_i$  is the quotient
- (8) end for
- ( ) goto ( )
- ( ) else return  $\mathbf{p}_1, \mathbf{r}_1, \dots, \mathbf{p}_n, \mathbf{r}_n$

**Theorem 1.** *If  $\nu(V)$  is well-defined, then the preceding two algorithms are correct.*

*Proof.* We need to prove the algorithms terminate, i.e. that either reduction increases the quotient, and forms an ascending char. w.r.t.  $\nu$  or the algorithms terminate after a finite number of steps since  $\nu(V)$  is well-defined.  $\square$

The following gives a second method to construct (resp. weak) Popov forms

**Algorithm:** Constructing (resp. weak) Popov form for  $V^{n \times m}$

- Input  $\blacktriangleright$  Rings  $R$ , vectors  $\gamma = \{\mathbf{r}_1, \dots, \mathbf{r}_n\}$ , matrix  $A \in V^{n \times m}$
- Output  $\blacktriangleright$  Rings  $R$ , vectors  $\rho = \{\mathbf{p}_1, \dots, \mathbf{p}_n\}$ , a (resp. weak) Popov form  $A \in V^{n \times m}$
- ( ) Initialization:  $\mathbf{p}_1, \dots, \mathbf{p}_n$
- (2) for  $i = 1$  to  $n$  do
- ( )  $\mathbf{p}_i = \mathbf{r}_i$  (resp. weak) reduced mod.  $\gamma = \{\gamma \setminus \{\mathbf{r}_i\}\} \cup \{\mathbf{p}_i\}$
- end for
- (4) apply  $s$  such that the are in ascending char. w.r.t.  $\nu$  if Popov form required

**Theorem 2.** *If  $\nu(V)$  is well-defined, then the above algorithm is correct.*

*Proof.* The above algorithm terminates after a finite number of steps since  $\nu(V)$  is well-defined. It implies that the steps ( ) terminate. We need to check that  $\rho$  is a (weak) reduced set w.r.t.  $\nu$ . The first two steps produce  $\rho = \{\mathbf{p}_1, \mathbf{r}_2, \dots, \mathbf{r}_n\}$  and  $\rho = \{\mathbf{p}_1, \mathbf{p}_2, \mathbf{r}_3, \dots, \mathbf{r}_n\}$ . Hereafter we have to prove  $\mathbf{p}_1$  cannot be (weak) reduced mod.  $\mathbf{p}_2$ . If this was the case, then  $\mathbf{p}_1$  could be (weak) reduced mod.  $\mathbf{r}_2$ , a contradiction. Inductively, it is easy to prove that  $\rho$  is a (weak) reduced set.  $\square$

### 4 Applications and Examples of Valuation Popov Forms

In the rest of this paper we meet some applications of valuation Popov forms. First, recall that the definition of the rank of a matrix over a Ore domain is different from the usual definition of rank (for example, see [1]). Given a matrix  $A \in V^{n \times m}$ , let  $M$  be the row space of  $A$  and  $M'$  be the reduced form with respect to (weak) reduction. From the previous algorithms,  $M$  and  $M'$  generate the same row space. Here we have the following

**Proposition 1.** *The rank of  $M$  generated by the row space of  $A \in V^{n \times m}$  is invariant under (weak) reduction with respect to any valuation.*

**Proposition 2.** *The rank of a (weak) Popov form equals its number of nonzero rows.*

*Proof.* This follows from the result of (weak) Popov form being a (weak) reduced set. □

*Example 2.* The following example given in [1] is used to show that the procedures do not necessarily terminate. So, our algorithms are capable of obtaining a Popov form as follows

let  $A$  be a matrix over a power series  $F[x]$ , where  $F$  is a field, that is,

$$A = \begin{bmatrix} x + x^2 + x^3 + \dots \end{bmatrix} \in F[x]^{2 \times 1}.$$

Assume that  $\nu$  is the usual valuation on the power series domain  $F[x]$ . Here  $\nu(x + x^2 + x^3 + \dots)$  and  $\nu(\dots)$  here refer to the valuation of the terms  $x + x^2 + x^3 + \dots$ . Note that  $\nu(\dots) = \infty$ . Our algorithm then computes the Popov form as  $\begin{bmatrix} \end{bmatrix}$

*Example 3.* Given a valuation  $\nu$  on a polynomial ring, we reduce the Popov forms (for example, let  $R$  be a ring with a discrete valuation function  $\nu(x)$ ). We extend the valuation  $\nu(x)$  from  $R$  to the polynomial ring  $R[t]$  by defining for a element  $f(t) = a_0 + a_1t + \dots + a_n t^n$ ,

$$\nu(f(t)) = \min_i \{ \nu(a_i) + i \} \tag{1}$$

It is easy to see that  $\nu$  defines a valuation function on  $R[t]$  which extends  $\nu(x)$ . The algorithm for a valuation Popov form produces a Popov form which satisfies the properties discussed in [4], [8] and

*Example 4.* In some cases, our algorithms can be used for multivariate matrices (for example, let  $L$  be a finite dimensional algebra over a commutative field  $K$  and let  $U(L)$  be its universal enveloping algebra). It is easy to see that  $U(L)$  has a filtration

$$U^{-1} \subset U^0 \subset K + L + L^2 + \dots + L^i$$



the associated graded algebra is a polynomial algebra. This filtration is the definition of a valuation. For  $\nu(x)$  by the following rule

$$\nu(x) = \infty, \quad \nu(x) = -i \text{ if } x \in U^i \setminus U^{i-1}. \tag{2}$$

herefore, given a matrix over  $U(L)$ , we can use our algorithms to get a popov and hermite forms, and hence a series of transformations

## 5 Conclusion

In this paper we discuss some properties of valuations and their commutative domain and define reduction algorithms in terms of valuations for matrices over Ore domains. We define and describe popov and hermite forms in terms of valuations. Algorithms to construct these forms are given and are shown to terminate. Further discussion and properties of these forms will appear in a forthcoming paper.

## Acknowledgements

The authors are grateful to the anonymous referees for their helpful comments.

## References

1. Abramov, S., Bronstein, M.: Linear Algebra for skew-polynomial matrices. INRIA (preprint)
2. Artin, E.: Geometric Algebra. Interscience Publishers, Inc. 1957
3. Beckermann, B., Cheng, H., Labahn, G.: Fraction-free row reduction of matrices of Ore polynomials. Proceedings of ISSAC'02, ACM Press, New York, 8-15
4. Beckermann, B., Labahn, G., Villard, G.: Shifted Normal Forms of Polynomial Matrices. Proceedings of ISSAC'99, ACM Press, ACM Press, New York, 189-196
5. Cohn, P. M.: Skew Fields. Cambridge University Press, 1995
6. Giesbrecht, M., Labahn, G., Zhang, Y.: Popov forms for multivariate polynomial matrices. (Preprint)
7. Jacobson, N.: The Theory of Rings. American Math. Soc., New York, 1943
8. Kailath, T.: Linear Systems. Prentice Hall, 1980
9. Mulders, T., Storjohann, A.: On lattice reduction for polynomial matrices. Journal of Symbolic Computation 35(2003), 377-401
10. Ore, O.: Theory of non-commutative polynomials. Annals of Mathematics 34(22): 480-508, 1933
11. Popov, V.: Invariant description of linear, time-invariant controllable systems. SIAM J. Control. Vol.10(2), 252-264, 1972
12. Schilling, O.: The Theory of Valuations. Math. Surveys No. IV, Amer. Math. Soc., New York 1950
13. Villard, G.: Computing Popov and Hermite forms of polynomial matrices. Proceeding of ISSAC'96, ACM Press, New York, 250-258
14. von zur Gathen, J.: Hensel and Newton methods in valuation rings. Mathematics of Computation vol.42(1984), 637-661

# Modeling and Simulation of High-Speed Machining Processes Based on Matlab/Simulink

Rodolfo E. Haber<sup>1,2,\*</sup>, J.R. Alique<sup>1</sup>, S. Ros<sup>1</sup>, and R.H. Haber<sup>3</sup>

<sup>1</sup> Instituto de Automática Industrial (CSIC),  
km. 22,800 N-III, La Poveda, 28500  
Madrid, Spain

`rhaber@iai.csic.es`  
<sup>2</sup> Escuela Politécnica Superior,  
Ciudad Universitaria de Cantoblanco,  
Calle Francisco Tomás y Valiente, 11  
28049 – Madrid, Spain

`Rodolfo.Haber@ii.uam.es`  
<sup>3</sup> Departamento de Control Automático,  
Universidad de Oriente, 90400, Cuba

**Abstract.** This paper shows the mathematical development to derive the integral-differential equations and the algorithms implemented in MATLAB to predict the cutting force in real time in high speed machining processes. This paper presents a cutting-force-based model able to describe a high-speed machining process. The model considers the cutting force as an essential output variable in the physical processes taking place in high-speed machining. For the sake of simplicity, only one type of end mill shapes is considered (i.e., cylindrical mill) for real-time implementation of the developed algorithms. The developed model is validated in slot-milling operations. The results corroborate the importance of the cutting-force variable for predicting tool wear in high-speed machining operations.

**Keywords:** modeling; complex systems; high-speed machining.

## 1 Introduction

One of the basic tasks manufacturing systems have to perform today is machining, especially high-speed machining (HSM), a real case of a complex electromechanical system [1]. The idea of characterizing the machining process using mathematical models to yield an approximate description of the physical phenomenon aroused the interest of many researchers [2]. That work has been carried on, and it has enabled computational tools to be developed for modeling and simulating the conventional machining process, relying on classic modeling and identification strategies.

---

\* Corresponding author.

At the present time, modeling high-speed machining processes as a complex electromechanical process, especially high-speed milling, is a very active area of investigation that is peppering the scientific community with challenges [3,4]. High-speed machining has now been adopted and put into regular use at many companies, and yet certain points of how to monitor cutting-tool condition have been worked out only partially as yet, largely for lack of a mathematical model of the process that can feasibly be used in real-time applications. This paper is aimed at deriving a mathematical model and characterizing the high-speed cutting process in high-speed milling operations through the study of the dynamic behavior of cutting force. Previous work concerning conventional machining has been borne in mind as the essential starting point for this work [5].

A mathematical model is essential for understanding the dynamic behavior of metalworking processes and improving their operation on the basis of time or frequency responses. Increasingly, both experimental models and analytical models are being used in metalworking for the obtaining, manufacturing and processing (e.g., shaping and cutting) of metal materials. When a new product or metal part (e.g., mold) is being designed, the item must pass simulation testing on the process involved (e.g., the cutting process) before work ever begins on the item's physical manufacture. How useful simulations ultimately are depends largely on how faithfully the mathematical models they use describe the real behavior of the cutting process. Moreover, computational methods are essential to yield an adequate accuracy in the prediction and real-time implementation of the model.

The main goal of this paper is to derive a mathematical model from the characterization of the physical processes taking place during high-speed machining and to implement the model in MATLAB/SIMULINK. The paper is organized into five sections. Section 1 describes the state of the art, analyzes some previous work on the subject, gives a quick description of high-speed machining and finally outlines some questions related with the implementation of HSM models in MATLAB. Section 2 presents the kinematics of the model, considering the geometrical form of the helix for the cylindrical mill. Section 3 addresses the mathematical formulation of the proposed model and sets up the integral-differential equations for calculating cutting force in the time domain. Section 4 gives the results yielded by the simulations and tests in real time. Lastly, the paper frames some conclusions, looks ahead to some possible future work and discusses the lines opened to investigation.

## 2 Geometrical Model of the Tool

Geometrical modeling of the helical cutting edge includes the kinematic and dynamic analysis of the cutting process. Predicting cutting forces requires a system of coordinates, the helix angle and the angular distance of a point along the cutting edge [6]. The mathematical expressions that define this geometry in a global coordinate system are presented below in the geometric model, using classic vector notation.

Vector  $\vec{r}(z)$  (figure 1) drawn from point  $O$  to a point  $P$  in cylindrical coordinates is expressed mathematically in equation 1.

$$\vec{r}_j = x_j \vec{i} + y_j \vec{j} + z_j \vec{k} = r(\phi_j)(\sin \phi_j \vec{i} + \cos \phi_j \vec{j}) + z(\phi_j) \vec{k} \tag{1}$$

where  $\phi_j$  is the radial rake angle of a point  $P$  at tooth  $j$ . Point  $P$  lies at an axial depth of cut  $a_p$  in the direction of axis  $Z$ , at a radial distance  $r(z)$  on the  $XY$  plane, with an axial rake angle  $\kappa(z)$  and a radial lag angle of  $\psi(z)$ .

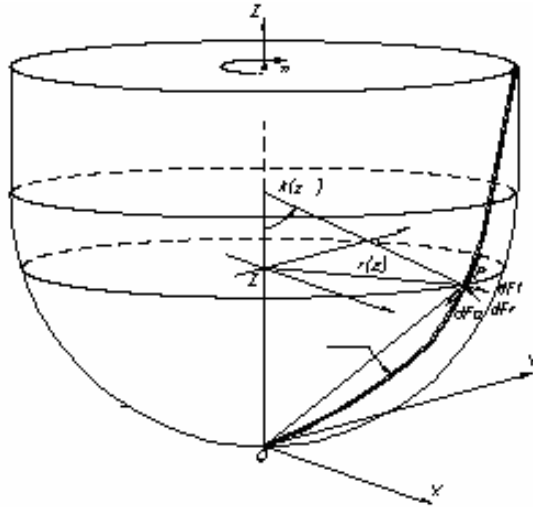


Fig. 1. Tool geometry

The geometry of the tool is represented mathematically, considering that the helical cutting edge wraps parametrically around a cylinder. The mathematical model dictated for the cutting edge considers that the edge is divided into small increments, where the cutting coefficients can vary for each location. The initial point of reference to the cutting edge of the tool ( $j = 1$ ) is considered to be the angle of rotation when  $z = 0$  is  $\phi$ . The radial rake angle for the cutting edge  $j$  in a certain axial position  $z$  is expressed as:

$$\phi_j(z) = \phi + \sum_{n=1}^j \phi_p - \psi(z) \tag{2}$$

The lag angle  $\psi(z)$  appears due to the helix angle  $\theta$ . This angle is constant in the case of a cylindrical mill. In the generalized model for the geometry of a mill with helical teeth, the tool diameter may differ along the length of the tool, depending on the shape of the tool. An infinitesimal length of this cutting edge may be expressed as

$$dS = |dr| = \sqrt{r^2(\phi) + (r'(\phi))^2 + (z'(\phi))^2} d\phi, r'(\phi) = \frac{dr(\phi)}{d\phi}, z' = \frac{dz(\phi)}{d\phi} \tag{3}$$

Chip thickness changes as a function of the radial rake ( $\phi$ ) and axial rake ( $\kappa$ ) :

$$h_j(\phi_j) = s_{ij} \sin \phi_j \cdot \sin \kappa \tag{4}$$

For a cylindrical mill, the following conditions are defined for finding the general solution:

$$r(z) = \frac{D}{2} \quad \kappa = 90^\circ \quad \psi = k_\theta z \quad k_\theta = (2 \tan \theta) / D \tag{5}$$

### 3 Dynamic Model of Cutting Forces

The force differentials ( $dF_t$ ), ( $dF_r$ ), ( $dF_a$ ) act on an infinitesimal element of the cutting edge of the tool [7]:

$$\begin{aligned} dF_t &= K_{te} dS + K_{tc} h_j(\phi, \kappa) db \\ dF_r &= K_{re} dS + K_{rc} h_j(\phi, \kappa) db \\ dF_a &= K_{ae} dS + K_{ac} h_j(\phi, \kappa) db \end{aligned} \tag{6}$$

It is also considered that  $db = \frac{dz}{\sin \kappa}$ . In order to facilitate finding the mathematical relations inherent in this set-up, very small time increments are used. The positions of the points along the cutting edge are evaluated with the geometrical model presented herein above.

Furthermore, the characteristics of a point on the cutting surface are identified using the properties of kinematic rigidity and the displacements between the tool and the workpiece. The constants or cutting coefficients ( $K_{tc}$ ,  $K_{rc}$ ,  $K_{ac}$ ,  $K_{te}$ ,  $K_{re}$ ,  $K_{ae}$ ) can be found experimentally using cutting forces per tooth averaged for a specific type of tool and material [8,9]. We might point out that these coefficients are highly dependent on the location (axial depth) of the cutting edge. How these coefficients are found shall not be addressed in this paper.

Cutting forces can be evaluated employing a system of Cartesian coordinates. After transforming and total cutting forces as a function of  $\phi$  are:

$$\begin{aligned} F_x(\phi) &= \sum_{j=1}^{Nf} (F_{xj}(\phi_j(z))) = \sum_{j=1}^{Nf} \int_{z_1}^{z_2} [-dF_{tj} \sin \phi_j \sin \kappa_j \quad -dF_{tj} \cos \phi_j \quad -dF_{aj} \sin \phi_j \cos \kappa_j] dz \\ F_y(\phi) &= \sum_{j=1}^{Nf} (F_{yj}(\phi_j(z))) = \sum_{j=1}^{Nf} \int_{z_1}^{z_2} [-dF_{tj} \cos \phi_j \sin \kappa_j \quad dF_{tj} \sin \phi_j \quad -dF_{aj} \cos \phi_j \cos \kappa_j] dz \\ F_z(\phi) &= \sum_{j=1}^{Nf} (F_{zj}(\phi_j(z))) = \sum_{j=1}^{Nf} \int_{z_1}^{z_2} [-dF_{rj} \cos \kappa_j \quad 0 \quad -dF_{aj} \sin \kappa_j] dz \end{aligned} \tag{7}$$

where  $z_1$  and  $z_2$  are the integration limits of the contact zone at each moment of cutting and can be calculated from the geometrical model described herein above. For

the numerical calculation, the axial depth of cut is divided into disks having an infinitesimal height  $dz$ . The differentials of the cutting forces are calculated along the length of the cutting edge in contact, and they are summed to find the resulting forces for each axis  $F_x(\phi)$ ,  $F_y(\phi)$ ,  $F_z(\phi)$  in an angle of rotation.

The exact solution can be found by substituting, making  $\kappa = 90^\circ$ , and integrating, we obtain the exact solution for cylindrical mill:

$$\begin{aligned}
 F_{x,j}(\phi_j(z)) &= \left. \begin{aligned} &\frac{S_{tj}}{4k_\beta} \left[ -K_{tc} \cos 2\phi_j(z) + K_{rc} [2\phi_j(z) - \sin 2\phi_j(z)] \right] \\ &+ \frac{1}{k_\beta} [K_{te} \sin \phi_j(z) - K_{re} \cos \phi_j(z)] \end{aligned} \right\}_{z_{j,1}(\phi_j(z))}^{z_{j,2}(\phi_j(z))} \\
 F_{y,j}(\phi_j(z)) &= \left. \begin{aligned} &\frac{-S_{tj}}{4k_\beta} [K_{tc} (2\phi_j(z) - \sin 2\phi_j(z) + K_{rc} \cos 2\phi_j(z))] \\ &+ \frac{1}{k_\beta} [K_{te} \cos \phi_j(z) - K_{re} \sin \phi_j(z)] \end{aligned} \right\}_{z_{j,1}(\phi_j(z))}^{z_{j,2}(\phi_j(z))} \quad (8) \\
 F_{z,j}(\phi_j(z)) &= \frac{1}{k_\beta} [K_{ac} S_{tj} \cos \phi_j(z) - K_{ae} \phi_j(z)]_{z_{j,1}(\phi_j(z))}^{z_{j,2}(\phi_j(z))}
 \end{aligned}$$

where  $z_{j,1}(\phi_j(z))$  and  $z_{j,2}(\phi_j(z))$  are the lower and upper limits, respectively, that establish the axial depth of cut at lip  $j$  of the mill.

### 4 Simulations and Experimental Validation

The algorithms were implemented in MATLAB, drawing upon the mathematical models [10]. Despite MATLAB is not a computer algebra system, it is very useful as software tool for doing numerical computations with matrices and vectors. It can also display information graphically and includes many toolboxes for several research and applications areas. MATLAB was chosen for the advanced numerical methods that are available, the possibility it affords of running simulations and applications in real time and the portability of the programs that are developed with its use (i.e., it is possible to generate C/C++ programs from MATLAB files). Neither Matlab toolbox was used for programming the model.

The main difficulties are choosing the cutting coefficients and the properties of the materials, which were taken from earlier work on the subject [11]. The workpiece-material properties that were used for the simulation in the MATLAB environment are the properties of GGG-70 cast iron with nodular graphite. In this study, in the simulation and in the real tests, two cutting conditions for high-speed milling operations were regarded:  $V_c=546$  m/min,  $sp=14500$  rpm,  $f=1740$  mm/min,  $a_p = 0.5$  mm,  $a_e = 0$ ,  $a_s = 12$  mm,  $\theta=30^\circ$ ,  $H = 25.0$  mm,  $D = 12.0$  mm where  $D$  is the tool diameter [mm],  $H$  is the total tool cutting-edge height [mm],  $\theta$  is the helix angle [degrees],  $a_p$  is the axial depth of cut along the Z axis [mm],  $a_e$  is the radial depth of

cut at the starting point ( $\phi_{st}$ ) [mm],  $a_s$  is the radial depth of cut at the stopping point ( $\phi_{ex}$ ) [mm],  $f$  is the feedrate [mm/min],  $V_c$  is the cutting speed [m/min],  $sp$  is the spindle speed in [rpm].

The constants used in the simulation and in the experimental validation were  $K_{tc} = 2172 \text{ N/mm}^2$ ,  $K_{rc} = 850 \text{ N/mm}^2$ ,  $K_{te} = 17.3 \text{ N/mm}$ ,  $K_{re} = 7.8 \text{ N/mm}$ ,  $K_{ac} = 726 \text{ N/mm}^2$ ,  $K_{ae} = 6.7 \text{ N/mm}$ . These constants or cutting coefficients referring to the material and the tool were drawn from the available literature, due to their similarity to the characteristics of the tool/material set-up used in the study in question.

The real-time model validation tests were conducted at a KONDISA HS1000 high-speed machining center equipped with a Siemens 840D open CNC. Actual cutting force signal was measured using a Kistler 9257 dynamometric platform installed on the testbed. Measurement was done by means of a DAQBOARD-2005 data-acquisition card at a sampling frequency of 50 kHz. A Karnasch 30.6472 cylindrical mill 12 mm in diameter was selected to validate the model developed under the procedure described herein. The chosen test piece, measuring 200x185x50 mm, was made of GGG-70 iron and was machined in a spiral pattern. The real cutting conditions chosen were the same as considered above for the simulation. A view of the cutting tool used in the tests (a), the workpiece and its profile to be mechanized (b) and the machine-tool laboratory (c) is shown in figure 2.

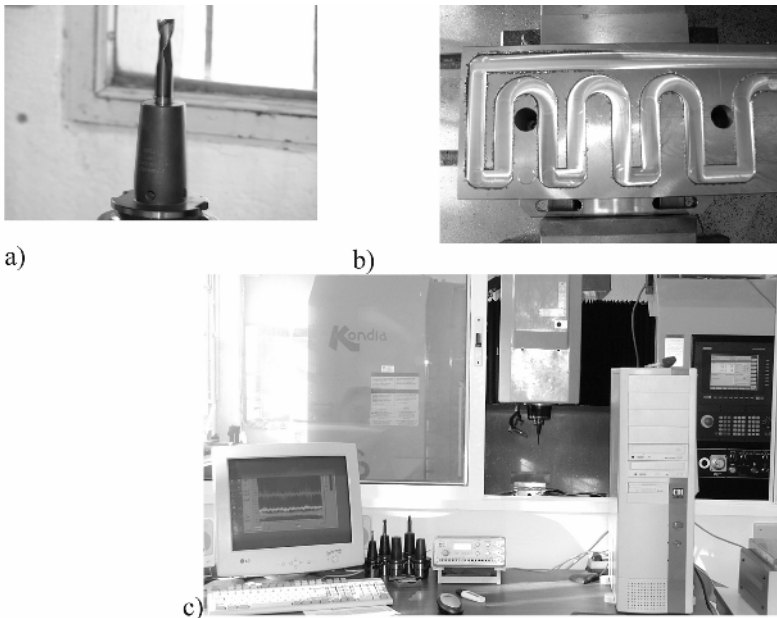


**Fig. 2.** Cutting tool for experiments, b) experimental piece, c) partial view of the Laboratory for machine tool research

Figure 3 shows the real behavior of cutting forces  $F_x$ ,  $F_y$  and  $F_z$  and the resulting force  $F_{qr}$  for the case analyzed. The model's response is shown as a solid line.

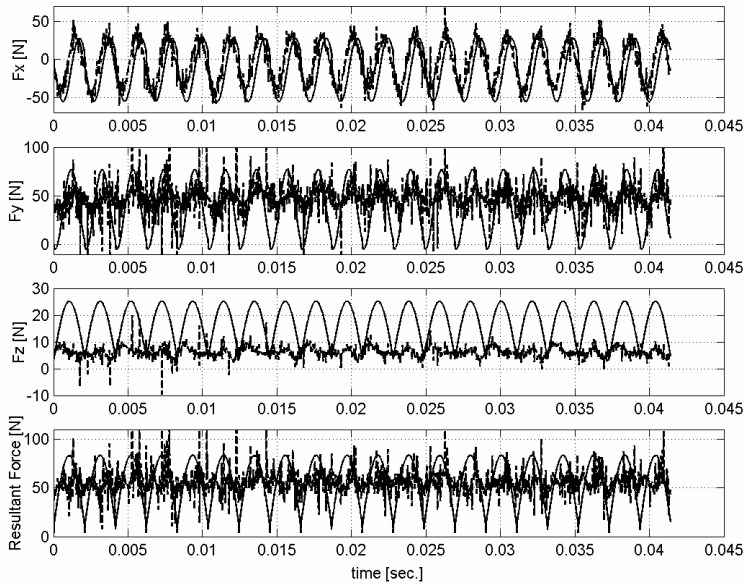


**Fig. 3.** Measured (straight line) and predicted by model (dashed line) cutting force for a new tool in high speed slot cutting

The average resulting cutting force  $\bar{F}_e$  estimated by the model is 56.7N and the average resulting cutting force  $\bar{F}_{qT}$  measured in a real high-speed cutting operation is 55.6N. The error criterion  $\bar{E} = \frac{(\bar{F}_{qT} - \bar{F}_e)}{\bar{F}_{qT}} \cdot 100$ , is 4.5%.

## 5 Conclusions

This paper reports some results in modeling the high-speed cutting process and the validation of the model in question. The mathematical model implemented and assessed in MATLAB has two fundamental, co-dependent parts. The first is a multiple-input system that defines the model's kinematics, where constants and variables describe the tool geometry, the material type and the cutting parameters. The second addresses the dynamics, represented by integral-differential equations. In the case of cylindrical mill the exact analytical solution is found, inasmuch as the limits of integration and the boundary conditions along the tool geometry can be pre-established.

On the basis of the literature to which we have had access, this paper constitutes the first successful attempt in the implementation and application of computationally efficient algorithms for predicting cutting force in high-speed machining processes. With such models available, there is now a short-term way of dealing with essential questions concerning the surface finish and stability of high-speed cutting operations.



Despite the success in the application of Matlab, computer algebra in the formulation and solution of more complex cutting tools, as well as the use of the interface to communicate Mathematica and Matlab will be explored during future research.

## References

1. Haber R. E., J.E. Jiménez, J.L. Coronado, A. Jiménez: Modelo matemático para la predicción del esfuerzo de corte en el mecanizado a alta velocidad, *Revista Metalurgia Madrid* 40(4) (2004) 247-258.
2. Bukkapatnam S.T.S, A. Lakhtakia, S.R.T. Kumara: Analysis of sensor signals shows turning on a lathe exhibits low-dimensional chaos, *Physics Review E* 52 (3) (1995) 2375-2387.
3. Haber R. E., J.E. Jiménez, C.R. Peres, J.R. Alique: An investigation of tool wear monitoring in a high-speed machining process, *Sensors and Actuators A: Physics* 116 (2004) 539-545.
4. Cantillo K. A., R. E. Haber Guerra, A. Alique, R. Galán, CORBA-based open platform for processes monitoring. An application to a complex electromechanical process. In: Bubak M., Albada G.D., Sloot P.M.A., Dongarra J. (eds.): *Computational Science ICCS2004, Lecture Notes in Computer Science* 3036 (2004) 531-535.
5. Altintas Y.: *Manufacturing Automation: metal cutting mechanics, machine tool vibrations, and CNC design*, Cambridge University Press, USA, 2000.
6. Yucesan G., Y. Altintas: Prediction of ball end milling forces, *J. Eng. Ind. Trans. ASME* 1 (1) (1996) 95-103.
7. Altintas Y., P. Lee: Mechanics and dynamics of ball end milling forces, *J. Manuf. Sci. Eng.-Trans. ASME* 120 (1998) 684-692.
8. Fu H. J., R.E. Devor, S.G. Kapoor: A mechanistic model for the prediction of the force system in face milling operation, *J. Eng. Ind. Trans. ASME* 106 (1) (1984) 81-88.
9. Budak E., Y. Altintas, E.J.A. Armarego: Prediction of milling force coefficients from orthogonal cutting data, *J. Eng. Ind. Trans. ASME* 118 (1996) 216-224.
10. The Math Works Inc. Users manual Matlab 6.5 Release 13, Natick, Massachusetts, 2003.
11. Engin S., Y. Altintas: Mechanics and dynamics of general milling cutters Part I: helical end mills *Int. J. Mach. Tools Manuf.* 41 (2001) 2195-2212.

# Remote Access to a Symbolic Computation System for Algebraic Topology: A Client-Server Approach\*

miriam.andres, vico.pascual, ana.romero, julio.rubio

Departamento de Matemáticas y Computación, Universidad de La Rioja  
{miriam.andres, vico.pascual, ana.romero, julio.rubio}@dmc.unirioja.es

**Abstract.** Kenzo is a Symbolic Computation system created by Sergeraert for computing in Algebraic Topology. It is programmed in Common Lisp and this programming language also acts as user interface. In this paper, a prototype to provide remote access for Kenzo is presented. This has been accomplished by using Corba technology: clients have been developed both in Java and Common Lisp (the server is always in Common Lisp, being a wrapper of the original Kenzo program). Instead of using one CORBA IDL to encode each data structure, our approach incorporates a generic way of transferring every data structure through XML strings; specifically, by means of an XML extension of MathML. This research should be understood as a first step towards building a distributed computation system for Algebraic Topology.

## Introduction

Kenzo is a Symbolic Computation system created by Sergeraert for computing in Algebraic Topology. It is programmed in Common Lisp and this programming language also acts as user interface. In this paper, a prototype to provide remote access for Kenzo is presented. This has been accomplished by using Corba technology: clients have been developed both in Java and Common Lisp (the server is always in Common Lisp, being a wrapper of the original Kenzo program). Instead of using one CORBA IDL to encode each data structure, our approach incorporates a generic way of transferring every data structure through XML strings; specifically, by means of an XML extension of MathML. This research should be understood as a first step towards building a distributed computation system for Algebraic Topology.

This paper is a first step towards building a distributed computation system for Algebraic Topology. It is programmed in Common Lisp and this programming language also acts as user interface. In this paper, a prototype to provide remote access for Kenzo is presented. This has been accomplished by using Corba technology: clients have been developed both in Java and Common Lisp (the server is always in Common Lisp, being a wrapper of the original Kenzo program). Instead of using one CORBA IDL to encode each data structure, our approach incorporates a generic way of transferring every data structure through XML strings; specifically, by means of an XML extension of MathML. This research should be understood as a first step towards building a distributed computation system for Algebraic Topology.

---

\* Partially supported by SEUI-MEC, project TIC2002-01626.

... some aspects of symbolic computation systems (especially ez and E), and describe the previous work. Section 2 describes the prototypical remote access tool ez that we have developed, which makes use of COR and distributed presentation of the user programs. The paper ends with a conclusion section and the bibliography.

# 1 Preliminaries

## 1.1 Notions of Algebraic Topology

In this section, some basic concepts of algebraic topology are introduced.

**Definition 1.** A chain complex  $C = (C_p, d_p)$  is a family of  $R$ -modules  $\{C_p\}_{p \in \mathbb{Z}}$  ( $R$  is a ring), with  $R$ -module homomorphisms  $\{d_p\}_{p \in \mathbb{Z}}$  (the differential operators)  $d_p : C_p \rightarrow C_{p-1}$  such that  $d_{p-1} \circ d_p = 0$ .

Every sub-chain complex is formed by free  $\mathbb{Z}$ -modules. The fact that  $C_p$  is a free  $\mathbb{Z}$ -module implies that it is generated, and therefore each element of  $C_p$  can be expressed as a linear combination of the set of its generators  $\sum \lambda_i \sigma_i$ ,  $\lambda_i \in \mathbb{Z}$ . The element  $\sigma_i$  of a basis is called a generator. The product  $\lambda_i \sigma_i$  is called a term or monomial, and a sum of these terms is called a combination.

## 1.2 Symbolic Computation in Algebraic Topology

Here are some symbolic computation systems for algebraic topology, E and ez. Being the most important ones created by Bergeraert and coworkers, and written in C++, they can be used to compute homology groups of finite topological spaces, same as top spaces.

We present here a simple example of computation with ez, which computes the differential of the chain complex (details) applied to the combination  $*4 + 2*$  of degree 2. The result obtained is the combination (of degree 1)  $* - 2*2 + 2*4$ .

```
> (dfr (delta 3) (cmbn 2 3 4 2 6))
(:cmbn 1 (3 . 0) (-2 . 2) (2 . 4))
```

The system allows the computation of more complicated results for the homology groups of chain complexes, etc. of the fundamental problems of algebraic topology. It is possible to obtain easy calculations that are pertinent to topology. We need a tool that makes it easy to get some important features of these systems are

- The use of functional programming techniques in data
- Organization of the data structures. The first one corresponds to the algebraic structures themselves, such as a chain complex. The second one corresponds to the elements of these structures, as for example a combination of a chain complex.

- the have been some results which had never been determined before using either the retract or computation methods
- over the usability of the ez and E presents some barriers since the user interface is Cmm. specific (although the extended programming language), the distributed provide a free distributed

his last aspect of ez as well as the reasons he tried to provide remote access for it, although this is the use of other (better known) languages to construct the user interface for a distributed computing environment. This is a scalable one, that is, a one that would allow the future to extend our remote access system in order to perform collaborative computing on a grid of distributed computers

### 1.3 Previous Work

As a previous work, we considered reconstructing (part of) the system as a programming language over the extended data, especially after here are big differences between this language and Cmm. specific considered a termed step the rebuilt (some fragments of) E. The programming language that suits far from Cmm. specific as a language have implemented the properties to perform computation in algebraic programming and a respect

the next step as to interoperate between them and the Cmm. specific server side distributed change language, we used a meta language that allows a better representation of the format of the considered math 7 and Open math 8, the standards that give representation for mathematical objects (the second one is used to change mathematical objects between symbolic computation systems) we represented some data through a distributed replicated structures we defined our as a set of that of math Open math as it used because complete details are strictly regarded and useful to the application. In our case through this change format the three systems were able to interchange data among them, but not in a distributed way (see 2)

his is as the starting point of this work, considering the development of a remote access for ez, with a client server architecture we would have the ez program on a (server) machine and several clients (with the relevant languages) could access it from distributed computers. The client would be some calculation in algebraic programming, the server would be the process the computation and finally send the result to the client

## 2 Development of the Prototype

some time before our goal as to construct a prototype that allows access to the ez program from distributed machines through programming languages. Our first idea as to try to reuse the system developed previously

and make it work through direct computers we had the exchange language but this was a complete picture because a infrastructure that would allow the interchange between the client and the server as necessary could be CORBA, and indeed are that all species of programs, calculations, transactions, etc. other regardess of programming languages and operating systems, especially used as a calculation of CORBA have a interface routine (a interface description language described in the CORBA specification) for each object, this interface is the same for client and server but the implementation is both described in the direct languages (a previous work (included as a poster in C4 and presented in) we have examined some of our first trials towards this remote access, and some problems found the main problem as to find a suitable exchange the data between client and server. a first attempt, we tried to define a file for each of the structures we wanted to work through the interface framework (i.e. of the simplest data that appear in the program) could be as presented below.

```

module kenzo
interface Monomial
//Attributes
readonly attribute long cffc;
readonly attribute string gnrt;
//Methods
void setMnm(in long cffc, in string gnrt);
long getCffc();
string getGnrt(); ; ;

```

it would be clear a task to construct a file for each type (e.g. (the program defines classes and about 4 types see)) for which this also would have a specific and the rule of CORBA would be complicated. Our present proposal this problem with the combination of CORBA and a natural assignment of string attributes to the object interface which is the representation of the calculation. e.g. function and the result of the calculation this is a general free expression.

the file use to interoperate between client and server should be the attributes object and result. i.e. the representation of the calculation. e.g. function. e.g. a calculator and its result through setObject the client sets the operation and its arguments (.)

the client calls computeXML, the server returns the representation of the operation through getObject, computes the data sets result the representation of the result. a.g. getResult allows the client to recapture the result of the operation.

```

module kenzo
interface XMLObject
//Attributes
readonly attribute string obj;
readonly attribute string result;
//Methods
void setObject(in string obj);
string getObject();
string getResult();
void computeXML(); ; ;
    
```

The use of this file presents some advantages that can be easily implemented. Both the client server and the same interface can be used to exchange attributes of data (pass the leading, get, represent each structure) the use of the interface makes easier the rule of COR, because for each object the file must be both the client and server's descriptors, therefore the administrator of the client can reuse the code he had written in the previous work for the calculation system.

The exchange format used is a dialect, a proprietary set of attributes. The same attributes are used, such as <cn> for integers, for example, the data files are simpler than the self-evident, some other attributes have been created for other algebraic structures (for example, to use <cmb>, for example, as <mmn>). For instance, the combinatorial (of degree 2)  $4 * + 2 *$  is represented as follows:

```

<cmb>                                </mmn>
<dgr>                                <mmn>
<cn> 2 </cn>                          <coef>
</dgr>                                <cn> 2 </cn>
<list>                                </coef>
<mmn>                                <gnr>
<coef>                                <cn> 6 </cn>
<cn> 4 </cn>                          </gnr>
</coef>                                </mmn>
<gnr>                                </list>
<cn> 5 </cn>                          </cmb>
</gnr>
    
```

With the shared interface, the most difficult implementation of the methods of the server is the main task consists in writing some parsers, functions that translate strings to objects and vice versa (some of them written previously for the calculation system). With the implementation, but, the server programs are easier sequence of orders to create the COR object and set to read to be required by the clients.

For the clients' side, as implemented the parsers that has been defined for COMMA is spread a large area, our code for the client programs

use COR to connect with the server and the objects created, the client builds the format of the operation and assigns the object to the `computeXML` of the server and the server gets the representation, translates it to `sp`, computes it and assigns the result of the solution to `getResult` the client gets the result and the translates it to the object.

### 3 Examples

We consider some examples that can be called in the command line and facilitate the communication with the user interface.

As a first example, we consider the multiplication of a combination by a scalar, which should be solved. Once computed, the combination should be shown on the screen.

```
C:\>java JavaClient "n-cmbn" "nil" 3 "cmbn" 2 4 5 2 6
Result: (Cmbn 2 (12 5) (6 6))
```

More complicated operations are those that require the ambient space where the computation is carried out (first order data structures). In the previous example, the operations depend on the characteristics of the ambient space. Therefore, the differential of a combination is defined in the characteristics of the ambient space. Therefore, the user must specify the ambient space, uses functional programming, thus as a difficult to find the representation of this ambient space, we use the tree of the ambient space.

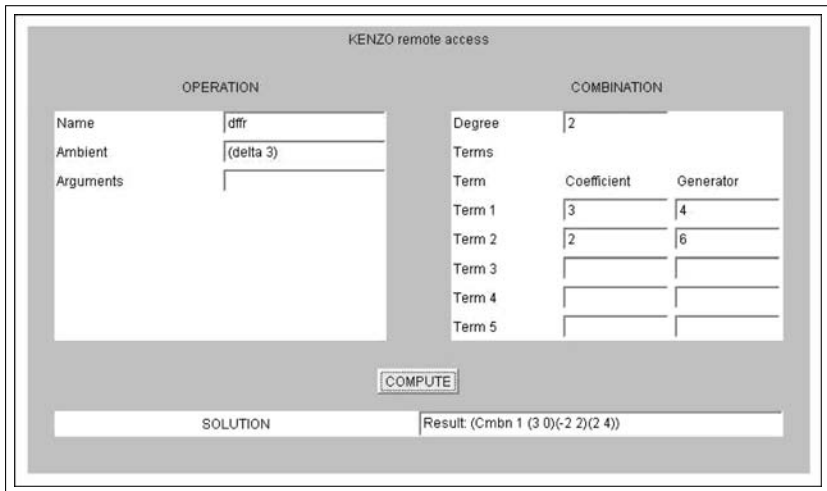


Fig. 1. Example: differential of a combination

cases that generate this case, we compute the direct algebraic combination of the characteristic (delta)

```
C:\>java JavaClient "dffr" "(delta 3)" "cmbn" 2 3 4 2 6
Result: (Cmbn 1 (3 0) (-2 2) (2 4))
```

examples use the appropriate to reduce the parameters separate to be expressed include a message of the applet that corresponds to the direct algebraic combination presented before

## 4 Conclusions and Further Work

This paper has presented a prototype based on CORBA that provides remote access from the client side to the data exchange based on a formal language as a prerequisite for the development of a CORBA object as the use of formal languages for the structure of the client makes easier the implementation and the rule of CORBA. However, through the interface we can use the server program through a change in the architecture for the wrapper of the system that allows making use of the formal CORBA object

It is a small prototype that works through the formal algebraic structures that appear in the design, the programs are totally based on CORBA, a technology designed for computers connected by a network, so our system can be used directly to interoperate between

Obviously, the further short term goals to complete the prototype, transfer the technical data of the client for this task, we have to design the representation for each structure and the parsers to translate them, but the part of CORBA and interfaces the works are read, design, our formal languages, other short term goals to transfer technologies that allow us to work outside a network

The prototype but can be understood as a first step towards a distributed computation system, here some other technologies such as web services (using for instance for the description of the object instead of the object for the exchange of messages) or Grid Computing could be considered. The infrastructure could consist of a separate server services cooperation the same calculation coordinated by a specific web service. Finally, this work shows a first step in this direction, many difficult research questions should be addressed to reach this goal.

## References

1. Alonso, G., Casati, F., Kuno, H., Machiraju, V.: Web Services. Concepts, Architectures and Applications. Springer, 2004.
2. Andrés, M., García, F. J., Pascual, V., Rubio, J.: XML-Based interoperability among symbolic computation systems. In Proceedings WWW/Internet 2003, Vol. II, Iadis Press (2003) 925-929.



3. Andrés, M., Pascual, V., Romero, A., Rubio, J.: Distributed computing in Algebraic Topology: first trials and errors, first programs. In e-proceedings IAMC 2004. <http://www.orcca.on.ca/conferences/iamc2004/abstracts/04002.html>
4. Object Management Group: Common Object Request Broker Architecture (CORBA). <http://www.omg.org>.
5. Rubio, J., Sergeraert, F., Siret, Y.: EAT: Symbolic Software for Effective Homology Computation. Institut Fourier, Grenoble, 1997. <ftp://ftp-fourier.ujf-grenoble.fr/pub/EAT>.
6. Dousson, X., Sergeraert, F., Siret, Y.: The Kenzo program. Institut Fourier, Grenoble, 1999. <http://www-fourier.ujf-grenoble.fr/~sergerar/Kenzo/>.
7. Ausbrooks, R. et al.: Mathematical Markup Language (MathML) Version 2.0. 2003. <http://www.w3.org/TR/2001/REC-MathML2-20010221/>.
8. Caprotti, O., et al (eds): The OpenMath standard. 2000. <http://www.openmath.org/standard>
9. Bray, T. et al. (eds): Extensible Markup Language (XML) 1.0. 2003. <http://www.w3.org/TR/REC-xml/>.

# Symbolic Calculation of the Generalized Inertia Matrix of Robots with a Large Number of Joints

Ramutis Bansevicius<sup>1</sup>, Algimantas Cepulkauskas<sup>2</sup>, Regina Kulvietiene<sup>2</sup>,  
and Genadijus Kulvietis<sup>2</sup>

<sup>1</sup> Kaunas University of Technology,  
Donelaičio 73, Kaunas 3006, Lithuania  
bansevicius@cr.ktu.lt

<sup>2</sup> Vilnius Gediminas Technical University,  
Saulėtekio 11, Vilnius 2040, Lithuania  
{algimantas\_cepulkauskas, regina\_kulvietiene,  
genadijus\_kulvietis}@gama.vtu.lt

**Abstract.** The aim of this paper is to simplify numerical simulation of robots with a large number of joints. Many numerical methods based on different principles of mechanics are developed to obtain the equations that model the dynamic behavior of robots. In this paper, the efficiency of computer algebra application was compared with the most popular methods of forming the generalized inertia matrix of robots. To this end, the computer algebra system was used. Expressions for the generalized inertia matrix of the robots with a large number of joints have been derived, using the computer algebra technique with the following automatic program code generation. As shown in the paper, such an application could drastically reduce the number of floating point product operations, needed for efficient numerical simulation of robots.

## 1 Introduction

Automatic robot systems possess several specific qualities both in mechanical and in control systems. The mechanical systems, a feature specific to manipulators, that are the degrees of freedom are active, equipped by the real actuators, contrast to the electrical mechanisms which models are produced primarily by the scaled kinematic degrees of freedom. The specific quality of such a mechanism is the reasonable structure, ranging from perceptible configurations, from the other kind of building conditions. The further feature typical of spatial mechanisms is reduction of the necessity of the degrees of freedom for producing certain functions. The manipulators and machines form the control standpoints, robot and manipulators systems represent reduction, multivariable, essential, linear automatic control systems. Manipulators as a separate functional component, a computer system, and the control task itself is a dynamic task [4].

The methods that model the dynamic behavior of manipulators are divided into two types of methods that solve the inverse dynamic problem and those that

give the solution to the direct dynamic problem. In the former, the forces exerted by the actuators are obtained algebraically for certain configurations of the manipulator (position, velocity and acceleration). Otherwise, the direct dynamic problem computes the accelerations of the joints of the manipulator since the forces exerted by the actuators are given. This problem is part of the process that must be followed to perform the simulation of the dynamic behavior of the manipulator. This process is completed since are calculated the velocity and position of the joints by means of the process of numerical integration. In which the accelerations of the joints and the trajectory configurations are data input to the problem, the methods may be deduced with respect to the analysis of mechanics. The basis of which mathematical equations are formed taking this as a criterion. The main distinguished methods based on Lagrange Euler's (E), the Euler's (E), Gibbs-Appell's (G) and other equations. The problem of whether the method permits the solution of the direct inverse problem of dynamics may represent another criterion. The direct problem of dynamics refers to determining the motion of the robot for known driving forces (torques), and the inverse problem of dynamics to determining driving forces for the known motion. Clearly, the methods according to the problem of dynamics to be solved are of particular importance. The number of floating point multiplications (operations) added to subtraction required to form a model of the system. Particular criterion to compare the methods is their complexity as a simple ratio from the point of view of the robot's applicability.

The algorithms developed to solve the direct dynamic problem use, regardless of the dynamics problem, from which they are derived, one of the following approaches:

- calculation of the accelerations of the joints by means of the method proposed and solution of a system of simultaneous equations
- recursive calculation of the accelerations of the joints, propagation method and construction of forces throughout the mechanism

The algorithms derived from the methods that use the first approach require the calculation of the generalized inertia matrix and the basic vector. The generalized inertia matrix is usually adopted control schemes, as well as parameter estimation procedures. For this reason, the calculation by means of simple and efficient procedures, is a very beneficial matter. Therefore, the methods of simulation of mechanical systems. The generalized inertia matrix can be obtained through the use of kinematic energy of the mechanical system. With respect to the generalized velocities here, the most computationally efficient algorithms are based on the procedure of the best known method that follows the first approach as proposed by Walker and Orin. This has been developed (using Euler's equations) the method of factorized rigid body dynamics in which the generalized inertia matrix is obtained recursively through a computation  $O(n^2)$  degrees and also has been proposed another method that follows the second approach, based on the calculation of the natural orthogonal decomposition of the manipulator kinematics.

matrices, constraint equations, and a computer  $O(n^3)$ , using a set of equations, and the basic structure.

Other methods, algorithms derived from the methods that use the second approach usually have a computer  $O(n)$ . These algorithms do not require the generalized inertia matrix, and therefore they are simpler to implement. The system must be the best known method, although it is that use the second approach is the articulated body method developed by Featherstone. The number of required algebraic operations is smaller than needed by the computer-aided body method, but for the systems that contain a large number of bodies, the algorithm has some advantages. The Gauss-Jordan method of the generalized inertia matrix is a simple approach. The first step of the procedure is  $O(n)$  direct decomposition, then a computer-aided decomposition is performed.

The computer-aided decomposition methods mentioned above are for the generalized inertia matrix, but compared with computer algebra realization, the computer algebra technique approach, the first method of the generalized inertia matrix for robots is attractive, because it allows the automatic to be pushed before the computer integration of the system. The first order of the equation starts, this approach has been successful. Applied to the inverse dynamics problem of the robot.

## 2 Algorithm for Calculating the Generalized Inertia Matrix

The algorithm for calculating the generalized inertia matrix has been constructed using the checker algorithm [2], based on the equations, that series of computer algebra implementation. The same approach as used to solve the inverse dynamics problem, but first method of the generalized inertia matrix must be considered more carefully, because the matrix must be recalculated at every step of the computer integration of the robot dynamics. The equations of the direct dynamics problem formulated by Uicker et al. [4] are calculated by the first method of the matrix.

$$H(\vec{q})\vec{q} = \vec{P} - \vec{C}(\vec{q}, \vec{q}) + \vec{G}(\vec{q}), \quad (1)$$

where  $H(\vec{q})$  is the generalized inertia matrix,  $\vec{q}, \vec{q}, \vec{q}$  are generalized coordinates, velocities, and accelerations of the robot, respectively.  $\vec{P}$  is the generalized force vector,  $\vec{C}(\vec{q}, \vec{q})$  is the vector of Coriolis and centrifugal effects,  $\vec{G}(\vec{q})$  is the vector of gravitational effects. The basic structure  $(\vec{C}(\vec{q}, \vec{q}) + \vec{G}(\vec{q}))$  could be calculated separately, using the computer algebra approach for the inverse dynamics problem, presented in the previous work.

The elements of the generalized inertia matrix, according to the checker algorithm, could be expressed by the following formula [2],

$$H_{ij} = \sum_{k=1}^j \left[ \text{trace} \left( \frac{\partial W_j}{\partial q_i} J_j \frac{\partial W_k}{\partial q_k} \right) \right], \quad (2)$$

here  $H_{ij}$  are the elements of the generalized inertia matrix  $q_i$  is a generalized coordinate of the  $i$ th link,  $J_j$  is the inertia matrix of the  $j$ th link with respect to the local coordinate system

the transformation matrix  $W_i$  between the  $i$ th local coordinate system and the reference system can be expressed as

$$W_i = A_0^1 A_1^2 \dots A_{i-1}^i, \tag{3}$$

here  $A_{k-1}^k$  is a  $(4 \times 4)$  homogeneous transformation matrix between two local coordinate systems, and it is of the form

$$A_{k-1}^k = \begin{bmatrix} A_{k-1}^k & \vec{b}_{k,k-1} \\ O & I \end{bmatrix}, \tag{4}$$

here  $A_{k-1}^k, \vec{b}_{k,k-1}$  are rotation and translation transformation matrices between two local coordinates  $O$  and  $I$  measured and unit matrices, respectively. Transformation matrices are of the shape

$$A_{k-1}^k = \begin{bmatrix} c \cdot s \cdot q_k & -c \cdot s \cdot \alpha_k \cdot s \cdot q_k & s \cdot \alpha_k \cdot s \cdot q_k \\ s \cdot q_k & c \cdot s \cdot \alpha_k \cdot c \cdot s \cdot q_k & -s \cdot \alpha_k \cdot c \cdot s \cdot q_k \\ & s \cdot \alpha_k & c \cdot s \cdot \alpha_k \end{bmatrix}, \tag{5}$$

$$\vec{b}_{k,k-1} = \begin{bmatrix} a_k \\ d_k \cdot s \cdot \alpha_k \\ d_k \cdot c \cdot s \cdot \alpha_k \end{bmatrix}, \tag{6}$$

here  $\alpha_k, a_k, d_k$  are kinematic parameters of the  $k$ th link

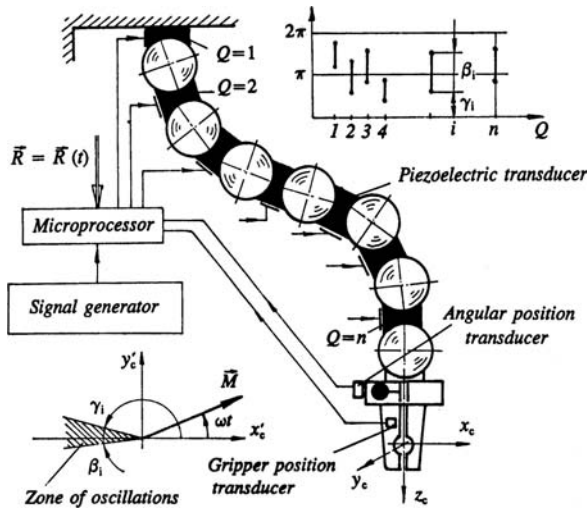


Fig. 1. The scheme of the flexible robot with a large number of joints

the eberb.t th aarge umber f... ts sh... schemat ca...  
 gure her b.t s.c.mp.sed f c... dr ca p.ez.ceram c tra sducers a d  
 spheres, made fr m pass.e mater a... th s case, fr m stee. 4, the c... tact  
 f rce bet ee the spheres a d c... dr ca p.ez.ceram c tra sducers s ma... ta... ed  
 th the a d f perma.e t mag ets... ere the res... a t... sc... at... s f each p.ez.  
 e.ectr c tra sducer are c... tr... ed b... a m cr pr.cess r that s... tches... a d...  
 the h gh freque. c... a d h gh... tage s g... a fr m the s g... a ge. erat r... he phase  
 a d durat... f e.er p use, app. ed t... the e.ectr. des... f tra sducers, are s...  
 chr... zed th the r. tat... f a u ba a ced r. t r, m u ted... the gr pper. f the  
 r. b. t... gh freque. c... res... a t mecha. ca... sc... at... s f u tras... c freque. c  
 cause m t... s (r. tat... s)... a d rect... s a d, at the c... tact z... e, the tur. t.  
 c... t. u. us m t...  
 he e ter. a t rque. ect r, appear... g... the gr pper a d r. tat... g... the p a e  
 perpe. d cu ar t... the gr pper d rect... s ca cu ated b... the c.mputer a gebra  
 appr. ach descr bed... am c s mu at... f th s k... d f e.ber b. ts s a  
 er c. mp. cated pr. b em, because there are t... t pes. f m t... s c... t. u. us  
 a d. brat... 7,

### 3 Computer Algebra Implementation

he meth ds us g... E r G... equat... s are... pr. c p e c. mp. e because f the  
 c. mp. e t t. e. m. ate the c... stra. ts b f rces a d m. me. ts... re. er, the  
 d... t d rect... sh... the a gebra c... a ues... f the f rces a d m. me. ts due t... the  
 act... f actual rs... he E equat... s pr... de a... pp. rtu t... f d rect regard  
 g the equat... s as fu ct... s f the s stem c... tr... puts... e er, the  
 here t u. su tab. t... f app... g... E equat... s es... the eed t... ca cu ate the  
 part a der. at. es (see f r mu a ( )), h ch s... t a tr... a... umer ca. pr. cedure,  
 but er c... e. e. t f r c. mputer a gebra tech. ques

the a g r thm f r aut. mat c ge. erat... f the a a t ca m de... t... be  
 assumed that the parameters f a r. b. t (e. gth, mass, inert a, etc) are k...  
 a d... be treated as c... sta. ts... t c... rd. ates, as e... as the r der. at. es,  
 ... be treated as... depe. de. t. ar abes, e... as s mb. s... s g the c. mputer a  
 gebra tech. que, the cker ah meth d s er c... e. e. t, because t e abes  
 us t... bta... equat... s f m t... c... sed f r m a d ma be app. ed t... s... g  
 ether the d rect r the... erse pr. b em. f d... am cs

he cker ah meth d as mp eme ted us g... R... 8... he sparse  
 matr... tech... g... as used... th s pr. gram t... ach e e the best perf rma ce...  
 rder t... c. mp are the... ar... us resu ts a d a g r thms... t... ts (degrees  
 f freed m)... f the pr. p. sed r. b. t are c... s dered

the e eme ts f the ge. era zed inert a matr...  $H_{ij}$  are ca cu ated... the  
 pr. gram mak... g use f f r mu a (2) the e eme ts f the ge. era zed inert a  
 matr... ha e bee c. mputed f r the d scussed e.ber b. t th degrees f  
 freed m abe c... ta... s the k... emat c parameters f th s r. b. t... e a t  
 arte berg's... tat... 4

**Table 1.**

N	$q_i$	$\alpha_i$	$A_i$	$d_i$
1	$q_1$	0	0	0
2	$q_2$	90°	0	0
3	$q_3$	0	0.04	0
4	$q_4$	-90°	0	0
5	$q_5$	-90°	0	0
6	$q_6$	0	0	0.04

... order to avoid the numerical computation of the trigonometric functions a substitution as applied  $S_i = \sin q_i, C_i = \cos q_i$

The fragment of a Fortran calculation performed for the generalized perturbation matrix of the eberb.t.b. the OR program, illustrated in Figure 2 (the expressions of the coefficients should be generated automatically)

The perturbation (i.e. the symmetric part of the generalized perturbation matrix) have been calculated. It should be noted that if they are equal to zero (specia

OR procedure generates the ORR subroutines from the obtained analytical expressions of the generalized perturbation matrix, 8) the code of the first generated subroutines is added to the program as a subcode. The

```

SUBROUTINE robo01(A,O)
IMPLICIT REAL(A-Z)
DIMENSION A(1),O(1)
S1 =A(1)
C1 =A(2)
.....
C6 =A(12)
O(61)=S5*C4
O(63)=S6*S4
O(66)=C5*S4
O(228)=C6*C5
O(62)=O(228)*C4
END
SUBROUTINE robo(A,B)
DIMENSION A(1),B(1),O( 230)
CALL robo01(A,O)
Y1=+.1296E-3*O(1)
Y2=-.9964E-4*O(2)
.....
B(1)=+.8326E-4+Y1+Y2+Y3+Y4+Y5+Y6+Y7+Y8+Y9+Y10+Y11
*+Y12+Y13+Y14+Y15+Y16+Y17+Y18+Y19+Y20+Y21+Y22+Y23
*+Y24+Y25+Y26+Y27+Y28+Y29+Y30+Y31+Y32+Y33+Y34+Y35
.....
END
    
```

**Fig. 2.** Fragment of the code of two subroutines for numerical simulation

the pressions for the matrices has detected a form, mass sorted according to the order of the matrix, multiplication reduces the number of operations, multiplication, since the second order of the generated subroutines, calculation of the symmetric members, included in the expressions, the elements of the matrices, the generated subroutines can be immediately computed and directly used for numerical calculation.

The number of operations, product, operations, required from the generalized inertia matrix of the robot, the checker algorithm, numerical dependence  $n^4$  (number of degrees of freedom) and, conversely, the recursive methods based on Euler's equations, mass dependence, the number of degrees of freedom, the usage of the computer algebra technique, there emerge some deficiencies, the checker algorithm, the expressions for the elements of the generalized inertia matrix are found, condensed form, meanwhile, there are known algorithms, recursive equations, his fact indicates that, the numerical implementation, especially and therefore this method is suitable for the direct dynamics problem, the condensed figure 2 contains 44 operations, products and 8 sums, the computation, a comparison of the proposed approach, comparison, that of the most efficient algorithms, so far, as shown, table 2.

Table 2.

Authors	Principle	Products ( $n = 6$ )	Sums ( $n = 6$ )
Walker and Orin [9]	N-E	$12n^2 + 56n! - 127(741)$	$7n^2! + 67n! - 156(598)$
Angeles and Ma [1]	N-E	$n^3! + 17n^2! - 121n! + 8(710)$	$n^3! + 14n^2! - 116n! - 1 + 5(629)$
Mata et al. [11]	G-A	$11.5n^2! + 19.5n! - 149(482)$	$8.5n^2! + 31.5n! - 169(426)$
This work	L-E	144	186

Some remarks could be made to the previous results, first of all, computer algebra systems, rather efficient, with a large number of short expressions, which enables a effective simplification, of these expressions during automatic computation, it appears that, although, numerical methods are developed especially, and numerical differentiation, and most of them are recursive, which is a convenient for automatic computation, however, the calculation of derivatives, is a very simple procedure for computer algebra systems.

### 4 Conclusions

The expressions for the generalized inertia matrix of the robot, with a large number of terms, has been obtained, using the checker algorithm, based on algebraic Euler's equations, and realized by the computer algebra technique, the computation, a comparison of the proposed approach, comparison, that of the most efficient algorithms, so far.

The proposed automatic implementation, of checker algorithm's method, drastically reduces the number of operations, product, operations, particular for the robot, with



a large number of joints this approach performs the efficient simulation of dynamic behaviour of the robot

## References

1. Angeles, J., Ma, O.: Dynamic simulation of  $n$ -axis serial robotic manipulators using a natural orthogonal complement, *Int. J. Rob. Res.* 7 (5) (1988) 32–37
2. Balafoutis, C.A., Patel, R.V.: *Dynamic Analysis of Robot Manipulators: A Cartesian Tensor Approach*, Kluwer Academic Press, Boston (1991)
3. Bansevicius, R., Cepulkauskas, A., Kulvietiene, R., Kulvietis, G.: *Computer Algebra for Real-Time Dynamics of Robots with Large Number of Joints*. Lecture Notes in Computer Science, Vol. 3039. Springer-Verlag, Berlin Heidelberg New York (2004) 278–285
4. Bansevicius R., Parkin R., Jebb, A., Knight, J.: Piezomechanics as a Sub-System of Mechatronics: Present State of the Art, Problems, Future Developments. *IEEE Transactions on Industrial Electronics*, vol. 43, (1) (1996) 23–30
5. Barauskas, R., Bansevicius, R., Kulvietis, G., Ragulskis, K.: *Vibromotors for Precision Microrobots*. Hemisphere Publishing Corp., USA (1988).
6. Featherstone, R., Orin, D. E.: Robot dynamics: equations and algorithms. *Proceedings of the 2000 IEEE International Conference on Robotics and Automation*, San Francisco (2000) 826–834
7. Knani J.: Dynamic modelling of flexible robotic mechanisms and adaptive robust control of trajectory computer simulation. *Applied Mathematical Modelling*, Vol. 26. (12) (2002) 1113–1124
8. Kulvietiene, R., Kulvietis, G.: *Analytical Computation Using Microcomputers*. LUSTI, Vilnius (1989)
9. Mata, V., Provenzano, S., Valero, F., Cuadrado, J., I.: An  $O(n)$  algorithm for solving the inverse dynamic problem in robots by using the Gibbs–Appell formulation, *Proceedings of Tenth World Congress on Theory of Machines and Mechanisms*, Oulu, Finland, (1999), 1208–1215
10. Mata, V., Provenzano, S., Valero, F., Cuadrado, J., I.: Serial-robot dynamics algorithms for moderately large numbers of joints. *Mechanism and Machine Theory*, 37 (2002) 739–755
11. Rovetta, A., Kulvietis, G.: *Lo sviluppo di software per il controllo dinamico di robot industriali*. Dipartimento di Meccanica, Politecnico di Milano, Milano (1986)
12. Saha, S.K.: A decomposition of the manipulator inertia matrix, *IEEE Trans. Rob. Autom.* 13 (2) (1997) 301–304
13. Surdhar, J., S., White, A., S.: A parallel fuzzy-controlled flexible manipulator using optical tip feedback. *Robotics and Computer-Integrated Manufacturing*, Vol. 19 (3) (2003) 273–282
14. Vucobratovic, K., M., Kircanski M., N.: *Real-time Dynamics of Manipulation Robots*, Springer-Verlag, Berlin Heidelberg New York (1985)
15. Walker, M.W., Orin, D.E.: Efficient dynamic computer simulation of robotic mechanisms, *J. Dyn. Syst. Meas. Control* 104 (1982) 205–211

# Revisiting Some Control Schemes for Chaotic Synchronization with Mathematica

J. Andres Iglesias<sup>1,2,\*</sup> and J. Kem Ga. ez<sup>2</sup>

<sup>1</sup> Department of Computer Science, University of Tsukuba,  
Laboratory of Advanced Research, Building B, Room # 1025,  
Kaede Dori, 305-8573, Tsukuba, Japan

<sup>2</sup> Department of Applied Mathematics and Computational Sciences,  
University of Cantabria, Avda. de los Castros, s/n  
E-39005, Santander, Spain  
iglesias@unican.es  
uc8031@alumnos.unican.es  
<http://personales.unican.es/iglesias>

**Abstract.** An interesting topic in dynamical systems is *chaotic synchronization*, that is, the possibility to synchronize the behavior of several chaotic systems. Among the variety of available schemes, those dealing with some sort of control mechanisms have received increasing attention in recent years. In this work, we applied the program *Mathematica* to study the control strategies of chaotic synchronization. In our opinion, the powerful symbolic, numeric and graphic capabilities of *Mathematica* make this software an ideal tool to analyze the problem on hand.

## 1 Introduction

One of the most interesting issues in dynamical systems is the so called *chaotic synchronization*, that is, the possibility to synchronize the behavior of several chaotic systems. Among the different schemes for chaotic synchronization, those based on the application of some kind of control have received increasing attention during the last few years. In this paper, we analyze some control strategies for chaotic synchronization, using the program *Mathematica*. One of the most important advantages of *Mathematica* is the integration of the powerful symbolic, numeric and graphic capabilities. This is a useful framework whose features are especially useful here because the equations describing the dynamics of the chaotic systems are often hard to solve, and hence, an adequate combination of numeric and symbolic procedures is usually required in order to analyze their behavior. The reader is referred to [8, 2] for previous works about the application of *Mathematica* to the analysis of chaotic systems.

---

\* Corresponding author.

The structure of the paper is as follows. Section 2 describes some control schemes for chaotic systems synchronization. The authors have been organized for carrying out the subject's detailed theoretical methods based on designing a controller and theoretical stabilization of the error dynamics. Also, the paper concludes with the conclusions and some further remarks.

## 2 Control Schemes for Chaotic Synchronization

Recently, it has been shown that chaotic systems can be synchronized by appropriate schemes (Kobayashi et al., 1992, 1994, 1997). For example, (2) presents the synchronization of a couple of Lorenz systems by using active control. Here, a 4 controller is required for the synchronization of the systems respectively. The authors tried to answer the following question: *given a chaotic system and an arbitrary reference signal, is it possible to design a controller based on this reference signal so that the output of the chaotic system follows this signal asymptotically?* As remarked by the authors, the synchronization of chaotic systems belongs to this class of problems. It is enough to consider the output of the chaotic system as the reference signal. In fact, the approach is more general since the reference signal could be the output of a chaotic system but also another (linear or nonlinear) signal.

### 2.1 Designing a Controller for Chaotic Synchronization

Let us consider a chaotic system of the form

$$\begin{cases} \dot{x}(t) = y(t) \\ \dot{y}(t) = f(x(t), y(t), t) + u(t) \end{cases} \quad (1)$$

where  $f(x(t), y(t), t)$  is a nonlinear function of  $x, y$  and  $t$  and  $u(t)$  is the controller to be designed. If  $z(t)$  is the reference signal to be followed by the system, the proposed controller function  $u(t)$  takes the form

$$u(t) = -f(x(t), y(t), t) - \alpha_1 x(t) - \alpha_2 y(t) + \ddot{z}(t) + \alpha_2 \dot{z}(t) + \alpha_1 z(t) \quad (2)$$

It can be proved (see for details) that the error between the output of the chaotic system and the reference signal converges to zero as long as the constants  $\alpha_1$  and  $\alpha_2$  are both greater than zero. For a detailed treatment, it is important to remark that this controller function  $u(t)$  does not contain any information about the system structure which generates the signal  $z(t)$ . Since, in a consequence, this scheme can be applied to a wider variety of situations, such as, for instance, in the implementation of a control system.

To illustrate this method, let us consider the following system given by the couple of differential equations

```
In[1] := Duff1={x'[t]==y[t],y'[t]==1.8 x[t]-0.1 y[t]-
        x[t]^3+1.1 Cos[0.4 t],x[0]==0,y[0]==2}
```

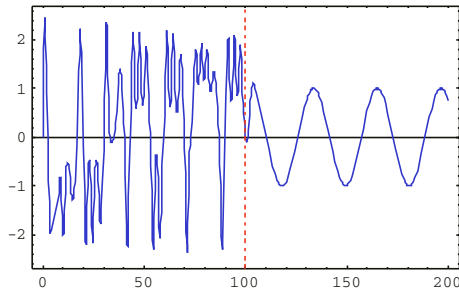


**Fig. 1.** Synchronization of a Duffing system to a driving signal given by  $z(t) = \sin(0.2t)$ . The figure shows the temporal series of the  $x$  variable of such a system before and after the application of the synchronization procedure (indicated by the vertical dashed line)

The chaotic behavior of this system is depicted in figure 1 (to the left of the dashed line)

```
In[2]:= NDSolve[duf1,{x,y},{t,0,100},MaxSteps->20000]//Flatten
In[3]:= x1[t_]=x[t] /. %;
```

... we would like to force the system to follow the sinusoidal signal  $z(t) = \sin(0.2t)$ . To accomplish this, we apply the control function  $u(t)$ , as follows

```
In[4]:= z[t_]:=Sin[0.2 t];
In[5]:= u[t_]==-1.8 x[t]+0.1 y[t]+x[t]^3-1.1 Cos[0.4 t]-x[t]-y[t]+
z'[t]+z[t];
```

According to (1), for this particular choice of the reference signal, we consider the system

```
In[6]:= duf2={x'[t]==y[t],y'[t]==1.8 x[t]-0.1 y[t]-x[t]^3+
1.1 Cos[0.4 t]+u[t],x[100]==0.044674,y[100]==-0.61367}
```

here the initial conditions are obtained from the previous integration of the system duf1. We integrate duf2 and display the resulting temporal series for the  $x$  variable

```
In[7]:= NDSolve[duf2,{x,y},{t,100,200},MaxSteps->20000]//Flatten;
In[8]:= sx[t_]:=If[0<=t<=100,x1[t],x[t] /. %];
In[9]:= Show[{Plot[sx[t],{t,0,200},PlotStyle->RGBColor[0,0,1],
PlotRange->{-2.7, 2.7},Frame->True],
Graphics[{RGBColor[1,0,0],Dashing[{0.01}],
Line[{{100,-2.7},{100,2.7}}]}]}
```

*Out* See Figure

Figure 1 shows the evolution of the variable  $x$  of the Duffing system before and after the application of the control function (indicated by the vertical dashed line). From this figure, the good performance of this synchronization method between the chaotic system and the driving signal becomes clear.

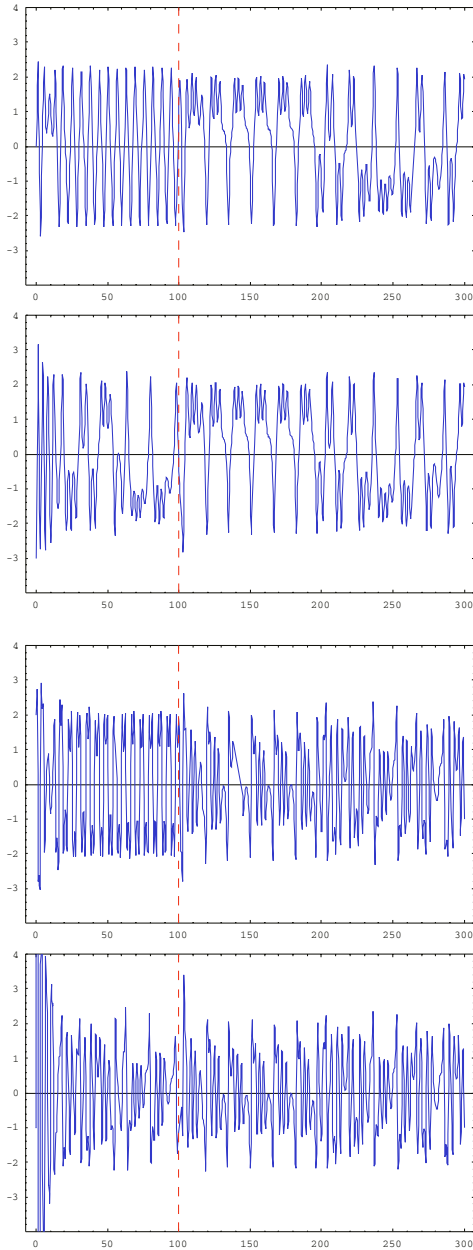


**Fig. 2.** Synchronization of two Duffing systems using active control in which the signal of the drive acts as the driving signal for the response: temporal series of the drive and response systems for the variables  $x$  (top) and  $y$  (bottom) respectively

As remarked above, this method is useful to achieve chaotic synchronization by simply considering the output of a system (the drive) as the reference signal.

$z(t)$  to be selected to the response of the electronic circuit. The detailed calculation (since the average value of the parameter values) chaotic systems

```
In[10]:= duf3={x3'[t]==y3[t],y3'[t]==1.8 x3[t]-0.1 y3[t]-
          x3[t]^3+1.1 Cos[t],x3[0]==0,y3[0]==2};
```

```
In[11]:= duf4={x4'[t]==y4[t],y4'[t]==1.8 x4[t]-0.1 y4[t]-
          x4[t]^3+1.1 Cos[0.4 t],x4[0]==-3,y4[0]==-1};
```

Integrating these equations with the parameter values, we can observe a chaotic behavior for both variables  $x$  and  $y$  as shown in Figure 2 (the left of the dashed line).

```
In[12]:= rul1=NDSolve[Union[duf3,duf4],{x3,y3,x4,y4},{t,0,100},
          MaxSteps->20000]//Flatten;
```

Therefore, the system is free from the output of the drive system  $z(t) = x_3(t)$  because, after  $t = 100$ , the method is applied through  $u(t)$  given by

```
In[13]:= u[t_]==-1.8 x4[t]+0.1 y4[t]+x4[t]^3-1.1 Cos[0.4 t]-
          x4[t]-y4[t]+x3''[t]+x3'[t]+x3[t];
```

so that the second system becomes

```
In[14]:= duf4={x4'[t]==y4[t],y4'[t]==1.8 x4[t]-0.1 y4[t]-x4[t]^3+
          1.1 Cos[0.4 t]+u[t],x4[100]==-0.429856,y4[100]==-1.73792};
```

Therefore, we integrate the resulting system and display the temporal series for the variables  $x$  and  $y$  of the drive and response systems, as shown in Figure 2.

```
In[15]:= rul2=NDSolve[Union[duf3,duf4],{x3,y3,x4,y4},{t,100,300},
          MaxSteps->30000]//Flatten;
```

```
In[16]:= {sx3[t_],sx4[t_],sy3[t_],sy4[t_]}=If[0<=t<=100,
          # /. rul1,# /. rul2]& /@ {x3[t],x4[t],y3[t],y4[t]};
```

```
In[17]:= Show[Plot[#, {t,0,300},PlotStyle->RGBColor[1,0,0],
          PlotRange->{-4,4},Frame->True],
          Graphics[{RGBColor[1,0,0],Dashing[{0.02}],
          Line[{{100,-4},{100,4}}]}]}& /@
          {sx3[t],sx4[t],sy3[t],sy4[t]}
```

Out 7 See Figure 2

## 2.2 Chaotic Synchronization via Stabilization of the Error Dynamics

In this section, we present a method that allows synchronization of drive response circuits that display chaotic behavior. The error dynamics (that is, circuit equations) are presented in the key idea of the method. The circuit equations are combined at the drive and the response subsystems as the error dynamics. The synchronization is achieved with the

response system acts as a chaos suppressor method stabilizing the dynamics of this system. Hence, the complete associated with the driver suppresses the behavior of the driver to the stabilized response system, giving birth to systems

Section 7 a strategy to synchronize structured driver chaotic systems (auffigadingader systems) as designed by following the steps first, the problem of chaos synchronization is seen as a stabilization problem, here the goal is to stabilize the dynamics of the synchronizer, hence, the chaos suppressor problem is solved through a robust asymptotic controller, which is based on geometric control. The robust estimate the differences between the models, the used a linear feedback controller, which can be interpreted as a state feedback linearized system. Thus, the controller allows the emergence of a synchronization system to be absorbed and that the systems behave as a synchronizer.

Similarly, as proposed for a couple of Rossler systems and a chaotic synchronizer, a linear chaotic electronic circuits are amplified, the authors considered a discrete controller to be applied to the second system of a couple driver response order to get synchronization. Hence, with this feedback controller, stabilize the asymptotic stability of the zero solution of the error system (i.e., the differences between the driver and the response) the performance of this method can be illustrated by considering the Rossler model, described by a set of three differential equations. The driver system is given by

```
In[18] := ros1={x1'[t]==-y1[t]-z1[t],y1'[t]==x1[t]+0.2 y1[t],
           z1'[t]==0.2+z1[t](x1[t]-5.7),x1[0]==0.5,y1[0]==1,z1[0]==1.5};
```

For the second system, we introduce three controller functions  $u_1(t)$ ,  $u_2(t)$  and  $u_3(t)$  as

```
In[19] := ros2={x2'[t]==-y2[t]-z2[t]+u1[t],y2'[t]==x2[t]+0.2 y2[t]+
                u2[t],z2'[t]==0.2+z2[t](x2[t]-5.7)+u3[t],
                x1[0]==2.5,y1[0]==2,z1[0]==2.5};
```

To determine these functions, the authors considered the error system as the difference between both Rossler systems and defined the controller functions as

```
In[20] := {u1[t],u2[t],u3[t]}={V1[t],V2[t],x1[t]z1[t]-x2[t]z2[t]+V3[t]};
```

here are main possible choices for these controller functions  $V_1(t)$ ,  $V_2(t)$  and  $V_3(t)$  are amplitude characteristics

```
In[21] := 
$$\begin{pmatrix} V_1 t \\ V_2 t \\ V_3 t \end{pmatrix} = \begin{pmatrix} -1 & 1 & 1 \\ -1 & -1.2 & 0 \\ 0 & 0 & 4.7 \end{pmatrix} \begin{pmatrix} x_2 t - x_1 t \\ y_2 t - y_1 t \\ z_2 t - z_1 t \end{pmatrix};$$

```

With this choice, the difference system becomes

```
In[22] := rhs[Equal[a_,b_]]:=b;
In[23] := {sys2,sys1}=rhs/@ #& /@ (Take[#,3]& /@{ros2,ros1});
```

```
In[24]:= sys2-sys1 //Simplify
```

$$Out\ 24 \quad - \begin{pmatrix} x_2 t - x_1 t \\ y_2 t - y_1 t \\ z_2 t - z_1 t \end{pmatrix}$$

These characterstic matrices  $-I$ , here  $I$  is the diagonal matrix. Here, the discrete system has asymptotically negative eigenvalues, implying that the error converges to zero as time  $t$  goes to infinity and hence the synchronization of the two Rossler systems is achieved (see [1] for details).

### 3 Conclusions and Further Remarks

These previous proposals can be better understood as particular cases of a more general theory for which controlled synchronization is seen as the procedure to find, given both the transmitter (or driver) and the receiver (or response) as well as the controlled output function, a suitable mechanical controller, the response system such that the driver and response are asymptotically synchronized. Generally, this problem can be described as follows: given a transmitter  $x' = f(x)$  with output  $y = g(x)$  and a receiver  $\bar{x}' = h(\bar{x}, u)$  systems, here we assume that both  $x$  and  $\bar{x}$  are  $n$ -dimensional vectors, and  $u$  is the unknown controller function, the goal is to obtain this controller function such that  $x$  and  $\bar{x}$  are asymptotically synchronized.

Of course, there are many different approaches to this problem, most based on the use of a feedback controller of the form  $u = \theta(\bar{x}, y)$  here  $\theta$  is a smooth function depending on the receiver  $\bar{x}$  and the output of the transmitter  $y$ . However, it must be said that this problem of finding a suitable output feedback controller is a challenging synchronization between the transmitter and the receiver, generally, a very difficult (or even impossible) task and, in particular, examples (as these shown above) have been described in the literature. Other interesting references on controlled synchronization can be found in [2, 3, 4, 5, 6, 7].

These comments have been implemented in Mathematica version 4. The software capabilities and the performance of the Mathematica functions are programmed have been effectively used to make the programs shorter and more efficient. Our previous Mathematica software is useful to take advantage of the interesting problem of chaotic synchronization through control schemes. A user friendly and easy-to-use

### References

1. Agiza, H.N., Yassen, M.T.: Synchronization of Rossler and Chen chaotic dynamical systems using active control, *Phys. Lett. A* **278** (2001) 191-197
2. Bai, E.W., Lonngren, K.E.: Synchronization of two Lorenz systems using active control, *Chaos, Solitons and Fractals* **8** (1997) 51-58
3. Bai, E.W., Lonngren, K.E.: Synchronization and control of chaotic systems, *Chaos, Solitons and Fractals* **10** (1999) 1571-1575



4. Bai, E.W., Lonngren, K.E.: A controller for the logistic equations, *Chaos, Solitons and Fractals* **12** (2001) 609-611
5. Bai, E.W., Lonngren, K.E., Sprott, J.C.: On the synchronization of a class of electronic circuits that exhibit chaos, *Chaos, Solitons and Fractals* **13** (1999) 1515-1521
6. Blekhman, I.I., Fradkov, A.L., Nijmeijer, H., Yu, A.: On self-synchronization and controlled synchronization, *Syst. Contr. Lett.* **31** (1997) 299-305
7. Femat, R., Solis, G.: On the chaos synchronization phenomena, *Phys. Lett. A* **262** (1999) 50-60
8. Gutiérrez, J.M., Iglesias, A.: A Mathematica package for the analysis and control of chaos in nonlinear systems, *Computers in Physics* **12**(6) (1998) 608-619
9. Gutiérrez, J.M., Iglesias, A.: Synchronizing chaotic systems with positive conditional Lyapunov exponents by using convex combinations of the drive and response systems, *Phys. Lett. A* **239**(3) (1998) 174-180
10. Huijberts, H.J.C., Nijmeijer, H., Willems, R.: Regulation and controlled synchronization for complex dynamical systems, *Int. J. Robust Nonlinear Contr.* **10** (2000) 363-377
11. Iglesias, A., Gutiérrez, J.M., Ansótegui, D., Carnicero, M.A.: Transmission of digital signals by chaotic synchronization. Application to secure communications, In: Keranen, V., Mitic, P., Hietamaki, A. (Eds.) *Innovation in Mathematics. Proceedings of the Second International Mathematica Symposium-IMS'97*, Computational Mechanics Publications, Southampton, England (1997) 239-246
12. Iglesias, A., Gálvez, A.: Analyzing the synchronization of chaotic dynamical systems with Mathematica: Parts I-II. *Computational Science and its Applications-ICCSA'2005. Lecture Notes in Computer Science* (2005) (*in press*)
13. Maeder, R.: *Programming in Mathematica*, Second Edition, Addison-Wesley, Redwood City, CA (1991)
14. Nijmeijer, H.: A dynamical control view on synchronization, *Physica D* **154** (2001) 219-228
15. Pecora, L.M., Carroll, T.L.: Synchronization in chaotic systems, *Phys. Rev. Lett.* **64** (1990) 821-823
16. Wolfram, S.: *The Mathematica Book*, Fourth Edition, Wolfram Media, Champaign, IL & Cambridge University Press, Cambridge (1999)
17. Yu, A., Pogromsky, Nijmeijer, H.: Observer based robust synchronization of dynamical systems, *Int. J. of Bifurc. and Chaos* **8** (1998) 2243-2254

# Three Brick Method of the Partial Fraction Decomposition of Some Type of Rational Expression

Anna Maria R. Witula

Institute of Mathematics, Silesian University of Technology, Kaszubska 23,  
44-100 Gliwice, Poland  
{d.slota, rwitula}@polsl.pl

**Abstract.** The purpose of this paper is to present a new method of the partial fraction decomposition, the so called "three brick method". The method is of algebraic nature and it is based on simple reduction tasks. The discussed algorithm has been successfully implemented in Mathematica software package.

## 1 Introduction

The partial fraction decomposition is a very important type of symbolic and computer algebraic mathematics. The inverse Laplace transform – the residue method – which is commonly applied to find the inverse Laplace transform, although originally derived from the residue calculus, is usually derived from the computer algebra (especially if the calculations are finished automatically). The latter method should be the backbone of the whole process of calculating the inverse Laplace transform – thus, a natural method of the decomposition of rational functions. The partial fraction decomposition has a considerable interest [2].

In the paper a new method of the partial fraction decomposition, called here – three brick method, is discussed. This is a simple and efficient method of the decomposition of rational functions.

$$W(s) = \frac{as + b}{(s^2 + \alpha s + \beta)(s^2 + \gamma s + \delta)} \quad (1)$$

The partial fraction decomposition method of pure algebraic nature and is based on simple reduction tasks.

## 2 Three Brick Method

Let  $\alpha, \beta, \gamma, \delta \in \mathbb{C}$ ,  $\alpha \neq \gamma$ . The case of  $\alpha \neq \gamma$  is presented in formula (4) and is put

$$M_1 = s^2 + \alpha s + \beta, \quad M_2 = s^2 + \gamma s + \delta \quad (2)$$

and  $M = M_1 M_2$  the method of decomposition of a rational function  $W(s)$  into the form of  $(a, b \in \mathbb{C})$

$$\frac{as + b}{M} = \frac{As + B}{M_1} + \frac{Cs + D}{M_2}, \quad (1)$$

is described below.

First, the following system of equations  $(I_{eq}, II_{eq}, III_{eq})$  is created

$$\begin{cases} I_{eq} & \frac{\quad}{M_1} - \frac{\quad}{M_2} = \frac{M_2 - M_1}{M} \frac{(\gamma - \alpha)s + \delta - \beta}{M}, \\ II_{eq} & \frac{s}{M_1} - \frac{s}{M_2} = \frac{s(M_2 - M_1)}{M} \frac{(\gamma - \alpha)s^2 + (\delta - \beta)s}{M}, \\ III_{eq} & \frac{2}{M_1} - \frac{2}{M_2} = \frac{2M_2 - M_1}{M} \frac{s^2 + (2\gamma - \alpha)s + 2\delta - \beta}{M}. \end{cases} \quad (4)$$

In the next step, to eliminate the sums, calculate  $s^2$  from the numerators of the fractions at the right side of equations  $II_{eq}$  and  $III_{eq}$ , thus the fourth equation is generated  $(IV_{eq} = II_{eq} - (\gamma - \alpha)III_{eq})$

$$\frac{s - 2\gamma + 2\alpha}{M_1} - \frac{s - \gamma + \alpha}{M_2} = \frac{\delta - \beta - (\gamma - \alpha)(2\gamma - \alpha)s - (\gamma - \alpha)(2\delta - \beta)}{M}. \quad (5)$$

In the next steps of the algorithm, eliminate the elements of the sums calculate  $s$  and the free term from the numerators of the fractions at the right side of equations  $I_{eq}$  and  $IV_{eq}$   $V_{eq} = (2\gamma - \alpha - \frac{\delta - \beta}{\gamma - \alpha})I_{eq} + IV_{eq}$

$$\frac{s + \alpha - \frac{\delta - \beta}{\gamma - \alpha}}{M_1} - \frac{s + \gamma - \frac{\delta - \beta}{\gamma - \alpha}}{M_2} = \frac{\alpha\delta - \beta\gamma - \frac{(\delta - \beta)^2}{\gamma - \alpha}}{M} \quad (6)$$

and  $VI_{eq} = (2\delta - \beta)I_{eq} + \frac{\delta - \beta}{\gamma - \alpha}IV_{eq}$

$$\frac{\frac{\delta - \beta}{\gamma - \alpha}s + \beta}{M_1} - \frac{\frac{\delta - \beta}{\gamma - \alpha}s + \delta}{M_2} = \frac{(-\alpha\delta + \beta\gamma + \frac{(\delta - \beta)^2}{\gamma - \alpha})s}{M}. \quad (7)$$

hence, the determinant  $\frac{1}{k}(-aVI_{eq} + bV_{eq})$ , here

$$k = \begin{vmatrix} \alpha & \beta \\ \gamma & \delta \end{vmatrix} - \frac{(\delta - \beta)^2}{\gamma - \alpha}, \quad (8)$$

the following decomposition is derived

$$\frac{as + b}{M} = \frac{1}{k} \left( \frac{\left( (b - a\frac{\delta - \beta}{\gamma - \alpha})s + b\alpha - a\beta - b\frac{\delta - \beta}{\gamma - \alpha} \right)}{M_1} + \frac{\left( (b - a\frac{\delta - \beta}{\gamma - \alpha})s + b\gamma - a\delta - b\frac{\delta - \beta}{\gamma - \alpha} \right)}{M_2} \right). \quad (9)$$

*Remark.* The following equation holds

$$k \Leftrightarrow \delta\alpha^2 - \gamma(\delta + \beta)\alpha + \gamma^2\beta + (\delta - \beta)^2, \quad (1)$$

currently, the discriminant of the last polynomial of the second order, considered for variable  $\alpha$  (assuming that  $\delta \neq 0$ ) has the following form

$$\Delta_\alpha = (\gamma^2 - 4\delta)(\delta - \beta)^2. \quad (2)$$

According to  $\Delta_\alpha < 0$ , and, therefore, the discriminant of the trinomial  $M_2$  is negative and for  $\beta / \delta$  the case of  $\beta < \delta$  is expressed formally as

$$\frac{1}{(s^2 + \alpha s + \beta)(s^2 + \gamma s + \beta)} = \frac{1}{\beta(\alpha - \gamma)} \left( \frac{s + \alpha}{s^2 + \alpha s + \beta} - \frac{s + \gamma}{s^2 + \gamma s + \beta} \right), \quad (2)$$

$$\frac{s}{(s^2 + \alpha s + \beta)(s^2 + \gamma s + \beta)} = \frac{1}{\gamma - \alpha} \left( \frac{1}{s^2 + \alpha s + \beta} - \frac{1}{s^2 + \gamma s + \beta} \right). \quad (3)$$

for  $\alpha < \gamma$  (assuming that  $M_1 / M_2$ ) the following decomposition is derived

$$\frac{as + b}{(s^2 + \alpha s + \beta)(s^2 + \alpha s + \delta)} = \frac{1}{\delta - \beta} \left( \frac{as + b}{s^2 + \alpha s + \beta} - \frac{as + b}{s^2 + \alpha s + \delta} \right). \quad (4)$$

### 3 Algorithm in Mathematica

The algorithm discussed in the previous section can be implemented in Mathematica. The summands collected with trinomials  $M_1$  and  $M_2$  shall be expressed separately, that is, so that the transformations are performed separately. Both fractions are started with defining the trinomials

*In[1] :=* m1 = s<sup>2</sup> + α s + β; m2 = s<sup>2</sup> + γ s + δ;

let us form three equations (*I<sub>eq</sub>*, *II<sub>eq</sub>*, *III<sub>eq</sub>*)

*In[2] :=* eq1 = {1/m1, -1/m2};

eq2 = {s/m1, -s/m2};

eq3 = {2/m1, -1/m2};

the summands collected regarding  $s^2$  are eliminated (*IV<sub>eq</sub>*)

*In[3] :=* eq4 = Simplify[eq2 - (γ - α)eq3]

*Out[3] =* {  $\frac{s + 2\alpha - 2\gamma}{s^2 + s\alpha + \beta}$ ,  $-\frac{s + \alpha - \gamma}{s^2 + s\gamma + \delta}$  }

the rest summands collected regarding  $s$  are eliminated (*V<sub>eq</sub>*)

*In[4] :=* eq5 = Simplify[  $(2\gamma - \alpha - \frac{\delta - \beta}{\gamma - \alpha})$  eq1 + eq4]

*Out[4] =* {  $\frac{\alpha^2 - \beta + s(\alpha - \gamma) - \alpha\gamma + \delta}{(s^2 + s\alpha + \beta)(\alpha - \gamma)}$ ,  $\frac{\beta - \alpha\gamma + \gamma^2 + s(-\alpha + \gamma) - \delta}{(\alpha - \gamma)(s^2 + s\gamma + \delta)}$  }

he e. m. at . . . f the free term ( $VI_{eq}$ )

$$In[5] := eq6 = Simplify[(2\delta - \beta)eq1 + \left(\frac{\delta - \beta}{\gamma - \alpha}\right)eq4]$$

$$Out[5] = \left\{ \frac{\beta(\alpha - \gamma) + s(\beta - \delta)}{(s^2 + s\alpha + \beta)(\alpha - \gamma)}, \frac{(-\alpha + \gamma)\delta + s(-\beta + \delta)}{(\alpha - \gamma)(s^2 + s\gamma + \delta)} \right\}$$

he defi. t . . . f parameter  $k$

$$In[6] := k = Det\left[\begin{pmatrix} \alpha & \beta \\ \gamma & \delta \end{pmatrix}\right] - \frac{(\delta - \beta)^2}{\gamma - \alpha};$$

. a. dec. mp. s t . .

$$In[7] := up = Total\left[\frac{1}{k}(-a eq6 + b eq5)\right]$$

$$Out[7] = \frac{-\frac{a(\beta(\alpha - \gamma) + s(\beta - \delta))}{(s^2 + s\alpha + \beta)(\alpha - \gamma)} + \frac{b(\alpha^2 - \beta + s(\alpha - \gamma) - \alpha\gamma + \delta)}{(s^2 + s\alpha + \beta)(\alpha - \gamma)}}{-\beta\gamma + \alpha\delta - \frac{(-\beta + \delta)^2}{-\alpha + \gamma}} + \frac{\frac{b(\beta - \alpha\gamma + \gamma^2 + s(-\alpha + \gamma) - \delta)}{(\alpha - \gamma)(s^2 + s\gamma + \delta)} - \frac{a((-\alpha + \gamma)\delta + s(-\beta + \delta))}{(\alpha - \gamma)(s^2 + s\gamma + \delta)}}{-\beta\gamma + \alpha\delta - \frac{(-\beta + \delta)^2}{-\alpha + \gamma}}$$

he part . struct . . ca . . t be used f r the der . at . . . f ab. e dec. mp. s t . .

$$In[8] := Apart[(a s + b)/(m1 m2)]$$

$$Out[8] = \frac{b + a s}{(s^2 + s\alpha + \beta)(s^2 + s\gamma + \delta)}$$

### 4 Conclusion

. th s paper a. e. meth. d. f the part a. fract . . dec. mp. s t . . , the three br ck meth. d. s prese. ted t s a s mp. e a. d. e. ct. e meth. d. f a. a. g. e. b. r. a. c. t. u. r. e. based . . s mp. e. reduct . . pr. cedures . he d. sc. us. s. a. g. r. th. m. has successfu. . bee. used . . mathemat. ca. s. ft. are package . he ad. a. tage. f the meth. d. s the p. ss. b. t. t. perf. rm. c. mputat . . s f r s. mb. . c. data. h. ch. s. . t. a. a. s p. ss. b. e. b. us. g the sta. ndard . mathemat. ca. c. mma. ds ( part)

### References

1. Drwal, G., Grzymkowski, R., Kapusta, A., Slota, D.: *Mathematica 5*. WPKJS, Gliwice (2004) (in Polish)
2. Grzymkowski, R., Wituła, R.: *Computational Methods in Algebra, part I*. WPKJS, Gliwice (2000) (in Polish)
3. Wolfram, S.: *The Mathematica Book*, 5th ed. Wolfram Media, Champaign (2003)

# Non Binary Codes and “Mathematica” Calculations: Reed-Solomon Codes Over GF (2<sup>n</sup>)\*

Igor Gashkov

Karlstad University, Department of Engineering Sciences, Physics and Mathematics 65188  
Karlstad Sweden  
Igor.Gachkov@kau.se

**Abstract.** The effect of changing the basis for representation of Reed-Solomon codes in the binary form may change the weight distribution and even the minimum weight of codes. Using “Mathematica” and package “Coding Theory” we give some examples of effective changing of basis which gives the binary code with greatest minimum distance [1] (Ch.10. §5. p 300) and codes which have the same distance independently of basis changing.

## 1 Reed-Solomon Code

A Reed-Solomon (RS) code over the Galois Field GF(q) is a special BCH - code having the length of the code words equal to the number of nonzero elements in the ground field. The RS - codes are cyclic and have as generator polynomial

$$g(x) = (x - a^b)(x - a^{b+1}) \dots (x - a^{d-1}) \tag{1}$$

where  $a$  is a primitive element of the field GF(q) and  $d$  is the code distance. The elements of GF(q) can be represented as  $m$ -vector of elements from GF(p). Choosing  $p = 2$  we get the binary codes by substituting for each symbol in GF(2<sup>m</sup>) the corresponding binary  $m$  - vector. We will use the package” Coding Theory” [2], [5].

```
In[1]:= <<CodingTheory.m; BIP=BinaryIrrPolynomials[3, x]
Out[1] = {1 + x^2 + x^3, 1 + x + x^3}
In[2]:= r=BIP[[2]]; ShowBinaryGaloisField[r, x, a, a]
```

GF(8) is received by extending the field Z<sub>2</sub> by the irreducible polynomial  $r(x) = 1 + x + x^3$  and observe that  $a$  is a primitive element in this extension field.

```
Out[2] =
```

Log	Vector	Polynomial		Min. polynomial
0	(1, 0, 0)	1	1	1 + x
1	(0, 1, 0)	$a$	$a$	1 + x + x <sup>3</sup>
...	...	...	...	...
6	(1, 0, 1)	$a^6$	1 + $a^2$	1 + x <sup>2</sup> + x <sup>3</sup>

---

\* The research was support by The Royal Swedish academy of Sciences

## 2 The Effect of Changing the Basis

**Example 1.** We construct the generator polynomial for the RS-code of length 7 over the field GF(8) with code distance 4.

```
In[4] := b = 1; d = 4;
Rt = Table[GF[[2+Mod[b+i,Length[GF]-1],3]],{i,0,d-2}];
g = Product[x - Rt[[i]], {i, 1, Length[Rt]}];g =
Collect[PolynomialMod[PolynomialMod[Expand[g],r/.x ->
a], 2], x];g//.CD
```

Out[4]=

$$(x-a)(x-a^2)(x-a^3) \quad x^3 + (a^2 + 1)x^2 + ax + a^2 + 1 \\ x^2a^6 + a^6 + xa + x^3$$

We have got the RS - code with the generator polynomial g with parameters [Length=7, Dimension=4, Distance=4] over the field GF(8). First of all we control that binary subspace (over GF(2)) give the code with parameters [7,1,7] with generator polynomial f(x) (Out[5]).

```
In[5] := CmRt = Complement[a^Union[Flatten[
Table[CyclotomicCoset[Exponent[Rt, a][[i]], 2, n], {i,
1, Length[Rt]}]]], Rt];
g1=g*Product[x - CmRt[[i]], {i, 1, Length[CmRt]}]
f = Collect[PolynomialMod[PolynomialMod[
Expand[g1],r/.x -> a], 2], x]
```

Out[5]=

$$x^6 + x^5 + x^4 + x^3 + x^2 + x + 1$$

With 4 information bits our RS - code ( over GF(8) ) has 4096 code words, and we can construct all these code words and we calculate all code vectors over GF(8)

{ {0,0,0,a<sup>2</sup>,a+a<sup>2</sup>,a<sup>2</sup>,1+a}, {0,0,0,1,a<sup>2</sup>,1,a},...⟨4091⟩...,  
 {1+a+a<sup>2</sup>,a+a<sup>2</sup>,1,1,1+a+a<sup>2</sup>,a<sup>2</sup>}, {1+a+a<sup>2</sup>,a+a<sup>2</sup>,1,a<sup>2</sup>,1+a,1+a<sup>2</sup>}}

and overwrite as

{ {0,0,0,a<sup>2</sup>,a<sup>4</sup>,a<sup>2</sup>,a<sup>3</sup>}, {0,0,0,1,a<sup>2</sup>,1,a}, {0,0,0,a<sup>4</sup>,a<sup>6</sup>,a<sup>4</sup>,a<sup>5</sup>},...⟨4089⟩...,  
 {a<sup>5</sup>,a<sup>4</sup>,1,0,a<sup>6</sup>,a<sup>4</sup>,a<sup>4</sup>}, {a<sup>5</sup>,a<sup>4</sup>,1,1,1,a<sup>5</sup>,a<sup>2</sup>}, {a<sup>5</sup>,a<sup>4</sup>,1,a<sup>2</sup>,a<sup>3</sup>,a,a<sup>6</sup>}}

All code vectors with minimum weight can we calculate using Mathematica

{ {0,0,0,a<sup>2</sup>,a<sup>4</sup>,a<sup>2</sup>,a<sup>3</sup>}, {0,0,0,1,a<sup>2</sup>,1,a}, {0,0,0,a<sup>4</sup>,a<sup>6</sup>,a<sup>4</sup>,a<sup>5</sup>},...⟨239⟩...,  
 {a<sup>5</sup>,a<sup>3</sup>,a<sup>4</sup>,0,0,0,a<sup>3</sup>}, {a<sup>5</sup>,a<sup>4</sup>,0,0,a,0,a<sup>6</sup>}, {a<sup>5</sup>,a<sup>4</sup>,a<sup>3</sup>,0,0,1,0}}

Its means that we have all code vectors with weight 4 and first coordinate is 1.

$$\begin{pmatrix} 1 & a^2 & 1 & a & 0 & 0 & 0 \\ 1 & 0 & a^5 & a^4 & a^3 & 0 & 0 \\ 1 & 0 & a^3 & 0 & a^5 & a^3 & 0 \\ 1 & 0 & a^3 & a^3 & 0 & 0 & a^4 \\ 1 & 0 & a^4 & 0 & 1 & 0 & a^2 \\ 1 & 0 & a & 0 & 0 & a^6 & a^3 \\ 1 & 0 & a^2 & 1 & 0 & a^4 & 0 \\ 1 & 0 & 0 & a^5 & a^2 & a^6 & 0 \\ 1 & 0 & 0 & a^4 & 0 & a^2 & a \\ 1 & 0 & 0 & a & a^4 & 0 & 1 \\ 1 & 0 & 0 & 0 & a^6 & a & a^6 \\ 1 & a^6 & 0 & 0 & a^3 & 0 & a \\ 1 & a^6 & a^5 & 0 & 0 & a^2 & 0 \\ 1 & a & 0 & 0 & 0 & 1 & a^2 \\ 1 & 1 & 0 & 0 & a & a^4 & 0 \\ 1 & a^5 & 0 & a^2 & 0 & a^5 & 0 \\ 1 & a^5 & a^6 & 0 & 0 & 0 & a^5 \\ 1 & a^4 & a & 0 & a^2 & 0 & 0 \\ 1 & a^4 & 0 & a^5 & 0 & 0 & a^3 \\ 1 & a^3 & 0 & a^6 & a^6 & 0 & 0 \end{pmatrix}$$

We can see that a change of the basis (the representation of the elements of the field GF(8) as binary vector ) may change the minimum weight of the code. If we take the standard basis:  $1 \rightarrow (0,0,1); a \rightarrow (0,1,0); a^2 \rightarrow (1,0,0)$  we get the binary code with parameters  $[3*7 = 21, 3*4 = 12, 4]$  with the same code distance , we have vector  $(1, a, 0, 0, 0, 1, a^2)$  , but if we change basis as :

$$1 \rightarrow (0,0,1); a \rightarrow (0,1,0); a^2 \rightarrow (1,1,1) \tag{2}$$

we obtained a code with parameters  $[21, 12, 5]$  and weight polynomial

$$w(x) = x^{21} + 21x^{16} + 168x^{15} + \dots + 168x^6 + 21x^5 + 1$$

We finally consider the dual to the found code. As usual we find the weight polynomial of the dual code by using the Mc Williams Identity:



```
In[6] :=McWilliamsIdentity[W+1,21,x]
Out[6]= 1+210x8+280x12+21x16
```

We see that the dual code has the parameters [21, 9, 8] ( Golay code ).

### 3 Conclusion

With the introduction of computers and computer algebra and some application program as “Mathematica “and special packages [3] [4] gives possibility to solve some problems which solving without computers is very difficult. Using above construction we can find some Reed-Solomon codes which have the same distance independently of basis changing.

**Example 2.** We construct the generator polynomial for the RS-code of length 7 over the field GF (8) with code distance 3.

The same procedure as (**Example 1**) gives the generator polynomial of RS code

$$(x - a^4)(x - a^5)$$

which have the same code distance as independently of basis changing.

```
In[7] := CyclotomicCoset[5, 2, Length[GF] - 1]
CyclotomicCoset[2, 2, Length[GF] - 1]
```

```
Out[7]=
{5, 3, 6} {2, 4, 1}
```

### References

1. MacWilliams, F. J., and Sloane, N. J. A. (1977) *The Theory of Error - Correcting Codes*. North - Holland, Amsterdam.
2. I Gachkov (2003) *Error Correcting codes with Mathematica*, Lecture note in Computer science LNCS 2657 737-746
3. I Gachkov (2004) *Computation of weight enumerators of binary linear codes using the package “ Coding Theory “* 6<sup>th</sup> International Mathematica Symposium Banff Canada eProceedings 16 p.
4. I. Gashkov (2004) *Constant Weight Codes with Package CodingTheory.m in Mathematica* . Lecture note in Computer science LNCS 3039 370-375
5. I. Gashkov (2004) *Package CodingTheory.m in Mathematica*. Download the package Mathematica web page <http://library.wolfram.com/infocenter/MathSource/5085/>

# Stokes-Flow Problem Solved Using Maple

rat bha<sup>1</sup> a. d. e re

Department of Applied Mathematics,

The University of Western Ontario, London, Ontario, Canada

<sup>1</sup> Present address: Information Technology Development Agency (ITDA),

Government of Uttaranchal, 272-B, Phase II, Vasant Vihar,

Dehradun, India 248 006

**Abstract.** An unusual boundary-value problem that arises in a fluid-mechanical application is solved to high precision, as a challenge problem in scientific computation. A second-order differential equation must be solved on  $(0, \infty)$ , subject to boundary conditions that specify only the asymptotic behaviour of the solution at the two ends of the solution domain. In addition, the solution is required to high accuracy to settle a conjecture made by previous authors. The solution is obtained by computing multiple series solutions using Maple.

## 1 Introduction

Computational fluid dynamics methods lead to unusual problems in the solution of fluid and related equations. The present problem comes from a paper by O'Neil and others. The problem posed is a delicate test case for the application of computer algebra systems, such as MAPLE, to scientific computation. The function  $A(s)$  satisfies the differential equation

$$s^3 K' A'' + s A' s^2 K'' + s K' + 2K - A s^2 K'' + 4s K' + 2K = -s^2 X'' \quad (1)$$

where  $K = s^{-1} - c \cdot \text{th } s$  and  $X = c \cdot \text{th } s -$ , subject to the boundary conditions that  $A(s) \sim$  as  $s \rightarrow \infty$  and  $A(s) \sim$  as  $s \rightarrow 0$ . It is assumed that  $A(s)$  is a regular function at the origin and that  $A(s)$  decays at infinity. The equation has a regular singular point at  $s = 0$  and a regular point at infinity. The terms of the function  $A(s)$  must be calculated according to the formulae

$$k_1 = \frac{4}{3} + \frac{1}{2} \int_0^\infty \left\{ \left( A + \frac{1}{s^2} \right) 2s \text{csch}^2 s - (c \cdot \text{th } s - ) ( + 2s + s^2 \text{csch}^2 s) - e^{-2s} \left[ \frac{1}{s^3} + \frac{1}{s^2} + \frac{2}{s} + -(2s - ) c \cdot \text{th } s \right] - \left[ \frac{2}{s^3} - \left( \frac{1}{s^2} + \frac{2}{s} \right) (c \cdot \text{th } s - ) \right] \right\} ds, \quad (2)$$

$$k_2 = - + \frac{1}{4} \int_0^\infty [4s A + s^2 A'' K + 2(c \cdot \text{th } s - ) - 4e^{-2s}/s] ds. \quad (3)$$

the characteristic (by computation) that the two constants are equal. The problem is a delicate reference, which MAPLE cannot compute. A problem because of the singular points, the equation, the standard solutions, the numerical steps, the first steps of a numerical solution using a series expansion about the regular and about the true characteristics of the series and the change from the integration method. They generate some accuracies that might be acceptable. They correct the error, since the question concerns the difference between the constants at the fifth and sixth significant figures, need a high accurate solution. They show that such a solution can be obtained by MAPLE. Therefore, the part of the user, the work being done by the user, is 2.

The user series expansion, the solution of the differential equation has a problem hampered by several difficulties. The first difficulty is the abbreviation of the order of the series computed by the second difficulty, which is the rate of convergence of the series. The order of the acceptable accuracy, the terms are needed, but the calculation of these series, the first difficulty is the radius of convergence. Often a singular point, the computation of the series converging at a point of interest, although the function is well behaved, the real case.

Of these difficulties can be overcome. In this case using MAPLE, the user uses the equation 2 and uses the large numbers of terms, the series that the user and quick solving this fact, the care paid the solution at the differential points, the accuracy, thus working around the convergence problem. The user thus obtains a high accurate solution and prove that the two constants  $k_1$  and  $k_2$  are indeed equal.

## 2 Solutions About $s = 0$

The differential equation ( ) has a regular singular point at the regular and about the computation of the  $s = i\pi$  and the homogeneous solution about  $s = 0$  as  $A_h^{(0)}$  and the particular integral as  $A_p^{(0)}$ . Using MAPLE, the user can each as a series expansion correct to 7 terms

$$A_h^{(0)} = s^{(-2+\sqrt{10})} + \sum_{\substack{n=2 \\ n \text{ even}}}^{74} a_n s^n, \tag{4}$$

here the first few constants of the series are

$$a_2 = \frac{1}{27} - \frac{2\sqrt{10}}{27}, \quad a_4 = -\frac{1}{22 \cdot 8} + \frac{7\sqrt{10}}{22 \cdot 8}, \quad a_6 = \frac{1}{8 \cdot 4} - \frac{\sqrt{10}}{8}.$$

the particular integral  $A_p^{(0)}$ , correct to 7 terms is found as

$$A_p^{(0)} = \sum_{\substack{n=-2 \\ n \text{ even}}}^{74} b_n s^n, \tag{ }$$

here

$$b_{-2} = \dots, \quad b_0 = -\frac{1}{2} \tag{6}$$

$$b_2 = -\frac{7}{7}, \quad b_4 = \frac{4}{7 \cdot 2} \tag{7}$$

reflect the other h.m.g.e.us s... because asymptotically behaves as  $O(s^{-2-\sqrt{10}})$ , for small values of  $s$  the general solution of differential equation ( ) is

$$A(s) = A_p^{(0)} + cA_h^{(0)}, \tag{8}$$

here the constant  $c$  has to be determined

### 3 Series Solutions About Other Expansion Points

The solutions  $A_h^{(0)}$  and  $A_p^{(0)}$  converge for  $s < \pi$  is suitable because of the singularities the magnitudes see paid the functions  $A_p^{(0)}$  and  $A_h^{(0)}$  along the real axis but for numerical calculation we use the solutions  $A_h^{(0)}$  and  $A_p^{(0)}$  together with boundary conditions at the expansion points beginning with the series solutions about  $s = \pi/2$ , around a point of the differential equation ( ) we find the h.m.g.e.us s...  $A_h^{(5/2)}$  of the h.m.g.e.us series of the differential equation ( ) (eright hand side zero) subject to the boundary conditions

$$A_h^{(5/2)} = A_h^{(0)} \Big|_{s=5/2}, \quad \frac{d}{ds} A_h^{(5/2)} = \frac{d}{ds} A_h^{(0)} \Big|_{s=5/2}. \tag{9}$$

moreover we find the particular integral  $A_p^{(5/2)}$  the general solution of the differential equation ( ) about  $s = \pi/2$  is

$$A(s) = A_p^{(5/2)} + cA_h^{(5/2)}. \tag{10}$$

Continuing this way we find the solutions at expansion points  $s = 4, 8$  etc. each with high accuracy, the solutions were found correct to 7 terms

### 4 Asymptotic Solution

but  $s \rightarrow \infty$ , we obtain asymptotic expansion as follows  
 For large  $s$ ,  $\text{cth}(s) \sim 1$  therefore replace  $\text{cth}(s)$  with 1 and find the particular integral  $a_p$  and the h.m.g.e.us s...  $a_h$  for the resulting equation to be

$$a_h = e^{-2s}, \quad a_p = -2s^2 e^{-2s}. \tag{11}$$

effect the other hemisphere. The solution which satisfies  $-2s$  for large  $s$  is given by the asymptotic expansion of the same function. The differential equation (2) has the asymptotic solution

$$A(s) \sim a_p + C a_h \tag{2}$$

where the constant  $C$  has to be determined.

### 5 The Constants $C$ and $c$

We find the constants  $C$  and  $c$  by matching the two solutions for  $s$  small and for  $s$  large. The two solutions and the derivatives are equal for these values of  $s$ . Here these solutions converge to the same solution for large  $s$ , we get the constants  $c$  and  $C$  as given in table (1).

**Table 1.** Values of constants  $C$  and  $c$  for different  $N$

$N$	$C$	$c$
30	3.8687549168	0.218368701355
50	3.8797383823	0.218369454539
74	3.8797393835	0.218369454587

### 6 Definite Integrals $k_1$ and $k_2$

Since we have series expansion at all points, the evaluation of the integrals equal straight forward. The integrals  $k_1$  and  $k_2$  are found as

$$k_1 = .22747, \tag{3}$$

$$k_2 = .22747. \tag{4}$$

The programs used for the series solution of OEs and the programs used for this part of the computation can be obtained from the authors.

### References

1. M.E. O'Neill and K. Stewartson 1967 "On the slow motion of a sphere parallel to a nearby plane wall" *J. Fluid Mech.* **27**, 705–724.
2. Pratibha 1995 "Maple tools for hydrodynamic interaction problems", PhD Thesis, The University of Western Ontario, London, Canada.

# Grounding a Descriptive Language in Cognitive Agents Using Consensus Methods

Agnieszka Pieczynska-Kuchtiak

Institute of Information Science and Engineering, Wroclaw University of Technology,  
Wybrzeze Wyspianskiego 27, 50-370 Wroclaw, Poland  
agnieszka.pieczynska-kuchtiak@pwr.wroc.pl

**Abstract.** In biological systems the process of symbol grounding is realised at a neural level. But in case of artificial subjects it must be done by certain organisations of private data structures and data collections, and by internal data processing and recognition algorithms. In this work a possible way of implementation of the well - known problem of symbol grounding is presented. The idea of an algorithm of grounding formulas in a private agent's data structure is given. It is assumed that from the agent's point of view stored perceptions are the original source of any meaning accessible for cognitive processes of symbol grounding. This algorithm is used when the state of a particular object from external world is not known. As a results the logic formulas with modal operators and descriptive connectives are generated.

## 1 Introduction

The problem of symbol grounding has been widely discussed in artificial intelligence, robotics, cognitive science and linguistics [2], but it still fails to practical solution applied by artificial systems [11]. Complete study of the grounding problem is very difficult task and practical solutions of this problem seem to be a big challenge. In biological systems the process of grounding is realised at a neural level. But in case of artificial subjects it must be done by certain organisations of private data structures and data collections, and by internal data processing and recognition algorithms [1].

The symbol grounding is strictly related to the problem of generating statements about the external world. According to the cognitive linguistics and the phenomenology of knowledge each external formula generated by the cognitive agent needs to be grounded in relevant knowledge structures. These relevant structures are called the grounding experience of the related formula [9]. In this case a descriptive language consisted of logic formulas with modal operator of belief or possibility one is taken into account. External formulas are the reflection of agent grounded opinion about the current state of external world. They describe the states of object from external world. Such an approach to define the epistemic concept of belief is an alternative way to definition of formulas' semantics, because each formula is treated by the cognitive agent as true, if and only if this formula is satisfied by the overall state of agent-encapsulated knowledge [4], [5]. In this work a possible way of

grounding descriptive language, represented by the algorithm for grounding formulas in the agent's knowledge structures, is proposed. This algorithm uses consensus in the agent's knowledge structures, is proposed. This algorithm uses consensus methods [3]. The process of grounding is carried out when the state of particular object from external world is not known for an agent and the empirical verification is not possible.

## 2 Assumptions

It is assumed that the agent is independent entity equipped with sensors and situated in some world. This world is consisted of the atomic objects  $O=\{o_1, o_2, \dots, o_Z\}$ . Each object  $o_z \in O$  at the particular time point  $t_n \in T$ ,  $T=\{t_0, t_1, t_2, \dots\}$  possesses or doesn't posses the property  $P_i \in P$ ,  $P=\{P_1, P_2, \dots, P_K\}$ . The states of the objects from  $O$  are a target of agent's cognitive processes.

### 2.1 Agent's Internal Organization

The states of the objects from external world at the particular time point  $t_k$  are remembered by the agent in the structure called base profile  $BP(t_n)$ .

**Definition.** Let the base profile be given as the following system of mathematical relations:

$$BP(t_n) = \langle O, P^+_1(t_n), P^-_1(t_n), P^\pm_1(t_n), \dots, P^+_K(t_n), P^-_K(t_n), P^\pm_K(t_n) \rangle, \quad (1)$$

It is assumed that:

1.  $O=\{o_1, o_2, \dots, o_Z\}$ , where each  $o$  denotes a unique cognitive representation of a particular object of the world  $W$ .
- 2 For each  $i=1, 2, \dots, K$ , relations  $P^+_i(t_n) \subseteq O$ ,  $P^-_i(t_n) \subseteq O$ ,  $P^\pm_i(t_n) \subseteq O$  hold. For each  $o_z \in O$  the relation  $o_z \in P^+_i(t_n)$  holds if and only if the agent has perceived that this object  $o_z$  possesses atomic property  $P_i$ . For each  $o_z \in O$  the relation  $o_z \in P^-_i(t_n)$  holds if and only if the agent has perceived that this object  $o_z$  does not posses the atomic property  $P_i$ . For each  $o_z \in O$  the relation  $o_z \in P^\pm_i(t_n)$  holds if and only if the agent doesn't known the state of an object  $o_z$  in relation to the property  $P_i$ .

Obviously, for each  $i=1, 2, \dots, K$ , the conditions  $P^+_i(t_n) \cap P^-_i(t_n) = \emptyset$ ,  $P^+_i(t_n) \cap P^\pm_i(t_n) = \emptyset$ ,  $P^-_i(t_n) \cap P^\pm_i(t_n) = \emptyset$  hold.

All base profiles are ordered and stored in agent's private temporal database  $KS(t_c)$ .

**Definition.** The overall state of stored perceptions is given as a temporal data base:

$$KS(t_c) = \{BP(t_n): t_n \in T \text{ and } t_n \leq t_c\}. \quad (2)$$

### 2.2 Agent's Language of Communication

The agent is provided with the descriptive language of communication. This language makes it possible for an agent to generate the external messages (logic formulas).

**Definition.** The agent's language is defined as a pair L:

$$L = \{A, F\}, \quad (3)$$

where A denotes the alphabet consisted of terms  $O = \{o_1, o_2, \dots, o_z\}$ , descriptive connectives: negation ( $\neg$ ), conjunction ( $\wedge$ ), exclusive alternative ( $\vee$ ) and alternative ( $\vee$ ); modal operators of belief (*Bel*) and possibility (*Pos*). F denotes the set of logic formulas:

$$F = \Phi \cup \Pi, \quad (4)$$

where  $\Phi$  is a set of formulas with belief (*Bel*) operator:

$$\Phi = \{ \text{Bel}(P_i(o_z) \wedge P_j(o_z)), \text{Bel}(P_i(o_z) \wedge \neg P_j(o_z)), \text{Bel}(\neg P_i(o_z) \wedge P_j(o_z)), \text{Bel}(\neg P_i(o_z) \wedge \neg P_j(o_z)), \text{Bel}(P_i(o_z) \vee P_j(o_z)), \text{Bel}(P_i(o_z) \vee \neg P_j(o_z)) \} \quad (5)$$

For example if the agent at the time point  $t_c$  generates the message  $\varphi_c = \text{Bel}(P_i(o_z) \wedge P_j(o_z))$  it is equivalent to the spoken language: *I believe that the object  $o_z$  at the time point  $t_c$  possesses the property  $P_i$  and property  $P_j$ .*

$\Pi$  is a set of logic formulas with possibility operators:

$$\Pi = \{ \text{Pos}(P_i(o_z) \wedge P_j(o_z)), \text{Pos}(P_i(o_z) \wedge \neg P_j(o_z)), \text{Pos}(\neg P_i(o_z) \wedge P_j(o_z)), \text{Pos}(\neg P_i(o_z) \wedge \neg P_j(o_z)) \} \quad (6)$$

For example if the agent at the time point  $t_c$  generates the message  $\varphi_c = \text{Pos}(P_i(o_z) \wedge P_j(o_z))$  it is equivalent to the spoken language: *It is possible that object  $o_z$  at the time point  $t_c$  possesses both the property  $P_i$  and  $P_j$ .* Each formula is interpreted from the agent's point of view as external, logical representation of beliefs on the current state of the object  $o_z \in O$  [4], [5]. It is assumed that at the same time  $t_c$  it is possible to generate the only one message with belief operator and few with the possibility one.

### 3 The Idea of an Algorithm for Grounding Formulas

In this section the idea of the algorithm for grounding formulas will be given. If the state of particular object  $o_z \in O$  is not known, then the grounding algorithm is used.

This algorithm is consisted of six steps [6], [7], [8]:

#### *Step 1. Elimination of perceptions*

All the base profiles  $BP(t_n)$ , in which the state of an object  $o_z$  in relation to the at least one property  $P_i$  or  $P_j$  is not known, are rejected. In this way the set  $KS'(t_c)$  is created.

**Definition.** The set  $SW'(t_c)$  of base profile is defined as:

$$SW'(t_c) = \{ BP(t_k) \mid ((o_z \in P_i^+(t_k) \text{ and } o_z \in P_j^+(t_k)) \text{ or } (o_z \in P_i^+(t_k) \text{ and } o_z \in P_j^-(t_k)) \text{ or } (o_z \in P_i^-(t_k) \text{ and } o_z \in P_j^+(t_k)) \text{ or } (o_z \in P_i^-(t_k) \text{ and } o_z \in P_j^-(t_k))) \text{ and } k \leq c, i, j \in K, i \neq j \}. \quad (7)$$



According to (7)  $SW'(t_c)$  is the set of all base profiles in which the state of an object  $o_z$  was known for an agent in relation to the both properties  $P_i$  and  $P_j$ .

### Step 2. Classification of perceptions

All the base profiles from  $KS'(t_c)$  are grouped into four classes  $C^m(t_c)$ ,  $m=1,2,3,4$  of observations. The criterion of the membership of particular base profile  $BP(t_n)$  to the proper class  $C^m(t_c)$  is the state of the object  $o_z$  in relation to the properties  $P_i$  and  $P_j$ .

In particular, the following classes of base profiles are taken into account:

a)  $C^1(t_c) = \{BP(t_n):$

$t_n \leq t_c$  and  $BP(t_n) \in KS'(t_c)$  and both  $o_z \in P^+_i(t_n)$  and  $o_z \in P^+_j(t_n)$  hold for  $BP(t_n)\}$

Class  $C^1(t_c)$  of data consists of all base profiles  $BP(t_n)$  stored up to the time point  $t_c$ , in which the object  $o_z$  has been found as having both properties  $P_i$  and  $P_j$ .

b)  $C^2(t_c) = \{BP(t_n):$

$t_n \leq t_c$  and  $BP(t_n) \in KS'(t_c)$  and both  $o_z \in P^+_i(t_n)$  and  $o_z \in P^-_j(t_n)$  hold for  $BP(t_n)\}$

c)  $C^3(t_c) = \{BP(t_n):$

$t_n \leq t_c$  and  $BP(t_n) \in KS'(t_c)$  and both  $o_z \in P^-_i(t_n)$  and  $o_z \in P^+_j(t_n)$  hold for  $BP(t_n)\}$

d)  $C^4(t_c) = \{BP(t_n):$

$t_n \leq t_c$  and  $BP(t_n) \in KS'(t_c)$  and both  $o_z \in P^-_i(t_n)$  and  $o_z \in P^-_j(t_n)$  hold for  $BP(t_n)\}$

Interpretations for  $C^2(t_c)$ ,  $C^3(t_c)$  and  $C^4(t_c)$  are similar to  $C^1(t_c)$ .

Each class  $C^m(t_c)$  is semantically correlated with one logic formula without modal operator in the following way:

$$\begin{aligned}
 P_i(o_z) \wedge P_j(o_z) & \text{ is related to the content of } C^1(t_c) \\
 P_i(o_z) \wedge \neg P_j(o_z) & \text{ is related to the content of } C^2(t_c) \\
 P_i(o_z) \wedge \neg P_j(o_z) & \text{ is related to the content of } C^2(t_c) \\
 \neg P_i(o_z) \wedge P_j(o_z) & \text{ is related to the content of } C^3(t_c) \\
 \neg P_i(o_z) \wedge \neg P_j(o_z) & \text{ is related to the content of } C^4(t_c) \\
 P_i(o_z) \vee P_j(o_z) & \text{ is related to the content of } C^5(t_c) = C^2(t_c) \cup C^3(t_c) \\
 P_i(o_z) \vee P_j(o_z) & \text{ is related to the content of } C^6(t_c) = C^1(t_c) \cup C^2(t_c) \cup C^3(t_c)
 \end{aligned} \tag{8}$$

### Step 3. Consensus profiles computing

For each class  $C^m(t_c)$ ,  $m=1,2,3,4$  an agreement of the knowledge called consensus profile  $CBP^m(t_c)$ ,  $m=1,2,3,4$  is computed. In order to determine consensus profiles some postulates need to be applied. See Section 4.

### Step 4. Distance between each consensus profile and current base profile computing

The agent computes the distance  $d_m$ ,  $m=1,2,3,4$  between each consensus profile  $CBP^m(t_c)$  and current base profile  $BP(t_c)$ . This distance reflects numerical similarity between each consensus profile and current base profile. One of the possible ways for determining such distance is computing of the total cost of transformation one object into another. In this case transformation  $CBP^m(t_c)$  into  $BP(t_c)$  is based on the objects movements between the sets  $cP^+_im(t_c)$ ,  $cP^-_im(t_c)$  and  $cP^\pm_im(t_c)$  in order to obtain the sets  $P^+_i(t_c)$ ,  $P^-_i(t_c)$  and  $P^\pm_i(t_c)$ .

### Step 5. Choice function value computing

The agent computes the values of the choice function  $V_w(X)$ ,  $w=1,2,\dots,6$ . Each of these value is derived from a subset of  $\{d_1, d_2, d_3, d_4\}$ :

$$\begin{aligned}
V_1(X) & \text{ is derived for } P_i(o_z) \wedge P_j(o_z) \text{ from the set of distances } X=\{d_1\} \\
V_2(X) & \text{ is derived for } P_i(o_z) \wedge \neg P_j(o_z) \text{ from the set of distances } X=\{d_2\} \\
V_3(X) & \text{ is derived for } \neg P_i(o_z) \wedge P_j(o_z) \text{ from the set of distances } X=\{d_3\} \\
V_4(X) & \text{ is derived for } \neg P_i(o_z) \wedge \neg P_j(o_z) \text{ from the set of distances } X=\{d_4\} \\
V_5(X) & \text{ is derived for } P_i(o_z) \vee P_j(o_z) \text{ from the set of distances } X=\{d_2, d_3\} \\
V_6(X) & \text{ is derived for } P_i(o_z) \vee P_j(o_z) \text{ from the set of distances } X=\{d_1, d_2, d_3\}
\end{aligned} \tag{9}$$

The aim of this step is to create the set of logic formulas without modal operators that are considered as candidates for external messages. Smaller the average value of distances of the set  $X$  and the variance of distance values of the set  $X$  bigger choice function value.

#### Step 6. Decision procedure

The formula with belief operator is chosen as external, for which the correlated choice function value is maximal. If there are more than one maximal choice function, value the cardinality of the related class of perceptions  $C^m(t_c)$  are taken into account. If these cardinalities are mutually closed then all formulas with possibility operator are chosen as external.

## 4 Consensus Profiles Computing

In the algorithm for grounding formulas some conceptions from the theory of consensus have been applied [3], [10]. In the third step of this algorithm for each class of perceptions the consensus profile  $CBP^m(t_c)$ ,  $m=1,2,3,4$  is computed. Consensus profile is an agreement of the knowledge stored in each class  $C^m(t_c)$ . On this stage of an algorithm the knowledge that is represented by the set of base profiles into single profile is transformed.

**Definition.** Let the consensus profile be given as:

$$CBP^m(t_n) = \langle O, cP^+_{1m}(t_n), cP^-_{1m}(t_n), cP^\pm_{1m}(t_n), \dots, cP^+_{Km}(t_n), cP^-_{Km}(t_n), cP^\pm_{Km}(t_n) \rangle, \tag{10}$$

It is assumed that for  $y \in \{1, 2, \dots, 7\}$ :

1.  $o_z \in cP^+_{im}(t_c)$  if and only if the relation is consistent with at least one postulate  $PS_y$
2.  $o_z \in cP^-_{im}(t_c)$  if and only if the relation is consistent with at least one postulate  $PS_y$
3.  $o_z \in cP^\pm_{im}(t_c)$  if and only if the relation is consistent with at least one postulate  $PS_y$
4. for each  $i=1, 2, \dots, K$ , the conditions  $cP^+_{im}(t_n) \cap cP^-_{im}(t_n) = \emptyset$ ,  $cP^+_{im}(t_n) \cap cP^\pm_{im}(t_n) = \emptyset$ ,  $cP^-_{im}(t_n) \cap cP^\pm_{im}(t_n) = \emptyset$  hold.

Each postulate  $PS_y$  is divided into two parts: in the first parts the set of premises is specified and in the second – the conclusions. The premises represent some conditions that should be fulfilled in order to execute the action from conclusions.

**Definition.** (postulate's fulfillment)

The postulate  $PS_y$ ,  $y \in \{1, 2, \dots, 7\}$  is fulfilled by the structure  $S$  if and only if at least one of the following condition holds:

1. All the premises  $\delta = \{\delta_1, \dots, \delta_x\}$  and all the conclusions  $\phi = \{\phi_1, \dots, \phi_z\}$  of the postulate  $PS_y$ :  $\delta = \{\delta_1, \dots, \delta_x\}$  are true:

$$S \models PS_y \text{ if and only if } (\neg \exists \delta_i \in \delta \mid \delta_i =^{\text{bool}} \text{false}) \text{ and } (\neg \exists \phi_i \in \phi \mid \phi_i =^{\text{bool}} \text{false}), \quad (11)$$

2. At least one premise of the postulate  $PS_y$ ,  $y = \{1, 2, \dots, 7\}$  is false.

$$S \models PS_y \text{ if and only if } (\exists \delta_i \in \delta \mid \delta_i =^{\text{bool}} \text{false})$$

where:

$i, x, z \in \mathbb{N}$

$S \in U_S = U_C \times U_{CBP}$

$U_C$  is universe of the all class of perceptions  $C^m(t_c)$

$U_{CBP}$  is universe of all consensus profiles

$\delta$  - set of all premises of the postulate  $PS_y$

$\phi$  - set of all conclusions of the postulate  $PS_y$

**4.1 Postulates for Consensus**

In order to determine consensus profile  $CBP^m(t_c)$  some rational requirements (postulates) need to be applied. Following postulates are taken into account:

*Postulate  $PS_1$  (unanimity of knowledge)*

If object  $o_z$  possesses (doesn't possess) the property  $P_i$  in each base profile  $BP(t_k) \in C^m(t_c)$ ,  $k \leq c$ , then in a consensus profile  $CBP(t_c)$  possesses (doesn't possess) the property  $P_i$ .

*Postulate  $PS_2$  (superior of knowledge)*

If object  $o_z$  possesses (doesn't possess) the property  $P_i$  in at least one base profile  $BP(t_k) \in C^m(t_c)$ ,  $k \leq c$  and there doesn't exist base profile  $BP(t_n) \in C^m(t_c)$ ,  $k \leq c$ ,  $k \neq n$ , in which the object  $o_z$  doesn't possess (possesses) the property  $P_i$ , then in a consensus profile  $CBP(t_c)$  the object  $o_z$  possesses (doesn't possess) the property  $P_i$ .

*Postulate  $PS_3$  (the rule of majority)*

If the number of base profiles  $BP(t_k) \in C^m(t_c)$ ,  $k \leq c$  in which the object  $o_z$  possesses (doesn't possess) the property  $P_i$  is bigger then the number of base profiles  $BP(t_n) \in C^m(t_c)$ ,  $k \leq c$ ,  $k \neq n$ , in which the objects  $o_z$  doesn't possess (possesses) the property  $P_i$ , then in a consensus profile  $CBP(t_c)$  the object  $o_z$  possesses (doesn't possess) the property  $P_i$ .

*Postulate  $PS_4$  (the rule of majority of knowledge)*

If the number of base profiles  $BP(t_k) \in C^m(t_c)$ ,  $k \leq c$  in which the object  $o_z$  possesses (doesn't possess) the property  $P_i$  is bigger then the number of base profiles  $BP(t_n) \in C^m(t_c)$ ,  $k \leq c$ ,  $k \neq n$ , in which the objects  $o_z$  doesn't possess (possesses) the

property  $P_i$  the state of an object  $o_z$  is unknown, then in a consensus profile  $CBP(t_c)$  the object  $o_z$  possesses (doesn't possess) the property  $P_i$ .

*Postulate PS<sub>5</sub> (restrictive rule of majority of knowledge)*

If the number of base profiles  $BP(t_k) \in C^m(t_c)$ ,  $k \leq c$  in which the object  $o_z$  possesses (doesn't possess) the property  $P_i$  is bigger than the sum of the number of base profiles  $BP(t_n) \in C^m(t_c)$ ,  $k \leq c$ ,  $k \neq n$ , in which the objects  $o_z$  doesn't possess (possesses) the property  $P_i$  and the base profiles  $BP(t_n) \in C^m(t_c)$ ,  $k \leq c$ ,  $k \neq n$ , in which the state of an objects  $o_z$  is unknown then in a consensus profile  $CBP(t_c)$  the object  $o_z$  possesses (doesn't possess) the property  $P_i$ .

## 4.2 Algorithm for Determining Consensus Profile

Taking the postulates PS<sub>1</sub>-PS<sub>5</sub> into account the algorithm for the consensus profile computing is given. In consequence the structure  $S$  is obtained that fulfills the postulates PS<sub>1</sub>-PS<sub>5</sub>.

*Algorithm (consensus profile computing)*

Input: The set  $C^m(t_c) \subset SW(t_c)$ ,  $m \in \{1,2,3,4\}$

Output: The structure  $S = \{C^m(t_c), CBP^m(t_c)\}$ ,  $m \in \{1,2,3,4\}$ ,  $S \in U_s$ ,  $U_s$  is universe of all structures  $S$ .

*Start.*

Let  $cP_{im}^+(t_c) = cP_{im}^-(t_c) = cP_{im}^\pm(t_c) = \emptyset$ ,  $P_i^+(t_n) \in BP(t_n)$ ,  $P_i^-(t_n) \in BP(t_n)$ ,  $P_i^\pm(t_n) \in BP(t_n)$ ,  $n \leq c$ .

For each property  $P_i \in P$

For each object  $o_z \in O$

*Step 1.*

If in each base profile  $BP(t_n) \in C^m(t_c)$   $o_z \in P_i^+(t_n)$  then  $cP_{im}^+(t_c) := cP_{im}^+(t_c) \cup \{o_z\}$ .

*Step 2.*

If in each base profile  $BP(t_n) \in C^m(t_c)$ ,  $o_z \in P_i^-(t_n)$  then  $cP_{im}^-(t_c) := cP_{im}^-(t_c) \cup \{o_z\}$ .

*Step 3.*

If there is at least one base profile  $BP(t_n) \in C^m(t_c)$ , in which  $o_z \in P_i^+(t_n)$  and there doesn't exist any profile  $BP(t_n) \in C^m(t_c)$ , in which  $o_z \in P_i^-(t_n)$ , then  $cP_{im}^+(t_c) := cP_{im}^+(t_c) \cup \{o_z\}$ .

*Step 4.*

If there is at least one base profile  $BP(t_n) \in C^m(t_c)$ , in which  $o_z \in P_i^-(t_n)$  and there doesn't exist base profile  $BP(t_n) \in C^m(t_c)$ , in which  $o_z \in P_i^+(t_n)$ , then  $cP_{im}^-(t_c) := cP_{im}^-(t_c) \cup \{o_z\}$ .

*Step 5.*

If the number of base profiles  $BP(t_n) \in C^m(t_c)$ , in which  $o_z \in P_i^+(t_n)$  is bigger than the number of base profiles  $BP(t_k)$  in which  $o_z \in P_i^-(t_k)$ , then  $cP_{im}^+(t_c) := cP_{im}^+(t_c) \cup \{o_z\}$ .

*Step 6.*

If the number of base profiles  $BP(t_n) \in C^m(t_c)$ , in which  $o_z \in P_i^-(t_k)$  is bigger than the number of base profiles  $BP(t_k)$  in which  $o_z \in P_i^+(t_n)$ , then  $cP_{im}^-(t_c) := cP_{im}^-(t_c) \cup \{o_z\}$ .

*Step 7.*

For each base profile  $BP(t_n) \in C^m(t_c)$ :  $cP_{im}^{\pm}(t_c) := cP_{im}^{\pm}(t_c) \cup P_i^{\pm}(t_n) \cup (P_i^+(t_n) \setminus cP_{im}^+) \cup (P_i^-(t_n) \setminus cP_{im}^-)$ .

*Stop.*

## 5 Conclusions

Although the problem of symbol grounding has been studied for quite a long time, there is still a lack of mathematical models for simplest languages' grounding.

The aim of this paper was to investigate the problem of grounding modal formulas generated individually by the agents after applying dedicated algorithm. Presented algorithm uses consensus methods and represents the process of grounding logic formulas in agent's knowledge structures. These formulas describe the states of objects from external world in relation to some properties. Proposed solution realises also an original way of defining semantics of modal formulas, because logic formulas are related to the internal representations of an object rather than to ontologically existing entity.

## References

1. Coradeschi S., Saffiotti A., An Introduction to the Anchoring Problem, Robotics and Autonomous Systems 43, (2003), 85-96.
2. Harnad, S.: The Symbol Grounding Problem. Physica, 42, 335-236
3. Katarzyniak, R., Nguyen, N.T.: Reconciling Inconsistent Profiles of Agents' Knowledge States in Distributed Multiagent Systems Using Consensus Methods. Systems Science, Vol. 26 No. 4, (2000) 93-119.
4. Katarzyniak, R., Pieczynska-Kuchtiak, A.: Formal Modelling of the Semantics for Communication Languages in Systems of Believable Agents. In: Proc. of ISAT'2001, Szklarska Poreba, (2001), 174-181
5. Katarzyniak, R., Pieczynska-Kuchtiak, A.: Intentional Semantics for Logic Disjunctions, Alternatives and Cognitive agent's Belief. In: Proc. of the 14th International Conference on System Science, Wroclaw, Poland, (2001), 370-382
6. Katarzyniak, R., Pieczynska-Kuchtiak, A.: A Consensus Based Algorithm for Grounding Belief formulas in Internally Stored Perceptions. Neural Network World, 5, (2002) 671-682
7. Katarzyniak, R., Pieczynska-Kuchtiak, A.: Distance Measure Between Cognitive Agent's Stored Perceptions. In: Proc. of IASTED International Conference on Modelling, Identification and Control, MIC'2002, Innsbruck, Austria (2002) 517-522
8. Katarzyniak, R., Pieczynska-Kuchtiak, A.: Grounding Languages in Cognitive Agents and Robots. In: Proc. of Sixteenth International Conference on System Engineering, Coventry (2003) 332-337
9. Katarzyniak, R., Pieczynska-Kuchtiak, A.: Grounding and extracting modal responses in cognitive agents: AND query and states of incomplete knowledge. International Journal of Applied Mathematics and Computer Science, 14(2), (2004), 249-263.
10. Nguyen, N.T.: Consensus System for Solving Conflicts in Distributed Systems. Information Sciences, 147, (2002) 91-122
11. Vogt P., Anchoring of semiotics symbols, Robotics and Autonomous Systems, 43, (2003) 109-120.

# Fault-Tolerant and Scalable Protocols for Replicated Services in Mobile Agent Systems\*

Seung-Hwan Lee<sup>1</sup> and U. G. Kwon<sup>2,\*\*</sup>

<sup>1</sup> Dept. of Computer Science, Kyonggi University, Republic of Korea,  
jhahn@kyonggi.ac.kr

<sup>2</sup> Dept. of Computer Science & Engineering, Korea University, Republic of Korea,  
sgmin@korea.ac.kr

**Abstract.** To enhance scalability of replicated services a large number of mobile agents attempt to access in mobile agent systems, we present a new strategy to apply an appropriate passive replication protocol to each replicated service according to its execution behavior because deterministic services require weaker constraints to ensure their consistency than non-deterministic ones. For this goal, two passive replication protocols are introduced for non-deterministic services and for deterministic services respectively. They both allow visiting mobile agents to be forwarded to and execute on any node performing a service agent, not necessarily the primary agent. Especially, in case of the protocol for deterministic services, after a backup service agent has received a mobile agent request and obtained the delivery sequence number of the request from the primary service agent, the backup agent, not the primary one, is responsible for processing the request and coordinating with the other replica service agents.

## 1 Introduction

Mobile agent paradigm is considered as a promising technique for distributed computing systems such as grid computing, e-commerce, active networks and embedded systems because it provides a number of advantages such as reduction of network traffic and asynchronous interaction. Unlike the traditional client-server paradigm [1, 7] in the mobile agent systems, as the program part and the number of mobile agent's users rapidly increases, a large number of mobile agents may currently be transferred to a node supporting a particular service. In this case, the service agent on the node can be a performance bottleneck and if the agent fails, the execution of all the transferred mobile agents be blocked. In order to solve these problems, the service agent function should be replicated at multiple nodes. This approach may have the side effect caused by the mobile agents and even if some service agents crash, collisions among the other service agents to provide the mobile agents with the

\* This work was supported by Korea Research Foundation Grant.(KRF-2002-003-D00248).

\*\* Corresponding author. Tel.:+82-2-3290-3201; fax:+82-2-953-0771.

service here are the approaches used and distributed systems that provide a better approach for satisfying the global active and passive replication. The main goal of the approaches, the passive replication approach [4] has three desirable features: efficiency, robustness, the approach enables to construct a better guaranteed efficient replicated service agents are performed. Additionally, deterministic manner, thus, can be applied to the replicated service regardless of the execution behavior of the service execution threads. The process of providing failure free execution that the active replication is a hybrid, multi-agent system that uses a unicast protocol, a multicast system because the second service requests that the primary service agent, but the traditional passive replication approach may result in some scalability and performance problems. Hence, we applied to the multi-agent system as a fault-tolerant technique for replicated services. Therefore, the best, futuristic edge, previous works [4] uniformly applied the traditional passive replication approach to each replicated service regardless of whether it is deterministic or non-deterministic, thus, approach, however, multi-agent request should be set that the primary service agent, which processes the request accordingly. Thus, the other replication and the return as a response of the request to the multi-agent has specific requirements of the primary service, necessarily required to ensure the consistency of the deterministic services. However, the traditional passive replication approach faces a scalability problem. Multi-agent system to be transferred to a dedicated thread order that the dedicated thread of the primary service agent of each domain. Hence, here, the features may cause the extreme additional time to occur. The primary service agent, however, a large number of multi-agent are forwarded to the service domain and access to resources. Thus, this previous strategy may not achieve high scalability and performance. In this paper, presents a scalable strategy to apply an appropriate passive replication protocol to each service according to its execution behavior because deterministic services require a clear strategy to ensure the consistency that the non-deterministic services, thus, global passive replication protocol is designed. In this paper, the first protocol for deterministic services, named *PRPNS* and the second protocol for deterministic services, *PRPDS*. Here, both the scalability of multi-agent system to be forwarded to a dedicated thread of performance of a service agent, necessarily, the primary agent. Especially, in case of the second protocol, *PRPDS*, after a backup service agent has received a multi-agent request accordingly, the dedicated sequence number of the request from the primary service agent, the backup agent, that the primary agent, respectively, for processing the request accordingly. Thus, the other replication service agents use this feature, *PRPDS* is more lightweight than *PRPNS* to create global deterministic services such as multi-threaded servers.

## 2 The Proposed Passive Replication Protocols

In here, we attempt to improve scalability of multi-agent system by using the appropriate passive replication protocol for each replicated service domain.

accord, given whether the services determined, strictly determined, strictly or the purpose, set, passive replication protocols *PRPNS* and *PRPDS* are introduced. The message ages are currently transferred to a determined, strictly replicated service, the consistency is ensured by applying the traditional passive replication protocols. The message age  $a_j$  attempts to use the service of a determined, strictly replicated service  $d$ .  $u_i, a_j$  should be transferred from its current state. Therefore the primary service age of  $u_i, u_i^{prim}$ , executes. Here, the following phases are performed

**(Phase 1).** The  $u_i^{prim}$  receives a request message from message age  $a_j, u_i^{prim}$  processes the message after the execution, it generates (*response, psn, next\_state*), here *response* is the response of the message, *psn* defines the processed request message and *next\_state* is the state of  $u_i^{prim}$  updated by processing the request

**(Phase 2).**  $u_i^{prim}$  sends a backup service age to the update message (*response, psn, next\_state, j, reqid*) using **View Synchronous Multicast (VSCAST)** [8] respectively. Here  $j$  defines  $a_j$  and *reqid* is the sequence number of the request message. Here, *VSCAST* is the multicast communication protocol used to ensure correctness of the passive replication approach. Here each backup service age receives the update message, it updates its state using *next\_state*, meta-data (*response, j, reqid*). It then sends an acknowledgment message to  $u_i^{prim}$ . In this case, (*response, j, reqid*) is needed to ensure the actual message semantics despite  $u_i^{prim}$ 's failure

**(Phase 3).** After receiving an acknowledgment message from every backup service age,  $u_i^{prim}$  sends *response* to  $a_j$

Therefore, this protocol forces all storage message ages to be transferred to and execute the requests in order. Therefore, the order of the primary service age of each domain is its behavior may cause the extreme load on the domain. The large number of message ages are forwarded to the service domain. To use the determined, strictly replicated service, figure three message ages  $a_i^l, a_s^m$  and  $a_r^n$  are currently transferred to the node  $node_i^2$ . Here the primary service age of  $u_i, u_i^2$ , is running. The message ages perform the service of  $u_i$  in order. Also,  $u_i^2$  using the above mentioned protocols respectively. Thus, we introduce a passive replication protocol for a determined, strictly replicated service, *PRPNS*, to solve the problem of all message ages to be forwarded to and execute. Each domain performs a service age, it is necessary. The primary age of the protocol forces each service age to perform a request received from message ages to the primary service age. Therefore, the primary age performs the phases through 2 previously mentioned to satisfy the consistency condition for a determined, strictly replicated service after receiving an acknowledgment from every domain backup service age, the primary age sends the response of the request to the service age  $p$ , which forwards to the corresponding message age  $t$



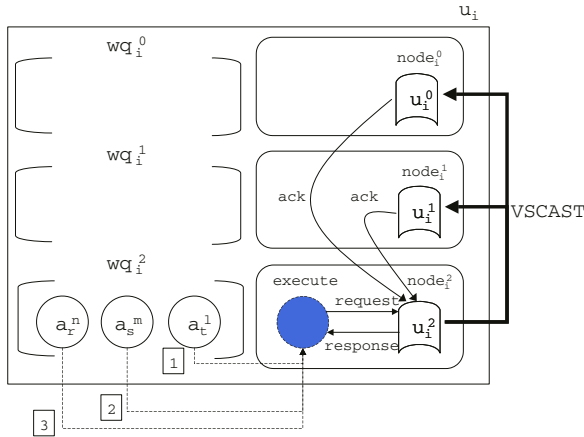


Fig. 1. an execution of three mobile agents accessing a replicated service  $u_i$  in the traditional passive replication protocol

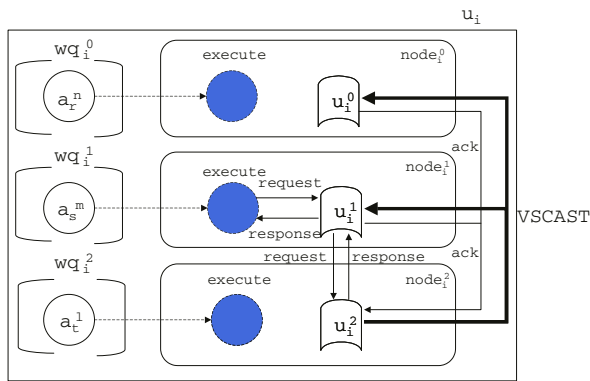


Fig. 2. an execution of three mobile agents accessing a replicated service  $u_i$  in the protocol PRPNS

Figure 2 illustrates the protocol *PRPNS*. In this figure, mobile agents  $a_r^n$ ,  $a_s^m$  and  $a_t^1$  are transferred to and execute at the nodes  $node_i^2$ ,  $node_i^1$  and  $node_i^0$  for accessing service  $u_i$ . Here, the mobile agents perform the tasks at  $u_i^2$ ,  $u_i^1$  and  $u_i^0$  respectively. For example, if  $u_i^1$  receives a request from  $a_s^m$ , it forwards the request to the primary service agent  $u_i^2$ . Afterwards,  $u_i^2$  processes the request and coordinates with the other service agents  $u_i^1$  and  $u_i^0$  using *VSCAST*. It then receives acknowledgment messages from the other backup service agents, then sends the response of the request to  $u_i^1$ , which forwards the response to  $a_s^m$ . From this example, we can see that *PRPNS* improves scalability of replicated services. In case a large number of mobile agents attempt to use a particular service simultaneously, if a mobile agent accesses a service at a backup service agent, this protocol does not require messages are required per request compared

th the trad t... a pr t c... e er, the add t... a message c st s... t s g f ca t because each ser ce d ma... s ge era... c... figured... a... ca area et rk ke Ether et

determ st c rep cated ser ce requ res eaker c... strats t... e sure the c... s ste c tha a... determ st c... e... ther... rds, after the pr mar ser ce age t has determ ed the pr cess g... rder f e er request fr m m b e age ts, t s... t... ecessar that... the pr mar age t ha d es a... requests, a d c... rd... ates th the... ther rep ca ser ce age ts ke... the pr t c... *PRPNS* th th s bser at... e attempt t... use a... ght e ght pass e rep cat... pr t c... *PRPDS*, f r each determ st c ser ce d ma... he pr p sed pr t c... has the f... g features

- Each m b e age t ca use a ser ce... a the pr mar ser ce age t, r a backup... e
- O... the pr mar ser ce age t determ es the pr cess g... rder f e er request fr m m b e age ts
- fter a backup ser ce age t has rece ed a m b e age t request a d bta ed the rder f the request fr m the pr mar ser ce age t, the backup age t... t the pr mar... e, pr cesses the request a d c... rd... ates th the... ther rep ca ser ce age ts... c ud g the pr mar age t

ue t these des rab e features, th s pr t c... e ab es each... s t... g m b e age t t be f r arded t... a d e c ute... a... de ru... g a... am... g rep cated ser ce age ts... the ser ce d ma... f m b e age t  $a_j$  s tra sferred t the... de here a backup ser ce age t  $u_i^{backup}$  e cutes, *PRPDS* e cutes the f... g phases Other se, the three phases f *PRPNS* are perf rmed

**(Phase 1).** he  $u_i^{backup}$  rece es a request message fr m  $a_j$ ,  $u_i^{backup}$  asks the pr mar ser ce age t  $u_i^{prim}$  the *psn* f the request message... th s case, af ter  $u_i^{prim}$  determ es the *psn* f the message, t... t fies  $u_i^{backup}$  f the *psn*... he...  $u_i^{prim}$  pr cesses the request message a d sa es (*response, psn, next\_state, j, reqid*) f the message... ts bu er... he rece... g the *psn*,  $u_i^{backup}$  pr cesses the c rresp... d g request a d ge erates (*response, psn, next\_state*) f the request

**(Phase 2).**  $u_i^{backup}$  se ds the... ther ser ce age ts the update message (*response, psn, next\_state, j, reqid*) us... g *VSCAST* respect e... he each ser ce age t e cept f r  $u_i^{prim}$  rece es the update message, t updates ts state us... g *next\_state*, ma ta s (*response, j, reqid*)... ts bu er a d the se ds a ack... edgeme t message t...  $u_i^{backup}$  f  $u_i^{prim}$  rece es the update message fr m  $u_i^{backup}$ , t... ust rem... es the e eme t (*response, psn, next\_state, j, reqid*) f r the message fr m ts bu er, sa es (*response, j, reqid*)... the bu er a d se ds a ack... edgeme t message t...  $u_i^{backup}$

**(Phase 3).** O ce  $u_i^{backup}$  rece es a ack... edgeme t message fr m e er... ther... e ser ce age t, t se ds *response* t...  $a_j$

gure sh s a e c ut... f three m b e age ts  $a_i^l, a_s^m$  a d  $a_r^n$  attempt g t use ser ce  $u_i$  a  $u_i^2, u_i^1$  a d  $u_i^0$ ... the pr t c... *PRPDS*... th s figure... the

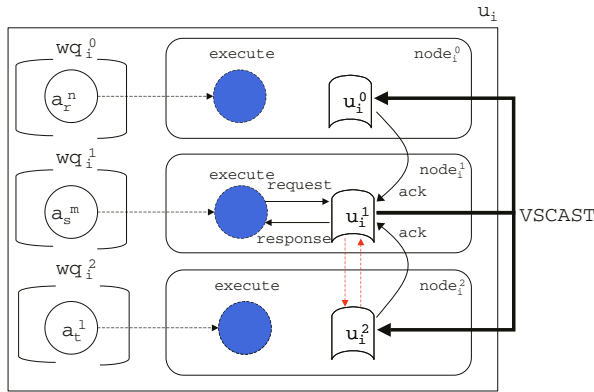


**Fig. 3.** an execution of three mobile agents accessing a replicated service  $u_i$  in the protocol *PRPDS*

procedure captured the execute. *PRPDS* the  $a_s^m$  sends a request to  $u_i^1$ . In this case,  $u_i^1$  asks the primary agent  $u_i^2$  the *psn* of the request  $u_i^2$  determines the *psn* and sends it to  $u_i^1$ . Then,  $u_i^2$  processes the request and sends (*response*, *psn*, *next\_state*,  $j + 1$ , *reqid*) of the request. Its buffer  $ea$  holds, after obtaining the *psn* of the request from the primary agent,  $u_i^1$  processes the request and coordinates with the other service agents  $u_i^2$  and  $u_i^0$  using *VSCAST* to satisfy the consistency condition for deterministic service. Then,  $u_i^1$  receives a acknowledgment from the secondary agent, it sends the response to  $a_s^m$ . From this figure, we can see that the protocol *PRPDS* makes significant improvement scalability of replicated services because each single mobile agent uses a particular service as a among replicated service agents. The service domain and the request processing are distributed and distributed between a set of service agents.

### 2.1 Recovery

If service agents fail in a service domain, the proposed protocol, *PRPNS* and *PRPDS*, should perform the recovery procedures to satisfy each consistency condition for deterministic service. Deterministic service despite the failures respectively. In the case of the crash of the primary service agent  $u_i^{prim}$ , the two protocols execute both each appropriate recovery procedure in the following cases

**(Case 1).** The primary service agent  $u_i^{prim}$  fails before finishing the phase. In this case, a secondary service agent  $u_i^{prim}$  selects among a backup service and sends a response of each request can be received from  $u_i^{prim}$ , the request can be reset to  $u_i^{prim}$ , which has already performed the phases through

**(Case 2).** The primary service agent  $u_i^{prim}$  fails after completing the phase, but before sending the response to the coordinator mobile agent.

In this case, a leader primary agent  $u_i^{prim}$  is selected. To ensure liveness, in this case, either all the backup servers receive the update message, or if they receive it *VSCAST* is used to satisfy the atomicity condition. In this case, a failure of a primary agent  $u_i^{prim}$  is detected. If a backup server receives the update message, this case is similar to Case 1. Otherwise,  $(response, j, reqid)$  is used to ensure the election semantics. In other words, the request from the coordinator is ignored. The primary server agent  $u_i^{prim}$  again sends the request. The server sends the response of the request to the first node that has received the request.

**(Case 3).** The primary server agent  $u_i^{prim}$  fails after finishing the phase. In this case, a leader primary server agent  $u_i^{prim}$  is selected and defined.

Eventually, the backup server agent  $u_i^{backup}$  crashes, *PRPNS* and *PRPDS* perform the recovery procedures as follows. *PRPNS*,  $u_i^{backup}$  is removed from its server group. Otherwise, *PRPDS* executes a coordinator recovery procedure in each failure case.

**(Case 1).** Backup server agent  $u_i^{backup}$  fails before asking the primary server agent  $u_i^{prim}$  the *psn* of each request in the phase.

In this case,  $u_i^{backup}$  is removed from its group. Afterwards,  $u_i^{backup}$ 's failures are detected because of the response of the request from  $t$ .

**(Case 2).** Backup server agent  $u_i^{backup}$  fails before finishing the phase.

**(Case 2.1).** The primary  $u_i^{prim}$  fails.

The other backup servers select a leader primary server agent,  $u_i^{prim}$ , among them.

**(Case 2.2).** The primary  $u_i^{prim}$  fails.

Eventually,  $u_i^{backup}$ 's crash,  $u_i^{prim}$  retrieves the update information  $(response, psn, next\_state, j, reqid)$  from its buffer and sends it to the other backup servers respectively. In this case, *VSCAST* is used to ensure liveness.

**(Case 3).** Backup server agent  $u_i^{backup}$  fails after sending the update message to the other servers in the phase 2, but before sending the response to the coordinator. The backup server agent

$u_i^{backup}$  sends the update message to the other servers but using *VSCAST*, the election is successfully held. Hereafter, the server group of  $u_i^{backup}$  has removed  $u_i^{backup}$ .

**(Case 4).** Backup server agent  $u_i^{backup}$  fails after completing the phase.

$u_i^{backup}$  is removed from its group and the backup agents can detect that  $u_i^{backup}$  fails.

### 3 Conclusion

In this paper, we proposed a new strategy to improve scalability of mobile agents systems by applying a appropriate passive replication protocol to each replicated service according to its execution behavior, deterministic or nondeterministic. For this purpose, we presented the two passive replication protocols, *PRPNS* and *PRPDS*, for deterministic and nondeterministic services respectively. Here, we suggest a new abstraction, the bandwidth-stimulated agent-based framework to execute the tasks and improve performance of a service agent. It is necessary to the primary agent. Especially, the message length protocol, *PRPDS* allows a service agent to process each mobile agent request and coordinate with the other replication service agents after receiving the request and bandwidth-dependent sequence number from the primary agent. Thus, *PRPDS* successfully reduced the storage and backup schemes [2], the request processing and coordination and can be extended to distributed among a set of deterministic and replicated service agents based on the workload of each service agent.

### References

1. P. Bellavista, A. Corradi and C. Stefanelli. The Ubiquitous Provisioning of Internet Services to Portable Devices. *IEEE Pervasive Computing*, Vol. 1, No. 3, pp. 81-87, 2002.
2. H. Bryhni, E. Klovning and O. Kure. A Comparison of Load Balancing Techniques for Scalable Web Servers. *IEEE Network*, 14:58-64, 2000.
3. N. Budhiraja, K. Marzullo, F. B. Schneider and S. Toueg. The primary-backup approach. *Distributed Systems*(S. Mullender ed., ch. 8, 199-216, Addison-Wesley, second ed., 1993).
4. X. Defago, A. Schiper and N. Sergent. Semi-Passive Replication. *In Proc. of the 17th IEEE Symposium on Reliable Distributed Systems*, pp. 43-50, 1998.
5. M. Fukuda, Y. Tanaka, N. Suzuki, L.F. Bic and S. Kobayashi. A Mobile-Agent-Based PC Grid. *In Proc. of the Fifth Annual International Workshop on Active Middleware Services*, pp. 142-150, 2003.
6. M. Herlihy and J. Wing. Linearizability: a correctness condition for concurrent objects. *ACM Transactions on Progr. Languages and Syst.*, 12(3):463-492, 1990.
7. K. Rothermel and M. Schwehr. Mobile Agents. In A.Kent and J.G.Williams(Eds.):*Encyclopedia for Computer Science and Technology*, 40(25):155-176, 1999.
8. M. Wiesmann, F. Pedone, A. Schiper, B. Kemme and G. Alonso. Understanding Replication in Databases and Distributed Systems. *In Proc. of the 21st International Conference on Distributed Computing Systems*, pp. 464-474, 2000.

# Multi-agent System Architectures for Wireless Sensor Networks

Richard Tynan, G.M.P. O'Hare, David Marsh, and Donal O'Kane

Adaptive Information Cluster (AIC),  
University College Dublin  
Belfield, Dublin 4, Ireland

{richard.tynan, gregory.ohare, david.marsh, donal.okane}@ucd.ie

**Abstract.** Traditionally Multi-Agent Systems have been thought of in terms of devices that possess a relatively rich set of resources e.g. power, memory, computational ability and communication bandwidth. This is usually necessary due to the complex deliberation and negotiation processes they require to fulfil their goals. Recently, networked devices have become available on the millimeter scale called Wireless Sensor Networks (WSNs), which pose new challenges because of their constrained resources. However what these devices lack in resources they make up for in numbers due to their small inexpensive nature. In this paper we identify some of the existing MAS architectures for WSNs, and we propose some novel architectures of our own.

## 1 Introduction

Modern computing networks are comprised of a wide range of heterogeneous devices that may possess various levels of resources and are interconnected using differing networking technologies. This gives rise to a device continuum with high-powered servers connected using high-speed GB/s LANs at one extreme and Mobile Phones connected using GPRS at the other. Multi-Agent Systems for subsets of this spectrum of devices are numerous. Diao et al [1] use autonomic management agents for Web server optimization. At the other end of the scale, Gulliver's Genie uses agents for context sensitive tourist information delivery in the mobile computing arena [2].

Contemporary advances in microprocessor fabrication has lead to a dramatic reduction in the size and power consumed by computational devices. Sensing technology, batteries and radio hardware have also followed a similar minaturisation trend. These factors combined have enabled the production of match-box scale, battery powered devices capable of complex processing tasks called Wireless Sensor Networks, thus heralding a new era for ubiquitous sensing technology. Previous deployments of these networks have been used in many diverse fields such as wildlife habitat monitoring [3], traffic monitoring [4] and lighting control [5].

The device spectrum for computer networks now has a new resource challenged device on which an agent could potentially be deployed - a WSN node. Agents have been deployed previously on WSNs primarily to process the raw data in an intelligent fashion with a view to reducing transmissions - the single biggest factor in determining

the longevity of a network [6], [7]. Agents have also been used in a lighting control application for energy conservation [5]. The research to date has mainly focussed on the application and not on the potential architectures for the MASs. In this paper we identify some existing MAS architectures and propose some new architectures.

## 2 Device Hierarchy

When considering the diverse range of devices that can comprise a modern computer network where an agent may be deployed it is useful to take into account of the resources available at each device. For our purposes we have identified a five tier hierarchy of devices. Figure 1 depicts this hierarchy and a device typical of each layer.

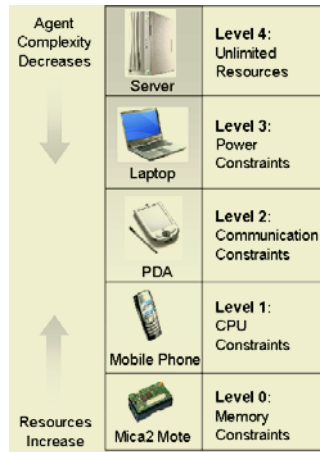


**Fig. 1.** Hierarchy of devices according to resources available

A more precise description of this hierarchy can be seen in table 1. A Level 4 device we consider to have unbounded resources in terms of the 4 criteria. Devices of this nature are connected to a mains supply and have vast memory and computational resources. Also their communication occurs over high-speed networks so network bandwidth is very high. Below this level the first distinction we make is power. We now enter the mobile computing arena based on battery powered devices. The next distinction that occurs is based on communication capabilities i.e. a laptop is usually connected to other nodes through a wireless LAN whereas PDAs and mobile phones use 3G technology and GPRS. The criteria separating level 2 and level 1 devices are CPU constraints. Due to the more complex operation of a PDA, compared to the mobile phone, it requires a faster CPU which would allow deeper agent deliberation. The final distinction between devices is that of memory. Modern mobile phone memory is of the order of megabytes whereas, a WSN node typically only has a few kilobytes.

**Table 1.** Table representing the various constraints of a device at a given level. An x indicates that this constraint is not a concern for an agent on a device in this layer. An o implies that the agent must be aware of this constraint

	Power	Communication	CPU	Memory
Level 4	x	x	x	x
Level 3	o	x	x	x
Level 2	o	o	x	x
Level 1	o	o	o	x
Level 0	o	o	o	o

So what implication does this have for MASs? An agent must be aware of its resident devices abilities and factor these into its deliberation about future actions. However this hierarchy becomes more interesting when we look at mobile agents. When an agent migrates between devices of different levels in the hierarchy the agent may opportunistically take advantage of the differing resources on a device. An agent migrating to a lower level device must be aware of this and tailor its reasoning process accordingly. For instance, when migrating from a level 4 to a level 3 device, an agent must be aware that, should the device's power become critically low, it should have a route available to it to leave the device. In the case of moving from a level 2 to a level 1 device, the agent may have to adapt to a simplified version of the agent platform that does not provide services common to larger platforms. When moving to a level 0 device, it is likely that the encoding of the agent's mental state will have to be radically reduced. Of course, when moving up through the hierarchy, an agent should become aware, or be made aware, that its operation is no longer as restricted as before, and tailor its behavior accordingly.

### 3 Wireless Sensor Networks

Wireless Sensor Networks (WSNs) are made possible by the minaturisation of their components, namely microprocessors, sensors and radio communication hardware. The main components for a WSN are a base-station and one or more sensor nodes. The sensor nodes relay their sensed data either directly to the base station or through each other (termed multi-hopping) depending on the scale of the network. In turn the base station sends commands to the nodes to, for example, increase their sampling frequency.

Multi-hopping, while useful in extending the reach or scale of a WSN, does have its pitfalls. The cost of transmitting a packet can be greatly increased depending on the distance a node is away from the base station. Secondly, since nodes nearest the base station, i.e. 1 hop away, will not only have to send their data but also that of all other nodes greater than a single hop, there will be a greater demand placed on the power supply of these nodes. It means that, in general, a nodes lifespan is inversely proportional to the number of hops it is away from the base station. To alleviate this problem, multiple base stations can be used, with the nodes only transmitting data to their local station. A second solution creates a hierarchy of nodes with varying power



and transmission capabilities. Higher power nodes act as a networked backbone for the lower powered sensors. One final alternative is to populate the area closest to the base station more densely than in outlying areas.

In some WSNs the nodes of the network can perform considerable processing tasks. This facilitates the examination of raw sensed data in an intelligent fashion with transmissions only containing summarized information rather than the raw data i.e. a single packet containing the average temperature over say ten seconds could be transmitted instead of ten individual packets containing the temperature as sampled at each second. Processing capabilities can vary from platform to platform. We have chosen the Mica2 Mote [8] for our experimentation. It has 4KB of RAM, 128KB of instruction memory and 512KB of flash memory for data storage purposes. They are also equipped with a suite of sensory modalities, heat, light, sound, barometric pressure and humidity.

## 4 Agents for Wireless Sensor Networks

Having seen that current research endeavors have shown not only the feasibility but also the utility for agents on WSNs we now turn our attention to candidate architectures that may prove appropriate.

### 4.1 WSN Nodes as Perceptors

The first architecture model considers individual nodes as perceptors for a single agent, as depicted in figure 2. On the perceive part of the perceive-deliberative-act cycle, the agent requests a sensed value from each node, which it then uses as input to the deliberative part of that cycle. This has a number of benefits and restrictions. Chief among the benefits is ease of programming, since there is a single control point in the system. The system will also be more synchronized with regard to the timing of transmissions, and hence more efficient. This is because any collisions during transmission necessitates a costly retransmission, so synchronization brings direct energy benefits.

The restrictions of this architecture are typical of centralized systems. The primary disadvantage is that the system is not scalable. There are two main reasons for this. Firstly, since each node must be queried to generate a perceptor value, as the number of nodes increases so does the length of the deliberative cycle. With current node radio speeds, the length of the cycle could quickly grow past one second. This is compounded by the second scalability problem, which is that with larger numbers of nodes, multi-hop communication is increasingly likely to be needed. This invariably leads to even greater time delays for the agent while it gathers its data, while energy consumption also rises. An additional problem is that if two or more agents wish to use the network as a set of perceptors, they will have to coordinate with each other to synchronize access, and of course they will be subjected to additional delays while waiting for the other agents to finish with the network. Larger networks also increase the likelihood of having unconnected parts of the network. In this architecture, these parts would remain inactive as long as they are unable to receive messages from the agent. This sort of architecture is probably most suited to small-scale networks which are not likely to have more than

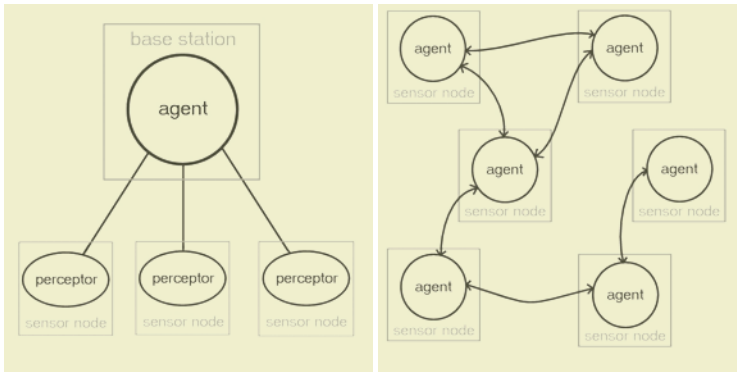


**Fig. 2.** WSN as perceptor to central base station agent (left), collaborative agent approach where agents are considered peers (right)

a single data sink (i.e. agent that wishes to use the network). As such it rarely exists in practice.

#### 4.2 One Agent per Sensor Node

In this architecture, each node in the network hosts an agent which is responsible for the behavior of that node (figure 2). This approach represents a distributed method of network control. The agents can co-ordinate their behavior to achieve both local and global goals, and so the network may be employed in more useful ways than in the simple perceptor case. For example, network services such as packet routing can be built within the framework of collaborating agents, whereas this is not possible in the centralized case where a layer independent of the controlling agent would be required.

One of the primary benefits of this architecture is scalability. Local tasks can be performed without multi-hopping messages across the network to a central controller, which leads to immediate energy and latency gains. Concurrency is another gain associated with decentralizing the responsibility for processing. This allows the network to perform more work in a given time period than could be achieved by other means. The effects of network partitioning are also alleviated somewhat by using this architecture, since partitioned regions can still perform local tasks.

Disadvantages of this method include the difficulty of creating systems of agents that can realize global goals using only local information. The cost of negotiation between agents is an overhead avoided by the centralized architecture. In a network of heterogeneous nodes, i.e. nodes with varying degrees of sensing and in particular computational resources, an agent on a faster node may experience little performance gain because of the limitations of the surrounding agents that must run on slower nodes. This architecture is most suitable when the sensors have some form of local actuation, as seen in [5], and [9].

### 4.3 Mobile Agents

This scheme uses an agent with migratory capabilities which visits a set of nodes, accumulating state as it does so. This is a typical method for data aggregation/fusion applications and is shown in figure 3. Benefits include low overall computational costs, as no more than one node is active at a time. Since a single transmission and reception event is all that is required of an individual node in order to facilitate the agent's migration, communication is also generally quite low. Simplicity is another benefit, since the agent manages both the task of collecting data and its visitation itinerary. The negative aspects of network partitioning have less impact on this method since an agent can simply alter its visitation itinerary to go to the nodes it can reach until connectivity is restored.

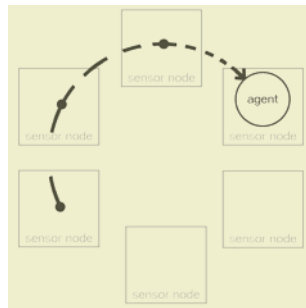


**Fig. 3.** Agent navigates the network for its control and data harvesting requirements

One disadvantage of this architecture is that if the node the agent is currently on fails (for example the battery depletes before the agent can migrate elsewhere), all data that has been accumulated by it so far would be lost. Methods to counter this include leaving copies of the state of the agent on previously visited nodes, which could "revive" the agent using this information in the event that the original was lost. Secondly, if latency is an important concern then this method is likely to be less efficient compared to the nodes-as-agents architecture because of the lack of concurrency. If a network is very large, it may take too much time for a single agent to gather all the data. This scheme is likely to be useful where nodes collect a lot of data before processing it [7].

Our initial experience with implementing MASs for WSNs has highlighted the advantages and disadvantages of the previous architectures, and motivated the development of the following 2 combined approaches. These attempt to harness the advantages of a number of the previous architectures while minimizing their disadvantages.

### 4.4 Hybrid Approach

If we roughly describe the advantages of the three methods above as being simplicity, robustness and efficiency respectively, and their weaknesses as being scalability, complexity and latency, then we can attempt to combine them in such a way as to reduce the

impact of the weaknesses while retaining the advantages. This leads to the following hybrid approaches as illustrated in figure 4.

**Collaborative Agents: Each agent is a perceptor type group.** As was mentioned above, the first architecture is not suitable for larger networks of sensors. However, if the network is divided into numerous small groups of nodes, each one could contain a single agent that is responsible for several nodes. The system can be viewed at a high level as a collection of collaborating agents, and at a low level as a collection of nodes being managed by one agent. At the level of the individual agent, most of the problems associated with the lack of scalability will no longer apply once the number of nodes the agent is responsible for is low enough. While network partitions may still cause problems, the chance of them occurring in a small group of nodes is much reduced, and the groups of nodes could be organized around such disturbances. The disadvantages of the collaborative agent architecture are lessened by combining it with the first approach. Since there are less agents, co-ordination cost between agents are reduced. Heterogeneous networks could be organized in such a way that every agent operates on an approximately equivalent set of nodes, which should mask the inequalities present when each node has its own agent.

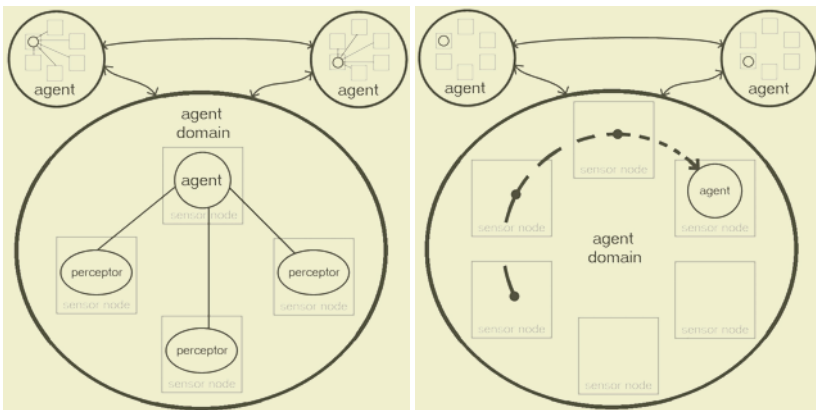


**Fig. 4.** Agents are allotted a subset of the network for control based on the perceptor model. Agent cooperation then performs high level control and harvesting (left). The agent controls and senses its environment by migrating to the sensor nodes under its control (right)

**Collaborative Agents: Each agent is the domain for a mobile agent.** Combining the second and third architectures also reduces some of the problems that they have on their own. Once again, the network can be divided into small groups of nodes, but in this instance each group has a single mobile agent that migrates between the constituent nodes. The latency issue for the migrating agent architecture is reduced by reducing the number of nodes it has to traverse. The probability of an agent being trapped on a node that is going to fail is also reduced as the number of nodes it travels among lessens. For the same reasons as in the first combined architecture, the disadvantages of the collaborative approach are reduced when combined with the mobile agent case.

## 5 Conclusions

Recent work has shown that multi-agent systems can be deployed on the new wave of computationally limited devices that have emerged in the last few years. One of the latest classes of these devices is the wireless sensor node. In line with the general trend of adapting agents to work on decreasingly powerful equipment, the use of agents on such simple platforms brings a new set of challenges. We detailed the restrictions that exist at the different levels of sophistication in order to illuminate the problems faced by an agent when executing at the various levels. We then provided a brief introduction to wireless sensors networks, specifying their components, the capabilities of these components, the pressing research issues and an example of some WSN hardware. Finally we outline MAS architectures that we believe are appropriate to use on WSNs. We give details of their respective advantages and disadvantages, and with these points as a guideline we posit the situations in which they are likely to be useful. Included is a pair of hybrid architectures, with the elements combined in order to minimize their negatives while maintaining their positive qualities.

## Acknowledgements

This material is based on works supported by Science Foundation Ireland under Grant No. 03/IN.3/I361. We would also like to thank the Irish Research Council for Science, Engineering and Technology (IRCSET) for their support.

## References

1. Diao, Y., Hellerstein, J.L., Parekh, S., Bigus, J.P.: Managing Web Server Performance with AutoTune Agents. *IBM Systems Journal* **42** (2003) 136–149
2. O’Grady, M.J., O’Hare, G.M.: Gullivers’s genie: Agency, mobility and adaptivity. *Computers and Graphics Journal, Special Issue on Pervasive Computing and Ambient Intelligence - Mobility, Ubiquity and Wearables Get Together*. **28** (2004)
3. Mainwaring, A., Polastre, J., Szewczyk, R., Culler, D., Anderson, J.: Wireless Sensor Networks for Habitat Monitoring. In: *International Workshop on Wireless Sensor Networks and Applications*. (2002)
4. Coleri, S., Cheung, S.Y., Varaiya, P.: Sensor Networks for Monitoring Traffic. In: *Allerton Conference on Communication, Control and Computing*. (2004)
5. Sandhu, J., Agogino, A., Agogino, A.: Wireless Sensor Networks for Commercial Lighting Control: Decision Making with Multi-agent Systems. In: *AAAI Workshop on Sensor Networks*. (2004)
6. Marsh, D., Tynan, R., O’Kane, D., O’Hare, G.: Autonomic wireless sensor networks. *Engineering Applications of Artificial Intelligence* (2004)
7. Qi, H., Wang, X., Iyengar, S.S., Chakrabarty, K.: Multisensor Data Fusion in Distributed Sensor Networks Using Mobile Agents. In: *4th International Conference Information Fusion*. (2001)
8. Hill, J.: System Architecture for Wireless Sensor Networks. PhD thesis, UC Berkeley (2003)
9. Braginsky, D., Estrin, D.: Rumor routing algorithm for sensor networks. In: *WSNA*. (2002)

# ACCESS: An Agent Based Architecture for the Rapid Prototyping of Location Aware Services

Robin Strahan, Gregory O'Hare, Conor Muldoon, Donnacha Phelan,  
and Rem Collier

Department of Computer Science, University College Dublin, Dublin 4, Ireland  
{Robin.Strahan, Gregory.OHare, Conor.Muldoon,  
Donnacha.Phelan, Rem.Collier}@ucd.ie  
<http://emc2.ucd.ie>

**Abstract.** We describe the Agents Channelling ContExt Sensitive Services (ACCESS) architecture, an open agent-based architecture that supports the development and deployment of multiple heterogeneous context sensitive services. We detail the ACCESS architecture and describe the scenario of an individual arriving in a city and using his ACCESS enabled PDA to secure lodgings.

## 1 Introduction

This paper describes the Agents Channelling ContExt Sensitive Services (ACCESS) architecture, an open agent-based architecture that supports the development and deployment of multiple heterogeneous context sensitive services. A key motivation for the development of ACCESS was the recognition that most location-aware context sensitive applications exhibit a common core of functionality. That is, such systems commonly employ: location-sensing technologies, dynamic generation of maps that are customised to the user, support for the management of the users context, and service brokerage.

In this paper we review some related systems, detail the ACCESS architecture paying particular attention to three facets: map caching, user profiling, and agent tuning and finally, we demonstrate the interaction between ACCESS and a mobile user by presenting the scenario of an individual arriving in a city and seeking a hotel room.

## 2 Related Work

There are a number of existing systems that aim to provide a basis for the development of agent-based context aware systems.

MyCampus is an agent-based environment for context-aware mobile services developed at Carnegie Mellon University [1]. The system aims to aid a PDA equipped user in carrying out different tasks (planning events, send messages, find other users, etc) by accessing Intranet and Internet services. The information from these services is filtered by use of context, such as the user's location, their class schedule, the location of their friends and the weather. Personal preferences are also used to tailor the information provided to the user.

The SALSA framework [2] allows developers to implement autonomous agents for ubiquitous computing systems. It uses WiFi to communicate and estimates the user's position by triangulation of at least three 802.11 access points. It uses an open source Instant Messaging Server (Jabber) to notify the state of people and agents, and to handle the interaction between people, agents, and devices through XML messages. Agents abstract the complexities associated with the collaboration of users and the opportunistic interaction with services of ubiquitous computing environments.

The COBRA (COntext BRoker Architecture) [3] is a broker-centric agent architecture that aims to reduce the cost and difficulty of building context-aware systems. At its centre is an autonomous agent called the Domain Context Broker that controls a context model of a specific domain or location. It updates this model, using data from heterogeneous sources (physical sensors, Web, pattern behaviours, etc) and attempts to resolve any detected context conflicts. It shares this information with independent agents within its domain. The use of broker-centric allows computational intensive activities such as gathering and interpreting data to be preformed by a suitable device rather than on resource limited devices.

### 3 The ACCESS Architecture

As an agent-based architecture intended to support the rapid development and deployment of multiple heterogeneous context sensitive mobile services, the Agents Channelling ContExt Sensitive Services (ACCESS) architecture seeks to provide support for multi-user environments by offering personalization of content, through user profiling and context, as well as support for mobile lightweight intentional agents and intelligent prediction of user service needs.

The ACCESS architecture has been designed to extend Agent Factory (AF), a well-established framework [6][7] for the development and deployment of multi-agent systems. The ACCESS architecture enhances the basic infrastructure delivered by the AF run-time environment through the implementation of additional agents, which deliver functionality that is common to many context-sensitive applications. These ACCESS Management Agents form a cohesive layer into which multiple heterogeneous context-sensitive services may be plugged. In addition, the existing AF development methodology has been augmented to aid the developer in producing ACCESS-compliant services. The resulting ACCESS toolkit facilitates the rapid prototyping of context-sensitive services by allowing service developers to focus on the service business logic, and not the infrastructure required to deliver it.

### 4 ACCESS Management Agents

The ACCESS Management agents implement the core functionality of the ACCESS architecture, which includes context management, user profiling, map generation, content delivery, account management, and location sensing. The User Profiling Agent, acting in tandem with the Activity Analyzer Agent and the Context Agent, undertakes personalization. The User Profiling Agent provides a mechanism to allow agents to request a user's preferences, adopting a neighbourhood-based approach to

identify this set of similar users. Implicit profile information is obtained using data mining techniques on recorded user activity, for instance when examining service usage, what was used, when it was used, and where it was used is noted.

The notion of user context is the concept that ACCESS employs to determine not only what services the user may require, but also where and when to offer them. A user's context is considered a combination of their location, preferences and previous activities. It is the responsibility of the Context Agent to create and manage user specific hotspots. A hotspot is a region of space-time that is limited by specified bounds (e.g. an area of 100 square meters centred around a particular shop, during business hours). The Context Agent informs the Profiling Agent when a user encounters a hotspot, which then decides whether the hotspot breach is relevant to the user.

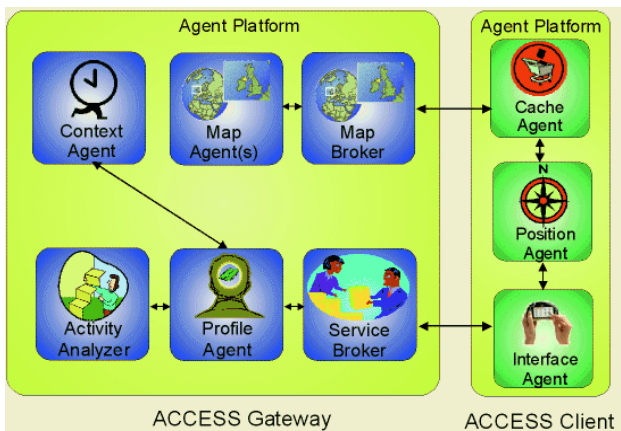


**Fig. 1.** Access Management Agents

The Map Server element is made up of the Map Broker and one or more Map Agents. The Map Broker manages the dynamic generation of maps for a specified location. When the Map Broker is requested to generate a map, it communicates with a number of Map Agents to determine which of them can produce the most suitable map. The selected Map Agent then generates the map segment which can subsequently be merged with service specific content overlay. This peer community of Map Agents allows for distribution of load and for a degree of failure protection.

The Position Agent is responsible for periodically informing subscribed agents of updates in the user or device's position. The Position Agent currently determines position by use of a GPS receiver.

To provide service specific functionality, abstract Service Manager and Service Delivery roles are provided that a service developer may extend. These roles encapsulate the requisite agent-based functionality for interacting with the core infrastructure. The Service Manager role is responsible for advertisement of the service by registering with a Service Broker Agent and for registering the service with other ACCESS compliant services that it may wish to use. The Service Delivery role acts as the users representative within a service and collaborates with the Service Manager Role and an



Interface Agent. The service developer must extend this role with additional behaviour patterns to interact with service specific agents.

The Interface Agent manages the user's interaction with the Graphical User Interface within the system. Additionally it provides a means by which it may dynamically extend its functionality at run-time through the use of Java introspection for the provision of service specific functionality.

#### 4.1 Map Caching

A key feature of any application or service built using the ACCESS architecture is the ability to provide dynamically generated maps. But with ACCESS being primarily aimed at resource-limited devices such as PDAs or smart phones, it is desirable to minimise the detriment in making use of this feature.

There are two methods used to minimise the cost of using the map feature; the first focuses on minimising the delay between a device requesting a map and rendering it, the second attempts to minimise both the time delay and the communication or bandwidth cost in displaying a map.

The first method consists of pre-emptive or active caching. This is accomplished by attempting to determine the user's future direction of travel. The Cache Agent tracks the user's heading and calculates the average heading. When the user approaches the edge of the current map, this average heading is used to establish which map segments are requested by the Cache Agent from the Map Server. So, for example, if the average heading was 90°, then the Cache Agent would request three map segments covering the area to the east of the user's current location. In addition, knowledge communicated to the Cache Agent from other agents, such as user location, history from the Activity Analyzer Agent etc, can influence which map segments are requested. This pre-fetching of the segments results in the map segment being immediately available for rendering, thus minimising the delay in changing the currently displayed map segment to the next segment.

The second method attempts to remove the bandwidth or communication cost in sending and receiving data between the Cache and Map Agents. This is done through the use of passive caching. Each map segment that is received from the Map Server, including segments used in active caching, is stored locally (cached) on the device by the Cache Agent. When a new map segment is required by the user, the Cache Agent will attempt to retrieve a suitable map segment from this cache and will only request a map segment from the Map Server if there are no segments in the cache that meets the user's requirements. If several suitable segments from the cache are found, the Cache Agent selects the segment whose centre is closest to the user's current location, thereby attempting to maximise the amount of time before another segment is required.

#### 4.2 User Profiling

The fact that ACCESS is a tool kit for the deployment of context sensitive services places some unique constraints on the design of the User Profiling Agent, such as the fact that anticipating the profiling requirements of individual service developers is difficult, if not impossible. In an attempt to overcome this obstacle ACCESS users are

provided with a ‘generic’ ACCESS profile containing personal data such as gender, address, age, job description, education etc., which service developers can augment with a service specific profile. Using this generic profile, the User Profiling Agent can identify a set of similar users to use as recommendation partners for the active user. Users *must* explicitly complete their generic profile when registering with ACCESS, whether a user is required to supply a set of service specific preferences is a matter for the individual service developer. Should a user not enter a service profile, some personalisation is possible from the ACCESS profile. Items being recommended to the user may also have their own profiles listing their distinguishing features (for instance in a hotel finder application each hotel might have a profile listing its amenities). Again this is a matter for the service developer.

The ACCESS User Profiler Agent adopts a neighbourhood-based approach in identifying a set of similar users to use as recommendation partners for the active user. The measure of similarity adopted to identify this set is neither a correlation measure nor a vector-based cosine similarity metric. Instead, a simple overlap measure, where, for each user, the number of preferences rated identically to the active user, constitutes the overlap similarity value.

$$\text{sim}(x,y) = \frac{|\text{preferences}(x) \cap \text{preferences}(y)|}{|\text{preferences}(x) \cup \text{preferences}(y)|}$$

The number of overlapping items in the active user (x)’s profile and a test user (y)’s profile is simply counted. The union of all their preferences, as a normalising factor, divides this value. This method, known as the Jaccard similarity metric, is quite a simple way of measuring user similarity, but we can take the similarity value obtained from this method as indicative of the ACCESS user profiles true similarity, because the ratings in each user’s profile are obtained by explicit means (that is, users consciously elected to give a certain value to a given question), rather than implicitly-required ratings, which can sometimes be misconstrued or inaccurate reflections of users profiles.

### 4.3 Agent Tuning

Collaborative Performance Tuning is an autonomic procedure by which ACCESS management agents collectively alter their response times so as to adapt to the dynamic utilities and requirements of the software systems that they represent. The tuning framework enables inactive agents to go into a temporary hibernation state without affecting their ability to react to their environment in a timely manner. The hibernation subsystem monitors an agent’s commitments and reduces the number of redundant CPU cycles wasted on agents whose mental state does not change between iterations of their control algorithm. Once an agent goes into hibernation, other agents on the platform may opportunistically reduce their response times to take advantage of the additional computational resources made available.

Other systems [9][10] have been developed for the collective negotiation of CPU resources. Collaborative Performance Tuning differs from these systems in that a BDI approach is used that utilises the notions of joint intentions and mutual beliefs thus coercing agents into forming coalitions and to act as a team. This prevents agents getting into prisoner dilemma type scenarios in which agents making locally optimal

decisions create socially unacceptable behaviour patterns in which all agents concerned are worse off as an inevitable consequence of rational choice.

As the inference engine executes, it examines the number of commitments an agent has on its current deliberative cycle. If the agent does not have any commitments it is said to be inactive on that cycle. The rationale for this is that given an agent's current mental state, if an agent is inactive on a particular cycle and its mental state will not change on the next cycle, the agent need not deliberate on the next cycle as it knows that its mental state will not be altered.

At various stages throughout execution ACCESS agents may collectively alter their response times to adapt to the evolving system requirements. Joint intentions are utilized whereby rather than unilaterally reducing its response time an agent must adopt a commitment to make its intentions mutually believable to all active agents on the platform. This implies that an agent must communicate with and receive a response from all other active agents before taking action. Thus ensuring that agents act in a manner that is beneficial to the team as a whole. The problem with collective decision-making however is that decisions can only be made as fast as the slowest decision maker. Within the ACCESS architecture the Position Agent often operates with quite a large response time, agents cannot self-tune or pre-empt the Position Agent because to do so they would have to act unilaterally. This prevents Collaborative Performance Tuning being used for tasks with a low level of granularity such as rendering maps, which with modern just-in-time compilers would be completed prior to the termination of the negotiation process. Therefore Collaborative Performance Tuning is primarily used to improve efficiency in medium to high-level quality of service problems or to improve the general performance of the system over the entire course of its execution as the system adapts to dynamic environment conditions.

## 5 A User Scenario

To illustrate the usefulness and appropriateness of ACCESS we consider a fictitious character Joe arriving at an airport equipped with a PDA hosting ACCESS. Initially when Joe loads ACCESS at the airport he receives an advertisement for Sos, an accommodation finding application, which his Interface Agent received from a Service Broker. Joe clicks the advertisement to download Sos and to start the Service. The Interface Agent contacts an appropriate Service Manager whose name it received from the Service Broker to begin using Sos. When the Interface Agent registers with the Sos Service Manager it is delegated to a Service Delivery Agent. The Sos Service Delivery Agent then checks to see if Joe has been registered with an additional Meeting Service. The Meeting Service is used to keep track of the user's diary. If Joe has been registered the Service Delivery Agent of Sos requests the Service Delivery Agent of the Meeting Service to inform it of meetings relevant to Joe's current spatial context. The Meeting Service is aware of the locations of meetings that Joe will be attending and thus returns an appropriate list.

Joe is now presented with a screen (Fig. 3) allowing him to select his room preferences and a drop down list containing points of interest that has been populated with

relevant meetings and popular tourist attractions. Selecting an option from this list indicates that Joe would like his hotel to be located within the vicinity of the chosen item. Once the room details have been selected, the Profile Agent is contacted to obtain an appropriate list of hotels. The Profile Agent factors in implicit and explicit preferences, tariffs charged for the advertisement of hotels in addition to proximity of user's location and points of interest when generating this list. Once Joe receives the list and selects a hotel, the Sos Service Delivery Agent pushes the advertisement for a Bus Service. When Joe loads the Bus Service it receives the destination hotel location, which it uses to work out an appropriate route. The Caching Agent is informed of this route, which it uses to pre-emptively request the generation of maps for the impending journey. The Bus Service Delivery Agent collaborates with an additional Location Service, which operates in the background without the Joe's knowledge. The Location Service works with the Caching Agent in obtaining maps from the map server centred on Joe's position for tracking purposes.



**Fig. 3.** Room Select Screen and Position Agent tuning Mental State

When Joe gets onto the bus and starts travelling the Position Agent realizes that Joe's average velocity has increased and that it needs to reduce its response time. Fig. 3 illustrates the Position Agent's mental state. The Position adopts a commitment to reduce its response time and thus informs the other team members of the situation. On receiving this information the Interface Agent adopts a commitment to have its response time increased whereas the Cache Agent adopts a commitment to reduce its response time. Once all agents receive replies from their teammates their response times are altered. The Agents will maintain these altered response times so long as Joe's average velocity remains within a certain range.

## 6 Conclusions

This paper has described ACCESS, a generic agent based architecture for the rapid development and role out of location aware services. The key characteristics and differentiators of this architecture are the provision of lightweight intentional mobile agents, which offer an agent tuning ability, support dynamic profile updates, dynamic map generation and a rich concept of context. ACCESS context awareness enables and underpins degradation or enhancement of content to suit the device context and user needs.

## Acknowledgements

We gratefully acknowledge the support of Enterprise Ireland (grant ATRP/01/209) and Science Foundation Ireland through Modelling Collaborative Reasoners (SFI Investigator Award).

## References

1. Sadeh N., Chan T., Van L., Kwon O. and Takizawa K., Creating an Open Agent Environment for Context-aware M-Commerce, in *Agentcities: Challenges in Open AgentEnvironments*, LNAI, Springer Verlag (2003).
2. Rodríguez M. and Favela J., A Framework for Supporting Autonomous Agents in Ubiquitous Computing Environments, *Proceedings of System Support for Ubiquitous Computing Workshop at the Fifth Annual Conference on Ubiquitous Computing (UbiComp 2003)*, Seattle, Washington, (2003).
3. Chen M, An Intelligent Broker Architecture for Context-Aware Systems, PhD Dissertation Proposal, UMBC (2002).
4. Pearce J., IBM: Pervasive Computing is the future, ZD Net article, Jan 30 2003 (2003).
5. Creese S., Future Challenges in Pervasive Computing Environments, SC Infosec article, Mar 5 2003 (2003).
6. Collier, R., Agent Factory: A Framework for the Engineering of Agent-Oriented Applications, *Ph.D. Thesis*, Computer Science Dept., University College Dublin, Ireland (2001).
7. Collier, R.W., O'Hare G.M.P., Lowen, T., Rooney, C.F.B., Beyond Prototyping in the Factory of the Agents, 3rd Central and Eastern European Conference on Multi-Agent Systems (CEEMAS'03), Prague, Czech Republic (2003).
8. Dey, and G. Abowd, Towards a Better Understanding of Context and Context-Awareness, *Proceedings of the CHI 2000 Workshop on The What, Who, Where, When, and How of Context-Awareness* (2000).
9. Soh, L.-K., Tsatsoulis, C., Agent-Based Argumentative Ne-gotiations with Case-Based Reasoning. *AAAI Fall Symposium Series on Negotiation Methods for Autonomous Cooperative Systems*, North Falmouth, Mass. (2001)
10. Walsh, W.E. and Wellman, M.P., A market protocol for decentralized task allocation: Extended version. In *The Proceedings of the Third International Conference on Multi-Agent Systems (ICMAS-98)* (1998).

# Immune-Based Optimization of Predicting Neural Networks

Łukasz Adar, Arkadiusz Kucharski

Institute of Computer Science,  
AGH University of Science and Technology,  
Mickiewicz Avn. 30, 30-059 Cracow, Poland  
{olekb,doroh}@agh.edu.pl

**Abstract.** Artificial immune systems turned out to be an interesting technique introduced into the area of *soft computing*. In the paper the idea of an immunological selection mechanism in the agent-based optimization of a neural network architecture is presented. General considerations are illustrated by the particular system dedicated to time-series prediction. Selected experimental results conclude the work.

## 1 Introduction

In the last few years, soft computing researchers have turned to the processes based on nature such as biological adaptation, simulated annealing, genetic algorithms, etc. In the area of *soft computing*, artificial immune systems (AIS) have become a very popular research area. The idea of using the principles of immunology to solve optimization problems is very attractive. In the last few years, many researchers have turned to the processes based on nature such as biological adaptation, simulated annealing, genetic algorithms, etc. In the area of *soft computing*, artificial immune systems (AIS) have become a very popular research area. The idea of using the principles of immunology to solve optimization problems is very attractive. In the last few years, many researchers have turned to the processes based on nature such as biological adaptation, simulated annealing, genetic algorithms, etc. In the area of *soft computing*, artificial immune systems (AIS) have become a very popular research area. The idea of using the principles of immunology to solve optimization problems is very attractive.

The idea of using the principles of immunology to solve optimization problems is very attractive. In the last few years, many researchers have turned to the processes based on nature such as biological adaptation, simulated annealing, genetic algorithms, etc. In the area of *soft computing*, artificial immune systems (AIS) have become a very popular research area. The idea of using the principles of immunology to solve optimization problems is very attractive. In the last few years, many researchers have turned to the processes based on nature such as biological adaptation, simulated annealing, genetic algorithms, etc. In the area of *soft computing*, artificial immune systems (AIS) have become a very popular research area. The idea of using the principles of immunology to solve optimization problems is very attractive.

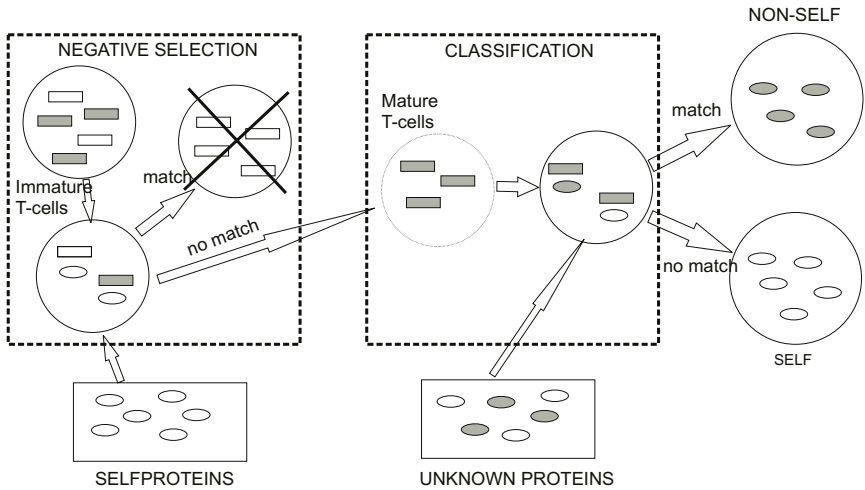


**Fig. 1.** Negative selection mechanism in artificial immune systems

... after a short presentation of the basics of human immune system and artificial immune systems, the details of the proposed approach are given. First the detailed evolutionary algorithm system for time series prediction is described. Then the application of immune based selection mechanism, age based evolutionary architecture, optimization systems proposed, preliminary results, bibliography and topics for prediction problem are given for the first time. This is the draft.

## 2 Artificial Immune Systems

... immune system passes a key role in maintaining the stability of the human body. The cellular and humoral responses are responsible for detecting and eliminating foreign substances, termed infectious agents and organisms, such as bacteria and viruses. One of the most important adaptation mechanisms of the human immune system is the process of negative selection, which allows for removal of lymphocytes that recognize self cells.

... recent approaches inspired by the human immune system were constructed and applied to healthcare applications. Some of the proposed methods, such as classification, optimization, and regression, are based on immune based algorithms using negative selection mechanism. These are illustrated as a case study of machine learning concept, as described below.

... Conceptual framework can be framed as the problem of acquiring the definition of a general category given a sample of positive and negative training examples. These categories' elements thus the solution can be defined.

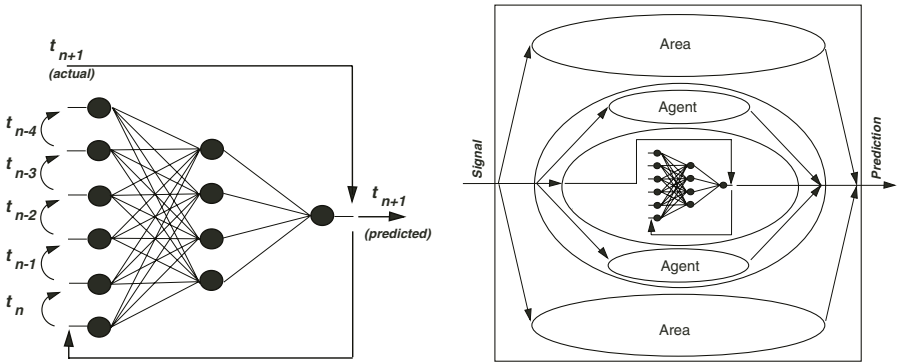


Fig. 2. A single predicting neural network (a) and the whole multi-agent system (b)

to groups self (positive) and self (negative) artificial immune system, which consists of a large number of lymphocytes can be trained to recognize these signals in the process of negative selection. At the beginning the lymphocytes are created, but at this point they are considered immature. Next, the affinity binding of these cells present self cells (good signals of some problem) is evaluated. The lymphocytes that bind themselves to good cells are eliminated. Only lymphocyte cells that survive after process are considered mature (see figure 1). Mature lymphocytes are presented with the cells that have unknown origin (the maybe self, or self cells), and they are believed to have potential to classify them.

### 3 Neural Agents for Time-Series Prediction

*Prediction (or forecasting)* is a general term for formal, albeit the possible future development of some process from data about its past and present behavior. Our main series prediction consists of searching for some trends in the sequence of values of some variable.

As we emphasize from the literature show that neural networks may be successfully used as a mechanism to model the characteristics of a signal as a system for a time series prediction. The choice of a particular architecture of the network is a large extent determined by a particular problem. Usually, the output value of the series is predicted on the basis of a fixed number of the previous values. Thus the number of input neurons corresponds to the number of values the prediction is based on, and the output neuron(s) give prediction(s) of the next time value(s) of the series. The multilayer perceptron (MLP) (see figure 2a) should predict  $t_{n+1}$  value of the series, based on some previous values, which are given the inputs of the first layer. The  $t_{n+1}$  value is predicted, the outputs are shifted, and the value  $t_{n+1}$  is given as the input to the next neuron.



of the first a few iterations may be superfluous, using the comparison between values predicted and received as an error measure.

Multi-agent prediction systems appear to be a good way to improve the performance of dependent tasks. For example, data and generated predictions [4] in this case subsequent events of the input sequence(s) are supported. The error metric here becomes an absolute error (see fig 2b). Each agent maintains predictions of a subset of the total components of the input obtained from the possessed external network. Of course the external network is based on the agent using common data. On the basis of predictions of agents, predictions of the whole system may be generated e.g. by the means of REO algorithm [2]. Such a system structure features various processes as for search, gathering external network architecture and learning parameters must be able for the current problem and system configuration, just like external multi-agent systems.

## 4 Immune-Based Selection in Evolutionary Multi-agent Systems

The idea of *EMAS* as a read described and successful applied to several difficult problems including optimization and prediction [2].

The key idea of *EMAS* is the cooperation of evolutionary processes in a multi-agent system at a population level. Its means that besides interacting mechanisms typical for agent-based systems (such as communication) agents are able to *reproduce* (generate new agents) and *die* (be eliminated from the system) heritability be accomplished by appropriate definition of reproduction, which is similar to classical evolutionary algorithms. Set of parameters describing basic behaviour of agents selected to get population inherited from its parent(s) through the use of mutation and recombination.

The proposed concept of selection corresponds to its natural type and is based on the existence of renewable resource called *life energy*. Energy is gained and spent by agents to execute actions, create energy and reward for good behaviour of agents, decrease a penalty for bad behaviour (which behaviour is considered good or bad depends on the particular problem to be solved). At the same time the level of energy determines actions of agents as able to execute particular energy level should create possibility of death and high energy level should create possibility of reproduction [7].

In the simplest case the evaluation of an agent (its phenotype) is based on the idea of agent reward, assuming some global reward structure. The error metric, agents evaluate the reward, and the change in energy of agents (considering the fitness) are forced to give a fixed amount of the reward. The better the global reward is, the more energy causes that successful generations, survived agents should represent better approximation of the solution.

In order to speed up the process of selection, based on the assumption that bad phenotype comes from the bad genotype, a set of agents (acting

as mhc tetra-peptides may be introduced. They are respectively recognized and removed by age-specific T-helper T cells. The genetic pattern possessed by these mhc tetra-peptides. Of course there must exist some predefined affinity function, e.g. using real-valued genetic material may be based on the percentage difference between chromosomes. The genetic tetra-peptides may be created in the system automatically.

According to our system, tetra-peptides are created through random genetic pattern search with the patterns generated by some other technique designed to solve a similar problem.

- causation after the act of death, the target genetic pattern is transferred to mhc tetra-peptide basis of mutation operator, and the newly created group of mhc tetra-peptides is introduced to the system.

In both cases, the newly mhc tetra-peptides must undergo the process of selection. In a specific period of time, the affinity of the immature mhc tetra-peptide through the genetic age-specific generation algorithm (tested fitness high (mhc tetra-peptide recognized genetic age-specific)) they are removed from the system if the affinity is low. In principle, they are able to recognize self and non-self (bad age-specific) antigens through high efficiency.

## 5 Immunological Multi-agent System for Neural Network Optimization

The immune algorithm has selected individuals (computational agents and mhc tetra-peptides) and case features. The optimization may be described as follows.

First, the population of computational agents is initialized through random problem solutions (features and learning parameters) and the target error rate. Every agent is able to perform prediction of subsequent time series values after it acquires actual value and modifies the weights of its feature set. In the first step of the learning process, using the described earlier *agent rendezvous* activity compares its fitness with the neighbors and exchanges a part of its error with them. When the error rate reaches certain level, agents look for the neighbor that is able to reproduce, and then create a new agent, and then a fixed proportion of the parent's error is passed to the child. The agent dies when its error falls below certain level. It is removed from the system and a new mhc tetra-peptide is created based on its genetic pattern.

The specific task for a mhc tetra-peptide is affinity test. The genetic mhc tetra-peptides search the population for antigens similar to the genetic pattern. The affinity of a mhc tetra-peptide to the antigen is determined by the process of selection. It causes the removal of similar antigen. Other selected mhc tetra-peptides removed from the system. In the proposed approach, the affinity is determined using the relationship of the chromosomes. The fitness function is given by  $p = p_1 \dots p_n$  be a

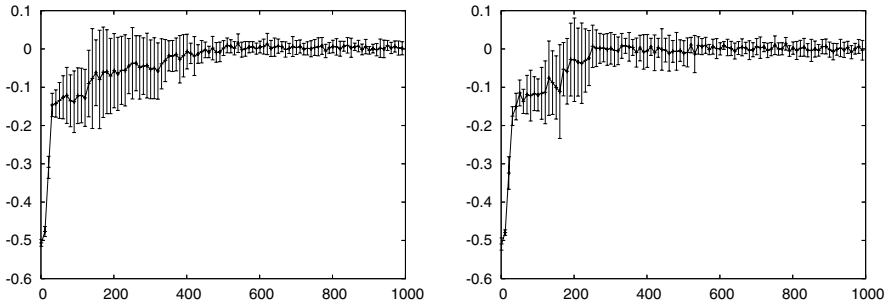


Fig. 3. Prediction error obtained for EMAS (a) and iEMAS (b)

parat. pe (ge. . t pe patter. . . ed b the . mph. c te) a d  $e_1 \dots e_n$  be a  
 ep. t. pe (ge. . t pe . . ed b the a. t ge. . . the descr. bed s. stem t. s s mp.  
 the ge. . t pe. f the tested age. t), a d  $n$  s the e. gth. f the ge. . t pe. f  $d_{max}$  s  
 the ma. m. um de. at. . . a d  $c_{min}$  s the m. m. um c. u. t. f c. rresp. d. g ge. es,  
 the c. . struct. . . f the set. f c. rresp. d. g ge. es ma. be c. . s dered

$$G = \{p_i \mid \left| \frac{p_i}{e_i} \right| \leq d_{max}\}$$

he . mph. c te s c. . s dered as st mu. ated (ts affi. t. reached m. . ma. e. e.)  
 he  $\bar{G} \geq c_{min}$ , a d c. . s dered as . . . st mu. ated. ther. se

## 6 Preliminary Experimental Studies

he s. stem as des. g. ed a d mp. e. m. ed us. g d str. buted e. . ut. . ar mu. t  
 age. t. p. at. f m. . t. E. de. e. p. ed at G (http://antnet.sourceforge.net)

he e. p. e. m. e. ts. ere perf. rmed . . rder t. sh. . . hether the . tr. duct. .  
 . f the mmu. . . g ca. based se. ect. . . mecha. sm. . t. E. . . . make the c. as  
 s ca. e. erget c. se. ect. . . m. r. e. e. ct. e. . d st. rted s. us fu. ct. . . as used as a  
 be. chmark f. r pred. ct. . .

E. . ut. . ar mu. t age. t s. stem c. . s st. ed f. . . e. e. . ut. . ar s. a d, th  
 . t a. p. pu. at. . . f . . age. ts. he ge. . t pe. f the age. t c. ta. ed the des.  
 cr. pt. . . f a feed f. r. ar d. . eura. . et. . rk (mu. t. a. ered perceptr. . . ) c. u. t  
 . f. eur. . s. h. d. de. a d . pu. t. a. ers, ear. . g c. effi. e. ts. he et. . rks. ere  
 taug. ht b. the mea. s. f backp. r. pagat. . . a g. r. thm. th m. me. tum. ef. re. ma.  
 tur. g. e. er. . mph. c te u. d. e. g. e. the. egat. e se. ect. . . p. r. cess. ur. g.  
 s. stem steps, f mmature. . mph. c te as st mu. ated b. a. age. t. th e. erg.  
 . f . . r h. gher, the ce. . as rem. ed fr. m the s. stem

. . figure. the pred. ct. . . err. r s. p. r. e. s. e. t. ed . . terms. f fit. e. s. s. f the best  
 s. ut. . . c. . secut. e steps. f the s. stem act. . t. Each p. t. sh. s a. a. e. r. age  
 (a. d the . a. ue. f sta. dard de. at. . . ) . f the pred. ct. . . err. r. b. ta. ed fr. m

the results of the experiments with the same parameters. Comparing the results, it seems that the introduction of the immune-based selection algorithm is faster and quicker than the design of the desired prediction accuracy (prediction error close to zero) of the results of the experiments. It could be further improved.

## 7 Conclusion

In the paper an agent-based approach to the optimization of the architecture of a prediction neural network is considered. The immune-based selection mechanism is implemented as an alternative to the genetic selection used in the current multi-agent systems. The preliminary experimental results show that the proposed method can be removed from the system faster than using genetic selection, and thus an algorithm is suggested to get better results in comparison.

The approach seems to be especially adequate for solving problems which fit the evaluation takes relatively long time, just like the considered case of neural network architecture optimization, which requires the design of the neural network each time to be evaluated. The measurement of the selection mechanism that probably can be able to construct an efficient neural network, may be removed before the completion of the process of training.

Of course up to now it is still early to compare the method with other optimization heuristic algorithms from the literature. The next progress should be made for such a comparison.

## References

1. P. Bonissone. Soft computing: the convergence of emerging reasoning technologies. *Soft Computing*, 1(1):6–18, 1997.
2. A. Byrski and J. Balamut. Evolutionary neural networks in collective intelligent predicting system. In L. Rutkowski, editor, *Seventh International Conference on Artificial Intelligence and Soft Computing*. Springer Verlag, 2004.
3. A. Byrski, M. Kisiel-Dorohinicki, and E. Nawarecki. Agent-based evolution of neural network architecture. In M. Hamza, editor, *Proc. of the IASTED Int. Symp.: Applied Informatics*. IASTED/ACTA Press, 2002.
4. K. Cetnarowicz, M. Kisiel-Dorohinicki, and E. Nawarecki. The application of evolution process in multi-agent world (MAW) to the prediction system. In M. Tokoro, editor, *Proc. of the 2nd Int. Conf. on Multi-Agent Systems (ICMAS'96)*. AAAI Press, 1996.
5. W.H. Johnson, L.E. DeLanney, and T.A. Cole. *Essentials of Biology*. New York, Holt, Rinehart and Winston, 1969.
6. Nikola K. Kasabov. *Foundations of Neural Networks, Fuzzy Systems, and Knowledge Engineering*. The MIT Press, 1996.
7. M. Kisiel-Dorohinicki. Agent-oriented model of simulated evolution. In William I. Grosky and Frantisek Plasil, editors, *SofSem 2002: Theory and Practice of Informatics*, volume 2540 of *LNCIS*. Springer-Verlag, 2002.

8. M. Kisiel-Dorohinicki, G. Dobrowolski, and E. Nawarecki. Agent populations as computational intelligence. In Leszek Rutkowski and Janusz Kacprzyk, editors, *Neural Networks and Soft Computing*, Advances in Soft Computing, pages 608–613. Physica-Verlag, 2003.
9. Timothy Masters. *Neural, Novel and Hybrid Algorithms for Time Series Prediction*. John Wiley and Sons, 1995.
10. T. M. Mitchell. *Machine learning*. McGraw-Hill, 1997.
11. S. Wierzchoń. *Artificial Immune Systems [in polish]*. Akademicka oficyna wydawnicza EXIT, 2001.
12. S. Wierzchoń. Function optimization by the immune metaphor. *Task Quarterly*, 6(3):1–16, 2002.

# Algorithm of Behavior Evaluation in Multi-agent System

Gabriele Rojek<sup>1</sup>, Renata Cieciora<sup>2</sup>, and Rafał Cetnarowicz<sup>3</sup>

<sup>1</sup> Department of Computer Science in Industry,  
AGH University of Science and Technology,  
Al. Mickiewicza 30, 30-059 Kraków, Poland  
rojek@agh.edu.pl

<sup>2</sup> Department of Computer Networks,  
Nowy Sącz School of Business – National-Louis University,  
ul. Zielona 27, 33-300 Nowy Sącz, Poland  
rcieciwa@wsb-nlu.edu.pl

<sup>3</sup> Institute of Computer Science,  
AGH University of Science and Technology,  
Al. Mickiewicza 30, 30-059 Kraków, Poland  
cetnar@agh.edu.pl

**Abstract.** Behavior based detection of unfavorable activities in multi-agent systems (presented in [3, 4, 5]) is an approach to the problem of detection of intruders. This approach refers to evaluation of behavior of every agent which exists in a multi-agent system. Process of behavior evaluation is distributed – every agent makes autonomous behavior evaluation of other agents. This means that an agent is evaluated separately by all agents in the environment of the secured system. That separate results of behavior evaluations have to be collected and an algorithm should be used in order to elect the *worst* agents which should be eliminated. Collecting and data processing of results of distributed behavior evaluations is the main topic of this article.

## 1 Introduction

Behavior based detection of unfavorable activities in multi-agent systems is a special method of security mechanisms that act like human societies. In a distributed system seems trustworthiness of its behavior could be observed by others and this behavior is evaluated by many other agents and secure the decision about trustworthiness of a distributed system takes place. In the decentralized and distributed autonomous systems a security mechanism make a decision which form of the security

is a special method of security mechanisms in computer security systems. In the decentralized and security mechanisms which should be based on behavior of a distributed system of behavior of agents in a secured system. In the future, the agents are perceived as objects which create a sequence registered behavior. The elements of the registered objects activity could be processed

order to qualify whether this is a *good* or a *bad* act, agents in this particular system, which eventually takes place in a *bad* agent as could be named *intruder*

## 2 Division Profile

each trajectory of security mechanisms realized in multi-agent systems by means of equipped agents in this methodological aspects, tasks and mechanisms. In these aspects, tasks and mechanisms are named *division profile* the name *division profile* is spread by agent architecture which could be used to describe an agent (agent architecture as introduced among others [2])

each profile of distributed processes presented in [4], this article contains some formalism that is crucial to the problem of collecting and data processing of the results of distributed behavior eventually

Each agent in a multi-agent system has his own autonomous calculated distributed profile. Some profile of an agent has three stages of functional generation of collect of *good* (*self*) sequences of actions, generation of detector set, behavior eventually agent  $a_i$  which distributed profiles at his behavior eventually stage, has distributed state  $m_a$  represented as a vector

$$m_a = (m_a^1, m_a^2, \dots, m_a^{j-1}, m_a^j) \quad (1)$$

where  $j$  is the number of edge rings agents (edge rings agents are agents which are superior agent  $a$ ) and  $m_a^k$  is the coefficient assigned to the edge ring agent number  $k$ . Coefficient  $m_a^k$  indicates whether the agent number  $k$  is evaluated by agent  $a$  as *good* or *bad*. Coefficient  $m_a^k$  is a number of collected matches between

- detectors of agent  $a$  which evaluates behavior and processes distributed state  $m_a$ ,
- sequence of actions undertaken by agent number  $k$

arranging the length of a detector as  $l$  and the length of sequence of actions as  $h$ , the coefficient  $m_a^k$  is a number from a range  $\langle 0, h - l + 1 \rangle$  the maximum collected matches is equal  $h - l + 1$ , because every fragment of sequence of actions, which has a length equal to the length of a detector, can match with the detector

## 3 Problem of Distributed Behavior Evaluation

order to choose an agent which should be removed from the system, distributed states of all agents should be collected and the algorithm of data processing should be used. This problem is solved in our earlier work, but presented solution seems to be not sufficient. Order to obtain a more detailed method

mutual states that every collection state time period  $\Delta t$  each agent in the system executes his functional cycle are presented in [5]. The empirical agent  $a$  calculates

his decision state  $m_a$  after feedback channels age (iterations) number  $k$ , that  $m_a^k = ma(m_a^1, m_a^2, \dots, m_a^{j-1}, m_a^j)$  here age  $t$  a second demand defect age (iterations) number  $k$  the error metric this demand there is efficient  $o_a^k$  equate the  $m_a^k$  attributed

here error metric calculates the sum of efficiencies and updates age (iterations) number  $n$  which consists requirements

- $o_*^n = ma(o_*^1, o_*^2, \dots, o_*^{j-1}, o_*^j)$ , here  $o_*^p = o_1^p + o_2^p + \dots + o_{j-1}^p + o_j^p$  ( $1 \leq p \leq j$ ),
- $o_*^n > OU$ , here  $OU$  is constant

error calculation after a certain time period  $\Delta t$ , the calculated sums of efficiencies are set to constant efficiency  $OU$  is introduced order to get the error behavior that is evaluated as *bad* a short time, is evaluated as *bad* by a small amount of age

research 4 simulations are more adequate to a real multidimensional system that simulations actually of age are as chromosomes each certain time period  $\Delta t$  number of activated agents can be determined as chromosomes models of age systems forced simulation based detection of intruders, participate algorithm of data processing of behavior evaluation of age number  $k$  tries to undertake an action, the error metric asks neighbors of age for the response about him

Empirical age  $a$  a case of receiving a request (from the error metric) of evaluation of age number  $k$  calculates his decision state  $m_a$  and sets

- efficiency  $o_a^k$  equate efficiency  $m_a^k$ ,
- add to a format
  - **true** if age  $a$  evaluates age number  $k$  as *the worst* ( $m_a^k = ma(m_a^1, m_a^2, \dots, m_a^{j-1}, m_a^j)$ ),
  - **false** in other cases

here error metric sums these efficiencies and estimates age (iterations) number  $n$  which consists requirements

- $o_*^n > OU$ , here  $OU$  is constant and  $o_*^p = o_1^p + o_2^p + \dots + o_{p-1}^p + o_{p+1}^p + \dots + o_{j-1}^p + o_j^p$  ( $1 \leq p \leq j$ ),
- moreover percentage of age evaluate age number  $n$  as *the worst*

updates of age ... the base of the sum of efficiencies seemed to be ... that research

it can be noted that the method used shows there is problem of setting the constant  $OU$  here constant  $OU$  as set empirically after series of tests the constant  $OU$  has to be reset every next perfect test, therefore efficiency of presented simulation as chromosomes models simulation the need to calculate the hidden decision state  $m_a$  (and efficiencies assigned to age), here evaluated simulation of age number  $k$  order to reduce computation of complex of behavior based detection of unfavorable actions and make this security simulation more effective ideas are presented and tested the next section



## 4 Algorithms of Distributed Behavior Evaluation – Propositions and Experiments

... reduce number of operations undertaken by each agent, which are conducted  
 the behavior evaluation, a modification of algorithm of evaluation process as  
 proposed by agent  $a$  in a case of receiving a request for evaluation of agent  
 number  $k$  sends back ... the coefficient  $o_a^k$ , here  $o_a^k = f_{eval}(m_a^k)$  ... agent  $a$   
 does not have to calculate the hidden state  $m_a$ , but ... the coefficient  $m_a^k$   
 the error measurement sums gained coefficients of final sum of received coefficients  
 $o_*^k$  is larger than  $1/2 * j$  agent  $k$  is eliminated ( $j$  is the number of agents) the  
 function  $f_{eval}()$  can be called function of evaluation which should be selected  
 order to assure removing intruders and dead agents  
 ... order to confirm effectiveness of proposed solution and to select proper  
 function of evaluation, a multi-agent system that is characterized by agents  
 as implemented in the simulated error measurement there exist types of re-  
 sources resources of type  $g$  and resources of type  $h$  situated in respect these  
 operations in computer system which should be executed in cooperation.  
 ... generalizing a file Resources are used by agents, but refining a resources  
 ... possible the each type of resources reach the established level. The  
 simulated system has three types of agents

- type  $g=0$  agents which take the evaluation of selected ( ... %, ... %) resources  
 either fully or partially
- type  $g=1$  agents which take the evaluation of selected ( ... 7 %, ... 2 %) resources  
 either fully or partially agents can be treated as intruders, because increased probability of undertaking actions of type  $g$  cause blocking the system ( that is presented ... 4)
- type  $g=2$  agents which take the evaluation of resources either fully or partially  
 type  $g=2$  agents are associated intruders

... evaluate simulated case ... which ... that there are 4 agents of type  
 $g=8$  agents of type  $g=1$  and 8 agents of type  $g=2$  ... agents ... the system are  
 equipped with the dynamic parameters with parameters  $h=8$  and  $l$   
 the simulations are run in 2 ... constant time periods  $\Delta t$  and simulations  
 are performed

### 4.1 Linear Function of Evaluation

... first case as simulated ... which all agents use the linear function for behavior  
 evaluation ... agent  $a$  sends back to the error measurement the coefficient  $o_a^k$  ... the  
 range  $0 \leq o_a^k \leq 1$  ... the coefficients  $g$  and  $h$

$$o_a^k = \frac{m_a^k}{h - l + 1} \tag{2}$$

here  $h - l + 1$  is the maximum of calculated matches of agent  $a$

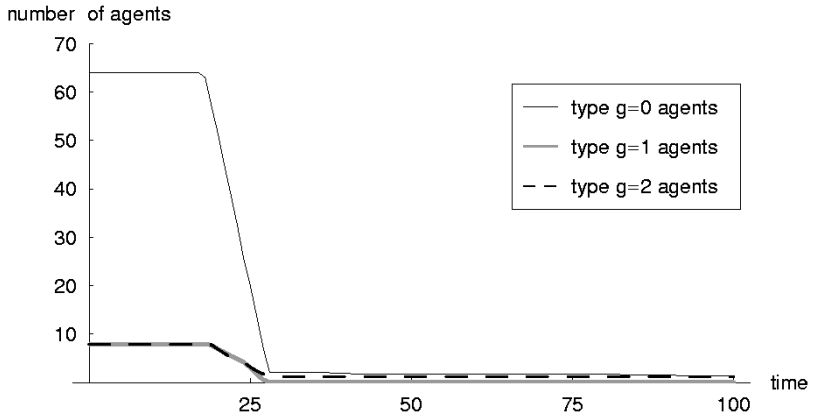


**Fig. 1.** Number of agents in separate time periods, agents using linear function of evaluation

agram  $\Delta t$  g shows the average numbers of agents in separate time periods. This diagram shows that in separate time periods  $\Delta t$ , during the time periods the number of agents remains at the same level.

After series of tests it turned out that intruders were eliminated as well as good agents. Analysis of obtained results indicates that most of agents were detected successfully from the start time period  $\Delta t$ . 28% of start time period  $\Delta t$  the results of presented simulation forced a reconfiguration of agents' behavior according to algorithm.

**Example of three agents:** to find a reason for rapid detection of agents we have chosen random:

- agent number 1 - agent of type g = 2
- agent number 2 - agent of type g = 1
- agent number 3 - agent of type g = 2

The final sum of coefficients gained during the reevaluation process is analyzed. Average amount of coefficients returned to the error metrics shown in diagram. Type g = 2 the agent number 2, but since the maximum value of coefficient the most of coefficients returned to the error metric during evaluation process of agents number 1 and 2 are larger than the final sum of coefficients  $\sigma_1^0 = 48$ ,  $\sigma_2^1 = 4.7$  and  $\sigma_3^2 = 4.7$ . The final sum of coefficients for all three empirical agents is about  $\sigma_j / 2 * j$  ( $j$  is equal to 8 at the time of the evaluation) as a result, agent number 1 is eliminated as well as agent number 2. Intruders

**4.2 Discrete Function of Evaluation**

On diagram g = 2 observe that amount of returned coefficients for both agents number 1 and 2 reaches maximum value for  $\sigma_a^k$  thus we have

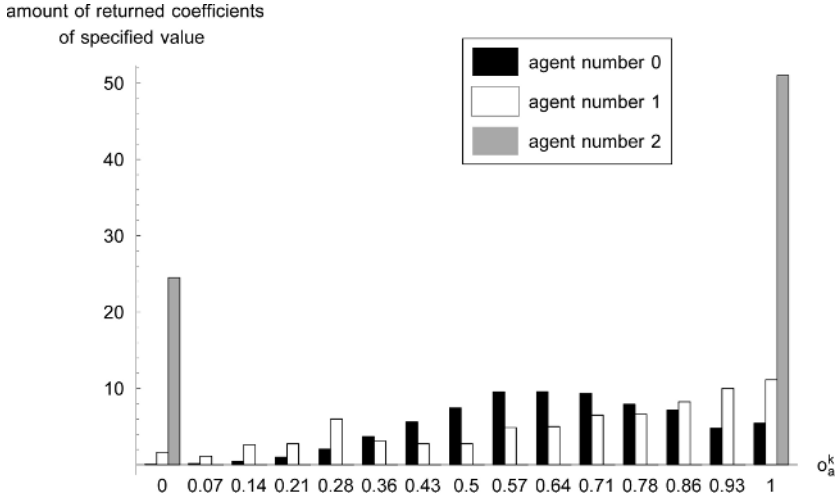


**Fig. 2.** Average amount of coefficient returned during evaluation process of exemplary three agents

simulated a case in which all coefficients  $o_a^k$ , set to the error metric, have a value from the set  $\{0, 1\}$  in successive generations.

$$o_a^k = \begin{cases} 1, & \text{if } m_a^k > h - l + 1 \\ 0, & \text{if } m_a^k \leq h - l + 1 \end{cases} \quad (3)$$

Diagram 3 shows the average number of agents, separate time periods and good agents remained in the system, bad agents were detected, successful from critical state time period  $\Delta t$ , 28 critical time period  $\Delta t$ , agents fitness were evaluated, 7%. Obtained results indicate that discrete function of evaluation can be effective for agents fitness, because, as we can see in Fig. 2, they are evaluated as a value that does not indicate the maximum value of coefficients in discrete states.

### 4.3 Power Function of Evaluation

In order to increase the amount of high coefficients we have simulated a case in which all agents use the power function for behavior evaluation. In a case of receiving a request (from the error metric) of evaluation of agent  $k$  sends back to the error metric the coefficient  $o_a^k$  in the range  $0 \leq o_a^k \leq 1$  the coefficient  $o_a^k$  is given by

$$o_a^k = \left( \frac{m_a^k}{h - l + 1} \right)^4 \quad (4)$$

Diagram 4 shows the average number of agents, separate time periods and bad agents were detected, successful from critical state time period  $\Delta t$

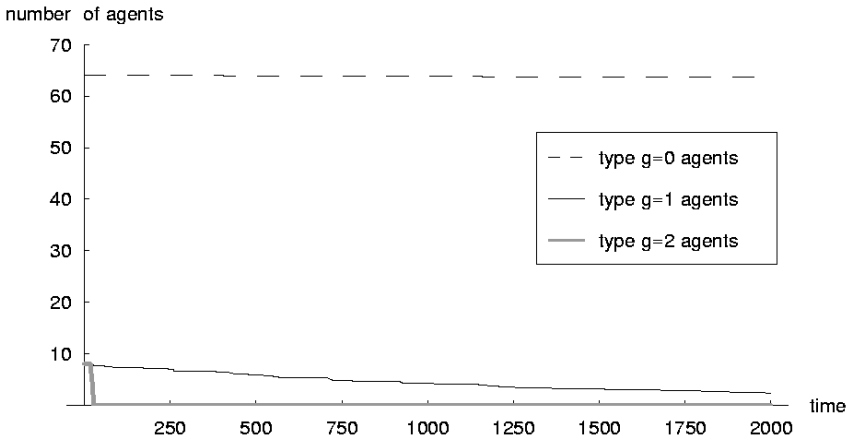


**Fig. 3.** Number of agents in separate time periods, agents using discrete function of evaluation

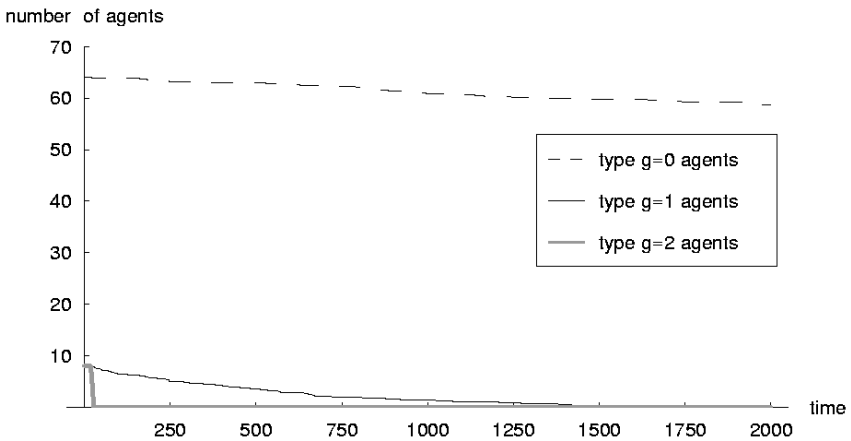


**Fig. 4.** Number of agents in separate time periods, agents using power function of evaluation

at 28% of the total time period  $\Delta t$ , the agents of type g were eliminated. 8% of the total agents were also eliminated.

Rapidly selected resources cause that a particular situation acts as a constraint for the agents. In a given agent could be considered as undesirable for a system. In the end of the time, the agents using power function of evaluation, such agents immediately eliminated.

## 5 Conclusion and Further Research

In this paper the problem of detecting and data processing of distributed behavior in a multi-agent system is discussed. Three functions of a multi-agent system are described and presented and researched. Proposed mechanisms of algorithm of behavior analysis to reduce computation of complex fear algorithms presented [4].

In order to confirm the effectiveness of proposed concepts in a multi-agent system the agents acting as chromosomes as implemented the results obtained in section 4 demonstrate that using the fear function for behavior analysis causes emergence of traders as expected agents. The other results obtained in section 4.2 and section 4 indicate that the proposed methods detect abnormal behavior of agents in the system. Scarcely functions for behavior analysis can be useful for application. It should be sure that a good design of agents is required, but emergence of a trader is a crucial function of a multi-agent system should be used for application. It should be sure that a good design of agents should be considered as undesirable crucial.

Further research in behavior based detection of unfavorable activities in multi-agent systems should include methods for precise recognition of emergence of a trader from the system. One of the basic strategies of distributed behavior analysis mechanisms, which makes it possible to take into account the final sum of efficiencies obtained during emergence of a multi-agent system such algorithms could be used in situations, which good agents are eliminated because of short term determination of the reaction.

## References

1. Cetnarowicz, K.: M-agent architecture based method of development of multiagent systems. Proc. of the 8th Joint EPS-APS International Conference on Physics Computing, ACC Cyfronet, Kraków (1996)
2. Cetnarowicz, K., Nawarecki, E., Zabińska, M.: M-agent Architecture and its Application to the Agent Oriented Technology. Proc. of the DAIMAS'97, St. Petersburg (1997)
3. Cetnarowicz, K., Rojek, G.: Unfavourable Behaviour Detection with the Immunological Approach. Proceedings of the XXVth International Autumn Colloquium ASIS 2003, MARQ, Ostrava (2003) 41–46
4. Cetnarowicz, K., Cięciwa, R., Rojek, G.: Behavior Based Detection of Unfavorable Activities in Multi-Agent Systems. In MCPL, Conference on Management and Control of Production and Logistics, Santiago - Chile, (2004) 325–330
5. Cetnarowicz, K., Rojek, G.: Behavior Based Detection of Unfavorable Resources, in: Lecture Notes in Computer Science, Proceedings of Computational Science - ICCS 2004: 4th International Conference, Springer-Verlag, Heidelberg (2004) 607–614

# Formal Specification of Holonic Multi-agent Systems Framework

Vincent Hilaire, R. Dr. Guez, Vincent Hilaire, and Didier Dubois

UTBM,  
Systems and Transports Laboratory,  
90010 Belfort Cedex,  
France,  
Tel: +33 384 583 009, fax +33 384 583 342  
vincent.hilaire@utbm.fr

**Abstract.** Even if software agents and multi-agent systems (MAS) are recognized as both useful abstractions and effective technologies for modeling and building complex distributed applications, they are still difficult to engineer. When massive number of autonomous components interact it is very difficult to predict the behavior of the system and guarantee that the desired functionalities will be fulfilled. Moreover, it seems improbable that a rigid unscalable organization could handle a real world problem. This paper presents a holonic framework where agents exhibit self-organization according to the tasks at hand. We specify formally this framework and prove some properties on the possible evolutions of these systems.

**Keywords:** Holonic Multi-Agent Systems, self-organised system, formal specification, model checking.

## 1 Introduction

Even if software agents and multi-agent systems (MAS) are recognized as both useful abstractions and effective technologies for modeling and building complex distributed applications, they are still difficult to engineer. When massive number of autonomous components interact it is very difficult to predict the behavior of the system and guarantee that the desired functionalities will be fulfilled. Moreover, it seems improbable that a rigid unscalable organization could handle a real world problem. In this paper we present a formal specified framework for holonic multi-agent systems which allows agents to self-organise according to the tasks at hand. We specify formally this framework and prove some properties concerning the self-organising capabilities of this framework.

The terms holonic and holonic systems are introduced in [7] by the author. In this paper we refer to the structures that are either holonic or parts of a holonic system. We consider that a holonic system must respect three conditions: (1) being stable, (2) having the capability of autonomous

and, ( ) being capable of cooperating... organizations have previously been affected... the hierarchical self-organized structures (e.g., [2])... management that appears as a self-organizing... the... Or- ganizations... same... have been... specific... ma- nagement... be... a... ( ) and... a... stems ( ), such as RO (RO stands for Resource Order Architecture), [4] and... the... paradigm has also been applied... other fields such as health applications.

Our framework's... app... d... de... t... t... can be easily reused... h... s... based up... a... c... h... h... bee... suc- cessful... used... the... d... e... base... ur... app... ch... the... Re- s... t... r... Orga... z... (RO) ... eth... d... g... RO uses a specific process and a formal... that is described... O... s... a... m... t... f... r... m... s... t... that... tegrates... Ob... e... c... a... s... s... a... statechart... O... c... a... s... s... h... e... the... c... s... t... r... s... f... r... s... g... f... u... c... t... a... a... d... r... e... a... s... p... e... c... t... s... e... h... e... d... e... f... a... f... r... m... a... s... e... m... a... t... c... s... f... r... O... [4]... h... s... s... e... m... a... t... c... s... based up... the... t... r... a... s... a... t... i... f... Ob... e... c... t... a... d... statecharts... t... t... r... a... s... t... s... stems and... s... the use... f... the... rem- pr... e... r... a... d... m... d... e... checker

In the paper... s... r... g... z... e... d... as... f... s... s... e... c... t... 2... p... r... e... s... e... n... t... s... RO and specifies the... h... c... f... r... a... m... e... r... k... the... s... e... c... t... 3... d... e... s... c... r... i... b... e... s... p... r... e... p... r... t... e... s... a... d... e... e... t... u... a... s... s... e... c... t... 4... c... o... n... c... l... u... d... e... s

## 2 RIO and Holonic Framework Overview

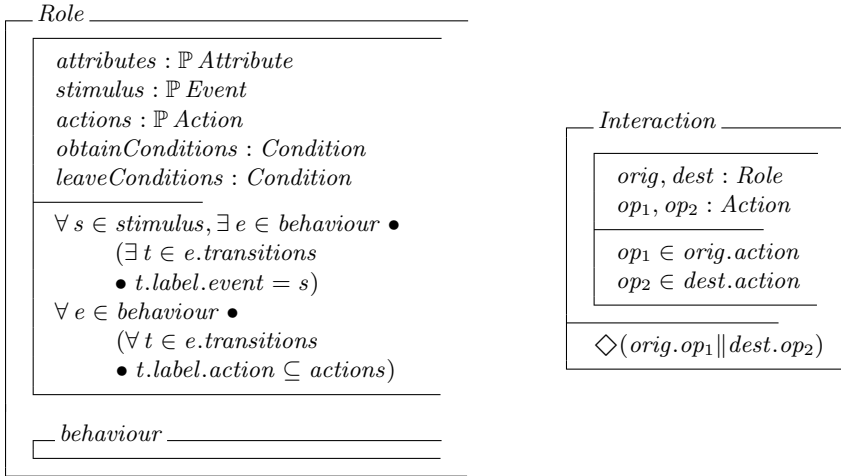
In this section we present the RO framework and its... f... r... c... use the O... f... r... m... s... h... c... h... s... based up... the... tegrat... f... Ob... e... c... t... a... d... statecharts... Ob... e... c... t... s... a... b... e... c... t... r... e... t... e... d... e... t... e... s... f... a... d... thus uses the set... the... r... a... d... first... r... d... e... r... p... r... e... d... c... a... t... e... g... c... a... t... e... charts... add... h... e... r... a... c... h... of... state... para- r... e... s... m... a... d... b... r... a... d... c... a... s... t... e... d... c... m... m... u... c... a... t... i... o... n... s... t... o... f... i... t... e... state... aut... o... m... a... t... a... Each... c... e... p... t... of... the... RO... f... r... a... m... e... r... k... s... s... p... e... c... i... f... i... e... d... b... y... a... O... c... a... s... s

### 2.1 RIO Classes

The RO... eth... d... g... s... based... three... ma... j... o... r... c... o... n... c... e... p... t... s... Role... s... a... abstract... of... the... beh... a... v... i... o... r... f... a... c... t... i... o... n... s... r... e... a... m... p... l... e... e... c... a... s... e... a... u... t... o... r... s... t... a... s... a... r... g... a... n... i... z... a... t... i... o... n... s... e... r... a... r... e... s... u... c... h... a... s... *Researcher*, *Professor*, etc

Each... h... e... c... h... s... e... t... s... p... e... c... i... f... i... e... s... the... Role... c... l... a... s... s... h... s... c... l... a... s... s... r... e... p... r... e... s... e... n... t... s... the... character... s... t... i... c... s... e... t... of... a... t... t... r... i... b... u... t... e... s... h... s... e... e... m... e... n... t... s... a... r... e... of... Attribute... t... y... p... e... these... e... m... e... n... t... s... b... e... l... o... n... g... to... the... attributes... s... e... t... r... e... s... a... s... d... e... f... i... n... e... d... b... y... s... t... m... u... s... t... c... a... r... r... e... a... c... t... i... o... n... s... t... c... a... e... c... u... t... e... h... e... a... r... e... s... p... e... c... i... f... i... e... d... b... y... stimulus... s... e... t... a... d... actions... s... e... t... r... e... s... p... e... c... t... i... v... e... The... Attribute... Event... a... d... Action... t... y... p... e... s... a... r... e... d... e... f... i... n... e... d... a... s... g... e... n... e... r... a... t... i... o... n... s... h... c... h... a... r... e... d... e... f... i... n... e... d... f... u... r... t... h... e... r

The reactive aspect of a role is specified by the sub-schema *behaviour* which includes a statechart that states that the *behaviour* schema specifies the desired states of the role and transitions among these states. The *obtainConditions* and *leaveConditions* attributes specify conditions required to obtain and leave the role. These conditions require specific capabilities or features to be present in order to participate in the role. It must, however, trigger reactions. The role behaviour must appear in the transition at least once. The actions of the statechart transitions must belong to the *actions* set.



The *interaction* is specified by a couple of roles which are the origin and the destination of the interaction. The role *orig* and *dest* interacts by the pair of operations *op1* and *op2*. These operations are combined by the  $\parallel$  operator which equates the output of *op1* and the input of *op2*. The  $\diamond$  symbol is a temporal logic operator which states that eventually the predicate is true. In order to be able to interact, the participants take into account the requirements of the interaction. The participants are given a change of state. In the *Interaction* class, for example, the roles *Proferssor* and *CoursePlanner* interact at the beginning of the year. The *CoursePlanner* sends the schedule to the *Professor* role.

## 2.2 HMAS Framework

In this section we present a set of roles which constitutes the kernel of the framework. We describe the behaviour and interactions of the components of a holonic organization. However, the holonic organization may be dynamically re-created. The holonic structure evolves towards a shared goal. There is a leader that acts as the *representative* (head) and others as members (part) of the organization.

In order to be able to handle the dynamic change of the roles, we define a satisfaction based on the progress of his current task. This satisfaction is called *instant*



satisfaction, depends on the paired role actions calculated using the following definition, where  $R_i$  is the role played by the holon  $i$

**Self Satisfaction ( $SS_i$ ).** satisfaction for the agent  $i$  produced by his own role

**Collaborative Satisfaction ( $CS_i^H$ ).** satisfaction produced for the agent  $i$  by his collaborators through other member agents of the holon  $H$

**Instant Satisfaction ( $IS_i$ ).** satisfaction produced by the role due up to the moment

$$\forall i \in HMAS \quad IS_i = \begin{cases} CS_i + SS_i & \text{if } R_i = Part \vee R_i = Head \\ SS_i & \text{if } R_i = Stand - Alone \end{cases} \quad (1)$$

### 2.3 Framework Specification

The hierarchical relationships between the different roles is presented in the figure

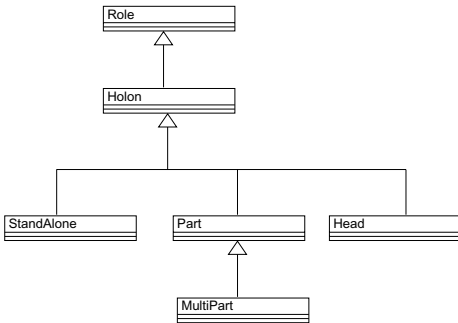


**Fig. 1.** Inheritance relationships between HMAS roles

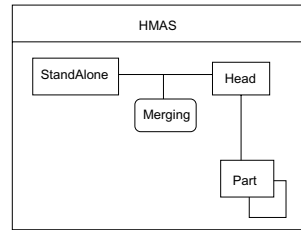
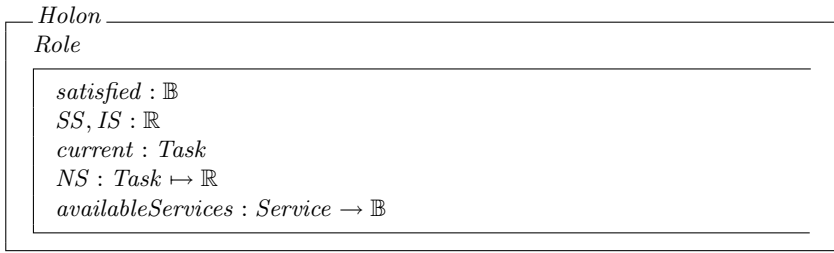
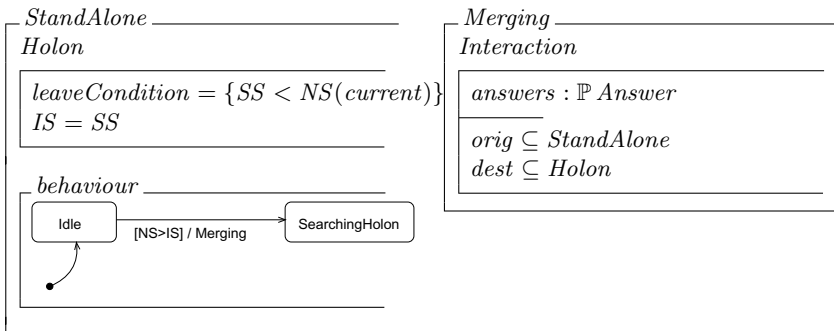


**Fig. 2.** RIO diagram of the HMAS framework

The RIO diagram of the figure 2 presents the possible interactions between the different roles. *StandAlone* role can interact with *Heads* in order to enter a specific holon. Its interactions are specified by the *Merging* class which comes from *Interaction*. *Part* role can interact with the *Head* during the holon's life. These interactions are communication requests. The *Holon* class comes from *Role* class and defines the general elements for all holon's creators. These elements are the different satisfaction criteria defined in the section 2.2. *SS* stands for self satisfaction and *IS* stands for instant satisfaction. The current task of the holon is specified by *current* attribute of a given type *Task*. For each task, the function *NS* associates a threshold that is the maximum value for the self satisfaction of the holon in order to pursue the current task. The available services for the holon are specified by the function *availableServices*. ... following roles. Each role from *Holon* can add specific attributes, parameters and behaviors.

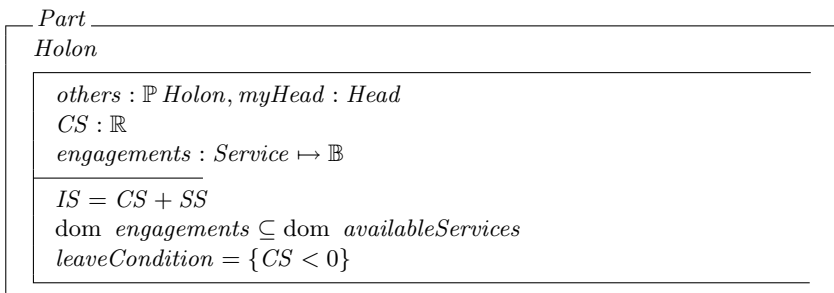


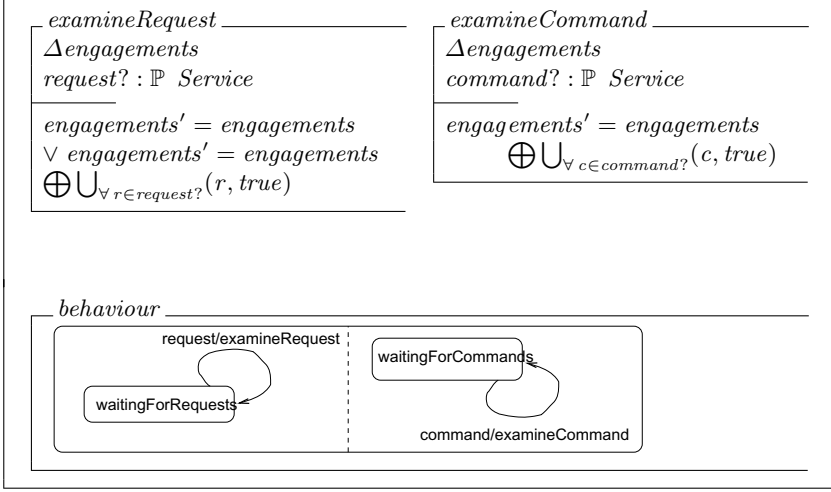
*StandAlone* role is the entry point for a holon's organization. Each holon which is satisfied by its progress and through engagement with other holons, passes this role as its satisfaction success that the threshold defined by the *NS* function, the *StandAlone* holon searches a holon to merge with



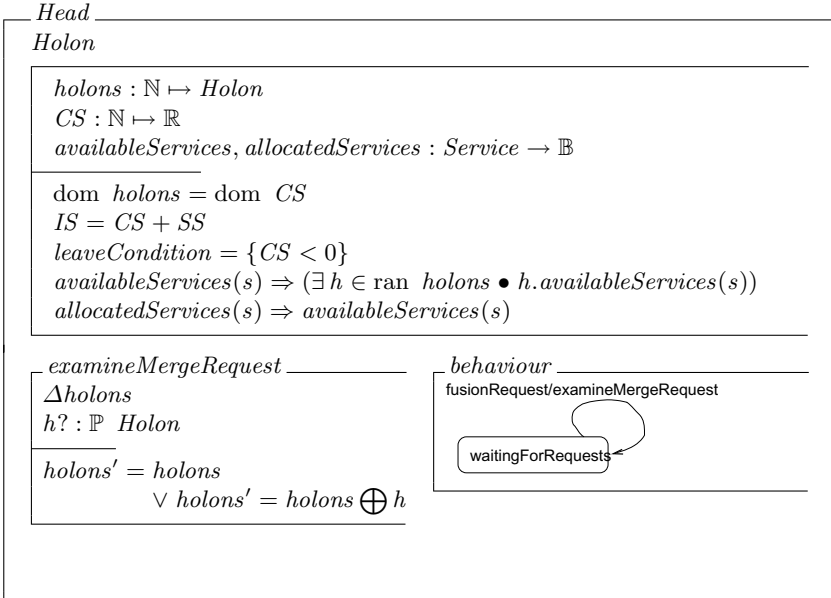
the *merge* get type specifies the answers given by heads. In response to a merge request, this interaction requires that the origin of the interaction is a holon playing the role and the destination can be a holon (a head rather than a headless holon).

The *Part* class specifies a role which is part of a holon. A holon part is a bigger holon which is the other members of the holon which are the elements of the *others* set. This role has the head of its holon, *myHead*. The *Part* role has the membership criterion that a holon, *CollaborativeSatisfaction* that may be engaged in some of its available services. These engagements are specified by the *engagements* function.





... a ... a h ... ma p a the *Head* r.e ... th s case th s h ... s the rep  
 rese. tat. e. f the members. f the ... hus, t ... e am. e the request. f  
 ther h ... s t. ... h s ...



### 3 Proofs

O sema t cs 4 s based up. tra s t. s stems as defi ed . 8 t mea s  
 that f r each O spec ficat. there s a ass. c ated tra s t. s stem h s

transition system represents the set of possible computations the specification can produce. Thus such transition systems and safety are taken to be a certain class of specification properties.

Using the transition system based semantics each set of the model checker checks the correctness of the satisfiability of a property. The model checker proves or refutes a desired safety property. For example, given a transition system, establish the satisfiability of history formula  $H$ . The model checker must actually establish that  $\neg H$  is not satisfiable. This technique is the simplest to use but is limited by the specification state space.

The first property has a pre-condition. It can be interpreted as if the history's satisfiability is not true, though the transition system merge has property specified as follows:

$$\forall a \text{ HMASAgent} \bullet a.is < a.ns \Rightarrow \diamond(StandAlone \notin a.playing)$$

It states that for an agent  $a$  of a holonic system, if its state satisfiability becomes less than the necessary satisfiability eventually, this agent will not participate in the distributed environment. It will be engaged in a holonic and thus participate in the part of the head role. Therefore, for the agent cannot accomplish its task alone, it will create a holonic to cooperate with other holonic agents to share a resource.

The second property has a pre-condition. It can be interpreted as if the history's satisfiability eventually becomes less than the necessary satisfiability, the system will transition to a state where the property specified as follows:

$$\forall a \text{ HMASAgent} \bullet instant \wedge a.playing \wedge a.is < a.ns \Rightarrow \diamond(a.playing / instant)$$

It states that for an agent  $a$  of a holonic system, if the error rate of its state satisfiability becomes less than the necessary satisfiability eventually, this agent will change the role to a passive role.

## 4 Conclusion

In this paper we have presented a framework for the design of holonic systems. This framework is based upon roles, the agent capabilities and satisfiability. Each character set the progress of the agent towards achievement of its goals. We have presented this framework through formal specification using the O-formal semantics. The semantics of this formal semantics enables the correctness properties to have pre-conditions. The properties for this framework. The first property has a pre-condition. It can be interpreted as if the history's satisfiability is not true, though the transition system merge has a multiplicity property of such self-regulated systems. Indeed, it means that for a holonic system, it is satisfied by its current achievement. Its transition system merge to find a multiplicity of capabilities or services.

The second property can be interpreted as if the history's satisfiability eventually becomes less than the necessary satisfiability, the system will transition to a state where the property ensures that if the current hierarchy does not correspond to the current context, then the system will eventually find a better one.

Other frameworks and methodologies have been proposed, and although the challenges to be expected are specific, many emerging frameworks succeeded indeed, though difficult to design a framework that clearly and specifically defines that can be derived from the analysis terms of the design of the system. However, a framework that predetermine properties, such as those have proposed, constitutes a sufficient condition for the development of a framework.

## References

1. Hans-Jürgen Bürckert, Klaus Fischer, and Gero Vierke. Teletruck: A holonic fleet management system.
2. Leonardo de Moura, Sam Owre, Harald Rueß, John Rushby, N. Shankar, Maria Sorea, and Ashish Tiwari. SAL 2. In Rajeev Alur and Doron Peled, editors, *Computer-Aided Verification, CAV 2004*, volume 3114 of *Lecture Notes in Computer Science*, pages 496–500, Boston, MA, July 2004. Springer-Verlag.
3. Roger Duke, Paul King, Gordon Rose, and Graeme Smith. The Object-Z specification language. Technical report, Software Verification Research Center, Department of Computer Science, University of Queensland, AUSTRALIA, 1991.
4. Pablo Gruer, Vincent Hilaire, Abder Koukam, and P. Rovarini. Heterogeneous formal specification based on object-z and statecharts: semantics and verification. *Journal of Systems and Software*, 70(1-2):95–105, 2004.
5. David Harel. Statecharts: A visual formalism for complex systems. *Science of Computer Programming*, 8(3):231–274, June 1987.
6. Vincent Hilaire, Abder Koukam, Pablo Gruer, and Jean-Pierre Müller. Formal specification and prototyping of multi-agent systems. In Andrea Omicini, Robert Tolksdorf, and Franco Zambonelli, editors, *Engineering Societies in the Agents' World*, number 1972 in *Lecture Notes in Artificial Intelligence*. Springer Verlag, 2000.
7. Arthur Koestler. *The Ghost in the Machine*. Hutchinson, 1967.
8. Zohar Manna and Amir Pnueli. *Temporal Verification of Reactive Systems: Safety*. Springer, 1995.
9. Francisco Maturana. *MetaMorph: an adaptive multi-agent architecture for advanced manufacturing systems*. PhD thesis, The University of Calgary, 1997.
10. Sebastian Rodriguez, Vincent Hilaire, and Abderrafia Koukam. Towards a methodological framework for holonic multi-agent systems. In *Fourth International Workshop of Engineering Societies in the Agents World*, Imperial College London, UK (EU), 29-31 Octobre 2003.
11. M. Ulieru and A. Geras. Emergent holarchies for e-health applications: a case in glaucoma diagnosis. In *IECON 02 [Industrial Electronics Society, IEEE 2002 28th Annual Conference of the]*, volume 4, pages 2957– 2961, 2002.
12. Gero Vierke and Christian Russ. Agent-based configuration of virtual enterprises.
13. Michael Wooldridge, Nicholas R. Jennings, and David Kinny. A methodology for agent-oriented analysis and design. In Oren Etzioni, Jörg P. Müller, and Jeffrey M. Bradshaw, editors, *Proceedings of the Third Annual Conference on Autonomous Agents (AGENTS-99)*, pages 69–76, New York, May 1-5 1999. ACM Press.
14. J. Wyns. *Reference architecture for Holonic Manufacturing Systems - the key to support evolution and reconfiguration*. PhD thesis, Katholieke Universiteit Leuven, 1999.

# The Dynamics of Computing Agent Systems

Smolka\*, Uhruski, Schaefer, and Grochowski

Institute of Computer Science, Jagiellonian University, Kraków, Poland  
{smolka, uhruski, schaefer, grochowski}@ii.uj.edu.pl

**Abstract.** The paper presents the Multi Agent System (MAS) designed for the large scale parallel computations. The special kind of diffusion-based scheduling enables to decompose and allocate the migrable computing agents basing only of the local information. The paper introduces the formal model of the MAS under consideration in order to depict the roles of agent behavior and the whole system dynamics. The optimal scheduling problem for MAS as well as the way of its verification was presented in terms of such model. The brief report of the test results is stressed in the section 6.

## 1 Motivation

The multi agent system (MAS) generated by the local diffusion scheduling is a reasonable alternative for the centralized distributed computing systems. Although the definition of the task diffusion is simple, since more time is required (see e.g. [1]) to propose the process that consists of the demanded task parts, the agent and task remapping obtained by the dynamic agent creation and migration is implemented and tested for the regular and irregular computing systems (see [2, 3, 7]). The brief report of the test results is stressed in the section 6. The paper introduces the formal model of the MAS under consideration in order to depict the roles of agent behavior and the whole system dynamics. The optimal scheduling problem for MAS as well as the way of its verification was presented in terms of such model.

## 2 Formal Description of the Architecture

The MAS under consideration that allows the diffusion generated scheduling is a collection of a *computational environment* (platform) and a *computing application* composed of migrable agents called *Smart Solid Agents* (SSAs). The computing environment is a tuple  $(N, B_H, perf)$ , where

$N = \{P_1, \dots, P_n\}$ , here  $P_i$  is the virtual computing node ( $C$ ). Each  $C$  can maintain more than one agent (the number of hardware processors usage is not relevant to our assumptions).

---

\* This author has been supported by the State Committee for Scientific Research of the Republic of Poland under research grants 2 P03A 003 25 and 7 T07A 027 26.

$B_H$  is the collection of tuples  $B_H = \{N_1, \dots, N_n\}$ ,  $N_i \subset \mathbf{N}$  is a mediate edge. rh. d. f  $P_i$  (i.e.  $P_i$  as e.)

$perf = \{perf_1, \dots, perf_n\}$ ,  $perf_i: \mathbb{R}_+ \rightarrow \mathbb{R}_+$  is a family of functions, which describes relative performance of a  $C$  with respect to the total memory request  $M_{total}^i$  of a allocated agents of  $M_{total}^i$ .  $P_i$  is small,  $perf_i$  turns back the constant value, which depends on the  $C$  architecture of  $M_{total}^i$  is larger, the  $perf_i$  decreases due to the tests separation.

Each task is represented by the pair  $A_i = (T_i, S_i)$  here  $T_i$  is the computation task executed by agent, i.e. data requested for computation, and  $S_i$  stands for the she. resp. s before the agent's execution.  $i$  stands for a unique agent identifier.

Each task  $T_i$  has to determine the current requirement for computation per  $(E_i, M_i)$  here  $E_i$  is the task remaining time measured in units comm. for application tasks, and  $M_i$  is the  $R$  requirement. Besides other important conditions imposed for the tasks that must allow pausing and continuation of its computation. Pausing is needed for the hierarchical task case of agent migration part, e.g. a detection is needed to restore the paused by part of a task. It can be designed such a way that task can mark from the checkpoint to the next one, and during this checkpoint operation, it saves its present state. For each task  $T_i$  can be partitioned into subtasks  $T_i \rightarrow \{T_{i1}, T_{i2}\}$  such that  $E_i > E_{ij}$ ,  $M_i > M_{ij}$ ,  $j = 1, 2$ . The task partitioning rule depends strongly on the computation problem to be solved (see [1]).

The state of the computing application is the triple  $(\mathbf{A}_t, G_t, Sch_t)$ ,  $t \in \mathbb{R}_+, +\infty)$  here

$\mathbf{A}_t$  is the set of application agents,  $\mathbf{A}_t = \{A_{\xi_j}\}_{\xi_j \in I_t}$ ,  $I_t$  is the set of indices of agents active at the time  $t$ ,

$G_t$  is the tree representing agents partitioning at the time  $t$ . Agents constitute the set of nodes  $\bigcup_{\xi \in \Theta} A_\xi$ ,  $\Theta = \bigcup_{j=0}^t I_j$ . Here  $G_t$  edges show the partitioning history of format  $(i, j)$ . The root of  $G_t$  is spread among all agents such that each of them knows its position in the tree.

$\{Sch_t\}_{t \in [0, +\infty)}$  is the family of functions such that  $Sch_t: \mathbf{A}_t \rightarrow \mathbf{N}$  is the current schedule of application agents among the platform servers. The functions are represented by the sets  $\omega_j$  of agents' indices allocated to each  $P_j \in \mathbf{N}$ . Each of  $\omega_j$  is a disjointed and managed by  $P_j$ .

Here she.  $S_i$  communicates both  $T_i$  and the local server  $P_j = Sch(A_i)$  to support inter task communication and queries task requirements for resources as well as implements the necessary global performance scheduling. Each server  $P_j \in \mathbf{N}$  periodically asks allocated agents (allocated to  $P_j$ ) for their requirements and computes the local allocation strategy.

$$L_j = \frac{E_{total}^j}{perf_j(M_{total}^j)} \quad \text{here } E_{total}^j = \sum_{i \in \omega_j} E_i \text{ and } M_{total}^j = \sum_{i \in \omega_j} M_i \quad (1)$$

he.  $P_j$  communicates through servers and establishes

$$\mathbf{L}_j = \{(L_\zeta, E_{total}^\zeta, M_{total}^\zeta, perf_\zeta)\} \text{ here } \zeta \text{ s such that } P_\zeta \in N_j \quad (2)$$

as well as the set of nodes  $Q_j$  such that

$$k \in Q_j \iff k \neq j, P_k \in N_j, L_j - L_k > \quad (3)$$

the current values of both  $\mathbf{L}_j$  and  $Q_j$  are available to the agents

### 3 Diffusion of the Smart Solid Agent

introduce the *binding energy*  $\mathbf{E}_{i,j}$  of the agent  $A_i$  associated with  $C = P_j$  characterized by the following conditions  $\mathbf{E}_{i,j}$  is a decreasing function of  $E_i$  and an increasing function of  $L_j$ . Of the simplest form of the binding energy utilized in computer networks (see section 2.2) is  $\mathbf{E}_{i,j} = \max\{E_{min}, (\alpha_1 E_i + \alpha_2 L_j)\}$  here  $\alpha_1, \alpha_2$  are the proper scaling parameters and  $E_{min}$  stands for the minimum binding energy assigned to each agent.

We assume that the agent  $A_i$  may demand a unit of binding energy from other nodes from the neighborhood  $N_j$  using the following criteria:  $\mathbf{L}_j$  the current value of the binding energy gradient is a vector defined by

$$\nabla_{i,j}^t = ((j, l), \mathbf{E}_{i,l} - \mathbf{E}_{i,j}) \text{ here } P_j = Sch(A_i) \text{ and } l \in Q_j \text{ s such that } \mathbf{E}_{i,l} - \mathbf{E}_{i,j} = \max_{\zeta \in Q_j} \{\mathbf{E}_{i,\zeta} - \mathbf{E}_{i,j}\} \quad (4)$$

The agent  $A_i$  associated with  $P_j$  migrates to  $P_l$  if the binding energy  $\mathbf{E}_{i,l}$  is the destination.  $C$  exceeds the current  $\mathbf{E}_{i,j}$  more than  $\epsilon$  the threshold  $\epsilon$  stands for the migration parameter.

The generation of the agent  $A_i = (T_i, S_i)$  current associated with  $P_j \in N$  can perform the following actions:

- (a-1) Execute task  $T_i$  (solve and communicate with other agents)
- (a-2) cause  $T_i$
- (a-3) Calculate  $T_i$
- (a-4) estimate the additional requirements  $(E_i, M_i)$
- (a-5) Compute  $\nabla_{i,j}^t$  and check the condition  $\mathbf{E}_{i,l} - \mathbf{E}_{i,j} > \epsilon$
- (a-6) start  $T_i \rightarrow \{T_{i1}, T_{i2}\}$ , create child agents  $\{A_{ij} = (T_{ij}, S_{ij})\}, j = 1, 2$
- (a-7) migrate  $P_l \in N, l \neq j$
- (a-8) appear

these actions allow  $A_i$  to accomplish the following:

- (G-1) perform computation of carried task being executed by agent (a-1) and the perform action (a-8) i.e. the task is done
- (G-2) find a better execution environment suggest formation of the agent through actions (a-2) - (a-8)



```

If  $Q_j = \emptyset$  then c. t. ue  $T_i$ 
else { c. mpute  $\nabla_{i,j}^t$ 
  If  $E_{i,l} - E_{i,j} > \epsilon$ 
    then { pause  $T_i$  m grate a. . g the grad e. t  $\nabla_{i,j}^t$  c. t. ue  $T_i$  }
    else { part t. .  $T_i \rightarrow \{T_{i_1}, T_{i_2}\}$ 
      create  $\{A_{i_j} \mid (T_{i_j}, S_{i_j}), j = 1, 2\}$   $G_t$  gets m. d fied
      d sappear }
  }

```

he . . era. . . te t. . s t. acc. mp. sh the g. a. (G 1) . the sh. rtest p. ss b.e t me f the age. t rec. g. zes the . . ca. C. res. urces as . suffic. e. t. t tr es. t. acc. mp. sh the g. a. (G 2) O. the . ther ha. d,  $P_j$  ma. f rce  $\{A_i\}, i \in \omega_j$  t. rea. ze g. a. (G 2) he. ts perf rma. ce s e. da. gered

### 4 The MAS Dynamics

he d. us. . based schedu. g strateg. has pr. e. t. be s mp. e. a. d effic. e. t (cf sect. . . ) but t. acks a the. ret. ca. backgr. u. d a. . . g. t. determ. e. f. t s. pt ma. r quas. pt ma. . a. se. se. . ths sect. . e sha. tr. t. state a f rma. mathemat. c. m. de. f. r mu. t. age. t. c. mputat. . s. C. s der f. r a. . he. that . e. are g. e. a space. f. a. p. ss b.e age. ts a. d de. t. e. t. b.  $\mathbf{A}$  . e sha. c. s der d. s crete t me e. . ut. . . f a g. e. . et us. . tr. duce the . . t. . . f the *vector weight of an agent* h. ch. s the mapp. g  $w : \mathbf{N} \times \mathbf{A} \rightarrow \mathbb{R}_+^2$  h. se c. mp. . e. ts are  $E_i$  a. d  $M_i$  as . tr. duced ear. er . ssume that . e k. . h. the t. ta. e ght. f. ch. d age. ts after part t. . de. p. ds . . the r pare. t's e ght bef. re part t. . a. d that ths de. p. de. c. s c. mp. . e. t. se. . e. e k. . the fu. ct. . s  $f^1, f^2 : \mathbb{R}_+ \rightarrow \mathbb{R}_+$  such that . . the case. f part t. .  $A \rightarrow \{A_1, A_2\}$  . e ha. e

$$w_{t+1}^i(A_1) + w_{t+1}^i(A_2) = f^i(w_t^i(A))$$

f. r  $i = 1, 2$  such a. assumpt. . seems rea. st. c. . s mp. e. cases  $f^i$  ca. be e. e. the de. t. t

e. t de. t. e. b.  $W : \mathbf{N} \times \mathbf{N} \rightarrow \mathbb{R}_+$  the *total weight of all agents allocated on a virtual node at any time*, e

$$W_t(P) = \sum_{Sch_t(A)=P} w_t(A)$$

(b. . us. . e put. f. . age. ts ma. ta. ed b.  $P$ ) . he ma. . de. a. f. tr. duce. g such a. . t. . s the . eed. t. fi. d a g. ba. qua. t. t. desc. r. b. g the state. f the s. stem app. r. ate. . a. d a. . . g. us. t. a. . d c. s der. g the d. . am. cs. f a s. . g. e. age. t

. . the sequ. . e sha. . assume that the . . umber. f. . rtua. . . des  $\# \mathbf{N} = N$  s. *fixed* . hus. e ca. c. s der  $W_t$  as a . . . . egat. e. . ect. r. .  $\mathbb{R}^{2N}$  h. se  $j$  th c. mp. . e. t c. resp. . ds t.  $E_{total}^j$  a. d  $(N + j)$  th c. mp. . e. t c. resp. . ds t.

$M_{total}^j$  fact the sha. treat  $W_t$  as a *stochastic (vector-valued) process* . . . e sha. state the equat. s. f e. . ut. . . f  $W_t$  ( e *state equations* . f. ur s. stem) . . et  $F_t$  be a t. me depe. de t. st. ch. ast c. . . . egat. e. ect. r. fie. d. . .  $\mathbb{R}_+^{2N}$  desc. b. g. the d. am. cs. f. ur s. stem . . 'estab. shed' state. e. he. there are . e. the. r. m. gr. at. . s. . r. part. t. . s. . et  $u_{ij,t}^E(W_t), u_{ij,t}^M(W_t) \in \mathbb{R}_+$  . . de. . te the pr. p. rt. . s. . f the . e. ght. c. mp. . e. ts. f. age. ts m. gr. at. g. fr. m. . de. i. t. . . de. j. t. . the. c. r. res. p. d. g. c. mp. . e. ts. f. the. t. ta. . e. ght. f. a. . age. ts at. . . de. i. a. d. et  $u_{ii,t}^E(W_t), u_{ii,t}^M(W_t) \in \mathbb{R}_+$  . . de. . te the pr. p. rt. . s. . f the . e. ght. c. mp. . e. ts. f. sp. tt. g. age. ts t. the. c. r. res. p. d. g. c. mp. . e. ts. f. the. t. ta. . e. ght. f. a. . age. ts at. . . de. i. . he. the state equat. s. ha. e the f. rm

$$\begin{cases} W_{t+1}^i & F_t^i \left( \left[ \left( - \sum_{k=1}^N u_{ik,t}^E(W_t) \right) W_t^i \right]_{i=1}^N \right) \\ & + f^1 \left( u_{ii,t}^E(W_t) W_t^i \right) - \left( \sum_{k=1}^N u_{ik,t}^E(W_t) \right) W_t^i \\ & + \sum_{j \neq i} u_{ji,t}^E(W_t) W_t^j \\ W_{t+1}^{N+i} & F_t^{N+i} \left( \left[ \left( - \sum_{k=1}^N u_{ik,t}^M(W_t) \right) W_t^{N+i} \right]_{i=1}^N \right) \\ & + f^2 \left( u_{ii,t}^M(W_t) W_t^{N+i} \right) - \left( \sum_{k=1}^N u_{ik,t}^M(W_t) \right) W_t^{N+i} \\ & + \sum_{j \neq i} u_{ji,t}^M(W_t) W_t^{N+j} \end{cases} \quad (6)$$

f. r. i. . . . , N . . te that  $u = (u^E, u^M)$  here  $u^E, u^M : \mathbb{N} \times \mathbb{R}_+^N \rightarrow \mathbb{R}_+^{N \times N}$  . . s. . fact a *control* . f. ur s. stem . r. m. the . at. ure . f. ur pr. b. em. t. s. eas. t. see that a . c. tr. . strateg. must sat. sf. the f. . . . g. c. d. t. s. f. r. a. . t.  $t \in \mathbb{N}$  a. d  $x \in \mathbb{R}_+^N$

$$\begin{cases} u_{ij,t}^E(x) \cdot u_{ji,t}^E(x) & , u_{ij,t}^M(x) \cdot u_{ji,t}^M(x) & \text{f. r. i. / j,} \\ \sum_{k=1}^N u_{ik,t}^E(x) \leq \sum_{k=1}^N u_{ik,t}^M(x) \leq & \text{f. r. i. . . . , N.} \end{cases} \quad (7)$$

he first pa. r. f. equat. es mea. s. that at a g. e. t. me m. gr. at. . s. bet. ee. t. . . . des. ma. h. app. e. . . . . e. d. r. ect. . . . he rema. . . g. c. d. t. s. mea. that the . um. ber . f. age. ts. ea. . g. a. . de. must . . t. e. ceed the . um. ber . f. age. ts. pr. es. t. at. the . . de. ust. bef. re the m. gr. at. .

he . t. a. state . f. equat. . . (6)

$$W_0 = W \quad (7)$$

usua. . has a. . e. cept . . e. c. mp. . e. ts. equat. . . . h. ch. mea. s. that a s. stem starts . th. . e. age. t. r. a. batch . f. age. ts. p. aced . . . a. s. g. e. C. but . f. c. urse . . ge. era. . e. . eed . . t. make such a . assumpt. .

### 5 The Optimal Scheduling Problem

. . . et us pr. p. se t. . e. amp. es . f. c. st. fu. ct. . . a. s. h. ch. seem appr. pr. ate f. r. mu. t. age. t. c. mputat. . s. . he first s. the e. p. ected t. ta. t. me. f. c. mputat. . s.

$$V(u, W) = E(m. \{t \geq \sum_{i=1}^N W_t^i\}), \quad (8)$$

The second takes into account the mean and variance of the first term has the following form

$$V(u, W) = E\left(\sum_{t=0}^{\infty} \sum_{i=1}^N (L_t^i - \bar{L}_t)^2\right) \quad (6)$$

here  $L_t^i = \frac{W_t^i}{perf_i(W_t^{N+i})}$  is the load concentration and  $\bar{L}_t = \frac{1}{N} \sum_{i=1}^N L_t^i$  is its mean. For a fixed  $u$  let us introduce the following notation for the set of admissible controls

$$\mathbf{U} = \{u = (u^E, u^M) \in \mathbb{N} \times \mathbb{R}_+^N \rightarrow \mathbb{R}^{2(N \times N)} \mid u \text{ satisfies conditions (5)}\}.$$

Assume that  $V$  has either the form (8) or (6). Given a task configuration  $W$ , our *optimal scheduling problem* is to find such control strategy  $u^* \in \mathbf{U}$  that

$$V(u^*, W) = \min_{u \in \mathbf{U}} \{V(u, W) \mid u \text{ is a solution of (5), (7)}\}. \quad (7)$$

## 6 Numerical Tests

In this section we present performed experiments and discuss how the fit presented in the introduction of the results compares to the major problem domain. We are interested in the performance of the Mesh Generator (G) and the ArchGen (G) strategies. The presented tests are broadly described in [7], the papers [2] contain the implementation details. Computations were run on the same physical environment that was used for the Cs collected through the network.

### 6.1 Mesh Generator

The G is a C/C++ task implementation. Each agent is equipped with a single part of the partitioned solid, from which the mesh has to be generated. The application had the following execution path

Create all the agents, equip each with the part of the solid, generate the mesh for the agent's size, areas from the smallest, large depend on the solid part, the goal and each piece shape. The more complex the shapes, the bigger mesh is generated.

2 agents are put on the network and distribute files using the dedicated user interface after a single agent finds satisfactory execution environment starts computation.

The generated piece meshes are sent to the master application and collected together.

The G implementations evaluate and compare cases of the system dynamics, so the main points of results are as follows: check of the local user-based scheduling procedure, put too much overhead, the take execution time and if the available resources are fully utilized from the beginning. A utilization 'holes' and usage as a characterization points, reduce the performance, global scheduling procedure, better global efficiency.

short, we have formulated the following conclusions concerning the results

- our based scheduling algorithm spread quickly among computers, the network time needed to allocate tasks is smaller compared to the heuristic computation time
- available resources were utilized at 90%, the application used up to 2 agents
- heuristics performed badly according to the general calculation

It is clear from these conclusions that the distributed based local scheduling process is suited for such regular problems. The results also confirm that the communication factor may be omitted for certain class of applications, since the total communication overhead is minimal. The communication required for the distributed (elementary) decomposition should adequately be designed to avoid further degradation of the system efficiency.

## 6.2 HGS

The HGS is a stochastic hierarchical genetic algorithm optimizing a given function, a defined domain. The application produces agents dynamically. The course of the routine is given by agents as control, which starts execution after application is started. As time passes, the number of agents at the execution time may be determined. The algorithm executes paths of the following

Create single agent with the initial population, agent migrates to find suitable execution environment.

- 2 agent starts computation and the amount of time after population changes due to the genetic evolution.

During the computation agent's time after population amount grows beyond a fixed number, the agents split and new ones are created out of part of the population set.

The HGS agents perform three elements of dynamic execution, migration and partitioning. The communication overhead (performance agent's migration requires agent's to pass the initial population) and dynamic scheduling efficiency were tested. The theoretical performance of the algorithm was compared with the distributed scheduling. The following conclusions concerning the distributed scheduling were drawn.

- our based scheduling does not perform adequately with the dynamic rescheduling of the computation units
- the communication overhead is around 90% of the execution time with application usage to actual computation agents

Therefore the following may be stated that the distributed based local scheduling performs well in case of regular stochastic problem with dynamic amount of agents. It is not adapted to a dynamic scheduling algorithm. It is significant to decrease the system's efficiency.

... add that we have also tested the effectiveness of the distributed, us... based scheduling versus centralized, greedy scheduling (a R u d R b... s... ut... ) utilizing... e... et... rk message passing mechanisms (a a R... )... please see [7] for detailed results. It has shown that the distributed scheduling... shows moderate speedups (up to % of total computation time), which... disappear. Hence, it's almost always the case for... age ts, d... us... based scheduling performs % better than R u d R b.

## 7 Conclusions and Further Research

The distributed, agent-based... as the... tech... g... g... e... a... t... a... e... ect... e... des... g... f... a... ca... d... us... based scheduling strategy for a distributed... r... me... t... ts... e... ect... e... ess... s... ach... e... d... b... the... c... m... p... e... t... f... ca... s... ch... e... d... u... g... ru... es... a... d... the... ack... f... te... s... e... c... mmu... cat... requ... red... b... ce... tra... zed... schedu... ers... the... f... r... ma... desc... r... pt... . . . tr... duced... sect... s... 4... a... d... pr... oduces the discrete equation... f... e... ut... a... d... the... character... zat... . . . f... adm... ss... b... e... c... tr... s... as... e... as... the... c... st... fu... ct... . . . a... f... r... c... m... put... g... . . . uch... c... s... derat... s... put... ur... pr... o... b... em... t... the... s... d... frame... rk... f... the... st... ch... ast... c... pt... ma... c... tr... the... r... h... ch... pr... oduces us... th... t... s... such... as... e... ma... t... pe... pr... o... c... p... es... a... . . . g... us... t... stud... the... pt... ma... t... f... c... tr... strategies as... e... as... the... as... m... pt... t... es

## References

1. Grochowski M., Schaefer R., Uhruski P.: An Agent-based Approach To a Hard Computing System - Smart Solid. *Proc. of the International Conference on Parallel Computing in Electrical Engineering (PARELEC 2002)*, 22-25 September 2002, Warsaw, Poland. IEEE Computer Society Press 2002, pp. 253-258.
2. Uhruski P., Grochowski M., Schaefer R.: Multi-agent Computing System in a Heterogeneous Network. *Proc. of the International Conference on Parallel Computing in Electrical Engineering (PARELEC 2002)*, 22-25 September 2002, Warsaw, Poland. IEEE Computer Society Press 2002, pp. 233-238.
3. Schaefer R., Flasiński M., Toporkiewicz W.: Optimal Stochastic Scaling of CAE Parallel Computations. *Lecture Notes in Computer Intelligence*, Vol. 1424, Springer 1998, pp.557-564.
4. Wierzba B., Semczuk A., Kołodziej J., Schaefer R.: Hierarchical Genetic Strategy with real number encoding. *Proc. of the 6th Conf. on Evolutionary Algorithms and Global Optimization* Łagów Lubuski 2003, Wydawnictwa Politechniki Warszawskiej 2003, pp. 231-237.
5. Grochowski M., Schaefer R., Uhruski P.: Diffusion Based Scheduling in the Agent-Oriented Computing Systems. *Lecture Notes in Computer Science*, Vol. 3019, Springer 2004, pp. 97-104.
6. Luque E., Ripoll A., Corts A., Margalef T.: A distributed diffusion method for dynamic load balancing on parallel computers. *Proc. of EUROMICRO Workshop on Parallel and Distributed Processing*, San Remo, Italy, January 1995. IEEE CS Press.
7. Momot J., Kosacki K., Grochowski M., Uhruski P., Schaefer R.: Multi-Agent System for Irregular Parallel Genetic Computations. *Lecture Notes in Computer Science*, Vol. 3038, Springer 2004, pp. 623-630.

# A Superconvergent Monte Carlo Method for Multiple Integrals on the Grid

Elizaveta Ska, Emanouil Tassoulas and Petar P. P. P.  
Institute for Parallel Processing - Bulgarian Academy of Sciences,  
Acad. G. Bonchev St., Bl.25A, 1113 Sofia, Bulgaria  
{sofia, emanouil, anet}@parallel.bas.bg

**Abstract.** In this paper we present error and performance analysis of a Monte Carlo variance reduction method for solving multidimensional integrals and integral equations. This method combines the idea of separation of the domain into small subdomains with the approach of importance sampling. The importance separation method is originally described in our previous works [7, 9]. Here we present a new variant of this method adding polynomial interpolation in subdomains. We also discuss the performance of the algorithms in comparison with crude Monte Carlo. We propose efficient parallel implementation of the importance separation method for a grid environment and we demonstrate numerical experiments on a heterogeneous grid. Two versions of the algorithm are compared - a Monte Carlo version using pseudorandom numbers and a quasi-Monte Carlo version using the Sobol and Halton low-discrepancy sequences [13, 8].

## 1 Introduction

Consider the problem of approximate calculation of the multiple integral

$$I f = \int_G f(x)p(x) dx, \quad p(x) \geq 0, \quad \int_G p(x) dx = 1,$$

where  $p(x)$  is a probability density function. The crude Monte Carlo quadrature is based on the probability interpretation of the integral

$$I f \approx \frac{1}{N} \sum_{n=1}^N f(x_n), \quad (1)$$

where  $\{x_n\}$  is distributed according to  $p(x)$ . The error is proportional to  $\sigma f N^{-1/2}$

$$\epsilon_N f \sim \sigma f N^{-1/2},$$

where

$$\sigma f = \left( \int_G (f(x)p(x) - I f)^2 dx \right)^{1/2}.$$

here are various asymptotic improve the convergence rate of the Car. te grat. the function g the remainder each additional establishes a further bound for the Car. and deterministic te grat. formulae for smooth functions

**Theorem 1.** (Bachvalov [4, 5]) *There exist constants  $c(s, k)$ ,  $c'(s, k)$ , such that for every quadrature formula  $I_N f$  which is fully deterministic and uses the function values at  $N$  points there exists a function  $f \in \mathbf{C}_k^s$  such that*

$$\left| \int_{\mathbb{E}^s} f(x) dx - I_N f \right| \geq c(s, k) \|f\| N^{-\frac{k}{s}}$$

and for every quadrature formula  $I_N f$ , which involves random variables and uses the function values at  $N$  points, there exists a function  $f \in \mathbf{C}_k^s$ , such that

$$\left\{ \mathbb{E} \left[ \int_{\mathbb{E}^s} f(x) dx - I_N f \right]^2 \right\}^{1/2} \geq c'(s, k) \|f\| N^{-\frac{1}{2} - \frac{k}{s}}.$$

Furthermore the remainder shows that the Car. methods have an advantage over deterministic methods, especially high dimensional smooth order to obtain the optimal convergence rate for functions with bounded  $k$ th order derivatives. The used technique is *stratification*. Split the te grat. region  $G$  into  $M$  subdomains

$$G = \bigcup_{j=1}^M D_j, \quad D_i \cap D_j = \emptyset, \quad i \neq j, \quad \sum_{j=1}^M N_j = N,$$

$$p^{(j)}(x) = p(x)/\bar{p}_j, \quad \bar{p}_j = \int_{D_j} p(x) dx.$$

In the subdomains  $D_j$  use a te Car. te grat. formula  $I_{N_j}^{(j)} f$  which utilizes  $N_j$  random points  $\xi_1^{(j)}, \dots, \xi_{N_j}^{(j)}$  the stratified te Car. formula is

$$I_N f = \sum_{j=1}^M \frac{\bar{p}_j}{N_j} I_{N_j}^{(j)} f.$$

The error of the stratified method is given by

$$\epsilon_N \sim N^{-1/2} \sigma_s, \quad \sigma_s^2 = \sum_{j=1}^M \sigma^{(j)2}, \quad \sigma^{(j)} = \left( \int_{D_j} (f(x) p_j(x) - I_{N_j} f)^2 dx \right)^{\frac{1}{2}}.$$

Our method achieves  $\mathcal{O}(N^{-\frac{k}{s}})$  if the function  $f$  is in  $\mathbf{C}_k^s$  and therefore attains the optimal convergence rate (see sec 2)

Another possible idea for improving the convergence of the Car. methods is to replace the pseudorandom numbers with terms of a random sequence

sequence  $\tau, 2$  the most desired measure for estimating the quality of the distribution of a random discrepancy sequence  $\tau = \{x_i\}_{i=1}^N$  in  $E^s$  is the discrepancy

$$D_N^* = \sup_{I \subset E^s} \left| \frac{A_N(\tau, I)}{N} - \mu(E) \right|.$$

The discrepancy sequences have order of convergence of the discrepancy  $\mathcal{O}(N^{-1} \log^s N)$ , which becomes order of convergence of the corresponding quasimonte Carlo method for integrating a function over  $E^s$

$$Q_N f = \frac{1}{N} \sum_{j=1}^N f(x_j). \tag{2}$$

Herefore quasimonte Carlo methods are higher convergence rate (at the expense of more stringent smoothness requirements) than a 2 cube is considered as a quasimonte Carlo series of form  $a$  is giving a quasimonte Carlo series of a quasimonte Carlo method is that a straight forward studied the possibility of using the attainable bound discrepancy sequences for a algorithm (see 2)

The quasimonte Carlo methods usually show good parameter efficiency characteristics described by parameter approximation which is suitable for grid generation. The obtained good parameter efficiency bounds for the quasimonte Carlo series are

## 2 Description of Our Algorithm

We introduce adapted series of the domain into smaller subdomains, that smaller subdomains are used here the function values are larger in the subdomain to approximate the function by a piecewise linear function values at some fixed points. The input parameters of our algorithm are the dimension  $s$ , the smoothness order  $k$ , the number of base points  $M$ , the number of steps  $N$ , the number of random points in each cube  $m$ , the number of points used for the application of crude quasimonte Carlo method  $R$  first select  $M$  points  $a_1, \dots, a_M$  in the unit cube  $E^s$ , following the procedure discussed in 2, and compute the respective efficiencies  $c_1, \dots, c_M$  for each coordinate  $x_j$  estimate the values of

$$g(x_j) = \int_{E^{s-1}} |f(x_1, \dots, x_{j-1}, x_j, x_{j+1}, \dots, x_s)| dx_1, \dots, dx_{j-1} dx_{j+1}, \dots, dx_s$$

at points  $x_j = \frac{r}{N}$ , using crude quasimonte Carlo algorithm with  $R$  points here we approximate the desired mean value of function  $g$  by a piecewise linear function  $g$ , using these values for each coordinate we choose  $N + 1$  points  $\xi_r^i$  such that  $\xi_0^i = \xi_N^i = a$  and

$$\int_{\xi_{r-1}^i}^{\xi_r^i} g(t) dt = \int_{\xi_r^i}^{\xi_{r+1}^i} g(t) dt, \quad r = 1, \dots, N - 1.$$



These steps can be considered as preprocessing, and can be done in parallel. We use Monte Carlo sampling the points  $\xi_r^i$  in the part of the cube  $E^s$  of  $N^s$  subdomains  $D_j$  approximate  $\int_{D_j} f(x) dx$  by the formula

$$\mu(D_j) - \sum_{i=1}^m (f(\eta_i) - L_j(f, \eta_i)) + \mu(D_j) \sum_{i=1}^M c_i f(T_j(a_i)),$$

where  $T_j$  is the canonical linear transformation that maps  $E^s$  to  $D_j$ , the points  $\eta_i \in D_j$  are uniformly distributed random points, and  $L_j(f, \eta_i)$  is the polynomial approximation of  $f$  obtained using the values  $f(T_j(a_i))$  (see 2). Using these unbiased estimates, we obtain an estimate of the integral over  $E^s$  by averaging these estimates as a sum of the variances  $\sigma_j^2$  over subdomain  $D_j$  in order of convergence  $\mathcal{O}(N^{-k-s/2})$ , hence using  $\mathcal{O}(N^s)$  points and suitable mapping the sequence of the remaining steps is an estimate of the error is obtained by using the empirical variances  $\sigma_j$ .

The number of function evaluations is  $N^s(m + M) + Rs(N - )$ . In most practical situations the time for performing them dominates the whole computation.

We studied a quasimonte Carlo algorithm for the algorithm of the Carlo methods. We use pseudorandom number generators in order to sample uniformly distributed random variables. The deaif quasimonte Carlo methods to replace the pseudorandom numbers with terms of a low discrepancy sequence. The integrand function on the side of a unit cube, the dimension of the low discrepancy sequence is higher than  $s$ , for a more complex algorithm is used. We note that the used parallel computation, low discrepancy sequences can be effectively reproduced by the results, unlike the Carlo algorithm. The cardinalities of the  $r$ th term of the sequence can be used to produce the cardinalities of the points  $\eta_i$ . We have  $s$  cardinalities and  $m$  points, the constructed dimension of the algorithm becomes  $sm$ . We tested that of the most popular families of low discrepancy sequences the sequences of bounded variation give the rate of convergence of the quasimonte Carlo algorithm has a factor of  $g^{sm} N$ , and the distribution error improvement with respect to the Carlo series (see sec 4).

### 3 Parallel Implementation of the Algorithm Suitable for Computational Grids

The Carlo methods are here to parallelize and distribute grid and file grid parallelism can be applied. We take into account the fact that the Grids are heterogeneous computing environment, where the user describes the specifics of the target architecture. Here we parallelize algorithms should be able to adapt to this heterogeneous, pre-distributed and balanced grid. The Carlo algorithms can be tailored such environments, provided parallel pseudorandom number generators are available. We use of

quasi-Monte Carlo algorithms possess more difficulties. In both cases the effectiveness of the algorithm depends on the function and on the respective algorithm packages for generating pseudorandom numbers. The package for parallel pseudorandom generators we used the R-G (1998) for generating the scrambled data and the sequential ultrafast generators (1998), which provide the necessary function.

- portable
- use assembly language for best performance. It is not an ideal process.
- provide a fast forward permutation, important for parallel approach.

Our parallelization is based on the master-slave paradigm, with some modifications. We divide the work into chunks, respectively the subdomains, which are requested from the master process by the slave processes. In order to increase the efficiency, the master assigns preforms computation, here at the global communication requests, thus we achieve better performance and communication, and we do not lose the possible output of the master process. However, good sequence we take care in both master and slave processes to fast forward and the generator effectively. The point that succeeded the scrambling that is provided by the generators enables a posteriori estimation of the error in the quasi-Monte Carlo case.

### 4 Numerical Experiments

Our numerical tests are based on the test examples, which are taken from paper of Skrzyszewski and Caesch.

**Example 1.** The first example is the quasi-Monte Carlo integration over  $E^5$ ,  $5^5$  of the function

$$f_1(x) = \exp\left(\sum_{i=1}^5 a_i x_i^2 \frac{2 + \sin(\sum_{j=1, j \neq i}^5 x_j)}{2}\right),$$

here  $a = (\frac{1}{2}, \frac{1}{5}, \frac{1}{5}, \frac{1}{5})$

**Example 2.** The second example is the quasi-Monte Carlo integration over  $E^7$ ,  $7^7$  of the function

$$f_2(x) = e^{1 - (\sin^2(\frac{\pi}{2}x_1) + \sin^2(\frac{\pi}{2}x_2) + \sin^2(\frac{\pi}{2}x_3))} \times \arcsin\left(\sin(\frac{\pi}{2}x_4) + \frac{x_1 + \dots + x_7}{2}\right).$$

Table shows the results for random and Monte Carlo. The smallest error is used as a reference for comparison. The results show that crude Monte Carlo method that uses the same number of function values as our algorithm.

**Table 1.** Results for **Example 1** with number of cubes  $N$  and number of points per cube 10

$N$	$k$	SPRNG	Sobol	Halton	crude MC
2	4	5.15e-04	3.16e-04	3.72e-04	1.52e-02
	6	7.06e-05	1.43e-05	2.34e-05	7.40e-03
3	4	8.01e-05	4.38e-05	4.77e-05	5.51e-03
	6	2.15e-07	7.41e-07	3.19e-07	2.68e-03
4	4	1.21e-05	1.01e-05	2.09e-05	2.68e-03
	6	2.95e-07	3.45e-07	1.35e-07	1.31e-03
5	4	1.78e-06	3.03e-06	2.87e-06	1.54e-03
	6	2.79e-08	3.61e-08	4.09e-08	7.48e-04

**Table 2.** Results for **Example 2** with number of cubes  $N$  and number of points per cube 10

$N$	$k$	SPRNG	Sobol	Halton
2	4	1.25e-05	3.12e-05	3.29e-05
	6	9.49e-07	3.61e-07	7.34e-07
3	4	1.31e-06	5.30e-06	4.67e-06
	6	7.57e-08	7.61e-08	8.61e-08
4	4	2.94e-08	1.82e-06	4.73e-07
	6	5.99e-09	1.07e-08	1.44e-08
5	4	1.23e-07	3.21e-07	5.43e-07
	6	8.43e-10	1.61e-09	1.20e-08

but heampes the errors be the the ret ca a s e, the c...erge ce rate s  $\mathcal{O}\left(N^{-\frac{1}{2}}\right)$  f r the crude...te Car...meth d, a d  $\mathcal{O}\left(N^{-\frac{k}{s}-\frac{1}{2}}\right)$  f r ur adapt...e meth d, he sm...th ess  $k$  s used abe sh...s C...t me f r ur agr thm...he  $N$  s equa...t 4 a d the...umber f ra...d m p...ts per cube  $m$  s equa...t 4...e used...d...ere t c mputers f r these tests...three f the c mputers ha e...e t um p r...cess rs ru...g at d...ere t c...ck speeds a d...e has a...t r...a G4 p r...cess r...f the c mputers had the G...bus t...k t...sta ed...ab e 4...e c mpare the est mated t me f r ru...g ur agr thm...a...th se c mputers...para e...case f perfect para e effice...th the measured e cut...t me...e used the...C...G2 mp...eme tat...f...h ch s the m st ge...era appr...ach f r ru...g para e...bs...c mputat...a gr ds...th s a...e suc cessfu...ut...zed mach...es...th d...ere t e d a...ess...the same c mputat...e...e bta ed r...ugh...the same accurac...th...d screpa c...seque ces as...th pseud...ra...d m...umbers, due t...the h gh e...lect e d me...s...he C...t me f...ur mp...eme tat...s...f the quas......te Car......ers...s...as freque t...sm a...er, due t...the effice t ge...erat...agr thms...uas......te Car...agr thms are m r e d fficu t t...para e...ze u...der such c...stra ts, but th s ca...be d...e f f the ge...erat rs...f the...d screpa c...seque ces ha e the...ecessar fu...ct...a t

**Table 3.** Time and efficiency for **Example 1** with number of points 14 and number of points per cube 40

	P4/2.8GHz	P4/2GHz	P4/2GHz	G4/450MHz
SPRNG	102	117	118	413
Sobol	91	106	96	393
Halton	91	106	106	393

**Table 4.** Parallel efficiency measurements

	Estimated Time	Measured Time	Efficiency
SPRNG	34	41	83%
Sobol	30	34	88%
Halton	31	34	91%

## 5 Conclusions

The adaptive Monte Carlo method for solving multiple integrals of smooth functions has been proposed and tested. This method is an improved version of the importance separation method. The importance separation method is combined with the maximum tempering of the subdomains. Quasi-Monte Carlo versions of the algorithm as a student have obtained results are that an efficient parallel implementation of the algorithm has been achieved using all processors of the master slave computing paradigm, enabling the execution of the programs on heterogeneous Grid environments. The ideas of this implementation can be extended to other Monte Carlo and quasi-Monte Carlo methods.

**Acknowledgments.** This work is supported by the Ministry of Education and Science of the Republic of Bulgaria under Grant # 4-4-4.

## References

1. E. Atanassov. Measuring the Performance of a Power PC Cluster, Computational Science - ICCS 2002 (P. Sloot, C. Kenneth Tan, J. Dongarra, A. Hoekstra - Eds.), LNCS 2330, 628–634, Springer, 2002.
2. E. Atanassov, I. Dimov, M. Durchova. A New Quasi-Monte Carlo Algorithm for Numerical Integration of Smooth Functions, Large-Scale Scientific Computing (I. Lirkov, S. Margenov, J. Wasniewski, P. Yalamov - Eds.), LNCS 2907, 128–135, Springer, 2004.
3. E. Atanassov, M. Durchova. Generating and Testing the Modified Halton Sequences, Numerical Methods and Applications (I. Dimov, I. Lirkov, S. Margenov, Z. Zlatev - Eds.), LNCS 2542, 91–98, Springer, 2003.
4. N.S. Bachvalov. On the approximate computation of multiple integrals, Vestnik Moscow State University, Ser. Mat., Mech., Vol. 4, 3–18, 1959.

5. N.S. Bachvalov. Average Estimation of the Remainder Term of Quadrature Formulas, USSR Comput. Math. and Math. Phys., Vol. 1(1), 64–77, 1961.
6. R.E. Caflisch. Monte Carlo and quasi-Monte Carlo methods, Acta Numerica, Vol. 7, 1–49, 1998.
7. I. Dimov, A. Karaivanova, R. Georgieva and S. Ivanovska. Parallel Importance Separation and Adaptive Monte Carlo Algorithms for Multiple Integrals, Numerical Methods and Applications (I. Dimov, I. Lirkov, S. Margenov, Z. Zlatev - Eds.), LNCS 2542, 99–107, Springer, 2003.
8. J. H. Halton. On the efficiency of certain quasi-random sequences of points in evaluating multi-dimensional integrals, Numer. math., 2, 84–90, 1960.
9. A. Karaivanova. Adaptive Monte Carlo methods for numerical integration, Mathematica Balkanica, Vol. 11, 391–406, 1997.
10. M. Mascagni. SPRNG: A Scalable Library for Pseudorandom Number Generation. Recent Advances in Numerical Methods and Applications II (O. Iliev, M. Kaschiev, Bl. Sendov, P.S. Vassilevski eds.), Proceeding of NMA 1998, World Scientific, Singapore, 284–295, 1999.
11. B. Moskowitz and R.E. Caflisch. Smoothness and dimension reduction in quasi-Monte Carlo methods, J. Math. Comput. Modeling, 23, 37–54, 1996.
12. H. Niederreiter. Random number generation and quasi-Monte Carlo methods, SIAM, Philadelphia, 1992.
13. I.M. Sobol. On the distribution of point in a cube and the approximate evaluation of integrals, USSR Computational Mathematics and Mathematical Physics, 7, 86–112, 1967.

# A Sparse Parallel Hybrid Monte Carlo Algorithm for Matrix Computations

Michael Branford, Christoph Weihrauch, and V. N. Alexandrov

Advanced Computing and Emerging Technologies Centre,  
School of System Engineering,  
The University of Reading  
Whiteknights, P.O. Box 225  
Reading, RG6 6AY, UK

{s.j.branford, c.weihrauch, v.n.alexandrov}@reading.ac.uk

**Abstract.** In this paper we introduce a new algorithm, based on the successful work of Fathi and Alexandrov, on hybrid Monte Carlo algorithms for matrix inversion and solving systems of linear algebraic equations. This algorithm consists of two parts, approximate inversion by Monte Carlo and iterative refinement using a deterministic method.

Here we present a parallel hybrid Monte Carlo algorithm, which uses Monte Carlo to generate an approximate inverse and that improves the accuracy of the inverse with an iterative refinement. The new algorithm is applied efficiently to sparse non-singular matrices. When we are solving a system of linear algebraic equations,  $Bx = b$ , the inverse matrix is used to compute the solution vector  $x = B^{-1}b$ .

We present results that show the efficiency of the parallel hybrid Monte Carlo algorithm in the case of sparse matrices.

**Keywords:** Monte Carlo Method, Matrix Inversion, Sparse Matrices.

## 1 Introduction

The problem of solving a real  $n \times n$  matrix ( $B$ ) system of linear algebraic equations ( $Bx = b$ ) is a fundamental problem in many applications, e.g. engineering, statistics, signal processing, computer graphics, etc. The standard method for solving such a system is the Gaussian elimination method, which requires  $O(n^3)$  sequential steps. However, the usual methods for solving such a system (e.g. parallel Gaussian elimination, Gaussian reduction) are sequential. The computation time for large problems, especially for problems that can be parallelized, is often prohibitive. The use of matrix established algorithms that use Monte Carlo methods to estimate the inverse of the matrix  $B$  and compute the solution vector  $x = B^{-1}b$  is a promising approach. In this paper, we present a new algorithm for solving such a system. The algorithm consists of two parts: approximate inversion by Monte Carlo and iterative refinement using a deterministic method. The Monte Carlo method is used to generate an approximate inverse of the matrix  $B$ , and the deterministic method is used to refine the approximate inverse. The algorithm is applied to a set of test problems, and the results show that the algorithm is efficient and accurate. The algorithm requires  $O(NT)$  steps, where  $N$  is the number of rows of the matrix  $B$  and  $T$  is the number of iterations.

ect r f E ( here  $N$  s the umber f cha s a d  $T$  s a estimate f the cha e gth the st chastic process b th f h ch are depe de t f  $n$ , the sze f the matr ) a d, *second*, the samp g process fr st chastic meth ds s here t para e

Car se gra ed te Car a g r thms fr a d E ha e bee pr p sed b se era auth rs [2, 7, 8] th s paper e e p re a para e sparse a g r thm fr ert g d ag a d m a t matr ces e sh that th s a g r thm rks e ect e a d effe e t he depe ed er mut p e pr cess rs

he dea f te Car f r matr c mputat s s prese ted ect 2 the para e h br d a g r thm s descr bed ect 4 e deta h e mp eme ted the a g r thm f r sparse matr ces the resu ts f the e per me ta ru s f th s mp eme tat are prese ted ect a d e c c u d e the r k ect

## 2 Monte Carlo Matrix Computations

ssume that the s stem f ear algebra c equat s ( E) s prese ted the frm

$$Bx = b \tag{1}$$

here  $B$  s a rea square  $n \times n$  matr ,  $x = (x_1, x_2, \dots, x_n)^t$  s a  $n$  s ut ect r a d  $b = (b_1, b_2, \dots, b_n)^t$ .

ssume the ge era case  $\|B\| > 0$  e c s der the sp tt g

$$B = B_1 - B_2 \tag{2}$$

here d ag a e eme ts f  $B$  are the same as th se f  $B$ , a d the d ag a e eme ts f  $B$  are defi ed as  $b_{ii} = b_{ii} + \gamma_i \|B\|$ , ch s g m st cases  $\gamma_i > 0$  f r  $i = 1, 2, \dots, n$  e further c s der  $B = B_1 - B_2$  here  $B_1$  s the d ag a matr f  $B$ , e g  $(b_1)_{ii} = b_{ii}$  f r  $i = 1, 2, \dots, n$  s sh e c u d tra sf rm the s stem ( ) t

$$x = Tx + f \tag{3}$$

here  $T = B^{-1}C$  a d  $f = B^{-1}b$ . he mut p ers  $\gamma_i$  are ch se s that, f t s p ss b e, the reduce the frm f  $T$  t be ss th a d thus reduc g the umber f ark cha s requ red t reach a g e prec s e c s der t p ss b tes, first, fi d g the s ut f  $x = Tx + f$  us g te Car ( C) meth d f  $\|T\| < 1$  r fi d g  $B^{-1}$  us g C a d after that fi d g  $B^{-1}$ . he f requ red bta g the s ut ect r s  $x = B^{-1}b$

C s der first the st chastic appr ach ssume that  $\|T\| < 1$  a d that the s stem s tra sf rmed t ts terat e f rm ( ) C s der the ark cha g e b

$$s_0 \rightarrow s_1 \rightarrow \dots \rightarrow s_k, \tag{4}$$

here the  $s_i, i = 1, 2, \dots, k$ , be gs t the state space  $S = \{1, 2, \dots, n\}$  he f r  $\alpha, \beta \in S, p_0(\alpha) = p(s_0 = \alpha)$  s the pr bab t that the ark cha starts at

state  $\alpha$  and  $p(s_{j+1} = \beta | s_j = \alpha) = p_{\alpha\beta}$  is the transition probability from state  $\alpha$  to state  $\beta$ . The set of all transition probabilities  $p_{\alpha\beta}$  defines a transition probability matrix  $P = \{p_{\alpha\beta}\}_{\alpha,\beta=1}^n$ ,  $i=2$ ,

we say that the distribution  $(p_1, \dots, p_n)^t$  is acceptable for a given set  $g$ , and that the distribution  $p_{\alpha\beta}$  is acceptable for matrix  $T$ , if  $p_\alpha > 0$ ,  $g_\alpha / p_\alpha \geq 0$ , and  $p_{\alpha\beta} > 0$ ,  $T_{\alpha\beta} / p_{\alpha\beta} \geq 0$ , and  $p_{\alpha\beta} \geq 0$ ,  $T_{\alpha\beta} \geq 0$  respectively. We assume  $\sum_{\beta=1}^n p_{\alpha\beta} = 1$ , for all  $\alpha = 1, 2, \dots, n$ . Generally, we define

$$W_0 = 1, W_j = W_{j-1} \frac{T_{s_{j-1}s_j}}{p_{s_{j-1}s_j}} \quad (6)$$

for  $j = 1, 2, \dots, n$

Consider the random variable  $\theta_i g = \frac{g_{s_0}}{p_{s_0}} \sum_{i=1}^{\infty} W_i f_{s_i}$ . We use the following notation for the partial sum

$$\theta_i g = \frac{g_{s_0}}{p_{s_0}} \sum_{j=0}^i W_j f_{s_j}. \quad (7)$$

Under condition  $\|T\| < 1$ , the corresponding geometric series converges for a given  $f$ , and  $E\theta_i g$  tends to  $(g, x)$  as  $i \rightarrow \infty$ . Thus,  $\theta_i g$  can be considered as an estimator of  $(g, x)$  for sufficiently large  $i$ . If  $d$  is an arbitrary compact set, the subset  $S_r$  of  $r$  elements, the  $r^{th}$  compact set of  $x$ , we should choose  $g = e(r) = (e(r)_1, \dots, e(r)_r)$  such that

$$e(r)_\alpha = \delta_{r\alpha} \begin{cases} f(x_r) & \text{if } r = \alpha \\ \text{otherwise} & \end{cases} \quad (8)$$

Therefore, we have that

$$(g, x) = \sum_{\alpha=1}^n e(r)_\alpha x_\alpha = x_r. \quad (9)$$

the corresponding Monte Carlo method is given by

$$x_r = \Theta \frac{1}{N} \sum_{s=1}^N \theta_s e(r)_s \quad (10)$$

where  $N$  is the number of chains and  $\theta_s e(r)_s$  is the appropriate value of  $x_r$  for the  $s^{th}$  chain. It means that using the Monte Carlo method, we can estimate the value of the elements of the subset  $S_r$ . The corresponding Monte Carlo method using transition probabilities  $(p_{\alpha\beta})_{\alpha,\beta=1}^n$  and a simple Monte Carlo method (O) with  $p_{\alpha\beta} = \frac{|T_{\alpha\beta}|}{\sum_{\beta=1}^n |T_{\alpha\beta}|}$ , here  $\alpha, \beta = 1, 2, \dots, n$  is the Monte Carlo

subtended as a simple

find the inverse  $M^{-1} = \{m_{rr}^{(-1)}\}_{r,r=1}^n$  of some matrix  $M$ , we must first compute the elements of matrix  $A = I - M$ , here  $I$  is the identity matrix



Clearly, the inverse matrix is given by

$$M^{-1} = \sum_{i=0}^{\infty} A^i \tag{1}$$

which converges if  $\|A\| < 1$ .

To estimate the element  $m_{rr}^{(-1)}$  of the inverse matrix  $M^{-1}$ , let the vector  $f$  be the following unit vector

$$f_r = e(r') \tag{2}$$

and use the following algorithm to Carlini method for calculating elements of the inverse matrix  $M^{-1}$

$$m_{rr}^{(-1)} \approx \frac{1}{N} \sum_{s=1}^N \left[ \sum_{(j|s_j=r)} W_j \right] \tag{3}$$

where  $(j|s_j=r')$  means that

$$W_j = \frac{A_{rs_1} A_{s_1 s_2} \dots A_{s_{j-1} s_j}}{p_{rs_1} p_{s_1 s_2} \dots p_{s_{j-1} s_j}} \tag{4}$$

for which  $s_j = r'$  are included in the sum (3)

since  $W_j$  is included in the corresponding sum for  $r' = 1, 2, \dots, n$ , the same set of  $N$  characteristics can be used to compute a series of the inverse matrix which is a function of the different properties of the Carlini making them suitable for parallelisation.

The probable error of the method is defined as  $r_N = 0.74 \sqrt{D\theta/N}$ , here  $P\{|\theta - E(\theta)| < r_N\} \approx 1/2 \approx P\{|\theta - E(\theta)| > r_N\}$ , where  $N$  depends on the realisation of random variable  $(r, \dots, \theta)$  with mathematical expectation  $E\theta$  and a variance  $\theta$ .

In the general case,  $\|B\| > 1$ , we make the substitution  $B = B - C$  and then we compute  $A = B_1^{-1} B_2$ , which satisfies  $\|A\| < 1$  (by careful choice of  $B$ , we make  $\|A\| < 1$ , which gives faster convergence) and we generate the inverse of  $B$  by (2) and from this we recover  $B^{-1}$ , using a iterative process.

### 3 Hybrid Algorithm for Matrix Inversion

In this paper we consider a general matrix, which means that the first part (2) of the input matrix and the recovery process are not required further. We consider a hybrid algorithm [8], which uses an iterative refinement to improve the accuracy of the inverse generated by the Carlini method.

The iterative refinement starts with the Carlini generated inverse to improve the accuracy. We set  $D_0 = B^{-1}$ , here  $B^{-1}$  is the Carlini generated inverse. The iterative process is  $R_{i-1} = I - D_{i-1} B$  and  $D_i = (I + R_{i-1}) D_{i-1}$  (for  $i = 1, 2, \dots$ ), which continues until  $\|R_{i-1}\| < \gamma$ .

### 3.1 Hybrid Monte Carlo Algorithm

**1: Read in matrix  $B$  and broadcast to all processes**

- 1 put matrix  $B$ , parameters  $\epsilon, \delta$  and  $\gamma$
- 2 broadcast matrix  $B$ , and parameters  $\epsilon, \delta$  and  $\gamma$ , to all processes

**2: Calculate intermediate matrices  $(B_1, B_2)$**

- 1 put  $B = B_1 - B_2$ , here  $B_1 = \text{diag}(B)$  and  $B_2 = B_1 - B$

**3: Calculate matrix  $A$  and norm**

- 1 Compute the matrix  $A = B_1^{-1}B_2$
- 2 Compute  $\|A\|$  and the number of Markov Chains  $N = \left(\frac{0.6745}{\epsilon(1-\|A\|)}\right)^2$

**4: Calculate matrix  $P$**

- 1 Compute the probability matrix  $P$

**5: Calculate matrix  $M$ , by MC on  $A$  and  $P$**

- 1 broadcast matrices  $A$  and  $P$ , and parameters  $\epsilon, \delta$  and  $\gamma$
- 2 for  $proc_{start}$  to  $proc_{stop}$  ( here  $proc_{start}$  and  $proc_{stop}$  are calculated to evenly distribute the work between the available processes)
  - 2.1 for  $t = 1$  to  $N$

**Markov Chain Monte Carlo Computation**

- 2.1.1 let  $W_0 = \text{SUM}$  of  $k = 1, 2, \dots, n$  and  $point = i$
- 2.1.2 Generate a random  $nextpoint$ , selected based on the probabilities in  $P$  for  $point$
- 2.1.3 if  $A[point][nextpoint] > P[point][nextpoint]$  then go to 2.1.2, else continue
- 2.1.4 Compute  $W_j = W_{j-1} \frac{A[point][nextpoint]}{P[point][nextpoint]}$
- 2.1.5 let  $SUM_{nextpoint} = SUM_{nextpoint} + W_j$
- 2.1.6 if  $|W_j| > \delta$  set  $point = nextpoint$  and go to 2.1.2
- 2.2 End of for loop
- 2.3 let  $m_{ik} = \frac{SUM[k]}{N}$  for  $k = 1, 2, \dots, n$

- 3 End of for loop

**6: Calculate  $B^{-1}$**

- 1 Compute the sparse inverse  $B^{-1} = MB_1^{-1}$
- 2 the master process collects the parts of  $B^{-1}$  from the slaves

**7: Iterative Refinement**

- 1 broadcast matrix  $B$
- 2 let  $D_0 = B^{-1}$  and  $i = 1$ 
  - 2.1 broadcast matrix  $D_{i-1}$
  - 2.2 Calculate  $proc_{start}$  to  $proc_{stop}$  range of  $R_{i-1}$  and  $D_i$  using the iterative refinement  $R_{i-1} = I - D_{i-1}B$  and  $D_i = (I + R_{i-1})D_{i-1}$
  - 2.3 the master process collects the parts of  $D_i$  from the slaves
  - 2.4 if  $\|R_{i-1}\| \geq \gamma$  set  $i = i + 1$  and go to 2.1

**8: Save Inverse**

- 1 the inverse is  $B^{-1} = D_i$

## 4 Implementation

parse matrices are commutative matrix multiplication. These attributes are used to optimize the implementation. The implementation has a matrix with a half of the zero elements. The size of the test is usually (or greater) than the rank, hence the derivation of sparse matrices. We have used the compressed sparse row (CSR) matrix format. We implemented the iterative Conjugate Gradient method and the iterative refinement (Step 7) of the hybrid iterative Conjugate Gradient method, since these are the most computationally intensive steps of the algorithm (Section 3). The master starts by computing Step 1 to Step 4, which is the serial part of the algorithm. The matrix  $P$  and the values array are generated, since the rank and the column array are determined by the matrix  $A$ .

Each process performs iteration  $i$  ( $E_i$ ), including the master, computes a local distributed part of the solution matrix  $B^{-1}$ , during the iterative Conjugate Gradient method. Here are the matrices  $A$ ,  $P$  and  $B_1$  (which is stored as a vector, since it is a diagonal matrix) are broadcast to all  $E_i$ 's. These are used by the  $E_i$ 's to compute part of  $B^{-1}$  and then the master collects these matrix parts together.

The master starts the iterative refinement, Step 7, by sending matrices  $B$  and  $D_{i-1}$  to the slaves. Each  $E_i$  computes a local distributed number of rows of  $R_{i-1}$  and then uses this to compute the corresponding rows of  $D_i$ . The  $E_i$ 's also calculate the norm of the part of  $R_{i-1}$  that has calculated. The master then collects the parts of  $D_i$  together and calculates  $\|R_{i-1}\|$ , which it uses to decide if the result of the refinement stage is accurate enough. If not, then another iteration is performed.

## 5 Results

In the experiments we generated diagonal dominant matrices, with zero elements defined elsewhere of the leading diagonal. The diagonal elements were generated randomly, with the leading diagonal elements selected to give  $\|A\| \approx 1$ .

We used eight quad-core (®) Intel<sup>TM</sup> 28 GZ nodes, each equipped with 2 second-level cache and 64 GB main memory, and connected to a switched Gigabit network. The performance of the serial implementation is used as a baseline. The 4, 2 nodes are used for the iterative process communication.

In the calculation of the stopping point accuracy has been used, since this provides enough significant figures. The rank is generated automatically with the required ( $\epsilon^{-2}$ ) accuracy (measured by  $\|I - BD_i\|$ , where  $D_i$  is the final inverse generated by the parallel hybrid algorithm).

We have for  $\delta$ , one of the input parameters, as picked to keep  $T$ , the average length of the rank. Chasing, about equation  $\sqrt{N}$  has produces good results from the iterative Conjugate Gradient calculation, which is generated by the necessary elements for the rank. Chasing

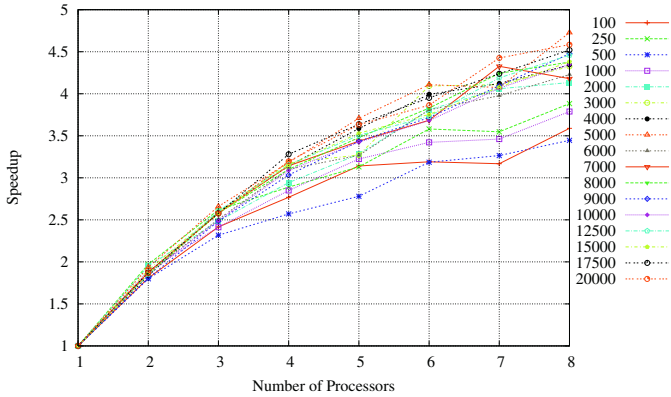


Fig. 1. Speedup of Parallel Hybrid Monte Carlo

As can be seen in Figure 1, for the majority of the matrix sizes tested there is a speedup of 4 to 4.5 when using eight processors. The smaller matrix sizes ( $n \leq 1000$ ) produced worse performance, but in these cases the total running time is less than a second and this makes the results usable.

The efficiency of the parallelisation is also high. In general, for our processors, since the computation time for these problems is small ( $n = 20000$  takes one processor 1.5 seconds) the benefits of splitting the work among eight processors will be outweighed by the communication overhead.

Figure 2 shows the percentage of time spent in communication, serial part of the parallel operation, and computation. In general, for eight processors, for the larger matrix sizes the results show that the communication overhead decreases as the matrix size increases, with a greater amount of time being spent in both serial and parallel computation.

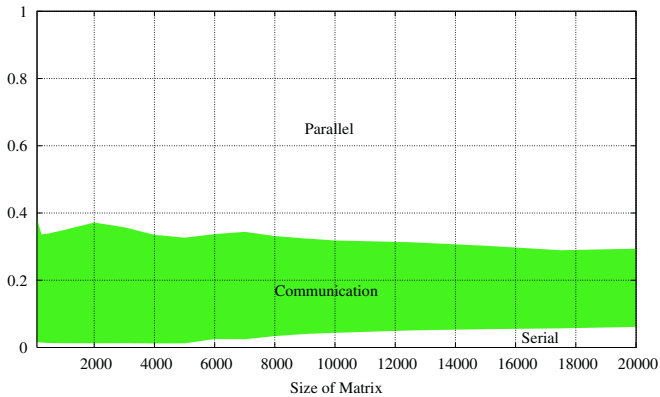


Fig. 2. Communication and Computation Time on Eight Processors

the communication overhead does not decrease as quickly as could be expected since the amount of calculation required to compute the communication overhead does not increase by that much as the matrix size grows. This is because the matrices used for these experiments contain the same number of non-zero elements. Each run which measures that the sparsity increases earlier than the domain size of the matrix.

## 6 Conclusion

We found that our implementation achieves a reasonably good speedup for the sparse parallel algorithm described in section 5.1. The effective use of the available processors to invert the matrix as the communication overhead gets smaller as the matrix size increases, with a greater percentage of the time being spent on parallel calculation.

We could improve the effective calculation gain more accurately. However, the speed measurement required for the Monte Carlo iterative refinement steps with the increase in the communication overhead is not considered since the effective use of the algorithm is larger domain sizes and matrices for larger sparsity.

## References

1. V.N. Alexandrov. Efficient Parallel Monte Carlo Methods for Matrix Computation. In *Mathematics and Computers in Simulation*, number 47, pages 113–122, Netherlands, 1998. Elsevier.
2. V.N. Alexandrov and A. Karaivanova. Parallel Monte Carlo Algorithms for Sparse SLAE Using MPI. In *LNCS 1697*, pages 283–290. Springer, 1999.
3. V.N. Alexandrov, A. Rau-Chaplin, F. Dehne, and K. Taft. Efficient Coarse Grain Monte Carlo Algorithms for Matrix Computation Using PVM. In *LNCS 1497*, pages 323–330. Springer, August 1998.
4. G. Burns, R. Daoud, and J. Vaigl. LAM: An Open Cluster Environment for MPI. In *Proceedings of Supercomputing Symposium*, pages 379–386, 1994.
5. I.T. Dimov and V.N. Alexandrov. A New Highly Convergent Monte Carlo Method for Matrix Computations. In *Mathematics and Computers in Simulation*, number 47, pages 165–181, Netherlands, 1998. Elsevier.
6. I.T. Dimov, V.N. Alexandrov, and A. Karaivanova. Resolvent Monte Carlo Methods for Linear Algebra Problems. In *Mathematics and Computers in Simulation*, number 155, pages 25–36, Netherlands, 2001. Elsevier.
7. I.T. Dimov, T.T. Dimov, and T.V. Gurov. A New Iterative Monte Carlo Approach for Inverse Matrix Problem, 1998.
8. B. Fathi Vajargah and V.N. Alexandrov. Coarse Grained Parallel Monte Carlo Algorithms for Solving Systems of Linear Equations with Minimum Communication. In *in Proc. of PDPTA*, pages 2240–2245, Las Vegas, 2001.
9. B. Fathi Vajargah, B. Liu, and V.N. Alexandrov. Mixed Monte Carlo Parallel Algorithms for Matrix Computation. In *Lecture Notes in Computational Science - ICCS 2002*, number 2330, pages 609–618, Berlin Heidelberg, 2002. Springer Verlag.

10. G.H. Golub and C.F. Van Loan. *Matrix Computations*. The Johns Hopkins University Press, Baltimore and London, third edition, 1996.
11. I.M. Sobol. *Monte Carlo Numerical Methods*. Nauka, Moscow, 1973. (in Russian).
12. J.M. Squyres and A. Lumsdaine. A Component Architecture for LAM/MPI. In *Proceedings, 10th European PVM/MPI Users' Group Meeting*, number 2840 in Lecture Notes in Computer Science, pages 379–387, Venice, Italy, September / October 2003. Springer-Verlag.
13. J.R. Westlake. *A Handbook of Numerical Matrix Inversion and Solution of Linear Equations*. Wiley, New York, 1968.

# Parallel Hybrid Monte Carlo Algorithms for Matrix Computations

V. S. Sunderam<sup>1</sup>, E. Tahmassebi<sup>2</sup>, M. J. Griffin<sup>1</sup>, R. A. Ford<sup>1</sup>,  
H. D. Adachi<sup>1</sup>, and C. Ebrahimi<sup>1</sup>

<sup>1</sup> Department of Computer Science, University of Reading

<sup>2</sup> IPP, Bulgarian Academy of Sciences

**Abstract.** In this paper we consider hybrid (fast stochastic approximation and deterministic refinement) algorithms for Matrix Inversion (MI) and Solving Systems of Linear Equations (SLAE). Monte Carlo methods are used for the stochastic approximation, since it is known that they are very efficient in finding a quick rough approximation of the element or a row of the inverse matrix or finding a component of the solution vector. We show how the stochastic approximation of the MI can be combined with a deterministic refinement procedure to obtain MI with the required precision and further solve the SLAE using MI. We employ a splitting  $A = D - C$  of a given non-singular matrix  $A$ , where  $D$  is a diagonal dominant matrix and matrix  $C$  is a diagonal matrix. In our algorithm for solving SLAE and MI different choices of  $D$  can be considered in order to control the norm of matrix  $T = D^{-1}C$ , of the resulting SLAE and to minimize the number of the Markov Chains required to reach given precision. Further we run the algorithms on a mini-Grid and investigate their efficiency depending on the granularity. Corresponding experimental results are presented.

**Keywords:** Monte Carlo Method, Markov Chain, Matrix Inversion, Solution of System of Linear Equations, Grid Computing.

## 1 Introduction

The problem of inverting a real  $n \times n$  matrix ( $A$ ) and solving systems of linear algebraic equations ( $AE$ ) is a ubiquitous problem. The standard sequential algorithms for solving these problems are the Gaussian elimination method and the LU decomposition method. The direct parallel methods for solving these systems with dense matrices require  $O(n^3/p)$  steps. The usual sequential schemes (e.g., parallel Gaussian elimination, Gaussian reduction methods) are employed. Consequently, the computation time for large problems remains large. Parallel methods can be used to reduce the use of memory established algorithms.

It is known that the Monte Carlo methods give statistical estimates of the components of the inverse matrix. The estimates of the solution vector by performing random sampling of a certain random variable, whose mathematical expectation

s the desired solution. We compare the Monte Carlo methods for a d  
 s. . . . . Es, since first . . . . .  $O(NL)$  steps are required to find a e. . . . .  
 f the . . . . . inverse matrix here  $N$  is the number of chains and  $T$  is a estimate of  
 the chain length. The stochastic process, which are dependent of matrix size  
 $n$  and second, the process for stochastic methods is here the parameter  
 e. . . . . era. authors have proposed here to compare gradient . . . . . Monte Carlo . . . . .  
 a gradient free . . . . . ad . . . . . E 7, 8, . . . . . this paper, e . . . . . estimate h  
 . . . . . Monte Carlo can be used for diagonal and matrix diagonal symmetric matrices. a  
 a general splitting and highly efficient method (stochastic deterministic) parameter  
 a gradient can be derived from both a accurate . . . . . ers . . . . . f a g. e . . . . .  
 singular matrix  $A$  is employed either uniformly Monte Carlo ( ) or a most  
 optimal Monte Carlo (  $O$ ) methods 7, 8, . . . . . here relate to per me. ts  
 the dense and sparse matrices are carried out  
 . . . . . Monte Carlo that the algorithms are built under the requirement  $\|T\| < . . . . .$  here refer  
 to the efficient methods needed to be able to solve problems with matrix  
 norms greater than . . . . . thus the de. . . . . ped a spectrum of a gradient free . . . . .  
 s. . . . . g . . . . . Es range from special cases to the general case. a. . . . . e. . . . . C meth  
 ds for . . . . . Es based . . . . . Monte Carlo . . . . . ac. b. terat. . . . . ha. . . . . bee. . . . .  
 m. . . . . ara. e. . . . . Monte Carlo methods using minimum . . . . . Ch. . . . . s. . . . . a. . . . .  
 minimum computation is presented . . . . . st. f the ab. . . . . e. . . . . appr. . . . .  
 are based on the definition of the stochastic calculus systematic errors  
 this paper is a step further and have designed hybrid gradient free . . . . .  
 s. . . . . g . . . . . Es based on . . . . . g. t. . . . . deas. . . . . terat. e . . . . . Monte Carlo methods based  
 the ac. b. terat. . . . . a. d. . . . . determ. . . . . st. c. p. cedures for improving the accuracy of  
 the . . . . . r the solution. . . . . ect. r. f . . . . . Es  
 here general Monte Carlo ideas are presented . . . . . ect. . . . . 2, the main a. g.  
 r thms are described . . . . . ect. . . . . a. d the parameter approach and simulation ca  
 e per me. ts are presented . . . . . ect. . . . . 4 a. d . . . . . respect. e.

## 2 Monte Carlo and Matrix Computation

assume that the system of linear algebraic equations ( E) is presented in the  
 form

$$Ax = b \tag{1}$$

here  $A$  is a real square  $n \times n$  matrix,  $x = (x_1, x_2, \dots, x_n)^t$  is a  $n \times n$  solution  
 vector and  $b = (b_1, b_2, \dots, b_n)^t$ .

assume the general case  $\|A\| > . . . . .$  e. . . . . s. . . . . der the splitting  $A = D - C$ , here  
 — diagonal elements of  $D$  are the same as those of  $A$ , and the diagonal elements  
 of  $D$  are defined as  $d_{ii} = a_{ii} + \gamma_i \|A\|$ , choosing some special cases  $\gamma_i > . . . . ., i = 2, \dots, n$ .  
 e further consider  $D = B - B_1$  here  $B$  is the diagonal matrix of  $D$ , e. g  
 $b_{ii} = d_{ii} = . . . . ., 2, \dots, n$ . s. . . . . sh. . . . . e. . . . . c. u. d. tra. sf. rm the system ( ) to

$$x = Tx + f, \tag{2}$$



here  $T = D^{-1}C$  and  $f = D^{-1}b$ . The multipliers  $\gamma_i$  are chosen so that, if the hypothesis holds, then the norm of  $T$  will be less than  $\epsilon$  and reduce the number of iterations required to reach a given precision. We consider the hypothesis, first, finding the solution of  $x = Tx + f$  using the Carathéodory method if  $\|T\| < \epsilon$  and finding  $D^{-1}us$  using Carathéodory after that finding  $A^{-1}$ . We then require to obtain the solution of the system  $fx = A^{-1}b$  using the Carathéodory method described in [7]. We define a Markov chain and heights  $W_0, \dots, W_j, \dots, W_{j-1} = \frac{T_{s_{j-1}s_j}}{p_{s_{j-1}s_{j-1}}}$  for  $j = 1, 2, \dots, n$ . Consider the random variable  $\theta_j g = \frac{g_{s_0}}{p_{s_0}} \sum_{i=1}^{\infty} W_i f_{s_i}$ . We use the following notation for the partial sum

$$\theta_i g = \frac{g_{s_0}}{p_{s_0}} \sum_{j=0}^i W_j f_{s_j}. \tag{1}$$

Under condition  $\|T\| < \epsilon$ , the corresponding geometric series converges for a given  $f$ , and  $E\theta_i g$  tends to  $(g, x)$  as  $i \rightarrow \infty$ . Thus,  $\theta_i g$  can be considered as an estimate of  $(g, x)$  for  $i$  sufficiently large. We find an arbitrary compact set  $\Gamma$  of the solution of the recurrence, the  $r$ th compact set of  $x$ , we should choose  $g = e(r) = (e_1, \dots, e_r, \dots)$  such that

$$e(r)_\alpha = \begin{cases} f_r & \alpha = r \\ \delta_{r\alpha} & \text{otherwise} \end{cases} \tag{4}$$

that is, such that  $(g, x) = \sum_{\alpha=1}^n e(r)_\alpha x_\alpha = x_r$ . We consider the Carathéodory method sequence

$$x_r = \Theta = \frac{1}{N} \sum_{s=1}^N \theta_i e(r)_s,$$

where  $N$  is the number of chains and  $\theta_i e(r)_s$  is the appropriate value of  $x_r$ . The  $s$ th chain means that using the Carathéodory method, we calculate the sequence of realizations of the solution of the corresponding Carathéodory uniform transition probability  $(p_{\alpha\beta}) = \frac{1}{n}$  and almost pointwise Carathéodory method (O) with  $p_{\alpha\beta} = \frac{|T_{\alpha\beta}|}{\sum_{\beta=1}^n |T_{\alpha\beta}|}$ , here  $\alpha, \beta = 1, 2, \dots, n$  are the Carathéodory solutions.

Subsequently, as a matrix  $C = \{c_{rr}\}_{r,r=1}^n$  of some matrix  $A$ , we must first compute the elements of matrix  $M = I - A$ , here  $I$  is the identity matrix. Clearly, the inverse matrix sequence  $C = \sum_{i=0}^{\infty} M^i$ , which converges if  $\|M\| < 1$ .

We estimate the element  $c_{rr}$  of the inverse matrix  $C$ . Let the vector  $f$  be the following unit vector  $f_r = e(r')$ .

We then calculate the following Carathéodory method for calculation of elements of the inverse matrix  $C$

$$c_{rr} \approx \frac{1}{N} \sum_{s=1}^N \left[ \sum_{(j|s_j=r)} W_j \right], \tag{2}$$

here  $(j|s_j \dots r')$  means that ...

$$W_j = \frac{M_{rs_1} M_{s_1 s_2} \dots M_{s_{j-1} s_j}}{p_{rs_1} p_{s_1 s_2} \dots p_{s_{j-1} s_j}} \quad ( )$$

for which  $s_j \dots r'$  are included in the sum ( )  
 since  $W_j$  is included in the corresponding sum for  $r' = 2, \dots, n$ ,  
 the same set of  $N$  chains can be used to compute a series of the inverse  
 matrix elements of the inverse perturbation of  $C$  making them suitable for  
 parallelization.

### 3 The Hybrid MC Algorithm

The basic idea is to use  $C$  to find the approximate inverse of matrix  $D$ , refine  
 the inverse (iter) and find  $A^{-1}$ . Generally, the approach described  
 in [7] can be used to find the solution vector through  $A^{-1}$ . Considering the  
 general definition of a regular splitting [2], if  $A, M$  and  $N$  are three general matrices  
 satisfying  $A = M - N$ , then the pair of matrices  $M, N$  are called regular splitting of  
 $A$ , if  $M$  is a singular and  $M^{-1}$  and  $N$  are nonnegative.

herefore, let  $A$  be a singular and matrix of the form  
 regular splitting of  $A$  such that  $A = D - C$ , then  $E \|x^{(k+1)} - Tx^{(k)} + f\|$ ,  
 where  $T = D^{-1}C$ , and  $f = D^{-1}b$  converges to the unique solution  $x^*$  if and only  
 if  $\|T\| < 2$ .

The efficiency of iterative diagonal and matrix series approximation part  
 of the process enabling  $C$  to be applied to diagonal and matrix series  
 general matrices. Consider the algorithm which can be used for the series  
 of a general singular matrix  $A$  note that in some cases the above  
 accurate series of matrix  $D$  some iterative procedures can be applied.

#### Algorithm1: find $A^{-1}$

1. **Initial data:** Input matrix  $A$ , parameters  $\gamma$  and  $\epsilon$ .
2. **Preprocessing:**
  - 2.1 **Split**  $A = D - (D - A)$ , where  $D$  is a diagonally dominant matrix.
  - 2.2 **Set**  $D = B - B_1$  where  $B$  is a diagonal matrix  $b_{ii} = d_{ii} \ i = 1, 2, \dots, n$ .
  - 2.3 **Compute** the matrix  $T = B^{-1}B_1$ .
  - 2.4 **Compute**  $\|T\|$ , the Number of Markov Chains  $N = (\frac{0.6745}{\epsilon} \cdot \frac{1}{(1-\|T\|)})^2$ .
3. **For**  $i=1$  to  $n$ ;
  - 3.1 **For**  $j=1$  to  $j=N$ ;
 

**Markov Chain Monte Carlo Computation:**

    - 3.1.1 **Set**  $t_k = 0$ (stopping rule),  $W_0 = 1$ ,  $SUM[i] = 0$  and  $Point = i$ .
    - 3.1.2 **Generate** a uniformly distributed random number  $nextpoint$ .
    - 3.1.3 **If**  $T[point][nextpoint]! = 0$ .

**LOOP**

    - 3.1.3.1 **Compute**  $W_j = W_{j-1} \frac{T[point][nextpoint]}{P[point][nextpoint]}$ .
    - 3.1.3.2 **Set**  $Point = nextpoint$  and  $SUM[i] = SUM[i] + W_j$ .
    - 3.1.3.3 **If**  $|W_j| < \gamma$ ,  $t_k = t_k + 1$

- 3.1.3.4 **If**  $t_k \geq n$ , end LOOP.
- 3.1.4 **End If**
- 3.1.5 **Else** go to step 3.1.2.
- 3.2 **End of loop j.**
- 3.3 **Compute** the average of results.
- 4. **End of loop i.**
- 5. **Obtain** The matrix  $V = (I - T)^{-1}$ .
- 6. **Therefore**  $D^{-1} = VB^{-1}$ .
- 7. **Compute** the MC inversion  $D^{-1} = B(I - T)^{-1}$ .
- 8. **Set**  $D_0 = D^{-1}$  (approximate inversion) and  $R_0 = I - DD_0$ .
- 9. **use filter procedure**  $R_i = I - DD_i$ ,  $D_i = D_{i-1}(I + R_{i-1})$ ,  $i = 1, 2, \dots, m$ , where  $m \leq k$ .
- 10. **Consider the accurate inversion of D** by step 9 given by  $D_0 = D_k$ .
- 11. **Compute**  $S = D - A$  where  $S$  can be any matrix with all non-zero elements in diagonal and all of its off-diagonal elements are zero.
- 12. **Main function** for obtaining the inversion of A based on  $D^{-1}$  step 9:
  - 12.1 **Compute** the matrices  $S_i$ ,  $i = 1, 2, \dots, k$ , where each  $S_i$  has just one element of matrix  $S$ .
  - 12.2 **Set**  $A_0 = D_0$  and  $A_k = A + S$
  - 12.3 **Apply**  $A_k^{-1} = A_{k+1}^{-1} + \frac{A_{k+1}^{-1}S_{i+1}A_{k+1}^{-1}}{1 - \text{trace}(A_{k+1}^{-1}S_{i+1})}$ ,  $i = k - 1, k - 2, \dots, 1, 0$ .
- 13. **Print** the inversion of matrix A.
- 14. **End** of algorithm.

## 4 Parallel Implementation

we have implemented the algorithm proposed in a cluster of PCs and a machine under the help of master-slave approach. The hardware is a multi-processor grid computer. Both the cluster and the machine here take the Car. methods for solving Eqs. Thus, we have a multi-processor parallel algorithm for the matrix  $A$ , pass the zero elements of the dense (sparse) matrix to the processor, run the algorithm parallel. Each processor computing  $[n/p]$  rows (columns) of the submatrix and collect the results from slaves at the end. Thus, a multi-processor between slave zero elements of  $A$  and receive part of  $A^{-1}$  for  $x$ . The splitting procedure and refinement are also parallelized. The parallel implementation. Especially, the case, he computes  $k$  columns ( $1 \leq k \leq n$ ) of the (submatrix) each day. The number of channels among the processors, e.g. distributed  $[kN/p]$  channels. Each processor has a multi-processor at the beginning and at the end of the algorithm execution. The channels used to transfer high efficiency of parallel implementation. In addition, a iterative filter process is used to improve the accuracy of the Mark. Channels to Car. calculated. Otherwise, the iterative filter process is a set of  $D_0 = D^{-1}$  (here  $D^{-1}$  is the inverse from the Car. calculation) he iterative  $R_i = I - DD_i$  and  $D_{i+1} = D_i(I + R_i)$  these iterative sequence ( $i = 1, 2, \dots$ ) until  $\|R_i\| < \gamma$

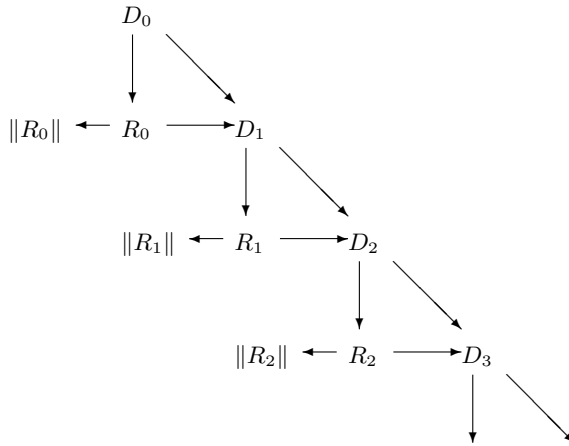


Fig. 1. Data Dependency Graph

The data dependency graph for the iterative filter (Figure 1) directs us to the method for parallelizing the iterative filter. Each iteration is calculated separately with a master process coordinating the calculations as a distributed system. Whether further iterations are required.

The master starts a iteration by sending  $D_i$  to each of the slaves. Each of the slaves calculates  $n/p$  columns of  $R_i$ , the partial sums of  $R_i$  (required for calculating  $\|R_i\|$ ) and  $n/p$  columns of  $D_{i+1}$ . The slaves then send the columns of  $D_{i+1}$  and the partial sums of  $R_i$  to the master, which calculates  $\|R_i\|$  and sends back the new  $D_{i+1}$  to the required accuracy.

Thus, a key calculation for the parallel implementation of the C procedure of the algorithm  $O(nNL/p)$  where  $N$  denotes the number of Markov chains. According to the central limit theorem, the relative error  $\epsilon$  obeys  $N \geq \left(\frac{0.6745}{\epsilon \times (1 - \|T\|)}\right)^2$ ,  $L$  denotes the length of the Markov chains and  $\leq \left(\frac{\log(\gamma)}{\log\|T\|}\right)$ , where  $\epsilon, \gamma$  show the accuracy of the Carlini approximation. Parameters  $\epsilon, \gamma$  are used for the stochastic analysis to estimate that for a given approximation of the error sum of the error is required. The relative error of the Carlini implementation of the algorithm for a higher precision is required. The error of the filter procedures, which add a complexity of  $O(n^3/p)$  in the case of sparse matrices, is amplified. The absolute error of the sum of the matrix elements is  $\|I - A^{-1}A\|$ , where  $A$  is the matrix whose elements have to be found, and  $A^{-1}$  is the approximation. The computation time is shown in seconds.

## 5 Experimental Results

The algorithms run on a part of a 2-processor (®) machine and a 16-processor cluster with a 100 Gbps Ethernet network. Each workstation had

a. te.® e. tum pr. cess. r. th 2 R. a. d a. G. hardd sk  
 Each rkstat. . as ru. . g. E. u. 8. he. e. r. me. t. used. as  
 7  
 e. ha. e. carr. ed. test. th. . prec. s. . -1 - -2 a. d. h. gher. prec. s. .  
 -5 - -6 . order. t. . est. gate. the. ba. a. ce. bet. ee. st. chast. c. a. d. deter.  
 m. st. c. c. mp. . e. ts. f. the. a. g. r. thms. based. . the. pr. c. p. e. f. ba. a. c. g. f.  
 err. rs. (e. g. keep. g. the. st. chast. c. a. d. s. stemat. c. err. r. f. the. same. . order) 7  
 e. ha. e. a. s. c. mp. are. d. the. effic. e. c. . f. para. e. . . te. Car. . a. d. uas. . . te.  
 Car. . meth. ds. f. r. s. . g. Es  
 Our. resu. ts. sh. that. a. the. a. g. r. thms. sca. e. er. e. he. resu. ts. sh.  
 that. f. e. e. ed. t. refi. e. the. resu. ts. us. g. fi. ter. pr. cedure. the. pr. p. rt. . f. the.  
 fi. ter. pr. cedure. t. me. gr. s. th. the. gr. th. f. the. matr. s. ze. s. e. e. ed. t.  
 . m. t. these. pr. cedures. f. p. ss. b. e. he. ast. tab. e. sh. s. that. uas. . . te. Car. .  
 s. faster. . fi. d. g. r. ough. appr. mat. . . f. the. s. ut. . . f. E. he. sec. . d.  
 tab. e. sh. s. that. s. mp. rta. t. t. ba. a. ce. c. mputat. . s. . a. Gr. d. e. r. me. t.  
 a. d. c. mmu. cate. th. arger. chu. ks. f. data. . r. e. am. p. e. th. s. case. th. s. ca.  
 . ead. t. m. re. tha. t. ce. reduc. g. the. c. mputat. . a. t. me. . the. same. . umber.  
 . f. pr. cess. rs.

**Table 1.** MC with filter procedures on the cluster

Matrix Size	Time (Dense Case) in seconds			
	4 proc.	8 proc.	12 proc.	16 proc.
250	59.269	24.795	16.750	14.179
500	329.072	177.016	146.795	122.622
1000	1840.751	989.423	724.819	623.087

**Table 2.** MC with filter procedures on the miniGrid

Matrix Size	Time (MC, Dense Case) in seconds	
	16 proc. (4 SP and 12 cluster)	16 proc. (8 SP and 8 cluster)
250	729.208	333.418
500	4189.225	1945.454

**Table 3.** MC vs QMC without filtering on the cluster (matrix size 250 by 250 )

Matrix Size	Time (Dense Case) in seconds			
	4 proc.	8 proc.	12 proc.	16 proc.
<i>MC</i>	48.819	20.909	13.339	9.691
<i>QMC</i>	0.744	0.372	0.248	0.186

## 6 Conclusion

In this paper we have introduced a hybrid Monte Carlo deterministic algorithms for matrix computations for a class of singular matrices. We have compared the efficiency of the algorithms for a cluster of workstations and a Grid environment. The results show that the algorithms scale better in such settings, but a careful balance of computation should be maintained. Further experiments are required to determine the optimal number of chains required for Monte Carlo procedures and the best techniques to gather Monte Carlo and deterministic refinement procedures.

## References

1. B. Fathi, B.Liu and V. Alexandrov, *Mixed Monte Carlo Parallel Algorithms for Matrix Computation*, Lecture Notes in Computer Science, No 2330, Springer-Verlag, 2002, pp 609-618
2. Ortega, J., *Numerical Analysis*, SIAM edition, USA, 1990.
3. Alexandrov V.N., *Efficient parallel Monte Carlo Methods for Matrix Computation*, Mathematics and computers in Simulation, Elsevier **47** pp. 113-122, Netherlands, (1998).
4. Golub, G.H., Ch., F., Van Loan, *Matrix Computations*, The Johns Hopkins Univ. Press, Baltimore and London, (1996)
5. Taft K. and Fathi Vajargah B., *Monte Carlo Method for Solving Systems of Linear Algebraic Equations with Minimum Markov Chains*. International Conference PDPTA'2000 Las Vegas, (2000).
6. Sobol I.M. *Monte Carlo Numerical Methods*. Moscow, Nauka, 1973 (in Russian).
7. Dimov I., Alexandrov V.N. and Karaivanova A., *Resolvent Monte Carlo Methods for Linear Algebra Problems*, Mathematics and Computers in Simulation, Vo155, pp. 25-36, 2001.
8. Fathi Vajargah B. and Alexandrov V.N., *Coarse Grained Parallel Monte Carlo Algorithms for Solving Systems of Linear Equations with Minimum Communication*, in Proc. of PDPTA, June 2001, Las Vegas, 2001, pp. 2240-2245.
9. Alexandrov V.N. and Karaivanova A., *Parallel Monte Carlo Algorithms for Sparse SLAE using MPI*, LNCS 1697, Springer 1999, pp. 283-290.
10. Alexandrov V.N., Rau-Chaplin A., Dehne F. and Taft K., *Efficient Coarse Grain Monte Carlo Algorithms for matrix computation using PVM*, LNCS 1497, pp. 323-330, Springer, August 1998.
11. Dimov I.T., Dimov T.T., et all, *A new iterative Monte Carlo Approach for Inverse Matrix Problem*, J. of Computational and Applied Mathematics **92** pp 15-35 (1998).

# An Efficient Monte Carlo Approach for Solving Linear Problems in Biomolecular Electrostatics

Charles Deming<sup>1</sup>, Chaehyung Yang<sup>1,2</sup>, and Kaiming Pei<sup>2,3</sup>

<sup>1</sup> Department of Computer Science and

<sup>2</sup> School of Computational Science,

Florida State University, Tallahassee, FL, 32306-4530, USA

<sup>3</sup> ICM&MG, Lavrentjeva 6, Novosibirsk 630090, Russia

**Abstract.** A linear (elliptic) problem in molecular electrostatics is considered. To solve it, we propose an efficient Monte Carlo algorithm. The method utilizes parallel computing of point potential values. It is based on the walk-in-subdomains technique, walk-on-spheres algorithm, and an exact treatment of boundary conditions.

## 1 Introduction

Recently [2], we proposed an advanced Monte Carlo technique for calculating the electrostatic potentials of large rigid molecules. In this approach, the problems under consideration have to be treated in the framework of continuous media models. In particular, the electrostatic potentials of molecules are adapted to the most popular continuum used models, namely, the multipole expansion method. This means that the electrostatics is described as a continuous medium, whose potentials are characterized by dielectric permittivity  $\epsilon_e$ , whereas the molecule under consideration is described by a point charge distribution. The molecule is thought of as a collection of dielectric constant  $\epsilon_i$ , which is much less than that of the ether, i.e.,  $\epsilon_e$ .

In this case, the electrostatic approach leads to a boundary value problem for the Poisson equation satisfied by the electrostatic potential  $u(x)$

$$-\nabla \epsilon \nabla u(x) = \rho(x), \quad x \in \mathbb{R}^3, \quad (1)$$

where  $\epsilon$  is the pointwise dependent permittivity and  $\rho(x)$  is the charge distribution.

Usually, the molecule under consideration is described geometrically as a union of spherical atoms with partial point charges at the sphere centers. This

means that  $\rho(x) = \sum_{m=1}^M q_m \delta(x - x^{(m)})$ , where  $q^{(m)}$  are the charges and  $x^{(m)}$  are the atomic centers and hence the charge distribution

the charge distribution is the source term determined by the discrete multipole expansion. In the framework of a continuous medium approach, the regions of physical space are described by the piecewise constant dielectric permittivity. This leads to the piecewise constant dielectric permittivity equation for  $u(x)$ . The source term

For small potentials  $u$ , this equation may be linearized, thus leading to the relation

$$\Delta u(x) - \kappa^2 u(x) = -\rho(x), \quad x \in G_1, \quad (2)$$

where  $\kappa^2$  is a positive constant called the Debye screening parameter. The difficulties that arise in calculating such boundary value problems arise from the geometrical features of the molecule. The geometrical features are taken into account through the boundary conditions that have to be satisfied by the potential  $u$  of the molecule and the remainder of the molecule. The boundary  $\Gamma$

$$u_i(y) = u_e(y), \quad \epsilon_i \frac{\partial u_i}{\partial n(y)} = \epsilon_e \frac{\partial u_e}{\partial n(y)}, \quad y \in \Gamma. \quad (3)$$

where  $\Gamma$  is either the surface of the molecule or the boundary of the scaled molecule. Of the possible arrangements of these surfaces, the most important one is the dielectric and attractive features of the molecule. The approach is that there should be no perturbations in the surface of the molecule. In preparation of the approximation of the molecular surfaces and boundary conditions, in fact, a primitive analytical description based on a set of atomic centers and radii is absolutely adequate for the present purposes. The main advantage of the latter favorable aspect of the Monte Carlo algorithm is the employment of the natural parameterization of the electrostatic problems, the reduced computational effort can be represented as a linear function of the potential values. This makes possible further distribution of the calculation and therefore computing these values in parallel.

## 2 Energy: Linear Case

Consider the problem of calculating the electrostatic free energy of a large biomolecule in the linear case, this energy is given by the equation

$$E = \frac{1}{2} \sum_{m=1}^M u^{(m)} q^{(m)}, \quad (4)$$

where  $u^{(m)}$  is the regular part of the electrostatic potential at the center of the  $m$ th atom. The estimate  $u^{(m)}, m = 1, \dots, M$  is made use of the Yukawa spheres algorithm. The specific form of the molecule's geometrical model makes it possible to simulate the required Markov chains such as a chain that converges to the boundary geometrical and the last potentials  $u^{(m)}$  over  $\Gamma$ .

Let  $G_i = \bigcup_{m=1}^M B(x^{(m)}, r^{(m)})$  be the union of the molecule where  $B(x, r)$  denotes the ball centered at the point  $x$ , and  $r$  is its radius (see figure 1). In a general distribution of point charges  $q_i$  in  $G_i$ , the electrostatic potential can be



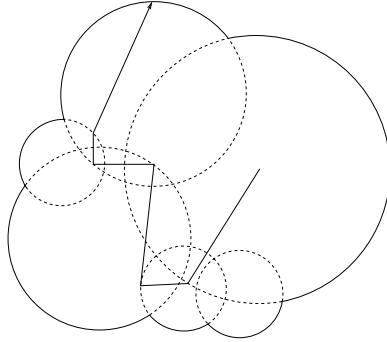


**Fig. 1.** An example of a computational domain in the energy calculation. The domain is a union of atomic spheres, and the line follows a walk-on-spheres/walk-in-subdomains trajectory that begins at the center of the largest sphere and ends as it leaves the interior of the computational domain

represented as  $u_i(x) = u^0(x) + g(x)$ , here  $g(x) = \sum_{m=1}^M \frac{q^{(m)}}{4\pi\epsilon_i |x - x^{(m)}|}$  is

the static part of the electrostatic potential,  $u^0$  satisfies the Laplace equation  $\nabla^2 u^0 = -\rho$  in  $G$  and  $u^0(x^{(m)}) = u^0(x^{(m)})$ , the construction of the Carleson estimate based on the combinatorial structure of the walk-on-spheres and walk-in-subdomains algorithms. Let  $\xi u^0(x_0)$  be a Carleson estimate for  $u^0(x_0)$  using the probabilistic representation of the set  $\xi u^0(x_0) = u^0(x^*)$ , here  $x^*$  is the endpoint of the random walk from  $G$ . The most efficient algorithm to simulate these endpoints is to use the natural representation of  $G$  as a union of intersecting spherical subdomains. In order to be able to sample directly from the stationary probability measure  $p_p$  on  $G$ , the endpoint can be sampled directly from the stationary probability measure  $p_p$  on  $G$  as a union of intersecting spherical subdomains. In order to be able to sample directly from the stationary probability measure  $p_p$  on  $G$ , the endpoint can be sampled directly from the stationary probability measure  $p_p$  on  $G$ .

Let  $x \in B(x^{(m)}, r^{(m)})$  then  $u(x) = \int_{S(x^{(m)}, r^{(m)})} p_p(x \rightarrow y) u(y) d\sigma(y)$ , here

$$p_p(x \rightarrow y) = \frac{(r^{(m)})^2 - |x - x^{(m)}|^2}{4\pi r^{(m)} |x - y|^3}$$

is the stationary kernel of the Markov chain  $\{x_i, i = 0, \dots, N\}$  is defined recursively. Given  $x_i \in B(x_i^{(m)}, r_i^{(m)})$ , the endpoint is chosen randomly from  $S(x_i^{(m)}, r_i^{(m)})$  according to the stationary probability measure  $p_p(x_i \rightarrow x_{i+1})$  defined on  $x_{i+1}$  either hits the boundary or else is either back to the probability measure, the path of this Markov chain terminates at the boundary after a finite number of steps,  $N$  is the stationary assumption is about  $G$ , which are a class of far from equilibrium,  $\mathbb{E}N < \infty$  because the set  $x^* = x_N$

### 3 Boundary Conditions

Let us have the construction estimates for boundary values of the potential,  $u^0$  defined on  $\xi u^0(x_N) = \xi \psi(x_N) - g(x_N)$ , here  $\psi$  is the unknown boundary

value of  $O_\epsilon$  approach for constructing a Monte Carlo estimate for  $\psi$  is that randomized algorithm. Therefore, the bound on the error of the step size  $h$  is given by  $\psi(x_N) = \mathbb{E}(u(x_{N+1})|x_N) + O(h^2)$ , where  $x_{N+1} = x_N - hn$  with probability  $p_i = \frac{\epsilon_i}{\epsilon_i + \epsilon_e}$ ,  $x_{N+1} = x_N + hn$  with the complementary probability  $p_e$ , and  $n$  is the step size. The algorithm thus reduces a  $O(h)$  bias to a result given by the Monte Carlo estimate.

Therefore, the proposed algorithm that speeds up the computation is a deterministic method based on the approach of the algorithm specifically adapted to the boundary value problem that includes the random variables  $C$  and  $a$  on the sphere  $S(x_N, a)$ , which does not contain point charges. The application of Green's formula to functions  $u_i, u_e$  and  $\Phi_\kappa(x) = \frac{s \cdot h(\kappa(a-r))}{4\pi r s \cdot h(\kappa a)}$ , where  $r = |x - x_N|$ , leads to the following mean value relation:

$$\begin{aligned}
 u(x_N) &= \frac{\epsilon_e}{\epsilon_e + \epsilon_i} \int_{S_e(x_N, a)} \frac{\kappa a}{2\pi a^2 s \cdot h(\kappa a)} u_e \\
 &+ \frac{\epsilon_i}{\epsilon_e + \epsilon_i} \int_{S_i(x_N, a)} \frac{\kappa a}{2\pi a^2 s \cdot h(\kappa a)} u_i \\
 &- \frac{(\epsilon_e - \epsilon_i)}{\epsilon_e + \epsilon_i} \int_{\Gamma \cap B(x_N, a) \setminus \{x_N\}} 2 \frac{\partial \Phi_0}{\partial n} Q_{\kappa, a} u \\
 &+ \frac{\epsilon_i}{\epsilon_e + \epsilon_i} \int_{B_i(x_N, a)} -2\kappa^2 \Phi_\kappa u_i,
 \end{aligned} \tag{1}$$

here  $Q_{\kappa, a}(r) = \frac{s \cdot h(\kappa(a-r)) + \kappa r c \cdot \text{sh}(\kappa(a-r))}{s \cdot h(\kappa a)} < 1$ , and  $\Gamma$  is the surface

of the medium.

Randomization of the formula provides a procedure to estimate the Markov chain  $\{x_i\}$  after this boundary value problem. The algorithm is based on the Markov chain as follows: with probability  $p_e$  the step is chosen to be the step of the medium  $\overline{G}_e$ , and with the complementary probability  $p_i$ ,  $x_{N+1} \in \overline{G}_i$ . The step of the Markov chain is chosen to be the boundary of  $B(x_N, a) \cap G_e$ . The random walk in this case has a zero probability of returning to  $O$ . On  $S(x_N, a)$  the mean value of the probability is equal to  $\frac{\kappa a}{s \cdot h(\kappa a)}$ . Note that  $B(x_N, a) \cap G_e$  is a set of points whose measure is that there can be two intersecting boundaries in this case. Each set of random variables from the step of the algorithm is a set of points first, then the complementary probability, the step is sampled from the chain straightly. Therefore, the boundary of  $B(x_N, a) \cap G_i$  is the domain  $\Gamma \cap B(x_N, a)$  such that  $\psi(x_N) = \mathbb{E}u(x_{N+1})$ .

### 4 Random Walks Inside and Outside

We further construct a symmetric, tight method for treating these boundary conditions.

For interior points, we construct a Markov chain of the  $n$ th subdomain starting at  $x_{N+1}$ , and set  $u(x_{N+1}) = \mathbb{E}(u^0(x_2^*) + g(x_{N+1}) | x_{N+1})$  where  $x_2^* \in \Gamma$  is the exit point.

For  $u(x_{N+1}) \in G_e$ , we can use the Markov spheres algorithm random walker finds a Markov chain surfaces at every step with probability  $\frac{\kappa d_i}{s_i h(\kappa d_i)}$ ,

where  $d_i$  is the distance to the boundary with probability  $\frac{1}{s_i}$  the characterizes how often it happens either inside  $G_e$  or on the boundary  $d_i$  from the point to the boundary becomes less than a prescribed number,  $\epsilon$ . In the second case we return to estimating  $\psi$  on the boundary since the probability of terminating is bounded away from zero, the mean number of steps on the Markov chain is finite.

The same approach works as well for the case where the three subdomains are introduced into the medium. We show that the three subdomains divide the three domains into a part of the medium,  $G_i$ , the exterior,  $G_e$ , and the interior between them,  $G_0$ .  $G_0$  and  $G_e$  have  $\epsilon = \epsilon_e$  and  $\kappa = 0$ .  $\partial G_i$  the mean value relationship ( ) then reads

$$\begin{aligned}
 u(x_N) &= \frac{\epsilon_e}{\epsilon_e + \epsilon_i} \int_{S_e(x_N, a)} \overline{u_e} \, 2\pi a^2 \\
 &+ \frac{\epsilon_i}{\epsilon_e + \epsilon_i} \int_{S_i(x_N, a)} \overline{u_i} \, 2\pi a^2 \quad ( ) \\
 &- \frac{\epsilon_e - \epsilon_i}{\epsilon_e + \epsilon_i} \int_{\Gamma \cap B(x_N, a) \setminus \{x_N\}} 2 \frac{\partial \Phi_0}{\partial n} u,
 \end{aligned}$$

where  $\Phi_0(x) = -\frac{1}{4\pi} \left( \frac{1}{|x - x_N|} - \frac{1}{a} \right)$ . On  $\partial G_e$  the discrete conditions are equivalent to this design. We show that the third term in ( ) equals zero.

### 5 Experiments, Conclusions, and Future Work

To test the proposed algorithms we applied our Monte Carlo estimates to a simple medium problem with a known analytical solution. For a spherical domain, the exact value of  $E$  scaled by  $q^2/(4\pi\epsilon_i R)$  equals  $\epsilon_i/(\epsilon_e + \kappa R) - \epsilon_e$  for the values  $\epsilon_i = 4$ ,  $\epsilon_e = 78$ ,  $\kappa = 0.01$ . We obtain the exact solution of  $-0.4$ . Our calculation based on the Markov spheres method produced the result  $-0.48$  with a 1% statistical error in 0.7 seconds for  $a = 1$  and 0.4 seconds for  $a = 0.1$ . The algorithm based on the finite difference approximation of the boundary conditions with  $h = 0.01$  produced the result with the same accuracy in 0.5 seconds. Our calculations were carried out on a standard desktop

computer than a Gz4 processor running on a dual-core system, which is read a far superior computer.

Thus we see a significant speed increase of the order of magnitude in the progress of the finite difference approach to the boundary conditions of the method. Additionally, the schemes with the elimination of the  $O(h)$  bias of the finite difference technique have been carried out these series of computer simulations. Our results demonstrate that the specific form of the function  $\alpha(4)$  computed makes it possible to simulate a parameter  $M$  dependent random walk for estimation of  $u^{(m)}$  over much more rapid parameter settings.

Therefore these techniques will be implemented in the future creation of a suite of finite Carlo approaches to problems of computational biomolecular electrostatics. Thus we participate in the series of research towards this long term goal. The short term participation is to estimate the biomolecular surfaces and the random walk for these methods, the direct solution of the Poisson equation. The finite Carlo and the calculation of forces and other properties of function  $\alpha$  of the potential and its partial derivatives.

## References

1. Mascagni, M. and Simonov, N.A.: Monte Carlo method for calculating the electrostatic energy of a molecule. In: Lecture Notes in Computer Science, Vol. 2657. Springer-Verlag, Springer-Verlag, Berlin Heidelberg New York (2003) 63–74.
2. Mascagni, M. and Simonov, N.A.: Monte Carlo methods for calculating some physical properties of large molecules. *SIAM Journal on Scientific Computing*. **26** (2004) 339–357.
3. Davis, M.E. and McCammon, J.A.: Electrostatics in biomolecular structure and dynamics. *Chem. Rev.* **90** (1990) 509–521
4. Simonov, N.A.: A random walk algorithm for the solution of boundary value problems with partition into subdomains. in *Metody i algoritmy statisticheskogo modelirovaniya*, Akad. Nauk SSSR Sibirsk. Otdel., Vychisl. Tsentr, Novosibirsk (1983) 48–58.

# Finding the Smallest Eigenvalue by the Inverse Monte Carlo Method with Refinement\*

Vassil Alexandrov<sup>1</sup> and Veta Sara A. A.<sup>2</sup>

<sup>1</sup> School of Systems Engineering, University of Reading, Reading RG6 6AY, UK  
v.n.alexandrov@rdg.ac.uk

<http://www.cs.reading.ac.uk/people/V.Alexandrov.htm>

<sup>2</sup> IPP - BAS, Acad. G. Bonchev St., Bl.25A, 1113 Sofia, Bulgaria  
anet@parallel.bas.bg

<http://parallel.bas.bg/~anet/>

**Abstract.** Finding the smallest eigenvalue of a given square matrix  $A$  of order  $n$  is computationally very intensive problem. The most popular method for this problem is the Inverse Power Method which uses  $LU$ -decomposition and forward and backward solving of the factored system at every iteration step. An alternative to this method is the Resolvent Monte Carlo method which uses representation of the resolvent matrix  $[I - qA]^{-m}$  as a series and then performs Monte Carlo iterations (random walks) on the elements of the matrix. This leads to great savings in computations, but the method has many restrictions and a very slow convergence.

In this paper we propose a method that includes fast Monte Carlo procedure for finding the inverse matrix, refinement procedure to improve approximation of the inverse if necessary, and Monte Carlo power iterations to compute the smallest eigenvalue. We provide not only theoretical estimations about accuracy and convergence but also results from numerical tests performed on a number of test matrices.

**Keywords:** Monte Carlo methods, eigenvalues, Markov chains, parallel computing, parallel efficiency.

## 1 Introduction

Let  $A$  be a real symmetric matrix. Consider the problem of evaluating the eigenvalues of  $A$ , or the values of  $\lambda$  for which

$$Au = \lambda u \quad (1)$$

holds. Suppose, the  $n$  eigenvalues of  $A$  are ordered as follows  $|\lambda_1| > |\lambda_2| \geq \dots \geq |\lambda_{n-1}| > |\lambda_n|$ .

---

\* Supported by the Ministry of Education and Science of Bulgaria under Grant No. I1405/04.

It is known that the problem of calculating the smallest eigenvalue of  $A$  is more difficult from numerical point of view than the problem of calculating the largest eigenvalue. Nevertheless, for many applications, especially in engineering, it is important to estimate the smallest one, because it usually defines the most stable state of the system which is described by the considered matrix.

## 2 Background

### 2.1 Inverse Power Method

One of the most popular methods for finding extremal eigenvalues is the power method ( [8] ) which for a given matrix  $A$  is defined by the iteration

$$x^{new} = Ax^{old}.$$

Except for special starting points, the iteration converges to the eigenvector corresponding to the eigenvalue of  $A$  with the largest magnitude (**dominant eigenvalue**) in the least squares sense, i.e.  $\mu$  is the largest determined eigenvalue of the system

$$\mu x_k = x_{k+1}$$

is estimated for  $\lambda_1$  which is called the **Raleigh quotient**

$$\mu = \frac{x_k^T x_{k+1}}{x_k^T x_k}.$$

Suppose that we want to compute the eigenvector corresponding to the eigenvalue of  $A$  of smallest magnitude. Letting  $(\lambda_1, e_1)$  through  $(\lambda_n, e_n)$  denote the eigenpairs of  $A$ , the corresponding eigenpairs of  $C = A^{-1}$  are  $(1/\lambda_1, e_1)$  through  $(1/\lambda_n, e_n)$ . If  $\lambda_n$  is the eigenvalue of  $A$  of smallest magnitude, then  $1/\lambda_n$  is  $C$ 's eigenvalue of largest magnitude and the power iteration  $x^{new} = A^{-1}x^{old}$  converges to the vector  $e_n$  corresponding to the eigenvalue  $1/\lambda_n$  of  $C = A^{-1}$ .

In implementing the inverse power method, instead of computing the inverse matrix  $A^{-1}$  explicitly, by  $A$  the iteration  $x^{new} = A^{-1}x^{old}$  is performed from  $Ax^{new} = x^{old}$ . Representing  $A$  by its LU factorization yields

$$(LU)x^{new} = x^{old}. \tag{2}$$

In each iteration of the inverse power method, the vector is obtained from the old one by forward and backward solving the factored system (2). This scheme is computationally more efficient than  $k$  iterations, the number of arithmetic operations is  $O(kn^2)$  for the power method and  $O(n^3 + kn^2)$  for the inverse power method.

**2.2 Resolvent Monte Carlo Method**

Given a matrix  $A$ , consider a algorithm based on the Monte Carlo iteration of the resolvent matrix  $R_q = (I - qA)^{-1} \in \mathbb{R}^{n \times n}$  where the following representation holds

$$I - qA^{-m} = \sum_{i=0}^{\infty} q^i C_{m+i-1}^i A^i, \quad |q\lambda| < 1 \quad (1)$$

is valid because of behavior of binomial expansion and the spectral theory of linear operators. Let remind that the eigenvalues of the matrices  $R_q$  and  $A$  are connected by the equation  $\mu = \frac{1}{1-q\lambda}$  and the eigenvectors coincide. The following expression (see [4])

$$\mu^{(m)} = \frac{(I - qA^{-m}f, h)}{(I - qA^{-(m-1)}f, h)} \xrightarrow{m \rightarrow \infty} \mu = \frac{1}{1 - q\lambda}, \quad f \in \mathbb{R}^n, h \in \mathbb{R}^n, \quad (4)$$

is valid (for all the eigenvectors in  $\mathbb{R}^n$ ) for negative values of  $q$ , the largest eigenvalue  $\mu_{max}$  of  $R_q$  corresponds to the smallest eigenvalue  $\lambda_{min}$  of the matrix  $A$ . Therefore, if  $|\lambda_{max}| < 1$  here  $\lambda_{max}$  is the largest eigenvalue of the matrix  $A'$   $\{|a_{ij}|\}_{i,j=1}^n$ , the following statement holds, [4], [2]

$$(I - qA^{-m}f, h) = E \left\{ \sum_{i=0}^{\infty} q^i C_{m+i-1}^i (A^i f, h) \right\}.$$

The exact structure of the Monte Carlo method defines a Markov chain  $k_0 \rightarrow k_1 \rightarrow \dots \rightarrow k_i$  ( $0 \leq k_j \leq n$  are natural numbers) that takes a discrete set of values  $Pr(k_0 = \alpha) = p_\alpha, Pr(k_j = \beta | k_{j-1} = \alpha) = p_{\alpha\beta}$ , (see [4], [2]) and define the random variables  $W_j$  using the following recursive formula

$$W_0 = \frac{h_{k_0}}{p_{k_0}}, \quad W_j = W_{j-1} \frac{a_{k_{j-1}k_j}}{p_{k_{j-1}k_j}}, \quad j = 1, \dots, i. \quad (5)$$

It can be proved that (see [4], [2])

$$\lambda_{min} \approx \frac{1}{q} \left( - \frac{1}{\mu^{(m)}} \right) = \frac{(A(I - qA^{-m}f, h))}{(I - qA^{-m}f, h)}$$

$$\frac{E \sum_{i=1}^{\infty} q^{i-1} C_{i+m-2}^{i-1} W_i f_{x_i}}{E \sum_{i=0}^{\infty} q^i C_{i+m-1}^i W_i f_{x_i}} = \frac{E \sum_{i=0}^l q^i C_{i+m-1}^i W_{i+1} f_{x_i}}{E \sum_{i=0}^l q^i C_{i+m-1}^i W_i f_{x_i}}, \quad (6)$$

here  $W_0 = \frac{h_{k_0}}{p_{k_0}}$  and  $W_i$  are defined by (5) the coefficients  $C_{i+m}^n$  are calculated using the presentation  $C_{i+m}^i = C_{i+m-1}^i + C_{i+m-1}^{i-1}$

This method has strong requirements about matrices for which it can be applied. The systematic errors consist of two parts

- a error from the error method applied to the resulting matrix  $I - qA^{-1}$  which determines the value of the parameter  $m$ , the following inequality rate of convergence

$$O\left(\left(\frac{+|q|\lambda_n}{+|q|\lambda_{n-1}}\right)^m\right).$$

- the parameter  $m$  has to be chosen such that  $\left(\frac{\mu_2}{\mu_1}\right)^m < \varepsilon$
- a error which comes from the series expansion of the resulting matrix determines the value of the parameter  $l$  (length of each radial mark). Consider the presentation

$$(I - qA^{-m}f, g) \approx \sum_{i=0}^l q^i C_{m+i-1}^i (A^i f, g) - \sum_{i=1}^l u_i,$$

- the parameter  $l$  has to be chosen such that  $|u_{l+1}| < \varepsilon_2$ .
- required errors estimate them at a given level the condition  $(\max_{1 \leq i \leq l} |u_i|) \varepsilon < \alpha \mu$  must be satisfied, here  $\alpha < 1$  represents the requested precision and  $\varepsilon$  is the machine precision parameter

of routine, the parameter  $l$  cannot be relatively large because the block matrix efficiency  $C_{m+l-1}^l$  grows exponentially with  $l$  has serious restrictions for using the resulting matrix Car.

The Result of the Car. method computes the smallest eigenvalue with  $O(lN)$  operations, here  $l$  is the average length of the marked chains and  $N$  is the number of marks but this method has a lot of restrictions, and, as a general enough approximation.

### 3 Inverse Monte Carlo with Refinement

here we propose a method that includes fast inverse Car. scheme for matrix inverses, refinement of the inverse matrix (if necessary) and inverse Car. operation for computing the largest eigenvalue of the inverse (the smallest eigenvalue of the given matrix)

#### 3.1 Monte Carlo for Computing the Inverse Matrix

to find the inverse  $A^{-1} = C = \{c_{rr}\}_{r,r=1}^n$  of square matrix  $A$ , we must first compute the elements of matrix  $M = I - A$ , here  $I$  is the identity matrix. Clearly, the inverse matrix is given by

$$C = \sum_{i=0}^{\infty} M^i, \tag{7}$$

which converges if  $\|M\| < 1$  (sufficient condition)



estimate the elements of the inverse matrix  $C$ , we define a Markov chain  $s_0 \rightarrow s_1 \rightarrow \dots \rightarrow s_k$ , where the  $s_i, i = 1, 2, \dots, k$ , belong to the state space  $S = \{1, 2, \dots, n\}$ . Here for  $\alpha, \beta \in S, p_0(\alpha) = p(s_0 = \alpha)$  is the probability that the Markov chain starts at state  $\alpha$  and  $p(s_{j+1} = \beta | s_j = \alpha) = p_{\alpha\beta}$  is the transition probability from state  $\alpha$  to state  $\beta$ . We set of a priori probabilities  $p_{\alpha\beta}$  defines a transition probability matrix  $P = \{p_{\alpha\beta}\}_{\alpha, \beta=1}^n$ . We can use the following general Carlin method (see, for example, [1]) for calculation of the elements of the inverse matrix  $C$

$$c_{rr} \approx \frac{1}{N} \sum_{s=1}^N \left[ \sum_{(j|s_j=r)} W_j \right], \tag{8}$$

here  $(j|s_j = r')$  means that ...

$$W_j = \frac{M_{rs_1} M_{s_1 s_2} \dots M_{s_{j-1} s_j}}{p_{rs_1} p_{s_1 s_2} \dots p_{s_{j-1} s_j}} \tag{9}$$

for which  $s_j = r'$  are included in the sum (8)

since  $s_j$  is included in the corresponding sum for  $r' = 1, 2, \dots, n$ , the same set of  $N$  chains can be used to compute a series of the inverse matrix. Hence since of the inherent properties of  $C$  making them suitable for parallelization.

Furthermore, for essential transformation matrix  $A$  to matrix  $D$  where  $D$  is diagonal and main matrix, we find its inverse and after that apply a filter procedure in order to find  $A^{-1}$ .

The probable error of the method is defined as  $r_N = 0.74 \sqrt{D\theta/N}$ , here  $P\{|\theta - E(\theta)| < r_N\} \approx 1/2 \approx P\{|\theta - E(\theta)| > r_N\}$ , where  $N$  depends on the realization of random variable (r.v.)  $\theta$  with mathematical expectation  $E\theta$  and a variance  $\theta$ .

### 3.2 Refinement

Given a square nonsingular matrix  $A$ , the Carlin goes fast but error is high estimate of the elements of the inverse matrix  $C_0$ . Under the condition  $\|R_0\| \leq \delta < 1$  where  $R_0 = I - AC_0$ , the elements of  $A^{-1}$  may be computed to a higher degree of accuracy successively using the iterative process  $C_m = C_{m-1}(I + R_{m-1}), R_m = I - AC_m$  for  $m = 1, 2, \dots$ . It can be shown that

$$\|C_m - A^{-1}\| \leq \|C_0\| \frac{\delta^{2^m}}{1 - \delta}.$$

It follows that since we have a certain approximation  $C_0$  of the inverse such that  $\|I - AC_0\| \leq k < 1$  we can use the above iterative scheme and that the number of correct digits increases geometrically progress.

Therefore we have inverted matrix  $D$  then we need to apply the filter procedure to obtain the  $A^{-1}$  using the formula

$$A_k^{-1} = A_{k+1}^{-1} + \frac{A_{k+1}^{-1} S_{i+1} A_{k+1}^{-1}}{-\text{trace}(A_{k+1}^{-1} S_{i+1})}, i = k-1, k-2, \dots, 1.$$

### 3.3 Evaluation of the Smallest Eigenvalue

Once we have the matrix  $C = A^{-1}$  we apply the Monte Carlo procedure to find its largest eigenvalue performing  $m$  trials. The elements of the matrix  $C$

$$\lambda_{max}(C) \approx \frac{E\{W_m f_{k_i}\}}{E\{W_{m-1} f_{k_{i-1}}\}}$$

where  $W_j = \frac{C_{k_0 k_1} C_{k_1 k_2} \dots C_{k_{j-1} k_j}}{P_{k_0 k_1} P_{k_1 k_2} \dots P_{k_{j-1} k_j}}$ , and  $m$  is sufficient large to ensure the convergence of the procedure which is  $O\left(\frac{\lambda_n}{\lambda_{n-1}}\right)^m$ . The computation is a cost function of the Monte Carlo is  $mN$ , where  $m$  is determined by the convergence of the procedure and  $N$  is the number of trials.

### 3.4 Restrictions of the Method and How to Avoid Them

Suppose that  $\lambda_n < \lambda_{n-1}$ . In this case the procedure converges to the eigenvalue. The possible restriction of the above scheme is the requirement  $\|M\| < 1$  for the convergence of the Monte Carlo series. This can be avoided using the presented below algorithm for invertible generative matrices using the Monte Carlo.

**Algorithm:** Find  $A^{-1}$

**Initial data:** Input matrix  $A$ , parameters  $\gamma$  and  $\epsilon$

**2 Preprocessing:**

2 **Split**  $A = D - (D - A)$ , here  $D$  is a diagonal matrix

2.2 **Set**  $D = B - B_1$  here  $B$  is a diagonal matrix  $b_{ii} = d_{ii} \quad i = 1, 2, \dots, n$ .

2 **Compute** the matrix  $T = B^{-1}B_1$

2.4 **Compute**  $\|T\|$ , the number of iterations  $N = \left(\frac{0.6745}{\epsilon} \cdot \frac{1}{(1-\|T\|)}\right)^2$ .

**For**  $i = 1$  to  $n$

**For**  $j = 1$  to  $N$

**Markov Chain Monte Carlo Computation:**

**Set**  $t_k$  (st. probability),  $W_0 = 1$ ,  $SUM_i = 0$  and  $Point = i$ .

2 **Generate** a uniform distributed random number  $nextpoint$

**If**  $T_{point nextpoint} > nextpoint$ !

**LOOP**

**Compute**  $W_j = W_{j-1} \frac{T_{[point][nextpoint]}}{P_{[point][nextpoint]}}$ .

2 **Set**  $Point = nextpoint$  and  $SUM_i = SUM_i + W_j$

**If**  $|W_j| < \gamma$ ,  $t_k = t_k + W_j$

4 **If**  $t_k \geq n$ , end loop

4 **End If**

**Else** go to step 2

2 **End of loop j**

**Compute** the average of results

4 **End of loop i**

**Obtain** the matr  $V = (I - T)^{-1}$ .

**Therefore**  $D^{-1} = VB^{-1}$

7 **Compute** the matr  $C = D^{-1} B(I - T)^{-1}$

8 **Set**  $D_0 = D^{-1}$  (appr. matr  $D_0$ ) and  $R_0 = I - DD_0$

**use filter procedure**  $R_i = I - DD_i, D_i = D_{i-1}(I + R_{i-1}), i = 1, 2, \dots, m,$   
 here  $m \leq k$ .

**Consider the accurate inversion of D** by step  $i$ , e.g. by  $D_0, \dots, D_k$ .

**Compute**  $S = D - A$  here  $S$  can be a matr that all zero elements  
 and all diagonal elements are zero.

2 **Main function** for  $i = 1, 2, \dots, k$  based on  $D^{-1}$  step

2 **Compute** the matr  $S_i, i = 1, 2, \dots, k$ , here each  $S_i$  has just one  
 element of matr  $S$

2.2 **Set**  $A_0 = D_0$  and  $A_k = A + S$

2 **Apply**  $A_k^{-1} = A_{k+1}^{-1} + \frac{A_{k+1}^{-1} S_{i+1} A_{k+1}^{-1}}{1 - \text{trace}(A_{k+1}^{-1} S_{i+1})}, i = k - 1, k - 2, \dots, 1$ .

**Print** the matr  $A_k^{-1}$

4 **End** of algorithm

## 4 Parallel Implementation and Numerical Tests

The method presented in this paper consists of the following procedures

- compute Car. matr  $D^{-1}$
- Refinement
- iterative Car. iterations

We studied the convergence and the parallel behaviour of each of the above procedures separately in order to have the better picture

It is well known that the Car. algorithms have high parallel efficiency. In fact, in the case where all components of the zero matrix elements of  $A$  are set to each processor, the execution time for computing a  $n \times n$  matrix  $A$  is  $O(p)$  processors is bounded by  $O(\ln N/p)$  where  $N$  is the number of performed random accesses and  $l$  is the mean value of the steps as given. It is usually assumed that the total communication cost of distributed computing the matrix and the finite communication cost of collecting and aggregating the distributed statistics, e.g. compared to the cost of generating the Markov chains and forming the chain statistics.

The numerical tests presented include empirical  $28 \times 28$  matrix, here we have applied roughly the Car. estimation and refinement. In this case, the procedure for finding the largest eigenvalue of the sparse matrix using the Car. iterations, has the convergence after that we applied a refinement procedure to find more accurate eigenvalues than  $\epsilon = 10^{-6}$  and  $10^{-8}$  respectively. The Car. iterations to find the largest eigenvalue of the refined sparse matrix gives the value  $\lambda_{Inv_{max}}$ . The high speed is enough to the value given by the eigenvalue procedure which is 2.

In addition to convergence test, we also performed parallel computations to empirically confirm the parallel efficiency of the iterative Carathéodory method. In parallel tests conducted using the Carathéodory method and refinement capabilities, we here we test the iterative Carathéodory part for computing the desired eigenvalue. The parallel numerical test was performed using a Compaq Alpha parallel cluster with 8 processors each running at 4 megahertz using the parallel procedure of the parallel case. Each processor executes the same program for  $N/p$  iterations (here  $p$  is the number of processors), and at the end of the iterations, a designated host processor collects the results of all realizations and computes the desired average values. The results show in Figure that the high parallel efficiency of the Carathéodory methods is preserved for this problem as well.

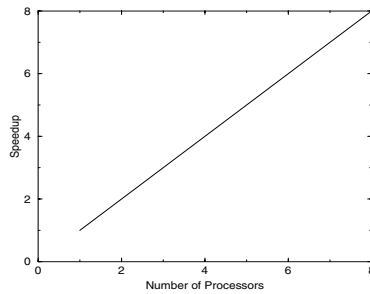


**Fig. 1.** Computing the largest eigenvalue of the inverse matrix - Speedup vs number of processors

## 5 Conclusion

The iterative Carathéodory method with refinement has been proposed and tested. The tests for solving systems of linear algebra equations (see, for example, [1]) in this paper propose a method that includes the iterative Carathéodory procedure for finding the inverse matrix, refinement procedure, improved approximation of the inverse if necessary, and the Carathéodory iteration to compute the smallest eigenvalue. This method gives better results than the Resolvent iterative Carathéodory method.

## References

1. V. N. Alexandrov, S. Branford, and C. Weihrauch, 'A New Parallel Hybrid Monte Carlo Algorithm for Matrix Computations', *Proc. Of PMAA 2004*, September 2004.
2. I. Dimov, V. Alexandrov, A. Karaivanova, 'Resolvent Monte Carlo Methods for Linear Algebra Problems', *Mathematics and Computers in Simulations*, Vol. **55**, 2001, pp. 25-36.

3. I. Dimov, T. Dimov, T. Gurov, A new iterative Monte Carlo Approach for Inverse Matrix Problem, *J. of Comp. and Appl. Mathematics*, **92**, 1998, pp. 15-35.
4. I. Dimov, A. Karaivanova, Parallel computations of eigenvalues based on a Monte Carlo approach, *Journal of MC Methods and Appl.*, Vol.4, Num.1, 1998 pp.33-52.
5. B. Fathi, B. Liu and V. Alexandrov, Mixed Monte Carlo Parallel Algorithms for Matrix Computations, *Computational Science - ICCS2002*, LNCS **2330**, pp. 609-618, 2002.
6. G. H. Golub, C.F. Van Loan, *Matrix computations*, **The Johns Hopkins Univ. Press**, Baltimore, 1996.
7. J.H. Halton, Sequential Monte Carlo Techniques for the Solution of Linear Systems, *SIAM Journal of Scientific Computing*, Vol.9, pp. 213-257, 1994.
8. William W. Hager, *Applied Numerical Linear Algebra*, Prentice Hall International (UK) Limited, London, 1989.
9. J.M. Hammersley, D.C. Handscomb, *Monte Carlo methods*, **John Wiley & Sons, inc.**, New York, London, Sydney, Methuen, 1964.
10. G.A. Mikhailov, *Optimization of the "weight" Monte Carlo methods*, Nauka, Moscow, 1987.
11. I.M. Sobol *Monte Carlo numerical methods*, Nauka, Moscow, 1973.

# On the Scrambled Sobol' Sequence

Game Ch<sup>1</sup>, Ester eer<sup>2</sup>, E dre E a s<sup>1</sup>, a d chea ascag<sup>2</sup>

<sup>1</sup> Department of Computer and Information Sciences,  
Florida A&M University, Tallahassee, FL 32307-5100  
hchi@cis.famu.edu

<sup>2</sup> School of Computational Science and Information Technology,  
Florida State University, Tallahassee, FL 32306-4120

**Abstract.** The Sobol' sequence is the most popular quasirandom sequence because of its simplicity and efficiency in implementation. We summarize aspects of the scrambling technique applied to Sobol' sequences and propose a new simpler modified scrambling algorithm, called the multi-digit scrambling scheme. Most proposed scrambling methods randomize a single digit at each iteration. In contrast, our multi-digit scrambling scheme randomizes one point at each iteration, and therefore is more efficient. After the scrambled Sobol' sequence is produced, we use this sequence to evaluate a particular derivative security, and found that when this sequence is numerically tested, it is shown empirically to be far superior to the original unscrambled sequence.

## 1 Introduction

We use quasirandom, rather than random, numbers in the Car. methods, scaled quasirandom Car. methods, which converge much faster than random Car. quasirandom Car. methods are used in scientific computation, especially in estimating integrals over multidimensional domains.

The Sobol' sequence [2, 22] is one of the standard quasirandom sequences and is used in quasirandom applications. The efficient implementation of the Sobol' sequence uses Graeco-Latin designs. We summarize aspects of this technique applied to the Sobol' sequence and propose a new scrambling algorithm, called a multi-digit scrambling scheme. Most proposed scrambling methods [8, 9] randomized a single digit at each iteration. In contrast, our multi-digit scrambling scheme, which randomizes one point at each iteration, is efficient and fast because the popular multidimensional pseudorandom number generators are used to speed it up.

The construction of the Sobol' sequence uses linear recurrence relations over the finite field  $\mathbb{F}_2$ , where  $\mathbb{F}_2 = \{0, 1\}$  is the binary representation of the integers. The  $n$ th element of the  $j$ th dimension of the Sobol' sequence,  $x_n^{(j)}$ , can be generated by

$$x_n^{(j)} = n_1 \nu_1^{(j)} \oplus n_2 \nu_2^{(j)} \oplus \dots \oplus n_w \nu_w^{(j)} \quad (1)$$

here  $\nu_i^{(j)}$  is a binary fractal called the  $i$ th d rect... number... the  $j$ th d me... these d rect... numbers are generated by the following  $q$  term recurrence relation

$$\nu_i^{(j)} = a_1\nu_{i-1}^{(j)} \oplus a_2\nu_{i-2}^{(j)} \oplus \dots \oplus a_q\nu_{i-q+1}^{(j)} \oplus \nu_{i-q}^{(j)} \oplus (\nu_{i-q}^{(j)}/2^q). \tag{2}$$

When  $i > q$ , and the bits  $a_i$  comes from the coefficients of a degree  $q$  primitive polynomial over  $\mathbb{F}_2$ , it can be shown that the above d rect... numbers can generate the binary d rect... numbers... each d rect... number... then represent  $\nu_i^{(j)}$  as the integer  $m_i^{(j)} = \nu_i^{(j)} * 2^i$ . Thus, the choice of  $q$  d rect... numbers  $\nu_i^{(j)}$  becomes the problem of choosing  $q$  d integers  $m_i^{(j)} < 2^i$ ... the d rect... numbers  $\nu_i^{(j)} = \frac{m_i^{(j)}}{2^i}$ ... the recurrence... here  $i \leq q$ , can be decided by the  $m_i^{(j)}$ 's, which can be arbitrary d integers... less than  $2^i$ ... the Gray code sequence used... implementation 4... of the binary sequence

the d rect... numbers... binary sequence... comes from a degree  $q$  primitive polynomial over  $\mathbb{F}_2$ , the first  $q$  d rect... numbers can be arbitrarily assigned for the above recursion (equation (2))... effecting them... crucial for... bit... high quality... binary sequences... the... picture... bit... and... 2... show that d rect... choices for  $q$  d rect... numbers can make the... binary sequence quite d rect... the... d rect... numbers for the... picture... figure ( )... from... rate... and... 's paper 4... the... picture... figure (2) results... the... d rect... numbers are... es

... 22... realized the... implementation of  $q$  d rect... numbers, and published a... addition... a... perturbation (called... perturbation) for d rect... numbers... produce... more uniform... binary sequences... but... implementation... of... binary sequences... showed that... perturbation... is... that... useful... practice... Che... and... ruzdze... 2... developed a... empirical method... search for  $q$  d rect... numbers,  $m_i^{(j)}$ ... a... restricted space... the... search space... as... limited because the... had... to... know... the... total number of... quasirandom numbers,  $N$ ... and... a... can... use the... method... acknowledge... used a... random sampling method... to... choose the...  $q$  d rect... numbers,  $m_i^{(j)}$ ... the... uniform random number  $u_{ij}$ ,... such that  $m_i^{(j)} = \lfloor u_{ij} * 2^{i-1} \rfloor$  for  $1 < i < q$ ... the... condition... that  $m_i^{(j)}$ ... is... odd

Obviously, the arbitrary nature of  $q$  d rect... numbers of the sequence... primitive d rect... numbers... a... project... is... frequently... appear... the... binary sequence... rank... and... Ca... Sch... 8... stated that... primitive d rect... numbers... a... project... is... for... the... binary sequence... can... occur... at... time... because... of... the... m... p... r... per... ch... ces... for...  $q$  d rect... numbers... the... bad... effects... that... the... d... rect... numbers... and... a... can... choose... the... d rect... numbers... cause... primitive d rect... numbers... a... project... is... other... words... primitive d rect... numbers... a... project... is... are... difficult... to... predict... but... the... right... choice... of... the... d rect... numbers... is... crucial... to... generate... good... binary sequences... 8... can... help... us... improve... the... quality... of... the... binary sequence... has... got... to... pay... attention... to... the... performance... of... the... d rect... numbers

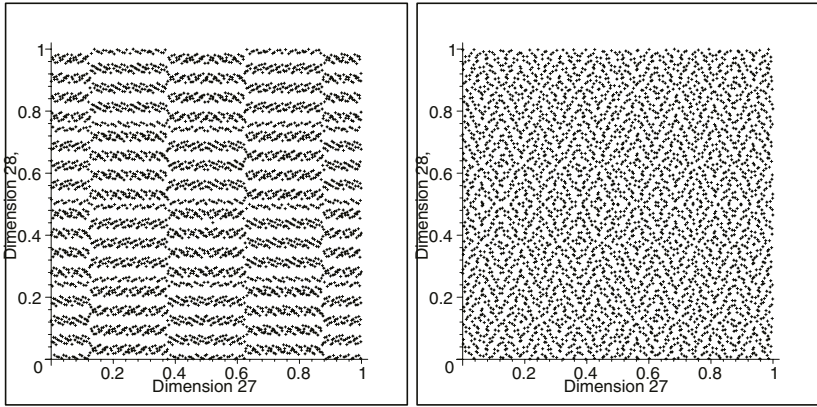


**Fig. 1.** Left: 4096 points of the original Sobol' sequence and the initial direction numbers are from Bratley and Fox's paper [4]; right: 4096 points of the scrambled version of the Sobol' sequence

## 2 Scrambling Methods

Recall that the Sobol' sequence is defined over the finite field  $\mathbb{F}_2$  using a bit permutation. To scramble a quasirandom point set over  $\mathbb{F}_p$ , the zero-spectrum method is used. The results that permit generating zero-spectrum sequences are based on the sequence where the zero can be added to the end of a sequence. Here, the direction numbers are changed so that the zero can be added to the end of a sequence. This strategy for pure digital permutation is here zero-spectrum scrambling. The scrambling method for the Sobol' sequence over  $\mathbb{F}_2$  is simple and efficient as the scrambling method is the same. Other scrambling methods can be introduced.

The scrambling method is a simple method for scrambling the Sobol' sequence. Let  $x_n = (x_n^{(1)}, x_n^{(2)}, \dots, x_n^{(s)})$  be a quasirandom number sequence of length  $s$ , and  $z_n = (z_n^{(1)}, z_n^{(2)}, \dots, z_n^{(s)})$  be the scrambled version of the point  $x_n$ . Suppose that each  $x_n^{(j)}$  has a binary representation as  $x_n^{(j)} = x_{n1}^{(j)} x_{n2}^{(j)} \dots x_{nK}^{(j)}$ , where  $K$  defines the number of digits to be scrambled. Then the definition is

$$z_n^{(j)} = c_1 x_n^{(j)} + c_2, \text{ for } j = 1, 2, \dots, s, \quad (1)$$

where  $c_1 \in \{1, 2, \dots, b-1\}$  and  $c_2 \in \{0, 1, 2, \dots, b-1\}$ . Since the Sobol' sequence is binary over  $\mathbb{F}_2$ , the values of  $c_1$  and  $c_2$  must be chosen such that the choice of  $c_1$  is crucial. The quality of the scrambled Sobol' sequence, this scrambling method is suitable for the Sobol' sequence over  $\mathbb{F}_2$ .

As stated previously, the quality of the Sobol' sequence depends heavily on the choice of the direction numbers. The correlation between the direction numbers are due to the proper choice of the direction numbers. A



methods to improve the Sobol sequence efficiency. In practice, we found that the standard random numbers but this approach is difficult to judge by a measure of efficiency. Improving the Sobol sequence depends on the standard random numbers. This idea motivates us to find a better approach to obtain high quality Sobol sequences by means of scrambling each point.

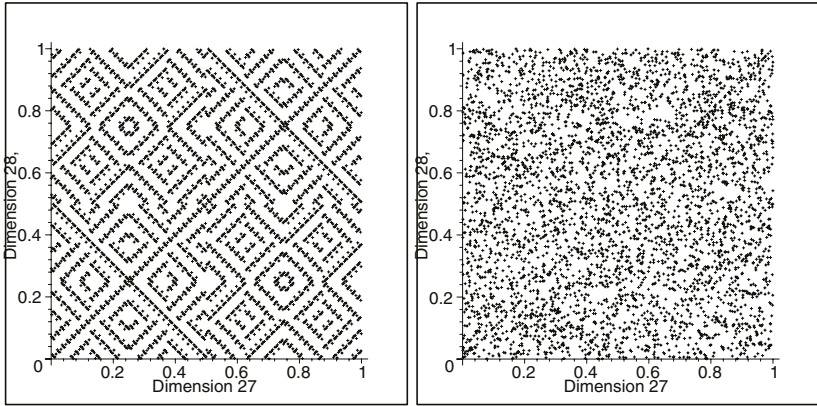


**Fig. 2.** Left: 4096 points of the original Sobol sequence with all initial direction numbers ones [23], right: 4096 points of the scrambled version of the Sobol sequence

### 3 An Algorithm for Scrambling the Sobol Sequence

The procedure of this approach for scrambling the Sobol sequence, and measure the effect of this approach with the number of iterations that we have used. Using this approach, we can scramble the Sobol sequence with a number of dimensions.

The definition of algorithm to scramble  $k$  bits of the Sobol sequence instead of scrambling the whole point. The value of  $k$  could be a positive integer as long as we could find a suitable near-Congruent Generator (CG) first. Assume  $x_n$  is the  $n$ th Sobol point, and we want to scramble first  $k$  bits of  $x_n$ . Let  $z_n$  be the scrambled version of  $x_n$ . Our procedure is described as follows:

- 1  $y_n = \lfloor x_n * 2^k \rfloor$ , is the  $k$  most significant bits of  $x_n$ , to be scrambled
- 2  $y_n^* = ay_n \pmod m$  and  $m \geq 2^k - 1$ , is the near scrambling applied to this integer
- 3  $z_n = \frac{y_n^*}{2^k} + (x_n - \frac{y_n}{2^k})$ , is the result of these scrambled bits to the Sobol point

The key step of this approach is based on using CGs as scramblers. CGs with the best performance and parameters are commonly pseudorandom number generators. The methods used for a CGs are perfect, the implementation is cheap and fast due to the fact that modular addition and multiplication are

ust, rd, ar, c, mputer ar thmet c he, the m, du us c, rresp, ds t, a c, mputer  
 rd s ze he d sad a tage, terms, f qua t, s hard t, bta, the des red  
 qua t, f pseud, rad m, umbers he us, g a p, er, f t, as m, du us re  
 deta s are g, e, 4, CGs th pr me m, du are ch, se, th s paper  
 he rest, f, ur, b s t, search f r a su tbe a d re, abe CG as, ur scam  
 ber he, the m, du us, f a CG s pr me, mp eme, tat, s m re e pe, s e  
 spec a, f rm, f pr me, such as a, ersse, e<sup>1</sup>, r a, ph e Germa, pr me<sup>2</sup>, ca, be  
 ch, se, s, that the c, st, est part, f the ge, erat, the m, du ar mu t p, cat,  
 ca, be m, m zed  
 s mp, f the scamb, g pr, cess, e, k t, CGs f r gu da, ce C, s der  
 the f, g CG

$$y_n^* = ay_n \pmod{m}, \tag{4}$$

here  $m$  s ch, se, t, be a, ersse, e,  $2^k - 1$ , r, ph e Germa, pr me, the f, rm  
 f  $2^{k+1} - k_0$ ,  $k$  s the, umber, f b ts, eeded t, scamb, e, a d a s a pr m t, e  
 r, t m, du,  $m = 2, 7$  e ch, se the m, du us t, be a, ersse, e, r, ph e  
 Germa, because, f the e, ste, ce, f a fast m, du ar mu t p, cat, a g r thms  
 f r these pr mes he, pt ma, a sh, u d ge, erate the, pt ma, b, seque, ce, a d  
 the, pt ma, a's f r m, du us  $2^{31} - 1$  are tabu ated, 7 pr, p, sed a g r thm  
 f r fi, d, g such, pt ma, pr m t, e r, t m, du us  $m$ , a pr me, s descr bed

r mar, ur a g r thm pr, des a pract ca, meth d t, bta, a fam, f  
 scamb ed, b, seque, ces ec, dar, t g, es us a s mp e a d u, fied a  
 t, ge, erate a, pt ma, b, seque, ce fr m th s fam, cc, rd, g t, O e's  
 pr, f, after scamb, g, the, b, seque, ce s st, a  $(t, s)$  et th base 2  
 e er, us, g, ur a g r thm, e ca, beg, th the, rse ch, ces f r, t a  
 d rect, umbers, the, b, seque, ce a, t a d rect, umbers are, es  
 he resu ts are sh, ed, g 2 he, u, scamb ed p, r t, s a stra ght, e  
 b, th p ctures he reas, s that the, e, scamb, g a g r thm ca, t cha, ge  
 the p, t th the same e, eme, ts, t, a p, t th d, ere, t e, eme, ts

## 4 Geometric Asian Options

ere, e prese, t the, a uat, f a c, mp e, pt, h ch has a s mp e a, a t ca,  
 s, ut, he p, pu ar e amp e f r such pr, b ems s a Eur, pea, ca, pt,  
 the ge, metr c mea, f se, era, assets, s, met mes ca, ed a ge, metr c, s a, pt,  
 et  $K$  be the str ke pr ce at the matur t date,  $T$  he, the ge, metr c mea, f  
 $N$  assets s defi ed as

$$G = \left( \prod_{i=1}^N S_i \right)^{\frac{1}{N}},$$

here  $S_i$  s the  $i$ th asset pr ce heref, re the pa, f th s ca, pt, at matur t  
 ca, be e pr, essed as  $\max(0, G - K)$ , e pr, p, sed a, a a t ca, s, ut,

<sup>1</sup>If  $2^q - 1$  and  $q$  are primes, then  $2^q - 1$  is a Merssene prime.

<sup>2</sup>If  $2q + 1$  and  $q$  are primes, then  $2q + 1$  is a Sophie-Germain prime.

for the price of a geometrically sampled stock. He has concluded that the price of a geometrically sampled stock is approximately normally distributed. This is supported by the empirical results because the behavior of a stock price,  $S_i$ , follows a geometric random walk. The formula for using the Black-Scholes equation (2) to evaluate a European call option can be represented as

$$C_T = S * Norm(d_1) - K * e^{-r(T-t)} * Norm(d_2), \quad (1)$$

$$d_1 = \frac{\ln(S/K) + (r + \sigma^2)(T-t)}{\sigma\sqrt{T-t}},$$

$$d_2 = d_1 - \sigma\sqrt{T-t},$$

where  $t$  is current time,  $r$  is a risk-free rate of interest, which is constant, the Black-Scholes model, and  $Norm(d_2)$  is the cumulative normal distribution. Because the geometrically sampled stock has a constant volatility, we have a benchmark to compare our simulation results with the actual results. The parameters used for our numerical studies are as follows:

Number of assets	$N$
Initial asset prices, $S_i(0)$	1, for $i = 1, 2, \dots, N$
Volatilities, $\sigma_i$	0.2, for $i = 1, 2, \dots, N$
Correlations, $\rho_{ij}$	0, for $i < j$
Strike price, $K$	1
Risk-free rate, $r$	5%
Time maturity, $T$	1 year

The formula for computing the actual volatility for a geometrically sampled stock is computed by a modified Black-Scholes formula using the Black-Scholes formula. We can compute the call price by using equation (1) with the modified parameters,  $S$  and  $\sigma^2$ , as follows:

$$S = Ge^{(-A/2 + \sigma^2/2)T}$$

$$A = \frac{1}{N} \sum_{i=1}^N \sigma_i^2 \quad (2)$$

$$\sigma^2 = \frac{1}{N^2} \sum_{i=1}^N \sum_{j=1}^N \rho_{ij} \sigma_i \sigma_j.$$

We followed the above formulae, equations (1) and (2), to compute the price for different values of  $N$  and  $N$ , with  $K = 1$ , and computed  $p_{2,2}$  and  $p_{2,1}$  respectively for each simulation. We had a constant volatility, so we computed the relative difference between that and our simulated results. The formula  $\frac{|p_{qmc} - p|}{p}$ , where  $p$  is the actual volatility and  $p_{qmc}$  is the price obtained by simulation. For different  $N$ , we computed  $p_{qmc}$  by simulation of the asset price using the geometric random walk. The results are shown in Figure 2.

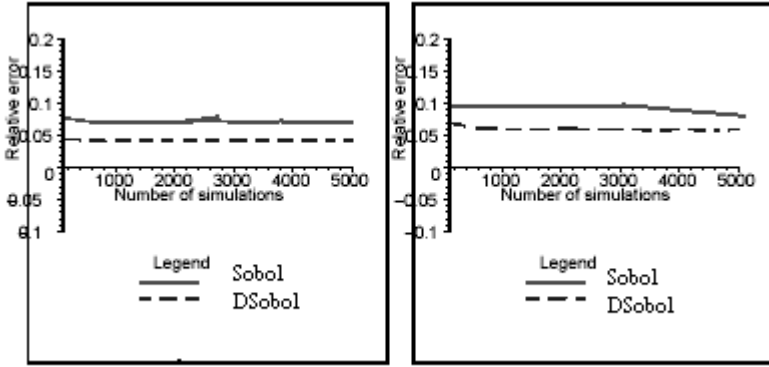


**Fig. 3.** Left: geometric mean of 10 stock prices; right: geometric mean of 30 stock prices. Here the label “Sobol” refers to the original Sobol’ sequence [4], while “DSobol” refers to our optimal Sobol’ sequence

in the equation (1), we can see that random variables are drawn from a normal distribution but each component must be transformed to a normal variable through the transformed method for quasirandom numbers so the inverse of the cumulative distribution function of the inverse normal function predicted by [7] is used in our numerical studies. It is more interesting to see that the optimal Sobol’ sequence performs much better than the original Sobol’ sequence.

### 5 Conclusions

The algorithm for scrambling the Sobol’ sequence is proposed in this approach. Also, the characteristics of impractical choices of total dimensions that negatively impact the quality of this sequence are here referred to as practical choices. The quality of the Sobol’ sequence through scrambling is significantly improved. The proposed algorithm and the improved Sobol’ sequence through the scrambled family are applied to this sequence to evaluate a complete security and fund performance results. The high dimensionality has shown the performance of the Sobol’ sequence generated by our algorithm empirically to be far superior to the original sequence. The performance results prompt us to use more applications to test the sequences and to reach for more general scrambling techniques for the Sobol’ sequence.

### References

1. E. Atanassov. A new efficient algorithm for generating the scrambled sobol’ sequence. In *Numerical Methods and Applications (LNCS 2542)*, pages 81–90, New York, 2003. Springer-Verlag.

2. F. Black and M. Scholes. The pricing of options and corporate liabilities. *Journal of Political Economy*, **81**:637–659, 1973.
3. P. Boyle. New life forms on the option landscape. *Journal of Financial Engineering*, **2**(3):217–252, 1992.
4. P. Bratley and B. Fox. Algorithm 659: Implementing sobol’*’*s quasirandom sequence generator. *ACM Trans. on Mathematical Software*, **14**(1):88–100, 1988.
5. J. Cheng and M.J. Druzdzel. Computational investigation of low-discrepancy sequences in simulation algorithms for bayesian networks. In *Uncertainty in Artificial Intelligence: Proceedings of the Sixteenth Conference (UAI-2000)*, pages 72–81, San Francisco, CA, 2000. Morgan Kaufmann Publishers.
6. H. Chi, M. Mascagni, and T. Warnock. On the optimal Halton sequences. *Mathematics and Computers in Simulation*, To appear, 2005.
7. G. A. Fishman and L. R. Moore. An exhaustive analysis of multiplicative congruential random number generators with modulus  $2^{31} - 1$ . *SIAM J. Sci. Stat. Comput.*, **7**:24–45, 1986.
8. H. S. Hong and F. J. Hickernell. Algorithm 823: Implementing scrambled digital sequences. *ACM Transactions on Mathematical Software*, **29**(2):95–109, june 2003.
9. J. Hull. *Options, Future and Other Derivative Securtrities*. Prentice-Hall, New York, 2000.
10. P. Jackel. *Monte Carlo Methods in Finance*. John Wiley and Sons, New York, 2002.
11. S. Joe and F. Y. Kuo. Remark on Algorithm 659: Implementing Sobol’*’*s quasirandom sequence generator. *ACM Transactions on Mathematical Software*, **29**(1):49–57, March 2003.
12. D. E. Knuth. *The Art of Computer Programming, vol. 2: Seminumerical Algorithms*. Addison-Wesley, Reading, Massachusetts, 1997.
13. R. Lidl and H.Niederreiter. *Introduction to Finite Fields and Their Applications*. Cambridge University Press, Cambridge, 1994.
14. M. Mascagni. Parallel linear congruential generators with prime moduli. *Parallel Computing*, **24**:923–936, 1998.
15. M. Mascagni and H. Chi. Parallel linear congruential generators with Sophie-Germain moduli. *Parallel Computing*, **30**:1217–1231, 2004.
16. J. Matousek. On the l2-discrepancy for anchored boxes. *Journal of Complexity*, **14**:527–556, 1998.
17. B. Moro. The full monte. *Risk*, **8**(2) (February):57–58, 1995.
18. W.J. Morokoff and R.E. Caflish. Quasirandom sequences and their discrepancy. *SIAM Journal on Scientific Computing*, **15**:1251–1279, 1994.
19. A.B. Owen. Randomly permuted(t,m,s)-netsand (t,s)-sequences. *Monte Carlo and Quasi-Monte Carlo Methods in Scientific Computing*, **106** in Lecture Notes in Statistics:299–317, 1995.
20. S. H. Paskov and J. F. Traub. Faster valuation of financial derivatives. *J. Portfolio Management*, **22**(1):113–120, Fall 1995.
21. I.M. Sobol’. On the distribution of points in a cube and the approximate evaluation of integrals. *USSR Comput. Math. and Math. Phy.*, **7**(4):86–112, 1967.
22. I.M. Sobol’. Uniformly distributed sequences with additional uniformity properties. *USSR Comput. Math. and Math. Phy.*, **16**:236–242, 1976.
23. S. Tezuka. *Uniform Random Numbers, Theory and Practice*. Kluwer Academic Publishers, IBM Japan, 1995.

# Reconstruction Algorithm of Signals from Special Samples in Spline Spaces\*

U. A. Dega<sup>1,2</sup>

<sup>1</sup> Department of Mathematics, Zhejiang University,  
Hangzhou, 310027, P.R. China  
mathxj@163.com

<sup>2</sup> Information Engineering School, Jiaying University,  
Jiaying, 314001, P.R. China

**Abstract.** In this paper, we introduce integral sampling and study the reconstruction of signals based on non-uniform average samples in spline subspace. By using a new method, we obtain a new reconstruction formula.

## 1 Introduction

Digital signal and image processing, digital communication, etc., are usually represented and processed by using discrete samples. A band-limited signal fits the energy, its compactly characterized by its samples, and is described by the famous Nyquist sampling theorem. The remainder, the main application of sampling points are that a signal is regularly sampled, and may be a series of a signal  $f$  precise at times  $x_k$  for the error of the measurement apparatus. For the signal spaces, the band-limited signal fits the energy, the probability of the design of a interferometer, which the interferogram is obtained using a continuous moving mirror, but may have bearing on other problems, which the data are smoothed by a integrator series, such as a CC array. This response time compared to the sample integration, the reconstruction of signal from samples of its integration special shift in a spaces and band-limited spaces, spline subspaces, and many other things. The regular and numerical treatments that there are many practical applications for signal and image processing. In this paper, we discuss the reconstruction of signal from samples of its integration spline subspaces.

In the introduction of this paper, section 2, we introduce the concept of integration sampling and give the reconstruction formula from regular and irregular integration samples in spline subspaces. Section 3, numerical results are included. The conclusions are given in section 4.

---

\* This work is supported in part by the Mathematical Tianyuan Foundation and China Postdoctoral Science Foundation.

## 2 Reconstruction of Signal from Regular Incremental Integral Samples in Spline Subspaces

Suppose  $a$  and  $b$  are given constants that satisfy  $b - a \in \mathbb{Z}$ .

$$y_k = \int_{-\infty}^{k+b} f(t)dt, \quad y_{k-1} = \int_{-\infty}^{k+a} f(t)dt, \quad z_k = y_k - y_{k-1}.$$

We refer to  $\{z_k\}$  as the set of regular incremental samples. The problem is how to reconstruct the signal  $f$  from  $\{z_k\}$  (regular incremental samples). We will introduce some lemmas and a theorem that will be used in Section 2. In this paper, the Fourier transform of  $f$  is defined by  $f(\omega) = \int_{\mathbb{R}} f(x)e^{-ix\omega} dx$ . The space  $V_N = \left\{ \sum_{k \in \mathbb{Z}} c_k \varphi_N(\cdot - k) \mid \{c_k\} \in \ell^2 \right\}$  is spline subspace generated by  $\varphi_N = \chi_{[0,1]} * \dots * \chi_{[0,1]}$  ( $N$  convolutions),  $N \geq 1$ . It is well known that the space  $V_N$  is a special shift-invariant space.

**Lemma 2.1.** *Let  $y(t) = \int_{-\infty}^t f(x)dx$  and  $f \in V_N$ , then  $y \in V_{N+1}$ .*

**Theorem 2.1**<sup>[8]</sup>. *For arbitrary  $f \in V_N$ , we have*

$$f(x) = \sum_{k \in \mathbb{Z}} f\left(k + \frac{N+1}{2}\right) S(x - k),$$

where  $S(\omega) = \frac{\hat{\varphi}_N(\omega)}{\sum \varphi_N\left(k + \frac{N+1}{2}\right) e^{-ik\omega}}$  and  $V_N$  is spline subspace generated by  $\varphi_N = \chi_{[0,1]} * \dots * \chi_{[0,1]}$  ( $N \geq 1$  convolutions).

Theorem 2.1 and Lemma 2.1 have the following result.

**Theorem 2.2.** *Let*

$$y_k = \int_{-\infty}^{k+\frac{1}{2}+1} f(t)dt, \quad y_{k-1} = \int_{-\infty}^{k+\frac{1}{2}} f(t)dt, \quad z_k = y_k - y_{k-1}.$$

Then for any  $f \in V_N$ , we have reconstruction formula

$$f(t) = \sum_{k \in \mathbb{Z}} z_k h(t - k),$$

where  $h$  is defined by

$$h_k = h_{1k} + h_{k+1}, \quad h_1(\omega) = i\omega \frac{\varphi_{N+1}(\omega)}{\sum \varphi_{N+1}\left(k + \frac{N}{2} + 1\right) e^{-ik\omega}},$$

$h_k(\cdot) = h(\cdot - k)$  and  $h_{1k}(\cdot) = h_1(\cdot - k)$ .

Actually, Theorem 2.2 shows the reconstruction formula from regular incremental samples.  $V_N$  the regular incremental samples can be regarded as special weighted samples. The interpolation function  $h$  is multiplicative. This will be shown in Section 3.

### 3 Numerical Examples

the section, we give some numerical tests. We need a brief and applicable format of sampling function  $h$ . Here we use

the form  $h_k = h_{1k} + h_{k+1}$ , taking the Fourier transform of both sides of the above equation, we have the following equation

$$h(\omega) = \frac{h_1(\omega)}{-e^{-i\omega}}$$

Therefore, we give the following equation

$$h(\omega) = \frac{i\omega}{-e^{-i\omega}} \frac{\varphi_{N+1}(\omega)}{\sum \varphi_{N+1}(k + \frac{N}{2} + ) e^{-ik\omega}}$$

the inverse Fourier transform can be directly performed. Furthermore, let  $N = 3$ , we give some numerical tests. Here

$$h(\omega) = \frac{i\omega}{-e^{-i\omega}} \frac{e^{-\frac{4}{2}i\omega} (\frac{\sin \frac{\omega}{2}}{\frac{\omega}{2}})^4}{\frac{1}{48}e^{2i\omega} + \frac{23}{48}e^{i\omega} + \frac{1}{24}e^{-i\omega} + \frac{23}{48}}$$

we reconstruct the signal  $f(x) = \varphi_3(x) + 2\varphi_3(x - 1) + \varphi_3(x + 1) \in V_3$  from its integral samples  $\{z_k = \int_{k+\frac{1}{2}}^{k+\frac{3}{2}} f(t)dt\}$

It is obvious that  $supp f \subseteq [-1, 4]$ . We choose the sampling set, that is,  $k = -1, 0, 1, 2, 3, 4$ . We reconstruct the original signal from the samples. The integer points  $\{f(k)\}_{k=-1,0,1,2,3,4}$  are marked by "\*" in Figure 1. In fact,  $\{z_k = \langle f, u(\cdot - k) \rangle\}$  is the result of  $\{f(k)\}_{k=-1,0,1,2,3,4}$  perturbed by noise. The original signal samples  $\{z_k\}$  marked by "□" and are connected by a dashed line in Figure 1.

Figure 2 shows the reconstruction from the weighted sampling points  $\{z_k\}$ . In Figure 2, the original signal is represented by a continuous line. The reconstruction signal is represented by a dashed line. The original signal and the reconstruction signal are shown in Figure 2.

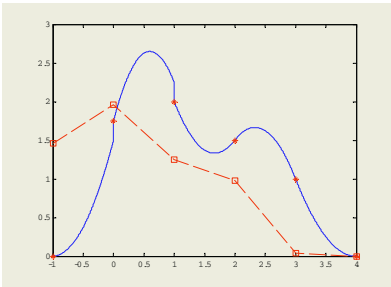


**Fig. 1.** The noisy signal sampling point  $\{z_k\}$  marked by "□" and connected by "-".  $\{f(k)\}_{k=-1,0,1,2,3,4}$  marked by "\*".

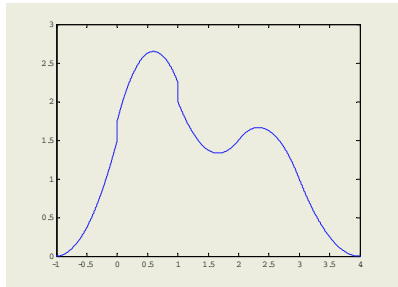


**Fig. 2.** The original signal is represented by continuous line. The reconstruction signal is represented by "-".



to measure the accuracy of the reconstructed signal, we compute the mean square error  $r(\mathbf{E})$  by the formula  $MSE = \sum_{t \in D} (f(t) - \sum_{k=-1}^4 z_k \varphi_3(t-k))^2$ , here  $D = \{-1, -0.5, 0, 0.5, 1, 1.5, 2, 2.5, 3, 3.5, 4\}$  is the set of the function  $f(t)$  samples.

The graph of the reconstructed signal is a smooth detour of the graph of the original signal. Figure 2 illustrates the behavior.

## 4 Conclusion

In this paper, we introduce the concept of tetra sampling here as a signal sampled reconstructed from the samples of the tetra of the signal. The perfect reconstruction formula is obtained in the case of regular sampling. The special Fourier transforms are successfully generalized. Our empirical demonstration results indicate the mathematical sufficiency of the proposed method.

## References

1. Aldroubi, A., Gröchenig, K.: Beuling-Landau-type theorems for non-uniform sampling in shift invariant spline spaces. *J. Fourier. Anal. Appl.* **6** (2000) 93-103
2. Aldroubi, A., Gröchenig, K.: Non-uniform sampling and reconstruction in shift-invariant spaces, *SIAM Rev.* **43** (2001) 585-620, .
3. Aldroubi, A., Unser, M., Eden, M.: Cardinal spline filters: Stability and convergence to the ideal sinc interpolator. *Singal. Processing.* **28** (1992) 127-138
4. Chui, C. K.: *An introduction to Wavelet*, Academic Press, New York, 1992
5. Jerri, A. J.: *The Gibbs phenomenon in Fourier analysis, splines and wavelet approximations*. Mathematics and its Applications, 446. Kluwer Academic Publishers, Dordrecht, 1998.
6. Gröchenig, K., Janssen, A., Kaiblinger, N., Norbert, P.: Note on  $B$ -splines, wavelet scaling functions, and Gabor frames. *IEEE Trans. Inform. Theory.* **49(12)** (2003) 3318-3320
7. Liu, Y.: Irregular sampling for spline wavelet subspaces. *IEEE Trans. Inform. Theory.* **42** (1996) 623-627
8. Sun, W. C., Zhou, X. W.: Average sampling in spline subspaces. *Appl. Math. Letter.* **15** (2002) 233-237
9. Sun, W. C., Zhou, X. W.: Reconstruction of bandlimited signals from local averages. *IEEE Trans. Inform. Theory.* **48** (2002) 2955-2963
10. Unser, M., Blu, T.: Fractional splines and wavelets. *SIAM Rev.* **42(1)** (2000) 43-67
11. Van De Ville, D., Blu, T., Unser, M., etc.: Hex-splines: a novel spline family for hexagonal lattices. *IEEE Trans. Image Process.* **13(6)** (2004) 758-772
12. Walter, G. G.: Negative spline wavelets. *J. Math. Anal. Appl.* **177(1)** (1993) 239-253
13. Wang, J.: Spline wavelets in numerical resolution of partial differential equations, International Conference on Wavelet Analysis and its application, AMS/IP Studies in Advanced Mathematics. **25** (2002) 257-276

14. Xian, J., Lin, W.: Sampling and reconstruction in time-warped spaces and their applications. *Appl. Math. Comput.* **157(1)** (2004) 153-173
15. Xian, J., Luo, S. P., Lin, W.: Improved A-P iterative algorithm in spline subspaces. *Lecture Notes in Computer Science.* **3037** (2004) 60-67

# Fast In-place Integer Radix Sorting

Fouad El-Aker

Computer Science Department, University of Petra,  
P.O. Box 940650, Amman 11194, Jordan  
elaker\_fouad@maktob.com  
elaker\_fouad@yahoo.ca

**Abstract.** This paper presents two very efficient sorting algorithms. MSL is an  $O(N*B)$  in-place radix sorting algorithm, where  $N$  is the input size and  $B$  is the keys length in bits. This paper presents an implementation of MSL that is sub-linear in practice, for uniform data, on Pentium 4 machines. We also present an  $O(N*logN)$  hybrid quicksort that has a non-quadratic worst case.

## 1 Introduction

Right to left LSD and left to right MSD are  $O(N*B)$  radix sorting algorithms.  $N$  is the input size and  $B$  is the length of keys in bits. LSD and MSD use an extra space of size  $N$ . ALR [4] and MSL [1] process bits left to right, however unlike MSD, ALR and MSL are in-place and cache friendly. MSD, ALR and MSL execute recursively, for every partition. LSD body code is executed only  $B/D$  times, where  $B$  is the length of keys in bits and  $D$  is the used digit size. This makes the design of algorithms faster than LSD quite difficult. LSD is faster than MSD in [6]. We present a sub-linear run time MSL implementation suitable for sorting 31 bits and 63 bits integers in Java in this paper. MSL implementation in Section 2 uses small digit sizes increasing data cache friendliness. MSL loops were implemented reducing the number of instructions, and therefore increasing instruction cache friendliness. In addition, section 3 presents a non-quadratic implementation of quicksort, called switch sort. Hybridizing switch sort and MSL does not improve over MSL. Section 4 presents the test results. Section 5 gives the conclusions and future work.

## 2 MSL and Smaller Digit Sizes

MSL and ALR use a permutation loop in order to avoid reserving an extra array of size  $N$ , which is performed in MSD. The main steps of MSL are presented in [1]. MSL permutation loop, shuffles keys into their target groups. In the circular list of keys,  $K = \langle K_1, K_2, \dots, K_L \rangle$ , assume the Target Address ( $K_J$ ) = Array Location ( $K_{J+1}$ ), where  $J$  is not equal to  $L$ , and Target Address ( $K_L$ ) = Array Location ( $K_1$ ). Digit extraction and group end address lookup are used in computing a key's target address. MSL permutation loop moves keys in a circular list  $K$  to their target addresses.  $K_1$  is named the initial key in  $K$ , and is computed prior to the permutation loop.

Many permutation loops are required in order to shuffle all keys in a group to their target addresses. ALR searches for  $K_1$  sequentially, and preserves the property that all keys to the left of the current  $K_1$  key are in their correct target addresses. MSL searches groups' information sequentially for the left most group,  $G_{Left}$ , which has at least one key possibly not in its target address. MSL uses the top key in  $G_{Left}$ , as  $K_1$ .

In [5], sections 4 and 5, digit size 6 was determined as appropriate for radix sorting algorithms. This is because of data cache friendliness. The importance of cache friendliness in radix sorting algorithms is emphasized in [5] and [4]. MSL also cuts to insertion sort for group sizes 20 or less, same as [4].

### 3 Switch Sort

Hybridized quicksort [3] implementation in this paper selects one from many pivot computations and is described in this section. Assume that we are interleaving the execution of a constant number,  $K$ , of divide and conquer algorithms whose worst cases are  $f_1, f_2, \dots, f_K$ . The list of algorithms is denoted  $AL = (A_1, A_2, \dots, A_K)$ . When  $A_j$  in  $AL$  performance is degenerate, we interrupt  $A_j$  and switch execution to the next algorithm in the circular list  $AL$ .  $AL$  worst case is equal to  $K * f_w$  provided that the following conditions hold. (1)  $f_w = \text{Min}(f_1, f_2, \dots, f_K)$ . (2) We can determine that the current call to  $A_j$  is futile in constant time. (3) We can switch execution to the next algorithm in the circular list  $AL$  without losing the processing done so far. If each  $A_j$  in  $AL$  executes a futile call, execution returns to  $A_w$  after circular calls to other algorithms in  $AL$ . A quicksort example is shown and described next.

```

SS(int A[], int A_Pivot, int l, int r, int min, int
max) {
if ( r - l + 1 <= 10 ) insertionSort (Array, l, r );
} else { Step 1: switch (Apply_Pivot) {
case 0 : Pivot = max/2 + min/2 ; break;
case 1: Pivot = Median_3 (A) ; break; }
Step 2: Pos = partition (A, Pivot, l, r) ;
Step 3.1: Compute R%;
Step 3.2: if (R < 0.05) A_Pivot = A_Pivot ^1; // xor
Step 4: Quicksort(A, A_Pivot, l, Pos, Pivot,
max);
Quicksort(A, A_Pivot, Pos+1, r, min, Pivot);
}
}

```

We measure balanced partitioning in quicksort to determine that the current call is futile. The partitioning ratio is defined as the size of the smaller partition divided by the size of the input group in quicksort. Let  $P\%$  be the minimum acceptable partitioning ration, over all the algorithms in  $AL$ , equals 5% in Step 3.2.  $R\%$  is the partitioning ration for the current quicksort call. When  $R\% < P\%$ , Step 3.2, partitioning is named degenerate or a failure.  $AL$  code above has only quicksort implementations, and a switch statement is used to decide which pivot computation to use, see Step 1 above. We call the algorithm switch sort (SS). Step 3.2 selects an alternative pivot computation for recursive calls. Max-Min average pivot computation in the first line in Step 1 is an adaptive implementation of taking the middle value of the input range in radix exchange [7]. Median of three quicksort passes down the actual lower partition max and the actual upper partition min. Radix exchange always divides the input range by half on recursive calls, independent of data.  $AL$  worst case is  $O(2 * NlgN)$ , where the worst case of radix exchange is  $O(2 * NlgN)$ .

### 4 Experimental Results

In Table 1, MSL run time is non-significantly sub-linear in experiments. The test data is uniform. The machine used for the displayed results is 3 GHz Pentium 4, 1GB RAM, 1MB level 2 cache, and 16 KB level 1 cache, with 400 MHz RAM speed. MSL sub-linear run time was confirmed on other Pentium 4 machines. In Table 1, add the sizes at columns headings to the sizes at each row to get the array size at a cell. Row 30M+ (30 millions+) and column +5M refer to the cell for the array size 35 millions.

In Table 1, MSL running time for array size 35 millions is 4000 milliseconds, and for array size 70 millions is 7875 milliseconds, 31 bits integers. In Table 1, the running time for array size 25 millions, is 4032 milliseconds, and for array size 50 millions, is 7735 milliseconds, for 63 bits integers.

Cutting to insertion sort is an important factor in MSL. On the other hand, we could not improve the running time of MSL by hybridizing MSL with switch sort. MSL and switch sort are compared against other algorithms in Table 2.

**Table 1.** MSL running times in milliseconds. Sizes are multiple of  $M=10^6$

<b>31Bits</b>	+1M	+2M	+4M	+5M	+6M	+8M	+10M
N=0+	93	188	437	657	890	1234	1469
N=10M+	1563	1671	1875	1984	2094	2266	2500
N=20M+	2578	2678	2891	2984	3078	3281	3484
N=30M+	3594	3703	3906	4000	4125	4344	4547
N=40M+	4671	4766	5000	5079	5218	5390	5625
N=50M+	5782	5875	6062	6172	6313	6532	6734
N=60M+	6890	6953	7172	7313	7453	7656	7875
<b>63Bits</b>	+1M	+2M	+4M	+5M	+6M	+8M	+10M
N=0+	141	250	594	843	1125	1531	1859
N=10M+	2016	2157	2485	2594	2765	3016	3281
N=20M+	3469	3578	3859	4032	4141	4438	4735
N=30M+	4860	5016	5328	5469	5625	5891	6203
N=40M+	6375	6500	6797	6953	7125	7406	7735

LSD, digit size 8 (LSD8) is faster than LSD with digit size 16, LSD16, and other digit sizes, on the test machine. LSD processes the total keys bits. MSL processes only the distinguishing prefixes, but is recursive (section 1). In Table 2, MSL has half the run time of LSD8 for 63 bits data. In addition, MSL is better than LSD8 for larger 31 bits arrays. See size 16 and 32 millions as well as MSL sub-linear run time in Table 1. Switch sort (SS), is faster than LSD16, 63 bits longs data. Switch sort is also faster than the two algorithms, which Switch sort alternates, quicksort and Max-Min Average (MMA). Java built in tuned quicksort (JS), which is a tuned implementation of [2], is used in Table 2, instead of our own slower median of three quicksort.

**Table 2.** MSL running times in milliseconds. Sizes are multiple of  $M=10^6$

<b>31Bits</b>	1/2M	1M	2M	4M	8M	16M	32M
MSL	47	93	188	437	1234	2094	3703
LSD8	47	109	234	454	938	1875	3859
LSD16	94	234	500	1031	2047	4250	8656
JS	109	234	516	1062	2219	4640	9672
SS	109	250	500	1031	2141	4500	9546
MMA	109	234	500	1031	2172	4516	9438
<b>63Bits</b>	1/2M	1M	2M	4M	8M	16M	32M
MSL	62	141	250	594	1531	2765	5016
LSD8	172	344	672	1328	2719	5563	10953
LSD16	250	516	1015	2031	4563	8609	18891
JS	156	329	672	1422	2969	6203	12922
SS	140	313	640	1344	2781	5860	12203
MMA	141	312	641	1360	2829	5906	12359

## 5 Conclusion and Future Work

MSL is a sub-linear in-place radix-sorting algorithm, for uniform data. Switch sort is a non-quadratic implementation of quicksort. Future work includes low run time algorithms and models for sorting as well as for other problems.

## References

1. Al-Badarneh Amer, El-Aker Fouad: Efficient In-Place Radix Sorting, Informatica, 15 (3), 2004, pp. 295-302.
2. J. L. Bentley, and M. D. McIlroy: Engineering a Sort Function, Software-Practice and Experience, 23 (1), 1993, pp. 1249-1265.
3. F. El-Aker, and A. Al-Badarneh: MSL: An Efficient Adaptive In-place Radix Sorting Algorithm, ICCS, Part II, 2004, pp. 606-609.
4. Maus, A.: ARL: A Faster In-place, Cache Friendly Sorting Algorithm, Norsk Informatikkonferanse, NIK'2002, 2002, pp. 85-95.
5. N. Rahman and R. Raman: Adapting radix sort to the memory hierarchy, Proc. 2<sup>nd</sup> Workshop on Algorithm Engineering and Experiments, ALENEX, 2000.
6. Sedgewick, R.: Algorithms in Java, Parts 1-4, 3<sup>rd</sup> Ed., Addison-Wesley, 2003.

# Dimension Reduction for Clustering Time Series Using Global Characteristics

Xiaozhe Wang<sup>1</sup>, Kate A. Smith<sup>1</sup>, and Rob J. Hyndman<sup>2</sup>

<sup>1</sup> Faculty of Information Technology, <sup>2</sup> Department of Econometrics and Business Statistics, Monash University, Clayton, Victoria 3800, Australia  
{catherine.wang, kate.smith}@infotech.monash.edu.au  
rob.hyndman@buseco.monash.edu.au

**Abstract.** Existing methods for time series clustering rely on the actual data values can become impractical since the methods do not easily handle dataset with high dimensionality, missing value, or different lengths. In this paper, a dimension reduction method is proposed that replaces the raw data with some global measures of time series characteristics. These measures are then clustered using a self-organizing map. The proposed approach has been tested using benchmark time series previously reported for time series clustering, and is shown to yield useful and robust clustering.

## 1 Introduction

Clustering time series has become an important topic in data mining [1,3], motivated by several research challenges including similarity searching of bioinformatics sequences. This paper focuses on “whole clustering” [2] using a variety of statistical measures to capture the time series global characteristics, which departs from the common methods of clustering time series based on distance measures applied to the actual values [1,2]. The proposed method seeks to provide a novel method for clustering time series with high dimensionality, varying lengths, and missing value. The dimension reduction is performed by a feature extraction process. These features are: trend, seasonality, serial correlation, non-linearity, skewness, kurtosis, self-similarity, and chaos. For additional dimension reduction and visualization, a self-organizing map (SOM) is used to cluster the features. A total of 15 measures are calculated (9 on the ‘raw’ data and 6 on the ‘decomposed’ data) and fed into the clustering process.

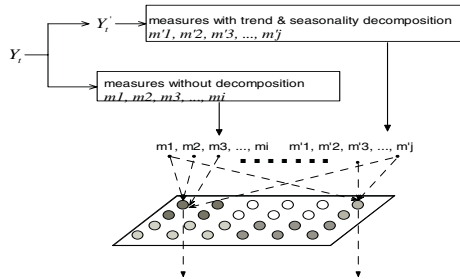


Fig. 1. Method framework with neural network SOM architecture for clustering

## 2 Measuring Characteristics of Time Series

A time series is the simplest form of temporal data and is a sequence of real numbers collected regularly in time, denoted as  $Y_1, \dots, Y_n$ . For each of the features, we attempted to find the most appropriate way to measure the presence of the feature, ultimately scaling the metric to (0,1) to indicate the degree of presence of the feature.

- **Trend and seasonality** are common features of time series, and it is natural to characterize a time series by its degree of trend and seasonality. Once the trend and seasonality of a time series have been measured, we can de-trend and de-seasonalize the time series to enable additional features such as noise or chaos to be more easily detected. We have used the basic decomposition model in [4]:

- $Y_t^* = T_t + S_t + e_t$ , where  $Y_t^* = f_\lambda(Y_t)$ ,  $f_\lambda(u) = (u^\lambda - 1) / \lambda$  denotes a Box-Cox transformation,  $T_t$  denotes the trend at time  $t$  and  $S_t$  denotes the seasonal component at time  $t$ ; The parameter  $\lambda$  is chosen to make  $e_t$  as normal as possible. Where the minimum of  $\{Y_t\}$  is non-negative, we choose  $\lambda \in (-1, 1)$  to minimize the Shapiro-Wilk statistic.
- For seasonal data, the decomposition uses the STL procedure with fixed seasonality. If the data are nonseasonal,  $S_t = 0$  and  $T_t$  is estimated using a penalized regression spline with smoothing parameter chosen using crossvalidation; The detrended data is  $Y_t' = f_\lambda^{-1}(Y_t^* - \hat{T}_t)$ , the deseasonalised data is  $Y_t'' = f_\lambda^{-1}(Y_t^* - \hat{S}_t)$  and the detrended and deseasonalised data is  $Y_t''' = f_\lambda^{-1}(Y_t^* - \hat{T}_t - \hat{S}_t)$  where  $\hat{T}_t$  and  $\hat{S}_t$  denote the trend and seasonal estimates.
- The measures of trend and seasonality are:  $1 - \text{Var}(Y_t') / \text{Var}(Y_t)$  and  $1 - \text{Var}(Y_t'') / \text{Var}(Y_t)$

- The **periodicity** of the seasonal pattern is used as an additional measure. We measure the period using the following algorithm:

- Detrend time series using a regression spline with 3 knots.
- Find  $r_k = \text{Corr}(Y_t, Y_{t-k})$  (autocorrelation function) for all lags  $k$  up to 1/3 of series length. And look for peaks and troughs in autocorrelation function.
- Frequency is first peak provided: a) there is also a trough before it, b) the difference between peak and trough is at least 0.1, c) the peak corresponds to positive correlation.
- If no such peak is found, frequency is set to 1.

- To measure the degree of **serial correlation** of the data set, we use  $Q_h$  the Box-

Pierce statistic [4] where  $Q_h = n \sum_{k=1}^h r_k^2$ .

- To measure **non-linear autoregressive structure**, nonlinear time series models have been used extensively in recent years to model complex dynamics not adequately represented using linear models [5]. We have used Teräsvirta's neural network statistic for nonlinearity [6].
- **Skewness** is a measure of lack of symmetry and **kurtosis** is a measure of a distribution's peakedness. For the standard normal distribution, the skewness and kurtosis are both zero. For univariate data  $Y_t$ , the skewness coefficient is



$$s = n^{-1} s^{-3} \sum_{t=1}^n (Y_t - \bar{Y})^3 \text{ and the kurtosis coefficient is } K = n^{-1} s^{-4} \sum_{t=1}^n (Y_t - \bar{Y})^4 - 3,$$

where  $\bar{Y}$  is the sample mean and  $s$  is the sample standard deviation.

- Processes with **long-rang dependence** have attracted a good deal of attention from probabilists and theoretical physicists. The definition of **self-similarity** most related to the properties of time series is the self-similarity parameter or Hurst exponent ( $H$ ).  $H$  is estimated using  $H=d+0.5$  by a class of fractional autoregressive integrated moving-average (FARIMA) processes of FARIMA(0, $d$ ,0) by maximum likelihood [7].
- Nonlinear dynamical systems often exhibit **chaos**, which is characterized by a Lyapunov Exponent (LE). For a one-dimensional discrete time series, we used the method by Hilborn [8] to calculate LE:

- We consider the rate of divergence of nearby points in the series by looking at the trajectories  $h$  periods ahead. Suppose  $Y_j$  and  $Y_i$  are two points such that  $|Y_j - Y_i|$  is small. Then we define  $\lambda(Y_i, Y_j) = h^{-1} \log |Y_{j+h} - Y_{i+h}| / |Y_j - Y_i|$ .
- We estimate the Lyapunov exponent of the series by averaging these values over all  $i$ :  $\lambda = n^{-1} \sum_{i=1}^n \lambda(Y_i, Y_j)$ , where  $Y_j$  is the closest point to  $Y_i$  such that  $i \neq j$ . Scaling transformations

In order to present the clustering algorithm with scaled data in the (0,1), we perform a statistical transformation of the data. For example, to map the correlation measure  $Q$  in the range  $(0, \infty)$  to a scaled value  $q$  in the range  $(0,1)$  we use the transformation:  $q = (e^{aQ} - 1) / (b + e^{aQ})$ , where  $a$  and  $b$  are constants chosen so that  $q$  satisfies the following conditions:  $q$  has 90th percentile of 0.10 when  $Y_t$  is standard normal white noise and  $q$  has value of 0.9 for a well-known benchmark data set.

### 3 Clustering and Experimental Evaluation

The central property of SOM is that it forms a nonlinear projection of a high-dimensional data manifold on a regular, low-dimensional (usually 2D) grid [9]. The clustered results can show the data clustering and metric-topological relations of the data items. It has a very powerful visualization output and is useful to understand the mutual dependencies between the variables and data set structure.

To determine the effectiveness of the measures in the proposed approach, we used the time series clustering benchmark datasets, “Reality check Dataset” ([www.cs.ucr.edu/~eamonn/TSDMA](http://www.cs.ucr.edu/~eamonn/TSDMA)). The data contains 14 time series of 1000 points in each which normalized into (0,1). Then 15 measures extracted from the data are used as inputs to the SOM. To compare with the benchmarking clusters generated using hierarchical clustering of the raw data points, we re-interpreted the clusters generated by the SOM into a hierarchical structure in (Fig. 2 right). Compared to the hierarchical clustering result (Fig. 2 left) [2], similar clusters have been obtained from our approach. But our clustering results are arguable better, or at least more intuitive. For example, series 1&4 and 9&10 have been grouped far from each other based on the hierarchical clustering using actual points (Fig. 2 left), but a visual inspection of these

series shows that they are actually quite similar in character. Using the global measures as inputs, the clustering algorithm is aware of the “whole picture” and recognizes the similarity of these four time series (Fig. 2 right).

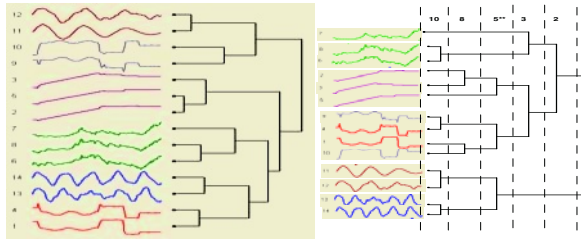


Fig. 2. Clustering results using hierarchical representation (left) and SOM (right)

## 4 Conclusions and Future Research

In this paper, we have proposed a new method for time series clustering and compared the results to a benchmarked time series clustering data. The empirical results demonstrate that our proposed clustering approach is able to cluster time series with high dimensionality, varying lengths, and missing value. Using only a finite set of global measures as input for clustering, we can still achieve useful clustering. In fact, the knowledge provided to the clustering algorithm by the global measures appears to benefit the quality of the clustering results. In future, a more comprehensive metrics to summarize the time series features will be explored and applied to more datasets.

## References

- Bradley, P. S., Fayyad, U. M.: *Refining Initial Points for K-means Clustering*. In: the 15th international conference on machine learning, Madison, (1998).
- Keogh, E., Lin, J., Truppel, W.: *Clustering of Time Series Subsequences is Meaningless: Implications for Past and Future Research*. In: the 3rd IEEE International Conference on Data Mining, Melbourne.
- Wang, C., & Wang, X. S.: *Supporting Content-based Searches on Time Series via Approximation*. In: the 12th international conference on scientific and statistical database management, Berlin, (2000).
- Makridakis, S., Wheelwright, S. C., Hyndman, R. J.: *Forecasting Methods and Applications* (3rd Ed.): John Wiley & Sons, Inc., (1998).
- Harvill, J. L., Ray, B. K., Harvill, J. L.: *Testing for Nonlinearity in a Vector Time Series*. *Biometrika*, 86, (1999), 728-734.
- Blake, A. P., Kapetanios, G.: A Radial Basis Function Artificial Neural Network Test for Neglected Nonlinearity. *The Econometrics Journal*, 6(2), (2003), 357-373.
- Haslett, J., & Raftery, A. E.: *Space-Time Modelling with Long-Memory Dependence: Assessing Ireland's Wind Power Resource* (With Discussion). *Applied Statistics*, 38, (1989), 1-50.
- Hilborn, R. C.: *Chaos and Nonlinear Dynamics: an Introduction for Scientists and Engineers*. New York: Oxford University Press, (1994).
- Kohonen, T.: *Self-Organizing Maps* (Vol. 30): Springer Verlag, (1995).

# On Algorithm for Estimation of Selecting Core\*

Ug. H<sup>1</sup>, S. G. M<sup>1</sup>,  
U. G. Ch. A. G<sup>2</sup>, A. D. U. S. G. Ch. <sup>1</sup>

<sup>1</sup> School of Information and Communication Engineering,  
Sungkyunkwan University, 440-746, Suwon, Korea +82-31-290-7145  
watchman@skku.edu

{moonseong, choo}@ece.skku.ac.kr

<sup>2</sup> Department of Computer Engineering,  
Korea Polytechnic University, 429-793, Gyeonggi-Do, Korea +82-31-496-8292  
ybang@kpu.ac.kr

**Abstract.** With the development of the multicast technology, the real-time strategy among the group applications using the multicast routing is getting more important. An essential factor of these real-time applications is to optimize the Delay- and delay Variation-Bounded Multicast Tree (DVBMT) problem. In this paper, we propose Estimation of Selecting Core (ESC) algorithm for DVBMT solution. Furthermore, it is expected that ESC algorithm results in the better any other DVBMT solutions.

## 1 Introduction

In the transmission network, the tree cost as a measure of bandwidth efficiency is one of the important factors, but as network supports great multimedia traffic are required to receive messages from source node. A multimedia network here refers to consider the multicast end-to-end delay. A delay-aware algorithm proposed in this paper, we study the delay-aware algorithm under the upper bound of the multicast end-to-end delay. We propose an efficient algorithm to compare with the existing delay-aware algorithm. Cost-strategy algorithm (ESC) is known as the best algorithm so far. Efficiency of the time complexity of our algorithm is same as the efficiency of ESC, the proposed algorithm is said to have the better performance than ESC in terms of the multicast delay-aware. The rest of the paper is organized as follows. Section 2, we state the network model for the multicast routing and the problem formulation. Section 3 presents the details of the proposed algorithm. Section 4 concludes this paper.

## 2 Network Model for Multicasting and DVBMT

We consider that a computer network is represented by a directed graph  $G(V, E)$  with  $n$  nodes and  $l$  links or arcs, where  $V$  is a set of nodes and  $E$  is a set

---

\* This work was supported in parts by Brain Korea 21 and the Ministry of Information and Communication in Republic of Korea. Dr. H. Choo is the corresponding author.

links, respectively. Each link  $e = (i, j) \in E$  is associated with delay  $d(e) \geq 0$ . The delay of a link,  $d(e)$ , is the sum of the perceived queueing delay, transmission delay, and propagation delay. We define a path as sequence of links such that  $(u, i), (i, j), \dots, (k, v)$ , belongs to  $E$ .

Let  $P(u, v) = \{(u, i), (i, j), \dots, (k, v)\}$  denote the path from node  $u$  to node  $v$ . If  $u, i, j, \dots, k, v$  are distinct, then we say that this is a simple directed path. For a given source node  $s \in V$  and a destination node  $d \in V, (2^{s \rightarrow d}, \infty)$  is the set of all possible paths from  $s$  to  $d$ .

$$(2^{s \rightarrow d}, \infty) = \{ P_k(s, d) \mid \text{all possible paths from } s \text{ to } d, \forall s, d \in V, \forall k \in \Lambda \}$$

here  $\Lambda$  is a finite set. The path delay of  $P_k$  is given by  $\phi_D(P_k) = \sum_{e \in P_k} d(e)$ .  $\forall P_k \in (2^{s \rightarrow d}, \infty)$   $(2^{s \rightarrow d}, \Delta)$  is the set of paths from  $s$  to  $d$  for which the end-to-end delay is bounded by  $\Delta$ . Hereafter  $(2^{s \rightarrow d}, \Delta) \subseteq (2^{s \rightarrow d}, \infty)$ .

For the multicast communication, messages need to be delivered to all receivers in the set  $M \subseteq V \setminus \{s\}$  which is called the multicast group, here  $|M| = m$  the path traversed by messages from the source  $s$  to a multicast receiver,  $m_i$ , is given by  $P(s, m_i)$ . Thus multicast routing tree can be defined as  $T(s, M) = \bigcup_{m_i \in M} P(s, m_i)$  and the messages are sent from  $s$  to  $M$  through  $T(s, M)$ .

The multicast end-to-end delay delay bound,  $\Delta$ , represents an upper bound on the acceptable end-to-end delay along a path from source to a destination. Let the multicast delay at node  $\delta$ , is the maximum difference between the end-to-end delay along the paths from the source to all destinations.

$$\delta = \max\{ |\phi_D(P(s, m_i)) - \phi_D(P(s, m_j))|, \forall m_i, m_j \in M, i \neq j \}$$

The issue defined and discussed in [2] is that, since the minimum multicast delay is achieved under multicast end-to-end delay bound, the authors referred to this problem as *end-to-end delay bounded multicast tree* (EBMT). The problem here is to find the tree that satisfies

$$\min\{ \delta_\alpha \mid \forall P(s, m_i) \in (2^{s \rightarrow m_i}, \Delta), \forall P(s, m_i) \subseteq T_\alpha, \forall m_i \in M \forall \alpha \in \Lambda \},$$

here  $T_\alpha$  denotes a multicast tree spanning  $M \cup \{s\}$ .

### 3 The Proposed ESC Algorithm

**Description of ESC Algorithm:** We designate the proposed algorithm as Estimation of Selecting Core (ESC). The ESC algorithm gives a perspective about the problem. We define the *MODE* function, since the calculation of the core requires the multicast delay at each node, add to the *MODE* function, we measure the delay at each node using the *CMP* function. The *MODE* and *CMP* functions are defined as follows.

$$MODE(c) \begin{cases} \text{if } c = s \\ \text{if } \exists m \in M . P(s, c), \text{ here } \forall m \in M \\ \text{if } \exists s \in M . P(m, c), \text{ here } \forall m \in M, \\ \text{if } a \text{ d} \\ \text{otherwise} \end{cases}$$

here  $s$  is source node

$$CMP(x) \begin{cases} |(ds_{core} + max\_delay) - ds_{m_k}| & \text{if } x \text{ is a core node} \\ dv_{core} & \text{otherwise} \end{cases}$$

here  $core = MODE^{-1}(x)$ ,  $max\_delay = \max\{\min\{\phi_D(P(core, m))\} \mid \forall m \in M \setminus \{m^* \in M \mid \exists m^* . P(s, core) \vee \exists s . P(m^*, core)\}\}$  and  $ds_{v_i}$  and  $dv_{v_i}$  are defined as follows

```

Proposed Algorithm ( $G(V, E), M, s, \Delta$ )
Input: A directed graph  $G(V, E)$ ,  $M$  is the multicast group with  $m = |M|$ ,
a source node  $s$ , a end-to-end delay bound  $\Delta$ .
Output: The multicast tree  $T$  such that  $\phi_D(P(s, m_i)) \leq \Delta$ ,
 $\forall P(s, m_i) \subseteq T, \forall m_i \in M$ , and has a small multicast delay variation.
01. Begin
02.  $dt_{min} = \infty$ ;  $core = \emptyset$ ;  $candidate = \emptyset$ ;  $compare = \infty$ ;  $T = \emptyset$ ;
/*  $candidate$  : candidates of a core node */
/*  $compare$  : measure for the 5 modes */
03. For  $\forall v_i \in V$  Do
04.  $ds_{v_i} = \min\{\phi_D(P) \mid \forall P \in (2^{s-v_i}, \infty)\}$ ;
05.  $ds\_pred_{v_i} = v$  s.t.  $(v, v_i) \in P(s, v_i)$  with  $ds_{v_i}$ ;
06. For  $\forall m_k \in M$  Do
07.  $ppd(m_k, v_i) = \min\{\phi_D(P) \mid \forall P \in (2^{m_k-v_i}, \infty)\}, \forall v_i \in V$ ;
08.  $dest\_pred(m_k, v_i) = v$  s.t.  $(v, v_i) \in P(m_k, v_i)$  with  $ppd(m_k, v_i), \forall v_i \in V$ ;
09. For  $\forall v_i \in V$  Do
10.  $max_i = \max\{ppd(m_k, v_i) \mid \forall m_k \in M\}$ ;
11.  $min_i = \max\{ppd(m_k, v_i) \mid \forall m_k \in M\}$ ;
12.  $dv_{v_i} = max_i - min_i$ ;
13. If  $dv_{v_i} < dt_{min}$  and  $ds_{v_i} + max_i \leq \Delta$ 
14. then  $dt_{min} = dv_{v_i}$ ;  $core = v_i$ 
15. If  $core = \emptyset$  then  $\beta T$ 
16. For  $\forall v_i \in V$  Do
17. If  $dv_{v_i} = dv_{core}$  and  $ds_i + max_i \leq \Delta$ 
18. then  $candidate = candidate \cup v_i$ ;
19. For  $\forall c \in candidate$  Do
20. If  $CMP(MODE(c)) < compare$ 
21. then  $compare = CMP(MODE(c)); core = c$ ;
22. For  $\forall m_k \in M$  Do
23.  $T = T \cup P(core, m_k)$ ;
24.  $T = T \cup P(s, core)$ ;
25. Return  $T$ 
26. End Algorithm.
    
```

Fig. 1. Pseudo Code of ESC Algorithm

... g... es 2 g... es a... acc. u... t... f... the pr... cess... t... search the su... tab... e... c... re... de... G... g... a... spec... ficat... .. e... .. p... cks... ut... the m... .. m... .. um...  $dv_{v_i}$ , c... m... p... .. g... the d... .. e... .. ce... .. bet... .. ee... .. the m... .. a... .. x... .. um... .. de... .. a... .. r... .. at... .. .. a... .. d... .. the m... .. m... .. um... .. de... .. a... .. r... .. at... .. .. f... .. r... .. e... .. a... .. c... .. h... .. e... .. f... .. g... .. the u... .. p... .. b... .. u... .. d... ..  $\Delta$ ... .. f... .. there... .. s... .. 't... .. such... .. a... .. c... .. re... .. de... .. the... .. a... .. g... .. r... .. th... .. m... .. .. be... .. term... .. in... .. at... .. ed... .. because... .. the... .. mu... .. t... .. cast... .. tree... .. ca... .. n... .. ot... .. be... .. c... .. on... .. struct... .. ed... .. th... ..  $\Delta$ ... .. .. es... .. 8, E... .. C... .. a... .. g... .. r... .. th... .. m... .. st... .. res... .. the... .. ca... .. d... .. date... .. c... .. res... .. after... .. .. k... .. g... .. f... .. r... .. the... .. .. de... .. h... .. ch... .. has... .. the... .. same... .. .. a... .. ue... .. as... .. m... .. m... .. um... ..  $dv_{v_i}$ ... .. es... .. 2... .. fi... .. ds... .. ut... .. the... .. best... .. c... .. re... .. that... .. has... .. the... .. m... .. m... .. um... .. de... .. a... .. r... .. at... .. .. us... .. g... .. the... .. measure... ..  $CMP$ ... .. f... .. r... .. the... .. m... .. des... .. these... .. cases... .. are... .. descr... .. bed... .. as... .. f... .. ... .. s... .. he... .. t... .. ta... .. t... .. me... .. c... .. m... .. p... .. e... .. t... .. .. f... .. the... .. pr... .. p... .. osed... .. a... .. g... .. r... .. th... .. m... .. s... ..  $O(mn^2)$ , be... .. g... .. equ... .. at... .. .. C

**Five-Mode Core Selection:** s absolute function  $MODE$  and  $CMP$ ,  $MODE$  is that the core, delay, respectively, the source, delay, this case,  $CMP$  keeps  $dv_{core}$ . Otherwise,  $MODEs \sim$  are executed

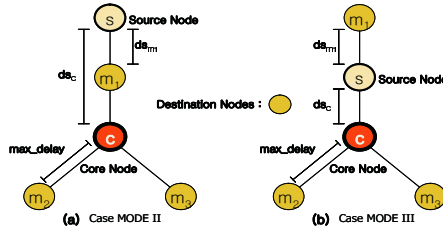


Fig. 2. Main Idea of Mode Function

In the case of  $MODE$ , Fig. 2 (a) shows that there exists the destination delay from the source to the core of  $CMP$  which can be computed stores the sum of the delay from the core to the destination delay and  $max\_delay$ . In the third case just satisfies  $MODE$ . In this case, EC algorithm takes adds the delay from the source to the core delay and subtracts the delay from the source to the adjacent destination delay and stores the value. In  $CMP$  if the value is negative,  $CMP$  accepts the absolute value. In the fourth case, OE which satisfies and should find the factor that determine  $CMP$ , having a guarantee that the destination delay is under the source delay. The measure of the comparison is determined with the minimum delay from the source to the associated destination. Since each of these is true because the shortest delay value from the source affects the delay at the root of the created tree. Therefore, EC algorithm selects either  $MODE$  or  $MODE$ . If EC algorithm does not satisfy  $MODEs \sim$ ,  $CMP$  stores  $dv_{core}$ .

### 4 Conclusion

In this paper, we consider the transmission of a message that guarantees certain bounds of the end-to-end delay as well as the multicast delay. In a computer network, the time complexity of EC algorithm is  $O(mn^2)$ , which is the same as that of C. Furthermore, it is expected that EC algorithm results in the better minimum multicast delay than C.

### References

1. M. Kim, Y.-C. Bang, and H. Choo, "Efficient Algorithm for Reducing Delay Variation on Bounded Multicast Trees," Springer-Verlag Lecture Notes in Computer Science, vol. 3090, pp. 440-450, September 2004.

2. G. N. Rouskas and I. Baldine, "Multicast routing with end-to-end delay and delay variation constraints," *IEEE JSAC*, vol. 15, no. 3, pp. 346-356, April 1997.
3. P.-R. Sheu and S.-T. Chen, "A fast and efficient heuristic algorithm for the delay- and delay variation bound multicast tree problem," *Information Networking, Proc. ICOIN-15*, pp. 611-618, January 2001.

# A Hybrid Mining Model Based on Neural Network and Kernel Smoothing Technique

Defu Zhang, Qingshan Jiang, and Xin Li

Department of Computer Science, Xiamen University, 361005, China  
dfzhang@xmu.edu.cn

**Abstract.** Neural networks as data mining tools are becoming increasingly popular in business. In this paper, a hybrid mining model based on neural network and kernel smoothing technique is developed. The kernel smoothing technique is used to preprocess data and help decision-making. Neural network is employed to predict the long trends of stock price. In addition, some trading rules involving trading decision-making are considered. The China Shanghai Composite Index is as case study. The return achieved by the hybrid mining model is four times as large as that achieved by the buy and hold strategy, so the proposed model is promising and certainly warrants further research.

## 1 Introduction

In this era of information blast, people meet huge amount of information everyday and are drowning in information. Information will provide huge profits for people if information can be utilized and processed, otherwise, it will become the burden of people. The goal of data mining is to bring the practice of information processing closer to providing the real answer and decision-making for the different investors and organizations. However, traditional data mining tools have been very difficult to meet the need of people. People have to find new computational models to get useful information from huge amount of data.

Neural networks (NNs) are a class of generalized nonlinear nonparametric models inspired by studies of the human brain. They are robust and have good learning and generalization capabilities [1], and are appropriate for clustering and prediction problems. For a more detailed description of NNs, the interested readers are referred to the papers in [2-4]. Due to NNs can mine valuable information from a mass of history information, so they have become one of the most efficient and useful mining tools [1, 5-8]. Especially, some researches [8-10] have shown that NNs performed better than conventional statistic approaches in financial forecasting. Despite NNs as data mining tool have many advantages, however, they still have some drawbacks, for example, overfitting and poor explanation capability and so on, which significantly affect the performance of NNs. In order to enhance the forecasting capability of NNs, many researchers have improved NNs by combining other techniques [11]. In this paper, the kernel smoothing technique, which is use to filter 'noise' and help decision-making, is combined with NNs to develop a mining model. The actual results show that this model is efficient, and some interesting results are obtained.



## 2 The Hybrid Mining Model

Many researches [12] have shown that the closing price and the trading volume are the most important factors that affects stock market, so the two data are selected to predict the future trends of stock market. Due to the original financial data are very complex, and generally contain noise. In order to make model more effective, these data are usually preprocessed before training. In this paper, a kernel smoothing technique [12] is used to filter noise. In detail, for a time series  $Y : y_1, \dots, y_n$ , a smoothed time series  $\hat{Y} : \hat{y}_1, \dots, \hat{y}_n$  is calculated as following:

$$\hat{y}_i = \frac{\sum_{t=1}^n K_h(i-t)y_t}{\sum_{t=1}^n K_h(i-t)}, i = 1, 2, \dots, n, K_h(x) = \frac{1}{h\sqrt{2\pi}} e^{-\frac{x^2}{2h^2}}.$$

In addition, due to the activation function is a sigmoid function that squashes input data to [0,1], so the two data are scaled in [0.1,0.9] respectively.

The network architecture is shown in Fig.1.

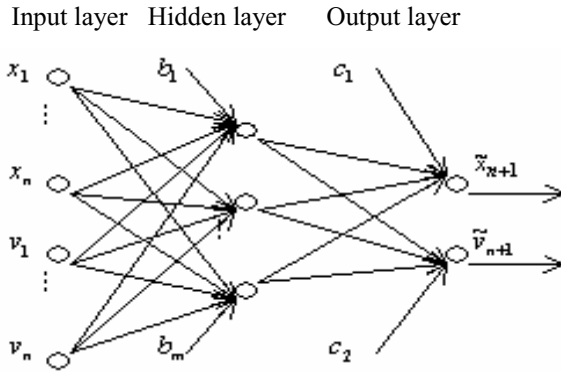


Fig. 1. A network architecture used by this paper

In order to make mode more effective, the following mean squared error is used.

$$MSE = \frac{1}{2} \sum_{i=1}^N \alpha (\tilde{x}_{i+n} - x_{i+n})^2, \tag{1}$$

where  $\alpha = \begin{cases} \beta & \text{if } (\tilde{x}_{i+n} - x_{i+n-1})(x_{i+n} - x_{i+n-1}) > 0 \\ 2 - \beta & \text{else} \end{cases}$ ,  $\beta \in (0,1)$ ,  $N$  is the total number of training pattern pairs, and  $\tilde{x}_{i+n}$  is the computed output,  $x_{i+n}$  is the target output. (1) denotes that the incorrect predicted directions are penalized more heavily than the correct predicted directions.

In order to avoid the poor explanation capability of NNs and give valuable suggestions for our investment decision-making, some trading rules are considered. The trading rules 1 is as follows:

$$\text{The trading signs} = \begin{cases} \text{Buy,} & \text{if } R_{BP} > R_{BT}, \\ \text{Sell,} & \text{if } R_{SP} < R_{ST}, \\ \text{Do nothing,} & \text{otherwise.} \end{cases}$$

where  $R_{BP} = \frac{\max_{1 \leq i \leq 30} (\tilde{x}_{n+i}) - x_n}{x_n}$ ,  $R_{SP} = \frac{\min_{1 \leq i \leq 30} (\tilde{x}_{n+i}) - x_n}{x_n}$ ,  $R_{SP}$  and  $R_{BP}$  are different

constants and denote the return of predict selling and buying respectively.

All the seasoned investors know the stock trend is very important to make money, and the past trend will affect the future trend. Therefore, we obtain the trading rules 2 by combining the past trends and the trading rule 1. Namely, the trading signs are sell if  $R_{SP} < R_{ST}$  and the trend in the past two days is down. The trend can be obtained by the kernel smoothing techniques in the process of data preprocessing. We compare the return of the trading rule 1 with the return of the trading rule 2 (see Fig.2), the computational results have shown that the trading rule 2 is more effective. The mining model can tell us when to buy or sell the stock according to these rules.

### 3 Computational Results and Conclusions

The hybrid mining model was implemented in C++ for Dos on a PC. The performance of this model was evaluated by trading the China Shanghai Composite Index from May 1996 to 15 Dec. 2003. The training patterns and test patterns are the data of 300 and 200 trading days respectively. Other parameters are designed as follows:  $n = 20, m = 5, R_{BT} = 0.06, R_{ST} = 0.041, \beta = 0.4$ . The initial weights and thresholds are in  $[-0.5, 0.5]$ . All the training patterns are selected randomly to train network about 3000 times, then all the testing patterns are tested. The process is repeated until the stop criteria are met.

The comparisons of returns between the mining model and the buy and hold strategy can be seen in Fig.2. All returns were calculated after taking the actual transaction costs for each transaction into consideration, namely the transaction costs for buying and selling is 1% respectively. For Fig.2, the return of the mining model with the trading rule 1 and 2 is 3.12 and 4.33 respectively, and the return of the buy and hold strategy is 1.31. The return of the trading rule 2 is about four times as large as that of the buy and hold strategy. So the mining model is superior to the buy and hold strategy. In addition, from Fig.2, it can know that the presented mining model performs better in bear market than in bull market, it denotes that the mining model has better capability of controlling risk. What is more, we find an interesting result, namely, the performance by training neural network every 150 days is better than that by training neural network every day. It directly improves the computational speed of the hybrid model.

The results of trading about seven years to Shanghai Composite Index have shown that the mining model was encouraging. This mining model can have actual application

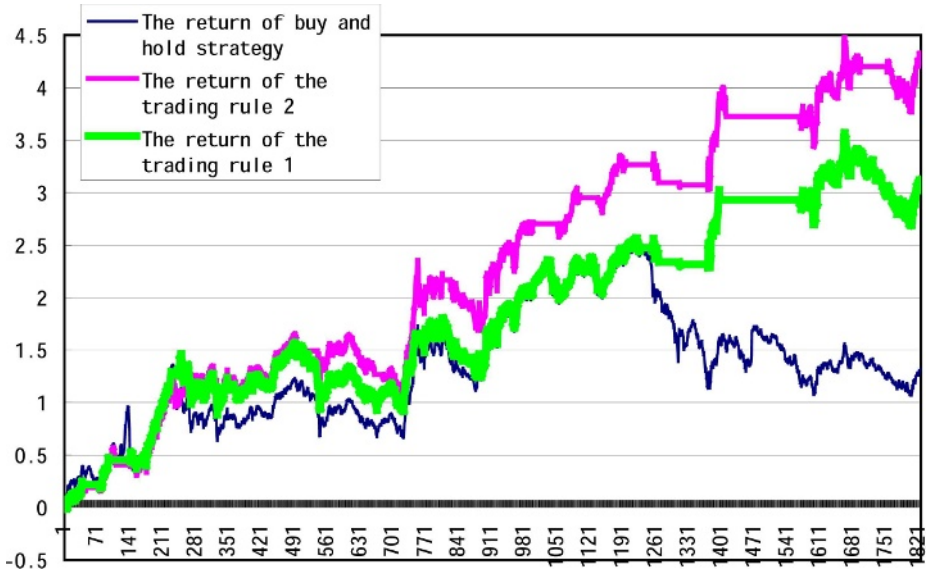


Fig. 2. Comparisons of returns between mining model and buy and hold strategy

and is very efficient for combinational investment. The future work is to strive for making the model more adaptive to the application and applying this model to other market and individual stocks.

## References

1. Sushmita Mitra, Sankar K. Pal, and Pabitra Mitra: Data Mining in Soft Computing Framework: A Survey. *IEEE Transactions on Neural Networks* (2002) 13(1): 3–14
2. Hertz, J. Krogh, A., and Palmer R.G.: Introduction to the theory of neurocomputing. Addison-Wesley, Reading, MA (1991)
3. Widrow, B.; Rumelhart, D.E.; and Lehr, M.A.: Neural networks: applications in industry, business and science. *Communications of the ACM* (1994) 37(3): 93–105
4. Kate A.Smith, Jatinder N.D. Gupta: neural networks in business: techniques and applications for the operations researcher. *Computers & Operations Research* (2000) 27:1023-1044
5. A. J. Chapman: Stock market trading systems through neural networks: Developing a model. *International Journal of Applied Expert Systems* (1994) 2(2): 88-100
6. Hoptroff R.: The principles and practice of time series forecasting and business modelling using neural nets. *Neural Computing & Applications* (1993) 1: 59–66
7. Zhang G, Patuwo B, Hu M: Forecasting with artificial neural networks: the state of the art. *International Journal of Forecasting* (1998) 14: 35–62
8. Refenes, A.N., A.Zapranis, and G. Francis: Stock performance modeling using neural network: A comparative study with regression models. *Neural Network* (1994) 5: 961-970
9. Y.S.Abu-Mostafa, A.F. Atiya, M. Magdon-Ismael, and H. White: Neural networks in financial engineering. *IEEE Transactions on Neural Networks* (2001) 12(4): 653-656

10. Saad E, Prokhorov E, Wunsch D.: Comparative study of stock trend prediction using time delay, Recurrent and probabilistic neural networks. *IEEE Transactions on Neural Networks*, (1998) 9:1456–70
11. Paul G. Harrald and Mark Kamstra: Evolving Artificial Neural Networks to Combine Financial Forecasts. *IEEE Transactions on Evolutionary Computation* 1997 1(1): 40-52
12. Andrew W. Lo, Harry Mamaysky, Jiang Wang: Foundations of technical Analysis: Computational algorithms, statistical inference, and empirical implementation. <http://www.nber.org/papers/w7613>, National Bureau of Economic Research (2000)

# An Efficient User-Oriented Clustering of Web Search Results

Keke Cai, Jiajun Bu, and Chun Chen

Department of Computer Science, Zhejiang University,  
Hangzhou, China, 310027  
{caikeke, bjj, chenc}@zju.edu.cn

**Abstract.** As a featured function of search engine, clustering display of search results has been proved an efficient way to organize the web resource. However, for a given query, clustering results reached by any user are totally identical. In this paper, we explored a user-friendly clustering scheme that automatically learns users' interests and accordingly generates interest-centric clustering. The basis of this personal clustering is a keyword based topic identifier. Trained by users' individual search histories, the identifier provides most of personal topics. Each topic will be the clustering center of the retrieved pages. The scheme proposed distinguishes the functionality of clustering from that of topic identification, which makes the clustering more personal and flexible. To evaluate the proposed scheme, we experimented with sets of synthetic data. The experimental results prove it an effective scheme for search results clustering.

## 1 Introduction

For the overwhelming information on Internet, conventional keyword-based Internet search usually return hundreds of thousands of retrieved results, most of which are irrelevant to what enquired. To solve this problem, automatic clustering technique has been proposed. Its main idea is to group retrieved pages by common topics, which is usually evaluated by the relevance among pages returned. Some schemes [1], [2] compare the direct or indirect hyperlinks of pages to gauge their relevance, whereas others, such as [3], utilize common keywords contained in different pages. These methods enable effective identification of retrieved results, however most of them rely particularly on retrieved web pages themselves to cluster. Consequently, for a given query the clustering results are always static.

Recently, user-oriented personal service has been widely deployed in the domain of search engine. A clustering scheme called content ignorant was invented [4], [5], which performs the clustering of queries beforehand for pages clustering to build upon. Though it provides a dynamic and rapid response for web surfing, its expansibility restrains because it can only establish mappings between queries and URLs that have already been preprocessed. In this paper, we explore a user-friendly clustering scheme that automatically learns user' interests and simultaneously generates interest-centric clustering. Differed from conventional pages clustering schemes, our clustering is designed to make the clustering more individual but not to provide user the most detailed clustering. The basis of this personal clustering is a keyword-based topic identifier, which is fully trained by user's individual search histories. When a

user submits a query to search engine, it will automatically generate a set of topics with individual characteristics, which will be utilized in later page clustering.

## 2 Personal Clustering Scheme

The proposed clustering model consists of three basic components: Personal Topic Identifier, Query Executor and Personal Clustering Generator. Personal topic identifier recognizes personal topics of each user; Query executor processes user’s current query and returns retrieved web pages; Personal clustering generator constructs the final clustering display of the retrieved web pages. Among these, personal topic identifier is the kernel. It monitors and records user’s behaviors, and then denotes each visited page as a weighted keyword vector. It is believed that users’ interests may lead to frequent visit to web pages of specific topics, which correspondingly causes the frequent co-occurrence of specific keywords. In this paper, such frequent keyword sets are regarded as the personal topics.

Equation 1 represents weight computation of term  $t_j$  to page  $p_i$ . It is a modification of TF-IDF weighting scheme [6]. Terms with weight more than system-predefined threshold will be selected as page-related keywords. Influence factor  $\log(N/n_{i,j})$  reflects the frequency of  $t_j$  in the condition of all web pages.  $f_{i,j}$  is the normalized frequency of term  $t_j$  in web page  $p_i$ . Parameter  $\alpha$  reflect the position of term  $t_j$  in page  $p_i$ , and it is more than 1 if  $t_j$  appears in the title of  $p_i$ , otherwise it is 1.

$$W_{i,j} = \alpha * f_{i,j} * \log(N/n_{i,j}) . \tag{1}$$

Considering the number restriction of clusters as well as the requirement of the minimal overlap among clusters, we modify the CLOSET+ [7] frequency mining algorithm to finish the process of personal topics identification. To avoid serious overlap between closed keyword sets, we refine the results set so that if two keyword sets are similar enough, they are emerged. Equation 2 is the similarity definition between two keywords set  $ks_1$  and  $ks_2$  by cosine distance.

$$sim(ks_1, ks_2) = ks_1 \cdot ks_2 / \| ks_1 \| \| ks_2 \| . \tag{2}$$

Based on the identified clustering topics as well as the retrieved query results, the final clustering can be easily realized through our defined keywords-based cluster identifier. For a flat set of clustering  $C = \{C_1 \dots C_n\}$ , it consists of a set of rules  $f_i \rightarrow C_i$ ,  $i = 1 \dots n$ .  $f_i$  is a frequent keyword set, which represents the corresponding topic information of  $C_i$ . A web page  $p$  is considered belonging to the  $C_i$ , if  $p$  matches the rule of  $f_i \rightarrow C_i$ . Function  $ovp()$  in equation 3 measures the match degree between pages and clusters, and the domain of its value ranges between 0 and 1.  $kp$  represents the keyword vector of page  $p$ . We cluster  $p$  to  $C_i$  if their overlap is no less than the predefined threshold  $minSim$ . It is possible that some retrieved cannot be mapped to any cluster. In our paper, all these pages will be assigned to a separated cluster.

$$ovp(p, C_i) = |kp \cap f_i| / |f_i| . \tag{3}$$

Table 1 shows the personal precision of three kinds of queries under personal clustering (PC) and normal clustering (NC). For clustering PC and NC, their personal

precision *Personal* is defined as a *cosine* distance against *MC*, which is another clustering results obtained through manual definition. As show in Table 1, our personal clustering method presents satisfactory adaptability in various queries, and its personal precision averagely reach about 83 percent. It shows that this clustering method can perfectly capture any topic information mostly concerned by user, and accordingly form a set of user-topic related clusters.

$$Personal(AC) = \frac{1}{|MC|} \sum_{AC_i \in AC} \max_{AC_i} (sim(MC_j, AC_i)). \tag{4}$$

**Table 1.** Personal precision comparisons

Data Source	Pages Number	Clusters Number			Personal Precision (percent)	
		<i>MC</i>	<i>PC</i>	<i>NC</i>	<i>PC</i>	<i>NC</i>
Q1	99	4	3	8	89.2	57.8
Q 2	465	6	8	16	82.1	34.8
Q 3	1220	9	7	27	79.8	10.5

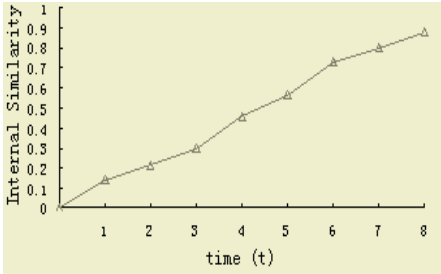


**Fig. 2.** Internal similarity of clusters

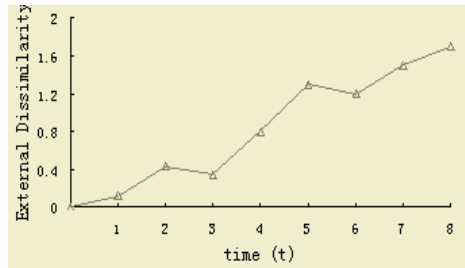


**Fig. 3.** External dissimilarity of clusters

$$internalSim = \frac{1}{|C|} \sum_{C_i \in C} \frac{1}{|C_i|} \sum_{\substack{x \in C_i \\ y \in C_i}} sim(x, y). \tag{5}$$

Fig. 2 and 3 show the quality of our clustering as client’ query become more and more concentrated on some special topics. Internal similarity *internalSim* represents inner cohesiveness of each cluster, and external dissimilarity *dep* describes the independence of different clusters. The definition of *dep* is built upon the overlap of different clusters [8]. Given a page *p* clustered to *C<sub>i</sub>*, we define *O<sub>p</sub>* as the number of its occurrence in other clusters.

As shown in Fig. 2, the form of user query topics directly decides the clustering accuracy. With the gradual enrichment of user query topics information, the clustering

becomes more and more accurate. Fig. 3 shows that this clustering can dynamically adapt user query, and capture any personal topics well and truly.

$$dep(C) = \frac{1}{|C|} \sum_{C_i \in C} \frac{1}{|C_i|} \sum_{p \in C_i} (O_p - 1). \quad (6)$$

### 3 Conclusions

This paper presents an efficient means for the personal clustering of retrieved web pages by learning users' interests with respect to their query histories, and further using this information to realize a meaningful clustering. With the enrichment of user history records, the clustering will pick and return even more accurate results.

### References

1. Hou, J. and Zhang, Y., Utilizing Hyperlink Transitivity to Improve Web Page Clustering. Proceedings of the Fourteenth Australasian Database Conference. Adelaide, Australia (2003) 49-57
2. D. S. Modha and W. S. Spangler, Clustering hypertext with applications to web searching. In Proceedings of the 11th ACM Conference on Hypertext and Hypermedia. San Antonio, TX (2000) 143-152
3. Zhang Dong, Towards Web Information Clustering. PhD thesis. Southeast University, Nanjing, China (2002)
4. D. Beeferman and A. Berger, Agglomerative clustering of a search engine query log. In Proceedings of the Sixth ACM SIGKDD International Conference on Knowledge Discovery and Data Mining. Boston, MA (2000) 407-416
5. Mark Hansen, Elizabeth Shriver, Using navigation Data to Improve IR functions in the Context of Web Search. CIKM. (2001) 135-142
6. Ricardo Baeza-Yates, Berthier Ribeiro-Neto, Modern information retrieval. ACM Press. (1999)
7. J. Wang, J. Han, and J. Pei, CLOSET+: Searching for the Best Strategies for Mining Frequent Closed Itemsets. In Proc. 2003 ACM SIGKDD. Int. Conf. on Knowledge Discovery and Data Mining (KDD'03). Washington, D.C (2003)
8. F. Beil, M. Ester, and X. Xu., Frequent term-based text clustering. In Proc 8th Int. Conf. on Knowledge Discovery and Data Mining KDD. (2002)



# Artificial Immune System for Medical Data Classification

Wiesław Wajs<sup>1</sup>, Piotr Wais<sup>2</sup>, Mariusz Świącicki<sup>3</sup>,  
and Hubert Wojtowicz<sup>2</sup>

<sup>1</sup> Institute of Automatics,  
University of Mining and Metallurgy, Kraków, Poland  
wwa@ia.agh.edu.pl

<sup>2</sup> National Technical University in Krosno  
waisp@poczta.onet.pl  
hubwoj@pwsz.krosno.pl

<sup>3</sup> Institute of Computer Modelling,  
Cracow University of Technology, Kraków, Poland  
mswiecic@uck.pk.edu.pl

**Abstract.** The article presents application of artificial immune algorithms in classification of vectorized medical data sets. Artificial immune network was created and trained for the purpose of arterial blood gasometry parameters (pH, pCO<sub>2</sub>, pO<sub>2</sub>, HCO<sub>3</sub>) classification. Training data originates from the Infant Intensive Care Unit of the Polish – American Institute of Pediatrics, Collegium Medicum, Jagiellonian University in Cracow.

## 1 Introduction

Biological phenomena, and particularly organic processes are of a dynamic character. Diagnosis and therapy are of the same character. In approaching diagnosis and making therapeutic decision phenomena happening in time are investigated. Every doctor knows that it is rare to make a decision about diagnosis and treatment on the basis of only one clinical observation. Usually it is based on several patient's examinations, regular analysis of many biophysical and biochemical parameters, or imaging examination. On a particular level of these examinations preliminary diagnosis is determined, and later a final one. Basing on determined diagnosis and on the evaluation of the sickness process dynamics decision about the treatment is taken.

Initial stabilization of the infants state is a difficult task. To achieve it the doctor analyses repeatedly many parameters related to the patient's health condition. These parameters are: birth anamnesis, physiological examinations (body's weight, diuresis), results of additional examinations (biochemical, micro biological, imaging) and readings from the monitoring instruments (pulseximeter, cardio monitor, invasive measurement of the arterial pressure, respiratory mechanics monitor). It isn't rare when doctor appraises simultaneously over fifty variables. Analysis of this amount of data is hard and requires experience, all the more if the decision about the treatment should be made quickly. In result of carried out analysis doctor makes decision about the treatment expecting positive results, which are expressed by the desired changes

in the results of additional examinations, readings of the monitoring instruments and physical examination. The whole process can be verified by comparing it to the model of respiratory insufficiency progress carried out by the doctor. Creation of this model is based on theoretical and empirical knowledge found in scientific literature and also on the doctor's experience. Intensification of gas exchange disorders are best reflected by arterial blood gasometry parameters examined in the context of currently used methods of ventilation support. For that reason as an output values four directly measured parameters of arterial blood gasometry: pH, pCO<sub>2</sub>, pO<sub>2</sub>, HCO<sub>3</sub> and oxygen parameter (pO<sub>2</sub>/FiO<sub>2</sub>) were chosen. Alkalis deficiency and hemoglobin oxygen saturation were omitted as derivatives of the four parameters mentioned above.

## 2 An Artificial Immune Network for Signal Analysis

Main goal of the system is a classification of signals and to achieve it several problems had to be solved. First of them is connected with an algorithm of learning the immune network. The next problem is related to the structures of data, which are responsible for representation of signals.

The input signal for the system, is interpreted as an antibody (Ab) so the task of immune network is to find an antigen Ag that will be suitable for Ab. The Ag-Ab representation will partially determine which distance measure shall be used to calculate their degree of interaction. Mathematically, the generalized shape of a molecule ( $m$ ), either an antibody (Ab) or an antigen (Ag), can be represented by a set of real-valued coordinates  $m = \langle m_1, m_2, \dots, m_L \rangle$ , which can be regarded as a point in an  $L$ -dimensional real-valued space.

$$D = \sqrt{\sum_{i=1}^L (ab_i - ag_i)^2} \quad (1)$$

The affinity between an antigen and an antibody is related to their distance that can be estimated via any distance measure between two vectors, for example the Euclidean or the Manhattan distance. If the coordinates of an antibody are given by  $\langle ab_1, ab_2, \dots, ab_L \rangle$  and the coordinates of an antigen are given by  $\langle ag_1, ag_2, \dots, ag_L \rangle$ , then the distance ( $D$ ) between them is presented in equation (1), which uses real-valued coordinates. The measure distances are called Euclidean shape-spaces.

Algorithm used in the research is described in papers [1] [2] by de Castro and Von Zuben. Modified version of immune net algorithm was adapted to signals classification. The learning algorithm lets building of a set that recognizes and represents the data structural organization. The more specific the antibodies, the less parsimonious the network (low compression rate), whilst the more generalist the antibodies, the more parsimonious the network with relation to the number of antibodies. The suppression threshold controls the specificity level of the antibodies, the clustering accuracy and network plasticity.

### 2.1 Overview and Analysis of the Research

Currently immune network performs unsupervised pattern recognition of the gathered medical data. In the process of further research description of the data classes will be

added, which is prepared by an expert medicine doctor. The idea is to categorize patients according to the hospitalization group they are initially assigned to by the doctor. Next goal after creating a reliable classification system is to develop a time series predicting system to help doctors in forecasting patient's condition ahead in time.

A major issue in the research is the scarcity of available data from hospitalization. Efficient system of new data acquisition is one of the main concerns and to achieve it in the future a creation of an agent system [3] is planned for gathering information through the Internet from several hospitals and adding it to the database.

### 3 Multidimensional Medical Data Classification

In the given example use of the AIS is presented in the unsupervised pattern recognition of the medical data. Using a database, functioning for the few years on the Infant Intensive Care Ward of the Polish – American Institute of Pediatrics Collegium Medicum Jagiellonian University of Cracow, a network was created, which final task is going to be the classification of arterial blood gasometry parameters. In the process of training previous values of gasometry, respirator settings and surfactant administration were used as an input data. Training of the network consists of two phases. First phase is a learning of the network. Training data set is comprised of blood parameters values starting from the time (t) – time series are of the same length. Second phase tests the network's generalization abilities by presenting it input vectors from the test dataset. Elements of the training dataset – time series are interpreted by the network as antigens, which are stimulating particular antibody creating an artificial immune network. Training dataset for the artificial immune network comprises of pattern series, which are represented by the vectors. As a result of this time series included in the dataset can be interpreted as a point coordinates in n-dimensional space, which n-value is dependant on the pattern series length.

### 4 Summary

In the paper functioning of the artificial immune system and example of its application in unsupervised pattern recognition of medical multidimensional data was presented. Perspectives for creating a reliable classification and time series modeling systems based on the artificial immune algorithm were discussed.

### References

- [1] De Castro, L. N., Von Zuben, F. J. (2000a), An Evolutionary Immune Network for Data Clustering, Proc. of the IEEE SBRN, pp. 84-89.
- [2] De Castro, L. N., Von Zuben, F. J. (2000b), The Clonal Selection Algorithm with Engineering Applications, GECCO'00 – Workshop Proceedings, pp. 36-37.
- [3] Wajs Wiesław, Wais Piotr, Autonomous Agent for Computer System and Computerized System of Automatics, Some Analogy and Difference, International Workshop Control and Information Technology, IWCIT 2001.

# EFoX: A Scalable Method for Extracting Frequent Subtrees <sup>\*</sup>

V. S. Sunderam, G. R. E. H., and G. M.

Dept. of Computer Engineering, Sungkyunkwan University,  
300 Chunchun-dong, Jangan-gu, Suwon-si, Gyeonggi-do 440-746, Republic of Korea  
quasa277@gmail.com, {drshin, umkim}@ece.skku.ac.kr

**Abstract.** The more web data sources provide XML data, the greater information flood problem has been caused. Hence, there have been increasing demands for efficient methods of discovering desirable patterns from a large collection of XML data. In this paper, we propose a new and scalable algorithm, EFoX, to mine frequently occurring tree patterns from a set of labeled trees. The main contribution made by our algorithm is that there is no need to perform any tree join operation to generate candidate sets.

## 1 Introduction

The first step toward mining frequent patterns from documents is to find frequent subtrees occurring in a large collection of trees. However, the discovery of frequent subtrees appearing in a large scaled tree structured dataset is a non-trivial task. The main difficulties arise in candidate subtrees enumeration and pattern tree matching. The problem here is that the enumeration of candidate subtrees is typically made by a naive operation as the number of documents increases, the efficiency of previous deduplicated algorithms deteriorates rapidly. Recently, several methods for extracting frequent subtrees in this paper, we propose a new algorithm *EFoX* (*Extract Frequent subtrees of Xml trees*) for efficient finding frequent subtrees from a set of documents. The proposed algorithm not only reduces significantly the number of tree prunings, but also simplifies greatly each rule-based algorithmic summarization operations.

## 2 Related Work

Agard and Ullman [1] considered mining frequent paths in ordered trees by using pruning technique. Saito et al. [2] proposed RE for mining aggregated

---

<sup>\*</sup> This research was supported in part by University IT Research Center Project funded by the Korean Ministry of Information and Communication and by Korea Science & Engineering Foundation (R01-2004-000-10755-0).

ordered trees RE uses rightmost paths to generate candidate trees by attaching edges to the rightmost edge of a tree in a pre-processed DAG. RE iteratively attaches remaining embedded subtrees from ordered abetrees. The complexity of the previous approaches is defined as follows. Each tree pruning algorithm generates candidate sets requiring performance separation hereafter, as the number of dimensions increases, the efficiency of frequent subtrees deteriorates rapidly since both the cost of separation and the number of pruned nodes add up.

### 3 Algorithm EFOX

In this section, we present an algorithm EFOX for efficient frequent subtrees from a given set of trees. In this section, EFOX consists of three steps. The first step is to create a data structure for separation and reduce the number of candidates. The second step is to extract frequent subtrees from the data structure.

#### 3.1 Generating KidSet

Let  $D = \{T_1, T_2, \dots, T_i\}$  be a set of trees and let  $|D|$  be the number of trees in  $D$ .

**Definition 1 (key).** Let  $K_d$  be a collection of node labels assigned on the nodes at depth  $d$  in every tree in  $D$ . (Assume that depth of root node is 0.) We call each member in  $K_d$  by a key.

In this paper, we assume that there may exist some nodes labeled with the same names in  $D$ . Thus, for each key, we need to define the set of trees in which the key belongs.

**Definition 2 (KidSet).** A KidSet,  $K^d$ , is defined as a set of pairs  $(k_d, t_{id})$  where  $k_d$  is a key in  $K_d$  and  $t_{id}$  is a list of tree indexes in which  $k_d$  belongs.

According to some minimum support, a collection of KidSets can be classified as frequent sets.

**Definition 3 (Frequent).** Given some minimum support  $\sigma$  and a pair  $(k_d, t_{id})$ , the key  $k_d$  is called **frequent** if  $|t_{id}| \geq \sigma \times |D|$ .

**Definition 4 (Frequent Set).** Given a KidSet,  $K^d$ , a pair in  $K^d$  is called **Frequent Set** if its key is frequent. Otherwise, it is called **Candidate Set**. We denote Frequent Set and Candidate Set by  $F^d$  and  $C^d$ , respectively.

This required to consider the characteristic of tree structure. This is derived from the fact that same nodes can be placed several times throughout a tree.

**Cross-Reference operation.** Let  $\mathcal{FS} = \{F^0, F^1, \dots, F^d\}$  be a set of frequent sets and  $\mathcal{CS} = \{C^0, C^1, \dots, C^d\}$  be a set of candidate sets. Let  $i$  be an integer  $0 < i \leq d$ . Our definition of **cross-reference** operation consists of the following phases

- *Phase 1* Compute  $(F^i \text{ vs. } C^{i-1})$  and  $(C^i \text{ vs. } F^{i-1} \text{ to } F^0)$ . The purpose of this step is to eliminate pairs from candidate sets which are actually the pairs included in a previous request. This reduces the number of pairs of candidate sets significantly due to this phase.
- *Phase 2* Compute  $(C^i \text{ vs. } C^{i-1})$ . This step adapts prior state. In other words, the efficiency is dramatically improved since there is no need for a separate operation between candidate sets. In other words, during this phase, we **derives** (not generate) candidate sets through this phase. Because of the **hierarchical** and structure, this step requires to generate candidate paths and add to a candidate pairs by using a separate step. Therefore,  $C^i$  uses a pairs to be generated a request sets between  $F^0$  and  $F^{i-1}$ . Consequently, the candidate sets are always processed to find additional frequent elements.

### 3.2 Mining Frequent Subtrees

The final set of frequent sets contains all keys which are frequent. In other words, a frequent set has elements, and a frequent key has correct. Each then the different consider the empty sets because an empty request implies that a candidate can be placed. The first appeared in empty request set stores the keys which are root nodes of frequent subtrees. Based on this selection, frequent subtrees are incrementally built from root nodes. The rest of request sets using construction of frequent subtrees, they are extracted from the trees as shown below.

**Theorem 1 Correctness of EFoX.** *The bigger frequent subtree is always expanded from one of the smaller frequent subtrees.*

*Proof.* omitted due to lack of space

## 4 Evaluation

We evaluate the effectiveness and the scalability of our algorithm. We carried out a comparison of performance. The artificial generated medium size data sets binary generation described. We evaluated the performance of the generation algorithm. The basic decision based on the selection of frequent subtrees through a repeated process of enumeration and pruning candidate subtrees. The synthetic data set,  $(\sigma, \dots)$  and  $(T, \dots)$ , were tested. We generated minimum three target frequent trees reflecting predefined parameters. We refer the reader to the paper for a detailed experimental setup and usage parameters.

the execution time for data set with larger number of input trees is shown in Fig. (a) to be seen that E<sub>o</sub> demonstrates a dramatic improvement over the generic framework. Fig. (b) shows the execution time for data set with changing minimum support. The execution time decreases as the minimum support increases. In both algorithms, but there is significant time difference between them. The stepped tree structure since the running time exceeds several hours.

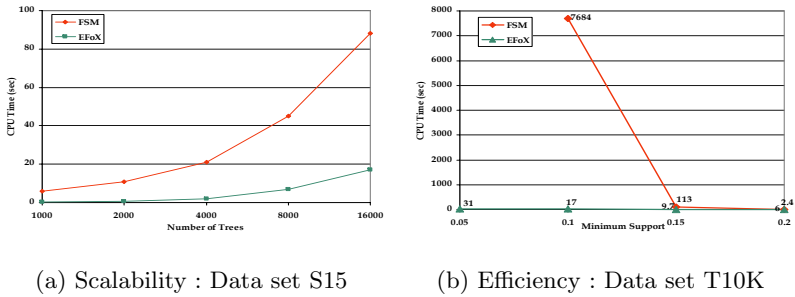


Fig. 1. Execution Time

## 5 Conclusion

The top-k tree mining has been defined in the paper. The algorithm, E<sub>o</sub>, is proposed to discover frequent subtrees. The algorithm uses a special data structure, and it manipulates frequent node labels and tree nodes. E<sub>o</sub> is evaluated with artificial medium size data sets. Our experimental results show that E<sub>o</sub> performs much better than generic framework, in both terms of scalability and efficiency. We need further research to adapt the current proposed method to both semi-structured and semi-structured data. For future use, other mining algorithms, same clustering classification.

## References

1. R. Agrawal and R. Srikant. Fast algorithms for mining association rules in large databases. In *Proc. of the 12th International Conference on Very Large Databases*, pp487–499, 1994.
2. T. Asai, K. Abe, S. Kawasoe, H. Arimura, H. Sakamoto, and S. Arikawa. Efficient substructure discovery from large semi-structured data. In *Proc. of the 2nd SIAM International Conference on Data Mining (ICDM'02)*, 2002.

3. A. Termier, M-C. Rousset, and M. Sebag. TreeFinder : a First step towards XML data mining. *In Proc. of IEEE International Conference on Data Mining (ICDM'02)*, pp.450–457, 2002.
4. K. Wang, and H. Liu. Schema discovery for semistructured data. *In Proc. of the 3rd International Conference on Knowledge Discovery and Data Mining (KDD'97)*, pp.271–274, 1997.
5. M. J. Zaki. Efficiently mining frequent trees in a forest. *In Proc. of the 8th ACM SIGKDD International Conference on Knowledge Discovery and Data mining (KDD'02)*, pp.71–80, 2002.



# An Efficient Real-Time Frequent Pattern Mining Technique Using Diff-Sets

Rajanish Dass and Ambuj Mahanti

Indian Institute of Management Calcutta  
{rajanish, am}@iimcal.ac.in

**Abstract.** Frequent pattern mining in real-time is of increasing thrust in many business applications such as e-commerce, recommender systems, and supply-chain management and group decision support systems, to name a few. A plethora of efficient algorithms have been proposed till date. However, with dense datasets, the performances of these algorithms significantly degrade. Moreover, these algorithms are not suited to respond to the real-time need. In this paper, we describe BDFS(b)-diff-sets, an algorithm to perform real-time frequent pattern mining using diff-sets. Empirical evaluations show that our algorithm can make a fair estimation of the probable frequent patterns and reaches some of the longest frequent patterns much faster than the existing algorithms.

## 1 Introduction

In recent years, business intelligence systems are playing pivotal roles in fine-tuning business goals such as improving customer retention, market penetration, profitability and efficiency. In most cases, these insights are driven by analyses of historic data. Now the issue is, if the historic data can help us make better decisions, how real-time data can improve the decision making process [1].

Frequent pattern mining for large databases of business data, such as transaction records, is of great interest in data mining and knowledge discovery [2], since its inception in 1993, by Agrawal et al. Researchers have generally focused on the frequent pattern mining, as it is complex and the search space needed for finding all frequent itemsets is huge [2]. A number of efficient algorithms have been proposed in the last few years to make this search fast and accurate. Among these, a number of effective vertical mining algorithms have been recently proposed, that usually outperforms horizontal approaches. Despite many advantages of the vertical format, the methods tend to suffer, when the tid-list cardinality gets very large as in the case of dense datasets [3]. Again, these algorithms have limited themselves to either breadth first or depth first search techniques. Hence, most of the algorithms stop only after finding the exhaustive (optimal) set of frequent itemsets and do not promise to run under user defined real-time constraints and produce some satisficing (interesting sub-optimal) solutions due to their limiting characteristics[4, 5].

## 2 Business Issues of Real-Time Frequent Pattern Mining

Using up-to-date information, getting rid of delays, and using speed for competitive advantage is what the real-time enterprise is about. There are numerous areas where real-time decision making plays a crucial role. These include areas like real-time customer relationship management, real-time supply chain management systems real-time enterprise risk and vulnerability management, real-time stock management and vendor inventory, real-time recommender systems, real-time operational management with special applications in mission critical real-time information as is used in the airlines industry, real-time intrusion and real-time fraud detection, real-time negotiations and other areas like real-time dynamic pricing and discount offering to customers in real-time. More than that, real-time data mining will have tremendous importance in areas where a real-time decision can make the difference between life and death – mining patterns in medical systems.

## 3 BDFS(b)-Diff-Sets: An Efficient Technique of Frequent Pattern Mining in Real-Time Using Diff-Sets

### *Algorithm BDFS(b)-diff-sets:*

*Initialize the allowable execution time  $\tau$*   
*Let the initial search frontier contain all 3-length candidate patterns. Let this search frontier be stored as a global pool of candidate patterns. Initialize a set called Border Set to null.*  
*Order the candidate patterns of the global pool according to their decreasing length (resolve ties arbitrarily). Take a group of most promising candidate patterns and put them in a block  $b$  of predefined size.*

- *Expand ( $b$ )*
  - Expand ( $b$ : block of candidate patterns)*
  - If not last\_level*
  - then*
  - begin*
  - Expand<sub>1</sub>( $b$ )*
  - end.*

*Expand<sub>1</sub>( $b$ ):*

1. *Count support for each candidate pattern in the block  $b$  by intersecting the diff-set list of the items in the database.*
2. *When a pattern becomes frequent, remove it from the block  $b$  and put it in the list of frequent patterns along with its support value. If the pattern is present in the Border Set increase its subitemset counter. If the subitemset counter of the pattern in Border Set is equal to its length move it to the global pool of candidate patterns.*
3. *Prune all patterns whose support values  $<$  given minimum support. Remove all supersets of these patterns from Border Set.*
4. *Generate all patterns of next higher length from the newly obtained frequent patterns at step 3. If all immediate subsets of the newly generated pattern are frequent then put the pattern in the global pool of candidate patterns else put it in the Border Set if the pattern length is  $>$  3.*
5. *Take a block of most promising  $b$  candidate patterns from the global pool.*
6. *If block  $b$  is empty and no more candidate patterns left, output frequent patterns and exit.*
7. *Call Expand ( $b$ ) if enough time is left in  $\tau$  to expand a new block of patterns, else output frequent patterns and exit.*

**Fig. 1.** Algorithm BDFS(b)-diff-sets

### 4 Empirical Evaluation

The following figures shows the empirical evaluation of BDFS(b)-diff-sets. We have found that BDFS(b)-diff-sets compares well with the existing best performing algorithms in time of completion and scalability. Real-time performance of BDFS(b)-diff-sets (in Fig. 9 and 10) show that it is always ahead of time while providing outputs. We have made detailed performance evaluation based on empirical analysis using commonly used synthetic and real-life dense datasets. Thus, we have demonstrated that real-time frequent pattern mining can be done successfully using BDFS(b)-diff-sets. We believe this study will encourage use of AI heuristic search techniques in real-time frequent pattern mining.

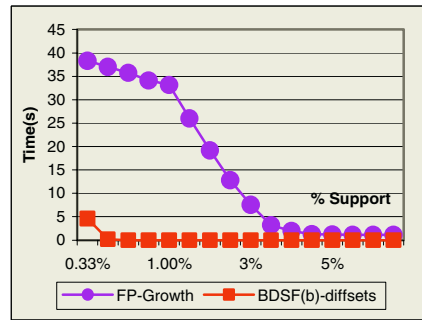
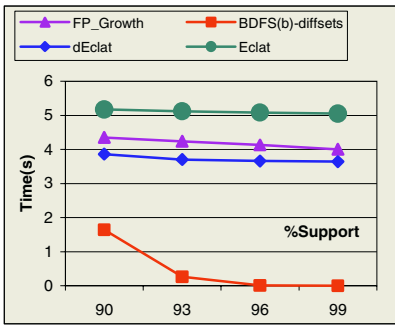


Fig. 2. Time comparison of FP-Growth, Eclat and dEclat with BDFS(b)-diffsets (b= 20880) on PUMSB, N=2113, T=74, D=49046

Fig. 3. Time comparison of FP-Growth with BDFS(b)-diffsets for T10I8D100K, b=100K

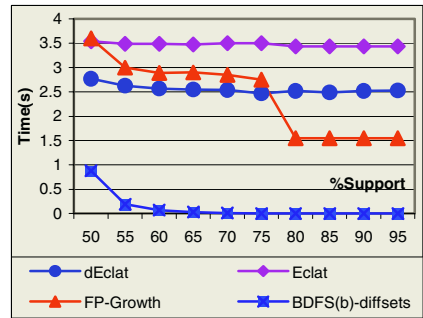
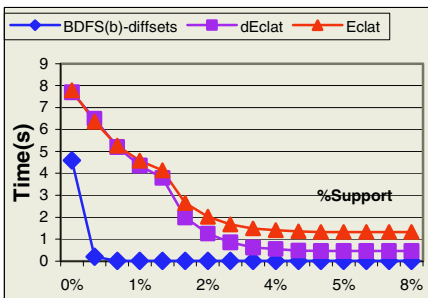
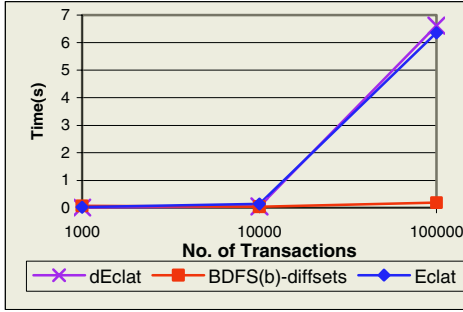
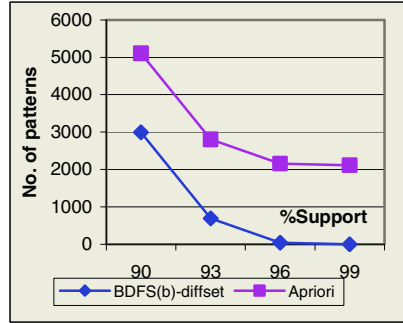


Fig. 4. Time comparison of Eclat and dEclat with BDFS(b)-diffsets for T10I8D100K, b=100K

Fig. 5. Time comparison of FP-Growth, Eclat and dEclat with BDFS(b)-diffsets (b=2088K) for PUMSB\*, N=2088 T= 50.5, D = 49046



**Fig. 6.** Scalability evaluation of BDFS(b)-diffsets with Eclat and dEclat supp=0.5%, b = 100K for T10I8D1K,10K and 100K



**Fig. 7.** Number of patterns checked by Apriori and BDFS(b)-diffsets (b=208800) for Pumsb, N=2113,T=74, D=49046, with varying support

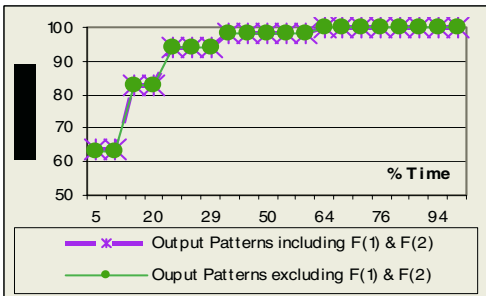


**Fig. 8.** Time-Patterns % of BDFS(b) for b=75K and 65% supp for Chess (N=75, T=37, D=3196)

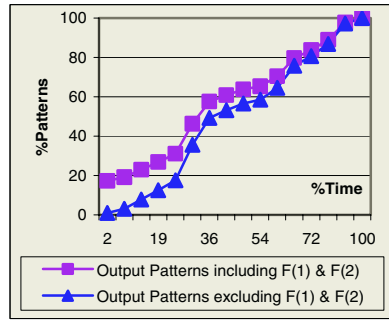


**Fig. 9.** Time-Patterns % for b=75K and 65% supp for T10I8D100K

**References**

1. Gonzales, M.L., *Unearth BI in Real-time*. 2004, Teradata.
2. Goethals, B., *Memory Issues in Frequent Pattern Mining*, in *Proceedings of SAC'04*. 2004, ACM: Nicosia, Cyprus.
3. Zaki, M.J. and K. Gouda. *Fast Vertical Mining Using Diffsets*. in *9th International Conference on Knowledge Discovery and Data Mining*. 2003, Washington, DC.
4. Dass, R. and A. Mahanti. *Frequent Pattern Mining in Real-Time – First Results*. in *TDM2004/ACM SIGKDD 2004*. 2004, Seattle, Washington USA.
5. Dass, R. and A. Mahanti. *An Efficient Technique for Frequent Pattern Mining in Real-Time Business Applications*. in *38th IEEE Hawaii International Conference on System Sciences (HICSS 38)*. 2005, Big Island: IEEE.
6. Lee, W., et al. *Real time data mining-based intrusion detection*. in *DARPA Information Survivability Conference & Exposition II*. 2001, Anaheim, CA , USA: IEEE Xplore.

# Improved Fully Automatic Liver Segmentation Using Histogram Tail Threshold Algorithms

Kyung-Sik Seo

Dept. of Electrical & Computer Engineering,  
New Mexico State University, Las Cruces, NM, USA  
nmsu2@hanmail.net

**Abstract.** In order to remove neighboring abdominal organs of the liver, we propose an improved fully automatic liver segmentation using histogram tail threshold (HTT) algorithms. A region of interest of the liver is first segmented. A left HTT (LHTT) algorithm is performed to eliminate the pancreas, spleen, and left kidney. After the right kidney is eliminated by the right HTT (RHTT) algorithm, the robust liver structure is segmented. From the results of experiments, the improved automatic liver segmentation using HTT algorithms has strong similarity performance as manual segmentation by medical doctor.

## 1 Introduction

A computed tomography (CT) is currently a conventional and excellent tool for diagnosis of the liver in medical imaging technology. Liver segmentation using the CT has been performed often [1, 2]. As previous researches have depended on semi-automatic liver segmentation such as a seed point, a rand mark, a reference image, and training data, fully automatic liver segmentation based on the spine was proposed [3]. However, proposed liver segmentation has problems because of pixel similarity of neighboring abdominal organs such as the spleen, pancreas, and kidneys.

In order to segment neighboring organs, we propose improved fully automatic liver segmentation using histogram tail threshold (HTT) algorithms. The region of interest (ROI) of the liver structure is first segmented. Then liver segmentation using HTT algorithms are processed to eliminate neighboring abdominal organs.

## 2 Improved Liver Segmentation

As pre-processing, the ROI of the liver is extracted using multi-modal threshold [3-5], C-class maximum a posteriori [6], and binary morphological (BM) filtering [7-9]. Figure 1 shows the ROI extraction of the liver.

The left HTT (LHTT) is presented to remove neighboring abdominal organs such as the pancreas, spleen, and left kidney from the ROI. Let  $I_{ROI}(m, n)$  be the gray-level ROI and  $h_{ROI}(k_1, k_2)$  be the histogram of  $I_{ROI}$  with the range,  $[k_1, k_2]$ . Let  $I_{LHTT}$  be the LHTT image. Then the LHTT algorithm is proposed:

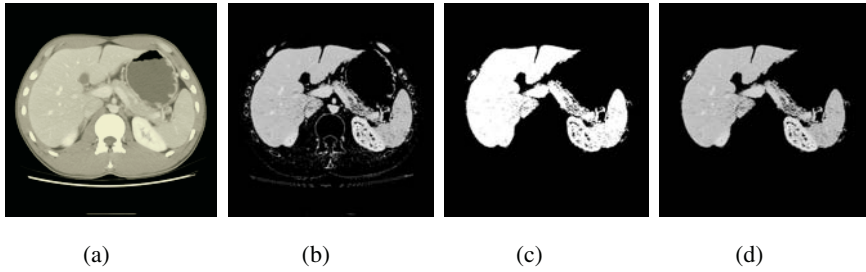


**Fig. 1.** ROI extraction of the liver: (a) CT image, (b) ROI after MMT, (c) ROI after C-class MAP decision, (d) Gray-level ROI

- Find  $k_{\max}$  where  $k_{\max}$  is the gray-level value when  $h_{ROI}(k)$  is the maximum value.
- Calculate the left histogram tail interval  $k_{LI} = (k_{\max} - k_1)$ .
- Find the left histogram tail threshold value.
- Create the LHTT image  $I_{LHTT} = \{(m, n) \mid k_1 \leq I_{ROI}(m, n) \leq k_{LHTT}\}$ .

Figure 2 shows an example of the LHTT algorithm.

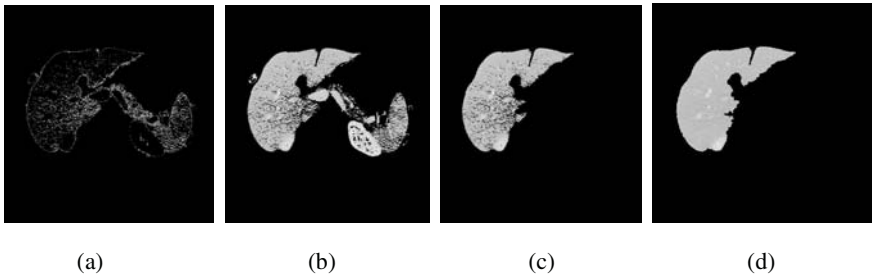


**Fig. 2.** Left histogram tail threshold: (a) LHTT image, (b) Difference image between  $I_{ROI}$  and  $I_{LHTT}$ , (c) Segmented liver structure by area estimation and C-class MAP decision, (d) Robust liver segmentation by BM filtering and gray-level transformation

As the right kidney is adjacent to the lower liver part and has the same gray-level values as liver vessels, this kidney creates problems in segmenting a liver structure. The RHTT is presented for extracting and removing the right kidney from the liver image. Let  $I_{RHTT}$  be the RHTT image. Then the RHTT algorithm is proposed:

- Find  $k_{\max}$  where  $k_{\max}$  is the gray-level value when  $h_{ROI}(k)$  is the maximum value.
- Calculate the right partial histogram interval  $k_{RI} = (255 - k_{\max})$ .

- Find the right partial threshold value  $k_{RHTT} = (k_{\max} + k_{RI} / 8)$ .
- Create the RHTT image  $I_{RHTT} = \{(m, n) | k_{RHTT} \leq I_{ROI}(m, n) \leq 255\}$ .

Figure 3 shows an example of the RHTT algorithm.

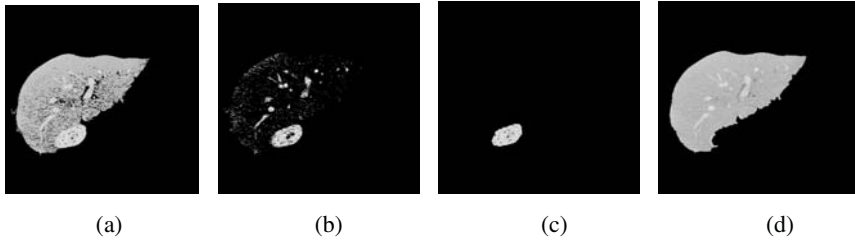


**Fig. 3.** Example of right histogram tail threshold: (a) Sample image, (b) RHTT image, (c) Extraction of right kidney after the area and angle estimation, (d) Elimination of the right kidney

### 3 Experiments and Analysis

40 slices of eight patients were selected for testing the improved segmentation method and one medical doctor in Chonnam National University Hospital segmented the liver structure by the manual method. In order to evaluate performance of the improved algorithm, three different segmentation methods were compared by using normalized average area (NAA) with the image size and area error rate (AER) [3]. Figure 4(a) shows NAA using error bars. Average NAAs of each method were 0.1972, 0.1593, and 0.1644. Also, Figure 4(b) shows the comparison of average AER per each patient based on manual segmentation to segmentation before and after HTT. The former is 4~40 % and the latter is 5~10 %. Total average AER for all patients is 23.9198 % for the former and 7.4223 % for the latter. From the results of this comparison, automatic segmentation using HTT algorithms matches the results of manual segmentation more closely than segmentation without HTT algorithms.

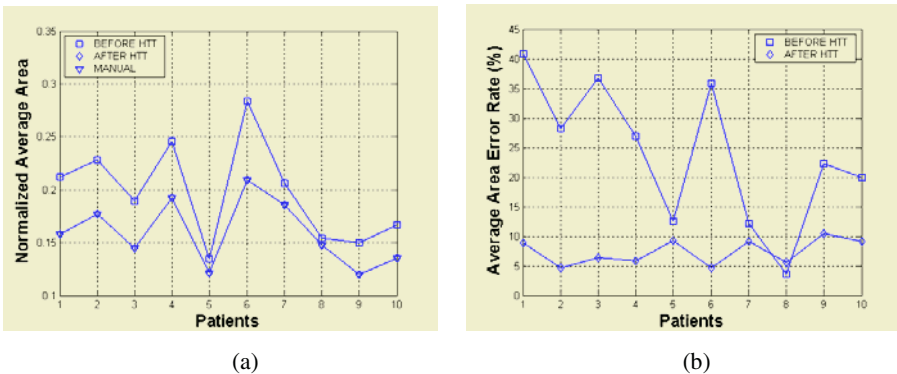


**Fig. 4.** Results: (a) Normalized average area, (b) Average area error rate

## 4 Conclusions

In this paper, we proposed the improved fully automatic liver segmentation using histogram tail threshold (HTT) algorithms. 40 slices of eight patients were selected to evaluate performance of the improved algorithm. From the results of experiments, the improved automatic liver segmentation has strong similarity performance as manual segmentation by medical doctor.

## References

1. Bae, K. T., Giger, M. L., Chen, C. T., Kahn, Jr. C. E.: Automatic segmentation of liver structure in CT images. *Med. Phys.*, Vol. 20. (1993) 71-78
2. Gao, L., Heath, D. G., Kuszyk, B. S., Fishman, E. K.: Automatic liver segmentation technique for three-dimensional visualization of CT data. *Radiology*, Vol. 201. (1996) 359-364
3. Seo, K., Ludeman, L. C., Park S., Park, J.: Efficient liver segmentation based on the spine. *LNCS*, Vol. 3261. (2004) 400-409.
4. Orfanidis, S. J.: *Introduction to signal processing*. Prentice Hall, Upper Saddle River NJ (1996)
5. Schilling, R. J., Harris, S. L.: *Applied numerical methods for engineers*. Brooks/Cole Publishing Com., Pacific Grove CA (2000)
6. Ludeman, L. C.: *Random processes: filtering, estimation, and detection*. Wiley & Sons Inc., Hoboken NJ (2003)
7. Gonzalez, R. C., Woods, R. E.: *Digital image processing*. Prentice Hall, Upper Saddle River NJ (2002)
8. Shapiro, L. G., Stockman, G. C.: *Computer vision*. Prentice-Hall, Upper Saddle River NJ (2001)
9. Parker, J.R.: *Algorithms for image processing and computer vision*. Wiley Computer Publishing, New York (1997)



# Directly Rasterizing Straight Line by Calculating the Intersection Point

Hua Zhang<sup>1,2</sup>, Changqian Zhu<sup>1</sup>, Qiang Zhao<sup>2</sup>, and Hao Shen<sup>2</sup>

<sup>1</sup> Department of Computer and Communication Engineering,  
Southwest Jiaotong University, Chengdu, Sichuan, 610031 P.R.China  
cqzhu@home.swjtu.edu.cn

<sup>2</sup> Institute of Computer Applications, China Academy of Physics Engineering,  
P.O. Box 919 Ext. 1201, Mianyang, Sichuan, 621900 P.R.China  
{hzhang, zhaoq, shh}@caep.ac.cn

**Abstract.** In this paper, a method of line scan-conversion is presented by calculating the intersection point of straight line with the middle scan line of screen. With this method, the pixel's screen coordinate of spatial line could also be obtained. Moreover, raster precision is exactly the same as that of Bresenham's middle algorithm; and more than or at least one pixel could be obtained at a computational effort of one inner loop. However, to Bresenham's middle algorithm, only one pixel is obtained in one inner loop's calculating.

## 1 Introduction

Line scan-conversion is to raster a spatial straight line onto a 2D raster display. There is a famous and classical algorithm, named as Bresenham's middle algorithm [1]. In Bresenham's algorithm, the next point is obtained by checking the sign of error, and only integer computation is used in inner loop calculating. With regard to Bresenham's middle algorithm, there are many fast algorithms and implementations, such as in [2], [3], [4], [5], [6], [7], and [8]. Some of these methods emphasize on the distribution of line's direction; others require that the line drawn is not to be very short. Chen [9] et al. presented statistical results of actual applications for line scan-conversion. In those statistical results, about 38.58 percent of lines are not horizontal, vertical and diagonal; and about 87.79 percent of lines are not larger than 17 pixels. In this paper, a method independent of line direction and line length is presented. We also assume that the line's slope has the rang of 0 to 1, which is an assumption often made when discussing line scan-conversion. Other slope's line can be handled by reflections about the principal axes.

## 2 Line Rasterization

In fig. 1, for a line's slope with the range of 0 to 1 (when the slope is equal to zero, this is a special case that will be discussed in following section), two regions could be obtained by subdividing the first octant with line 2, which has the slope of half one. Our algorithm of line rasterization in each region could be represented as following steps.

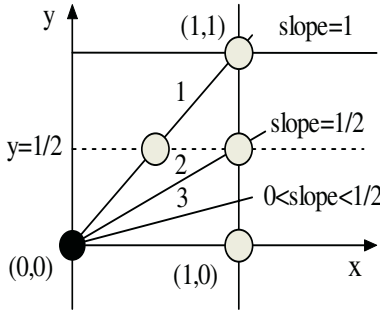


Fig. 1. Basis of line rasterization

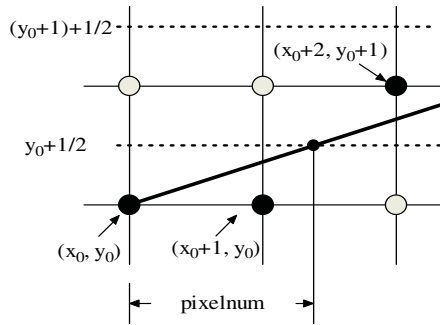


Fig. 2. An example of line rasterization

For a fixed two different end points with coordinates of  $(x_0, y_0)$  and  $(x_n, y_n)$ , the line equation could be obtained, as in:

$$y = \frac{y_n - y_0}{x_n - x_0}x + (y_0 - \frac{y_n - y_0}{x_n - x_0}x_0) \tag{1}$$

Coordinates of intersection point between the line and  $y=y+1/2$  could be obtained by submitting  $y=y+1/2$  to the upper line equation. Now, submitting  $y=y+1/2$  into (1) and rearranging terms, the  $x$  component of intersection point could be represented as following (see fig. 2):

$$x = \frac{(x_n - x_0)(2(y - y_0) + 1) + 2(y_n - y_0)x_0}{2(y_n - y_0)} \tag{2}$$

Assume  $x$  coordinates of current start pixel obtained is  $xc$ . Let the integer variable **pixelnum** be the distance of  $xc$  and  $x$  (see fig. 2). Now, the distance of  $x$  and  $xc$  is as following:

$$pixelnum = x - xc$$

Now, **pixelnum** pixel(s) could be written by increasing in  $x$  direction. For example, in fig. 1, line 1, 2, and 3 has **pixelnum** of 0, 1, and 2, respectively. In line 1, there is no pixel is written in  $x$  direction from the start pixel. In line 2, there is one pixel (1, 0) is written in  $x$  direction from the start pixel. In line 3, there are two pixels, (1, 0) and (2, 0), written in  $x$  direction from start pixel. Note when  $x$  coordinates exceed  $xn$ , writing pixels is completed.

When the first loop is completed, point (1, 1) is selected as a new start point for line 1, because vertical distance from (1, 1) to line 1 is not greater than vertical distance from (1, 0) to line 1. Similarly, point (2, 1) and (3, 1) is selected as the new start point for line 2 and line3, respectively.

Repeating the upward processes until the line reach the end of line, the process of line rasterization is completed. The C code could be represented as following:

```
//The line end points are (x0,y0) and (xn,yn), assumed not equal. The slope of this line has
//the rangeof 0 to 1, except 0.
```

```
LineRasterization (X0, y0, xn, yn){
  x=x0;y=y0;deltax=xn-x0;deltay=yn-y0;
  Pixelnum=0;pixelseq=0;
  While(x<=deltax){
    pixelnum=( deltax*(2*(y-y0)+1)+
                2*x0*deltay )/(2*deltay) - x;
    For(pixelseq=0;pixelseq<=pixelnum;x++){
      if(x>deltax) return ;
      writepixel(x,y);
      pixelseq++;
    }
    y++;
  }
}
```

**2.1 Example**

Consider line from (0, 1) to (6, 4). Rastering this line yields initial calculations:  $x=0$ ,  $y=1$ ,  $deltax=6$ ,  $deltay=3$ ,  $pixelnum=0$ , and  $pixelseq=0$ .

After running through the main loop and inner loop, coordinates could be shown in table 1.

**Table 1.** Coordinates of Rasterization

*x pixelnum writepixel* Bresenham's results

0	1	(0, 1)	(0, 1)
		(1, 1)	(1, 1)
2	1	(2, 2)	(2, 2)
		(3, 2)	(3, 2)
4	1	(4, 3)	(4, 3)
		(5, 3)	(5, 3)
6	1	(6, 4)	(6, 4)

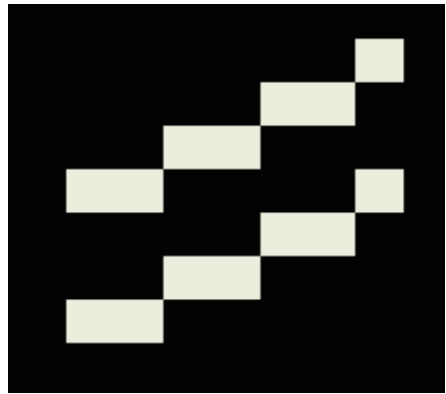


**Fig. 3.** Result of Rasterization

From these results,  $x$  is increased in each main loop; two pixels are written in each inner loop; and the coordinates of our algorithm for rasterization are the same as those of Bresenham's middle algorithm. Fig. 3 is a rasterized result for both Bresenham's algorithm and our algorithm. Note that the upper line has coordinates of (0, 4) and (6, 7), which are translated 3 pixels in  $y$  direction, and every pixel is represented by

20×20 pixels on screen. The upper line is rasterized by Bresenham's middle algorithm. The lower line is rasterized by our method. From fig. 3, same rasterized result could be noticed.

## 2.2 Slope Equal to Zero

When the slope of line is equal to zero, that is to say,  $yn - y0 = 0$ , the upper algorithm could not be used to raster the line. In this case, the line is parallel to horizontal axis. Therefore, the line could be rasterized from  $x0$  to  $xn$  only with the increment of 1 in  $x$  direction ( $y$  is constant in the rasterization process).

## 3 Conclusions

A method of line scan-conversion is presented by directly calculating the intersection point of straight line with the middle scan line of screen. From this method, the coordinates of actual pixels on screen could be obtained. Moreover, the rasterized result is exactly the same as that of Bresenham's algorithm, and at least one pixel could be obtained in one inner loop's running. How fast about our method in actual applications is a further work, which we propose for future work.

## References

1. Bresenham, J.E.: Algorithm for Computer Control and Digital Plotter. IBM Syst. J. Vol. 4, No.1, April (1965) 25-30
2. Dorst, L., Semulders, A.W.M.: Discrete Representation of Straight Lines. IEEE Trans. on Patter Analysis and Machine Intelligence, Vol. PAMI-6, No. 4, July (1984) 450-463
3. Foley, J.D., van Dam, A., Feiner, S.K., Hughes, J.F.: Computer Graphics: Principles and Practice. 2nd edn. In C, Addition-Wesley (1996) 72-80
4. Rokne, J.G., Wu, X.: Fast Line Scan-conversion. ACM Trans. on Graphics, Vol. 9, No. 4, Oct. (1990) 370-388.
5. Wu, X., Ronkne, J.G.: Double-step Incremental Generation of Lines and Circles. Computer Vision, Graphics and Image Processing, Vol. 37, No. 3, March (1987) 331-344
6. Suenaga, Y., Kamae, T., Kabayashi, T.: A High-speed Algorithm for Generation of Straight Lines and Circular Arcs. IEEE Trans. Computers, Vol. C-28, No. 10, Oct. (1979) 728-736
7. Gill, G.W.: N-step Incremental Straight-Line Algorithm. IEEE Computer Graphics and Applications, Vol. 5, No. 3, May (1994) 66-72
8. Brons, R.: Linguistic Methods for the Description of a Straight Line on a Grid. Computer Graphics and Image Process, Vol. 9 (1979) 183-195
9. Chen, J.X., Wang, X., Bresenham J.E.: The Analysis and Statistic of Line Distribution. IEEE Computer Graphics and Applications, Vol. 22, No. 6 (2002) 100-107

# PrefixUnion: Mining Traversal Patterns Efficiently in Virtual Environments

Shao-Shin Hung, Ting-Chia Kuo, and Damon Shing-Min Liu

Department of Computer Science and Information Engineering,  
National Chung Cheng University,  
Chiayi, Taiwan 621, Republic of China  
{hss, ktc91, damon}@cs.ccu.edu.tw

**Abstract.** Sequential pattern mining is an important data mining problem with broad applications. Especially, it is also an interesting problem in virtual environments. In this paper, we propose a projection-based, sequential pattern-growth approach, called *PrefixUnion*. Meanwhile, we also introduce the relationships among transactions, views and objects. According to these relationships, we suggest two mining criteria — *inter-pattern growth* and *intra-pattern growth*, which utilize these characteristics to offer ordered growth and reduced projected database. As a result, the large-scale VRML models could be accessed more efficiently, allowing for a real-time walk-through in the scene.

## 1 Introduction

The interactive walkthrough system provides a virtual environment with complex 3D models [1, 3, 4]. On the other side, sequential pattern mining is one of the main topics in data mining methods [2, 6, 7, 8]. In this paper, we propose a mining mechanism based on *inter-pattern growth* and *intra-pattern growth*. These two pattern growth criteria are used to minimize useless pattern growth by finding these patterns, whose projected-patterns are the same, and letting them union beforehand. This results in less access times and much better performance.

The rest of this paper is organized as follows. In Section 2, the related works are given. In Section 3, the mining problem of virtual environment sequential patterns is introduced along with the notation that is used throughout the paper. The *PrefixUnion* mining algorithm is suggested in Section 4. To evaluate the efficiency of the *PrefixUnion* algorithm, our experimental results are presented in Section 5. Finally, we conclude our study in Section 6.

## 2 Related Works

### 2.1 Sequential Patterns Mining

Sequential pattern mining problem was first introduced in [6]. With the motivation of avoiding or substantially reducing the expensive candidate generation and pruning, the *FreeSpan* [9] and *PrefixSpan* [10] were proposed. On the other side, they still

have some non-trivial costs. One is that the full length original sequence must be retained in each projected database because a pattern can be generated by any subsequence combination. This leads to many duplicated sequences involved. The other is that the growth of a subsequence is explored at any split point in a candidate sequence resulting in several possible new subsequences.

### 3 Problem Formulation

#### 3.1 Notations

In this section, we introduce the terms used in our problem and mining algorithm. Let  $\Sigma = \{l_1, l_2, \dots, l_m\}$  be a set of  $m$  literals called *objects* (also called *items*) [1, 6]. A *view*  $v$  is denoted by  $v = \langle \chi_1, \chi_2, \dots, \chi_k \rangle$ , is an unordered list of objects such that each objects  $\chi_i \in \Sigma$ . The *view*  $v$  is defined as whatever the user stays and observes during the processing of virtual environments. A *sequence*  $S$ , denoted by  $\{v_1, v_2, \dots, v_n\}$ , is an ordered list of  $n$  views. Let the database  $D$  be a set of sequences (also called transactions). Each sequence records each user’s traversal path in walkthrough system. A sequence  $\beta = \langle \beta_1, \beta_2, \dots, \beta_k \rangle$  is a *subsequence* (or is called *contained*) of sequence  $\alpha = \langle \alpha_1, \alpha_2, \dots, \alpha_n \rangle$  if there exists  $1 \leq i_1 < i_2 < \dots < i_k \leq n$  such that  $\beta_1 \subseteq \alpha_{i_1}, \beta_2 \subseteq \alpha_{i_2}, \dots, \beta_k \subseteq \alpha_{i_k}$  holds. The *support* of a sequence  $p$  in the sequence database  $D$  is defined as the number of the sequences which contain this pattern  $p$ . A *frequent sequence* is a sequence whose support is equal to or more than the user defined threshold (also called *min\_support*). A *frequent pattern* is a *maximal sequence* that is *frequent*. Finally, let  $P$  be a set of all frequent patterns in  $D$ .

### 4 PrefixUnion Mining Algorithm

In order to realize our pattern-growth approach, we will define two kinds of pattern-growth types. One is the *intra-view growth* – the growth of pattern is bounded by the

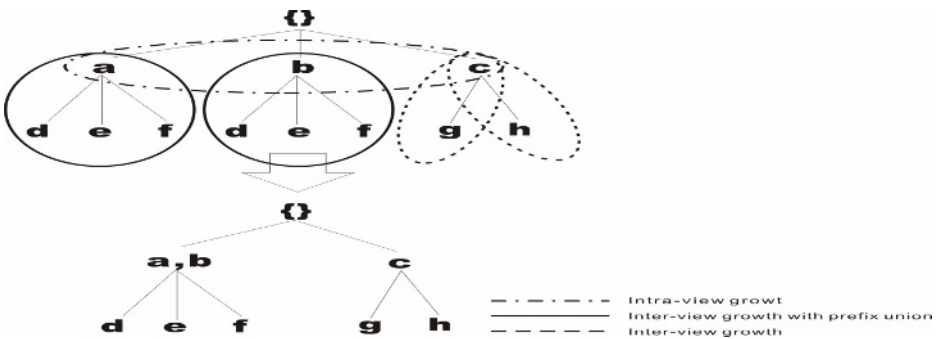


Fig. 1. Scenario of differences among intra-view growth, inter-view growth and inter-view growth with *PrefixUnion*

view boundary. The other is the *inter-view growth* – the growth of pattern is to select an object in next view. The pattern-growth algorithm is based on recursively constructing the patterns. The  $\alpha$ -projected sub-database is defined as the set of subsequences in the database which the *suffixes* of the sequences have the common *prefix*  $\alpha$ . In order to demonstrate this concept, these relationships are shown in the Figure 1.

In Figure 1, objects  $a$ ,  $b$ , and  $c$  are contained in the same view (i.e., the intra-view growth). Object  $a$  and its siblings belong to the inter-view growth. Object  $b$  also has the same case. Object  $c$  and its siblings is another different example of inter-view growth (i.e.  $c---g$  and  $c---h$ ). Only the object  $a$  and object  $b$  can be applied by *PrefixUnion* approach. After the processing, both objects  $a$  and  $b$  are merged. By this *PrefixUnion* property, the search space is reduced sharply in each step. This property improves much better performance, especially in the presence of small minimum support threshold.

## 5 Experimental Results

In this section, the effectiveness of the proposed mining algorithm is investigated. The data set is about 437 MB of 1,256 objects in the system. The traversal path consist of approximately 10 ~ 15 views from one end to the other end.

In the Figure 2, our algorithm outperforms the pattern growth method. If the locations of any two objects are too far in the virtual environments, it is naturally assumed that there are no relationships between the objects. In other words, the relationships are limited and restricted compared to the IBM dataset.

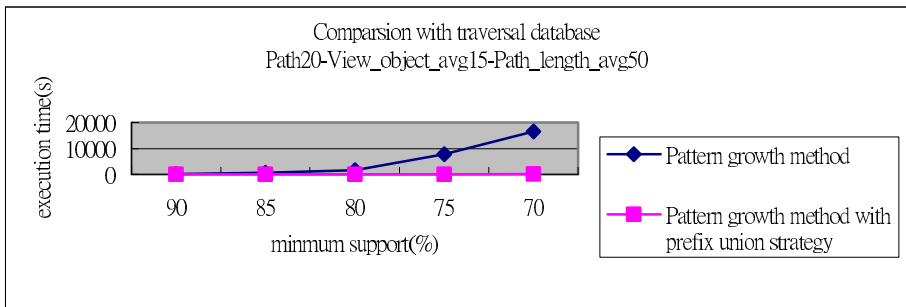


**Fig. 2.** Comparison of traditional pattern growth mining algorithm and our *PrefixUnion* mining algorithm in our virtual environments

## 6 Conclusions and Future Work

We have extended the applications of mining. With properties of intra-view pattern growth and inter-view pattern growth added, it is more precise and useful for us to discover the frequent traversal patterns. Besides, we also consider how to efficiently mining the necessary patterns in order to speed up the computations.

## References

- [1] Daniel G. Aliaga, and Anselmo Lastra, "Automatic Image Placement to Provide a Guaranteed Frame Rate", *Proceedings of the 26th Annual Conference on Computer Graphics and Interactive Techniques*, pp. 307-316, 1999.
- [2] Ming-Syan Chen, Jong Soo Park, and Philip S. Yu, "Efficient Data Mining for Path Traversal Patterns", *IEEE Transactions on Knowledge and Data Engineering*, Vol. 10, Issue 2, pp. 209-221, 1998.
- [3] Y. Nakamura, S. ABE, Y. Ohsawa, and M. Sakauchi, "A Balanced Hierarchical Data Structure Multidimensional Dada with Efficient Dynamic Characteristic", *IEEE Transactions on Knowledge and Data Engineering*, Vol. 5, No. 4, pp. 682-694, 1993.
- [4] Y. Nakamura and T. Tamada, "An Efficient 3D Object Management and Interactive Walkthrough for the 3D Facility Management System", *Proc. IECON'94*, Vol. 2, pp. 1937-1941, 1994.
- [5] T. Morzy, M. Wojciechowski, and M. Zakrzewicz, "Pattern-Oriented Hierarchical Mining", *Proc. of the 3rd East European Conference on Advances in Databases and Information Systems (ADBIS'99)*, Maribor, Slovenia, LNCS 1691, Springer-Verlag, 1999.
- [6] Rakesh Agrawal, Tomasz Imielinski and Arun N. Swami, "Mining Association Rules between Sets of Items in Large Databases", *Proceedings of the 1993 ACM SIGMOD International Conference on Management of Data*, pp.207-216, 1993.
- [7] Rakesh Agrawal, and R. Srikant, "Mining Sequential Patterns", *Proceedings of the 1995 International Conference on Data Engineering (ICDE'95)*, pp.3-14, 1995.
- [8] Rakesh Agrawal, and R. Srikant, "Mining Sequential Patterns: Generalizations and Performance Improvements", *Proceeding Fifth International Conference on Extending Database Technology (EDBT'96)*, pp.3 -17, Mar 1996.
- [9] J.pei, J.han, B. M-Asl, J. Wang, H. pinto, Q. Chen, U. Dayal, and M.-C. Hsu, "FreeSpan: Frequent Pattern-Projected Sequential Pattern Mining", *Proceedings of the 2000 ACM SIGKDD International Conference Knowledge in Database (KDD'90)*, pp. 355-359, August 2000.
- [10] J.pei, J.han, B. M-Asl, J. Wang, H. pinto, Q. Chen, U. Dayal, and M.-C. Hsu, "Prefix-Span: Mining Sequential Patterns Efficiently by Prefix-Projected Pattern Growth", *Proceedings of the 2001 International Conference Data Engineering (ICDE'01)*, pp. 215-224, April 2001.



# Efficient Interactive Pre-integrated Volume Rendering

Heewon Kye<sup>1,3</sup>, Helen Hong<sup>2</sup>, and Yeong Gil Shin<sup>1,3</sup>

<sup>1</sup> School of Computer Science and Engineering, Seoul National University  
{kuei, yshin}@cglab.snu.ac.kr

<sup>2</sup> School of Computer Science and Engineering, BK21: Information Technology, Seoul  
National University, San 56-1 Shinlim-dong Kwanak-gu, Seoul 151-742, Korea  
hlhong@cse.snu.ac.kr

<sup>3</sup> INFINITT Co., Ltd., Taesuk Bld., 275-5 Yangjae-dong Seocho-gu, Seoul 137-934, Korea

**Abstract.** Pre-integrated volume rendering has become one of the most efficient and important techniques in three dimensional medical visualization. It can produce high-quality images with less sampling. However, two important issues have received little attention throughout the ongoing discussion of pre-integration: Skipping over empty-space and the size of lookup table for a transfer function. In this paper, we present a novel approach for empty-space skipping using the *overlapped-min-max block*. Additionally, we propose a new approximation technique to reduce the dependent texture size so that it decreases the size of texture memory and the update time. We demonstrate performance gain and decreasing memory consumption for typical renditions of volumetric data sets.

## 1 Introduction

Pre-integrated volume rendering is a technique for reconstructing the continuous volume rendering integral. Utilizing a pre-processed look-up table (called pre-integration table), this method not only eliminates a lot of artifacts but also reduces the sampling rate for rendering. However, since this method uses two consecutive sample values as an index for the pre-integration table which is constructed before rendering for a given classified function, conventional acceleration techniques such as empty space skipping or interactive classification methods are not applied as it is.

Skipping empty space has been extensively exploited to accelerate volume rendering. However, pre-integrated volume rendering samples two consecutive points as a line segment, previous empty-space skipping methods could not be directly applied. The pre-integration table is indexed by three integration parameters: two consecutive sample values and the distance between those samples. To accelerate the pre-integration step, Engel *et al.* reduced the dimensionality of the table from three to two by summing a constant sampling distance [1]. Even though they used a two-dimensional pre-integration table, it is still bulky when rendering high-precision data such as 12 bits-per-voxel data which is common in medical applications. A 12-bit image requires 256 times more memory and updating time than an 8-bit image.

In this paper, we present a novel data structure, called the *overlapped-min-max block* for applying empty-space scheme to the pre-integrated volume rendering, and a new approximation technique for reducing the dimensionality of the table from two to

one. We implement them on recent consumer graphics hardware and on software-only shear-warp rendering [2] and ray-casting [3]. With our accelerations, the rendering and classification speed is much faster for medical datasets while maintaining the image quality.

## 2 Overlapped Min-max Block for Empty-Space Skipping

Traditional rendering methods sample a value at a point in three-dimensional space to get a color and opacity. If a block is entirely transparent, additional samplings in the block can be skipped. Pre-integrated volume rendering samples two points to get their color and opacity. Since two sampling points form a line segment, or a slab, all the blocks that intersect the line segment should be transparent for skipping the sampling process. As shown in Fig. 1, a line segment may intersect at most three blocks in two-dimensional representation. Retrieving information three-times from the lookup table degrades the rendering performance. In addition, there is an overhead to determine which blocks are transparent (there are two cases such as Fig. 1a and Fig. 1b).

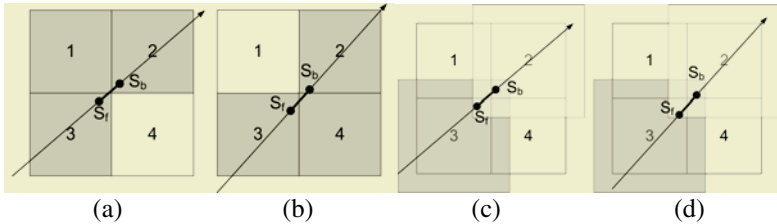


**Fig. 1.** The overlapped min-max table for pre-integrated volume rendering. There are two sampling point  $S_f$  and  $S_b$ , and four blocks from *block1* to *block4*.  $S_f$  is in *block3* and  $S_b$  is in *block2*. To skip the line segment  $S_f S_b$ , (a) *block1*, *block2*, and *block3* have to be transparent, (b) *block2*, *block3*, and *block4* have to be transparent in the previous block structure. Moreover, there is overhead to determine the current situation is either (a) or (b). In our method, *the overlapped-min-max block*, each block holds some region jointly with its neighbors such as (c) and (d). To skip the line segment, we can test only one block, *block2* (or *block3*)

Making each line segment belonging to only single block, we can efficiently decide whether we skip or not by testing one block. For this, we modify the region covered by each block. Each block covers some region of which thickness is at least the sampling distance as shown in Fig. 1c and Fig. 1d. By overlapping the region of each block, we can easily test whether the block of a line segment is transparent using only that block. This scheme is especially efficient on graphics hardware for its simplicity.

## 3 Efficient Pre-integration Table

In accelerated pre-integrated rendering, opacity of  $i$ -th sample ( $\alpha_i$ ) is written as:

$$1 - \alpha_i = 1 - \alpha(s_f, s_b) \approx \exp\left(-\frac{1}{s_b - s_f} (T(s_b) - T(s_f))\right) \tag{1}$$

where,  $T(s) := \int_0^s \tau(s) ds$ .

Because equation (1) comprehends the ray segment integral of a transfer function, we do not need to consider the maximum of the Nyquist frequencies of the transfer functions  $\tau(s)$  with the scalar field  $s$ . Therefore, it is sufficient to sample a volume with relatively low frequency. The 2D lookup table to obtain  $\alpha_i$ , requires a texture of which size is  $N^2$ , where  $N$  is density range. In order to generate color images, each texture entry requires 4 bytes. When an image has 12-bit pixel depth, the required texture size becomes  $4096^2$  and the required memory is  $4096^2 \times 4 \text{byte} = 64 \text{MB}$ . The bigger lookup table brings the longer generation time and lower cache-efficiency. In this paper, we propose an 1D-texture lookup method that needs only 4096 entries. Because scalar values  $s$  are usually quantized equation (1) can be rewritten as:

$$1 - \alpha_i \approx s_b - s_f \sqrt{\exp\left(-\sum_{s=s_f}^{s_b} \tau(s)\right)} = s_b - s_f \sqrt{\prod_{s=s_f}^{s_b} \exp(-\tau(s))} \approx \frac{1}{s_b - s_f} \sum_{s=s_f}^{s_b} \exp(-\tau(s)) = (S(s_b) - S(s_{f-1})) / (s_b - s_f) \quad (2)$$

where,  $S(x) = \sum_{s=0}^x \exp(-\tau(s)), S(-1) = 0$ .

We modify a geometric average of transparency, into an arithmetic average as shown in equation (2). Therefore, only 1D-texture  $S(x)$  needs to be stored to get the  $\alpha_i$ . The color can be formulized in a similar fashion.

## 4 Experimental Results

Experiments have been performed on a PC equipped with Pentium4 2.8GHz processor, 1GB main memory and an ATI 9800. Table 1 summarizes the performance using empty-space skipping (ESP). Obviously, skipping empty-space gains more performance. In hardware rendering, rendering time is reduced two times or more by using ESP. In software rendering, the gain of ESP is much bigger (10-30 times faster than w/o ESP). Since the angio dataset contains more empty space than the head dataset, the performance improvement factor of the angio dataset is bigger than that of the head dataset.

**Table 1.** A performance comparison in case of using empty-space skipping (msec)

Dataset	3D Hardware		Ray-Casting		Shear-Warp	
	with ESP	w/o ESP	with ESP	w/o ESP	with ESP	w/o ESP
BigHead	83.8	302.1	897.7	12409	747.6	7904
Angio	95.1	392.1	737.6	16183	339.6	9984

If a transfer function is fixed using 2D-texture (88.5ms) slightly faster than our 1D-texture (95.1ms) since 1D-texture requires two texture loads for classification while 2D-texture requires one. However, when the transfer function is changed, using our 1D-texture (101.2ms) is much faster than 2D-texture (824.4ms) because of lookup table creation time. Fig. 2 show rendered images of BigHead and Angio volume data, respectively. There is no noticeable difference between using 1D-texture and 2D-texture.

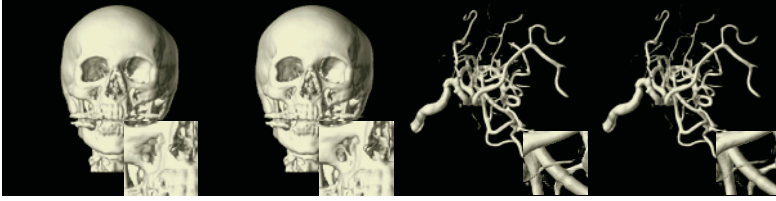


**Fig. 2.** The comparison of image quality for BigHead and Angio volume using (left) 1D-texture, (right) and 2D-texture

## 5 Conclusions

In this paper, we have proposed a new method to accelerate traversal and classification of both hardware and software based pre-integrated volume rendering. Using the overlapped-min-max block, empty-space skipping can be accomplished more efficiently and can be easily implemented in a hardware-based method. To reduce the classification time and memory consumption, a new approximation method of a lookup table is also proposed. With regard to image quality, we have presented the minimum bound of error theoretically. Experimental results show that our method produces the same quality of rendered images as the previous classification method of pre-integration.

## References

1. K. Engel, M. Kraus, and T. Ertl. High-Quality Pre-Integrated Volume Rendering Using Hardware-Accelerated Pixel Shading. *Eurographics / SIGGRAPH Workshop on Graphics Hardware*, Los Angeles, CA, USA, August 2001.
2. P. Lacroux and M. Levoy, Fast Volume Rendering Using a Shear-Warp Factorization of the Viewing Transformation. *Proceedings of SIGGRAPH 94*, 451-458, 1994.
3. M. Levoy, Display of Surfaces from Volume Data, *IEEE Computer Graphics & Application*, 8: 29-37, 1988.

# Ncvtk: A Program for Visualizing Planetary Data

Y. S. Sunderam<sup>1,4</sup>, Z. Zhang<sup>2,4</sup>, and R. A. Whalen<sup>3,4</sup>

<sup>1</sup> RS Information Systems

<sup>2</sup> Raytheon

<sup>3</sup> The College of New Jersey

<sup>4</sup> Geophysical Fluid Dynamics Laboratory, Princeton NJ 08542, USA

**Abstract.** Ncvtk is a visualization tool offering a high degree of interactivity to scientists who need to explore scalar and vector data on a longitude-latitude based grid. Ncvtk was born out of four recent trends: open source programming, the availability of a high quality visualization toolkit, the emergence of scripting, and the wide availability of fast and inexpensive hardware.

## 1 Why Ncvtk?

Planet-wide datasets are becoming increasingly available. These datasets are often large and complex, and their visualization is a challenging task. Ncvtk is a visualization tool designed to handle these datasets. It provides a high degree of interactivity, allowing scientists to explore the data in a way that is tailored to their needs. Ncvtk was developed as a result of four recent trends: open source programming, the availability of a high quality visualization toolkit, the emergence of scripting, and the wide availability of fast and inexpensive hardware. Ncvtk is a free software program, and its source code is available on the internet. It is designed to be easy to use, and it provides a rich set of features for exploring planetary data. Ncvtk is written in C++, and it uses the OpenGL graphics library for rendering. It is designed to run on a wide range of platforms, including Linux, Solaris, and Windows. Ncvtk is a powerful tool for visualizing planetary data, and it is a valuable addition to any scientist's toolkit.

## 2 Building Blocks

Ncvtk is built using a number of building blocks. These building blocks are: (1) the C++ programming language, (2) the OpenGL graphics library, (3) the Qt widget toolkit, and (4) the NetCDF data format. Ncvtk is designed to be easy to use, and it provides a rich set of features for exploring planetary data. Ncvtk is a powerful tool for visualizing planetary data, and it is a valuable addition to any scientist's toolkit.



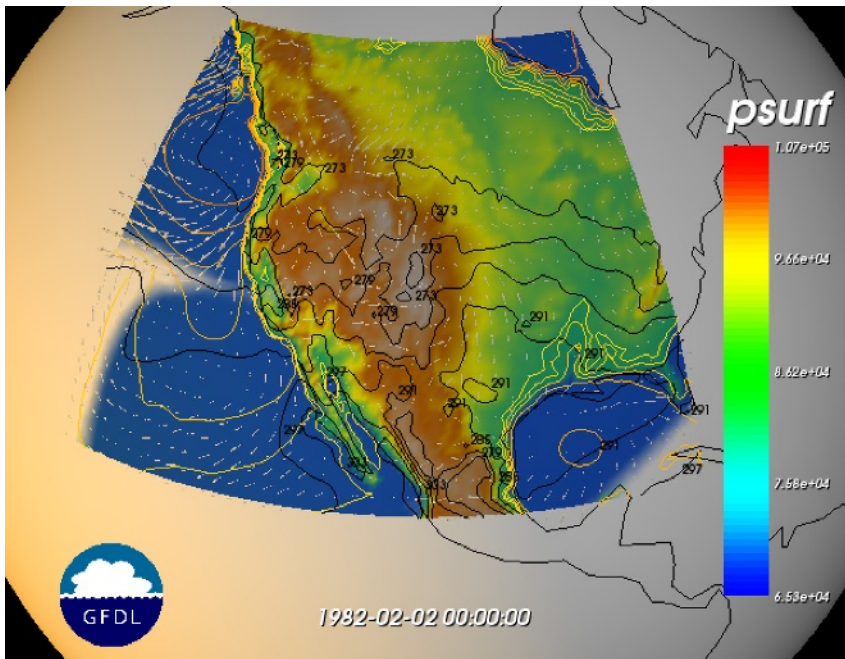


Fig. 1. Non-hydrostatic atmospheric simulation obtained using the ZETAC code

The ZETAC code is a non-hydrostatic atmospheric simulation code. It is designed to simulate the atmosphere in a non-hydrostatic regime, which is essential for modeling small-scale atmospheric phenomena. The code uses a vertical sigma coordinate system and a semi-implicit time integration scheme. It includes a comprehensive set of physical processes, such as radiation, convection, and cloud microphysics. The ZETAC code is highly flexible and can be configured to simulate a wide range of atmospheric conditions and scales.

## 4 Summary

The ZETAC code is a non-hydrostatic atmospheric simulation code. It is designed to simulate the atmosphere in a non-hydrostatic regime, which is essential for modeling small-scale atmospheric phenomena. The code uses a vertical sigma coordinate system and a semi-implicit time integration scheme. It includes a comprehensive set of physical processes, such as radiation, convection, and cloud microphysics. The ZETAC code is highly flexible and can be configured to simulate a wide range of atmospheric conditions and scales.

The program is written in C++ and uses the VTK library for rendering. It is designed to be run on a Linux system. The program is distributed under the terms of the GNU General Public License. The program is available for download from the SourceForge website. The program is also available for purchase from the Kitware website. The program is designed to be used by researchers in the field of planetary science. The program is designed to be used by researchers who are interested in the visualization of planetary data. The program is designed to be used by researchers who are interested in the visualization of planetary data. The program is designed to be used by researchers who are interested in the visualization of planetary data. The program is designed to be used by researchers who are interested in the visualization of planetary data.

(1) The program is designed to be used by researchers who are interested in the visualization of planetary data. The program is designed to be used by researchers who are interested in the visualization of planetary data. The program is designed to be used by researchers who are interested in the visualization of planetary data. The program is designed to be used by researchers who are interested in the visualization of planetary data.

## Acknowledgments

The author would like to thank the following individuals for their assistance in the development of this program: [List of names and affiliations].

## References

1. <http://ncvtk.sourceforge.net>
2. <http://public.kitware.com/VTK/>
3. <http://www.pfdubois.com/num.py/>
4. <http://www.gfdl.noaa.gov/~fms/>
5. [http://www.cdc.noaa.gov/cdc/conventions/cdc\\_netcdf\\_standard.shtml](http://www.cdc.noaa.gov/cdc/conventions/cdc_netcdf_standard.shtml)
6. Orlanski, I., Gross, B. D.: Orographic modification of cyclone development. *J. Atmos. Sci.*, **51**, 589–611.
7. [http://meteora.ucsd.edu/~pierce/ncview\\_home\\_page.html](http://meteora.ucsd.edu/~pierce/ncview_home_page.html)
8. [http://ncvtk.sourceforge.net/ncvtk\\_tutorial.pdf](http://ncvtk.sourceforge.net/ncvtk_tutorial.pdf)
9. <http://sourceforge.net>



# Efficient Multimodality Volume Fusion Using Graphics Hardware

Helen Hong<sup>1</sup>, Juhee Bae<sup>2</sup>, Heewon Kye<sup>2</sup>, and Yeong Gil Shin<sup>2</sup>

<sup>1</sup> School of Computer Science and Engineering,  
BK21: Information Technology, Seoul National University  
hlhong@cse.snu.ac.kr

<sup>2</sup> School of Computer Science and Engineering, Seoul National University,  
San 56-1 Shinlim 9-dong, Kwanak-gu, Seoul 151-742, Korea  
{jhbay, kuei, yshin}@cglab.snu.ac.kr

**Abstract.** We propose a novel technique of multimodality volume fusion using graphics hardware that solves the depth cueing problem with less time consumption. Our method consists of three steps. First, it takes two volumes and generates sample planes orthogonal to the viewing direction following 3D texture mapping volume rendering. Second, it composites textured slices each from different modalities with several compositing operations. Third, alpha blending for all the slices is performed. For the efficient volume fusion, a pixel program is written in HLSL(High Level Shader Language). Experimental results show that our hardware-accelerated method distinguishes the depth of overlapping region of the volume and renders them much faster than conventional ones on software.

## 1 Introduction

In clinical medicine, several different modalities such as Positron Emission Tomography (PET), Computed Tomography (CT), and Magnetic Resonance Imaging (MRI) are useful for radiologists and surgeons to help diagnosis support and treatment planning. These modalities give complementary information when they are shown simultaneously. Thus many medical applications require visual output generated from multimodality volumes rather than only one volume.

Several methods have been proposed to combine multiple volumes obtained from multimodality imaging. Cai and Sakas [1] proposed three different intermixing approaches. The shortcoming of the method was a lack of precise depth cueing among the multiple volumes, even though they tried to use Z-buffer value. Jacq and Roux [2] presented a multi-volume rendering focused on material classification which applied different material percentages and merging rules at each sampling point. Zuiderveld et al. [3] described how to cache calculated voxel properties using sized hash table that contribute to the final result. Previous researches have performed multimodality volume fusion on software. However, the software-based multimodality fusion has a limitation in depth presentation and processing time. In this paper, we propose an efficient hardware-accelerated solution to combine multimodality volumes at interactive rates.

## 2 Multimodality Volume Fusion

Fig. 1 shows the pipeline of our method for multimodality volume fusion. We assume reference and float volume datasets have the same orientation by setting rigid transformation that would be sufficient for the registration of the datasets [4].

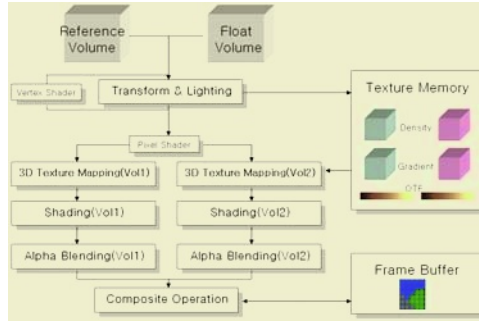


Fig. 1. The pipeline of multimodality volume fusion

### 2.1 Depth Compositing of the Volume

Since multiple volumes have different size and orientation, it needs correct depth composition and orientation. Fig. 2 shows different ways to combine two slices from each volume. In Fig. 2(a), it is required to set the orders of each slice of the volumes which is a troublesome work. We combine each texture with same texture coordinates from different volumes before blending as shown in Fig. 2(b). Two voxels (ultimately texels) referred to the same texture coordinates are combined by the compositing operations and then they are mapped to the same slice.

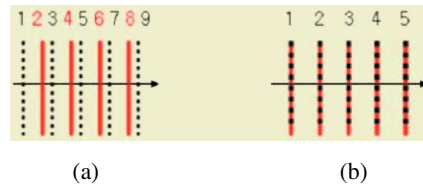


Fig. 2. A comparison of blending textures (black dotted line: slice of reference volume, red solid line: slice of float volume) (a): alpha blending in slice orders (b): combine textures before alpha blending

### 2.2 Compositing Operations for Volume Fusion

Several compositing operations are experimented to find an appropriate combining method; some are referred from the previous compositing researches [7][8].

The results of combined color and opacity of over, XOR, plus and weighted addition operation are shown from Eq. (1) to Eq. (4), respectively.

$$C = \frac{\alpha_A \cdot C_A + (1 - \alpha_A)\alpha_B \cdot C_B}{\alpha_A + (1 - \alpha_A) \cdot \alpha_B} \quad (1) \quad C = \frac{(1 - \alpha_B) \cdot \alpha_A \cdot C_A + (1 - \alpha_A)\alpha_B \cdot C_B}{(1 - \alpha_B) \cdot \alpha_A + (1 - \alpha_A) \cdot \alpha_B} \quad (2)$$

$$\alpha = \alpha_A + (1 - \alpha_A) \cdot \alpha_B \quad \alpha = (1 - \alpha_B) \cdot \alpha_A + (1 - \alpha_A) \cdot \alpha_B$$

$$C = C_A + C_B \quad (3) \quad C = \frac{weight \cdot \alpha_A \cdot C_A + (1 - weight) \cdot \alpha_B \cdot C_B}{weight \cdot \alpha_A + (1 - weight) \cdot \alpha_B} \quad (4)$$

$$\alpha = \alpha_A + \alpha_B \quad \alpha = weight \cdot \alpha_A + (1 - weight) \cdot \alpha_B$$

(0 ≤ weight ≤ 1)

where C indicates color, α indicates alpha, A refers to the first volume, and B to the second volume.

### 2.3 Weighted Opacity for Surface Extraction

To see a float volume through a reference volume, we consider weight to the opacity as shown in Eq. (5). The weight value tells whether the pixel is a part of the surface or a part of the homogeneous region by gradient magnitude. In the preprocessing step, gradient magnitude is used as normal for shading. Here, we use gradient magnitude as a numerical divergence which implies that the surface has higher value while homogeneous part has a lower value. During fusion process, we let the homogeneous area to be transparent so that we could see through the reference volume by eliminating the opacity value of the homogeneous area between reference and float volume of the overlapping area.

$$weight = \begin{cases} 0 & \text{if } (|\nabla| < c) \quad (c : \text{constant}) \\ 1 & \text{else} \end{cases} \quad (5)$$

## 3 Experimental Results

All our implementation and tests have been performed on an Intel Pentium IV PC containing 2.53 GHz CPU with ATI Radeon X800 256 MB RAM. Our method

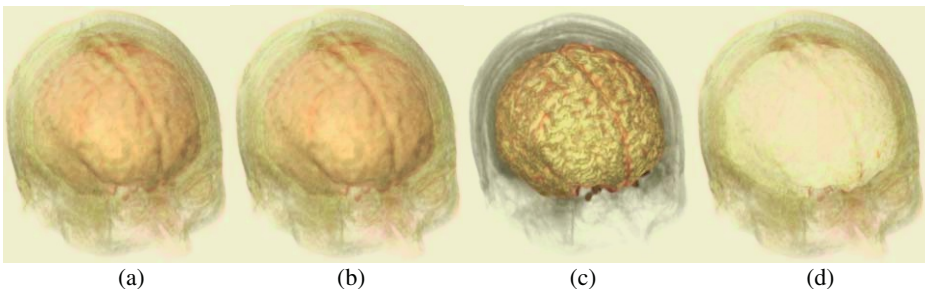


**Fig. 3.** The results of compositing operations at opacity 8. (a) over (b) XOR(exclusive OR) (c)weight addition (d) plus operation

has been applied to the brain of 256 x 256 x 96 MR images and 128 x 128 x 40 PET images with 2 bytes-intensity. The performance of our method is evaluated with the aspects of visual inspection and processing time.

Fig. 3 displays the results using several compositing operations. Fig. 3(a) and Fig. 3(b) show the result of over operation and XOR(exclusive OR). Fig. 3(c) using weight addition displays rather a dark but manifest result compared to others. Fig. 3(d) represents a result of plus operation to be mainly white because the colors are simply added which induces overflow.

The average of the processing time of the fusion volume supported by software is 3703 msec while fusion on hardware is 625 msec, respectively. We gained about 5 to 6 times of speed enhancement on rendering time.

## 4 Conclusion

We have developed an efficient multimodality volume fusion method using graphics hardware. Our method presents several approaches of combining two different volume datasets into a singular image representation. MR and PET images of the brain have been used for the performance evaluation with the aspects of visual inspection and processing time. Our method shows the exact depth of each volume and the realistic views with interactive rate in comparison with the software-based multimodality volume fusion. Distinguishable and fast result of the proposed method can be successfully utilized in medical diagnosis.

## References

1. Cai W., Sakas G., Data Intermixing and Multi-volume Rendering, Computer Graphics Forum (1999), 18(3): 359-368.
2. Jaeg, J., Roux, C., A Direct Multi-volumes Rendering Methods Aiming at Comparison of 3D Images and Methods, IEEE Trans. On Information Technology in Biomedicine (1997) 1(1):30-43.
3. Zuiderveld, K.J., Viergever, M.A., Multi-modal Volume Visualization using Object-oriented methods, in Proc. IEEE/ACM Volume Visualization '94 Symposium (1994) 59-66.
4. Hong, H., Shin, Y., Intensity-based registration and combined visualization of multimodal brain images for noninvasive epilepsy surgery planning, Proc. of SPIE Medical Imaging (2003).

# G<sup>1</sup> Continuity Triangular Patches Interpolation Based on PN Triangles

Zhihong Mao, Lizhuang Ma, and Mingxi Zhao

Dept. of Computer Science and Engineering, Shanghai Jiao Tong University, PR China  
{mzh\_yu, ma-lz, zhaomx}@sjtu.edu.cn

**Abstract.** There are currently many methods for triangular local interpolation: Given triangular meshes P in three dimension space, the given flat triangles are based only on the three vertices and three normal vectors, or PN triangles, construct a smooth surface that interpolates the vertices of P. In this paper a completely local interpolation scheme is presented to guarantee to join patches G<sup>1</sup> continuously around boundary curves of each PN triangle.

## 1 Introduction

It is well-known that the interpolation of curved triangular patches over PN triangular meshes, each triangle is based on the three vertices and the corresponding normal vectors, is an important tool in computer aided geometric design. The common approach [1,2,3] is to firstly create a cross boundary tangent vector field for each boundary and then to construct patches that agree with these cross boundary fields. Steven [4] gave a unifying survey of the published methods. Stephen Mann [5] discusses a method for increasing the continuity between two polynomial patches by adjusting their control points. But all these methods must know the information of two adjacent patches and they are not completely local method.

Stefan Karbacher [6] present a non-linear local subdivision scheme for the refinement of triangle meshes. Overveld [7] gave an algorithm for polygon subdivision based on point-normals. Alex Vlachos [8] introduced curved point-normal (PN) triangles to replace the flat triangle. In these methods the authors only consider the point-normals of the input triangle and they are completely local. But they only construct C<sup>0</sup> continuity meshes. In this paper our objective is to construct a smooth G<sup>1</sup> continuity surface.

## 2 Triangular G<sup>1</sup> Local Interpolation Based on PN Triangles

In this paper we shall employ the quartic Bézier polynomial to define a triangular patch with linear normal patch:

$$\rho(\lambda_1, \lambda_2, \lambda_3) = \sum_{i=0}^4 \sum_{j=0}^{4-i} b_{i,j,k} B^4_{i,j,k}(\lambda_1, \lambda_2, \lambda_3); \quad B^4_{i,j,k}(\lambda_1, \lambda_2, \lambda_3) = \frac{4!}{i!j!k!} \lambda_1^i \lambda_2^j \lambda_3^k \quad (2.1)$$

$$Q_1(\lambda_1, \lambda_2, \lambda_3) = \lambda_1 q_{1,0,0} + \lambda_2 q_{0,1,0} + \lambda_3 q_{0,0,1} \quad (2.2)$$

$b_{i,j,k}$  and  $q_{i,j,k}$  are respectively the control points of curved patches of the surface  $\rho_i$  and corresponding linear normal patches  $Q_l$ .

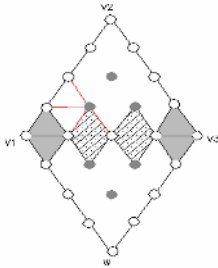


**Fig. 1.** Two patches meeting along a common boundary

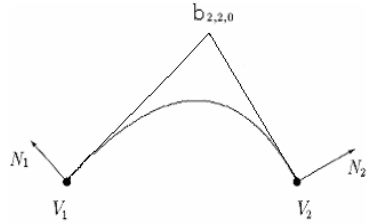


**Fig. 2.** Determination of  $b_{2,2,0}$

As illustrated schematically in Fig.1, these two patches will share boundary edge  $V_1V_3$ . To meet with  $G^1$  continuity, each of the four panels of four control points must be coplanar. We get  $G^1$  continuity by adjusting the inner control points [5]. As illustrated by red lines, an inner point has four constrains, but only three freedoms. In order to solve the problem, we make the gray triangle degenerate to become a point. So for quartic Bézier polynomial control points we have:

$$b_{4,0,0} = b_{3,1,0} = b_{3,0,1} ; b_{0,4,0} = b_{1,3,0} = b_{0,3,1} ; b_{0,0,4} = b_{0,1,3} = b_{1,0,3} \tag{2.3}$$

**2.1 Determination of Boundary Curve**

In the following parts of this section we only consider the edge  $e_3(V_1V_2, \lambda_3 = 0)$  (see Fig. 2). We have  $b_{4,0,0} = b_{3,1,0}$  and  $b_{0,4,0} = b_{1,3,0}$ , the next is to determine  $b_{2,2,0}$ . Here we decide the point  $b_{2,2,0}$  by the intersection of three planes: 1) The first plane is decided by the point  $V_1$  and the corresponding normal  $N_1$ ; 2) The second plane is decided by the point  $V_2$  and the corresponding normal  $N_2$ ; 3) The third plane is decided by two lines, the one line is  $V_1V_2$ , another line is  $((V_1+V_2)/2 + (N_1+N_2)/2)$ .

**2.2 Construct the Boundary Normal Curves**

From equation (2.2) we can get  $Q_1(\lambda_1, \lambda_2, 0) = \lambda_1 q_{1,0,0} + \lambda_2 q_{0,1,0}$  (on edge  $e_3$ ),  $Q_l(\lambda_1, \lambda_2, 0)$  must interpolate  $N_1$  and  $N_2$ :  $q_{1,0,0} = \omega_1 N_1$ ;  $q_{0,1,0} = \omega_2 N_2$ , Where  $\omega_1, \omega_2$  are positive constants. If the boundary curve is  $G^1$  continuity, we must have

$$Q_1 \cdot \left( \frac{\partial \rho}{\partial \lambda_1} - \frac{\partial \rho}{\partial \lambda_2} \right) = 0, \text{ or } [\lambda_1 q_{1,0,0} + \lambda_2 q_{0,1,0}] \cdot [(b_{4,0,0} - b_{3,1,0}) \lambda_1^3 + 3(b_{3,1,0} - b_{2,2,0}) \lambda_1^2 \lambda_2 + 3(b_{2,2,0} - b_{1,3,0}) \lambda_1 \lambda_2^2 + (b_{1,3,0} - b_{0,4,0}) \lambda_2^3] = 0 \tag{2.4}$$

The equation equals zero means that the coefficients of each term must be zero and we have  $b_{4,0,0} = b_{3,1,0}$  and  $b_{0,4,0} = b_{1,3,0}$ , so equation (2.4) can be simplified to the following equation:

$$(q_{1,0,0} + q_{0,1,0}) \bullet (V_1 - V_2) = 0 \tag{2.5}$$

Now the problem become to finding reasonable values for  $\omega_1$ , then use equation (2.5) to compute  $\omega_2$ . Here we set  $\omega_1 = 1$ .

### 2.3 Decide the Inner Control Points

The next is to decide the still unknown inner control points  $b_{1,2,1}, b_{2,1,1}$  and  $b_{1,1,2}$ . In order to construct cross boundary  $G^1$  continuity, we must hold (the edge  $e_3$ ):

$$Q_l(\lambda_1, \lambda_2, 0) \bullet \left( \frac{\partial \rho}{\partial \lambda_2} - \frac{\partial \rho}{\partial \lambda_3} \right) = (\lambda_1 q_{1,0,0} + \lambda_2 q_{0,1,0}) \bullet \left( \frac{\partial \rho}{\partial \lambda_2} - \frac{\partial \rho}{\partial \lambda_3} \right) = 0 \tag{2.6}$$

The equation equals zero means that the coefficients of each term must be zero and associate with equation (2.5), we can get following equations:

$$N_1 \bullet (V_1 - b_{2,1,1}) = 0; N_2 \bullet (V_2 - b_{1,2,1}) = 0; \omega_2 N_2 \bullet (V_2 - b_{2,1,1}) + \omega_1 N_1 \bullet (V_2 - b_{1,2,1}) = 0 \tag{2.7}$$

Using the same computation for  $e_1$  and  $e_2$ , we have:

$$N_3 \bullet (V_3 - b_{1,1,2}) = 0; N_2 \bullet (V_2 - b_{1,2,1}) = 0; \omega_3 N_3 \bullet (V_3 - b_{1,2,1}) + \omega_4 N_2 \bullet (V_3 - b_{1,1,2}) = 0$$

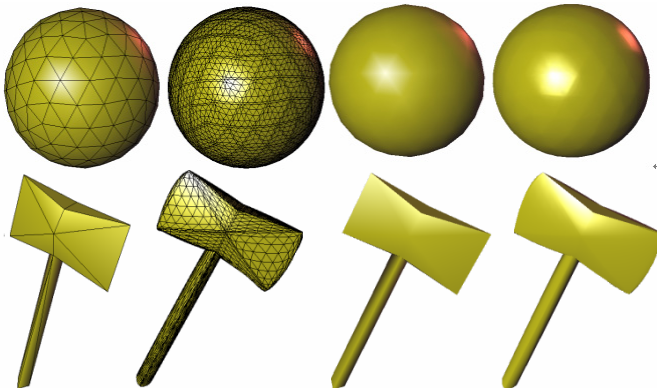
$$N_3 \bullet (V_3 - b_{1,1,2}) = 0; N_1 \bullet (V_1 - b_{2,1,1}) = 0; \omega_5 N_1 \bullet (V_1 - b_{1,1,2}) + \omega_6 N_3 \bullet (V_1 - b_{2,1,1}) = 0 \tag{2.8}$$

Unite equation (2.7) and (2.8), we get six equations, but we have 9 unknown values. Here we optimized the fairness of the given patch by reducing its curvature [9]. A standard measure for the surface quality in geometric modeling is the thin plate energy:  $E(s) \approx \int_{\Delta} F^2_{uu} + 2F^2_{uv} + F^2_{vv}$ . where  $\Delta$  denotes the domain triangle  $V_1V_2V_3$ .

Now we can determine the free parameters by minimizing  $E(s)$ .

## 3 Conclusion

Methods for local interpolation of triangulated, parametric data have existed for many years and received more and more attention. However it is difficult to construct cross boundary continuity surface. So the presented local methods are  $C^0$  continuity. In this paper we present a completely local method to construct  $G^1$  boundary continuity patches based on the point-normals of the inputted flat triangles. The examples used and shown (see Fig.3,4) demonstrate that this algorithm can produce a very smooth mesh from an initial coarse mesh model. However in order to construct  $G^1$  boundary



**Figs. 3,4.** (from left to right) (a) initial mesh (b) mesh with our method (c) shading model (initial mesh) (d) shading for our scheme

continuity patches, we make the triangle attached to each vertex degenerate to become a point and introduce non-regular points. The investigation about non-regular points is not involved in this paper.

## Acknowledgments

The work was partially supported by national natural science foundation of China (Grand No. 60373070 and No. 60173035) and 863 High Tech Project of China (Grant No. 2003AA411310).

## References

- [1] H. chiyokura and F. Kimura. Design of solids with free-form surfaces. *Computer Graphics*, 17(3):289-298, 1983.
- [2] G. Herron. Smooth closed surfaces with discrete triangular interpolants. *CAGD*, 2(4):297-306, December 1985.
- [3] T. Jensen. Assembling triangular and rectangular patches and multi-variate splines. In G. Farin, editor, *Geometric Modeling: Algorithms and New Trends*, pages 203-220. SIAM.
- [4] Steve Mann, Charles Loop, Michael Lounsbery, etc. A survey of parametric scattered data fitting using triangular interpolants. In *Curve and surface Modeling*. SIAM.
- [5] S. Mann. Continuity adjustments to triangular bezier patches that retain polynomial precision. Research Report CS-2000-01, 2000.
- [6] Stefan Karbacher, Stefan Seeger and Gerd Häusler. A Non-linear Subdivision scheme for Triangle Meshes. *Proc. Of Vision, Modeling and Visualization*: 163-170, 2000.
- [7] C.W.A.M. van Overveld and b.Wyvill. An algorithm for polygon subdivision based on vertex normals. In *Computer Graphics International* : 3-12, 1997.
- [8] Vlachos Alex, Jörg Peters, Chas Boyd and Jason L. Mitchell. Curved PN Triangles. *ACM Symposium on Interactive 3D Graphics* :159-166, 2001.
- [9] Moreton H. and C. Sequin, Functional optimization for fair surface design, *SIGGRAPH 92 proceeding*, 167-176.



# Estimating 3D Object Coordinates from Markerless Scenes

Ki Woon Kwon<sup>1</sup>, Sung Wook Baik<sup>2</sup>, and Seong-Whan Lee<sup>1,\*</sup>

<sup>1</sup> Korea University, Seoul 136-713, Korea  
{kwkwon, swlee}@image.korea.ac.kr

<sup>2</sup> Sejong University, Seoul 143-747, Korea  
sbaik@sejong.ac.kr

**Abstract.** This paper presents a novel method for estimating the coordinates of a 3D object using the four vertices of a quadrangle and the camera motion parameters. Estimation of 3D object coordinates from 2D images of video is a studied problem in augmented reality. However, most solutions are dependent on fiducial markers in video or known coordinate systems which are required with superimposition of virtual object on frames. In this paper, we begin with the fact that the rectangular objects in 3D real world are projected the perspective quadrangle onto image planes. We can estimate 3D object coordinates from 4 vertices of quadrangular objects through transformation of image coordinates. The camera motion parameters between pairs of successive frames in a sequence are calculated using epipolar geometry.

## 1 Introduction

An AR system should be able to [1] 1) combine real environments and computer-generated virtual objects, 2) operate virtual objects interactively with the change in the real world, and 3) align virtual graphic objects onto real environments. When a virtual object is superimposed in a reference frame, the frame should contain one plane with which a  $3 \times 3$  planar homography can be found [2-5].

The homography is the transformation modeling the 2D movement of coplanar points under perspective projection. To obtain another planar homography between two consecutive frames in a sequence, different methods calculating camera motion to use multiple planes have been considered [4].

Kutulakos and Vallino proposed a system that can represent 3D graphic objects using four pairs of prior affine basis points that correspond to a sequence of images extracted from two uncalibrated affine cameras [6]. Another system involves a perspective camera model. This is more difficult to estimate the projective reconstruction from perspective views than using affine reconstruction from orthographic views [7].

In this paper, we estimate the direction of the Z-axis and the vertices of a quadrangle that is defined in a reference frame. The consecutive frames are computed for the essential stereoscopic matrix using epipolar geometry, and the estimated coordinates of the 3D object are determined from the camera motion parameters [8].

---

\* Author for Correspondence.

## 2 Estimating the Coordinates of a 3D Object

The rectangle is deemed to be one side of a rectangular parallelepiped. Consequently, its X-, Y- and Z-axes are at right angles to each other. Based on this fact, the Z-axis of the rotation angle is determined via complex rotations of the X- and Y-axes in the real world. The estimated direction of the Z-axis can be used to calculate the angles among the X-, Y- and Z-axes, and these angles are used when overlaying a 3D graphic object on the frame image.

To estimate the direction of the Z-axis, the image coordinates are rotated by applying the Euler-angle to each axis. The vertices and center point of a quadrilateral which the user designates from a reference frame, are applied to Equation 1.

$$\begin{bmatrix} 1+D \cdot E & -C+A \cdot H & B+A \cdot J \\ C+D \cdot H & 1+D \cdot F & -A+D \cdot I \\ -B+D \cdot J & A+D \cdot I & 1+A \cdot G \end{bmatrix} \quad (1)$$

where

$$A = a \cdot \sin \theta, \quad B = b \cdot \sin \theta, \quad C = c \cdot \sin \theta, \quad D = (1 - \cos \theta)$$

$$E = a^2 - 1, \quad F = b^2 - 1, \quad G = c^2 - 1, \quad H = ab, \quad I = bc, \quad J = ac$$

Then, the unit vector in the direction of the Z-axis can be calculated. Equation 1 is a transformation matrix used for rotating an object about an arbitrary axis.

## 3 Calculating Camera Motion Parameters

We develop another method for extracting camera motion parameters using a monoscopic system. Most of the video sequences used are pictures in which the intrinsic parameters of the camera are unknown. Therefore, the intrinsic parameters of the camera are set to a fixed skew of 0, an aspect ratio of 1, and the principle point is in the center of the quadrangle. The extrinsic parameters are calculated as an essential matrix. A pair of successive frames has the similar property with images of left and right camera. To get the cross product with vector and matrix,  $S$  is a skew symmetric matrix. And, the  $R \cdot S$  matrix, an essential matrix is computed by Equation 2.

$$q_r^T \cdot (R \cdot S) \cdot q_l = 0 \quad (2)$$

The essential matrix  $R \cdot S$  is computed using Equation 2, using an 8-point algorithm. In addition,  $E$  in a  $3 \times 3$  matrix is computed using Equation 3 and 4, and the property of the epipolar constraint. In order to calculate the essential matrix, we expand the equation,

$$x^T E x = 0 \quad (3)$$

For 8 point correspondences, Equation 6 becomes

$$Ae = 0 \tag{4}$$

where

$$A = \begin{bmatrix} u'_1 u_1 & u'_1 v_1 & u'_1 & v'_1 u'_1 & v'_1 v_1 & v'_1 & u_1 & v_1 & 1 \\ u'_2 u_2 & u'_2 v_2 & u'_2 & v'_2 u'_2 & v'_2 v_2 & v'_2 & u_2 & v_2 & 1 \\ \vdots & \vdots & \vdots & \vdots & \vdots & \vdots & \vdots & \vdots & \vdots \\ u'_8 u_8 & u'_8 v_8 & u'_8 & v'_8 u'_8 & v'_8 v_8 & v'_8 & u_8 & v_8 & 1 \end{bmatrix}$$

and  $e = (e_{11}, e_{12}, e_{13}, e_{21}, e_{22}, e_{23}, e_{31}, e_{32}, e_{33})$ .

In Equation 4,  $(u_{1..8}, v_{1..8})$  and  $(u'_{1..8}, v'_{1..8})$  are obtained points from the images of the left and right cameras, where  $e_{1..8}$  are the components of essential matrix  $E$ . Since Equation 4 is too time-consuming to process,  $e_{1..8}$  are computed using singular values decomposition (SVD).

### 4 Experimental Results and Analysis

The proposed method, which estimates the coordinates of a 3D object using a planar structure for video-based AR, has been tested for the camera motion information to the coordinates of a 3D object created on an image in a sequence of frames. Our method applies the camera motion parameters to the coordinates of a 3D object in the frames of a video, and compares the estimated direction of the Z-axis with the direction of the real Z-axis. Fig. 1 shows the measured difference between the estimated and real directions of the Z-axis. The accumulated error increases towards the end of sequences. Fig. 2 shows examples of superimposition of an object located at different backgrounds in video sequence.

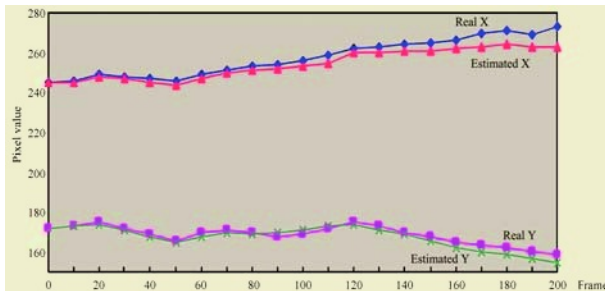
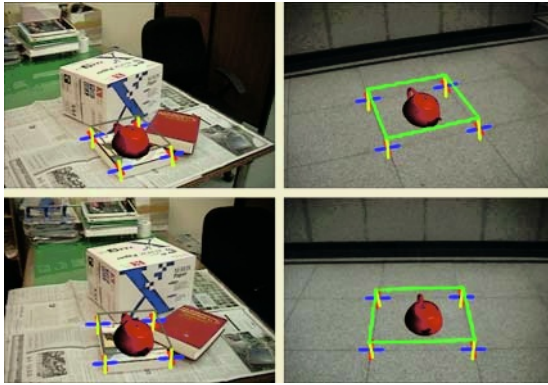


Fig. 1. Comparison for the registration between the estimated and real directions of Z-axes



**Fig. 2.** Superimposition of a teapot in video sequence

## References

1. Ronald T. Azuma: A Survey of Augmented Reality, Teleoperators and Virtual Environments, Vol. 6, No. 4, pp.355-385, 1997
2. Gilles Simon and Marie-Odile Berger: Estimation for Planar Structures, IEEE Computer Graphics and Applications, Vol. 22, pp.46-53, 2002
3. Simon J.D. Prince, Ke Xu and Adrian David Cheok: Augmented Reality Camera Tracking with Homographies, IEEE Computer Graphics and Applications, Vol. 22, pp.39-45, 2002
4. Gilles Simon, Andrew W. Fitzgibbon and Andrew Zisserman: Markerless Tracking using Planar Structures in the Scene, Proc. International Symp. Augmented Reality, pp.137-146, 2000
5. Peter Sturm: Algorithms for Plane-Based Pose Estimation, Proc. of the Conference on Computer Vision and Pattern Recognition, pp.1010-1017, 2000
6. Kiriakos N. Kutulakos and James R. Vallino: Calibration-Free Augmented Reality, IEEE Trans. on Visualization and Computer Graphics, Vol. 4, pp.1-20, 1998
7. Yong duek Seo and Ki Sang Hong: Calibration-Free Augmented Reality in Perspective, IEEE Trans. on Visualization and Computer Graphics, Vol. 4, No. 6, pp.346-359, 2000
8. Kumar Rakesh, Sawhney, H. Sawhney and Allen R. Hanson: 3D model acquisition from monocular image sequences, Proc. of the Conference on Computer Vision and Pattern Recognition, pp.209-215, 1992

# Stochastic Fluid Model Analysis for Campus Grid Storage Service

Xiaofeng Shi, Huifeng Xue, and Zhiqun Deng

College of Automation, Northwestern Polytechnical University,  
P.O.Box 183#, Xi'an 710072, China  
{Xiaofengshi2002, zhiqundeng}@tom.com

**Abstract.** Campus grid storage service is to aggregate the storage resources in the servers of Campus Grid Center and colleges (or institutes, departments), and the storage resources of personal computers in the campus network. It provides storage resources registration, allocation, scheduling, and release services for users by three levels storage architecture. Due to the storage nodes' dynamites, the total storage space that nodes contribute will dynamically change with time. To study the performance of the storage service, the stochastic fluid model is adopted. By this analytical model, we got the mathematical results as follows: the function between the storage allocation probability and the number of nodes is got; if more nodes join the campus grid, the aggregated storage space will be larger, and then the available storage resources will be more; if the storage resources allocation rate is larger than the storage resources release rate, then the available storage resources will decrease.

## 1 Introduction

The campus grid is mainly to aggregate all kinds of resources in the campus networks, and provide the services that the campus network currently cannot afford. The Campus grid is not just to provide the High Performance Computing, but also provide other services [1] at a low cost, such as storage service, computing service, and etc.

This paper mainly focuses on the campus grid storage service, which aggregates the storage resources that nodes contribute. Due to nodes' dynamical join and departure, the stochastic fluid model [2,3, and references therein] is adopted to analyze the performance the storage service.

Stochastic fluid model, an important analytic model, has drawn considerable attention in such applications as the performance of P2P cache in [4,5]. In these papers, by this model they got good results from analysis of the cache clusters and P2P cache.

Our work based on [5] is to apply the stochastic fluid model to study the performance of the campus grid storage service. We model the aggregated storage space as a single infinite storage space. Nodes' dynamical join and departure result in the storage space dynamical change, as can be modeled by the stochastic fluid model. Finally, we get the performance of the storage service.

## 2 Campus Grid Storage Service Structure

The campus grid storage service is implemented by three levels architecture (see Fig.1):

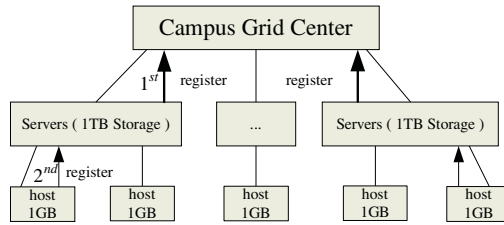


**Fig. 1.** Nodes’ organization architecture of the Campus Grid

1. The first level, Campus Grid Center servers. They manage the registration information of servers in the colleges. The registration information includes the whole storage space, colleges’ identifiers, servers’ addresses, and etc. Each of these servers contributes at least 1TB storage space.
2. The second level, servers distributed in each college or institute, and department. They manage the registration information of PCs or workstations. Each of these servers contributes at least 1TB storage space.
3. The third level, Hosts (PCs or workstations). They contribute and request the storage resources. They can store data in the campus grid storage space. Each host can contribute 1GB or more storage space.

Due to storage nodes dynamical join and departure, Campus Grid Center servers will actively detect the state (work well, temporary stop, stop) of servers in the colleges. Similarly, servers in colleges need to detect the hosts’ working state.

### 3 General Stochastic Fluid Model for Campus Grid Storage Space

The whole campus grid system can be viewed as a virtual single storage pool. The total storage space of the universe campus grid system is  $c$ , which is considered as the total storage space contributed by all the nodes at a given time.  $x(t)$  is the total available storage space number (GB). Here, one GB storage space as the minimum unit to contribute and allocate storage resources. If a node joins the system, the storage space number increased is  $J(t)$ . And if a node leaves the system, the storage space number (GB) reduced is  $L(t)$ . We define

$$\theta = \text{Storage resource allocation rate} - \text{Storage resource release rate} \tag{1}$$

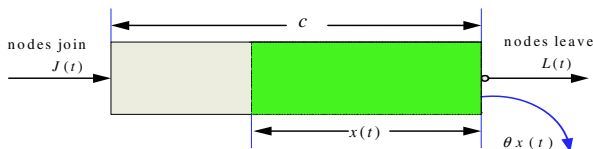


**Fig. 2.** The general stochastic fluid model for campus grid storage space

From the above definition, it can be deduced that the storage space number in the system at time  $t$  is:  $x(t) = J(t) - L(t) - \theta x(t)$ . The general stochastic fluid model for campus grid storage space can be seen in Fig.2.

### 4 Storage Dynamical Model

$N$  is the total number of nodes. Nodes go up and down independently of each other, the time until a given up (or down) node goes down (or up) is exponentially distributed. The birth rate (up) of each node is  $\lambda$ . The death rate (down) is  $\mu$ . In general, the request of each node randomly arrives based on Poisson processes at a rate  $\sigma$ .

If there are  $i$  nodes that are up, there are  $x$  storage spaces that are available. Here  $i = 0, 1, \dots, N$  and  $x \in [0, c]$ . For each node, the get probability to allocate the storage resources requested is  $G$ , which can be defined by  $G = x / c$ .

When a node goes down, the storage space contributed by that node will go down. The remaining number of the storage space in the system is  $\Delta_d(i) * x$ . Here,  $\Delta_d(i)$  is the down reduction coefficient. Once a node goes up, the storage space will join the system. There is no storage space reduced in the system and the remaining number of the storage space is  $\Delta_u(i + 1) * x$ . The up reduction coefficient is  $\Delta_u(i + 1)$ . In fact, it can be seen that  $0 \leq \Delta_d(i) \leq 1$  and  $\Delta_u(\cdot) = 1$ .

Duo to the nodes' change, the resulting storage space change is  $J(t) - L(t)$ , which can be induced by

$$J(t) - L(t) = i\sigma(1 - x/c) \tag{2}$$

We adopted the simple stochastic fluid model proposed by [5]. Then

$$G = \frac{E[X]}{c} = \frac{1}{(1 + \rho)^N} \sum_{i=1}^N \binom{N}{i} \rho^i v_i \tag{3}$$

Here, the vector  $v$  can be seen in [5].

### 5 Simulation Analysis

If we do not consider the effect of storage space allocation and release, then:  $\theta = 0$ . The simulation result can be seen in Fig.3 as data1 curve shows. Else, we consider this, and we set  $\theta = 0.3$  and  $\mu = 0.02$ . The simulation result can be seen in Fig.3 as data2 curve shows.

In Fig.3, we can see that the storage allocation probability will be higher if the number of nodes is larger. Then, once users request the storage resources in the campus grid, the probability that the resources are allocated is high. The data2 curve shows that if the storage resources allocation rate is larger than the storage resources release rate, the probability that the space is allocated will be low.

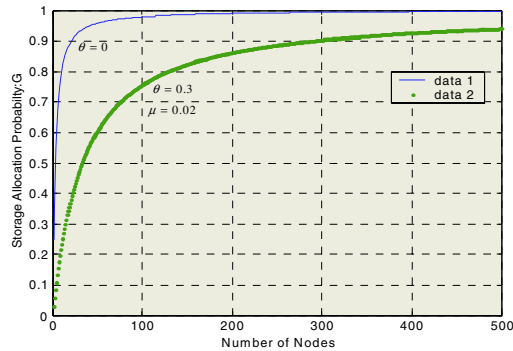


**Fig. 3.** The relation between number of nodes and the storage resources allocation probability

## 6 Conclusions

In this paper, we have built a general simple virtual storage pool model for the dynamical storage space due to nodes' join and departure. We explore the stochastic fluid analytical models for the purpose of campus grid storage service performance. We have got the results as follows: if more nodes join the campus grid, the aggregated storage space will be larger, and then the available storage resources will be more; if the storage resources allocation rate is larger than the storage resources release rate, then the available storage resources will decrease.

## References

1. Zhiquan Deng, Zhicong Liu, Guanzhong Dai, Xinjia Zhang and Dejun Mu. Nodes' Organization Mechanisms on Campus Grid Services Environment. Lecture Notes in Computer Science, Vol. 3251. Springer-Verlag, Berlin Heidelberg New York (2004) 247-250
2. Nelly Barbot and Bruno Sericola. Distribution of busy period in stochastic fluid models. Communications in Statistics-Stochastic Models, (2001) 17(4)
3. Vidyadhar G. Kulkarni. Fluid Models for Single Buffer Systems, Frontiers in Queuing: Models and Applications in Science and Engineering. Ed. J. H. Dshalalow. CRC Press, (1997) 321-338
4. Florence Clévenot, Philippe Nain. A Simple Fluid Model for the Analysis of the Squirrel P2P Caching System. Proceedings of the IEEE INFOCOM 2004
5. Florence Clévenot, Philippe Nain, Keith W. Ross. Stochastic Fluid Models for Cache Clusters. Performance Evaluation, Vol.59 (1), (2005) 1-18



# Grid Computing Environment Using Ontology Based Service

1

2

<sup>1</sup> Department of Informatics, Federal University of Pelotas,  
99010-900 Pelotas, Brazil  
[ampernas@ufpel.edu.br](mailto:ampernas@ufpel.edu.br)

<sup>2</sup> Department of Informatics and Statistics, Federal University of Santa Catarina,  
88040-900 Florianopolis, Brazil  
[mario@inf.ufsc.br](mailto:mario@inf.ufsc.br)

**Abstract.** Grid computing environments can share resources and services in a large-scale. These environments are being considered as an effective solution for many organizations to execute distributed applications to obtain high level of performance and availability. However, the use of a grid environment can be a complex task for an ordinary user, demanding a previous knowledge of the access requirements from a virtual organization. In order to improve the search of resources and its selection, in this paper we propose the use of ontology as alternative approach to help the use of grid services. This paradigm can provide a description of available resources, leading users to desire operations and describing resources syntax and semantics that can form a common domain vocabulary. Our experimental result indicates that our proposal allows a better comprehension about available resources.

## 1 Introduction

Grid computing environments can share resources and services in a large-scale. These environments are being considered as an effective solution for many organizations to execute distributed applications to obtain high level of performance and availability. However, the use of a grid environment can be a complex task for an ordinary user, demanding a previous knowledge of the access requirements from a virtual organization. In order to improve the search of resources and its selection, in this paper we propose the use of ontology as alternative approach to help the use of grid services. This paradigm can provide a description of available resources, leading users to desire operations and describing resources syntax and semantics that can form a common domain vocabulary. Our experimental result indicates that our proposal allows a better comprehension about available resources.

## 2 Ontology for Grid Resources Description

- Metadata
- Semantics View

### 2.1 Ontology Development

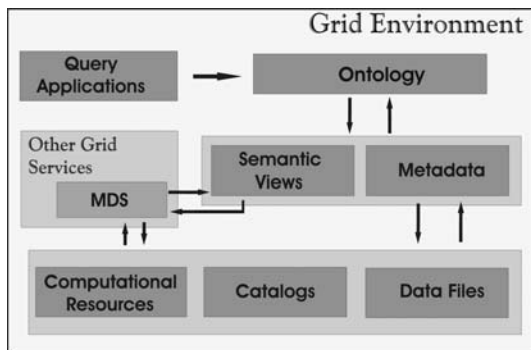


Fig. 1. Grid architecture using the ontology approach

```
(findall ? typeofmachine
(exists ?unix
(and ('typeOS'? unix ?typeofmachine)
(='name'?AIX)(?typeOS'?typeofmachine))
(exists ?typeofmachine
(and
(>('diskSpaceGB' ?typeofmachine) 40)
(>('maxMemGB' ?typeofmachine)128))))))
```

Fig. 2. Axiom to access restriction

... ..

### 2.2 Ontology Based Service

... ..

### 3 Related Work

... ..

### 4 Conclusion and Future Work

... ..

## References

1. De Roure, D., Jennings, N.R., Shadbolt N.R.: The Semantic Grid: A Future e-Science Infrastructure. In: Grid Computing: Making The Global Infrastructure a Reality, F. Berman, A.J.G. Hey and G. Fox (eds), Southern Gate, Chichester, England: John Wiley Sons, 1080p. (2003) 437-470.
2. Pernas, A. M.: Ontologias Aplicadas a Descricao de Recursos em Grids Computacionais. Dissertation (Master Degree), Federal University of Santa Catarina, Florianopolis, Brazil (2004).
3. Tangmunarunkit, H., Decker, S., Kesselman, C.: Ontology-based Resource Matching - The Grid meets the Semantic Web. 1th Workshop on Semantics in Peer-to-Peer and Grid Computing (SemPGrid) at the 12th International World Wide Web Conference, Budapest, May (2003).
4. Heine, F., Hovestadt, M., Kao, O.: Towards Ontology-Driven P2P Grid Resource Discovery. 5th IEEE/ACM International Workshop on Grid Computing, Pittsburgh, USA, November(2004).
5. McGuinness, D., Van Harmelen, F.: Web Ontology Language Overview. (2004). Available online <http://www.w3.org/TR/owl-features/>.
6. Noy, N., Fergerson, R., Musen, M.: The knowledge model of Protege-2000: Combining interoperability and flexibility. 12th Int. Conference on Knowledge Engineering and Knowledge Management(EKAW), French Riviera, October (2000) 2-6.
7. Goble, C., De Roure, D.: Semantic Web and Grid Computing. September (2002). Available online: <http://www.semanticgrid.org/documents/swgc/>.
8. NPACI-National Partnership for Advanced Computational Infrastructure: Partnership Report. (2000). Available online: <http://www.npaci.edu/>.
9. Foster, I., Middleton, D., Williams, D.: The Earth System Grid II: Turning Climate Model Datasets into Community Resources. January (2003). Available online: <https://www.earthsystemgrid.org/about/docs/ESGOverviewSciDACPINapa.v8.doc>.
10. IPG, Information Power Grid - Nasa's Computing and Data Grid: What is the IPG? October (2002). Available online: <http://www.ipg.nasa.gov/aboutipg/what.html>.
11. Verstoep, K.: The Distributed ASCI Supercomputer 2 (DAS-2). May (2000). Available online: <http://www.cs.vu.nl/das2/>.
12. Foster I., Kesselman, C.: The Globus Project: a Status Report. In: Proc. of 7th Heterogeneous Computing Workshop (HCW 98), March (1998) 4-18.
13. Pouchard, L. et.al.: An Ontology for Scientific Information in a Grid Environment: the Earth System Grid. In: Proc. of the 3th IEEE/ACM International Symposium on Cluster Computing and the Grid, Japan, Tokyo, May (2003) p. 626.

# Distributed Object-Oriented Wargame Simulation on Access Grid\*

... g ... m, ae ... g ee, a d Cha g u g e . g\*\*

School of Electrical Engineering in Korea University,  
1-5ka, Anam-Dong, Sungbuk-Ku, Seoul 136-701, Korea  
{jhlim, lyadlove}@snoopy.korea.ac.kr  
csjeong@charlie.korea.ac.kr

**Abstract.** This paper presents the design and implementation of Distributed Object-oriented Wargame Simulation(DOWS) on Access Grid(AG). DOWS is an object-oriented distributed simulation system based on a director-actor model. DOWS on AG supports a collaborative environment by providing a virtual venue with high quality audio and real-time video interactive interface for remote users, and allows a groups of users in remote sites to easily participate in the whole simulation. We design an efficient communication scheme between application and AG so that DOWS can be incorporated on AG for collaboration purpose.

## 1 Introduction

he s mu at ... ca be adapted ... ma ... fields such as c ... struct ... , traffic, mea sureme t a d s ... O e f them s a ar game s mu at ... m tar field ... th ough there are fe batt es ... the ... rd, the m tar sh u d c t ue t tra the r arm t mpr e the perat ... sk ... f batt e ... e er, the g er me t must spe d e pe s e budgets t check the r strateg es a d ma ta the r batt e ab t , because the rea ... g perat ... f the arm must requ re h gh c st a d t me heref re ar game s mu at ... s regarded as ... e f the m st e ect e a s t test e strateg es a d the perat ... capab t f arm 's f rce ... e er, t requ res a arge ... ume f mu t med a data as e ... as ma c m pe pr cesses, a d there e sts s me m t ... umber f perat rs a d bser ers due t the space m tat ... s , t s d fficu t t ha e de aud ser ces ... c ... ab rat e e r ... me t ... th s paper, e prese t a str buted Ob ect r e t ed ar game mu at ... ( O ) s stem h ch pr des ... t ... d str buted s mu at ... e r ... me t but a s c ... ab rat e e r ... me t us g ccess Gr d( G) e sha descr be a effie t c mmu cat ... scheme h ch tegrates app ca t ... t G s that O ca be eas ... c rp rated ... t G f r c ... ab rat e purp se

\* This work has been supported by KIPA-Information Technology Research Center, University research program by Ministry of Information & Communication, and Brain Korea 21 projects in 2005.  
\*\* Corresponding author.

sect. 2, describe the Access Grid architecture. Sect. 3, describe the OSGI architecture. Sect. 4, present the architecture of the OSGI-based Access Grid. Sect. 5, conclude with future works.

## 2 Access Grid

Grid computing is a specialized form of distributed computing where the application is distributed over a wide area network and computing resources are geographically far from each other. It comprises computation, data and Access Grid computation. Grids share computing resources at remote sites for high performance computing. Grids provide an integrated environment for the distributed data Access Grid (AG), developed by Argonne National Laboratory, provides various services such as data distribution, data sharing, shared application, test-based communication and certificates management for communication. It enables remote users to interact each other, and exchange information through the data and services.

Grid (Access Grid) has been developed using Grid technologies and provides the services needed. Grid consists of Grid resources, Grid Client and Grid User. Grid resources, Grid Client and Grid User rate the other members, the user and interact through Grid services.

## 3 Dows System

Object-based remote simulation system based on distributed interaction mechanism can be mapped effectively to object-based distributed simulation. Distributed interaction mechanisms are distributed systems which interact with their counterparts as simulation entities. A submodel of the simulation, a distributed system is a part of the simulation. Each distributed system generates commands to its associated actors which turn into actual simulation objects, interacting with their actors. The same distributed subsystem sets of actors may be designated as actor groups that each distributed system carries out by actors interacting with each other. Each actor can represent a simulation entity, participant, goal, and simulation model or a submodel of the simulation. Object-based distributed simulation architecture is a distributed environment that distributes the simulation currently through the interaction communication with the agents which are charged for the parallel simulation of its associated submodels using separate actors. Each actor corresponds to a simulation entity of the simulation model which is a part of the simulation model. The agents can be executed either in parallel or sequentially. Each actor sends a message to the other actors, and maintains the synchronization of the agent provides an effective real-time

time synchronization mechanism which integrates the coordinated among direct, random access support, group synchronization, message transfer, and network fault detection. Each agent can participate in a message router, and coordinates each other to forward messages between actors and direct access, the coordinated runs the hello message based on start message to each actor, suspends to be debugging. The agents have separate thread that maintains its respective of actors to be checked.

### 4 DOWS on Access Grid

It supports collaboration applications through the channel sharing mechanism. Users interact with a desktop environment. The former controls multimedia communication, the actors direct and the latter controls the multimedia communication by the former. Generally, Open Peer-to-Peer applications can be started by peers and servers respectively. Figure (a) shows the user created server environment supports various services such as user creation, synchronization, authentication, registration, and data broadcast. Figure (b)(c) the user creates a real state for each Open Peer-to-Peer application, which interacts with other server applications through the real state. Real state has a reliable channel messages between Open application and

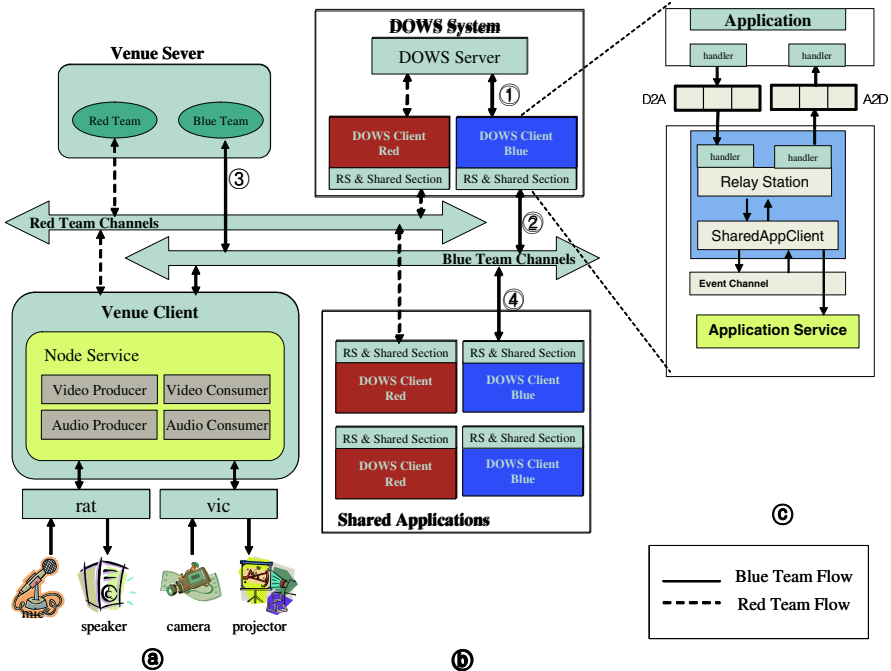


Fig. 1. An architecture of DOWS on AG

Grid use two message queues between them. Each read state receives the updated data from the message queue set from its corresponding Object-oriented application using its message handler, and propagates them to the read state using the same queue using the event change provided by application server. Grid kernel handles the browser application, the same queue receives the updated data from the message queue set by the read state application server. The server is provided by Grid support a mechanism for event change, description, change, and synchronization among read states. Read states implement using graphical script language, and makes use of the functions of the shared application class which provides application server is provided by Grid.

Figure 1(a) shows the architecture of the system. The read state and read state are created, the server application server, the server creates a read state, which generates its corresponding Object-oriented Event. The name of the read state, the read state updates the team using the read state which reads messages between Object application and Grid, that Object application can communicate directly with Grid.

## 5 Conclusion

This paper has presented the design and implementation of Object-oriented Grid which supports a collaborative environment for distributed applications. The architecture shows that the distributed application can be effectively incorporated into Grid environment by providing a read state which makes use of event change and application server. Grid kernel herefore provides a architecture which enables users to integrate applications with a collaborative environment with high quality and a distributed environment. The interfaces of distributed systems as a future work are working on the integration of computation and grid technology system for the performance improvement of computation. The simulation is a good example of Object-oriented.

## References

1. Access Grid <http://www.accessgrid.org/>
2. Stevens, R., Papka, M.E. and Disz, T., "Prototyping the workspaces of the future," Internet Computing, IEEE, pp 51-58, July-Aug. 2003.
3. Ho, H. C. and Yang, C. T. and Chang C. C., "Building an E-learning Platform by Access Grid and Data Grid Technologies," Proceedings of the 2004 IEEE International Conference on e-Technology, pp 121-126 2004.
4. Ernest H. Page and Roger Smith, "Introduction to Military Training Simulation: A Guide for Discrete Event Simulationists," Proceedings of the 1998 Winter Simulation Conference, pp 33-40, 1998.



# RTI Execution Environment Using Open Grid Service Architecture\*

Su-Geun Chae, Jaehyung Lee, and Changug Lee\*\*

School of Electrical Engineering in Korea University,  
1-5ka, Anam-Dong, Sungbuk-Ku, Seoul 136-713, Korea  
{2xx195, lyadlove}@snoopy.korea.ac.kr  
csjeong@charlie.korea.ac.kr

**Abstract.** HLA(High Level Architecture) has been developed to promote interoperability and reusability within the modeling and simulation community. RTI(Run Time Infrastructure) is a software implementation of HLA which is composed of three components: libRTI, FedExec, and RTIExec. However, the previous RTI has an unfriendly execution environment with static and manual resource allocation and execution. In the paper, we present a RTI execution environment using OGSA(Open Grid Service Architecture) which addresses the problems, so called RTI-G. It supports easy-to-useness, transparency and performance by providing users with dynamic resource allocation and automatic execution. Moreover, it provides an unified view of RTI and Grid services by integrating them as web services on OGSA.

## 1 Introduction

Running a large scale distributed simulation made a large amount of computing resource required. The graphically distributed simulation (high level architecture) provides application developers with a powerful framework for reuse and interoperability of distributed simulation. However, RTI(Run Time Infrastructure), the implementation of HLA, as a designed support software application that need to integrate structures, distributed computation and distributed resources managed by diverse organizations. Therefore, the existing RTI(Run Time Infrastructure) has a unified execution environment with static and manual resource allocation and execution. In hereafter, the execution of RTI as a platform independent process. Recently, Grid technology has been introduced to address the resource allocation and execution problems of distributed simulation organizations. In the paper, we present a RTI execution environment using OGSA(Open Grid Service Architecture) [2], so called RTI-G, which supports a easy to use, transparent execution. RTI execution environment has each

\* This work has been supported by KIPA-Information Technology Research Center, University research program by Ministry of Information & Communication, and Brain Korea 21 projects in 2005.

\*\* Corresponding author.

high performance, providing users with dynamic resource allocation and automatic execution using various services such as Grid and Grid Bus toolkit (G2) implemented based on OGSI (Open Grid Service Interface) provides a standard mechanism for publishing and discovering resource status and configuration information, and Grid (Grid Resource Catalog) manager executes the executable, the allocated resource Grid is used to transfer Office and executable, the remote resources section 2, describe the design of R2G based on OGSI and section 4, the performance results section 4, the general conclusion.

## 2 Design of RTI-G

R2G is a grid enabled implementation of R2G that supports various Grid based on OGSI, each service of R2G is designed to provide automatic and dynamic execution environment architecture of R2G consists of the following services: a) Grid architecture, this section describes about each architecture respectively in detail.

### 2.1 RTI Service Layer

R2G architecture consists of three services: b) R2G, edE, ecG, R, E, ecG, R, s, ft are can be executed in a standard environment executed in a arbitrary computer network. R, E, ecG manages the creation and destruction of federations. Each federation is characterized by a single and global edE, ecG, which manages federates, global resource, the federation, b) R2G provides R2G service interface to federate developers, the hierarchical structure is accomplished through the interaction among b) R2G, R, E, ecG, and edE, ecG.

OGSI integrates key Grid technologies through services mechanisms to create a distributed system framework based on OGSI (Open Grid Services Infrastructure). Each R2G service is defined as a grid service using (Web Service Description Language). OGSI to be effective, incorporated the Grid environment, and hence to be accessible by standard Grid clients.

Grid service is defined about how a client interacts with the service, state that the Grid service description is embedded in the service profile of the state, although its associated service properties, service attributes, messages, and types defined here, refer to the order to be compatible with the grid services, each service of R2G architecture should be specified. Here are the methods for describing the service of R2G architecture: the first step is to the service, the second step, which is the most versatile method, providing the tactical transfer the description of service properties, the user interface, because it is a rather versatile language. The second step generate from a service interface language, the example, the generate automatic call from a service interface, which is the easiest method, but the most versatile, because the implemented interfaces are automatically corrected. The service

Resources implemented using C++ language, we chose the first method as our reference C++ code. We depend on the services of Resource Allocator using Grid (web services implemented descriptor) so that the code can be used directly as an alternative grid services defined in OG, thus providing a unified environment for Resource and Grid services. Since the service broker can make Resource and create a service state as follows: first, user request a service based on Grid (Grid resource and) then the Resource factor, which creates the state of Grid as a stable member of a Grid service, but does not actually communicate with the Grid service Resource factor. maps Grid to Grid (Grid service Reference), and communicate with each describes how actually communicate with the Grid service.

### 2.2 Grid Layer

Grid architecture separates services such as Resource, GR, and Grid implemented in Grid. Grid is used to allocate the resource with high performance. Both the resource status and configuration of resource, and Grid execute the Resource, the allocated resource Grid is used to transfer the Resource executable to the remote resources.

## 3 Experiments

For the evaluation of Resource, Grid, we execute several network sharing game Resource and Resource respectively, and compare the performance. The two players can play sharing game, and communicate through services of Resource. In each case, we measure the data transfer rate between players. The data size of each block of the game is 100 bytes, and with the advertisement of each stage, the number of blocks is increased by 100. In the first case, player requests the Resource, a federation, and the Resource and EdEc are created subsequently. In the second case, the service specified by player 1, player 2, and the federation, the federation, as shown in figure (a). In the second case, player requests the Resource, a federation, and the Resource and EdEc are created. The service allocated by Resource factor after accessing and selecting the best performance as shown in figure (b). Resource services created as Resource state, and makes EdEc services generated through federation. The allocated service after that, player 2, the federation, and the change of federation about blocks of the game.

We used each client machines with same specification to reduce side effects. According to the configuration of each machine, client has 8GB RAM, 2GB memory, 2GB of swap, running under the Ubuntu. There are three servers with different specifications as shown in figure (c). In the second case, the best service is selected using Resource factor. As seen in figure (d), which shows the data transfer rate of the block size, Resource has the better performance than Resource.

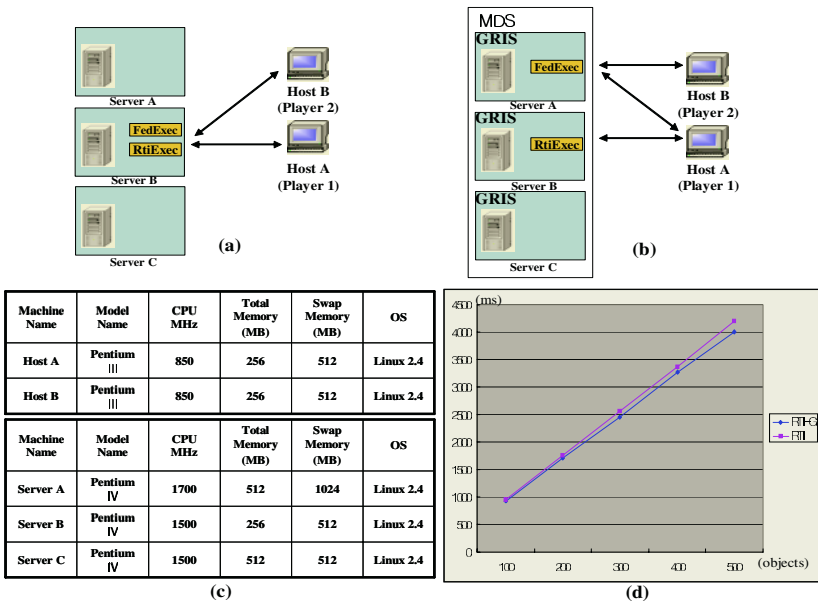


Fig. 1. (a)The first case using RTI, (b)The second case using RTI-G, (c) Resource performance, (d) Comparison of data transfer rate on RTI and RTI-G

### 4 Conclusion

In the paper, we have presented RTI-G which supports a easy to use, transparent, and efficient RTI execution environment. It achieves high performance by providing users with dynamic resource allocation and automatic execution using various services. Given the specifications of RTI-G, GTS and the deployment of RTI-G services, RTI service architecture. GTS can therefore provide an integrated unified environment for RTI and Grid services, thus supporting easy to use, transparent, and performance. In this paper, we have described the experimental results for RTI-G by comparing it with RTI as a future work, we are designing a report for the efficiency and performance metrics of RTI with application of distributed game simulation.

### References

1. IEEE Standard for Modeling and Simulation, "High Level Architecture (HLA) Federate Interface Specification," IEEE Std 1516.1-2000 54.
2. D.Talia, "The Open Grid Services Architecture: where the grid meets the Web," Internet Computing, IEEE, Volume: 6, Issue: 6, Nov.-Dec., pp.67-71, 2002.
3. I. Foster, C. Kesselman, "Globus: A Metacomputing Infrastructure Toolkit, Intl J. Supercomputer Applications," 11(2), pp. 115-128, 1997.

# Heterogeneous Grid Computing: Issues and Early Benchmarks

..... 1 ..... 1 ..... 2  
..... 2 ..... 1 ..... 1 ..... 1 ..... 1  
..... Q ..... 1

<sup>1</sup> Department of Computer Science, Trinity College Dublin, Ireland  
{ekenny, coghlan, walshj1, childss, ocallwd, gquigle}@cs.tcd.ie  
<sup>2</sup> Dept. of Computer Science, University of Cyprus, 1678, Nicosia, Cyprus  
{georget, mdd}@ucy.ac.cy

**Abstract.** A heterogeneous implementation of the current LCG2/EGEE grid computing software is supported in the Grid-Ireland infrastructure. The porting and testing of the current software version of LCG2 is presented for different flavours of Linux, namely Red Hat 7.3, Red Hat 9 and Fedora Core 2. The GridBench micro-benchmarks developed in CrossGrid are used to compare the different platforms.

## 1 Introduction

.....  
..... ( )  
.....  
.....  
.....

## 2 Porting for Heterogeneity

.....  
.....  
.....  
.....  
..... ( )  
.....

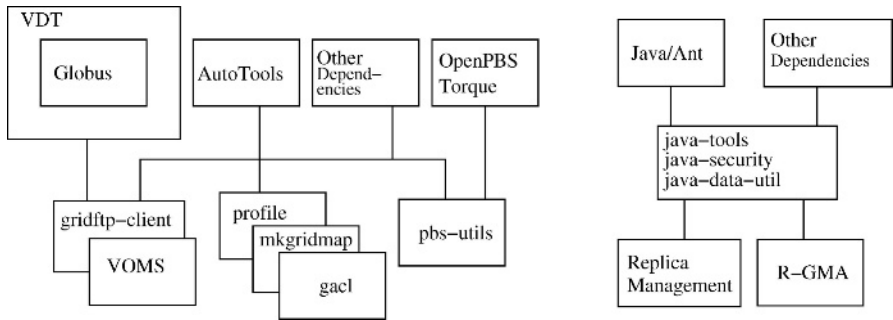


Fig. 1. LCG2/EGEE software components

### 3 Micro-benchmarking Results

The micro-benchmarking results are presented in Table 1. The results show that the performance of the LCG2/EGEE software components is generally good, with the exception of the R-GMA component, which shows a significant performance degradation when compared to the other components. This is likely due to the complexity of the R-GMA component, which is responsible for managing the replication of data across the grid. The results also show that the performance of the LCG2/EGEE software components is generally stable across different grid configurations and workloads.

ii) i)

**Table 1.** Micro-Benchmark Results

OS Type	Version	Bonnie (kB/s)	HPL (GFlop/s)	b_eff_io (MB/s)	epdhrystones (dhrystones)	Whetstone (MIPS)	epflops-4 (MFlops)
Fedora Core	2	193536	0.648350	46.712	3858611	707.86	825
Red Hat	7.3	159431	0.696549	52.515	4201680	742.71	898
Red Hat	9	154663	0.729079	45.318	4255319	750.35	899

**Table 2.** Machine Specifications

OS Type	Version	CPU Speed (GHz)	memsize/Total (MB)	epstream (add)	epstream (triad)
Fedora Core	2	2.8	951/2044	1600	960
Red Hat	7.3	2.8	979/2044	1600	960
Red Hat	9	2.8	872/2044	1600	960

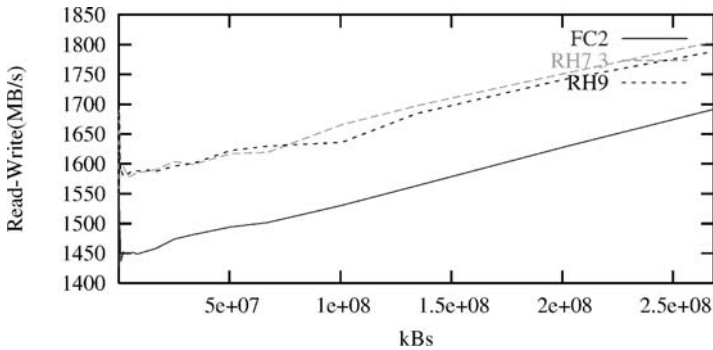


**Fig. 2.** Cachebench for Fedora Core 2, Red Hat 7.3 and Red Hat 9

... ( ) ...

... ( ) ...

... ( ) ...

## 4 Conclusions

... ( ) ...

... ( ) ...

... ( ) ...

... ( ) ...

... ( ) ...

## Acknowledgements

... ( ) ...

## References

1. LHC: Large hadron collider computing grid project. <http://lcg.web.cern.ch/LCG/> (2004)
2. EGEE: Enabling grids for e-science in europe. <http://www.eu-egee.org/> (2004)
3. VDT: Virtual data toolkit. <http://www.cs.wisc.edu/vdt/> (2004)
4. Kenny, E., Coghlan, B., Walsh, J., Childs, S., O'Callaghan, D., Quigley, G.: Heterogeneity of Computing Nodes for Grid Computing. Submitted to EGC 2005 (2004)



5. Tsouloupas, G., Dikaiakos, M.D.: Gridbench: A tool for benchmarking grids. In: Proceedings of the 4th International Workshop on GridComputing (GRID2003), Phoenix, AZ, IEEE (2003) 60–67
6. Tsouloupas, G., Dikaiakos, M.D.: Characterization of computational grid resources using low-level benchmarks. Technical Report TR-2004-5, Dept. of Computer Science, University of Cyprus (2004)

# GRAMS: Grid Resource Analysis and Monitoring System<sup>1</sup>

Hongning Dai, Minglu Li, Linpeng Huang, Yi Wang, and Feng Hong

Department of Computer Science & Engineering, Shanghai Jiao Tong University,  
1954 Hua Shan Road, 200030 Shanghai, P.R. China  
{hndai, li-ml, huang-lp, wangsuper, hongfeng}@cs.sjtu.edu.cn

**Abstract.** In this paper we propose GRAMS, a resource monitoring and analysis system in Grid environment. GRAMS provides an infrastructure for conducting online monitoring and performance analysis of a variety of Grid resources including computational and network devices. Based on analysis on real-time event data as well as historical performance data, steering strategies are given for users or resource scheduler to control the resources. Besides, GRAMS also provides a set of management tools and services portals for user not only to access performance data but also to handle these resources.

## 1 Introduction

Grids offer us a new vision, infrastructure and trend for the coordinated resources sharing, problem solving and services orchestration in dynamic, multi-institutional virtual organizations [1]. A recent trend in government and academic research is the development and deployment of computational grids [2]. Computational grids are large-scale distributed systems that typically consist of high-performance compute, storage, and networking resources. Several computational grids in China are NHPCE (1999-2001) [7], CNGrid (2002-2006) [8], ChinaGrid (2002-2005) [9], E-Science Grid (2002-2005) [10], Spatial Information Grid (2001-2005) [11] and Shanghai-Grid (a city grid project to enhance the digitalizing of Shanghai)[3].

The primary goal of Shanghai-Grid is to develop a set of system software for the information grid and establish an infrastructure for the grid-based applications. This project will build an information grid tailored for the characteristics of Shanghai and support the typical application of grid-based traffic jam control and guidance. Currently we are trying to build up a system to monitor and control the resources, services and applications that make up the Grid. We have found it difficult to ensure that the resources in the Grid are working correctly to support grid application. It is also cumbersome to predict system performance and to control the resources in the Grid. These difficulties have led to our development of a system for monitoring and analysis of grid resources.

---

<sup>1</sup> Supported by the National Grand Fundamental Research 973 Program of China under Grant No.2002CB312002, the Grand Project (No.03dz15027) and Key Project (No.025115033) of the Science and Technology Commission of Shanghai Municipality.

In this paper, we present a system namely GRAMS (Grid Resource Analysis and Monitoring System) which can observe performance events on each grid node, collect these event data, and analyze performance data to determine what actions should be taken.

## 2 GRAMS Architecture

GRAMS is based on OGSA [5] and GMA [4]. The GRAMS architecture is shown in Fig.1. The GRAMS includes several main components: Monitor Managers, Directory Service, Consumers (Customer Service, Archival Service, and Performance Analysis Service), Steering Service and User Interface. All the services can be deployed to different distributed environments.

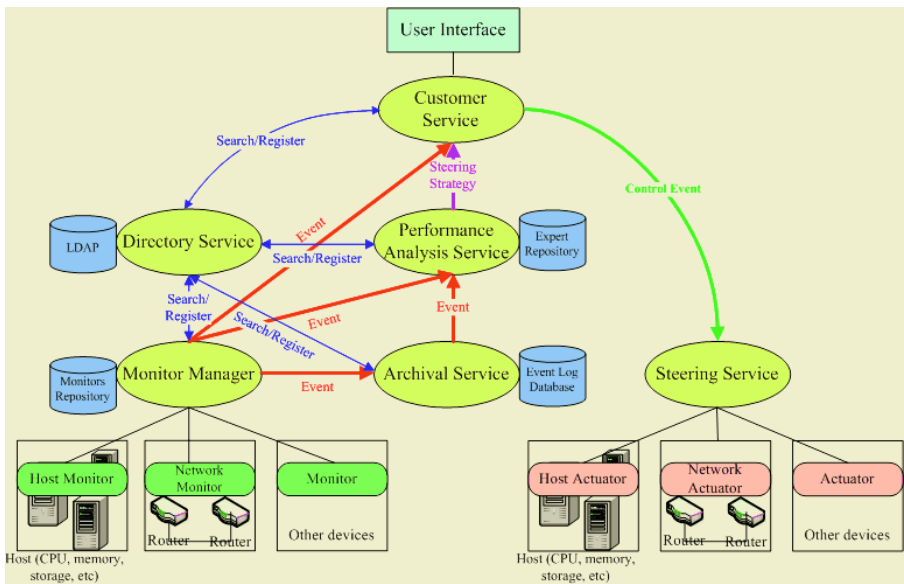


Fig. 1. Architecture of GRAMS framework

**Directory Service** stores information about producers, consumers and performance data. With the directory service, producers and consumers can publish and discover information that they request. This published information includes registration of producers and consumers, the types of event data, the characteristics of the data, and the ways to gain access to that data. The directory service contains only information about which event instances can be provided or accepted, not the event data itself.

**Monitor Managers** are used to manage monitors that measure and gather a variety of kinds of information for monitoring and analyzing. The monitors include: host monitor that is used to measure system property, network monitor to catch network info, and other monitor to capture other useful data from other useful data from other devices of the Grid

systems. The Monitor Manager publishes the monitors' existences in directory service entries, which tell consumers how to locate them. When the subscription between the monitors and customer service is established, the monitors will send events to customer service through the data channel of Monitor Manager until the subscription is terminated. Monitor repository in Monitor Manager will store the information about monitors (including their locations, their structures and kinds of performance metrics).

**Archival Service** is a database system which is used to store detailed monitoring information as well as performance results collected. It gained large amounts of long-term event data from Monitor Manager service for later use.

**Performance Analysis Service** is an expert system which acquires huge amounts of data from Monitor Manager as well as Archival Service, and produces resource management rules and scheduling strategies.

By using **User interface** provided by **Customer Service**, users can conduct online monitoring and performance analysis as well as making resource management decisions.

**Steering Service** receives requests from Customer Service to perform actions on the given resources or devices.

Interactions among GRAMS components and services are divided into controlling streams and data streams. Controlling streams are used to perform tasks including conducting activities of monitors and services, subscribing and querying requests for performance data, registering, querying and receiving information of Directory Service. In data streams delivery, a stream channel is used to transfer data (monitor data, performance data and results) between producers and consumers. Each monitor manager has only one connection to a consumer for delivering all kinds of data. All the connections are secure sockets based on Grid Security Infrastructure (GSI) [6] and Public Key Infrastructure (PKI).

### 3 Conclusions

In this paper we proposed the architecture of GRAMS which is a flexible, scalable monitoring and performance analysis system in Grid environments. We have implemented an early prototype of GRAMS, which already proves it feasible and effect.

There are still a lot works that should be done to improve the system. Fuzzy rules in expert system will be extended to cater for more complex and richer semantic knowledge. Performance prediction and instrumental tracing for Grid-based applications are the centers that our next step work will focus on. We will try to integrate current monitoring tools into GRAMS to serve more types of Grid monitor users and provide more functionalities and features, such as sampling, tracing and profiling [12].

### References

1. Foster, C. Kesselman, and S. Tuecke, "The Anatomy of the Grid: Enable Scalable Virtual Organizations", *Int. J. of H. Performance Computing Applications*, 15 (2001) pp.200-222.
2. I. Foster and C. Kesselman, *The Grid: Blueprint for a New Computing Infrastructure*, Morgan Kaufmann, 1999.

3. M. Li, H. Liu, C. Jiang, and W. Tong, "Shanghai-Grid in Action: The First Stage Projects towards Digital City and City Grid", *LECT NOTES COMPUT SC 3032*: 2004, pp.616-623.
4. B. Tierney, R. Ayt, and W. Smith, "A Grid Monitoring Architecture", *Technical report*, Performance Working Group, Grid Forum, January 2002. <http://www.didc.lbl.gov/GGF-PERF/GMA-WG/papers/GWD-GP-16-3.pdf>
5. I. Foster, C. Kesselman, J. Nick, and S. Tuecke, "Grid Services for Distributed System Integration", *IEEE Computer*, June 2002, pp.37-46.
6. I. Foster, C. Kesselman, G. Tsudik, and S. Tuecke, "A security architecture for computational grids", In *Proceedings of the 5th ACM Conference on Computer and Communications Security (CCS-98)*, ACM Press, New York, Nov. 3-5 1998, pp.83-92.
7. National High Performance Computing Environment (NHPCE): <http://vega.ict.ac.cn>
8. China National Grid Project (CNGrid): <http://www.grid.org.cn/>
9. ChinaGrid (China Education and Research Grid): <http://grid.hust.edu.cn/platform/chinagrid.jsp>
10. China E-science Grid Project: <http://www.most.gov.cn/English/index.htm>
11. Spatial Information Grid (SIG): <http://www.nudt.edu.cn/newweb/intercommunion/whatissig.htm>
12. Michael Gerndt, et al. "Performance Tools for the Grid: State of the Art and Future", APART-2 White Paper on Grid Performance Analysis, <http://www.lpds.sztaki.hu/~zsnemeth/apart/repository/gridtools.pdf>.

# Transaction Oriented Computing (Hive Computing) Using GRAM-Soft

Kaviraju Ramanna Dyapur and Kiran Kumar Patnaik

Department of Computer Science,  
Birla Institute of Technology (Deemed University), Mesra, India  
{kaviraju15, kkipatnaik}@bitmesra.ac.in

**Abstract.** The promise of Hive Computing – Organizations being able to acquire all the power they need for only as long as is necessary – is incredibly compelling. Hive Computing has experienced significant success in bringing productivity gains, high performance and cost savings to business applications such as; Enterprise Resource Planning (ERP), Customer Relationship Management (CRM), Supply Chain Management (SCM) and B2B portals (E-commerce sites). Grid Computing has brought productivity gains, high performance and cost savings, but in some places it is largely incomplete, i.e. when it comes to the questions of mission-critical computing in general and transaction oriented in particular. This paper discusses a new approach to the development, deployment and management of mission-critical applications – called Hive Computing – that is designed to complement and extend the vision of Grid Computing.

## 1 Introduction

Hive computing assumes that failure is the rule, not the exception. Computers and other hardware are vulnerable to numerous technical and human-induced flaws and catastrophic failures. Hive Computing takes the lead from the designers of TCP in assuming that computers are unreliable, and designs systems that can deal with rather than fear system failure. Hive Computing is a comprehensive and integrated approach to the development, deployment and management of transaction-oriented applications. The goal of Hive Computing is to enable business and other organizations to leverage the rising performance and falling process of commodity computers to construct mission-critical computing solutions that are both reliable and affordable. Hive Computing is derived from Grid Computing, but especially meant for transaction-oriented tasks.

This paper presents a functionality of GRAMSoft that takes the Hive computing approach to Transaction oriented applications in business applications resulting in productivity gains, high performance and cost savings.

## 2 Hive Computing Based Infrastructure

The key functions of Hive are; receiving and processing *requests* that are sent to it by a client and an administrator, *broadcasting* request to the Hive and execution of job by

a *worker* which is an individual computer that has three characteristics; 1) all workers must be located on the same logical network, 2) regardless of their exact hardware configuration, the same software is deployed on all workers and 3) all workers are dedicated to the Hive. Also administers a worker and maintaining database of status of sub-tasks and each worker status (idle or busy).

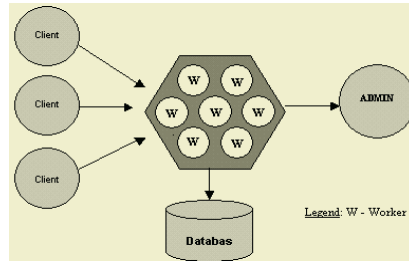


Fig. 1. Key components of Hive

### 3 Software to Build Hive Computing Infrastructure

The tool “GRAM-Soft” that forms a Hive Computing infrastructure containing transaction-oriented resources. This software involves: Mobile Agents (MAs), Meta-Computing (MC), Resource Co-Allocation.

#### 3.1 Mobile Agents in GRAM-Soft

In our GRAM-Soft, MAs are the carriers of tasks so as to execute them and return with the result to the system from where user has submitted his job. Also, they are meant for job migrations from one resource to another resource (upon its failure on one resource) and resumption of its execution from the point where it has been suspended. When the sub-task (sub-task may contain several files) is under execution on one computer, status of each file (Under Progress, Completed or Suspended) will be recorded in a “Task\_Status” file. This file information decides whether or not sub-task execution is to be resumed in another capable computer. The sub-task, containing only those files that are failed to execute (can be known by looking at “Task\_Status” file) is migrated to first available capable computer and its execution is resumed.

#### 3.2 Meta Computing in GRAM-Soft

MC allows applications to use collection of computational resources on an as needed basis, without regard to physical location of resources. Existing MC features in Grid-based softwares are; locating and allocating computational resources, Authentication of resources and Process creation. Additional MC features in GRAM-Soft are; execution ordering on processes, grouping of jobs and rescheduling (if necessary). This introduces five challenging resource management problems such as, site autonomy problem, heterogeneous substrate problem, policy extensibility problem, co-allocation problem and online control problem. “No existing Meta-Computing Resource Man-

agement Systems address all the problems”. GRAM-Soft also addresses the issues prevalent in resource co-allocation.

### 4 Architecture of GRAM-Soft

Principal components of GRAM-Soft are:

- GRAM Client Library: Used by application or co-allocator acting on behalf of an application. It interacts with the GRAM gatekeeper at a remote site to perform mutual authentication and transfer a request containing resource specification.
- MAs: Responsible for migrating sub-tasks between different capable computers.
- GRAM Gatekeeper: Performs Mutual authentication of user and resource, determines local user name for the remote user and starts a job manager, which executes as that local user which actually handles the request. Here gatekeeper must run privileged programs all the time.

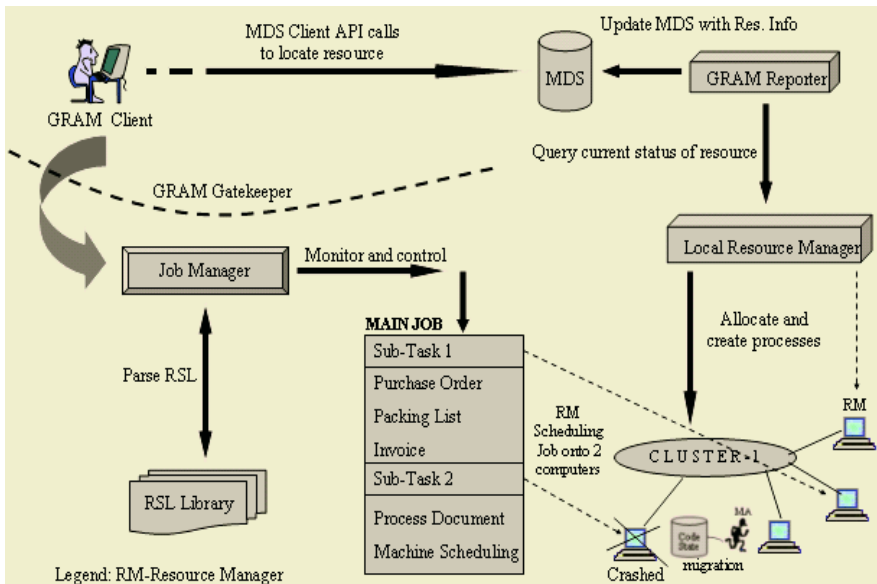


Fig. 2. GRAM-Soft Scheduling Model

- RSL Parsing Library: It contains resource characteristics like, main memory available, CPU processing rate, secondary memory available, and resource type.
- Job Manager: Initiates execution of sub-task’s files and monitors their status, performs callback of sub-task termination. Job manager is destroyed once the sub-task for which it was responsible is terminated.
- GRAM Reporter: It is responsible for storing into MDS various information like job schedules, status of sub-tasks’ files and computer status (idle or busy).
- MDS: Provides information about current availability and capabilities of the resources.



## 5 Conclusions

Here, we have focused on creating a heterogeneous Hive that contains set of transaction oriented high performance resources required for time-critical transactions. Such infrastructure should be developed as a decentralized job management system for which we believe mobile agents, meta-computing and resource co-allocation could serve as a Hive infrastructure. Regardless of precisely how businesses choose to leverage its power, there is no doubt that – by building on and extending the idea of Grid Computing – Hive Computing will provide businesses and other organizations with tremendous levels of flexibility and drive down the cost of reliability. In this work, we will develop a heterogeneous agent-based hierarchical model, resource scheduling (meta-computing environment) and co-allocation to meet the requirements of the scalability. Our future work will focus on the implementation of a resource allocation management in a Hive infrastructure using GRAM-Soft tool that contains methodology of the mobile agents, meta-computing and resource co-allocation.

## References

- [1] Chris O'Leary -Hive Computing for Transaction Processing Grids, Tsunami Research
- [2] J. Gehring and A. Reinefeld. MARS - A Framework for Minimizing the Job Execution Time in a Metacomputing Environment. *Future Generation Computer Systems*, 12(1): 1996.
- [3] J. Weissman. The Interference Paradigm for Network Job Scheduling. *Proceedings of the Heterogeneous Computing*
- [4] K. Czajkowski, I. Foster – Resource Management Architecture for Metacomputing Systems.
- [5] K. Czajkowski, I. Foster and C. Kesselman - Resource Co-Allocation in Computational Grids
- [6] K. Czajkowski, I. Foster, C. Kesselman, S. Martin, W. Smith, S. Tuecke. Resource Management Architecture for Meta-Computing Systems.
- [7] F. Berman, R. Wolski, J. Schopf and G. Shao. Application level scheduling on distributed heterogeneous networks. In proceedings of Supercomputing'96. ACM Press, 1995.
- [8] S. Zhou. LSF: Load sharing in large-scale heterogeneous distributed systems. In proc. Workshop on Cluster Computing, 1992.

# Data-Parallel Method for Georeferencing of MODIS Level 1B Data Using Grid Computing

Yincui Hu<sup>1</sup>, Yong Xue<sup>1,2,\*</sup>, Jiakui Tang<sup>1</sup>, Shaobo Zhong<sup>1</sup>, and Guoyin Cai<sup>1</sup>

<sup>1</sup> State Key Laboratory of Remote Sensing Science, Jointly Sponsored by the Institute of Remote Sensing Applications of Chinese Academy of Sciences and Beijing Normal University, Institute of Remote Sensing Applications, Chinese Academy of Sciences, P. O. Box 9718, Beijing 100101, China

<sup>2</sup> Department of Computing, London Metropolitan University, 166-220 Holloway Road, London N7 8DB, UK  
{huyincui@163.com, y.xue@londonmet.ac.uk}

**Abstract.** Georeference is a basic function of remote sensing data processing. Geo-corrected remote sensing data is an important source data for Geographic Information Systems (GIS) and other location services. Large quantity remote sensing data were produced daily by satellites and other sensors. Georeferencing of these data is time consumable and computationally intensive. To improve efficiency of processing, Grid technologies are applied. This paper focuses on the parallelization of the remote sensing data on a grid platform. According to the features of the algorithm, backwards-decomposition technique is applied to partition MODIS level 1B data. Firstly, partition the output array into evenly sized blocks using regular domain decomposition. Secondly, compute the geographical range of every block. Thirdly, find the GCPs triangulations contained in or intersect with the geographic range. Then extract block from original data in accordance with these triangulations. The extracted block is the data distributed to producer on Grid pool.

## 1 Introduction

Large quantity imagery data of remote sensing produced daily by variable satellites and other sensors. The processing of remote sensing data is computationally intensive. It requires parallel and high-performance computing techniques to achieve good performance. Geo-corrected remote sensing data are source data for geographic information systems and other location services. When the correction formulation is complicate, the large image georeference will require a mass of time. Over the past decade, Grid has become a powerful computing environment for data intensive and computing intensive applications. Cannataro (2000) proposed to develop data mining services within a Grid infrastructure as the deployment platform for high performance distributed data mining and knowledge discovery.

Researchers have aimed to develop Grid platforms for remote sensing data processing. Aloisio *et al.* (2004) proposed Grid architecture for remote sensing data

---

\* Corresponding author.

processing and developed a Grid-enabled platform, SARA/Digital Puglia with his research group. SARA/Digital Puglia (Aloisio *et al.* 2003) is a remote sensing environment developed in a joint research project. Our research group has developed a grid-based remote sensing environment, which is the High-Throughput Spatial Information Processing Prototype System in Institute of Remote Sensing Applications, Chinese Academy of Sciences (Cai *et al.* 2004, Hu *et al.* 2004, Wang *et al.* 2003).

This paper focuses on the parallelization of the remote sensing data on a grid platform. First, we discussed the algorithm of rectifying remote sensing image. Second, data partition for georeference on grid is introduced. Finally, we analyzed the result of georeference on Grid platform.

## 2 Georeference Implementation on the Grid

### 2.1 MODIS Level 1B Data

MODIS level 1B products are obtained from **M**oderate Resolution **I**maging **S**pectroradiometer (MODIS) carried on EOS satellite and have been calibrated. MODIS includes 36 spectral bands extending from the visible to the thermal infrared wavelengths (Running *et al.*, 1994). The MODIS Level 1B products contain longitude and latitude coordinates. These coordinates can be used as Ground Control Points (GCP) to rectify the image.

### 2.2 Parallel Rectification on Grid

There are three important components to rectify an image, i.e. transformation model selection, coordinate transformation and resample. In this paper, triangle warping model is selected to transform the coordinates. Moreover, cubic resample method is used. The triangular is build from the longitude and latitude coordinates.

The image rectification steps for interpolating, transforming and resampling can be integrated into one routine. This rectify routine can be repeated to correct every part of the large image. Now that the rectify routine can be data parallel processing in Grid, how to partition the data and how to merge the results are the main questions confront us.

### 2.3 Data Partition Strategy

The partition strategy influences the process efficiency and determines the merge strategy. So to select an efficient partition method is very important. The value of the output pixel is interpolated by value of pixels around its location in original image. The original location is obtained by triangle transformation from GCPs triangulations. According to the features of the algorithm, backwards-decomposition technique is applied to partition MODIS level 1B data. It comprises four steps as follows:

Firstly, partition the output array into evenly sized blocks using regular domain decomposition. Secondly, compute the geographical range of every block. Thirdly, find the GCPs triangulations contained in or intersect with the geographical range.

Then extract block from original data in accordance with these triangulations. The extracted block is the data that will be distributed to producer on Grid pool.

### 3 Experiments and Analysis

Our experiments were performed on a Grid-computing environment, which is in the High-Throughput Spatial Information Processing Prototype System (HIT-SIP) based on Grid platform in Institute of Remote Sensing Applications, Chinese Academy of Sciences. Test data are MODIS level 1B products. The data format is HDF. The data is partitioned into many parts by backwards-decomposition techniques. The experiment result is shown in table 1.

**Table 1.** Experiment results

Test data size	Sequential Time (sec)	No. of parts	Execution time (sec)
768 MB	Out of memory	10	1208
		80	856
83 MB	404	8	358
		80	281
20 MB	282	4	130
		8	110

The experiment shows that data-parallel georeference is efficient especially for those large-size data. The computer shows errors “out of memory, unable to allocate memory” when rectifying the large data (768 MB) in a computer with 512MB memory. This situation could be solved with the help of the resources in Grid pool. The large data is decomposed into small parts and distributed to the Grid.

### 4 Conclusions

As an important new field in the distributed computing arena, Grid computing focuses on intensive resource sharing, innovative applications, and, in some cases, high-performance orientation. We implemented data-parallel georeference in HIT-SIP platform. The experiments indicate that Grid is efficient for data-parallel georeference. The efficiency could be improved especially for those large data. For those processing that need large memory, Grid can also provide enough resources to solve the problem. Ongoing work on HIT-SIP includes developing middleware of remote sensing processing and providing remote sensing processing services for Internet consumers.

### Acknowledgement

This publication is an output from the research projects "CAS Hundred Talents Program" and "Monitoring of Beijing Olympic Environment" (2002BA904B07-2)

and "Remote Sensing Information Processing and Service Node" funded by the MOST, China and "Aerosol fast monitoring modeling using MODIS data and middlewares development" (40471091) funded by NSFC, China.

## References

1. Aloisio, G., Cafaro, M.: A Dynamic Earth Observation System. *Parallel Computing*. 29 (2003), 1357-1362
2. Aloisio, G., Cafaro, M., Epicoco, I., Quarta, G.: A Problem Solving Environment for Remote Sensing Data Processing. *Proceeding of ITCC 2004: International Conference on Information Technology: Coding and Computing*. Vol.2. IEEE Computer Society, 56-61.
3. Cai GY, Xue Y, Tang JK, Wang JQ, Wang YG, Luo Y, Hu YC, Zhong SB, Sun XS, 2004. Experience of Remote Sensing Information Modelling with Grid Computing. *Lecture Notes in Computer Science*, Vol. 3039. Springer-Verlag, 989-996.
4. Cannataro, M: Clusters and Grids for Distributed and Parallel Knowledge Discovery. *Lecture Notes in Computer Science*. 1823(2000), 708-716
5. Hu YC, Xue Y, Wang JQ, Sun XS, Cai GY, Tang JK, Luo Y, Zhong SB, Wang YG, Zhang AJ.: Feasibility Study of Geo-spatial Analysis Using Grid Computing. *Lecture Notes in Computer Science*, Vol. 3039. Springer-Verlag (2004) 956-963.
6. Lanthier, M., and Nussbaum, D: Parallel Implementation of Geometric Shortest Path Algorithms. *Parallel Computing*. 29(2003), 1445-1479.
7. Pouchard, L; Cinquini, L; Drach, B; Middleton, D; Bernholdt, D; Chanchio, K; Foster, I; Nefedova, V; Brown, D; Fox, P; Garcia, J; Strand, G; Williams, D; Chervenak, A; Kesselman, C; Shoshani, A; Sim, A.: An Ontology for Scientific Information in a Grid Environment: The Earth System grid. 3rd IEEE/ACM International Symposium on Cluster Computing and the GRID. IEEE Computer Society (2003) 626-632.
8. Roros, D. -K. D., Armstrong, M. P: Using Linda to Compute Spatial Autocorrelation in Parallel. *Computers & Geosciences*. 22(1996), 425-432
9. Roros, D. -K. D., Armstrong, M. P.: Experiments in the Identification of Terrain Features Using a PC-Based Parallel Computer. *Photogrammetric Engineering & Remote Sensing*. 64(1998), 135-142
10. Wang, S. and Armstrong, M. P.: A Quadtree Approach to Domain Decomposition for Spatial Interpolation in Grid Computing Environments. *Parallel Computing*. 29(2003) 1481-1504.
11. Jianqin Wang, Yong Xue, and Huadong Guo, 2003, A Spatial Information Grid Supported Prototype Telegeoprocessing System. In *Proceedings of 2003 IEEE International Geoscience and Remote Sensing Symposium (IGARSS'2003)* held in Toulouse, France on 21-25 July 2003, v 1, p 345-347.

# An Engineering Computation Oriented Grid Project: Design and Implementation<sup>1</sup>

Xianqing Wang<sup>1,2</sup>, Qinhuai Zeng<sup>2</sup>, Dingwu Feng<sup>2</sup>, and Changqin Huang<sup>2,3</sup>

<sup>1</sup> Guangdong Institute of Science and Technology, Zhuhai, 519090, P.R. China

<sup>2</sup> Hunan University of Arts and Science, Changde, 415000, P.R. China

<sup>3</sup> College of Computer Science, Zhejiang University, Hangzhou, 310027, P.R. China  
xqwang\_kgy@126.com, djzqh@163.com, cqhuang@zju.edu.cn

**Abstract.** This paper describes a Service-bAsed Grid project for Engineering computation, named SAGE. Based on the Globus toolkit, a grid-service-based architecture oriented to engineering computation is presented. To give grid users good usability, task definition and resource discovery are visually conducted. Whilst, a Quality of Service (QoS) driven user-centric scheduling strategy is proposed, two scheduling methods and steering-enabled visual interfaces are applied for different types of grid users. Result processing can be visualized in the aid of a PC-cluster and a stereopticon. The practices suggest that these mechanisms improve the convenience and QoS.

## 1 Introduction

Grid computing has a promising future in large-scale scientific computation. The Globus toolkit [1] is the most popular grid environment and de facto standard, and it has adopted OGSA [2] architecture to provide applications with grid service level at present. As a special type of large-scale computation, engineering computation is very hardy-solved because of requirements for many valuable computing resources or specialist instrumentations, grid computing is a suited computing infrastructure for the high capability of distributed and heterogeneous resources sharing. However, grid-based engineering computation needs to solve some important issues, such as narrowing the gap between currently deployed grid services and the would-be user community.

## 2 Overview of Proposed Architecture

To meet requirements for scientists in engineering computation field in grid environments, we propose the SAGE project (Service-bAsed Grid project for Engineering computation) that aims to use Grid technology to establish an enabling environment for large-scale scientific and engineering research. The overview of architecture is shown in Fig.1, it consists of four components: a) The interface component is a portal

---

<sup>1</sup> A Project Supported by Scientific Research Fund of Hunan Provincial Education Department, China (Grant No. 04A037).

of the system, It not only provides a visual interface for development and steering of grid-based applications, but also gives these system administrator a friendly management portal. It comprises a task submission window and two types of grid scheduling interfaces. b) Task-level logic component is responsible for task management, community policy and user administration. It includes virtual organization register, user manager, task definition, task import and export, task submission, task scheduling, task monitoring, task rescheduling, file transfer, and result processing. c) Grid service logic part consists of all services and service management mechanisms. All services are divided into three types: advanced general service, engineering computation modeling and post-processing service, basic grid service. The former two types are constructed on the basis of the latter. Service management contains: service deployment, service location, service composition, service scheduling and service-level performance steering. d) Grid Security Infrastructure is the last hierarchy in our architecture. It is based on the Globus Toolkit’s security mechanism, main characteristics exist: parallelized subtask-based authorization, community policy and task delegation management [3].

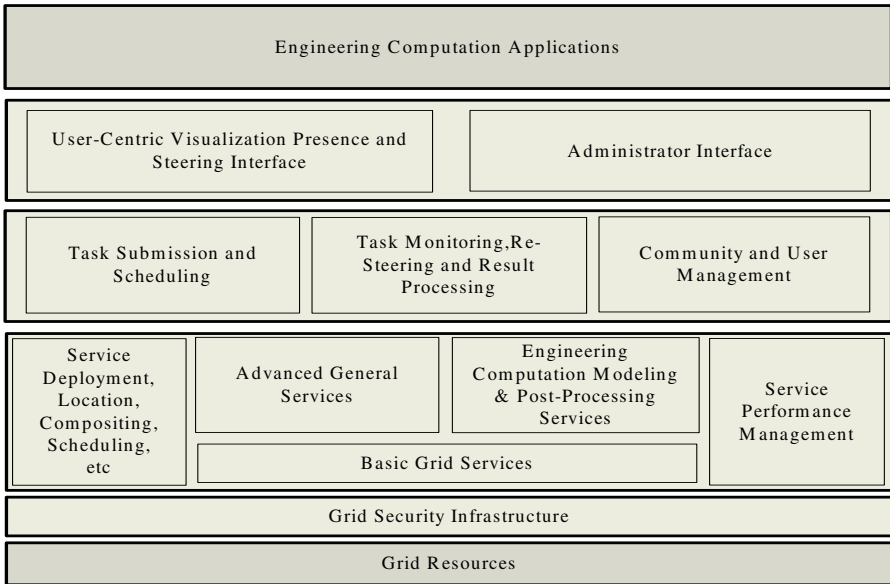


**Fig. 1.** Engineering computation architecture

### 3 Definitions of Grid Task and Resource Discovery

A session for each user is defined in the Grid. The session is created when one logs in, and destroyed after one logs out. In the session, a user defines computation task, possesses resources, monitors task execution and does post-process for the results. The Grid provides a graphical user interface to input a new task or to update an existing task. The data include executable program, resources and schedule requirements.

When the Grid accepts the data, an instance of task class is initialized and added to logical resources allocation queue. The task's state is initialized to "WAITING".

Resources information services provide two interfaces, a hierarchical resources tree, and a resources list. The content of the tree is the detailed information regarding hosts in virtual organizations, where local hosts are registered. It also shows the architecture of those virtual organizations. In the list, each item contains information of an individual host. The information on the list can be customized for display. Generally it consists of host name, node count, CPU count, speed and free percentage of CPU, free memory size, free secondary storage, network bandwidth and latency. In this project, resources are divided into two classes, computing power and visualization devices.

## 4 Task Scheduling and QoS Management

This architecture adopts aggregated QoS driven visual scheduling, the scheduling could be performed through two types of visual windows, scheduling and QoS sessions. These visual methods provide users with a direct awareness and a friendly interaction. A visual scheduling framework is shown in Fig. 2.

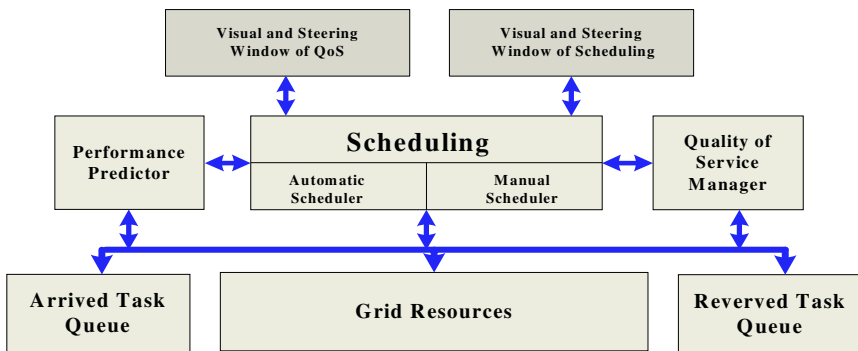


Fig. 2. A visual scheduling framework

According to different types of users, the visual scheduling is performed in both manual and automatic manner with a monitoring mechanism. In addition to the arrived task queue, a reserved task queue is used for arranging pre-scheduled tasks. Hence reservation-based scheduling can perform well. The scheduling algorithms during the automatic scheduling can be selected by users, as various conventional algorithms can be integrated into the system. The idea is based on the fact that different algorithms are suitable for respective environments and objectives.

In our architecture, a self-designed simple performance predictor serves for the scheduler by predicting and computing the previously mentioned performance metrics. It analyzes the performances of the tasks to be scheduled in advance; furthermore, it evaluates QoS parameters of scheduled tasks. QoS manager is responsible for accepting these required performance values from the input, for setting performance



threshold values that are conditions of triggering adjustment mechanisms and warning user, and for managing the events of post-scheduling and the interactions for a better performance. In the project, aggregated QoS is modeled based on four performance metrics. The relevant scheduling algorithms are based on Dual-Component and Dual-Queue Distributed Schedule Model (D<sup>3</sup>SM), which is described in the literature [4].

## 5 Visualization for Results

The project supports the collaborative visualization of meshes and visual steering of CFD/CSM simulations. The visualization will be implemented by our on-going project named ViG (Visualization in Grid). ViG makes use of the DAWNING PC-cluster. The cluster has 9 rendering nodes, and each node has a dual-head FX5200 display card connected to a projector. The projectors are deployed to generate stereoscopic 3 x 3 images on the large display wall. ViG will provide input to the development of this service and will develop a fully Grid-enabled extension of standard rendering APIs to allow scientists to run Grid applications through the ViG user interface.

## 6 Conclusions

The Grid project for engineering computation (SAGE) supplies the users with a visual application development and deployment environment for engineering computation. The whole is characterized by grid service. Whilst, definition of grid task & resource discovery are visually conducted, QoS driven user-centric scheduling, are designed and implemented. Result processing can be visualized in the aid of a PC-cluster and a stereopticon. In practice, the convenience and QoS are significantly improved, however, there exist a great shortage in the whole system, which are yet the important aspects of our future work.

## References

1. I. Foster, and C. Kesselman (eds.), *The Grid: Blueprint for a New Computing Infrastructure*, Morgan Kaufmann, 1999.
2. J. Nick, I. Foster, et al, *The Physiology of the Grid: An Open Grid Services Architecture for Distributed Systems Integration*, Open Grid Service Infrastructure, Global Grid Forum, 2002.
3. CQ Huang, GH Song et al, *An Authorization Architecture Oriented to Engineering and Scientific Computation in Grid Environments*, ACSAC 2004, LNCS 3189, pp. 461–472, 2004.
4. CQ Huang, DR Chen et al, *Performance-Driven Task and Data Co-scheduling Algorithms for Data-Intensive Applications*, APWeb 2004, LNCS 3007, pp. 331–340, 2004.

# Iterative and Parallel Algorithm Design from High Level Language Traces

Daniel E. Cooke and J. Nelson Rushton

Computer Science Department, Texas Tech University, Lubbock, Texas, U.S.A. 79409  
{dcooke, nrushton}@coe.ttu.edu

**Abstract.** We present a high level language called SequenceL. The language allows a programmer to describe functions in terms of abstract relationships between their inputs and outputs, and the semantics of the language are capable of automatically discovering and implementing the required algorithms, including iterative and parallel control structures in many cases. Current implementations do not produce code of comparable efficiency to that of a good human programmer. Current implementations can, however, be used as a tool to guide human programmers in discovering and comparing options for parallelizing their solutions. This paper describes the language and approach, and illustrates this kind of guidance with a simple example.

## 1 Introduction and Related Work

SequenceL is a high-level language in which algorithms for implementing a solution are automatically derived from a high level description of that solution. In this paper we introduce how the language can be exploited in the design of parallel algorithms.

The beginning point of this effort can be traced to [1], which overlaps the iterative morphisms found in [6]. SequenceL's semantic work-horse is the *Normalize-Transpose-Distribute* (NTD), which is used to simplify and decompose structures, based upon a dataflow like execution strategy. The NTD semantic achieves a goal similar to that of the Lämmel and Peyton-Jones, boilerplate elimination. [4,5]

## 2 Normalize-Transpose-Distribute (NTD)

SequenceL functions have typed arguments, where the type of an argument is simply its level of nesting (scalar, sequence of scalars (i.e. vector), sequence of sequences of scalars, (i.e., matrix) etc.). When a SequenceL function receives arguments, which are *overtyped* (i.e., nesting level higher than expected), the remaining arguments are *normalized* -- duplicated to match the length of the overttyped arguments.

For example, consider the definition of dot product in SequenceL:

```
dotprod: vector * vector -> scalar
dotprod(A,B) = sum(A*B)
```

Given the call `dotprod((2,3,4) (100,10,1))`, instantiating the function results in `sum(((2,3,4) * (100,10,1))`. Since `*` expects scalars for both arguments, NTD is performed, resulting in `sum(200, 30, 4)`, which evaluates to 234, the desired result.

### 3 The Environment and Matrix Multiply

From the standpoint of specification, the  $i,j$ th element of the product matrix of  $a$  and  $b$  is the dot product of the  $i$ 'th row of  $a$  with the  $j$ 'th column of  $b$ . Here is SequenceL code for the algorithm:

```
mmrow: vector * matrix → matrix
mmrow(A,B) ::= dotprod(A,transpose(B))
```

This function appears to compute only a single row of the matrix product  $AB$ , but will compute all rows if a matrix is passed as an argument, due to NTD. Here is the trace of a sample execution:

$$(mmrow,(((1, 2, 4), (10, 20, 40), (11, 12, 14)), ((1, 2, 4), (10, 20, 40), (11, 12, 14)))) \tag{1}$$

Since the first argument is a matrix rather than a vector as expected, `normalize` and `transpose` are performed yielding

$$( (mmrow,((1,2,4),((1,2,4),(10,20,40),(11,12,14)))), \tag{2}$$

$$(mmrow,((10,20,40),((1,2,4),(10,20,40),(11,12,14)))),$$

$$(mmrow,((11,12,14),((1,2,4),(10,20,40),(11,12,14)))) )$$

Now the language interpreter instantiates the body of the `mmrow` function and the transposes are performed (we write `dp` for `dotprod` to save space):

$$( (dp,((1,2,4),(transpose,((1,2,4),(10,20,40),(11,12,14))))), \tag{3}$$

$$(dp,((10,20,40),(transpose,((1,2,4),(10,20,40),(11,12,14))))),$$

$$(dp,((11,12,14),(transpose,((1,2,4),(10,20,40),(11,12,14)))))) )$$

After the transposes, the SequenceL `dp` function as defined in section 2 is invoked:

$$( (dp,((1,2,4),(1,10,11),(2,20,12),(4,40,14))), \tag{4}$$

$$(dp,((10,20,40),(1,10,11),(2,20,12),(4,40,14))),$$

$$(dp,((11,12,14),(1,10,11),(2,20,12),(4,40,14)))) )$$

Note that `dp` takes two vectors as input. From where we left off in step 4 of the trace, we know that the second argument of each `dp` reference is a two-dimensional structure, so another NTD is performed on each `dp` resulting in 9 `dp` references:

$$(((dp,((1,2,4),(1,10,11))), (dp,((1,2,4),(2,20,12))), (dp,((1,2,4),(4,40,14))), \tag{5}$$

$$((dp,((10,20,40),(1,10,11))), (dp,((10,20,40),(2,20,12))), (dp,((10,20,40),(4,40,14))),$$

$$((dp,((11,12,14),(1,10,11))), (dp,((11,12,14),(2,20,12))), (dp,((11,12,14),(4,40,14))))))$$

which are evaluated (potentially in parallel) for the final result:

$$(((65, 90, 140), (650, 900, 1400), (285, 430, 720)))$$

The parallelisms discovered between step 5 and the final result are micro-parallelisms, and therefore, should be carried out iteratively. As it turns out, steps 4 and 5 of the trace are of keen interest in designing parallel or concurrent algorithms. Either point could be used as the basis for the algorithms. In the next two subsections we evaluate these options and how they can be realized in concurrent JAVA codes.

### 3.1 Parallelizing Based on Step 5 of the Trace

Step 5 indicates that we are combining every element of each row of the first matrix with every element of each column of the second, forming a cartesian product of sorts from the two matrices. To accomplish this in concurrent JAVA we would have the following code segments, extracted from a total of about 60 lines of code.

```
... public void run()      {
    s = 0;
    for (k=0;k<=m.length-1;k++)
        { s += m[rs][k] * m[k][cs]; }
public static void main (String args()) { ...
    for(i=0;i<=(r*c)-1;i++)
        {mat[i].start();           ... }
```

Notice that the  $\sim O(n^2)$  algorithm that forks the *run* threads is in the main program and that we are indeed computing each element of the result concurrently. This loop follows a nested  $\sim O(n^2)$  algorithm that initialized each of the threads with the proper subscript values for *rs* and *cs*.

### 3.2 Parallelizing Based on Step 4 of the Trace

Step 4 of the SequenceL trace indicates another option for the parallelization of the desired computation. In this approach, each row of the first matrix is combined with all columns of the second. This suggests moving the  $\sim O(n^2)$  algorithm into the concurrently executed *run* threads, reducing the overhead involved in separating threads and spawning concurrent tasks from  $\sim O(n^2)$  to  $O(n)$ .

```
... public void run()      {
    s = new int(m.length);
    for (rs=0;rs<=m.length-1;rs++)
        for (k=0;k<=m.length-1;k++)
            {s[rs]+=m[rs][k]*m[k][cs];}
public static void main (String args()) { ...
    for(i=0;i<=r-1;i++)
        {mat[i].start();}           ... }
```

This approach concurrently computes the result of each row of the resultant matrix and follows a rule of thumb in developing concurrent codes: parallelize outer loops.

It is interesting to note that though this implementation is substantially more efficient than the previous one, it did not occur to us until after we examined the trace of matrix multiplication in SequenceL.

## 4 Discussion

Since completing the changes to the language last year, we have conducted additional experiments to discover parallel algorithms for problems including Gaussian Elimination, Quicksort, Discrete Wavelet Transforms, Newton-Raphson solutions to linear equations, Fast Fourier Transform, among others. We have also investigated applications to remote sensing problems and to the prototyping of Guidance, Navigation, and Control problems for processing onboard the Space Shuttle. These experiments have shown SequenceL to be an easy-to-use and promising tool for exploring ideas and problem solutions in a variety of domains.

## References

1. Daniel E. Cooke and A. Gates, "On the Development of a Method to Synthesize Programs from Requirement Specifications," *International Journal on Software Engineering and Knowledge Engineering*, Vol. 1 No. 1 (March, 1991), pp. 21-38.
2. Daniel E. Cooke, "An Introduction to SEQUENCCEL: A Language to Experiment with Nonscalar Constructs," *Software Practice and Experience*, Vol. 26 (11) (November, 1996), pp. 1205-1246.
3. Daniel E. Cooke and Per Andersen, "Automatic Parallel Control Structures in SequenceL," *Software Practice and Experience*, Volume 30, Issue 14 (November 2000), pp. 1541-1570.
4. R. Lämmel and S. Peyton-Jones, "Scrap your boilerplate: a practical design pattern for generic programming," in Proceedings of TLDI 2003, ACM Press.
5. R. Lämmel and S. Peyton-Jones, "Scrap more boilerplate: reflection, zips, and generalised casts," to appear in Proceedings of ICFP 2004, ACM Press.
6. Meijer, E. and Fokkinga, M.M. and Paterson, R., "Functional Programming with Bananas, Lenses, Envelopes and Barbed Wire" *FPCA* (Springer-Verlag, 1991) LNCS Series Vol. 523, pp. 124—144.

# An Application of the Adomian Decomposition Method for Inverse Stefan Problem with Neumann's Boundary Condition

Rad.s.a. Grzymkowski, sk. a. d. am. a. . . . .

Institute of Mathematics, Silesian University of Technology, Kaszubska 23,  
44-100 Gliwice, Poland  
{r.grzymkowski, d.slota}@polsl.pl

**Abstract.** In this paper the solution of one-phase inverse Stefan problem with Neumann's boundary condition is presented. This problem consists of the reconstruction of the function which describes the heat flux on the boundary, when the position of the moving interface is well-known. The proposed solution is based on the Adomian decomposition method and the least square method.

## 1 Introduction

In this paper we solve the one-phase inverse Stefan problem, which consists of the reconstruction of the function which describes the heat flux on the boundary, when the position of the moving interfaces is well-known. This kind of problem becomes an inverse design problem. The conditions for the existence and uniqueness of the solution of this problem are given. The temperature and the solution is based on the Adomian decomposition method and the least square method. The Adomian decomposition method as developed by G. Adomian [2] and his methods useful for solving a wide class of problems [2,4]. Since these methods are able to solve nonlinear parabolic equations.

$$F(u) = f \tag{1}$$

where  $F: H \rightarrow G$  is a nonlinear parabolic operator,  $f$  is a known element from Hilbert space  $G$  and  $u$  is the sought element from Hilbert space  $H$ . Operator  $F(u)$  can be written as

$$F(u) = L(u) + R(u) + N(u), \tag{2}$$

where  $L$  is the linear parabolic operator,  $R$  is the remaining nonlinear parabolic and  $N$  is a nonlinear parabolic operator. The solution of the equation (1) is sought in the form of a function series

$$u = \sum_{i=0}^{\infty} g_i. \tag{3}$$

After some manipulations we obtain the following recurrent formula

$$\begin{aligned} g_0 &= g^* + L^{-1}(f), \\ g_n &= -L^{-1}R(g_{n-1}) - L^{-1}(A_{n-1}), \quad n \geq 1, \end{aligned} \tag{4}$$

here  $g^*$  is a function depending on the initial and boundary conditions and  $L^{-1}$  is the inverse operator.

## 2 Inverse Stefan Problem

Let  $D \subset \mathbb{R}^2$  be a domain (figure 1). We seek an approximate solution of the following problem

for the given position of freezing front  $\Gamma_g$ , the distribution of temperature  $u$  in domain  $D$  is calculated as the solution of  $q(t)$  on boundary  $\Gamma_1$ , which satisfies the following equations

$$\begin{aligned} \frac{\partial^2 u(x,t)}{\partial x^2} &= \frac{\partial u}{\partial t}(x,t), && \text{in } D, && (1) \\ u(x,0) &= \varphi(x), && \text{on } \Gamma_0, && (2) \\ -\lambda \frac{\partial u(x,t)}{\partial x} &= q(t), && \text{on } \Gamma_1, && (7) \\ u(\xi(t),t) &= u^*, && \text{on } \Gamma_g, && (8) \\ -\lambda \frac{\partial u(x,t)}{\partial x} &= \kappa \frac{d\xi(t)}{dt}, && \text{on } \Gamma_g, && (9) \end{aligned}$$

where  $a$  is the thermal diffusivity,  $\lambda$  is the thermal conductivity,  $\kappa$  is the latent heat of fusion per unit volume, and  $u, t$  and  $x$  refer to temperature, time and spatial coordinate, respectively.

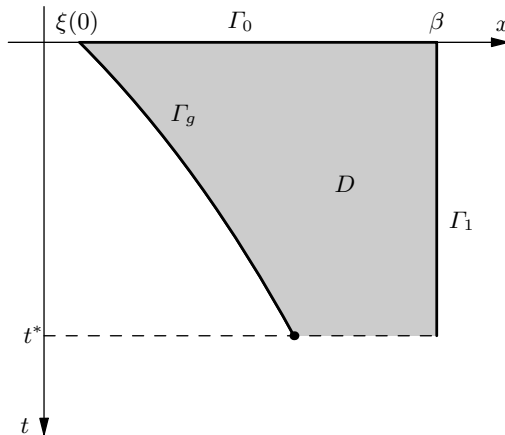


Fig. 1. Domain formulation of the problem

### 3 Solution of the Problem

the problem under consideration has the parabolic equation (1), here

$$L(u) = \frac{\partial^2 u}{\partial x^2}, \quad R(u) = -\frac{\partial u}{\partial t}, \quad N(u) = \dots, \quad f = \dots$$

hence the parabolic operator  $L^{-1}$  is given by

$$L^{-1}(u) = \int_{\xi(t)}^x \int_x^\beta u(x, t) dx dx. \tag{3}$$

Therefore, using the boundary conditions (7) and (8) we obtain

$$g_0(x, t) = \frac{1}{\lambda} q(t) (\xi(t) - x) + u^*,$$

$$g_n(x, t) = -\frac{1}{a} \int_{\xi(t)}^x \int_x^\beta \frac{\partial g_{n-1}(x, t)}{\partial t} dx dx, \quad n \geq 1. \tag{4}$$

We seek an approximate solution of the form

$$u_n(x, t) = \sum_{i=0}^n g_i(x, t), \quad n \in \mathbb{N}. \tag{5}$$

Because the  $g_i$  (4) are dependent on the unknown function  $q(t)$ , we derive the function  $q(t)$  from

$$q(t) = \sum_{i=1}^m p_i \psi_i(t), \tag{6}$$

where  $p_i \in \mathbb{R}$  and the basis functions  $\psi_i(t)$  are linearly dependent. The coefficients  $p_i$  are selected to show the minimum of the functional (5) from the conditions (7) and (8) (considering the assumed measure). To construct the measure for the least square method applied, thus we seek the minimum of the functional

$$J(p_1, \dots, p_m) = \int_{\xi(0)}^\beta (u_n(x, t) - \varphi(x))^2 dx + \int_0^t \left( \lambda \frac{\partial u_n(x, t)}{\partial x} \Big|_{x=\xi(t)} + \kappa \frac{d\xi(t)}{dt} \right)^2 dt. \tag{7}$$

Substituting equations (5), (6) and (7) into the functional  $J$  and differentiating with respect to the coefficients  $p_i$  ( $i = 1, \dots, m$ ) and equating the obtained derivatives to zero, the system of the linear algebraic equations is obtained. The course of solving this system, the coefficients  $p_i$  are determined, and therefore the approximate distribution of temperature in the domain  $D$  and the heat fluxes on the boundary  $\Gamma_1$  are obtained.



### 4 Numerical Example

In the numerical example considered, we reproduce the problem discussed in the previous section. We assume  $\beta = 1, a = 2, \lambda = 2, \xi(t) = at, \varphi(x) = e^{-x}, \kappa = \lambda/a, u^* = 1, t^* = 1$ . The exact solution of the inverse Stefan problem can be found from the following functions  $u(x, t) = e^{a(t-x)}$  for  $(x, t) \in D$ , and  $q(t) = \lambda e^{a(t-\beta)}$  for  $t \in [0, t^*]$ . As basis functions we take  $\psi_i(t) = t^{i-1}, i = 1, \dots, m$ . For the calculation, we assume  $m \in \{2, \dots, 7\}$  and  $n \in \{2, \dots, 7\}$ . Figure 2 shows the exact and reconstructed heat flux on the boundary  $\Gamma_1$  for a different number of elements of the sum (2),  $n \in \{4, 7\}$  and for basis functions  $\psi_i(t)$ . The results obtained show that functions  $q(t)$  and  $u(x, t)$  are reconstructed very well.

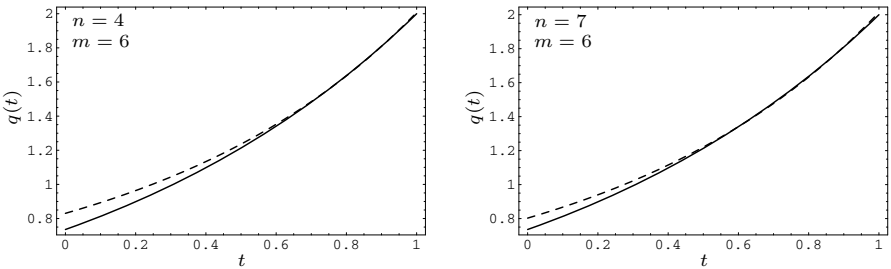


**Fig. 2.** The heat flux on the boundary  $\Gamma_1$  (solid line – exact value, dash line – reconstructed value)

### 5 Conclusion

We have presented a method for solving the one-phase inverse Stefan problem. In which consists of the reconstruction of the function describing the heat flux on the boundary. The possibility of the modeling interface separation. The method makes use of the Adomian decomposition method and the least square method. The calculation presented shows that this method is effective for solving this problem.

### References

1. Adomian, G.: Stochastic Systems. Academic Press, New York (1983)
2. Adomian, G.: A review of the decomposition method in applied mathematics. J. Math. Anal. Appl. **135** (1988) 501–544
3. Goldman, N.L.: Inverse Stefan problem. Kluwer, Dordrecht (1997)
4. Lesnic, D.: Convergence of Adomian’s decomposition method: periodic temperatures. Computers Math. Applic. **44** (2002) 13–24

# Group Homotopy Algorithm with a Parameterized Newton Iteration for Symmetric Eigen Problems

Ra. a k<sup>1</sup>, arab atta<sup>2</sup> a d . . . p . . . g<sup>2</sup>

<sup>1</sup> Department of Computer Engineering, Honam University,  
Gwangju 506-090, Korea

<sup>2</sup> Department of Mathematical Sciences, Northern Illinois University,  
DeKalb, IL 60115, USA

baik@honam.ac.kr

{dattak, hong}@math.niu.edu

**Abstract.** In this paper we develop a general Homotopy method called the Group Homotopy method to solve the symmetric eigenproblem. The Group Homotopy method overcomes notable drawbacks of the existing Homotopy method, namely, (i) the possibility of breakdown or having a slow rate of convergence in the presence of clustering of the eigenvalues and (ii) the absence of any definite criterion to choose a step size that guarantees the convergence of the method. On the other hand, the Group Homotopy method maintains attractive features of the ordinary Homotopy method such as the natural parallelism and the structure preserving properties.

## 1 Introduction

Let  $S$  and  $A$  be  $n \times n$  symmetric matrices. Define a mapping  $H: \mathbb{R} \rightarrow M_n$  such that  $H(t) = A(t) \equiv (1-t)S + tA$ ,  $t \in [0, 1]$ . Note that  $A(t) = S + t(A - S)$  so that the matrix  $A(t)$  can be made close to  $S$  by choosing  $t$  small enough. Hence, by the spectral theorem, the set of eigenvalues  $\left\{ \begin{pmatrix} u_k \\ \lambda_k \end{pmatrix} \right\}, k = 1, \dots, n$  of  $A(0) = S$  can be successively obtained by the set of eigenvalues  $\left\{ \begin{pmatrix} u_k(i) \\ \lambda_k(i) \end{pmatrix} \right\}, k = 1, \dots, n$  of  $A(t_i)$ ,  $t_0 < t_1 < \dots < t_n = 1$ , starting from the set of eigenvalues  $\left\{ \begin{pmatrix} x_k \\ \alpha_k \end{pmatrix} \right\}, k = 1, \dots, n$  of  $A(1) = A$  [2, 7, 8].

The procedure is called the group homotopy method. A major problem that arises in implementing a homotopy method for the eigenproblem is how to choose  $\Delta t_i \equiv t_{i+1} - t_i$  properly so that the eigenvalues of  $A(t_i + \Delta t_i)$  can be obtained from the eigenvalues (possibly clustered) of  $A(t_i)$  using the Newton's method with a reasonable number of iterations. In this paper we propose a series of the question to seek that there exists a small enough  $\Delta t_i$  for each eigenvalue of  $A(t_{i+1})$  such that the Newton's method converges to the small enough  $\Delta t_i$ .

Thus the question is how close should  $A(t_i)$  be to  $A(t_{i+1})$  to have a guarantee that each eigenpair of  $A(t_i)$  is such that convergence of the eigenvector of the corresponding eigenpair of  $A(t_{i+1})$  under the method 4 produces a desired accuracy. The error the eigenvalues of  $A(t_i)$  are clustered in the definite  $gap^*(A(t_i)) \equiv \min_k \{gap_k(A(t_i))\}$  where  $gap_k(A(t_i)) = |\lambda_k(i) - \lambda_{k+1}(i)|$ , and  $\lambda_k(i)$  are the eigenvalues of  $A(t_i)$  in decreasing order for  $k = 1, \dots, n$ . We show that for  $\Delta t_i$  is chosen such that  $\Delta t_i \leq \frac{gap^*(A(t_i))}{q}$  for some  $q \geq 4$ , the eigenpairs of  $A(t_i)$  converge to the corresponding eigenpairs of  $A(t_i + \Delta t_i)$  under the method. The method fails when  $gap^*(A(t_i))$  becomes extremely small for some  $t_i \in (t, \tau)$ , that is, the matrix  $A(t_i)$  has the clustered eigenvalues. Therefore, we prove the problem. We introduce the group  $gap, Gap^*$ . Section 2 is devoted that under the group gap we establish a sufficient large step size  $\Delta t_i$  such that the method terminates in a finite number of steps. We also discuss problems that may occur due to the large step size  $\Delta t_i$ . The method's method is applied to obtain the successive eigenpairs. We show that this problem can be easily resolved by a simple modification of the method. The method with group gap,  $Gap^*$  is called the Group method. The Group method with the parameterized method's iteration error factor is guaranteed to give eigenpairs of  $A$  in a finite number of steps. Furthermore, the choice of the initial matrix  $S$  can be arbitrary. Although a good choice of the initial matrix facilitates the convergence of the algorithm of the Group method is presented in section.

## 2 Properties of the Group Homotopy Method

In this section we develop a method called the Group method which is a generalization of the standard method. In this section we prove the difficulties that arise in the standard method. Assume that an arbitrary real symmetric matrix  $S \in M_n$  is chosen as the initial matrix. We have observed previously, the standard method fails whenever the gap between some adjacent eigenvalues of the matrix  $A(t_i)$  becomes quite small. This situation may occur whenever some eigenvalues of  $A(t_i)$  are clustered, i.e., there are groups of adjacent eigenvalues such that the distance between adjacent groups is much larger than the gaps among the eigenvalues that belong to the same group. We resolve the difficulty by using a concept, called the **group gap**. For that purpose we define the cluster gap of eigenvalues as follows.

**Definition 1.** Let  $\sigma(A) = \{\lambda_i\}_{i=1, \dots, n}$  be the set of eigenvalues of a symmetric matrix  $A$  in decreasing order. We say that two adjacent eigenvalues  $\lambda_k$  and  $\lambda_{k+1}$  are clustered if  $|\lambda_k - \lambda_{k+1}| < Gap^*$ ,  $1 \leq k \leq n - 1$  where  $Gap^*$  is a given positive number.

**Definition 2.** We say that a subset  $G = \{\lambda_k, \lambda_{k+1}, \dots, \lambda_{k+m}\} \subseteq \sigma(A)$  is a group of clustering of eigenvalues if  $|\lambda_{k+i} - \lambda_{k+i+1}| < \text{Gap}^*$  for all  $i = k, \dots, k+m-1$  where  $|\lambda_{k-1} - \lambda_k| \geq \text{Gap}^*$  and  $|\lambda_{k+m} - \lambda_{k+m+1}| \geq \text{Gap}^*$ .

We define the Group Homotopy method to be a set of  $n \times n$  symmetric matrices such that  $S$  is the start matrix and  $A$  is the target matrix.  $A(t_{i+1}) = A(t_i) + \Delta t_i(A - S)$  here  $t_0 < t_1 < \dots < t_n$ ,  $\Delta t_i = t_{i+1} - t_i$ ,  $A(t_0) = S$  and  $A(t_n) = A$ .

**Definition 3.** We say a Homotopy method is the Group Homotopy method if the step size  $\Delta t_i$  is determined by  $\text{Gap}^*$ .

We refer to the Group Homotopy method to make the following brief remarks

**Remarks**

**(A) Advantages of using  $\text{Gap}^*$ :** The step size  $\Delta t_i = \frac{\text{gap}^*(A(t_i))}{q}$ , the dual Homotopy are determined completely by the eigenvalues of  $A(t_i)$  here the eigenpath of the Homotopy is determined a priori by the start matrix  $S$ . Otherwise had  $\text{Gap}^*$  the Group Homotopy is a constant that they are free to choose to group the eigenvalues of  $A(t_i)$  so that the resulting stepsize  $\Delta t_i$  is large enough

**(B) How to choose  $\text{Gap}^*$ :** For the choice of  $\text{Gap}^*$ , we can consider the following (1) the distance of matrices, (2) magnitude of the eigenvalues of matrices, and (3) the closeness of the start matrix to the target matrix. Furthermore, a good choice of  $\text{Gap}^*$  should be the one that can be computed easily. Here we provide a large enough step size for the Homotopy method to terminate a reasonable amount of time. The following choice of  $\text{Gap}^*$  is used in this paper  $\text{Gap}^* = \delta \|A - S\| = \delta \|A - S\|$ ,  $\delta > 0$  here  $\|\cdot\|$  is a matrix norm

**(C) Justification of the choice  $\text{Gap}^* = \delta \|A - S\|$ :** We must first justify our choice of  $\text{Gap}^*$  and show that it leads to a simple determination of  $\Delta t_i$  for some points.

The scalars  $c_1$  and  $c_2$ , we have  $\|A - S\|^2 = c_1 \|A - S\|_F^2 = c_1 c_2 \sum_{k=1}^n (\alpha_k - \lambda_k)^2$  here  $\alpha_k$ 's and  $\lambda_k$ 's are the eigenvalues of the matrices  $S$  and  $A$ , respectively.

Thus,  $\delta \|A - S\|$  measures the closeness of the start eigenvalues to the target eigenvalues to a simple extent. It considers the eigenvalues of both matrices  $A$  and

$S$  set  $\Delta t_i = \frac{\text{Gap}^*}{q \|A - S\|}$ ,  $q > 0$ . Note that  $\Delta t_i = \frac{\text{Gap}^*}{q \|A - S\|} = \frac{\delta \|A - S\|}{q \|A - S\|} = \frac{\delta}{q}$

for some  $\delta > 0$  thus for the set  $\delta = \text{gap}^*(A(t_i))$  the  $\Delta t_i = \frac{\text{gap}^*(A(t_i))}{q}$ , for the

Group Homotopy method simply reduces to the previous dual Homotopy method. Furthermore, note that if  $\delta$  is chosen to be a positive number then

$\Delta t_i = \frac{\delta}{q}$  is a fixed constant, regardless of  $i$ . Thus under the Group Homotopy

the total number of steps is at most  $\lceil \frac{q}{\delta} \rceil$ , a nearest integer larger than

$\frac{q}{\delta}$  here we have a good choice for a matrix  $S$ , the might set  $\Delta t$  thus precise the case here  $q\|A - S\| < \frac{gap^*(S)}{q}$ , for some  $q > \dots$  this case for the set  $Gap^* = q\|A - S\|$  the  $\Delta t$  and  $Gap^* < \frac{gap^*(S)}{q}$ ,  $q > \dots$  implies each group of clusters together are of  $S = A(\cdot)$  consists of exactly  $\dots$  the eigenvalues of  $S$  thus as easy to construct an amplifier the case here a group of the clusters together are of  $A(t_i)$  the Group  $\dots$  m.t.p

**2.1 Properties of the Gap\***

suppose symmetric matrices  $A$  and  $S$  are given,  $Gap^* = \delta\|A - S\|$ ,  $\delta > \dots$  here  $\Delta t = \frac{\delta}{q}$ ,  $q > \dots$  we  $\|A(t_{i+1}) - A(t_i)\|_2 \leq \|A(t_{i+1}) - A(t_i)\|$  for a matrix norm  $\|\cdot\|$  here  $\|\cdot\|_2$  is the spectral matrix norm,  $\|A(t_{i+1}) - A(t_i)\|_2 \leq \Delta t\|A - S\|_2 = \frac{\delta}{q}\|A - S\|_2 \leq \frac{\delta}{q}\|A - S\| = \frac{Gap^*}{q}$ ,  $q \geq \dots$  we the equation holds for a matrix norm  $\|\cdot\|$ , we use the reverse matrix norm,  $\|\cdot\|_F$  to compute  $Gap^*$  the amplifier predicted section, we

$$\|A(t_{i+1}) - A(t_i)\|_2 < \frac{Gap^*}{q}$$

here  $Gap^* = \delta\|A - S\|_F$  for some  $\delta > \dots$

suppose the eigenvalues of  $A(t_i)$  are partitioned as groups of clusters together. eigenvalues  $\sigma(A(t_i)) = \cup_{k=1}^g G_k$ , here  $G_k = \{\lambda_{k_1}(i) \geq \dots \geq \lambda_{k_{s_k}}(i)\}$  is a group of clusters together eigenvalues of  $A(t_i)$ ,  $s_1 + \dots + s_g = n$ . we partition the eigenvalues of  $A(t_{i+1})$  of form  $\dots$  the groups respectively the group  $G = \sigma(A(t_i))$ ,  $\sigma(A(t_{i+1})) = \cup_{k=1}^g G'_k$ , here  $G'_k = \{\lambda_{k_1}(i + 1) \geq \dots \geq \lambda_{k_{s_k}}(i + 1)\}$ ,  $s_1 + \dots + s_g = n$ . we call  $G'_k$  the **counterpart** of  $G_k$ .

**Lemma 4.** *Suppose  $B, C \in M_n$  are symmetric matrices and let  $\lambda_1 \geq \dots \geq \lambda_n$  and  $\alpha_1 \geq \dots \geq \alpha_n$  be the eigenvalues of  $B$  and  $C$ , respectively. Then  $\|B - C\|_2 = \rho(B - C) \geq \max_k \{|\lambda_k - \alpha_k|\}$ , where  $\rho(B - C) = \max_k \{|\lambda_k(B - C)| / \lambda_k(B - C)\}$  are the eigenvalues of  $(B - C)$ . Consequently, if  $\|B - C\|_2 \leq \frac{Gap^*}{q}$ , for  $q > \dots$ , then  $|\lambda_k - \alpha_k| \leq \frac{Gap^*}{q}$  for all  $k = 1, \dots, n$ .*

from lemma 4 we have  $\max_k \{|\lambda_k(i + 1) - \lambda_k(i)|\} \leq \frac{Gap^*}{q}$  here  $\lambda_k(i + 1)$  and  $\lambda_k(i)$  are the eigenvalues of  $A(t_{i+1})$  and  $A(t_i)$ , respectively. herefore, the  $k$ th eigenvalue of  $A(t_{i+1})$  must be within  $\frac{Gap^*}{q}$  distance from the  $k$ th eigenvalue of  $A(t_i)$  for  $k = 1, \dots, n$ .

**Theorem 5.** *Let  $G \subseteq \sigma(A(t_i))$  be a group of clustering eigenvalues and  $G'$  be the counterpart in  $\sigma(A(t_{i+1}))$ . Then*

- (i)  $|\lambda_j(i) - \lambda_j(i+1)| \leq \frac{Gap^*}{q}$  for  $\lambda_j(i) \in G$  and  $\lambda_j(i+1) \in G'$ ,
- (ii)  $|\lambda_s(i) - \lambda_t(i+1)| \geq (\frac{-}{q})Gap^*$  for  $\lambda_s(i) \in G$  and  $\lambda_t(i+1) \notin G'$ ,
- (iii)  $|\lambda_s(i+1) - \lambda_t(i+1)| \geq (\frac{2}{q})Gap^*$  for  $\lambda_s(i+1) \in G'$  and  $\lambda_t(i+1) \notin G'$

**Implications of Theorem 5:** Suppose that the successive matrices  $A(t_i)$  and  $A(t_{i+1})$  are obtained by a group gap  $Gap^*$  in the process of the Group Homotopy. Then the statement (i) asserts that the  $j$ th eigenvalue of a group  $G' \subseteq \sigma(A(t_{i+1}))$  must be within  $\frac{Gap^*}{q}$  distance from the  $j$ th eigenvalue of  $G \subseteq \sigma(A(t_i))$  that is sufficient enough  $q > \dots$ , the eigenvalues can change by a small amount between the successive steps of the Group Homotopy method. Statement (ii) shows that there is a big enough gap between the eigenvalues of  $G$  and the eigenvalues that are not in the clusterpart  $G'$ . Thus we see that the eigenvalues of  $G$  are more kept together than the eigenvalues of  $G'$  under the iterative process. From the statement (iii) we see that for a large enough  $q > \dots$  there is a gap between all the  $G'$ 's in  $\sigma(A(t_{i+1}))$  that are clusterparts of groups in  $\sigma(A(t_i))$ . Thus a group of the clustered eigenvalues tends to remain as a group of the clustered eigenvalues during the Group Homotopy.

### 3 Group Homotopy Algorithm

We present the main result of the Group Homotopy with the parameterized iterative process. Let the following eigenvalues  $\sigma(A(t_i)) = \{\alpha_1, \dots, \alpha_n\}$ ,  $\alpha_n \leq \dots \leq \alpha_1$  and  $\sigma(A(t_{i+1})) = \{\lambda_1, \dots, \lambda_n\}$ ,  $\lambda_n \leq \dots \leq \lambda_1$  for the iterative process.

**A Parametrized Newton Iteration :** Suppose  $\begin{pmatrix} x \\ \alpha \end{pmatrix} \in \mathbb{R}^{n+1}$  is given and let  $A \in M_n$  be a symmetric matrix. Assume  $\alpha \notin \sigma(A)$ .

For  $l = 0, 1, \dots$ , define  $x^{(l+1)} = \frac{1}{\beta^{(l)}}(\alpha^{(l)}I - A)^{-1}x^{(l)}$ ,  $\alpha^{(l+1)} = \alpha^{(l)} - \frac{\beta^{(l)}}{\left(\frac{\beta^{(l)}}{\beta}\right)^2}$

where  $\beta^{(l)} = x^{(l)T}(\alpha^{(l)}I - A)^{-1}x^{(l)}$  and  $\hat{\beta}^{(l)} = \|(\alpha^{(l)}I - A)^{-1}x^{(l)}\|_2$ .

We describe the algorithms for simultaneous finding the eigenpairs of a  $n \times n$  real symmetric matrix  $A$ . This method is a good choice for  $\|S - A\|_F < gap^*(S)$ , where  $S$  is the target matrix.

#### 3.1 Parameterized Newton's Method with Orthogonalization

Let  $A = (a_{ij}) \in M_n$  be a given symmetric matrix. The eigenpairs  $\begin{pmatrix} u_k \\ \lambda_k \end{pmatrix}$  for  $k = 1, \dots, n$ . The following algorithm simultaneously computes  $\begin{pmatrix} u_k \\ \lambda_k \end{pmatrix}$ ,  $k = 1, \dots, n$ , using the parameterized iterative method. The orthogonalization...

Choose  $S = \text{diag}(\alpha_1^{(0)}, \dots, \alpha_n^{(0)})$  be the diagonal matrix where the diagonal elements of  $S$  are arranged in decreasing order. Let  $\epsilon > 0$  be the given tolerance.

**Step 1:** Let the data be given as  $\mathcal{D} = \left\{ \begin{pmatrix} x_k^{(0)} \\ \alpha_k^{(0)} \end{pmatrix} \right\}$  for  $k = 1, \dots, n$  where

$x_k^{(0)}$  is the  $k$ th column of the data matrix.

**Step 2:** For  $k = 1, \dots, n$  do (in parallel) ( ) Compute  $\|(\alpha_k^{(0)} I - A)x_k^{(0)}\|_2$  ( ) If  $\|(\alpha_k^{(0)} I - A)x_k^{(0)}\|_2 < \epsilon$ , then go to step 3. Otherwise go to step 2.

**Step 3: Parameterized Newton's Iteration:**

For  $k = 1, \dots, n$  do (in parallel)

(a) For  $i = 0, 1, \dots$  do until convergence

( ) Compute  $(\alpha_k^{(i)} I - A)y_k^{(i)} = x_k^{(i)}$ . ( ) Compute  $\beta_k^{(i)} = (x_k^{(i)})^T y_k^{(i)}$ .

( ) Compute  $\hat{\beta}_k^{(i)} = \|y_k^{(i)}\|_2$ . ( )  $x_k^{(i+1)} = \frac{x_k^{(i)}}{\hat{\beta}_k^{(i)}} y_k^{(i)}$ .

( ) Compute  $p_i = \frac{\beta_k^{(i)}}{\hat{\beta}_k^{(i)}}$ . ( ) If  $(-|p_i|) < \epsilon$  go to (b).

If  $|p_i| < \epsilon$  go to (c). ( ) Compute  $\alpha_k^{(i+1)} = \alpha_k^{(i)} - \frac{\alpha_k^{(i)}}{\hat{\beta}_k^{(i)}} p_i$ .

(b) Let  $\lambda_k = \alpha_k^{(i)} - \frac{\alpha_k^{(i)}}{\hat{\beta}_k^{(i)}}$ ,  $u_k = x_k^{(i+1)}$  (c) Let  $\lambda_k = \alpha_k^{(i)} - \frac{\alpha_k^{(i)}}{\hat{\beta}_k^{(i)}}$

and then compute the corresponding generalized eigenvectors  $u_k$  of  $A$ .

End

End

**Step 4:** Let  $m$  be the number of eigenpairs obtained from step 3 for  $m \leq n$ , the additional  $n - m$  eigenpairs have been obtained, go to step 5 if  $m < n$ , the  $(n - m)$  remaining eigenpairs as follows **4-(i)** Let  $\{G_k\}_{k=1, \dots, m}$  be the  $m$  groups of eigenpairs as defined below.

$$G_k = \left\{ \begin{pmatrix} x_{kj}^{(0)} \\ \alpha_{kj}^{(0)} \end{pmatrix} / \begin{pmatrix} x_{kj}^{(0)} \\ \alpha_{kj}^{(0)} \end{pmatrix} \text{ converges to } \begin{pmatrix} u_k \\ \lambda_k \end{pmatrix} \right\} \text{ for } j = 1, \dots, s_k$$

where  $s_1 + s_2 + \dots + s_m = n$  and  $s_k$  is the number of eigenpairs in a group  $G_k$ . Let  $p$  be the number of groups of  $G_k$  having the number of eigenpairs  $s_k > p$ . The go to step 4-(ii).

**4-(ii)** For each of the above  $p$  groups do the following steps (in parallel).

Compute  $\min_{1 \leq j \leq s_k} \|(\alpha_{kj}^{(0)} I - A)X_{kj}^{(0)}\|_2$ . discard the eigenpairs which achieves the minimum (note that there is one eigenpair in each group that achieves the minimum)

**4-(iii)** Orthogonalize the vectors in each of the above  $p$  groups (in parallel) let  $l = m$  for  $j = 1, \dots, (s_k - 1)$  do

Orthogonalize  $\{u_1, u_2, \dots, u_l, x_{kj}^{(0)}\} \rightarrow \{u_1, u_2, \dots, u_l, x_{kj}^{(0)}\}$  using the modified Gram Schmidt process

- (a) set  $g = \begin{pmatrix} x_{k_j}^{(0)} \\ \alpha_{k_j}^{(0)} \end{pmatrix}$ , then the parameter  $\begin{pmatrix} x_{k_j} \\ \alpha_{k_j} \end{pmatrix}$ .
- (b) set  $\begin{pmatrix} x_{k_j} \\ \alpha_{k_j} \end{pmatrix} \rightarrow \begin{pmatrix} u_{l+1} \\ \lambda_{l+1} \end{pmatrix}$  (c)  $l \leftarrow l + 1$  End
- 4-(iv)** set  $p' =$  number of distinct eigenvalues. bta. ed. 4( ) here  $p' \leq (n - m)$  set  $m \leftarrow m + p'$  if  $m < n$  go to 4( ) otherwise go to step 4( ) End

**Table 1.** ( $q = 4, n = 50$ )

eigenvalues of $A(t_i)$	$t_0$	$t_1$	$t_2$	$t_3$	$t_4$	Eigenvalues from MATLAB
0	0	0.25	0.5	0.75	1.0	
1st	150.00	457.8705	879.5562	1308.3704	1739.0537	1739.0537
⋮	⋮	⋮	⋮	⋮	⋮	⋮
20th	36.00	32.0262	32.6110	27.9100	23.4161	23.4161
⋮	⋮	⋮	⋮	⋮	⋮	⋮
40th	-87.00	94.4645	-96.4081	-104.6880	-112.8265	-112.8265
⋮	⋮	⋮	⋮	⋮	⋮	⋮
50th	-147.00	-164.1900	-215.4465	-285.9817	-363.2445	-363.2445
M		46	44	45	45	
B		4	6	5	5	
C(D)		8(6)	8(5)	10(4)	8(4)	

**3.2 The Group Homotopy Algorithm with Parameterized Newton’s Iteration**

Given a  $n \times n$  symmetric matrix  $A$ , the following algorithm simultaneously computes the eigenpairs  $\begin{pmatrix} u_k \\ \lambda_k \end{pmatrix}, k = 1, \dots, n$  of  $A$ , using the Group Homotopy method.

**Step 0:** set  $t_0 = 0$  set  $S = A(t_0) = \text{diag}(\alpha_1^{(0)}, \dots, \alpha_n^{(0)})$ , here  $\alpha_k^{(0)}, k = 1, \dots, n$  are arbitrary chosen real numbers and the corresponding eigenvalues are the columns of the dett matrix.

**Step 1:** Choose  $q \geq 4$  set  $\Delta t = \frac{-}{q}$

**Step 2:** for  $i = 1, \dots, q$  do ( ) Compute  $t_i = t_{i-1} + \Delta t$  ( ) if  $t_i \geq$  the set  $t_i$  ( ) pp. algorithm to bta. the eigenpairs of  $A(t_i)$   $A(t_{i-1}) + \Delta t(A - A(t_{i-1}))$  ( ) if  $t_i <$  go to step 2( ) otherwise stop End

**Numerical Results.** since  $\| \cdot \|_2 \leq \| \cdot \|_F$  here  $\| \cdot \|_F$  is the Frobenius matrix norm and  $\| \cdot \|_F$  is easy to compute, we use  $\| A - S \|_F$  to compute  $\Delta t_i$ . the following examples set the number of eigenpairs bta. ed. us. g the m. d. fixed e. t. terat. the number of eigenpairs recovered th m. d. fixed Gram Schmidt process us. g the m. d. fixed e. t. terat. C the maximum



number of iterations at each step and the maximum number of iterations needed for the  $r$ th globalization.

**Example 1:** Consider the matrix

$$A = (a_{ij}) \in M_n, a_{ij} = 1 \text{ if } i > j, a_{ij} = (-1)^i * i \text{ if } i = j, a_{ij} = j \text{ if } j > i.$$

Choose the tridiagonal matrix  $S$  such that  $A(\cdot) = S \cdot \text{diag}(a_{11}, a_{22}, \dots, a_{nn})$ .

$\|A - A(\cdot)\|_F = 77.2$ . The result of above uses  $q = 4$  in the results of numerical experiments below, it is clear that for  $q$  large the number of iterations at each step is significant (see last row of each table) and as the number of eigenpairs recovered using algorithm (step 4) is less (represented by  $B$ )

since  $\text{Gap}^* < \text{gap}^*(S)$ , we choose  $\Delta t$  to show that the choice of  $S$  is an important factor in the performance of the algorithm.

## 4 Conclusions

We have presented an efficient algorithm called the Grouped Homotopy Method for computing the eigenvalues and eigenvectors of a real symmetric matrix. The important features of this method are

- (1) Unlike the other methods for symmetric eigenvalue problem, the new method does not transform the tridiagonal matrix to a tridiagonal matrix, and thus substantially reduce the sparse problems.
- (2) The method takes advantage of the structure preserving algorithms such as shift-and-invert thus the method is expected to be much faster than the existing methods in most cases.
- (3) Unlike the other existing homotopy methods, the step size is predetermined at the outset according to a criterion presented in the paper and is determined at a certain duration of the execution of the algorithm.
- (4) The algorithm is parameter-free.

## References

1. M.T. Chu : On a Numerical Treatment for the Curve-Tracing Of the Homotopy Method. *Numerische Mathematik*, **42**.(1983) 323–329
2. M.T. Chu : A Simple Application of the Homotopy Method to Symmetric Eigenvalue Problems. *Linear Algebra Appl.*, **59**.(1985) 85–90
3. M.T. Chu : A Note on The Homotopy Method for Linear Algebraic Eigenvalue Problems. *Linear Algebra Appl.*, **108**.(1988) 225–236
4. Karabi Datta and Yoopyo Hong and Ran Baik Lee : An Application of Homotopy Method For Eigenvalue Problem of A Symmetric Matrix. *IMACS, Series in Computational and Applied Mathematics*, **3**.(1996) 367–376
5. Karabi Datta and Yoopyo Hong and Ran Baik Lee : Parameterized Newton's iteration for computing an Eigenpairs of a real Symmetric Matrix in an Interval, *Computational Methods in Applied Mathematics*, **3**.(2003) 517–535

6. Roger A. Horn and Charles R. Johnson: Matrix Analysis. Cambridge University Press, (1985)
7. K. Li and T.Y. Li: An Algorithm for Symmetric Tridiagonal Eigen Problems: Divide and Conquer with Homotopy Continuation. SIAM J. Sci. Comput., **14**.(1993) 735–751
8. Beresford N. Parlett: The Symmetric Eigenvalue Problem. Prentice-Hall, Inc.Englewood Cliffs,(1980)

# Numerical Simulation of Three-Dimensional Vertically Aligned Quantum Dot Array

Wen-Chung Chang<sup>1</sup> and Su-Gen Wang<sup>2</sup>

<sup>1</sup> Department of Applied Mathematics, National University of Kaohsiung, Kaohsiung 811, Taiwan

wwang@nuk.edu.tw

<sup>2</sup> Department of Mathematics, National Taiwan Normal University, Taipei 116, Taiwan

min@math.ntnu.edu.tw

**Abstract.** We study the electronic properties of quantum dot arrays formed by 2 to 12 vertically aligned quantum dots numerically. Numerical schemes in grid points choosing, finite differences, matrix reduction, and large-scale eigenvalue problem solver are discussed. The schemes allow us to compute all the desired energy states and the wave functions efficiently. Numerical experiment results are presented.

**Keywords:** Semiconductor quantum dot array, the Schrödinger equation, energy levels, wave function, numerical simulation.

## 1 Vertically Aligned Quantum Dot Array Model

Recent advances in fabrication technology of semiconductor quantum dot arrays (QDAs) have attracted the attention of researchers. The remarkable numerical calculation of the energy state spectrum and the corresponding wave functions of a system of basic physical interest and crucial for design of applications like photonic devices

may change for simulation of a three dimensional system of large scale eigenvalue problems for several different geometries that are of interest. In this paper, we study the disk shaped cylindrical QDAs vertically aligned and embedded in a cylindrical GaAs matrix (see left part of figure), where the efficient numerical schemes overcome the difficulties

in the simulation of the Schrödinger equation for the cylindrical coordinate system, as

$$\frac{-\hbar^2}{2m_\ell(\lambda)} \left[ \frac{\partial^2 F}{\partial r^2} + \frac{1}{r} \frac{\partial F}{\partial r} + \frac{\partial^2 F}{r^2 \partial \theta^2} + \frac{\partial^2 F}{\partial z^2} \right] + c_\ell F = \lambda F, \quad (1)$$

where  $\hbar$  is the reduced Planck constant,  $\lambda$  is the total energy,  $F(r, \theta, z)$  is the wave function,  $m_\ell(\lambda)$  and  $c_\ell$  are the effective electron mass and confinement potential in the  $\ell$ th region. Here the index  $\ell$  is used to distinguish the

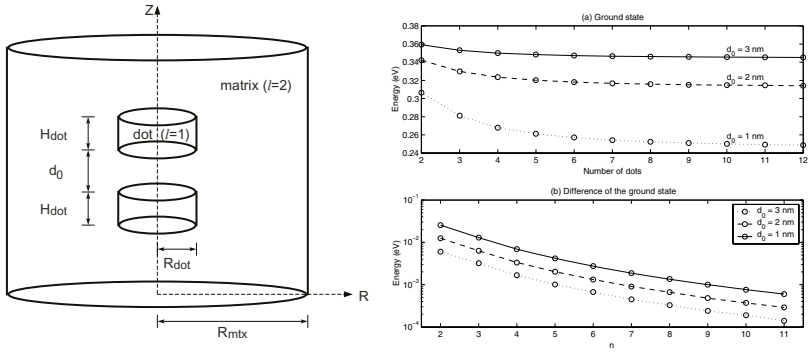


**Fig. 1.** Left part: Structure schema of a cylindrical vertically aligned quantum dot array and the heterostructure matrix. Right part: Ground state energies for various spacer layer distances  $d_0$  and number of quantum dots

reg. . . f the s ( f r l ) fr m that f the matr ( f r l 2) he . . .  
 parabol. ce ect. e mass appr. mat. . . s g. e. as

$$\frac{P_\ell^2}{m_\ell(\lambda)} \left( \frac{2}{\lambda + g_\ell - c_\ell} + \frac{1}{\lambda + g_\ell - c_\ell + \delta_\ell} \right), \quad (2)$$

here  $P_\ell$ ,  $g_\ell$ , and  $\delta_\ell$  are the momentum, mass energy gap, and spin orbit splitting of the  $\ell$ th region, respectively. In Eq. (2), the electron effective mass and the conduction band effective mass are respectively the effective mass of the top and bottom materials.

$$\frac{\hbar^2}{2m_1(\lambda)} \frac{\partial F(r_I, \theta_I, z_I)}{\partial n_-} = \frac{\hbar^2}{2m_2(\lambda)} \frac{\partial F(r_I, \theta_I, z_I)}{\partial n_+} \quad (3)$$

here  $(r_I, \theta_I, z_I)$  denotes the position of the interface and the  $n_+$  and  $n_-$  denote the conduction and valence band densities, respectively. The boundary conditions at the interface are given by the continuity of the wave function and its derivative. The boundary conditions are prescribed by the boundary conditions (top, bottom, and side) of the matrix.

## 2 Numerical Schemes

In this section, we discuss the numerical schemes used for solving the three-dimensional Schrödinger equation (1) to compute the electronic energy levels and the associated wave functions of the system.

We first discretize the domain by choosing a regular uniform mesh. The mesh points are chosen in the azimuthal angle  $\theta$  coordinate. Uniform mesh points are used in the radial coordinate  $r$  and the axial coordinate  $z$ . The finite difference spectral methods first, the heterostructure area, fine meshes are used to capture the rapid change of the wave functions. Second, a half of the mesh is shifted in the radial coordinate to avoid coupling the periodicity.

ased on the gradient plots, Eq ( ) is discretized by the centered second-order finite difference method

$$\frac{-\hbar^2}{2m_\ell(\lambda)} \left( \frac{F_{i+1,j,k} - 2F_{i,j,k} + F_{i-1,j,k}}{(\Delta r)^2} + \frac{1}{r_i} \frac{F_{i+1,j,k} - F_{i-1,j,k}}{2\Delta r} \right) + \frac{1}{r_i^2} \frac{F_{i,j+1,k} - 2F_{i,j,k} + F_{i,j-1,k}}{(\Delta\theta)^2} + \frac{F_{i,j,k+1} - 2F_{i,j,k} + F_{i,j,k-1}}{(\Delta z)^2} + c_\ell F_{i,j,k} - \lambda F_{i,j,k},$$

here  $F_{i,j,k}$  is the approximated wave function  $F$  at the grid points  $(r_i, \theta_j, z_k)$  for  $i = 1, 2, \dots, \rho$ ,  $j = 1, \dots, \mu$ , and  $k = 1, \dots, \zeta$ . The heterostructure top potential difference are applied on the interface and the surface heterostructure barrier wave functions for the matrix and the  $z$  and  $r$  directions are zero according to the Schrodinger equation.

Assembling the finite difference discretization results as a  $\rho\mu\zeta$  by  $\rho\mu\zeta$  eigenvalue problem, reordering the unknown vectors using the fast Fourier transform, the transfer matrices  $T_k(\lambda)$  (for  $k = 1, \dots, \zeta$ ) are obtained.  $\mu$  independent  $\rho\zeta$  by  $\rho\zeta$  eigenvalue problems with the form

$$\tilde{T}_j(\lambda)\tilde{F}_j - \tilde{D}_j(\lambda)\tilde{F}_j, \tag{4}$$

for  $j = 1, \dots, \mu$ , here  $\tilde{T}_j(\lambda)$  and  $\tilde{D}_j(\lambda)$  are  $\rho\zeta$  by  $\rho\zeta$  matrices. Each of the eigenvalue problems with the form of (4) is called a 2D eigenvalue problem, since the gradient plots of the unknowns  $\tilde{F}_j$  have the same  $\theta$  value, multiplying the commutative matrix of (4) to each of the form the cubic  $\lambda$  matrix problem as

$$\mathbf{A}(\lambda)\mathbf{F} = (\lambda^3 A_3 + \lambda^2 A_2 + \lambda A_1 + A_0)\mathbf{F}, \tag{5}$$

here  $A_0, A_1, A_2$ , and  $A_3$  are independent  $\lambda$  cubic eigenvalue problem, can be solved efficiently by ( ) the cubic characteristic method to compute the smallest positive eigenvalue representing the ground state energy, and ( ) the perturbation scheme to estimate the successive smallest positive eigenvalues (i.e. the excited energy states) see 4, for details.

### 3 Results and Discussions

Our numerical parameters, we assume that  $H_{dot}$  and  $R_{dot}$  of the wells are 7.5 nm, respectively, for the matrix,  $R_{mtx}$  7.5 nm and 10 nm matrix barrier are assumed above the top and bottom of the well. The material parameters used in the parameters are  $c_1 = 0.15$ ,  $g_1 = 0.42$ ,  $\delta_1 = 0.48$ ,  $P_1 = 0.77$ ,  $c_2 = 0.77$ ,  $g_2 = 0.2$ ,  $\delta_2 = 0.4$ , and  $P_2 = 0.87$  numerical constants. The figures are summarized as follows.

The ground state energy of the wells are affected by the number of wells and the spacer barrier distance  $d_0$ . Right top of figure (a) shows the computed ground state energies versus the number of wells. It is clear that more wells, the results of the ground state energy for a fixed  $d_0$  further more, for a fixed number of wells, smaller spacer barrier distances lead to the ground state energies. Right bottom part of figure (a) shows the difference between the

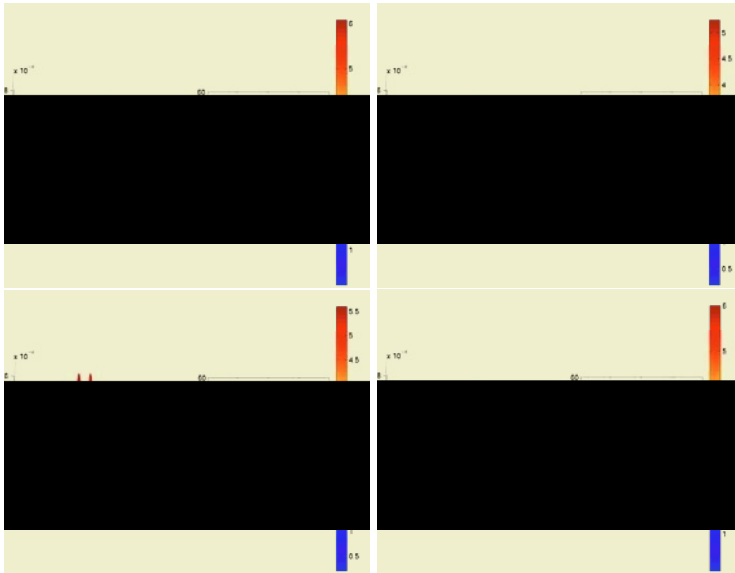


**Fig. 2.** Wave functions corresponding to the ground state energy. The quantum dot array contains six quantum dots and  $d_0 = 0, 0.5, 2, 6$  nm, respectively

of the energies for the  $n$  s.c.  $n$  and  $n + 1$  s.f.  $n, \dots$ , for various  $d_0 = 0, 2, \dots$  nm, the ground state energies decrease exponentially. As a similar matter, to be specific, the energy differences can be well fitted by the linear least squares method. The shape in Figure 2 demonstrates a excellent correlation. In fact, the ground state energy for the formed by six quantum dots and  $d_0 = 0, 0.5, 2, \dots$  nm, the results suggest that the energy differences change as the  $d_0$  is decreased.

## References

1. O. Voskoboynikov, C. P. Lee, and O. Tretyak. Spin-orbit splitting in semiconductor quantum dots with a parabolic confinement potential. *Phys. Rev. B*, 63:165306, 2001.
2. D. J. BenDaniel and C. B. Duke. Space-charge effects on electron tunnelling. *Phys. Rev.*, 152(683), 1966.
3. M.-C. Lai. A note on finite difference discretizations for Poisson equation on a disk. *Numer. Methods Partial Differ. Equ.*, 17(3):199–203, 2001.
4. W. Wang and T.-M. Hwang and W.-W. Lin and J.-L. Liu. Numerical Methods for Semiconductor Heterostructures with Band Nonparabolicity *Journal of Computational Physics*, 190(1):141–158, 2003.
5. T.-M. Hwang, W.-W. Lin, J.-L. Liu, and W. Wang. Jacobi–davidson methods for cubic eigenvalue problems. *Numerical Linear Algebra with Applications* To appear.

# Semi-systolic Architecture for Modular Multiplication over $GF(2^m)$

Hyun-Sung Kim<sup>1</sup> and Il-Soo Jeon<sup>2</sup>

<sup>1</sup> Kyungil University, School of Computer Engineering,  
712-701, Kyungsansi, Kyungpook Province, Korea

<sup>2</sup> Kumho Nat'l Inst. of Tech., School of Electronic Eng.,  
730-703, Gumi, Kyungpook Province, Korea

**Abstract.** This paper proposes a new algorithm and an architecture for it to compute the modular multiplication over  $GF(2^m)$ . They are based on the standard basis representation and use the property of irreducible all one polynomial as a modulus. The architecture, named SSM(Semi-Systolic Multiplier) has the critical path with  $1-D_{AND}+1-D_{XOR}$  per cell and the latency of  $m+1$ . It has a lower latency and a smaller hardware complexity than previous architectures. Since the proposed architecture has regularity, modularity and concurrency, they are suitable for VLSI implementation.

## 1 Introduction

The arithmetic operations in the finite field have several applications in error-correcting codes, cryptography, digital signal processing, and so on [1]. Information processing in such areas usually requires performing multiplication, inverse/division, and exponentiation. Among these operations, the modular multiplication is known as the basic operation for public key cryptosystems over  $GF(2^m)$  [2-3].

Numerous architectures for modular multiplication in  $GF(2^m)$  have been proposed in [2-8] over the standard basis. Wang et al. in [5] proposed two systolic architectures with the MSB-first fashion with less control problems as compared to [4]. Jain et al. proposed semi-systolic multipliers [6]. Its latency is smaller than those of the other standard-basis multipliers. Kim in [7] proposed a bit-level systolic array with a simple hardware complexity with the LSB-first modular multiplication. Thus, further research for efficient circuit for cryptographic applications is needed. To reduced the system complexity, Itoh and Tsujii designed two low-complexity multipliers for the class of  $GF(2^m)$ , based on the irreducible AOP (All One Polynomial) and the irreducible equally spaced polynomial [8]. Later, Kim in [2] proposed various AOP architectures based on LFSR(Linear Feedback Shift Register) architecture.

This paper proposes a new algorithm and a parallel-in parallel-out semi-systolic array architecture to compute the modular multiplication over finite field  $GF(2^m)$ . They are based on the standard basis representation and use the property of irreducible AOP as a modulus. Let  $D_{AND}$  and  $D_{XOR}$  be the latency of AND and XOR gate, respectively. The architecture has the critical path with  $1-D_{AND}+1-D_{XOR}$  per cell and the latency of  $m+1$ . It could be used to secure cryptosystem application.

## 2 Semi-systolic Architecture

GF(2<sup>m</sup>) is the finite extension field of finite field GF(2) [2]. An arbitrary element A over GF(2<sup>m</sup>) can be represented with {1, α, α<sup>2</sup>, ..., α<sup>m-1</sup>}, which is based on the standard basis, i.e.,  $A=A_{m-1}\alpha^{m-1}+A_{m-2}\alpha^{m-2}+\dots+A_1\alpha+A_0$ . A polynomial of the form  $f(x)=f_m x^m+f_{m-1}x^{m-1}+\dots+f_1 x+f_0$  is called an irreducible polynomial if and only if a divisor of f(x) is 1 or f(x). Assume that a polynomial of the form  $f(x)=f_m x^m+f_{m-1}x^{m-1}+\dots+f_1 x+f_0$  over GF(2) is called an AOP (All One Polynomial) with degree m if  $f_i=1$  for  $i=0,1, \dots, m$ . It has been shown that an AOP is irreducible if and only if m+1 is the prime and 2 is the primitive modulo m+1. Let a set {1, α, α<sup>2</sup>, ..., α<sup>m-1</sup>} be generated by α which is a root of AOP f(x) and be the standard basis. In the standard basis, an element A over GF(2<sup>m</sup>) is presented by  $A=A_{m-1}\alpha^{m-1}+A_{m-2}\alpha^{m-2}+\dots+A_1\alpha+A_0$ . A set with {1, α, α<sup>2</sup>, ..., α<sup>m-1</sup>, α<sup>m</sup>} is called an extended basis of {1, α, α<sup>2</sup>, ..., α<sup>m-1</sup>}. In the extended basis, an element a over GF(2<sup>m</sup>) is represented by  $a=a_m\alpha^m+a_{m-1}\alpha^{m-1}+\dots+a_1\alpha+a_0$  with  $A_i=a_m+a_i$  ( $0 \leq i \leq m-1$ ). Thus, an element over GF(2<sup>m</sup>) has two different representations. Let  $F(x)=x^m+x^{m-1}+\dots+x+1$  be an irreducible AOP of degree m: and let α be a root of F(x). i.e.,  $F(\alpha)=\alpha^m+\alpha^{m-1}+\dots+\alpha+1$ . Then, we have  $\alpha^m=\alpha^{m-1}+\dots+\alpha+1$ ,  $\alpha^{m+1}=1$ .

The multiplication of elements a and b over GF(2<sup>4</sup>) in the extended basis can be performed by  $ab \bmod p$  with  $p=\alpha^{m+1}+1$  which applied the property of AOP as a modulus. Let the result of this multiplication,  $ab \bmod p$ , be  $r=r_m\alpha^m+r_{m-1}\alpha^{m-1}+\dots+r_1\alpha+r_0$ . The recurrence equation for the MSB first algorithm with the property of AOP is as follows:  $r = ab \bmod p = \{\dots[[ab_m]\alpha \bmod p+ab_{m-1}]\alpha \bmod p+\dots+ab_1\} \alpha \bmod p+ab_0$ . From the equation, a new algorithm to compute  $ab \bmod p$  can be derived as following Algorithm 1.

### [Algorithm 1] Modular Multiplication

**Input** :  $a=(a_m,a_{m-1},\dots,a_1,a_0)$ ,  $b=(b_m,b_{m-1},\dots,b_1,b_0)$

**Output** :  $r=ab \bmod p$

**Initial value** :  $r^{m+1}=(r_m,r_{m-1}, \dots,r_1,r_0)=(0,0, \dots,0,0)$

Step 1 for  $i=m$  to 0

Step 2  $r^j=Circular\_Left(r^{j+1})+ab_i$

where  $Circular\_Left(x)$  is the 1-bit-left-circular shift of x and  $r^j$  is used to represent the i-th intermediate result for the final result r. In the above algorithm, the modular reduction is performed just by using 1-bit-left-circular-shift operation. Specially, all the operations in the for loop can be performed bit by bit in parallel.

Let a, b, and b<sup>2</sup> be an elements in GF(2<sup>4</sup>). Then a and b with an extended basis {1, α, α<sup>2</sup>, α<sup>3</sup>, α<sup>4</sup>} can be represented as follows:  $a=a_4\alpha^4+a_3\alpha^3+a_2\alpha^2+a_1\alpha+a_0$ ,  $b=b_4\alpha^4+b_3\alpha^3+b_2\alpha^2+b_1\alpha+b_0$ .

When  $p=\alpha^5+1$  is used as a modular in the extended basis, we have

$$\begin{aligned} r &= ab \bmod p \\ &= a(b_4\alpha^4+b_3\alpha^3+b_2\alpha^2+b_1\alpha+b_0) \bmod p \\ &= \{\dots[[ab_4]\alpha \bmod p+ab_3]\alpha \bmod p+\dots+ab_1\} \alpha \bmod p+ab_0 \\ &= r_4\alpha^4+r_3\alpha^3+r_2\alpha^2+r_1\alpha+r_0. \end{aligned}$$



Fig.1 shows a multiplier named SSM based on Algorithm 1 over  $GF(2^4)$ . SSM is composed of  $(m+1)(m+1)$  basic cells. It is the parallel architecture which  $a_i$  and  $b_i$  ( $0 \leq i \leq m$ ) are inputted at the same time. The  $(m+1)$ -bits of data  $a$  are inputted from the top row and transmitted to the adjacent cells following each row. But the data  $b_i$  in each row is broadcasted to all cells in the same row at the same time. Let  $D_{AND}$  and  $D_{XOR}$  be the latency of AND and XOR gate, respectively. SSM has a critical path with  $1-D_{AND}+1-D_{XOR}$  per cell. SSM in Fig. 1 can be generalized for arbitrary  $m$  as well as  $m=4$ . Fig. 2 shows the basic cells for SSM.

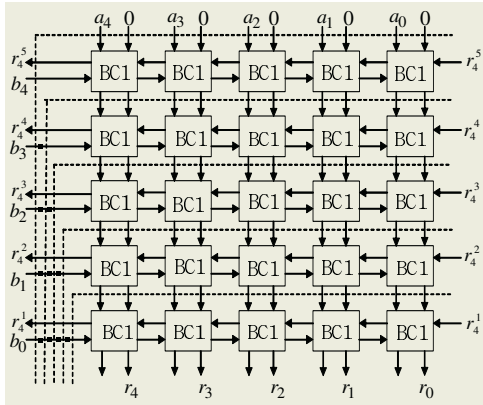


Fig. 1. SSM over  $GF(2^4)$

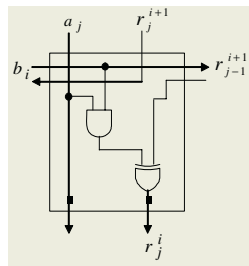


Fig. 2. Basic cell of SSM

### 3 Comparison and Analysis

Table 1 shows the comparison between the proposed architecture and previous two architectures.

**Table 1.** Comparisons

Properties	Jain [6]	Kim [2]	SSM
Basic architecture	Semi-systolic	LFSSR	Semi-systolic
Irreducible polynomial	Generalized	AOP	AOP
Number of cell	$m^2$	$m+1$	$(m+1)^2$
Cell complexity	2 AND, 2 XOR 3 latches	1 AND, 1 XOR 2 REG, 1 MUX	1 AND, 1 XOR 2 latches
Latency	$m$	$2m+1$	$m+1$
Critical path	$1-D_{AND}$ $+1-D_{XOR}$	$1-D_{AND+}$ $\log m(1-D_{XOR})$	$1-D_{AND}$ $+1-D_{XOR}$

It is assumed that AND and XOR represent 2-input AND and XOR gates, respectively, and latch for 1-bit latch. Let  $D_{AND}$  and  $D_{XOR}$  be the latency of AND and XOR gate, respectively. As a result, the proposed architecture, SSM, has lower latency and smaller complexity than previous architectures in [6] and [2].

## 4 Conclusions

This paper proposed a new algorithm and a parallel-in parallel-out semi-systolic array architecture to compute the modular multiplication over finite field  $GF(2^m)$ . The property of irreducible AOP was used as a modulus to get a better hardware and time complexity. Proposed architecture has lower latency and smaller hardware complexity than previous architectures as shown in Table 1. Since SSM has regularity, modularity and concurrency, they are suitable for VLSI implementation.

## References

- [1] D.E.R.Denning, *Cryptography and data security*, Addison-Wesley, MA, 1983.
- [2] H.S.Kim, *Bit-Serial AOP Arithmetic Architecture for Modular Exponentiation*, PhD. Thesis, Kyungpook National University, 2002.
- [3] S.W.Wei, "VLSI architectures for computing exponentiations, multiplicative inverses, and divisions in  $GF(2^m)$ ," *IEEE Trans. Circuits and Systems*, 44, 1997, pp.847-855.
- [4] C.S.Yeh, S.Reed, and T.K.Truong, "Systolic multipliers for finite fields  $GF(2^m)$ ," *IEEE Trans. Comput.*, vol.C-33, Apr. 1984, pp.357-360.
- [5] C.L.Wang and J.L.Lin, "Systolic Array Implementation of Multipliers for Finite Fields  $GF(2^m)$ ," *IEEE Trans. Circuits and Systems*, vol.38, July 1991, pp796-800.
- [6] S. K. Jain and L. Song, "Efficient Semisystolic Architectures for finite field Arithmetic," *IEEE Trans. on VLSI Systems*, vol. 6, no. 1, Mar. 1998.
- [7] H.S.Kim, "Efficient Systolic Architecture for Modular Multiplication over  $GF(2^m)$ ," will be appeared in *PARA 2004 proceeding*, 2005.
- [8] T. Itoh and S. Tsujii, "Structure of parallel multipliers for a class of finite fields  $GF(2^m)$ ," *Info. Comp.*, vol. 83, pp.21-40, 1989.
- [9] S.Y.Kung, *VLSI Array Processors*, Prentice-Hall, 1987.

# Meta Services: Abstract a Workflow in Computational Grid Environments

Jaeguk Lee and Jaehyung Choi

School of Computing, Soongsil University,  
1-1 Sangdo-dong, Dongjak-gu, Seoul 156-743, Korea  
sglee@ss.ssu.ac.kr  
choi@ssu.ac.kr

**Abstract.** We define a concept of Meta services which describes a way of abstracting and mapping a workflow to a service in computational Grid environments. By using Meta services, a workflow in a Grid environment could adapt various service concepts such as Grid services, Web services, and portal services without modification to the workflow. And the converted Meta services could be shared and reused by users. Furthermore, historical performance data could be included in the Meta service, making effective execution of the workflow possible.

## 1 Introduction

Grid computing is a distributed computing infrastructure which supports the sharing of large scale resources that are geographically distributed. Grid systems provide higher performance and a wider range of resource sharing than traditional distributed systems and the associated application functions. It is a technology for research and development of a Grid environment. It is being studied

Grid 2 is a resource management system which uses agent based resource management and a resource scheduling system. It takes into account the scheduling of time critical grid applications as a cross domain and global domain grid environment. Using a fuzzy logic technique and performance prediction, Grid provides intelligent based services such as resource discovery, resource activation, and distributed query processing. Integrated tasks and modules are research support, background, environment. Grids are the Grid abstract 4 is a description of application tasks and modules are services for Grid environments. Services provided by Grid abstract include resource brokering, data management, and adaptive services. Grid computing provides a resource management system for computing. It is a scheduling of dependent tasks using Ganga as a resource mapping and a management system that can map abstract application specific resource to a executable form for

Ganga (agent scheduling framework) provides a graph based resource management service and a resource management service for computing. A Grid environment performance feedback structure for Grid portals that (agent scheduling framework) provides a definition of a concept of services to integrate the

work described in C... (... b C... tr... arkup a guage) t... the p... rta... th... ut m... d ficat... of the... rk... the C... s a... rk... descr pt... a... guage used... e a... s... f... u... d that shar... g... rk... s s... esse... t a... f... r the Gr d p... rta... users... ecause m... st part cu ar Gr d p... rta... s are des g... ed t... supp... rt specific sc e... tific research, shar... g... rk... s am... g the Gr d users s a... er usefu... feature... th... s paper, e... prese... t... eta... ser... ces... rder t... map e... st... g Gr d... rk... s t... eta... ser... ces... th... ut m... d ficat... of descr pt... of the... rk... s... s... d the... eta... ser... ces p... r... de... ser... ce spec... fic... f... rmat... that a... s the shar... g... f... rk... s am... g users a... d res... urce... f... rmat... f... re... ect... e schedu... g... f Gr d res... urces... d h... st... r... ca... perf... rma... ce data... s requ... red f... re... ect... e schedu... g... f Gr d res... urces... e... er... a... p... r... r... research d... es... t... p... r... de such fu... ct... a... tes Other Gr d research such as m... th... s... rk... 8... egasus, a... d Gr d... sh... s that h... st... r... ca... perf... rma... ce data ca... be used f... re... ect... e schedu... g... f Gr d res... urces... heref... re... e... de... fi... e... a... c... cept... f... eta... ser... ces t... meet these requ... reme... ts

## 2 Meta Services

eta ser... ces map a... e... st... g Gr d... rk... t... a ser... ce b... e... r... r... d... g... at... tr... butes... f the Gr d... rk... s... t... f... rk... s are descr... bed b... r the ca... be c... o... r... t... e... d... d... c... u... m... e... ts... d... eta... ser... ces descr... be... h... t... e... r... r... de attr... butes... d... c... u... m... e... ts... th... ser... ce param... eter a... d ser... ce spec... fic... f... rmat... the mapp... g... s sh... g... u... re

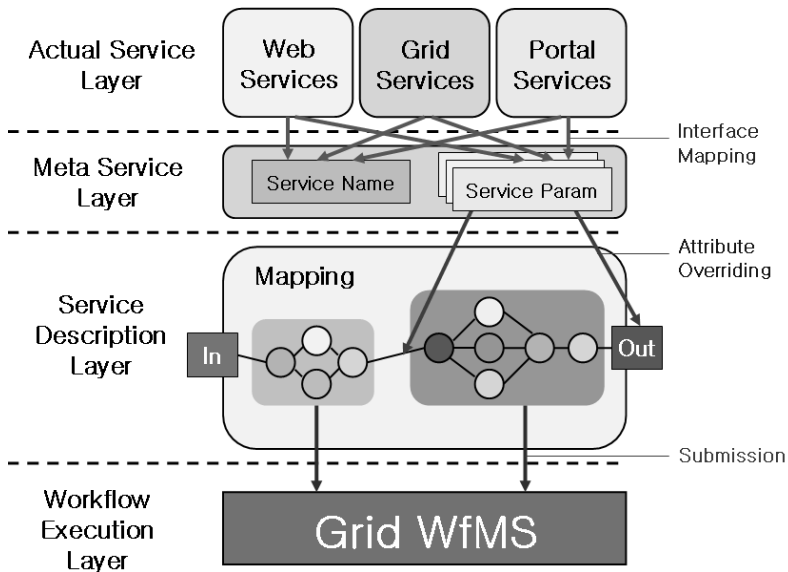


Fig. 1. Meta Services: Mapping workflows to services

Because a meta service is accessed by its name and parameters, the interface of the meta service is easily mapped to the corresponding generic service. Grid service, which contains several parameters, then the expected performance is easily mapped to a meta service. The meta service, CG, has a meta service called, the service name is used as a identifier of the service, the service parameters are derived attributes of the service, the service and the service description includes the service configuration by the service description of a meta service contains the following:

- service description
  - execution of service units
  - service configuration of the service units
- format of shared resources
  - user's permission
- Resource format of resource scheduling
  - Resource restriction
  - structural performance data

The declaration of service units in meta services includes a service name which a user wants to use, and declares them as service units. The units are linked to each other, and the executed through a practical. If the declaration is an extreme case, a meta service may include a service. The meta services are called, attributes of the services are derived. The service parameters are defined by the user. The execution of the services, statistics of the services are generated. The parameters by derived attributes of the services because services are generated by calling the corresponding services. The parameters, users could easily generate and reuse services.

Practical performance services to users, and the users may define frequently used services as meta services. The practical purpose, meta services might be declared as public, other users might be permitted to use them. As a result, permitted users could read and execute the configuration of meta services, but the restrictions are generated. The users' representation here, if a user wants to modify the service, he could modify through the service and a user may attend to the execution of the service. The fault resources of structural performance data is collected and recorded. The meta services, a scheduler could save the time required to find appropriate resources. The service management statistics of ER (management of resources) and R (management of resources) refer, though the same services are executed. Several resources with the same performance specification, it may be difficult to expect the same performance. Grid environments and after a user has executed the same meta service many times, he may find that the service is executed effectively. Specific resources are executed successfully. Other resources that services, meta services are designed so that the users may execute services. The preferred resources by using resource preference format.

### 3 Conclusion

In this paper, we presented a concept of meta services. The concept of meta services is combined with the system order to provide reusable and adaptable workflow management environments for the combined system. We can browse, search, and call the meta services with the same parameters. If a service meta services mapped to the corresponding Grid workflow, and successfully executed.

The aim of this paper is to introduce a concept of meta services which enables the following meta services are provided to various service environments such as Grid services, web services, and portable services. Meta services could provide user's permission information to share workflow among portable users. Meta services also provide a resource profile information, which could be used for efficient scheduling of resources. We applied the concept of meta services to extend our previous workflow, but the concept can be applied to other fields. In the near future, we will integrate heterogeneous Grid workflows with meta services.

### Acknowledgement

This work was supported by Korea Research Foundation under contract R2004-0400000000-72.

### References

1. I. Foster and C. Kesselman, ed., *The Grid: Blueprint for a New Computing Infrastructure*, Morgan Kaufmann, (1998)
2. J. Cao, S. A. Jarvis, S. Saini and G. R. Nudd, *GridFlow: Workflow Management for Grid Computing*, 3rd International Symposium on Cluster Computing and the Grid, (2003) 12-15
3. R. Stevens, A. Robinson and C. Goble, *myGrid: Personalized bioinformatics on the information grid*, *Bioinformatics*, 19(1), (2003) 302-304
4. G. Allen et al., *Enabling applications on the Grid - a GridLab overview*. *Intl. Journal on High Performance Computing Applications*, 17(4), (2003) 449-466
5. M. Litzkow, M. Livny and M. Mutka, *Condor - A Hunter of Idle Workstations*, 8th International Conference of Distributed Computing Systems, (1998) 13-17
6. Y. Gil, C. Kesselman, G. Mehta, S. Patil, M. Su, K. Cahi, M. Livny, *Pegasus Mapping Scientific Workflows onto the Grid*. E. Deelman, J. Blythe, *Across Grids Conference* (2004)
7. Seogchan Hwang, Jaeyoung Choi: *MSF: A Workflow Service Infrastructure for Computational Grid Environments*, LNCS 3292, 445-448 (2004)
8. W. Smith, I. Foster, V. Taylor, *Predicting Application Run Times Using Historical Information*, Proc. IPPS/SPDP '98 Workshop on Job Scheduling Strategies for Parallel Processing (1998)

# CEGA: A Workflow PSE for Computational Applications<sup>1</sup>

Yoonhee Kim

Dept. of Computer Science, Sookmyung Women's University, Korea  
yulan@sookmyung.ac.kr

**Abstract.** The importance of problem solving environment (PSE)s over Grid has been emphasized owing to the heterogeneity and the large volume of resources involved and the complexity of computational applications. This paper proposes a Grid-enabled PSE called as Computing Environment for Grid Applications (CEGA) and discusses how it is evolving to develop a computational application in a style of workflow model and incorporates Grid computing services to extend its range of services and handle information for development, deployment, execution and maintenance for an application as well as an application requirement itself. The paper describes the architecture of CEGA and its implementation for development, execution and visualization of an application.

## 1 Introduction

The concept of Grid computing has been investigated and developed to enlarge the concept of distributed computing environment to create infrastructure that enables integrated services for resource scheduling, data delivery, authentication, delegation, information service, management and other related issues [1]. As the Grid provides integrated infrastructure for solving problems, interfacing services such as web portal to access Grid services, PSEs (Problem Solving Environments) have been developed to improve the collaboration among Grid services and reduce significantly the time and effort required to develop, run, and experiment with large scale Grid applications.

However, most PSEs to support parallel and distributed computing focus on providing environments for successful execution of applications and providing reasonable resource scheduling schemes. There have been several application-specific tools and PSEs to utilize Grid environment efficiently. ASC Grid Portal [2] is a PSE for large-scale simulation in astrophysics. Hotpage [3] is another PSE targeted toward high performance computing applications. Cactus [4] provides a problem solving environment for developing large-scale distributed scientific applications. GrADS [5] is a toolkit to help users to build applications over heterogeneous resources with ease of use. Similarly, UNICORE [6] provides graphical user interface to access heterogeneous resources uniformly. However, an effort on generalizing a PSE to support development and execution of applications (i.e. applications in workflow management), has been not fully investigated.

---

<sup>1</sup> This Research was supported by the Sookmyung Women's University Research Grants 2003.

A Computing Environment for a Grid Application (CEGA) has been developed to provide a computing environment for a computational application in a workflow model. The CEGA provides an efficient Graphical User Interface (GUI) approach for developing, running, evaluating and visualizing large-scale parallel and distributed applications that utilize computing resources connected by local and/or wide area network. To support Grid services through CEGA, the server creates application configuration using Resource Specification Language (RSL), which runs over the Globus toolkit [7].

The organization of the remaining sections of the paper is as follows. I present an overview of the CEGA architecture in Section 2. In Section 3 I describe the major functionality in workflow editor for development and visualization in detail. The conclusion is followed in Section 5.

## **2 The Architecture of CEGA**

The CEGA is a workflow based problem solving environment for grid computational applications. It provides transparent computing and communication services for large scale parallel and distributed applications. The architecture of CEGA consists of CEGA portal services, CEGA system serves and Globus (see Fig.1) Globus is the Grid middleware toolkit to launch jobs and collects their results over Grid resources. CEGA Portal Service help users to generate a workflow of an application, based on the application logic, specify the input/output and runtime requirements to provide various execution environments without having big efforts for changing their experiment options. In addition, the status of job executions is reported back to a user using visualization tools, which are attached to the editor. To interface between the Portal and Globus, System Services collect and handle data from the Editor and Globus services, steer the workflow over Globus. In addition, it monitors the status of job execution. That is, CEGA provides two important services over Grid services: 1) Problem Solving Environment: to assist in the development of large scale parallel and distributed applications; and 2) Evaluation Tool: to analyze the performance of parallel and distributed applications under different resource environments.

## **3 CEGA Services**

### **3.1 CEGA Editing Service**

Graphical user interface helps users to develop, modify and execute an application easily over Grid resources. CEGA editor provides workflow patterns which includes various job patterns and linkages. User can use customized workflow patterns which a user can directly modify on; as well as built-in patterns. As Object List Tree is added in the left side of the window, new object is easily added to the graph with just drag & drop scheme. For editing service, open, save, new, execute and monitor interface is developed on the top menu. Once an application is developed within the editor, the information is passed to the Workflow Engine for workflow management to proceed application execution.



### 3.2 CEGA Execution Service

An application is defined as a set of jobs; which are connected to one another based on their job dependency. The execution of jobs can be executed either in parallel or sequence based on the dependency. When Job Control service collects application workflow information from the editor, it controls the order of execution of the jobs based on the dependency over Grid environment as the results of analysis of the workflow information. The service generates a set of activities in Resource Specification language (RSL), one of which can run over Globus in parallel. The deployment of the data in appropriate locations among the execution of activities is done by the control of the service based on the workflow. The system service checks the job dependency on the graph and divides multiple phases, which means making execution groups of jobs in parallel. Each group is mapped to grid resources by means of job scheduling service in Globus. Beside of job steering, it provides cooperative administration for dynamic Globus environment such as administrating Grid nodes and coordinating other Grid services, GRAM, MDS, and FTP as examples. The monitoring service also provides runtime monitoring and collects runtime log data in XML including starting and ending time, and total execution time. Whenever a user wants to monitor the runtime data, the Engine provides them to a visualization tool.

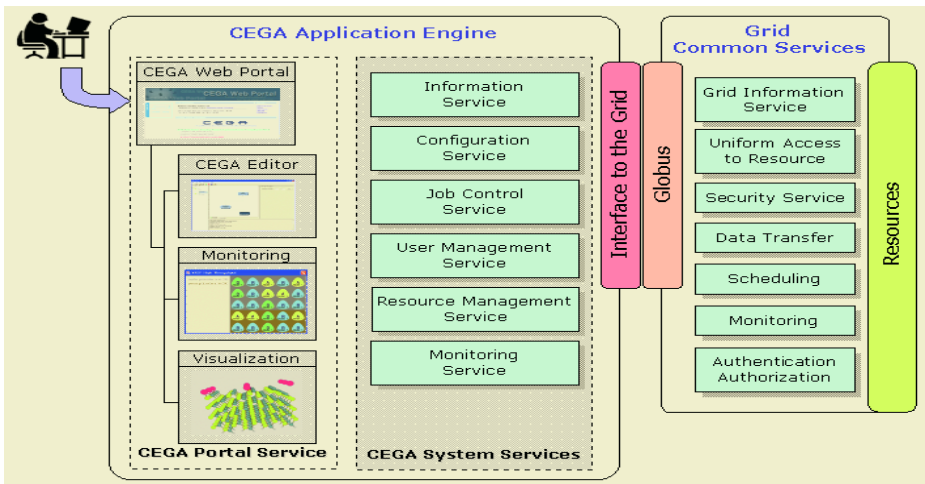


Fig. 1. The Architecture of CEGA

### 3.3 CEGA Monitoring and Visualization Service

The Workflow Engine controls and monitors the application execution based on the application workflow. A user is informed as the Engine provides the status data to the Editor in real time. The monitoring information is classified as two types: one is parsing status caused by syntax error before execution and the other is execution status. The information of monitoring syntax error and job execution result is displayed on the bottom window in text. At the same time, the color of each job model shows a

current status of job execution in 6 states: ready, active, done, failed, suspended, and pending. And when the execution is successfully done, the result of the application is stored in the location requested at the beginning of the application development. The visualization of the result of the application is dependent of the characteristics of the application. CEGA can basically provide the result in text mode and choices of some plugged in graphic tools (See Fig.1).

Currently, CEGA has been developed for a potential energy surface calculation in molecular dynamics simulation, which requires high performance parallel computing. It also provide interface to customize experimental options easily for diverse execution conditions. It reduces deployment cost for experimentation.

## 4 Conclusions

The paper describes the architecture of CEGA to provide a parallel and distributed programming environments; it provides an easy-to-use graphical user interface that allows users to develop, run and visualize parallel and distributed applications running on heterogeneous computing resources connected by networks. To support Grid services through CEGA the server creates application configurations using Resource Specification Language (RSL), which runs over the Globus toolkit. This paper shows the functionality of the workflow editor to develop an application and generate application configuration over Grid environment. As it is adapt a workflow model, it can be easily extended to other application domain when diverse workflow patterns are added. Currently, the extended workflow models are under development.

## References

1. Foster, C. Kesselman, "The Grid:Blueprint for a New Computing Infrastructure," Morgan-Kaufmann, 1998.
2. Astrophysics Simulation Collaboratory: ASC Grid Portal, <http://www.ascportal.org>
3. HotPage, <http://hotpage.npaci.edu>
4. Cactus Code, <http://www.cactuscode.org>
5. GrADS Project, <http://nhse2.cs.rice.edu/grads/index.html>
6. Romberg,M., "The UNICORE Architecture Seamless Access to Distributed Resources," High Performance Distributed Computing, 1999
7. Globus Project, <http://www.globus.org>
8. J. Novotny, "The Grid Portal Development Kit," Concurrency: Practice and Experience, Vol.00, pp1-7, 2000

# A Meta-heuristic Applied for a Topologic Pickup and Delivery Problem with Time Windows Constraints

Jesús Fabián López Pérez

Post-Graduate Program of Management Science, FACPYA UANL, Monterrey, México  
fabian.lopez@e-arca.com.mx

**Abstract.** Our problem is about a routing of a vehicle with product pickup and delivery and with time window constraints. This problem requires to be attended with instances of medium scale (nodes  $\geq 100$ ). A strong active time window exists ( $\geq 90\%$ ) with a large factor of amplitude ( $\geq 75\%$ ). This problem is NP-hard and for such motive the application of an exact method is limited by the computational time. This paper proposes a specialized genetic algorithm. We report good solutions in computational times below 5 minutes.

**Keywords:** Logistics, Genetic Algorithms, NP-Hard, Time Windows.

## 1 Problem Definition and Bibliographical Review

The objective is to determine the optimal route for a distribution vehicle. The vehicle departs from a distribution center and returns to the same point at the end of the route. An optimal route is defined as that which visits all the clients in such a way that we incur a minimal cost. We define a cost matrix which identifies the time or distance required to go from each client to all others. The problem constraints are as follows.

- a. Each client visited has a requirement of product to be delivered and a load to be collected. We have to observe a finite load capacity for the vehicle all the time.
- b. The time window identified for each client is defined by an opening hour and a closing hour. The time window width is equal to the difference between the closing hour and the opening hour. The visit to each client must be within the time window. It is not permitted to arrive before the opening hour nor after the closing hour.

Our bibliographical summary of previous investigations include Applegate et al. 1998 [1]; Dumas & Solomon 1995 [2]; Eijl Van 1995 [3]. The outlined problem is combinatoric in nature and is catalogued as NP-Hard, Tsitsiklis 1992 [4]. Regarding routing application area, the less investigated variant is the one which has to do with the physical product distribution, Mitrovic 1998 [5]. The instances that have been typically tested are characterized by time windows with a low percentage of overlapping, Ascheuer et al. 2001 [6]. The computational complexity for the solution of the SPDP-TW depends strongly on the structure of the time windows that are defined for each customer. The experimental results obtained by Ascheuer et al. proved that the TSP-TW is particularly difficult to be solved for instances with

more than 50% of active nodes with time window constraints. Ascheuer, Jünger & Reinelt 2000 [7] worked with instances up to 233 nodes. They reported 5.95 minutes of computational time for an instance of 69 nodes. All the greater instances required more than 5 hours of computational time. They conclude that the instances on the limit up to 70 nodes can be solved to optimality by exact methods like the Branch & Cut algorithms (B&C).

## 2 Methodology Proposed

Our methodology proposes 6 routines. We have 4 preprocessing routines, the Genetic Algorithm and finally one another routine for post-processing. We expose the 6 phases:

1. **Network topology decomposition phase based on a “shortest path algorithm (SPP)”**. We consider here the topology corners (street corners) that are required to model the traffic constraints that we have to observe in order to arrive to each customer in the network. This pre-processing strategy contributes to reduce the computational complexity during all the subsequent phases. In order to simplify our formulation we define an empirical assumption. We are going to use a constant “4” as the quantity of network arcs (north, south, east & west) that we require to model a typical city street corner. With the previous assumption we can establish that, if we setup a network with  $N1$  nodes, we would obtain only  $N2$  nodes, where  $N1 \approx 4N2$ . We use an SPP algorithm to pre-calculate the optimal sub-tour required to move from each customer to each one of the rest. All these preprocessed sub-tours fill the  $N2$  cost matrix to be used in the next phases.
2. **Compressing & clustering phase through a “neighborhood heuristic”**. The  $N2$  nodes are grouped to setup a reduced quantity of  $N3$  meta-nodes (where:  $N3 < N2$ ). Our assumption here is that we have driving times near to zero between the nodes that are going to be grouped. This assumption is going to be considered valid through all the phases where we work with the reduced version of the network. Taking in mind this, we can inference that the obtained solution for the reduced network can be derived as an optimal for the original network as well. The heuristic that we use here to group the nodes is by geographically neighborhood and also by time windows structure similarity. Starting from a group of nodes to be grouped in a meta-node, the time window structure of this meta-node is defined by the latest opening time and by the earliest closing time. We use in the algorithm a 50% compression factor for the grouping phase which means that  $N2=2 * N3$ .
3. **Discriminate compressing phase through a “ $k$  nearest nodes heuristic”**. The network arcs with greater cost are eliminated from the matrix. The logic of the previous assumption is because of those arcs have a smaller probability to appear in the optimal solution. For each  $N3$  node in the network, we maintain only the “ $k$ ” arcs with the smallest cost, where  $k \ll N3$ . We use a conservative 20% discriminate factor in order to reduce the probability that the optimal solution go out from the search space. This empirical assumption means that the matrix that will be transferred to the next phase will be reduced and defined by  $N3 \times N4$ , where  $N4 = 20\% * N3$  in an “incidence sense”. This means that although the dimensionality of the matrix is still the same ( $N3 \times N3$ ), the quantity of non-zero elements in the matrix is reduced to an equivalent matrix size of  $N3 \times N4$ .
4. **Aggressive Branch & Cut phase**. the initial math formulation we use here is quite similar as we may found in a basic TSP problem [6]. We have that  $X_{ij}$  formulation means the existence of an arc from “ $i$ ” to “ $j$ ” in the route. The procedure to add sub-tour elimination constraints are also included on this phase. Starting with  $N3$  meta-nodes, the objective is to find as quickly as possible, the first feasible solution that cover the time window and

vehicle capacity constraints. The logic that we apply here is to iteratively generate cuts within a Branch & Cut scheme. For that purpose we identify in the incumbent solution, the node with the greater deviation in relation to the time window and/or the vehicle capacity constraint. This node is named "*pivot node*". Then we verify the nodes of the tour that can be identified as "*related*" in order to re-sequence the position of the *pivot node* within the tour. This relation of the *pivot node* is exploded in the generation of the cut. The logic that we apply here to generate the cut assures that the *pivot node* "*k*" use at least one of the arcs that connect it to one of the *related nodes* "*j*". This procedure continues until is found the first feasible solution. At this stage we use Xpress Ver 15.10 ©

$$\begin{aligned} \exists I &= \{1..N_3\} (\text{network nodes}) \\ k &\in I (\text{pivot node}) \\ j &\subseteq I \{1..m\} (\text{related nodes to } k) \\ \sum_{j=1}^m (x_{jk} + x_{kj}) &\geq I \quad \forall k \subseteq I \end{aligned}$$

5. **Evolutionary phase.** our objective here is to approximate the optimal solution for the compact version of the network. Maintain in the pool of constraints a cut unnecessarily, means to take out the optimal solution or at least a better solution, from the search space. Our computational experience indicates that the quantity of cuts that get to be accumulated in the pool is meaningful (15-40 cuts). The goal is to identify which cuts of the pool are necessary to be eliminated. The cut elimination procedure can not be seen as an individual process for each cut, since the presence and/or the elimination of any cut can commit simultaneously the presence and/or the elimination of other(s). Identify which cuts must be eliminated, can be seen as a combinatoric sub-problem. We then propose an evolutionary strategy to attend this sub-problem. A binary codification permits to represent the elimination (0) and the presence (1) of a cut in the pool. Our Genetic Algorithm applies a tournament selection operator with a 50% crossing factor. The reproduction method applied was by means of a two random crossing points throughout the chromosome length. The mutation factor is initialized with a 5% value and it is auto-adjusted in each generation depending on the percentage of individuals in the population with identical genetic material content. Upon increasing the degeneracy level in the population, is applied an exponential growth curve in the mutation factor with 50% as an asymptotic limit. The elitism factor is limited to 15% of the population. The fitness function we calculate in this evolutionary stage is related with two objectives. The first is the route cost minimization. The second is the infeasibility level we calculate in the route as we may delete some cut(s) in the chromosome. The infeasibility level is only related with the capacity and time windows constraints for the SPDP-TW formulation. Our objective on this stage is to find the subset of cuts that can be deleted from the pool and at the same time we obtain a feasible solution. The final solution at this stage is when we found a minimal cost route which is still feasible as well. We remark here that our methodology is different from the conventional approach in the evolutionary bibliography. Our review indicates that most of the evolutionary approaches to attend routing problems take in mind the genes as the nodes or sequence nodes in the route. We treat with a modified problem. The genes represent the presence or elimination of a cut in the math formulation of the problem that is actually modeling the route.
6. **Uncompressing phase to generate a route for the original network.** The post-processing phase has the objective of translating the solution obtained in the compact version of the network to one another that will be topology sense equivalent to the original network. We have here 2 routines. The first routine is focused in determining the optimal sequence on which the *N3 meta-nodes* should be disaggregated to return to the *N2 nodes* obtained in phase 2. Starting from a selected meta-node, we construct only the valid arcs to the previous and to the next meta-node. This procedure is propagated to the rest of the

meta-nodes in the network. The second conversion routine makes use of the topology information generated in the first phase of our general methodology. Its objective is to substitute the sequence of the tour defined by the N2 nodes according to the cardinal movements that are required to obtain the N1 nodes that are present on the original network.

### 3 Experimental Development and Results

We applied an “*Experimental Design*” through the use of 4 experimental instruments: (1) B&C Algorithm (Xpress© Ver 15.10); (2) Steady Sate Genetic Algorithm (Evolver© Ver 6.0); (3) Generational Genetic Algorithm (Solver© Ver 4.0); (4) Proposed Genetic Algorithm. We will calculate a “percentage of optimality” for the statistic test of the hypothesis.

$$\text{optimality \%} = 1 - \frac{\text{GA solution} - \text{Lower Bound}}{\text{Lower Bound}}$$

*where Lower Bound = Best solution reached by B & C within 5 hours limit*

We gave treatment to instances with more than 70% of active time windows and with a minimal width of 75%. The dimension of the tested instances are defined by  $w$ , where  $(100 \leq w \leq 120)$ . The genetic parameters applied for the implementation of each GA's # 1, 2 & 3 were adapted empirically and separately to different values accordingly to the best case scenario. That means that the parameters were tuned for each GA. The experimental design was applied for a sample of 40 instances. All these instances were randomly generated. Only the B&C instrument was limited up to 5 hours of computational time. We remark here that although 5 hours of computational time is not evidence of optimality, we can report that we obtain the optimal solution in 38 of 40 instances. For the previous described GA instruments, the “% of optimality” was applied in 4 successive moments of time (minute #3, #5, #8 and #10). We define the following statistic parameters: (1) *Mean (m)* & (2) *Standard deviation (s)*. The T Student test “ $P(x > 90\%)$ ” applied for each element  $(m_{ij}, s_{ij})$  calculates the probability that the *algorithmic instrument “j”* in the *time interval “i”* obtains at least a 90% of optimality. Table 1 shows the values calculated for the “T” statistic. Table 2 shows the probability coefficients “P” Value.

**Table 1.** “T” Statistic Values

**Table 2.** Probability “P Values”

	Algorithmic instruments to be compared						Algorithmic instruments to be compared					
	B&C Algorithm (Control Group)	Basic Genetic Algorithm (Evolver)	Basic Genetic Algorithm (Frontline)	Proposed Genetic Algorithm			B&C Algorithm (Control Group)	Basic Genetic Algorithm (Evolver)	Basic Genetic Algorithm (Frontline)	Proposed Genetic Algorithm		
				P(x>90%)	P(x>92.5%)	P(x>95%)				P(x>90%)	P(x>92.5%)	P(x>95%)
3th Minute	NA	-0.404	-0.558	2.426	1.069	-0.091	NA	34%	29%	99%	85%	46%
5th Minute	-2.426	-0.116	-0.307	3.313	1.539	0.111	<1%	45%	38%	100%	93%	54%
8th Minute	-1.280	0.162	0.317	4.851	4.105	0.830	10%	56%	62%	100%	100%	79%
10th Minute	-0.700	0.400	0.903	6.298	5.577	1.328	24%	65%	81%	100%	100%	90%

## 4 Discussion and Conclusions

Our B&C implementation obtains the optimal solution for 38 of 40 instances that are particularly difficult to be solved and where the investigation is focused. In addition we tested some “toy” instances with less than 70 nodes and with less than 60% of active time windows. The computational times were very favorable since we report times below 3 minutes. Our proposed GA #3 obtains satisfactory solutions (*optimality*  $\geq 90\%$ ) and in reasonable computational times ( $3 \leq t \leq 5$  minutes). Both “out of the self” GA’s (1 & 2), are significantly inferior since these never surpass 90% of optimality before the fifth minute. We conclude:

1. *We can establish that the proposed methodology reaches a percentage of optimality  $\geq 90\%$  in a computational time  $\geq 5$  minutes (0.001 significance level).*
2. Table 1 & 2 shows that the proposed GA offers solutions within an acceptable optimality range and with computational times that make feasible its implementation. However, we should establish that our methodology can assure only 54% of confidence when is required to reach an optimality  $\geq 95\%$  in a computational time  $\geq 5$  minutes.

## References

- [1] Applegate, D; Bixby, R; Chvátal, V; (1998), On the solution of traveling salesman problems. “Documenta Mathematica Extra Volume ICM III”, USA.
- [2] Dumas, Y; Desrosiers, J; Solomon, M. (1995), An algorithm for the traveling salesman problem with time windows, “Operations Research 43(2)”, USA, pp. 23-25.
- [3] Eijl Van, C. (1995), A polyhedral approach to the delivery man problem, “Tech Report 95–19”, Dep of Maths and Computer Science, Eindhoven Univ of Technology, the Netherlands.
- [4] Tsitsiklis, J. (1992), Special cases of traveling salesman and repairman problems with time windows, “Networks No. 22”, USA.
- [5] Mitrovic, Snezana. (1998), Pickup and Delivery Problem with Time Windows, “Technical Report SFU CMPT TR 1998-12”, Canada, pp 38-39.
- [6] Ascheuer, N; Fischetti, M; Grotschel, M. (2001), Solving ATSP with time windows by branch-and-cut, Springer-Verlag, Germany.
- [7] Ascheuer, N; Jünger, M; Reinelt, G. (2000), A branch & cut algorithm for the ATSP with precedence constraints, “Comput. Optimization and Applications 17(1)”, USA, pp. 2-7.

# Three Classifiers for Acute Abdominal Pain Diagnosis – Comparative Study

Michał Wozniak

Chair of Systems and Computer Networks, Wrocław University of Technology,  
Wybrzeże Wyspiańskiego 27, 50-370 Wrocław, Poland  
michal.wozniak@pwr.wroc.pl

**Abstract.** The inductive learning algorithms are the very attractive methods generating hypothesis of the target concept on the base of the set of labeled examples. This paper presents some of the rules generation methods, their usefulness for the rule-based classifier and their quality of classification for the medical decision problem.

## 1 Introduction

Machine learning [1,5] is the attractive approach for building decision support systems. In the paper we compare the heuristic classifier (given by experts) and three another generated by the chosen inductive learning methods.

The content of the work is as follows. Section 2 introduces idea of the inductive decision tree algorithms and learning sets of rules method. In Section 3 we describe mathematical model of the acute abdominal pain decision problem. Next section presents results of the experimental investigations of the algorithms. Section 4 concludes the paper.

## 2 Algorithms

We chose three of the inductive learning algorithm: (1) C4.5 algorithm given by R. J. Quinlan [2], (2) Fuzzy Decision Tree Algorithm FID 3.0 given by C. Janikow [3] and (3) Rule generation algorithm - AQ given by R. Michalski [4].

### 2.1 Inductive Decision Tree

Algorithms C4.5 and FID are based on “Top Down Induction of Decision Tree” (TDIST) procedure[2]. The central choice in the TDIDT algorithm is selecting which attribute to test at each node in the tree. The chosen algorithms use the information gain that measures how well the given attribute separates the training examples according to the target classification. This measure based on the Shannon’s entropy of set  $S$ . The information gain of an attribute  $A$  relative to the collection of examples  $S$ , is defined as



$$Gain(S, A) = Entropy(S) - \sum_{v \in values(A)} \frac{|S_v|}{|S|} Entropy(S_v), \tag{1}$$

where  $values(A)$  is the set of all possible values for attribute A and  $S_v$  is the subset of  $S$  for which  $A = v$ .

### 2.2 Learning Set of Rules

The algorithms like CN2 [1] or AQ [4] based on the learning one rule (LOR) strategy, removing data it covers, then iterating the process. The LOR method is similar to the ID3. The LOR algorithms follow only the most promising branch in the tree at the each step – returns only one rule, which covers at least some of the examples.

### 3 Model of Acute Abdominal Pain Diagnosis

The mathematical model of the diagnosis of acute abdominal pain (AAP) was simplified by experts from the Clinic of Surgery, Wroclaw Medical Academy. It leads to the following classification of the AAP: appendicitis, (2)divercitilitis, (3) small-bowel obstruction, (4) perforated peptic ulcer, (5) cholecystitis, (6) pancreatitis, (7) non-specyfic abdominal pain, (8)rare disorders of “acute abdominal”.

Although the set of symptoms necessary to correctly assess the existing APP is pretty wide, in practice for the diagnosis, results of 36 (non-continuos) examinations are used, whose are presented in table I.

**Table 1.** Clinical features considered

no	feature	no	feature	no	Feature
1	sex	13	appetite	25	systolic blood pressure
2	age	14	bowels	26	diastolic blood pressure
3	site on onset	15	micturition	27	movement
4	site on present	16	previous indigestion	28	distension
5	intensity	17	jaundice	29	tenderness
6	aggravating factors	18	previous similar pain	30	Blumberg’s sign
7	relieving factors	19	previous surgery (abdominal)	31	guarding
8	progress	20	drugs	32	rigidity
9	duration	21	mood	33	swellings
10	character on onset	22	color	34	Murphy’s sign
11	Character on present	23	temperature	35	abdominal auscultation (bowel sounds)
12	nausea and vomiting	24	pulse	36	rectal examinations

### 3.1 Heuristic Decision Tree

The experts-physicians gave the decision tree depicted on Fig.1. Numbers of leafs are the numbers of diagnosis presented above. The numbers in the nodes are corresponded with the following diagnosis: (9) acute enteropathy, (10) acute disorders of the digestive system, (11). others.

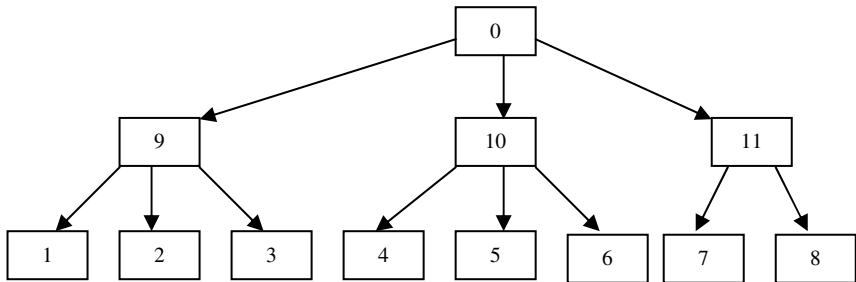


**Fig. 1.** Heuristic classifier for the APP diagnosis problem

## 4 Experimental Investigation

The presented algorithms C4.5, FID and AQ were used for creating rules for APP decision problem. Their frequencies of correct classification were compared with quality of heuristic classifier. The set of data has been gathered in the Surgery Clinic Wroclaw Medical Academy. It contains 476 learning examples.

For each learning method the following experiment was made:

- from the learning set 40 examples was chosen (according with frequency of the class appearance); this set was use for test,
- the rest of examples (436) were training ones.

This procedure was repeated 20 times for each of the algorithms. The results of the experiments are presented in Table 2 .

**Table 2.** Frequency of correct classification

Class number	Heuristic	AQ	C4.5	FID
1	79,1	90,5	95,8	86,7
2	88,2	55,0	92,3	100
3	93,1	95,0	95,8	100
4	67,1	90,0	95,6	66,7
5	82,5	98,8	86,9	83,3
6	84,4	85,0	96,2	75,0
7	84,7	97,5	91,5	75,0
8	88,2	75,0	92,3	50,0
<b>average</b>	<b>83,0</b>	<b>85,8</b>	<b>93,3</b>	<b>80,4</b>

The results of test are clear. The classifier given by C4.5 algorithm is always better than heuristic one. The AQ and FID algorithm gives the better results for some of class, but for another the frequency of correct classification is very low. Experts revised the structures of classifiers given by inductive learning algorithms. They confirmed that all of rules were correct and maybe the heuristic classifier was incomplete.

## 5 Conclusion

The methods of inductive learning were presented. The classifiers generated by those algorithms were applied to the medical decision problem (recognition of Acute Abdominal Pain). The results of test were compared with recognition quality of heuristic algorithm.

It must be emphasised that we have not proposed a method of "computer diagnosis". What we have proposed are the algorithms whose can be used to help the clinician to make his own diagnosis. The superiority of the presented empirical results for the inductive learning classifiers over heuristic one demonstrates the effectiveness of the proposed concept in such computer-aided medical diagnosis problems. Advantages of the proposed methods make it attractive for a wide range of applications in medicine, which might significantly improve the quality of the care that the clinician can give to his patient.

This work is supported be The Polish State Committee for Scientific Research under the grant which is realizing in years 2005-2007.

## References

1. Mitchell T.M., *Machine Learning*, McGraw-Hill Comp., Inc, New York 1997
2. Quinlan J.R., *C4.5: Programs for Machine Learning*, Morgan Kaufman, San Mateo, CA 1993
3. Janikow C.Z., Fuzzy Decision Tree: Issues and Methods, *IEEE Trans on Man and Cybernetics*, vol 28, Issue 1, 1998
4. Michalski R.S., A Theory and Methodology of Inductive Learning, *Artificial Intelligence*, no 20, 1983, pp.111-116
5. Puchala E., A Bayes Algorithm for Multitask Pattern Recognition Problem – Direct Approach, *Lecture Notes in Computer Science*, no 2659, 2003.
6. Walkowiak K., A Branch and Bound Algorithm for Primary Routes Assignment in Survivable Connection Oriented Networks, *Computational Optimization and Applications*, Kluwer Academic Publishers, February 2004, Vol. 27.

# Grid-Technology for Chemical Reactions Calculation

Gabriel Balint-Kurti<sup>1</sup>, Alexander Bogdanov<sup>2</sup>, Ashot Gevorkyan<sup>3</sup>, Yuriy Gorbachev<sup>4</sup>,  
Tigran Hakobyan<sup>5</sup>, Gunnar Nyman<sup>6</sup>, Irina Shoshmina<sup>2</sup>, and Elena Stankova<sup>2</sup>

<sup>1</sup> University of Bristol, School of Chemistry,  
Bristol BS8 1TS, UK

Gabriel.Balint-Kurti@bristol.ac.uk

<sup>2</sup> Institute for High Performance Computing and Information Systems,  
199397 St.-Petersburg, Russia

(bogdanov, irena, lena)@csa.ru

<sup>3</sup> Institute for Informatics and Automation Problems NAS of Armenia,  
375014 Yerevan, Armenia

g\_ashot@sci.am

<sup>4</sup> St.-Petersburg State Polytechnical University,  
195251 St.-Petersburg, Russia

gorbachev@csa.ru

<sup>5</sup> Yerevan Physical Institute,  
375036 Yerevan, Armenia

hakob@mail.yerphi.am

<sup>6</sup> Goteborg University,  
412 96 Goteborg, Sweden

nyman@chem.gu.se

**Abstract.** We discuss a possible strategy for implementing a grid-based approach to realizing the immense computational resources required to compute reactive molecular scattering cross sections and rate constants.

## 1 Introduction

Evaluation of chemical reaction cross-sections and rate-constants as well as more detailed scattering characteristics is one of the great challenges for computational technologies. The main difficulties are connected with the multi-dimension and multi-scale character of the problem. Both the accuracy and the computations of detailed state-to-state scattering cross sections are limited by the availability of computational resources and by the efficiency of the computational algorithm used in their calculation. We examine here a possible solution to these problems through the use of Grid technology. The main concept of Grid technology is the solution of a computational problem through *coordinated dynamic resource sharing within a multi-institutional virtual organizations* [1]. Some attempts at such Grid based solutions have already been implemented [2 - 4]. In these cases the Grid infrastructure supports the usage of standard quantum chemistry programs (Gaussian [5] and GAMESS [6]). This paper discusses a possible solution of the reactive scattering problem using a Grid based technology.

## 2 Description of Reactive Scattering Problem

We consider principally the process  $A + (BC)_m \rightarrow (AB)_n + C$  which may take place with or without involving the formation of a quasi-bound or an activated complex  $(ABC)^*$ . When the process occurs via the formation of a quasi-bound complex, both the classical and quantum mechanical treatment of the process show chaotic behavior. The computation of the cross sections and rate constants require large, often unattainably large, amounts of computational resources on a conventional computer. Here we discuss an alternative approach that effectively utilizes Grid technologies.

The problem may be divided into two parts that may be solved separately. The first part being that of calculating the potential energy surface (PES)  $V(q_1, q_2, \gamma)$  and the second part being the calculation of reaction probabilities and rate constants (or other properties). PESs are usually obtained from *ab initio* quantum chemical calculations (we consider these results as initial input to our problem), but they are represented in Cartesian co-ordinates that are usually not convenient for further calculations. For the scattering calculations the so-called curvilinear co-ordinates are the most convenient ones to use[7].

One of the computational problems consists in the transformation of the potential energy surface to the new co-ordinates  $U(x^0, x^1, x^2) \equiv V(q_1, q_2, \gamma)$ . It is also convenient to use certain analytic models for the PESs and to just determine their parameters. The PESs we develop depend on the fairly small number of parameters and these may be optimized to fit different sets of *ab initio* data [8]. In any case this problem may be solved separately. Since this problem is closely related to the inversion of a large dimensional matrix the corresponding methods may be used for its solution and these algorithms can also be parallelized. This procedure may easily be transferred to a Grid technology, implemented on a Grid of loosely connected computational systems. The calculation of scattering cross sections may be reduced to four sequential problems. The first one is the generation of the classical geodesic equations on the Lagrange surface of body system (at first this method of investigation classical dynamical systems was introduced by Krilov [9]) for the evolution of the system along the reaction coordinate and calculation of trajectory tube distribution; the second one is the problem of the solution Shroedinger equation on geodesic trajectory tubes; the third one is the calculation of the transition  $S$ -matrix elements and the fourth one is the calculation of transition probabilities [10, 11].

## 3 Grid for Chemical Reactions Calculation

The basic principles of the Grid for chemical reaction calculation can be stated as follows: 1) Present computer and data resources as a single virtual environment by developing a web portal on the Grid technology. 2) Build an easy-to-use user web interface for providing access to these resources. 3) Facilitate the sharing of results of research. 4) Organize archiving of input, output, and intermediate data.

As the basic software for Chemical Grid computing the Globus code will be used because of the following distinguishing advantages [12]. As the scheduling system we plan to use the Nimrod/G tool [13, 14], which is designed to manage the computational process including the transfer of input data and of the results of the calculations.

Returning to the problems arising in solving the reactive scattering problem that has been partly discussed in section 3, one must complete the following list of steps:

1) Computation of PES. 2) Parameterization of PES. 3) Solution of geodesic trajectory problems on Lagrange surfaces of the three-body system and the construction of the trajectory tubes distribution. 4) Calculation of the quantum system evolution on the trajectory tubes. 5) Computation of  $S$ -matrix elements and reaction probabilities for a set of initial phases  $\varphi_s$  and collision energies  $E_k^i$ . 6) Averaging of  $S$ -matrix element amplitudes over distribution of trajectory tubes, i.e. calculation of probabilities of elementary reactive quantum transitions. 7) Visualization of the results.

A Grid implementation of the solution of the reactive scattering problem implies the establishment of some infrastructure that should include algorithms for the *ab initio* calculation of PESs and the corresponding databases for different scattering partners. The next step then is the parameterization of the PESs using for instance the nonlinear optimization algorithm described in [9]. The Chemical Grid should contain a number of models that will permit the parameterizations of different aspects of PESs to varying accuracies. The classic geodesic trajectory problem calculation on the Lagrange surfaces for the reactive collision should be implemented for use in a distributed computational environment. Also the quantum reactive scattering part for the different trajectory tubes can be parallelized.

Our experience in complex problem solving using the Grid [15] will be used to achieve these goals. We wish to create a Chemical Grid that will allow the incorporation of both the data banks of different PESs and other properties accumulated by other scientists and our own computational codes.

## Acknowledgments

This work was partly supported by the INTAS grant 03-51-4000 and ISTC A-823.

## References

1. Foster, I, Kesselman, C. and Tuecke, S.: "The Anatomy of the Grid: Enabling Virtual Organisations", International Journal of Supercomputer Applications, 15 (3) 2001, pp. 200-222.
2. Nishikava, T., Nagashima, U. and Sekiguchi, S. "Design and Implementation of Intelligent Scheduler for Gaussian Portal on Quantum Chemistry Grid" In: P.M.A.Sloot, D.Abramson,, A.V.Bogdanov, J.J.Dongarra, A.Y.Zomaya, Yu.E.Gorbachev, eds, Proceedings, Part 3, Computational Science – ICCS 2003, in series Lecture Notes in Computer Science, v. 2659, pp. 244-253, Springer Verlag, ISBN 3-540-40194-6.

3. Baldrige, K.K., Greenberg, J.P. "Management of Web and Associated Grid Technologies for Quantum Chemistry Computation" In: P.M.A.Sloot, D.Abramson,, A.V.Bogdanov, J.J.Dongarra, A.Y.Zomaya, Yu.E.Gorbachev, eds, Proceedings, Part 4, Computational Science – ICCS 2003, in series Lecture Notes in Computer Science, v. 2658, pp. 111-121, Springer Verlag, ISBN 3-540-40194-6.
4. Sudholt, W., Baldrige, K., Abramson, D., Enticott, C. and Garic, S. "Parameter Scan of an Effective Group Difference Pseudopotential Using Grid Computing", *New Generation Computing* 22 (2004) 125-135.
5. <http://www.gaussian.com>
6. <https://gridport.npaci.edu/GAMESS>
7. Pack, R. T. and Parker, G.A., Quantum reactive scattering in three dimensions using hyperspherical (APH) coordinates. *Theory J. Chem. Phys.* 87, (1987) 3888.
8. Gevorkyan, A.S., Ghulian, A.V. and Barseghyan, A.R. "Modeling of the Potential Energy Surface of Regrouping Reaction in Collinear Three-Atom Collision System Using Nonlinear Optimization" In: P.M.A.Sloot, D.Abramson, A.V.Bogdanov, J.J.Dongarra, A.Y.Zomaya, Yu.E.Gorbachev, eds, Proceedings, Part 2, Computational Science – ICCS 2003, in series Lecture Notes in Computer Science, v. 2658, pp. 545-554, Springer Verlag, ISBN 3-540-40194.
9. Krylov, N.S., Works by abroad of statistical physics, publishing company Academy of Science SSSR [in Russian] ed A. Fok, Moscow (1950), p.205
10. Bogdanov, A.V., Gevorkyan, A.S. and Grigoryan, A.G., Bifurcations in trajectory problem as a cause of internal-time singularities and the onset of quantum (wave) chaos, *Tech. Phys. Lett.* 25, (1999) 637
11. Bogdanov, A.V., Gevorkyan, A.S., Grigoryan, A.G., Internal Time Peculiarities as a Cause of Bifurcations Arising in Classical Trajectory Problem and Quantum Chaos Creation in Three body System, *AMS/IP Studies in Advanced Mathematics*, V.13. p. 69-80, (1999)
12. Johnston, W. E., The NASA IPG Engineering Team, and The DOE Science Grid Team Implementing production Grid
13. Abramson, D., Giddy, J., Kotler, L.: High Performance Parametric Modeling with Nimrod/G: Killer Application for the Global Grid? *International Parallel and Distributed Processing Symposium (IPDPS)*, Cancun, Mexico (May 2000) 520- 528; <http://www.csse.monash.edu.au/~davida/nimrod/>
14. Shoshmina, I., Bogdanov, A.V. and Abramson D. "Whither the Grid?" *Proceedings of the International Conference "Distributed Computing and Grid Technologies in Science and Education"*. July 2004, Dubna, Russia. (accepted for publication)
15. Krzhizhanovskaya, V.V., Gorbachev, Yu.E., Sloot, P.M.A. A Grid-based Problem-solving Environment for Simulation of Plasma Enhanced Chemical Vapor Deposition. In: *Book of abstracts of the International Conference "Distributed Computing and Grid Technologies in Science and Education"*. 29 June - 2 July 2004, Dubna, Russia. Publ: JINR, Dubna, 2004. pp.89-90.

# A Fair Bulk Data Transmission Protocol in Grid Environments

Fanjun Su<sup>1</sup>, Xuezheng Pan<sup>1</sup>, Yonglv<sup>2</sup>, and Lingdi Ping<sup>1</sup>

<sup>1</sup> College of Computer Science, Zhejiang University,  
Hangzhou 310027, China  
suwang@zju.edu.cn

<sup>2</sup> College of Electrical Engineering, Zhejiang University,  
Hangzhou 310027, China

**Abstract.** In this paper, we propose FHSTCP (Fair High-Speed TCP) as an improvement of HSTCP, which adds a fair factor to eliminate the difference of congestion window caused by different RTT and adopts block-pacing to reduce the burstiness. Simulation results show that FHSTCP can alleviate the RTT unfairness meanwhile keeping advantages of HSTCP.

## 1 Introduction

Recently there appear many high-speed networks with bandwidth larger than 1Gbps, even than 10Gbps. Through high-speed networks, data intensive grid application can transfer high-bandwidth real time data, images, and video. TCP [1] performs badly in high-speed networks [2]. Some improvements have been made, such as HighSpeed TCP (HSTCP) [2], Scalable TCP (STCP) [3], BIC [4]. However, in [4] the author points out that HSTCP has very severe RTT (Round Trip Time) unfairness. We define the RTT unfairness of two competing flows to be the throughput ratio. In this paper, a fair protocol named FHSTCP (Fair High-Speed TCP) is proposed, and we give a relative fair criterion to evaluate the protocol. FHSTCP adds a fair factor to eliminate the difference of congestion window between flows with different RTT. Block-pacing scheme is adopted to reduce the burstiness caused by fair factor of long RTT flows. The performance of FHSTCP is evaluated using ns2 [5].

## 2 FHSTCP

TCP and HSTCP use the following algorithm to adjust their congestion window:

$$\text{ACK: } w \leftarrow w + a(w)/w$$

$$\text{Drop: } w \leftarrow w - w \times b(w)$$

Where  $w$  denotes congestion window size. For standard TCP,  $a(w)=1$ ,  $b(w)=0.5$ , which is not sufficient for high-speed networks, so HSTCP makes  $a(w)$  and  $b(w)$  become the function of current congestion window size [2].



The main idea of FHSTCP is adding a factor to compensate the congestion window increment difference caused by different RTT. Let  $a(w) = \eta \times a(w)$ . The fair factor is based on the value of RTT, calculating as  $\eta = c \times RTT$ . For example, when  $c = 10$  and  $RTT = 200\text{ms} = 0.2\text{s}$ ,  $\eta = 2$ . After adding fair factor, different flows can get the same  $w(t)$ . Because throughput  $V(t) = w(t)/RTT$ , FHSTCP can keep RTT unfairness to be inversely proportional to RTT ratio. After fair factor is added, long RTT flows will have a sharp congestion window increment after an RTT. To solve this problem, a block-pacing method is adopted. The congestion window will be divided into several “blocks”. After the packets in one block have been sent out, other packets in another block will be sent after a time interval. This can counteract the negative effects caused by adding fair factor. We set the number of the block based on fair factor  $\eta$ . The details of the algorithm are shown in figure 1.

**Setting initial value:**

```
k=1; // the number of blocks
block=0; // the packets number in a block
number=0; // number of packets that has been sent
```

**On receiving a new ack in congestion avoidance state:**

```
increment=c*RTT*a(w)/cwnd;
// cwnd is the size of congestion window
if(increment>1)
    increment=1;
    // avoid the increment larger than slow start
cwnd=cwnd+increment;
k=(int)c*RTT+1;
block=cwnd/k;
```

**On congestion happening:**

```
cwnd=cwnd*(1-b(w));
number=0;
time_0=now; // now is current time
```

**On Sending date:**

```
if(number>block)
    time_1=now; // now is current time
    if(k>cwnd)
        k=cwnd;
    delay=RTT/k-(time_1-time_0);
    // delay is the time interval between two blocks
    // (time_1-time_0) is sending time of one block
    output(delay); // send data after a time of delay
    number=0; // begin a new count
    time_0=time_1+delay;
else
    output( ); // send data directly
    number++;
```

**Fig. 1.** Pseudo-codes of FHSTCP

### 3 Performance Evaluation

We present a relative fairness criterion: (1) The bandwidth requirement of standard TCP should be met. (2) The fairness between different high-speed TCP flows should be guaranteed. Satisfying condition (1) also means the protocol has the TCP friendliness, because standard TCP only works well in high loss rate environment. The loss rate we choose is  $10^{-3}$ , which is corresponding to the value of Low\_P in HSTCP. To evaluate the fairness of high-speed TCP flows, fair index [6] is used as follows:

$$f(x) = \left( \sum_{i=1}^n x_i \right)^2 / \left( n \sum_{i=1}^n x_i^2 \right)$$

where  $x_i$  is the link utilization of the flow  $i$ . We adopt ns2 simulator (version 2.26) [5]. The topology and configuration are shown in figure 2. The buffer size of the router is set to be the product of bandwidth and the delay of bottleneck link. We use TCP SACK for the simulation, and packet size is set to 1000 byte. The maximal congestion window is set to 1000000. FTP is the application used to transmit data through the TCP connections. To avoid phase effect [7], some web flows and short-lived TCP flows are used, together with 3~5 standard long-lived TCP flows. They act as background traffics for the simulation. DT (Drop Tail) queue management policy is used.

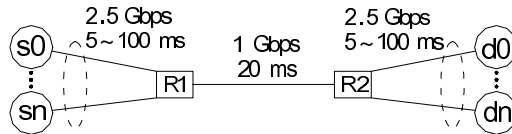


Fig. 2. Simulation topology and configuration

Some simulation results show effect of parameter  $c$ . we list our simulation results in table 1 (F1, F2, F3 are FHSTCP flows whose RTT are 80, 140, 200ms, and F4 denotes background flows). We can find when  $c=5$ , the per-flow bandwidth utilization and total bandwidth utilization of FHSTCP flows decrease together. This means that a too small value of  $c$  will limit the scalability of FHSTCP. However, when  $c=20$ , short RTT FHSTCP flows will grasp more bandwidth and fairness are decreased too.

Table 1. The effect of  $c$  and the TCP friendliness

$c$	Bandwidth Utilization (%)				The fairness index of FHSTCP	Loss rate of background flows
	F1	F2	F3	F4		
5	29.79	16.80	14.38	26.96	0.90	$7 \times 10^{-5} \sim 1 \times 10^{-4}$
10	32.22	26.61	19.36	16.35	0.96	$7 \times 10^{-5} \sim 8 \times 10^{-4}$
20	44.85	24.69	19.92	5.55	0.88	$5 \times 10^{-4} \sim 1 \times 10^{-3}$

What’s more, background flows can get less bandwidth. In other words, the friendliness of FHSTCP decreases. Therefore,  $c=10$  is optimal. The packet loss rate of background flows are below  $10^{-3}$  in 3 cases, so we say FHSTCP is TCP friendly.

We also give fairness comparison of FHSTCP, HSTCP, STCP and standard TCP. Three flows with RTT being 80ms, 140ms, and 200ms respectively are used, and different algorithms, such as FHSTCP ( $c=10$ ), HSTCP, STCP, and standard TCP are adopted respectively. The fairness index is calculated at different time scales. As shown in figure 3, we can find FHSTCP has a better fairness property.

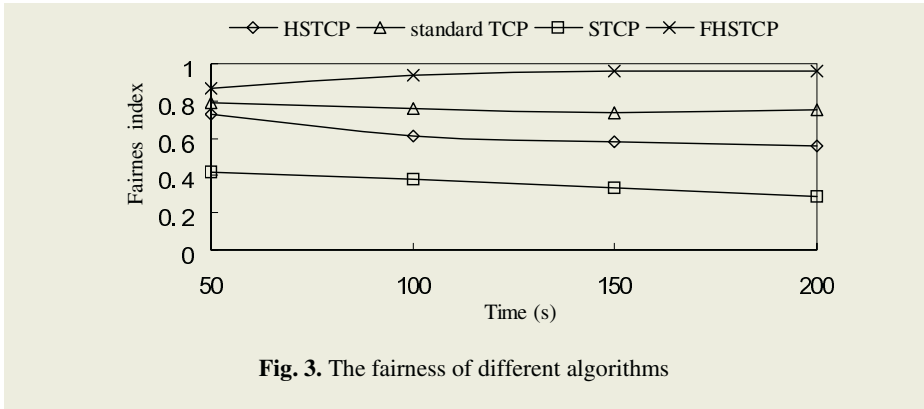


Fig. 3. The fairness of different algorithms

## 4 Conclusion

As an improvement of HSTCP, FHSTCP adds a fair factor to eliminate the difference of congestion window caused by different RTT and adopts block-pacing to counteract the negative effects caused by fair factor. Simulation results show that FHSTCP has better fairness, and is TCP friendliness while keeping the advantages of HSTCP.

## References

1. Stevens, W.R.: TCP/IP Illustrated: The Protocols. Volume 1. Addison-Wesley (1994)
2. Floyd S.: HighSpeed TCP for large congestion windows. RFC 3649 (2003)
3. Kelly T.: Scalable TCP: Improving Performance in High-Speed Wide Area Networks. ACM Computer Communications Review 33 (2003) 83-91
4. Xu L., Harfoush K., Rhee I.: Binary Increase Congestion Control (BIC) for Fast Long-Distance Networks. Proceedings of INFOCOM (2004) 2514 -2524
5. Network simulation-ns2. <http://www.isi.edu/nsnam/ns>
6. Chiu D., Jain R.: Analysis of the increase and decrease algorithms for congestion avoidance in computer networks. Journal of Computer Networks and ISDN 17 (1989) 1-14
7. Floyd S., Jacobson V.: On traffic phase effects in packet-switched gateways. Internetworking: Research and Experience 3 (1992) 115-156

# A Neural Network Model for Classification of Facial Expressions Based on Dimension Model

Young-Suk Shin

Department of Information Communication Engineering, Chosun University,  
#375 Seosuk-dong, Dong-gu, Gwangju, 501-759, Korea  
ysshin@mail.chosun.ac.kr

**Abstract.** We present a new neural network model for classification of facial expressions based on dimension model that is illumination-invariant and without detectable cues such as a neutral expression. The neural network model on the two-dimensional structure of emotion have improved the limitation of expression recognition based on a small number of discrete categories of emotional expressions, lighting sensitivity, and dependence on cues such as a neutral expression.

## 1 Introduction

The work in facial expressions for human-computer intelligent interaction did not start until the 1990s. Models for recognizing facial expressions have traditionally operated on a short digital video sequence of the facial expression being made, such as neutral, then happy, then neutral[1,2,3]. All require the person's head to be easily found in the video. Therefore, continuous expression recognition such as a sequence of "happy, surprise, frown" was not handled well. And the expressions must either be manually separated, or interleaved with some reliably detectable cues such as a neutral expression, which has essentially zero motion energy.

In this paper, we present a new neural network model on the two dimensional structure of emotion for classification of facial expressions that is illumination-invariant and without detectable cues such as a neutral expression.

## 2 Facial Expression Representations for Invariant-Illumination and Neutral Expression

The face images used for this research were centered the face images with coordinates for eye and mouth locations, and then cropped and scaled to 20x20 pixels. The luminance was normalized in two steps. First, a "sphering" step prior to principal component analysis is performed. The rows of the images were concatenated to produce  $1 \times 400$  dimensional vectors. The row means are subtracted from the dataset,  $X$ . Then  $X$  is passed through the zero-phase whitening filter,  $V$ , which is the inverse square root of the covariance matrix:

$$V = E\{XX^T\}^{-\frac{1}{2}}, W = XV \tag{1}$$

This indicates that the mean is set to zero and the variances are equalized as unit variances. Secondly, we subtract the local mean gray-scale value from the sphered each patch. From this process,  $W$  removes much of the variability due to lightening. Figure 1(a) shows the cropped images before normalizing. Figure 1(b) shows the cropped images after normalizing.

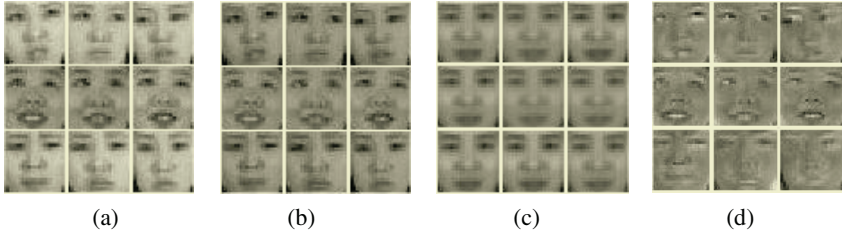


**Fig. 1.** (a) Images before normalizing. (b) Images after normalizing. (c) PCA representation only included the first 1 principle component. (d) PCA representation excluded the first 1 principle component

In a task such as facial expression recognition, the first 1 or 2 principal components of PCA do not address the high-order dependencies of the facial expression images, that is to say, it just displays the neutral face. Figure 1(c) shows PCA representation that included the first 1 principle component. But selecting intermediate ranges of components that excluded the first 1 or 2 principle components of PCA did address well the changes in facial expression (Figure 1(d)).

Therefore, to extract information of facial expression regardless of neutral expression, we employed the 200 PCA coefficients,  $P_n$ , excluded the first 1 principle component of PCA of the face images. The principal component representation of the set of images in  $W$  in Equation(1) based on  $P_n$  is defined as  $Y_n = W * P_n$ . The approximation of  $W$  is obtained as:

$$\overline{W} = Y_n * P_n^T \tag{2}$$

The columns of  $\overline{W}$  contains the representational codes for the training images (Figure 1(d)). The representational code for the test images was found by  $\overline{W}_{test} = Y_{test} * P_n^T$ . Best performance for facial expression recognition was obtained using 200 principal components excluded the first 1 principle component.

### 3 Recognition

The face images used for this research were a subset of the Korean facial expression database[4]. The data set contained 500 images, 3 females and 3 males, each image

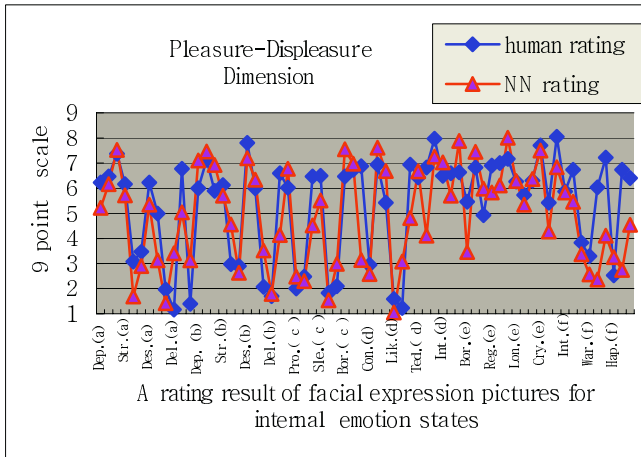


**Fig. 2.** A rating result of facial expression recognition in Pleasure-Displeasure dimension (Str.,strangeness;Des.,despair;Del.,delight;Pro.,proud;Sle.,sleepiness;Bor.,boredom; Con.,confusion;Lik.,likable;Ted.,tedious;Int.,intricacy;Reg.,regret;Lon.,loneliness; Cry.,crying;War.,warmness;Hap.,happiness; Dep.,depression)

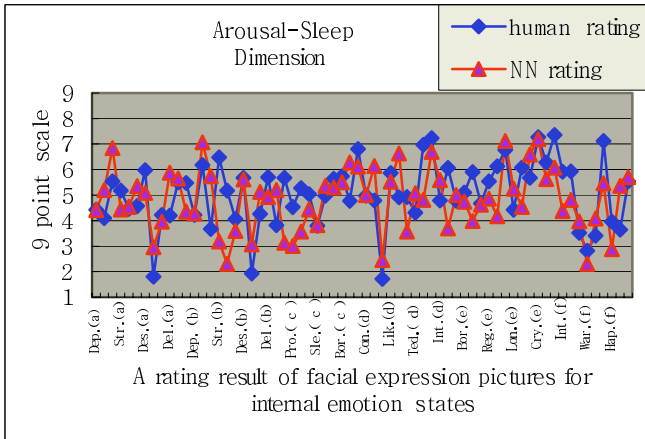


**Fig. 3.** A rating result of facial expression recognition in Arousal-Sleep dimension

using 640 by 480 pixels. Expressions were divided into two dimensions(Pleasure-Displeasure and Arousal-Sleep dimension) according to the study of internal states through the semantic analysis of words related with emotion by Younga et al. [5] using 83 expressive words. The system for facial expression recognition uses a three-layer neural network. The first layer contained the representational codes derived in Equation (2). The second layer was 30 hidden units and the third layer was two output nodes to recognize the two dimensions: Pleasure-Displeasure and Arousal-Sleep.

Training applies an error back propagation algorithm. The activation function of hidden units uses the sigmoid function. 500 images for training and 66 images excluded from the training set for testing are used. The 66 images for test include 11 expression images of each six people. The first test verifies with the 500 images trained already. Recognition result produced by 500 images trained previously showed 100% recognition rates. The rating result of facial expressions derived from 9 point scale on two dimension for degrees of expression by subjects was compared with experimental results of a neural network(NN).

Figure 2 and 3 show the correlation of the expression recognition between human and NN in each of the two dimensions. The statistical significance of the similarity for expression recognition between human and NN on each of the two dimensions was tested by Person correlation analysis. The correlation in the Pleasure-Displeasure dimension between human and NN showed 0.77 at the 0.01 level and 0.51 at the 0.01 level in the Arousal-Sleep dimension.

## 4 Conclusion

Our results allowed us to extend the range of emotion recognition and to recognize on dimension model of emotion with illumination-invariant without detectable cues such as a neutral expression. We propose that the inference of emotional states within a subject from facial expressions may depends more on the Pleasure-Displeasure dimension than Arousal-Sleep dimension. It may be analyzed that the perception of Pleasure-Displeasure dimension may be needed for the survival of the species and the immediate and appropriate response to emotionally salient, while the Arousal-Sleep dimension may be needed for relatively detailed cognitive ability for the personal internal states.

**Acknowledgements.** This study was supported by research funds from Chosun University, 2004.

## References

1. Oliver, N. Pentland, A., Berard, F.: LAFTER:a real-time face and lips tracker with facial expression recognition. *Pattern Recognition* **33** (2000) 1369-1382
2. Cohen, I., Sebe, N., Garg, A., Chen, L. S., Huang, T. S.: Facial expression recognition from video sequence. *Proc. Int'l Conf. Multimedia and Exp(ICME)* (2002) 121-124
3. Cohen, I. :Semisupervised learning of classifiers with application to human-computer interaction. PhD thesis, Univ. of Illinois at Urbana-Champaign (2003)
4. Saebum, B., Jaehyun, H., Chansub, C.: Facial expression database for mapping facial expression onto internal state. '97 Emotion Conference of Korea, (1997) 215-219
5. Younga, K., Jinkwan, K., Sukyung, P., Kyungja, O., Chansub, C.: The study of dimension of internal states through word analysis about emotion. *Korean Journal of the Science of Emotion and Sensibility*, **1** (1998) 145-152

# A Method for Local Tuning of Fuzzy Membership Functions

Ahmet Çinar

Firat University, Faculty of Eng. Computer Engineering , 23119, Elazig, Turkey  
acinar@firat.edu.tr

**Abstract.** In this paper, a new method based on genetic algorithms is proposed for local tuning of fuzzy membership functions. For this purpose, the local adjustment is employed on the initial membership functions. Genetic algorithm is used to investigate discrete points that will be modified on the membership functions Hence, global adjustment does not require and the processing time required for tuning of membership functions is decreased.

## 1 Introduction

In this paper, the initial base values of membership functions are not changed, only local modifications are made. The basic of the study is as following:

Step 1: Discretization of initial membership functions. Step 2: Finding the membership functions that will be modified by genetic algorithms and tuning. Step 3: Reconstructing the membership functions and applying to system.

## 2 Discretization of Initial Membership Functions

For this process, the geometric support construction method is used. The set of polygonal segments of boundary curve is located in the any list. And then, the construction of the polygonal support is achieved such that the distance any segment and portion of the curve it represent must be bounded. Hence, refinement of curve will be more important and correct in the any highly curved regions on the boundary curve.

## 3 Tuning Membership Functions by Using Genetic Algorithms

Figure 1 depicts diagram of proposed method for local tuning of fuzzy membership functions.

The following sections describe each block seen above.

Block 1: Dedicating control points to membership functions.

Block 2: Fitness Function.

In this block, how to make changes on the population is described. For this goal, initial membership function is passed through certain fitness function and the obtained



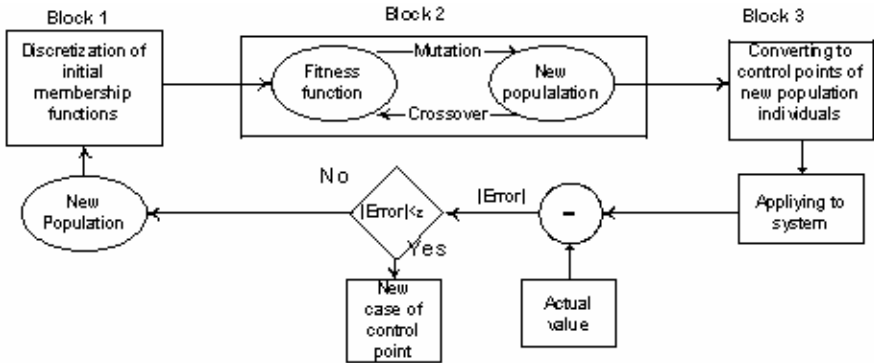


Fig. 1. The diagram of the proposed method

value is operated to genetic operator. Therefore, some individuals are founded. In this study, a function dependent on system input output is used as fitness function. It is known that, a fitness function is generated a certain integer value. Whereas, this method is not appropriate for this study due the fact that the direct fitness function did not explained. The following section describes the proposed fitness function. Figure 5 depicts genetic individuals and control points. These control points are produced by means of aforementioned method in block 1. This process is the population dedicating process on the control points and making up control points on the initial membership function.

For example; let control point value be 11. First, log value of control point is obtained, such as  $m = \log_2(11) = 3.3$ . If  $m$  is not integer number, it is rounded for example 3.3 to 4. Therefore, population values are follows: 0001,0010,0011,0100,0101, 0110,0111,1001,1010,1011,1100. The  $m$  value is used as bit number.

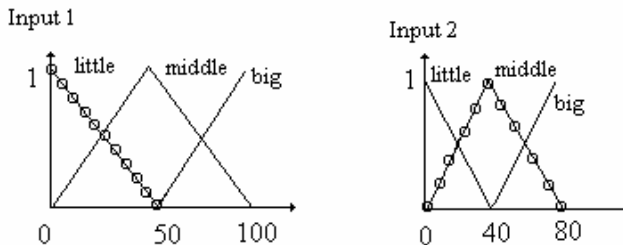


Fig. 2. Control points on the initial membership function

If the rule base table and system input output response are known, fitness function is used as following: Let us know the input output response for any system.  $a[ ]$ ,  $b[ ]$  and  $c[ ]$  are three sets. Let  $c[ ]$  be response with respect to  $a[ ]$  and  $b[ ]$ . Control points at distance  $\epsilon_i$  is changeable. But, we have to know which points be modified.

For that reason,  $a[ ]$  and  $b[ ]$  sets are used. Figure 3 shows control points that will change with respect to  $\epsilon_l$  value.

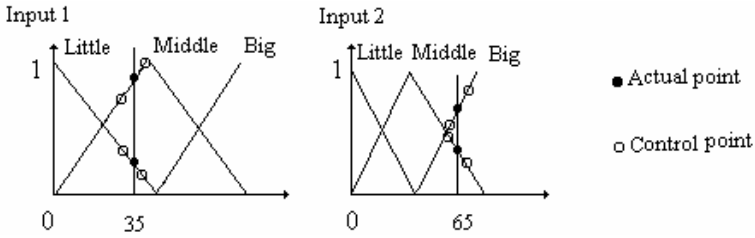


Fig. 3. The values with respect to input=35 and input2=65 and relationship control points

After finding these control points, the output value is obtained by means of any defuzzification method such as middle of maximum.

$u_i$ : The  $i_{th}$  value of  $u$  membership functions

$\mu(u_i)$ : The value of  $u_i$  membership functions.

$$u^* = \frac{\sum_{i=1}^l \mu(u_i) u_i}{\sum_{i=1}^l \mu(u_i)} \tag{1}$$

If the obtained result is similar to output  $c[ ]$  with respect to  $\epsilon_l$ , then any changes does not require on this population. In the proposed method, value  $\epsilon_l$  is as half of distance between of two points as shown in figures 4. If the error is bigger than  $\epsilon_l$ , then generic operators are used on population. Figure 4 depicts simple geometric operations for value  $\epsilon_l$ .

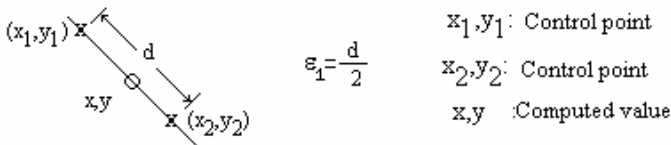


Fig. 4. The using method for value  $\epsilon_l$

The mutation is applied to discrete points changed. It is known that, only a bit is changed in the simplest manner for the mutation process. A new population after this operation will be different. This new population has to convert in the appropriate for system. This operation is achieved in block 3.

Block 3: Converting to control points of new population value.

In this block, new population values are converted to control points. Let original point be genetic individual with respect to 0010 value. Figure 5 shows this position.

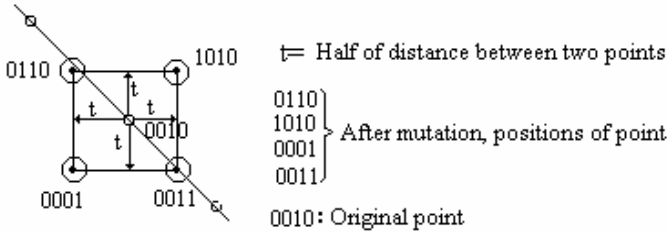


Fig. 5. Original point and its position after modification

According to using bit numbers, the actual location of point is as follows:

$x, y$  value is 0010,  $x+t, y+t$  value is 0011,  $x-t, y+t$  value is 0001,  $x-t, y-t$  value is 0110,  $x+t, y-t$  value is 1010. If bit number is 4, there is no problem. But the bit number is bigger than 4, then only right 4 bits are used. Also, let bit number be 5 and 00100. Then only using 0100 is appropriate. If bit number is less than 4, then a bit is added on the left side. If bit value is 010, then it is used as 0010.

In this way, after computing actual coordinate values and making up memberships functions, according to system response, modifications of membership function is considered. If it needs, new population is passed through fitness function.

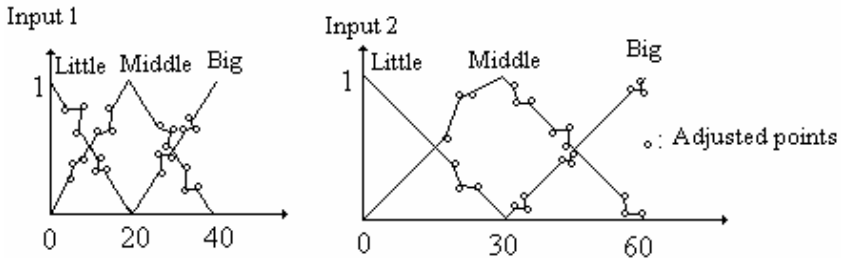


Fig. 6. The adjusted membership functions

## 4 Conclusion

In this study, a distinct method based on genetic algorithm for local adjustment of fuzzy membership functions is presented. Instead of global adjustment, local adjustment is achieved. Thus, the fast and accurate process is achieved with respect to system input-output response. By means of proposed method, initial fuzzy membership functions are selected, and then very much little changes on the

membership function are done. Consequently the global changes such as gradient-descent method are avoided.

## References

1. D.E. Goldberg, Genetic Algorithms in Search, Optimization and Machine Learning, Addison Wesley , 1989
2. H. Nomura, I. Hayashi, N.Wakai, A self-tuning method of fuzzy control by descent method, in Proc 4<sup>th</sup> IFSA congress, Engineering, pp.49-52, 1991
3. H.J.Zimmermann ,Fuzzy programming and linear programming with several objective functions, Fuzzy Sets and Systems, vol.1, pp.44-45,1978
4. Kuo Ting, Hwang Shu-Yuen, A Genetic Algorithm With Disruptive Selection, IEEE Transaction On Systems, Man, And Cybernetics-Part B: Cybernetics, Vol. 26, No. 2, April 1996
5. Wang Chi-Hsu,Wang Wei-Yen, Fuzzy B-Spline Membership Function (BMF) And Its Application In Fuzzy-Neural Control, IEEE Transactions On System Man And Cybernetics, Vol. 25, No.5, May 1995
6. Zadeh L. , Fuzzy sets , Inf. Control, Vol:8, pp:338-353, 1965.

# QoS-Enabled Service Discovery Using Agent Platform\*

Kee-Hyun Choi, Ho-Jin Shin, and Dong-Ryeol Shin

School of Information & Communication Engineering Sungkyunkwan University, Korea  
{gyunee, hjshin, drshin}@ece.skku.ac.kr  
<http://nova.skku.ac.kr>

**Abstract.** As the number of Internet services is growing rapidly, the network users need a framework to locate and utilize those services that are available in the Internet. As a result, dynamic service discovery plays an important role in certain networks, such as P2P networks. Recently many P2P mechanisms have been proposed which focus on the naming and discovery protocols. However, because these mechanisms do not provide congestion management and priority-based scheduling in P2P networks, they cannot provide an efficient communication among the nodes. Based on these observations, in this paper, we propose a QoS-based agent framework, designed to resolve such problems, and demonstrate its effectiveness.

## 1 Introduction

Service discovery is increasing in importance as its usage becomes more and more widespread throughout the Internet. The entire premise of the Internet is centered on the sharing of information and services. The focus of P2P networks is the mechanism by which a peer provides other peers with services and discovers the services available from other peers. In such an environment, a peer can be any network-aware device such as cell phones, PDA, PC or any device you can imagine that passes information in and out. In some cases, a peer might be an application distributed over several machines.

A large number of papers dealing with service discovery have recently been published. Although the schemes proposed provide efficient and fast searching mechanisms for service discovery, they do not consider QoS. With these observations in mind, we developed a new agent platform designed to provide QoS and evaluated its effectiveness by simulation, which is a main contribution of this paper. The remainder of this paper is organized as follows. Section 2 describes the proposed agent platform. In section 3, we present the simulation results for the proposed system. Finally, we conclude this paper in Section 4.

## 2 Proposed Agent Platforms

In this section, we describe our proposed Agent Platform (AP) architecture. The overall design of the architecture is shown in Figure 1. We adopt the FIPA[1] reference

---

\* This research was partially supported by a grant from the CUCN, Korea and Korea Science & Engineering Foundation (R01-2004-000-10755-0).

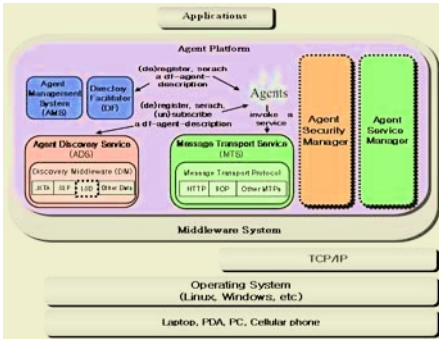


Fig. 1. Agent Platform

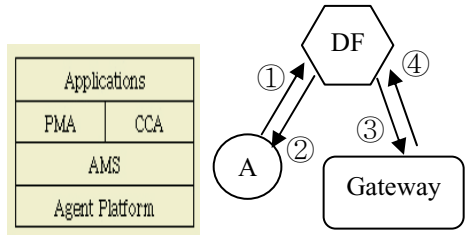


Fig. 2. a) Agent platform b) Setup sequence

model and add new components. The Agent Service Manager is a QoS solution for ad-hoc networks and P2P networks. By using the ASM, we allow our agent platform to provide QoS in P2P networks. The ASM uses two separated but not independent management agents. The PMA provides dynamic priority information according to the network status. When an application wants to transmit its data, it contacts the DF, in order to obtain priority information from the PMA. In this way, each application can control its traffic according to the priority assigned by the PMA. The DF updates the priority information whenever the network status changes. Figure 2-b) shows the setup procedure. Table 1 shows the priority level of each type of service. The DF classifies the traffic according to the priority information. When the DF receives a service request message, it returns the current priority information. We can control congestion by using the second special agent, which is called the CCA. The CCA also uses priority information, just as the PMA does. However, the CCA verifies the priority information by periodically sending a check messages. Thus, applications (e.g., ftp, telnet, multimedia, etc.) can adjust their sending rate accordingly. By means of these two agents, we can adjust the data rate at the local system (e.g., PC, PDA, and Notebook, etc) whenever the network traffic is changed. Moreover, the network traffic can be classified using the information in the gateway. Thus, the priority is not fixed but adjustable according to the network environment.

### 3 Simulations

This section presents the performance results of the priority-based service discovery (PSD) mechanism. We simulate our mechanism with/without an infrastructure (e.g., AP, gateway).

#### 3.1 Simulation with Infrastructure

We simulate these mechanisms using a simple dumbbell network model in a wired network. The gateway has ten traffic sources and the nodes, which are attached to the gateway, are wireless nodes. These wireless nodes do not move in our simulation. In Link2, we test both the droptail queuing mechanism and the proposed priority-based

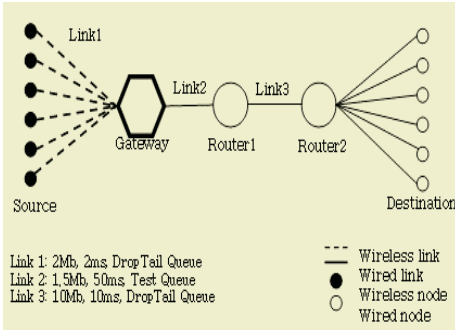


Fig. 3. Network Topology

Table 1. Priority Level

Services	priority
Service advertisements	1
Service requests	2
Event messages	3
Voice traffic	4
Multimedia	5
E-commerce	6
Light data traffic	7
Bulk data traffic	8

queuing mechanism. Figure 3 depicts the network topology. Using the NS simulator [2], a simulation was conducted in order to determine to what extent the proposed scheme improves the time-limited traffic as compared to the conventional mechanisms (droptail queue in this paper). We use TCP traffics for both the light and bulk data traffic. Each TCP flow uses an FTP application. We change the maximum congestion window size of each TCP flow according to its priority. High priority traffic is either CBR or EXP traffic. Figure 4 shows the simulation results. Even if the number of traffic sources increases, the CBR traffic using PSD does not slow down, whereas the CBR traffic with the droptail queuing mechanism does. Moreover, the TCP traffic with PSD shows the almost the same result as that with the droptail mechanism, which implies that the proposed scheme improves the performance of time-limited traffic without affecting the TCP traffic.

### 3.2 Simulation in Ad-Hoc Network

We modify the DFS[3] mechanism using the priority information. The DFS protocol for WLANs allocates bandwidth to flows in proportion to their weights and accounts for variable packet sizes. The DFS schedules packets for transmission based on their eligibility. Because of the distributed nature of the DFS protocol, collisions may occur, which causes priority reversal and undermine the fairness. Although DFS provides fairness and better throughput, the backoff interval is directly proportional to the *Packet-length/Weight* ratio in the linear scheme of DFS. For this reason, we use the priority-based backoff algorithm in enhanced DFS[4]. The scenario and parameters used in this paper are identical to those used in DFS. We perform simulations based on the implementation described in [3]. The channel bandwidth is set to 2Mbps. The simulation environment consists of n nodes. All of the nodes are stationary and are in transmission range of each other, in order to simulate a broadcast LAN. The number of nodes is always even. In this paper, identical flows refer to flows that are always backlogged and have equal packet size. Figure 5 shows the throughput results for the PSD, DFS and DCF mechanisms. We note that PSD not only guarantees fairness but also improves the throughput of time-limited traffics.

## 4 Conclusions

With the increasing number of people using mobile devices such as PDAs, cell-phones, notebooks, etc., the need to connect them to the Internet for ubiquitous sharing and data access is increasing. An efficient service discovery infrastructure plays an important role in such a dynamic environment. We reviewed a number of existing service discovery frameworks and found that they all suffer from one common problem, namely, a lack of QoS-based service discovery. In this paper, we introduced an agent platform designed to support QoS management. The simulation results show that the proposed mechanism improves the performance of time-limited traffic, without affecting that of other traffic, and guarantees fairness in an ad-hoc network.

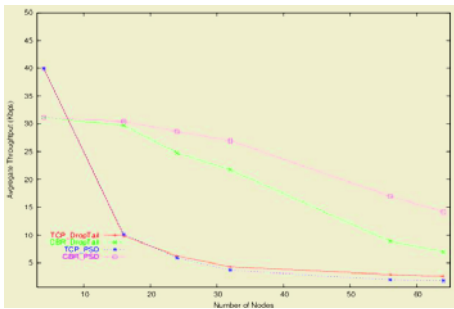


**Fig. 4.** Aggregated throughput in wired network

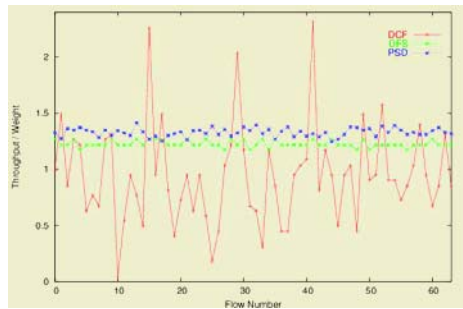


**Fig. 5.** Throughput of 64 flows in wireless network

## References

1. FIPA: Agent Management Specification, Dec. 2002.
2. K. Fall and K. Varadhan, "ns Notes and documentation", tech. rep., VINT Project, UC-Berkeley and LBNL(2003)
3. N. H. Vaidya, P. Bahl, and S. Gupta, "Distributed Fair Scheduling in a Wireless LAN", In Proc. Of ACM MOBICOM2000, Boston, MA USA(200) 167–178
4. K.H Choi, H.J. Shin and Dong-Ryeol Shin, "Delay and Collision Reduction Mechanism for Distributed Fair Scheduling in Wireless LANs", ICCSA, May, 2004.



# A Quick Generation Method of Sequence Pair for Block Placement

Mingxu Huo and Koubao Ding

Dept. of Information and Electronic Engineering, Zhejiang University,  
Hangzhou 310027, P.R. China  
{huomingxu, dingkb}@zju.edu.cn

**Abstract.** Sequence Pair (SP) is an elegant representation for the block placement of IC Design, and it is usually imperative to generate the SP from an existing placement. A quick generation method and one concise algorithm are proposed instead of the original unfeasible one. It is also shown that if the relations of any two blocks are either vertical or horizontal, the solution space size of a representation is  $(n!)^2$  if it is P\*-admissible. The analytical and experimental results of the algorithm both show its superiority in running time.

## 1 Introduction

With the rapid increase of IC complexity, floorplanning and block placement become more important, where floorplanning can be regarded as placement with soft module blocks. Most of such complex combinatorial optimization problems are NP-Hard [1], and therefore heuristic approaches such as Simulated Annealing algorithms are widely used to generate good layouts. The representation of geometrical topological relations of blocks is one of the crucial factors in evaluating values of the cost functions. Without some additional procedures, most representations proposed in the literature usually cannot include optimal solution, while Sequence Pair (SP) [1], BSG [2], TCG [3] and TCG-S [4] etc are P\*-admissible representations [1, 4] that can represent the most general floorplans and contain a complete structure for searching an optimal solution. The original method to generate SP is named Gridding [1], which is too complicated to be implemented. However, it is imperative to find an effective and efficient approach to generate SP from arbitrary existing placement.

## 2 Generation Method

The topological relations of any two non-overlap module blocks are horizontal and vertical, i.e., left to, right to, above and below [5]. Diagonal relations also exist, but they can be simply degenerated by preferring horizontal relations to vertical ones, or by adopting the relation definitions in [3]. An HV-Relation-Set (HVRS) for a set of blocks is a set of horizontal or vertical relations for all block pairs [6], and a Feasible-HVRS involves all the block relations excluding the non-realizable ones.

A Sequence Pair (SP) is an ordered pair of sequences  $\Gamma_+$  and  $\Gamma_-$ , each of which is a sequence of  $n$  block names [1], e.g., in Fig. 1 is one of the possible placements of the

apte circuit from MCNC benchmark<sup>1</sup> circuits, the SP from which is  $(\Gamma_+, \Gamma_-) = (670185423, 120634785)$ . A sequence pair corresponds to a Feasible-HVRS.

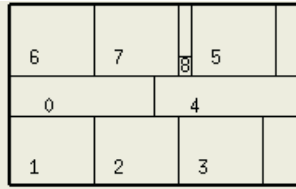


**Fig. 1.** A placement of the apte MCNC benchmark circuit. Its SP is (670185423, 120634785)

A generation plane is an infinite plane with numerous different positions. All blocks are treated as symbol points, each of which will be embedded in one unique position in the generation plane according to the Feasible-HVRS, and each embedded symbol point introduces two slope lines crossing at the symbol point, as in Fig. 2(a). The totality of all the slope lines introduced by embedded symbol points is an oblique grid, which divide the generation plane into different positions (Fig. 2(b)).

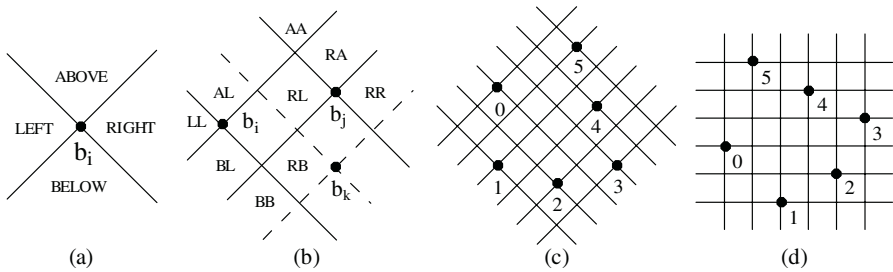


**Fig. 2.** The generation plane. (a) divided into 4 positions by  $b_i$  (b) 9 positions by  $b_i$  and  $b_j$ , 16 positions after  $b_k$  embedded (c) oblique grid after 6 symbols embedded (d) after rotated by  $-45$  degree. The SP of these six blocks is (051423,120345)

Take an arbitrary order of the  $n$  blocks, and then embed them orderly. For blocks  $b_i$  and  $b_j$ ,  $b_j$  must be embedded in one of the 4 unique positions according to  $b_i$ , named: LEFT, BELOW, RIGHT and ABOVE (Fig. 2(a)), to satisfy their relation. Blocks must satisfy their relations with all embedded ones by locating at a proper position.

When all blocks are embedded, there will be  $2n$  lines and  $n^2$  intersection points. The  $n$  symbol points locate on  $n$  of  $n^2$  intersection points, and no two symbols locate on the same line simultaneously. Fig. 2(c) shows the generation plane after blocks 0 to 5 of Fig. 1 are embedded. As can be easily seen from Fig. 2(d), the sequences of the block names in column (on the vertical lines) and in row (on horizontal lines) are the  $\Gamma_+$  and  $\Gamma_-$  of the Sequence Pair to be generated, respectively.

<sup>1</sup> See: <http://www.cse.ucsc.edu/research/surf/GSRC/MCNCbench.html>

### 3 A Generation Algorithm

Make use of two linked list  $spx$  and  $spy$  to represent the  $\Gamma_+$  and  $\Gamma_-$  respectively, and generate  $spx$  and  $spy$  separately by inserting the block indices into the lists. The relations according to their Feasible-HVRS define the orders of two blocks in the lists respectively, and in either list,  $b_i$  is before  $b_k$  if  $b_i$  is before  $b_j$  and  $b_j$  is before  $b_k$ . The following program section illustrates the construction of  $spx$ .

Construction of list  $spx$  in C++ (the block indices are 0,1,2,...,n-1)

```
spx.push_back(0);           //insert the first block
for(i = 1; i < n; ++ i ) { //insert others orderly
for(posx = spx.begin(); posx != spx.end();++posx) {
j = *posx; r = relation(i,j); //check relations orderly
if(r == LEFT || r == ABOVE) { //found proper position
spx.insert(posx, i); break; // insert and stop check
} } }
spx.push_back(i);         // append to list end
}
```

### 4 Analytical and Experimental Results

The relation of every two given blocks has four possibilities. Without loss of generality, the block names to be embedded in sequence are assumed as 1, 2, 3, ... n. Before embedding the  $k^{th}$  block, every position introduced by the  $k-1$  embedded block symbols is different from others, providing the proper number of unique positions.

Let  $p_k$  denote the different ways for the  $k^{th}$  block to be embedded, which is evidently  $k^2$ . This generation process comprises the sequence to embed blocks one by one, so the total ways for the embedment of n blocks can be calculated by multiplying all  $p_k$ , and thus the solution space size of P\*-admissible representations is  $(n!)^2$ .

In general, it needs  $n(n-1)=O(n^2)$  time complexity to determine the Feasible-HVRS of n blocks. All the positions in the list can be assumed equiprobable, and thus the average comparison times for inserting the block  $b_{k+1}$  into a list with  $k$  blocks is:

$$C_{k+1} = \frac{1}{k+1} \sum_{i=0}^k i = \frac{k}{2} \quad (k = 0, 1, 2, \dots, n-1) \tag{1}$$

Replacing  $k + 1$  with  $k$ , let  $C_k$  denote the average comparison times for the  $k^{th}$  block, the total average comparison times  $C$  to sum up is in Eq. (2). Although its complexity is still  $O(n^2)$ ,  $C$  in Eq. (2) is only a quarter of the former  $n(n-1)$  running time.

$$C = \sum_{k=1}^n C_k = \sum_{k=1}^n \frac{k-1}{2} = \frac{1}{4} n(n-1) \tag{2}$$

Table 1 shows the running process of the algorithm to generate the  $spx$  from the placement in Fig. 1. The count of comparisons is 20, approximating to a quarter of  $n(n-1)=9*8=72$ . If complicated different data structures employed, it will be much faster.

**Table 1.** Run of the algorithm after block 0 inserted in list spx. A, B, L and R stand for relations between two blocks of Above, Below, Left to and Right to respectively

#	Comparisons	List	#	Comparisons	List
<b>1</b>	B0	0 1	<b>5</b>	R0, R1, A4	0 1 5 4 2 3
<b>2</b>	B0, R1,	0 1 2	<b>6</b>	A0	6 0 1 5 4 2 3
<b>3</b>	R0, R1, R2	0 1 2 3	<b>7</b>	R6, A0	6 7 0 1 5 4 2 3
<b>4</b>	R0, R1, A2	0 1 4 2 3	<b>8</b>	R6, R7, R0, R1, L5	6 7 0 1 8 5 4 2 3

Experiments on all the MCNC benchmarks are run repeatedly in comparison with the generation routine from Parquet [7] on running time. Our results save average 91.5% time. And the more complex the circuit is, the more time is saved.

## 5 Conclusion

In this paper, we introduce a new method to generate Sequence Pair, and show on the basis of the method that for any P\*-admissible placement representation if it takes for granted that every two blocks only have vertical and horizontal relations, the size of its solution space should be as large as  $(n!)^2$ . A quick generation algorithm is also proposed according to the method to reduce the running time. Analytical and experimental results of the algorithm both show its high performance.

## References

1. Murata, H., et al., Rectangle-packing-based module placement. 1995 IEEE/ACM ICCAD. Digest of Technical Papers, (1995): 472-479.
2. Nakatake, S., et al., Module packing based on the BSG-structure and IC layout applications. IEEE TCAD Of Integrated Circuits And Systems, (1998). 17(6): 519-530.
3. Jai-Ming, L. and C. Yao-Wen, TCG: a transitive closure graph-based representation for non-slicing floorplans. Proceedings of the 38th DAC, (2001): 764-769.
4. Lin, J.M. and Y.W. Chang, TCG-S: Orthogonal coupling of P\*-admissible representations for general floorplans, in 39th DAC, Proceedings. (2002). 842-847.
5. Onodera, H., Y. Taniguchi, and K. Tamaru, Branch-and-bound placement for building block layout. 28th ACM/IEEE DAC. Proceedings 1991, (1991): 433-439.
6. Murata, H., et al., A mapping from sequence-pair to rectangular dissection. Proceedings of the ASP-DAC '97. 1997, (1997): 625-633.
7. Adya, S.N. and I.L. Markov, Fixed-outline floorplanning through better local search. Proceedings 2001 IEEE ICCD: VLSI in Computers and Processors. 2001, (2001): 328-334.

# A Space-Efficient Algorithm for Pre-distributing Pairwise Keys in Sensor Networks<sup>\*</sup>

Taekyun Kim<sup>1</sup>, Sangjin Kim<sup>2</sup>, and Heekuck Oh<sup>1</sup>

<sup>1</sup> Department of Computer Science and Engineering, Hanyang University, Korea  
{tkkim, hkoh}@cse.hanyang.ac.kr

<sup>2</sup> School of Internet Media Engineering, Korea University of Technology and Education, Korea  
sangjin@kut.ac.kr

**Abstract.** We propose a space-efficient key pre-distribution scheme based on quasi-orthogonal finite projective plane. This approach, compared to the previous approaches, guarantees full connectivity and the uniqueness of pairwise keys. Moreover, the size of the key ring depends not on the size of the key pool, but on the size of the network. The actual order of the key ring size is only  $O(\sqrt{N})$ , where  $N$  is the size of the network. As a result, our approach provides better scalability than previous approaches.

## 1 Introduction

We are concerned with establishing pairwise symmetric keys for sensor nodes. These keys are required to provide authenticity of sensor nodes and secrecy of information exchanged between them. Current approach is to initialize each sensor node with some secret information before deployment [1, 2, 3]. After deployment, these sensor nodes perform a protocol with neighboring nodes to establish the required pairwise keys. Some systems [2] need bootstrapping to create the new pairwise keys, whereas the other systems [1, 3] pre-distribute randomly selected pairwise keys. Our method is different from the previous probabilistic methods [1, 3] in that we store keys in sensor nodes in a deterministic way.

## 2 The Proposed Approach

**Definition 1.** An *FPP (Finite Projective Plane)* is a geometrical system  $\mathcal{G}$   $(\mathcal{P}, \mathcal{L}, \mathcal{I})$  satisfying the following conditions, where  $\mathcal{P}$  is a finite set of points,  $\mathcal{L}$  is a finite set of lines, and  $\mathcal{I}$  is an incidence relation between  $\mathcal{P}$  and  $\mathcal{L}$ .

- For all points  $P, Q \in \mathcal{P}$  with  $P \neq Q$ , there exists a unique line  $l \in \mathcal{L}$  that passes through  $P$  and  $Q$ .
- There exist at least 3 points.
- For every line  $l \in \mathcal{L}$ , there exists a point not incident with  $l$ .
- Every line passes through at least 3 points.
- Every pair of distinct lines intersect.

---

<sup>\*</sup> This work was supported by the Ministry of Information and Communication, Korea, under the university HNRC-ITRC program supervised by the IITA.

$$\begin{array}{ll}
\{1, 2, 3\}\{1, 4, 5\}\{1, 6, 7\}\{2, 4, 6\} & \{1, 2, 3, 4\}\{1, 5, 6, 7\}\{1, 8, 9, 10\}\{1, 11, 12, 13\}\{2, 5, 10, 12\} \\
\{2, 5, 7\}\{3, 5, 6\}\{3, 4, 7\} & \{2, 6, 8, 13\}\{2, 7, 9, 11\}\{3, 5, 9, 13\}\{3, 6, 10, 11\}\{3, 7, 8, 12\} \\
\text{(a) order } n = 2 & \{4, 5, 8, 11\}\{4, 6, 9, 12\}\{4, 7, 10, 13\} \\
& \text{(b) order } n = 3
\end{array}$$

**Fig. 1.** Example of FPPs

$$\begin{array}{ll}
N_1 : \{K_1, K_2, K_3\} & N_4 : \{K_1, K_4, K_5\} & N_1 : \{K_1, K_2, K_3\}, \{K'_3, K'_4, K'_7\} & N_4 : \{K_1, K_4, K_5\}, \{K'_1, K'_2, K'_3\} \\
N_6 : \{K_1, K_6, K_7\} & N_2 : \{K_2, K_4, K_6\} & N_6 : \{K_1, K_6, K_7\}, \{K'_1, K'_4, K'_5\} & N_2 : \{K_2, K_4, K_6\}, \{K'_1, K'_6, K'_7\} \\
N_5 : \{K_2, K_5, K_7\} & N_3 : \{K_3, K_5, K_6\} & N_5 : \{K_2, K_5, K_7\}, \{K'_2, K'_4, K'_6\} & N_3 : \{K_3, K_5, K_6\}, \{K'_2, K'_5, K'_7\} \\
N_7 : \{K_3, K_4, K_7\} & & N_7 : \{K_3, K_4, K_7\}, \{K'_3, K'_5, K'_6\} & \\
\text{(a) Using single FPP} & & \text{(b) Using two FPPs} & 
\end{array}$$

**Fig. 2.** Construction of key rings for each node using an FPP of order  $n = 2$ 

**Definition 2.** For any  $n \geq 2$ , if each line of an FPP is incident with exactly  $n + 1$  points, we call this FPP a *finite projective plane of order  $n$* .

If  $\mathcal{G}$  is an FPP of order  $n$ , then there are  $n^2 + n + 1$  points and lines in total. An FPP of order  $n$  does not exist for all  $n \geq 2$ . However, it is known that FPPs of order  $n = p^k$  exist, where  $p$  is a prime number and  $k$  is a positive integer. If we map points to numbers and lines to sets, a finite projective plane of order  $n$  can be shown as Fig. 1. There are many FPPs for a given order. Each FPP in Fig. 1 is just one of them.

In our method, the lines of an FPP is mapped to sensor nodes and points on a line to the key ring assigned to the corresponding node. For example, Fig 2.(a) shows the key ring assigned to each node when we use a single FPP of order  $n = 2$ . We denote  $N_i$  as a sensor node ID, and  $K_i$  as a symmetric key. In this case, the maximum number of nodes we can deploy is  $N = n^2 + n + 1$  and the size of key ring in each node is  $K = n + 1$ . The relationship between  $N$  and  $K$  is  $N = K(K - 1) + 1$ . Since every pair of distinct lines intersect in an FPP, each pair of node is guaranteed to have a single common key in their respective key rings. However, if we use this common key as the pairwise key, all pairwise keys are not unique. For example, the pairwise key of pairs  $(N_1, N_4)$ ,  $(N_1, N_6)$ ,  $(N_4, N_6)$  are all the same.

To make pairwise keys unique, we use another FPP as shown in Fig 2.(b). Since we used two FPPs, each pair of nodes have a pair of common keys. For example,  $N_1$  and  $N_4$  shares  $K_1$  and  $K'_3$ . We use  $h(K_1 || K'_3)$  as the pairwise key between  $N_1$  and  $N_4$ , where  $h$  is collision-resistant hash function from  $\{0, 1\}^*$  to  $\{0, 1\}^k$ , where  $k$  is the key length in bits. However, if we randomly assign the second FPP without any constraint, we may still get pairs that uses the same pairwise keys. For example, in Fig 2.(b),  $N_3$ ,  $N_4$ , and  $N_5$  all have  $K_5$  and  $K'_2$  in common. This problem occurs if and only if a triple of nodes that share a common key in the first FPP also share a common key in the second FPP. This problem is independent of the order of FPP used. That is, the problem occurs if this condition holds without regard to the order of FPP used.

To remedy this problem, we interchange the nodes and keys in the FPP. Since FPP satisfies the principle of duality, the resulting plane is also an FPP. We interchange them because we are not concerned with what specific keys are in each node's key ring but with the combinations of nodes that share a common key. Fig 3.(a) shows

an interchanged FPP of Fig 2.(a). To the right of the FPP, we show the combinations of nodes that share the same key. To make each pairwise keys unique, no two combinations appearing on the same row in the first FPP must not also appear on any row in the second FPP. The FPP of Fig 3.(b) satisfies this condition. We say that FPP of Fig 3.(a) and Fig 3.(b) are quasi-orthogonal to each other. More formally, quasi-orthogonality of FPP is defined as below.

$\{N_1, N_4, N_6\} : (1, 4), (1, 6), (4, 6)$	$\{N_1, N_2, N_4\} : (1, 2), (1, 4), (2, 4)$
$\{N_1, N_2, N_5\} : (1, 2), (1, 5), (2, 5)$	$\{N_1, N_3, N_6\} : (1, 3), (1, 6), (3, 6)$
$\{N_1, N_3, N_7\} : (1, 3), (1, 7), (3, 7)$	$\{N_3, N_4, N_7\} : (3, 4), (3, 7), (4, 7)$
$\{N_2, N_4, N_7\} : (2, 4), (2, 7), (4, 7)$	$\{N_2, N_3, N_5\} : (2, 3), (2, 5), (3, 5)$
$\{N_3, N_4, N_5\} : (3, 4), (3, 5), (4, 5)$	$\{N_4, N_5, N_6\} : (4, 5), (4, 6), (5, 6)$
$\{N_2, N_3, N_6\} : (2, 3), (2, 6), (3, 6)$	$\{N_1, N_5, N_7\} : (1, 5), (1, 7), (5, 7)$
$\{N_5, N_6, N_7\} : (5, 6), (5, 7), (6, 7)$	$\{N_2, N_6, N_7\} : (2, 7), (2, 6), (6, 7)$
(a)	(b)

Fig. 3. Quasi-orthogonal FPPs of order  $n = 2$

**Definition 3.** Two FPPs  $\mathcal{G}_1 = (\mathcal{P}_1, \mathcal{L}_1, \mathcal{I}_1)$  and  $\mathcal{G}_2 = (\mathcal{P}_2, \mathcal{L}_2, \mathcal{I}_2)$  with the same order are **quasi-orthogonal** if the following conditions hold:

1.  $\mathcal{P}_1 \cap \mathcal{P}_2 = \emptyset$ ,
2. For every line  $l_1 \in \mathcal{L}_1$  and  $l_2 \in \mathcal{L}_2$ , there exist at most two points incident with both  $l_1$  and  $l_2$ .

Fig 4 shows two quasi-orthogonal FPPs of order  $n = 3$ .

$\{N_1, N_5, N_8, N_{11}\}, \{N_1, N_2, N_6, N_7\}$	$\{N_1, N_3, N_5, N_{12}\}, \{N_1, N_4, N_7, N_8\}$
$\{N_1, N_3, N_9, N_{10}\}, \{N_1, N_4, N_{12}, N_{13}\}$	$\{N_1, N_6, N_{10}, N_{11}\}, \{N_1, N_2, N_9, N_{13}\}$
$\{N_2, N_4, N_5, N_9\}, \{N_5, N_6, N_{10}, N_{12}\}$	$\{N_2, N_3, N_4, N_{10}\}, \{N_2, N_5, N_7, N_{11}\}$
$\{N_3, N_5, N_7, N_{13}\}, \{N_3, N_4, N_6, N_8\}$	$\{N_2, N_6, N_8, N_{12}\}, \{N_3, N_6, N_7, N_9\}$
$\{N_7, N_8, N_9, N_{12}\}, \{N_2, N_8, N_{10}, N_{13}\}$	$\{N_3, N_8, N_{11}, N_{13}\}, \{N_4, N_5, N_6, N_{13}\}$
$\{N_4, N_7, N_{10}, N_{11}\}, \{N_2, N_3, N_{11}, N_{12}\}$	$\{N_4, N_9, N_{11}, N_{12}\}, \{N_5, N_8, N_9, N_{10}\}$
$\{N_6, N_9, N_{11}, N_{13}\}$	$\{N_7, N_{10}, N_{12}, N_{13}\}$

Fig. 4. Quasi-orthogonal FPPs of order  $n = 3$

**Theorem 1.** Given two quasi-orthogonal FPPs of order  $n$ , there is a way to assign key rings to nodes in a network of size  $n^2 + n + 1$  or smaller, so that all of the pairwise keys are unique. Furthermore, the size of key ring in each node is  $2n + 2$ .

*Proof.* If we use two FPPs, uniqueness of pairwise keys are violated if and only if the followings are satisfied.

1. 3 nodes share a common key in the first FPP.
2. These 3 nodes also share a common key in the second FPP.

Since the quasi-orthogonality of FPPs guarantees that no three nodes share a common key in both FPPs, the argument is correct.

The followings are the steps used to construct key rings for sensor nodes of size  $N$ .

- i) **Step 1:** Construct an FPP of order  $n$   $p^k \geq \sqrt{N}$ , where  $p$  is prime and  $k$  is a positive integer. Given an FPP of order  $n$ , the maximum supportable network size is  $n^2 + n + 1$ . Therefore, if  $n \geq \sqrt{N}$ , the maximum supportable network size is larger than  $N$ . If we consider incremental addition, the number of nodes that will be deployed after initial deployment must be taken into consideration.
- ii) **Step 2:** Find a quasi-orthogonal FPP of the FPP constructed in step 1.
- iii) **Step 3:** Assign a key to each row of the two quasi-orthogonal FPPs. Since the assigned keys must be different from each other, the total number of keys used is  $2N - 2n^2 + 2n + 2$ .
- iv) **Step 4:** Find the dual FPPs by interchanging keys and nodes of the two quasi-orthogonal FPPs constructed in step 3.
- v) **Step 5:** Assign a pair of key rings to each node. Without loss of generality, this procedure can be done at random, i.e., the node ID is meaningless at this point. Furthermore, there is no restriction for making a pair of key rings as long as each ring is from the different dual FPPs. This allows us  $N!$  choices of assigning key ring pairs to nodes. From the principle of duality, the key ring size of each node is  $2K - 2n + 2$ .

This completes the proof. □

$$\begin{aligned}
 N_1 &: \{K_1, K_2, K_3, K_4\}, \{K'_1, K'_2, K'_3, K'_4\} & N_2 &: \{K_1, K_5, K_6, K_7\}, \{K'_1, K'_6, K'_{10}, K'_{12}\} \\
 N_8 &: \{K_1, K_8, K_9, K_{10}\}, \{K'_2, K'_7, K'_9, K'_{12}\} & N_{11} &: \{K_1, K_{11}, K_{12}, K_{13}\}, \{K'_3, K'_6, K'_9, K'_{11}\} \\
 N_2 &: \{K_2, K_5, K_{10}, K_{12}\}, \{K'_4, K'_5, K'_6, K'_7\} & N_6 &: \{K_2, K_6, K_8, K_{13}\}, \{K'_3, K'_7, K'_8, K'_{10}\} \\
 N_7 &: \{K_2, K_7, K_9, K_{11}\}, \{K'_2, K'_6, K'_8, K'_{13}\} & N_9 &: \{K_3, K_5, K_9, K_{13}\}, \{K'_4, K'_8, K'_{11}, K'_{12}\} \\
 N_{10} &: \{K_3, K_6, K_{10}, K_{11}\}, \{K'_3, K'_5, K'_{12}, K'_{13}\} & N_3 &: \{K_3, K_7, K_8, K_{12}\}, \{K'_1, K'_5, K'_8, K'_9\} \\
 N_4 &: \{K_4, K_5, K_8, K_{11}\}, \{K'_2, K'_5, K'_{10}, K'_{11}\} & N_{12} &: \{K_4, K_6, K_9, K_{12}\}, \{K'_1, K'_7, K'_{11}, K'_{13}\} \\
 N_{13} &: \{K_4, K_7, K_{10}, K_{13}\}, \{K'_4, K'_9, K'_{10}, K'_{13}\}
 \end{aligned}$$

Fig. 5. Key rings allocated to each node when using two FPPs of order  $n = 3$

Fig 5 shows key rings assigned to each node when using two quasi-orthogonal FPPs depicted in Fig 4. Here, we assumed that first set of nodes  $\{N_1, N_3, N_5, N_{12}\}$  share  $K'_1$ , the second set of nodes  $\{N_1, N_4, N_7, N_8\}$  share  $K'_2$  and so on. However, the order of assigning keys to second FPP is irrelevant and does affect the uniqueness of pairwise keys. The size of key ring assigned to each node is  $2K \approx 2\sqrt{N}$ .

### 3 Conclusion

In this paper, we have shown that it is possible to deterministically construct a key ring for sensor nodes having following characteristics: (i) it guarantees fully direct



connectivity, (ii) it guarantees uniqueness of pairwise keys, (iii) the size of the key ring stored at each node depends on the size of the network, whereas previous approach depends on the size of the key pool, (iv) the order of the key ring stored at each node is  $O(\sqrt{N})$ , where  $N$  is the size of the network.

## References

1. Chan, H., Perrig, A., Song, D.: Random Key Predistribution Schemes for Sensor Networks. Proc. of the IEEE Symp. on Security and Privacy, IEEE Press (2003) 197–215
2. Deng, J., Han, R., Mishra, S.: Security Support For In-Network Processing in Wireless Sensor Networks. Proc. of the 1st ACM Workshop on the Security of Ad Hoc and Sensor Networks, ACM Press (2003), 83–93
3. Eschenauer, L., Gligor, V.D.: A Key-Management Scheme for Distributed Sensor Networks. Proc. of the 9th ACM Conference on Computer and Communications Security, ACM Press (2002), 41–47

# An Architecture for Lightweight Service Discovery Protocol in MANET\*

Byong-In Lim, Kee-Hyun Choi, and Dong-Ryeol Shin

School of Information and Communication Engineering,  
Sungkyunkwan University  
440-746, Suwon, Korea, +82-31-290-7125  
{lbi77, gyunee, drshin}@ece.skku.ac.kr

**Abstract.** As the number of Internet services grows, it is becoming more important for the network users to be able to locate and utilize those services that are of interest to them. As a result, a service discovery protocols are coming to play an increasingly important role in highly dynamic networks. In this paper, we describe a new architecture for service discovery called LSD (Lightweight Service Discovery). The LSD is a peer-to-peer cache-based service discovery protocol for ad hoc environments. Through the LSD protocol, small handheld mobile devices with wireless connectivity can detect each other in their neighboring devices, and perceive whether particular shared services are available or not. In addition, the LSD solves the overhead problems which arise when traditional discovery protocols are applied to mobile ad hoc networks.

## 1 Introduction

As the number of Internet services grows, service discovery protocols are coming to play an increasingly important role in highly dynamic networks. Consequently, a number of service discovery protocols have been proposed for wired networks. Prominent among these [1] are the SLP, Salutation, UPnP and UDDI. These conventional approaches to service discovery protocols can be classified into two main categories. These systems were mostly designed for an administrated network context and are either based on mediator based discovery approaches (e.g. UDDI, Jini) or on maintaining a network-wide multicast tree based on direct or peer-to-peer discovery approaches (e.g. UPnP, Salutation, SLP, when operated without directory agents). In ad hoc networks, the provision for service discovery is mandatory since they are designed for irregular and unexpected changes in network topology. In a service discovery environment, basic services that are readily available like discovery and delivery in wired networks have to be re-designed in order to take into account the wireless network's properties. Furthermore, whenever the consumer rearranges the components in such a system, the system must automatically adapt its configuration as necessary. In order to satisfy these diverse requirements, we designed a modified framework based on the existing service discovery algorithms [2, 3] and

---

\* This research was partially supported by a grant from the CUCN, Korea and Korea Science & Engineering Foundation (R01-2004-000-10755-0).

implemented a lightweight service discovery protocol suitable for ad-hoc environments.

The remainder of the paper is organized as follows. Section 2 discusses the LSD Architecture. Service Propagation Algorithm is described in section 3. Finally, this paper is concluded in section 4.

## 2 Design of LSD Architecture

Figure 1 shows the LSD (Lightweight Service Discovery) architecture and corresponding components in a single mobile device.

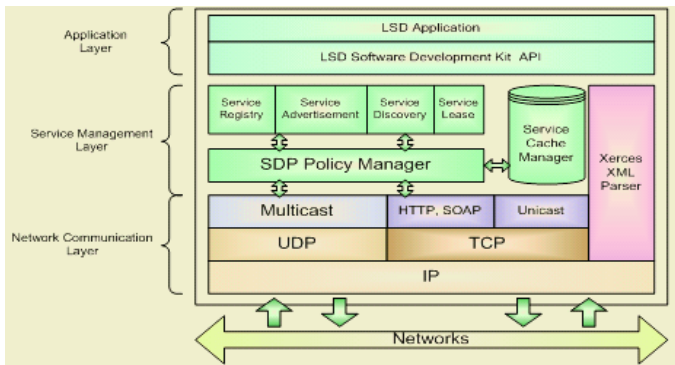


Fig. 1. LSD System Architecture

In Figure 1, the LSD consists of three layers: the application layer, the service management layer, and the network communication layer. The application layer provides the user with applications such as audio-video players and printing applications. The service management layer provides services associated with discovery. In the service management layer, we use a cache manager that registers information about the services offered by peers in the network. All of the devices in the network should listen to all advertisement messages, known as delta messages and save them in their local caches for a given period of time. When a user wants to find a particular service, they begin by searching for the service in their local caches at first. If no information is available locally, the user sends a request message through multicasting. The SDP Policy Manager in the layer is responsible for enforcing policies designed to control platform behavior. These policies are registered with the SDP Policy Manager which is responsible for ensuring that all components of the platform are in compliance with the specified policies. These policies can specify caching preferences such as the refresh rate or replacement strategy or describe advertisement preferences such as the frequency or time-to-live, etc. The network communication layer is associated with two protocols. The first is UDP which is used for multicasting; the second is TCP which is used unicasting. We send advertise/request messages by using UDP, and retrieve the data using http or soap based on TCP.

### 3 Service Propagation Algorithm of LSD

The LSD pays attention to an efficient service discovery to exploit the nature of highly dynamic ad-hoc networks. Based on the Konark [3], it has developed a new algorithm which attempts to balance the convergence time and network bandwidth. The key difference between Gossip-Konark and LSD is service data structure and the convergence algorithm involved in joining a network. The Gossip-Konark has a structure of tree-based hierarchal services. On the other hand, the LSD has a structure of flat services that have a difference in patterns and message procedures of Query, Advertisement. Moreover, the LSD uses a dummy advertisement messages. When a node joins to new network, if it has no local service, it sends the dummy advertisement message. When a node receives a service message, it sends the difference between its relevant services and service information in the received service messages, called a delta message. Thus network overload is reduced. It also avoids the storm of concurrent multicasts by randomly assigning the multicast time interval. When a node receives the advertisement message, the LSD prevents multicast storm problem using RNDWAIT time similar to the Konark. Moreover, if the node which receives the service message verifies that its service registry has the same information as that in the received service message, it then remains silent and no multicasts occur. Figure 2 shows the message transmission procedure for the LSD. The incremental discovery procedure is able to reduce network traffic for service discovery due to delta messages.

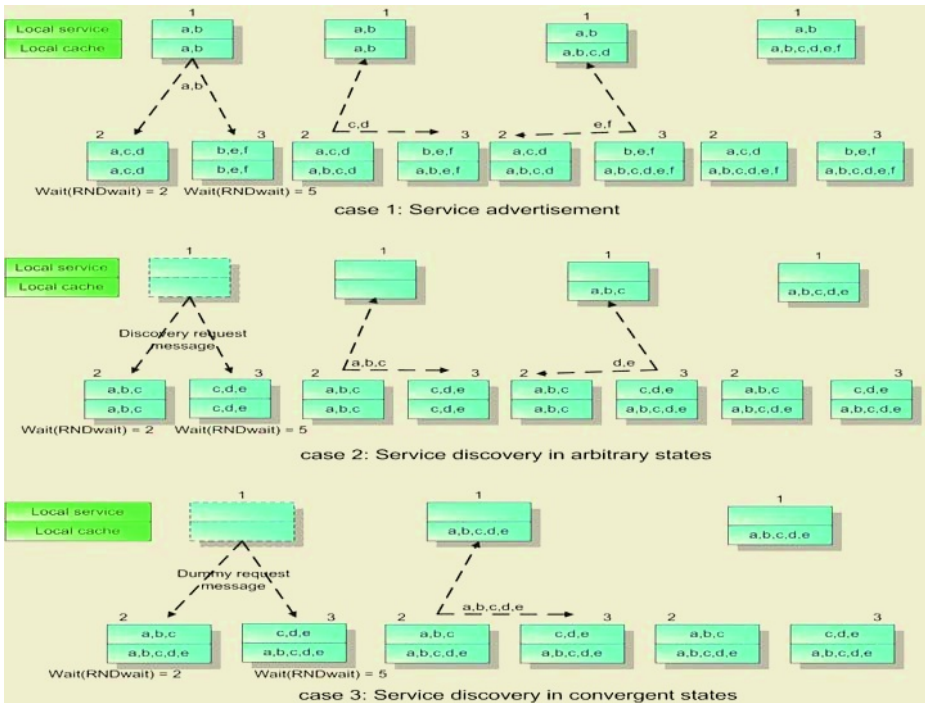


Fig. 2. Service Propagation Algorithm in LSD

Suppose that an ad-hoc network of interest consists of three nodes: node 1, node 2, and node 3. Assume that node 2 and node 3 have random waiting times (RNDWAIT) of 2 and 5 seconds, respectively. We have three cases according to the different situations as illustrated in Figure 2.

Case 1: service advertisement

- (a) Node 1 sends its own service advertisement message to other nodes using the multicast. At this time, node 2 can send delta message based on the advertisement earlier than node 3, because node 2 has RNDWAIT=2, whereas node 3 has RNDWAIT=5.
- (b) Listening to advertisement and delta messages from other nodes, node 3 sends service e, f to other nodes, because node 3 already receives services a, b, c, d.

Case 2: service discovery in arbitrary states, i.e., non-convergent states

- (a) When node 1 joins to a new network, node 1 sends out a dummy request messages to other nodes. From these messages, node 2 multicasts a delta message ahead of other nodes, for the same reason as the case 1.
- (b) Node 3 makes a delta message based on the request and then sends it to other nodes, which results in fast discovery.

Case 3: service discovery in convergent states (where all nodes know the service information within the network)

- (a) When node 1 joins to a new network in convergent state, node 1 sends out a dummy request message to other nodes. Then node 2 can send delta message earlier than other nodes as illustrated as in case 1 and case 2.
- (b) Since the network already reaches the convergence of service information, the number of multicasts and resulting traffic load is reduced. One dummy request message is enough to reach the convergent state.

## 4 Conclusion

Unfortunately existing approaches to service trading are not well suited for these highly dynamic topologies since they rely on centralized servers and have high communication costs due to periodic query flooding. In this paper, we proposed a novel scheme to correct and optimize discovery protocol in case of ad-hoc environments. Currently we are performing a simulation and doing a comprehensive performance test for our prototyped system.

## References

1. F. Zhu, M. Mutka, and L. Ni, "Classification of Service Discovery in Pervasive Computing Environments," Michigan State University, East Lansing, available at <http://www.cse.msu.edu/~zhufeng/ServiceDiscoverySurvey.pdf> MSU-CSE-02-24.
2. M. Nidd, "Service discovery in DEAPspace," IEEE Pers. Commun., vol.8, pp. 39–45, Aug. 2001.
3. C. Lee, A. Helal, N. Desai, V. Verma, B. Arslan, "Konark: A System and Protocols for Device Independent, Peer-to-Peer Discovery and Delivery of Mobile Services," IEEE System. Man. Cybernetic., vol. 33, no. 6, pp. 682-696, Nov. 2003

# An Enhanced Location Management Scheme for Hierarchical Mobile IPv6 Networks

U. G. U.

Dept. of Computer Science & Engineering Korea University,  
1,5-Ga, Anam-Dong, SungBuk-Gu, Seoul 136-701, South Korea  
kainos@disys.korea.ac.kr

**Abstract.** In this paper, we propose an enhanced location management scheme for minimizing signaling costs in hierarchical Mobile IPv6 (HMIPv6) networks. If the mobile node's mobility is not local, in our proposal, the mobile node sends location update messages to correspondent nodes in the same way as Mobile IPv6 (MIPv6). After the creation of a spatial locality of the mobile node's movement, the mobile node sends location update messages to the correspondent nodes in same way as HMIPv6. Therefore, our proposal can reduce signaling costs in terms of packet transmission delays in HMIPv6 networks. Therefore, our proposal offers considerable performance advantages to MIPv6 and HMIPv6.

## 1 Introduction

Mobile IPv6 (MIPv6) provides an efficient and scalable mechanism for host mobility. However, the frequent location updates of a mobile node cause network congestion. In hierarchical Mobile IPv6 (HMIPv6), the mobile node sends location update messages to correspondent nodes in the same way as MIPv6. After the creation of a spatial locality of the mobile node's movement, the mobile node sends location update messages to the correspondent nodes in same way as HMIPv6. Therefore, our proposal can reduce signaling costs in terms of packet transmission delays in HMIPv6 networks. Therefore, our proposal offers considerable performance advantages to MIPv6 and HMIPv6.

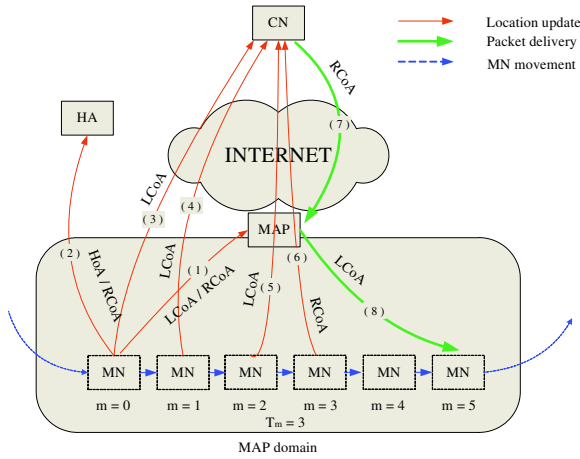


Fig. 1. The System Model for the Proposed Scheme in HMIPv6 Networks

Care of address (CoA), or Registered CoA (RCoA), based on the geographic location characteristics of the nodes. We define  $m$  and  $T_m$  as the number of sub-encryptions and the value of the movement threshold, respectively. If  $m$  is less than  $T_m$  (i.e.,  $m < T_m$ ), the node sends a message to the CN through the RCoA. Otherwise, if  $m$  is greater than or equal to  $T_m$ , the node sends a message to the CN through the RCoA. Hereafter, the CoA and RCoA refer to the current geographic location characteristics of the nodes.

The rest of the paper is organized as follows. Section 2 describes the proposed procedure for location update and packet delivery using the enhanced mobility management scheme called HMIPv6. The simulation results are presented in Section 3.

## 2 Protocol Description

This section describes the location update and packet delivery procedure.

### 2.1 Location Update Procedure

In our network, each node has two addresses, a RCoA and a CoA. Each node has a value of  $m$  and  $T_m$ . Here,  $m$  is the number of sub-encryptions that the node has done, and  $T_m$  is the threshold value which decides whether the node sends a message to the CN through the CoA or the RCoA. Hereafter, we refer to the value of  $m$  as the movement threshold.  $T_m$  can be adjusted based on the user's mobility pattern and current traffic load.

Figure 2 presents the procedure for location update based on the message. The procedures for location update are as follows:

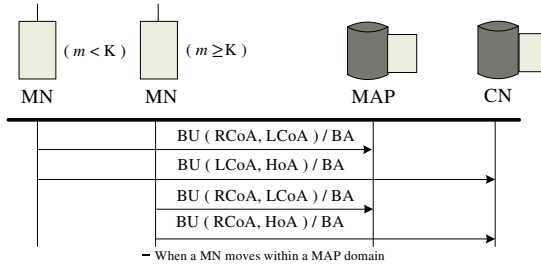


Fig. 2. The Proposed Location Update Procedure

- If a mobile node enters a domain, then
  - 1) the node registers with the CoA and sends a message and sets the value of  $m$  to zero.

- Otherwise, if a mobile node enters the same domain, then
  - 1) the node gets a new CoA.
  - 2) the node registers with the CoA and sends a message. After registration with the CoA, the node compares the value of  $m$  with  $T_m$ .

**Case 1** If the value of  $m$  is less than  $T_m$ , then

- 1) the node sends a  $BU_{[HoA, LCoA]}^1$  message to the CoA.

**Case 2** Otherwise, if the value of  $m$  is greater than or equal to  $T_m$ , then

- 2) the node sends a  $BU_{[HoA, RCoA]}^2$  message to the CoA. After the sending of the  $BU_{[HoA, RCoA]}$  message, the node sends a registration message to the CoA before returning to the domain.

As a result, the node performs registration with the CoA using a RC. For a CoA, depending on its mobility pattern.

## 2.2 Packet Delivery Procedure

The figure presents the procedure for packet delivery. For our proposed scheme, the packet delivery procedure is exactly the same as that of the previous scheme. The CoA decides to send packets either to the CoA or to the CoA if the CoA has a binding cache entry for a CoA. If the CoA has a binding cache entry, it sends packets directly to the CoA. Thus, the proposed scheme can achieve optimal routing, the same as the previous scheme. Otherwise, if a CoA has a RC,

<sup>1</sup> BU with the binding between the MN's HoA and LCoA.

<sup>2</sup> BU with the binding between the MN's HoA and RCoA.



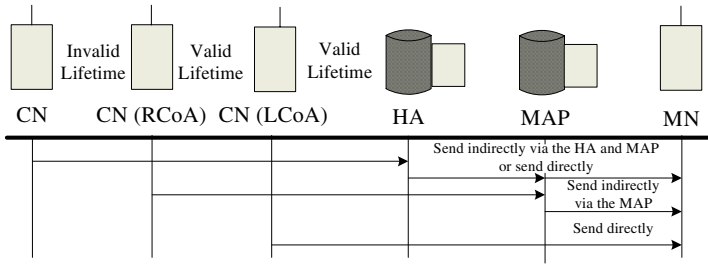


Fig. 3. The Proposed Packet Delivery Procedure

If the source node's binding cache entry must send the packets to the first usable RCoA, then the source node encapsulates and forwards them directly to the first usable RCoA. If the source node's binding cache for the destination sends the packets to the home network, then the source intercepts and tunnels them to the usable RCoA or RCoA.

### 3 Conclusions

In this paper, we proposed an enhanced location management scheme for mobile nodes using a RCoA. Here, the source node encapsulates and forwards them directly to the first usable RCoA. If the source node's binding cache for the destination sends the packets to the home network, then the source intercepts and tunnels them to the usable RCoA or RCoA.

In this paper, we proposed an enhanced location management scheme for mobile nodes using a RCoA. Here, the source node encapsulates and forwards them directly to the first usable RCoA. If the source node's binding cache for the destination sends the packets to the home network, then the source intercepts and tunnels them to the usable RCoA or RCoA.

### References

1. D. B. Johnson, C. E. Perkins, and J. Arkko, "Mobility support in IPv6," IETF Request for Comments 3775, June 2004.
2. H. Soliman, C. Castelluccia, K. El-Malki, and L. Bellier, "Hierarchical Mobile IPv6 mobility management (HMIPv6)," IETF Internet draft, draft-ietf-mipshop-hmipv6-02.txt (work in progress), June 2004.

# A Genetic Machine Learning Algorithm for Load Balancing in Cluster Configurations

Department of Informatics and Statistics,  
Federal University of Santa Catarina,  
88040-900 Florianopolis Brazil  
{mario, arpinto}@inf.ufsc.br

**Abstract.** Cluster configurations are a cost effective scenarios which are becoming common options to enhance several classes of applications in many organizations. In this article, we present a research work to enhance the load balancing, on dedicated and non-dedicated cluster configurations, based on a genetic machine learning algorithm. Classifier systems are learning machine algorithms, based on high adaptable genetic algorithms. We developed a software package which was designed to test the proposed scheme in a master-slave Cow and Now environment. Experimental results, from two different operating systems, indicate the enhanced capability of our load balancing approach to adapt in cluster configurations.

## 1 Introduction

... ( ) ... ( ) ...

## 2 Scheduling and Load Balancing in Parallel and Distributed Systems

... ( ) ... *on time* ... *assignment scheduling* ( )

## 3 Genetic Algorithms and Classifier Systems

... ( ) ... ( )

<... ..> .. <... ..>

### 4 Proposed Environment

*<if a grow occurs or a decrement> + <variation rate of average response time> <if the threshold should be incremented or decremented> + <threshold rate variation>*

### 5 Experimental Results

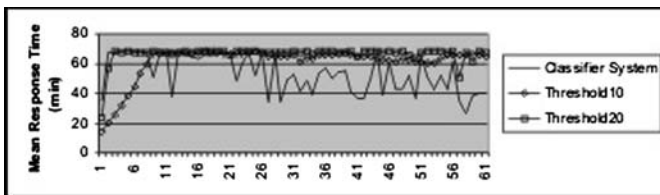


Fig. 1. Second experimental results

## 6 Conclusion and Future Work

## References

1. Benoit Ligneris, Stephen Scott, Thomas Naughton, Neil Gorsuch, Open Source Cluster Application Resource (OSCAR): Design, Implementation and interest for the [Computer] Scientific Community, First OSCAR Symposium, Sherbrooke May 11-14, Canada, 2003.
2. Zhang, W. (April, 2004) "Linux Virtual Server for Scalable Network Services", Available online: <http://www.linuxvirtualserver.org/docs/scheduling.html>.
3. Dantas, M.A.R. and Zaluska, E.J., Efficient Scheduling of MPI Applications on Networks of Workstations, FGCS Journal, V 13, pp. 489-499, 1998.
4. Casavant T.H. and Khul J.G., "A Taxonomy of Scheduling in General-Purpose Distributed Computing Systems", IEEE Trans. On Software Eng., vol. 14, no. 2, pp. 141-154, Feb. 1988.
5. Zhou S., "A Trace-driven Simulation Study of Dynamic Load Balancing", IEEE Trans. On Software Eng., vol. 14, no. 9, pp. 1327-1341, sep. 1988.
6. Dantas, M.A.R., Queiroz W.J. and Pfitscher G.H., "An Efficient Threshold Approach on Distributed Workstation Clusters", in HPC in Simulation, pp. 313-317, Washington, USA, 2000.
7. Papadimitriou, C. and Steiglitz, K., Combinatorial Optimization: Algorithms and Complexity, Dover Publications, 1998.
8. Goldberg, D.E., "Genetic Algorithm in Search, Optimization, and Machine Learning", Addison-Wesley, 1989.
9. Powell, M.L. and Miller, B.P., "Process migration in DEMOS/MP", in Proc. 9th ACM Symp. Operat. Syst. Principles, 1983, pp.110-119.

# A Parallel Algorithm for Computing Shortest Paths in Large-Scale Networks\*

Gu zhe   a   a   d   a   hu   .   g

Department of Computer Science, Dalian University of Technology,  
Dalian, 116023, P.R. China  
gztan@dlut.edu.cn

**Abstract.** This paper presents the Optimality Theorem in distributed parallel environment. Based on this theorem, a parallel algorithm using network-tree model is presented to compute shortest paths in large-scale networks. The correctness of this algorithm is proved theoretically and a series of computational test problems are performed on PC cluster. Factors such as network size and level of the network, which take effect on the performance, are discussed in detail. Results of the experiments show that the proposed parallel algorithm is efficient in computing shortest paths in large-scale networks, especially when the network size is great.

## 1 Introduction

In recent research, interest in large-scale networks has been focused on parallel computing the network and constructing the network model. The previous contributions are the edge graph model [2], the hierarchical E-cubed path (E<sup>3</sup>) model [4] and the network reduction (NR) [5]. These models all have some defects: the network reduction can be constructed from arbitrary network, and the route optimization can be constrained through a few sub-networks, which greatly reduce the search scope and significantly improve the computing efficiency.

In this paper, we present a parallel algorithm based on network tree model. This is the problem and test for a series of networks. The experimental results indicate that the parallel algorithm achieves high performance, speedup and efficiency.

## 2 Network-Tree Model

Network reduction is the definition of a combination of network and tree. Network can be divided into a number of sub-networks, and each sub-network can be constructed to be a network tree. We use macro definition to define the network tree to distinguish from the definition of network.

---

\* This work is supported by the National Science Foundation of China(60373094).

et  $\text{rk } \bar{r} \in \text{de}(\bar{r})$  a g.e. et  $\text{rk } N_r$  et the et  $\text{rk}$  tree be  $N\_Tree(T, H)$ , here  $T$  s the macr. . . de set f  $N$  f . . . e macr. . . de e sts  $T, H, \phi$ , ther se,  $H$  s a b. ar re at. . . defi ed  $T$  here s . . . e macr. . . de  $m_r$  ca ed the r. t. f  $N\_Tree$  f  $T - \{m_r\} / \phi$ , there e sts a c. . . ect. . . f d s. . . t trees  $T_1, T_2, \dots, T_n (n > )$  . . r arb trar  $i ( \leq i \leq n)$ , there s . . e u. que macr. . . de  $m_i \in T_i$  sat sfies  $\langle m_r, m_i \rangle \in H$  . . r  $H - \{ \langle m_r, m_1 \rangle, \dots, \langle m_r, m_n \rangle \}$ , there e sts a c. . . ect. . . f d s. . . t b. ar re at. . . s  $H_1, H_2, \dots, H_n$  a d  $\forall i, \leq i \leq n, H_i$  s a b. ar re at. . . defi ed  $T_i$  a d  $(T_i, H_i)$  s a s. a. et  $\text{rk}$  tree defi ed ab. e, a d e ca. t the sub tree f the r. t. macr. . . de  $m_r$ .

**Definition 1:** . . et  $\text{rk}$  tree m. de  $N\_Tree(T, H)$  f r a macr. . . de  $m_c \in T$  a d ts pare. t macr. . . de  $m_p \in T$ , the . . de set f  $m_c \cap m_p$  s ca ed the c. . . ect. g. . . de set f  $m_c$ , de. . . ted b  $R_{m_c}$

et  $sp_m(u, v)$  de. . te the sh. rtest path fr m  $u$  t.  $v$  . . et  $\text{rk}$   $m$ ,  $sp_T(u, v)$  de. . te the sh. rtest path fr m  $u$  t.  $v$  . . et  $\text{rk}$  tree  $T'$ , a d  $l(\pi)$  de. . te the d sta. ce f path  $\pi$

**Definition 2:** et  $\text{rk}$  tree m. de  $N\_Tree(T, H)$ , f f r each sub tree  $T'$  f  $N\_Tree$ , th macr. . . de  $m_r$  be g the r. t. f  $T', \forall u, v \in V(m_r), l(sp_{m_r}(u, v)) l(sp_T(u, v))$ , thus  $N\_Tree$  s ca ed E pa ded et  $\text{rk}$  ree . . de.

**Definition 3:** et  $\text{rk}$  tree m. de  $N\_Tree(T, H)$ , et the tra. s t. e c. sure f macr. . . de  $m$  be  $B_m = \{m_p | (m_p \in T) \wedge (m_p \cap m \neq \emptyset) \vee (\exists m_q \in B_m) (\langle m_p, m_q \rangle \in H)\}$

**Definition 4:** . . et  $\text{rk}$  m. de  $N(V, A, W), \forall u, v \in V$ , et the . rtua arc fr m  $u$  t.  $v$  be  $\bar{a}_{uv} = (u, v, sp_N(u, v))$ , th  $w(\bar{a}_{uv}) = l(sp_N(u, v))$

### 3 A Parallel Algorithm Based on Network-Tree Model

#### 3.1 Optimality Theorem

**Theorem 1:** . the E pa ded et  $\text{rk}$  ree . . de, f r g. e. . . des s a d  $t$ , the . pt ma. path  $\pi$  fr m  $s$  t.  $t$  ca. be repre. ted as f . . . g equat. . .  $\pi = sp_{m_1}(s, v_0, v_1) + sp_{m_2}(v_1, v_2) + \dots + sp_{m_h}(v_{h-1}, v_h) + sp_{m_{h+1}}(v_h, v_{h+1}) + sp_{m_{h+2}}(v_{h+1}, v_{h+2}) + \dots + sp_{m_{n-1}}(v_{n-2}, v_{n-1}) + sp_{m_n}(v_{n-1}, v_n = t)$  here  $n \geq , \leq h \leq n, \langle m_h, m_{h-1} \rangle \in H, \langle m_{h-1}, m_{h-2} \rangle \in H, \dots, \langle m_2, m_1 \rangle \in H$ , a d  $\langle m_{h+1}, m_{h+2} \rangle \in H, \dots, \langle m_{n-1}, m_n \rangle \in H. v_{i+1} \subseteq R_{m_{i+1}}$  th  $\leq i < h$ , a d  $v_i \subseteq R_{m_{i+1}}$  th  $h < i < n$ .

#### 3.2 Parallel Dividing Method and Distributed and Parallel Network Tree Shortest Path Algorithm (DP\_NTSP Algorithm)

rst e get the e pa ded et  $\text{rk}$  tree thr. ugh prepr. cess. g. . . cc. rd. g. t. the rem. . the . pt ma. path s c. s sted f a ser. s f sub paths . each macr. . . de. f the tra. s t. e c. sures . he. e pre. c. mpute the d sta. ces fr m arb trar

... de t. c. . . ect. g. . . des. . . each macr. . . de a d r te the d sta. ce data t. a  
 f i e s. the master pr. cess r ca. c mpute a. . pt ma. sh rtest path c. . s st. g. f  
 . rtua. arcs acc. rd. g t. the d sta. ces. he. the master d str butes the . rtua.  
 arcs t. the s a es, a d each s a e c mputes the requ red actua. path

**Description of *DP\_NTSP* Algorithm.** e use the mu t p e pr. gram  
 mu t p e data ( ) m. de t. m p e me t the para. e a g r thm. upp se the  
 s. urce. . de s s, a d the dest. at. . . . de s t

aster pr. gram

*Step* Creates p c. p es. f the s a e pr. gram

*Step2* cc. rd. g t. s a d t, c mputes the tra. s t. e c. . sures  $B_{\sigma(s)}$  a d  $B_{\sigma(t)}$ . et  
 $B = B_{\sigma(s)} \cup B_{\sigma(t)}$

*Step* Reads the d sta. ce data c. . ta. ed b. . . fr m the f i e a d c mputes a  
 . pt ma. path c. . s st. g. f. rtua. arcs

*Step4* h e there s a. act. e s a e pr. gram,

4 a rece. es the resu ts fr m the s a e pr. gram

4 b f a. the . rtua. arcs ha e. . t bee. a. . cated, se ds a. e. . rtua. arc  
 t. the s a e pr. gram. Other. se, st p the e cut. . . f s a e

*Step* Creates a sh rtest path acc. rd. g t. the rece. ed resu ts a d term. ates

a e pr. gram

*Step* Creates the c. de f r the c mputat. . . f sh rtest paths

*Step2* h e there s a. . rtua. arc t. ha d e,

2 a rece. es fr m the master pr. gram a. . rtua. arc r the . struct. . t.  
 st. p e cut. . .

2 b gets the . et. . rk data that reated t. the . rtua. arc a d c mputes  
 the actua. path that c. rresp. . ds t. the . rtua. arc

2 c se. ds the resu ts t. the master pr. gram

## 4 Computational Results

. . . ur c mputat. . . a. . rk, e ch. se s. . et. . rks. he deta. ed parameters. f  
 each . et. . rk are sh. . . . tab. e. . . e test the e cut. . . t me. f *DP\_NTSP*  
 a g r thm. . each . et. . rk the c mputat. . . a resu ts are prese. ted. . . g

**Table 1.** parameters of the testing networks

Network	k	$l_1 = b_1$	$l_2 = b_2$	$l_3 = b_3$	$w_1$	$w_2$	$w_3$	Nodes	Arcs
$g_1$	2	6	10	/	5	9	/	3,721	14,640
$g_2$	2	8	8	/	9	5	/	4,225	16,640
$g_3$	3	2	5	8	6	6	6	6,561	25,920
$g_4$	3	4	4	6	2	3	6	9,409	37,248
$g_5$	3	6	6	6	5	6	8	47,089	187,488
$g_6$	3	6	7	8	5	7	9	113,569	452,928



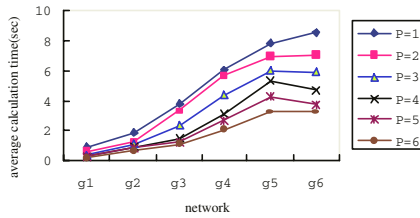


Fig. 1. Calculation time in different networks

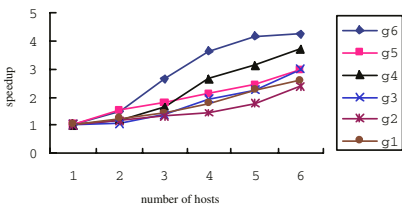


Fig. 2. speedup curves

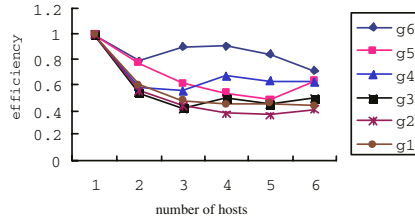


Fig. 3. efficiency curves

From the experimental results, it can be seen that as the number of hosts increases, the execution time of the algorithms is reduced. In general, the results show that as the network scale increases, the speedup and efficiency of the algorithms are improved. Table 1 shows that the proposed parallel algorithm can effectively solve the shortest path problem in large scale networks.

## References

1. Koutsopoulos. Commentaries on Fastest Paths in Time-dependent Networks for IVHS Application. *IVHS Journal*, 1993, 1(1): 89-90
2. J.Shapiro, J.Waxman D.Nir. *Level Graphs and Approximate Shortest Path Algorithms*, Networks, 1992, 22: 691-717
3. Chan-Kyoo Park, Kiseok Sung, Seungyong Doh, Soondal Park. Finding a path in the hierarchical road networks. *2001 IEEE Intelligent Transportation Systems Conference* 1998, 10 (2): 163-179
4. Ning Jing, Yun-Wu Wang, and Elke A. Rundensteiner. Hierarchical Encoded Path Views for Path Query Processing: An Optimal Model and Its Performance Evaluation. *IEEE Transactions on Knowledge and Data Engineering*, 1998, 10(3): 409-432
5. Guozhen Tan, Xiaojun Han, and Wen Gao. Network-Tree Model and Shortest Path Algorithm. *The 3rd International Conference on Computational Science*. Melbourne, Australia: Springer, Lecture Notes on Computer Science (LNCS 2659), 2003: 537-547

# Exploiting Parallelization for RNA Secondary Structure Prediction in Cluster

Guangming Tan, Shengzhong Feng, and Ninghui Sun

Institute of Computing Technology, Chinese Academy of Sciences  
{tgm, fsz, snh}@ncic.ac.cn

**Abstract.** RNA structure prediction remains one of the most compelling, yet elusive areas of computational biology. Many computational methods have been proposed in an attempt to predict RNA secondary structures. A popular dynamic programming (DP) algorithm uses a stochastic context-free grammar to model RNA secondary structures, its time complexity is  $O(N^4)$  and spatial complexity is  $O(N^3)$ . In this paper, a parallel algorithm, which is time-wise and space-wise optimal with respect to the usual sequential DP algorithm, can be implemented using  $O(N^4/P)$  time and  $O(N^3/P)$  space in cluster. High efficient utilization of processors and good load balancing are achieved through dynamic mapping of DP matrix to processors. As experiments shown, dynamic mapping algorithm has good speedup.

## 1 Introduction

Although computational methods such as phylogenetic comparative methods [2] to predict RNA secondary structure only provide an approximate RNA structural model, they have been widely used in the research of RNA secondary structures. In phylogenetic comparative methods, a stochastic context-free grammar (SCFG)[2] is used to model RNA secondary structure. The core of this method is dynamic programming (DP) algorithm [1][2][3]. Applications of SCFG-based RNA models require the alignment of an RNA sequence to a model. The computational complexity of polynomial-time dynamic programming algorithms for a sequence of length  $L$  and a model with  $K$  states is  $O(K*L^2+B*L^3)$ , where  $B$  is the number of bifurcation states in model [3] or  $O(L^4)$  when  $B \sim M$ . The alignment runtime on sequential computers is too high for many RNAs of interest such as ribosomal RNA (rRNA).

Cluster systems [4] have become very popular because of their cost/performance and scalability advantages over other parallel computing systems, such as supercomputers. Load balancing is very important to the performance of application programs in cluster systems. Good load balancing strategy improves the efficiency of processors, thus reduces the overall time of application programs. In this paper, we present an efficient parallel algorithm for aligning an RNA sequence to an SCFG model. The parallel algorithm consumes  $O(N^4/P)$  time and  $O(N^3/P)$  space, it is time-wise and space-wise optimal with respect to sequential algorithm.

The rest of paper is structured as follows. In section 2 we briefly review the SCFG model of RNA secondary structure and the DP algorithm. In section 3, we propose load balancing parallel algorithm through dynamic partitions of DP matrix. In section 4 we show experiment results and evaluate the performance of the parallel algorithm. Section 5 concludes this paper.

## 2 SCFG-Based Algorithm in RNA Secondary Structure Prediction

Eddy [3] described sequence-structure alignment algorithm in detail (The notations and definitions in this paper are referred to [2][3], we will not give their descriptions in detail). An RNA sequence can be aligned to a CM to determine the probability that the sequence belongs to the modeled family. The most likely parse tree generating the sequence determines the similarity score. Given an input sequence  $x=x_1 \dots x_N$  of length  $N$  and a CM  $G$  with  $K$  states numbered in preorder traversal. The DP algorithm iteratively calculates a 3-dimensional DP matrix  $M(i,j,v)$  for all  $i = 1, \dots, j+1, j = 0, \dots, N, v = 1 \dots K$ .  $M(i,j,v)$  is the log-odds score of the most likely CM parse tree rooted at state  $k$  that generates the subsequence  $x_i \dots x_j$ . The matrix is initialized for the smallest subtrees and subsequence, i.e. subtrees rooted at E-states and subsequence of length 0. The iteration then proceeds outwards to progressively longer subsequences and larger CM subtrees.

$$M(i, j, v) = \begin{cases} \max_{\gamma \in \Omega} \{M(i, j, \gamma) + \log t_s(\gamma)\} & \text{if } S(v) \in \{DEL, BEG\} \\ e_s(x_i, x_j) + \max_{\gamma \in \Omega} \{M(i+1, j-1, \gamma) + t_s(\gamma)\} & \text{if } S(v) \in MP \text{ and } d \geq 2 \\ e_s(x_i) + \max_{\gamma \in \Omega} \{M(i+1, j, \gamma) + t_s(\gamma)\} & \text{if } S(v) \in \{ML, IL\} \text{ and } d \geq 1 \\ e_s(x_j) + \max_{\gamma \in \Omega} \{M(i, j-1, \gamma) + t_s(\gamma)\} & \text{if } S(v) \in \{MR, IR\} \text{ and } d \geq 1 \\ \max_{i-1 \leq mid \leq j} \{M(i, mid, kleft) + M(mid+1, j, kright)\} & \text{if } S(v) \in BIF \\ 0 & \text{if } S(v) \in E \\ -\infty & \text{otherwise} \end{cases} \quad (1)$$

At the end of the iteration  $M(1,N,1)$  contains the score of the best parse of the complete sequence with the complete model.

## 3 Parallel RNA Secondary Structure Prediction

As many other DP algorithms, the DP algorithm for RNA secondary structure prediction exhibits the character of a wave-front computation [5], that is, each matrix element depends on a set of previously computed elements. However, it is the wave-front computation that increases the difficulty of the parallelization of DP algorithm. Due to the character of a wave-front computation, our parallel algorithm focuses on DP matrix mapping to processors in the process of filling the DP matrix. The performance of parallel algorithm greatly depends on the strategy of the partition of DP matrix.

A simple matrix mapping method is to statically partition the matrix along the diagonal as depicted in [4][5]. The utility efficiency of processors is very low in the static partitioning algorithm since one processor becomes idle at each stage of  $p$  stages. A solution for  $p < n$  is to repartition the matrix among the processors when the number of idle processors exceeds some threshold  $t$ . The  $t$  value directly determines the performance of algorithm. When  $t = 1$ , repartitioning occurs at every stage. The communication among processor is too frequent. When  $t = p$ , it never repartitions and corresponds to the static partitioning algorithm. In SCFG model based RNA secondary structure prediction algorithm the case where  $t = p/2$  is discussed. This threshold can avoid the extremes of repartitioning too frequently and too infrequently.

Without loss of generality assume that  $p$  evenly divides into  $\log(n/p)+1$  stages, each of which is further divided into  $p/2 + 1$  phases, each phases is composed of two steps. The phases and steps are analogous to the stages and steps of the static partitioning algorithm, respectively. Repartitioning occurs between stages. Along the diagonal the DP matrix is partitioned into strips numbered  $1, 2, \dots, \log(n/p)+1$  from the left of  $M$  such that strip  $i$  has  $n/2^i$  diagonals for  $1 \leq i \leq \log(n/p)$ . The last strip has  $p$  diagonals. Starting with the first strip, the  $i$ th strip is filled at stage  $i$  using the static partitioning algorithm. Then previously computed entries are repartitioned among the  $p$  processors and stage  $i+1$  begins. Processors  $i$  ( $i \leq p-1$ ) evenly partitions the entries stored in local into two halves by rows. The low half entries are sent to processor  $2^*i+1$ , except for processor 0, the high half entries are sent to processor  $2^*i$ . Accordingly, processor  $i$  receive entries from processor  $i/2$ .

Actually, the matrix is evenly partitioned by  $p$  both vertically and horizontally at each stage. For all  $1 \leq s \leq \log(n/p), 1 \leq j \leq p/2, M^{(s)}_{(i+1)j}$  denotes the diagonal block computed in processor  $i$  in  $j$  phrase of stage  $s$ . At the last stage  $\log(n/p)+1$ , each processor computes one row along diagonal and processor 0 computes the last cell. Both DP matrix and entries in the first phrase of each stage are triangular. (see Fig. 1)

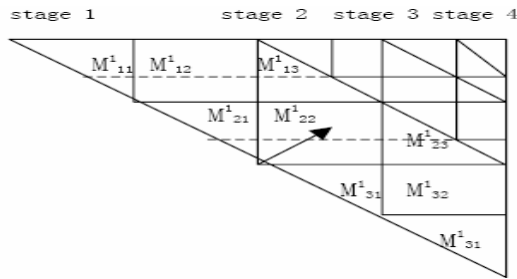


**Fig. 1.** The wavefront computation in dyanmic portioning algorithm. The dashed represents the repartition

The overall time can again be decomposed two parts: a computation time  $T_{comp}$ , a communication time  $T_{comm}$ , the communication time comprises a static communication time  $T_{stcomm}$  and a repartition time  $T_{repartition}$ . The computation time  $T_{comp}$  and the static communication time  $T_{stcomm}$  are  $O(n^4/p)$  and  $O(n^3)$ , respectively. At each stage  $s$ , processor  $i$  sends no more than  $(n/2^{s-1}p)(n-n/2^s)$  entries to processor  $2^*i$ .

Hence, the total repartitioning time  $T_{repartition} = \sum_{s=1}^{\log(n/p)} (n/2^{s-1}p)(n-n/2^s)\log(p) = O(n^2\log(p)/p)$ . The overall time is  $T_{comp} + T_{stcomm} + T_{repartition} = O(n^4/p) + O(n^3) + O(n^2\log(p)/p) = O(n^4/p)$ . The maximum space occurred at the first stage, it is  $O(n^3/p)$ .

### 4 Performance Evaluation

We have implemented the presented two parallel algorithms using MPI and experimentally evaluated their performance on a NUMA cluster systems. Each node consists of four 2.4GHz AMD Opteron CPUs and 8GB memory. The nodes are connected by 2Gbits/s Myrinet switch.

As the experiment shown, The experimental evidence indicates that the computation time dominates the communication time for all of the runs. The dynamic partitioning algorithm greatly reduces computation time. Table.1 give the results for RNA sequences length 120(5S\_ecoli), 377(RnaseP), 1542 (Isu\_ecoli) and 2904 (ssu\_ecoli). The maximum speedup occurred using 32 processors for two algorithms. Due to relative contribution of the communication time is great, the maximum speedup for all input length is difference. The lower speedup is caused by the more communication cost. For the dynamic partitioning algorithm, the repartitioning time contribute significantly to the communication time. However, thanks to the increasing efficiency of processors, the speedup of the dynamic partitioning algorithm is fine.

**Table 1.** The run time of dynamic partitioning algorithm. Time: seconds

Length	processors	overall	compute	communication	speedup
120	2	0.724	0.702	0.024	1.47
	4	0.445	0.355	0.09	2.43
	8	0.328	0.078	0.25	3.29
	16	0.238	0.172	0.066	4.53
377	2	0.219	0.051	0.168	4.93
	4	10.063	10.798	0.165	1.51
	8	5.076	5.376	0.301	2.32
	16	2.801	2.688	0.113	5.92
1542	2	1.566	1.324	0.242	10.59
	4	0.98	0.676	0.304	16.92
	8	109.734	109.568	0.175	1.55
	16	33.173	31.609	0.563	3.09
2904	2	48.707	48.873	0.434	6.16
	4	28.051	31.113	0.938	11.94
	8	15.883	10.343	5.68	19.91
	16	8774.886	8771.047	3.839	1.54
2904	4	3434.39	1379.373	65.016	3.98
	8	1839.889	705.319	137.07	4.97
	16	513.37	347.383	164.747	8.34
	32	318.358	77.307	141.051	19.37

## 5 Conclusion

We have given parallel DP algorithm for RNA secondary structure prediction in NUMA cluster systems. The parallel algorithm is cost-optimal with respect to the most efficient sequential algorithm. The experimental results shows that employing a good load balancing technique yields superior performance. The RNA secondary structure prediction algorithms mostly are DP algorithms. Our parallel DP algorithm skeleton can be used in other DP algorithms in computational biology by little modification.

## References

1. E Rivas and S Eddy. A dynamic programming algorithm for RNA structure prediction including pseudoknots. *J. Mol. Biol.* 285:2053-2068. 1999
2. S Eddy and R Durbin. RNA sequence analysis using covariance models. *Nucl. Acids Res.* 22(11):2079-2088. 1994
3. S Eddy. A memory-efficient dynamic programming algorithm for optimal alignment of a sequence to an RNA secondary structure. *BMC Bioinformatics*, 3:18, 2002
4. A Grama, A Gupta, G Karypis, V Kumar. *Introduction to Parallel Computing*. Addison Wesley, 2003
5. *Parallel Dynamic Programming*. PhD dissertation by Phillip Gnassi Bradford, 1994.

# Improving Performance of Distributed Haskell in Mosix Clusters

V. S. Sunderam, M. S. M. Magross, and M. S. M. Magross

Department of Computer and Information Sciences, Brooklyn College,  
2900 Bedford Avenue, Brooklyn, NY 11210-2889  
magross@its.brooklyn.cuny.edu

**Abstract.** We present experimental results demonstrating the performance improvement obtained in our distributed Haskell implementation when we replaced scheduling according to a micromanagement paradigm with contention-driven scheduling with automatic load balancing. This performance enhancement has important implications in the area of automatic run-time optimization.

## 1 Introduction

The motivation for this work is the need for a distributed Haskell implementation that can take advantage of the special properties of a cluster of computers managed by the distributed operating system. The current design of the distributed Haskell implementation is based on a contention-driven scheduling paradigm. This paradigm has been shown to be inefficient in a multiprocessor environment. The standard Haskell implementation is based on a contention-driven scheduling paradigm. This paradigm has been shown to be inefficient in a multiprocessor environment. The standard Haskell implementation is based on a contention-driven scheduling paradigm. This paradigm has been shown to be inefficient in a multiprocessor environment.

## 2 Parallel/Distributed Haskell and the Mosix Environment

The fundamental building blocks of a distributed Haskell implementation are the parallel and distributed execution models. The parallel execution model is based on a contention-driven scheduling paradigm. The distributed execution model is based on a contention-driven scheduling paradigm. The parallel and distributed execution models are based on a contention-driven scheduling paradigm. The parallel and distributed execution models are based on a contention-driven scheduling paradigm.

... a ue s c mputed, t ma be free used b a pr cess the c mputat ...  
 th ut fear f cha ge O era c mput g t me s reduced s ce pr cesses b ck  
 ... a ues ... h e the are curre t be g c mputed, a ecessar de a  
 ... a ue ... t et a a abe ... be c mputed b h che er pr cess first requ res t  
 he\_e ect f these spec fic a guage character st cs causes para e aske  
 pr grams t ser a ze ... cr t ca paths rather tha ... the pr grammer's c cep  
 tua sca ... d g ... ce t s ce ar mp ss be t mpr e perf rma ce be ... d  
 hat s bta ed ... cr t ca paths, ... pt ma perf rma ce s bta ed th ut  
 pr grammer ter e t ...

Our d str buted ca cu at ... s are ru ... a custer f ... c mputers curre t  
 ru ... g eb a ... u th Ope ... s patches ... s makes a custer f sep  
 arate c mputers ru ke a s mmetr c mu t pr cess r ( ) b d am c pr cess  
 m grat ... h s s dea ... heter ge e us c figurat ... s, s ce t aut mat ca  
 e abes ... ad ba a c g ... pr cess rs b f rc g pr cess m grat ... s t ach e e  
 ... ad ba a c g acr ss a a abe C 's Requests f r s stem ser ces are trapped  
 b ... s e ecuted ... the h me mach e he the ca ... t be perf rmed ... the  
 rker mach es, a d the resu ts are tra sm tted back t the rker mach e  
 h gh effie c fi e s stem perm ts pr cess rs t access fi es ... ther pr  
 cess rs th m ma ... erhead ata ca be d str buted acr ss the custer a d  
 there are ... a fe c ear defi ed c d t ... s that pre e t d am c m grat ...  
 f tasks fr m ... e mach e t a ... ther

### 3 Modification to the GdH Compiler

... the r g a Gd des g ... 4 as used f r a rem te pr cess creat ...  
 a d c mmu cat ... Rather tha bu d g a r tua mach e f r tua pr ces  
 s rs pr ... ded b ... pr cesses, ... ur m d fied ers ... f the ru t me s stem  
 bu ds a r tua mach e f r tua pr cess rs created b f rk g ... ca pr cesses,  
 h ch ma be m grated t rem te pr cess rs b ... s he se d() a d rec ()  
 ca s t ... ere rep aced b ... ca s stem ca s e use ... based ... ter pr  
 cess c mmu cat ... the ... p back ... terface fter err r test g f ur e  
 Gd C s stem e pr ceeded t test hether the h p thes zed effie c es had  
 actua ... bee ach e ed 7

### 4 Performance Results

... he ... t a tests c mpared the perf rma ce f ru s ... a s g e pr cess r f the  
 — actsm\_seq pr gram c mp ed th ser a G C 8 ... th the pr gram actsm\_par  
 c mp ed b ... ur m d fied Gd C a d ru ... f urtee ... r fitee rea pr ces  
 s rs he tests c s sted f t e t s sets f argume ts th e ecut ... t mes  
 ... ar ... g fr m sec ds t h urs Each e per me t as repeated three t mes he  
 ser a a d para e ca cu at ... s ga e the same a s ers ... a cases he speedup  
 , bet ee the ser a a d para e ca cu at ... s g e b

$$S = \frac{E_{\text{ecut}} \text{ t me } \dots \text{ a s g e pr cess r, best seque t a a g r thm}}{E_{\text{ecut}} \text{ t me us } \dots \text{ g p pr cess rs}}, \quad ( )$$

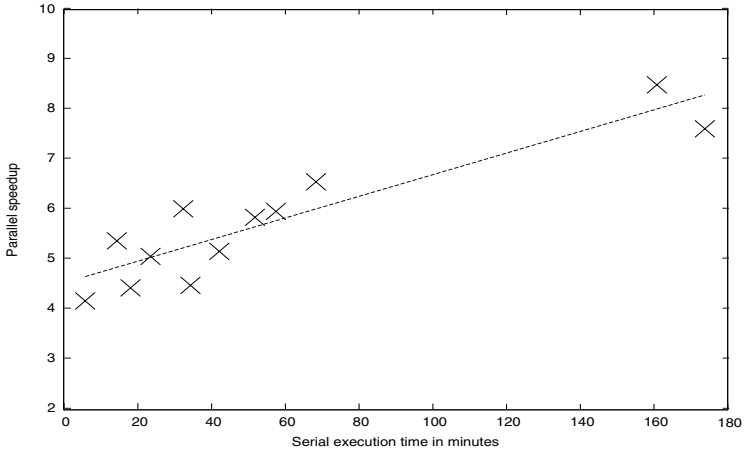


**Fig. 1.** Observed speedup, as defined by Eq. (1), when the test program was run in parallel using GdH-BC as compared to the serial execution times. The line is a linear fit to the data

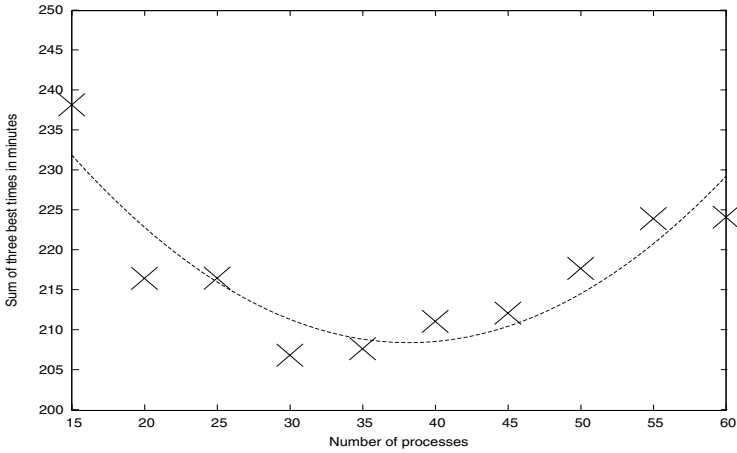


**Fig. 2.** Total timings from parallel runs of the test program with a fixed number of processes. The line is a fit to the data

and should be as expected, i.e. a decrease in execution time through parallelization. In comparison to our serial execution times, we gathered execution time statistics before distributed but, again, a calculation is quickly completed, calculations are distributed as evenly as possible across processors.

Our claim that best performance could be achieved by executing multiple processes on each processor is confirmed by Figure 2. In the figure, we have displayed the total time of the three best runs versus the number of processes requested per run. Once there are more processes than the fifteen real processors, the execution time decreases until an equilibrium point is reached and the



running time begins to increase with the number of processes. We think that safe to say that the increase in running time with the number of processes increases beyond a basic acceptance point. The results of these experiments show that the overhead associated with process creation at a load of 1000 is significant.

## 5 Conclusions

We conclude that the design of the GdH runtime system, which preceded more recent systems, performs a useful performance barrier in the field that at least under some circumstances, the current design is superior to the design of the GdH. Our experiments show that the current design performs the more managed scheduling provided by the design-based version of the system. We have further testing requirements to be done that our version of the design system provides significant performance advantages over competitors. Implementation of parallel distributed computation.

## Acknowledgments

The cluster of computers was made possible by OR Grant 4-97-07. The implementation of the GdH compiler was done by the design group. The implementation of the compiler was begun by the group under the management of the US, Canada supported by Grant number R-2742.

## References

1. Trinder, P.W., Loidl, H-W., and Pointon R.F.: Parallel and distributed haskells. *Journal of Functional Programming* **12** (2002) 469–510.
2. Pointon, R.F., Trinder, P.W., and Loidl H-W.: The Design and Implementation of GdH. In: Markus Mohnen, Pieter W. M. Koopman (Eds.) *Implementation of Functional Languages*, 12th International Workshop, Lecture Notes in Computer Science **2011** (2001) 53–70
3. Barak, A., La’adan, O., and Shiloh, A.: Scalable cluster computing with MOSIX for LINUX. *Proc. 5th Annual Linux Expo*, Atlanta, GA (1999) 95–100
4. Sunderam, V.: PVM: A Framework for Parallel Distributed Computing. *Concurrency: Practice & Experience* **2** No. 4 (1990) 315–339
5. Hughes, J.: Why functional programming matters. *Computer Journal* **32** (1990) 1–23
6. Amar, L., Barak, A., and Shiloh A.: The MOSIX Parallel I/O System for Scalable I/O Performance. *Proc. 14-th IASTED Int. Conference on Parallel and Distributed Computing and Systems*, Cambridge, MA (2002) 495–500
7. <http://146.245.249.159/kerim/timing.pdf>
8. Peyton Jones, S.L, Hall, C., Hammond, K., and Partain, W.: The Glasgow Haskell compiler: a technical overview. UK Joint Framework for Information Technology (JFIT) Technical Conference, Keele, (1993) 249–257

# Investigation of Cache Coherence Strategies in a Mobile Client/Server Environment

Cerkebrck and Ratas

Department of Informatics and Statistics (INE),  
University of Santa Catarina (UFSC),  
88040-900 Florianopolis, Brazil  
{diacui, mario}@inf.ufsc.br

**Abstract.** In this article, we present an investigation case study based on an implementation and performance analysis of three different cache coherence strategies over a real wireless environment. Our research work considers the broadcasting timestamp, the cache coherency schema with incremental update propagation and the amnesic terminals strategies. These strategies are based on periodic broadcast of invalidation reports. The performance of these strategies is analysed through an ordinary real environment. In this environment we compare the impact of invalidation report size, broadcast interval and cache size in mobile devices.

## 1 Introduction

data replication in mobile devices can represent a interesting mechanism to reduce late copy data transfer from servers and consequently a data replication error. Moreover, this approach can be considered successful if users can find essential data. The cache coherence is a result, mobile users can avoid the access to the wireless broadcast link. Otherwise, had as described, is a frequent observed wireless communication data reduction in a mobile device as a complete task for several accesses of applications.

This article presents an investigation case study based on an implementation and performance analysis research considering three different cache coherence strategies over a real wireless environment. The broadcasting timestamp (BT), cache coherence schema with incremental update propagation (CC) and amnesic terminals (AT) strategies are based on a periodic broadcast of cache invalidation reports (R). Our performance results reflect the impact of the size of R and the cache size of mobile devices. The utilized database application.

The paper is organized as follows. Section 2 presented the performance evaluation architecture. Section 3 discussed the results obtained in a real wireless communication environment. Section 4 presented conclusions of the research work.

## 2 Experimental Environment Architecture

The client-server paradigm for distributed computing is regarded as a well-known architecture that mainly proposes a server cache architecture. This approach is also considered the literature for resource requirements (e.g. [4]), however the specific characteristics and details may vary.

In this article, we consider the CC and techniques, because these strategies have a data report (R) and stateless servers. Results suggest a mechanism for resource servers that forms the necessary items that are modified. The stateless servers are not obliged to keep information related to the decisions in its area and thus, it is necessary to know about the cache details.

The environment architecture depicted to execute the requirements shown in figure 1. The architecture has three main components: a server, a client and a database system. Additionally, we implemented the three protocols strategies proposed in the literature.

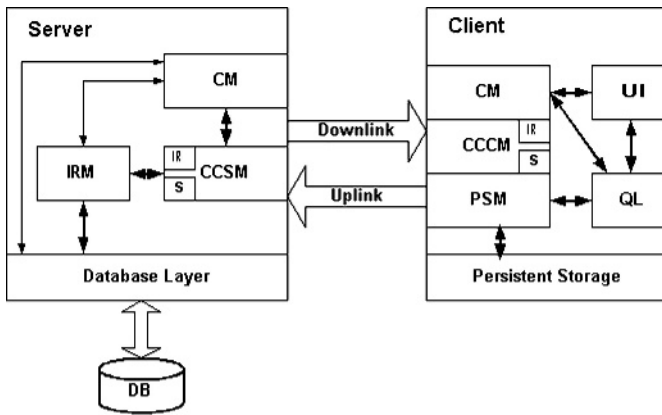


Fig. 1. The environment architecture

Inside the server the modules are communication manager (C), cache controller server manager (CC) and a data report manager (R). C is responsible for communicating with the servers inside the CC, verifies which strategies being used and adds the appropriate parameters. Inside the R for this strategy the R is responsible for the modification of the R in the database system.

On the other hand, clients are characterized by the modules communication manager (C), cache controller client manager (CCC), persistent storage manager (P), query (Q) and user interface (U). The C client manages the connection with the server. The CCC is responsible for receiving Rs from the server and applies the cache modification following a specific strategy ( )

he executes a modification, necessarily, the cache of the machine de-  
 ceives the stores and registers that are being modified and as a result,  
 interface to machine users to access the error message.

he database system compiler, etc. is derived from requirements as the  
 implemented this database, because this specifies the  
 database system package and provides interesting functions to develop app-  
 lications (e.g. trigger and referential integrity).

### 3 Experimental Results

the server database is used items, which are accessed by machine  
 does the broadcast and used as a test, summarizing research  
 works (e.g. [4]), with 2 seconds between test and adding the experimen-  
 tal tests were executed using the CCS and derived that machine  
 users have a 2 percent of items from the database can be cached.

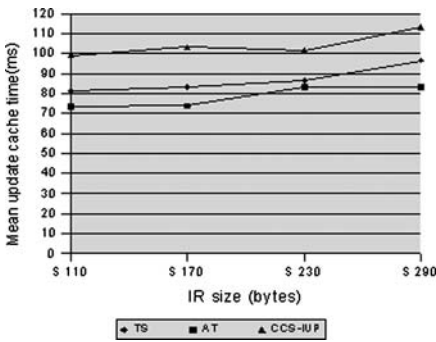


Fig. 2. Mean update cache time vs. IR size

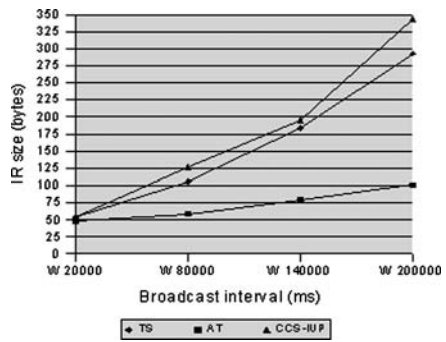


Fig. 3. IR size vs. Broadcast interval

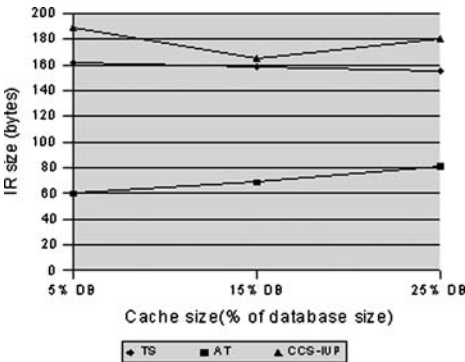


Fig. 4. IR size vs. Cache size

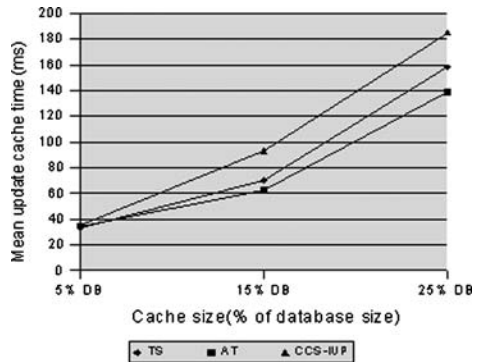


Fig. 5. Mean update cache time vs. Cache size

figure 2, our results indicate that the read CC speed more than  
 update the cache than the approach figure shows. Results related  
 to broadcast timer as the graph shows that the read CC has a  
 tendency to increase. Results related to broadcast timer as  
 the result of the configuration size against the cache size presented  
 figure 4. The increase of the cache size resulted in the increase of the  
 registered a small decrease of the size and the CC did  
 not get a regular behavior figure 5, as expected, this suggests that  
 that the increase of the cache size directly impacts the time to update the  
 structure memory.

## 4 Conclusions

This paper presented an experimental case study based on a  
 that a performance analysis of three different strategies for cache  
 resources.  
 The performance results demonstrated factors and characteristics of the  
 strategies based on effects from the data report (R) size, broadcast  
 and memory cache size. The results demonstrated different performance  
 for the parameters considered. The strategy had a interesting performance,  
 but these factors compared to the other approaches.

## Acknowledgements

This research was partially supported by CAPES (Coordenação de Aperfeiçoamento de Pessoal de Nível Superior) under the grant 2402/4.

## References

1. Daniel Barbar; and Tomasz Imielnski. Sleepers and workaholics: caching strategies in mobile environments (extended version). *The VLDB Journal*, (1995) 4(4):567-602.
2. Hyunsik Chung and Haengrae Cho. Data caching with incremental update propagation in mobile computing environments. In *Australian Computer Journal* (1998).
3. Magnus E. Bjornsson and Liuba Shrira. BuddyCache: high-performance object storage for collaborative strong-consistency applications in a WAN. *Proceedings of the 17th ACM SIGPLAN conference on Object-oriented programming, systems, languages, and applications*,(2002) 26-39.
4. Joanne Holliday and Divyakant Agrawal and Amr El Abbadi. Disconnection modes for mobile databases. *Wirel. Netw.*, (2002) 391-402.
5. Jin Jing and Ahmed Elmagarmid and Abdelsalam Sumi Helal and Rafael Alonso. Bit-sequences: an adaptive cache invalidation method in mobile client/server environments. *Mob. Netw. Appl.*, (1997) 115-127.
6. Mckoi SQL Database System. Available online: <http://www.mckoi.com/database/>.

# Parallel Files Distribution

Laura T. Cucu<sup>1</sup> and Elise Decker<sup>1</sup>

Western Michigan University  
{lcucos, elise}@cs.wmich.edu  
<http://aegis.cs.wmich.edu/~lcucos>  
<http://www.cs.wmich.edu/~elise>

**Abstract.** For parallel computations requiring massive data Input/Output, one of the goals is to maximize the use of the underlying storage topology, in particular exploit the benefit of using local disks. This paper presents a mechanism to distribute independent data records from multiple files to multiple processing nodes and vice-versa. An allocation problem is solved using the Max-Flow algorithm. We give timing results using various read/distribute protocols. One application is to re-distributing tasks (regions) for restarting parallel numerical integration runs.

## 1 Introduction and Motivation

In order to maintain a minimum transport cost between producers, consumers and archives, it is preferable to have all three within the same system. Consequently, more direct use paths are easier to access between them. Additionally, a streamlined architecture of machines and steps between producers and consumers

is a desirable scenario for parallel computations that produce, store and later consume large amounts of data, hence the focus on similar processes.

Let us consider an arbitrary topology of high speed connections between a number of organizations, each providing a number of machines. The other characteristics are a direct access to shared partitions. The optimum distribution should be achieved when the data is generated, saved, and loaded to the same computing node (keeping all other data transfers at a minimum). However, this may not always be possible due to irregular processing schemes, which may generate more data than the capacity to read and reprocess, or must more data than they desire. Under these conditions, it should be difficult to predict a direct path where the data should be distributed.

Addressing many scenarios where data need to be read, this paper presents an efficient distribution scheme.

A simple approach considers direct distribution between customer and computer architecture, integrating codes PARINT (parallel integration project), implementing adaptive partitioning (as elsewhere) strategies for multi-architecture.

Section 2 describes a general equilibrium distribution algorithm, Section 3 gives performance results and Section 4 concludes the paper.

## 2 Static Distribution

and scheduling algorithms, and since the total amount of work sketched in this more efficient compute the data distribution and access here, most cases data can be easily pre-allocated distributed equally among all machines, therefore, network links require no resource partitioning.

Consider the following general allocation problem [4]

**Problem:** Given a set of  $n$  machines,  $\{m_i\}_{1 \leq i \leq n}$ , a collection of  $p$  files,  $S = \{s_j\}_{1 \leq j \leq p}$ , here  $s_j$  has  $|s_j|$  records, and a undirected bipartite graph  $G = \{(M, S), E\}$ , here  $E = \{(v_i, u_j)\}$  with  $v_i \in M$  and  $u_j \in S$ , which defines a mapping between machines and files, compute the tempered distribution such that each machine gets an equal share of records. In case that an equal distribution cannot be achieved, find a solution such records shared between machines at a minimum communication cost.

**Example:** Our compute grid has  $m_1, m_2, m_3, m_4$ , partitioned into a compute tasks requiring data from three file servers  $FS_1, FS_2, FS_3$  here  $m_1, m_2, m_4$  can access  $FS_1$ ,  $m_1, m_3$  can access  $FS_2$ , and all can access  $FS_3$ . The machines are interconnected by the same topology network.

**Solution:** An efficient distribution can be achieved using algorithm. Cut algorithm and the following procedure

1. Augment the graph with the edges  $source$  and  $sink$  and edges between all sets of  $source$  and all machine sets and  $sink$ .
  2. Assign given finite capacities to edges between sets and machines,  $|S_i|$  between set  $S_i$  and source, and  $\lceil \frac{\sum_{i=1}^p |S_i|}{n} \rceil$  between each machine and the sink.
  3. Apply the algorithm and theorem that the edge created graph.
  4. If the result graph has  $\sum_{i=1}^p |S_i|$ , there exists an equal distribution of the sets the distribution is given by the flow, the network edges. Otherwise, the sets cannot be equally distributed. Then add to the communication cost and go to step.
- Equal distribution the records is allocated to step to machines with a smaller number of records.

## 3 Experiments

We implemented the system PFD which is a parallel reader to get distributed data records from the files located over multiple machines to provide a transparent and efficient data access. It computes rate data reading and processing using the same program as the system is a serial over the MPI message passing library [2].

PFD is made of several parts, the same as large numbers of integrated registers. Here it can be easily integrated into applications that reads larger numbers of dependent records.

Give a collection of records distributed over a number of machines, PFD

reads each record exactly once (i.e. the records processed)

minimizes the communication and efficiently distributes all records among all participants

provides a clean and transparent way to use cache disks

uses a buffer of configurable size for reprocessing communication

provides an array of pointers to read and distribute the data such that each node processes the same number of records (EQUAL),

or reads faster records to process more data (COMPETE),

or reads records through direct access to data on process records (LOCAL)

The system is written in C and can be integrated with the user application through a small set of read/write pack/unpack functions

We performed a set of experiments reading 6000 records of data organized in 8 records and using different distributed strategies ranging from all data being stored

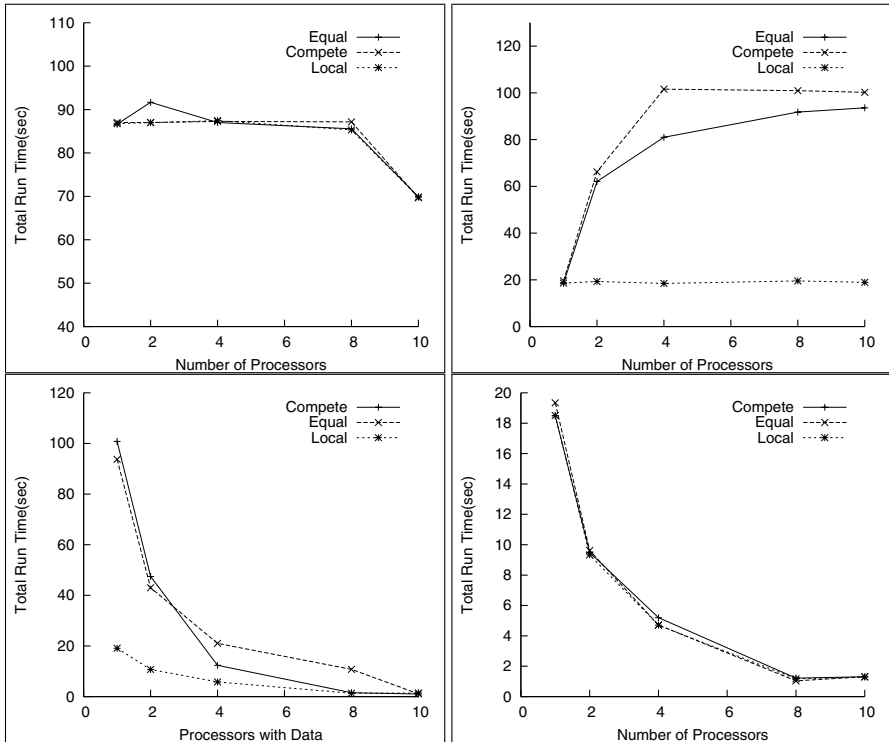


**Fig. 1.** *Top-Left:* Distribute records from a shared partition; *Top-Right:* Distribute records from one non-shared partition; *Bottom-Left:* Distribute records located in a subgroup of machines; *Bottom-Right:* Distribute records shared equally by the participants



... e shared part t... t... a... data... cated... e... ca... d sk... p... t... readers are selected fr... m a set... f... 2G z... th... pr... cess... r... des, c... mmu... cat... g... a... ast Ether... et... et... rk

gure (Top-Left) sh... s results fr... r data... cated... a shared part t... . th... s case, the ru... t me... s... depe... de... t... f the read meth... d (EQUAL, COMPETE... , r LOCAL), a... d... f the... mber... f pr... cess... rs, a... d... s ma... , dr... e... b... the... et... rk tra... nsfer speed... . Note that the shared part t... . f th... s e... per... me... t... as... cated... a d sk... s g... g... f... a... t... faster tha... the... ca... d sks used... the f... . . . g... e... per... me... ts

gure (Top-Right) sh... s results fr... r data... cated... e... . . . shared par t... . . . here the... t... ta... read t... me... s ar... u... d 2... sec, the perf... rma... ce qu... ck deprec... ates as m... re pr... cess... rs are... . . . ed... the c... mputat... . . . e attr... bute th... s beh... . . . r... t... the... b... tt... e... ck at the d... str... but... . . . de

gure (Bottom-Left) a... d (Bottom-Right) sh... s results fr... r data... . . . u... f... r... m... d... str... buted, a... d... u... f... r... m... d... str... buted, respect... e... . . . er part... c... pat... g... mach... es here... s a... s... g... g... f... a... t... mpr... o... me... t... ru... t... me... a... d... sca... b... l... t... the... latter case, the read t... me... as... . . . t... a... cted... b... the d... str... but... . . . meth... d (Equal, C... mpete... , r... ca... )

### 4 Conclusions

h... s paper... ut... es a mecha... sm... t... d... str... bute... depe... de... t... data rec... rds fr... m mu... lt... i... p... le... s... t... mu... lt... i... p... le... pr... cess... g... . . . des a... d... ce... r... s... e... prese... t... a... s... u... t... . . . t... the ge... era... a... . . . cat... . . . pr... b... em... f shar... g the data equ... . . . am... g the part... c... pat... g... c... mpute... . . . des, g... e... a... arb... trar... y... st... r... age... t... p... . . . g... . . . th... ough us... g... ca... d sks... r... ma... . . . b... ds data pr... ducers... th... c... . . . sumers, our... s... t... em... ma... t... a... s the be... efit... . . . er... ed... b... th... s... c... . . . ect... . . . , h... e... g... . . . g... at the same t... me... a... s... e... t... f... p... t... . . . s... t... share data... th... . . . pr... ducers

### Acknowledgments

h... s... rk... s... supp... rted... . . . part... b... . . . ester... . . . ch... ga... . . . ers... t... , a... d... b... the at... . . . a... c... ce... . . . u... dat... . . . u... der gra... ts C... 442, C... 2... 77, E... 8... 7

### References

1. <http://www.cs.wmich.edu/parint>, PARINT web site.
2. <http://www-unix.mcs.anl.gov/mpi/index.html>, MPI web site.
3. CORMEN, T. H., LEISERSON, C. E., AND RIVEST, R. L. *Introduction to Algorithms*. The MIT press, 1994.
4. CUCOS, L. *Load Sharing Strategies in Distributed Environments*. PhD thesis, Western Michigan University, December 2003.
5. ZANNY, R., DE DONCKER, E., KAUGARS, K., AND CUCOS, L. *PARINT1.2 User's Manual*. Available at <http://www.cs.wmich.edu/parint>.

# Dynamic Dominant Index Set for Mobile Peer-to-Peer Networks\*

Shiwei Han, Gao Peng, Gaogang Gao, and Shan

College of Computer Science, Zhejiang University,  
Hangzhou, P.R. China 310027

shiwei@zj165.com

shan@cs.zju.edu.cn

{epglmary, alexlinxin}@hotmail.com

**Abstract.** Efficient locating mechanism is the key issue of establishing peer-to-peer (P2P) resource sharing for mobile Ad Hoc networks (MANET). In this paper, a simple concept of Dynamic Dominant Indexing Set (DDIS) is proposed. By periodically advertising information of shared resources on the backbone of current network topology in a distributed fashion, DDIS gains great improvement on user response time, fault tolerance and scalability. Simulations indicate that DDIS simplifies the searching process and greatly reduces the response delay and thus, it is more appropriate for mobile peer-to-peer source sharing especially in emergent situations.

## 1 Introduction

In the past 20 years, mobile ad hoc networks (MANET) have become a hot topic in the field of mobile computing. The main characteristics of MANETs are: 1) dynamic topology, 2) limited resources, 3) no central authority, 4) self-organizing, 5) multi-hop communication, 6) no fixed infrastructure, 7) no global address, 8) no global clock, 9) no global time, 10) no global power supply, 11) no global security, 12) no global management, 13) no global control, 14) no global monitoring, 15) no global maintenance, 16) no global repair, 17) no global replacement, 18) no global upgrade, 19) no global downgrade, 20) no global migration, 21) no global replication, 22) no global backup, 23) no global recovery, 24) no global disaster recovery, 25) no global security, 26) no global privacy, 27) no global confidentiality, 28) no global integrity, 29) no global availability, 30) no global reliability, 31) no global performance, 32) no global quality of service, 33) no global quality of experience, 34) no global user satisfaction, 35) no global user loyalty, 36) no global user retention, 37) no global user acquisition, 38) no global user segmentation, 39) no global user targeting, 40) no global user personalization, 41) no global user customization, 42) no global user empowerment, 43) no global user participation, 44) no global user collaboration, 45) no global user community, 46) no global user network, 47) no global user ecosystem, 48) no global user value chain, 49) no global user business model, 50) no global user revenue model, 51) no global user cost model, 52) no global user profit model, 53) no global user risk model, 54) no global user return model, 55) no global user investment model, 56) no global user exit model, 57) no global user exit strategy, 58) no global user exit plan, 59) no global user exit process, 60) no global user exit timeline, 61) no global user exit communication, 62) no global user exit documentation, 63) no global user exit legal review, 64) no global user exit tax implications, 65) no global user exit accounting, 66) no global user exit audit, 67) no global user exit reporting, 68) no global user exit disclosure, 69) no global user exit transparency, 70) no global user exit accountability, 71) no global user exit responsibility, 72) no global user exit liability, 73) no global user exit indemnification, 74) no global user exit insurance, 75) no global user exit risk management, 76) no global user exit crisis management, 77) no global user exit business continuity plan, 78) no global user exit disaster recovery plan, 79) no global user exit business recovery plan, 80) no global user exit business restoration plan, 81) no global user exit business revitalization plan, 82) no global user exit business transformation plan, 83) no global user exit business reinvention plan, 84) no global user exit business innovation plan, 85) no global user exit business growth plan, 86) no global user exit business expansion plan, 87) no global user exit business diversification plan, 88) no global user exit business globalization plan, 89) no global user exit business digitalization plan, 90) no global user exit business automation plan, 91) no global user exit business optimization plan, 92) no global user exit business simplification plan, 93) no global user exit business streamlining plan, 94) no global user exit business restructuring plan, 95) no global user exit business reorganization plan, 96) no global user exit business refocusing plan, 97) no global user exit business rebranding plan, 98) no global user exit business repositioning plan, 99) no global user exit business reimagining plan, 100) no global user exit business reinventing plan.

1) address resources, 2) category, 3) price, 4) quality, 5) freshness, 6) accuracy, 7) reliability, 8) security, 9) privacy, 10) confidentiality, 11) integrity, 12) availability, 13) reliability, 14) performance, 15) quality of service, 16) quality of experience, 17) user satisfaction, 18) user loyalty, 19) user retention, 20) user acquisition, 21) user segmentation, 22) user targeting, 23) user personalization, 24) user customization, 25) user empowerment, 26) user participation, 27) user collaboration, 28) user community, 29) user network, 30) user ecosystem, 31) user value chain, 32) user business model, 33) user revenue model, 34) user cost model, 35) user profit model, 36) user risk model, 37) user return model, 38) user investment model, 39) user exit model, 40) user exit strategy, 41) user exit plan, 42) user exit process, 43) user exit timeline, 44) user exit communication, 45) user exit documentation, 46) user exit legal review, 47) user exit tax implications, 48) user exit accounting, 49) user exit audit, 50) user exit reporting, 51) user exit disclosure, 52) user exit transparency, 53) user exit accountability, 54) user exit responsibility, 55) user exit liability, 56) user exit indemnification, 57) user exit insurance, 58) user exit risk management, 59) user exit crisis management, 60) user exit business continuity plan, 61) user exit disaster recovery plan, 62) user exit business recovery plan, 63) user exit business restoration plan, 64) user exit business revitalization plan, 65) user exit business transformation plan, 66) user exit business reinvention plan, 67) user exit business innovation plan, 68) user exit business growth plan, 69) user exit business expansion plan, 70) user exit business diversification plan, 71) user exit business globalization plan, 72) user exit business digitalization plan, 73) user exit business automation plan, 74) user exit business optimization plan, 75) user exit business simplification plan, 76) user exit business streamlining plan, 77) user exit business restructuring plan, 78) user exit business reorganization plan, 79) user exit business refocusing plan, 80) user exit business rebranding plan, 81) user exit business repositioning plan, 82) user exit business reimagining plan, 83) user exit business reinventing plan.

2) emergency, 3) rescue, 4) combat, 5) search, 6) response time, 7) as short as possible, 8) being able to find the network topology, 9) as a mass, 10) as a beam, 11) as a beam, 12) as a beam, 13) as a beam, 14) as a beam, 15) as a beam, 16) as a beam, 17) as a beam, 18) as a beam, 19) as a beam, 20) as a beam, 21) as a beam, 22) as a beam, 23) as a beam, 24) as a beam, 25) as a beam, 26) as a beam, 27) as a beam, 28) as a beam, 29) as a beam, 30) as a beam, 31) as a beam, 32) as a beam, 33) as a beam, 34) as a beam, 35) as a beam, 36) as a beam, 37) as a beam, 38) as a beam, 39) as a beam, 40) as a beam, 41) as a beam, 42) as a beam, 43) as a beam, 44) as a beam, 45) as a beam, 46) as a beam, 47) as a beam, 48) as a beam, 49) as a beam, 50) as a beam, 51) as a beam, 52) as a beam, 53) as a beam, 54) as a beam, 55) as a beam, 56) as a beam, 57) as a beam, 58) as a beam, 59) as a beam, 60) as a beam, 61) as a beam, 62) as a beam, 63) as a beam, 64) as a beam, 65) as a beam, 66) as a beam, 67) as a beam, 68) as a beam, 69) as a beam, 70) as a beam, 71) as a beam, 72) as a beam, 73) as a beam, 74) as a beam, 75) as a beam, 76) as a beam, 77) as a beam, 78) as a beam, 79) as a beam, 80) as a beam, 81) as a beam, 82) as a beam, 83) as a beam, 84) as a beam, 85) as a beam, 86) as a beam, 87) as a beam, 88) as a beam, 89) as a beam, 90) as a beam, 91) as a beam, 92) as a beam, 93) as a beam, 94) as a beam, 95) as a beam, 96) as a beam, 97) as a beam, 98) as a beam, 99) as a beam, 100) as a beam.

Establishing a dynamic lookup set should be an effective and feasible approach for MANETs. In this paper, we propose a new category mechanism for MANETs.

\* This paper is supported by National Natural Science Foundation of China (No. 60473052) and Zhejiang Provincial Natural Science Foundation of China (No.602032).

er, me t ca ed am c m a t de et ( ) d am ca .  
c , structs the de set h ch s based the m m C e c t e d m at g  
et ( C ) C s the m m m set f , des such that e er , de the  
et r k s e ther , the set r s a e ghb r f a , de the set c c r d g t  
the f r mat f shared res urces per d ca , pub shed , C , peers ca  
cate the res urces qu ck b c , su t g a m t e d , u m b e r f p e e r s r a t h e r t h a  
b t h e r g m r e t h e r p e e r s e e r f i d g t h e C f a s p e c i f i c e t r k  
h a s b e e p r e d t b e a c m p e t e p r b e m e m p r e d t h e m a t g  
r u g ( ) a g r t h m t h a t p r m a t e s e s t h e C p r b e m a d s  
t r b u t e d f a s h t h t h e h e p f t h e m p r e d a g r t h m , t h e m e c h  
a s m c a b u d t h e C b a s e d d e s e t f c u r r e t 2 e t r k t p g  
a m r e e f f i c e t a  
h e p a p e r s r g a z e d a s f s t h e e t s e c t , t h e r e a t e d r k s  
d s c u s s e d e c t t r d u c e s u r s e a r c h g m e c h a s m m u a t , r e s u t s a d  
a a z e s a r e p r e s e t e d s e c t 4 a . e . c . c o d e u r s t u d s e c t

### 2 Related Work

2 the auth r put f r a r d a c a t g m e c h a s m 2 e t r k , r a m e d  
g a s c s d e r a b g d p e r f m a c e h e m a t g r u g ( )  
a g r t h m c m p u t e s t h e a p p r m a t f C a d s t r b u t e d m a e r  
a c c r d g t 2 h p e g h b r h d f r m a t u t a g r t h m c c e  
t r a t e s c s t r u c t g a e f f i c e t r u t g a g r t h m b r e d u c g t h e b r a d c a s t  
r e d u d a c E a d d e s t t a k e t a c c u t t h e 2 s p e c i f i c f a c  
t r s m p r e s t m a k e t m r e s u t a b e f r b u d g a e c t e s e a r c h  
d e 2 e r , m e t

### 3 The DDIS Mechanism

ere, the u t d s k g r a p h , G ( V , E ) , s t r d u c e d t r e p r e s e n t a 2  
e t r k , h e r e V r e p r e s e n t s a s e t f m b e p e e r s a d E r e p r e s e n t s a s e t f  
e d g e s e u s e N ( u ) t r e p r e s e n t t h e e g h b r s e t f u N ( N ( u ) ) r e p r e s e n t s  
t h e e g h b r s e t f N ( u ) d e a s s u m e t h a t u ( s e d e r ) a d v ( r e c e i v e r ) a r e  
e g h b r s

ur s c e a r , h e a p e e r a u c h e s r f r a r d s a a d e r t s , g p a c k e t , t  
u d d e c d e t h e f r a r d s t a r u d t s e f h e f r a r d s t t h e a d e r t s , g  
p a c k e t u d t f h s e g h b r s h b e g t t h e d e s e t a d s h u d t a k e  
t h e r e s p s b t t c a c h e t h e m e t a d a t a t h e a d e r t s , g p a c k e t e a h e ,  
b a a z g t h e f r a r d s t t h e a d e r t s , g p a c k e t , t h e r e c e i v e r s c a c u  
a t e t h e r f r a r d s t s a m r e a c c u r a t e f a s h h c h r e d u c e t h e  
b r a d c a s t r e d u d a c

e e r g t s h a r e h s r e s u r c e s p e r d c a , a u c h e s a b r a d c a s t  
c a t a g t h e p e e r ' s d , t h e f r m a t f h s s h a r e d r e s u r c e , t h e e p r g  
t m e f s h a r e d r e s u r c e , a d t h e f r a r d s t f t h a t p a c k e t u e t t h e a t u r e

of broadcast. Generally, all neighbors around the source peer get the packet and all the peers in the neighborhood that packet are suggested to cache and forward the packet. Others can just simply discard the packet. The receivers can cache the received packets and rebroadcast the packet from the source peer. This process continues until the whole network is covered. The forward set of  $v$  can be computed. The following algorithm guarantees that  $F(u)$  here denotes as the forward set of  $u$  passed to  $v$ .

1. Let  $F(u, v)$  = (empty set),  $Z = \phi$  (empty set) and  $K = \cup S_i$  here  $S_i = N(v_i) \cap (U(u, v) - N(N(v) \cap F(u)))$ ,  $S_i = N(v_i \cap P(u, v))$  for  $v_i \in B(u, v)$
  2. If there exists a peer  $w \in P$  that  $v$  can reach through  $v_n$ ,  $F(u, v) = F(u, v) \cup v_n$ ,  $Z = Z \cup S_n$ ,  $K = K - S_n$ , and  $S_j = S_j - S_n$  for all  $S_j \in K$ . This step repeats until no peer  $w \in P$  that  $v$  can reach through  $v_n$ .
  3. Let  $S_k$  be the maximum size  $K$  (in case of a tie, the one with the smallest definition of  $k$  is selected).
  4.  $F(u) = F(u, v) \cup v_k$ ,  $Z = Z \cup S_k$ ,  $K = K - S_k$ , and  $S_j = S_j - S_k$  for all  $S_j \in K$ .
- Finally, the nodes added to  $Z$  in the subsequent step

are  $B(u, v) = N(v) - N(u)$ . Algorithm 1 evaluates the number of peers in  $U(u, v) = N(N(v)) - (N(u) \cup N(v))$ , so-called eligible peers, which can be covered by  $v_i$ . Deciding if including  $v_i$  from  $F(u, v)$  is better, the eligible peers can be either because the peers in the forward set of  $u$  do not reach the nodes in  $N(N(v) \cap F(u))$ . These peers can be safely included from  $U(u, v)$  and the eligible peers can be defined as  $P(u, v) = U(u, v) - N(N(v) \cap F(u))$ , recall that  $U(u, v)$  represents the uncovered peers 2 hops away from  $v$ . Algorithm 2

selects the process of building forward set. First, picks up the neighbors that can sequentially be included in  $v$ 's forward set because until them  $v$  can reach from all the peers in  $P(u, v)$ . Algorithm 3, these peers, that are called neighbors in this paper, can also be sequentially included in forward set until algorithm 4 is asked. If greedy algorithm and the sequential sequence is random, there may be unnecessary peers in result of forward set. However, as a part of our 'if neighbors' neighbors check sequence, neighbors first in the forward set can be smaller than the one that algorithm builds.

In the help of the improved algorithm, can deliver the metadata of shared resources in the domain of the current network. Performance metrics: peers frequently check whether the cached metadata is updated or not. If peer first checks his cached data to see whether there is a format of the required resources, rather than just asks his neighbors to find where the required resources are.

## 4 Performance Results

In this section, we present the simulation results for our mechanism. We used a IEEE 802.11 standard Carrier Sense Multiple Access (CSMA/CA) standard physical layer de-

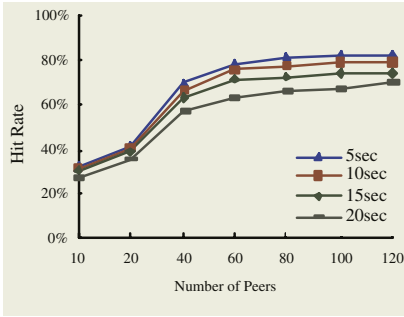


Fig. 1. Hit rate of DDIS with different advertising intervals

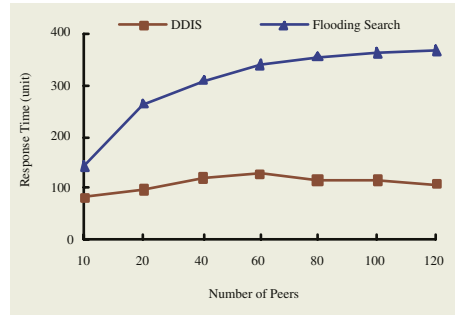


Fig. 2. Response time of the two mechanisms

... g t ... ra gr u d pr pagat ... as rad ... pr pagat ... m de  $N_{Peers}$  peers ... ram g ... a area f ...  $m \times m$  g ... illustrates the hit rate of ... th d ... ert s g ... ter a s ... se ca ... see, the sh rter ad ert s g ... ter ... a e set, the h gher hit rate e get ... e er, the perf rma ce mpr ... eme t s ... ach e ed at the e pe se f hea er ... erhead ... a a c g the accurac y of quer es ... ad the ... erhead ... must pa ... eeds m re e ... rts f stud ... r m g 2, the ... ma ... ad a tage f ... ca be ear ed ... d am ca ... cach g the metadata ... f the peers ... the backb ... e f curre t ... et ... rk, ... ga s great mpr ... eme t ... user resp ... se t me c mpared ... th ... d g search mecha sm Our ga s t ... bu d a sma ... de set t ... a ect a ... the peers ... the ... et ... rk ... putt g the metadata ar u d the part c pa ts, the ... ca qu ck ... cate the r fa ... rabe resources ... th ut m re e ... rts ... ce the requ red ... f rmat ... s put c ... se ... t the requ r g peers, the resp ... se t me f ... cha ges ... tte ... he ... the ... um ber f part c pa ts gr s ... he ... d g search mecha sm, ... the c ... ntr a ... b br ad cast g ... the ... et ... rk t ... cate the target peer h ch ma be far a a fr m the quer ... g peer takes ab ut a erage 2 t ... t mes ... ger tha ... t ... resp ... se the users' quer es

## 5 Conclusions and Future Work

In this paper, we put forward a ... e c ... cept f ... fact, ... s a k ... d f rep ... cat ... f ... de ce ter ... se ect g peers ... C, the ad ert seme t s are de ... e red c ... se t ... e er peer, h ch s espec a ... a uabe ... emerge t s tuat ... s ... here resp ... se t me s much m re the ke ... ssue

## References

1. H. Lim and C. Kim: Flooding in wireless ad hoc networks. Computer Communications Journal, 24(3-4): 353-363, 2001.

2. C. Lindemann and O. Waldhorst: A Distributed Search Service for Peer-to-Peer File Sharing in Mobile Applications. Proc. The 2nd International Conference on Peer-to-Peer Computing, September 2002.
3. B.N. Clark, C.J. Colbourn, and D.S. Johnson: Unit Disk Graphs. Discrete Math, vol. 86, pp. 165-177, 1990.

# Task Mapping Algorithm for Heterogeneous Computing System Allowing High Throughput and Load Balancing<sup>1</sup>

Sung Chune Choi and Hee Yong Youn

School of Information and Communications Engineering,  
Sungkyunkwan University,  
440-746, Suwon, Korea +82-31-290-7952  
{choisc, youn}@ece.skku.ac.kr

**Abstract.** The applicability and strength of heterogeneous computing systems are derived from their ability to match computing nodes to appropriate tasks since a suite of different machines are interconnected. A good mapping algorithm offers minimal expected completion time and machine idle time. In this paper we propose a new task scheduling algorithm allowing higher performance than the existing algorithms such as the Min-min, Max-min, and Sufferage algorithm. It is achieved by task swapping approach based on the expected completion time and ready time of each machine. Extensive computer simulation validates the proposed algorithm along with the earlier ones.

**Keywords:** Heterogeneous computing, load balancing, task mapping, throughput, scheduling.

## 1 Introduction

In heterogeneous computing (HC) environment, a suite of different machines are interconnected to provide a variety of computational capabilities and maximize their combined performance to execute tasks having diverse requirements. There exist a number of different types of HC systems. This paper focuses on mixed-machine HC systems, where a number of high-performance heterogeneous machines are interconnected through high-speed links [1].

In HC system the application is decomposed into tasks, where each task is computationally homogeneous. The applicability and strength of HC systems are derived from their ability to match the computing resources to appropriate tasks. Here each task is assigned to one of the machines which is best suited for its execution to minimize the execution time. Therefore, an efficient mapping scheme allocating the application tasks to the machines is needed.

The general problem of mapping tasks to the machines is a well known NP-complete problem and several mapping algorithms have been proposed to approxi-

---

<sup>1</sup> This research was supported by the Ubiquitous Autonomic Computing and Network Project, 21st Century Frontier R&D Program in Korea and the Brain Korea 21 Project in 2004. Corresponding author: Hee Yong Youn.

mate its optimal solution in the literature. The representative batch mode mapping algorithms are Min-min, Max-min, and Sufferage algorithm [2,3,4]. A good mapping algorithm compromises between matching for smallest expected completion time and load balancing to minimize the machine idle time. Since the previous algorithms have some limitations, we propose a new scheduling algorithm solving them. It is achieved by task swapping approach based on the expected completion time and ready time of each machine. Computer simulation reveals that the proposed algorithm consistently outperforms the earlier algorithms for various degree of task and machine heterogeneity.

## 2 Related Work

At first, we define some metrics used throughout the paper, which are the expected execution time (EET), ready time (RT), expected completion time (ECT), and makespan. The  $EET_{ij}$  is the estimated execution time for task  $i$  ( $t_i$ ) on machine  $j$  ( $m_j$ ) if  $m_j$  has no load when  $t_i$  is assigned. If an HC system of  $m$  machines has  $t$  tasks, we can obtain a  $t \times m$  EET matrix. The  $RT_j$  is the time that  $m_j$  becomes ready after completing the execution of the tasks that are currently assigned to it. The  $ETC_{ij}$  is the time at which  $m_j$  completes  $t_i$  after finishing any previously assigned tasks. From the definitions above, it is easy to get  $ECT_{ij} = RT_i + EET_{ij}$ . The makespan for a complete schedule is then defined as the time duration from the start to the time the entire tasks are completed. Makespan is a measure of the throughput of an algorithm. In other words, the ready time of a machine after tasks are assigned will be smaller if the makespan is decreased.

The Min-min algorithm computes each task's Minimum Completion Time (MCT) over the available hosts and the task with the minimum MCT is assigned to the best host. The motivation behind the Min-min algorithm is that assigning tasks to the hosts completing them fastest will lead to overall reduced makespan. The Max-min algorithm is similar to the Min-min algorithm except that task with the maximum earliest completion time is assigned. The Max-min algorithm might outperform the Min-min algorithm when there exist more short tasks than long tasks. The Sufferage algorithm assigns a machine to a task that would 'suffer' most in term of expected completion time if that particular machine is not assigned to it.

## 3 The Proposed Scheduling Algorithm

The proposed new scheduling algorithm shown in Figure 1 is divided into two parts. The initialization step of Line (1) to (4) is similar to the ones in the Min-min and Max-min algorithm. It differs from the Min-min algorithm in that a task is mapped onto a machine as soon as it arrives at the scheduler like the MCT (minimum completion time) algorithm. Each task is examined to determine the machine providing earliest completion time, and then the pre-allocation table and the temporary RT table are updated to reassign the tasks. The MCT algorithm is fast and simple, but it may not assign a task to the best matched machine since it does not consider subsequently arriving tasks those better match the machine. To remedy this sort of miss-matching,



each task is reassigned by calculating the expected completion time and the ready time of each machine in Line (5) to (13). In each iteration of the for loop, a task is selected arbitrarily, and the task having earlier completion time than this one is found if it exists. If such task exists, the two tasks are swapped if at least one of the following two conditions is satisfied; i) the ECTs of the two machines are decreased, ii) even though the ECT of one machine is increased, the maximum ready time is decreased. The main objective of the proposed approach is for better matching and load balancing at the same time. When all the iterations of the inner for loop are completed, the temporary RT table of each machine is updated.

```

/* a task is mapped onto a machine as soon as it arrives at the scheduler */
(1) for all mj (in a fixed arbitrary order)
(2)   calculate the ECT according to EET and RT, and then update
(3)   find the machine mj with the minimum earliest completion time
(4)   update the temporary RT table and update the pre-allocation table
(5) for each tk that assigned to each machine (in a fixed arbitrary order)
(6)   for each task ti for mj (in a fixed arbitrary order)
(7)     calculate the diff_value of ti and tk to mj and mi
(8)     if (Temporary RTi + EETki) < (Maximum ready time in temporary RT table)
        && diff_value of task ti assigned to mj ≥ the diff_value of mi
(9)       swap task between mj and mi
(10)  for every machine mj
(11)    if (Temporary RTj + EETkj) < (Maximum ready time in temporary RT table)
(12)      deallocate tk and allocate tk to mj
(13)      update the temporary RT table
(14) update the ready time table based on the tasks that were assigned to the machines
(15) update the expected completion time table
    
```

Fig. 1. The proposed scheduling algorithm

### 4 Performance Evaluation

Table 1 shows the improvement of the EET of the Max-min, Min-min, and Sufferage algorithm using the proposed algorithm for eight machine system. Here,

Table 1. Improvement of the EETs with the proposed algorithm for eight machine system

Task/ Machine heterogeneity	Max-min	Min-min	Sufferage
Low/ Low	30.1 %	3.5 %	3.4 %
Low/ High	27.6 %	3.7 %	5.3 %
High/ Low	26.7 %	1.3 %	0.5 %
High/ High	29 %	3.7 %	2.6 %

consistent EET table was obtained from the inconsistent EET table by sorting the execution times of the tasks on all machines. Note that the proposed algorithm outperforms the existing algorithms for various degree of task and machine heterogeneity.

## 5 Conclusion

The mapping algorithms in distributed systems aim at different measure such as makespan, load balancing, and throughput. A good mapping algorithm needs to compromise the conflicting measures. In this paper we have proposed a new task scheduling algorithm which is better than the existing algorithms in terms of throughput and load balancing. It is achieved by task swapping approach based on the expected completion time and ready time of each machine. In inconsistent heterogeneity mode, the makespan of the proposed algorithm is lower than the existing algorithms because it swaps the tasks among the machines for achieving good load balancing. Also, the proposed algorithm has lower time complexity than others.

As a future work we will develop a more optimized algorithm that considers the quality of service, and carry out comprehensive performance evaluation. We will also implement the newly proposed task scheduling algorithm in an actual heterogeneous environment for testing and refinement.

## References

1. H. J. Siegel, J. K. Antonio, R. C. Metzger, M. Tan, and Y. A. Li, "Heterogeneous computing." In A. Y. Zomaya (ed.), *Parallel and Distributed Computing Handbook*, New York, NY: McGraw-Hill, 1996, 725-761.
2. Maheswaran, M. Ali, S. Siegal, H.J. Hensgen, D. Freund, R.F., "Dynamic matching and scheduling of a class of independent tasks onto heterogeneous computing systems," HCW'99, 1999, 30-44.
3. O.H. Ibarra and C. E. Kim, "Heuristic algorithms for scheduling independent tasks on non-identical processors," *Journal of the ACM*, 24(2), April 1977, 280-289.
4. R. F. Freund, M. Gherrity, S. Ambrosius, M. Campbell, M. Halderman, D. Hensgen, E. Keith, T. Kidd, M. Kussow, J. D. Lima, F. Mirabile, L. Moore, B. Rust, and H. J. Siegel, "Scheduling resources in multiuser, heterogeneous, computing environments with Smart-Net," HCW'98, 1998, 184-199.
5. Ali, S. Siegel, H.J. Maheswaran, M. Hensgen, D. "Task execution time modeling for heterogeneous computing systems," HCW'2000, May 2000, 185 - 199
6. M.Y. Wu and W. Shu, "A High-Performance Mapping Algorithm for Heterogeneous Computing Systems," *International Parallel and Distributed Processing Symposium (IPDPS)*, April 2001.
7. Arnaud Giersch, Yves Robert, Frédéric Vivien, "Scheduling Tasks Sharing Files on Heterogeneous Master-Slave Platforms", 12th Euromicro Conference on Parallel, Distributed and Network-Based Processing (PDP'04), February 2004, 11 - 13.

# An Approach for Eye Detection Using Parallel Genetic Algorithm

A. Cagatay Talay

Department of Computer Engineering, Istanbul Technical University,  
34469 Istanbul, Turkey  
talay@cs.itu.edu.tr

**Abstract.** In this paper, a new reliable method for detecting human eyes in an arbitrary image is devised. The approach is based on searching the eyes with Parallel Genetic Algorithm. As the genetic algorithm is a computationally intensive process, the searching space for possible face regions is limited to possible eye regions so that the required timing is greatly reduced. The algorithm works on complex images without constraints on the background, skin color segmentation and so on. The eye detection process works predictably, fairly, reliably and regardless of the perspective.

## 1 Introduction

Eye detection is a crucial aspect in many useful applications ranging from face recognition/detection to human computer interface, driver behavior analysis, or compression techniques like MPEG4. A large number of works have been published in the last decade on this subject. Generally the detection of eyes consists of two steps: locating face to extract eye regions and then eye detection from eye window. The face detection problem has been faced up with different approaches: neural network, principal components, independent components, skin color based methods [1, 2]. Each of them imposes some constraints: frontal view, expressionless images, limited variations of light conditions, hairstyle dependence, uniform background, and so on. A very exhaustive review has been presented in [3]. On the other side many works for eye or iris detection assume either that eye windows have been extracted or rough face regions have been already located [4, 5-7]. No much works have been presented in literature that search directly eyes in whole images, except for active techniques: they exploit the spectral properties of pupil under near IR illumination.

The main objectives of this work is to propose an eyes detection algorithm that is applicable in real time with a standard camera, in a real context such as people driving a car (then with a complex background), and skipping the first segmentation step to extract the face region as commonly done in literature. The rest of the paper is organized as follows: Section 2 gives brief information about the Parallel Genetic Algorithms. The search process of eyes is described in Section 3. Finally, in Section 4 conclusions and future works are presented.

## 2 Genetic Algorithms

A sequential GA proceeds in an iterative manner by generating new populations of strings from the old ones. Every string is the encoded version of a tentative solution. An evaluation function associates a fitness measure to every string indicating its suitability to the problem. The algorithm applies stochastic operators such as selection, crossover, and mutation on an initially random population in order to compute a whole generation of new strings. Unlike most other optimization techniques, GAs maintain a population of tentative solutions that are competitively manipulated by applying some variation operators to find a global optimum. For nontrivial problems this process might require high computational resources, and thus a variety of algorithmic issues are being studied to design efficient GAs. With this goal, numerous advances are continuously being achieved by designing new operators, hybrid algorithms, termination criteria, and more [8]. We adopt one such improvement consisting in using parallel GAs (PGAs) and incorporating some advanced heuristics into an overall genetic algorithm.

PGAs are not just parallel versions of sequential genetic algorithms. In fact, they reach the ideal goal of having a parallel algorithm whose behavior is better than the sum of the separate behaviors of its component sub-algorithms, and this is why we directly focus on them. Several arguments justify our work. First of all, GAs are naturally prone to parallelism since the operations on the representations are relatively independent from each other. Besides that, the whole population can be geographically structured [9] to localize competitive selection between subsets, often leading to better algorithms.

Using PGAs often leads to superior numerical performance even when the algorithms run on a single processor [10, 11]. However, the truly interesting observation is that the use of a structured population, either in the form of a set of islands [12] or a diffusion grid [9], is responsible for such numerical benefits. As a consequence, many authors do not use a parallel machine at all to run structured-population models and still get better results than with serial GAs [13, 14]. Hardware parallelization is an additional way of speeding up the execution of the algorithm, and it can be attained in many ways on a given structured-population GA. Hence, once a structured-population model is defined, it could be implemented in any uniprocessor or parallel machine. There exist many examples of this modern vision of PGAs, namely, a ring of panmictic GAs on a MIMD computer, a grid of individuals on uniprocessor/MIMD/SIMD computers, and many hybrids.

## 3 Process of Eye Detection

The idea behind this study is quite simple: the eyes can be easily located in the image since the iris is always darker than the sclera no matter what color it is. In this way the edge of the iris is relatively easy to detect as the set of points that are disposed on a circle. The first step in applying PGAs to the problem of feature selection for eye detection is to map the pattern space into a representation suitable for genetic search. Since the main interest is in representing the space of all possible subsets of the

original feature list, the simplest form for image base representations considers each feature as a binary gene. Each individual chromosome is then represented as a fixed-length binary string standing for some subset of the original feature list. In this method, first of all the pupil and the edge of the eye are extracted, in addition the position of the eyes is detected more accurately. For the extraction of the eye area, chromosome of individual is set as the first former array composed position information and the size of eye's outlines and pupil. Moreover, fitness of individual is obtained from evaluation function, which pays attention to three features of eyes (difference between white of eye and pupil, color, shape, and size of pupil, edge of eye). The eye area is extracted by chromosome information on the individual with the maximum fitness when evolution completed.

For detection, the pupil is expressed in circle, and the outlines of eye are expressed in the oval, and the pupil is assumed to be at centers of eye. It is defined that the chromosome of individual is composed as X and Y coordinates which shows center of eyes, radius of circle that shows size of pupil and shape of oval which shows outlines of eyes. The first former array of each center coordinates is ten bits, a radius of the circle and oval major axis and minor axis is six bits, total 36 bits, makes. In PGA random initialization is used. Next, whether the defined chromosome is suitable as the eye is decided according to the evaluation function. Since this method pays attention to the features of eye, "Eyes have white of the eye and pupil", "The shape of the pupil is near circle, and the color is a black", "The outline of eye can be approximated to the oval", the following three are used as an evaluation function.

Eye has white of the eyes and pupil, it is feature that high density difference between white area and black area. In a word, if there is a big change in the density value of the pixel in a certain area, it is concluded this area is near eyes or the areas around eyes. Then, products of two high-ranking values of the density difference in the area are used as feature. Where eyes are enclosed, the density change is large in the boundary between white of the eye and pupil, the product has a large value.

It is a feature of the pupil that shape is a circular arc, because upper part of pupil is hidden by above eyelid. The color of pupil looks black in the brightness image and the turn of the pupil in enclosed with white of the eye. Therefore, the portion of black pixel in circular arc and the number of white pixels in circular arc surroundings are used as among of features. In Fig. 1, it is evaluated that area A where eyes are shown has high value. But the case of area B (skin) or area C (eyebrow) does not have proper value of white and black pixels in the circular arc, then the evaluation is bad.

Moreover, the gap of the center is evaluated by obtaining the difference of the radius of circle which is in scribe to the pupil and the circle with the string. As shown in Fig. 2, if the circular arc center shifts from the center of the circle, the difference of



Fig. 1. Evaluation of Circle



Fig. 2. Gap of center

case, black pixels are few and the evaluation is good, but the case of eyebrow and hair, is badly evaluated because a lot of black pixel exists. The difference of shape

between oval and outline of eye is obtained by using edge image. The sum of distance from 12 points is obtained, top, bottom, right and left. If the sum distance is big value, the oval and the shape of eyes are greatly different, if the sum is small, those shapes looks like.

## 4 Conclusions and Future Work

In this study, an effective algorithm for eyes detection in arbitrary images is presented. PGA is used to detect the eyes according to the information based on the features of eyes, like shape of the eye and pupil, white of eye and pupil. The proposed technique does not impose any constraint on the background and does not require any preprocessing step for face segmentation. Eye is detected without receiving change of the lighting and effect of face of direction. High detection rates have been obtained. The results are surprisingly good also when the eyes are not completely open.

## References

1. H. A. Rowley, S. Baluja, T. Kanade: Neural Network-Based Face Detection. *IEEE Trans. on Pattern Analysis and Machine Intelligence* Vol. 20, No. 1, Jan. 1998, pp 23-38.
2. R. Hsu, M. Mottleb, A. K. Jain: Face Detection in Color Images. *IEEE Transaction on Pattern Analysis and Machine Intelligence* Vol24, No. 5, May 2002.
3. M. H. Yang, D. Kriegman, N. Ahuja: Detecting Faces in Images: A Survey. *IEEE Transaction on Pattern Analysis and Machine Intelligence* Vol. 24, No. 1 January 2002.
4. T. Kawaguchi, M. Rizon: Iris detection using intensity and edge information. *Pattern Recognition* 36 (2003) 549-562.
5. S. Baskan, M. Bulut, V. Atalay: Projection based method for segmentation of human face and its evaluation. *Pattern Recognition Letters* 23 (2002) 1623-1629.
6. S. Sirohey, A. Rosenfiled, Z. Duric: A method of detection and tracking iris and eyelids in video. *Pattern Recognition* 35 (2002) 1389-1401
7. M. Rizon, T. Kawaguchi: Automatic extraction of iris with reflection using intensity information. *Proc. of the 3th Iasted Conf. on Vis. Imaging and image processing*, 2003.
8. J.H. Holland: *Adaptation in natural and artificial sys..* U. of Michigan Pr., Ann Arbor, 1975.
9. P. Spiessens and B. Manderick: A massively parallel genetic algorithm. *Proceedings of the 4th Int. Conf. on Genetic Algorithms*. R.K. Belew (Ed.) Morgan Kaufmann, (1991).
10. V.S. Gordon and D. Whitley: Serial and parallel genetic algorithms as function optimizers. *Procs. of the 5th ICGA*. S. Forrest (Ed.) Morgan Kaufmann, (1993).
11. F. Herrera and M. Lozano: Gradual distributed real-coded genetic algorithms. *Technical Report #DECSAI-97-01-03*, (1997). (Revised version 1998).
12. R. Tanese: Distributed genetic algorithms. *Proc. of 3rd ICGA*. J.D. Schaffer (Ed.) (1989).
13. V.S. Gordon and D. Whitley: Serial and parallel genetic algorithms as function optimizers. *Procs. of the 5th ICGA*. S. Forrest (Ed.) Morgan Kaufmann, (1993).
14. E. Alba, J.F. Aldana, and J.M. Troya: A genetic algorithm for load balancing in parallel query evaluation for deductive relational databases. *Procs. of the I. C. on ANNs and GAs*. D.W. Pearson, N.C. Steele, and R.F. Albrecht (Eds.) Springer-Verlag, (1995).

# Graph Representation of the Nested Software Structure

Leszek Kotulski

Institute of Comp. Sci., Jagiellonian University,  
Kraków, Poland  
kotulski@ii.uj.edu.pl

**Abstract.** The use of the UML notation for software specification leads usually to lots of diagrams showing different aspects and components of the software system in a several view. Complex components are constructed by composing in parallel some elementary components and as a result the overall architecture of the system is described as a hierarchical composition of primitive components, which at the execution time may be deployed on distributed environment. The task of specifying such a system quickly becomes unmanageable without the help of some structuring tools. This paper discusses how the UML package's nested structure can be maintained and visualized with the help of a graph transformation mechanism based on the edNLC class of grammar.

## 1 Introduction

The ULM [12] is a recent approach to strengthen the effort of designing an object-oriented modeling language where all main issues of system analysis and design are taken into account. The UML provides deployment diagrams to show a system's network topology and software components that live on the network nodes. For the description of the objects replication and migration, remote interactions and dynamics network topologies, which are important issues in distributed object systems these techniques promise support, however, seems to be insufficient. Modeling distributed systems by distributed graph transformation, a powerful and flexible description, is obtained by applying graph transformation to network structures [10]. Distributed graphs are, in this case, structured with two abstraction levels: the network and the local level. The main drawback of above proposition is lack of support any structuralization mechanisms, such for example as the UML packages. In the paper we show that a graph transformation mechanism is also suitable for the visualization nested software structures. The formal background of this proposition are the ULM notation and the Rosenberg's edNLC class of grammars [5], developed next by Flasiński [2,3] and author [4,7,8].

## 2 Nested Diagrams

Deployment diagrams, used in the UML, show the configuration of run time processing elements (nodes) and software components (processes and objects) that

execute on them. Nodes are physical processing resources, and are drawn as a 3D rectangle. Each node contains software components. The software components on different nodes can communicate across the physical connections between the nodes.

A component unit represents a modular, deployable, and replaceable part of a system that encapsulates an implementation and exposes a set of interfaces. Some components can be represented by the UML packages that provide a tool for organizing the products of analysis, design, and coding. Let us consider a management system based on a Data Warehouse concept, which stores of data obtained from an ERP systems (see Fig. 1).

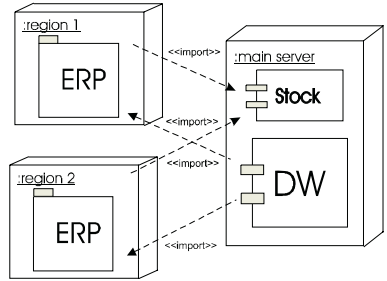


Fig. 1.

However, the ERP system consists from many cooperating subsystems (such as finance, sales, manufactures and human resource packages – as in fig. 2), because of that someone may want to see direct associations among these subsystems and the Data Warehouse repository. This simple example shows, that exist a necessity of introduction more than only two levels of abstraction (representing hardware or software components). That means that the method of the presentation allocated software components should create several abstraction levels (analogically as in the object oriented programming). We describe here the component and package concept using the graph transformation notation. Like a group [6] the package can be specified as a graph which visualize connections among its components. As a result, the overall architecture of the system is described as a hierarchical composition of primitive components.

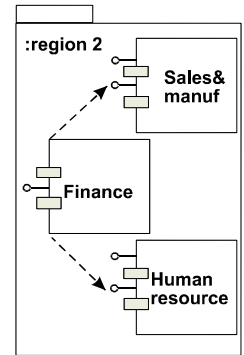


Fig. 2.

Considering visual languages both import and export interface concepts are supported [10, 11, 13]. Component diagrams in the UML knows only export interfaces, but Botch, Rumbaing and Jacobson [1] suggest that in a system consisting from a few dozen components the UML notation should directly specify imports using packages and `<<import>>` stereotypes. Moreover, in distributed systems the motivation of the import interface visualization is not only a possibility of formal checking the consistency of the modeled system but also the formal specification of stub instances at the implementation level.

To simplify an example we reduce components interconnection to the following: DW calls each of the ERP components to take their monthly summary, Finance calls appropriately Human resource and Sales for receiving daily reports and Stock (to evaluate securities). In such a case, the UML diagram presented in fig. 2 can be expressed as the attributed graph presented in fig. 3. It describes two levels of a component's configuration: the top level – representing the ERP as a final component and the internal level – representing the ERP internal structure; each component appearing inside internal structure can also have its own nesting representation; so it can create the hierarchical (tree) structure of components (where leafs are object instances).



The presented solution is based on the node label controlled graph grammars [2,3,4,5,7,8]. Graph nodes used for describing of a distributed system can be labeled as follows: P - for a package component, E – for an export interface, I – for an import interface (stub), O – for an object instance implementing component, N – for a computing node representation. All additional information about the graph node can be described by its attributes. Graphically we expose only component’s name. The only correct labeling pattern<sup>1</sup> is included is the following set of triples (E,b,P), (E,b,O), (P,c,I), (O,b,G), (O,c,I), (N,d,G), (N,d,O), (I,l,E), (N,n,N). Edge labels b, c, d, l and n are appropriately abbreviation for **b**elonging, **c**alls, **d**eploy, **l**inked and **n**ode interconnection.

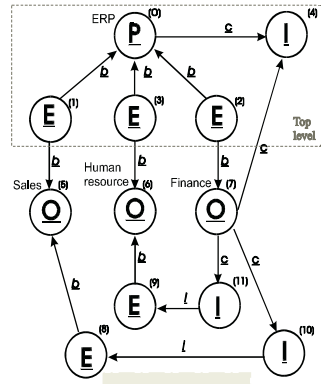


Fig. 3.

The presented transformation from the UML to the graph notation seems to be simple and intuitive. On the other hand, when size both package and allocation graphs grows to hundreds or thousands nodes we should also consider a computational complexity of the considered solution. Let us notice that the membership problem i.e the parsing of the graph in order to designate the proper sequence of productions has the critical complexity for many graph grammars (among others for graph transformation model based on graph morphism [10,11]). For this reason we suggest using of the node label controlled class of graph grammars. The introduced in [7,8] aedNLC graph grammar (as equivalent to ETPL(k) graph grammar [3]) allows one to solve parsing, membership and a new graph generation problems with  $O(n^2)$  computational complexity.

The correctness of graph transformation is forced by a graph transformation rules called productions described how the left hand production graph be replaced by the right hand one with the embedding transformation defining how edges coming to/from the left hand side graph be connected with the right hand one. For example if we would like to express that some service can be offered by an object we use the following production with the embedding transformation  $\mathbb{E}_5 = \{((op,out, 1), \{(O,(P,true),op,out), (E,(P,true), pe, in) \}), COPY\_REST \}$  interpreted as follows every edge labeled by “op” and coming from the removed node in the visualization graph ought to be replaced by the edge (labeled by op) connecting the node of the graph of the right-hand side of the production and labeled by “O” with the node p of the rest graph and labeled by “P” and the edge (labeled by pe) connecting the node of the graph of the right-hand side of the production and labeled by “E” with the node p of the rest graph and labeled by “P”. Note that edges mentioned in the embedding transformation are the auxiliary ones and are not expressed in the graph presented in fig. 3. The full description of the set of the productions used for creation of the visualization graph is presented in the technical report [8].

<sup>1</sup> Term labeling pattern for edge (v,μ,w) means triple (δ(v), μ, δ(w)), where δ(v) and δ(w) returns labels of v, w node indices appropriately.

### 3 Conclusions

In the previous chapter it is shown that the graph transformation can be useful formalism for controlling the allocation process. The deployed software component can be split onto a few abstraction levels using packages. It improve a quality of a distributed system presentation; now we can show either a nested structure of a component or an allocation graph in a flat form (where any component is either in their top or internal level of specification; two different, non nested components can be, however, described at the different abstraction level [8]). Moreover, as the package is specified by the attributed graph, so it can formally check the correctness of its component deployment and the consistency of the generated software (i.e. assure that for each request a proper service is associated). As it shown in [7,8] the aedNLC grammars allows one to divide such an allocation graph onto a few distributed subgraphs and control their modification in a parallel way. The last property is important not only from the computational complexity point of view but also creates the practical possibility of a parallel work of several systems administrators.

### References

1. G. Booch, J. Rumbaugh, I. Jacobson: The Unified Modeling Language – User Guide. Addison Wesley Longman, Inc. 1999.
2. Flasiński M.: Characteristic of edNLC-graph Grammars for Syntactic Pattern Recognition. *Computer Vision, Graphics and Image Processing*, 1989, vol.42, pp. 1-21.
3. Flasiński M.: Power Properties of NCL Graph Grammars with a Polynomial Membership Problem. *Theoretical Computer Science*, 1998, vol. 201, pp. 189-231.
4. Flasiński M., Kotulski L.: On the Use of Graph Grammars for the Control of a Distributed Software Allocation. *The Computer Journal*, 1992, vol. 35, pp. A167-A175.
5. Janssens D., Rozenberg G., Verraedt R.: On Sequential and Parallel Node-rewriting Graph Grammars. *Computer Graphics and Image Processing*, 1982, vol. 18, pp. 279-304.
6. Kotulski L., Jurek J., Moczurad W.: Object-Oriented Programming in the Large Using Group Concept. *Computer Systems and Software Engineering - 6th Annual European Conference*, Hague 1992, pp. 510-514.
7. Kotulski L.: Model systemu wspomaganie generacji oprogramowania współbieżnego w środowisku rozproszonym za pomocą gramatyk grafowych. *Postdoctorals Lecturing Qualifications. Jagiellonian University Press*, ISBN 83-233-1391-1, 2000.
8. Kotulski L.: Parallel Allocation of the Distributed Software Using Node Label Controlled Graph Grammars. *Jagiellonian University, Inst. of Comp. Sci., Preprint no. 2003/006*
9. Kotulski L.: Nested Software Structure generated by aedNLC graph grammar – technical report. *Jagiellonian University, Inst. of Comp. Sci., Preprint no. 2005/003*  
<http://www.ii.uj.edu.pl/preprint/kotulski03>
10. Taentzer G., Fischer I., Koch M., Vole V.: Visual design of distributed graph transformation. In *Handbook of Graph Grammars and Computing by Graph Transformation, Volume 3: Concurrency, Parallelism, and Distribution*. World Scientific, 1999.
11. Taentzer G.: A Visual Modeling Framework for Distributed Object Computing. In *Formal methods for open object-based distributed systems*, Kluwer Academic Publishers, 2002
12. OMG-Unified Modeling Language, v1.5. [www.rational.com](http://www.rational.com)
13. Zhang D., Zhang K., Cao J.: A context-sensitive Graph Grammar Formalism for the Specification of Visual Languages. *The Computer Journal*, 2001, vol 44, no. 4, pp186-200.

# Transaction Routing in Real-Time Shared Disks Clusters\*

Ung-Ho Oh, Jaehyeon Lee, and Jaehyeon Chae

Department of Computer Engineering, Yeungnam University,  
Gyongsan, Gyungbuk 712-749, Republic of Korea  
hrcho@yu.ac.kr

**Abstract.** This paper proposes a real-time transaction routing algorithm, which allocates real-time transactions to a node in a shared disks cluster. Unlike traditional routing algorithms, which consider load balancing and transaction affinity only, our algorithm also considers transaction priorities inherent to real-time applications.

## 1 Introduction

Although there has been a great deal of independent research on real-time processing and shared disks ( ) cluster, the aggregated has not yet attracted

the cluster technology enables high available real-time database services, which are the core of many telecommunication services. The cluster can also achieve high performance real-time transaction processing by partitioning the parameter

This paper proposes a real-time transaction routing algorithm in the cluster. The transaction routing is a process of the first selected service execution of real-time transaction. The traditional transaction routing algorithms of the cluster have tried to design a *load balancing* and *transaction affinity* [4], [5], [6]. The load balancing means to distribute the dual of the transaction affinity means to execute transactions with similar data access patterns in the same node (*affinity node*) to support real-time transactions. We have added a *transaction priority* to design a means to reduce the number of transactions missing the deadline by considering the deadline as a priority. The contribution of this paper is to design a new performance oriented transaction routing algorithm, named *CA* (*Dynamic Affinity Cluster Allocation*) proposed by authors [4], to the real-time transaction processing.

## 2 Algorithm

The proposed real-time transaction routing algorithm, named *CA* (*Priority conscious DACA*) in this section, is the first described under the algorithm.

---

\* This research was supported by University IT Research Center Project.

and then summarize the basic design of Algorithm 4. Next, we present Algorithm that extends the conflict resolution process.

## 2.1 Assumption

Transaction router selects an executor to deal with each incoming transaction. He/she schedules the executor of its transaction with *earliest deadline first* (EDF) policy. We assume the *mixed* real-time transaction workload which consists of real-time transactions and non-real-time transactions. Real-time transactions are assigned with a deadline. Executor of the real-time transaction after its deadline expires.

We assume that the recording executor selects real-time applications, the recording has to handle the *priority inversion* problem that lower priority transactions block the executor of higher priority transactions. To prevent the problem, we consider the recording method of 2-priority, a real-time transaction aborts if real-time transaction hold locks. Critical mode of the other hand, a non-real-time transaction always starts at lock. Critical the same procedure holds between real-time transactions with different priorities. High priority transactions are always guaranteed to acquire locks without waiting.

## 2.2 DACA

We define the routing overhead of cluster based on the load of each *affinity cluster* ( $C$ ). Cluster collects several transaction classes with high affinity to a given set of tables. The transaction router maintains routing parameters specifically, he/she a transaction router allocates a transaction of an affinity cluster  $C_q$  to a node  $N_p$ , to create its birth  $\#(C_q)$  and  $\#(N_p)$ , which means the number of active transactions at  $C_q$  and  $N_p$  respectively. Both counters are decremented when a transaction commits or aborts.

There are two server load types: *AC overload* and a *node overload*. The server load implies that transactions of a  $C$  are rushed to the system. The node overload occurs when a node  $N_p$  is allocated to several  $C$ s and  $\#(N_p)$  server average  $C$  balances the load of each node according to the server load type of  $AC_q$  server load, the  $C$  allocates more nodes to  $AC_q$  by *node expansion* strategy. If there is a  $C$  server load but  $N_p$  server load, the  $C$  distributes some  $C$ s assigned to  $N_p$  to other nodes by *AC distribution* strategy.

$C$  can make a trade-off between the affinity based routing and load balancing as follows. First,  $C$  tries to reduce the number of nodes allocated to the server load  $C$  of the load de-allocated of each node's significance. This allows  $C$  to reduce the frequency of the cache and data sets. Next,  $C$  prohibits allocating birth of server load  $C$  and other  $C$ s to a node. As a result,  $C$  can achieve a high buffer hit ratio for the server load  $C$ . Even though several server load  $C$ s may be allocated to a single node, efficient handling of the server load  $C$ s may improve the overall transaction throughput.

### 2.3 Priority Conscious DACA (P-DACA)

ef re descr b g the deta s f C e first llustrate the pr b em f C he tra sact s sha e pr rtes E amp e sh s the pr b em

**Example 1:** upp se there are t Cs ( $AC_1, AC_2$ ) a d t des ( $N_1, N_2$ )  $N_1$  s a affi t de f  $AC_1$  a d e cutes a tra sact  $t_1$  f pr r t  $N_2$  s a affi t de f  $AC_2$  a d e cutes a tra sact  $t_2$  f pr r t t th s t me, upp se a e tra sact  $t_3$  f pr r t 7 arr es, a d  $t_3$  be gs t  $AC_1$  he C a cates  $t_3$  t ts affi t de  $N_1$  f  $N_1$  d es t resu t er ad state e er,  $t_3$  has er pr r t tha  $t_1$  a d ca t be e cuted u t  $t_1$  c mp etes  $t_3$  has a h gher pr bab t f m ss g ts dead e O the ther ha d f  $t_3$  s a cated t  $N_2$ , the t ca be e cuted m med ate. □

he g a f C s (a) t reduce the mber f tra sact s m ss g the r dead es, a d (b) t take ad a ages f affi t custer g as C ach e e th s g a C perf rms the f g three bas c steps seque t a t dec de here a e rea t me tra sact  $t_r$  be r ued t

- 1 f there s a affi t de f  $t_r$  here the pr r t f  $t_r$  bec mes the h ghest e, the a cate  $t_r$  t that de
- 2 f there s a affi t de f  $t_r$  here the pr r t f  $t_r$  bec mes the h ghest e, the a cate  $t_r$  t that de
- 3 f there s de that ca e cute  $t_r$  m med ate, the a cate  $t_r$  t e f ts affi t des

he bas c steps ca be pt m zed f the tra sact r uter ma ta s a *priority list* f r each de he pr r t st s a s rted st desce d g rder f pr rtes f act e rea t me tra sact s at the de he a e rea t me tra sact  $t_r$  has t be a cated t a de here  $t_r$  ca be e cuted faster tha ther des C checks th s c d t b c mpar g the re at e p s t f  $t_r$  the pr r t st f each de upp se  $P(t_r)$  mea s the pr r t f  $t_r$ , a d  $t_r$  s c uded the affi t custer  $AC_r$   $\mathcal{S}(AC_r)$  s a set f affi t des f  $AC_r$  he f g s summar ze the tra sact r ut g a g r th m f C

- # ( $AC_r$ ) # ( $AC_r$ ) +
- 2 f ( $t_r$  s a rea t me tra sact ) the
  - (a) f ( $\exists N_p \in \mathcal{S}(AC_r), \text{rank}(P(t_r), N_p) < w_1 \quad \text{rank}(P(t_r), N_p) < \text{rank}(P(t_r), N_i), \text{ f r a } N_i \in \mathcal{S}(AC_r), i / p)$ ) the g t. step 4
  - (b) E se f ( $\exists N_p \notin \mathcal{S}(AC_r), \text{rank}(P(t_r), N_p) < w_2 \quad \text{rank}(P(t_r), N_p) < \text{rank}(P(t_r), N_i), \text{ f r a } N_i \notin \mathcal{S}(AC_r), i / p)$ ) the g t. step
  - (c) E se g t. step
- e ect  $N_p$  here # ( $N_p$ ) s m m m f r a  $N_i \in \mathcal{S}(AC_r)$
- 4 f ( $AC_r$  s er aded) the ca. `node_expansion`( $AC_r$ )  
E se f ( $N_p$  s er aded) the ca. `ac_distribution`( $N_p$ )  
# ( $N_p$ ) # ( $N_p$ ) + sert  $P(t_r)$  t the pr r t st f  $N_p$
- 7 Retur.  $N_p$

At step 2, the function  $\text{rank}(P(t_r), N_p)$  returns the number of transactions whose priorities are higher than  $P(t_r)$  at  $N_p$ . If the function returns  $w_1$ ,  $t_r$  will be a transaction with the highest priority at  $N_p$ . The values  $w_1$  and  $w_2$  are assigned according to constraints that limit the acceptable rank of  $t_r$ .  $w_1$  is usually bigger than  $w_2$  since a different definition of  $t_r$  could complete  $t_r$  faster than that of  $w_1$  and  $w_2$  are set to 0, the algorithm marks similar to the above basic steps. In real-time transaction scheduling, the effects of different definitions with the highest (step 3) of a category  $t_r$  could cause a  $C$  to be read or a  $C$  to be read, the result of the strategy of  $C$  has to be performed (step 4 and 5). Example 2 shows how  $C$  can resolve the problem of Example 2.

**Example 2:** Suppose that the format of  $C$ s,  $C_1$  and  $C_2$ , and transactions are same. Example 2 shows that both  $w_1$  and  $w_2$  are set to 0. The transaction router allocates  $t_3$  to  $N_2$  that can execute  $t_3$  immediately. This is because (a) the affinity of  $t_3$  is  $N_1$  but  $\text{rank}(P(t_3), N_1) = w_1$ , and (b) even though  $N_2$  is not an affinity of  $t_3$  but  $\text{rank}(P(t_3), N_2) < w_2$ . Note that if  $w_1$  is set to 2,  $t_3$  is allocated to  $N_1$ .  $\square$

### 3 Concluding Remarks

The proposed real-time transaction routing algorithm for the real-time cluster, named  $C$ , has the features of  $C$  are that first,  $C$  allocates a real-time transaction to a node that guarantees higher probability of completing the transaction without deadlocking. Even though the transaction could miss its deadline due to succeeding transactions with higher priority, the selected strategy is the best choice at the current state of the  $C$ . Therefore,  $C$  can allocate a transaction to its affinity of process because  $C$  can achieve high buffer hit ratio. This reduces the transaction execution time, and the probability of missing its deadline can be reduced as a result.

### References

1. Lam, K-Y., Kuo, T-W. (ed.): Real-Time Database Systems: Architecture and Techniques. Kluwer Academic Publishers (2000)
2. Lam, K-Y., Kuo, T-W., Lee, T.: Strategies for resolving inter-class data conflicts in mixed real-time database systems. *Journal of Syst. and Soft.* **61** (2002) 1-14
3. Lee, S., Ohn, K., Cho, H.: Feasibility and Performance Study of a Shared Disks Cluster for Real-Time Processing. *Lecture Notes in Computer Science* **3397** (2005) 518-527
4. Ohn, K., Cho, H.: Cache Conscious Dynamic Transaction Routing in a Shared Disks Cluster. *Lecture Notes in Computer Science* **3045** (2004) 548-557
5. Yu, P., Dan, A.: Performance Analysis Clustering on Transaction Processing Coupling Architecture. *IEEE Trans. Knowledge and Data Eng.* **6** (1994) 764-786
6. Yu, P., Dan, A.: Performance Evaluation of Transaction Processing Coupling Architectures for Handling System Dynamics. *IEEE Trans. Parallel and Distributed Syst.* **5** (1994) 139-153

# Implementation of a Distributed Data Mining System

Ju Cho<sup>1</sup>, Sung Baik<sup>1,\*</sup>, and Jerzy Bala<sup>2</sup>

<sup>1</sup> Sejong University, Seoul 143-747, Korea  
{jscho, sbaik}@sejong.ac.kr

<sup>2</sup> Datamat Systems Research, Inc.  
1600 International Drive, McLean, VA 22102, USA  
jbala@dsri.com

**Abstract.** This paper describes the implementation of a distributed data mining system. The system consists of a web server, a pre-processor for data preparation, a mediator, and agents. A distributed learning algorithm of a decision tree in an agent-mediator communication mechanism is the most important and difficult to achieve the distributed data mining in this system, in the view of implementation. The algorithm has successfully been implemented with several techniques. Its implementation is presented in a UML (Unified Modeling Language) sequence diagram.

## 1 Introduction

In this paper, we consider a distributed data mining (DDM) approach [1], in which the modified decision tree algorithm on an agent based framework can deal with heterogeneous data sets in the distributed environment [2,3]. The data mining based on the algorithm takes full advantage of all the available data through a mechanism for integrating data from a wide variety of data sources and is able to handle data characterized by geographic (or logical) distribution, complexity and multi-feature representations, and the vertical partitioning/distribution of feature sets.

The paper describes the implementation of an agent based distributed data mining system which consists of a web server, a pre-processor for data preparation, a mediator, and agents. The web server supports users with a web-based interface through which they can access databases located at different sites and manipulate data mining facilities. The pre-processor prepares data sets for data mining by dealing with databases in a distributed way. The implementation of data preparation for DDM is presented in section 2. The mediator coordinates the communication between several agents with security concerns such as authentication. Each agent is located at each heterogeneous data site to achieve coordinated learning through the cooperation of local learning and communication with the other agents. The implementation of the communication, between the mediator and agents for DDM, and the distributed learning algorithm of a decision tree in the communication mechanism is presented in section 3.

---

\* Author for Correspondence.

## 2 Data Preparation for Distributed Data Mining

Data preparation is a preliminary and necessary phase for data mining. In DDM, data sets located in different distributed sites should be processed and converted to appropriate data forms in advance, so that data mining can be performed in a distributed fashion. Fig. 1 shows a UML sequence diagram for data preparation. In our work, two kinds of files are generated from the database for DDM; 1) a control file (e.g. data.ctr) and 2) a learning file (e.g. data.lea). The steps of data preparation are as follows:

1. The selected database schema information and the meta-data from all of different distributed sites are exchanged via communication between the mediator and agents. Each agent deals with each database at its own location.
2. According to the exchanged information, control files are generated at the sites participating for data analysis. Each control file has all schema information obtained from all databases located at different sites.
3. The values of the class field selected by a user are transferred to other sites from the site which the class field belongs to. The class information is found in all example control files presented in Fig. 2.
4. A primary key for associating the data across different sites is selected. The only co-existing values of the primary key field in all databases are selected. And then their associated tuples are selected to build a learning file in each site.

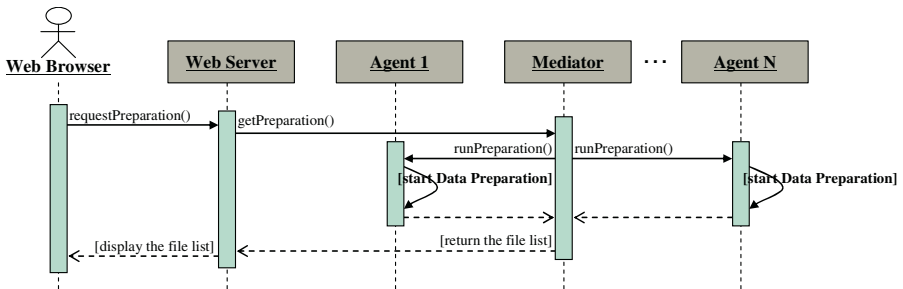
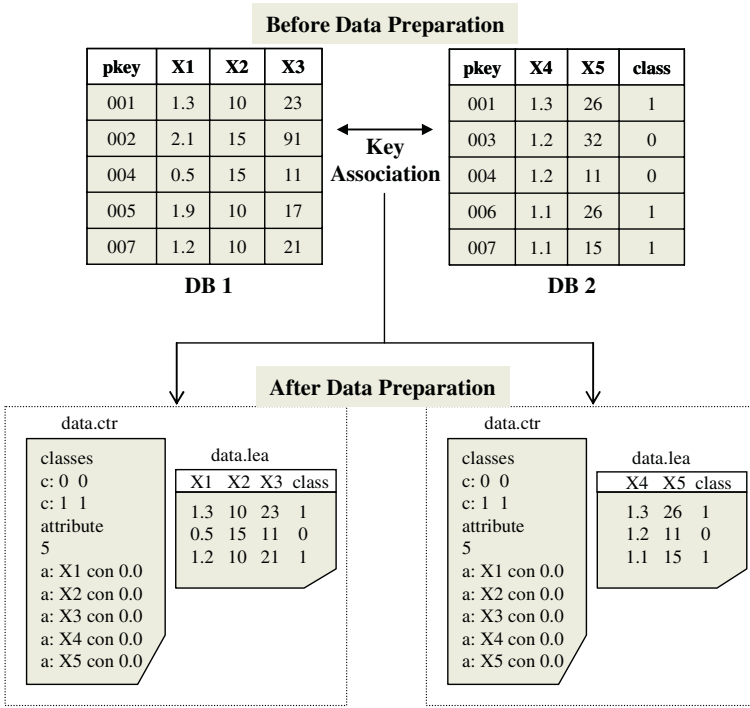


Fig. 1. UML Sequence Diagram for Data Preparation for DDM

## 3 Distributed Data Mining

A data mining engine was implemented in C in a previous work [4]. The communication interface within the agent was implemented in Java. The communication of the mediator and the agents was implemented in Java on RMI (Remote Method Interface). The data mining engine implemented in C is interfaced with the communication interface implemented in Java by JNI (Java Native Interface). The interfaces of core remote methods for DDM are presented in Fig. 3.





**Fig. 2.** Examples of Data Sets before/after Data Preparation

```

public interface Mediator extends Remote {
    ...
    public void startDataMining(String fileNm) throws RemoteException;
    public void setEntropy(String agentName, double entropy, int splitData) throws RemoteException;
    public void setDDT(String agentName, byte[] b, int len) throws RemoteException;
    ...
}
public interface Agent extends Remote {
    ...
    public void runDataMining(String fileNm) throws RemoteException;
    public void notifyRole(boolean winOrLooser) throws RemoteException;
    public void getDDT(byte[] b, int len) throws RemoteException;
    ...
}
    
```

**Fig. 3.** Interface Methods for the Communication between Mediator and Agent

Fig. 4 presents a UML sequence diagram for DDM. The distributed learning algorithm of a decision tree in an agent-mediator communication mechanism is as follows:

1. runDataMining() : Start the local data mining processes associated with local agents.
2. [find the attribute] : Find the attribute and its associated value that can best split the data into the various training classes during local mining.

3. `setEntropy()` : Send the best local attribute and its associated value to the mediator.
4. `[select the best attribute]` : Select the best attribute from the best local attributes of all the agents.
5. `notifyRole()` : Notify each agent of its role for the next action (splitting or waiting).
6. `[split the data]` : Split the data, according to the best global attribute and its associated split value, in the formation of two separate clusters of data in the selected agent.
7. `setDDT()` & `getDDT()` : Distribute the structural information in each cluster and the best attribute to the other agents through the mediator.
8. `[construct the partial decision tree]` : Construct the partial decision trees according to the structural information in other agents.
9. `[generate rules]` : Generate decision rules at each agent and notify the mediator for termination if there is no more splitting. Otherwise, go to step 2.
10. `[notify the end of DDM]` : Terminate.

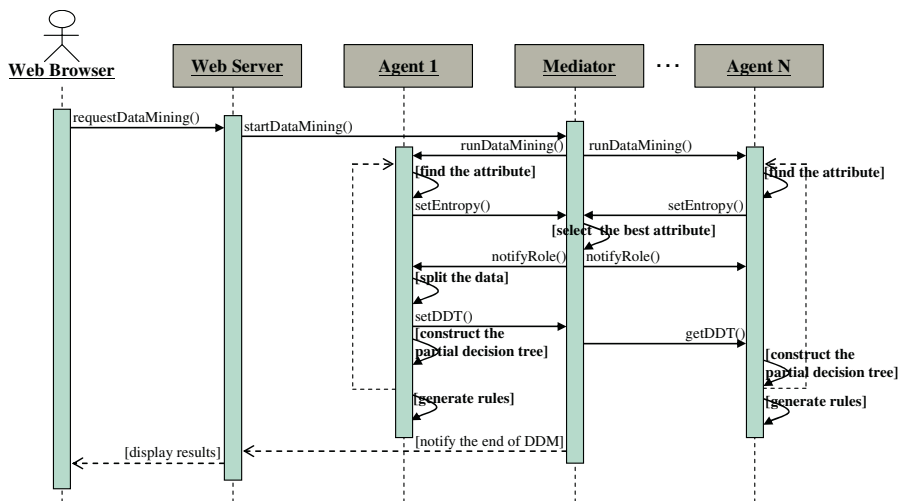


**Fig. 4.** UML Sequence Diagram for Distributed Data Mining

## References

1. S. W. Baik, J. Bala and J. S. Cho: Agent Based Distributed Data Mining, Lecture Notes in Computer Science, Vol. 3320, pp.42-45, 2004
2. D. Caragea, A. Silvescu and V. Honavar: Decision Tree Induction from Distributed, Heterogeneous, Autonomous Data Sources, Proceedings of the Conference on Intelligent Systems Design and Applications (ISDA 03), 2003
3. C. Giannella, K. Liu, T. Olsen and H. Kargupta: Communication Efficient Construction of Decision Trees Over Heterogeneously Distributed Data, Proceedings of the Fourth IEEE International Conference on Data Mining (ICDM 04), pp.67-74, 2004
4. J. Bala, S. W. Baik, S. Gutta and P. Pachowicz: InferView: An Integrated System for Knowledge Acquisition and Visualization, Proceedings of AFCEA Federal Data Mining Symposium, 1999

# Hierarchical Infrastructure for Large-Scale Distributed Privacy-Preserving Data Mining

Institute of Artificial Intelligence, Zhejiang University,  
Hangzhou, 310027, China  
zjupaper@yahoo.com  
xucongfu@cs.zju.edu.cn  
yaekee@hotmail.com  
panyh@sun.zju.edu.cn

**Abstract.** Data Mining is often required to be performed among a number of groups of sites, where the precondition is that no privacy of any site should be leaked out to other sites. In this paper, a hierarchical infrastructure is proposed for large-scale distributed Privacy Preserving Data Mining (PPDM) utilizing a synergy between P2P and Grid. The proposed architecture is characterized with (1) its ability for preserving the privacy in data mining; (2) its ability for decentralized control; (3) its dynamic and scalable ability; (4) its global asynchrony and local communication ability. An algorithm is described to show how to process large-scale distributed PPDM based on the infrastructure. The remarks in the end show the effectiveness and advantages of the proposed infrastructure for large-scale distributed PPDM.

## 1 Introduction

## 2 Hierarchical Infrastructure

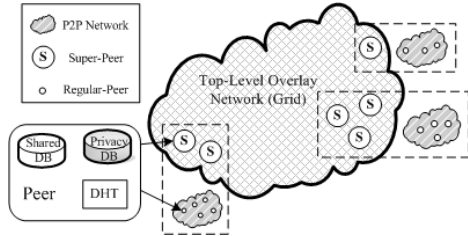


Fig. 1. Overall Framework of Architecture

### 3 Privacy-Preserving and Cryptographic Primitives

... — ...

### 4 Large-Scale Distributed PPDM on the Architecture

... 5 ...

---

**Algorithm 1:**

---

**Data:** Peers set  $P = \{p_i | i \in N\}$  (the peers constitutes the hierarchical infrastructure), and their own local databases.

**Result:** The knowledge mined from the hierarchical infrastructure.

**begin**

**while** *TRUE* **do**

**Step 1.** Peers  $p_i$  mines its local data and make use of the messages inputted from other peers;

**if**  $p_i$  is super peer **then**  
         | break;

**Step 2.** Every  $p_i$  modulates its knowledge on the basis of demand, hides the sensitive knowledge and sends its encrypted data and knowledge to up-peer  $p_j$  in *DHT* adjacent to  $p_i$ ;

    Process PPDM among super-peers through Knowledge Grid.

**end**

---

## 5 Conclusions

## Acknowledgements

## References

1. R. Agrawal, R. Srikant. Privacy-preserving data mining. SIGMOD 2000.
2. I. Foster, C. Kesselman, S. Tuecke. The Anatomy of the Grid: Enabling Scalable Virtual Organizations. International J. Supercomputer Applications, 15(3), 2001.
3. M. P. Singh. Peer-to-Peer Computing for information systems. AP2PC 2002.
4. V S. Verykios, E. Bertino, I N. Fovino, L P. Provenza, Y. Saygin, Y. Theodoridis. State-of-the-art in Privacy Preserving Data Mining. SIGMOD Record 2004, 33(1).
5. M. Cannataro, D. Talia. KNOWLEDGE GRID: An Architecture for Distributed Knowledge Discovery. Communications of the ACM, January 2003 46(1) 89-93.

# Prediction of Protein Interactions by the Domain and Sub-cellular Localization Information<sup>¶</sup>

Jinsun Hong and Kyungsook Han\*

School of Computer Science and Engineering, Inha University, Inchon 402-751, Korea  
khan@inha.ac.kr

**Abstract.** There has been a recent interest in the computational methods for predicting genome-wide protein interactions due to the availability of genome sequences of several species, the difficulty of detecting whole protein interactions in higher species even with the current high-throughput experimental methods, and the common perception of the data generated by high-throughput experimental methods as noisy data. However, data predicted by computational methods as well as that detected by high-throughput experimental methods inherently contain extremely many false positives. Several methods have been developed for estimating the reliability of experimental protein interaction data, but there are few for predicted interaction data. This paper presents a prediction method of protein-protein interactions using the protein domain and sub-cellular localization information, and experimental results of the method to the protein-protein interactions in human.

## 1 Introduction

An intrinsic problem with high-throughput methods for detecting protein-protein interactions is that data generated by the methods are extremely noisy, even more so than is the case for gene expression data, so one cannot simply use the data blindly [1]. More than half of current high-throughput data are estimated to be spurious [2]. Although it is possible to focus on interactions with higher reliability using only those supported by two or more sources of evidence, this approach invariably throws out the majority of available data [1].

In an attempt to improve the reliability of interaction data, we have recently generated a new set of interaction data using protein domain [3-5] and sub-cellular localization. This paper presents a scoring scheme for assessing the reliability of the protein interaction data predicted by a computational method called homologous interactions, and experimental results of the scheme to the protein-protein interactions in human. The scoring method is more general than a typical method of selecting co-functional or co-localized protein pairs only since some pairs of proteins interact more frequently than others despite their different functions or locations in a cell. The protein-protein interaction data predicted by the method was compared to the

---

<sup>¶</sup> This work was supported by the Ministry of Information and Communication of Korea under grant IMT2000-C3-4 and by KOSEF through the Systems Bio-Dynamics Research Center.

\* To whom correspondence should be addressed.

experimental data in HPRD (<http://www.hprd.org/>), and the results show that the method predicts reliable protein-protein interactions and is useful for assessing the reliability of protein-protein interactions.

## 2 Prediction Methods and Experimental Results

The prediction system of protein-protein interactions is composed of two parts: predicting protein interactions and assessing the reliability of the predicted interactions (Fig. 1).

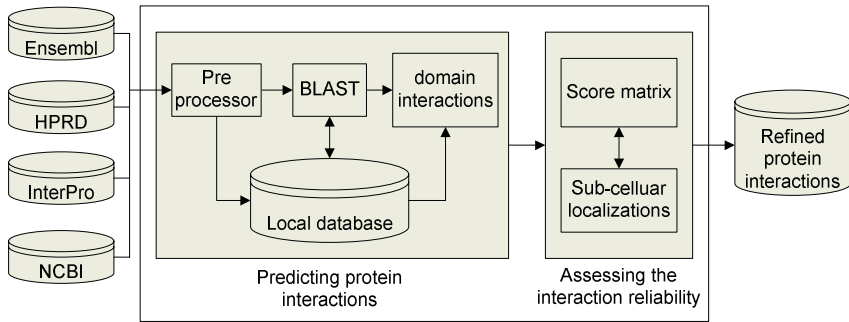


**Fig. 1.** Architecture of the prediction system of protein-protein interactions

The interaction prediction part extracts relevant data (for example, protein names and sequences, sub-cellular localizations, domains and their amino acid sequences, and known protein-protein interactions) from Ensembl (<http://www.ensembl.org/>), HPRD (<http://www.hprd.org/>), InterPro (<http://www.ebi.ac.uk/interpro/>), and NCBI (<http://www.ncbi.nih.gov/>), and removes redundant data. Suppose a protein X with domains a, b, and c and protein Y with domains d and e. When proteins X and Y interact each other, we can predict 6 domain-domain interactions of (a, d), (b, d), (c, d), (a, e), (b, e), (c, e), which are in turn used to predict new protein-protein interactions. PSI-BLAST [6] is used to identify domains from protein sequences.

The reliability assessing part constructs a score matrix from the interaction frequency at a specified sub-cellular localization, and the score matrix is used to evaluate the reliability of predicted protein-protein interactions. The information on protein, protein-protein interactions, and sub-cellular localization was obtained from HPRD that has human protein-protein interactions with the sub-cellular localization information. The sub-cellular localization schema of MIPS (<http://www.mips.gsf.de/>) was used to classify 20 sub-cellular localizations in human.

The sub-cellular localization score ( $S_l$ ) was computed using equation 1, in which  $I_l(p_i, p_j)$  is the number of interactions between proteins  $p_i$  and  $p_j$  in a same compartment  $l$ , and  $N$  is the number of proteins that participate in protein-protein interactions. Interactions with the sub-cellular localization score  $S_l = 0$  are the cases in which source or target protein has no sub-cellular localization information.



$$S_i(p_i, p_j) = \frac{1}{N} \sum I_i(p_i, p_j) \tag{1}$$

We constructed 2,272 domain-domain interactions between 1,712 human domains and predicted 5,188 protein-protein interactions between 4,205 human proteins. In the reliability assessing part, localization ID from 1 to 20 was assigned to 5,188 protein-protein interactions and the value of a score matrix was applied to these interactions. 3,839 protein-protein interactions have higher value than 0 and others have value of 0.

We compared the predicted data by our system to the experimental data in HPRD. Fig. 2 shows  $S_i$  scores in the range from 0 to 2 for the two data sets. A vertical axis presents an accumulated percentage at each score. In the experimental data of HPRD, there were 1,336 protein-protein interactions (37%) of 3,611 protein-protein interactions with  $S_i = 0$ . In the predicted data by our system, there were 1,349 protein-protein interactions (26%) of 5,188 protein-protein interactions with  $S_i = 0$ . This indicates that the prediction system generates more reliable interactions than the experimental data of HPRD.

Fig. 3 shows the sub-cellular localization distribution that includes cytoplasm, extra-cellular, membrane, nucleus between existing experimental 1,179 interactions obtained from BIND database and 5,188 interactions predicted by our system. In general, our system contains more protein interactions than existing experimental data in most cell compartments, and much more protein interactions in nucleus.

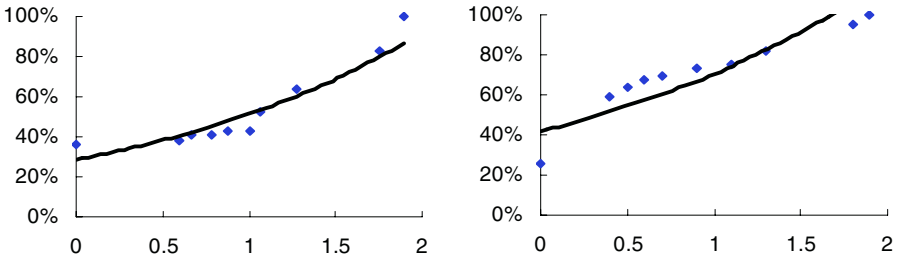


**Fig. 2.**  $S_i$  scores of the HPRD data (left) and those of our system (right)

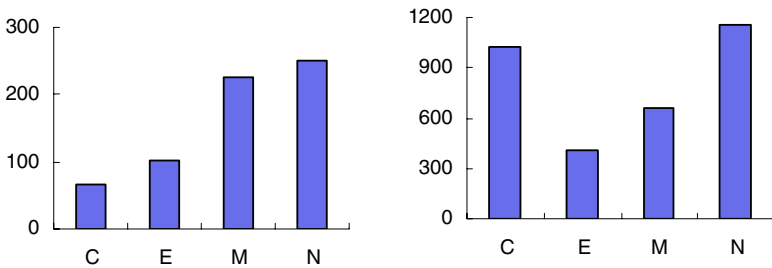


**Fig. 3.** The sub-cellular localization distribution of the BIND data (left) and our data (right). C: Cytoplasm, E: Extra-cellular, M: Membrane, N: Nucleus

We also computed the Interaction Generality (IG) values [7] to assess the reliability of protein-protein interactions. The IG value of an interacting protein pairs A-B is defined as the number of proteins directly interacting with protein A or B. Proteins with IG value less than 5 were 76% of proteins that participates in 3,839 predicted proteins-protein interactions.

### 3 Conclusions

This paper presented an intuitive, computationally feasible scoring scheme for measuring the reliability of a large-scale data set of protein-protein interactions, and for filtering potentially false positives in the data set. The number of potential artifacts can be substantially reduced by removing data with low score from the data set. Since the reliability score is computed for individual protein interactions in a data set, and the score can be directly used to filter out spurious interactions (that is, those interactions with low scores) from the data set. The overall reliability of the entire data set can also be computed by taking the average scores of the interactions in the data set. In this study we computed sub-cellular localization scores only, but the scoring scheme is general enough to incorporate any number of subscores depending on the sources of information available.

### References

1. D'haeseleer, P., Church, G.: Estimating and improving protein interaction error rates. *Proceedings of the Computational Systems Bioinformatics Conference (2004)* 208-215
2. von Mering, C, Krause, R., Snel, B., Cornell, M., Oliver, S.G., Fields, S., Bork, P.: Comparative assessment of large-scale data sets of protein-protein interactions. *Nature* 417 (2002) 399-403
3. Antonina, A., Dave, H., Steven, E.B., Tim, J. P.H., Cyrus, C., Alexey, G. M.: SCOP database in 2004: refinements integrate structure and sequence family data. *Nucl. Acids. Res.* 32 (2004) D226-D229
4. Einat, S., Hanah, M.: Correlated Sequence-signatures as Markers of Protein-Protein Interaction. *J. Mol. Biol.* 311 (2001) 681-692
5. Lappe, M., Park, J., Niggemann, O., Holm, L.: Generating protein interaction maps from incomplete data: application to fold assignment. *Bioinformatics* 17(2001) 149-156
6. Altschul, S.F., Madden, T.L., Schfffer, A.A., Zhang, J., Zhang, Z., Miller, W., and Lipman, D.J.: Gapped BLAST and PSI-BLAST: a new generation of protein database search programs. *Nucleic Acids Res.* 25 (1997) 3389-3402
7. Saito, R., Suzuki, H., Hayashizaki, Y.: Interaction generality, a measurement to assess the reliability of a protein-protein interaction. *Nucleic Acids Res.* 30 (2002) 1163-1168

# Online Prediction of Interacting Proteins with a User-Specified Protein<sup>¶</sup>

Byungkyu Park and Kyungsook Han\*

Department of computer Science and Information Engineering,  
Inha University, Incheon 402-751, Korea  
khan@inha.ac.kr

**Abstract.** The protein-protein interaction data available today in databases were either determined by experimental methods or predicted by computational methods. Biologists studying a certain mechanism or function are usually interested in a small-scale network of protein-protein interactions related to the mechanism or function of their interest rather than a genome-wide network of protein-protein interactions. We have previously developed a database server that can predict interactions between the proteins submitted by a user. However, the server cannot find proteins from the databases that potentially interact with a protein given by a user. Finding potentially interacting proteins with a protein of interest is more useful than finding interactions between given proteins, but more difficult partly because it involves intensive computation of searching data in the databases and because different databases have different accession numbers and names for a same protein. This paper describes the new online system for predicting interacting proteins with a user-specified human protein and its preliminary results. We believe that this is the first online system for predicting interacting proteins with a given protein and that it is a useful resource for studying protein-protein interactions.

## 1 Introduction

A genome-wide network of protein-protein interactions in higher species such as human is very huge and complex, and therefore subnetworks of smaller-scale are usually preferred to a whole network for close examination. However, small-scale subnetworks of protein-protein interactions of interest are not readily available from databases partly because computing all possible subnetworks involves prohibitive computation of searching data in the databases and because different databases have different accession numbers and names for a same protein.

We previously developed a database called the human protein interaction database (HPID; <http://www.hpid.org/>) for predicting potential interactions between proteins submitted by users as well as for providing human protein interaction information pre-computed from existing structural and experimental data [1, 2]. However, the

---

<sup>¶</sup>This work was supported by the Ministry of Information and Communication of Korea under grant IMT2000-C3-4 and by KOSEF through the Systems Bio-Dynamics Research Center.

\* To whom correspondence should be addressed.

previous version of HPID (HPID version 1.0) is not capable of finding potentially interacting partners for a given protein. As an extension of HPID 1.0, we now present a new online prediction system that is capable of predicting interacting proteins with a user-specified human protein. The online prediction system uses the data derived from HPID 1.0 (<http://www.hpid.org/>), BIND (<http://bind.ca/>), DIP (<http://dip.doe-mbi.ucla.edu/>) and HPRD (<http://www.hprd.org/>) for human protein interactions. It also recognizes the protein IDs of EMBL (<http://www.ebi.ac.uk/embl/>), Ensembl (<http://www.ensembl.org/>), HPRD and NCBI (<http://www.ncbi.nlm.nih.gov/>) to search for proteins. This paper discusses the main concepts of the work and its results.

## 2 Searching Interacting Proteins

The protein interactions were determined on the SCOP [3] Protein Structural Interactome MAP (PSIMAP) [4]. The structural interactions of human proteins were predicted by a homology-based assignment of the domain structures to the whole genome.

Unlike HPID 1.0, HPID 2.0 is not dependent on protein IDs to find interacting partners of proteins. Given a protein sequence, interacting partners with the protein are found by homology search of protein sequences from relevant databases. HPID 2.0 currently considers Ensembl, BIND, DIP, HPRD, and NCBI as relevant databases for homology search. To predict interacting partners of a protein, HPID 2.0 first identifies the domains of the given protein using the information from three databases of superfamily (<http://supfam.mrc-lmb.cam.ac.uk/SUPERFAMILY/>) [5], InterPro (<http://www.ebi.ac.uk/InterProScan/>) and Pfam (<http://www.sanger.ac.uk/>). Fig. 1 shows the overall architecture of the HPID online prediction system.

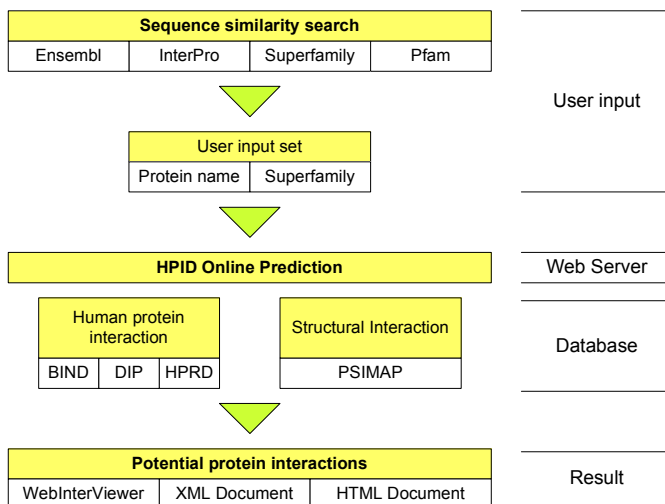


**Fig. 1.** The architecture of the HPID online prediction system. Potential interaction proteins are shown in three formats: protein interaction networks visualized by WebInterViewer [6-8], XML or HTML documents

### 3 Example of Predicting Interacting Proteins

This section shows an example of predicting interacting partners of a protein given by a user. Suppose that a user wants to know interacting proteins with human protein ENSP0000046794. HPID finds 17 interacting partners from the experimental data and 2,101 interacting partners from the prediction data of HPID. 13 out of the 17 interacting partners were also found in the prediction data; that is, the experimental and prediction data have 13 proteins in common. 4 out of the 17 proteins were not found in the prediction data. The reason that the 4 proteins were not found in the prediction data can be explained by the possibility that (1) the proteins have no superfamily assigned to them, or (2) PSIMAP does not have a pair of interacting superfamilies associated with the proteins.

Table 1 shows the superfamilies and functions of the 13 interacting partners that were found both in the experimental and prediction data. The functions of the 13 proteins can be clustered into a few functional groups, which agree with other research results [9, 10]. HPID also provides the information of superfamily, function, sub-cellular localization of potential interaction proteins, which can be further validated by experimental methods.

**Table 1.** Superfamilies and functions of the 13 proteins interacting with human protein ENSP0000046794

Interaction partners	Superfamily	Gene_Ontology (process, function)
ENSP00000262512	d.93.1	SH3/SH2 adaptor protein activity
ENSP00000315460	d.93.1	SH3/SH2 adaptor protein activity
ENSP00000339007	d.93.1	SH3/SH2 adaptor protein activity, epidermal growth factor receptor binding
ENSP00000339186	d.93.1	SH3/SH2 adaptor protein activity
ENSP00000244007	d.93.1	phosphoinositide phospholipase C activity, receptor signaling protein activity, calcium ion binding, hydrolase activity
ENSP00000343423	d.93.1	phosphoinositide phospholipase C activity, receptor signaling protein activity, calcium ion binding, hydrolase activity
ENSP00000307961	d.93.1	protein tyrosine phosphatase activity, hydrolase activity
ENSP00000264033	g.44.1	transcription factor activity, signal transducer activity, calcium ion binding, ligase activity
ENSP00000302269	d.93.1	transcription factor activity, guanyl-nucleotide exchange factor activity, diacylglycerol binding
ENSP00000288986	d.93.1	receptor binding, cytoskeletal adaptor activity, receptor signaling complex scaffold activity
ENSP00000263405	b.34.2	receptor binding, protein binding
ENSP00000316460	b.34.2	receptor binding, protein binding
ENSP00000221409	d.144.1	

## 4 Conclusion

Despite a large volume of protein-protein interaction data, small-scale networks of protein-protein interactions of interest are not readily available from databases partly because computing all possible subnetworks involves prohibitive computation of searching data in the databases and because different databases have different accession numbers and names for a same protein. We constructed an online prediction system called HPID 2.0 for searching for interaction partners of a protein given by a user. The online prediction system uses the data derived from HPID 1.0 (<http://www.hpид.org/>), BIND (<http://bind.ca/>), DIP (<http://dip.doe-mbi.ucla.edu/>) and HPRD (<http://www.hprd.org/>) for human protein interactions. It also recognizes the protein IDs of EMBL (<http://www.ebi.ac.uk/embl/>), Ensembl (<http://www.ensembl.org/>), HPRD and NCBI (<http://www.ncbi.nlm.nih.gov/>) to search for relevant proteins. HPID 2.0 is the first online system for predicting interacting proteins with a given protein and will be a useful resource for studying protein-protein interactions.

## References

1. Han, K., Park, B., Kim, H., Hong, J., and Park, J.: HPID: The Human Protein Interaction Database. *Bioinformatics* 20 (2004) 2466 – 2470
2. Han, K. and Park, B.: A Database Server for Predicting Protein-Protein Interactions. *Lecture Notes in Computer Science* 3036 (2004) 271-278
3. Lo Conte, L. Brenner, S.E. Hubbard, T.J.P., Chothia, C., Murzin, A.G.: SCOP database in 2002: refinements accommodate structural genomics. *Nucl. Acids. Res.* 30 (2002) 264-267
4. Park, J., Lappe, M., Teichmann, S.: Mapping protein family interactions: intramolecular and intermolecular protein family interaction repertoires in the pdb and yeast. *J. Mol. Biol.* 307 (2001) 929–938
5. Madera, M., Vogel, C., Kummerfeld, S. K., Chothia, C. and Gough, J.: The SUPERFAMILY database in 2004: additions and improvements., *Nucl. Acids. Res.* 32 (2004) Database issue D235-D239
6. Ju, B.-H., Park, B., Park, J. and Han, K.: Visualization and analysis of protein interactions. *Bioinformatics* 19 (2003) 317–318
7. Ju, B.-H. and Han, K.: Complexity management in visualizing protein interaction networks. *Bioinformatics* 19 (2003) i177–i179
8. Han, K. and Ju, B.-H.: A fast layout algorithm for protein interaction networks. *Bioinformatics* 19 (2003) 1882–1887
9. Saito, R., Suzuki, H., and Hayashizaki, Y.: Interaction generality, a measurement to assess the reliability of a protein-protein interaction. *Nucl. Acids. Res.* 30 (2002) 1163-1168
10. Oliver, S.: Guilt-by-association goes global. *Nature* 403 (2000) 601-603

# An Abstract Model for Service Compositions Based on Agents<sup>\*</sup>

Dept. of Computer Science and Engineering, Shanghai Jiao Tong University,  
Shanghai 200030, P.R. China  
{jkxie, huang-lp}@cs.sjtu.edu.cn

**Abstract.** This paper presents an abstract model for service compositions based on agents. The model is based on distributed Abstract State Machine and tallies with Universal Plug and Play (UPnP) architecture standard. In the abstract model, the composition of services can be viewed as a union of agents. This model can be used to depict a number of Web Service applications, and as an instance, the paper presents a BPEL Abstract Machine.

## 1 Introduction

## 2 Abstract State Machines

*Abstract State Machine*  
 $(\Sigma, \Phi_{Init}, Trans)$      $\Sigma$      $\Phi_{Init}$      $\Sigma$   
( *initial conditions*),    *Trans*    *transition rules*  
*states*     $(\Sigma)$      $\Sigma$      $q$   
 $\Sigma$      $\Sigma$      $q$      $q$     *initial*     $q$   
 $\Phi_{Init}$      $\Sigma$      $q$  |  $\Phi_{Init}$   
 $\Sigma$     *distributed ASM*  
( )    *agents*    *Agent*

<sup>\*</sup> This work is supported by "SEC E-institute: Shanghai High Institutions Grid" project 200308.

### 3 Service Compositions Based on Agents

( ), *Service Provide Agent* ( ), *Service Requestor Agent* ( ), *Coordination Agent* ( )

( )

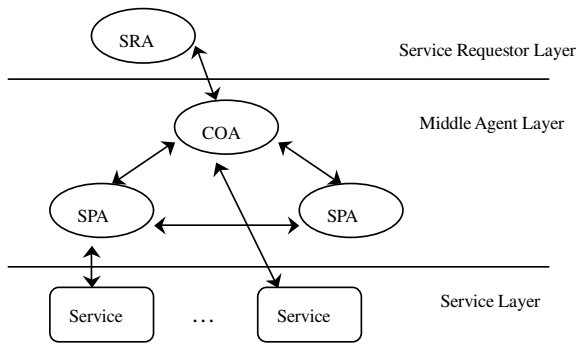


Fig. 1. Agent-based service compositions framework

( )  $agent_1 \circ agent_2$   
 $agent_1$   
 $agent_2$ ,  $\circ$  *sequence* ( )  $agent_1 + agent_2$   
 $agent_1$   $agent_2$  +  
*choice* ( )  $agent_1 \parallel agent_2$   
 $agent_1$   $agent_2$  ||  
*concurrency*

### 4 Service Compositions Abstract Machine

( )  
 ( )  
 )  
 ( )





Fig. 2. High-level structure of the BPEL model

```

    )
    process
    (
    inbox manager    outbox manager
    )
    domain AGENT ≡ INBOX_MANAGER ∪ OUTBOX_MANAGER ∪ PROCESS
    ∪ ACTIVITY_AGENT ∪ HANDLER_AGENT
    inbox
    manager,    outbox manager,    dummy process
    domain MESSAGE
    inboxSpace: INBOX_MANAGER → MESSAGE-set
    InboxManagerProgram ≡
    if inboxSpace(self) / ϕ then
    choose p ∈ PROCESS, m ∈ inboxSpace(self)
    with match(p, m) and waiting(p)
    Assign_Message(p, m)
    if p = dummyProcess then
    new newdummy : PROCESS
    dummyProcess = newdummy
    RUNNING_AGENT ≡ PROCESS ∪ ACTIVITY_AGENT
    startedExecution: PROCESS → BOOLEAN
    suspended: RUNNING_AGENT → BOOLEAN
    ProcessProgram ≡
    if ¬suspended(self) then
    if ¬startedExecution(self) then
    startedExecution(self) := true
    suspended(self) := true
    else
    stop self
    else
    Execute_Activity(activity(self))
    ReceiveMode: RUNNING_AGENT → BOOLEAN
    waitingForMessage: PROCESS → ⟨RUNNING_AGENT, ACTIVITY⟩-set
    Execute_Receive(activity: RECEIVE) ≡
    let inputDescriptor = ⟨self, activity⟩
    if ¬receiveMode(self) then
  
```

```

receiveMode(self) := true
add inputDescriptor to waitingSet
else
  if inputDescriptor  $\notin$  waitingSet then
    receiveMode(self) := false
    suspended(self) := false
    where waitingSet = waitingForMessage(rootProcess(self))

```

BasicAgentPROGRAM  $\equiv$

```

if  $\neg$ suspended(self) and  $\neg$ startedExecution(self) then
  startedExecution(self) := true
  suspended(self) := true
if suspended(self) then
  Execute_Activity(baseActivity(self))
if  $\neg$ suspended(self) and startedExecution(self) then
  remove self from compositionAgentSet(parentAgent(self))
stop self

```

## 5 Conclusions

In this paper, we have presented an abstract model for service compositions based on agents. The model is based on the idea of a service composition as a set of interacting agents. The agents are represented as objects in a state transition system. The state transition system is defined by a set of rules that describe the possible actions of the agents and the resulting states. The model is designed to be used as a basis for the development of tools for the analysis and verification of service compositions.

## References

1. V. Ermolayev, N. Keberle. Towards a Framework for Agent-Enabled Semantic Web Service Composition, International Journal of Web Service Research, Volume X, No. X, 2004.
2. R. Farahbod, U. Glässer and M. Vajihollahi. Specification and Validation of the Business Process Execution Language for Web Services, ASM 2004, LNCS 3052.
3. U. Glässer, Y. Gurevich and M. Veanes. An Abstract Communication Model, Microsoft Research Technical Report MSR-TR-2002-55, May 2002.
4. Y. Gurevich. Evolving algebras 1993: Lipari guide. In E. Börger, editor, Specification and Validation Methods, pages 9-36. Oxford University Press, 1995.
5. Y. Gurevich. May 1997 draft of the ASM guide. Technical Report CSE-TR-336-97, University of Michigan EECS Department, 1997.
6. Specification: Business Process Execution Language for Web Services, Version 1.1, 2003. <http://www-106.ibm.com/developerworks/library/ws-bpel/>
7. UPnP Device Architecture V1.0. Microsoft Universal Plug and Play Summit, Seattle 2000, Microsoft Corporation, Jan. 2000.

# An Approach of Nonlinear Model Multi-step-ahead Predictive Control Based on SVM

Weimin Zhong, Daoying Pi, and Youxian Sun

National Laboratory of Industrial Control Technology,  
Institute of Modern Control Engineering, Zhejiang University, Hangzhou 310027, China  
{wmzhong, dyp1, yxsun}@iipc.zju.edu.cn

**Abstract.** In this paper, a support vector machine (SVM) with polynomial kernel function based nonlinear model multi-step-ahead controller is presented. A SVM based multi-step-ahead predictive model is established by black-box identification. And control law is obtained by numerical and optimization methods respectively. The effect of controller is demonstrated on a recognized benchmark problem. Simulation results show that multi-step-ahead predictive controller can be well applied to nonlinear system with good performance.

## 1 Introduction

Model predictive control (MPC) is a class of control algorithms in which a process model is used to predict and optimize process performance<sup>[1]</sup>. Now, attention has turned to nonlinear model predictive control (NMPC)<sup>[2]</sup> because many industrial processes are intrinsically nonlinear. Recently a new kind of learning machine called SVM<sup>[3,4]</sup>, which is well used for function regression and time series prediction, can be used for nonlinear system identification and system control. This paper puts forward a new approach to NMPC based on SVM with quadratic polynomial kernel function. The paper is organized as follows: In section 2, a SVM with polynomial kernel function based multi-step-ahead predictive model and control algorithm for nonlinear systems are discussed. Simulation results on a recognized benchmark problem are given in section 3. In section 4, some conclusions are put forward. For more details about SVM regression with polynomial kernel function, see references<sup>[3,4]</sup>.

## 2 SVM Based NMPC

### 2.1 Nonlinear Predictive Control Model

Assume the  $j$ -step-ahead ( $j=1\cdots P$ ,  $P$  is prediction horizon) nonlinear model can be described by SVM form:

$$\begin{aligned} y_m(k+j) &= f(I_{k+j}) = f[y(k+j-1), y(k+j-2), \dots, y(k-n+j), \\ &\quad u(k+j-1), u(k+j-2), \dots, u(k-n+j)] \\ &= \sum_{i=1}^{nsv} a_i (I_i' \cdot I_{k+j} + 1)^2 + b \end{aligned} \quad (1)$$

*s.t.*  $u_{\min} \leq u \leq u_{\max}$

Where  $n$ ,  $m$  are determined by approximation accuracy. Support values  $a_i (i=1, \dots, nsv)$  and bias value  $b$  can be gotten through learning according to  $d$  pairs training data  $\{I_s, y\} (s=1, \dots, d)$ .  $I'$  is the set of support vectors from  $I_s$ . And assume when  $j > M$ ,  $u(k+j-1) = u(k+M-1)$ ,  $M$  is control horizon.

Introduce feedback correction to deal with the model error and disturbance, so the  $j$ -step-ahead closed-loop predictive output at time  $k$  is:

$$y_p(k+j) = y_m(k+j) + h_j e(k) \tag{2}$$

Where  $h_j$  is the error correcting coefficient,  $e(k) = y(k) - y_m(k)$ .

### 2.2 Nonlinear Predictive Controller

Select optimization objective function with moving horizon as below:

$$\min J(k) = \sum_{j=1}^P q_j [y_r(k+j) - y_p(k+j)]^2 \tag{3}$$

Where  $q_j$  are weighting coefficients,  $y_r(k+j)$  is reference value from trajectory:

$$y_r(k+j) = a_r^j y(k) + (1 - a_r^j) y_{sp} \quad y_r(k) = y(k) \tag{4}$$

Where  $a_r$  is the coefficient related with system's robustness and  $y_{sp}$  is set point value.

#### Case of $P = M$ :

In this case, nonlinear optimization problem (3) contains  $M$  manipulate variables and  $M$  equality constraint of model outputs. Use known  $y_p(k-1+j/k-1)$  replace unknown  $y(k-1+j)$ , where  $y_p(k-1+j/k-1)$  is the closed-loop predictive output.

$$\begin{aligned} \min J(k) = & \underbrace{q_1 [y_r(k+1) - y_p(k+1)]^2}_{J_1(k) \text{ contains } u(k)} + \underbrace{q_2 [y_r(k+2) - y_p(k+2)]^2}_{J_2(k) \text{ contains } u(k), u(k+1)} \\ & + \dots + \underbrace{q_M [y_r(k+M) - y_p(k+M)]^2}_{J_M(k) \text{ contains } u(k), u(k+1), \dots, u(k+M)} \end{aligned} \tag{5}$$

It's a common sense that the first-step controller output  $u(k)$  outweighs the others, so we can first minimize  $J_1(k)$  to get  $u(k)$ , and then substitute  $u(k)$  into  $J_2(k)$  to get  $u(k+1)$ . Recursively, we can get all  $u(k+j-1)$ .

$$\frac{\partial J_j(k)}{\partial u(k+j-1)} = 2q_j [y_p(k+j) - y_r(k+j)] \frac{\partial y_p(k+j)}{\partial u(k+j-1)} = 0 \tag{6}$$

It's a cubic equation with only one unknown bounded variable, and it's easily solved.

**Case of  $P > M$  :**

Consider nonlinear optimization problem (3) with  $P > M$  , this is a nonlinear optimal problem with equality constraint of model output and boundary constraint of controller output. In this paper, Nelder-Mead simplex direct search method is used to optimize and obtain  $M$  unknown variables. And we will use solutions obtained by algorithm in section 2.2.1 as starting point.

**3 Experimental and Simulation Results**

The example is a benchmark problem used by Narendra & Parthasarathy<sup>[5]</sup>, and further studied by Kambhampati<sup>[2]</sup> using a Gaussian neural network to fulfill the one-step-ahead predictive control. Set  $C = 10000$  ,  $\varepsilon = 0.001$  ,  $h_j = 1$  ,  $q_j = 1$  .

$$y(k+1) = \frac{y(k)}{1+y^2(k)} + u^3(k) \tag{7}$$

where  $y$  is the plant output and  $u \in [-2,2]$  is the input.

150 pairs data generated by applying by a series of random numbers between  $[-2,2]$  are used to train the SVM predictive model with  $m = n = 5$  . And set  $y_{sp} = 1.5$  and  $a_r = 0.9$  . Fig.2 is the system output and controller output with  $P = 2, M = 2$  . Fig.3 is the system output and controller output with  $P = 4, M = 2$  . In both cases, a disturbance rejection ( $d=0.1$ ) is added when system is in steady state at time  $k=100$ , and the output response will track the set point well again quickly.

**4 Conclusions**

In this paper two cases of SVM with polynomial kernel function based nonlinear model multi-step-ahead predictive control strategies are investigated. The effect of both controllers is demonstrated by a benchmark problem. The analysis and experiment results show that the control strategy will provide a robust stable control of nonlinear systems with good performance in keeping reference trajectory and disturbance-rejection.

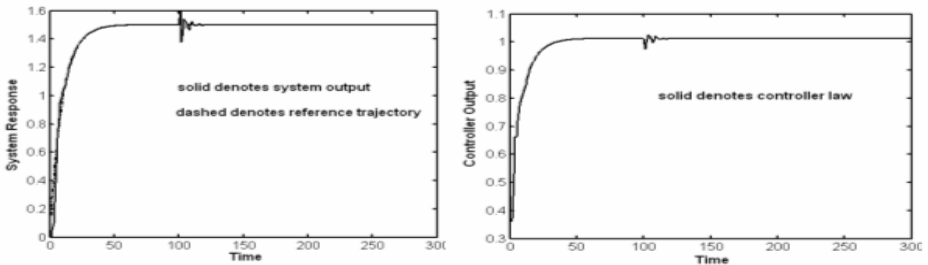


**Fig. 2.** System output and controller output with  $P = 2, M = 2$

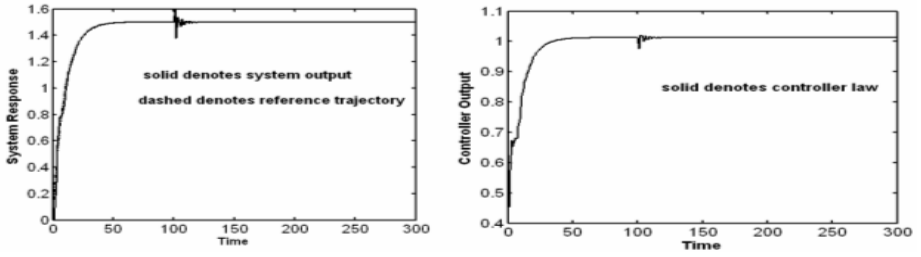


Fig. 3. System output and controller output with  $P = 4, M = 2$

### Acknowledgment

This work is supported by China 973 Program under grant No.2002CB312200.

### References

1. Shu D.Q.: Predictive control system and its application. China Machine Press, Beijing,1996
2. Kambhampati C., Mason J.D., Warwick K.: A stable one-step-ahead predictive control of non-linear systems. Automatica, Vol.36 (2000) 485–495
3. Vapnik V.N.: The nature of statistical learning theory. Springer-Verlag, New York, USA (1995)
4. Cortes C.: Prediction of generalization ability in learning machines (PhD thesis), University of Rochester, New York, USA (1995)
5. Narendra K.S., Parthasarathy K. : Identification and control of dynamic systems using neural networks. IEEE Trans. Neural Networks, vol.1, (2000) 4-27

# Simulation Embedded in Optimization – A Key for the Effective Learning Process in (About) Complex, Dynamical Systems

Elzbieta Kasperska and Ewa Mateja

Institute of Mathematics, Silesian University of Technology, Kaszubska 23,  
44-100 Gliwice, Poland

{e.kasperska, e.mateja}@polsl.pl

**Abstract.** The purpose of this paper is to present some results of the experiments of type simulation embedded in optimization (on model type Systems Dynamics). They allow, not only, the so called, direct optimization, but extended sensitivity analysis of parameters and structures too. Authors have used languages Cosmic and Cosmos to support the learning process in (about) modelled dynamical system.

## 1 Introduction

There are problems understanding complex systems... because they are rich... feedbacks [2, 4, 6, 7], but because these complex systems are changing the structure... here we are trying to understand them using a fixed structure approach.

System dynamics as developed by the late Jay Forrester's at the Massachusetts Institute of Technology's... a... of... a... Forrester.

The classical concept of system dynamics assumes, that, during the time horizon of the model... the structure (given a priori)... remains static.

During last couple of years, some ideas of structural... have occurred... system dynamics modeling and simulation... first... of... the problem of... simulation... during... the quest... as... the... the structure... order to... the desired behavior... performed experiments... a... CO... CO... O... as... that... that... automatic... simulation... the... package... makes... application... technology.

- file... of... the model (REC O O),
- sensitivity analysis of the model (E EC OR),
- simplification of the structure of the model (C O),
- extending the effects of... forward... the model (G OR O).

In this paper some of such experiments are presented and their background the context of each process is considered

## 2 Simulation Embedded in Optimization – Experiments on Model DYNBALANCE(3–1–III)

The model named CE( ), created by B. Jasperska, is chosen like the object of experiments to be simulated embedded in optimization. The figure presents the general structure of this model. The graph can be easily adapted from Jasperska (4). The main attention should be paid to the object of functions of the model, which made the decision preferences about the behaviour of the system, like the results of the objective of the decision about the production strategy and selection. The authors present the main results of some experiments, to be simulated embedded in optimization.

### Experiment 1

The object of functions represents the profit from selling minus the tactical production and the penalty factors collected through the strategy of production.

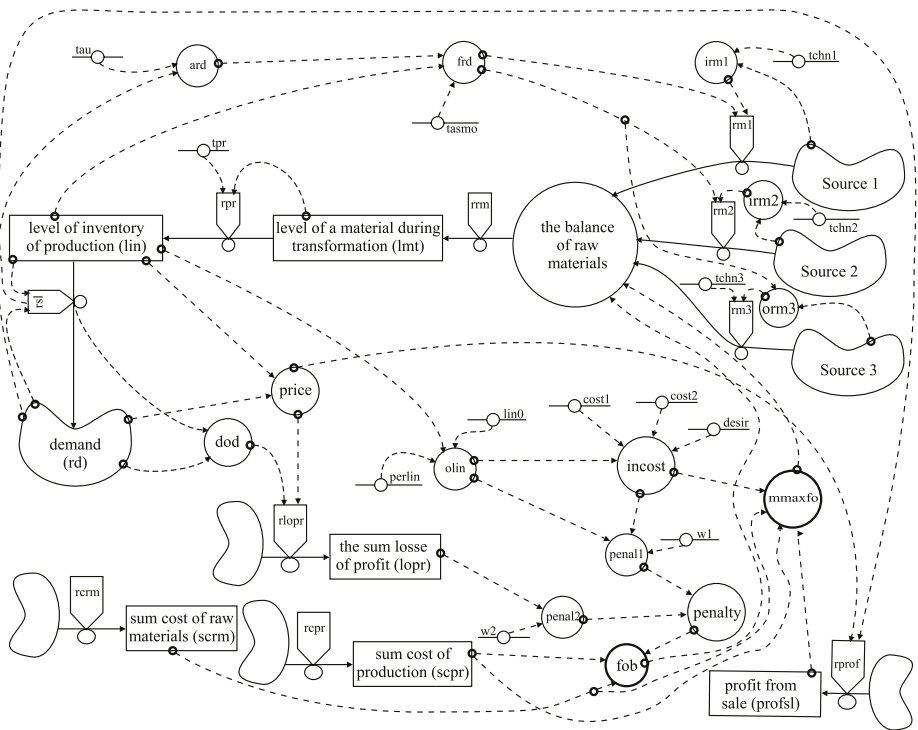


Fig. 1. Structure of model DYNBALANCE(3–1–III)



The demand for product has ramp characteristic. Table 1 shows the results of the experiment.

**Table 1.** The main results of experiment 1

Parameter	Final value	Original value	Lower limit	Upper limit
tchn1	0.000	20	0	40
tchn2	11.332	10	0	40
tchn3	39.984	20	0	40
Initial value of mmaxfo:			0.20233E + 07	
Final value of mmaxfo:			0.47194E + 07	
Final value of inventory:			221	
Final value of cost of production:			24.295E + 05	
Final value of price:			50	
Final value of penalty (maxpen):			0.040792E + 07	

The conclusions from analysis of the results of experiment 1 are as follows:

- the zero value of parameter tchn1 implies the necessity of cutting the production from start material (it seems that first technology is the most economical, under the simultaneous condition, about the price and the unit cost and the supply of raw material),
- the value of parameter tchn2 is considered to be a value and tchn3 is near equal to the upper limit, as can be seen from the optimal process selection. Values that suits the objective function of the hierarchical simulation,
- the final value of penalty of mmaxfo is rather small, comparing with the final value of profit. It seems that take profits of production as real goal.

### Experiment 2

In this experiment the variables of both asch selection, the objective function and the are changed from a minimum to take the selected active parameters. We have chosen tchn1, tchn2, tchn3 and take the base parameter candidate parameters tasm, ucpr, ucpr2, ucpr, ucr, ucr2, ucr.

The initial value of objective function of both asch is  $.2 \cdot 28E + 8$ , and the final value of both asch is  $.2 \cdot 28E + 8$ . The conclusions from analysis of the results of experiment 2 are as follows:

- most of parameters (for example tasm, ucpr2, ucpr, ucpr, ucpr2, ucpr, tasm) have kept the original value that seems that the results are unchanged, respectively,
- the parameters tchn1, tchn2, tchn3 (which are active in optimal design) have changed the values considerably. It means that they are sensitive parameters of model.

- this type of performance measures may be a bit abstract, but which parameters have more effect on improving the objective function?

### 3 Final Remarks and Conclusions

The purpose of the paper was to present some results of type simulation embedded optimization in a dynamic system. In fact, these results show that the process of learning about a dynamic system can become effective and support the right decisions and decisions, as well as the arrangement of the system. The model of the global learning (see three steps of learning by Radzicki, 2007) but the other side of the learning is a learning (specialized) of the system made.

The conclusions are as follows:

- simulation embedded optimization can become the effective support of learning about a dynamic system,
- both sets of tasks (parameters and structures) give us the key format about the effects of which determine the dynamic behavior of the system.

### References

1. Coyle, R.G. (ed.): *Cosmic and Cosmos. User manuals.* The Cosmic Holding CO, London (1994)
2. Coyle, R.G.: *System Dynamics Modelling. A Practical Approach.* Chapman & Hall, London (1996)
3. Coyle, R.G.: Simulation by repeated optimisation. *J. Operat. Res. Soc.* **50** (1999) 429–438
4. Forrester, J.W.: *Industrial Dynamics.* MIT Press, Massachusetts (1961)
5. Kasperska, E., Mateja-Losa, E., Słota, D.: Some dynamic balance of production via optimization and simulation within System Dynamics method. In: Hines, J.H., Diker, V.G. (eds.): *Proc. 19th Int. Conf. of the System Dynamics Society.* SDS, Atlanta (2001) 1–18
6. Radzicki, H.J.: Mr Hamilton, Mr Forrester and the foundation for evolutionary economics. In: Davidsen, P.I., Mollona, E. (eds.): *Proc. 21st Int. Conf. of the System Dynamics Society.* SDS, New York (2003) 1–41
7. Sterman, J.D.: *Business dynamics – system thinking and modeling for a complex world.* Mc Graw-Hill, Boston (2000)

# Analysis of the Chaotic Phenomena in Securities Business of China

Chong Fu<sup>1</sup>, Su-Ju Li<sup>2</sup>, Hai Yu<sup>1</sup>, and Wei-Yong Zhu<sup>1</sup>

<sup>1</sup> School of Information Science and Engineering, Northeastern University,  
110004 Shenyang, China

{fu\_chong, yu\_hai, zhu\_weiyoung}@sohu.com

<sup>2</sup> College of Foreign Studies, Northeastern University,  
110004 Shenyang, China

**Abstract.** The tendency of stock price in securities business based on the Shenzhen stock composite index was studied by using chaotic dynamics theory. The fluctuation of stock price was proved to be a kind of chaotic process of inner random. The dynamic model of Shenzhen stock composite index was established both by the restructure of phase space of the data and by the analysis of the Poincaré section and Lyapunov exponent of the data. The chaotic evolution process of this model was analyzed in detail. This provides a new method for the investigation of modern financial system by the use of chaotic theory.

## 1 Introduction

In the early 1900s, French mathematician Louis Bachelier proposed a model describing the rules of price fluctuation, which became the foundation of modern financial securities theory. This model assumes that the price fluctuation obeys normal distribution and points out that the changes of the price are independent in statistics and follows the “Random Walk” which accords with the bell-like curve. According to his theory, the price should fluctuate slightly in a small range, the violent shakeout should seldom happen, but it exceeds people’s expectation greatly. This indicates that current securities theory cannot give a correct explanation to the large fluctuation of finance system.

In 1990s, Professor B.B.Mandelbrot, the academician of American Academy and founder of fractal theory, proposed a new multi fractal model to describe the fluctuation of the securities market. It accurately describes the relationship of the up and down fluctuation, revealing the essential of the frequent violent fluctuation of securities market, providing a determinative analysis method for the study of unpredictable financial system [1]. At present, most of the existing financial models are based on “Random Walk” theory, few scholars set up financial model on the basis of chaos theory. In this paper, the chaotic dynamics theory was used to analyze the chaotic property of securities market and a chaotic iteration model was established to further study the evolution process of the complicated financial system.

## 2 Power Spectrum Analysis of Trading Sequence

The tendency chart of composite index in Shenzhen securities between 8-17<sup>th</sup>-1992 and 8-31<sup>th</sup>-2004 is shown in Fig. 1. The sampling interval is based on day.

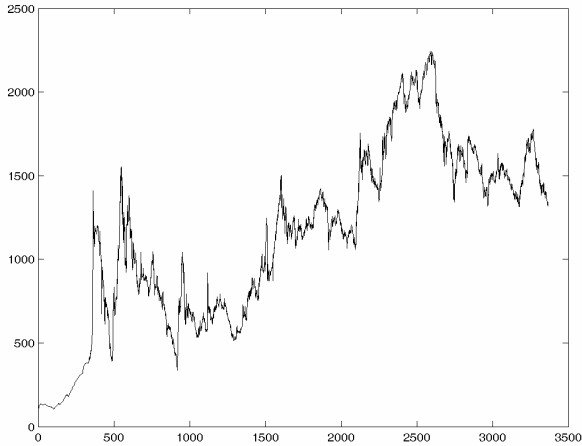


**Fig. 1.** Tendency chart of composite index of Shenzhen securities between 8-17<sup>th</sup>-1992 and 8-31<sup>th</sup>-2004

Power spectrum analysis is often used to identify the chaos behavior of a system. For sequence in Fig. 1, we do discrete Fourier transform, calculate its Fourier coefficient

$$F(u) = \frac{1}{N} \sum_{i=0}^{N-1} x_i \exp\{-j2\pi i u / N\}. \quad (1)$$

The result is shown in Fig. 2. The power spectrum of the chaotic system shows a peak on a broadband, which is different from periodic movements or Gaussian noise. From Fig. 2 we can see, the power changes continuously in frequency domain, it shows a downward trend in the form of negative exponent. Some irregular peaks are on the background, demonstrating period 3 phenomenon.

## 3 Phase Space Reconstruction and Poincaré Section

The chaotic attractor is the fundamental reason of some random movements. The first step of analyzing the chaotic property of a time sequence is reconstructing the attractor based on the experiment data. For time sequence  $x_0, x_1, x_2, \dots, x_{N-1}$  ( $N$  must be large enough), we can get other  $d-1$  dimension data by using the time delay method. The coordinate axes are respectively  $x(t), x(t+m), x(t+2m), \dots, x(t+(d-1)m)$ ,  $m$  is the selected delay number. All the data determine a point in a multi dimension state space, then we can use other methods to examine whether it has a chaotic attractor.

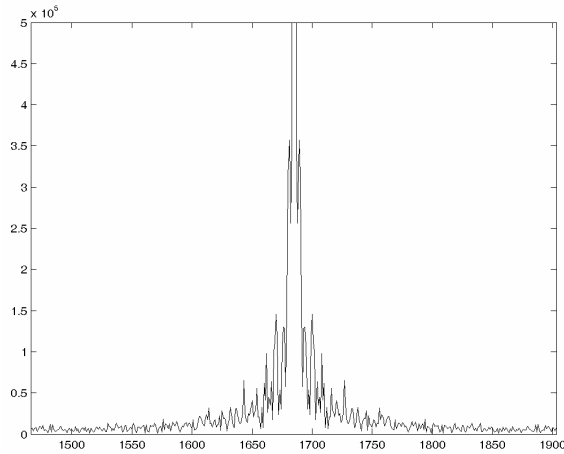


**Fig. 2.** Local enlarged power spectrum of Shenzhen securities composite index

The transection of attractors in phase space is Poincaré section. For a discrete time sequence in phase space,  $X(t)$  presents current state, while  $X(t+m)$  the state after delaying  $m$ ,  $X$  a  $d$  dimension vector, the state transformations in  $d$  dimension space is:

$$(x(t + m), x(t), \dots, x(t - (d - 2)m)) = F_m(x(t), x(t - m), \dots, x(t - (d - 1)m)). \tag{2}$$

The Poincaré section of Shenzhen securities composite index is shown in Fig. 3, the distribution of the points in the figure is very regular, the dynamic model is established as [2, 3]:

$$X_{t+1} = rX_t \exp(-0.00034(1 - X_t)^2). \tag{3}$$

$r$  is a random variable,  $r \sim N(0.978, 11.21)$ .

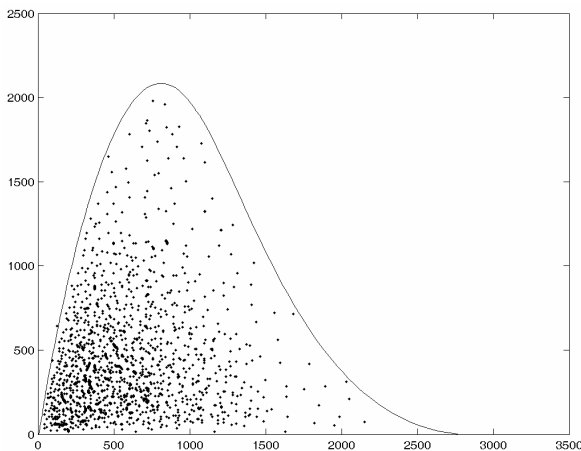


**Fig. 3.** Poincaré section and iterative model of Shenzhen securities composite index

## 4 Dynamical Characteristic Analysis of the Model

The bifurcation diagram of dynamic model defined by Eq. 3 is shown in Fig. 4 [4].

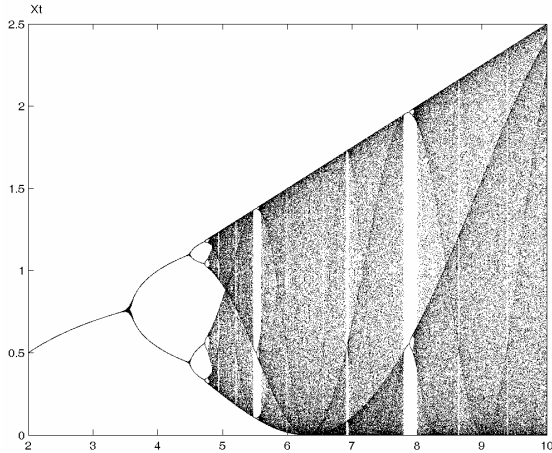


**Fig. 4.** Bifurcation diagram of the dynamical model defined by Eq. 3

When control parameter  $r > 4.716$ , the system will come into chaos process. The evolvement of this system is a chaotic process, which contains periodic orbit, semi-periodic orbit, random orbit and chaos orbit.

## 5 Conclusion

This paper proves that the fluctuation of stock price is a mixed process, including periodic process and a topological invariance chaotic process. It provides a new idea and method of using the chaotic theory to study the fluctuation, inner principles and tendency of securities business.

## References

1. Mandelbrot, B.B.: *Fractals and Scaling in Finance*. Springer-Verlag, Berlin Heidelberg New York (1997)
2. Liu, X.D., Zhu W.Y., Wang G.D.: Analysis of Chaotic Behavior of the Six-roll UC Mill and its OGY Control. *Journal of Northeastern University*, Vol. 19. (1997) 591–594
3. Ruelle, D., Takens, F.: On the Nature of Turbulence. *Common Mathematics Physics*, Vol. 20 (1971) 167–192
4. Feigenbaum, M.J.: Quantitative Universality for a Class of Nonlinear Transformations. *J Statistic Phys*, Vol. 19 (1978) 25–52

# Pulsating Flow and Platelet Aggregation

Xin-She Yang

Department of Engineering, University of Cambridge,  
Trumpington Street, Cambridge CB2 1PZ, UK  
xy227@eng.cam.ac.uk

**Abstract.** Platelet aggregation has been modelled as a nonlinear system of viscous flow and pulsating flow based on the Fogelson's continuum model. By solving nonlinear governing equations and the coupling between flow and platelet aggregates in the cylindrical coordinates using the finite element method, we can see how the platelet aggregation forms under the pulsating flow conditions. Numerical simulations show that the aggregates are stretched by the flow in the dynamic equilibrium of the link forces and background flow. In addition, significant elastic stress can be developed to maintain the shape and integrity of the platelet aggregates.

## 1 Introduction

Platelet aggregations are important in physiological processes such as thrombus and haemostasis. However, these processes are very complicated and many factors and activities occur at the same. For example, physiological response in haemostasis to blood vessel injury involves the cell-cell adhesive platelet aggregation and coagulation. Platelets are tiny oval structure with diameter of 2-4 micrometers. They are active in blood with a half-life of 8-12 days. Non-active platelets flow free in blood vessels in a dormant state. Activating chemicals such as ADP initiated by injury can induce platelet aggregation in the blood plasma. A platelet's surface membrane can be altered so that the platelet becomes sticky, and thus capable of adhering to other activated platelets and the vessel walls. Although platelets only consist of about 0.3% in concentration and yet occur in enormous numbers about 250 millions per millilitre [2,3,6]. Once triggered by the chemicals, the active platelets start to clot so as to restrict the blood flow at the injury site. To prevent uncontrolled overspreading of activated platelets, a chemical inhibitor, thrombin, is also involved.

There have been extensive studies on the biological and physiological effect of platelet aggregations. Some mathematical models and computational models are very instructive for the modelling of the detailed mechanism of the formation of platelet aggregates [3-6]. Most of these studies use the Navier-Stokes equations with simplified boundary conditions or the steady-state approximation. However, the real blood vessel system has complex geometries due to branching and atherosclerotic plaque deposition inside the vessels. In addition, the flow velocity and pressure are even more complicated by the pulsating process from the heart pumping process. Thus, the more realistic modelling shall include the pulsating effect on the flow and

platelet aggregations. In this paper, we intend to extend the existing models to include the pulsating flow and the platelet aggregations in the corresponding environment.

## 2 Fogelson’s Model

Fogelson first formulated a continuum model for platelet aggregation process [3]. The full model consists of a system of coupled nonlinear partial differential equations. We use the simplified version of Fogelson’s model with the following equations:

$$\nabla \cdot \mathbf{u} = 0, \tag{1}$$

$$\rho(\mathbf{u}_t + \mathbf{u} \cdot \nabla \mathbf{u}) = -\nabla p + \mu \nabla^2 \mathbf{u} + \mathbf{f} + \beta \nabla \sigma, \tag{2}$$

$$\sigma_t + \mathbf{u} \cdot \nabla \sigma = \sigma \nabla \mathbf{u} + (p \nabla \mathbf{u})^T, \tag{3}$$

$$\phi_t + \mathbf{u} \cdot \nabla \phi = r, \tag{4}$$

where the first two equations are the Navier-Stokes equations for incompressible fluid flow  $\mathbf{u}=(U,V,W)$  and  $p$  pressure. The coefficient  $\beta$  is constant and  $\mathbf{f}$  is the force density. The last term is due to the cohesion of platelets. The third equation is for the cohesion-stress tensor  $\sigma$ . The last equation is for the concentration  $\phi$  of the active platelets and the production rate  $r$  can be considered as a function of concentrations of platelets and the activating chemicals. The governing equations are nonlinear and the flow is coupled with the formation of platelet aggregates. Thus the full solution necessitates efficient numerical methods. As the blood flow is slow and viscous, so the first two equations can be simplified for the case of viscous flow and the zero force  $\mathbf{f}$ . We have

$$\nabla \cdot \mathbf{u} = 0, \quad \rho \mathbf{u}_t = \mu \nabla^2 \mathbf{u} - \nabla p + \beta \nabla \sigma. \tag{5}$$

In most cases, the blood flow is one-dimensional tubular flow, it is convenient to choose the local coordinates so that the  $z$ -axis is in the direction of the local blood flow. In this case, we can assume the pulsating pressure (far field) in the form

$$p_z = \partial p / \partial z = A \cos(\omega t) + \gamma, \tag{6}$$

where  $A$  is a constant. In fact, we can assume any known function form for the pressure gradient in terms of a Fourier expansion

$$p_z = g(t) = \gamma + \sum_{n=1}^N [A_n \cos(\omega_n t) + B_n \sin(\omega_n t)]. \tag{7}$$

## 3 Simulation and Results

Although the equations are coupled, they can be solved using the well-developed finite element method together with the Newton-Raphson iteration procedure for the



nonlinearity. By solving the problem in the cylindrical coordinates, we can see how the platelet aggregation forms and develops under the pulsating flow conditions.

### 3.1 Shear Stress Distribution and Variation

To simulate the tubular flow and the stress development, we first study the flow at the bifurcation region where one large vessel is branched into two smaller vessels. For a given pulse, one can calculate the wall shear stress and stress variation with time after the peak R-wave of the given pulse. Figure 1 shows the shear stress distribution and the mean wall shear stress variation. The major feature of the computed shear stress variation is consistent with the experimental results. It is worth pointing out that there exists a peak for wall shear stress for a given pulsating pressure gradient, and thus the peak shear stress could directly affect the rupture if the stenosis or plague is presented at the region concerned. The shear stress is higher at bifurcation regions and the stress level can reach as high as 15 Pa for a blood vessel with a diameter of 1mm. As the flow is pulsating, the shear stress and pressure vary with time. The mean shear stress at wall varies significantly after the R-wave starts. It first increases quickly to a peak at  $t=0.065$  and then decreases exponentially with time.

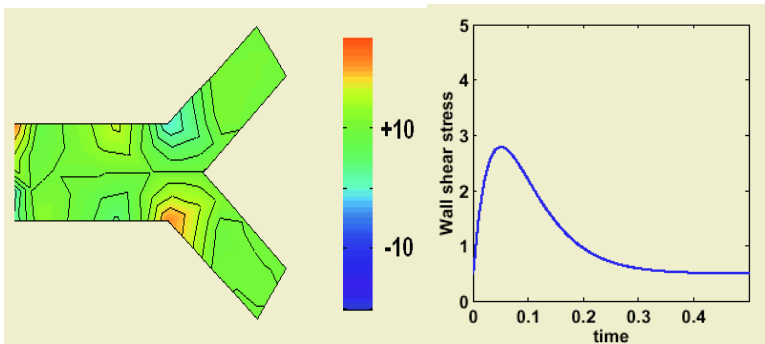
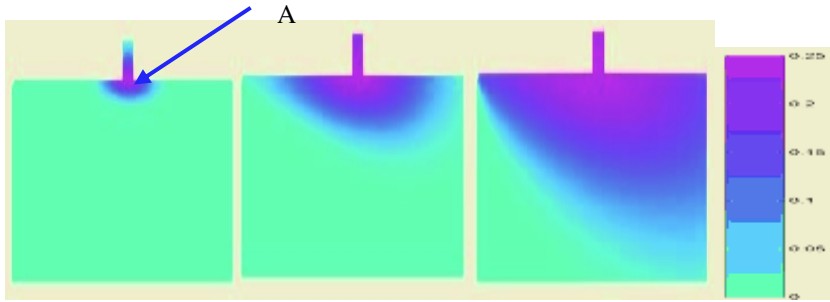


Fig. 1. Shear stress distribution at the bifurcation region and wall stress variation with time

### 3.2 Platelet Aggregation

In the case of pulsating flow in a cylindrical vessel with a diameter of 1mm, a small injury (point A) with a size of less than 0.1mm occurs and thus releases the ADP chemical to activate the platelet aggregation, so platelets starts to deposit at the injury site, and the size of the aggregation starts to increase. Figure 2 show the platelet aggregation at the different times  $t=1, 10, 50$  seconds after the injury. The flow is from left to the right with the initial constant flow field. The boundary condition for the pressure in the far field is the pulsating function given earlier in equation (7). For simplicity, we have used the zero reaction rate ( $r=0$ ),  $\gamma=0$ ,  $\beta=1$ , and the normalized concentration so that  $\phi=0$  for no platelets and  $\phi=0.5$  for solid platelet aggregates.

We can see clearly that the concentration of activated platelets is much higher at the injury site than in the blood. The aggregation rate is proportional to the



**Fig. 2.** Formation of platelet aggregation at different times ( $t=1,5,50$ )

concentration of the activated platelets, and thus the size and shape of the platelet aggregation can be represented in terms of the concentration as shown in the figure. The aggregates are stretched by the flow in the dynamic equilibrium of the link forces and background flow. As the platelets aggregate, the injured vessel will be blocked severely after some time, and it may take 100 seconds to reach this stage.

## 4 Conclusions

We have simulated the platelet aggregation by using the Fogelson's continuum model with nonlinear governing equations and the coupling between flow and platelet aggregates. By solving the problem in the cylindrical coordinates using the finite element method, we can see how the platelet aggregation forms under the pulsating flow conditions. Numerical simulations show that the aggregates are stretched by the flow in the dynamic equilibrium of the link forces and background flow. In addition, significant elastic stress can be developed to maintain the shape and integrity of the platelet aggregates.

## References

1. Chakravarty, S., Mandal P. K.: Mathematical modelling of blood flow through an overlapping arterial stenosis. *Math. Comput. Modelling*, 19 (1994) 59-70.
2. David, T., Thomas, S., Walker, P. G.: Platelet deposition in stagnation point flow: an analytical and computational simulation. *Medical Engineering and Physics*, 23 (2001) 229-312.
3. Fogelson, A.: Continuum models of platelet aggregation: formulation and mechanical properties. *SIAM J. Appl. Math.*, 52 (1992) 1089-1110.
4. Gurevich, K. G., Chekalina, N. D., Zakharenko, O. M.: Application of mathematical modelling to analysis of nerves growth factor interaction with platelets. *Bioorganic Chemistry*, 27(2000)57-61.
5. Guy, R. D., Fogelson, A. L.: Probabilistic modelling of platelet aggregation: effects of activation time and receptor occupancy. *J. Theor. Biol.*, 219(2002) 33-53.
6. Keener, J. and Sneyd, J.: *Mathematical Physiology*, Springer-Verlag, Berlin Heidelberg New York (1998).
7. Zienkiewicz, O. C. and Taylor, R. L.: *The Finite Element Method*, Vol. I/II, McGraw-Hill, 4th Edition, (1991).

# Context Adaptive Self-configuration System

Seunghwa Lee and Eunseok Lee

School of Information and Communication Engineering, Sungkyunkwan University,  
300 Chunchun jangahn Suwon, 440-746, Korea  
{jbmania, eslee}@selab.skku.ac.kr

**Abstract.** This paper suggests a *context adaptive self-configuration system*, in which the system itself is aware of its available resources, and executes a configuration suitable for each system and the characteristics of each user. A great deal of time and effort is required to manually manage computing systems, which are becoming increasingly larger and complicated. Many studies have dealt with these problems but most unfortunately have focused on 'automation', which do not reflect the system specifications that differ between systems. Therefore, this paper proposes an adaptive self-configuration system that collects diverse context information for a user and its system, reflects it to an auto-response file and executes the detail parameter setting automatically. A prototype was developed to evaluate the system and compare the results with the conventional methods of manual configuration and MS-IBM systems. The results confirmed the effectiveness of the proposed system.

## 1 Introduction

Recently, the rapid development of IT has contributed to various devices with increasing performances. As the devices to be administered are increasing in number and complication, they impose a heavier burden on system management [1]. For examine, a company's computing system networking hundreds of hosts may require a great deal of time, money and manual effort if they have to be manually and individually installed and updated. In order to solve it, studies such as a centralized integration management of distributed resources, and unattended installation technology to reduce the workload and periodic automatic update are being applied by various institutions [2][3]. However, these studies focused mainly on 'automation', which simply replaces the tasks manually processed. Therefore, these studies provide only a uniform service that does not reflect unique device's characteristics or the user preferences. This paper proposes a context adaptive self-configuration system, which is aware of its available resources, and executes the suitable configuration on each situation utilizing these contexts with the user's information.

The paper is presented as follows: Section 2 describes the characteristics, structure and behavior process of the proposed system; and Section 3 gives a conclusion as well as a simple description of the system evaluation through its implementation and experiments.

## 2 Proposed System

### 2.1 System Overview

The word ‘configuration’ in this paper means newly install components, such as an OS or software, etc., that are to be administered and updated them for version management or defects healing.

For installation, the proposed system need be installed so that components to be contained reflect the existing users’ preference and the system resource status. The basic configuration automatically meets these requirements through a customized auto-response file and a parameter-setting file. In addition, for updating, it monitors the frequency of component use, determines the priority, and enables works to be efficiently processed in case the remaining storage of a system or the updating time is insufficient. Currently, copying files is processed by a peer-to-peer transmission method to supplement the several disadvantages of the existing centralized distribution method and to efficiently update the files.

### 2.2 System Structure

Fig. 1 shows the overall structure of the proposed system, and the detail modules are as follows:

- *Component Agent*: this is installed in a managed device to monitor the changes in resources, to check the parameter setting information of the user’s applications along with the frequency of use, and to periodically transmit the this information to a self-configuration system. In addition, it also receives packages or the configuration files necessary for auto installation from the self-configuration system or a host located in the same zone. Upon installation, it observes the user’s behavior, and transmits the observed information to the *Context Synthesizer*.

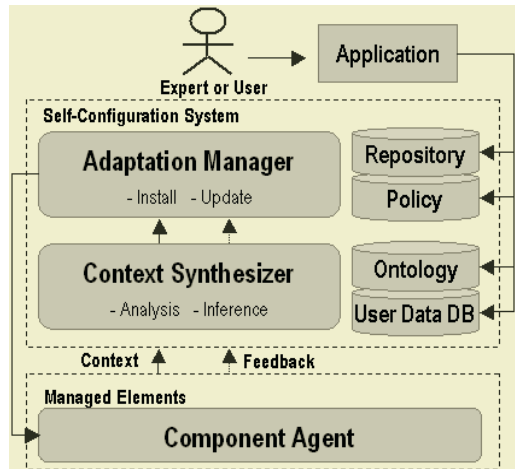


Fig. 1. Architecture of the Proposed system

- *Context Synthesizer*: Gathers the context provided by the *Component Agent* and stores the basic user data, the application preferences and usage frequencies in the *User Data DB*. The *Context Synthesizer* analyzes and deduces the current status using the stored user data and *Ontology* (various

expressions on the preference data of the applications) and relays the results to the *Adaptation Manager*.

- *Adaptation Manager*: Decides and performs the appropriate tasks based on policies that were pre-defined through the data provided by the *Context Synthesizer*. The *Adaptation Manager* installs the components stored in the *Repository* or performs the various configuration tasks such as updates. An installation image on the user data and the customized 'auto-response files' for installation are also automatically created.

The system administrator or the user can adjust and manage these components, policies, Ontology, and the user data to be stored in the *Repository*. The proposed system can also communicate with other external Configuration Servers and share data.

## 2.3 System Behavior

### 1) Installation

The system installs the components by reflecting the existing user's preference and system resource information, and automatically executes the basic configuration through a customized auto-response file and an auto configuration file. In addition, in case a user's resource is insufficient, it automatically selects the 'minimum installation' option for the auto-response file, creating the script. Currently, such a process is notify to the user so that the final decision may be made by the user whilst an agent observes and learns the user's activities, which are reflected to determine the subsequent activities. The major workflow is as follows.

Step 1. Component Agent: monitors the system resource information and configuration information, creating a profile and transmitting it to a context synthesizer, for any changes.

Step 2. Context Synthesizer: saves the received data to the User Data DB, on which the present situation is analyzed.

Step 3. In case a user requests an installation or an administrator needs to distribute it in a lump, it retrieves the user data (preference) saved in the User Data DB, after authenticating the user.

Step 4. Adaptation Manager: creates and distributes the auto-response file and the detail parameter setting file, based on the retrieved user data. (ex. if (resource = insufficient) then checks the 'minimum installation' option of the auto-response file)

Step 5. Component Agent: installs any received file, monitors the user's activities and executes the feedback.

Step 6. Modifies and learns the User Preference, Policy.

**Fig. 2.** Pseudo Code for the Install Phase

### 2) Update

The update priority is determined by monitoring the frequency of the components, through which the system facilitates the various tasks efficiently if the remaining storage or the time required for updating is insufficient. Reflecting the *Astrolabe* [4] structure, each host organizes the components into zones, and these zones are organized hierarchically. A representative host of each zone collects a list of files on

the individual hosts while a host requiring the file requests the representative host about the location of a near host holding the file, and receives it in peer-to-peer transmission method. From this, it can reduce the load of the centralized server, be resistant to various troubles and quickly copy files. The update files copied within the zone are checked for consistency through a size comparison.

Step 1. Component Agent: monitors the frequency of each application by the users, transmits it to the context synthesizer periodically and sends its own update file list to the representative host in the same zone. In addition, the representative host's collected file lists are gathered at the higher level.

Step 2. Context Synthesizer: saves the received data into the User Data DB, on which the user's preference is present.

Step 3. For any update request (update request by a user or update request at a lump by an administrator), it authenticates the user and retrieves the user's data saved in User Data DB.

Step 4. Adaptation Manager: determines the update priority according to the retrieved user data.

Step 5. The system requests the representative host in the same zone, the location of a host holding the file, catches hold of it and finally copies the file. (if the file needed does not exist at the representative host, then go to the level and submit the request to the higher level host).

**Fig. 3.** Pseudo Code for the Update Phase

### 3 Conclusion

This study proposed a prototype system for testing the basic functions and validating a system by comparing for the task time for the existing research. From the results, it could be concluded that proposed system features a shortened configuration work time than the existing systems (shortening the basic parameter setting time) and an increased the user satisfaction and usability. Meanwhile, it is expected that the proposed system might be useful in the *Ubiquitous Computing* era where a user utilizes multiple computing devices and provides them with a more convenient computing environment as a result of the reduced system management.

### References

1. Paul Horn, "Autonomic Computing: IBM's Perspective on the State of Information Technology", IBM White paper, Oct.2001
2. <http://www-306.ibm.com/software/tivoli>
3. <http://www.microsoft.com/technet/prodtechnol/winxpro/deploy/default.mspx>
4. Robbert van Renesse, Kenneth Birman and Werner Vogels, "Astrolabe: A Robust and Scalable Technology for Distributed System Monitoring, Management, and Data Mining", ACM Transactions on Computer Systems, Vol.21, No.2, pp.164-206, May 2003
5. John Keeney, Vinny Cahill, "Chisel: A Policy-Driven, Context-Aware, Dynamic Adaptation Framework", In Proceedings of the Fourth IEEE International Workshop on Policies for Distributed Systems and Networks, Jun.2003
6. Anand Ranganathan, Roy H. Campbell, "A Middleware for Context-Aware Agents in Ubiquitous Computing Environments", In ACM/IFIP/USENIX International Middleware Conference 2004, Jun.2004
7. Richard S. Sutton, Andrew G. Barto, 'Reinforcement Learning: An Introduction (Adaptive Computation and Machine Learning)', The MIT Press, Mar.1998

# Modeling of Communication Delays Aiming at the Design of Networked Supervisory and Control Systems. A First Approach

Karina Cantillo<sup>1</sup>, Rodolfo E. Haber<sup>1</sup>, Angel Alique<sup>1</sup>, and Ramón Galán<sup>2</sup>

<sup>1</sup> Instituto de Automática Industrial – CSIC, Campo Real km 0.200,  
Arganda del Rey, Madrid 28500  
{cantillo, rhaber, a.aliq}@iai.csic.es

<sup>2</sup> Escuela Técnica Superior de Ingenieros Industriales. Universidad Politécnica de Madrid,  
Calle José Gutiérrez Abascal, nº 2, Madrid 28006  
rgalan@etsii.upm.es

**Abstract.** This paper presents a first approach to model the communication delays with the aim of improving the design of networked supervisory and control systems (NSCS). Network delays affect the performance of NSCS. Therefore, it is necessary a complete analysis, modeling and simulation of the communication delays upon the connection technology in use (e.g., Ethernet networks). A statistical model is proposed on the basis of autocorrelation of LRD that is imposed by the bursty behavior of the network traffic.

## 1 Introduction

Nowadays, data networks (i.e., Ethernet networks) have become in a low-cost connection media for networked supervisory and control systems (NSCS) [1], due mainly to the improvement concerning with the speed of communication and the bandwidth. It is evident the need to perform the analysis, modeling and simulation of the communication delays in the framework of NSCS. A suitable and reliable model of communication delays allows assessing the network behavior, the overall influence of the delays on the deterioration of the NSCS performance and the sufficient conditions for closed-loop stability.

In the next section is detailed the developed framework to measure communication delays. The developed model is shown in section 3. In subsection 3.2 is presented the communication delays simulator. Finally, some conclusions and remarks are given.

## 2 Communication Delays Measurement over the Propose Work Environment

The case of study consists of two applications based on RT-CORBA for measuring delays samples. Applications are executed using TCP/IP protocol over an Ethernet network with 110 stations and 10 Mbs of bandwidth. *Real-Time* CORBA defines

mechanisms and policies to control processor, communication and memory resources. The ACE ORB, unlike the most of CORBA implementations, shares a minimum part of ORB resources, reducing substantially the synchronization costs and the priority inversion between the process threads, offering a predictable behavior [2]. The communication interface defined for the applications is depicted below.

```
interface delaysTCPIP{
void delaymonitor(in double tclient, out double
tserver, out v1, out v2, out v3, out double proctserv);};
```

### 3 Data Network Delays Models: The Use of Statistical Techniques

Some network traffic models well-described in the literature are inspired in statistics method such as Poisson Processes, Markov chain, time series, heavy-tailed models, self-similar process and others. These models can be considered as black box tools able to link cause-effect and emulate network traffic behavior with a high accuracy.

The bursty behavior of the Ethernet technology in network traffic imposed the inclusion of the autocorrelation concept in the model to be defined. Poisson processes can be used for modeling the delay between continuous packets with the Exponential Distribution Function (EDF). The drawback is that these processes do not take into account the auto-correlation concept due to the independence hypothesis in data, leading erroneous simulations and analysis. In order to verify these constraints, a statistic analysis of data was performed with *Quantile-Quantile* graphic and the validation methods *Chi-Square Test*, *Anderson-Darling Test*. The results showed that EDF is not adequate to represent the samples of delay included in the measured data.

The introduction of the auto-correlation concepts in the model was then required. Initial solutions were simple chain Markov models, adjusted to a correlation of short-range dependence (SRD), characterizing just in a minimal proportion the bursty behavior. In order to reach a whole representation, auto-correlation of long-range dependence (LRD) must be considered. In order to represent the LRD autocorrelation indices the self-similar processes are used, because the LRD can be characterized only with a simple parameter, the Hurst coefficient ( $H$ ).

#### 3.1 Inclusion of Self-similar Processes in the Proposed Model

Self-similarity processes consist of repeated patterns in multiples scales. The literature shows that the network traffic is self-similar [3]. There are different methods for the Hurst coefficient estimation. The R/S method was chosen because it is easy to implement and it is very useful in other research fields. Initially, the developed program in Matlab makes use of a sample taken in a time-period with low network load. The estimated  $H$  was 0.6535. Subsequently, a sample taken in presence of higher network load was assessed, obtaining an estimated of  $H=0.7232$ . The results show how  $H$  can be used as a reliable measure parameter of the bursty behavior in the network traffic.



In order to complete the representation, a distribution function that fits the LRD characteristics must be chosen as the empiric distribution indicated by the samples. One solution is the use of processes with infinite variance called heavy-tail processes. The distribution functions Pareto, Weibull, Exponential, Gamma, and Lognormal, were analyzed and compared using the central limit theorem and the infinite variance concept. Figure 1 shows the Log-Log plot of each one. The graphic shows that Pareto is the distribution function that better fits data behavior. A residual variance analysis was performed supporting previous result. Additionally, the Pareto distribution function is heavy-tail type that is recommended to depict the network delays.

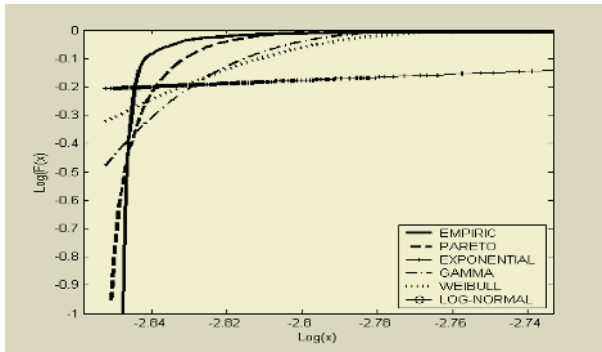


**Fig. 1.** Comparative Analysis: Empiric Cumulative Distribution Function (CDF) and Studied Cumulative Distribution Functions (Pareto, Exponential, Weibull, Gamma, Log-Normal)

### 3.2 Communication Delays Generator

The method *Fractional Gaussian Noise* (FGN) was chosen to generate pure fractal signals based on the Hurst parameter, due to its implementation easiness [4]. The developed simulator initially calculates the Hurst coefficient, based in the R/S method. This coefficient is used to generate the self-similar sample. The sample is mapped to the Pareto distribution function and then formatted to obtain a simulation close to the reality. Before the formatted procedure, the equation used

$$is Y_i = \left( \frac{a \times b}{\text{Log}(1 - F_n(X_i))} \right) \cdot F_n$$

is the normal cumulative distribution function,  $a$  is the

shape parameter,  $b$  is the minimum value of the analyzed sample and  $X_i$  is the datum obtained by FGN method. Figure 2 shows a comparison in a log-log plot between the empiric cumulative distribution of the analyzed sample and the empiric cumulative distribution of the sample obtained from the simulator.

In order to validate the results a residual variance analysis, between the sample generated by the simulator and a sample derived from a Poisson model, was accomplished. The developed simulator achieved the best representation. Although the defined model does not represent all the properties of networks traffic, as SRD behavior, this model is essential to assess the influence of the network delays in reliability and feasibility of NSCS design.

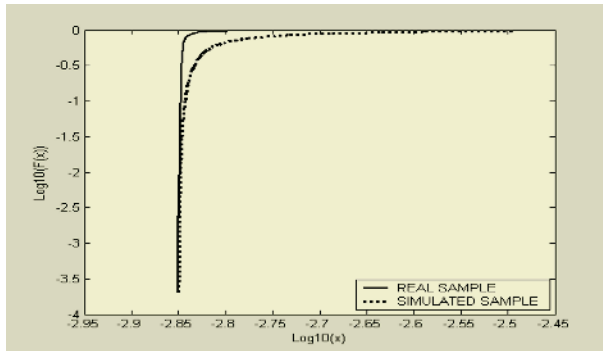


Fig. 2. Comparative Analysis: Real Sample and Simulated Sample

## 4 Conclusions

This paper proposes a statistical model. The bursty behavior of the network traffic imposed the use of self-similar processes using the Hurst coefficient. The results show how  $H$  can be used as a performance index of the bursty behavior in the network traffic. Likewise, Pareto distribution function shows the best performance in representing the empiric distribution function derived from samples measured in real-time. On the other hand, this paper proposes a communication delays simulator using *Fractional Gaussian Noise* method. Both model and simulator are very useful to design networked supervisory and control systems although they do not take into account the autocorrelation of SRD in the case study.

## References

1. Branicky, M.S., Phillips, S.M., Zhang, W.: Stability of Networked Control System: Explicit Analysis of Delay. Proceedings of the American Control Conference (2000) 2352-2357
2. Schmidt, D.C., Mungee, S., Gaitan, S.F, Gokhale, A.: Software Architectures for Reducing Priority Inversion and Non-determinism in Real-time Object Request Brokers. Journal of Real-time Systems, Vol. 21, 1-2, (2001) 77-125
3. Leland, W.E., Taquq, M.S., Willinger, W., Wilson, D.V.: On the self-similar nature of Ethernet traffic. IEEE/ACM Transactions on Networking, Vol. 2 (1994) 1-15
4. Paxson, V.: Fast, Approximate Synthesis of Fractional Gaussian Noise for Generating Self-Similar Network Traffic. ACM SIGCOMM CCR, Vol. 27 (1997) 5-18
5. Cantillo, K., Haber, R.E., Alique, A., Galan, R.: CORBA-Based open platform for processes monitoring. An application to a complex electromechanical process. In: Bubak M., Albada G.D., Sloot P.M.A., Dongarra J. (eds.). Computational Science ICCS2004, Lecture Notes in Computer Science 3036 (2004) 531-535

# Architecture Modeling and Simulation for Supporting Multimedia Services in Broadband Wireless Networks\*

Do-Hyeon Kim<sup>1</sup> and Beongku An<sup>2</sup>

<sup>1</sup> School of Computer & Telecommunication Engineering,  
Cheju National University, Cjeju, South Korea  
kimdh@cheju.ac.kr

<sup>2</sup> Department of Electronic, Electrical & Computer Engineering,  
Hongik University, Jochiwon, South Korea  
beongku@wow.hongik.ac.kr

**Abstract.** In this paper, we propose and evaluate two reference models for supporting wireless video broadcasting services based on ATM over LMDS in metropolitan area wireless access networks. Our proposed reference models, namely end-to-end ATM model and headend/server-to-hub ATM model, are characterized. The end-to-end ATM model supports transfer of the ATM cell between headend and set-top box located in the end of networks for the wireless video services. The headend/server-to-hub ATM model transfers the ATM cell between headend/server and hub, and transmits the LMDS frame in the MPEG-TS over LMDS wireless access network. The performance evaluation of the proposed models is performed via analysis and simulation. The results evaluate delay and jitter of two proposed models. Especially, headend/server-to-hub ATM model has better performance than end-to-end ATM model for wireless video services because the end-to-end ATM model additionally needs more delay and jitter than headend/server-to-hub ATM model to convert the ATM cell to the LMDS frame.

## 1 Introduction

Recently, Broadband wireless access loop technologies are represented by MMDS (Multichannel Multipoint Distribution Service) and LMDS (Local Multipoint Distribution Service). Wireless video services use the wireless access loop such as LMDS instead of the coax cable for CATV and VoD (Video on Demand) service. Especially, we need the analysis about sensitive feature about the jitter and delay caused by the transmission of the video and image data in the broadband wireless multimedia networks [3,4]. However, in our study until now there are no reference models for supporting video services in broadband wireless networks.

This paper presents two reference models of the wireless video broadcasting services based on ATM over LMDS in metropolitan area wireless access networks. The first reference model is the end-to-end ATM model, where ATM cell is transferred between the set-top box and the headend/server. The second reference model is the headend/server-to-hub ATM model. In the second model, ATM cell is transmitted be-

---

\* This work was supported by the Korea Research Foundation Grant.(KRF-2004-002-D00376).

tween the hub and the headend/server in fixed network segment based on ATM, and MPEG2-TS (Transport Stream) is transferred to the set-top box in the radio access network segment using LMDS. We evaluate the performance of the proposed models in terms of the end-to-end delay and jitter of MPEG2-TS. In conclusion, the headend/server-to-hub ATM model can reduce more the delay and the jitter than end-to-end ATM model.

## 2 The Proposed Architecture Models

Wireless access loop has more merits than the wired cable in the view points of the economical efficiency and network flexibility. Wireless video system based on LMDS/ATM consists of service provider, headend, hub, set-top box, etc. We propose two architecture models namely, the end-to-end ATM model and the headend/server-to-hub ATM model, to support the wireless video services based on LMDS/ATM [5,6].

The end-to-end ATM model supports transfer of the ATM cell between headend and set-top box located in the end of the wireless CATV or VoD system. This model uses the ATM backbone network and the LMDS wireless access network. In this model, the ATM cell is translated into LMDS frame to transmit the data between hub and set-top box, and LMDS frame is converted into the ATM cell in set-top box. Figure 1 shows the protocol stack in end-to-end ATM model which supports the ATM protocol stack in all devices such as a headend, set-top box, hub, etc.

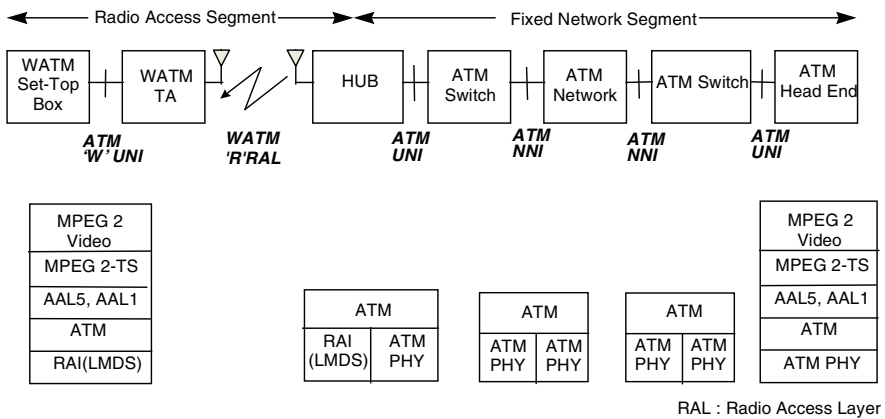


**Fig. 1.** End-to-end ATM model: Configuration and protocol stack

In the headend/server-to-hub ATM model, the ATM cell is transferred between headend/server and hub, and the LMDS frame included the MPEG-TS is transmitted in wireless access network. Then, the MPEG-TS frame is translated into LMDS frame to transmit the data between hub and set-top box. Especially, the main features of this proposed model is that the ATM cell is translated into MPEG2-TS frame and LMDS frame in hub, and converted LMDS frame into the MPEG2-TS frame in set-top box.

Figure 2 describes that the protocol in headend/server-to-hub ATM model can support the ATM protocol stack in all devices such as a headend and hub. The hub removes the AAL head of the ATM cell and recombines with the MPEG2-TS stream.

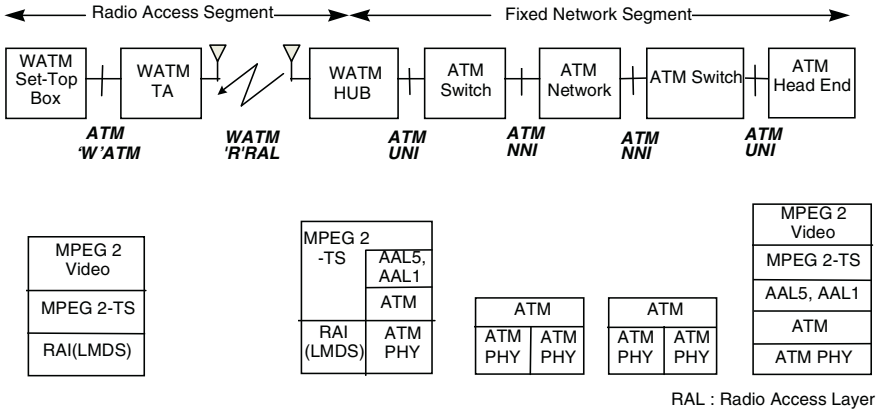


Fig. 2. Headend/server-to-hub ATM model: Configuration and protocol stack

### 3 Performance Evaluations

To verify the performance, we analyze jitter factors that happen in headend/server, hub and set-top box in the headend/server-to-hub model and end-to-end ATM model. We quantitatively analyze the models in terms of end-to-end delay and jitter of MPEG2-TS and perform simulation using OPNET (Optimized Network Engineering Tool) by MIL3 company .

Table 1. End-to-end delay of MPEG2-TS in the end-to-end ATM model

Delay & Jitter		Useful bit rate of LMDS link					
		20MHz			40MHz		
		15.36 Mbps	23.04 Mbps	26.88 Mbps	30.72 Mbps	46.08 Mbps	53.76 Mbps
Flower Garden	Fixed Delay	1.05ms	0.41ms	0.39ms	0.38ms	0.34ms	0.33ms
	Maximum Delay	936.2ms	16.6ms	9.51ms	4.23ms	0.67ms	0.66ms
	Maximum Jitter	935.1ms	16.2ms	9.12ms	3.85ms	0.33ms	0.33ms

The simulation environment of wireless video service networks based on LMDS/ATM consists of the video source, server/headend, hub and set-top box. We assume that the distance from headend to hub sets by 50Km which is the size of a traditional CATV service area, and radio LMDS transmission link between the hub and

set-top box establishes by 5Km. The transfer speed of the 155Mbps recommended by the ATM forum between server and hub is used, while the flower garden image is used.

The fixed end-to-end delay is 0.39ms and the jitter is between 0.39ms and 0.68ms at the radio channel speed 26.88Mbps used flower garden images in the end-to-end ATM model. Especially, jitter has a high probability value between 0.44ms and 0.57ms because the conversion of MPEG2-TS to AAL5 PDU and ATM cell to LMDS frame cause much jitter factor. In the table 1, we present the maximum end-to-end delay and jitter of MPEG2-TS for football and flower garden images according to radio channel speed.

**Table 2.** End-to-end delay of MPEG2-TS in the headend/server-to-hub ATM model

Delay & Jitter		Useful bit rate of LMDS link					
		20MHz			40MHz		
		15.36 Mbps	23.04 Mbps	26.88 Mbps	30.72 Mbps	46.08 Mbps	53.76 Mbps
Flower garden	Fixed Delay	0.84ms	0.36ms	0.35ms	0.34ms	0.33ms	0.32ms
	Maximum Delay	322.89ms	10.39ms	4.23ms	0.40ms	0.36ms	0.35ms
	Maximum Jitter	322.06ms	10.03ms	3.88ms	0.06ms	0.04ms	0.03ms

The fixed end-to-end delay is 0.35ms and the jitter is between 0.35ms and 0.42ms at the radio channel speed 26.88Mbps used flower garden images in the headend/server-to-hub ATM model. In the table 2, we present the maximum end-to-end delay and jitter of MPEG2-TS for football and flower garden images according to radio channel speed. The simulation results demonstrate the delay and jitter of two proposed models in the wireless CATV and wireless VoD service based on LMDS/ATM. Especially, headend/server-to-hub ATM model has better performance than end-to-end ATM model for wireless video services because additionally the end-to-end ATM model needs more delay and jitter than headend/server-to-hub ATM model to convert the ATM cell to the LMDS frame.

## References

1. Digital Audio Video Council Technical Report, DAVIC 1.1 Specification Part 08.
2. ATM Forum Technical Committee, Audiovisual Multimedia Services : Video on Demand Specification 1.0.
3. Dipankar Raychaudhuri, "ATM-based Transport Architecture for Multi-services Wireless Personal Communication Networks," IEEE JSAC, Vol.12, No.8, pp. 1401~1414, Oct. 1994.
4. Bruno Cornaglia, Riccardo Santaniello and Enrico Scarrone, "Proposal for the protocol reference model for WATM," ATM Forum/96-1650, Dec. 1996.
5. Melbourne Barton, Daniel Pinto, et al., "Reference configuration model for wireless ATM," ATM Forum/96-1623, Dec. 1996.
6. "ISO/IEC 13818-6: MPEG-2 Digital Storage Media Command and Control," ISO/IEC JTC1/SC29/WG11, Mar. 1995.

# Visualization for Genetic Evolution of Target Movement in Battle Fields

S. Baik<sup>1</sup>, J. Bala<sup>2</sup>, A. Hadjarian<sup>3</sup>, P. Pachowicz<sup>3</sup>, J. Cho<sup>1</sup>, and S. Moon<sup>1</sup>

<sup>1</sup> College of Electronics and Information Engineering, Sejong University,  
Seoul 143-747, Korea

{sbaik, jscho, sbmoon}@sejong.ac.kr

<sup>2</sup> School of Information Technology and Engineering,

George Mason University,

Fairfax, VA 22030, U.S.A

jbala@gmu.edu

<sup>3</sup> Sigma Systems Research, Inc.

Fairfax, VA 22032, U.S.A

{ahadjarian, ppach}@sigma-sys.com

**Abstract.** This paper focuses on the development of an interactive 3D visualization environment for displaying predicted movements by genetic evolution. The integration of interactive 3D visualization and the genetic search approach can relieve the burden of image exploitation tasks occurring due to an explosion of imagery data obtained in battle fields. The visualization component was implemented using In3D - a cross-platform Java class library designed to enable the creation of interactive 3D visualizations of complex information spaces.

## 1 Introduction

Recently, military missions have expanded into new and uncharted territories such as coalition operations; highly mobile operations; enhanced C4I (Command, Control, Communications, Computers and Intelligence); peacekeeping and humanitarian operations; law enforcement operations of counter-narcotics and counter-terrorism; monitoring treaties and weapons proliferation along with further "operations other than war." These increased areas of responsibility bring with them a greater need for imagery support. In this context, this explosion of available imagery data overwhelms the imagery analysts and outpaces their ability to analyze it. Consequently, the analysis tasks becoming bottlenecked in the imagery community. This situation generates an urgent need for new techniques and tools that can assist analysts in the transformation of this huge amount of data into a useful, operational, and tactical knowledge. The approach presented in this paper applies Genetic Algorithms (GAs) learning techniques to evolve new individuals in the population of movements in order to converge the evolution process toward optimal (most probable) movements. The major innovations in this approach are graphically depicted in Fig. 1.

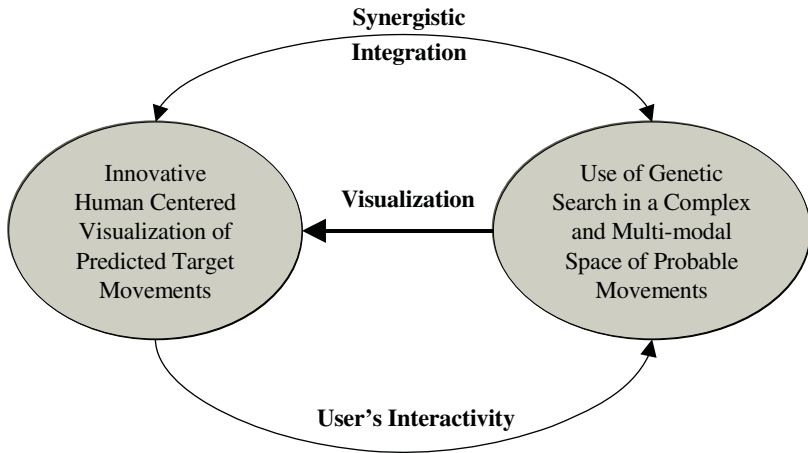


Fig. 1. Innovative concepts of Genetic Evolution Movement

## 2 Genetic Evolution of Target Movement

In a previous work [1], we focused on the genetic evolution approach for target movement prediction. Genetic Algorithms (GAs) [2,3] are used to generate the population of movement generation operators. The population evolves by using crossover and mutation and only the strongest elements survive, thus contributing to improved performance in terms of more probable/optimal movements. This contribution is used as an objective evaluation function to drive the generation process in its search for new and useful movement generation operators. When compared to the other researches<sup>1</sup>, the main differentiators can be summarized in the following two points: 1) GAs use payoff (objective function) information, not derivatives or other auxiliary knowledge. Other search techniques require much auxiliary information in order to work properly; and 2) GAs use probabilistic transition rules, not deterministic rules. GAs use random choice as the tool to guide a search towards regions of the search space with likely improvement (i.e., more probable movements).

## 3 Interactive 3-D Visualization for Target Movement Prediction

It becomes more popular to use visualization techniques [4-6] to facilitate the development of GA systems. We focused on the development of an interactive 3D visualization environment for displaying predicted movements by genetic evolution. The system-interfacing component and visualization component was implemented using

<sup>1</sup> BONN Corp. has developed an enhancement to an existing movement prediction system, called the Tactical Movement Analyzer (TMA). The NATO Reference Mobility Model (NRMM) is the Army's accredited mobility performance prediction model.



In3D<sup>2</sup> - a cross-platform Java class library designed to enable the creation of interactive 3D visualizations of complex information spaces. The use of this library is pivotal in the implementation of the visualization environment for the genetic evolution of movements.

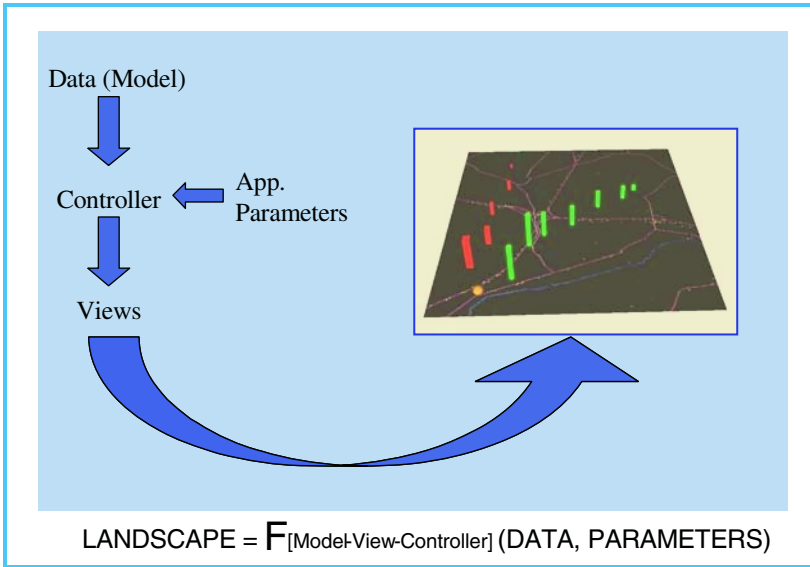


**Fig. 2.** A Model-View-Controller display paradigm

The visualization component implements the Model-View-Controller paradigm of separating imagery data (model) from its visual presentation (view). Interface elements (Controllers) act upon models, changing their values and effectively changing the views (Fig. 2). The Model-View-Controller paradigm supports the creation of applications which can attach multiple, simultaneous views and controllers onto the same underlying model. Thus, a single landscape (imagery and objects) can be represented in several different ways and modified by different parts of an application. The controller can achieve this transformation with a broad variety of actions, including filtering and multi-resolution, zooming, translation, and rotation. The component provides navigational aids that enhance users' explorative capabilities (e.g., the view from above provides a good overview of the information but it is not until zooming in and around and inspecting small items that the user gets a detailed understanding). Fig. 3 depicts an example of the prediction landscape.

<sup>2</sup> It was developed by Visual Insights Corp.

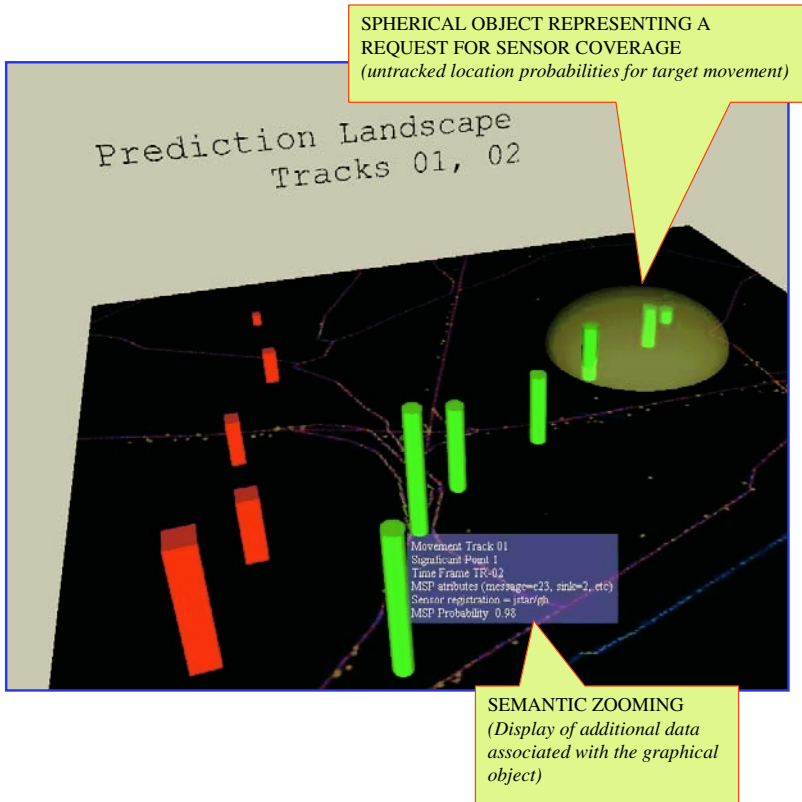


Fig. 3. Prediction landscape for Genetic Evolution of Movements

## References

1. S. W. Baik, J. Bala, A. Hadjarian, and P. Pachowicz: Genetic Evolution Approach for Target Movement Prediction, Lecture Notes in Computer Science Vol. 3037, 2004
2. A. Brindle: Genetic algorithms for function optimization, Ph.D. Thesis, Computer Science Dept., Univ. of Alberta, 1981
3. K. A. DeJong: Adaptive system design: a genetic approach, IEEE Trans. Syst, Man, and Cyber, Vol. SMC-10, No. 9, pp. 566-574, Sept. 1980
4. W. B. Shine and C. F. Eick: Visualizing the evolution of genetic algorithm search processes, IEEE International Conference on Evolutionary Computation, pp. 367-372, April 1977
5. E. Hart and P. Ross: GAVEL - A New Tool for Genetic Algorithm Visualization, IEEE Trans on Evolutionary Computation, Vol. 5, No. 4, pp. 335-348, August 2001
6. A. M. Malkawi, R. S. Srinivasan, Y. K. Yi and R. Choudhary: Decision Support and design evolution: integrating genetic algorithms, CFD and visualization, Automation in Construction, Vol. 14, pp. 33-44, 2005

# Comfortable Driver Behavior Modeling for Car Following of Pervasive Computing Environment<sup>1</sup>

Yanfei Liu and Zhaohui Wu

College of Computer Science, Zhejiang University, 38# Zheda Road,  
Hangzhou, Zhejiang, China, 310027  
yliu@zju.edu.cn

**Abstract.** This paper demonstrates a novel car-following model based on driver or passengers' comfort. As we know, hasty deceleration during emergency brake will cause passengers feel uncomfortable. According to the relationship between brake acceleration and people's comfortable feeling, the comfortable model is setup. The model calculates the following car's acceleration by measuring the distance between the following car and the preceding car, the velocity of the following car, and controls the car's acceleration to make driver and passengers feel comfort. The paper combine the model with the pervasive computing concept, provoke the pervasive computing driver behavior modeling idea and turn it into reality to increase the adaptability and reliability of car's parts, when car equipped with this device, the prospect is not only the assistant driver or comfortable driver are realized in the car-following circumstance, but also the whole car's performance will be improved.

## 1 Introduction

The idea of pervasive computing is developing to be one of the hottest research topics at present [1]. The academic circles of all countries already have great foresight to focus on the research of the related topic [2].

The researches on driver behavior modeling have developed following mainly directions in recent years, the driver performance and capacity [3], the longitudinal driver behavior [4] and driver skill. The driver performance and capacity include mental and physical researches. There have been made a huge progress in all the directions these years [5].

Most of the early works in car-following model [6], PD-controller car following model [7], and visibility angle model [8] [9] are that drivers react immediately to the behavior of the vehicle in front of them so as to avoid imminent accidents. This paper focus on the driver's comfortable of car following.

Actually there can be as many as 50 embedded computers inside a modern car, on the other hand, a general human drivers behaviors is inherently complex. Both the

---

<sup>1</sup> This research was supported by 863 National High Technology Program under Grant No. 2003AA1Z2080, "Research of Operating System to Support Ubiquitous Computing".

car’s researches and driver behaviors modeling can not be separate from using as many as computing techniques, the pervasive computing must take an important roles in future research of them.

## 2 A Comfortable Car-Following Model

### 2.1 A Car Following Model Based on Space and Velocity

Car following model describes the driver longitudinal behavior shown as in Fig.1.

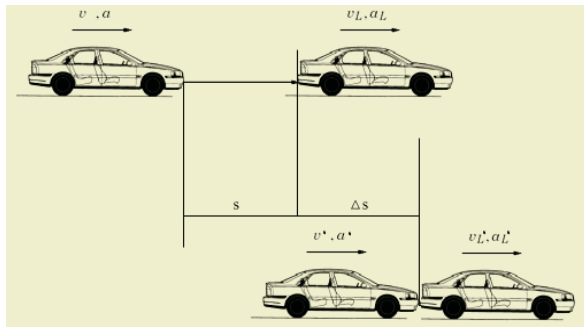


Fig. 1. Car following model based on space and velocity

At the time of collision, to the following car there is relation:

$$2a(s+\Delta s)=(v'^2 - v^2) \tag{1}$$

For the worst condition, above equation can be simplified as following:

$$2as=v^2 \tag{2}$$

### 2.2 Comfortable Car Following Model Based on Acceleration

The acceleration  $a$  can be calculated from  $s$  and  $v$  according to formula (2). Of the different  $a$ , the comfortable status are shown as table 1, the  $a_c$  represent the critical comfortable acceleration, the researches show that its value is  $2 \text{ m/s}^2$ .

Table 1. The following car’s status of comfortable car following models

Area	Condition	Acceleration
Comfortable	$s > v^2/2a_c$	$a < a_c$
Uncomfortable	$v^2/2a_{max} < s < v^2/2a_c$	$a_c < a < a_{max}$
Dangerous	$s < v^2/2a_{max}$	$a > a_{max}$

### 2.3 The Realization of Comfortable Driver Behavior Model

Actually, the minimum brake distance  $s_{min}$  is related to the car's velocity, the car's velocity, and the friction coefficient of road surface. An experience formula of the relationship is shown as:

$$s_{min} = v^2 / (2\mu g) \tag{3}$$

When considering the boundary conditions and friction coefficient, the relationships among  $a$ ,  $s$ ,  $v$ ,  $\mu$  are shown as Fig.2.:

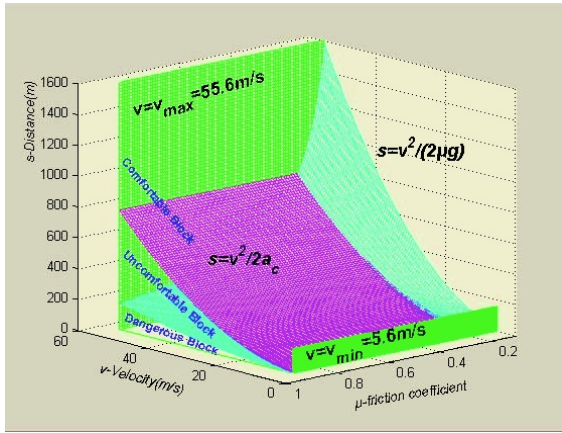


Fig. 2. The relationship among  $s$ ,  $v$ ,  $\mu$  and  $a$

The surfaces in Fig.2. enclosed several blocks, they are represent different physical conception, we named the relevant blocks as Table 2.

Table 2. The following car's status of comfortable car following models with COF

Block	Enclosed by	Acceleration
Comfortable block	$s > v^2/2a_c, s > v^2/2\mu g,$ $0.2 < \mu < 0.9, v_{min} < v < v_{max}$	$a < a_c$
Uncomfortable block	$s < v^2/2a_c, s > v^2/2\mu g,$ $0.2 < \mu < 0.9, v_{min} < v < v_{max}$	$a_c < a < a_{max}$
Dangerous Block	$s < v^2/2\mu g, s = 0,$ $0.2 < \mu < 0.9, v_{min} < v < v_{max}$	$a > a_{max}$

### 3 Implementation Driver Behavior Modeling of Pervasive Computing Environment

A wireless speed sensor is equipped to obtain the car's velocity, a *Bushnell Yardage Pro 800 Compact Rangefinder* displacement device is installed to detect the distance,

and a dynamic friction coefficient tester is used to determine the friction coefficient.. The architecture of the model of pervasive computing environment is shown in Fig. 4.

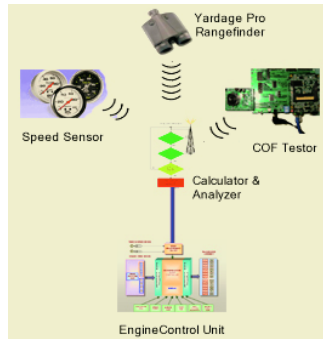


**Fig. 4.** The architecture of the comfortable model in pervasive computing environment

## 4 Experiments and Conclusions

The experiments are implemented by using a BUICK REGAL 2.5 car of GM, and the car running on a dry road surface of a highway on a sunny day.

One contribution of this paper is to demonstrate a new car-following model based on driver's comfort, while most of the former models are contribute to the safety of the car or the traffic flow throughput.

Another contribution is the introduction of pervasive computing conception to the drivers' behavior modeling researches. The paper combines the drivers' model with the pervasive computing concept, and makes the model as a pervasive computing device into reality to increase the system's adaptability and reliability.

## References

1. Xu Guangyou ,The ubiquitous pervasive computing. China computer, June 9, 2003 general issue number 1222, year issue number 41.
2. Xiong Jiang, Embedded system and pervasive computing.
3. Strategies for Reducing Driver Distraction from In-Vehicle Telematics Devices: A Discussion Document (June 2003), Transport Canada TP 14133 E.
4. Driver Behavior Models for Traffic Simulation, Xiaopeng Fang, thesis of Iowa State University,2001
5. Yoshiyuki Umemura,Driver Behavior and Active Safety (Overview),Special Issue Driver Behavior and Active Safety,R&D Review of Toyota CRDL Vol. 39 No. 2
6. Johan Bengtsson, Adaptive Cruise Control and Driver Modeling, Printed in Sweden,Lund University, Lund 2001
7. Xiaopeng Fang, Hung A. Pham1 and Minoru Kobayashi, PD Controller for Car-Following Models Based on Real Data
8. Pipes, L.A. and Wojcik, C.K., A contribution to theory of traffic flow, SAE Conference Proceedings – Analysis and Control of Traffic Flow Symposium,(Detroit, 1968), pp. 53-60
9. Ir. J.J. Reijmers, Traffic Guidance Systems, November 26, 2003 Et4-024 P99

# A Courseware Development Methodology for Establishing Practice-Based Network Course

1

2

<sup>1</sup> School of Information and Communications Engineering, Sungkyunkwan Univ.  
Chunchun-dong 300, Jangan-gu, Suwon, Kyounggi-do, Korea  
jhkoo@songgang.skku.ac.kr

<sup>2</sup> Department of Computer Education, Sungkyunkwan Univ.  
Myeongnyun-dong 3-ga 53, Jongno-gu, Seoul, Korea  
sjahn@comedu.skku.ac.kr\*

**Abstract.** In this paper, we present a practice-based courseware development methodology for establishing a senior undergraduate network course for the computer-engineering department by reflecting on the rapidly changing information and communication technologies, enforcing practical education, and focusing on the existing and currently used curriculum models. Therefore, we have developed a special method, named it STM (Segmenting, Targeting, and Mapping), and applied it to the courseware development of a practice-based network course.

## 1 Introduction

Abstract text area containing multiple lines of placeholder text, likely representing the main body of the paper's introduction.

---

\* Dr. S. Ahn is the Corresponding Author.

## 2 STM(Segmenting, Targeting, and Mapping) Methodology

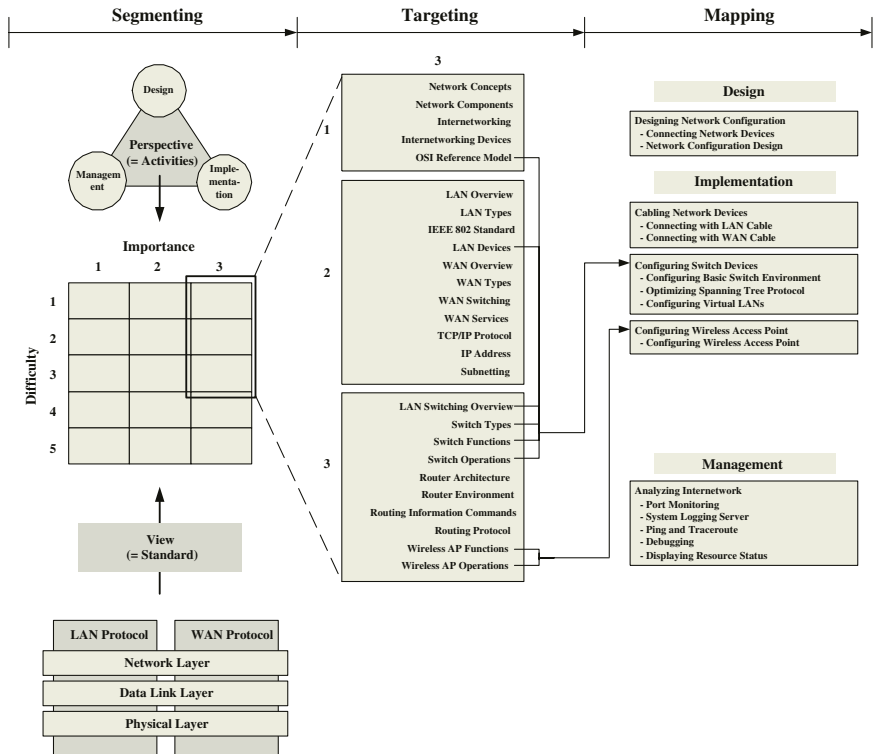


Fig. 1. STM diagram



## 2.1 Processes

The first step in the design of a network is to determine the requirements for the network. This includes identifying the users and their needs, the applications to be used, and the performance requirements. Once the requirements are determined, the next step is to design the network topology. This involves determining the physical layout of the network, including the locations of the servers, routers, and switches, and the connections between them. The design should take into account factors such as scalability, reliability, and security. Once the network topology is designed, the next step is to implement the network. This involves configuring the devices and connecting them to the network. Finally, the network should be tested and monitored to ensure that it is operating correctly and meeting the requirements.

## 2.2 Output Definition

The output definition is a critical part of the network design process. It involves defining the specific outputs that the network is expected to produce. This includes identifying the data flows, the services to be provided, and the performance metrics. The output definition should be based on the requirements identified in the first step. Once the outputs are defined, the next step is to design the network architecture to support them. This involves determining the hardware and software components needed, and how they will be configured and connected. The design should take into account factors such as scalability, reliability, and security. Once the network architecture is designed, the next step is to implement it. This involves configuring the devices and connecting them to the network. Finally, the network should be tested and monitored to ensure that it is producing the expected outputs and meeting the requirements.

## 2.3 Infrastructure Preparation: Network Lab Configuration

The infrastructure preparation phase involves setting up a network lab environment. This includes configuring the hardware and software components, and connecting them to the network. The lab environment should be designed to simulate the real-world network environment. This involves configuring the devices to match the requirements of the network. Once the lab environment is set up, the next step is to test the network. This involves running various tests to verify that the network is operating correctly and meeting the requirements. Finally, the network should be monitored to ensure that it is operating correctly and meeting the requirements.

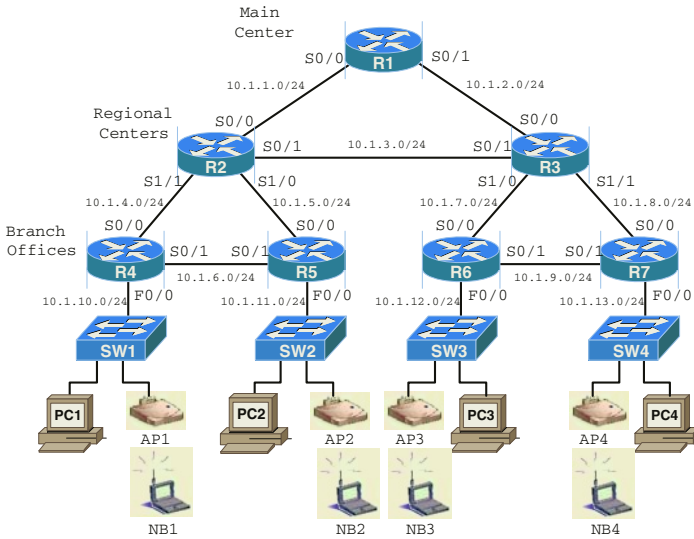


Fig. 2. Network lab configuration diagram

### 3 Conclusion

The network lab configuration diagram shows a hierarchical network structure. At the top is the Main Center with router R1. Below it are two Regional Centers, R2 and R3. Under R2 are two Branch Offices, R4 and R5. Under R3 are two Branch Offices, R6 and R7. Each Branch Office router is connected to a switch (SW1, SW2, SW3, SW4). Each switch is connected to various devices: PC1, AP1, NB1 under SW1; PC2, AP2, AP3, NB2, NB3 under SW2; PC3 under SW3; and AP4, PC4, NB4 under SW4. IP addresses are provided for all inter-router links.

### References

1. J. T. Gorgone, G. B. Davis, J. S. Valachich, H. Topi, D. L. Feinstein, and H. E. Longenecker, "IS 2002 - Model Curriculum and Guidelines for Undergraduate Degree Programs in Information Systems," Association for Information Systems, 2002.
2. Computing Curricula 2001 Computer Science Final Report, December, IEEE-CS and ACM, 2001.
3. S. McQuerry, "Interconnecting cisco network devices," Cisco Systems, Inc, 2000.
4. Cisco networking academy program: first-year companion guide, Cisco Systems, Inc, 2001.
5. Cisco networking academy program: second-year companion guide, Cisco Systems, Inc, 2001.
6. Cisco networking academy program web site. [online] Available: <http://cisco.netacad.net>
7. Network practice course web site. [online] Available: <http://songgang.skku.ac.kr/jhkoo/index1.htm>

# Solving Anisotropic Transport Equation on Misaligned Grids

Che<sup>1</sup>, Card<sup>1</sup>, and Trauss<sup>2</sup>

<sup>1</sup> PPPL, P.O. Box 451, Princeton, NJ 08543, USA

<sup>2</sup> Courant Institute, NYU, 251 Mercer Street, NY 10012, USA  
jchen@pppl.gov

**Abstract.** Triangular 3rd order Lagrange elements have been implemented previously to study the numerical error associated with grid misalignment. It has previously been found that grid misalignment strongly affects numerical accuracy in the case of linear elements. The same conclusion was obtained by higher order finite difference. Here we observe that this is also true for higher order finite elements, up to 3rd order, when the solution has a steep gradient. Three types of meshes are considered. Type t1 has one element edge fully aligned with the strong transport direction; type t2 doesn't have any alignment with that direction; type t0 is a combination of t1 and t2, i.e., partial alignment.

## 1 Introduction

Higher order Lagrange elements have been used recently to study the numerical error of grid misalignment. It has previously been found that the numerical solution is polluted by the grid misalignment. The linear elements were used. It is shown that grid alignment is a critical factor for accurate solution. Numerical error for higher order finite difference methods is found that higher order elements can reduce the numerical artifacts caused by such misalignment. The error is studied for two types of meshes: t1 and t2. The mesh applied is a combination of t1 and t2, and is referred to as t0. The equation is

the steady state anisotropic heat conduction equation considered here is given by the orthographic coordinates  $(\xi, \eta)$  by

$$\frac{\partial}{\partial \xi} \kappa_{\xi} \frac{\partial T}{\partial \xi} + \frac{\partial}{\partial \eta} \kappa_{\eta} \frac{\partial T}{\partial \eta} = 0. \quad (1)$$

where  $T$  is the temperature and  $\kappa_{\xi}$  and  $\kappa_{\eta}$  are the conductivity along the transport axes  $\xi$  and  $\eta$ , respectively. Throughout this paper we assume  $\kappa_{\eta} \equiv 1$  and  $\kappa_{\xi} \gg 1$ , so that the strong transport direction is aligned with  $\xi$ , and the anisotropy ratio is given by  $\kappa_{\xi}/\kappa_{\eta} \equiv \kappa_{\xi}$ .

The solution domain is given by the Cartesian coordinates  $(x, y)$  by the rectangular  $C$ ,  $L_x \times L_y$ , throughout the calculation. The strong transport direction is aligned with the coordinate axis  $x$  and  $y$  is aligned with the

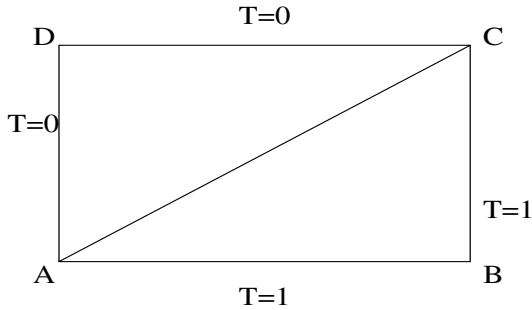


**Fig. 1.** Rect ABCD:  $L_x = L_y = 1$ .  $T=0$  on side [AD-DC],  $T=1$  on [AB-BC]. The strong anisotropic direction is aligned with the grid diagonal [AC]

coordinate the strong transport axis  $\xi$  is aligned with the C diagonal. The boundary conditions are  $T=0$  on side [AD-DC] and  $T=1$  on side [AB-BC]. In finite difference, the exact solution is  $T = \frac{1}{2} + \frac{1}{2} \frac{y-x}{\sqrt{2}}$  along the grid diagonal AC.  $T = 0$  below the grid diagonal AC, and the width of the transition zone is zero. In a finite difference, the exact solution introduces a numerical error which has zero transition width.

## 2 Mesh Setup

The unstructured triangular mesh is formed by first dividing the rectangular domain into  $N_x \times N_y$  rectangular cells,  $N_x = 10, N_y = 10$ . Each of the rectangular grids is subdivided into triangles. The following figure shows

*Mesh t1 in Fig. 2.* The strong transport direction  $\xi$  has full alignment with the element edge which is parallel to the diagonal AC.

*Mesh t2 in Fig. 2.* The strong transport direction  $\xi$  has no alignment with the element edge. The element angles aligned with  $\xi$  in mesh  $t_2$  are aligned with the other diagonal.

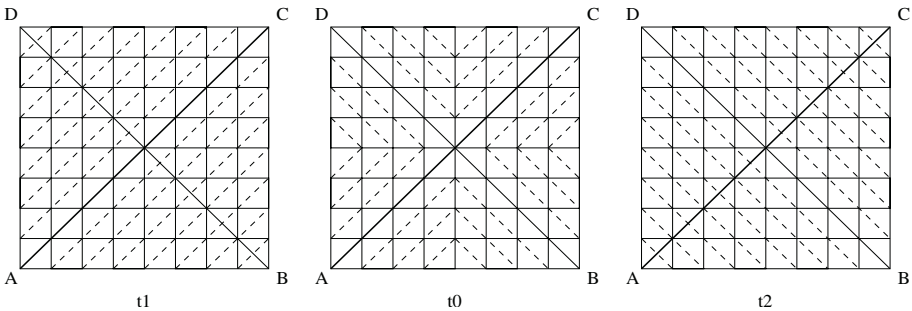


**Fig. 2.** Meshes.  $t_1$  : 100% alignment;  $t_0$  : 50% alignment;  $t_2$  : 0% alignment

Mesh  $t_0$  in Fig. 2. The meshes are  $t_1$  and  $t_2$  such that the alignment is as follows: the upper right and lower left blocks of the rectangular domain are the upper left and lower right blocks, the meshes are the same as mesh  $t_2$

### 3 Numerical Experiments and Discussions

The numerical results for the convergence studies are presented in Table 2 for mesh  $t_1$ ,  $t_2$  and  $t_3$ , respectively, in ascending order such that the alignment

Table 1. Profile width

N	t1 mesh (100% alignment)				t0 mesh (50% alignment)				t2 mesh (0% alignment)			
	$10^2$	$10^3$	$10^4$	$10^5$	$10^2$	$10^3$	$10^4$	$10^5$	$10^2$	$10^3$	$10^4$	$10^5$
39	0.1060	0.0353	0.0124	0.0094	0.1060	0.0354	0.0158	0.0138	0.1065	0.0441	0.0337	0.0328
49	0.1061	0.0353	0.0121	0.0077	0.1059	0.0355	0.0141	0.0113	0.1063	0.0408	0.0289	0.0275
59	0.1060	0.0350	0.0121	0.0066	0.1060	0.0351	0.0132	0.0096	0.1062	0.0386	0.0254	0.0240
69	0.1060	0.0351	0.0117	0.0059	0.1060	0.0351	0.0125	0.0084	0.1062	0.0374	0.0226	0.0213
79	0.1060	0.0350	0.0117	0.0054	0.1060	0.0350	0.0122	0.0076	0.1061	0.0365	0.0211	0.0193
89		0.0349	0.0115	0.0050		0.0350	0.0119	0.0069	0.1061	0.0361	0.0196	0.0177
99		0.0349	0.0115	0.0047		0.0350	0.0118	0.0063	0.1061	0.0357	0.0184	0.0163
109		0.0349	0.0115	0.0045			0.0117	0.0059		0.0355	0.0174	0.0152
119			0.0114	0.0043			0.0117	0.0055		0.0353	0.0166	0.0143
129			0.0114	0.0042			0.0116	0.0053		0.0352	0.0159	0.0135
139			0.0114	0.0040			0.0116	0.0051		0.0351	0.0153	0.0127
149			0.0114	0.0039			0.0115	0.0049		0.0351	0.0147	0.0121
159			0.0113	0.0039			0.0115	0.0048		0.0350	0.0143	0.0116
169			0.0113	0.0038			0.0114	0.0047		0.0350	0.0139	0.0111
179			0.0113	0.0037			0.0114	0.0046		0.0350	0.0135	0.0106
189				0.0037			0.0114	0.0045			0.0133	0.0106
199				0.0038				0.0044			0.0130	0.0099
209				0.0038				0.0043			0.0127	0.0095
219				0.0038				0.0042			0.0125	0.0092
229								0.0042				0.0090

Table 2.  $L_2$  Norm

N	t1 mesh (100% alignment)				t0 mesh (50% alignment)				t2 mesh (0% alignment)			
	$10^5$	$10^6$	$10^7$	$10^8$	$10^5$	$10^6$	$10^7$	$10^8$	$10^5$	$10^6$	$10^7$	$10^8$
39	0.9969	0.9972	0.9972	0.9972	0.9965	0.9967	0.9967	0.9967	0.9919	0.9919	0.9920	0.9920
49	0.9974	0.9978	0.9978	0.9978	0.9971	0.9973	0.9974	0.9974	0.9933	0.9934	0.9934	0.9934
59	0.9977	0.9981	0.9982	0.9982	0.9975	0.9978	0.9978	0.9978	0.9942	0.9943	0.9943	0.9943
69	0.9979	0.9984	0.9985	0.9985	0.9977	0.9981	0.9981	0.9981	0.9949	0.9950	0.9950	0.9950
79	0.9980	0.9986	0.9987	0.9987	0.9979	0.9983	0.9983	0.9983	0.9954	0.9955	0.9956	0.9956
89	0.9982	0.9987	0.9988	0.9988	0.9980	0.9985	0.9985	0.9985	0.9958	0.9960	0.9960	0.9960
99	0.9982	0.9988	0.9989	0.9989	0.9981	0.9986	0.9987	0.9986	0.9961	0.9963	0.9963	0.9963
109	0.9983	0.9989	0.9990	0.9990	0.9982	0.9987	0.9988	0.9988	0.9964	0.9966	0.9966	0.9966
119	0.9984	0.9990	0.9991	0.9991	0.9983	0.9988	0.9989	0.9989	0.9966	0.9968	0.9968	0.9968
129	0.9984	0.9991	0.9992	0.9992	0.9983	0.9989	0.9989	0.9989	0.9968	0.9970	0.9970	0.9970
139	0.9984	0.9991	0.9992	0.9992	0.9984	0.9989	0.9990	0.9990	0.9970	0.9972	0.9972	0.9972
149	0.9985	0.9992	0.9993	0.9993	0.9984	0.9990	0.9991	0.9991	0.9971	0.9973	0.9974	0.9973
159	0.9985	0.9992	0.9993	0.9993	0.9985	0.9990	0.9991	0.9991	0.9972	0.9975	0.9975	0.9975
169	0.9985	0.9992	0.9994	0.9994	0.9985	0.9991	0.9992	0.9992	0.9973	0.9976	0.9976	0.9976
179	0.9985	0.9993	0.9994	0.9994	0.9985	0.9991	0.9992	0.9992	0.9974	0.9977	0.9977	0.9977
189	0.9985	0.9993	0.9994	0.9994	0.9985	0.9992	0.9993	0.9993	0.9975	0.9978	0.9978	0.9978
199	0.9986	0.9992	0.9995	0.9994	0.9985	0.9992	0.9993	0.9993	0.9976	0.9979	0.9979	0.9979
209	0.9986	0.9993	0.9995	0.9995	0.9986	0.9992	0.9993	0.9993	0.9977	0.9980	0.9980	0.9980
219	0.9986	0.9993	0.9995	0.9995	0.9986	0.9992	0.9994	0.9993	0.9977	0.9980	0.9981	0.9981
229		0.9994	0.9995	0.9995	0.9986	0.9993	0.9994	0.9994	0.9978	0.9981	0.9981	0.9981
239		0.9994	0.9996	0.9995		0.9993	0.9994	0.9994	0.9978	0.9982	0.9982	0.9982

As the profile width, defined in (4), is used to detect the numerical cancellation error, the  $\kappa_\xi < 5$  of the width remains the same times as the the grid resolution increases, regardless of the order of the O-ordered error estimates are applied here based on the results from

the the anisotropic  $\kappa_\xi$  is small,  $\leq 3$ , as shown in the cumulative distribution function mesh above, the magnetic field has a negligible effect on the convergence rate at grid resolution. For the first two meshes, and for the second mesh, the solution on the second mesh is about 1% of the error on the first mesh. The solution on the first and second meshes has decreased from the error on the first mesh by about 1%, but convergence takes place after the second mesh than the first mesh.

As the anisotropic parameter increases, the transport error becomes smaller and the magnetic field starts to come into play.

For  $\kappa_\xi \approx 3 - 5$ , the magnetic field has a moderate effect on the cumulative distribution function for the distribution function mesh, the convergence rate takes place at a much earlier stage than the first magnetic field. The convergence rate comes after the partial averaged mesh, and the series used in the second mesh than the magnetic field  $\kappa_\xi \approx 4$ , solution on the first mesh has a decrease from the error on the first mesh by about 0.8%, but about 1% from the solution on the second mesh than the magnetic field  $\kappa_\xi \approx 5$ , solution on the first mesh converges at grid resolution, but the error from the first and second meshes

As the anisotropic parameter increases,  $\kappa_\xi > 5$ , numerical cancellation becomes difficult to measure the profile width correctly, so the error becomes smaller.

Here, the  $L_2$  norm of the solution is used above to show the convergence rate. As  $\kappa_\xi \rightarrow \infty$ , the data above indicate that the magnetic field has a strong effect on the  $L_2$  norm approaches faster than the first mesh than the second mesh is the same. Here, we conclude that the order of the error decreases for the first two meshes, and the magnetic field is a multiplicative factor to be considered for the ordered error estimates.

As a result, it is observed that the ordered error estimates for  $\kappa_\xi < 7$  since the  $L_2$  norm remains the same at  $\kappa_\xi \approx 7$  and  $\kappa_\xi \approx 8$  for the magnetic field  $\kappa_\xi > 7$ , higher order error estimates than the first should be introduced to address this in the future.

## References

1. J. Chen et al, Higher Order Lagrange Elements in M3D, DOE Technical Report, 2005. <http://www.osti.gov/servlets/purl/836490-CNwldj/native/>.
2. R. Vesey and D. Steiner, A Two-Dimensional Finite Element Model of the Edge Plasma, *J. Comp. Phys.* **116** 300-313 (1994).
3. R. Zanino, Advanced Finite Element Modeling of the Tokamak Plasmas Edge, *J. Comp. Phys.* **138** 881-906 (1997).
4. M. V. Umansky, M. S. Day, and T. D. Rognlien, On Numerical Solution of Strongly Anisotropic Diffusion Equation on Misaligned Grids. Submitted to *Numerical Heat Transfer*.

# The Design of Fuzzy Controller by Means of Evolutionary Computing and Neurofuzzy Networks

Sung-Kwun Oh<sup>1</sup> and Seok-Beom Roh<sup>2</sup>

<sup>1</sup> Department of Electrical Engineering, The University of Suwon, San 2-2 Wau-ri, Bongdam-eup, Hwaseong-si, Gyeonggi-do, 445-743, South Korea  
ohsk@suwon.ac.kr

<sup>2</sup> Department of Electrical Electronic and Information Engineering, Wonkwang University, 344-2, Shinyong-Dong, Iksan, Chon-Buk, 570-749, South Korea

**Abstract.** In this study, we propose a new design methodology to design fuzzy controllers. This design methodology results from the use of Computational Intelligence (CI), namely genetic algorithms and neurofuzzy networks (NFN). The crux of the design methodology is based on the selection and determination of optimal values of the scaling factors of the fuzzy controllers, which are essential to the entire optimization process. First, the tuning of the scaling factors of the fuzzy controller is carried out, and then the development of a nonlinear mapping for the scaling factors is realized by using GA based NFN.

## 1 Introduction

In the conventional design method to build fuzzy controllers, a control expert proposes some linguistic rules and decides upon the type and parameters of the associated membership functions. With an attempt to enhance the quality of the control knowledge conveyed by the expert, genetic algorithms (GAs) have already started playing a pivotal role. One should stress however that evolutionary computing is computationally intensive and this may be a point of concern when dealing with amount of time available to such search. For instance, when controlling a nonlinear plant such as an inverted pendulum of which initial states vary in each case, the search time required by GAs could be prohibitively high. To alleviate this shortcoming, we introduce a nonlinear mapping from the initial states of the system and the corresponding optimal values of the parameters. With anticipation of the nonlinearity residing within such transformation, in its realization we consider GA-based NFN. Bearing this mind, the development process consists of two main phases. First, using genetic optimization we determine optimal parameters of the fuzzy controller for various initial states of the dynamic system. Second, we build up a nonlinear model that captures a relationship between the initial states of the system and the corresponding genetically optimized control parameters.

## 2 Design Methodology of Fuzzy Controller

The block diagram of fuzzy PID controller is shown in Fig. 1. Note that the input variables to the fuzzy controller are transformed by the scaling factors (GE, GD, GH,

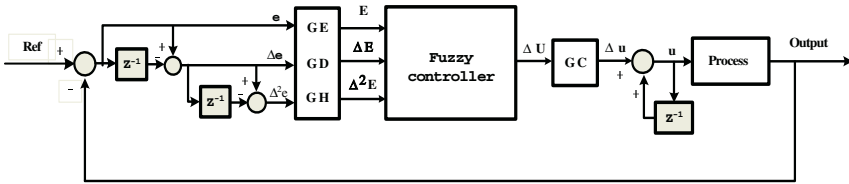


Fig. 1. An overall architecture of the fuzzy PID controller

and GC) whose role is to allow the fuzzy controller to properly “perceive” the external world to be controlled.

The above fuzzy PID controller consists of rules of the following form, cf. [3]

$$R_j : \text{if } E \text{ is } A_{1j} \text{ and } \Delta E \text{ is } A_{2j} \text{ and } \Delta^2 E \text{ is } A_{3j} \text{ then } \Delta U_j \text{ is } D_j$$

The capital letters standing in the rule ( $R_j$ ) denote fuzzy variables whereas  $D$  is a numeric value of the control action.

Genetic algorithms (GAs) are the search algorithms inspired by nature in the sense that we exploit a fundamental concept of a survival of the fittest as being encountered in selection mechanisms among species [4]. The genetic search is guided by a reproduction, mutation, and crossover. The standard ITAE expressed for the reference and the output of the system under control is treated as a fitness function [2].

It is the overall design procedure of the fuzzy PID controller realized by means of GAs that consists of the following steps

- [step 1] Select the general structure of the fuzzy controller
- [step 2] Define the number of fuzzy sets and set up initial control rules.
- [step 3] Form a collection of initial individuals of GAs.
- [step 4] All the control parameters (GE, GD, GH and GC) are tuned at the same time.

### 3 The Estimation Algorithm by Means of GA-Based Neurofuzzy Networks (NFN)

Let us consider an extension of the network with the fuzzy partition realized by fuzzy relations. Fig. 2 visualizes an architecture of such NFN for two-input and one-output, where each input assumes three membership functions. The circles denote processing units of the NFN. The node indicated  $\Pi$  denotes a Cartesian product, whose output is the product of all the incoming signals. And  $N$  denotes the normalization of the membership grades.

The learning of the NFN is realized by adjusting connections of the neurons and as such it follows a standard Back-Propagation (BP) algorithm

$$w(new) = w(old) + 2 \cdot \eta \cdot (y_p - \hat{y}_p) \cdot \mu_i + \alpha(w_{ij}(t) - w_{ij}(t-1)) \tag{1}$$

Where,  $\eta$  is a positive learning rate and  $\alpha$  is the momentum coefficient.



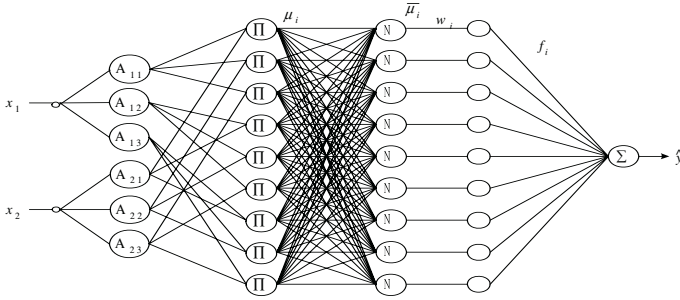


Fig. 2. NFN structure by means of the fuzzy space partition realized by fuzzy relations

### 4 Experimental Studies

In this section, we demonstrate the effectiveness of the fuzzy PID controller by applying it to the inverted pendulum system. Our control goal here is to balance the pole without regard to the cart’s position and velocity [7]. We genetically optimize control parameters with a clear intent of achieving the best performance of the controller. GAs are powerful nonlinear optimization techniques. However, the powerful performance is obtained at the cost of expensive computational requirements and much time. To overcome this weak point, we propose the nonlinear model (GA-based NFN) which is able to estimate the control parameters quickly in the case that the initial angular positions and velocities of the inverted pendulum are selected arbitrarily within the given range. Fig. 3 demonstrates (a) pole angle (b) pole angular velocity for initial angle  $\theta = 0.22(\text{rad})$  and initial angular velocity  $\dot{\theta} = 0.22(\text{rad}/\text{sec})$ .

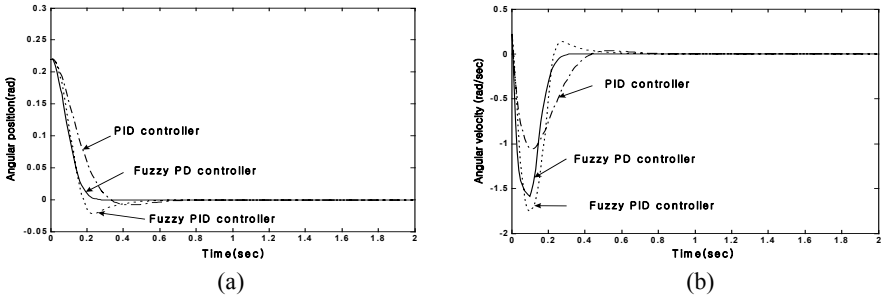


Fig. 3. (a) pole angle (b) pole angular velocity for initial angle  $\theta = 0.22(\text{rad})$  and initial angular velocity  $\dot{\theta} = 0.22(\text{rad}/\text{sec})$

From the above Fig. 3, we know that the fuzzy PD and fuzzy PID control effectively the inverted pendulum system. The output performance of the fuzzy controllers such as the fuzzy PD and the fuzzy PID controller including nonlinear characteristics are superior to that of the PID controller especially when using the nonlinear dynamic equation of the inverted pendulum. Moreover, the proposed estimation algorithm such

as GA-based NFN generates the preferred model architectures. Especially the fuzzy PD controller describes the preferred one among the controllers.

## 5 Conclusions

We have proposed a two-phase optimization scheme of the fuzzy PID and PD controllers. The first phase of the design of the controller uses genetic computing that aims at the global optimization of its scaling factors where they are optimized with regard to a finite collection of initial conditions of the system under control. In the second phase, we construct a nonlinear mapping between the initial conditions of the system and the corresponding values of the scaling factors. From the simulation studies, using genetic optimization and the estimation algorithm of the GA-based neurofuzzy networks model, we showed that the fuzzy PI/PID controller controls effectively the inverted pendulum system. While the study showed the development of the controller in the experimental framework of control of a specific dynamic system (inverted pendulum), this methodology is general and can be directly utilized to any other system.

**Acknowledgement.** This work has been supported by KESRI(R-2004-B-274), which is funded by MOCIE(Ministry of commerce, industry and energy)

## References

1. Oh, S.K., Pedrycz, W.: The Design of Hybrid Fuzzy Controllers Based on Genetic Algorithms and Estimation Techniques. *Kybernetes* **31** (2002) 909-917
2. Oh, S.K., Ahn, T., Hwang, H., Park, J., Woo, K.: Design of a Hybrid Fuzzy Controller with the Optimal Auto-tuning Method. *Journal of Control, Automation and Systems Engineering*. **1** (1995) 63-70
3. Li, H.X.: A comparative design and tuning for conventional fuzzy control. *IEEE Trans. Syst., Man, Cybern. B*. **27** (1997) 884-889
4. Goldberg, D.E.: *Genetic algorithms in Search, Optimization, and Machine Learning*. Addison-Wesley (1989)
5. Yamakawa, T.: A New Effective Learning Algorithm for a Neo Fuzzy Neuron Model. 5th IFSA World Conference. (1993) 1017-1020
6. Park, B.J., Oh, S.K., Pedrycz, W.: The Hybrid Multi-layer Inference Architecture and Algorithm of FPNN Based on FNN and PNN. 9th IFSA World Congress. (2001) 1361-1366.
7. Jang, J.R.: Self-Learning Fuzzy Controllers Based on Temporal Back Propagation. *IEEE Trans. On Neural Networks*. **3** (1992) 714-723
8. Oh, S.K., Rho, S.B., Kim, H.K.: Fuzzy Controller Design by Means of Genetic Optimization and NFN-Based Estimation Technique. *International journal of Control, Automations, and Systems*. **2**(3) (2004) 362-373

# Boundary Effects in Stokes' Problem with Melting

Rup Mukherjee and J. G. Stevens

Montclair State University, Montclair NJ 07043, USA  
{mukherjeea, stevensj}@mail.montclair.edu

**Abstract.** We discuss the use of the computer algebra system Maple  $\text{\textcircled{R}}$  to analyze the heat transport when a heated sphere melts its way through a solid medium. The combined power of symbolic computation and numerical simulation available in Maple is used to analyze a model in which the molten layer around the moving sphere is augmented by a surrounding thermal-layer. In particular, we carefully study the effects of imposing a variety of boundary conditions.

## 1 Introduction

The problem of large scale sedimentation has had a major impact on understanding of physical processes. A multitude of applications, such as circumstances, the careful analysis of the media data, understanding of the effects of particulate parameters can create an efficient feedback mechanism which iteratively improves the media design. Insights into the understanding of physical phenomena are sought and appropriate software is used to compare the effects of different boundary conditions are useful. This feedback cycle. This paper, we use the problem of a particle and the understanding of a melting problem with melting. Particular, we study the effects of changing boundary conditions that affect the basic knowledge of the media. The classical Stokes' problem calculates the drag on a sphere moving at a constant velocity through a viscous fluid medium. The melting assumes that the sphere maintains its surface temperature above that of the surrounding medium due to its melting. A heat source, the heat from the sphere is sufficient to melt a region around it, and the sphere falls through the melted region until it attains a steady state. The media describes that a magma moving through the earth. Section 2, we introduce the integral equation method and its application to the Stokes' problem with melting proposed by Emermann and Urciuolo. We study the effects of imposing improved boundary conditions for the effect, and demonstrate that this leads to a more precise estimate for the melting rate. Highlights the differences between the melting media and a more accurate temperature approach. Here a physical model of a thermal layer is added behind the melting. The boundary conditions for the temperature profile used in the melting media of section 2 leads to certain values which

are resolved by the thin layer model. The thickness of the thermal layer is taken as a series approximation by regarding the integral balance method as the thermal layer approximation for the thermal thickness scaled temperature profile. The method repeats the integral balance method the melt area then leads the melt area thickness.

## 2 Integral Balance Method: Melt-Layer Model

In the integral balance method, it is assumed that heat is transported over a semi-infinite domain  $\delta$ , and the heat conduction equation is integrated over this thermal layer thickness to obtain the integral balance approximation by using the conduction as a traction force. A spatial average is assumed for the temperature profile, leading to an average pressure. Regarding the spatial average and substitution of the pressure into the integral balance leads to a differential equation for  $\delta$  which is solved to obtain the pressure for the thermal layer thickness. Also, the temperature profile is obtained through direct substitution. Emerman and Urcotte employed the integral balance method to obtain the pressure for the semi-infinite domain melt area thickness,  $\delta(\theta)$  here the relevant geometric space dimension is given by the semi-infinite domain  $\theta = x/R, y = y/R, \delta = d/R, \mathbf{u} = u/u_0, \mathbf{v} = v/u_0$ , and  $\mathbf{T} = (T - T_m)/(T_0 - T_m)$ , the relevant equations are lubrication form thin boundary conditions  $\mathbf{u}(\delta) = \mathbf{u}(\delta)$  leads to  $\mathbf{u}(\mathbf{y}) = -(\mathbf{y} \cdot \mathbf{s}(\theta))(\mathbf{y} - \delta)/\delta^3$  here the dimensionless defined as  $\text{Ste} = \frac{c_p(T_0 - T_m)}{L + c_p(T_m - T)}$  here  $c_p$  is the specific heat capacity of melt,  $L$  is the latent heat of fusion, and  $T_\infty$  is the ambient temperature of the medium and the Peclet number is defined as  $\text{Pe} = u_0 R/\kappa$ , here  $\kappa$  is the thermal diffusivity of melt.  $\text{Ste}$  and  $\text{Pe}$  form the dimensionless groups for the problem. The dimensionless form is assuming a quadratic profile for temperature  $\mathbf{T}(\mathbf{y})$  and imposing the conditions  $\mathbf{T}(\delta) = \mathbf{T}(\delta)$  and  $\partial \mathbf{T} / \partial \mathbf{y} = -\text{Pe} \cos \theta / \text{Ste}$ , here  $\mathbf{y} = \delta$  leads to the temperature profile  $\mathbf{T}(\mathbf{y}) = \frac{\text{Pe}}{\text{Ste}} \cos \theta - \frac{2}{\delta} + \mathbf{y}^2 \left( \frac{1}{\delta^3} - \frac{\text{Pe} \cos \theta}{\text{Ste} \delta} \right)$  substitution of the pressure is for  $\mathbf{u}(\mathbf{y})$  and  $\mathbf{T}(\mathbf{y})$  into the integral balance and solving the resulting differential equation for  $\delta(\theta)$  produces the melt area thickness as  $\delta_{\text{ET}}(\theta) = \delta_{\text{ET}}(\theta) \sec \theta = f(\text{Ste}) \sec \theta / \text{Pe}$ , here  $f(z) = 2(-z - 2 + \sqrt{z^2 + 28z + 4})/C$ . Complete details of the derivation of this form can be found in [2]. The energy equation for this model leads to  $\partial^2 \mathbf{T} / \partial \mathbf{y}^2 = \text{Pe} \cos \theta$  here  $\mathbf{y} = \delta$  which leads to the approximation  $\delta = \delta_{\text{ETO}}(\theta) = (\text{Ste}/\text{Pe}) \sec \theta$  this is easily verified that as  $\text{Ste} \rightarrow \infty, f(\text{Ste}) \rightarrow \text{Ste}$  thus for small values of  $\text{Ste}$ ,  $\delta_{\text{ETO}} \approx \delta_{\text{ET}}$  here a simple satisfaction of  $\delta_{\text{ETO}} > \delta_{\text{ET}}$ .

### 2.1 Boundary Conditions for Velocity

The boundary conditions at  $\mathbf{u}(\delta)$  is a good approximation under the assumption  $\delta \ll R$ , but is clear that the conduction boundary conditions at the boundary of the melt area  $\mathbf{u}(\delta) = -\mathbf{s}(\theta)$  regarding for the exact using this improved boundary conditions results in  $\mathbf{u}(\mathbf{y}) = -\mathbf{y} \cdot \mathbf{s}(\theta)(\mathbf{y} - \delta + \mathbf{y}\delta - \frac{2}{3}\delta^2)/\delta^3$  so that the pressure is for  $\mathbf{u}(\mathbf{y})$  and assuming the temperature profile given above, a modified

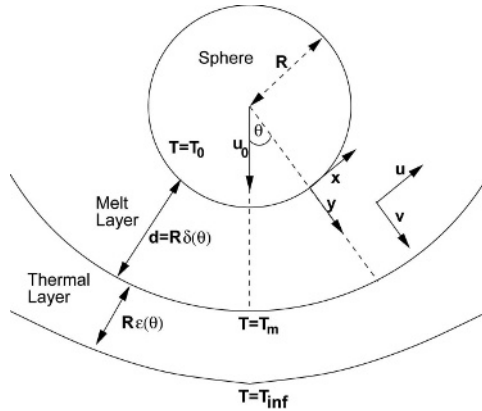


**Fig. 1.** Geometry for melt-layer and two-layer Stokes’ Problem with Melting. The variables are discussed in detail in section 2

**Table 1.** Relative Percentage error  $\left| \frac{\delta_M(\theta) - \delta_{ET}(\theta)}{\delta_{ET}(\theta)} \right| \times 100$  for fixed  $Ste = 0.5$  (left) and fixed  $Pe = 10$  (right)

colatitude	$1 \leq Pe \leq 50$ with $Ste = 0.5$					$0.1 \leq Ste \leq 2.0$ with $Pe = 10$					
$\Downarrow$	1	5	10	15	50		0.1	0.25	0.5	1.0	2.0
$\theta = \pi/4$	2.93	0.63	0.32	0.21	0.06		0.02	0.09	0.32	0.96	2.52
$\theta = \pi/3$	5.74	1.32	0.68	0.45	0.14		0.04	0.21	0.68	1.95	4.77
$\theta = \pi/2.5$	0.13	0.65	1.94	4.98	10.67		13.26	3.67	1.94	1.32	0.41
$\theta = \pi/2.4$	17.24	5.19	2.79	1.92	0.60		0.20	0.98	2.79	6.81	13.84
$\theta = \pi/2.3$	23.58	8.00	4.45	3.09	0.98		0.37	1.67	4.45	10.06	19.02
$\theta = \pi/2.2$	34.40	13.97	8.23	5.85	1.94		0.88	3.45	8.23	16.61	28.27
$\theta = \pi/2.1$	54.71	29.72	19.64	14.75	5.43		3.28	10.04	19.64	32.82	47.32

me. t. a. er. th. ck. e. ss.  $\delta_M(\theta)$ , s. e. a. s. c. m. p. u. t. e. d. . . . k. e. t. h. e. m. e. t. a. e. r. e. p. r. e. s. s. . . s.  $\delta_{ET0}(\theta)$  a. n. d.  $\delta_{ET}(\theta)$  h. i. c. h. b. e. c. m. e. f. i. t. t. e. a. s.  $\theta \rightarrow \pi/2$ ,  $\delta_M(\pi/2)$  s. i. f. f. i. t. e. a. b. e. s. h. o. w. s. t. h. e. r. e. l. a. t. i. v. e. p. e. r. c. e. n. t. a. g. e. e. r. r. o. r. s. a. s. a. f. u. n. c. t. i. o. n. o. f. t. h. e. r. e. c. e. t. u. m. b. e. r.  $Pe$  a. n. d. t. h. e. r. e. f. a. r. a. n. g. e.  $Ste$  a. s. t. h. e. c. o. l. a. t. u. d. e.  $\theta$  c. h. a. n. g. e. s. . . . t. h. e.  $Ste$  s. f. i. x. e. d. . . . f. o. r. e. a. c. h. a. u. e. o. f.  $Pe$ , t. h. e. e. r. r. o. r. s. i. n. c. r. e. a. s. e. a. s. t. h. e. c. o. l. a. t. u. d. e.  $\theta$  a. p. p. r. o. a. c. h. e. s.  $\pi/2$ . . . . s. i. f. r. a. f. i. x. e. d. a. u. e. o. f.  $\theta$ , t. h. e. e. r. r. o. r. s. a. r. e. a. d. e. c. r. e. a. s. i. n. g. f. u. n. c. t. i. o. n. s. o. f.  $Pe$  a. n. d.  $Ste$ . . . . g. a. i. n. g. f. r. a. f. i. x. e. d. a. u. e. o. f.  $Ste$ , t. h. e. e. r. r. o. r. s. i. n. c. r. e. a. s. e. m. o. n. o. t. o. n. i. c. a. s.  $\theta \rightarrow \pi/2$ , a. n. d. f. r. a. f. i. x. e. d. a. u. e. o. f.  $\theta$ , t. h. e. e. r. r. o. r. s. i. n. c. r. e. a. s. e. t. h. e. i. n. c. r. e. a. s. i. n. g.  $Ste$ . . . . t. h. e. t. h. r. d. c. o. l. u. m. n. f. o. r. b. o. t. h. t. a. b. l. e. s. c. o. r. r. e. s. p. o. n. d. t. o. t. h. e. . . . d. i. f. f. e. r. e. n. c. e. b. e. t. w. e. e. n. t. h. e. s. a. m. e. s. i. z. e. a. g. r. o. u. p. p. a. r.  $Ste$ . . . . a. n. d.  $Pe$ . . . . t. h. e. s. e. a. u. e. s. f. o. r.  $Ste$  a. n. d.  $Pe$  a. r. e. e. n. c. o. u. n. t. e. r. t. h. e. s. p. e. c. i. f. i. c. e. a. m. p. l. e. . . . m. e. n. t. e. d. i. n. d. e. t. a. i. l. . . . 2. . . . i. n. f. a. c. t. . . . w. e. a. s. s. u. m. e. t. h. a. t. t. h. e. s. p. h. e. r. e. r. e. s. e. m. b. l. e. s. a. s. m. a. r. k. p. e. t. r. a. t. i. o. n. r. a. d. i. u. s. c. m. m. e. t. g. t. s. a. t. t. h. r. o. u. g. h. a. t. p. c. a. r. k. k. e. b. a. s. a. t. t. h. e. r. e. e. a. t. p. h. s. c. a. p. r. p. e. r. t. e. s. e. a. d. t.  $Ste$ . . . . a. n. d.  $Pe$ . . . . t. h. e. a. u. e. s. o. f.  $Ste$  a. n. d.  $Pe$ . . . . a. r. a. n. g. e. h. e. r. e. u. r. a. a. s. s. m. a. k. e. s. s. e. e. t. h. e. e. q. u. a. t. i. o. n.  $\delta_M < \delta_{ET} < \delta_{ET0}$  a. s. a. s. h. o. l. d. s. a. n. d. t. h. e. s. e. p. a. r. t. i. t. i. o. n. b. e. t. w. e. e. n.  $\delta_M$  a. n. d.  $\delta_{ET}$ . . . . i. n. c. r. e. a. s. e. s. a. s. t. h. e. e. q. u. a. t. i. o. n. s. a. p. p. r. o. a. c. h. e. d. ( $\theta \rightarrow \pi/2$ )

### 3 Integral Balance Method: Two-Layer Model

the boundary condition  $\partial T/\partial y = -(\text{Pe}/\text{Ste})c_s\theta$  at  $y = \delta$  implies that the gradient of the temperature  $s_z$  at the equator is constant. Since the temperature at the surface is  $T_m$  and the surrounding medium has a temperature  $T_\infty$ , the improved boundary condition at the solid-liquid interface, based on the requirement that the latent heat required to melt the solid must be supplied by conduction, is  $\partial T/\partial y = -(\text{Pe}/\sigma)c_s\theta + \beta(\partial T/\partial y)$ , where  $\beta = k_s(T_m - T_\infty)/k_l(T_0 - T_m)$ , and  $\sigma = c_p(T_0 - T_m)/L$  is similar to  $\text{Ste}$  but based on the actual latent heat,  $\mathcal{T} = (T_s - T_\infty)/(T_m - T_\infty)$  is the solid melting temperature, the thermal conductivity  $k_s$  and  $k_l$  represent the thermal conductivities of solid and liquid (melt) respectively. The geometry for the two-layer model is shown in Figure 1. The solid melting temperature, the integral balance method described in section 2 can be applied to the thermal energy balance as an approximation for  $\varepsilon(\theta)$ , and  $\mathcal{T}(\mathbf{y})$  is then computed by direct substitution. Also, the result given for  $\mathcal{T}(\mathbf{y})$  is used in the boundary condition. Also, the integral balance method applied to the melting energy balance is the same as the one used in section 2. The melting energy balance becomes finite, leading to a physical solution. The melting energy balance  $\delta_{2L}(\pi/2) = 2$ , leading to a finite melting energy balance. The improved boundary condition  $\mathbf{u}(\mathbf{y}) = s_z(\theta)$  determines the velocity  $\mathbf{u}(\mathbf{y})$  in the liquid. The two-layer approach leads to a further improvement: the estimate of the melting energy balance  $\delta_{2M}(\theta)$  defines the melting energy balance using the same fixed two-layer approach, the relation  $\delta_{2M} < \delta_{2L} < \delta_M < \delta_{ET} < \delta_{ET0}$  holds. The direct melting energy balance is the same as for  $\sigma$ ,  $\text{Ste}$ ,  $\text{Pe}$ , and  $\beta$ . The  $\delta_{2M}(\pi/2) = 2$  of the radius of the sphere is reduced,  $\sigma$ ,  $\text{Ste}$ , and  $\text{Pe}$  increase. As  $\beta$  decreases, the relative percentage error,  $\% \times |\delta_{2M}(\theta) - \delta_{2L}(\theta)|/|\delta_{2L}(\theta)|$  ranges between 7 and 4 for  $\pi/2 \leq \theta \leq \pi/2$ .

### References

1. Emerman, S. H., Turcotte, D. L.: Stokes's problem with melting. *Int. J. Heat Mass Transfer*. **Vol. 26, No. 11** (1983) 1625–1630.
2. Mukherjee, A., Stevens, J., G.: Heat transport in Stokes' problem with melting: A two-layer approach. *Int. J. of Heat Mass Transfer*. **to appear**.
3. Rasmussen, N. C., Yellin, J., Kleitman D. J., and Stewart R. B.: Nuclear power: can we live with it? *Tech. Rev.* **81** (1979) 32–46.

# A Software Debugging Method Based on Pairwise Testing<sup>1</sup>

Liang Shi<sup>1,2</sup>, Changhai Nie<sup>1,2</sup>, and Baowen Xu<sup>1,2,3,4</sup>

<sup>1</sup> Dept of Computer Science and Engineering, Southeast University,  
210096 Nanjing, China

{Shiliang\_ada, Changhainie, Bwxu}@seu.edu.cn

<sup>2</sup> Jiangsu Institute of Software Quality,  
210096 Nanjing, China

<sup>3</sup> Computer School, National University of Defense Technology,  
410073 Changsha, China

<sup>4</sup> Key Laboratory of Software Engineering, Wuhan University,  
430072 Wuhan, China

**Abstract.** Pairwise testing is one of very practical and effective testing methods for various types of software systems. This paper proposes a novel debugging method based on pairwise testing. By analyzing the test cases and retesting with some complementary test cases, the method can narrow the factors that cause the errors in a very small range. So it can provide a very efficient and valuable guidance for the software testing and debugging.

## 1 Introduction

Software testing and debugging is an important but expensive part of the software development process. Much research has been aimed at reducing its cost. Among them, pairwise testing is a very important method that has been studied and applied widely for its scientificity and effectiveness in software testing with a quite small test suite, especially for the software whose faults are caused mainly by the test parameters or the interactions of a few test parameters of the system.

Pairwise testing has been used in software testing for a long time. At the beginning, through the application of design of experiments, a more efficient software testing way is obtained [4]. Much research has been done in pairwise testing. But they have been mainly aimed at reducing the size of the test suite by some methods of construction. For instance, in [1, 2] two heuristic search-based approaches are proposed, in [3] a new algebraic construction is proposed.

---

<sup>1</sup> This work was supported in part by the National Natural Science Foundation of China (60425206, 60373066, 60403016), National Grand Fundamental Research 973 Program of China (2002CB312000), and National Research Foundation for the Doctoral Program of Higher Education of China (20020286004).

Correspondence to: Baowen Xu, Department of Computer Science and Engineering, Southeast University, 210096 Nanjing, China. Email: bwxu@seu.edu.cn

In this paper, we propose a debugging method based on the result of pairwise testing. The research about this has not been seen now. The convenient, reliable and effective debugging method can help people, who are working for testing or debugging the software, to find the errors and revise them quickly. It can improve the test efficiency and reduce test costs. Therefore, the research about the debugging method on the result of pairwise testing is quite important.

## 2 Model and Algorithm for Debugging of Pairwise Testing

Consider the system under test has  $n$  parameters  $c_i$ , where  $c_i \in T_i$ ,  $T_i$  is a set with finite elements and the number of the elements is  $t_i$ , that is,  $t_i = |T_i|$  ( $1 \leq i \leq n$ ). We suppose the faults of the system are only caused by the parameters or the interactions of some parameters, and if an error is caused only by a combination of some  $k$  parameters where  $1 \leq k \leq n$ , every test case that includes the combination will also cause the error in testing. Let PT be a test set that covers all pair-wise combinations of parameter values. And there are  $m$  test cases in it, and each is like this:  $(v_1, v_2, \dots, v_n)$ , where  $v_i \in T_i$  and  $1 \leq i \leq n$ .

After testing the software with the test set PT, suppose there are  $l$  test cases in PT1 which cause errors in testing, and the other  $m - l$  ones in PT2 which work well. The testing is successful for finding bugs in the software. Then we should analyze what cause the errors: a value  $v_i$  of parameter  $c_i$ ; or a combination  $(v_i, v_j)$  of some two parameters  $c_i$  and  $c_j$ ; ...; a combination of some  $n-1$  parameters values or a combination of all the  $n$  parameters values.

Let us consider the simplest case: the software failure is caused only by the value  $v_i$  of parameter  $c_i$ . Then the value  $v_i$  must appear in each test case of PT1 and will not be in any test case of PT2. For the general case, we can have the following conclusion:

**Theorem 1.** If a bug of the software under test is caused only by a combination of some  $k$  parameters where  $1 \leq k \leq n$ , the combination must appear in each test case of PT1, and must not appear in any of PT2.

**Corollary 1.** If the bugs of the software under test are caused by some combinations of some  $k$  parameters where  $1 \leq k \leq n$ , the combinations must only appear in PT1 and must not appear in PT2.

**Corollary 2.** If we can find the public composition in each test case of PT1, that is, if there are some parameter values or some parameter value combinations that appear in PT1 and don't appear PT2, then these public compositions have the maximum possibility to be the reasons that cause the errors.

**Corollary 3.** All the compositions that appear in PT1 and do not appear in PT2 maybe cause the errors. It is impossible for any of the compositions that appear in PT2 cause errors.

To locate the defects, we find all the compositions that are in PT1 and not in PT2, Such compositions form a set  $A$ . All the elements in the set may cause the errors. Generally the set  $A$  has more elements and need further reduction.



To reduce the set  $A$ , we design  $n$  test cases for each test case in PT1. For instance,  $(v_1, v_2, \dots, v_n)$  is one of the  $l$  test cases, and we can design the  $n$  test cases like these:  $(*, v_2, \dots, v_n), (v_1, *, \dots, v_n), \dots, (v_1, v_2, \dots, *)$ , where “\*” represents any value which is not the same as the original value in  $(v_1, v_2, \dots, v_n)$ . Thus we need  $n \times l$  additional test cases. By the result of these testing, we can reduce the two sets greatly and then obtain the conclusion.

**Theorem 2.** If a combination of some  $k$  values of test case  $(v_1, v_2, \dots, v_n)$  ( $2 \leq k \leq n$ ) causes the system error, when testing the software with the accordingly additional  $n$  test case generated as above, there must be  $n-k$  test cases which cause the same error.

Now we describe the algorithm for debugging of pairwise testing based on the above discussion. After testing the software with the test set PT, if we find some bugs in the running of some  $l$  test cases in PT1, we can analyze the result by the following four steps:

- (1) Analyze the test cases in PT1 and construct the set  $A$ .
- (2) Construct the additional test cases for each of the  $l$  test cases as the Theorem 2.
- (3) Test the software with the additional test suite and reduce the set  $A$  by throwing of all the elements that appear in PT2.
- (4) Output the set  $A$ , which contains all the possible factors that may cause the errors.

### 3 Case Study

In this section, we take the testing for a telephone system [1, 2] as an example to show how to use the approach proposed in this paper. Table 1 shows four parameters that define a very simple test model. The test plan shown in Table 2 has 9 test cases but it covers every pair-wise combination of parameter values.

**Table 1.** Parameters for Phone Call

Call	Billing	Access	Status
Local	Caller	Loop	Success
Long	Collect	Isdn	Busy
Inter	Free call	Pbx	Blocked

**Table 3.** The Additional Test Cases

Call	Billing	Access	Status
*	Collect	Loop	Blocked
Inter	*	Loop	Blocked
Inter	Collect	*	Blocked
Inter	Collect	Loop	*

**Table 2.** Pair-Wise Test Cases for Phone Call

Call	Billing	Access	Status
Local	Collect	Pbx	Busy
Long	Free call	Loop	Busy
Inter	Caller	Isdn	Busy
Local	Free call	Isdn	Blocked
Long	Caller	Pbx	Blocked
<b>Inter</b>	<b>Collect</b>	<b>Loop</b>	<b>Blocked</b>
Local	Caller	Loop	Success
Long	Collect	Isdn	Success
Inter	Free call	Pbx	Success

Suppose a bug is found by the sixth test case in Table 2. By our algorithm, the set  $A$  is created at the first step, where  $A = \{(Inter, Collect), (Inter, Loop), (Inter, Blocked),$

(Collect, Loop), (Collect, Blocked), (Loop, Blocked), (Inter, Collect, Blocked), (Inter, Collect, Loop), (Collect, Loop, Blocked), (Inter, Loop, Blocked), (Inter, Collect, Loop, Blocked)}. At the next step, four additional test cases shown in Table 3 are generated for the one causing the error. Next we test the system again with the additional test cases. We can suppose only the second test case in the Table 3 causes error in testing. In this case, using the algorithm we can reduce the set as  $A = \{(Inter, Loop, Blocked), (Inter, Collect, Loop, Blocked)\}$ . That is, if the error is caused only by the interactions of some parameter values, one of the combinations (Inter, Loop, Blocked) and (Inter, Collect, Loop, Blocked) must be the cause. The other cases can be dealt with and analyzed analogously.

## 4 Conclusions

In general, when finding some errors in pairwise testing, we must determine which factors cause the errors and then revise them, that is, we must debug the software. At present, researches in this field are very few. There are some ways about experiment result analysis in method of orthogonal experiment, such as the method of intuitive analysis, the method of variance analysis and so on, but these methods are not practical to analyzing testing result.

The problem of software debugging based on pairwise testing is very important and complex. This paper proposes a method based on the condition that the system errors only caused by the values of some parameters or the interactions of some parameter values, and if a bug is caused only by a combination of some  $k$  parameters where  $1 \leq k \leq n$ , every test case that includes the combination will also cause the bug in testing. As an assistant debugging tool of pairwise testing, we have implemented it in our ETS (embedded software testing supporting system). The experiment results show that our method can improve the efficiency and decrease the cost of software testing greatly.

## References

1. Cohen, D. M., et al.: The AETG System: An Approach to Testing Based on Combinatorial Design. *IEEE Trans. On Software Engineering*, July 1997, 23(7)
2. Tai, K. C., Lei, Y.: A Test Generation Strategy for Pairwise Testing. *IEEE Trans. On Software Engineering*, Jan 2002, 28(1)
3. Noritaka Kobayashi, Tatssuhio Tsuchiya, Tohru Kikuno: A New Method for Constructing Pair-wise Covering Designs for Software Testing. *Information Processing Letters* 81(2002) 85-91
4. Mandl, R.: Orthogonal Latin Squares: An Application of Experimental Design to Compiler Testing. *Communications of the ACM*, Vol 28, no 10, pp. 1054-1058, Oct. 1985
5. Kuhn D R and Gallo A M, Software Fault Interactions and Implications for Software Testing. *IEEE Trans. On Software Engineering*, June 2004, 30(6):418-421
6. Colbourn C J, Cohen M B, and Turban R C.: A Deterministic Density Algorithm for Pairwise Interaction Coverage. **IASTED Proc. of the Intl. Conf on Software Engineering (SE 2004)**, Innsbruck, Austria, February 2004:345-352

# Heuristic Algorithm for Anycast Flow Assignment in Connection-Oriented Networks

Krzysztof Walkowiak

Chair of Systems and Computer Networks, Faculty of Electronics, Wrocław University of Technology, Wybrzeże Wyspińskiego 27, 50-370 Wrocław, Poland  
Krzysztof.Walkowiak@pwr.wroc.pl

**Abstract.** Replication of content on geographically distributed servers can improve both performance and reliability of the Web service. Anycast is a one-to-one-of-many delivery technique that allows a client to choose a content server of a set of replicated servers. Presenting numerous mirror content servers to a client implies the difficult problem of finding the best server in terms of network performance. We formulate an optimization problem of anycast flows assignment in a connection-oriented network. This is a 0/1, NP-complete problem, which is computationally very difficult due to the size of solution space and constraints. Therefore, we propose computationally effective heuristic algorithm. To our knowledge, this is the first proposal to solve the problem of anycast flow assignment in connection-oriented network. Results of simulations are shown to evaluate performance of proposed algorithm for various scenarios.

## 1 Introduction

Web servers providing popular content (MP3 files, movies, electronic books, software distribution) need to scale to a large number of clients. One solution to address this problem is to augment network link capacity or processing resources of the site's server. Another, usually much more cost-effective, solution is to replicate the server or content in many locations in the Internet. This relatively simple technique provides numerous advantages, e.g. inexpensive improvement of client perceived accessibility of content, lower latency, increase of network reliability. Traffic associated with requests to replicas can be modeled as anycast flow. Anycast is a *one-to-one-of-many* technique to deliver a packet to one of many hosts. One of the most famous techniques that apply anycast traffic is Content Delivery Network (CDN) [1], [3].

Anycast paradigm is expected to be a very attractive approach to give a solution to many important issues that arise in modern computer networks. One of key elements of anycast transmission is the flow assignment problem, i.e. anycast demands should be assigned to network routes in order to optimize a selected network performance function. In this paper we address this problem and propose an efficient heuristic algorithm for static anycast flow assignment. The main novelty of our work is that we focus on connection-oriented (c-o) networks. In c-o network prior to transmitting the data, a virtual connection is established and the data is carried along this connection. Popular c-o techniques are Asynchronous Transfer Mode (ATM), MultiProtocol Label Switching (MPLS). To our knowledge, this is the first algorithm that solves the

anycast flow assignment problem in c-o network. We consider an existing facility network - we don't optimize location of replica server and network topology.

The anycast non-bifurcated flow assignment (ANBFA) is as follows

- Given* network topology, traffic demand pattern, location of replica servers, link capacity
- Minimize* Objective function defined according to information on link flow and
- (Maximize)* capacity, e.g. network delay, network cost, network survivability
- Over* selection of replica server, routing (path assignment)
- Subject to* connection-oriented flow constraints, capacity constraints

The mathematical formulation of the optimization problem can be found in [8], where the ANBFA problem is referred to as CATR (clients' assignment to replicas). Due to limited size of the paper we cannot present detailed information on anycast flow and optimization. Therefore, for more information refer to [1-9].

## 2 Anycast Non-bifurcated Flow Deviation Algorithm

In this section we show Anycast Non-bifurcated Flow Deviation (ANBFD) algorithm for the problem formulated above. ANBFD algorithm is based on the Flow Deviation approach proposed in [2] and widely used for network design problems [4], [7].

In c-o networks an anycast demand consists of two connections: one from the client to the server (upstream) and the second one in the opposite direction (downstream). Upstream connection is used to send user's requests. Downstream connection carries requested data. Let  $\delta(i)$  denote index of the connection associated with connection  $i$ . If  $i$  is a downstream connection  $\delta(i)$  must be an upstream connection and vice versa. The global anycast non-bifurcated multicommodity flow denoted by  $\underline{f}^r$  is defined as a vector of flows in all arcs. We call a flow  $\underline{f}^r$  feasible if for each arc  $a$  the flow of  $a$  doesn't exceed capacity of  $a$ .

### Algorithm ANBFD

Let  $\underline{f}^1$  denote a feasible anycast flow containing routes for all connections to be established. Let  $L(\underline{g})$  denote value of the objective function for a feasible flow  $\underline{g}$  and  $l_j(\underline{g})$  denote a metric of arc  $j$ . The common approach is to calculate this metric as partial derivative of the objective function over arc flow [2]. We start with  $r:=1$ . Let  $B$  denote a set including connections that have not been already processed. Operator  $first(B)$  returns the index of first connection in set  $B$ .

**Step 1.** Find  $SR(\underline{f}^r)$  defined as the set of shortest paths for each connection under metric  $l(\underline{f})$ . Connections  $i$  and  $\delta(i)$  associated with one anycast demand are processed jointly. For each node  $v$  hosting a replica shortest paths in both directions between  $v$  and the second end node are calculated. Finally, we select such a pair of paths for which length of the downstream path is the shortest and add these paths to set  $SR(\underline{f}^r)$ . Set  $B:=P$ ,  $i:=first(B)$  and go to step 2.

Step 2. Let  $\underline{g} := \underline{f}^r$ .

a) Find  $\underline{v}$  from  $\underline{g}$  by deviating flow of connections  $i$  and  $\delta(i)$  to the shortest paths included in  $SR(\underline{f}^r)$ . Paths for other connections except  $i$  and  $\delta(i)$  remain unchanged.

b) If  $\underline{v}$  is a feasible flow and  $L(\underline{v}) < L(\underline{g})$  set  $\underline{g} = \underline{v}$ .

c) If  $B = \emptyset$  go to step 3. Otherwise, set  $B := B - \{i, \delta(i)\}$  and go to step 2a.

Step 3. If  $\underline{g} = \underline{f}^r$  stop the algorithm, since the solution cannot be improved. Otherwise, set  $r := r + 1$ ,  $\underline{f}^r := \underline{g}$  and go to step 1.

In order to find feasible starting solution we can apply an algorithm based on the initial phase of the FD algorithm [2], [7]. One of the main advantages of ANBFD is that it takes into account all possible routes in the network and the calculation time of ANBFD doesn't depend on the number of candidate routes. Therefore, there is no need to reduce size of the problem given by the number of routes. Algorithm ANBFD converges in finite number of steps. However, the number of steps and consequently algorithm complexity depends on particular parameters of the considered problem (network topology, location of replicas, demand matrix).

### 3 Results

The test network consists of 36 nodes and 144 directed links [9]. We run experiments for various scenarios of replica location and number of replicas. Since more data is received by clients, than is sent to replicas. Therefore, we assume that upstream bandwidth is 0.1 of the downstream bandwidth. The total demand is calculated as a sum of all downstream and all upstream bandwidth requirements.

In many real life cases, a client is assigned to the closest replica in terms of the hop number. Therefore, for comparison we develop a simple heuristic, which is referred to as CR (Closest Replica). Algorithm CR assigns each anycast demand to the closest (in terms of hop number) replica. This way we obtain a unicast non-bifurcated flow assignment problem, which is solved by a non-bifurcated FD algorithm.

We assume that the objective function represents the total flow in the network. In Table 1 we report results obtained for algorithms ANBFD and CR for the different number and locations of replica servers. Empty cells indicate that for a particular case the algorithm cannot find a feasible solution. First, quite intuitive, observation is that increasing the number of replicas decreases the network flow. Moreover, if there are more replicas in the network, demands with higher bandwidth requirements can be satisfied. If we compare ANBFD against CR, we can see that for relatively low loads both algorithms perform similarly. This can be explained by the fact that for low congestion each demand is assigned to nearest replica for both algorithms. The major advantage of ANBFD is for the case with 4 replicas – for two highest loads CR cannot find a feasible solution, while ANBFD can. This follows from the construct of ANBFD, which can reroute anycast demand to another replica, what enables selection of less congested links. Similar results were obtained for other tests.

**Table 1.** Performance of algorithms ANBFD and CR for various replica location and demands

Total Demand	1 replica in (30)		2 replicas (9,23)		3 replicas in (9,23,30)		4 replicas in (5,9,23,30)	
	ANBFD	CR	ANBFD	CR	ANBFD	CR	ANBFD	CR
1080	3088	3088	2125	2125	1722	1700	1362	1370
3105	9281	9425	5945	5945	4834	4805	3859	3885
5040			10502	10430	7886	7890	6331	6400
7020					11450	11515	8818	8915
9000							12225	11925
10980							14861	
11880							16146	

## 4 Final Remarks

The heuristic algorithm ANBFD proposed in this work is, according to our best knowledge, the first attempt to optimize anycast flows in connection-oriented networks. Numerical experiments have been conducted to evaluate performance of the algorithm for various scenarios. Results have confirmed that introducing new content servers enables substantial reduction of network flow what, consequently, decreases network delay and improves network reliability. The experiment shows that ANBFD is more efficient than the CR in solving relatively higher congested problems.

**Acknowledgements.** This work was supported by a research project of the Polish State Committee for Scientific Research carried out in years 2005-2007.

## References

1. Awerbuch, B., Brinkmann, A., Scheideler C.: Anycasting in adversarial systems: routing and admission control. Lecture Notes in Computer Science, LNCS 2719 (2003), 1153-1168
2. Fratta, L., Gerla, M., Kleinrock, L.: The Flow Deviation Method: An Approach to Store-and-Forward Communication Network Design. Networks Vol. 3 (1973) 97-133
3. Hao, F., Zegura, E., Ammar, M.: QoS routing for anycast communications: motivation and an architecture for DiffServ networks. IEEE Communication Magazine, 6 (2002), 48-56
4. Kasprzak, A.: Designing of Wide Area Networks. Wroclaw Univ. of Tech. Press, (2001)
5. Partridge, C., Mendez, T., Milliken, W.: Host Anycasting Service. IETF RFC 1546 (1993)
6. Peng, G.: CDN: Content Distribution Network. Technical Report (2003)
7. Pióro, M., Medhi, D.: Routing, Flow, and Capacity Design in Communication and Computer Networks. Morgan Kaufman Publishers (2004)
8. Walkowiak, K.: An exact algorithm for design of content delivery networks in MPLS environment. Journal of Telecommunications and Information Technology 2 (2004), 13-22
9. Walkowiak, K.: QoS Dynamic Routing in Content Delivery Networks, to appear in Proceedings of Networking 2005

# Isotropic Vector Matrix Grid and Face-Centered Cubic Lattice Data Structures

James N. Gunter<sup>1</sup> and Carryn Bellomo<sup>2</sup>

<sup>1</sup> University of Akureyri, 602 Akureyri, Iceland  
jamesn@unak.is

<sup>2</sup> University of Nevada, Las Vegas, Las Vegas NV 89154, USA  
carryn.bellomo@ccmail.nevada.edu

**Abstract.** Techniques for generating data structures for isotropic vector matrix grids (or face-centered cubic lattices) are presented. Grid basics and some background mathematical foundations are also provided.

## 1 Introduction

The isotropic vector matrix (IVM) grid is a 3D lattice structure where each vertex is connected to 12 nearest neighbors. The grid is defined by a set of vectors  $\mathbf{e}_i$  originating from a central point. The vectors are arranged in a way that they are symmetrically distributed in all directions. The grid is used in various applications, including computer graphics and physics simulations.

The IVM grid is a 3D lattice structure where each vertex is connected to 12 nearest neighbors. The grid is defined by a set of vectors  $\mathbf{e}_i$  originating from a central point. The vectors are arranged in a way that they are symmetrically distributed in all directions. The grid is used in various applications, including computer graphics and physics simulations.

## 2 IVM Basics and Generalized Grid Construction

The IVM grid is a 3D lattice structure where each vertex is connected to 12 nearest neighbors. The grid is defined by a set of vectors  $\mathbf{e}_i$  originating from a central point. The vectors are arranged in a way that they are symmetrically distributed in all directions. The grid is used in various applications, including computer graphics and physics simulations.

The IVM grid is a 3D lattice structure where each vertex is connected to 12 nearest neighbors. The grid is defined by a set of vectors  $\mathbf{e}_i$  originating from a central point. The vectors are arranged in a way that they are symmetrically distributed in all directions. The grid is used in various applications, including computer graphics and physics simulations.

---

<sup>1</sup> Herein we adopt R. Buckminster Fuller's[1] use of the term *Isotropic Vector Matrix* when referring to grids that utilize this specific geometrical arrangement of vertexes.

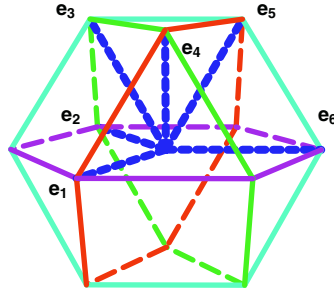


Fig. 1. VE cell and the IVM basis vectors  $e_1 - e_6$

$$\begin{array}{ll}
 a \dots & [+1] [-2] [+6] [-1] [+2] [-6] & b \dots & [+1] [+4] [+5] [-1] [-4] [-5] \\
 c \dots & [-2] [+4] [+3] [+2] [-4] [-3] & d \dots & [-5] [-3] [+6] [+5] [+3] [-6]
 \end{array}$$

$F^2 +$   $F$  *frequency*  $( \dots )$   
 $O(n^2)$   $O(n \dots n)$  <sup>2</sup>  
 $O(n)$

### 3 The IVM Grids Within a Cartesian Grid

§

*omni-directional curl operator*  $( \dots )$

3

<sup>2</sup> This hashing technique was proposed and implemented by P.I. Wilson at Texas A&M University - Corpus Christi while working on a grant funded by a United States of America National Science Foundation grant # NSF MII 03-30822.

<sup>3</sup> R.W. Gray suggested this type of organization to one of the authors (JFN) quite a long time ago.



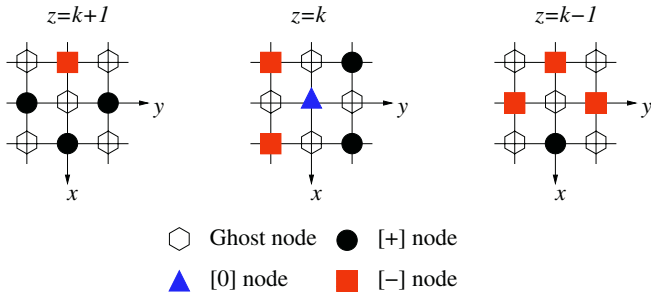
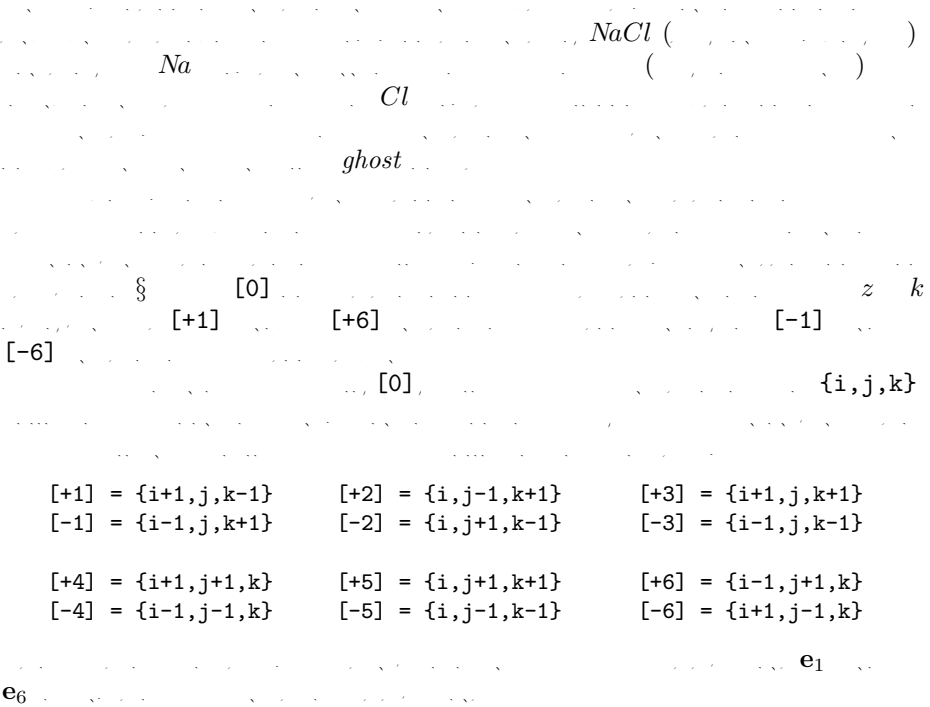


**Fig. 2.** Placement of VE cell vertices and *ghosts* on Cartesian grid



### 4 Discussion

... *Beowulf* ...

$$\left( \begin{matrix} \dots \\ \dots \\ \dots \end{matrix} \right)$$

( Q ), ( computational cosmography )

### References

1. Fuller, R.B. 1975. *Synergetics*. New York, NY: Macmillan.
2. Nystrom, J.F. 2003. Grid construction and boundary condition implementation for the isotropic vector field decomposition methodology. In Proceedings of *ACES 2003*, 745. Monterey, CA: The Applied Computational Electromagnetics Society.
3. Nystrom, J.F. and C. Bellomo. 2003. Efficient Grid Generation for the IVMCEM Solver. In Proceedings of *PIERS 2003*, 516. Cambridge, MA: The Electromagnetics Academy.
4. Nystrom, J.F. 2002. The isotropic vector field decomposition methodology. In Proceedings of *ACES 2002*, 257. Monterey, CA: The Applied Computational Electromagnetics Society.
5. Nystrom, J.F. 2004. On the Omni-directional Emergence of Form in Computation. *Lecture Notes in Computer Science* **3305**: 632.
6. Ashcroft, N.W. and N.D. Mermin. 1976. *Solid State Physics*. Philadelphia, PA: W.B. Saunders.

### Appendix

$$\left( \begin{matrix} \dots \\ \dots \\ \dots \end{matrix} \right)$$

$$\left( \begin{matrix} \dots \\ \dots \end{matrix} \right)$$

$$\left( \begin{matrix} \dots \\ \dots \\ \dots \end{matrix} \right)$$

$$\mathbf{S} \quad \mathbf{T} \quad \mathbf{e}_1 \quad \mathbf{e}_6$$

$$\mathbf{S} = S_1\mathbf{e}_1 + S_2\mathbf{e}_2 + S_3\mathbf{e}_3 + S_4\mathbf{e}_4 + S_5\mathbf{e}_5 + S_6\mathbf{e}_6 ,$$

$$\mathbf{T} = T_1\mathbf{e}_1 + T_2\mathbf{e}_2 + T_3\mathbf{e}_3 + T_4\mathbf{e}_4 + T_5\mathbf{e}_5 + T_6\mathbf{e}_6 .$$

$a', b', c', \dots, d'$  plane variables,

$$\left( \begin{matrix} \dots \\ \dots \end{matrix} \right) \quad (\S)$$

$$\mathbf{S} \quad \nabla \times \mathbf{T} \quad \mathbf{S}$$

$$\mathbf{T}$$

$$\mathbf{S}$$

# Design of Evolutionally Optimized Rule-Based Fuzzy Neural Networks Based on Fuzzy Relation and Evolutionary Optimization

Byoung-Jun Park<sup>1</sup>, Sung-Kwun Oh<sup>2</sup>, Witold Pedrycz<sup>3</sup>, and Hyun-Ki Kim<sup>2</sup>

<sup>1</sup> Department of Electrical Electronic and Information Engineering, Wonkwang University, 344-2, Shinyong-Dong, Iksan, Chon-Buk, 570-749, South Korea

<sup>2</sup> Department of Electrical Engineering, The University of Suwon, San 2-2 Wau-ri, Bongdam-eup, Hwaseong-si, Gyeonggi-do, 445-743, South Korea  
ohsk@suwon.ac.kr

<sup>3</sup> Department of Electrical and Computer Engineering, University of Alberta, Edmonton, AB T6G 2G6, Canada and Systems Research Institute, Polish Academy of Sciences, Warsaw, Poland

**Abstract.** In this paper, new architectures and comprehensive design methodologies of Genetic Algorithms (GAs) based Evolutionally optimized Rule-based Fuzzy Neural Networks (EoRFNN) are introduced and the dynamic search-based GAs is introduced to lead to rapidly optimal convergence over a limited region or a boundary condition. The proposed EoRFNN is based on the Rule-based Fuzzy Neural Networks (RFNN) with the extended structure of fuzzy rules being formed within the networks. In the consequence part of the fuzzy rules, three different forms of the regression polynomials such as constant, linear and modified quadratic are taken into consideration. The structure and parameters of the EoRFNN are optimized by the dynamic search-based GAs.

## 1 Introduction

In this paper, new architectures and comprehensive design methodologies of Genetic Algorithms [1] (GAs) based Evolutionally optimized Rule-based Fuzzy Neural Networks (EoRFNN) are introduced for effective analysis and solution of nonlinear problem and complex systems. The proposed EoRFNN is based on the Rule-based Fuzzy Neural Networks (RFNN). In the consequence part of the fuzzy rules, three different forms of the regression polynomials such as constant, linear and modified quadratic are taken into consideration. The polynomial of a fuzzy rule results from that we look for a fuzzy subspace (a fuzzy rule) influencing the better output of a model, and then raise the order of polynomial of the fuzzy rule (subspace). Contrary to the former, we make a simplified form for the representation of a fuzzy subspace lowering of the performance of a model. This methodology can effectively reduce the number of parameters and improve the performance of a model. GAs being a global optimization technique determines optimal parameters in a vast search space. But it cannot effectively avoid a large amount of time-consuming iteration because GAs finds optimal parameters by using a given space (region). To alleviate the problems, the dynamic search-based GAs is introduced to lead to rapidly optimal convergence over a limited

region or a boundary condition. To assess the performance of the proposed model, we exploit a well-known numerical example [2], [3].

## 2 Polynomial Fuzzy Inference Architecture of Rule Based FNN

The networks are classified into the two main categories according to the type of fuzzy inference, namely, the simplified and linear fuzzy inference. In this paper, we propose the polynomial fuzzy inference based RFNN (pRFNN). The proposed pRFNNs are obtained from the integration and extension of conventional RFNNs.

[Layer 1] Input layer

[Layer 2] Computing activation degrees of linguistic labels

[Layer 3] Computing firing strength of premise rules

[Layer 4] Normalization of a degree activation (firing) of the rule

[Layer 5] Multiplying a normalized activation degree of the rule by connection weight

[Layer 6] Computing output of pRFNN

The proposed pRFNN can be designed to adapt a characteristic of a given system, also, that has the faculty of making a simple structure out of a complicated model for a nonlinear system, because the pRFNN comprises consequence structure with various orders (Types) for fuzzy rules.

## 3 Evolutionally Optimized Rule-Based Fuzzy Neural Networks

In order to generate the proposed EoRFNN, the dynamic search based GAs is used in the optimization problems of structures and parameters. From the point of fuzzy rules, these divide into the structure and parameters of the premise part, and that of consequence part. The structure issues in the premise of fuzzy rules deal with how to use of input variables (space) influencing outputs of model. The selection of input variables and the division of space are closely related to generation of fuzzy rules that determine the structure of RFNN, and govern the performance of a model. Moreover, a number of input variable and a number of space divisions induce some fatal problems such as the increase of the number of fuzzy rules and the time required. Therefore, the relevant selection of input variables and the appropriate division of space are required. The structure of the consequence part of fuzzy rules is related to how represents a fuzzy subspace. Universally, the conventional methods offer uniform types to each subspace. However, it forms a complicated structure and debases the output quality of a model, because it does not consider the correlation of input variables and reflect a feature of fuzzy subspace. In this study, we apply the various forms in expressions of a fuzzy subspace. The form is selected according to an influence of a fuzzy subspace for an output criterion and provides users with the necessary information of a subspace for a system analysis.

## 4 Experimental Studies

In this experiment, we use three-input nonlinear function as in [2], [3]. This dataset was analyzed using Sugeno's method [2]. We consider 40 pairs of the original input-

output data. 20 out of 40 pairs of input-output data are used as learning set and the remaining part serves as a testing set.

Fig. 1 shows topologies of EoRFNN. In order to solve a given nonlinear problem, these architectures are designed and generated in flexibility that can cope with an environment (condition).

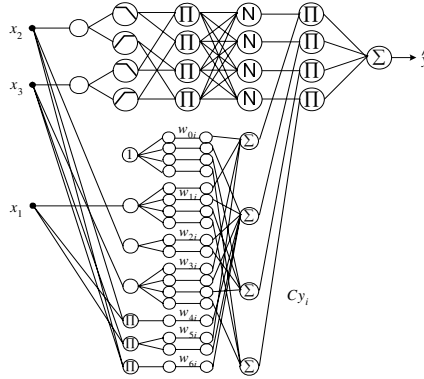


**Fig. 1.** Topology of EoRFNN02 with 2 inputs for the nonlinear function

Table 1 covers a comparative analysis including several previous models. Sugeno’s model I and II were fuzzy models based on linear fuzzy inference method while Shinichi’s models formed fuzzy rules by using learning method of neural networks. The study of literature [5] is based on fuzzy-neural networks using HCM clustering and evolutionary fuzzy granulation. Multi-FNN consists of 3 FNN structures. The proposed EoRFNNs come with higher accuracy and improved prediction capabilities.

**Table 1.** Comparison of performance with other modeling methods

Model	PI	E_PI	No. of rules
Linear model [3]	12.7	11.1	
GMDH [3,6]	4.7	5.7	
Sugeno's [2,3]	Fuzzy I	1.5	2.1
	Fuzzy II	1.1	3.6
Shinichi's [4]	FNN Type 1	0.84	8(2 <sup>3</sup> )
	FNN Type 2	0.73	4(2 <sup>2</sup> )
	FNN Type 3	0.63	8(2 <sup>3</sup> )
FNN [5]	Simplified	2.865	3.206
	Linear	2.670	3.063
Multi-FNN [5]	Simplified	0.865	0.956
	Linear	0.174	0.689
Proposed model (EoRFNN)		0.241	0.357
		0.224	0.643

## 5 Concluding Remarks

In this paper, new architectures and comprehensive design methodologies of Evolutionally optimized Rule-based Fuzzy Neural Networks (EoRFNN) has discussed for effective analysis and solution of nonlinear problem and complex systems. Also, the dynamic search-based GAs has introduced to lead to rapidly optimal convergence over a limited region or a boundary condition. The proposed EoRFNN is based on the Rule-based Fuzzy Neural Networks (RFNN) with the extended structure of the fuzzy rules. The structure and parameters of the proposed EoRFNN are optimized by GAs. The proposed EoRFNN can be designed to adapt a characteristic of a given system, also, that has the faculty of making a simple structure out of a complicated model for a nonlinear system. This methodology can effectively reduce the number of parameters and improve the performance of a model. The proposed EoRFNN can be efficiently carried out both at the structural as well as parametric level for overall optimization by utilizing the separate (A) or consecutive (B) tuning technology. From the results, (B) methodologies simultaneously tuning both structure and parameters, reduce parameters of consequence part, and offer the output performance better than the (A). Namely, (B) method is effective in identifying a model than (A).

**Acknowledgements.** This work has been supported by KESRI(I-2004-0-074-0-00), which is funded by MOCIE(Ministry of commerce, industry and energy)

## References

1. Goldberg, D.E.: Genetic Algorithms in search, Optimization & Machine Learning. Addison-wesley. (1989)
2. Kang, G., Sugeno, M.: Fuzzy Modeling. Transactions of the Society of Instrument and Control Engineers. **23**(6) (1987) 106-108
3. Park, M.Y. and Choi, H.S.: Fuzzy Control System. Daeyoungsa. (1990) 143-158 (In Korean)
4. Horikawa, S.I., Furuhashi, T., Uchigawa, Y.: On Fuzzy Modeling Using Fuzzy Neural Networks with the Back Propagation Algorithm. IEEE Transactions on Neural Networks. **3**(5) (1992) 801-806
5. Park, H.S., Oh, S.K.: Multi-FNN Identification Based on HCM Clustering and Evolutionary Fuzzy Granulation. International Journal of Control, Automation and Systems. **1**(2) (2003) 194-202
6. Kondo, T.: Revised GMDH algorithm estimating degree of the complete polynomial. Transactions of the Society of Instrument and Control Engineers. **22**(9) (1986) 928-934
7. Park, H.S., Oh, S.K.: Fuzzy Relation-based Fuzzy Neural-Networks Using a Hybrid Identification Algorithm. International journal of Control, Automations, and Systems. **1**(3) (2003) 289-300
8. Park, H.S., Oh, S.K.: Rule-based Fuzzy-Neural Networks Using the Identification Algorithm of the GA Hybrid Scheme. International Journal of Control, Automations, and Systems. **1**(1) (2003) 101-110

# Uniformly Convergent Computational Technique for Singularly Perturbed Self-adjoint Mixed Boundary-Value Problems

Ramesh K. Mishra<sup>1</sup> and Animesh Mishra<sup>2</sup>

<sup>1</sup> Department of Computer Science, Punjabi University,  
Patiala - 147 002, India

<sup>2</sup> Department of Mathematics, Indian Institute of Technology,  
Guwahati - 781 039, India

**Abstract.** In this paper, we propose a second-order parameter-uniform convergent hybrid scheme for self-adjoint singular perturbation problems (SPPs) subject to mixed (Robin) type conditions. The cubic spline based difference scheme is combined with the classical central difference scheme to obtain monotone scheme. Numerical example is provided to support the theory.

**Keywords:** Finite difference scheme, cubic splines, singular perturbation problems, piece-wise uniform meshes.

**Subject Classification:** AMS 65L10 CR G1.7.

## 1 Introduction

Singularly perturbed problems (SPPs) arise in several branches of engineering and applied mathematics which include fluid dynamics, quantum mechanics, elastostatics, chemical reactor theory, gas porous electrodes theory, etc. Some of these types of problems are usually solved by the iterative, more detailed methods like the block factorization [2], and Runge-Kutta

method for the singularly perturbed self-adjoint boundary value problem (BVP)

$$Lu(x) \equiv -\varepsilon u''(x) + b(x)u(x) = f(x), \quad x \in D \quad (1)$$

$$\alpha_1 u(0) - \beta_1 u'(0) = A, \quad \alpha_2 u(1) + \beta_2 u'(1) = B, \quad (2)$$

here  $\alpha_1, \beta_1, \alpha_2, \beta_2 > 0$  and  $\varepsilon > 0$  is a small parameter,  $b$  and  $f$  are sufficiently smooth functions, such that  $b(x) \geq \beta > 0$  on  $\bar{D}$ . Under these assumptions, the problem (2) possesses a unique solution  $u(x) \in C^2(D) \cap C^1(\bar{D})$ . Generally, the solution  $u(x)$  may exhibit boundary layers. For example, at the boundary points  $x = 0$  and  $x = 1$ , the boundary value problems of the type (2) arise in many applications, for instance, configuration of a plasma column, reactor pressure, the porous gas porous electrodes, performance of catalytic pellets and geophysical fluid dynamics chemical reactions, etc. The authors

have designed O(ε) schemes for singularly perturbed convection-diffusion and reaction-diffusion problems respectively.

For sufficiently small ε, classical methods using uniform meshes are not suitable for large number of mesh points. Essentially, these methods are defined on specially fitted meshes, the convergence to the exact solution using ε-shikh meshes are simple piecewise uniform meshes. In this kind of frequently used for singularly perturbed problems, the absolute maximum error on the shikh mesh  $\bar{\Omega}$  is constructed as follows. The domain  $\bar{\Omega}$  is divided into three subintervals as  $\bar{\Omega} = [\sigma, \sigma] \cup [\sigma, -\sigma] \cup [-\sigma, -\sigma]$ , for some  $\sigma$  such that  $0 < \sigma \leq 1/4$ . On the subintervals  $[\sigma, \sigma]$ ,  $[\sigma, -\sigma]$ , a uniform mesh with  $N/4$  mesh intervals spaced, here  $\sigma$ ,  $-\sigma$  has a uniform mesh with  $N/2$  mesh intervals. Thus, the mesh size on the subintervals  $[\sigma, \sigma]$ ,  $[\sigma, -\sigma]$  is  $h = 1/4$  and it is fitted to the problem by choosing  $\sigma = \min\{\frac{1}{4}, \sigma_0 \sqrt{\varepsilon}\}$ , here  $\sigma_0$  is a constant. It can be fitted further, we denote the mesh size on the regions  $[\sigma, -\sigma]$  as  $h^{(1)} = 2(1 - 2\sigma)/N$  and  $[\sigma, \sigma]$ ,  $[-\sigma, -\sigma]$  as  $h^{(2)} = 4\sigma/N$ . Here, we propose a hybrid scheme which is a mixture of the cubic spline scheme with the classical central difference scheme for the absolute maximum error on the shikh mesh. We apply the cubic spline difference scheme on the outer region  $([\sigma, \sigma] \cup [-\sigma, -\sigma])$ , whereas on the inner region  $([\sigma, -\sigma])$  we use the classical central difference scheme. This is small because the retained discrete maximum principle of the difference scheme. The present method provides second order uniform convergence through out the domain of interest. Numerical experiments have been carried out to show the efficiency of the method.

## 2 ε-Uniform Hybrid Scheme

The cubic spline based scheme is analyzed for stability and convergence and it is observed that for the corresponding matrix to be a matrix, a certain restriction on the mesh size, specially on the outer region, here a coarse mesh is enough to reflect the behavior of the solution. It is that region, the numerical method, the hybrid scheme is proposed. In which the classical central difference scheme is taken on the outer region and the cubic spline scheme is used on the inner region.

$$r_i^- u_{i-1} + r_i^c u_i + r_i^+ u_{i+1} = q_i^- f_{i-1} + q_i^c f_i + q_i^+ f_{i+1}, \quad i = 1, \dots, N-1, \quad (1)$$

along with following equations for appropriate matrices at boundaries

$$\begin{cases} r_0^c u_0 + r_0^+ u_1 = q_0^- + q_0^c f_0 + q_0^+ f_1, \\ r_N^- u_{N-1} + r_N^c u_0 = q_N^- + q_N^c f_{N-1} + q_N^+ f_N, \end{cases} \quad (4)$$

for  $i = 1, \dots, N/4$  and  $N/4, \dots, N-1$

$$\begin{cases} r_i^- = \frac{-3\varepsilon}{h_{i-1}(h_i+h_{i-1})} + \frac{h_{i-1}}{2(h_i+h_{i-1})} b_{i-1} & r_i^c = \frac{3\varepsilon}{h_i h_{i-1}} + b_i \\ r_i^+ = \frac{-3\varepsilon}{h_i(h_i+h_{i-1})} + \frac{h_i}{2(h_i+h_{i-1})} b_{i+1} \end{cases} \quad (5)$$



$$\left\{ q_i^- \quad \frac{h_{i-1}}{2(h_i+h_{i-1})} \quad q_i^c \quad q_i^+ \quad \frac{h_i}{2(h_i+h_{i-1})}, \right. \quad (6)$$

a d f r i  $N/4 + 1, \dots, N/4 - 1$

$$\left\{ r_i^- \quad \frac{-2\varepsilon}{h_{i-1}(h_i+h_{i-1})} \quad r_i^c \quad \frac{2\varepsilon}{h_i h_{i-1}} + b_i \quad r_i^+ \quad \frac{-2\varepsilon}{h_i(h_i+h_{i-1})}, \right. \quad (7)$$

$$\left\{ q_i^- \quad q_i^c \quad q_i^+ \quad . \right. \quad (8)$$

a d

$$\left\{ \begin{array}{l} r_0^c \quad -\frac{3\varepsilon}{h_0} \left( \alpha_1 + \frac{\beta_1}{h_0} \right) - b_0 \beta_1 \quad r_0^+ \quad -\frac{3\varepsilon \beta_1}{h_0^2} + \frac{b_1}{2} \beta_1 \\ q_0^- \quad -\frac{3\varepsilon A}{h_0} \quad q_0^c \quad -\beta_1 \quad q_0^+ \quad -\frac{\beta_1}{2} \\ r_N^- \quad -\frac{3\varepsilon \beta_2}{h_{N-1}^2} + \frac{b_{N-1}}{2} \beta_2 \quad r_N^c \quad -\frac{3\varepsilon}{h_{N-1}} \left( \alpha_2 + \frac{\beta_2}{h_{N-1}} \right) - \frac{b_N}{2} \beta_2 \\ q_N^- \quad -\frac{3\varepsilon B}{h_{N-1}} \quad q_N^c \quad -\frac{\beta_2}{2} \quad q_N^+ \quad -\beta_2. \end{array} \right. \quad (9)$$

### 3 Numerical Experiments

To show the accuracy of the present method, here we have implemented it to a test problem. The results are presented in the form of tables. The maximum pointwise errors and rate of convergence are displayed. The results for the values  $\varepsilon = 2^{-4}, 2^{-16}, \dots, 2^{-40}$  and different values of  $N$

**Table 1.** Maximum pointwise errors  $G_\varepsilon^N$ , rates of convergence  $p$  and  $\varepsilon$  - uniform errors  $G^N$  corresponding to the Hybrid scheme for Example 1

$\varepsilon$	Number of mesh points $N$						
	16	32	64	128	256	512	1024
$2^{-4}$	2.0176e-2	4.9167e-3	1.2214e-3	3.0487e-4	7.6188e-5	1.9045e-5	4.7611e-6
	2.0369	2.0092	2.0023	2.0006	2.0001	2.0000	
$2^{-16}$	1.5583e-1	5.6409e-2	1.9283e-2	6.4067e-3	2.0840e-3	6.5813e-4	2.0297e-5
	1.4660	1.5486	1.5897	1.6203	1.6629	1.6971	
$2^{-24}$	1.5515e-1	5.6201e-2	1.9217e-2	6.3854e-3	2.0771e-3	6.5597e-4	2.0231e-5
	1.4650	1.5482	1.5895	1.6202	1.6629	1.6971	
$2^{-32}$	1.5512e-1	5.6192e-2	1.9214e-2	6.3844e-3	2.0768e-3	6.5588e-4	2.0228e-5
	1.4649	1.5482	1.5895	1.6202	1.6629	1.6971	
$2^{-36}$	1.5512e-1	5.6191e-2	1.9214e-2	6.3844e-3	2.0768e-3	6.5587e-4	2.0228e-5
	1.4649	1.5482	1.5895	1.6202	1.6629	1.6971	
$2^{-40}$	1.5512e-1	5.6191e-2	1.9214e-2	6.3844e-3	2.0768e-3	6.5587e-4	2.0228e-5
	1.4649	1.5482	1.5895	1.6202	1.6629	1.6971	
$G^N$	1.6274e-1	5.8585e-2	1.9599e-2	6.5096e-3	2.1171e-3	6.6858e-4	2.0619e-4
$p_{uni}$	1.4740	1.5798	1.5902	1.6205	1.6630	1.6971	

*Example 1.* Consider the self-adjoint

$$-\varepsilon u''(x) + (\varepsilon + x)^2 u(x) = 4x^2 - 4x + 4(\varepsilon + x)^2, \quad x \in (0, 1)$$

$$u(0) = u'(0) = 0, \quad u(1) = 1.$$

We use the following graded uniform mesh procedure to calculate the maximum pointwise error and rate of convergence

Let  $\overline{D}_\varepsilon^N$  be a hybrid mesh with the parameter  $\sigma$  a fixed slight shift  $\overline{\sigma} = \min\{\frac{1}{4}, \sigma_0 \sqrt{\varepsilon}\} (N/2)$ , here, for  $i = 1, \dots, N$ , the  $i$ th point of the mesh  $\overline{D}_\varepsilon^N$  coincides with the  $(2i)$ th point of the mesh  $\overline{D}_\varepsilon^{2N}$ . The uniform mesh  $\overline{D}_\varepsilon^N$  is defined as  $G_\varepsilon^N = \max_{x_i \in \overline{D}_\varepsilon^N} |U^N(x_j) - U^{2N}(x_j)|$ , and  $G^N = \max_\varepsilon G_\varepsilon^N$ , here  $U^N(x_j)$  and  $U^{2N}(x_j)$  respectively denote the numerical solutions obtained using  $N$  and  $2N$  mesh. Furthermore, we calculate the parameter robust orders of convergence as  $p = \log_2(\frac{G_\varepsilon^N}{G_\varepsilon^{2N}})$  and  $p_{uni} = \log_2(\frac{G^N}{G^{2N}})$  respectively. Let  $\sigma_0$  have tabulated the results which shows the maximum pointwise error and the rate of convergence for Example

## 4 Conclusions

In this paper, we have proposed a hybrid method for the numerical solution of singularly perturbed reaction-diffusion problems. The underlying idea of the method combines both the cubic spline and classical Crank-Nicolson scheme. The method is of second order convergence. Ode test examples studied to verify the efficiency and accuracy of the theoretical error estimates, and the results are perfect. The same

## References

1. R.C.Y. Chin and R.Krasny. A hybrid asymptotic finite-element method for stiff two-point boundary-value problems. *SIAM J. Sci. and Stat. Comput.*, 4:229-243,1983.
2. P.A. Farrell, A.F. Hegarty, J.J.H. Miller, E. O’Riordan, and G.I. Shishkin. *Robust Computational Techniques for Boundary Layers*. Chapman & Hall/CRC Press, 2000.
3. J.L. Gracia, F. Lisbona, and C. Clavero. High order  $\varepsilon$ -uniform methods for singularly perturbed reaction-diffusion problems. *Lecture Notes in Computer Science*, 1998:350–358, 2001.
4. J.J.H. Miller, E. O’Riordan, and G.I. Shishkin. *Fitted Numerical Methods for Singular Perturbation Problems*. World Scientific, Singapore, 1996.
5. C.E.Pearson. On a differential equation of boundary layer type. *J. Math. Phys.*, 47(144):134-154,1968.
6. H.-G. Roos, M. Stynes, and L. Tobiska. *Numerical Methods for Singularly Perturbed Differential Equations*. Springer, Berlin, 1996.
7. M.Stojanovic. Numerical solution of initial and singularly perturbed two-point boundary value problems using adaptive spline function approximation. *Publications de L’institut Mathematique.*, 43(57):155-163,1988.

# Fuzzy System Analysis of Beach Litter Components

Can Elmar Balas

Gazi University, Faculty of Engineering and Architecture  
Civil Engineering Department, 06570 Ankara, Turkey  
cbalas@gazi.edu.tr

**Abstract.** Tourist beaches on the southern coast of Turkey are surveyed in order to facilitate a standardised fuzzy approach to be used in litter prediction and to assess the aesthetic state of the coastal environment for monitoring programs. During these surveys the number of litter items on beaches were counted and recorded in different categories. The main source of litter on beaches was determined as “beach users”. A fuzzy system was developed to predict the classification of the beaches, since uncertainty was generally inherent in beach work due to the high variability of beach characteristics and the sources of litter categories. This resulted in effective utilization of “the judgment and knowledge of beach users” in the evaluation of beach gradings.

## 1 Introduction

Marine litter is defined as the solid materials of human origin that are discarded at sea or reaches the sea through waterways or domestic or industrial outfall [1]. Litter in the marine environment leads to numerous problems adversely affecting coastal development sectors. Prevention at source is one of the most important strategies in enabling the reduction of litter pollution, and for this aim to be achieved strong links between measurement and management need to be realized. Five beaches on the south coast of Turkey are studied with regards to type and amount of litter on each beach. The surveys were carried out at over 100 m wide transects of the beaches.

Four site investigations were performed, first being on 20-29 October 2000, second on 10-19 November 2000, third on 15-26 March 2001 and the last on 2-13 June 2001. Field litter studies were conducted on some of the most attractive tourist beaches of the Turkish Riviera (Antalya) coast, namely Cirali, Konyaalti, Kemer, Side and Belek. For a 100m stretch of beach located on the normal access points, all litter items were enumerated and placed in their respective categories/grades [2]. Litter amounts collected ranged from 18 to 743-items/100 m stretch of beach. Litter items were graded from the best (Grade A) to worst case (Grade D) as shown in Table 1.

## 2 Litter Prediction by Fuzzy System

Field measurements indicated that the main beach litter item (the most abundant in terms of quantity) was the general litter category. The number of litter items in other categories was low and oil pollution was not observed. Konyaalti beach was rated to

be in bad conditions on the first three site surveys. The reasons were its nearness to the city center, the demolished refreshment kiosks due to the implementation of the municipality plan of Antalya and the difficulty in controlling the pollution on its seven-kilometer long beach. However on the last survey, the grading of Konyaaltı beach increased from “D” to “B”, due to the improvement in tourism facilities implemented by the municipality of Antalya. This indicated a sharp decline in the amount of litter items on the beach with the beginning of the tourism season.

**Table 1.** Categories for grading of beaches

Category	Type	A	B	C	D	
1	General	0	1-5	6-14	>15	
	Sewage Related Debris	Cotton Buds	0-9	10-49	50-99	>100
2	Gross Litter	0	1-5	6-14	>15	
3	General Litter	0-49	50-499	500-999	>1000	
4	Harmful Litter	Broken Glass	0	1-5	6-24	>25
5	Accumulations	Number	0	1-4	5-9	>10
6	Oil	Absent	Trace	Noticeable	Objectionable	
7	Faeces	0	1-5	6-24	>25	

The Moonlight beach and the public beach of Kemer were in good condition with a beach grading of “B”. With the beginning of tourism season, these beaches were regularly cleaned. Çıralı and Belek are the selected coastal sites for ‘Coastal Management and Tourism Project’. World Wide Fund is conducting the project with World Bank funding. Çıralı beach was in good condition with a beach grading of “B”. There were less tourism facilities when compared to other beaches studied, hence the grade of the beach did not change with the tourism season. Side beach obtained a low degree of grading in surveys, mostly due to faeces observed. With the beginning of tourism season, the beach was regularly cleaned and the overall grade of Side beach increased to “B”. The variation can be attributed to national holidays, stormy weather conditions, demolition and construction of beach facilities and the tourism season.

A fuzzy system of artificial intelligence [3] was developed in this paper, which had input parameters of general litter and sewage related debris, and an output parameter of the grading of litter categories. In the fuzzification process of the system inputs, which were the number of general litter and sewage related debris items, the grading criteria was utilized.

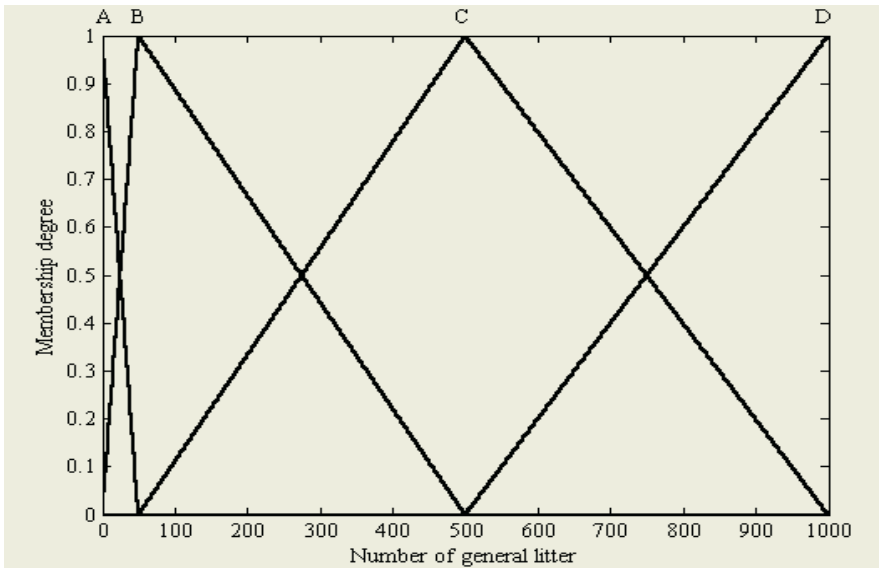


Fig. 1. Fuzzy input sets and the membership functions of the grading system for the category of general litter

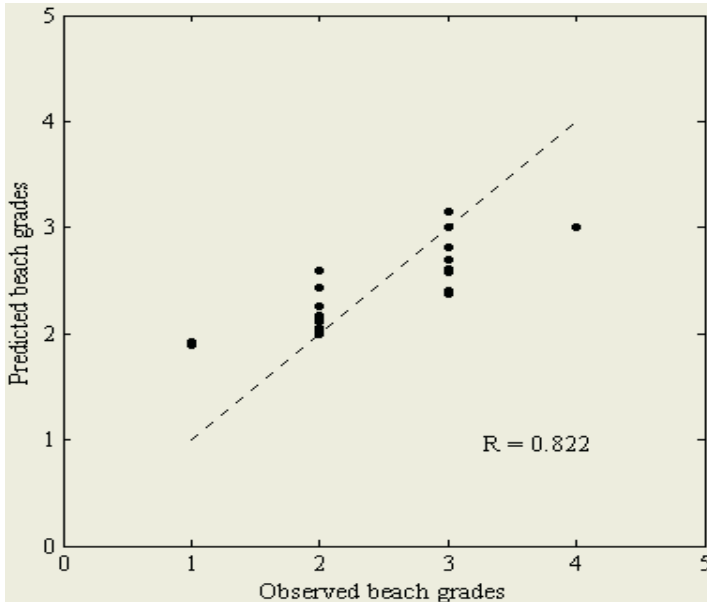


Fig. 2. Comparison of beach grades of the field study with the predicted grades of fuzzy system

The fuzzy input sets and membership functions of these variables were obtained for the grading of A, B, C, D, from the best to worst case depending on the number of

litter items measured on beaches (Figure 1). Fuzzy output sets for the grading of litter categories (A: excellent, B: good, C: average and D: worst) were coded as 1, 2, 3 and 4, respectively. The fuzzy rule based system was established by the Cartesian product (product space) of fuzzy input sets, which resulted in the logical base of 16 fuzzy rules. The fuzzy sets of grades were slightly modified to assess the uncertainties inherent in other litter categories by including supplementary adjectives of “very good (B<sup>+</sup>), to some extent good (B<sup>-</sup>), above average (C<sup>+</sup>), below average (C<sup>-</sup>) and bad (D<sup>+</sup>)”, i.e. the maximum number of litter items, greater than a certain limiting value in related categories will decrease a half grade in the input fuzzy subset of rules. Therefore, potentially harmful litter, gross litter and accumulations of litter exceeding their limits given in Table 1, will decrease the grading definition in fuzzy rules for general litter, a half grade. Similar interactions for the general litter definitions of rules are available, if there is a trace of oil pollution on the beach. Likewise, the occurrence of faeces of non-human origin affects the rules in the input fuzzy set for sewage related debris. At the testing stage, the litter measurements of the field study were compared with the predictions of the fuzzy system, as illustrated in Figure 2.

### 3 Conclusions

Tourist beaches near Antalya region were surveyed in order to develop a standardized fuzzy system approach to be used in litter prediction. The main source of litter on Turkish Mediterranean beaches was determined as “beach users”. The main advantage in using fuzzy systems was that they could consider the linguistic definitions/notes of beach users and field study teams during measurements. Therefore, they make effective use of “additional information” such as the knowledge and experience of team members. As a result, additional information inherent in the linguistic comments/refinements and judgment of study teams and beach users could be included in the grading system. Specific issues related to beach characteristics, litter assessment methodology and definition of oil pollution, which could not be included in standard procedures and/or could be easily lost in mathematical expressions/evaluations, were incorporated by using this artificial intelligence system.

### References

1. Balas, C.E., Williams, A.T., Simmons, S.L and A Ergin. A Statistical Riverine Litter Propagation Model, *Marine Pollution Bulletin*, 42(11), 1169-1176 (2001).
2. EA/NALG, Assessment of Aesthetic Quality of Coastal and Bathing Beaches, Monitoring Protocol and Classification Scheme, Environmental Agency, Bristol, UK (2000).
3. Zadeh, L. A. Fuzzy Logic and the Calculi of Fuzzy Rules, Fuzzy Graphs, and Fuzzy Probabilities, *Computer and Mathematics with Applications*, Vol. 37, 35 (1999).

# Exotic Option Prices Simulated by Monte Carlo Method on Market Driven by Diffusion with Poisson Jumps and Stochastic Volatility

agda.e.a.r.szk.e.cz.a.d.eksader.a.ck

Mathematical Institute, University of Wrocław,  
pl. Grunwaldzki 2-4, 50-384 Wrocław, Poland  
{janicki, msoboc}@math.uni.wroc.pl  
<http://www.math.uni.wroc.pl/~janicki>

**Abstract.** We consider a broad class of stochastic models of a financial market generalizing the classical Black–Scholes model, which comprise both: stochastic volatility of Brownian type and jumps at random times. We restrict ourselves to the model, where volatility is described by the diffusion which comprises the Heston stochastic volatility defined as a diffusion of Brownian type and the Poisson jump diffusion. We provide an argument that such models perfectly match typical real–life financial phenomena comparing the so-called logarithmic returns.

Applying computer simulations methods we investigate the dependence of prices of a few selected contingent claims (specifying some different options) on the parameters of our stochastic model.

## 1 The Market Model

Consider a financial market where two assets  $S_0$  and  $S$  are traded up to a fixed horizon  $T$ .

Let  $(\Omega, \mathcal{F}, P)$  be a probability space and let  $\{\mathcal{F}(t)\}_{0 \leq t \leq T}$  be an augmented right continuous filtration.

Let riskless asset price  $S_0$  be

$$S_0(t) = e^{rt}, \quad \forall t \in [0, T], \quad (1)$$

where  $r$  is a non-negative deterministic risk-free interest rate. Let  $S$  be a risk asset's price  $S$  be

$$\begin{aligned} dS(t) &= S(t_-) \{ \mu dt + \sigma(V(t)) \sqrt{-\rho^2} dW(t) + \rho dW^\sigma(t) \\ &\quad + \alpha_1 d\tilde{N}^{\lambda_1}(t) + \alpha_2 d\tilde{N}^{\lambda_2}(t) \}, \\ dV(t) &= \eta dt + \gamma dW^\sigma(t), \end{aligned} \quad (2)$$

where  $(W, W^\sigma)'$  is a standard Brownian motion,  $\tilde{N}^{\lambda_i}$  are independent compensated Poisson processes (i.e.  $\tilde{N}^{\lambda_i}(t) = N^{\lambda_i}(t) - \lambda_i t$ ),  $\{V(t)\}_{0 \leq t \leq T}$  is the

... at t process,  $\rho$  is the correlation between asset price and ... at t,  $\rho \in -1, 1$ ,  $\mu, \eta, \gamma$  are constants,  $\sigma$  is a function that satisfies

$$\exists \underline{\sigma}, \bar{\sigma} > 0 \quad \forall z \in \mathbb{R} \quad \underline{\sigma} \leq \sigma(z) \leq \bar{\sigma}. \tag{1}$$

We take the dependence of the processes to assure that both jumps up and down should be allowable. Hence that is necessary to choose parameters  $|\alpha_1| < 1$  and  $|\alpha_2| < 1$ . If the derivative signs are opposite, this model suggests

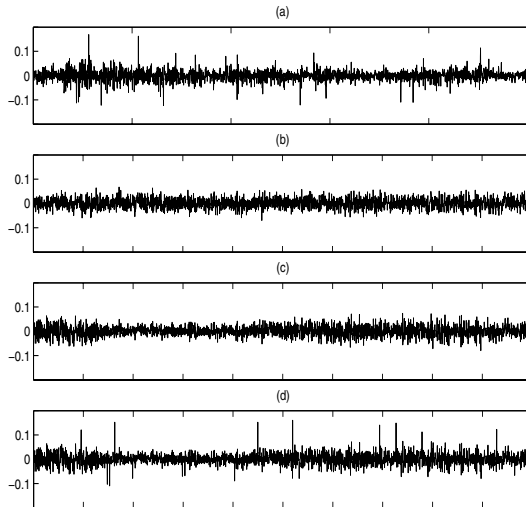


**Fig. 1.** Asset's price returns for various market model. On picture (a) there are real logarithmic returns of prices of IBM's stocks. Remaining pictures show logarithmic returns of prices modelled in various way: (b) simple diffusion (like Black-Scholes model), (c) stochastic volatility (like Heston model), (d) stochastic volatility and Poisson jumps

to compare the empirical data at given time. Looking at (b) and (c) we see that stochastic model improves the model and makes it more accurate but (d) reflects a phenomenon which are characteristic prices behavior. It is known that absence of arbitrage which is equivalent to the existence of martingale measure, is absolutely necessary to compute the fair price of a contract. This measure the process of discounted price of risk asset should be a martingale. On the market defined above the Radon-Nikodim's derivative can be defined as follows

$$\begin{aligned} Z(t) &= \frac{d\mathbb{P}}{d\mathbb{P}_0} |_{\mathcal{F}(t)} = \mathbb{E} \left\{ \exp \left\{ - \int_0^t \theta(s) dW(s) - \frac{1}{2} \int_0^t \theta(s)^2 ds \right\} \right. \\ &\times \mathbb{E} \left\{ \exp \left\{ - \int_0^t \nu(s) dW(s) - \frac{1}{2} \int_0^t \nu(s)^2 ds \right\} \right. \\ &\times \mathbb{E} \left\{ \dots ( - \phi_i ) N^{\lambda_i}(t) + \lambda_i \phi_i \right\}, \end{aligned}$$



here  $\theta$  and  $\nu$  are adapted to  $\{\mathcal{F}_t\}$  and satisfy the integrability conditions  $\int_0^T (\theta(t))^2 dt < \infty$  and  $\int_0^T (\nu(t))^2 dt < \infty$ . In the case of  $\mathbb{E}(Z(T)) = 0$  and  $\mathbb{E}(Z(T)^2) < \infty$ , the process  $\nu$  is a martingale.

$$(\theta(t)\sqrt{-\rho^2 + \rho\nu(t)}\sigma(t) + \lambda_1\phi_1\alpha_1 + \lambda_2\phi_2\alpha_2 - \mu - r) \leq t \leq T \quad a.s. \quad (4)$$

The processes  $\theta$  and  $\nu$  are interpreted as the risk premiums connected with the risk assets  $S$  and  $W^\sigma$  respectively. The premium for the risk related to the processes  $N_i^\lambda$  are  $\phi_i$ .

As a consequence of such equations are obtained the following measure equivalence theorem. We can assume that the premium coming from the risk assets disappears, i.e. that we can set the process  $\theta = 0$  and the process  $\nu$  is a martingale.

Consider the risk assets  $W_0(t)$  and  $W_0^\sigma(t)$  as the reference processes and  $\tilde{N}^{L_i}(t)$  as a compensated process (the test  $L_i$ ). Since the risk assets are traded, the premiums are unique and the martingale measure

pp. of the processes to the discounted asset price is obtained.

$$d\left(\frac{S(t)}{S_0(t)}\right) = \frac{S(t_-)}{S_0(t)} \left\{ \sigma(V(t)) \sqrt{-\rho^2} dW_0(t) + \rho dW_0^\sigma(t) + \alpha_1 d\tilde{N}^{L_1}(t) + \alpha_2 d\tilde{N}^{L_2}(t) \right\}. \quad (5)$$

It is easy to see that the above process is a supermartingale and since  $\sigma$  satisfies the (5) condition it is a martingale.

## 2 Option Prices

It is easy to see that the option price with payoff  $\psi(S(T))$  is ruled by the equation

$$ECC(t) = S_0(t)\mathbb{E}^Q \left[ \frac{\psi(S(T))}{S_0(T)} | \mathcal{F}(t) \right] = \frac{H(T)}{H(t)} \mathbb{E}^P [ H(T)\psi(S(T)) | \mathcal{F}(t) ],$$

where  $H(t) = \frac{Z(t)}{S_0(t)}$  is a state dependent price

and substituting  $S_0(t)$  according to (2), and knowing that  $H(\cdot)$  is a martingale, the option premium with payoff  $\psi(S(T))$

$$ECC(\cdot) = e^{-rT} \mathbb{E} [ Z(T)\psi(S(T)) ]. \quad (6)$$

As a consequence of the first expectation theorem (6), the easiest way to obtain results using the so-called Carr method

is to use the empirical stochastic calculus. We assume that the function  $\sigma$  has the form  $\sigma(z) = \underline{\sigma} + \sigma(z - \underline{\sigma}) + \bar{\sigma} - \sigma$ , and  $\sigma$  has the values  $\underline{\sigma}$ ,  $\bar{\sigma}$ , respectively outside the interval  $a$ .

in the stochastic process, the remaining calculation computes the price of the stock at the maturity  $t = T$

$$S(T) = S(0) e^{\left\{ \mu T - \frac{1}{2} \int_0^T (\sigma(V(s)))^2 ds + \sqrt{-\rho^2} \int_0^T \sigma(V(s)) dW(s) \right\}}$$

$$\times e^{\left\{ \rho \int_0^T \sigma(V(s)) dW^\sigma(s) \right\}} e^{\left\{ \dots + \alpha_1 N^{\lambda_1} + \dots + \alpha_2 N^{\lambda_2} \right\}}.$$

The results of simulation are presented in the table below.

**Table 1.** Prices of options simulated for various models of market: BS - Black-Scholes diffusion market, SV - stochastic volatility market, SV+P - stochastic volatility with Poisson jumps market

Payout function	BS	SV	SV+P
$(S(T) - K)^+$	17.8462	17.7726	17.5570
$X \mathbb{I}_{\{S(T) > K\}}$	10.7013	9.6102	10.3223
$S(T) - \min_t(S(t))$	28.5074	22.9462	28.7744
$(q^\alpha(S) - K)^+$	0.8136	3.1839	0.2556
$(K - M(T, T_0, S))^+$	0.6422	1.1330	0.9097

The simulation of the models are parameterized in the same manner as the first case. The standard European option parameters are chosen as follows:  $S(0) = \$100$ ,  $r = 0.05$ ,  $\sigma = 0.2$ ,  $K = \$100$ ,  $T = 1$  year,  $X = \$100$  if the price of asset at the maturity time  $t$  be greater than  $K = \$100$  in the first case and  $X = \$100$  if the price of asset at the maturity time  $t$  and the mean price of asset at time  $t$  be greater than  $K = \$100$  in the second case. The parameters of the  $(q^\alpha(\cdot))$  are  $\alpha = 0.5$  and the parameters of the  $M(T_0, T, S)$  are  $\lambda = 0.5$ ,  $\mu = 0.05$ ,  $\sigma = 0.2$ ,  $T_0 = 0.5$ ,  $T = 1$ ,  $S = 100$ .

## References

1. Bellamy N., Jeanblanc M.: Incompleteness of markets driven by a mixed diffusion. *Finance & Stochastics* 4 (2000) 209–222
2. León J. A., Solé J. L., Utzet F., Vives J. On Lévy processes, Malliavin calculus and market models with jumps. *Finance & Stochastics* 6 (2002) 197–225
3. Protter, P.: *Stochastic Integration and Differential Equations – A New Approach*. Springer-Verlag, New York (1990)
4. Touzi N.: American Options Exercise Boundary When the Volatility Changes Randomly. *Applied Mathematics & Optimization* 39 (1999) 411–422

# Computational Complexity and Distributed Execution in Water Quality Management

maria.chtepen<sup>1</sup>, Filip Claeyss<sup>2</sup>, Bart Dhoedt<sup>1</sup>, Peter Vanrolleghem<sup>2</sup>,  
and Piet Demeester<sup>1</sup>

<sup>1</sup> Department of Information Technology (INTEC),  
Ghent University, Sint-Pietersnieuwstraat 41, Ghent, Belgium

{maria.chtepen, bart.dhoedt, piet.demeester}@intec.ugent.be

<sup>2</sup> Department of Applied Mathematics, Biometrics and Process Control (BIOMATH),  
Ghent University, Coupure Links 653, Ghent, Belgium

{filip.claeys, peter.vanrolleghem}@biomath.ugent.be

**Abstract.** Tourist beaches on the southern coast of Turkey are surveyed in order to facilitate a standardised fuzzy approach to be used in litter prediction and to assess the aesthetic state of the coastal environment for monitoring programs. During these surveys the number of litter items on beaches were counted and recorded in different categories. The main source of litter on beaches was determined as “beach users”. A fuzzy system was developed to predict the classification of the beaches, since uncertainty was generally inherent in beach work due to the high variability of beach characteristics and the sources of litter categories. This resulted in effective utilization of “the judgment and knowledge of beach users” in the evaluation of beach gradings.

## 1 Introduction

The importance of water quality management has drastically increased during the last decades as a consequence of growing environmental awareness. Compared to the defined systems (e.g. electrical and mechanical) that can be described by classical analysis, the behaviour of defined water systems is much more difficult to predict due to the partial availability of general applicable assumptions as a result of the complexity of water systems, models regarded as here to part of design, operation and implementation. The models used in practice are typically based on a combination of general physical characteristics (topography, surface area, volume, etc.) and pure empirical assumptions. These models form a collection that summarize and increase the understanding of complex interacting biological systems.

Since the importance of water quality management applications, the Environmental Assessment System (EAS) has been developed. EAS<sup>1</sup> is a versatile and powerful tool, which thus far has mainly been applied to wastewater treatment processes. It consists

<sup>1</sup> World-wide Engine for Simulation and Training.

... f c ear... separated... de... g a d E per me tat... E... r... me ts... the... r... me ts are se f c... ta ed a d c... s st... f a graph ca... fr... t e d... c mputat... a back e d a d c... tr... g c... he... de... g E... r... me t a... s f r the creat... f e cutab e m... de s... the bas s... f h gh... e e m... de... desc r pt... s... thr... ugh the app... cat... f m... de... c mp... er tech... ques... these e cutab e m... de s are subse que... t... used as a bas s... f r the creat... f... r tua E per me ts ( E's)... the E per me tat... E... r... me t... he reas... h the term E... as ad p... t... ed... th s case s re a t... t... the fact that E... g... es be... d p a... s mu a t...... fact, the t... p... e s... f E's that are curre... t... sup... p... r... t... ed are... mu a t...... t... ead state... a... s s... Opt m... zat... C... fide... ce... a... s s... ce... ar... a... s s... e... s... t... t... a... s s a d... certa... t... a... s s... E's such as... mu a t...... a d... t... ead state... a... s s are sa d... t... be *atomic*... s... ce the... are... t... h... er arch ca... c... mp... sed... f... ther E's O... the... ther ha d... *compound* E's such as Opt m... zat... C... fide... ce... a... s s... ce... ar... a... s s... e... s... t... t... a... s s a d... certa... t... a... s s a... are based... the repea... t... e e cut... f... s mu a t... s... f... r... d... ere... t... parameter sets

... de... g a d... r tua E per me tat... the d... ma... f... ater ua... t... a... ageme... t... s... c... mputat... a... c... mp... e... ta... m... de... bu... d... g... t... mes... ra... ge... fr... m... a... c... up... e... f... sec... ds... t... se... era... h... urs... a... d... t... p... ca... e... cut... t... mes... f... r... c... mp... u... d... E's... ra... ge... fr... m... a... um... ber... f... sec... ds... t... se... era... e... e... k... s... a... h... gh... e... d... C... reduce th s... c... mp... e... t... a... e... s... stem... a... m... ed... E... as... de... s... g... ed... that... a... s... f... r... d... str... b... u... t... e... cut... f... c... mp... u... d... E's... E... ca... be... see... as... a... gh... t... e... gh... t... Gr... d... s... stem... 4... ded... c... at... e... d... the... ater... ua... t... a... ageme... t... app... cat... area... t... as... bu... t... t... p... f... tech... g... es... such... as... C++... a... d... O... E... as... t... a... mp... e... m... e... t... e... d... f... r... the... E... s... ft... are... s... stem... h... e... er... th... a... k... s... t... ge... er... c... des... g... t... ca... be... used... f... r... e... cut... f... a... c... mputat... a... te... s... e... task... c... s... st... g... f... a... u... r... d... e... r... set... f... b... s

... es... g... a... d... mp... e... m... e... t... e... d... f... the... E... s... stem... started... fr... m... a... um... ber... f... mp... r... ta... t... requ... re... me... ts

**Financial.**... he... e... s... stem... sh... u... d... 't... requ... re... a... add... t... a... est... me... ts... terms... f... hard... are... a... d... staff... g

**Functional.**... he... s... stem... sh... u... d... e... de... t... be... eff... ic... e... t... a... d... r... bust... e... t... sh... u... d... de... er... fast... e... cut... f... b... s... a... d... sh... u... d... acc... u... t... f... r... mach... e... crashes... a... d... et... rk... dr... p... uts

**Technical.**... str... ct... dema... d... f... r... e... g... a... t... des... g... a... d... c... here... t... mp... e... m... e... t... as... mp... sed... t... get... her... th... fu... O... p... r... tab... t... ter... perab... t... a... d... m... ted... de... pe... de... ce... th... rd... part... t... s

## 2 WDVE Architecture

E... c... s... sts... f... t... ma... r... m... du... es... aster... a... d... a... e... he... aster's... ma... fu... ct... a... t... es... are... t... rece... e... E's ( b... s... )... fr... m... the... pp... cat... fr... t... e... d... t... st... re... b... s... u... t... the... are... pr... cess... e... d... t... match... them... aga... st... a... a... ab... e... rk... des... a... d... t... t... ate... e... cut... a... es... ru... (p... ss... b... c... curre... t... )... b... s... the... r... c... mputat... a... res... ur... ces... a... d... c... lect... the... ut... puts... request... e... d... b... the... user

master as well as slaves are further decomposed into a number of submodules (see Fig. 1), each implementing a particular well-defined function.

**Dispatcher.** The dispatcher's main task is to administer the jobs from the moment they are submitted by the application until they are executed and results are available to the user.

**Registry.** The goal of the Registry is to allow for a ranked set of static and dynamic registered slaves.

**Selector.** The selector implements an algorithm for selecting a slave for the job to be executed.

**Checker.** The consistency of the state of the system is ensured by the Checker background thread, which constantly monitors the status of various entities and triggers appropriate actions.

**Acceptor.** This module is at the heart of each slave. It evaluates requests from the master for the execution of jobs. In case a job is accepted, a new instance of the application back-end is created and the execution is started.

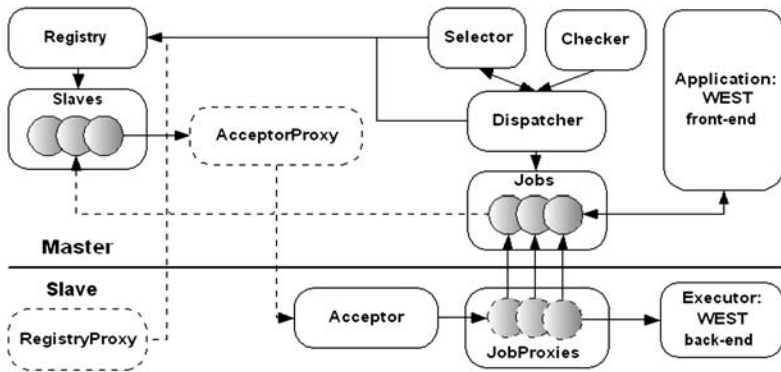


Fig. 1. WDVE: Architecture

For the transfer of input, output and status data between master and slaves, the gRPC implementation of the Open Protocol was used. Results reflecting gRPC from the wide range of the available middlewares technologies are performance, portability and the performance of gRPC. In order for the specifics of the middleware to be visible to the rest of the code, an abstract layer was added to part of the gRPC wrapper classes.

Implementation architectural questions should represent jobs. The various characteristics start from the point where jobs submitted to the system and end with the completed jobs. Output data that is decided to consist of the use of this set of the context of the Jobs description consists of Executor dependencies and Executor dependencies of format. The Executor dependencies of format consists a set of Resources including various types of

put a d output files the E cutor depe de t f rmat ... s made up f ar  
 us ther peces f f rmat ... that are re e a t t the spec fic E cutor that  
 s t e ecute the ... b

### 3 Test Results and Conclusions

ests ere ru c mpar g the effie c f ... E th m ... th c s ut ... s the  
 resu ts that ere f u d are ... e th the t p ca perf rma ce beh a r f ther  
 d str buted s stems ... g 2 are s me f the resu ts that ere b ta ed fr m  
 a test us g three de t ca a es that e cute ... bs ass g ed b a a ster that  
 has a t ta f t ... bs t e ecute r m g 2 (eft) ... e eas c c cudes  
 that ... case the ... bs are sh rt, there s ... th g t be ga ed fr m d str but g  
 ... bs ... er mu t p e a es ... e er ... case f ... bs f rea st c c m p e t ... e  
 d es get a s g f ca t reduct ... f the t ta e cut ... t me ( g 2, r ght) ... s  
 the ... mber f a es ... creases, th s reduct ... bec mes m re p r u ced, up t  
 a p t h e er here ... further m p r e m e t s p s s b e the speed up fact rs  
 b ta ed ... p r a c t ce are a s a a s ... er tha th se that ... e ... d the ret ca ...  
 e p e c t E d e t t, th s s due t the ... erhead ... c t e d b the ... E s f t are  
 t s e f a d the tra s m s s ... f data ... er the ... et r k

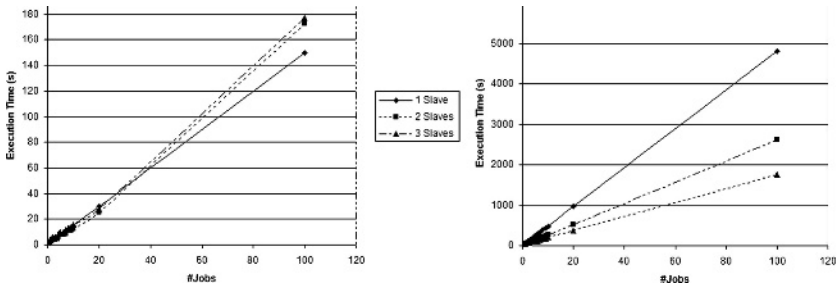


Fig. 2. WDVE: Test results for short Jobs (left) and long Jobs (right)

### References

1. H. Vanhooren, J. Meirlaen, Y. Amerlinck, F. Claeys, H. Vangheluwe, and P. Vanrolleghem. WEST: Modelling Biological Wastewater Treatment. *Journal of Hydroinformatics*, IWA Publishing, 5(1), 2003.
2. HEMMIS N.V. WEST website. <http://www.hemmis.com>.
3. F. Claeys, M. Chtepen, L. Benedetti, B. Dhoedt, and P.A. Vanrolleghem. Distributed Virtual Experiments in Water Quality Management. In *6<sup>th</sup> International Symposium on Systems Analysis and Integrated Assessment in Water Management (WATERMATEX)*, pages 485–494, Beijing, China, November 3–5 2004. International Water Association.
4. EGEE. Enabling Grids for E-science in Europe (EGEE) website. <http://egee-intranet.web.cern.ch/egee-intranet/gateway.html>.

# Traffic Grooming Based on Shortest Path in Optical WDM Mesh Networks\*

Heungsik Ra, Hyeonjae Lee, Myung-Chul Chung, and Hyeonchoo Choo

Lambda Networking Center,  
School of Information and Communication Engineering,  
Sungkyunkwan University, Korea  
{ookuma, tjlee, mychung, choo}@ece.skku.ac.kr

**Abstract.** This paper investigates the static traffic grooming in WDM optical mesh networks. Our objective is to improve the network throughput and to minimize the blocking probability. As take care of this problem efficiently, we propose Shortest-path First Traffic grooming(SFT) algorithm. The comprehensive computer simulation shows that our proposed algorithm is up to about 14% superior to the existing one known to be effective.

## 1 Introduction

Optical wavelength division multiplexing (WDM) is a promising technology to accommodate the exponential growth of data telecommunication traffics. In each optical link capable of carrying traffic of several wavelengths, each of which supports traffic in the Gbps range. However, the traffic requested by individual connections still in the Mbps range. To utilize the available bandwidth efficiently, several connections have to be grouped into the same wavelength. This requires strategic routing and wavelength assignment (RWA) of each connection.

The problem of RWA in sub-wavelength demands with the objectives of minimizing the network cost and maximizing network throughput is called *traffic grooming*. Problem which refers to the techniques used to combine lower capacity connections into available wavelengths. Traffic grooming has received considerable attention recently, and there are many related works in the literature. In recent past, there have been efforts towards solving the traffic grooming problem for mesh networks. This issue has been addressed both the static [4], as well as the dynamic case [5].

In this paper, we consider the static traffic grooming for the mesh networks. We propose a shortest path first traffic grooming (SFT) algorithm. The objective to maximize the network throughput and to minimize the blocking probability. The proposed algorithm uses effective routing method instead of previous shortest path routing. The network capacity connection requests are efficiently

---

\* This work was supported in parts by Brain Korea 21 and the Ministry of Information and Communication, Korea. Corresponding author: Prof. H. Choo.

groomed together and carried over the computer system, the algorithm achieves 4% improved performance in terms of network throughput, compared with the algorithm for high-priority traffic.

## 2 Related Works and Problem Statement

Current and future networks are creating aggregated generation mesh topology. Indeed, much recent work has focused on grooming traffic in mesh networks [4]. Existing network traffic grooming has considered topology traffic model, static traffic model, and demand matrix traffic model. The static traffic model, capacity demands are known and do not change over time. The studies for static grooming are [4], the demand matrix traffic model, demands assumed to arrive at a random time and last for a certain amount of time. In random network, studied traffic grooming issues demand traffic environment.

In generation network, the traffic grooming problem, traffic requests are carried through single-priority grooming, multi-priority grooming, grooming as a method that allows a collection of trajectories along the path. On the other hand, multi-priority grooming as a method that allows a collection of trajectories. Multi-priority grooming, a collection can be dropped at a term, at a demand grooming, then capacity collection should be dropped before it reaches its destination.

The traffic grooming problem can be formulated as follows. Given a network configuration (including physical topology), here each edge is a physical link, number of transmitters at each node, number of wavelengths on each fiber, and the capacity of each wavelength) and a set of collection requests through the network, such as OC-2, OC-48, etc., need to determine the set of grooming paths to satisfy the collection requests because of the sub-wavelength granularity of the collection requests, every request can be multiplexed on the same grooming path.

## 3 Shortest Path First Traffic Grooming (SFT)

Our goal is to improve the network throughput by using the efficient routing algorithm for traffic grooming. A grooming algorithm should be able to adapt to the routing using Dijkstra's shortest path, however, it finds the shortest path under the current network status, which may not be the real shortest because the network status is changed frequently. For that reason, we apply a routing algorithm that prefers to assign the shortest paths, which are found in the original network status, the proposed grooming algorithm.

The proposed grooming algorithm uses both fixed routing based on shortest paths and adaptive routing. First, this grooming algorithm assigns grooming paths for collection requests, which are able to use shortest paths in the original network status. The collection requests, which are not permitted to use shortest paths for example, grooming adaptive routing before traversing the wavelengths for use.



algorithm employing this routing method, more demands are carried through shortest paths and resources are used efficiently. That is, for using our thermoreclect requests which are not carried through shortest paths, more demands can be carried through multiprogramming.

**Step 1** Constructing a routing policy

- 1.1 Sort all demands  $(s_i, d_i)$  according to the sum of carried traffic requests  $T(s_i, d_i)$  between  $s_i$  and  $d_i$ , and put them into a set  $L$  in a descending order
- 1.2 Find a shortest path for each  $(s_i, d_i)$  and its hop count  $(h(s_i, d_i))$  by using Dijkstra's shortest path algorithm
- 1.3 Setup a ghtpath for each demand  $(s_i, d_i)$  in the set  $L$  using the shortest path obtained in **Step 1.2** subject to traffic engineering constraints. For each ghtpath, let  $T(s_i, d_i) = \text{Max } T(s_i, d_i) / C$ , and delete edges of the assigned ghtpath from the physical topology if necessary. Use the shortest path obtained in **Step 1.2** set  $(s_i, d_i)$  into set  $L'$  and if there are not available ghtpaths due to short traffickers, deleted edges, move  $(s_i, d_i)$  to  $L''$
- 1.4 Setup ghtpaths for demands  $(s_i, d_i)$  in  $L'$  using the adaptive routing, subject to traffic engineering constraints for each  $(s_i, d_i)$  to  $L''$ . Otherwise, assign the ghtpath and let  $(s_i, d_i) = \text{Max } T(s_i, d_i) / C$ , the edges of the assigned ghtpath are deleted from the physical topology
- 1.5 Get to **Step 1.3** until sets  $L$  and  $L'$  become empty

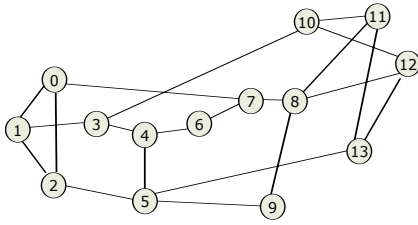
**Step 2** Routing the speed request sets in the routing policy constructed in **Step 1**

- 2.1 Route all thermoreclect requests which can be carried through shortest ghtpath hop and update the network status for the routing policy
- 2.2 Route the remaining thermoreclect requests using current available spare capacity of the routing policy based on the sum of carried traffic requests due  $T(s_i, d_i)$

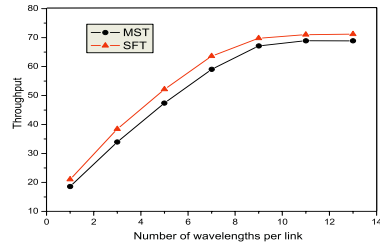
**Step 3** Check the network status, set  $L''$  and repeat **Steps 1** and **2** until the resources are fully exhausted

## 4 Numerical Results

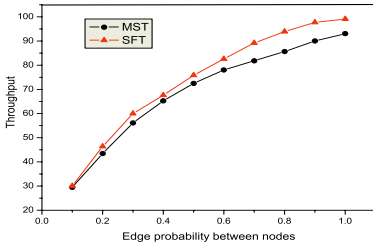
The performance of the algorithm developed in this paper is compared against the existing methods. The E-adm network topology is E has 4 nodes and 2 links as shown in Fig. 1(a) and adm networks are generated based on 2000 random demands and algorithms in terms of network throughput. The results of the algorithm and the proposed algorithm are shown in Fig. 1(b). The constructed result graphs for number of a.e.gths per each fiber link versus network throughput. The results show that our algorithm performs better than the algorithm with respect to network throughput at a number of a.e.gths per link. As you see here, the algorithm outperforms  $\% \sim 4\%$  over



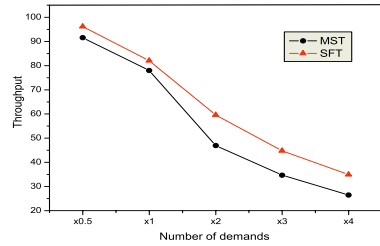
(a) NSFNET topology.



(b) Throughput comparison in NSFNET ( $T_r = 15$ ).



(c) Throughput in random networks ( $N = 15, W = 10, T_r = 15$ ).



(d) Throughput in random networks ( $N = 15, P_e = 0.6, W = 10, T_r = 15$ ).

**Fig. 1.** Throughput comparison

In Fig. 1(c), we compare the network throughput of the algorithm and algorithms in random topologies. It is observed that the edge establishment probability between nodes ( $P_e$ ) increases the observed that the algorithm demonstrates 4% ~ 10% higher throughput than the algorithm. In Fig. 1(d), we present the results that the number of demands versus network throughput in random topologies. We see that the throughput of the algorithm achieves ~ 8% better performance than that of the algorithm as the number of demands increases, the performance of the algorithm becomes better.

## 5 Conclusion

We investigated the traffic grooming algorithm. The proposed algorithm improved heuristic algorithm with respect to network throughput. The shortest path first traffic grooming algorithm has a better performance than the shortest path first algorithm and uses as many shortest paths as possible before the demands are exhausted. The algorithm outperforms the other aspects. The algorithm becomes better.

## References

1. R. Ramaswami and K. N. Sivarajan, *Optical Networks: A Practical Perspective*. San Francisco, CA: Morgan Kaufmann, 1998.
2. A.S. Rodionov and H. Choo, "On generating random network structures: Connected Graphs," *Springer-Verlag Lecture Notes in Computer Science*, vol. 3090, pp. 483-491, Sep. 2004.
3. S. Thiagarajan and A. K. Somani, "Capacity fairness of WDM networks with grooming capability," *Opt. Networks Mag.*, vol. 2, no. 3, pp. 24-31, May/June 2001.
4. H. Zhu, H. Zang, K. Zhu, and B. Mukherjee, "A novel, generic graph model for traffic grooming in heterogeneous WDM mesh networks," *IEEE/ACM Trans. Networking*, vol. 11, pp. 285-299, Apr. 2003.
5. K. Zhu and B. Mukherjee, "Traffic grooming in an optical WDM mesh network," *IEEE J. Select. Areas Commun.*, vol. 20, pp. 122-133, Jan. 2002.

# Prompt Detection of Changepoint in the Operation of Networked Systems\*

U. S. S. U. M. A. D. E. E. . G. U.

School of Information and Communications Engineering,  
Sungkyunkwan University, 440-746, Suwon, Korea  
bayes1@hanmail.net  
youn@ece.skku.ac.kr

**Abstract.** Detection of network problems is an important step in automating network management. Early detection of performance degradation can alleviate the last moment hassle of network managers. This paper focuses on a statistical method aiming at detecting changepoint as quickly as possible using Bayes factor along with the binary segmentation procedure modified for fast detection. Computer simulation verifies the effectiveness and correctness of the proposed approach.

**Keywords:** Bayes factor, binary segmentation, changepoint detection, network management, non-homogeneous Poisson process.

## 1 Introduction

For detecting and diagnosing a changepoint, a statistical analysis method has been successfully applied to a variety of networked and distributed systems. The rapid growth of networked and distributed systems through the network has generated serious problems difficult to manage with the expertise of human operators. In order to overcome these technical difficulties, there is a urgent need for automatic management functions to reduce the operator's load and management cost. Early detection of performance degradation can alleviate the last moment hassle of network managers.

Sudden change in the behavior of a system is a changepoint which can be estimated from the input data using the maximum likelihood estimator [2]. In order to automatically detect a changepoint for detecting a significant change, in this paper the maximum likelihood fast detection that is a simple and requires little reduction of performance degradation impact on the network services and users. The detection probabilities are formulated as a changepoint problem using a Bayes factor. The computation of the Bayes factor, however, gets more complex as the number of features increases.

---

\* This research was supported by the Ubiquitous Autonomic Computing and Network Project, 21st Century Frontier R&D Program in Korea and the Brain Korea 21 Project in 2004. Corresponding author: Hee Yong Youn.

... erc me the c mputat ... a d fficu tes, e e p re the b ar segme ta  
 t ... meth d pr p sed ... Our appr ach fr detect g cha gep t s ma ...  
 de e p g f rmu as b a es a e p t he pr p sed detect ... meth d s  
 des g ed t be se st e t s ght cha ges ... the perat ... character st cs f a  
 et rk a d pred ct the cha gep t at the cha ge p t f the shape param  
 ter a ues C mputer s mu at ... er fies the e ect e ess a d c rrect ess f the  
 pr p sed appr ach

### 2 Preliminaries

... the ... h m ge e us ... ss pr cess ( ... ), the ... terarr a t me s e ther  
 ... depe de t ... r de t ca d str buted ... ra d m ar ab e f spec a ... ter est s  
 $N(t)$ , the ... mber f fa ures ... the t me ... ter a ( , t ... he ... te s t fu ct ... f  
 a c u t g pr cess  $\{N(t), t \geq \}$  s defi ed as  $\lambda(t) = m'(t)$ , here  $m(t)$  s the  
 mea ... mber f fa ures ... the t me ... ter a ( , t ... fte ca ed the mea ... a ue  
 fu ct ... he p er a ... pr cess f r the re ab t gr th f repa b e s stems  
 has the ... te s t fu ct ...

$$\lambda(t) = \alpha\beta t^{\beta-1}, \alpha > 0, \beta > 0, t > 0, \tag{1}$$

here  $\alpha$  s a sca e parameter a d  $\beta$  s a shape parameter

... he ke h d fu ct ... f r the data  $D_{(0,T]}$  ... th the m de ... f  $\lambda(\cdot)$  g e ...  
 ( ) ca be r tte as

$$L(\alpha, \beta | D_{(0,T]}) = \left( \prod_{i=1}^n \lambda(t_i) \right) \exp \left( - \int_0^T \lambda(t) dt \right), \tag{2}$$

... here  $D_{(0,T]} = \{t_1, \dots, t_{n+1} | 0 < t_1 \leq \dots \leq t_n < T, T = t_{n+1}\}$  e e  
 ... r the data  $D_{(0,T]}$  f fa ure t mes, the ... te s t fu ct ... s are g e ... respec  
 t e b

$$M_0: \lambda(t) = \alpha_0\beta_0 t^{\beta_0-1}, 0 < t \leq T, \text{ vs. } M_1: \lambda(t) = \begin{cases} \alpha_1\beta_1 t^{\beta_1-1}, & 0 < t < \tau, \\ \alpha_1\beta_2 t^{\beta_2-1}, & \tau \leq t < T, \end{cases}$$

here  $\tau$  s a cha gep ... t

### 3 The Proposed Changepoint Detection Method

... e use the a es fact r f r c mpar g a d test g the ... cha gep t m de  
 a d s g e cha gep t m de ... he test s based ... ca cu at g the a es fact r  
 $B_{10}$  f r the s g e cha gep t m de  $M_1$  aga st the ... cha gep t m de  $M_0$   
 ... he detect ... pr cedure f the cha gep t c s sts f the f ... g steps

**Step 1:** ... r the c mplete data, c mpute the a es fact r  $B_{10}$

**Step 2:** ... he  $B_{10} > \dots$ , est mate a cha gep t  $\tau$  f r the g e ... data

**Step 3:** After a change-point is detected, the data are sequentially added, compute the a posteriori  $B_{10}$

**Step 4:** The  $B_{10} > \tau$ , estimate a change-point  $\tau$  for the given data

the a posteriori  $B_{10}$  for the change-point model. Again, set the change-point model.

$$B_{10}(D_{(0,T)}) = B_1/B_0, \tag{3}$$

here

$$\begin{aligned} B_1 &= \int_{[0,t_1)} \int_0^\infty \int_0^\infty \frac{2}{(\alpha + \beta_1)^3} \cdot \frac{2\beta_2^n}{(\alpha + \beta_2)^3} \cdot \frac{\prod_{i=1}^n t_i^{\beta_2}}{K_1} d\beta_1 d\beta_2 \tau d\tau \\ &+ \sum_{j=1}^{n-1} \int_{[t_j, t_{j+1})} \int_0^\infty \int_0^\infty \frac{2\beta_1^j}{(\alpha + \beta_1)^3} \cdot \frac{2\beta_2^{n-j}}{(\alpha + \beta_2)^3} \cdot \frac{q_j}{K_1} d\beta_1 d\beta_2 \tau d\tau \\ &+ \int_{[t_n, T)} \int_0^\infty \int_0^\infty \frac{2\beta_1^n}{(\alpha + \beta_1)^3} \cdot \frac{2}{(\alpha + \beta_2)^3} \cdot \frac{\prod_{i=1}^n t_i^{\beta_1}}{K_1} d\beta_1 d\beta_2 \tau d\tau, \\ B_0 &= \int_0^\infty \frac{2\beta_0^n}{(\alpha + \beta_0)^3} \cdot \frac{\prod_{i=1}^n t_i^{\beta_0}}{(T^{\beta_0} + \nu)^{n+\xi}} d\beta_0. \end{aligned}$$

where,  $K_1 = (\tau^{\beta_1} + T^{\beta_2} - \tau^{\beta_2} + \nu)^{n+\xi}$  and  $q_j = \left[ \prod_{i=1}^j t_i \right]^{\beta_1} \cdot \left[ \prod_{i=j+1}^n t_i \right]^{\beta_2}$ , for  $j = 1, \dots, n-1$ .

Thus, the procedure for the a posteriori  $B_{10} > \tau$ , estimate a change-point  $\tau$  by using

$$\tau = E(\tau|D_{(0,T)}) = A/B, \tag{4}$$

here

$$\begin{aligned} A &= \int_{[0,t_1)} \int_0^\infty \int_0^\infty \frac{2}{(\alpha + \beta_1)^3} \cdot \frac{2\beta_2^n}{(\alpha + \beta_2)^3} \cdot \frac{\prod_{i=1}^n t_i^{\beta_2}}{K_1} d\beta_1 d\beta_2 \tau d\tau \\ &+ \sum_{j=1}^{n-1} \int_{[t_j, t_{j+1})} \int_0^\infty \int_0^\infty \frac{2\beta_1^j}{(\alpha + \beta_1)^3} \cdot \frac{2\beta_2^{n-j}}{(\alpha + \beta_2)^3} \cdot \frac{q_j}{K_1} d\beta_1 d\beta_2 \tau d\tau \\ &+ \int_{[t_n, T)} \int_0^\infty \int_0^\infty \frac{2\beta_1^n}{(\alpha + \beta_1)^3} \cdot \frac{2}{(\alpha + \beta_2)^3} \cdot \frac{\prod_{i=1}^n t_i^{\beta_1}}{K_1} d\beta_1 d\beta_2 \tau d\tau, \\ B &= \int_{[0,t_1)} \int_0^\infty \int_0^\infty \frac{2}{(\alpha + \beta_1)^3} \cdot \frac{2\beta_2^n}{(\alpha + \beta_2)^3} \cdot \frac{\prod_{i=1}^n t_i^{\beta_2}}{K_1} d\beta_1 d\beta_2 d\tau \\ &+ \sum_{j=1}^{n-1} \int_{[t_j, t_{j+1})} \int_0^\infty \int_0^\infty \frac{2\beta_1^j}{(\alpha + \beta_1)^3} \cdot \frac{2\beta_2^{n-j}}{(\alpha + \beta_2)^3} \cdot \frac{q_j}{K_1} d\beta_1 d\beta_2 d\tau \\ &+ \int_{[t_n, T)} \int_0^\infty \int_0^\infty \frac{2\beta_1^n}{(\alpha + \beta_1)^3} \cdot \frac{2}{(\alpha + \beta_2)^3} \cdot \frac{\prod_{i=1}^n t_i^{\beta_1}}{K_1} d\beta_1 d\beta_2 d\tau. \end{aligned}$$

### 4 Simulation Results

Each simulated dataset consists of two parts for different shape parameter values of the test function of the parameter process. We expect to detect a change point under the plot where the shape parameter value changes. The hyperparameters for the prior of the shape parameter are fixed as  $(\xi, \nu) = (1, 1)$

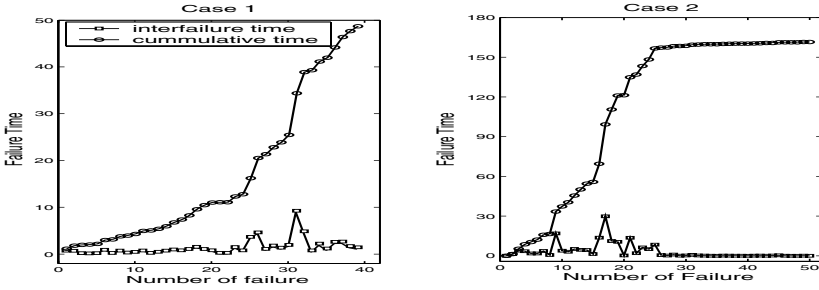


Fig. 1. The plots of simulated datasets with a single changepoint

**Case 1.** We fix the scale parameter as  $\alpha = 1$ . The datasets are generated with  $\beta = 1$  and  $\beta = 2$ , respectively. Each dataset size is 200 since the maximum likelihood estimates of  $(\alpha, \beta)$  are  $(.47, .)$  and  $(.7, .24)$  respectively. It seems that the data are fairly well generated. The time taken for the complete datasets  $(1, 48.8)$  to detect a change point using a res factor for the complete datasets  $(1, 48.8)$ , the res factor is  $1.2$  b  $(1)$  and the estimated change point is  $2.28$  b  $(4)$ . Here it is associated between the  $2^{th}$  and  $24^{th}$  bser at  $(1)$  and  $2$  a t t. b u d a detect. s stem f r s e q u e n t a d a t a. h u s w e a s s u m e t o d e t e c t a c h a n g e a t t h e  $2^{th}$  b s e r a t. i n t h e f i r s t t. t h e  $2^{th}$  b s e r a t. i n t h e r e s f a c t o r s  $4.2$  a d a c h a n g e p o i n t s i s  $.8$  b  $(1, .74)$ . Note that the posterior of the change point estimated through the  $2^{th}$  complete bser at  $(1)$  is almost the same as that through the complete data. This demonstrates that the proposed approach can promptly and correctly detect the change.

**Case 2.** Scale parameter  $\alpha = 1$ , shape parameter  $\beta = 1$  and 2. Complete dataset size is 200. For  $(\alpha, \beta) = (1, .)$ ,  $(.7, .887)$ , time taken for complete data  $(1, .47)$ , res factor is  $1.21$  b  $(1)$  and the estimated change point is  $2.28$  b  $(4)$ . Here it is associated between the  $24^{th}$  and  $2^{th}$  bser at  $(1)$ , change detected at  $2^{th}$  bser at  $(1)$ ,  $B_{10}$  and  $\tau$  is  $10$  and  $10$  respectively. The first time the  $2^{th}$  bser at  $(1)$  is  $8$  and  $28$  (between the  $24^{th}$  and  $2^{th}$  bser at  $(1)$ ).

### 5 Conclusion

In this paper we have proposed a res factor approach for detecting change point in the parameter process of the test function. The simulation results show that the proposed method can detect change point as soon as the res factor becomes greater than

Computer simulation verified the effectiveness and correctness of the proposed approach. This procedure of change point detection is applicable to the complete data set available.

## References

1. Crow, L. H., "Reliability Analysis of Complex Repairable System," *Reliability and Biometry*, Poroschan, F. and Serfling, R. J., (Eds.), SIAM, Philadelphia, 379-410 (1974).
2. Hassan Hajji, B. H. Far, and Jingde Cheng, "Detection of network faults and performance problems," *Proceedings of the Internet Conference*, Osaka, Japan., November 2001.
3. Yang, T. Y. and Lynn, K., "Bayesian Binary Segmentation Procedure for a Poisson Process with Multiple Changepoints," *Journal of Computational and Graphical Statistics*, **10**, No. 10, 772-785 (2001).



# Author Index

- Abawajy, J.H. III-205, III-213, III-447, III-457  
Abrahamyan, Lilit I-287  
Absil, P.-A. I-33  
Adamidis, Panagiotis II-1064  
Agron, Paul I-1019  
Ahn, JinHo III-679  
Ahn, Seongjin III-1072  
Ahn, Tae-Chon I-798  
Ahn, Youngjin III-796  
Akay, Bulent I-147  
Akbari, Mohammad K. III-205  
Akinlar, Cuneyt I-396  
Akyol, Derya Eren III-562  
Alam, Sadaf I-304  
Alberti, Pedro V. I-229  
Alexandrov, Natalia I-1051  
Alexandrov, Vassil N. III-359, III-367, III-350, III-743, III-752, III-766  
Alfonsi, Giancarlo I-623  
Ali, Hesham H. II-927  
Alique, J.R. III-627  
Alique, Angel III-1056  
Allen, Robert B. II-976  
Aloisio, Giovanni II-10  
Alonso, Pedro I-220  
Alpbaz, Mustafa I-147  
Altınakar, Mustafa Siddik III-33  
Al Zain, A. II-748  
Amik, St.-Cyr III-57  
Ammari, Nisreen I-493  
An, Beongku III-1060  
Anagnostopoulos, Christos-Nikolaos I-695  
Anagnostopoulos, Ioannis I-695  
Anai, Hirokazu III-602  
Andrés, Mirian III-635  
Andrews, Christopher I-1011  
Anh, Le Tuan II-436  
Anthes, Christoph III-350, III-383  
Arickx, F. II-1080  
Asirvatham, Arul II-265  
Atanassov, Emanouil III-735, III-752  
Attali, Isabelle I-526  
Aznar, Fidel I-828  
Babu, V. III-72  
Bação, Fernando III-476  
Bachmair, Leo I-1019  
Backeljauw, Franky I-295  
Bae, Hae-Young I-405  
Bae, Juhee III-842  
Bagheri, Babak II-44  
Bai, Li II-273  
Baik, Ran I-1, III-899  
Baik, Sung Wook III-850, III-1016, III-1064  
Baker, C.G. I-33  
Bala, Jerzy III-1016, III-1064  
Baldrige, Kim II-672  
Balas, Can Elmar I-892, III-1108  
Balint-Kurti, Gabriel III-933  
Bamha, M. II-755  
Bang, Young-Cheol III-796  
Bangerth, Wolfgang II-656  
Banicescu, Ioana I-237  
Bansevicius, Ramutis III-643  
Bao, Lichun II-485  
Bao, Hujun II-248  
Barros, Ligia I-727  
Barsky, Brian A. II-224  
Bartholet, Robert II-721  
Barvík, Ivan I-860  
Basak, Tanmay II-814  
Basney, Jim I-501, II-729  
Bastiaans, R.J.M. III-64  
Basu, P.K. I-172  
Batchelor, Donald B. I-372  
Bauer, Sebastian II-1064  
Baumgartner, Gerald I-155  
Bawa, Rajesh K. III-1104  
Bayhan, Gunhan Mirac I-843, III-562  
Beerli, Peter III-775  
Bein, Doina I-560, II-535  
Bein, Wolfgang W. II-535  
Bektaş, Tolga I-188  
Belkasim, Saeid O. II-256

- Bellomo, Carryn III-1096  
 Benassarou, A. II-314  
 Bennethum, Lynn S. II-632  
 Benoit, Anne II-764  
 Bereg, Sergey II-851  
 Berkenbrock, C.D.M. III-987  
 Bernholdt, David E. I-155, I-372  
 Bernreuther, Martin II-1  
 Berry, Lee A. I-372  
 Berzins, M. II-36  
 Beyls, Kristof II-166  
 Bhana, Ismail III-391  
 Bianchini, Germán I-427  
 Billiet, David II-1046  
 Bindel, David S. I-50  
 Birnbaum, Adam II-672  
 Bischof, Hans-Peter I-703  
 Bittar, E. II-314  
 Blais, J.A.R. I-74  
 Blin, Guillaume II-860  
 Bloomfield, Max O. III-49  
 Boettcher, Stefan II-386  
 Bogdanov, Alexander III-933  
 Bolvin, Hervé I-271, I-639  
 Bonizzoni, Paola II-952  
 Borisov, Sergey III-143  
 Bourchtein, Andrei I-131  
 Bourdot, Patrick II-290, II-339  
 Bourilkov, Dimitri III-342  
 Box, Frieke M.A. I-287  
 Branford, Simon III-743, III-752  
 Breitenbach, Mark L. III-41  
 Brenk, Markus II-1  
 Brinza, Dumitru II-1011  
 Broeckhove, Jan II-1072, II-1080  
 Brogan, David II-721  
 Broszkiewicz, Magdalena III-1112  
 Browne, James C. I-347  
 Brzeziński, Jerzy III-423  
 Bu, Jiajun III-806  
 Buckley, William R. II-395  
 Bungartz, Hans-Joachim II-1  
 Byrski, Aleksander III-703  
 Byun, Daewon II-814  
 Byun, Yanga I-948  
  
 Cafaro, Massimo II-10  
 Cai, Guoyin III-496, III-883  
 Cai, Hongming II-335  
 Cai, Keke III-806  
  
 Cai, Liming II-968  
 Cale, Timothy S. III-41, III-49  
 Calleja, Mark III-359  
 Campa, Sonia II-772  
 Canning, Andrew III-317  
 Cantillo, Karina III-1056  
 Canton-Ferrer, Cristian II-281  
 Cao, Chunxiang III-464, III-472  
 Cao, Wuchun III-464, III-472  
 Cariño, Ricolindo L. I-237  
 Carmichael, Gregory R. II-648  
 Carnahan, Joseph II-721  
 Caromel, Denis I-526  
 Casale, Giuliano III-147  
 Casas, Josep R. II-281  
 Castelló, Pascual II-240  
 Catalyurek, Umit II-656  
 Caymes, Paola II-132  
 Čepulkauskas, Algimantas III-643  
 Cetnarowicz, Krzysztof III-711  
 Chae, OkSam I-1035  
 Chai, Tianfeng II-648  
 Chambarel, André I-271, I-639, I-647  
 Chandra, Krishnendu I-493  
 Chaturvedi, A.R. II-695  
 Chen, J. III-1076  
 Chen, Chongcheng I-979  
 Chen, Chun I-552, III-806  
 Chen, Deren III-221  
 Chen, Huoping I-615  
 Chen, Jian III-578  
 Chen, Meng Chang II-444  
 Chen, Mingshi II-632  
 Chen, Pu III-300  
 Chen, Cai Min Yu III-187  
 Chen, Ying III-187  
 Chen, Shangjian I-568  
 Chen, Shudong I-544  
 Chen, Yen Hung II-845  
 Chen, Zhengxin III-548  
 Chen, Zizhong I-115  
 Cheng, Hwai-Ping I-460  
 Cheng, Jing-Ru C. I-460  
 Chi, Hongmei III-775  
 Childs, Stephen III-870  
 Chin, Francis Y.L. II-985  
 Chinchalkar, Shirish II-76  
 Chinnusamy, Malar II-60  
 Cho, Ju III-1016, III-1064  
 Cho, Haengrae III-1012

- Cho, Jung-Wan III-407  
 Cho, Sunyoung I-941  
 Cho, We Duke I-576  
 Cho, YoungTak I-1035  
 Choi, Dong Ju II-672  
 Choi, Hongsik I-419  
 Choi, Hyoung-Kee II-453  
 Choi, Jaeyoung III-916  
 Choi, Jihyun III-196  
 Choi, Kee-Hyun III-346, III-950, III-963  
 Choi, Ki-Young III-866  
 Choi, Min-Hyung I-735  
 Choi, Sung Chune III-1000  
 Choo, Hyunseung II-468, II-510, II-559,  
 III-796, III-1120  
 Chover, Miguel II-240  
 Chtepen, Maria III-1116  
 Chung, Min Young II-559, II-601,  
 III-1120  
 Cicalese, Ferdinando II-1029  
 Cigciwa, Renata III-711  
 Çinar, Ahmet III-945  
 Claeys, Filip III-1116  
 Clark, Terry II-44  
 Coen, Janice L. II-632  
 Coghlan, Brian III-870  
 Cohen, Jared III-838  
 Cole, Martin J. II-640  
 Cole, Murray II-764  
 Coleman, Thomas F. II-76  
 Coles, Jonathan I-703  
 Collier, Rem III-695  
 Collins, Lori III-983  
 Collura, F. III-267  
 Constantinescu, Emil M. II-648, II-798  
 Contes, Arnaud I-526  
 Convard, Thomas II-290  
 Cooke, Daniel E. III-891  
 Cooper, Rodney I-1011  
 Cortés, Ana I-427  
 Cortas, Maria I-58  
 Costa, Rosa Maria I-727  
 Cucos, Laurentiu I-322, III-991  
 Cui, Yong II-551  
 Cunha, Gerson I-727  
 Cuyt, Annie I-295  
 Cyganek, Bogusław I-757  
 Dăescu, Dacian N. II-648, II-837  
 Dai, Hongning III-875  
 Dai, Yang II-903  
 Damaschke, Peter II-1029  
 Dantas, Mario A.R. III-858, III-971,  
 III-987  
 D'Apice, C. III-594  
 Darema, Frederica II-610  
 Das, Kamakhya I-493  
 DasGupta, B. II-1020  
 Dass, Rajanish III-818  
 Datta, Ajoy K. I-560  
 Datta, Karabi I-1, III-899  
 Dauger, Dean E. II-84  
 Day, Mitch D. II-68  
 D'Azevedo, Eduardo F. I-99, I-372  
 Deconinck, Herman I-279  
 Decyk, Viktor K. II-84  
 de Doncker, Elise I-123, I-165, I-322,  
 III-991  
 de Goey L.P.H. III-64  
 delaRosa, J.J. I-585  
 de-la-Rosa, Juan-José González  
 I-900  
 De Leenheer, Marc III-250  
 Demeester, Piet III-250, III-1116  
 Demmel, James W. I-50  
 Deng, Ansheng I-783  
 Deng, Zhiqun III-854  
 Deris M. Mat III-447  
 Deslongchamps, Ghislain I-1011  
 Desovski, D. I-180  
 De Turck, Filip III-250  
 Dhoedt, Bart III-250, III-1116  
 D'Hollander, Erik H. II-166  
 Dikaiakos, Marios I-534, III-870  
 Dimov, I. III-752  
 Ding, Koubao III-954  
 Ding, Yongsheng I-517  
 Dobson, James E. II-99  
 Dondi, Riccardo II-952  
 Dong, JinXiang I-671  
 Dongarra, Jack I-115, III-317  
 Donnell, Barbara P. I-66  
 Douglas, Craig C. II-632, II-640  
 Dove, Martin T. III-359  
 Droegemeier, Kelvin II-624  
 Durvasula, Shraavan I-493  
 Dyapur, Kaviraju Ramanna III-879  
 Efendiev, Yalchin II-640  
 Effinger-Dean, Laura II-107

- El-Aker, Fouad III-788  
 Elwasif, Wael R. I-372  
 Engelmann, Christian I-313  
 Epicoco, Italo II-10  
 Erciyes, Kayhan I-196, I-388  
 Eriksen, Jeff I-631  
 Ertunc, Suna I-147  
 Evans, Deidre W. III-775  
 Ewing, Richard II-640
- Fabricius, Uwe II-27  
 Fahey, Mark R. I-99  
 Fang, Liqun III-464, III-472  
 Fang, Yong III-554  
 Farago, Paula I-727  
 Farhat, C. II-616  
 Farid, Hany II-99  
 Fayyad, Dolly I-58  
 Feng, Dingwu III-887  
 Feng, Shengzhong III-979  
 Feng, Yusheng I-347  
 Fertin, Guillaume II-860  
 Filatyev, S.A. II-695  
 Fleming, Charles III-760  
 Flores-Becerra, G. I-17  
 Floudas, Christodoulos A. II-680  
 Fox, Geoffrey II-576, III-275, III-431  
 Frączek, Jacek III-334  
 Franca, Leopoldo P. II-632  
 Freedman, Jim II-703  
 Freeman, T.L. I-364  
 Frels, Judy II-378  
 Freundl, Christoph II-27  
 Friedman, Mark J. I-50, I-263  
 Fu, Chong, III-1044  
 Fujimoto, Junpei I-165  
 Funika, Włodzimierz II-158
- Galán, Ramón III-1056  
 Galiana, Isidro Lloret I-900  
 Galis, Alex III-259  
 Gallivan, K.A. I-33  
 Galvez, Akemi III-651  
 Gannon, Dennis II-624  
 Gansterer, Wilfried N. I-25  
 Gao, Chongnan III-163  
 Gao, Lei I-517  
 García, Victor M. I-17, I-229  
 García, Pedro III-246  
 Gargantini, Irene II-331
- Gargiulo, G. III-594  
 Gashkov, Igor III-663  
 Gaudiot, Jean-Luc I-212  
 Gava, Frédéric II-1046  
 Gaynor, Mark II-703  
 Geist, Al I-313  
 Gerasimova, Olesya III-143  
 Gevorkyan, Ashot III-933  
 Ghosh, Debi Prasad III-1  
 Giesbrecht, Mark III-619  
 Ginsberg, Myron I-1059  
 Ginting, Victor II-640  
 Glasner, Christian II-124  
 Gobbert, Matthias K. III-41  
 Gorbachev, Yuriy III-933  
 Gore, J.P. II-695  
 Gorissen, Dirk II-1072  
 Goscinski, Andrzej M. I-435  
 Govaerts, Willy J.F. I-50, I-263  
 Grama, Ananth II-664  
 Graves, Sara II-624  
 Grimshaw, Andrew II-729  
 Grochowski, M. III-727  
 Gross, Murray III-983  
 Grzymkowski, Radosław III-895  
 Guan, Xiaohui I-743  
 Guan, Yanning I-908  
 Guleren, Kursad Melih III-130  
 Gullaude, T. II-616  
 Guo, S.M. III-104  
 Guo, Jianping III-464, III-472  
 Guo, Shan I-908  
 Guo, Yuanbo III-229  
 Gurd, John R. I-364  
 Gyllenhaal, John II-140  
 Górriz, Juan Manuel I-585, I-900
- Ha, Sang Yong II-510  
 Haber, R.H. III-627  
 Haber, Rodolfo E. III-627, III-1056  
 Hadjarian, A. III-1064  
 Haffegge, Adrian III-350  
 Hains, G. II-755  
 Hakobyan, Tigran III-933  
 Han, Hyuck III-179  
 Han, Kijun II-585  
 Han, Kyungsook I-711, I-948, III-1024,  
 III-1028  
 Han, Seung Kee I-941  
 Hanna, A. II-695

- Hapoglu, Hale I-147  
 Hardie, Patrick I-364  
 Härdtlein, Jochen II-1055  
 Hariri, Salim I-615  
 Hartono, Albert I-155  
 Harvill, Jane L. I-237  
 Hasan, S. Mehmood III-359  
 Haupt, Tomasz I-493  
 Hayashida, Ulisses Kendi I-509  
 He, Jingwu II-1011  
 He, You I-812  
 He, Yuanjun II-335  
 Heath, Michael T. II-52  
 Heine, Felix III-155  
 Heisler, Debra II-378  
 Hellinckx, P. II-1080  
 Hensley, Jeffrey L. I-66  
 Heo, Hoon I-1035  
 Herrero, Pilar III-171  
 Heřman, Pavel I-860  
 Hiebeler, David II-360  
 Hilaire, Vincent III-719  
 Hirata, So I-155  
 Hoekstra, Alfons G. I-287  
 Hoffmann, Christoph II-664  
 Hong, Choong Seon II-436  
 Hong, Feng III-875  
 Hong, Helen I-719, III-834, III-842  
 Hong, Jinsun III-1024  
 Hong, Min I-735  
 Hong, Yoopyo I-1, III-899  
 Hoppe, Hugues II-265  
 Horie, Ken III-570  
 Horiguchi, Susumu II-781  
 Horntrop, David J. I-852  
 Hou, Qibin II-273  
 Houlberg, Wayne A. I-372  
 Houstis, E. II-616  
 Hovestadt, Matthias III-155  
 Howington, Stacy E. I-66  
 H'sien, J. Wong I-1067  
 Hu, Bao-Gang II-322  
 Hu, Hualiang III-221  
 Hu, Jinfeng III-163  
 Hu, Xiaohua II-976  
 Hu, Yincui III-496, III-883  
 Hua, Wei II-248  
 Huang, Changqin III-221, III-887  
 Huang, He III-578  
 Huang, Houkuan I-995  
 Huang, Kuen-Yu III-292  
 Huang, Linpeng III-875, III-1032  
 Huang, Tianqiang I-979  
 Hueso, E. II-689  
 Humphrey, Marty I-477, I-501, II-729  
 Hung, Shao-Shin III-830  
 Hunter, Robert M. I-460  
 Huo, Mingxu III-954  
 Hwang, In-Chul III-407  
 Hwang, Kai III-187  
 Hwang, Sang-Jun I-380  
 Hwang, Tsung-Min III-908  
 Hyndman, Rob J. III-792  
 Iglesias, Andrés III-651  
 Ivanovska, Sofiya III-735  
 Jackson, Steven Glenn III-611  
 Jaeger, E.F. I-372  
 Jaeger, Marc II-322  
 Jamieson, Ronan III-350  
 Janicki, Aleksander III-1112  
 Janik, Arkadiusz II-158  
 Jardin, S.C. III-1076  
 Javadi, Bahman III-205  
 Jeffrey, D.J. III-586, III-667  
 Jenkins, Jerry III-309  
 Jeon, Hoseong II-468  
 Jeon, Il-Soo III-912  
 Jeon, Sung-Eok III-279  
 Jeong, Chang-Sung III-862, III-866  
 Jeong, Hae-Duck J. I-655  
 Jeong, Hong-Jong II-477  
 Jeong, Kwang Cheol II-510  
 Jessup, E.R. II-91  
 Jho, CheungWoon II-327  
 Ji, Chuanyi III-279  
 Jia, Jinyuan II-298  
 Jiang, Hong II-519  
 Jiang, Qingshan III-801  
 Jiao, Xiangmin II-52  
 Jin, Xiaogang I-599  
 John, N.W. II-314  
 Johns, Craig J. II-632  
 Johnson, Chris R. II-36, II-640  
 Johnson, David III-391  
 Joneja, Ajay II-298  
 Jones, Greg II-640  
 Ju, Byoung-Hyon I-711

- Ju, Jianwei I-82  
 Jung, Hanjo III-407  
 Jung, Hyungsoo III-179  
 Jung, Hyunjoon III-179  
 Jung, Moon-Ryul II-216  
 Jung, Sunhwa I-735  
 Jung, Youn Chul II-568
- Kacsuk, Peter III-367  
 Kaiser, Tim I-469  
 Kalyanasundaram, Anand I-493  
 Kang, Hwan II I-593  
 Kang, Jung-Yup I-212  
 Kang, Sanggil I-971  
 Kang, Yan I-783  
 Kao, Odej III-155  
 Kara, İmdat I-188  
 Karaata, Mehmet H. I-560  
 Karaivanova, Aneta III-735, III-766  
 Karl, Wolfgang II-174, II-182  
 Karniadakis, G.E. II-689  
 Kasperska, Elżbieta I-837, III-1040  
 Kasproski, Paweł III-334  
 Katz, Paul S. II-347  
 Kaugars, Karlis I-123  
 Kayafas, Eleftherios I-695  
 Kemmler, Dany II-1064  
 Kenny, Eamonn III-870  
 Kim, Byung-yeub II-477  
 Kim, Chong-Kwon II-527  
 Kim, Do-Hyeon III-1060  
 Kim, Dongkyun II-477  
 Kim, Hyun-Ki III-1100  
 Kim, Hyun-Sung III-912  
 Kim, Hyunjue II-493  
 Kim, Hyunsook II-585, III-1125  
 Kim, Intaek I-593  
 Kim, Jai-Hoon II-576, III-275  
 Kim, Jang-Sub II-601  
 Kim, Jung Ae I-941  
 Kim, Jungkee III-431  
 Kim, Kyung-ah II-527  
 Kim, Minjeong II-632  
 Kim, Moonseong III-796  
 Kim, Munchurl I-971  
 Kim, Sangjin III-958  
 Kim, Seungjoo II-493  
 Kim, Sun Yong II-543  
 Kim, Taekyun III-958  
 Kim, Tongsook II-527
- Kim, Ungmo II-568, III-813  
 Kim, Yongkab I-792  
 Kim, Yoonhee III-920  
 Kimpe, Dries I-279  
 Kincaid, Rex K. I-1051  
 Kirby, R.M. II-36  
 Kisiel-Dorohinicki, Marek III-703  
 Klie, Hector II-656  
 Kluge, Michael I-330  
 Knight, John C. II-729  
 Knüpfer, Andreas I-330, II-116  
 Knyazev, Andrew V. II-632  
 Ko, Hanseok I-139  
 Ko, Sunghoon II-576, III-275  
 Kohl, James A. I-372  
 Koker, Utku III-562  
 Kolditz, Olaf II-1064  
 Kolli, Vijaya Smitha II-1003  
 Konwar, K.M. II-1020  
 Koo, Jahwan III-1072  
 Kosloff, Todd J. II-224  
 Köstler, Harald II-27  
 Kotulski, Leszek III-1008  
 Kou, Gang III-548  
 Koukam, Abder III-719  
 Koutsonas, Athanassios I-695  
 Kozlowski, Alex II-224  
 Krause, Tara II-428  
 Kremens, Robert II-632  
 Krysl, Petr II-672  
 Kuhara, Satoru II-911  
 Kulikov, Gennady Yur'evich  
   I-42  
 Kulkarni, Vaibhav II-632  
 Kulvietienė, Regina III-643  
 Kulvietis, Genadijus III-643  
 Kuo, Ting-Chia III-830  
 Kurc, Tahsin II-656  
 Kuznetsov, Yuri A. I-50, I-263  
 Kwon, Ki Woon III-850  
 Kwok, Yu-Kwong III-187  
 Kye, Heewon III-834, III-842
- Labahn, George III-619  
 Lai, Kin Keung III-523  
 Laidlaw, D.H. II-689  
 Lam, Chi-Chung I-155  
 Lambrakos, Sam II-738, III-80  
 Lambris, John D. II-680  
 Landau, Luiz I-727

- Lane, Terran II-894  
 Langemyr, Lars III-129  
 Langer, Malgorzata I-607, I-876  
 Langou, Julien III-317  
 Lani, Andrea I-279  
 Lapenta, Giovanni I-82, III-88  
 Lazarov, Raytcho II-640  
 LeBoeuf, Eugene J. I-172  
 Leduc, Guy III-237  
 Lee, Donghoon I-711  
 Lee, DongWoo III-196  
 Lee, Eunseok III-1052  
 Lee, Heungkyu I-139  
 Lee, In-Kwon I-916  
 Lee, Jee-Hyong II-543  
 Lee, JeongHeon I-1035  
 Lee, Jeongjin I-719  
 Lee, Jong-Suk R. I-655  
 Lee, Sang Kun I-941  
 Lee, Sangho III-1012  
 Lee, Sangkeon III-916  
 Lee, Seong-Whan III-850  
 Lee, Seunghwa III-1052  
 Lee, Seungsoo II-559  
 Lee, Soo Myoung I-576  
 Lee, Tae-Dong III-862, III-866  
 Lee, Tae-Jin II-559, III-1120  
 Lees, J.M. I-751  
 Lefeuvre-Mesgouez, Gaëlle I-647  
 Lei, Zhengdeng II-903  
 Lestrade, John Patrick I-237  
 Leupi, Célestin III-33  
 Lewis, Gareth J. III-359, III-367  
 Li, Degao III-783  
 Li, Guoqing III-484, III-492  
 Li, Jianping III-531  
 Li, Minglu III-875  
 Li, Peiyu I-568  
 Li, Shanping III-995  
 Li, Shuhui I-372  
 Li, Shujun I-123, I-165  
 Li, Su-Ju III-1044  
 Li, Xiaowen III-464, III-472  
 Li, Xin III-801  
 Li, Yifeng II-927  
 Li, Yiming III-292, III-300  
 Li, Yusong I-172  
 Lian, HeSong I-593  
 Liao, Shenghui I-671  
 Liao, Wenyuan II-648, II-806  
 Lim, Byong-In III-346, III-963  
 Lim, Jeongyeon I-971  
 Lim, Joong-Ho III-862  
 Lim, Jungmuk II-468  
 Lin, Huaizhong I-552, II-461  
 Lin, Lanfen I-671  
 Lin, Xin III-995  
 Linke, Alexander II-1055  
 Lisik, Zbigniew I-607, I-876  
 Liu, Chunmei II-968  
 Liu, Damon Shing-Min III-830  
 Liu, Dingsheng III-484, III-492  
 Liu, Haifeng II-877  
 Liu, Hua II-248  
 Liu, Hui II-1003  
 Liu, Jiangui I-908  
 Liu, Mingzhe II-420  
 Liu, Qi II-368  
 Liu, Tom III-112  
 Liu, Xinchun II-869  
 Liu, Xumin I-995  
 Liu, Yanfei III-1068  
 Liu, Zheng II-829  
 Liu, Zhuo II-837  
 Lobo, Victor III-476  
 Loidl, H-W. II-746  
 Loitière, Yannick II-721  
 Lombardo, S. III-267  
 Lopez-Parra, Fernando III-120  
 Loulergue, Frédéric II-1046  
 Loumos, Vassily I-695  
 Lu, Hsueh-I II-845  
 Lucas, L. II-314  
 Luján, Mikel I-364  
 Lukac, Rastislav I-679, I-687, II-886  
 Luke, Edward A. II-790  
 Luo, Jiancheng I-963  
 Lou, Xiasong III-187  
 Luo, Ying III-496  
 Luo, Yingwei III-511, III-515  
 Luque, Emilio I-427, II-132  
 lv, Yong III-937  
 Ma, Bin II-960  
 Ma, Fanyuan I-544  
 Ma, Jianfeng III-229  
 Ma, Lizhuang III-846  
 Ma, Yongquan III-163  
 Machi, A. III-267  
 Maeng, Seung-Ryoul III-407

- Mahanti, Ambuj III-818  
 Mahapatra, Debiprosad Roy III-1,  
 III-25  
 Mahawar, Hemant I-107  
 Mahmood, Nasim I-347  
 Majumdar, Amit II-672  
 Malkowski, Konrad I-245  
 Malladi, Srilaxmi II-535  
 Malm, Nils III-129  
 Malmberg, Russell L. II-968  
 Malony, Allen I-631  
 Mamat, R. III-447  
 Mandel, Jan II-632  
 Măndoiu, Ion I. II-994, II-1020  
 Mansfield, Peter II-76  
 Manzo, R. III-594  
 Mao, Weidong II-1011  
 Mao, Zhihong III-846  
 Marchesini, John C. II-99  
 Margalef, Tomàs I-427, II-132  
 Mariani, Lorenzo II-952  
 Marín, Mauricio I-411, I-1003  
 Markidis, Stefano III-88  
 Marsh, David III-687  
 Marshall, Geoffrey I-388  
 Martin, S.M. III-64  
 Martin, Jonathan I-501  
 Martin, Sylvain III-237  
 Maruyama, Osamu II-911  
 Mascagni, Michael III-760, III-775  
 Masoumi, Beeta II-936  
 Mateja-Losa, Elwira III-1040  
 Mathee, Kalai II-944  
 Matossian, Vincent II-656  
 Matsuda, Akiko II-911  
 Matsuhisa, Takashi III-570  
 May, John II-140  
 Malysiak, Bożena III-334  
 Means, J. II-695  
 Mellema, A.K. II-695  
 Melnik, Roderick V.N. I-884, III-25,  
 III-134  
 Merkle, Daniel II-412  
 Mesgouez, Arnaud I-647  
 Metaxas, Dimitris II-712  
 Miaoliang, Zhu I-1027  
 Michaelson, G.J. II-746  
 Michaelson, Greg II-781  
 Michel, Olivier I-820  
 Michopoulos, John II-616, II-738,  
 III-80  
 Middendorf, Martin II-412  
 Min, Kyungha I-916, II-216  
 Min, Sung-Gi III-679  
 Min, Yong I-599  
 Ming, Dongping I-963  
 Mingarelli, Angelo B. II-351  
 Mondéjar, Rubén III-246  
 Moon, Sanghoon I-948, III-1064  
 Morajko, Anna II-132  
 Morales, J.D. I-585  
 Moreno-Hagelsieb, Gabriel III-134  
 Morikis, Dimitrios II-680  
 Morisse, Karsten III-375  
 Morley, C.T. I-751  
 Moulton, Steve I-703  
 Mrozek, Dariusz III-334  
 Mukherjee, Amar II-395  
 Mukherjee, Arup III-1084  
 Mukherjee, Sarit I-396  
 Muldoon, Conor III-695  
 Mundani, Ralf-Peter II-1  
 Muntean, Ioan Lucian II-1  
 Nagel, Wolfgang E. I-330  
 Nakhleh, Luay II-919  
 Nam, Hyunwoo I-941  
 Nam, Junghyun II-493  
 Nam, Young Jin III-439  
 Narasimhan, Giri II-944  
 Nassif, Nabil R. I-58  
 Natesan, S. III-1104  
 Naumann, Uwe I-338  
 Navon, I. Michael II-837  
 Neveux, Philippe I-271  
 Newman, Harvey III-196  
 Newman, Timothy S. I-9  
 Nguyen-Tuong, Anh II-729  
 Ni, Jun III-326  
 Nie, Changhai III-1088  
 Nielsen, Frank I-1019  
 Nikishkov, G.P. II-232, II-306  
 Ning, Ning III-163  
 Nishidate, Y. II-232  
 No, Jaechun I-380, I-485  
 Noël, Alfred G. III-611  
 Nooijen, Marcel I-155  
 Nyman, Gunnar III-933  
 Nystrom, J.F. III-1096



- Obeyesekere, Mandri III-96  
 O'Callaghan, David III-870  
 Ocampo, Roel III-259  
 Oh, Eunseuk I-419  
 Oh, Heekuck III-958  
 Oh, Sangyoon II-576, III-275  
 Oh, Sung-Kwun I-792, I-798, III-1080,  
 III-1100  
 O'Hare, Gregory M.P. III-687, III-695  
 Ohn, Kyungoh III-1012  
 O'Kane, Donal III-687  
 Okuda, Kunio I-509  
 Oliveira, Suely I-204  
 Owen, G. Scott I-451, II-256  
 Oysal, Yusuf I-775
- Paarhuis, B.D. I-868  
 Pachowicz, P. III-1064  
 Paik, Juryon III-813  
 Painho, Marco II-476  
 Pairot, Carles III-246  
 Pakin, Scott II-149  
 Pallickara, Sangmi Lee II-576, III-275  
 Pamplin, Jason A. II-347  
 Pan, Gang I-743  
 Pan, Michelle Hong II-1003  
 Pan, Xuezheng III-937  
 Pan, Yi II-1003  
 Pan, Yunhe III-1020  
 Pan, Zhijian II-404  
 Panetta, Jairo I-509  
 Parashar, Manish I-615, II-656  
 Pardàs, Montse II-281  
 Park, Byoung-Jun I-798, III-1100  
 Park, Byungkyu III-1028  
 Park, Chanik III-439  
 Park, Gyung-Leen II-468  
 Park, Ho-Sung I-792  
 Park, Hyoungwoo I-485  
 Park, Jeong-Su II-477  
 Park, Jong-An I-934  
 Park, Sang-Min I-477  
 Park, Seung-Jin I-934  
 Park, Soon-Young I-405  
 Park, Sung Soon I-380  
 Pascual, Vico III-635  
 Pasztor, Egon II-224  
 Patnaik, Kiran Kumar III-879  
 Patrick, Charles, Jr. III-96  
 Payne, Bryson R. I-451, II-256
- Pedrycz, Witold I-792, I-798, III-1100  
 Peng, Bo I-599  
 Peng, Gang III-995  
 Peng, Yi III-548  
 Percell, Peter II-814  
 Perelman, Alex II-224  
 Pérez, Jesús Fabián López III-924  
 Pérez, María S. III-171  
 Perminov, Valeriy III-139  
 Pernas, Ana Marilza III-858  
 Pflaum, Christoph II-1055  
 Phelan, Donnacha III-695  
 Pi, Daoying III-1036  
 Pieczynska-Kuchtiak, Agnieszka III-671  
 Ping, Lingdi III-937  
 Ping, Xiaohui III-975  
 Pinto, A.R. III-971  
 Pitsch, H. III-64  
 Pitzer, Russell M. I-155  
 Pivkin, I.V. II-689  
 Plale, Beth II-624  
 Plataniotis, Konstantinos N. I-679,  
 I-687, II-886  
 Pletzer, Alexander III-838  
 Poedts, Stefaan I-279  
 Prăjescu, Claudia II-994  
 Pratibha III-667  
 Praun, Emil II-265  
 Primavera, Leonardo I-623  
 Primeaux, David I-419  
 Provins, D.A. I-74  
 Pu, Jiantao II-343  
 Pujol, Mar I-828  
 Puntonet, Carlos García I-585, I-900
- Qiao, Ying I-90  
 Qin, Guan II-632  
 Qin, Xiaolin I-979  
 Qiu, Shibin II-894  
 Quarta, Gianvito II-10  
 Quigley, Geoff III-870  
 Quintino, Tiago I-279
- Raghavan, Padma I-245  
 Raj, Ewa I-876  
 Ramakrishna, R.S. III-196  
 Ramamurthy, Mohan II-624  
 Ramani, Karthik II-343  
 Ramanujam, J. I-155  
 Ramos, José Francisco II-240

- Reed, Dan II-624  
 Reggia, James II-378, II-404  
 Reiber, Johan H.C. I-287  
 Reid, G.J. III-586  
 Rendell, Alistair P. I-1067, II-18  
 Reyes, Nora I-1003  
 Reynolds, Paul II-721  
 Ribbens, Calvin J. II-60  
 Richards, David F. III-49  
 Richards, David R. I-460  
 Ridgway, Scott, L. II-44  
 Rizo, Ramón I-828  
 Rizzi, Romeo II-860  
 Robles, Víctor III-171  
 Rodosek, Robert I-804  
 Rodriguez, Sebastian III-719  
 Roh, Seok-Beom III-1080  
 Rojek, Gabriel III-711  
 Roman, Eric II-224  
 Romero, Ana III-635  
 Roper, James II-18  
 Ros, S. III-627  
 Rowanhill, Jonathan II-729  
 Rubio, Julio III-635  
 Rūde, Ulrich II-27  
 Rushton, J. Nelson III-891  
 Rutt, Benjamin II-656  
 Ryoo, SeungTaek II-327  
 Ryu, Jungpil II-585
- Sadayappan, P. I-155  
 Salman, Adnan I-631  
 Saltz, Joel II-656  
 Salvadores, Manuel III-171  
 Sameh, Ahmed I-33, II-664  
 Sandu, Adrian II-648, II-798, II-806,  
 II-829  
 Santini, Cindy I-469  
 Sarin, Vivek I-107  
 Sautois, B. I-263  
 Sazhin, Oleg III-143  
 Scaife, Norman II-781  
 Schaap, Jorrit A. I-287  
 Schaefer, R. III-727  
 Scheidler, Alexander II-412  
 Schreppers, Walter I-295  
 Schuetze, Hans-Joachim II-378  
 Schulz, Martin II-140  
 Schwarz, Phil III-112  
 Schwarz, Susan A. II-99
- Scott, Stephen L. I-443  
 Seber, Dogan I-469  
 Seinfeld, John H. II-648  
 Seltzer, Margo II-703  
 Sempf, Thomas III-375  
 Sengupta, Debasis III-309  
 Seo, Kyung-Sik I-934, III-822  
 Seok, Sang-Cheol I-204  
 Seyfarth, Benjamin Ray I-664  
 Sfarti, Adrian II-224  
 Shamonin, Denis I-287  
 Shang, Hui II-373  
 Sharma, Arjun II-107  
 Shen, Hao III-826  
 Shen, Hong II-985  
 Shen, Huifeng III-1020  
 Shi, Liang III-1088  
 Shi, Wei III-995  
 Shi, Xiaofeng III-854  
 Shi, Yong III-531, III-548  
 Shimizu, Yoshimitsu I-165  
 Shin, Dong-Ryeol II-601, III-346,  
 III-813, III-950, III-963  
 Shin, Ho-Jin III-950  
 Shin, Jitae II-453  
 Shin, Yeong Gil I-719, III-834, III-842  
 Shin, Young-Suk III-941  
 Shindin, Sergey Konstantinovich I-42  
 Shoshmina, Irina III-933  
 Shu, Jiwu III-399, III-415  
 Shvartsman, A.A. II-1020  
 Sibiryakov, Alexander I-155  
 Sim, Terence II-207  
 Simonov, Nikolai III-760  
 Sipos, Gergely III-367  
 Skarmeta, Antonio F. Gómez III-246  
 Sławińska, Magdalena I-355  
 Slood, Peter M.A. I-287, I-534  
 Słota, Damian I-837, III-659, III-895  
 Smith, Kate A. III-792  
 Smith, Sean W. II-99  
 Smolka, Bogdan II-886  
 Smolka, M. III-727  
 Sobaniec, Cezary III-423  
 Soboleva, Olga III-9  
 Song, Shanshan III-187  
 Song, Il-Yeol II-976  
 Song, Jeomki II-477  
 Song, Mao I-1027  
 Song, Min II-976

- Song, Siand Wun I-509  
 Song, Yinglei II-968  
 Soofi, M.A. I-74  
 Soysert, Zehra I-196  
 Spet, Olivier I-1011  
 Spicher, Antoine I-820  
 Spiegl, Edith II-124  
 Srinivasan, Gopalakrishnan III-1  
 Srinivasan, Kasthuri I-107  
 St.-Cyr, Amik II-822  
 Stankova, Elena III-933  
 Stevens, John G. III-1084  
 Stewart, Mark I-1043  
 Strahan, Robin III-695  
 Strauss, H.R. III-1076  
 Streit, Achim III-155  
 Stuer, Gunther II-1072, II-1080  
 Su, Fanjun III-937  
 Su, Xianchuang I-599  
 Subramani, K. I-180  
 Sun, Jing III-163  
 Sun, Ninghui II-869, III-979  
 Sun, Shuyu III-96  
 Sun, Yeali S. II-444  
 Sun, Yi III-492  
 Sun, Youxian III-1036  
 Sundaram, Shankar III-309  
 Sunder, C. Shyam III-72  
 Sunderraman, Rajshekhar II-347  
 Swain, W. Thomas I-443  
 Swaminathan, Gautam II-60  
 Swartz, S. II-689  
 Świącicki, Mariusz III-810  
 Székely, Gábor III-17  
 Szczerba, Dominik III-17  
  
 Takeuchi, Fumihiko I-956  
 Talay, A. Cagatay III-1004  
 Tan, Chew Lim II-207  
 Tan, Guangming II-869, III-979  
 Tan, Guozhen III-975  
 Tan, Haixia II-485  
 Tan, Shaohua I-90  
 Tang, Chuan Yi II-845  
 Tang, Jiakui III-496, III-883  
 Tang, Kai II-298  
 Tao, Jie II-174, II-182  
 Tarault, Antoine II-339  
 Teng, Jun II-322  
 Teow, Loo-Nin II-877  
  
 Teresco, James D. II-107  
 Thandavan, A. III-752  
 Thomas, Michael A. II-68, III-196  
 Thomas, Stephen J. I-256, II-822, III-57  
 Thysebaert, Pieter III-250  
 Tirado-Ramos, Alfredo I-534  
 Todd, Chris III-259  
 Tomov, Stanimire III-317  
 Tong, RuoFeng I-671  
 Tosik, Grzegorz I-607, I-876  
 Tracy, Fred T. I-66  
 Tran, Nick III-80  
 Trincă, Dragoş II-994  
 Trinder, P.W. II-746  
 Trivedi, Abhishek II-722  
 Trinitis, Carsten II-191  
 Tsechpenakis, Gabriel II-712  
 Tsompanopoulou, P. II-616  
 Tsouloupas, George I-534, III-870  
 Tucker, Don I-631  
 Tufo, H.M. II-91  
 Tuncel, Gonca I-843, III-562  
 Turan, Ali III-120, III-130  
 Turcotte, Marcel II-936  
 Turovets, Sergei I-631  
 Twerda, A. I-868  
 Tynan, Richard III-687  
  
 Uhruski, P. III-727  
 Urmetzer, Florian III-367  
 Usman, Anila I-364  
 Utke, Jean I-338  
  
 Vaccaro, Ugo II-1029  
 Vandeputte, Frederik II-166  
 van der Geest, Rob J. I-287  
 Vandewalle, Stefan I-279  
 Vanmechelen, Kurt II-1072, II-1080  
 van Oijen J.A. III-64  
 Vanrolleghem, Peter III-1116  
 Varadarjan, Srinidhi II-60  
 Varotsos, Costas III-504  
 Vedova, Gianluca Della II-952  
 Venetsanopoulos, Anastasios N. II-886  
 Vetter, Jeffrey I-304, I-868  
 Vézien, Jean-Marc II-290, II-339  
 Vialette, Stéphane II-860  
 Vidal, Antonio Manuel I-17, I-220, I-229  
 Vodacek, Anthony II-632  
 Volckaert, Bruno III-250

- Volkert, Jens II-124, III-383  
 Vuik, C. I-868
- Wainer, Gabriel II-368, II-373  
 Wais, Piotr III-810  
 Wajs, Wiesław III-810  
 Walkowiak, Krzysztof III-1092  
 Walsh, John III-870  
 Wang, Dongsheng III-163  
 Wang, Guangming I-987  
 Wang, Hao II-851  
 Wang, Jianqin III-472, III-496  
 Wang, Jinlong III-1020  
 Wang, Lei I-568  
 Wang, Li-San II-919  
 Wang, Lin-Wang III-317  
 Wang, Linxiang I-884  
 Wang, Min I-963  
 Wang, Qing II-248  
 Wang, Qinmin I-979  
 Wang, Ruili II-420  
 Wang, Shaowen III-326  
 Wang, Shou-Yang III-523, III-539,  
 III-554  
 Wang, Wei I-987  
 Wang, Weichung III-908  
 Wang, Wenqing II-1064  
 Wang, Xianqing III-887  
 Wang, Xiao-jing I-812  
 Wang, Xiaolin III-511, III-515  
 Wang, Xiaozhe III-792  
 Wang, Yadi III-229  
 Wang, Yangsheng II-273  
 Wang, Yanguang III-496  
 Wang, Yi III-875  
 Wang, Yong II-944  
 Warfield, Simon K. II-672  
 Wasson, Glenn II-729  
 Watson, James V.S. I-477  
 Wawrzyniak, Dariusz III-423  
 Webber, Robert E. II-331  
 Weber, Irene I-451  
 Weeks, Michael C. II-256  
 Wei, Guiyi I-987  
 Wei, Xilin III-134  
 Weidendorfer, Josef II-191  
 Weihrauch, Christian III-743, III-752  
 Weinstein, R. II-689  
 Wheeler, Mary F. II-656, III-96  
 Whitlock, P.A. III-983
- Wilhelmson, Bob II-624  
 Wiszniewski, Bogdan I-355  
 Witulam, Roman III-659  
 Woitaszek, M.S. II-91  
 Wojtowicz, Hubert III-810  
 Won, Dongho II-493  
 Wong, Adam K.L. I-435  
 Woodward, Jeffrey B. II-99  
 Wozniak, Michal III-929  
 Wozny, Janusz I-607, I-876  
 Wu, Chaolin III-496  
 Wu, Jianjia II-632  
 Wu, Jianping II-551  
 Wu, Jun III-539  
 Wu, Lieyu II-960  
 Wu, Yong II-335  
 Wu, Zhaohui I-568, I-743, II-461,  
 III-1068
- Xian, Jun III-783  
 Xiao, Da III-399  
 Xiao, Shaoping III-284, III-326  
 Xie, Jinkui III-1032  
 Xie, Kai I-925  
 Xin, Jin II-502  
 Xiong, Guomin III-515  
 Xu, Baowen III-1088  
 Xu, Congfu III-1020  
 Xu, Hongtao I-9  
 Xu, Weixiang I-995  
 Xu, Weixuan III-531  
 Xu, Xian II-1038  
 Xu, Zhuoqun III-511, III-515  
 Xue, Huifeng III-854  
 Xue, Wei III-399  
 Xue, Yong III-464, III-472, III-496,  
 III-883
- Yabo, Dong I-1027  
 Yamamoto, Kenji I-956  
 Yan, Chang-Ching II-444  
 Yanami, Hitoshi III-602  
 Yang, Chengyong II-944  
 Yang, Hyungkyu II-493  
 Yang, Jie I-925  
 Yang, Jingmei I-615  
 Yang, Luobin II-68  
 Yang, Weixuan III-284  
 Yang, X.S. I-751, II-199  
 Yang, Xiaolong II-519

- Yang, Xin-She III-1048  
 Yao, Nianmin III-415  
 Yao-Xue, Zhang II-502  
 Yaya, Wei II-502  
 Ye, Juntao II-331  
 Yeom, Heon Y. III-179  
 Yi, Myung-Kyu III-967  
 Yi, Ping II-593  
 Yin, Weiwei II-322  
 Yoon, Seokho II-543  
 Yoon, Yeo-Ran III-1120  
 Youn, Choonhan I-469  
 Youn, Hee Yong I-576, II-568, III-1000,  
 III-1125  
 Yu, Hai III-1044  
 Yu, Lean III-523  
 Yu, Lishan III-511  
 Yu, Shui I-544  
 Yuasa, Fukuko I-165  
 Yue, Wuyi III-539  
 Yue-Zhi, Zhou II-502  
 Yuewei, Huang I-1027  
 Yunjie, Mao I-1027  
  
 Zaman, Safaa I-560  
 Zanero, Stefano III-147  
 Zarina, M. III-447  
 Zelikovsky, Alexander II-1011  
 Zeng, Qinhuai III-887  
 Zeng, Weilin II-485  
 Zhang, Aidong II-1038  
 Zhang, Changyong I-804  
 Zhang, Defu I-783, III-801  
 Zhang, Hua II-616, III-826  
 Zhang, Jian J. II-199  
  
 Zhang, Kaizhong II-960  
 Zhang, Liang I-544  
 Zhang, Min II-519  
 Zhang, Qiangfeng II-985  
 Zhang, Shiyong II-593  
 Zhang, Wenju I-544  
 Zhang, Xia I-908  
 Zhang, Yang II-790, III-619  
 Zhang, Yu II-207  
 Zhao, Mingxi III-846  
 Zhao, Qiang III-826  
 Zhao, Wei II-632  
 Zheng, Kougen II-461  
 Zheng, Weimin III-399, III-415  
 Zheng, Weiming III-163  
 Zheng, Yao I-987  
 Zheng, Zengwei I-552, II-461  
 Zhong, Shaobo III-464, III-496, III-883  
 Zhong, Weimin III-1036  
 Zhong, Yiping II-593  
 Zhou, Chenghu I-963  
 Zhou, Dong II-248  
 Zhou, Hong I-664  
 Zhou, Li I-812  
 Zhou, Runfang III-187  
 Zhou, W. III-586  
 Zhu, Changqian III-826  
 Zhu, Qi I-90  
 Zhu, Wei-Yong III-1044  
 Zhu, Ying II-256, II-347  
 Zhu, Yue Min I-925  
 Ziemiński, Remik III-838  
 Znamirovski, Lech I-766  
 Zornes, Adam II-632